

Power Electronics, Drives, and Advanced Applications

Vinod Kumar
Ranjan Kumar Behera
Dheeraj Joshi
Ramesh Bansal



CRC Press
Taylor & Francis Group

Power Electronics, Drives, and Advanced Applications



Taylor & Francis

Taylor & Francis Group

<http://taylorandfrancis.com>

Power Electronics, Drives, and Advanced Applications

Vinod Kumar

EE Department, Maharana Pratap University of Agriculture
and Technology, Udaipur,
India

Ranjan Kumar Behera

Electrical Engineering Department, IIT Patna, India

Dheeraj Joshi

EE Department, Delhi Technological University, India

Ramesh Bansal

Electrical Engineering Department,
University of Sharjah, UAE



CRC Press

Taylor & Francis Group

Boca Raton London New York

CRC Press is an imprint of the
Taylor & Francis Group, an **informa** business

MATLAB® is a trademark of The MathWorks, Inc. and is used with permission. The MathWorks does not warrant the accuracy of the text or exercises in this book. This book's use or discussion of MATLAB® software or related products does not constitute endorsement or sponsorship by The MathWorks of a particular pedagogical approach or particular use of the MATLAB® software.

CRC Press
Taylor & Francis Group
6000 Broken Sound Parkway NW, Suite 300
Boca Raton, FL 33487-2742

© 2020 by Taylor & Francis Group, LLC
CRC Press is an imprint of Taylor & Francis Group, an Informa business

No claim to original U.S. Government works

Printed on acid-free paper

International Standard Book Number-13: 978-1-138-06239-9 (Hardback)

This book contains information obtained from authentic and highly regarded sources. Reasonable efforts have been made to publish reliable data and information, but the author and publisher cannot assume responsibility for the validity of all materials or the consequences of their use. The authors and publishers have attempted to trace the copyright holders of all material reproduced in this publication and apologize to copyright holders if permission to publish in this form has not been obtained. If any copyright material has not been acknowledged please write and let us know so we may rectify in any future reprint.

Except as permitted under U.S. Copyright Law, no part of this book may be reprinted, reproduced, transmitted, or utilized in any form by any electronic, mechanical, or other means, now known or hereafter invented, including photocopying, microfilming, and recording, or in any information storage or retrieval system, without written permission from the publishers.

For permission to photocopy or use material electronically from this work, please access www.copyright.com (<http://www.copyright.com/>) or contact the Copyright Clearance Center, Inc. (CCC), 222 Rosewood Drive, Danvers, MA 01923, 978-750-8400. CCC is a not-for-profit organization that provides licenses and registration for a variety of users. For organizations that have been granted a photocopy license by the CCC, a separate system of payment has been arranged.

Trademark Notice: Product or corporate names may be trademarks or registered trademarks, and are used only for identification and explanation without intent to infringe.

Visit the Taylor & Francis Web site at
<http://www.taylorandfrancis.com>

and the CRC Press Web site at
<http://www.crcpress.com>

Contents

Preface.....	.xxi
Acknowledgment	xxv
Authors.....	xxvii

SECTION I Power Semiconductor Devices

Chapter 1 Overview of Power Electronics	3
1.1 Introduction	3
1.2 Power Electronics Systems.....	3
1.3 Power Semiconductor Devices.....	4
1.4 Power Electronic Converters	7
1.5 Power Electronic Modules	9
1.6 Applications of Power Electronics	10
1.7 Computer Simulation of Power Electronic Circuits	11
1.7.1 Importance of Simulation.....	12
1.7.2 Benefits of Computer-Aided Simulation	12
1.7.3 Demerits of Computer-Aided Simulation.....	12
1.7.4 Simulation Tools.....	13
Review Questions.....	14
Summary	15
References/Further Reading	15
Chapter 2 Power Semiconductor Devices	17
2.1 Introduction	17
2.2 Power Diode	17
2.2.1 Working and V-I Characteristics.....	19
2.2.2 Diode Reverse Recovery Characteristics	19
2.3 DIAC	21
2.4 TRIAC.....	22
2.5 Characteristics of Power Transistors	23
2.5.1 Bipolar Junction Transistor	23
2.5.1.1 Steady-State Characteristics.....	24
2.5.1.2 Switching Characteristics of a BJT	25
2.5.2 Power MOSFETs	27
2.5.3 Insulated-Gate Bipolar Transistor	30
2.6 Characteristics of the Thyristor.....	32
2.6.1 Static V-I Characteristics of a Thyristor	33
2.6.1.1 Reverse Blocking Mode (RBM).....	34
2.6.1.2 Forward Blocking Mode	34
2.6.1.3 Forward Conducting Mode	34

2.6.2	Switching Characteristics of a Thyristor.....	35
2.6.3	Thyristor Gate Characteristics	38
2.7	Gate Turn-Off (GTO) Thyristor	40
2.7.1	Static V-I Characteristics.....	40
2.7.2	Switching Characteristics of GTO	41
2.8	Two-Transistor Model of a Thyristor	42
	Review Questions	44
	Summary	45
	References/Further Reading	45
Chapter 3	Silicon-Controlled Rectifier	47
3.1	Introduction	47
3.2	SCR Construction.....	47
3.2.1	Planer Diffused	47
3.2.2	Alloy Diffused.....	48
3.3	Specifications and Ratings	49
3.3.1	Voltage Ratings	49
3.3.2	Current Ratings	50
3.4	Methods of Turn On	51
3.4.1	Gate Triggering	51
3.4.2	Forward Voltage Triggering	53
3.4.3	dv/dt Triggering	53
3.4.4	Temperature Triggering.....	53
3.4.5	Light Triggering	53
3.5	Firing (Triggering) Circuits for SCR	54
3.5.1	Resistance (R) Triggering Circuit	55
3.5.2	Resistance-Capacitance (RC) Triggering Circuit.....	58
3.5.3	UJT Relaxation Oscillator.....	61
3.6	Series and Parallel Operation of SCR	62
3.6.1	Series-Connected SCRs	63
3.6.2	Parallel-Connected SCRs.....	65
3.7	String Efficiency.....	66
3.8	Protection of SCR.....	67
3.8.1	Overshoot Protection.....	67
3.8.2	Overcurrent Protection.....	68
3.8.3	dv/dt Protection	69
3.8.4	di/dt Protection.....	72
3.8.5	Gate Protection.....	72
3.9	Solved Problems	72
	Review Questions and Unsolved Problems.....	98
	Summary	98
	Main Formulas of the Chapter.....	98
	References/Further Reading	100

SECTION II Power Electronic Converters

Chapter 4	Phase-Controlled Rectifiers.....	105
4.1	Introduction	105
4.2	Classifications.....	105
4.3	Performance Indices for Line-Commutated Converter	107
4.4	Single-Phase Converters.....	110
4.4.1	Single-Phase Half-Wave-Controlled Rectifier with R Load	110
4.4.2	Single-Phase Half-Wave-Controlled Rectifier with RL Load	113
4.4.3	Single-Phase Half-Wave-Controlled Rectifier with RL Load and Freewheeling Diode (FD)	116
4.4.4	Single-Phase Full-Wave-Controlled Converter	118
4.4.4.1	Single-Phase Full-Wave Mid-Point Rectifier with R Load.....	119
4.4.4.2	Single-Phase Full-Wave Bridge-Type-Controlled Rectifier with R Load	121
4.4.4.3	Single-Phase Full-Wave Bridge-Type-Controlled Rectifier with RL Load	122
4.4.5	Single-Phase Half-Wave-Controlled Rectifier with RLE Load.....	125
4.4.6	Single-Phase Full Converter with RLE Load and Discontinuous Conduction	128
4.5	Three-Phase Converters	129
4.5.1	Three-Phase Half-Wave Converters with RL Load	129
4.5.2	Three-Phase Full Converter	133
4.6	Dual Converters	135
4.6.1	Ideal Dual Converter	136
4.6.2	Practical Dual Converter.....	137
4.6.2.1	Dual Converter without Circulating Current	138
4.6.2.2	Dual Converter with Circulating Current	139
4.6.3	Single-Phase Dual Converter	139
4.6.4	Three-Phase Dual Converters	142
4.7	Effect of Source Impedance.....	144
4.7.1	Single-Phase Fully Controlled Rectifier with Source and Load Inductance	144
4.8	Solved Problems	147
	Review Questions and Unsolved Problems.....	172
	Summary	174
	Main Formulas of the Chapter.....	174
	References/Further Reading	177

Chapter 5	Semiconverters	179
5.1	Introduction	179
5.2	Single-Phase Semiconverter with RL Load	179
5.3	Three-Phase Semiconverter with RL Load.....	186
5.4	Power Factor Improvement	188
5.4.1	Extinction Angle Control (EAC).....	188
5.4.2	Symmetrical Angle Control (SAC)	190
5.4.3	Pulse Width Modulation Control	192
5.4.4	Sinusoidal Pulse Width Modulation Control	194
5.5	Inversion Operation	195
5.6	Solved Problems.....	195
	Review Questions and Unsolved Problems.....	212
	Summary	213
	Main Formulas of the Chapter.....	214
	References/Further Reading	216
Chapter 6	Chopper	217
6.1	Introduction	217
6.2	Chopper Classifications	217
6.3	Principle of Chopper Operation	218
6.4	Control Strategies	220
6.4.1	Time Ratio Control.....	220
6.4.2	Current Limit Control	222
6.5	Step Up/Down Chopper	222
6.6	Chopper Configurations	223
6.6.1	First-Quadrant or Type-A Chopper.....	224
6.6.2	Second-Quadrant or Type-B Chopper	224
6.6.3	Two-Quadrant Type-A Chopper or Type-C Chopper.....	225
6.6.4	Two-Quadrant Type-B Chopper or Type-D Chopper.....	225
6.6.5	Four-Quadrant Chopper or Type-E Chopper	226
6.7	Analysis of Type-A (Step-Down) Chopper	227
6.7.1	With Resistive Load	227
6.7.2	With RLE Load	228
6.7.2.1	Steady-State Ripple	231
6.7.2.2	Limits of Continuous Conduction.....	231
6.7.2.3	Computation of Extinction Time (t_x).....	232
6.7.2.4	AC Ripple Voltage (V_r).....	233
6.7.2.5	Ripple Factor (RF)	233
6.8	Commutation of Chopper.....	233
6.8.1	Voltage-Commutated Chopper (Classical Chopper or Parallel Capacitor Turn-Off Chopper)	234

6.8.2	Current-Commutated Chopper.....	240
6.8.3	Load-Commutated Chopper.....	244
6.9	Switched-Mode Regulators	247
6.10	Solved Problems	261
	Review Questions and Unsolved Problems.....	288
	Summary	291
	Main Formulas of the Chapter.....	291
	References/Further Reading	294
Chapter 7	DC-to-AC Converter: Inverter	297
7.1	Introduction	297
7.2	Classifications.....	297
7.3	Performance Parameters of Inverters	298
7.4	Voltage Source Inverters	299
7.4.1	Single-Phase Voltage Source Inverters.....	299
7.4.1.1	With RL and RLC Overdamped Loads....	303
7.4.1.2	With RLC Underdamped Load	303
7.4.1.3	Fourier Analysis of Single-Phase Inverter Output Voltage	303
7.4.2	Three-Phase VSI Bridge Inverter	304
7.4.2.1	Three-Phase 180-degree Mode VSI	305
7.4.2.2	Three-Phase 120-degree Mode VSI	310
7.4.2.3	Merits and Demerits of 180°- and 120°-Mode VSIs	314
7.5	Current Source Inverters	315
7.5.1	Single-Phase CSI	315
7.5.2	Three-Phase CSI.....	316
7.6	CSI versus VSI.....	317
7.7	Voltage Control of Single-Phase Inverters	318
7.7.1	Control of Input DC Voltage	318
7.7.2	External Control of AC Output Voltage	318
7.7.3	Internal Control of Inverters.....	319
7.8	Pulse-Width Modulation.....	320
7.8.1	Single Pulse-Width Modulation	320
7.8.2	Multiple Pulse-Width Modulation.....	321
7.8.3	Sinusoidal Pulse-Width Modulation.....	322
7.9	Advanced Modulation Techniques	323
7.9.1	Trapezoidal Modulation	324
7.9.2	Staircase Modulation.....	325
7.9.3	Stepped Modulation.....	326
7.9.4	Harmonic-Injected Modulation	326
7.9.5	Delta Modulation.....	327
7.10	Space Vector Modulation	328
7.10.1	Implementation of Space Vector PWM.....	328

7.11	Harmonic Reduction.....	334
7.12	Solved Problems	334
	Review Questions and Unsolved Problems.....	352
	Summary	353
	Main Formulas of the Chapter.....	353
	References/Further Reading	354
Chapter 8	AC Voltage Controllers	357
8.1	Introduction	357
8.2	Principle of On-Off Control	357
8.3	Principle of Phase Control.....	360
8.4	Single-Phase AC Voltage Controllers.....	361
8.4.1	Single-Phase Full-Wave AC Voltage Controller with Resistive Load	361
8.4.2	Single-Phase Full-Wave AC Voltage Controller with RL Load	363
8.4.3	Single-Phase Full-Wave AC Voltage Controller with Purely Inductive Load	365
8.5	Three-Phase Full-Wave AC Voltage Controllers.....	366
8.6	Solved Problems	366
	Review Questions	372
	Summary	372
	Main Formulas of the Chapter.....	373
	References/Further Reading	373
Chapter 9	Cycloconverter.....	375
9.1	Introduction	375
9.2	Classifications.....	375
9.3	Principle of Operation of Single-Phase to Single-Phase Cycloconverter.....	375
9.3.1	Single-Phase to Single-Phase Step-Up Cycloconverter.....	375
9.3.1.1	Midpoint Cycloconverter.....	375
9.3.1.2	Bridge-Type Cycloconverter.....	377
9.3.2	Single-Phase to Single-Phase Step-Down Cycloconverter.....	378
9.3.2.1	Bridge-Type Cycloconverter.....	378
9.3.2.2	Midpoint Cycloconverter.....	380
9.4	Three-Phase to Single-Phase Cycloconverters.....	380
9.5	Three-Phase to Three-Phase Cycloconverters	382
9.6	Output Voltage Equation for the Cycloconverter	384
9.7	Reduction of Output Harmonics.....	385
9.8	Solved Problems	386

Review Questions	387	
Unsolved Problems	387	
Summary	388	
Main Formulas of the Chapter	388	
References/Further Reading	388	
Chapter 10	Switched-Mode Power Supplies	391
10.1	Introduction	391
10.2	Basic Working of Switched-Mode Power Supply	391
10.2.1	Forward-Mode-Type Switching Regulator	392
10.2.2	Flyback-Mode-Type Switching Regulator	393
10.3	Switched-Mode Power Supply (SMPS)	395
10.3.1	Flyback Switched-Mode Power Supply	395
10.3.2	Push-Pull Switched-Mode Power Supply	397
10.3.3	Half-Bridge Switched-Mode Power Supply	398
10.3.4	Full-Bridge Switched-Mode Power Supply	399
10.4	Resonant DC Power Supplies	400
10.5	Bidirectional DC Power Supplies	401
Review Questions	402	
Summary	402	
Main Formulas of the Chapter	402	
References/Further Reading	403	
Chapter 11	Multipulse Converter	405
11.1	Introduction	405
11.2	Multipulse Converter	405
11.2.1	Unidirectional AC-DC Converters	405
11.2.1.1	12-Pulse AC-DC Converters	405
11.2.1.2	18-Pulse AC-DC Converters	406
11.2.1.3	24-Pulse AC-DC Converters	406
11.3	Multilevel Inverters	407
11.3.1	Cascaded H-Bridge Multilevel Inverter	408
11.3.2	Neutral Point-Clamped Multilevel Inverter	410
11.3.3	Flying Capacitor Multilevel Inverter (FCMLI)	411
11.4	Power Converter Switching Techniques	413
11.4.1	Hysteresis Current Control of Inverters	413
11.4.2	Pulse-Width Modulation (PWM) Techniques	415
11.4.2.1	Sinusoidal PWM	416
11.4.2.2	Phase-Opposition Sinusoidal PWM	417
11.4.2.3	In-Phase Sinusoidal PWM	418
11.4.2.4	Third-Harmonic Injection Sinusoidal PWM (THISPWM)	418
11.4.2.5	Three-Phase Two-Level SVPWM	420

11.5	Resonant Converters	426
11.5.1	Soft-Switching Topologies.....	428
11.5.1.1	Resonant Load Converters	429
11.5.1.2	Resonant Switch Converters.....	430
11.5.1.3	Flyback Converter	431
11.5.1.4	Switched Mode Power Conversion (SMPC) with Regulated DC Source.....	432
11.5.1.5	Phase-Shift Bridge.....	432
11.5.1.6	Parallel Resonant Converter	433
11.5.1.7	Multielement Resonant Converters.....	434
11.6	Dual Active-Bridge Converter	435
11.7	Three-Phase AC-AC Matrix Converter	437
11.7.1	Three-Phase to Three-Phase DMC Modeling.....	439
11.7.2	Space Vector PWM	440
11.7.3	Commutation Methods in DMC	446
11.7.4	Deadtime Commutation	446
11.7.5	Current Commutation Based on Multiple Steps....	446
11.7.6	Simulation Results.....	447
	Review Questions	448
	Summary	450
	References/Further Reading	450

SECTION III Electrical Drives

Chapter 12	Introduction of Electrical Drives.....	455
12.1	Electric Drives Concepts.....	455
12.1.1	Electrical Motors	456
12.1.2	Power Modulator	457
12.1.3	Sources	458
12.1.4	Controller.....	459
12.1.5	Load Torques	459
12.2	Advantages of Electrical Drives	459
12.3	Characteristics of an Electrical Drive	460
12.4	Classifications	461
12.5	Quadrant Operation of the Drive	462
12.5.1	One Quadrant	462
12.5.2	Two Quadrants.....	463
12.6	Four-Quadrant Operation of Electrical Drives	463
12.7	Constant-Torque Drive	464
12.8	Constant-Power Drive	465
12.9	Nature and Components of Load	466
12.9.1	Fan-Type Load.....	466
12.9.2	Load Torque as a Function of Position	466

12.9.3	Hoisting Load	466
12.9.4	Load Torque as a Function of Angle of Shaft Displacement	467
12.9.5	Load Torques Varying with Time	468
12.10	Combined Motor Load Dynamics	469
12.11	Equivalent System.....	470
12.11.1	Equivalent Load Torque Referred to the Motor.....	471
12.11.2	Equivalent Moment of Inertia	471
12.11.3	Relating Translation Motion to Rotational Motor	472
12.12	Practical Determination of Moment of Inertia	473
12.12.1	Retardation Test.....	473
12.13	Rating of Electrical Drives.....	474
12.13.1	Heating Affects All Machines during Running Produce Losses	474
12.13.2	Loading Conditions	476
12.13.3	Load Inertia	476
12.13.4	Environmental Factors	477
12.14	Selection of Electrical Drives	477
12.14.1	Drive Considerations	479
12.15	Guides for Selection of Electrical Motors.....	480
12.16	Solved Problems.....	481
	Review Questions.....	483
	Unsolved Problems.....	484
	Summary	485
	References	485
Chapter 13	Control of DC Motor Drives	487
13.1	Introduction	487
13.2	Basics of DC Machines.....	487
13.2.1	Shunt and Separately Excited DC Motors.....	488
13.2.2	DC Series Motor.....	489
13.3	Effect of Change in Supply Voltage on Characteristics of DC Motors	491
13.3.1	Separately Excited DC Motor.....	491
13.3.2	DC Series Motor.....	491
13.4	Effect of Change in Load Torque	491
13.5	Speed Control of DC Motors	492
13.6	Phase-Controlled Rectifier Control of DC Motor.....	492
13.6.1	Single-Phase Fully Controlled Rectifier Control of DC Separately Excited Motor Drive	493
13.6.2	Single-Phase Half-Controlled Rectifier (or Semiconverter) Control of DC Separately Excited Motor Drive	495

13.6.3	Three-Phase Fully Controlled Rectifier Control of DC Separately Excited Motor Drive.....	497
13.6.4	Three-Phase Half-Controlled Rectifier Control of Separately Excited DC Motor	499
13.7	Chopper Control of DC Motor.....	500
13.7.1	Chopper Control of Separately Excited DC Motors	500
13.7.2	Chopper Control of DC Series Motor	506
13.8	Solved Problems.....	507
	Review Questions and Unsolved Problems.....	509
	Summary	510
	References/Further Reading	510
Chapter 14	Control of Induction Motor Drives.....	513
14.1	Introduction.....	513
14.2	Basics of the Induction Motor	513
14.3	Modeling and Characteristics of Induction Drives	516
14.4	No-Load Current of a Three-Phase Motor	518
14.5	Starting Performance of the Three-Phase Induction Motor.....	518
14.6	Modifying Torque-Speed Characteristics of the Three-Phase Induction Motors.....	519
14.6.1	Varying the Supply Voltage.....	519
14.6.2	Constant V/f Control	519
14.6.3	Adding Impedance in the Stator Circuit	521
14.6.4	Adding Resistance in the Rotor Circuit.....	521
14.6.5	Voltage Injection—The Rotor Circuit	523
14.6.6	Pole-Changing Drive	523
14.6.7	Pole-Amplitude Modulation	524
14.7	Transient Stability	524
14.8	Braking of the Induction Motor	524
14.8.1	Regenerative Braking	524
14.8.2	Plugging	526
14.8.3	Dynamic Braking	526
14.9	Speed Control of Three-Phase Induction Motors	527
14.9.1	Stator Voltage Control Method.....	527
14.9.2	Variable-Frequency Control Method.....	528
14.9.3	Rotor-Resistance Control.....	532
14.9.4	Injection of Voltage in the Rotor Circuit	533
14.10	Slip Power Control Using Power Semiconductor Converter	535
14.10.1	Static Rotor-Resistance Control.....	535
14.10.2	Static Scherbius Drive	539
14.10.3	Static Kramer Drive	543

14.11 Solved Examples	543
Review and Unsolved Questions.....	548
Summary	548
References	548
Chapter 15 FPGA-Based Fuzzy-Logic Control of DTC for Matrix-Converter-Fed Induction-Motor Drives	551
15.1 Introduction.....	551
15.2 Various Controllers for Induction Motor Drives.....	551
15.3 Integrated Circuits for IM Drives	552
15.4 Details of IM Drive under Investigation	553
15.4.1 Direct-Torque Control for Matrix-Converter-Fed Induction-Motor Drive.....	554
15.4.2 Estimation of Flux and Electromagnetic Torque ..	556
15.4.3 Development of Developed Fuzzy-Logic Controller.....	557
15.4.4 Control Implementation on the FPGA Board	559
15.5 Simulation Results of Performance Comparison between Developed Fuzzy-Logic DTC-Controller-Based IM Drive and Conventional DTC-Based IM Drive..	562
15.5.1 Response of the System at Constant Reference Speed 100 rad/s and No-Load Condition	562
15.5.2 Response of the System with Reference Speed Reversal at No-Load Condition.....	562
15.6 Experimental Results of Developed FLDTC-Based MC-Fed IM Drive	566
15.6.1 Response of the Drive with Constant Reference Speed (500 rpm) at No-Load Condition.....	566
15.6.2 Stability Analysis of the Developed System	566
15.6.3 Harmonic Analysis.....	566
Summary	572
References/Further Reading	572
Chapter 16 Control of Synchronous and Special Motor Drives	575
16.1 Introduction.....	575
16.2 Basics of the Synchronous Motor	575
16.3 Speed Control of the Synchronous Motor.....	578
16.3.1 True Synchronous Mode	578
16.3.2 Self-Controlled Mode.....	578
16.4 Stepper Motor.....	579
16.5 Variable-Reluctance Motor	580
16.5.1 Single-Stack Variable-Reluctance Stepper Motor....	581
16.5.2 Multistack Variable-Reluctance Stepper Motor	582

16.6 Permanent-Magnet Motors	582
16.7 Hybrid Stepper Motor.....	583
16.8 Drive Circuits for Stepper Motors	584
Unsolved Problems.....	585
Summary	586
References	586

SECTION IV Advanced Power Electronics Applications

Chapter 17 Electric/Hybrid Electric Vehicles.....	591
17.1 Introduction	591
17.2 Power-Train Architectures.....	591
17.2.1 Major Characteristics of BEVs, HEVs, and FCVs ..	591
17.2.2 Different Functions of the Various HEV Architectures	593
17.3 Drivetrain Analysis.....	594
17.3.1 BEV Drivetrain Topology	594
17.3.2 Series HEV Drivetrain Topology	594
17.3.3 Parallel HEV Drivetrain Topology	595
17.3.4 Series-Parallel HEV Drivetrain Topology	596
17.3.5 FCV Drivetrain Topology	596
17.4 Vibration and Vehicle Dynamics.....	598
17.4.1 Vibration.....	598
17.4.2 Vehicle Dynamics	598
17.5 Power Converter for Electric/Hybrid Electric Vehicles	601
17.5.1 Configurations of Engine-Based HEV	601
17.5.2 Configurations of FCV	601
17.5.3 Basic Bidirectional DC-DC Converters	602
17.5.4 Isolated Bidirectional DC-DC Converters	604
17.5.5 Multiphase Bidirectional DC-DC Converters	605
17.6 Vehicular Power Electronics	606
17.6.1 Power Converters for DC Motor Drives.....	606
17.6.2 Power Converters for AC Motor Drives.....	606
17.7 Selection of Motor Drives for Electric/Hybrid Electric Vehicles.....	607
17.7.1 Comparative Study	608
17.7.1.1 DC Motor (DC)	608
17.7.1.2 Induction Motor.....	608
17.7.1.3 Synchronous Motor (PM Brushless Motor)	609
17.7.1.4 Switched Reluctance Motor (SRM)	610

17.8	Solar and Fuel Cell Drives	611
17.9	PV Array Formations.....	611
17.10	Solar-Powered Variable-Speed Drive	614
17.10.1	Solar-Based Electric Vehicles.....	614
17.10.2	Solar-Based Pump Drive	615
17.11	Fuel-Cell-Powered Electrical Drives	616
17.12	Solved Problems.....	617
	Review Questions and Unsolved Problems.....	618
	Summary	619
	References/Further Reading	619
	Chapter 18 Power Electronics Applications in Power Systems	623
18.1	Introduction.....	623
18.2	General Aspects of DC Transmission.....	623
18.3	Converter Circuits and Their Analysis	624
18.4	High Voltage DC Transmission	625
18.5	Mechanism of Active and Reactive Power Flow Control	626
18.6	Basic FACTS Controllers: SVC, TCR, TSC, STATCOM, TCSC, UPFC.....	627
18.6.1	Static VAR Compensator.....	627
18.6.2	Thyristor-Controlled Reactor (TCR)	627
18.6.3	Thyristor-Switched Capacitor (TSC).....	628
18.6.4	Static Synchronous Compensator.....	629
18.6.5	TCSC	629
18.6.6	UPFC	631
18.7	Modeling of FACTS Controllers.....	633
18.7.1	Filter Modeling	633
18.7.2	STATCOM Modeling	634
18.8	System Dynamic Performance Improvement with FACTS Controllers.....	635
18.9	Interline Power Flow Controller (IPFC)	638
18.10	Unified Power Quality Conditioners (UPQC)	639
18.11	Power Electronics in Power Generation.....	640
	Review Questions	641
	Summary	641
	References/Further Reading	641
	Chapter 19 Power Electronics Application in Renewable Energy (Wind and PV) System Integration	643
19.1	Introduction.....	643
19.2	Grid-Connected Converters—Key Element for Grid Integration of WT and PV Systems	644

19.3	Power Electronics Converters for Renewable Energy Integration	645
19.3.1	Variable-Speed Double-Fed Induction Generator (DFIG).....	645
19.3.2	Variable-Speed Full-Power Converter	645
19.3.3	Boost Converter.....	647
19.4	Photovoltaic Inverter Structure	648
19.5	Grid Converter Structure for Wind Turbine System.....	652
19.5.1	Single-Cell (VSC or CSC)	653
19.5.2	Medium-Power Converter	653
19.5.3	High-Power Converter.....	653
19.6	Grid Requirements for Photovoltaic and Wind Turbine Systems.....	656
19.7	Grid Synchronization Using a Phase-Locked Loop	657
19.7.1	Basic Structure of a Phase-Locked Loop	658
19.7.2	Basic Equations of PLL.....	658
19.7.3	Linearized Small-Signal Model of a PLL	659
19.7.4	PLL Based on $T/4$ Transport Delay	660
19.7.5	PLL Based on the Inverse Park Transform.....	661
19.7.6	Second-Order Generalized Integrator	663
19.7.7	SOGI-QSG	666
19.8	Control of Grid Converter under Grid Fault	668
19.9	Design of Grid Filters	669
19.10	Solved Problems.....	671
	Review Questions	672
	Summary	673
	References/Further Reading	673
Chapter 20	Distributed Generation and Microgrids	675
20.1	Introduction.....	675
20.2	DG and MG Components	676
20.3	Microsources and Loads	677
20.4	Power Electronics Interface	677
20.4.1	DC-Bus Interface.....	677
20.4.2	AC-Bus Interface.....	678
20.5	Architecture (DC/AC/Hybrid) of Microgrids and Storage Systems	679
20.5.1	DC Microgrid	679
20.5.2	AC Microgrid	679
20.5.3	Hybrid Microgrid	680
20.5.4	Storage System	681
20.6	Integration Issues of Distributed Generation and Synchronization	681
20.6.1	Integration Issues.....	681
20.6.2	Grid Synchronization	682

20.7	Interconnection of Power Electronics Converters with Medium-Voltage Grid	684
20.8	Stability Aspects in Microgrids	684
20.8.1	Major Stability Issues in the Microgrid	684
20.8.2	Stability Improvement in Microgrid	685
20.9	Islanding Techniques.....	686
20.9.1	Active Islanding Detection.....	686
20.9.2	Passive Islanding Detection.....	687
20.10	Power Electronics in Smart-Grid Applications.....	687
20.11	Vehicle-to-Grid Interconnection	688
20.12	Grid-to-Vehicle.....	690
	Review Questions.....	691
	Summary	691
	References/Further Reading	691
Chapter 21	Wireless Power Transfer.....	695
21.1	Introduction	695
21.2	Wireless Charging Landscape.....	695
21.3	Wireless Power Transfer Model	695
21.3.1	Two-Coil Structures	695
21.3.2	Direct-Fed (DF) Coils	696
21.4	Magnetic Resonance WPT System	697
21.4.1	Multiterminal WPT System	697
21.4.2	Dual and Multiterminal Links	700
21.5	Inductive Wireless Power Transfer (IWPT).....	700
21.6	Technology Overview and Concepts of Wireless Charging System	701
21.6.1	Inductive-Coupling-Based Wireless Charging System	702
21.6.2	Magnetic-Resonance-Based Wireless Charging System	702
21.6.3	Microwave-Based Wireless Charging System	702
21.7	Analysis of Three Resonating Coupled Coils	702
21.8	Wireless Power Transfer in Online Electric Vehicle.....	705
21.9	Hardware Design of Wireless Power Transmitter and Receiver.....	706
	Review Questions.....	708
	Summary	708
	References/Further Reading	708
Appendix	711
Index	749



Taylor & Francis

Taylor & Francis Group

<http://taylorandfrancis.com>

Preface

With the integration of renewable energy sources into a power system, the role of power electronics has become extremely important.

Power Electronics, Drives, and Advanced Applications is suitable at both the under- and postgraduate levels. It also provides a comprehensive reference material for power electronics professionals and engineers. This textbook is supported by a large number of solved, unsolved, and review problems.

This book contains twenty-one chapters that are arranged in four sections. **Section I** in three chapters covers an overview of power electronics, power semiconductor devices, and silicon control rectifiers. **Section II** contains eight chapters and describes power converters, such as phase-controlled rectifiers, semiconverters, choppers, inverters, AC voltage controllers, multipulse converters, and switched-mode power supplies. The five chapters of **Section III** on electric drives presents control of DC, induction, FPGA-based fuzzy-logic control of DTC for matrix-converter-fed induction motor drives, and synchronous and special motor drives. **Section IV** in five chapters covers the areas of advanced power electronics applications, that is, electric/hybrid electric vehicles; power electronics applications in power, renewable energy, distributed generation, and microgrids; and wireless power transfer. Brief descriptions of the contents are as follows.

Chapter 1 presents an overview of power electronics, and **Chapter 2** explains the construction, working, and different characteristics of various power semiconductor devices for power applications. **Chapter 3** presents the construction, structure, working, and principles of operation of SCR with different characteristics for power applications.

Chapter 4 discusses the controlled rectifiers used at high power levels for controlled transfer of power between an AC source and the adjustable DC load by controlling the phase angle or delay angle of thyristors. This chapter discusses various types of rectifiers with the effect of source and load impedance. **Chapter 5** discusses half-controlled rectifiers or semiconverters that are used at high power levels for controlled transfer of power between an AC source and the adjustable DC load by controlling phase angle or delay angle of thyristors.

Chapter 6 covers in detail various converter topologies for DC-to-DC conversion. These converters are widely used for various types of DC power supplies. These are also very common in telecommunication systems and battery-operated systems. **Chapter 7** discusses in detail the voltage and current-source inverters with single- and three-phase AC outputs along with different voltage-control techniques. It also explains the different pulse-width modulation schemes.

Chapter 8 explains the working principles of different AC voltage controllers along with their controls. It can be seen that two types of control strategies, that is, phase control and integral cycle control, can be effectively used to control the power flow in AC voltage controllers. Few main applications of such converters are for industrial and domestic heating, lighting control, starting of induction motors, motion control of AC drives, etc. AC voltage controllers have replaced the use of

magnetic amplifiers, reactors, auto transformers, etc. for these applications due to faster control, higher efficiency, less maintenance, and being compact in size.

Chapter 9 deals in the detailed principles of operation of different step-up and step-down cycloconverters, such as single-phase to single-phase, three-phase to single-phase, and three-phase to three-phase. Various applications of cycloconverters include induction heating, motion control of AC drives, power supply in aircrafts and shipboards, and static VAr compensators. **Chapter 10** studies the concept and principle of operation of different switched-mode power supplies, resonant DC power supplies, and bidirectional power supplies. Due to factors such as increased switching speeds, low cost, low-power dissipation, higher current, and voltage ratings, the switching-power supplies have emerged significantly.

Chapter 11 discusses different kinds of multipulse converter structures for AC-DC converters and how they help in reducing harmonics. Detailed multilevel pulse-width modulation (PWM) voltage source converters (VSC) for high-power drive applications are discussed. The operating principles, characteristics, modulation methods, and latest developments of these converters, such as neutral-point clamped cascaded H-bridge and flying capacitor multilevel converters, are presented. Well-known PWM for industrial applications and hysteresis current control (HCC) techniques for VSC are discussed. The operation of dual active bridge (DAB) and matrix converter technology is explained.

Chapter 12 deals with the basic concepts of the electric drive. Each component of the electric drive is explained. Emphasis is also given on the load component, which is a deciding factor to select a suitable rating for the electric drive. **Chapter 13** presents the control of DC motors, which are highly suitable for the servo drive applications.

Chapter 14 presents the control of induction motors. AC drives have several advantages over DC drives, such as being cheaper, 30% lighter than DC motors, and low maintenance. **Chapter 15** presents the development of the fuzzy-logic-based DTC controller on the FPGA board for matrix converter-fed induction motor drives to achieve superior performance under different conditions with reduced harmonics. **Chapter 16** presents the control of synchronous and special motor drives. It converts variable reluctance, permanent magnet, hybrid stepper, and synchronous motors.

Chapter 17 provides the fundamentals of electric/hybrid electric vehicles and their drives technology that includes drivetrain analysis, vibration, vehicle dynamics, power converters, vehicular power electronics and selection of motor drives. General solar-powered electric drives and fuel cells with their motor drive are provided.

Chapter 18 presents a general introduction of power electronics application to the power system, which includes HVDC transmission; power-flow modeling; FACTS controllers such as SVC, STATCOM, TCSC, UPFC, and IPFC; and power-quality conditioners.

Chapter 19 explains the key elements for wind and PV systems for grid integration. A brief discussion of MPPT algorithms and robust inverter topologies are provided. The importance of the filter and their utilization for integration with the utility grid is discussed.

Chapter 20 presents distributed generation (DG) and microgrid (MG) technology. Microgrid integration, stability issues, synchronization, and its interconnection with

power electronics converters are explained for both grid connected and islanding modes. Few power electronics converters for smart-grid applications and an overview of vehicle-to-grid (V2G) and grid-to-vehicle (G2V) interconnection technologies with the microgrid are provided.

[Chapter 21](#) discusses how the wireless power transfer is a cutting-edge technology for modern portable electronics devices. The analysis of inductive coupling and the resonant-based coupled inductor system and analysis of two and three wireless power transmission system are discussed.

[Appendix A](#) provides, in detail, various MATLAB-based/Simulink models and programs for circuit computation, simulation, waveform plots, and spectrum analysis of various power electronic circuits.

MATLAB® is a registered trademark of The MathWorks, Inc. For product information, please contact:

The MathWorks, Inc.
3 Apple Hill Drive
Natick, MA 01760-2098 USA
Tel: 508 647 7000
Fax: 508-647-7001
E-mail: info@mathworks.com
Web: www.mathworks.com



Taylor & Francis

Taylor & Francis Group

<http://taylorandfrancis.com>

Acknowledgment

Authors sincerely thank Dr. Gagandeep Singh, Mouli Sharma, Prachi Mishra of CRC Press, Taylor & Francis Group; and Monica Felomina of Lumina Datamatics for their help in the timely publication of the book. Authors would like to thank their universities, authorities, and staff members for maintaining a cordial atmosphere and providing the facilities for the completion of the book. Authors would like to express gratitude and sincere regards to their family members who have provided great support during preparation of this book.

Also, Dr. Ranjan dedicates this book to HDG A. C. Bhaktivedanta Swami Prabhupada, Founder Acharya ISKCON. Dr. Ranjan would like to express his heartfelt gratitude to his father Sri Narayan, Mother Tara Rani, and teachers. He extends his sincere thanks to his wife Madhurya Rasa Devi Dasi. Thanks are due to Padma, Sanjay, Runu, Dr. Sanjoy Kumar Parida, Prof. Shayama Prasad Das of IIT Kanpur, Prof. David Gao, Prof. J. Ojo, and all his colleagues at IIT Patna. He thanks his students Utkal Muduli, Bheemaiah Chikondra, Md. Junaid Akhtar, Jitendra Kumar, Suryaprakash, Chintami Mahapatro, Bibhunandan Pradhan, Anish Ahmad, Rajalaxmi Rath, Jasmine Minz, and Omsmaran Mahapatra for writing, editing, and helping to develop the manuscript. He is highly indebted to his teacher Prof. Laxmidhardhar Behera, who taught him the very purpose of all his endeavors. He expresses his heartfelt gratitude to Lord Jagannath, Baladeva, and Mother Subhadra for unlimited blessing and strength.

Suggestions leading to the improvement of the book will be gratefully acknowledged and incorporated in future editions.



Taylor & Francis

Taylor & Francis Group

<http://taylorandfrancis.com>

Authors



Vinod Kumar has more than 15 years of teaching, research, and industrial experience. Currently, he is faculty in the Department of Electrical Engineering, Maharana Pratap University of Agriculture & Technology, Udaipur, India. He has published several books/book chapters and over 80 papers in journals and conferences. He has received the prestigious Career Award for Young Teachers from AICTE, the government of India, New Delhi. His current research interests include power electronics, power quality, and wind-power generation. He is an associate editor of the reputed

journal *IET-Renewable Power Generation*. He is a fellow at the Institution of Engineers (India).



Ranjan Kumar Behera received his BE degree in electrical engineering from the Regional Engineering College Rourkela, Rourkela, India, and M.Tech and PhD degrees from the Indian Institute of Technology Kanpur, Kanpur, India, in 1998, 2003, and 2009, respectively. He worked at Hindustan Aeronautic Limited, Sunabeda, as a trainee engineer. Since May 2009, he has been a faculty member in the Department of Electrical Engineering at IIT Patna, where he became head of the department in January 2016. From July 2008 to February 2009, he was as a visiting scholar at the Energy Systems Research Center, Tennessee Technological University, USA,

and a visiting research collaborator in the ECE department, University of Pretoria, in July 2016. His current research interests include power electronic, electric motor drives, and nonlinear control applications.



Dheeraj Joshi received an ME in electrical engineering from the Indian Institute of Technology, Roorkee, in 2000 and a PhD in electrical engineering from the National Institute of Technology, Kurukshetra, India, in 2010. He is presently working as professor in the Department of Electrical Engineering, Delhi Technological University, New Delhi, India. His present research interests are renewable power generation, power electronics, and application of AI techniques.



Professor **Ramesh Bansal** has more than 25 years of diversified experience of research, scholarship of teaching and learning, accreditation, industrial, and academic leadership in several countries. Currently, he is a professor in the Department of Electrical Engineering at University of Sharjah. Previously, he was professor and group head (Power) in the ECE Department at University of Pretoria (UP), South Africa. Prior to his appointment at UP, he was employed by the University of Queensland, Australia; University of the South Pacific, Fiji; BITS Pilani, India; and Civil Construction Wing, All India Radio.

Prof. Bansal has significant experience in collaborating with industry and government organizations. These utilities include NTPC (a 60 GW Indian power generation company), Powerlink, and ESKOM. During sabbaticals, he has worked with Powerlink, an Australian government-owned corporation responsible for Queensland's high-voltage electricity transmission network. He has made significant contributions to the development and delivery of BS and ME programs for utilities. He has extensive experience in the design and delivery of CPD programs for professional engineers. He has carried out research and consultancy and attracted significant funding from industry and government organizations.

Professor Bansal has published over 300 journal articles, presented papers at conferences, and wrote books and chapters in books. He has Google Citations of over 9000 and an h-index of 45. He has supervised 20 PhDs, 4 postdocs, and is currently supervising several PhD students. His diversified research interests are in the areas of renewable energy (wind, PV, DG, microgrid) and smart grid. Professor Bansal is an editor of several highly regarded journals: *IET-RPG*, *IEEE Systems Journal*, *Electric Power Components and Systems*, and *Technology and Economics of Smart Grids and Sustainable Energy*. He is a Fellow and Chartered Engineer at IET-UK, Fellow Engineers Australia, Fellow Institution of Engineers (India), Fellow SAIEE, and senior member of IEEE-USA.

Section I

Power Semiconductor Devices



Taylor & Francis

Taylor & Francis Group

<http://taylorandfrancis.com>

1 Overview of Power Electronics

1.1 INTRODUCTION

Power electronics deals with the use of electronics for the control and conversion of large amounts of electrical power. The design of power electronics involves interactions between the source and the load with the effective use of small-signal electronic control circuits as well as power semiconductor devices.

Definition: Power electronics is the study of electronic circuits meant to control the flow of electrical energy at higher levels than the individual device ratings.

A power electronics system consists of an electrical source, load, and a power electronic circuit containing switches, energy storage elements, and control functions as shown in [Figure 1.1](#). Power electronics is a vast, complex, and interdisciplinary subject that has undergone through a rapid technological evolution during the last 50 years. Due to advancement in technology with decreased apparatus cost and improved reliability, the applications of power electronics are expanding in industrial, commercial, aerospace, residential, military, and utility environments. Many innovations in the field of power semiconductor devices, converter topologies, electric machine drives, control, and estimation techniques contribute to this advancement. The frontier of this technology has been further advanced by the versatile use of artificial intelligence (AI) techniques, such as fuzzy logic and the artificial neural network, thus bringing more challenges to power electronics engineers.

This chapter presents an overview of the power devices, converters, applications of power electronics, and computer simulation for power electronics circuits.

1.2 POWER ELECTRONICS SYSTEMS

The major components of a power electronics system are shown in the form of a block diagram in [Figure 1.2](#) [3,4,6]. The main power source can be an AC or a DC supply system.

The output from the power electronics circuit can be variable AC or DC voltage, or it may be a variable voltage and frequency depending upon the requirements of the load. For example, if the load is a DC motor, the converter output must be adjustable direct voltage. In case the load is a three-phase induction motor, the converter should have adjustable voltage and frequency at its output terminals.

The feedback component in [Figure 1.2](#) measures various parameters of the load, say, speed in case of a rotating machine, and compares it with the command. The difference of the two, through the digital circuit components, controls the instant

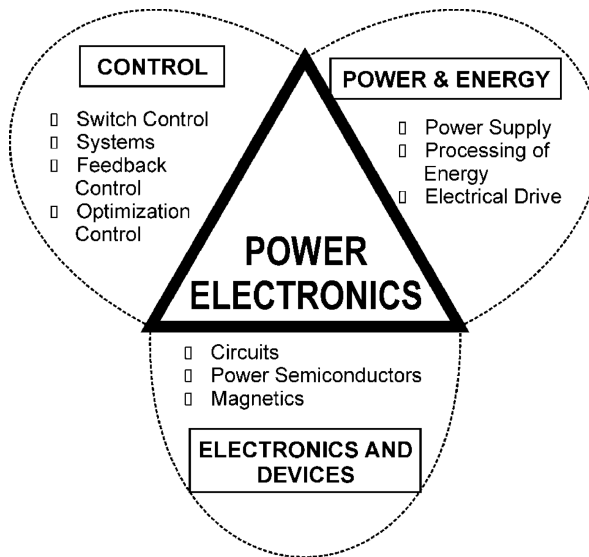


FIGURE 1.1 Control, energy and power electronics are interrelated.

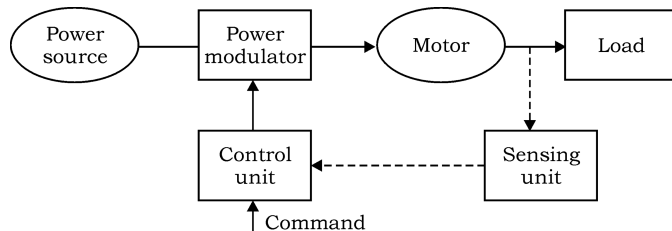


FIGURE 1.2 Block diagram of power electronics system.

of turn-on of semiconductor devices forming the power converter system. In this manner, the behavior of the load circuit can be controlled as desired over a wide range with the adjustment of the command.

1.3 POWER SEMICONDUCTOR DEVICES

In 1957, the silicon-controlled rectifier (SCR) was introduced, and later other power semiconductor devices have been developed with the advancement in the semiconductor technology, which is enumerated below [1–6].

Power diodes are available up to the ratings of 3,000 V, 3,500 A, and 1 kHz, whereas thyristors are available up to 6,000 V, 3,500 A, 1 kHz, and gate turn-off (GTO) thyristors up to ratings of 4,000 V, 3,000 A, and 10 kHz. MOS-controlled thyristors (MCTs) and TRIACS can work up to 600 V, 60 A, 20 kHz, and 1,200 V, 300 A, 400 Hz, respectively. Bipolar Junction Transistors (BJTs) are available in the market up to ratings of 1,200 V, 400 A, and 10 kHz, as shown in Table 1.1 [1–12].

TABLE 1.1
Comparison of Various Power Semiconductor Devices

S. No.	Parameters	Thyristor	BJT	Power MOSFET	GTO	IGBT
1.	Voltage and current ratings	10 kV/4 kA	2 kV/1 kA	500 V/200 A	5 kV/3 kA	1200 V/400 A
2.	Linear/trigger	Triggered	Linear	Triggered	Linear	Linear
3.	Gating	Current	Current	Current	Voltage	Voltage
4.	Voltage blocking	Symmetric/asymmetric	Asymmetric	Asymmetric	Symmetric/ asymmetric	Asymmetric
5.	SOA (Safe Operating Area)	Does not apply	Second Break down (SB) and T _j limited < 2 Volts	T _j limited	T _j limited	T _j limited
6.	Conduction drop	<2 Volts	<2 Volts	4–6 Volts	<4 Volts	33 Volts
7.	Temp. coeff. of resistivity	Negative	Negative	Positive	Negative	Approximately flat (positive at high current)
8.	Turn-off gain	—	200	—	3–5	—
9.	Switching frequency	500 Hz	10 kHz	up to 100 kHz	2 kHz	10 kHz
10.	Turn-on time	2 μ s	1 μ s	100 ns	2–4 μ s	2 μ s
11.	Turn-off time	200 μ s	2–5 μ s	150–200 ns	10 μ s	2 μ s
12.	Snubber	Unpolarized	Polarized	Polarized or unpolarized (operation is possible)	Polarized (Snubberless)	Polarized (Snubberless)
13.	Reapplied dv/dt (V/ μ s)	30	5 device	Limit for device loss	Limit for Miller effect and SOA 100	Limited by device loss

(Continued)

TABLE 1.1 (Continued)
Comparison of Various Power Semiconductor Devices

S. No.	Parameters	Thyristor	BJT	Power MOSFET	GTO	IGBT
14.	Turn-on dV/dt (A/us)	200	21	300	100	Very high
15.	Leakage current (mA)	3	1	30	2.5	0.2
16.	Protection	Gate inhibit or fast fuse	Gate inhibit or fast fuse	Gate inhibit or fast fuse	Base control	Gate control
17.	Applications	DC/AC motor drives, large power supplies, lighting and heating, static VAR compensators, electronic circuit breakers	Lamp heating control, zero voltage switched AC relay, AC motor starting and control	Gate inhibit or fast fuse. Motor drives, UPS systems, static VAR compensations, induction heating	Base control. Motor drives, UPS systems static VAR and harmonic compensators, switched mode power supplies	Gate control. Switching mode power supply. Brushless DC motor drive, electronic DC relay
18.	Comments	Large surge-current capability	Large surge-current capability	High uncontrollable surge current. Large snubber to limit device loss switching low frequency at high power	Current gain varies with C and collector current	Built-in body diode can carry full current but slow recovery. Becomes higher with voltage and current ratings

Power MOSFETs (metal oxide semiconductor field effect transistors) have relatively low ranges of approximately 1,000 V and 50 A with high frequency of 100 kHz, whereas insulated-gate bipolar transistors (IGBTs) are available up to power ratings of 1,200 V, 400 A, and 20 kHz.

On the basis of switching characteristics and gate-signal requirements, the power semiconductor devices can be classified as:

1. *Diodes*: These are uncontrolled power semiconductor devices. Their on and off states are not dependent on the control signals but controlled by the power supply and load circuit conditions.
2. *Thyristors*: These are controlled, switched on by a gate signal, and once they get turned on, they remain latched in the “on” state due to the internal regenerative action.
3. *Controllable switches*: These devices are switched on/off by applying control signals. The devices, which behave as controllable switches, are BJT, MOSFET, GTO, Static Induction Thyristor (SITH), IGBT, Static Induction Transistor (SIT), and MCT.

Some other important information regarding power semiconductor devices are pin-pointed as:

- SCR, GTO, SITH, and MCT require a pulse-gate signal for turning them on; whereas, BJT, MOSFET, IGBT, and SIT require a continuous signal for keeping them in turned-on state.
- BJT, MOSFET, IGBT, and MCT are unipolar devices; whereas, thyristors and GTOs are bipolar devices.
- The TRIAC and reverse conducting thyristor (RCT) possess a bidirectional current capability; whereas, all other remaining devices (diode, SCR, GTO, BJT, MOSFET, IGBT, SIT, SITH, MCT) are unidirectional current devices.
- Thyristors require an extra forced-commutation circuit, if the source is DC. But power transistors and GTOs do not require any extra commutation circuit.

1.4 POWER ELECTRONIC CONVERTERS

Any power electronic system may have one or more power electronic converters, which are made up of some power semiconductor devices controlled by integrated circuits. It is the switching characteristics of power semiconductor devices that permit the power converter to shape the input power of one form to the output power of some other form very efficiently. Broadly, power electronic converters can be classified into six types as discussed below [3–6]:

1. *Diode rectifiers*: A diode rectifier circuit converts AC input voltage into a fixed DC voltage. The input voltage may be single phase or three phase. Diode rectifiers find wide use in electric traction, battery charging, electroplating, electrochemical processing, power supplies, welding, and uninterrupted power supply (UPS) systems.

2. *AC-to-DC converters (phase-controlled rectifiers)*: These convert constant AC voltage to variable DC output voltage. These rectifiers use line voltage for their commutation; as such, these are also called line-commutated or natural commutated AC-to-DC converters. Phase-controlled converters may be fed from a one-phase or three-phase source and are mainly used in DC drives, metallurgical and chemical industries, excitation systems for synchronous machines, etc.
3. *DC-to-DC converters (DC choppers)*: A DC chopper converts fixed DC input voltage to a controllable DC output voltage. The chopper circuits require forced, or load commutation, to turn off the thyristors. For lower power circuits, thyristors are replaced by power transistors. The classification of chopper circuits is dependent upon the type of commutation and also on the direction of the power flow. Choppers find wide applications in DC drives, subway cars, trolley trucks, battery-driven vehicles, etc.
4. *DC-to-AC converters (inverters)*: An inverter converts fixed DC voltage to a variable AC voltage. The output may be a variable voltage and variable frequency. These converters use line, load, or forced commutation for turning off the thyristors. Inverters find wide use in induction motor and synchronous motor drives, induction heating, UPS, high-voltage direct current (HVDC) transmission, etc. Presently, conventional thyristors have been replaced by GTOs in high-power applications and by power transistors in low-power applications.
5. *AC-to-AC converters*: These convert fixed AC input voltage into variable AC output voltage. There are three types and discussed as follows:
 - a. *AC voltage controllers*: These circuits also termed as *AC voltage regulators*, which convert fixed AC voltage directly to a variable AC voltage at the same frequency. These circuits consist of two thyristors in anti-parallel, or a TRIAC, and are widely used for lighting control, speed control of fans, pumps, etc.
 - b. *Cycloconverters*: These circuits convert input power at one frequency to output power at a different frequency through one-stage conversion. Line commutation is more common in these converters, though forced and load commutated cycloconverters are also employed. These are primarily used for slow-speed large AC drives like rotary kiln, etc.
 - c. *Matrix converters*: A three-phase matrix converter circuit consists of nine fully controlled bidirectional switches arranged in three rows, each connecting an input line to an output line. The matrix converter can be considered to be a direct converter. In this respect, it's similar to a cycloconverter, because, first, it does not employ a DC link, and second, the output waveforms are composed of switched segments of the input waveforms. As the matrix converter employs fully controlled bidirectional switches, pulse-width modulation (PWM) control strategies can be implemented, similarly to those used by the

PWM controls. The matrix converter therefore possesses the advantages of both the cycloconverter and the PWM drive, as summarized below:

- i. It can be used as a direct frequency changer, converting a fixed AC or DC source into a variable AC or DC supply.
- ii. It requires fewer devices than a cycloconverter.
- iii. There is no DC link and therefore no requirement for energy storage devices.
- iv. It facilitates four-quadrant operation.
- v. The input power factor may be controlled across the whole speed range.
- vi. The harmonic distortion is incurred at high frequencies.
- vii. The output voltage and input current waveforms can be controlled such that they are near sinusoidal in form.

Unfortunately, the matrix converter suffers from the following disadvantages:

- i. The maximum output voltage is restricted.
 - ii. The required fast-acting bidirectional switches are not currently manufactured.
 - iii. Very precise control of the devices is necessary to ensure correct device commutation and to prevent short-circuiting of the source.
6. *Static switches:* The power semiconductor devices can operate as static switches or contactors and possess many advantages over mechanical and electromechanical circuit breakers. Depending upon the input supply, the static switches are called AC static switches or DC static switches.

1.5 POWER ELECTRONIC MODULES

For any application, a power electronic converter may require two, four, or more power semiconductor devices depending upon the circuit configuration. Presently in market, power modules consisting of two, four, or six semiconductor devices are available [3–6]. Therefore, a power converter can be assembled from such power modules instead of from individual semiconductor devices because these modules have better performance characteristics as far as their switching characteristics, operating speed, and losses are concerned. Gate-drive circuits for individual devices or power modules are also commercially available. Due to such advancement, intelligent power modules are available in the market.

An intelligent module, also called smart-power, is a state-of-the-art power electronic consisting of a power module and a peripheral circuit. The peripheral circuit comprises of microcomputer control; controlled power supply with interfacing of power module with the input/output through proper isolation from low and highvoltage power circuit; a drive circuit; and protection and diagnostic circuitry against maloperation, such as excess current or over voltage.

Advantages and Disadvantages of Power Electronic Converters

The advantages possessed by power-electronics systems are as follows:

1. High efficiency as there are negligible losses in semiconductor devices
2. High reliability
3. Long life with less maintenance due to the absence of any moving parts
4. Fast dynamic response as compared to electromechanical converter systems
5. Lower cost due to mass production semiconductor devices

Various demerits of power electronics are as follows:

1. These circuits generate harmonics in the supply as well as in the load circuit and therefore deteriorates the performance.
2. Certain converters like AC to DC or AC to AC under certain operating conditions operate at a low input power factor (PF).
3. Controllers used for power electronics have low overload capacity. Therefore, these converters must be rated for taking momentary overloads, which increases the cost of the power electronic controller.
4. Regeneration of power is difficult in power electronic converter systems.

1.6 APPLICATIONS OF POWER ELECTRONICS

Since 1957, there has been an emergence of many new power semiconductor devices. Power electronic systems today incorporate power semiconductor devices as well as microelectronic integrated circuits [1,3,5,6–12].

The term, “converter system,” in general, is used to denote a static device that converts AC to DC, DC to AC, DC to DC or AC to AC. Conventional power controllers based on thyratrons, mercury-arc rectifiers, magnetic amplifiers, rheostatic controllers, etc. have been replaced by power electronic controllers using semiconductor devices in almost all applications. The development of new power-semiconductor devices, new circuit topologies with their improved performance, and their fall in prices have opened up a wide field for the new applications of power electronic converters. A judicious use of power semiconductor devices, in conjunction with microprocessors or microcomputers, has further enhanced the control strategies, and synthesizing devices can be regarded as the muscle and the microelectronics as the intelligent brain in the modern power electronic systems [1–7].

No boundaries can be earmarked for the applications of power electronics, especially with the present trend of integrated design of power semiconductor devices, microprocessors, and the controlled equipment. The power ratings of power electronic systems range from a few watts in lamps to several hundred megawatts in HVDC transmission systems. It is believed that by 2020, almost 80% of the electric power consumed in utility systems will pass through power electronics, and this

figure will eventually reach 100% in the future because power electronic converters or controllers are better over other types of controllers (e.g., hydraulic, mechanical) in respect to the following aspects [2,3,6]:

1. *Efficiency*: Efficiency of a power electronic converter is very high (of order of 95%). Therefore, it results in low loss in the controller circuit.
2. *Compactness*: These are lighter in weight and occupy less space.
3. *Ease and speed*: Power electronic controllers are very fast in comparison to other controllers. Also, the automatic controls with complicated and sophisticated control strategies are easily accomplished.
4. *Reliability*: Probability of failure is low and life is longer in case of power electronic controllers as compared to others.

Some applications of power electronics are as under [1–7]:

1. In aerospace for power supplies in the space shuttle, satellite, and aircraft power systems.
2. In various commercial applications, such as advertising, heating, air-conditioning, central refrigeration, computer and office equipment, UPS, elevators, light dimmers, and flashers.
3. In various industries, such as arc and industrial furnaces, blowers and fans, pumps and compressors, industrial lasers, transformer-tap changers, rolling mills, textile mills, excavators, cement mills, welding.
4. Power electronics have wide applications in residential requirements, such as air conditioning, cooking, lighting, space heating, refrigerators, electric-door openers, dryers, fans, personal computers, other entertainment equipment, vacuum cleaners, washing and sewing machines, light dimmers, food mixers, electric blankets, food-warmer trays.
5. In the field of telecommunication, power electronics is required for battery chargers and power supplies.
6. Nowadays, power electronics plays a crucial role in transportation, such as battery chargers, traction control of electric vehicles, electric locomotives, street cars, trolley buses, subways, automotive electronics.
7. It has wide applications in HVDC transmission, excitation systems, static Var compensation (SVC), static circuit breakers, fans and boiler-feed pumps, supplementary energy systems (solar, wind).

1.7 COMPUTER SIMULATION OF POWER ELECTRONIC CIRCUITS

Computers have long been used to numerical and logical models or simulations of real-world systems. Indeed, a large part of the motivation for developing the first computers in the 1930s and 1940s were able to perform calculations to simulate and analyze physical systems, such as electrical circuits. Since then, there has been a desire to understand computer simulation and the behavior of complex systems. In this section, the concept of simulation is discussed in detail, and the names of a few simulation tools are also mentioned [2,3,5,6].

1.7.1 IMPORTANCE OF SIMULATION

Simulation has become a very powerful tool in industry applications as well as in academics. Now, it is essential for an electrical and electronics engineer to understand the concept of simulation for its use in various applications. Simulation is one of the best ways to study the system or circuit behavior without damaging it. However, computer simulation should not be looked upon as a substitute for a hardware (breadboard) prototype.

Many systems are so complex that their correctness and behavior cannot be easily or confidently predicted, either analytically or through experience and intuition. Beyond allowing engineers to see if their designs work, computer simulation allows the rapid comparison of alternative designs. By comparing the performance of various permutations of a given design, an engineer can optimize the performance, cost, or other desirable attributes of the design, subject to the constraints within which it must function.

1.7.2 BENEFITS OF COMPUTER-AIDED SIMULATION

The benefits of computer-aided analysis in power electronics circuits are enormous. They are listed as follows [2,3,5,6]:

1. Evaluating the effects of variations in elements, such as resistors, power semiconductor devices, transformers, and so on
2. The assessment of performance, improvements, or degradations
3. Evaluating the effects of noise and signal distortion without the need of expensive measuring instruments
4. Sensitivity analysis to determine the permissible bounds due to tolerances on each and every element value or parameter of active elements
5. Fourier analysis without expensive wave analyzers
6. Evaluating the effects of nonlinear elements on the circuit performance
7. Optimizing the design of electronic circuits in terms of circuit parameters

1.7.3 DEMERITS OF COMPUTER-AIDED SIMULATION

We need to realize that there are several factors that make simulation of power electronics systems very challenging:

1. Solid-state power semiconductor switches, including diodes and thyristors, present extreme nonlinearity during their transition from one state to the other. The simulation program ought to be able to represent this switching of states in an appropriate manner.
2. The simulation may take a long time. The time constants, or in other words the response time of various parts within the system, may differ by several orders of magnitude.
3. Accurate models are not always available. This is especially true for power semiconductor devices but is also the case for magnetic components, such as inductors and transformers.
4. The controller, which may be analog and/or digital needs to be modeled along with the power converters.

1.7.4 SIMULATION TOOLS

Simulation of power electronic converter and circuits can be done either by (a) circuit-oriented simulators (e.g., PSPICE, PSIM, TINAPRO, Electronics Workbench, etc.), or (b) mathematical model-based equation solvers using high-level languages (e.g., C, C++, Visual BASIC, FORTRAN, BASIC), or (c) high-level language-based packages (MATLAB®, MATHEMATICA, etc.). In this section, a few software simulation tools are listed, which are widely accepted by the engineering society, particularly by the engineers. These simulation tools are in use in industries as well as in academic institutions [2,3,5,6].

PSPICE: This tool is used for simulation of the digital and analog circuits.

The stability of the system and the optimization of the circuit components can also be done using this tool. This is the most powerful and popular tool for circuit-level analysis. It has the model of most of the components in its library. The library of this software simulation tool is very broad. Waveforms at different points in power electronic circuits are very important to be known. Waveforms can be seen at various points in the circuit using this tool. Even the analysis of these waveforms in terms of Fourier transforms, etc. can also be studied. The component-manufacturing vendors are giving the ready-made PSPICE model, which can be included in the library and can be used for the analysis. For example, Infineon, a manufacturer of semiconductor devices, has introduced a MOSFET and named it COOLMOS. It has different additional features (as compared to the conventional FET). They have given the PSPICE the model of the new MOSFET. Similarly, almost every manufacturer gives the SPICE model for their components. This software package is in use for very-large-scale integration (VLSI), power electronics, and other circuit designs.

Electronics workbench: This is another powerful tool from Interactive Image Technologies Ltd. It has a vast component library of electronic components and power semiconductor devices. It has similar computational facilities. The recently released package for this purpose is MULTISIM2001 from Electronics Workbench. It has schematic capture, simulation, and programmable logic facilities.

PSCAD: Power systems computer-aided design (PSCAD) is a package for simulating interactions between power electronic systems (converters, machine drives, static VAR controllers, HVDC power supplies, etc.) and power systems. It is extensively used for the study of HVDC systems. An evaluation version is available at <http://www.pscad.com>.

PSIM: Power SIM (PSIM) is a package for motor drives and digital control simulation. Sample circuits are available for motor control, power factor control, vector control (PWM), and SMPS. There is an evaluation version available, which can be obtained from <http://www.power simtech.com>.

PLECS: Piece-wise linear electrical circuit simulation (PLECS) is an add-on for Simulink for dynamic systems. It converts a circuit into a Simulink subsystem. The package is available free at <http://www.eth.ee.ethz.ch/plecs>.

VTB: Virtual test bed (VTB) is a free package for multi-disciplinary dynamic systems (e.g., renewable energy systems, battery systems, fuel cells, super capacitors). It is available on <http://vtb.engr.sc.edu>.

SABER: This is a very powerful tool for simulation of analog circuits and systems, digital systems, event-driven analog systems, and mixed-mode systems through all levels of description from the highest structural level down to the transistor level. With SABER's MAST language, even a combination of circuit blocks with different description levels in one model description is possible. For example, an electrical controller can be coupled with a mechanical system. Thus, the overall performance of the whole system can be analyzed by SABER tools. A library is also provided with a number of predefined templates, which can be used as circuit hierarchy and a number of predefined components.

ONLINE SIMULATION: Recently, Prof. Carlos A. Canesin of the Paulista State University, UNESP (Brazil), has developed a web-based power electronics educational tool for online simulation. It is an open WWW-HTML-based multimedia course in power electronics. The main purpose is to provide an interactive visual simulation and analysis of idealized uncontrolled and controlled rectifiers (single-phase and three-phase topologies). Moreover, JAVA, applet programs are implemented to solve some design-oriented equations for rectifier applications. The emphasis is on the interactive waveform analysis, stresses on devices, and average and RMS values of the main circuit variable that can be accessed free of charge at <http://www.dee.feis.unesp.br/Lep> Applets.

MATLAB and Simulink: These are very powerful mathematical-model-based equation-solver mathematical software tools. These are mainly used to study the system behavior. In this package, the mathematical model of any system or component can be simulated in form of its equation. It is also a user-friendly tool, mainly used to study the behavior of big systems by modeling it through their mathematical expressions. For example, a diesel-based distributed/dispersed generation (DG) system is a complex system, and its performance can be analyzed by modeling computation using MATLAB/Simulink. Recently, a WebMATHEMATICA package is also released by WOLFRAMResearch, for online computation and visualization (www.wolfram.com/webmathematica). There are many other tools that are also available in the market.

REVIEW QUESTIONS

- 1.1 Define power electronics.
- 1.2 List names of unidirectional power semiconductor devices.
- 1.3 What are unipolar and bipolar devices?
- 1.4 List various applications of power electronics.
- 1.5 List five motors and their functions in a typical household that utilize power electronic controllers to save energy.
- 1.6 List some applications of different power electronic converters.

- 1.7 Comment on the interdisciplinary nature of the power electronics.
- 1.8 What is smart power? Mention its advantages.
- 1.9 What are the advantages of a matrix converter over a cycloconverter?
- 1.10 List the different simulating tools used for the power electronic circuits.

SUMMARY

Today, the most common needs for electrical power conversion demanded by the industries is the conversion of voltage and frequency. A power electronic converter circuit is placed in between the source and the load with the primary objective to achieve 100% efficiency with very high reliability during energy conversion. Thorough research in the field of more advanced semiconductor material, devices, and power converters is in progress worldwide; therefore in the future, application requirements will not be limited by device capabilities.

REFERENCES/FURTHER READING

1. N. Mohan, Tore M. Undeland, and William P. Robbins, *Power Electronics: Converters, Applications and Design*, John Wiley & Sons, New York, 1996.
2. B. K. Bose, *Power Electronics and AC Drives*, Prentice Hall, Englewood Cliffs, NJ, 1986.
3. M. H. Rashid, *Power Electronics: Circuits, Devices, and Applications*, Pearson Education, Singapore, 2004.
4. P. T. Krein, *Elements of Power Electronics*, Oxford University Press, New York, 2003.
5. K. Thorborg, *Power Electronics*, Prentice Hall International, London, UK, 1988.
6. P. S. Bhimra, *Power Electronics*, 5th edn, Khanna Publications, New Delhi, India, 2012.
7. F. Mazda, *Power Electronics Handbook*, Newnes, Oxford, UK, 1997.
8. J. C. Whitaker, *The Electronics Handbook*, CRC Press, Boca Raton, FL, 2005.
9. R. W. Erickson, *Fundamentals of Power Electronics*, Chapman & Hall, New York, 1997.
10. V. R. Moorthi, *Power Electronics Devices, Circuits and Industrial Applications*, Oxford University Press, New Delhi, India, 2010.
11. T. Suntio, T. Messo, J. Puukko, *Power Electronic Converters*, Wiley-VCH, Verlag GmbH, Weinheim, Germany, 2018.
12. A. M. Trzynadlowski, *Introduction to Modern Power Electronics*, 3rd edition, John Wiley & Sons, Hoboken, NJ, 2010.



Taylor & Francis

Taylor & Francis Group

<http://taylorandfrancis.com>

2 Power Semiconductor Devices

2.1 INTRODUCTION

Presently, converters have found large numbers of applications along with some new topologies due to the advancement in power semiconductor devices in terms of ease and faster control, reduced costs with increased power-handling capabilities, etc. This chapter discusses in detail the structure, construction, working, terminal characteristics and the switching speed, current, and voltage capabilities of different power devices. The power semiconductor devices are considered ideal switches with switching functions having a value of either 0 or 1, that is, the switch is either off (carries no current) or on (carries current). It is lossless. A real switch differs from an ideal switch in characteristics, such as the on-state current is limited, nonzero on-state voltage drop, and some leakage current during the off state, and so the losses also occur.

As shown in [Table 2.1](#), on the basis of turn-on and turn-off characteristics, gate-signal requirements, and controllability, the power semiconductor devices can be classified as follows [1]:

1. **Diodes:** These are uncontrolled power semiconductor devices. Their on and off states are not dependent on the control signals but controlled by the power supply and load-circuit conditions.
2. **Thyristors:** These are controlled, turned on by a gate signal. After thyristors are turned on, they remain latched in the on-state condition due to internal regenerative action. These require extra forced-commutation circuits for their commutation (or turn-off), if the source is DC.
3. **Controllable switches:** These devices are turned on and turned off by the application of control signals. The devices, which behave as controllable switches, are BJT, MOSFET, GTO, SITH, IGBT, SIT, and MCT.

2.2 POWER DIODE

Power diodes are two-layered $p-n$ semiconductor devices having two terminals named the anode and cathode as shown in [Figure 2.1](#). Diffusing, alloying, and epitaxial growth are used to form one $p-n$ junction.

TABLE 2.1
Categorization of Semiconductor Power Devices

Devices that require pulse-gate signal for their turn on	GTO, SCR, SITH, MCT
Devices that require continuous control signal	BJT, MOSFET, IGBT
Devices that can withstand unipolar voltage	BJT, MOSFET, IGBT, MCT
Devices that can withstand bipolar voltage	Thyristors, GTOs
Bidirectional current capability	Triac and RCT (reverse conducting thyristor)
Unidirectional current capability	Diode, SCR, GTO, BJT, MOSFET, IGBT, SIT, SITH, MCT

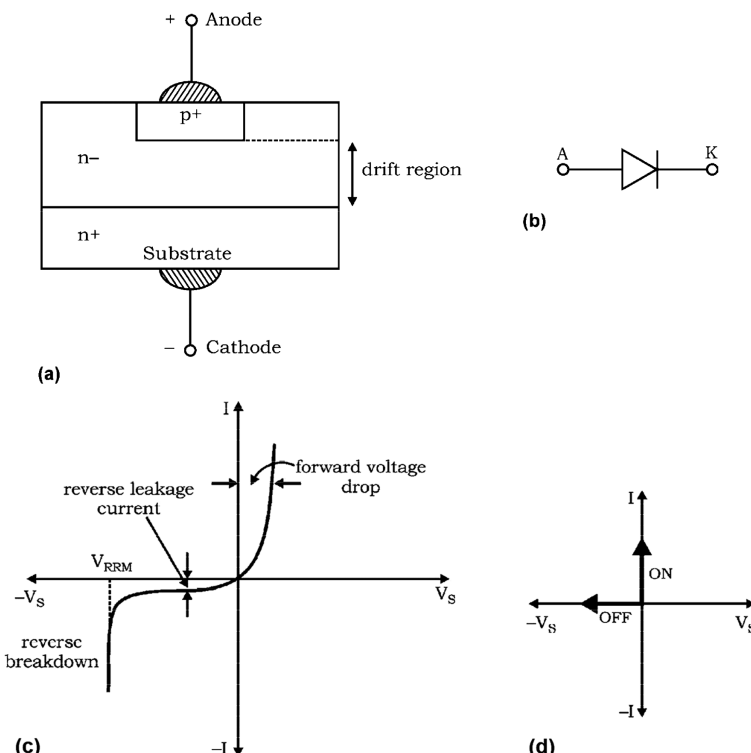


FIGURE 2.1 Power diode (a) structure, (b) symbol, (c) practical V-I characteristics, and (d) ideal V-I characteristics.

A power diode behaves as a switch with uncontrolled turn-on/turn-off characteristics. They perform various functions, such as the freewheeling of energy in inductive circuits, charge reversal in capacitors, and trapped-energy recovery in case of rectification.

Power diodes differ in structure from signal diodes. A signal diode constitutes a simple $p-n$ junction. But the power diode has some difference, as shown in [Figure 2.1a](#).

On a heavily doped n^+ substrate, a lightly doped n^- layer is epitaxially grown, and then the heavily doped p^+ layer is diffused into the n^- layer to form the anode of the power diode, as shown. Therefore, the n^- layer is the basic structural feature not found in signal diodes. The function of the n^- layer is to absorb the depletion layer to the reverse-biased (RB) $p^+ n^-$ junction J_1 . The drawback of the n^- layer is that ohmic resistance increases, so there is more power dissipation in power diodes and therefore requires proper cooling arrangements. These modifications make it appropriate for high-power applications [2,4,6–8].

2.2.1 WORKING AND V-I CHARACTERISTICS

Working and V-I characteristics of a power diode can be explained using its two basic modes of operation:

1. *Forward-biased (FB) mode*: In this mode, the anode is positive w.r.t. cathode, and the diode current increases gradually for low values of source voltage V_S . Beyond the cut-in voltage, the current rises rapidly, as shown in [Figure 2.1c](#). The diode is then in a conduction state, and the forward voltage drop in the device is about 1–2 V. The V-I characteristics under the FB mode appear in the first quadrant of voltage versus the current plot as shown in [Figure 2.1d](#).
2. *Reverse-biased mode*: In this mode, the cathode is a positive w.r.t. anode and a small reverse current, called leakage current (μA or mA), flows. The junction breaks down at some particular reverse voltage (breakdown or avalanche voltage) where a large reverse current flows as shown in [Figure 2.1c](#). It can be avoided by operating the diode below a specified peak repetitive reverse voltage V_{RRM} .

2.2.2 DIODE REVERSE RECOVERY CHARACTERISTICS

When the circuit conditions require the diode to switch off, the forward diode current first decays to zero, and then the diode continues to conduct in the reverse direction as shown in [Figure 2.2](#) [2–10]. It is because of the presence of stored charges in the two layers of the diode. The time duration for which the reverse current flows in the device is called *reverse recovery time* t_{rr} . During this time, t_{rr} , the charge carriers stored in the device are removed due to the flow of the reverse current. The diode regains its blocking capability until the reverse recovery current I_{rr} decays to zero, that is, until stored charges are completely removed from the layers of the device.

The reverse recovery time t_{rr} is composed of two time intervals, t_a and t_b , that is,

$$t_{rr} = t_a + t_b \quad (2.1)$$

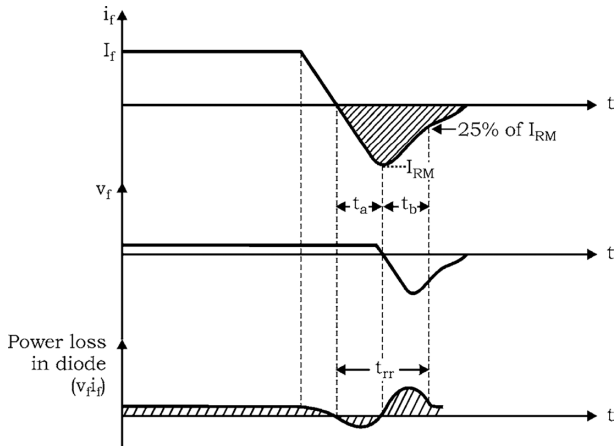


FIGURE 2.2 Reverse recovery characteristic of power diode, where I_f is the forward current, and v_f is the forward voltage drop.

Time t_a is the time between the zero crossing of the forward current and peak reverse current I_{RM} . During this time, charge carriers stored in the depletion region are removed.

Time t_b is the time interval between the instant current I_{rr} is maximum to the instant current I_{rr} is 25% of its peak value (i.e., 25% of I_{RM}). During this time, charge carriers from the two semiconductor layers are removed.

The shaded area in Figure 2.2 represents the stored charge or reverse recovery charge Q_R . The ratio of t_b/t_a is called the *softness factor* or *S-factor* [2,4,6–8].

for soft-recovery diode—*S*-factor is unity.

for fast-recovery diode—*S*-factor is less than unity.

From Figure 2.2, the peak reverse current can be expressed as:

$$I_{RM} = t_a \frac{di}{dt} \quad (2.2)$$

where $\frac{di}{dt}$ is the rate of change of the reverse current. Assuming the reverse recovery characteristic to be triangular, stored charge, Q_R , is given by:

$$Q_R = \frac{1}{2} I_{RM} t_{rr}$$

or

$$I_{RM} = \frac{2Q_R}{t_{rr}} \quad (2.3)$$

if $t_{rr} \cong t_a$, then from Equation (2.2),

$$I_{RM} = t_{rr} \cdot \frac{di}{dt} \quad (2.4)$$

From Equations (2.3) and (2.4), we get

$$t_{rr}, \frac{di}{dt} = \frac{2Q_R}{t_{rr}}$$

or

$$t_{rr} = \left[\frac{2Q_R}{di/dt} \right]^{\frac{1}{2}} \quad (2.5)$$

From Equation (2.2), with $t_{rr} \cong t_a$,

$$I_{rr} = t_{rr} \cdot \frac{di}{dt} = \left[\frac{2Q_R}{di/dt} \right] \cdot \frac{di}{dt}$$

or

$$I_{rr} = \left[2Q_R \left(\frac{di}{dt} \right) \right]^{\frac{1}{2}} \quad (2.6)$$

Therefore, it can be seen that t_{rr} and I_{RM} depend on storage charge and the rate of change of current $\frac{di}{dt}$. The stored charge depends upon the forward diode current I_F .

2.3 DIAC

DIAC, a member of the thyristor family, is a five-layer, four-junction device as shown in [Figure 2.3 \[2–6\]](#). It is an uncontrolled bidirectional device. The term “DIAC” stands for diode that can work on AC. When T_2 is made positive w.r.t. T_1 , the device $pnpn'$ becomes FB, and if voltage is further increased beyond the breakdown voltage V_{B02} , then the structure $pnpn'$ conducts in the third quadrant as shown in [Figure 2.3c](#).

When T_1 is made positive w.r.t. T_2 , the device $pnpn$ becomes FB, and if voltage is increased beyond the breakdown voltage V_{B01} , then it conducts in the first quadrant as shown in [Figure 2.3c](#). It has a symmetrical characteristic in the first and third quadrants if the doping density in $pnpn$ and $pnpn'$ are identical. The device exhibits negative resistance characteristics in both directions; therefore, DIAC is used in relaxation mode as a trigger device for TRIACs.

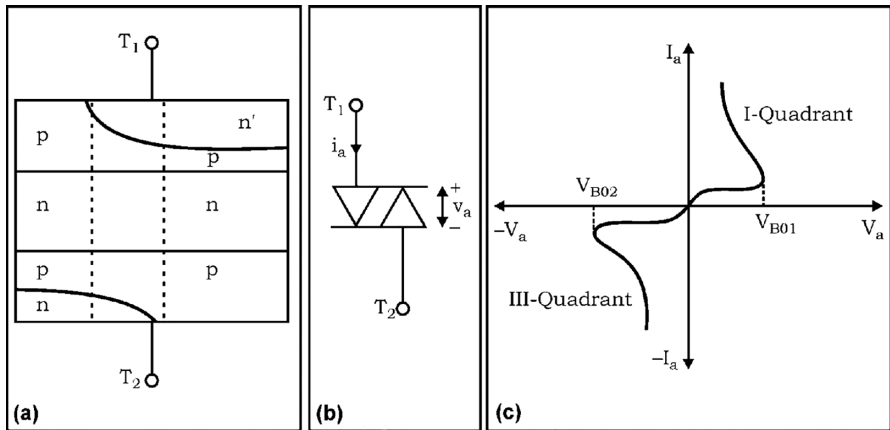


FIGURE 2.3 DIAC (a) structure, (b) symbol, and (c) V-I characteristic of DIAC.

2.4 TRIAC

TRIAC is one of the widely used devices of the thyristor family in power-control applications. It is a bidirectional device with three terminals MT_1 , MT_2 , and gate G as shown in Figure 2.4 [2–8]. It can be considered as an integration of two SCRs in antiparallel. The gate is near the terminal MT_1 with the gate open, and the TRIAC blocks both the polarities of voltage applied across MT_1 and MT_2 if the magnitude of the voltage is less than the breakdown voltage of the device.

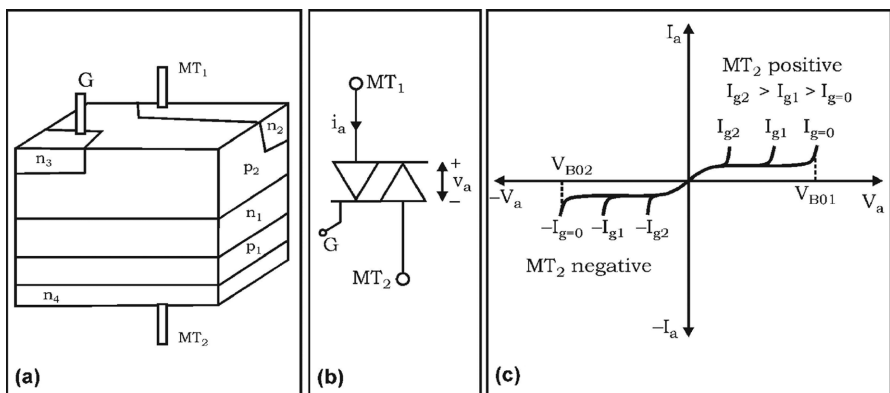


FIGURE 2.4 TRIAC (a) structure, (b) symbol, and (c) V-I characteristic of TRIAC.

With terminal MT_2 being a positive w.r.t. terminal MT_1 , the device is turned on by applying a positive gate current. On the other hand, when terminal MT_1 is a positive w.r.t. terminal MT_2 , a negative gate current can turn on the device. It means that a TRIAC can be turned on by both positive and negative gate signals and thus can be operated with four modes of operation:

Mode 1: MT_2 positive w.r.t. MT_1 and positive gate current

Mode 2: MT_2 positive w.r.t. MT_1 , gate current negative

Mode 3: MT_2 negative w.r.t. MT_1 , gate current negative

Mode 4: MT_2 negative w.r.t. MT_1 , gate current positive

Modes 1 and 3 are the recommended modes of operation for TRIAC because the gate sensitivity of the device is high during these modes.

2.5 CHARACTERISTICS OF POWER TRANSISTORS

Power transistors possess controlled characteristics. These can be turned on by applying a control signal to the base, or control terminal. The transistor remains in the on state as long as the control signal is present. With the removal of the control signal, it gets turned off. Therefore, a power transistor does not require any extra circuit for its turn-off (commutation). Presently available power transistors in the market are discussed as follows.

2.5.1 BIPOLAR JUNCTION TRANSISTOR

A bipolar junction transistor (BJT) is three-layered, two-junction *npn* or *pnp* semiconductor device, as shown in Figure 2.5. The term “bipolar” means that the flow of current is due to both majority- and minority-charge carriers (holes and electrons). It has three terminals named collector, emitter, and base. Here,

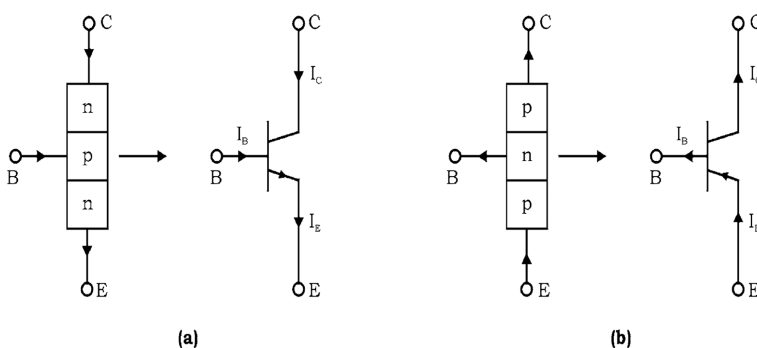


FIGURE 2.5 Bipolar junction transistor (a) *npn* type and (b) *pnp* type.

an arrow head indicates the direction of the emitter current. Out of three possible configurations, the common emitter is more commonly used for switching applications.

2.5.1.1 Steady-State Characteristics

The circuit shown in [Figure 2.6a](#) is used to draw the following steady-state characteristics of a BJT [2–8].

- 1. Input characteristics:** This represents the graph between the base current (I_B) and base-emitter voltage (V_{BE}), which is similar to the diode curve because the base-emitter junction of a transistor is like a diode. It can be seen from [Figure 2.6](#) that as the V_{CE} increases the base current decreases.
- 2. Output characteristics:** This represents the graph between the collector current (I_C) and collector-emitter voltage (V_{CE}). As the base current rises, collector current also rises.

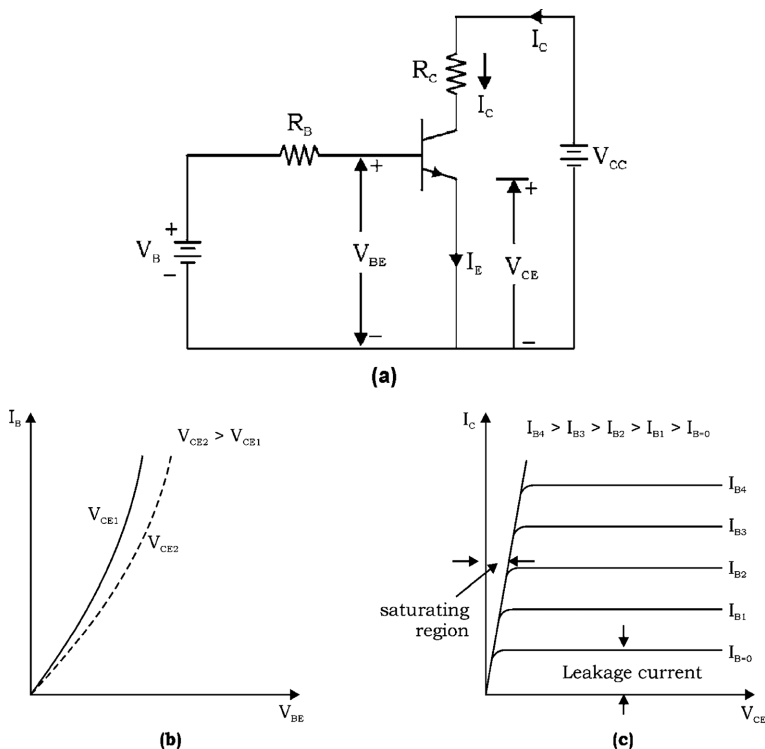


FIGURE 2.6 BJT transistor (a) *npn* BJT circuit characteristics, (b) input characteristics, and (c) output characteristics.

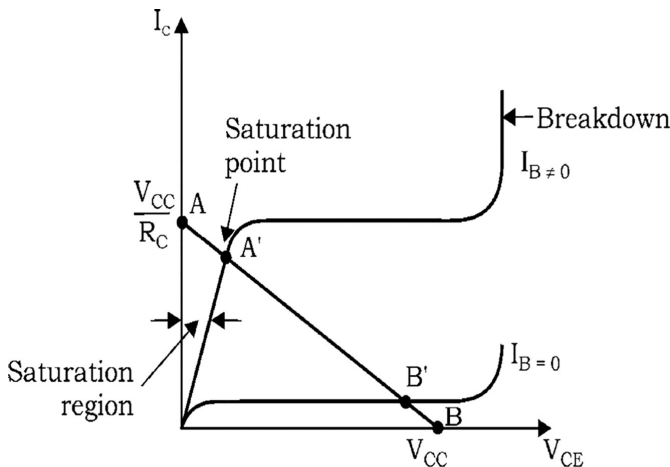


FIGURE 2.7 Output characteristics and load line for *npn* BJT.

The transistor operates as a switch when it operates either in saturation or in the cut-off region. As an ideal switch, the transistor operates as closed switch at Point A in the saturated state with $V_{CE} = 0$ and as an open switch at Point B in the cutoff state with $I_C = 0$, as shown in Figure 2.7.

But practically, the transistor operates at Point A' in the saturated region with a small saturation voltage V_{CES} (so $V_{CE} \neq 0$). Voltage V_{CES} represents the on-state voltage drop of the transistor, which is of the order of about IV.

When the control, or base signal, is reduced to zero, the transistor is turned off and its operation shifts to B' in the cutoff region, as shown in Figure 2.7. A small leakage current I_{CEO} flows in the collector circuit when the transistor is off.

2.5.1.2 Switching Characteristics of a BJT

Figure 2.8a is used to draw the switching characteristics of a BJT. A transistor cannot be turned on instantly because of the presence of an internal capacitance. Figure 2.8b shows the switching waveforms of an *npn* transistor with resistive load between collector and emitter.

1. **Turn-on time (t_{on}):** It consists of two time intervals, that is,

$$t_{on} = \text{delay time} (t_d) + \text{rise time} (t_r)$$

Delay time (t_d): When the base-emitter voltage V_{BE} is applied, I_B rises to I_{BS} ; the collector current I_C remains zero or equal to the collector-emitter leakage current (I_{CEO}) as shown in Figure 2.8. After some delay time (t_d), I_C begins to rise. This delay is due to the time required to charge the base-emitter capacitance to $V_{BES} = 0.7$ V.

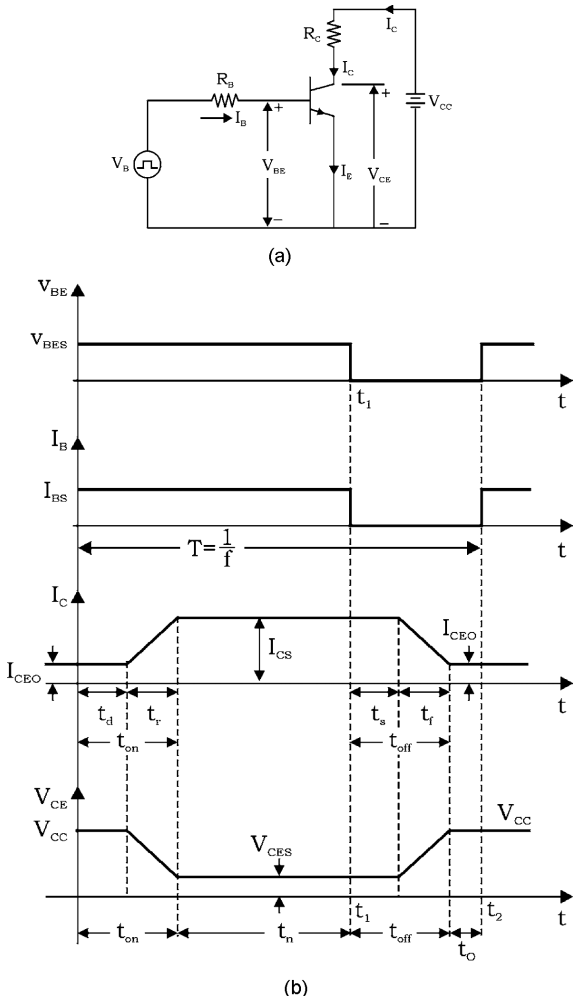


FIGURE 2.8 (a) BJT with resistive load and (b) switching turn-on and turn-off characteristics of *npn* BJT (where t_n = conduction period, t_o = off period).

Rise time (t_r): During this time interval, I_C rises to a steady-state value I_{CS} , and V_{CE} falls from V_{CC} to V_{CES} . It depends on the input capacitances. The transistor remains in the on and saturated state as long as the forward base current is maintained.

2. **Turn-off time (t_{off}):** Total turn-off time consists of two time intervals, that is,

$$t_{off} = \text{storage time } (t_s) + \text{ fall time } (t_f)$$

Storage time (t_s): After the removal of the base-emitter voltage V_{BE} at time t_1 , I_C does not change for a time called storage time t_s . During t_s , saturating charges are removed from the base.

Fall time (t_f): During this time, the collector current I_C begins to fall, and the collector voltage starts building up, that is, the I_C decreases to I_{CEO} (almost zero) and V_{CE} rises to V_{CC} .

2.5.2 POWER MOSFETs

Power metal-oxide semiconductor field-effect transistors (MOSFETs) are recent power semiconductor devices that have been developed using the field-effect concept and MOS technology. It has three terminals, drain (D), source (S), and gate (G), in place of a corresponding three-terminal collector, emitter, and base for the BJT as shown in [Figure 2.9](#) [2–8].

Here, the arrow indicates the direction of electron flow.

Construction: On a p-substrate (or body), two heavily doped n^+ regions are diffused as shown in [Figure 2.9b](#). An insulating layer of silicon dioxide (SiO_2) is grown on the surface, and then it is etched to embed a metallic source and drain terminals. The n^+ region makes contact with the source and drain terminals. A layer of metal is also deposited on the SiO_2 layer to form a gate of MOSFET.

In a power MOSFET, conduction is due to the majority charge carriers only, and therefore, time delays caused by the removal or recombination of minority carriers are eliminated. Thus, the power MOSFET can work at a high-switching frequency (in the range of MHz).

MOSFET Characteristics: The basic circuit diagram shown in [Figure 2.10a](#) is used to draw the static characteristics of a power MOSFET.

1. **Transfer characteristics:** It is a graph between the drain current (I_D) and gate-source voltage (V_{GS}). [Figure 2.10b](#) shows the typical transfer characteristics of a power MOSFET. From the characteristics, it can be seen that below V_{GST} (threshold voltage) the device is off.

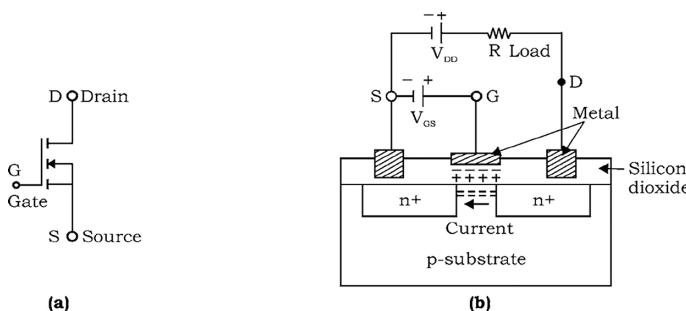


FIGURE 2.9 Power MOSFET (a) circuit symbol and (b) basic structure.

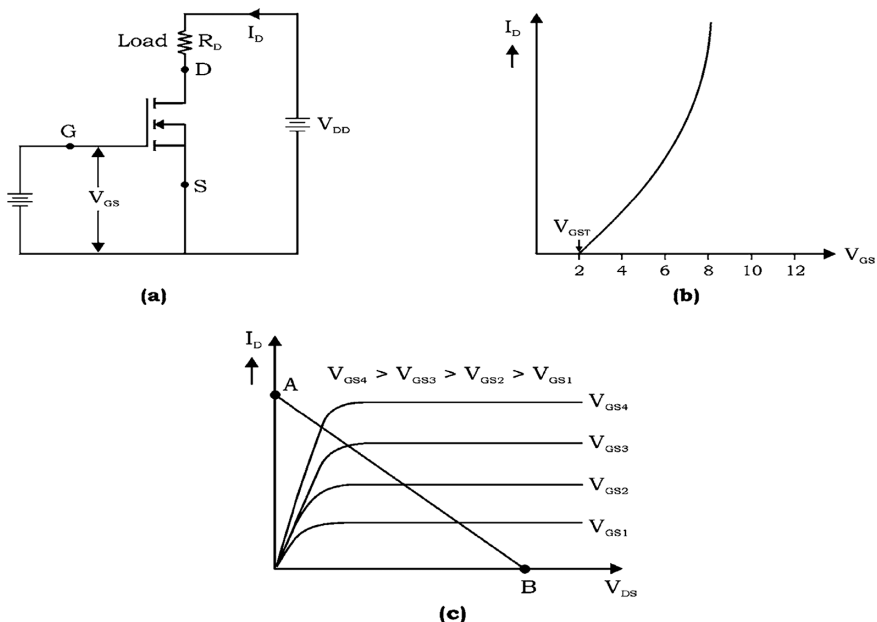


FIGURE 2.10 (a) Power MOSFET circuit diagram, (b) transfer characteristics, and (c) output characteristics.

2. **Output characteristics:** It is a graphical variation between the drain current I_D and drain-source voltage V_{DS} . For low values of V_{DS} , the graph between I_D and V_{DS} is linear.
 3. **Switching characteristics:** Switching characteristics (see Figure 2.11) of a power MOSFET are influenced by its internal capacitance and impedance of a gate-drive circuit.
- Turn-on time (t_{on}):** It consists of two time intervals, that is,

$$t_{on} = \text{turn-on delay time } (t_{dn}) + \text{rise time } (t_r)$$

During delay time (t_{dn}), the input capacitance charges to the gate-threshold voltage (V_{GST}).

During rise time (t_r), the gate voltage rises to the final value V_{GSP} , and the drain current rises from zero to full on the current I_D . The total turn-on time can be reduced by using a low-impedance gate-drive source.

Turn-off time: Because the MOSFET is a majority-charge carrier device, the turn-off process is initiated soon after removal of the gate voltage at time t_1 . It consists of two time intervals, that is,

$$t_{on} = \text{turn-off delay time } (t_{df}) + \text{fall time } (t_f)$$

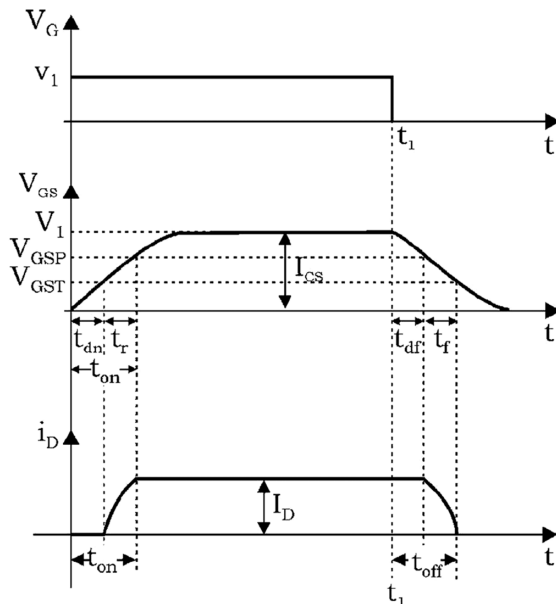


FIGURE 2.11 Switching characteristics of power MOSFET.

During turn-off delay time (t_{df}), the input capacitance discharges from the overdrive gate voltage V_1 to V_{GSP} .

During fall time (t_f), the input capacitance discharges from V_{GSP} to the threshold voltage V_{GST} , and the drain current falls from I_D to zero. So, when $V_{GS} \leq V_{GST}$, MOSFET gets turn off completely. A detailed performance comparison between MOSFET and BJT have been summarised in [Table 2.2](#).

TABLE 2.2
Comparison of MOSFET and BJT

Performance Criteria	Power MOSFET	Power BJT
Switching losses	Low	High
On-resistance and conduction losses	High	Low
Applications	For high-frequency applications	For low-frequency applications
Type of device	Voltage controlled	Current controlled
Temperature coefficient for resistance	Positive (so parallel operation is easy)	Negative
Secondary breakdown	Does not occur	Occurs

2.5.3 INSULATED-GATE BIPOLAR TRANSISTOR

The insulated-gate bipolar transistor (IGBT) is the most recent and efficient semiconductor device that has the advantages of both MOSFET and BJT. It has high input impedance like a MOSFET and low on-state power loss as in a BJT. Also, it is free from the second breakdown problem present in the BJT. It is also called MOSIGT or COMFET or IGT. The basic structure and circuit symbol of the IGBT is shown in [Figure 2.12 \[2–6\]](#). It has three terminals called gate (G), emitter (E), and collector (C).

IGBT Characteristics: The circuit used to draw IGBT characteristics is shown in [Figure 2.13a](#).

1. **Static V-I characteristics (or output characteristics):** It is a graph between the collector current (I_C) and collector-emitter voltage (V_{CE}), for various values of the gate-emitter voltage as shown in [Figure 2.13b](#). Here, the controlling parameter is the gate-emitter voltage (V_{GE}) because IGBT is a voltage-controlled device. This characteristic is similar to that of the BJT.
2. **Transfer characteristics:** It is a graph between the collector current (I_C) and gate-emitter voltage (V_{GE}), which is identical to that of power MOSFET. When V_{GE} is less than the threshold voltage V_{GET} , IGBT is in the off state.
3. **Switching characteristics:** Switching characteristics includes both turn-on and turn-off characteristics.

During turn-on time: It is defined as the time between the instants of forward blocking to the forward on state. It consists of delay time (t_{dn}) and rise time (t_r), that is,

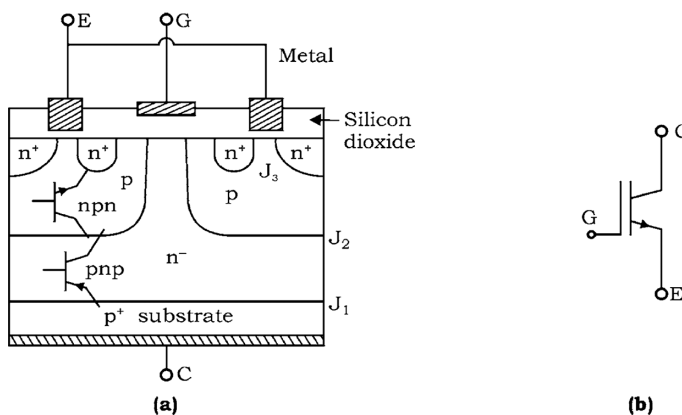


FIGURE 2.12 IGBT (a) basic structure and (b) circuit symbol.

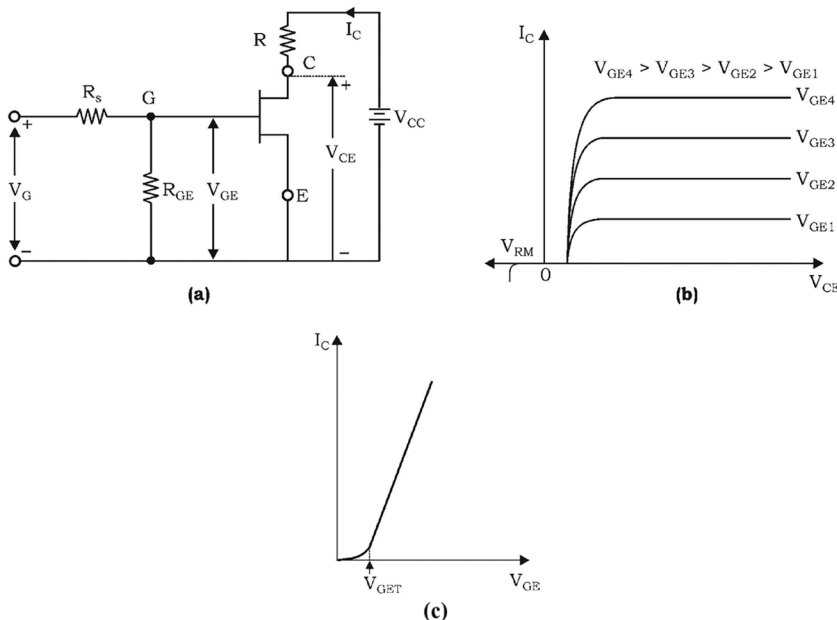


FIGURE 2.13 IGBT (a) circuit diagram, (b) static V-I characteristics, and (c) transfer characteristics.

$$t_{on} = \text{turn-on delay time } (t_{dn}) + \text{rise time } (t_r)$$

The delay time is defined as the time for the collector-emitter voltage (V_{CE}) to fall from V_{CE} to $0.9 V_{CE}$ or time for the collector current to rise from the initial leakage current to $0.1 I_C$, where I_C is the final value of the collector current.

The rise time t_r is the time during which the collector-emitter voltage falls from $0.9 V_{CE}$ to $0.1 V_{CE}$ or the collector current rises from $0.1 I_C$ to its final value I_C .

During turn-off time: It consists of three time intervals, that is, the delay time (t_{df}), initial fall time (t_{f1}), and final fall time (t_{f2}):

$$t_{off} = t_{df} + t_{f1} + t_{f2}$$

The delay time is the time during which the gate voltage falls from V_{GE} to the threshold voltage V_{GET} . As V_{GE} falls to V_{GET} , the collector current falls from I_C to $0.9 I_C$ and V_{CE} the voltage begins to rise.

The first fall time (t_{f1}) is defined as the time during which the collector current falls from 90% to 20% of its initial value I_C or the time when the V_{CE} voltage rises from V_{CES} to $0.1 V_{CE}$.

The final fall time is the time during which I_C falls from 20% to 10% of I_C or the V_{CE} voltage rises from $0.1 V_{CE}$ to the final value V_{CE} , as shown in Figure 2.14.

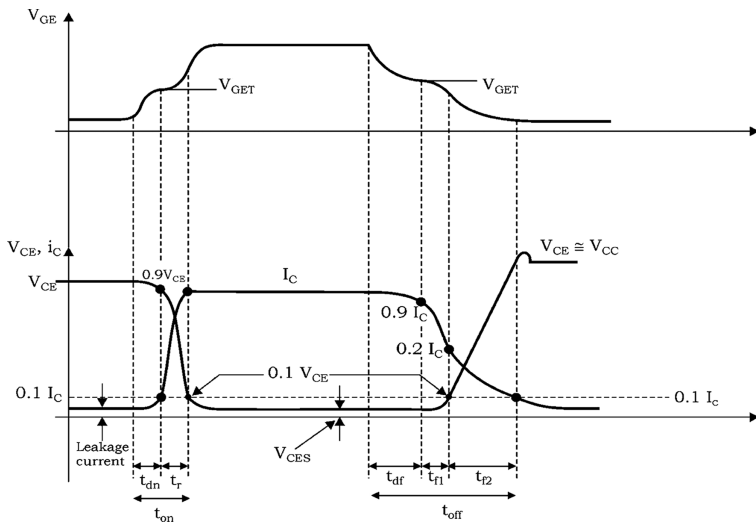


FIGURE 2.14 IGBT turn-on and turn-off characteristics.

2.6 CHARACTERISTICS OF THE THYRISTOR

The thyristor is a silicon-based semiconductor device having four layers ($p-n-p-n$); three junctions J_1 , J_2 , and J_3 ; and three terminals, anode (A), cathode (K), and gate (G). [Figure 2.15](#) gives the schematic diagram and circuit symbol of a thyristor. Other semiconductor devices having similar characteristics with the thyristor are DIAC, TRIAC, GTO, silicon-controlled switch, RCT, etc. This whole family of semiconductor devices is given the name thyristor. One oldest and

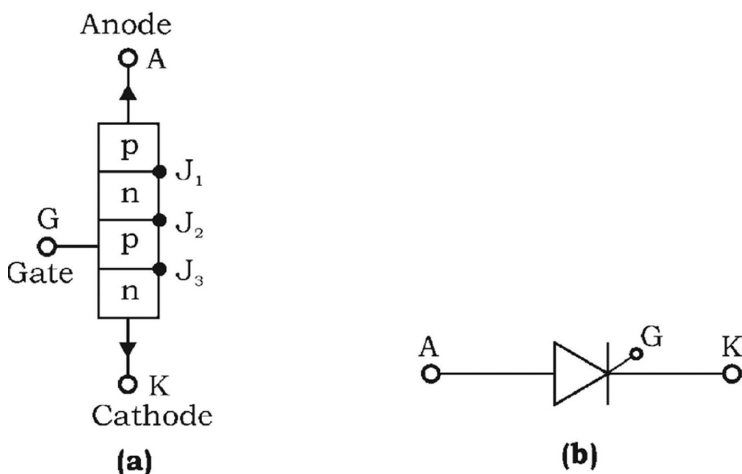


FIGURE 2.15 (a) Schematic diagram and (b) circuit symbol.

most widely used member of this family is the silicon-controlled rectifier (SCR). At present, the use of SCR is so vast and wide that the word *thyristor* has become synonymous with SCR.

The thyristor has a characteristic similar to a thyratron tube, but from the construction point of view, it is similar to a transistor. The name “thyristor” is derived by a combination of “thyratron” and “transistor.” So, thyristor is a solid-state device like a transistor, but its characteristic is similar to thyratron tube.

2.6.1 STATIC V-I CHARACTERISTICS OF A THYRISTOR

A circuit diagram for obtaining the static V-I characteristics of a thyristor is shown in Figure 2.16a.

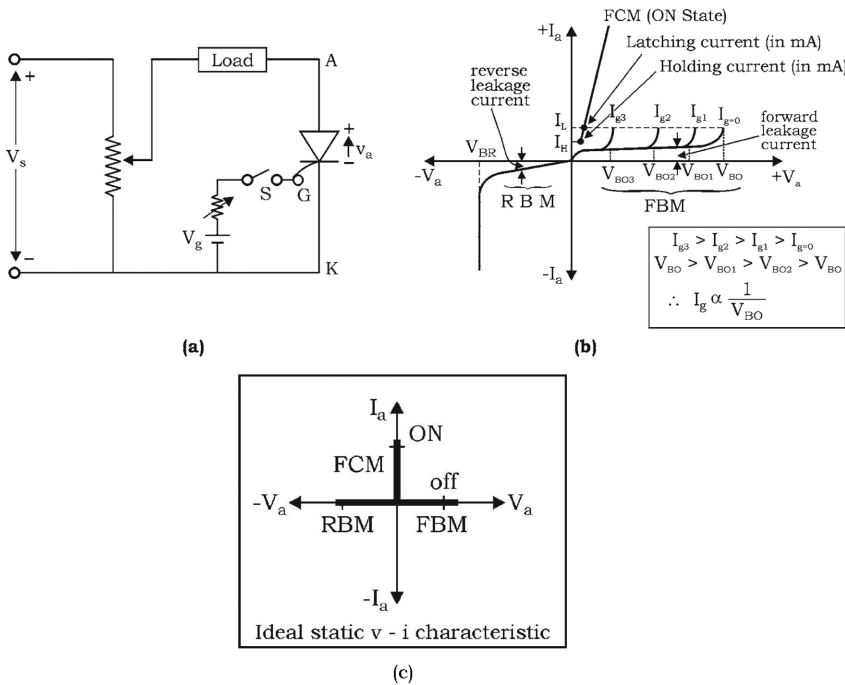


FIGURE 2.16 (a) Circuit for obtaining thyristor V-I characteristics, (b) static V-I characteristics of thyristor, and (c) ideal V-I characteristics of a thyristor.

where RBM = reverse blocking mode

FBM = forward blocking mode

FCM = forward conduction mode

V_{BO} = forward breakover voltage

V_{BR} = reverse breakover voltage

I_g = gate current

V_a = anode voltage across thyristor terminals A and K

I_a = anode current

Static V-I characteristics of thyristor as shown in [Figure 2.16b](#) and [Figure 2.16c](#) indicates that it has three basic modes of operation which are discussed as follows.

2.6.1.1 Reverse Blocking Mode (RBM)

During this mode, the cathode is a positive w.r.t. anode with switch S open, that is, no gate pulse is applied. So the thyristor is RB, as shown in [Figure 2.17a](#). The junctions J_1 and J_3 are RB, whereas junction J_2 is FB. The device behaves like two diodes connected in series with reverse voltage applied across them. So, a small reverse leakage current (of order of mA or μ A) flows from the cathode to anode during this mode.

If the reverse voltage is further increased to the critical breakdown level called as reverse breakdown voltage (V_{BR}), an avalanche occurs at junctions J_1 and J_3 . As a result, the reverse current increases rapidly. This large reverse current gives rise to more losses, which may damage the device due to the rise in junction temperature beyond its permissible limit. So, it must be ensured that the maximum working reverse voltage across the thyristor does not exceed V_{BR} .

2.6.1.2 Forward Blocking Mode

During the FBM, the anode is a positive w.r.t cathode, with the gate circuit open, that is, no gate pulse is applied. So, the junctions J_1 and J_3 are FB, whereas junction J_2 is RB, and therefore, a small current called the forward leakage current flows from the anode to cathode, as shown in [Figure 2.17b](#). In this mode, the device offers high impedance, and therefore, the thyristor is treated as an open switch (OFF state).

2.6.1.3 Forward Conducting Mode

During the FCM, the anode is a positive w.r.t. cathode, and the gate pulse is applied between the gate and cathode. So, all three junctions J_1 , J_2 and J_3 become FB, and therefore, a large current starts flowing from the anode to cathode with a very small voltage drop across it (1–2 V). In this mode, the thyristor is in the on state and behaves like a closed switch.

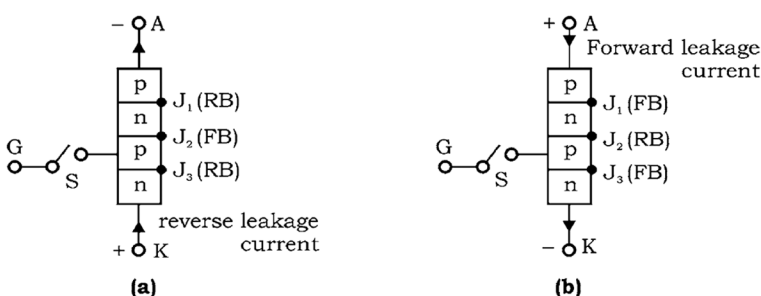


FIGURE 2.17 (a) RBM: J_1J_3 —RB and J_2 —FB and (b) FBM: J_1J_3 —FB and J_2 —RB.

2.6.2 SWITCHING CHARACTERISTICS OF A THYRISTOR

During the turn-on/turn-off process, the thyristor is subjected to different voltages and currents. So, the time variations of these voltages and currents during turn-on/turn-off of the thyristor gives the dynamic or switching or transient characteristics of a thyristor.

Switching characteristics during turn-on: The thyristor is generally turned on by applying a positive gate voltage between the gate and cathode of an FB thyristor (i.e., the anode is a positive w.r.t. cathode). The thyristor turn-on time is a transition time that can be defined as the time during which it changes from the FBM to the final on state. The total turn-on time is divided into three time intervals, that is, the delay time (t_d), rise time (t_r), and spread time (t_p), as shown in Figure 2.18.

$$t_{on} = t_d + t_r + t_p$$

Delay time (t_d): It is measured from the instant at which the gate current reaches $0.9 I_g$ to the instant at which the anode current reaches $0.1 I_a$. It can also be defined as the time during which the anode voltage falls from V_a to $0.9 V_a$.

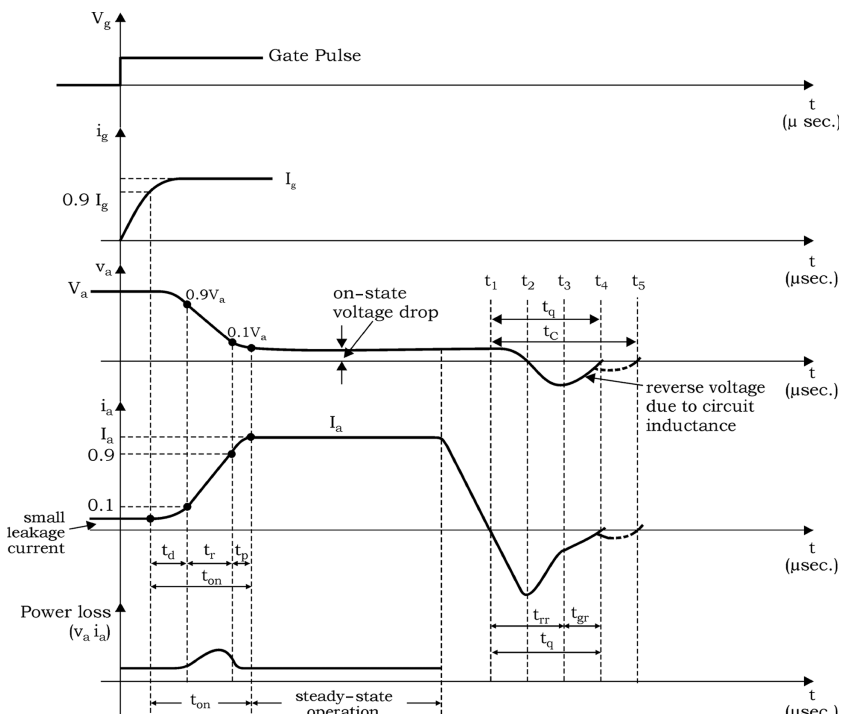


FIGURE 2.18 Thyristor switching characteristics during turn-on and turn-off.

Delay time (t_d) $= 0.9 I_g$ to $0.1 I_a$ or V_a falls from V_a to $0.9 V_a$ or I_a rises from forward leakage current to $0.1 I_a$

Rise time (t_r): It is the time taken by the anode current to rise from $0.1 I_a$ to $0.9 I_a$ or time required for forward blocking off-state voltage to fall from $0.9 V_a$ to $0.1 V_a$.

Rise time (t_r) $= I_a$ rises from $0.1 I_a$ to $0.9 I_a$ or V_a falls from $0.9 V_a$ to $0.1 V_a$

Rise time is inversely proportional to the magnitude of the gate current and its build-up rate. So, the rise time can be reduced if high, and steep current pulses are applied to the gate.

for series RL circuit— t_r is morefor series RC circuit— t_r is less

During rise time, turn-on losses in thyristor are highest due to high anode voltage (V_a) and current (I_a)

Spread time (t_p): It is the time taken by the anode current to rise from $0.9 I_a$ to I_a or voltage to fall from $0.1 V_a$ to the on-state voltage drop (1 to 1.5 V). During this time, conduction spreads over the entire section of the cathode.

Spread time (t_p) $= I_a$ rises from $0.9 I_a$ to I_a or V_a falls from $0.1 V_a$ to on-state voltage drop (1 to 1.5 V)Total turn-on time (t_{on}) —→ (1 to 4) μ sec

– It depends on anode circuit parameter and gate signal waveshapes

During turn-on, the thyristor is a charge-controlled device. The higher the magnitude of the gate current, lesser the time it takes to inject charges into the gate region, and so lesser one will be the total turn-on time.

Hard firing or overdriving: The thyristor is said to be hard fired or overdriven when the gate current is several times higher than the required minimum gate current, which results into a reduction of its turn-on time with enhanced di/dt capabilities.

Switching characteristics during turn-off: Turning off the device means changing from the on to off state with forward voltage blocking capability. This process of turning off the thyristor is also called a commutation.

The gate loses its control once the thyristor gets turned on. Therefore, it can be turned off by bringing its anode current below the holding current through natural or forced commutation. At this instant, the device is not capable of blocking the forward voltage due to the presence of charge carriers (holes and electrons) present in four layers of the thyristor. So, the device may go into conduction mode even if the gate signal is not applied. Therefore, two essential requirements for completely turning off the device are:

1. Anode or forward current must be brought below holding current and then,
2. Thyristor must be reversed biased for some finite time after the anode current becomes zero.

The turn-off time, t_q , of a thyristor is defined as the time between the instant anode current (I_a) becoming zero to the instant device regaining its forward blocking capability. During this time, all the excess charge carriers from four layers of thyristor are removed by the following two processes:

- a. Sweeping out of holes from output p -layer and e^- from outer n -layer
- b. Recombination of charge carriers around junction J_2 (i.e., holes and electrons from inner p and n layer)

The duration of the turn-off time is generally 3 to 100 μ sec. The turn-off time consists of two time intervals, that is, the reverse recovery time (t_{rr}) and gate recovery time (t_{gr}):

$$t_q = t_{rr} + t_{gr}$$

Reverse recovery time (t_{rr}): During this period, the reverse anode current flows with the same slope due to the presence of charge carriers stored in the layers of thyristor. This reverse recovery current removes excess charge carriers from the outer p and n layers between the instant t_1 and t_3 . In other words, the reverse recovery current flows due to the sweeping out of holes and electrons from outer p and n layers. Reverse recovery time can also be defined as the time between the instant anode current being zero to the instant I_{rr} being 25% of the maximum reverse recovery current.

At instant t_2 , most of the stored charge carriers are removed from outer two layers, so the charge density and reverse recovery current (I_{rr}) begin to decrease. Because the decay of I_{rr} is fast, a reverse voltage appears across the device due to circuit inductance, as shown in [Figure 2.18](#).

At instant t_3 , when the reverse recovery current I_{rr} falls near to zero, junctions J_1 and J_3 recover. This reverse recovery process between t_1 and t_3 is similar to that of the diode.

Gate recovery time (t_{gr}): During this period, excess charge carriers from the inner p and n layers (i.e., around junction J_2) are removed by a recombination process through maintaining a small reverse voltage across the thyristor. It can be defined as the time between the instant reverse recovery current (I_{rr}) being 25% of $(I_{rr})_{\max}$ to the instant the thyristor is capable of blocking the forward voltage (or reverse voltage reaches zero).

The total turn-off time depends on:

1. Magnitude of anode or forward current at the time of commutation
2. dil/dt at the time of commutation
3. Junction temperature

An increase in magnitude of above factors increases the thyristor turn-off time.

Circuit turn-off time (t_c): This is the turn-off time provided to the thyristor by the practical circuit, which can be defined as the time between the instant anode current becoming zero to the instant the reverse voltage reaches zero, as shown in [Figure 2.18](#).

The comparison between the converter grade and inverter grade SCRs is presented in [Table 2.3](#).

2.6.3 THYRISTOR GATE CHARACTERISTICS

This presents the relationship between gate voltage and current as shown in [Figure 2.19](#) [2,4,6]. These characteristics are similar to that of a diode.

TABLE 2.3
Comparison of Converter- and Inverter-Grade SCRs

Performance Criteria	Converter-Grade SCRs	Inverter-Grade SCRs
Turn-off time	Slow	Fast
Cost	Cheaper	Costly
Applications	Phase-controlled rectifiers, AC-voltage controllers, cycloconverters, etc.	Inverters, choppers, and force-commutated converters

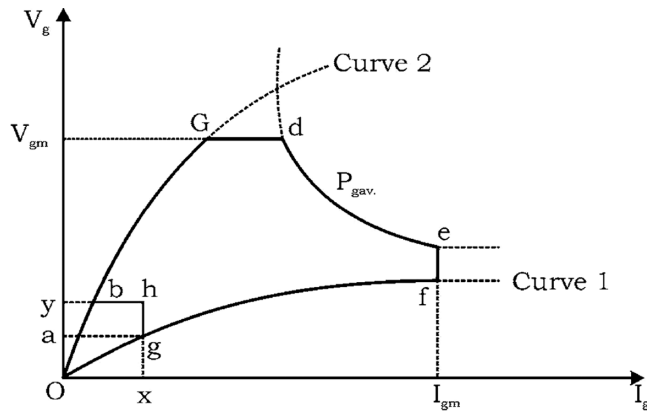


FIGURE 2.19 Forward gate characteristics of a thyristor.

where,

oy, ox → minimum gate voltage and current to trigger thyristor

V_{gm} , I_{gm} → maximum gate voltage and current

oa → nontriggering gate voltage

P_{gav} → average gate power dissipation.

Curve 1 represents the lowest voltage magnitude, which is applied to turn on the device, whereas the Curve 2 represents the highest possible voltage magnitude that can be safely applied to the gate circuit.

If V_{gm} , I_{gm} and P_{gav} are exceeded, the thyristor can be damaged. So, the preferred gate drive area for a thyristor is bGdefghb as shown in Figure 2.19. It must be ensured that all spurious noise or unwanted signals should be less than nontriggering voltage (oa).

For Figure 2.20a:

$$E_s = V_g + I_g R_s \quad (2.7)$$

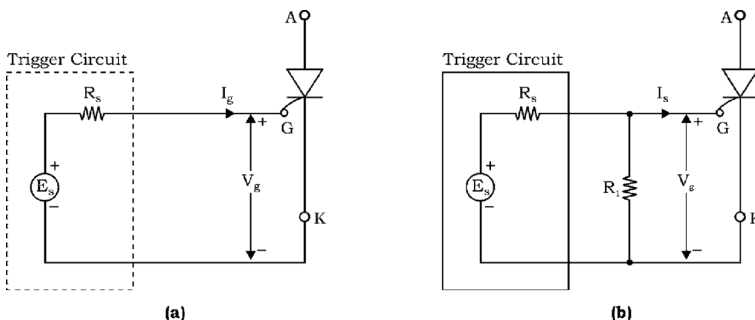


FIGURE 2.20 Trigger circuit.

The magnitude of internal resistance R_s must be such that current (E_s/R_s) is not harmful to the source and gate circuit when thyristor is turned on.

For [Figure 2.20b \[2,4,6\]](#):

$$E_s = \left(I_{gmn} + \frac{V_{gmn}}{R_l} \right) R_s + V_{gmn} \quad (2.8)$$

R_1 is connected to provide an easy path to leakage current.

Also, it should be ensured that the pulse width is sufficient to allow the anode current to exceed the latching current. If T is the pulse width, then $T > t_{on}$, that is, the gate-pulse width is taken equal or greater than thyristor turn-on time.

$$\text{Also, } \frac{P_{gm}T}{T_1} \geq P_{gav} \text{ or } P_{gm}Tf \geq P_{gav}$$

or

$$\boxed{\frac{P_{gav}T}{fT} \leq P_{gm}} \quad (2.9)$$

where $f = 1/T_1$ = Frequency of firing in Hz.

T = Pulse width in sec.

$$\text{Duty cycle } \delta = \frac{T}{T_1} = f T$$

$$\therefore \boxed{\frac{P_{gav}T}{\delta} \leq P_{gm} \text{ or } \frac{P_{gav}}{\delta} = P_{gm}} \quad (2.10)$$

2.7 GATE TURN-OFF (GTO) THYRISTOR

The GTO is a four $p-n-p-n$ -layered, three-terminal anode (A), cathode (K), and gate (G) device, which can be turned on like an ordinary thyristor by applying a positive gate pulse between the gate and cathode terminals. But unlike a thyristor, it can be turned off simply by applying a negative gate pulse of appropriate magnitude between the gate and cathode terminals.

Therefore, for the applications where the supply is DC, such as in a chopper and inverter, GTO is preferred because this does not require any forced commutation circuit for its turn off. So, it becomes more compact and economical. The negative gate current required to turn off a GTO is 15%–25% of the anode current at the time of commutation, which is very high ([Figure 2.21](#)).

2.7.1 STATIC V-I CHARACTERISTICS

From static V-I characteristics of GTO, it can be seen that latching current is in Amp. (here 2A) as compared to 100–500 μ A for a normal thyristor of the same rating [[2-7](#)].

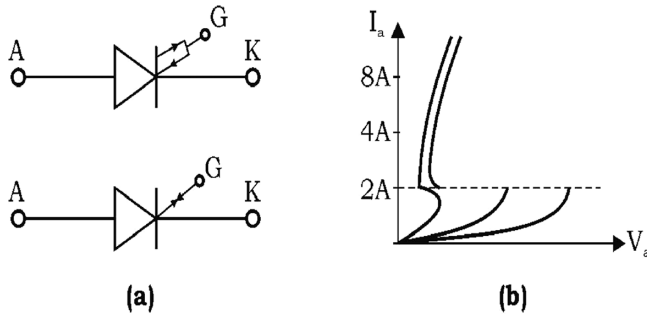


FIGURE 2.21 GTO (a) circuit symbol and (b) static V-I characteristics.

2.7.2 SWITCHING CHARACTERISTICS OF GTO

During gate turn-on: The turn-on process for the GTO is similar to that of normal thyristor, that is, t_{on} time consists of delay time, rise time, and spread time:

$$t_{on} = t_d + t_r + t_p$$

Turn-on time can be reduced by increasing its forward gate current like in a thyristor.

During gate turn-off: The turn-off characteristics of a GTO are different from those of a normal thyristor or SCR. It can be turned off by applying a negative pulse between gate and cathode terminals. The turn-off time of the GTO consists of three time intervals, that is, storage time, fall time, and tail time:

$$t_q = t_s + t_f + t_t$$

Storage time (t_s): During the storage period, the anode current (I_a) and anode voltage (equal to on-state voltage drop) remain constant. The excess charges (holes in p -base) are removed by negative gate current during this period, that is, it prepares the GTO for turning off (or commutation).

Fall time (t_f): During fall time, the anode current falls rapidly and the anode voltage rises. The fall period is measured from the time the instant gate current is at a maximum negative to the instant the anode current falls to its tail current, as shown in [Figure 2.22](#).

Tail time (t_t): During tail time, the anode current and voltage keep moving toward their turn-off values. After t_f , the anode current reaches zero and the anode voltage v_a undergoes a transient overshoot due to the presence of R_s and C_s .

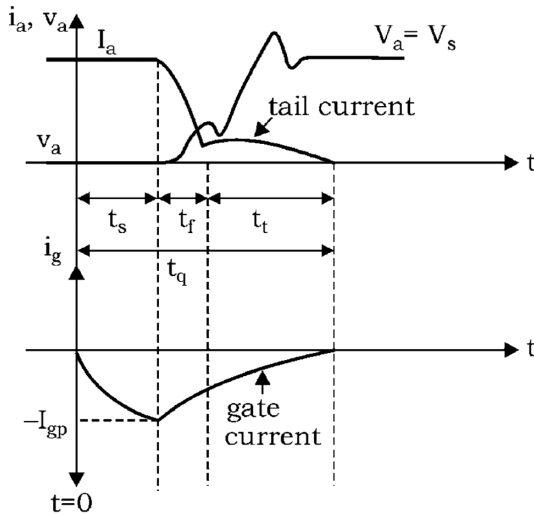


FIGURE 2.22 Switching turn-off characteristics of GTO.

2.8 TWO-TRANSISTOR MODEL OF A THYRISTOR

With the help of the two-transistor model, the principle of thyristor operation can be explained. The two-transistor model is obtained by bisecting the two middle layers in two separate halves as shown in Figure 2.23a [2–7].

So, it constitutes the two *pnp* and *npn* transistors separately, as shown in Figure 2.23b and c.

In the off state of a transistor, the collector current I_C is related to the emitter current I_E as follows:

$$I_C = \alpha I_E + I_{CBO} \quad (2.11)$$

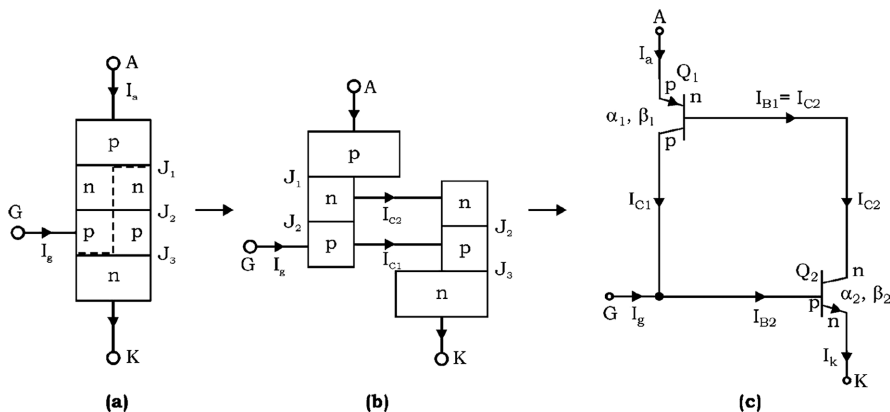


FIGURE 2.23 Thyristor (a) layered diagram, (b) and (c) two-transistor models.

where

α = common-base current gain

I_{CBO} = common-base leakage current

For transistor Q_1 ,

$$I_{C1} = \alpha_1 I_a + I_{CBO1} \quad (2.12)$$

where

α_1 = common-base current gain of transistor Q_1 ,

I_{CBO1} = common-base leakage current of transistor Q_1 ,

I_a = anode current or forward current.

Similarly,

$$I_{C2} = \alpha_2 I_k + I_{CBO2} \quad (2.13)$$

where α_2 and I_{CBO2} are the common-base current gain and leakage current of transistor Q_2 and I_k = emitter current of transistor Q_2 .

From [Figure 2.19](#) I , it can be seen that the sum of the two collector currents given by Equations (2.6) and (2.7) is equal to the external circuit current I_a entering at anode terminal A .

$$\therefore I_a = I_{C1} + I_{C2}$$

or

$$I_a = \alpha_1 I_a + I_{CBO1} + \alpha_2 I_k + I_{CBO2} \quad (2.14)$$

When the gate current is applied, then

$$I_k = I_a + I_g \quad (2.15)$$

Substituting the value of I_k in Equation (2.14), we get

$$I_a = \alpha_1 I_a + I_{CBO1} + \alpha_2 (I_a + I_g) + I_{CBO2}$$

or

$$I_a = \frac{\alpha_2 I_g + I_{CBO1} + I_{CBO2}}{1 - (\alpha_1 + \alpha_2)}$$

(2.16)

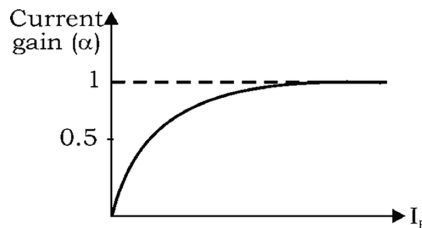


FIGURE 2.24 Variation of current gain with emitter current of thyristor.

Current gain α is very low at low emitter current. With an increase in emitter current, α increases rapidly as shown in [Figure 2.24](#).

If, by some means, the emitter current of two transistors Q_1 and Q_2 is increased so that $(\alpha_1 + \alpha_2)$ approaches unity, then as per Equation (2.16), I_a would tend to become infinite, which implies that the device has turned on.

Therefore, the methods of turning on the device are nothing but the methods of making $(\alpha_1 + \alpha_2)$ to approach unity, that is, $(\alpha_1 + \alpha_2) \geq 1$. Various methods for turning on a thyristor are [\[2,3,5,8\]](#):

1. Gate triggering
2. Forward-voltage triggering
3. dV/dt triggering
4. Temperature triggering
5. Light triggering

REVIEW QUESTIONS

- 2.1 Differentiate between the thyristor and transistor family semiconductor power devices.
- 2.2 Describe static V-I characteristics and switching characteristics of SCR, IGBT, and MOSFET.
- 2.3 Draw ideal and practical V-I characteristics of a power diode and SCR.
- 2.4 Differentiate between a simple diode and power diode.
- 2.5 What is the softness factor for a power diode?
- 2.6 What factors affect the reverse recovery time of a power diode?
- 2.7 Make a detailed comparison between BJT and IGBT.
- 2.8 How does GTO differ from SCR?
- 2.9 What is the importance of the two-transistor model of SCR?
- 2.10 What are various methods for turning on the SCR?
- 2.11 Draw switching characteristics of power MOSFET and power IGBT.
- 2.12 Draw switching characteristics of a GTO thyristor.
- 2.13 List members of the thyristor and transistor family members.

SUMMARY

This chapter has studied in detail the construction, structure, working, and different characteristics of various power semiconductor devices intended for power applications. The power devices of the thyristor family do not require continuous control signals for their conduction, which is required in the case of the transistor family.

REFERENCES/FURTHER READING

1. M. S. Adler, K. W. Owayang, B. Jayant Baliga, and R. A. Kokosa, “The evolution of power device technology,” *IEEE Trans. Electron. Dev.*, vol. ED-31, no. 11, pp. 1570–1591, 1984.
2. M. H. Rashid, *Power Electronics: Circuits, Devices, and Applications*, Pearson Education, Singapore, 2004.
3. *SCR Manual*, 6th ed., General Electric Company, New York, 1979.
4. P. T. Krein, *Elements of Power Electronics*, Oxford University Press, New York, 2003.
5. K. Thorborg, *Power Electronics*, Prentice Hall International, London, UK, 1988.
6. P. S. Bhimra, *Power Electronics*, 5th edition, Khanna Publications, New Delhi, 2012.
7. R. W. Erickson, *Fundamentals of Power Electronics*, Chapman & Hall, New York, 1997.
8. V. R. Moorthi, *Power Electronics Devices, Circuits and Industrial Applications*, Oxford University Press, 2010.
9. T. Suntio, T. Messo, J. Puukko, *Power Electronic Converters*, Wiley-VCH, Verlag GmbH, Germany, 2018.
10. A. M. Trzynadlowski, *Introduction to Modern Power Electronics*, 3rd edition, John Wiley & Sons, Hoboken, NJ, 2010.



Taylor & Francis

Taylor & Francis Group

<http://taylorandfrancis.com>

3 Silicon-Controlled Rectifier

3.1 INTRODUCTION

The silicon-controlled rectifier (SCR) is very commonly used and a popular member of the SCR family where sometimes thyristors are termed SCRs. It is the oldest power device with the highest power-handling capacity even today. It is a latching switch with four-layered construction, which is turned on by applying a gate pulse but cannot be turned off by gate. This chapter discusses in detail the construction, working, terminal characteristics, switching speed, current, and voltage capabilities of different available power devices [1–19].

3.2 SCR CONSTRUCTION

SCR consists of four layers of alternate *p*- and *n*-type semiconductors forming three *p*–*n* junctions, J_1 , J_2 , and J_3 . It has three terminals named as anode (A), cathode (K), and gate (G). The anode terminal is connected to the outer *p*-region, the cathode terminal with the outer *n*-region, and the gate to the inner *p*-region as shown in Figure 3.1. The threaded stud is to tighten the SCR on the heat sink for dissipating the heat.

It is called a “silicon-controlled rectifier” because silicon is used for its construction, and its operation as a rectifier can be controlled. It is a unidirectional device that blocks the current flow from cathode to anode. Unlike the diode, the SCR also blocks the current flow from anode to cathode until it is triggered. So, it is a controlled device.

The “pellet” of the alternate *p*- and *n*-type semiconductor material are fabricated by any one of the following most popular methods [2,7–9,4–19]:

1. Planar diffused (all diffused)
2. Alloy diffused

The manufacturing of both alloy- and planar-diffused “*p*–*n*–*p*–*n*” pellets start with preparation of a large area of “*p*–*n*–*p*” wafers. These are formed by gaseously diffusing *p*-type impurities into both faces of a thin wafer of *n*-type silicon. The finished “*p*–*n*–*p*–*n*” wafers are then divided into individual pellets.

3.2.1 PLANER DIFFUSED

The SCR consists of a four-layer pellet of *p*- and *n*-type semiconductor material. Silicon is used as the intrinsic semiconductors doped with proper impurities. The junctions are the diffused type. It therefore describes a type of pellet where all *pn* junctions come out to a single surface on the silicon pellet as shown in cross-sectional view in Figure 3.2a [7–9].

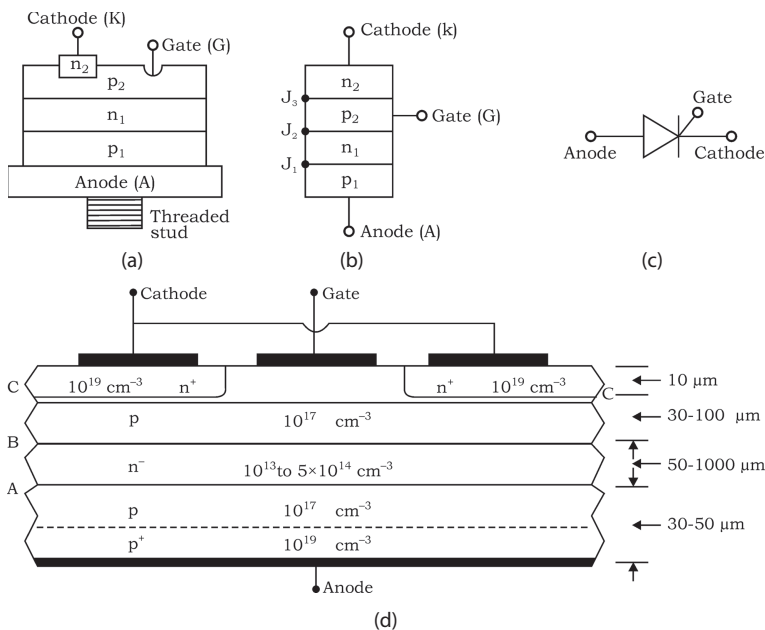


FIGURE 3.1 Construction and structure of SCR: (a) construction, (b) layered structure, (c) circuit symbol, and (d) cross section.

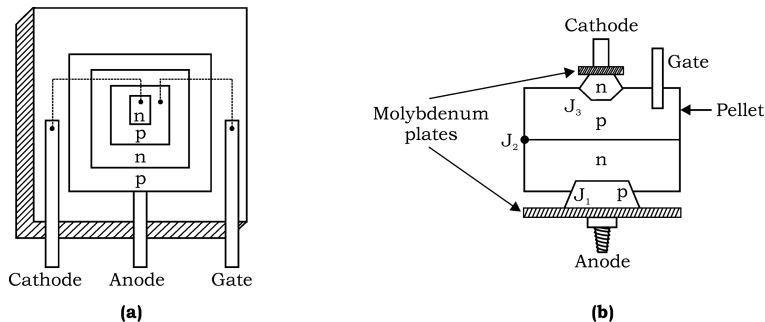


FIGURE 3.2 (a) Cross-sectional view of planar type SCR, and (b) cross-sectional view of alloy diffused SCR.

3.2.2 ALLOY DIFFUSED

The inner junction J_2 is obtained by diffusion, and then the outer two layers are alloyed to it as shown in cross-sectional view in [Figure 3.2b](#). To provide greater mechanical strength to handle large currents, the $p-n-p-n$ pellet is braced with tungsten or molybdenum plates.

3.3 SPECIFICATIONS AND RATINGS

For reliable and satisfactory operation of the SCR, it is ensured that its current, voltage, power, temperature, dv/dt , and di/dt ratings do not exceed above its manufacturer specifications. Ratings and specifications serve as links between designer and the user of the SCR [2,3,6,8,10,11]. Some subscripts are associated with voltage and current ratings for convenience.

Let X_{123} , where X may be voltage (V) or current (I). Where the first subscript “1” indicates the direction or state, that is,

D = forward-blocking region

T = on state

R = reverse

F = forward

Second subscript “2” indicates:

W = working value

R = repetitive value

S = surge or nonrepetitive value

T = trigger

Third subscript “3” indicates:

M = maximum or peak value

3.3.1 VOLTAGE RATINGS

1. **V_{DWM} : Peak working forward-blocking voltage:** It is the maximum value of the forward voltage that an SCR can withstand when it is in the off state (Figure 3.3).
2. **V_{DRM} : Peak repetitive forward-blocking voltage:** It is the peak transient voltage that an SCR can withstand repeatedly when it is in on or off state (FBM)*. It is specified at a maximum allowable junction temperature. It appears when the SCR is turned off due to an abrupt in the change in the reverse recovery current and circuit inductance voltage ($L \frac{di}{dt}$).
3. **V_{DSM} : Peak surge (or nonrepetitive) forward-blocking voltage:** It is the maximum value of any nonrepetitive surge voltage that an SCR can withstand when in off state. It is 130% of V_{DRM} but less than the forward break over voltage (V_{BO}).
4. **V_{RWM} : Peak working reverse voltage:** It is the maximum reverse voltage that an SCR can withstand repeatedly.
5. **V_{RRM} : Peak repetitive reverse voltage:** It is the maximum value of reverse voltage that may be applied repeatedly to the SCR.
6. **V_{RSM} : Peak surge (or nonrepetitive voltage):** It is the maximum transient reverse surge voltage that does not repeat. It is 130% of V_{RRM} but less than the reverse breakdown voltage (V_{BR}).

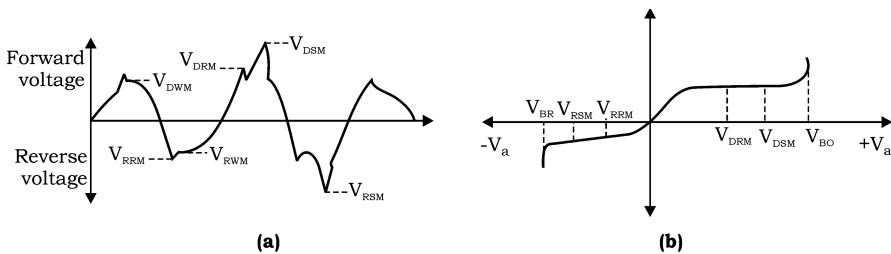


FIGURE 3.3 Voltage ratings during blocking state of SCR.

7. **V_T : on-state voltage drop:** It is the voltage drop across the SCR when conducting (on state) at the specified value of forward current and junction temperature. It is about 1.0–1.5 V.
8. **V_{GT} : Gate trigger voltage:** It is the maximum gate voltage required to produce the gate-triggering current.
9. **Forward $\frac{dv}{dt}$ rating:** It is the maximum rate of rise of the anode voltage that will not trigger SCR if the gate signal is not applied. If $\frac{dv}{dt}$ exceeds the rated value, the SCR may be turned on even in the absence of gate signal due to the flow of charging current ($i_c = C_j \frac{dv}{dt}$).

3.3.2 CURRENT RATINGS

The current carrying capacity of a thyristor is determined by the allowable junction temperature. If the current exceeds the rated value, the junction temperature rises, which may lead to damage of the SCR.

1. **I_{TAV} : Average on-state (forward) current:** It determines the power loss in the SCR because the voltage drop across the conducting SCR is low. The current I_{TAV} depends on the temperature of the case, and data sheets of manufacturers indicate this fact.
2. **I_{RMS} : RMS on-state current:** It is also repetitive type and is specified at the maximum junction temperature.
3. **I_{TSM} : Impulse (surge) current rating:** It is the maximum surge current (nonrepetitive) that the SCR can withstand. It is determined by equating the energies involved in one cycle surge and subcycle surge, that is,

$$I_{sub}^2 t = I^2 T$$

or

$$I_{sub} = I \sqrt{\frac{T}{t}} \quad (3.1)$$

where

I = current rating of one-cycle surge, A

I_{sub} = current rating of subcycle surge, A

T = time duration of half-cycle, s
 t = time duration of subcycle surge, s
for 50 Hz, $T = 10 \times 10^{-3}$ s

$$\therefore I_{sub} = I \sqrt{\frac{10 \times 10^{-3}}{t}}$$

or

$$I_{sub} = \frac{0.1I}{t} \quad (3.2)$$

4. **I^2t rating:** It is the maximum allowable nonrepetitive value of a square of instantaneous current integrated over time.
5. **$\frac{di}{dt}$ rating:** It indicates the maximum allowable rate of an increase of the anode current. If the rate of rise of the anode current is very rapid compared to the spreading velocity of carriers across junctions during turn-on time, the local hot-spot heating occurs based on which junction temperature rises beyond its safe limits, and the device may be damaged.

Typical range of $\frac{di}{dt} = (20 - 500)$ A/micro seconds

6. **Holding Current (I_H):** It is defined as the minimum value of anode current below which it must fall for turning off the SCR. It is associated with the turn-off process.
7. **Latching Current (I_L):** It is defined as the minimum value of anode current that it must attain during the turn-on process to maintain conduction when the gate signal is removed.

$$I_L > I_H$$

8. **Minimum and Maximum Gate Current:** Minimum gate current ($I_{g\ min.}$) indicates that value of gate current that is sufficient to turn on the SCR. Whereas the maximum gate current ($I_{g\ max.}$) indicates the safe value of the gate current. The gate current should not exceed $I_{g\ max.}$.

$$I_{g\ min.} \leq I_g < I_{g\ max.}$$

3.4 METHODS OF TURN ON

With the anode positive with respect to the cathode, an SCR can be turned on by any one of the following methods [2.7–9, 14–19]:

3.4.1 GATE TRIGGERING

It is a simple, reliable, and efficient method to turn on an SCR, where a positive gate pulse is applied between the gate and cathode terminal of the device. In this,

the SCR is turned on at reduced forward breakdown voltage (V_{BO}). By applying the gate pulse, the gate current (I_g) is established. As a result, charges are injected into the inner p layer and voltage at which the forward breakdown occurs is reduced. V_{BO} depends on magnitude of the gate current. The higher the gate current the lower the forward breakdown voltage, that is,

$$V_{BO} \propto \frac{1}{I_g} \quad \text{i.e., } I_g \uparrow V_{BO} \downarrow$$

The effect of the gate current on the forward breakdown voltage of an SCR is shown by means of a curve in [Figure 3.4a](#).

[Figure 3.4b](#) explains the chemistry of turning on the SCR by gate triggering. When a positive gate pulse is applied, the I_g current flows, as shown in [Figure 3.4b](#), due to which electrons from the outer n layer are injected into inner p layer, as a result of which the width of the depletion layer around the reverse biased junction J_2 reduces. This causes the junction J_2 to break down at an applied voltage lower than forward breakdown voltage V_{BO} (at $I_g = 0$). If the magnitude of the gate current I_g is increased, more electrons reach the junction J_2 , as a result of which, the width of the depletion layer around junction J_2 reduces to zero very fast; thus, the SCR will get turned on at a reduced forward voltage.

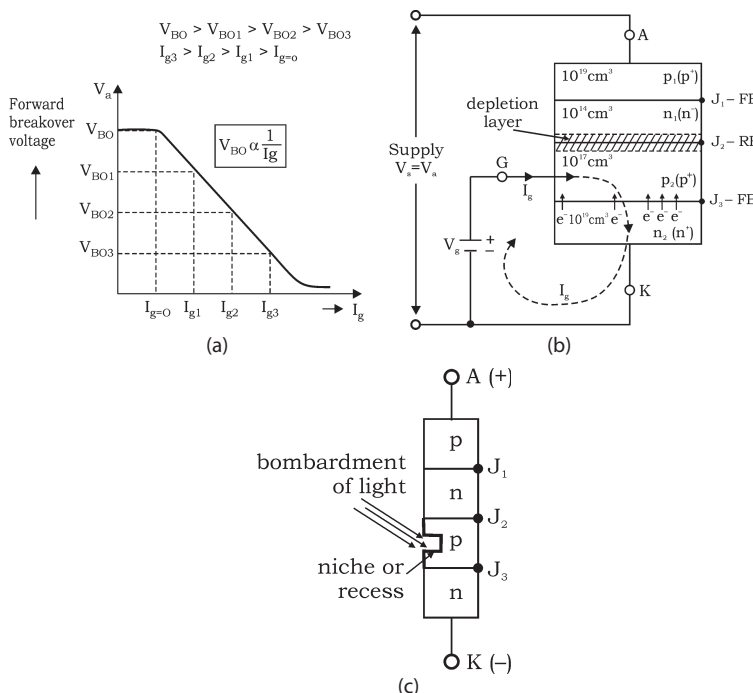


FIGURE 3.4 (a) Forward breakdown voltage V_{BO} versus gate current I_g , (b) circuit showing chemistry of turning on of SCR by gate triggering, and (c) light-activated SCR.

3.4.2 FORWARD VOLTAGE TRIGGERING

In this method of turn on, the anode to cathode forward voltage is increased with the gate circuit open, so the reverse-biased junction J_2 breaks. This is called an avalanche breakdown, and the voltage at which the avalanche breakdown occurs is called the forward breakdown voltage V_{BO} . As other junctions J_1, J_3 are already forward biased, the breakdown of junction J_2 allows the free movement of charge carriers across three junctions, and therefore large forward current flows. Generally, this method of turn on is not used because the SCR may get damaged due to the application of a high voltage.

V_{BO} & V_{BR} are temperature dependent and $V_{BR} > V_{BO}$.
Therefore, V_{BO} is taken as highest voltage rating.

3.4.3 dv/dt TRIGGERING

Reverse-biased junction J_2 of the SCR during the forward-blocking mode behaves like capacitance due to the presence of space-charge carriers around it. Let the capacitance of this junction be C_j . For any capacitor, $i_c = C \frac{dv}{dt}$. The entire forward voltage V_a appears across the reverse-biased junction J_2 . So, the charging current i_c is established, that is,

$$i_c = C_j \frac{dv_a}{dt}$$

Due to a large $\frac{dv_a}{dt}$, this charging current i_c becomes so large that it can play the role of a gate current, and this may turn on the SCR. Such a turn on of the SCR is called an “unwanted” or “spurious” turn on, which is avoided by keeping $\frac{dv_a}{dt}$ within the prescribed limits.

3.4.4 TEMPERATURE TRIGGERING

During the forward-blocking mode, junctions J_1 and J_3 are forward biased, whereas junction J_2 is reverse biased. So the whole applied voltage appears across the reverse biased junction J_2 . As a result, junction J_2 gets associated with leakage current, which raises the temperature of junction J_2 . With an increase in temperature, the leakage current through junction J_2 further increases, and finally this cumulative process may turn on the SCR at some high temperature.

3.4.5 LIGHT TRIGGERING

In this method, a recess or niche is made inside the inner p layer as shown in [Figure 3.4c](#). When a pulse of light of appropriate wavelength guided by optical fibers is irradiated, free charge carriers (hole and electrons) are generated inside the inner p layer just like when gate signal is applied between the gate and cathode. Such an SCR is called a light-activated SCR (LASCR). LASCRs are used in high-voltage direct current (HVDC) transmission systems.

3.5 FIRING (TRIGGERING) CIRCUITS FOR SCR

Circuits used for turning on the SCR are called firing or triggering circuits. Along with their design considerations, these circuits are discussed as follows.

Main Features of Firing Circuits

The most common method for controlling the onset of conduction or a firing angle (α) of an SCR is gate triggering. The gate-control circuit, also called the firing or triggering circuit, is usually a low-power electronic circuit. A firing circuit should fulfill the following requirements:

1. It must be capable of producing gate pulses for each SCR at a desired instant, in case the power circuit has more than one SCR.
2. Pulses produced by it must be periodic in nature.
3. It should have a driver circuit consisting of a pulse amplifier and pulse transformer to ensure turning on of the SCR.

A general layout of the firing-circuit scheme for SCRs is shown in [Figure 3.5a \[2,8,10\]](#). Shielded cables are used to transmit the amplified pulses to pulse transformers.

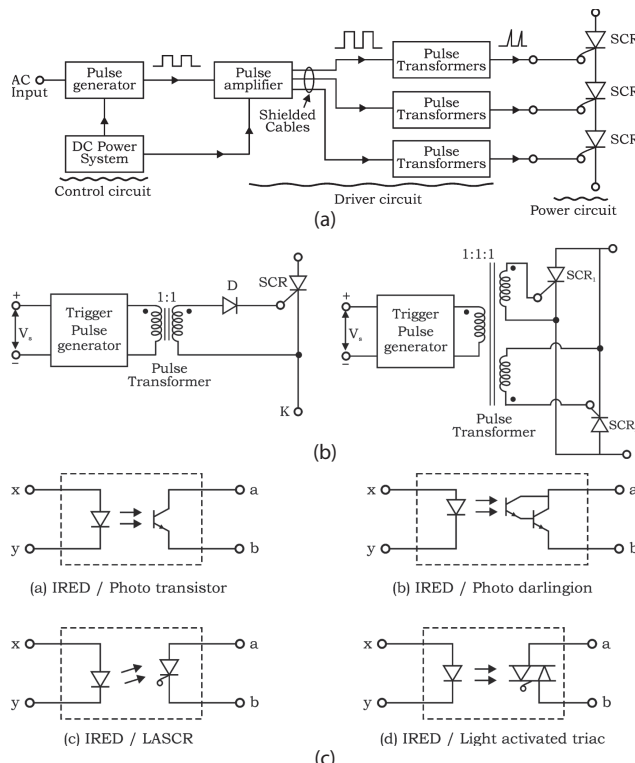


FIGURE 3.5 (a) General layout of firing circuit for SCR, (b) pulse transformer in triggering circuits, and (c) common optoisolators.

The pulse transformer is used to isolate the low-voltage gate-cathode circuit from the high-voltage anode–cathode circuit.

Pulse Transformer: Pulse transformers are basically the transformers that isolate the low-voltage gate-cathode circuit from the high-voltage anode–cathode circuit. In power electronics, pulse transformers have 1:1 two-winding or 1:1:1 three winding as shown in [Figure 3.5b \[2,8,10\]](#). These are also used to produce gate pulses for more than one SCR in a power circuit. It is one of the important components of the driver circuit.

Optical Isolator (OPTOISOLATORS): Optical isolators or optoisolators are used to isolate the low-power control circuit from the high-power load circuit. But these use light energy to couple the control signal to the load.

Optoisolators consist of a light source, usually an infrared-emitting diode (IRED), a light-sensitive device (e.g., a photo transistor), and a switching device. [Figure 3.5c](#) shows some of the available optoisolators. In each case, the devices inside the dotted lines are integrated into a single light-tight package with only input terminals x and y , and output terminals a and b for users. The input circuit is an IRED, which emits IR radiation when it is sufficiently forward biased. This radiation is focused on a light-sensitive device so that it switches “ON” whenever sufficient current flows through the IRED.

3.5.1 RESISTANCE (R) TRIGGERING CIRCUIT

This is the simplest and most economical firing circuit for an SCR. As shown in [Figure 3.6](#), R_2 is a variable resistor, and R is a stabilizing resistor.

Design considerations:

Design of R_1 : When R_2 is zero, the gate current I_g may flow through the source, load, R_1 , D , and gate to the cathode. This current should not exceed the maximum permissible gate current $I_{g\max}$. Therefore, R_1 can be find out from the relation [\[2,7–9\]](#):

$$\frac{V_m}{R_1} \leq I_{g\max} \quad \text{or} \quad R_1 \geq \frac{V_m}{I_{g\max}} \quad (3.3)$$

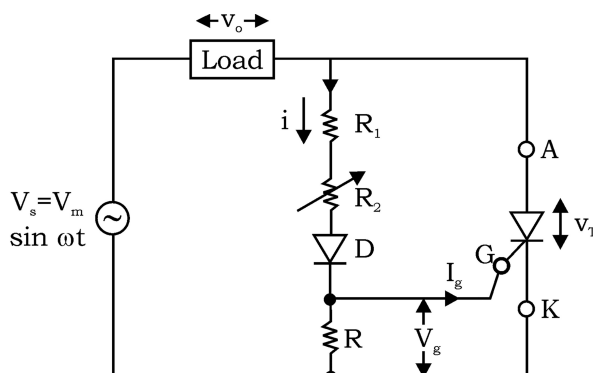


FIGURE 3.6 Resistance (R) triggering circuit.

where V_m is the maximum value of the source voltage V_s . The role of resistor R_1 is to limit the magnitude of the gate current to a safe value when R_2 is varied.

Design of R : Resistor R should have such a value that the maximum voltage drop across it does not exceed the maximum possible gate voltage ($V_{g \max}$). It can happen only when R_2 is zero. Under such conditions:

$$iR \leq V_{g \max}$$

or

$$\frac{V_m}{R_1 + R} \cdot R \leq V_{g \max}$$

or

$$R \leq \frac{V_{g \max} \cdot R_1}{V_m - V_{g \max}}$$

(3.4)

Diode D is used to allow the flow of current during possible half-cycles only, that is, the gate voltage V_g is a positive half-wave DC pulse. The amplitude of this DC pulse is controlled by varying resistor R_2 .

Case 1. When $V_{gp} < V_{gt}$: When R_2 is large, the current, i , is small, and so voltage across R , that is, $V_g = iR$ is also small, as shown in Figure 3.7a [2,8].

Therefore, when the peak of the gate voltage (V_{gp}) is less than the gate-trigger voltage (V_{gt}), then SCR will not turn on:

$$\therefore V_0 = 0, \quad i_0 = 0$$

$V_T = V_S$, as shown in Figure 3.7a

Case 2. When $V_{gp} = V_{gt}$: For this, R_2 is so adjusted such that $V_{gp} = V_{gt}$. This gives the firing angle $\alpha = 90^\circ$. Various waveforms for this case are shown in Figure 3.7b.

Case 3. When $V_{gp} > V_{gt}$: For this to occur, R_2 is reduced such that V_{gp} becomes larger than V_{gt} . When V_g becomes equal to V_{gt} for the first time, SCR is turned on. So by reducing R_2 , V_g is increased more than V_{gt} , and therefore, SCR turns on at an angle α less than 90° , as shown in Figure 3.7c.

A relationship between V_{gp} and V_{gt} can be found out as:

When V_g becomes equal to V_{gt} for the first time, SCR turns on, that is,

$$V_g = V_{gt}$$

or

$$V_{gp} \sin \alpha = V_{gt}$$

or

$$\alpha = \sin^{-1} \left(\frac{V_{gt}}{V_{gp}} \right)$$

As

$$V_{gp} = \frac{V_m \cdot R}{R_1 + R_2 + R}$$

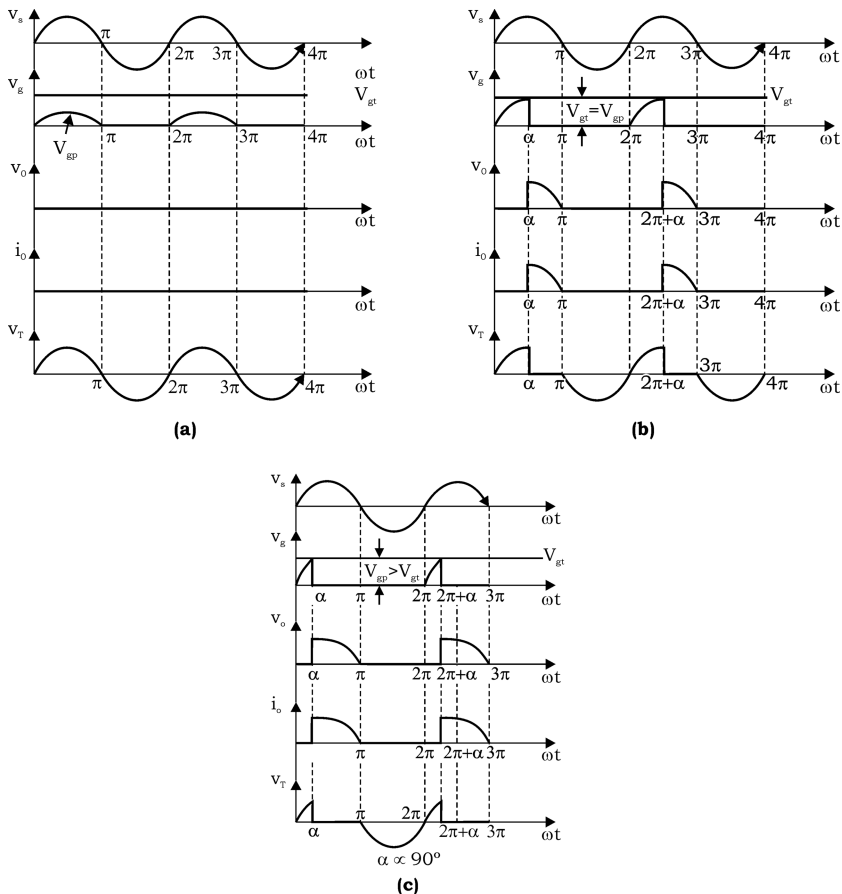


FIGURE 3.7 Resistance “R” triggering of SCR: (a) no triggering of SCR ($V_{sp} < V_{gt}$, large R_2), (b) $\alpha = 90^\circ$ ($V_{sp} = V_{gt}$), and (c) $V_{sp} > V_{gt}$ (small R_2 and $\alpha < 90^\circ$).

$$\therefore \alpha = \sin^{-1} \left[\frac{V_{gt} \cdot (R_1 + R_2 + R)}{V_m \cdot R} \right] \quad (3.5)$$

Therefore, firing angle α is directly proportional to variable resistor R_2 , that is, $\boxed{\alpha \propto R_2}$.

Advantages:

1. It is simple.
2. It is more economical.

Disadvantages:

1. It has limited range of firing angle (0° – 90°), that is, $0 < \alpha < 90^\circ$.
2. It is temperature dependent.

3.5.2 RESISTANCE-CAPACITANCE (RC) TRIGGERING CIRCUIT

- 1. RC half-wave trigger circuit:** RC half-wave triggering circuit is shown in Figure 3.8 [2,8].

In this case, by varying the magnitude of variable resistor “ R ,” the firing angle α can be varied from 0° to 180° . During a negative half cycle, capacitor C charges through diode D_2 with a lower plate positive and at $\omega t = -90^\circ$; it charges to a voltage V_m (peak supply voltage) as shown in Figure 3.9.

After $\omega t = -90^\circ$, as the source voltage V_s decreases from $-V_m$ to zero at $\omega t = 0^\circ$, the capacitor voltage V_c also falls from $-V_m$ to some lower voltage $-ob$ at $\omega t = 0^\circ$, as shown in Figure 3.9. Now, as the supply voltage increases in the positive direction after $\omega t = 0^\circ$, then capacitor C begins to charge through resistor R from the initial voltage $-ob$. When it charges to a

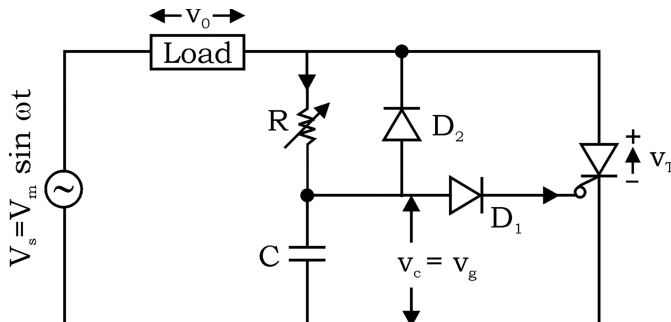


FIGURE 3.8 RC half-wave triggering circuit.

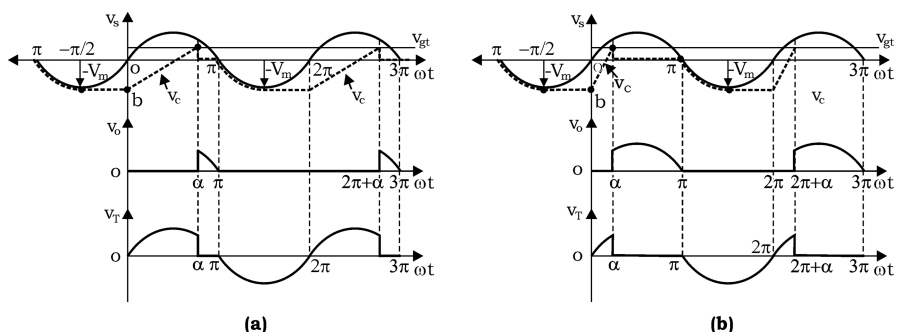


FIGURE 3.9 Waveforms of RC half-wave triggering circuit: (a) for high value of R and (b) for low value of R .

positive voltage equal to the gate-trigger voltage V_{gt} , the SCR is turned on and V_c becomes almost zero. Diode D_1 is used to protect the gate–cathode junction during negative half cycle.

If Magnitude of resistor R is

More, time taken for C to charge to V_{gt} is more, So α is more
therefore V_o is less.

Less, time taken for C to charge to V_{gt} is Less, So α is less
therefore V_o is more.

Design considerations:

RC for zero output voltage is given by

$$\boxed{RC \geq \frac{1.3T}{2} \cong \frac{4}{w}} \quad (3.6)$$

SCR is turned on when $V_c = V_{gt} + V_{d1}$. Maximum value of R is given by

$$V_s \geq RI_{gt} + V_c$$

or

$$V_s \geq RI_{gt} + V_{gt} + V_{d1}$$

or

$$\boxed{R \leq \frac{V_s - V_{gt} - V_{d1}}{I_{gt}}} \quad (3.7)$$

Advantage: The range of firing angle (α) is from 0° to 180° , that is, $0^\circ \leq \alpha \leq 180^\circ$.

Disadvantage: It produces a pulse during the positive half cycles only.

2. **RC full-wave trigger circuit:** Circuit diagram for RC full-wave triggering circuit for SCR is shown in [Figure 3.10 \[2,8\]](#). In this circuit, diodes D_1 – D_4 form a full-wave diode bridge and give a voltage V_d , which is a full-wave positive DC pulse. Here, capacitor C charges through variable resistor R.

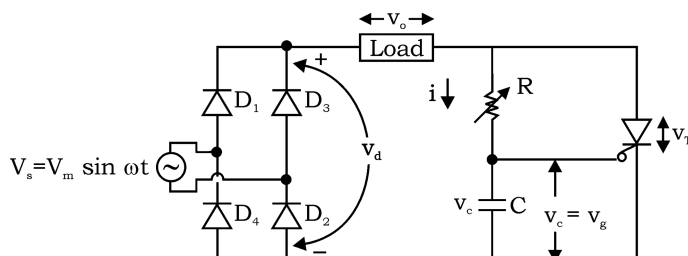


FIGURE 3.10 RC full-wave trigger circuit.

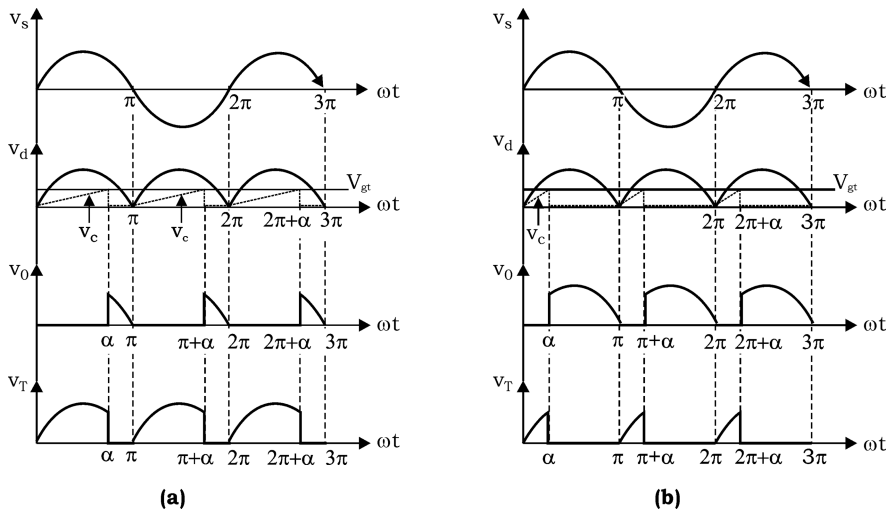


FIGURE 3.11 Waveform of RC full-wave trigger circuit: (a) for high value of R and (b) for low value of R .

When it charges to a voltage equal to the gate-triggering voltage V_{gt} , the SCR turns on, and the rectified voltage V_d appears across the load as v_0 , as shown in Figure 3.11.

If value of resistor R is high, then the time taken by capacitor C to charge the gate-triggering voltage V_{gt} will be more. So, firing angle α will be more, and therefore, the output voltage V_0 will be less.

But, if value of resistor R is low, then the time taken by capacitor C to charge the gate-triggering voltage V_{gt} will be less. So, firing angle α will be less, and therefore, the output voltage V_0 will be more.

Design consideration: Value of RC is calculated by the relation:

$$RC \geq 50 \frac{T}{2} \cong \frac{157}{\omega} \quad (3.8)$$

and

$$R \ll \frac{V_s - V_{gt}}{I_{gt}}$$

(3.9)

Advantages:

1. The range of firing angle (α) is from 0° to 180° , that is, $0 \leq \alpha \leq 180$.
2. It produces firing pulses during both the positive and negative half cycles of the AC supply.

Disadvantages of R and RC-triggering circuit:

1. It produces prolonged pulses, so the power dissipation in the gate circuit is more.
2. It cannot be used for automatic or feedback control circuit.

3.5.3 UJT RELAXATION OSCILLATOR

The uni-junction transistor (UJT) consists of *n*-type silicon base to which *p*-type emitter is embedded, as shown in Figure 3.12a [2,8]. It has three terminals, emitter (*E*), base (*B*₁) and (*B*₂), as shown in Figure 3.12b. Between base *B*₁ and *B*₂ it behaves like an ordinary resistance.

A UJT is a highly efficient switch with a switching time in the range of nanoseconds. It exhibits a negative resistance characteristic. Therefore, it is used as a relaxation oscillator for pulse triggering of an SCR. Figure 3.12c shows the circuit diagram with a UJT working in oscillator mode [2,8,10]. Here, *R*₁ and *R*₂ are the external resistors, *R* is the charging resistor through which capacitor *C* charges to a voltage *V*_p (peak point voltage) required to forward bias the *E*–*B*₁ junction. The magnitude of resistor *R* should be such that the load line intersects the device characteristic in the negative resistance region, for working it as a relaxation oscillator.

Working: When input voltage *V*_{BB} is applied, capacitor *C* begins to charge through resistor *R* exponentially toward *V*_{BB} with the upper plate positive. The capacitor voltage *V*_c equal to emitter voltage *V*_e is given by:

$$V_c = V_e = V_{BB}(1 - e^{-t/RC}) \quad (3.10)$$

where *RC* is the charging time constant (*τ*).

When capacitor voltage *V*_c (or *V*_e) reaches the peak-point voltage *V*_p ($= \eta V_{BB} + V_D$), the *E*–*B*₁ junction breaks down, and as a result, the UJT turns on. Capacitor *C*,

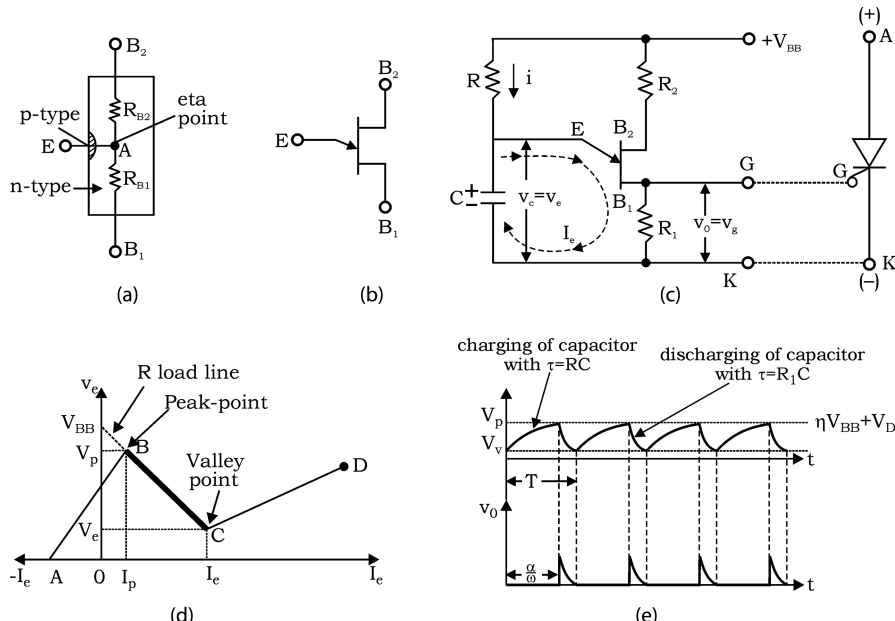


FIGURE 3.12 UJT (a) structure, (b) symbol, (c) circuit diagram of the UJT in relaxation oscillator mode, (d) V–I characteristic of UJT, and (e) voltage waveforms of the UJT relaxation oscillator circuit.

therefore, now discharges rapidly through resistor R_1 with the discharging time constant (τ) = R_1C , as shown in Figure 3.12d and 3.12e.

When capacitor voltage V_C (or V_e) decays to the valley-point voltage (V_v), the UJT gets turned off.

Design considerations:

The time T required for capacitor C to charge from initial voltage V_v to peak-point voltage V_p through resistor R can be obtained as:

$$V_p = \eta V_{BB} + V_D = V_v + V_{BB} (1 - e^{-T/RC}) \quad (3.11)$$

where:

η = intrinsic stand-off ratio of UJT ($\eta = 0.5\text{--}0.8$).

V_p = peak-point voltage

V_v = valley-point voltage

V_D = forward voltage drop of $E-B_1$ junction ($p-n$ junction)

As seen from the V-I characteristic of UJT (Figure 3.12d), it has a negative resistance characteristic between peak point B and valley point C .

Assuming $V_D = V_v$, Equation (3.11) becomes

$$\eta = (1 - e^{-T/RC})$$

or

$$T = \frac{1}{f} = RC \ln \left(\frac{1}{1-\eta} \right) \quad (3.12)$$

Neglecting the small discharge time, T becomes the time period of output pulse duration, then firing angle α is:

$$\alpha = \omega T = \omega RC \ln \left(\frac{1}{1-\eta} \right) \quad (3.13)$$

where ω is angular frequency of the UJT.

The maximum value of R is determined by the peak-point values V_p and I_p . When voltage across C reaches V_p , then voltage across R is $(V_{BB} - V_p)$

$$R_{\max} = \frac{V_{BB} - V_p}{I_p} = \frac{V_{BB} - (\eta V_{BB} + V_D)}{I_p} \quad (3.14)$$

and the minimum value of R , is governed by valley-point values V_v and I_V :

$$R_{\min} = \frac{V_{BB} - V_v}{I_V} \quad (3.15)$$

3.6 SERIES AND PARALLEL OPERATION OF SCR

SCRs are connected in series to meet the high-voltage demand and in parallel to fulfill the high-current requirement [2,7–9,14–19].

3.6.1 SERIES-CONNECTED SCRs

SCRs connected in series should have identical V-I characteristics. But due to inherent variations in their characteristics, the voltage shared by each SCR may not be equal. Figure 3.13a and 3.13b show the symbol and V-I characteristic of two SCRs [2,8,10]. It is seen that their forward- and reverse-blocking voltages (V_{BO} and V_{BR}) are different even for same current. These unequal voltages cause unnecessary voltage stresses across some SCRs in the series string.

A uniform voltage distribution in steady state can be achieved by using a static equalizing circuit and during dynamic or transient conditions using dynamic equalizing circuits.

Static Equalizing Circuit: Figure 3.14 shows a string of series-connected SCRs. Shunt resistor R forms the static equalizing circuit, whereas R_c and C form the dynamic equalizing circuit [2,8,10]. It has been found that an SCR having lower leakage current has a higher forward-blocking voltage across it.

Let

I_{l1} —forward leakage current carried by SCR_1

I_{l2} —forward leakage current carried by remaining SCRs like $\text{SCR}_2, \text{SCR}_3 \dots, \text{SCR}_n$.

$I_1, I_2 \dots I_n$ —currents through resistor R , forming static equalizing circuit

I —total string current

$V_{b1}, V_{b2}, \dots V_{bn}$ —forward-blocking voltages across $\text{SCR}_1, \text{SCR}_2 \dots, \text{SCR}_n$.

$n_s \rightarrow$ number of series-connected SCRs

Also, let

$$I_2 = I_3 = \dots I_n. \text{ Then}$$

$$I_{l1} + I_1 = I_{l2} + I_2 = I$$

or

$$I_{l1} - I_2 = I_2 - I_1 = \Delta I_1$$

The voltage across SCR_1 is $V_{b1} = RI_1$

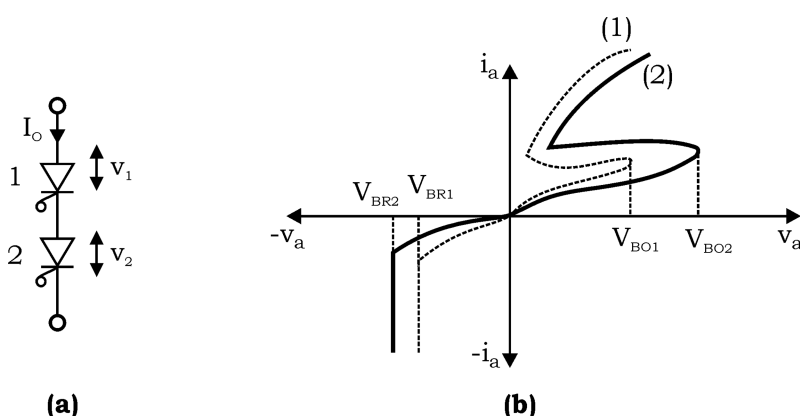


FIGURE 3.13 Series-connected SCRs: (a) Symbol and (b) V-I characteristic of two SCRs.

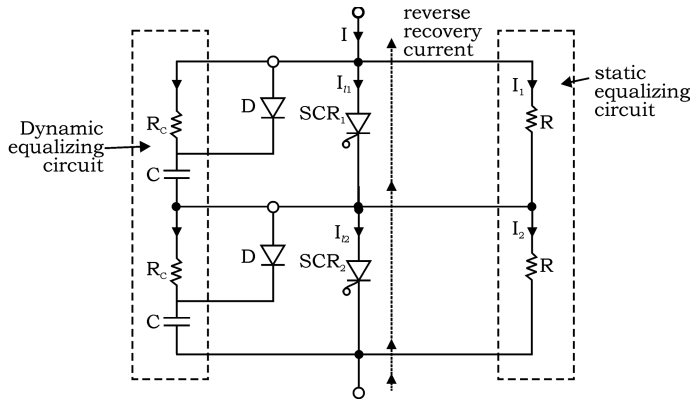


FIGURE 3.14 Equalizing circuits (dynamic and static) for SCRs connected in series.

For a string voltage V_s , the voltage equation for the series circuit (KVL) can be written as:

$$V_s = V_{b1} + (n_s - 1) I_2 R = V_{b1} + (n_s - 1) (I_1 + \Delta I_l) R$$

$$= V_{b1} + (n_s - 1) I_1 R - (n_s - 1) R \Delta I_l$$

or

$$V_s = n_s V_{b1} - (n_s - 1) R \Delta I_l \quad (3.16)$$

The worst situation occurs when $I_{l1} = 0$. Then $\Delta I_l = I_B$, the maximum blocking current of SCR. Under this condition $V_{bl} = V_b$ where V_b is maximum voltage rating of each SCR.

Then

$$V_s = n_s V_b - (n_s - 1) R I_B \quad (3.17)$$

or

$$R = \frac{n_s V_b - V_s}{(n_s - 1) I_B}$$

(3.18)

where:

V_b = maximum voltage rating of each SCR

I_B = maximum blocking current of SCR

n_s = number of series-connected SCRs

Dynamic Equalizing Circuit

Voltage equalization under transient or dynamic conditions like turn-on and turn-off periods of SCRs is achieved by employing shunt capacitors across each SCR. The capacitor C tends to equalize the transient voltage. It also improves the dv/dt rating of SCR.

Damping resistor R_C is used in series with capacitor C to limit the discharge current spikes and to damp out high-frequency oscillations. The combination of R_C and C is called the dynamic equalizing circuit, as shown in [Figure 3.14](#). The main uses of this circuit are:

1. To equalize the voltage during dynamic or transient conditions
2. To protect SCR against high dv/dt

The value of C can be determined by the reverse recovery characteristics of SCRs. Let ΔQ = maximum difference between reverse recovery charge of SCR_1 and other SCRs.

SCR_1 recovers first and goes into a blocking state. So, it does not allow the passage of ΔQ ; rather, ΔQ passes through C .

$$\therefore \Delta V_s = RI_b = \frac{\Delta Q}{C} \quad (3.19)$$

Substitute Equations (3.19) in (3.17), and we get

$$V_s = n_s V_b - (n_s - 1) \frac{\Delta Q}{C}$$

or

$$C = \frac{(n_s - 1)\Delta Q}{n_s V_b - V_s} \quad (3.20)$$

3.6.2 PARALLEL-CONNECTED SCRs

To meet the large current requirements, SCRs are connected in parallel in a string. For equal sharing of currents, V-I characteristics of SCRs during forward conduction must be identical.

The dynamic resistances of SCRs in parallel may not be equal, and this causes unequal currents through them. If current through one of them is more, its power dissipation will be more. This will raise its temperature and lower its dynamic resistance. It will further increase the current through this SCR. This cumulative process is known as **thermal runaway**.

In DC circuits, the effect of unequal currents can be minimized by connecting resistors in series with SCRs, as shown in [Figure 3.15a](#) [2,8]. The values of R_1 , R_2 are so selected that the total anode-to-cathode voltage across each branch is the same.

Thus,

$$V_{T1} + I_{T1} (R_{T1} + R_1) = V_{T2} + I_{T2} (R_{T2} + R_2) \quad (3.21)$$

where:

V_{T1} , V_{T2} = voltage drops across SCR_1 and SCR_2 ,

I_{T1} , I_{T2} = current through SCR_1 and SCR_2

R_{T1} , R_{T2} = dynamic resistance of SCRs

In AC circuits, uniform current distribution is made by magnetic coupling, as shown in [Figure 3.15b](#). If currents I_{T1} and I_{T2} are equal, the fluxes produced by two inductors

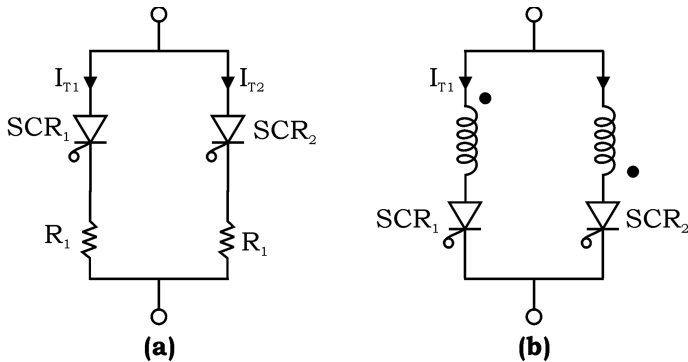


FIGURE 3.15 (a,b) Equalizing circuits for SCRs connected in parallel.

cancel each other, and the net voltage drop in inductors is zero. But if currents I_{T1} and I_{T2} are unequal, the net flux linkage is not zero. So unequal voltages are induced in two inductors, which reduce the difference between I_{T1} and I_{T2} .

3.7 STRING EFFICIENCY

String efficiency is a term that is used to measure the degree of utilization of SCRs in a string, and it can be defined as:

$$\text{String efficiency} = \frac{\text{Actual voltage/current rating of whole string}}{\left[\frac{\text{Individual voltage/current}}{\text{rating of one SCR}} \right] \left[\frac{\text{no. of SCRs}}{\text{in string}} \right]} \quad (3.22)$$

If SCRs connected in a string share equal voltage/current, then string efficiency is one and the utilization of SCRs is maximum. But in practice, string efficiency is less than one. Various equalizing circuits explained earlier in [Section 3.5](#) helps in improving the string efficiency.

Derating Factor (DRF): It is a measure of the reliability of string and defined as:

$$\boxed{\text{DRF} = 1 - \text{string efficiency}} \quad (3.23)$$

When SCRs are connected in parallel, current derating is:

$$\boxed{\text{Current derating} = 1 - \frac{I_m}{n_p I_T}} \quad (3.24)$$

where:

I_m = total circuit current

n_p = number of parallel-connected SCRs

I_T = current rating of each SCR

When SCRs are connected in series, the voltage derating is:

$$\boxed{\text{Voltage derating} = 1 - \frac{V_s}{n_s V_b}} \quad (3.25)$$

where:

V_s = total voltage across the string (supply voltage)

n_s = number of SCRs connected in series

V_b = forward voltage rating of each SCR

Derating helps in improving the reliability of operation because actual voltage/current of each SCR will be lesser than the rated voltage/current.

Finger Voltage: It is that minimum forward voltage across the anode–cathode of SCRs, which is required to turn its number. If voltage across the SCR drops to a value less than its finger voltage, then the SCR will not turn on.

3.8 PROTECTION OF SCR

For reliable and successful operation of the SCR, it must be ensured that its specified ratings are not exceeded. The SCR should be protected from various abnormal conditions, such as overvoltages, overcurrents, large di/dt during turn on, or false or unwanted turn on by high values of dv/dt [2–6].

3.8.1 OVERVOLTAGE PROTECTION

SCR may be subjected to overvoltage due to the following causes:

- a. SCR commutation
- b. Current chopping
- c. Lightning strikes
- d. Transformer in-rush current

Overvoltages cause either maloperation of the circuit by unwanted turn on of the SCR or permanent damage to the SCR.

During the commutation of the SCR, internal overvoltages are produced. During the turn off of an SCR, reverse recovery current (I_{rr}) flows to sweep out the stored charges from the layers of SCR. This I_{rr} current increases to its maximum value (I_{rr})_{max}, and then decays rapidly. This fast decay of I_{rr} causes a high internal overvoltage $L \frac{di}{dt}$ due to circuit inductance L .

External overvoltage may be caused due to current chopping, that is, interruption of the current by a circuit breaker; lightning strikes on lines feeding the SCR system; and transformer in-rush current during energization and de-energization of primary winding of transformers. The SCR can be protected from such overvoltage by using RC circuits and nonlinear resistors called *voltage clamping devices*. RC circuits called snubber circuits are connected across the device, as shown in Figure 3.16 [2,8,11,19]. It provides a local path for internal overvoltage caused by a reverse-recovery current during the turn-off process of the SCR.

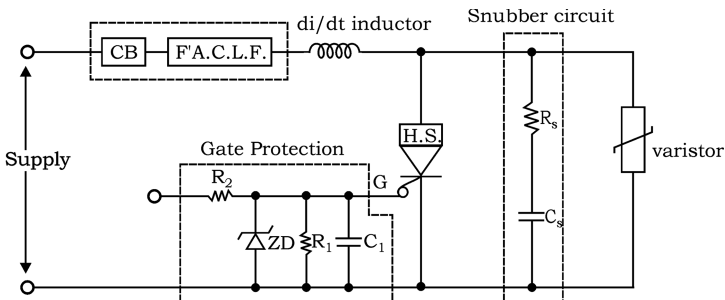


FIGURE 3.16 Overall protection of SCR (CB = circuit breaker, FACLF = fast-acting current-limiting fuse, HS = head sink, ZD = Zener diode).

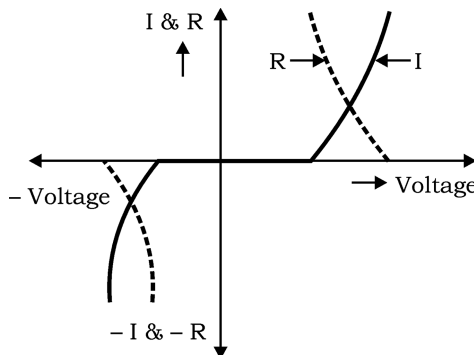


FIGURE 3.17 V-I and V-R characteristics of VC device.

A voltage-clamping (VC) device is a nonlinear resistor connected across the SCR as shown in [Figure 3.16](#). These devices have falling resistance characteristics with increasing voltage ([Figure 3.17](#)). Under normal working conditions of voltage, the device has high resistance and draws only a small leakage current. But when a voltage surge (overvoltage) appears, the VC device operates in a low-resistance region and produce a virtual short circuit across the SCR, and thus the SCR is protected.

3.8.2 OVERCURRENT PROTECTION

The SCR can be subjected to overcurrents due to

1. faults
2. short circuits
3. surge currents

Because SCRs have small thermal time constants, the junction temperature may exceed the rated value, and the device may be damaged. Overcurrent protection in SCR circuits is achieved through the use of circuit breakers and fast-acting current-limiting fuse (FACLF) as shown in [Figure 3.16](#). The operation of the FACLF is

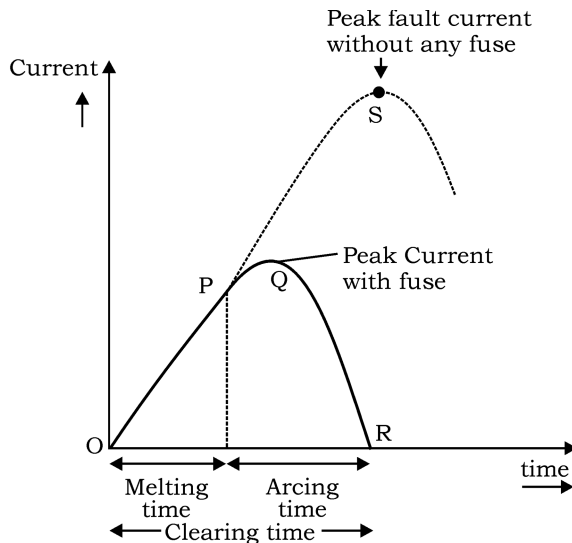


FIGURE 3.18 Action of FACLF in an AC circuit.

illustrated in [Figure 3.18](#). These fuses consist of fine silver ribbons having very short fusing times. As shown in [Figure 3.18](#), without a fuse, the fault current would rise up to point S, whereas with FACLF, it rises up to point Q only.

3.8.3 dv/dt PROTECTION

During forward-blocking mode, junctions J_1 and J_3 are forward biased, whereas junction J_2 is reverse biased. This reverse-biased junction J_2 behaves like a capacitance due to space charges around it. If the entire anode-to-cathode forward voltage V_a appears across the J_2 junction, and the charge is denoted by Q , then a charging current develops, which is given as:

$$\begin{aligned} i_c &= \frac{dQ}{dt} = \frac{d}{dt}(C_j \cdot V_a) \\ &= C_j \frac{dV_a}{dt} + V_a \frac{dC_j}{dt} \end{aligned}$$

Because C_j is almost constant, the charging current is given by:

$$i = C_j \frac{dV_a}{dt} \quad (3.26)$$

If the rate of rise of forward voltage dV_a/dt is high, the charging current i_c will be more. This i_c current can play the role of a gate current and therefore may turn on the SCR even when gate signal is zero. Such turning on of the SCR is called the dv/dt turn on or unwanted turn on, which must be avoided.

Typical values of $\frac{dv}{dt}$ are $(20 - 500) \text{ v}/\mu\text{sec}$

The SCR is protected from such unwanted or false or dv/dt turn-on, by using snubber circuit connected in parallel with the device.

Snubber circuit: The snubber circuit consists of a series combination of resistor R_s and capacitor C_s connected in parallel with the SCR as shown in Figure 3.19a,b [2,8,10].

When switch S is closed, a sudden voltage appears across the SCR. Snubber capacitor C_s behaves like a short circuit, so the voltage across SCR is zero. With the passage of time, voltage across C_s develops gradually. Thus, dv/dt across C_s and so across SCR is less than the specified maximum dv/dt rating of the device. Resistor R_s is inserted in series with C_s to limit the magnitude of discharging current when SCR is turned on when SCR is fired, then C_s , which is charged to voltage V_s , discharges through SCR with the discharging current given by

$$i = \frac{V_s}{\text{resistance of load path} + R_s}$$

Design of snubber circuit: When switch (S) is closed, the snubber capacitor C_s behaves like short circuit, and the SCR in forward-blocking mode offers very high resistance. So, the equivalent circuit soon after the instant of closing the switch S is shown in Figure 3.19c. It gives:

$$V_s = (R_s + R_L) i + L \frac{di}{dt} \quad (3.27)$$

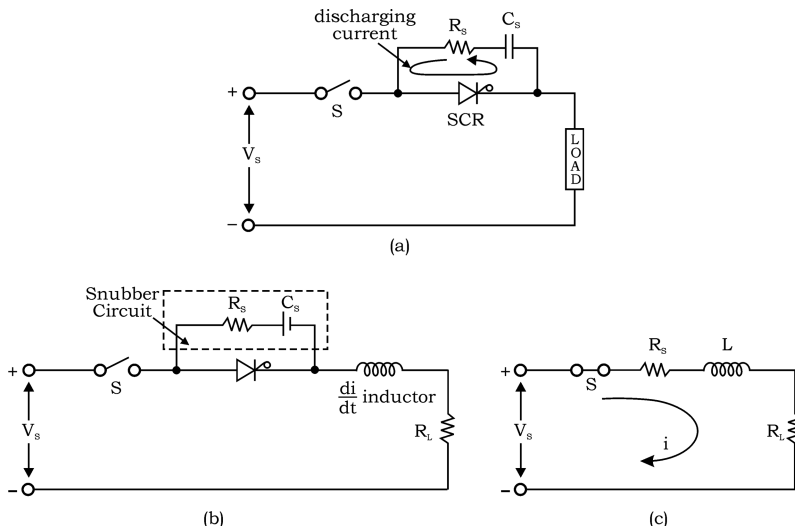


FIGURE 3.19 (a) Snubber circuit across SCR, (b) snubber circuit, and (c) equivalent circuit when switch S is closed.

Its solution gives,

$$i = I(1 - e^{-t/\tau}) \quad (3.28)$$

where $I = \frac{V_s}{R_s + R_L}$ and $\tau = \frac{L}{R_s + R_L}$

Differentiating Equation (3.28) w.r.t. time t , we get

$$\begin{aligned} \frac{di}{dt} &= I \cdot e^{-\frac{t}{\tau}} \cdot \frac{1}{\tau} = \frac{V_s}{R_s + R_L} \cdot \frac{R_s + R_L}{L} e^{-\frac{t}{\tau}} \\ &= \frac{V_s}{L} e^{-\frac{t}{\tau}} \end{aligned}$$

The value of $\frac{di}{dt}$ is maximum at $t = 0$

$$\therefore \left(\frac{di}{dt} \right)_{\max} = \frac{V_s}{L} \quad (3.29)$$

or

$L = \frac{V_s}{(di/dt)_{\max}}$

(3.30)

The voltage across SCR is, $v_a = i \cdot R_s$

or

$$\frac{dv_a}{dt} = R_s \cdot \frac{di}{dt}$$

or

$$\left(\frac{dv_a}{dt} \right)_{\max} = R_s \cdot \left(\frac{di}{dt} \right)_{\max} \quad (3.31)$$

From Equations (3.29) and (3.31),

$$\left(\frac{dv_a}{dt} \right)_{\max} = \frac{R_s \cdot V_s}{L}$$

or

$R_s = \frac{L}{V_s} \left(\frac{dv_a}{dt} \right)_{\max}$

(3.32)

The value of R_s can also be obtained from the relation:

$R_s = 2 \xi \sqrt{\frac{L}{C_s}}$

(3.33)

where ξ is the damping factor or damping ratio (generally, $\xi = 0.65$) and has the range $0.5 < \xi < 1$. Thus, from Equations (3.30), (3.32), and (3.33), the values of L , C_s , and R_s can be suitably designed.

3.8.4 di/dt PROTECTION

When the gate pulse is applied to a forward-biased SCR, the conduction of the anode current begins in the immediate neighborhood of the gate-cathode junction, and later this current spreads across whole area of the junction.

If the rate of rise of the anode current di/dt is large as compared to the spread velocity of carriers, local hot spots are formed. This produces localized heating, which may destroy the SCR. So, the magnitude of the di/dt at the time of turn on should be kept below the specified rating. SCR is protected from a large di/dt by using a small inductor, called a di/dt inductor, as shown in [Figure 3.18](#).

The typical range of is $\frac{di}{dt}$ in the range of (20–500) A/microseconds

The formation of local hot spots can also be avoided by ensuring that the conduction spreads to the whole area as rapidly as possible. This can be achieved by applying a gate current nearer to the maximum specified gate current (but never greater than $I_{g\ max}$).

3.8.5 GATE PROTECTION

The gate circuit should also be protected from overvoltage and overcurrents because an overvoltage across gate circuits can cause false (or unwanted) turn on of the SCR. Whereas overcurrents may raise the junction temperature beyond the specified limit, leading to damage of the SCR.

It is protected against overvoltage by connecting the Zener diode (ZD) across the gate circuit, as shown in [Figure 3.18](#). Against overcurrents, the gate circuit is protected by connecting resistor R_2 in series with the gate circuit. Capacitor C_1 and resistor R_1 connected across the gate to cathode terminals are used to bypass the unwanted noise or spurious signals.

3.9 SOLVED PROBLEMS

Example 3.1: Find the anode current if gain of NPN transistor of two-transistor model = 0.5; gain of PNP transistor of two transistor model = 0.4; gate current = 50 mA. Ignore leakage current.

SOLUTION

Transistor T_1 is PNP

Therefore, $\alpha_1 = 0.4$

Transistor T_2 is NPN and $\alpha_2 = 0.5$

Using two transistor models of SCR, the anode current is given as

$$I_a = \frac{\alpha_2 I_g + I_{CBO1} + I_{CBO2}}{1 - (\alpha_1 + \alpha_2)}$$

Neglecting I_{CBO1} and I_{CBO2}

$$\therefore I_a = \frac{0.5 \times 50 \times 10^{-3}}{1 - (0.56 + 0.4)} = 250 \text{ mA}$$

Example 3.2: Find the equivalent capacitance of the depletion layer of an SCR if $\frac{dv_a}{dt}$ is 180 V/ μ s and capacitive current flowing through the junction is 7 mA.

SOLUTION

$$I_c = C_j \frac{dv_a}{dt}$$

$$\therefore 7 \times 10^{-3} = C_j \times 180 \times 10^6$$

or

$$C_j = 38.9 \times 10^{-12} \text{ F}$$

Example 3.3: If an SCR with a holding current of 5 mA has a trigger voltage and current of 0.6 V and 7 mA, respectively, (a) What will be the output voltage when the SCR is in off state? (b) Calculate the voltage V_s necessary to turn off the SCR, if the SCR is ideal. (c) To what value should V_{CC} be reduced to turn off the SCR if a voltage of 0.5 V exists across it when it is conducting? Take $R_g = 2000 \Omega$, $V_{CC} = 30 \text{ V}$, and $R = 200 \Omega$.

SOLUTION

(a) No current flows through SCR when it is in off state.

$$\therefore V_0 = 30 \text{ V.}$$

$$(b) V_s = 0.6 + (7 \times 10^{-3})(2000) = 8.4 \text{ V.}$$

(c) To turn off the SCR, its current must be reduced below the holding current. When current is 5 mA, voltage drop across resistor R is $5 \times 10^{-3} \times 200 = 1 \text{ V}$. Hence, V_{CC} should be reduced to less than 1 V. Hence, V_{CC} should be reduced to less than $(1 + 0.5)$ or 1.5 V.

Example 3.4: If gate voltage current relation for an SCR is $V_g = 1 + 9 I_g$. The gate signal is a rectangular pulse of 30 V and duration π radian during each cycle. It is expected that average gate power loss be limited to 0.8 W. Find V_g , I_g and the resistance R_g to be connected in series with the gate circuit to limit the gate power loss to this value.

SOLUTION

The voltage-current equation for the gate circuit is, $V_g = V_g + I_g R_g$

$$\therefore 0 = R_g I_g + 1 + 9 I_g$$

or

$$9 I_g + R_g I_g = 29$$

$$\text{Average power loss} = 0.8 \text{ W}$$

$$\text{Power loss during conduction} = \frac{0.8 \times 2\pi}{\pi} = 1.6 \text{ W}$$

$$1.6 = V_g I_g = (1 + 9 I_g) I_g$$

or

$$9I_g^2 + I_g - 1.6 = 0$$

or

$$I_g = 0.4 \text{ A}$$

$$V_g = 1 + 9 \times 0.4 = 4.6 \text{ V}$$

$$R_g = \frac{29 - 9I_g}{I_g} = 63.5 \Omega$$

Example 3.5: The DC supply of 120 V feeds an inductance of 10 H through an SCR. Find the minimum width of the gate so that the SCR is triggered. The latching current of SCR is 80 mA.

SOLUTION

$$120 = L \frac{di}{dt}$$

or

$$i = \frac{120}{10} t = 12 t$$

SCR will trigger when $i = 80$ mA.

$$\therefore t = \frac{80 \times 10^{-3}}{12} = 6.7 \text{ ms}$$

Therefore, the pulse width should be more than 6.7 ms.

Example 3.6: The DC supply of 120 V feeds a load having a resistance of 10 ohms and an inductance of 5 H through an SCR as shown in Figure 3.20. The latching current of the SCR is 50 mA. Find the minimum width of the gate pulse.

SOLUTION

The circuit is shown in Figure 3.20. The current at any time t is

$$i = \frac{120}{10} (1 - e^{-Rt/L}) = 12(1 - e^{-2t})$$

SCR will trigger when $i = 50$ mA

$$50 \times 10^{-3} = (1 - e^{-2t})$$

or

$$e^{-2t} = 0.995$$

or

$$t = 0.0025 \text{ s} = 2.5 \text{ ms}$$

Hence, the minimum width of the gate pulse is 2.5 ms.

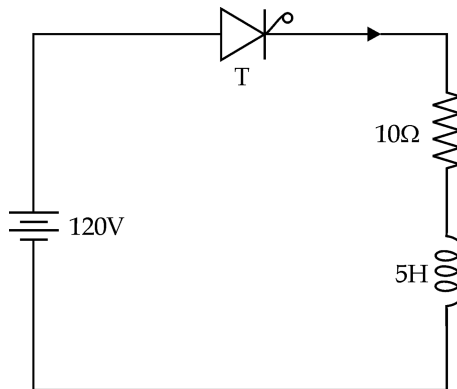


FIGURE 3.20 An SCR circuit of Example 3.6.

Example 3.7: *Figure 3.21 shows an SCR circuit. Assume that switch S is open. The SCR has a latching current of 40 mA and is fired by a pulse of width 40 μs. (a) Find whether the SCR will turn on, and (b) find the maximum value of resistor R so that SCR may turn on (switch is closed).*

SOLUTION

- (a) When switch (S) is open, then resistor R is not in circuit. Therefore, the circuit current is expressed as, $i = \frac{120}{25}(1 - e^{-25t/0.5}) = \frac{120}{25}(1 - e^{-50t})$. At the end of the gate pulse, that is, at $t = 40 \times 10^{-6}$ s

$$i = \frac{120}{25}(1 - e^{-50 \times 40 \times 10^{-6}}) = 0.0096 \text{ A}$$

Because this current is less than the latching current, the SCR will not get turned on.

- (b) Value of resistor, $R = \frac{120}{40 \times 10^{-3} - 0.0096} = 3947 \Omega$. Therefore, R should be less than 3,947 Ω.

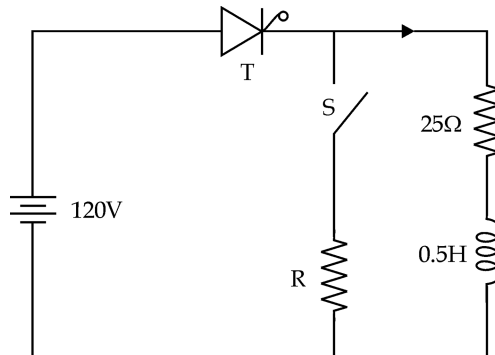


FIGURE 3.21 An SCR circuit of Example 3.7.

Example 3.8: The SCR in Figure 3.22 has a holding current of 60 mA, and it is fired by a pulse of length 50 μ s. Show that without resistance R, the SCR will fail to remain on when the firing pulse ends. Find the maximum value of R to ensure firing. Ignore the voltage drop across the SCR.

SOLUTION

Let resistor R be infinite. The circuit current is

$$R = \frac{120}{40 \times 10^{-3} - 0.0096} = 3947 \Omega$$

When the firing pulse ends, $t = 50 \times 10^{-6}$ s

$$\begin{aligned} \text{The circuit current is } i &= 6 \left(1 - e^{-40 \times 50 \times 10^{-6}}\right) \\ &= 0.012 \text{ or } 12 \text{ mA} \end{aligned}$$

Because this current is less than the holding current, the SCR will fail to remain on and return to the off state.

For an SCR to remain on, the current through the SCR at $t = 50 \mu$ s should at least be equal to the holding current.

Therefore, current through $R = 60 - 12 = 48$ mA

$$\text{Therefore, the maximum value of resistor } R = \frac{120}{48 \times 10^{-3}} = 2.5 \text{ ohm}$$

Example 3.9: What are various requirements for turning on the SCR by gate triggering?

SOLUTION

Various requirements that must be satisfied for turning on the SCR can be summarized as follows:

1. SCR must be forward biased, that is, the potential of the anode must be more than that of the cathode.
2. The gate signal must be positive, that is, the potential of the gate must be more than that of the cathode.

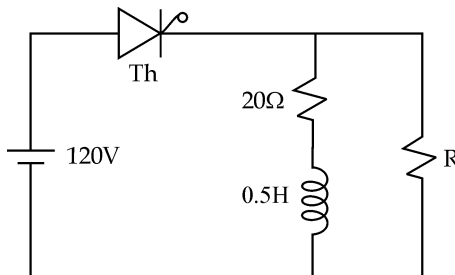


FIGURE 3.22 An SCR circuit of Example 3.8.

3. The gate pulse width should be more than the turn-on time of the SCR.
4. The anode-to-cathode voltage should be more than knee voltage.
5. The magnitude of the gate current should be more than the minimum gate current required for triggering but less than maximum possible gate current (otherwise the SCR may be destroyed).

Example 3.10: Find the one-cycle surge current rating and corresponding I^2t rating for an SCR if the half-cycle surge current rating is 2,500 A for 50 Hz AC.

SOLUTION

We know, $I_{\text{sub}}^2 t = I^2 T$

$$I_{\text{sub}} = 2,500 \text{ A},$$

$$T = \text{duration of half cycle} = 10 \times 10^{-3} \text{ s}$$

$$t = 5 \times 10^{-3} \text{ s}$$

$$I = \left[\frac{(2,500)^2 \times 5 \times 10^{-3}}{10 \times 10^{-3}} \right]^{0.5} = \frac{2,500}{\sqrt{2}} = 1,768$$

$$I^2 t \text{ rating} = (1,768)^2 \times 10 \times 10^{-3} = 3 \times 10^4 \text{ A}^2 \text{s}$$

Example 3.11: The $V_g - I_g$ characteristics of an SCR is given by $V_g = 1 + 9 I_g$. The gate pulses are rectangular with an amplitude of 15 V and duration of 40 μs . The duty cycle is 0.3. (a) Find the series resistance R_g in the gate circuit to limit the peak power loss to 8 W and (b) find the average gate power loss.

SOLUTION

(a) Since peak power loss in the gate circuit is $V_g I_g$, we have

$$6 = V_g I_g = (1 + 9 I_g) I_g$$

or

$$9 I_g^2 + I_g - 6 = 0$$

or

$$I_g = 0.763 \text{ A}$$

The KVL equation of the gate circuit is

$$15 = V_g + R_g I_g = 1 + 9 I_g + R_g I_g = 1 + (9 + R_g) I_g$$

or

$$14 = (9 + R_g) (0.763)$$

or

$$R_g = 9.35 \Omega$$

(b) Average power loss,

$$P_{\text{gav}} = \text{peak power loss } (P_{\text{gm}}) \times \delta$$

$$= 8 \times 0.3 = 2.4 \text{ W}$$

Example 3.12: An SCR is triggered from a 12 V source. The load line has a slope of -100 V/A . The minimum gate current for successful triggering is 18 mA. Find the source resistance, trigger current, and voltage for the gate-power dissipation of 0.2 W.

SOLUTION

$$V_g I_g = 0.2 \text{ or } V_g = \frac{0.2}{I_g}$$

The KVL for the gate circuit is

$$V_g = V_g + I_g R_g$$

or

$$12 = \frac{0.2}{I_g} + I_g R_g$$

Since the load line has a slope of -100 V/A , the source resistance for the gate circuit is 100Ω .

$$12 = \frac{0.2}{I_g} + 100 I_g$$

or

$$100 I_g^2 - 12 I_g + 0.2 = 0$$

or

$$I_g = 85 \text{ mA or } 36 \text{ mA}$$

Let $I_g = 36 \text{ mA}$

$$V_g = \frac{0.2}{36 \times 10^{-3}}, \text{ i.e., } 5.56 \text{ V}$$

Example 3.13: The parameters of a relaxation oscillator using UJT are $V_{BB} = 36 \text{ V}$, $\eta = 0.65$, $I_p = 10 \text{ mA}$, $V_V = 3.5 \text{ V}$, $I_v = 10 \text{ mA}$, forward voltage drop across p-n junction 0.5 V , frequency of oscillation 500 Hz , and width of triggering pulse $50 \mu\text{s}$. Assume a suitable value of C . Design a UJT relaxation oscillator circuit.

SOLUTION

Given: $V_{BB} = 36 \text{ V}, \eta = 0.65$,

$$I_p = 10 \mu\text{A}, V_V = 3.5 \text{ V}, I_v = 10 \text{ mA},$$

$$V_D = 0.5 \text{ V},$$

$$f = \frac{1}{T} = 500 \text{ Hz},$$

width of triggering pulse $\tau = R_l C = 50 \mu\text{s}$.

Assuming value of $C = 0.04 \mu\text{F}$

Now, the value of the charging resistor R is given by,

$$\begin{aligned} R &= \frac{T}{C \ln \frac{1}{1-\eta}} = \frac{1}{fC \frac{1}{1-\eta}} \\ &= \frac{1 \times 10^6}{500 \times 0.04 \ln \frac{1}{1-0.65}} = \frac{10^6}{500 \times 0.04 \ln \frac{1}{0.35}} \\ &= \frac{10^6}{20 \ln 2.86} = 47.58 \times 10^3 \Omega \end{aligned}$$

$$V_p = \eta V_{BB} + V_D = 0.65 \times 36 + 0.5 = 22.9 \text{ V}$$

The value of resistor R_2 can be calculated from the relation,

$$R_2 = \frac{10^4}{\eta V_{BB}} = \frac{10^4}{0.65 \times 36} = 427.35 \Omega$$

the width of the triggering pulse, $\tau = R_l C = 50 \times 10^{-6}$

$$\therefore R_1 = \frac{50 \times 10^6}{0.04 \times 10^6} = 1250 \Omega$$

$$\text{Also, } R_{\max} = \frac{V_{BB} - V_p}{I_p} = \frac{36 - 22.9}{10 \times 10^{-6}} = 1.31 \times 10^6 \Omega$$

$$R_{\min} = \frac{V_{BB} - V_v}{I_v} = \frac{36 - 3.5}{10 \times 10^{-3}} = 3.25 \times 10^3 \Omega$$

\therefore The value of R is within maximum and minimum limits.

Example 3.14: A relaxation oscillator is to be designed to generate 2-kHz output. $V_{BB} = 12 \text{ V}$, $\eta = 0.6$, peak discharge current = 5 mA. Neglect the discharge time for the calculation of frequency. Find the values of various components of the circuit.

SOLUTION

The operating points of the UJT should be in the negative resistance region of characteristics of UJT, that is, on the right of the peak point.

Let voltage drop across $p-n$ junction = 0.5 V

$$V_p = \eta V_{BB} + V_D = 0.6 \times 12 + 0.5 = 7.7 \text{ V}$$

$$R_{\max} = \frac{V_{BB} - V_p}{I_p} = \frac{12 - 7.7}{5 \times 10^{-3}} = 860 \Omega$$

$$\therefore R < 860 \Omega$$

Now, Assume, $C = 0.5 \mu F$

$$T = \frac{1}{2000} = 0.5 \times 10^{-3} s$$

$$T = RC \ln \frac{1}{1-0.6} = RC \ln (2.5)$$

or

$$0.5 \times 10^{-3} = R \times 0.5 \times 10^{-6} \ln (2.5)$$

or

$$R = 1091 \Omega$$

This value of R is not suitable because R must be less than 860Ω .

Now, Assuming again $C = 1 \mu F$

$$\therefore 0.5 \times 10^{-3} = R (1 \times 10^{-6}) \ln (2.5)$$

or

$$R = 545.7 \therefore R < R_{\max}$$

Therefore, C must be $1 \mu F$ and $R = 545.7 \Omega$.

Example 3.15: In the RC half-wave triggering circuit of Figure 3.23a, $V_s = 220 V_{rms}$. Resistance R is a variable from 1 to $22 k\Omega$. The gate-triggering voltage is 3 V. If $C = 0.47 \times 10^{-6} F$, find the range of firing angle possible with this circuit.

SOLUTION

Figure 3.23b shows the phasor diagram for the RC series circuit of Figure 3.23a.

V_s is the supply voltage. The current I leads V_s by angle θ . Voltage across resistor R is V_R and is in phase with I . Voltage across C is V_C and lags I by 90° .

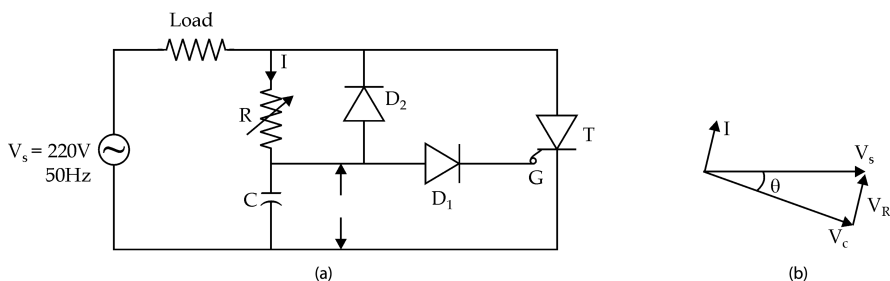


FIGURE 3.23 An RC-triggering circuit of Example 3.15: (a) triggering circuit and (b) phasor diagram.

$$\theta = \tan^{-1} \frac{R}{X_C} = \tan^{-1}(\omega CR) = \tan^{-1}(2\pi \times 50 \times 0.47 \times 10^{-7} R)$$

$$= \tan^{-1}(147.65 \times 10^{-6})$$

Moreover, $V_C = V_s \cos \theta$ and $v_c = V_C \sin(\omega t - \theta)$
When

$$R = 1\text{k}\Omega, \theta = \tan^{-1}(147.65 \times 1000 \times 10^{-6}) = 8.4^\circ$$

$$V_C = 220 \cos(8.4^\circ) = 217.63$$

$$v_c = (217.63) \sin(\omega t - 8.4^\circ) = 307.78 \sin(\omega t - 8.4^\circ)$$

Since gate voltage required for triggering is 3 V,

$$3 = 307.78 \sin(\omega t - 8.4^\circ)$$

or

$$\sin(\omega t - 8.4^\circ) = \frac{3}{307.78}$$

$$\text{Firing angle} = \left(\sin^{-1} \frac{3}{307.78} \right) + 8.4^\circ = 8.95^\circ$$

When

$$R = 22\text{k}\Omega, \theta = \tan^{-1}(147.65 \times 22000 \times 10^{-6}) 72.9^\circ$$

$$V_C = 220 \cos(72.9^\circ) = 64.69$$

$$v_c = (64.69) \sin(\omega t - 72.9^\circ) = 91.48 \sin(\omega t - 72.9^\circ)$$

Since gate voltage required for triggering is 3 V,

$$3 = 91.48 \sin(\omega t - 72.9^\circ)$$

or

$$\sin(\omega t - 72.9^\circ) = \frac{3}{91.48}$$

$$\text{Firing angle} = \sin^{-1} \left(\frac{3}{91.48} \right) + 72.9^\circ = 74.78^\circ$$

∴ Therefore, the range of the firing angle is $8.95^\circ < \alpha < 74.78^\circ$.

Example 3.16: In an AC circuit using an SCR having a dv/dt rating of $30\text{ V}/\mu\text{s}$, the source inductance is 0.2 mH . The RMS value of the supply voltage is 220 V . If the damping factor is 0.65 , find the values of R and C of the snubber circuit.

SOLUTION

$$V_m = 220 \times \sqrt{2} = 311.12\text{ V}$$

$$L = 0.2 \times 10^{-3} \text{ H}$$

$$\frac{dv}{dt} = 30 \text{ V}/\mu\text{s} = 30 \times 10^6 \text{ V/s}$$

Snubber capacitor,

$$C = \frac{1}{2 \times 0.2 \times 10^{-3}} \left[\frac{0.564 \times 325.27}{25 \times 10^6} \right]^2 = 134.62 \times 10^{-9} \text{ F}$$

Snubber resistance,

$$R = 2 \times 0.65 \left[\frac{0.2 \times 10^{-3}}{134.62 \times 10^{-9}} \right]^{0.5} = 50.1 \Omega$$

Example 3.17: An SCR circuit has an input voltage of 300 V and a load resistance of 10 ohm. The circuit inductance is negligible. The operating frequency of the circuit is 2000 Hz. The required dv/dt is 100 V/ μ s and the discharge current is to be limited to 100 A. Find (a) value of R and C of snubber circuit, (b) power loss in snubber circuit, (c) power rating of resistance R of snubber circuit.

SOLUTION

$$V = 300 \text{ V}, R_L = 10 \Omega, L = 0, I_{Th} = 100 \text{ A}, \frac{dv}{dt} = 100 \times 10^6 \text{ V/s}$$

(a) KVL equation during charging of capacitor C is

$$V = (R + R_L)i + \frac{1}{C} \int idt + v_C(0^-)$$

Assuming that $v_C(0^-)$ is zero, we get the solution of above equation as

$$i = \frac{V}{R + R_L} e^{-t/(R+R_L)C}$$

The forward voltage across the SCR is

$$v_{Th} = V - R_L i = 300 - \frac{10 V}{R + R_L} e^{-t/(R+R_L)C}$$

$$\text{At } t = 0, v_{Th} = V - \frac{R_L}{R + R_L} V$$

$$\text{At } t = \tau = (R + R_L)C,$$

$$v_{Th} = V - \frac{0.368 R_L}{R + R_L} V$$

$$\frac{dv}{dt} = \frac{v_{Th}(\tau) - v_{Th}(0)}{\tau} = \frac{0.632 R_L V}{C(R + R_L)^2}$$

$$R = \frac{300}{100} = 3 \Omega$$

$$\frac{dv}{dt} = 100 \times 10^6 = \frac{0.632 \times 10 \times 300}{C(3+10)^2}$$

or

$$\frac{dv}{dt} = 100 \times 10^6 = \frac{0.632 \times 10 \times 300}{C(3+10)^2}$$

(b) Snubber power loss = $\frac{1}{2}CV^2f = \frac{1}{2} \times 0.112 \times 10^{-6} \times 300^2 \times 2000 = 10.08 \text{ W}$

All the energy stored in capacitance C is dissipated in resistance R .
Hence, the power rating of R is 10.08 W.

Example 3.18: *R, L, and C in an SCR circuit meant for protecting against dv/dt and di/dt are 4 Ω, 6 μH, and 6 μF, respectively. If the supply voltage is 300 V, find the maximum permissible values of dv/dt and di/dt .*

SOLUTION

$$\left(\frac{di}{dt}\right)_{\max} = \frac{V}{L} = \frac{300}{6 \times 10^{-6}} = 50 \times 10^6 \text{ A/s}$$

When the circuit is switched on, the rate of change of voltage across the capacitor is given by

$$\frac{dv_C}{dt} = R \frac{di}{dt} + \frac{I_{sc}}{C}$$

$$I_{sc} = \text{short circuit current} = \frac{300}{4} = 75 \text{ A}$$

Therefore

$$\frac{dv_C}{dt} = 4 \times 50 \times 10^6 + \frac{75}{6 \times 10^{-6}} = 212.5 \times 10^6 \text{ V/s}$$

Hence, the maximum permissible value of $\frac{dv}{dt}$ is $212.5 \times 10^6 \text{ V/s}$.

Example 3.19: *An SCR is used to feed a load resistance 8 ohms from a 230 V single-phase supply. The ratings of SCR are: repetitive peak current = 200 A, $\left(\frac{di}{dt}\right)_{\max} = 40 \text{ A/μs}$ and $\left(\frac{dv}{dt}\right)_{\max} = 150 \text{ V/μs}$. Design a snubber circuit for protection of the SCR. Allow a safety factor of 2 for SCR ratings.*

SOLUTION

When the safety factor is 2, the maximum permissible ratings are:

Repetitive peak current = 100 A

$$\left(\frac{di}{dt}\right)_{\max} = 20 \text{ A/μs} = 20 \times 10^6 \text{ A/s}$$

and

$$\left(\frac{dv}{dt}\right)_{\max} = 75 \text{ V/μs} = 75 \times 10^6 \text{ V/s}$$

The protection must be designed for the peak value of input voltage, which is $\sqrt{2}$ (230) = 325.27 V. An inductance L is connected in series to limit $\frac{dv}{dt}$. Using equation $L = V/(di/dt)_{\max}$

$$\therefore L = \frac{325.27}{20 \times 10^6} = 16.26 \times 10^{-6} \text{ H}$$

$$\therefore R = \frac{L \left(\frac{dv}{dt} \right)_{\max}}{V} = \frac{16.26 \times 10^{-6}}{325.27} (75 \times 10^6) = 3.75 \Omega$$

When the SCR is turned on, the current through it is the sum of the load current and capacitor discharge current. The capacitor is charged to the peak of the supply voltage.

$$\text{Peak load current} = \frac{325.27}{8} = 40.66 \text{ A}$$

$$\text{Peak capacitor discharge current through } R = \frac{325.27}{3.75} = 86.74 \text{ A}$$

$$\text{Total current through capacitor} = 40.66 + 86.72 = 127.37 \text{ A}$$

Since the total current through the capacitor is more than permissible value of 100 A, the value of resistance R should be increased. The maximum capacitor discharge current = 100 – 40.66 = 59.35 A. Therefore

$$R = \frac{325.27}{59.35} = 5.48 \Omega$$

Let

$$R = 6 \Omega$$

taking $\zeta = 0.65$,

$$R^2 = 4\zeta^2 \frac{L}{C}$$

or

$$C = \frac{4\zeta^2 L}{R^2} = \frac{4(0.65)^2 (16.26 \times 10^{-6})}{6^2}$$

or

$$C = 0.7633 \times 10^{-6} F$$

Using the above value of C , the current through the capacitor at the instant of switching on the circuit is $C \frac{dv}{dt}$.

Hence,

$$C \frac{dv}{dt} = \frac{325.27}{R + R_L} = \frac{325.27}{6 + 8}$$

or

$$\frac{dv}{dt} = \frac{325.27}{14} \left(\frac{1}{0.7633 \times 10^{-6}} \right) = 30.43 \times 10^6 \text{ V/s}$$

Since the value of dv/dt is within the specified limit, the design is safe. Hence, $R = 6 \Omega$, $C = 0.7633 \mu F$, and $L = 16.26 \mu H$.

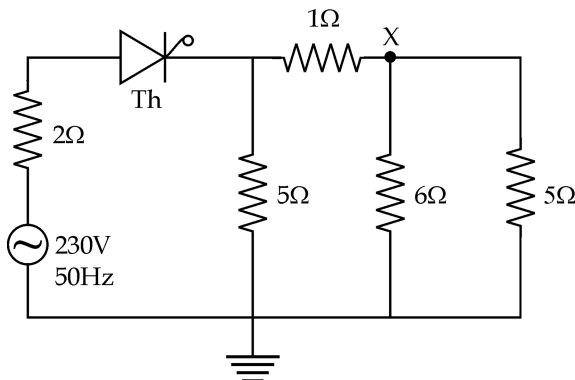


FIGURE 3.24 An SCR circuit of Example 3.20.

Example 3.20: An SCR having I^2t ratings of $30 \text{ A}^2\text{s}$ is used in the circuit of Figure 3.24. If a ground fault occurs on node X, find the fault-clearing time so that the SCR is not damaged.

SOLUTION

When node X is grounded, the net resistance to the source is equal to $2 + \frac{5 \times 1}{6} = \frac{17}{6} \Omega$.

The current in the circuit will be maximum when the source voltage is at its peak value of $230\sqrt{2} \text{ V}$.

Therefore, the initial fault current = $\frac{230\sqrt{2}}{\frac{17}{6}} = 114.78 \text{ A}$

$$\int_0^{t_c} i^2 dt = \int_0^{t_c} (114.78)^2 dt = 30$$

or

$$(114.78)^2 t_c = 30$$

or

$$t_c = \frac{30}{114.78^2} = 2.277 \times 10^{-3} \text{ seconds}$$

Example 3.21: Find the number of SCRs in series and parallel for a 3 kV, 750 A power electronics circuit having SCRs with 700 V and 150 A ratings. Use a derating factor of 25%.

SOLUTION

Current derating is given by = $1 - \frac{I_m}{n_p I_T}$

$$\therefore 0.25 = 1 - \frac{750}{n_p \times 150}$$

or

$$n_p = 6.66 \text{ or } 7$$

and voltage derating = $1 - \frac{V_s}{n_s V_D}$

$$\therefore 0.25 = 1 - \frac{300,000}{n_s \times 750}$$

or

$$n_s = 5.33 \text{ or } 6.$$

Example 3.22: The SCR used in the circuit of Example 3.21 has a maximum forward leakage current of 8 mA. If $\Delta Q = 30 \times 10^{-6} \text{ C}$, find the value of R and C for static and dynamic equalizing circuits.

SOLUTION

Resistance R forming the static equalizing circuit,

$$R = \frac{n_s V_D - V_s}{(n_s - 1) I_B} = \frac{6 \times 750 - 3000}{(6 - 1) \times 8 \times 10^{-3}} = 37.5 \times 10^3 \Omega$$

Capacitor C forming the dynamic equalizing circuit,

$$C = \frac{(n_s - 1) \Delta Q}{n_s V_D - V_s} = \frac{(6 - 1) \times 30 \times 10^{-6}}{6 \times 750 - 3000} = 0.1 \times 10^{-6} \text{ F}$$

Example 3.23: Twelve SCRs are used in a string to withstand a DC voltage of 16 kV. The maximum leakage current and recovery charge difference of SCRs are 10 mA and $150 \times 10^{-6} \text{ C}$, respectively. Each SCR has a resistance of $56 \text{ k}\Omega$ and capacitance of $0.5 \times 10^{-6} \text{ F}$ for stabilization. Find (a) maximum steady-state voltage rating of each SCR, (b) the steady-state voltage derating factor, (c) the maximum transient-state voltage rating of each SCR, and (d) the transient-state voltage derating factor.

SOLUTION

Given:

$$n_s = 12, V = 16 \text{ kV},$$

$$I_B = 10 \times 10^{-3} \text{ A},$$

$$R = 56 \times 10^3 \Omega,$$

$$\Delta Q = 150 \times 10^{-6} \text{ C},$$

$$C = 0.5 \times 10^{-6} \text{ F}$$

(a) $V = n_s V_D - (n_s - 1) R I_B$

$$16000 = 12 V_D - 11 \times 56 \times 10^3 \times 10 \times 10^{-3}$$

or

$$V_D = \frac{16000 + 11 \times 56 \times 10}{12} = 1846.67 \text{ V}$$

$$(b) \text{ Voltage derating} = 1 - \frac{V_s}{n_s V_D} = 1 - \frac{16000}{12 \times 1846.67} = 0.278 \text{ or } 27.8\% \text{ F}$$

$$(c) V = n_s V_D - (n_s - 1) \frac{\Delta Q}{C}$$

$$\therefore 16000 = 12 V_D - (11) \frac{(150 \times 10^{-6})}{0.5 \times 10^{-6}}$$

or

$$V_D = \frac{16000 + 11(150 \times 10^{-6}) / (0.5 \times 10^{-6})}{12} = 1608.33 \text{ V}$$

$$(d) \text{ Voltage derating} = 1 - \frac{V_s}{n_s V_D}$$

$$= 1 - \frac{16000}{12 \times 1608.33} = 0.171 \text{ or } 17.1\%$$

Example 3.24: For a circuit with total voltage and current rating of 7.5 kV and 1 kA, find the number of SCRs each with a rating of 500 V and 75 A required for each branch of a series parallel combination. Take the derating factor of 14%.

SOLUTION

$$\text{Voltage derating} = 1 - \frac{V_s}{n_s V_D}$$

where V_s is the circuit voltage, V_D is the SCR-rated voltage, and n_s is the number of SCRs in series.

$$0.14 = 1 - \frac{7500}{n_s(500)} = \text{or } n_s = 17.44 \text{ or } 18$$

$$\text{current derating} = 1 - \frac{I_m}{n_p I_T}$$

where I_m is circuit current, I_T is rated current of SCR, and n_p is the number of SCRs in parallel.

$$0.14 = 1 - \frac{1000}{n_p(75)} = \text{or } n_p = 15.5 \text{ or } 16.$$

Example 3.25: Three SCRs are connected in series to form a string. The string must withstand an off-state voltage of 8 kV. The static-equalizing resistance is 20 kΩ. The dynamic-equalizing circuit has an $RC = 25 \text{ ohm}$ and $C = 0.1 \mu\text{F}$. The leakage currents of the SCRs are 22 mA, 20 mA, and 18 mA, respectively. Find (a) voltage across each SCR during off state, and (b) discharge current through each SCR at the time of turn on.

SOLUTION

- (a) Let I be the total string current in the off state. A part of this current flows through the SCR, and the remaining current flows through the static-equalizing resistance R . Voltage across an SCR is equal to that across its static-equalizing resistance since they are in parallel.

$$V_1 = \text{Voltage across SCR 1} = (I - 22 \times 10^{-3})(20000)$$

$$V_2 = \text{Voltage across SCR 2} = (I - 20 \times 10^{-3})(20000)$$

$$V_3 = \text{Voltage across SCR 3} = (I - 18 \times 10^{-3})(20000)$$

$$V_1 + V_2 + V_3 = 8000$$

$$= (I - 22 \times 10^{-3}) + (I - 20 \times 10^{-3}) + (I - 18 \times 10^{-3}) 2000$$

or

$$20000(3I - 60 \times 10^{-3}) = 8000$$

or

$$I = \frac{0.4 - 60 \times 10^{-3}}{3} = 0.15333 \text{ A}$$

Using this value of I , the values of V_1 , V_2 , V_3 are

$$V_1 = (0.15333 - 22 \times 10^{-3}) 20000 = 2626.67 \text{ V}$$

$$V_2 = (0.15333 - 20 \times 10^{-3}) 20000 = 2666.67 \text{ V}$$

$$V_3 = (0.15333 - 18 \times 10^{-3}) 20000 = 2706.67 \text{ V}$$

(Check $V_1 + V_2 + V_3 = 8000$)

$$(b) \text{ Discharge current through SCR 1} = \frac{V_1}{R_C} = \frac{2666.67}{25} = 106.66 \text{ A}$$

$$\text{Discharge current through SCR 2} = \frac{V_2}{R_C} = \frac{2666.67}{25} = 106.66 \text{ A}$$

$$\text{Discharge current through SCR 3} = \frac{V_3}{R_C} = \frac{2706.67}{25} = 108.26 \text{ A}$$

Example 3.26: Make a comparison between transistors and SCRs.

SOLUTION

Both transistors and SCRs are semiconductor devices. The base material in their manufacture is silicon. However, they have major differences in their characteristics, operation, and application.

1. A transistor is a three-layer two-junction device, but an SCR is a four-layer three-junction device.
2. A transistor requires a continuous base signal for conduction. However, an SCR requires only a gate pulse to start conduction and continues to conduct thereafter till commutated.
3. In a transistor, the forward voltage drop during conduction is about 0.3 to 0.8 V. However, in an SCR, the forward voltage drop during conduction is about 1.2 to 1.8 V.
4. Transistors are manufactured in low and medium current and voltage ratings. However, SCRs are manufactured in very high voltage and current ratings also.
5. Transistors do not require commutation in most of their applications while SCRs require commutation.
6. Power transistors can withstand only low di/dt and cannot withstand surges. However, SCRs have high di/dt ratings and can withstand surges also.
7. Transistors have very small switching times. However, the switching times of SCRs are more than those of transistors.
8. Transistors find applications in amplifier circuits, oscillator circuits, whereas SCRs are used in rectifiers, inverters, choppers, etc.
9. Transistors are generally used in low-power circuits but the main field of application of SCRs is in high-power circuits.

Example 3.27: Find the absolute maximum operating or switching frequency of a converter-grade SCR whose turn-on/turn-off time are 4 μs and 180 μs , respectively.

SOLUTION

A device turns on and turns off in each switching cycle of converter. The absolute minimum period of the switching cycle should be greater than or equal to the total switching period (turns on and turns off). The minimum period is, therefore, given by

$$T_{\min} = t_{\text{turn-on}} + t_{\text{turn-off}} = 4 + 180 = 184 \mu\text{s}$$

The absolute maximum operating frequency of the SCR is given by

$$f_{\max} = \frac{1}{T_{\min}} = \frac{1}{184 \times 10^{-6}} = 5.4 \text{ kHz}$$

Example 3.28: A 400-V, 50-Hz AC source is connected with an SCR and a resistance load circuit. During the forward-blocking condition, the blocking junction capacitance (C_{j2}) is 1.6 nF . The parameters and rating of the SCR at 25°C are: $IT (\text{rms}) = 120 \text{ A}$, $VDRM = VRRM = 900 \text{ V}$, $VRSM = 1000 \text{ V}$, $VF = 1.5 \text{ V}$, $VGT = 2.5$, $IGT = 50 \text{ mA}$, $T_j \text{ max} = 120^\circ\text{C}$, $dv/dt = 100 \text{ V}/\mu\text{s}$ and $di/dt = 30 \text{ A}/\mu\text{s}$. Show that if the snubber circuit is not used, even a spike of 250 V and 2- μs duration will be sufficient to trigger the device undesirably (when the device is in the forward-blocking condition).

SOLUTION

The rate of the rise of the voltage of the spike is given by

$$\frac{dv_a}{dt} = \frac{250}{2} \mu\text{s} = 125 \text{ V}/\mu\text{s}$$

This value is higher than the $\frac{dv_a}{dt}$ limit of the device (i.e., 100 V/ μ s). The charging current through the capacitor that reaches the p_2 layer is,

$$i_{Cj2} = C_{j2} \frac{dv_a}{dt} = 1.6 \times 10^{-9} \text{ (125 V}/\mu\text{s}) = 200 \text{ mA}$$

Since this current is greater than the minimum gate current required to trigger the SCR, (i.e., $IGT = 50 \text{ mA}$), the SCR will be falsely triggered. It may be noted that this current is negligibly small at the normal forward-blocking condition with a higher steady-state voltage (i.e., 400 V). That is

$$I_{Cj2} = \frac{V_a}{1/(\omega C_{j2})} = V_a(2\pi f C_{j2}) = 400 \times 100 \times 1.6 \times 10^{-9} = 201 \mu\text{A}$$

Example 3.29: Following are the parameters and ratings of UJT (2N2646) at $T_j = 25^\circ\text{C}$:

Maximum interbase voltage (V_{BB}) = 35 V

Maximum average power dissipation = 300 mW

Range of interbase resistance (R_{BB}) = 4.7 – 9.1 k Ω (typical 5.6 k Ω at $V_{BB} = 12 \text{ V}$)

Valley-point current, $I_V = 4 \text{ mA}$ at $V_{BB} = 20 \text{ V}$

Intrinsic stand-off ratio, $\eta = 0.56$ to 0.75 (0.63 typical)

Valley-point voltage, $V_V = 2 \text{ V}$ at $V_{BB} = 20 \text{ V}$

Peak-point current, $I_P = 5 \text{ mA}$ (maximum) at $V_{BB} = 25 \text{ V}$

The maximum gate voltage (V_{GD}) that will not trigger-on the SCR = 0.18 V

Design a suitable UJT-based trigger circuit for a single-phase converter (rectifier) operating with a 50-Hz AC mains supply.

SOLUTION

The switching angle α varies from 0° to 180° , that is, a halftime period of the AC mains supply. Therefore, the required maximum delay of the switching pulse is

$$\frac{T}{2} = \frac{1}{2f} = \frac{1}{2 \times 50} = 10 \text{ ms}$$

Let

$$V_{BB} = 12 \text{ V},$$

then

(i) The minimum value of resistance:

$$R_{\min} > \frac{V_{BB} - V_V}{I_V} = \frac{12 - 2}{4 \times 10^{-3}} = 2.5 \text{ k}\Omega$$

Take $R_{\min} = 2.7 \text{ k}\Omega$ (the nearest value of commercially available carbon resistor).

(ii) *The peak-point voltage:*

$$V_p \cong \eta V_{BB} = 0.63 \times 12 \text{ V} = 7.56 \text{ V}$$

$$\text{Then } R_{\max} < \frac{V_{BB} - V_p}{I_p} = \frac{12 - 7.56}{5 \times 10^{-6}} = 888 \text{ k}\Omega$$

Then value of R is given by

$$R = R_{\max} - R_{\min} = 888 - 2.7 = 885.3 \text{ k}\Omega$$

Take $R = 1 \text{ M}\Omega$, then the new value of $R_{\max} = 1002.7 \text{ k}\Omega$.

(iii) *Selection of base resistances:* The empirical formula for R_2 is given by

$$R_2 = \frac{10000}{\eta V_{BB}} = \frac{10000}{0.63 \times 12} = 1.32 \text{ k}\Omega$$

The nearest value of commercially available resistors is selected, that is, $R_2 = 1.2 \text{ k}\Omega$. Then R_1 can be found as

$$\frac{V_{BB}}{R_1 + R_2 + R_{BB(\min)}} R_1 < V_{GD}$$

or

$$\frac{12}{R_1 + 1200 + 5600} R_1 < 0.18$$

It gives, R_1 less than 103Ω . Therefore, take $R_1 = 100 \Omega$.

(iv) *Selection of capacitor:* Let the triggering circuit be designed for a maximum delay period, that is, millisecond. The maximum delay period corresponds to the minimum frequency of oscillator, which is given by

$$\tau = 10 \text{ ms} = R_{\max} C \ln \frac{1}{1-\eta}$$

Therefore,

$$C = \frac{10^{-2}}{R_{\max} \times \ln [1/(1-\eta)]} = \frac{10^{-2}}{1002.7 \times 10^{-3} \ln [1/(1-0.63)]} = 0.01 \mu\text{F}$$

Although a capacitor of $0.01 \mu\text{F}$ can be selected, the pulse width of the triggering pulse will be small ($R_1 C = 100 \times 0.1 = 1 \mu\text{s}$). Sometimes, this may not be sufficient to trigger an SCR successfully. Then it should be increased (about $5 \mu\text{s}$). Moreover, sometimes, the voltage (peak) across R_1 may not be sufficient to drive the SCR, then the value of R_1 has to be increased.

The minimum delay period (ideal) is given by

$$\tau_{\min} = R_{\min} C \ln \frac{1}{1-\eta} = 2.7 \times 10^3 \times 0.01 \times 10^{-6} \times 0.99425 = 0.0268 \text{ ms}$$

Minimum value of α = minimum delay period (in ms)

$$\times \frac{360^\circ}{20 \text{ ms}} = \frac{0.0268 \times 360}{20} = 0.483^\circ$$

Similarly, the maximum delay period (ideal) is given by

$$\tau_{\max} = R_{\max} C \ln \frac{1}{1-\eta} = 1002.7 \times 10^3 \times 0.01 \times 10^{-6} \times 0.994 = 9.967 \text{ ms}$$

The maximum value (ideal) of α is given by

$$\alpha_{\max} = \text{minimum delay period (in ms)} \times \frac{360^\circ}{20 \text{ ms}} = \frac{9.967 \times 360^\circ}{20} = 179.4^\circ$$

Example 3.30: For an SCR, the gate-cathode characteristic has a straight-line slope of 120. For a trigger-source voltage of 20 V and allowable gate-power dissipation of 0.5 W, calculate the gate-source resistance.

SOLUTION

Here

$$V_g I_g = 0.5 \text{ W}$$

and

$$\frac{V_g}{I_g} = 120 \Omega$$

$$120 I_g^2 = 0.5$$

This gives

$$I_g = [0.5/120]^{1/2} = 0.064 = 64 \text{ mA}$$

$$\therefore \text{Gate voltage, } V_g = 120 \times 64 \times 10^{-3} = 7.6 \text{ V}$$

$$\text{For the gate circuit, } E_g = I_g R_s + V_g = 0.064 R_s + 7.6 = 20 \text{ V}$$

$$R_s = \frac{20 - 7.6}{0.064} = 194 \Omega$$

Example 3.31: For an SCR, the gate-cathode characteristic is given by $V_g = 1 + 10I_g$. Gate source voltage is a rectangular pulse of 15 V with 20 μs duration. For an average gate power dissipation of 0.3 W and a peak gate drive power of 5 W, compute

- (a) the resistance to be connected in series with the SCR gate,
- (b) the triggering frequency, and
- (c) the duty cycle of the triggering pulse.

SOLUTION

- (a) Here $V_g = 1 + 10I_g$

For the pulse triggering of SCRs,

(Peak gate voltage) (peak gate current) during pulse-on period
= peak gate drive power, P_{gm} .

Because the gate pulse width is 20 μs (less than 100 μs), the DC case does not apply. Had the gate pulse width been more than 100 μs , the

relation $(1 + 10 I_g) I_g = 0.3 \text{ W}$ will hold good. But as the DC date does not apply, we have here

$$(1+10 I_g) I_g = 5 \text{ W}$$

or

$$10 I_g^2 + I_g - 5 = 0$$

Its solution gives,

$$I_g = 0.659 \text{ A}$$

\therefore Amplitude of current pulses = 0.659 A

During the pulse-on period, $E_s = R_s I_g + V_g$

or

$$R_s = \frac{15-1}{0.659} - 10 = 11.244 \Omega$$

(b) $P_{gm} = \frac{P_{gav}}{f T}$.

Here $T = 20 \mu\text{sec}$

\therefore Triggering frequency, $f = \frac{0.3 \times 10^6}{5 \times 20} = 3 \text{ kHz}$

(c) Duty cycle, $\delta = f T = 3 \times 10^3 \times 20 \times 10^{-6} = 0.06$.

Example 3.32: An SCR operating from a peak supply voltage of 400 V has the following specifications:

Repetitive peak current, $I_p = 200 \text{ A}$, $(di/dt)_{max} = 50 \text{ A}/\mu\text{s}$, $(dv/dt)_{max} = 200 \text{ V}/\mu\text{s}$.

Choosing a factor of safety of 20 for I_p , $(di/dt)_{max}$ and $(dv/dt)_{max}$ design a suitable snubber circuit. The minimum value of load resistance is 10 Ω .

SOLUTION

For a factor of safety of 2, the permitted values are $I_p = \frac{200}{2} = 100 \text{ A}$, $(\frac{di}{dt})_{max} = \frac{50}{2} = 25 \text{ A}/\mu\text{s}$, $(\frac{dv}{dt})_{max} = \frac{200}{2} = 100 \text{ V}/\mu\text{s}$.

In order to restrict the rate of rise of current beyond specified value, (di/dt) inductor must be inserted in series with SCR.

$$L = \frac{R_s \cdot V_s}{(dv_a/dt)_{max}} = \frac{400 \times 60^{-6}}{300} = 16 \mu\text{H}$$

$$R_s = \frac{L}{V_s} \cdot \left(\frac{dv}{dt} \right)_{max} = \frac{16 \times 10^{-6}}{400} \times \frac{100}{10^{-6}} = 4 \Omega$$

Before SCR is turned on, C_s is charged to 400 V. When SCR is turned on, the peak current through the SCR is $= \frac{V_s}{R_L} + \frac{V_c}{R_s}$, where $V_c = V_s$

$$= \frac{400}{10} + \frac{400}{4} = 140 \text{ A}$$

As the peak current through SCR is more than the permissible peak current of 100 A the magnitude of R_s must be increased. Taking R_s as 8 Ω , the peak current through the SCR $= \frac{400}{10} + \frac{400}{8} = 90 \text{ A}$, which is less than the allowable peak current. So choose $R_s = 8 \Omega$.

$$\text{Also } C_s = \left(\frac{2\xi}{R_s}\right)^2 L = \left(\frac{1.3}{8}\right)^2 \times 16 \times 10^{-6} = 0.4225 \mu\text{F}$$

The value of C_s may be lowered as discussed in the previous example, so C_s may be taken as $0.30 \mu\text{F}$.

At the instant switch S is closed, the SCR is open circuited, and the current through C_s is given by

$$C_s \frac{dv}{dt} \cong \frac{V_s}{R_s + R_L}$$

or

$$0.3 \times 10^{-6} \frac{dv}{dt} = \frac{400}{10 + 8}$$

$$\frac{dv}{dt} = \frac{400}{18} \times \frac{1}{0.3 \times 10^{-6}} = 74.07 \text{ V}/\mu\text{s}$$

Since the designed value of (dv/dt) is less than the specified maximum value of $100 \text{ V}/\mu\text{s}$, the value of chosen C is correct. So, choose $L = 10 \mu\text{H}$, $R_s = 8 \Omega$, and $C_s = 0.3 \mu\text{F}$.

Example 3.33: A string of four series-connected SCRs is provided with static and dynamic equalizing circuits. This string has to withstand an off-state voltage of 10 kV . The static equalizing resistance is $25,000 \Omega$ and the dynamic equalizing circuit has $RC = 40 \mu\text{s}$ and $C = 0.08 \mu\text{F}$. The leakage currents for four SCRs are $21, 25, 18$, and 16 mA , respectively. Determine voltage across each SCR in the off-state and the discharge current of each capacitor at the time of turn on.

SOLUTION

Let I be the string current in the off state. Then the current through the static-equalizing resistance R of $25,000 \Omega$ is (I -leakage current), the current through each SCR is its own leakage current, and no current flows through series combination of R_C and C .

\therefore Voltage across R = voltage across each SCR

$$\text{Voltage across SCR1} = (I - 0.021) \times 25,000 = V_1$$

$$\text{Voltage across SCR2} = (I - 0.025) \times 25,000 = V_2$$

$$\text{Voltage across SCR3} = (I - 0.018) \times 25,000 = V_3$$

$$\text{Voltage across SCR4} = (I - 0.016) \times 25,000 = V_4$$

The sum of V_1 , V_2 , V_3 and, V_4 gives

$$25,000(4I - 0.08) = V_1 + V_2 + V_3 + V_4 = \text{string voltage, } 10,000 \text{ V}$$

or

$$I = 0.12 \text{ A}$$

From above, voltage across SCR1

$$= (0.12 - 0.021) \times 25,000 = 2,475 \text{ V}$$

Similarly, $V_2 = 2,375 \text{ V}$, $V_3 = 2,550 \text{ V}$ and $V_4 = 2,600 \text{ V}$.

Discharge current through SCR1 at the time of turn on

$$= \frac{V_1}{R_C} = \frac{2,475}{40} = 61.875 \text{ A}$$

Similarly, discharge currents through SCRs 2, 3, and 4 are respectively 59.375 A, 63.75 A, and 65 A.

Example 3.34: Calculate the number of series and parallel units required in case derating factor is (a) 0.1 and (b) 0.2 for SCRs with a rating of 1,000 V and 200 A are to be used in string to handle 6 kV and 1 kA.

SOLUTION

(a) Derating factor, DRF = 1-string efficiency

$$\therefore 0.1 = 1 - \frac{6,000}{n_s \times 1,000} = 1 - \frac{1,000}{n_p \times 200}$$

\therefore Number of series-connected SCRs

$$n_s = \frac{6,000}{1,000 \times 0.9} = 6.6 \cong 7$$

Number of parallel-connected SCRs,

$$n_p = \frac{1,000}{200 \times 0.9} = 5.5 \cong 6$$

(b) As above, number of series-connected SCRs,

$$n_s = \frac{6,000}{1,000 \times 0.8} = 7.5 \cong 8$$

and the number of parallel-connected SCRs,

$$n_p = \frac{6,000}{1,000 \times 0.8} = 7.5 \cong 8$$

With the higher value of DRF, more SCRs are required, and therefore voltage and current shared by each device are lower than their normal rating. This increases the string reliability, though at an increased investment.

Example 3.35: It is required to operate a 250-A SCR in parallel with a 350-A SCR with their respective on-state voltage drops of 1.6 V and 1.2 V. Calculate the value of resistance to be inserted in series with each SCR so that they share the total load of 600 A in proportion to their current ratings.

SOLUTION

$$\text{Dynamic resistance of 250-A SCR1} = \frac{1.6}{250} \Omega$$

$$\text{Dynamic resistance of 350-A SCR2} = \frac{1.2}{350} \Omega$$

Let R be the resistance inserted in series with each SCR. With this, the current shared by

$$SCR1 = 600 \frac{\frac{1.2}{350} + R}{\text{Total resistance}} \approx 250$$

and current shared by

$$SCR2 = 600 \frac{\frac{1.6}{250} + R}{\text{Total resistance}} \approx 350$$

From above,

$$\frac{\frac{1.2}{350} + R}{\frac{1.6}{250} + R} = \frac{250}{350} = \frac{5}{7}$$

Its simplification gives

$$R = 0.004 \Omega$$

Thus, the resistance to be inserted in series with each SCR is 0.004Ω .

Example 3.36: A relaxation oscillator using an UJT is to be designed for triggering an SCR. The UJT has the following data:

$\eta = 0.72$, $I_p = 0.6 \text{ mA}$, $V_p = 18.0 \text{ V}$, $V_v = 1.0 \text{ V}$, $I_v = 2.5 \text{ mA}$, $R_{BB} = 5 \text{ k}\Omega$,
normal leakage current with emitter open = 4.2 mA .

The firing frequency is 2 kHz . For $C = 0.04 \mu\text{F}$, compute the values of R , R_1 , and R_2 .

SOLUTION

The value of charging resistor R is:

$$R = \frac{T}{C \ln \frac{1}{1-\eta}} = \frac{1}{fC \ln \frac{1}{1-\eta}} = \frac{10^6}{2000 \times 0.04 \ln \frac{1}{0.28}} = 9.82 \text{ k}\Omega$$

As V_D is not given, $V_p = \eta V_{BB}$

$$\therefore V_{BB} = \frac{V_p}{\eta} = \frac{18.00}{0.72} = 25 \text{ V}$$

The value of R_2 is calculated from the relation, $R_2 = \frac{10^4}{\eta V_{BB}}$

$$R_2 = \frac{10^4}{0.72 \times 25} = 555.55 \Omega$$

With emitter open, V_{BB} = leakage current ($R_1 + R_2 + R_{BB}$)

$$\therefore R_1 = \frac{25}{4.2 \times 10^{-3}} - 5,000 - 555.55 \Omega = 396.83 \cong 397 \Omega$$

Example 3.37: If the firing frequency of the SCR in Example 3.36 is changed by varying the charging resistor R , obtain the maximum and minimum values of R and the corresponding frequencies.

SOLUTION

$$R_{\max} = \frac{V_{BB} - V_P}{I_P} = \frac{V_{BB} - (\eta V_{BB})}{I_P} = \frac{V_{BB}(1-\eta)}{I_P}$$

$$R_{\max} = \frac{25(1-0.72)}{0.6 \times 10^{-3}} = 11.67 \text{ k}\Omega$$

or

$$R_{\min} = \frac{V_{BB} - V_V}{I_V}$$

$$\begin{aligned} f_{\min} &= \frac{1}{T_{\max}} = \frac{1}{R_{\max} C \ln \frac{1}{1-\eta}} \\ &= \frac{10^3}{11.67 \times 0.04 \ln \frac{1}{0.28}} = 1682.8 \text{ Hz} \cong 1.683 \text{ kHz} \end{aligned}$$

and

$$f_{\max} = \frac{10^3}{9.6 \times 0.04 \ln \frac{1}{0.28}} = 2045.7 \text{ Hz} \cong 2.05 \text{ kHz}$$

Example 3.38: The holding current of SCRs in the single-phase full converter is $I_H = 600 \text{ mA} = 0.6 \text{ A}$, and the delay time is $t_d = 1.5 \text{ ms}$. The converter is supplied from a $220 \text{ V}, 50 \text{ Hz}$ with a delay supply and has a load of $L = 20 \text{ mH}$ and $R = 20 \Omega$. The converter is operated with a delay angle of $\alpha = 45^\circ$. Determine the minimum value of gate pulse width t_G .

SOLUTION

$I_H = 600 \text{ mA} = 0.6 \text{ A}$, $t_d = 1.5 \mu\text{s}$, $\alpha = 45^\circ = \frac{\pi}{4}$, $L = 20 \text{ mH}$, and $R = 20 \Omega$. The instantaneous value of the input voltage is $v_s(t) = V_m \sin \omega t$, $V_m = \sqrt{2} \times 220 = 311.12 \text{ V}$.

At $\omega t = \alpha$,

$$V_1 = v_s(\omega t = \alpha) = 311.12 \times \sin \frac{\pi}{4} = 219.99 \text{ V}$$

The rate of rise of the anode current di/dt at the instant of triggering is approximately:

$$\frac{di}{dt} = \frac{V_1}{L} = \frac{219.99}{20 \times 10^{-3}} = 10,999 \text{ A/s}$$

If di/dt is assumed constant for a short time after the gate triggering, the time t_1 required for the anode current to rise to the level of holding current is calculated from $t_1 \times \frac{di}{dt} = I_H$ or $t_1 \times 10999 = 0.6$, and this gives $t_1 = 0.6/10999 = 54.55 \mu\text{s}$. Therefore, the minimum width of the gate pulse is $t_G = t_1 + t_d = 54.55 + 1.5 = 56.05 \mu\text{s}$.

REVIEW QUESTIONS AND UNSOLVED PROBLEMS

- 3.1 Find the equivalent capacitance of the depletion layer of an SCR if $\frac{dv_a}{dt}$ is 230 V/ μs and the capacitive current flowing through the junction is 5 mA?
- 3.2 The $V_g - I_g$ characteristics of an SCR is given by $V_g = 1 + 5 I_g$. The gate pulses are rectangular with an amplitude of 10 V and duration of 20 μs . The duty cycle is 0.4. (a) Find the series resistance R_g in the gate circuit to limit the peak power loss to 6 W, and (b) find average gate power loss.
- 3.3 Find the number of SCRs in series and parallel for a 5 kV, 750 A power electronics circuit having SCRs with 600 V and 100 A ratings. Use a derating factor of 20%.
- 3.4 What are the main features of a firing circuit?
- 3.5 List the advantage and disadvantage of the R, RC, and UJT relaxation oscillator triggering circuit?
- 3.6 What is the need for series and parallel operation of SCRs?
- 3.7 What is thermal runaway? How it can be avoided?
- 3.8 What is light triggering? Name any application where it is used?
- 3.9 Why temperature triggering is not used for turning on the SCR?
- 3.10 What is a snubber circuit? What is the role of the resistor in a snubber circuit?
- 3.11 Calculate the number of series and parallel connected SCRs (rating of 1,200 V and 250 A) required for a string to handle 8 kV and 1.5 kA, if the derating factor is (a) 0.25 and (b) 0.3.
- 3.12 Make a detailed comparison of different triggering circuits for the SCR.

SUMMARY

This chapter has studied in detail the construction, structure, working, and principles of operation of the SCR with different characteristics intended for power applications. The SCR is turned on when the gate pulse is applied to the gate terminal, but then the gate loses its control, and hence, the external power circuit is used for its turn off. It is a minority charge device with the highest voltage-blocking capabilities and largest current conduction amongst all switching devices. It is a slow-switching device as compared to MOSFETs and BJTs.

MAIN FORMULAS OF THE CHAPTER

- **Impulse (surge) current rating:** $I_{sub} = I \sqrt{\frac{T}{t}}$
- Typical rate of $\frac{di}{dt} = (20 - 500) \text{ A/micro seconds}$

- **Resistance (R) triggering circuit**

$$\frac{V_m}{R_l} \leq I_{g\max} \quad \text{or} \quad \boxed{R_l \geq \frac{V_m}{I_{g\max}}}$$

$$\boxed{R \leq \frac{V_{g\max} \cdot R_l}{V_m - V_{g\max}}}$$

$$\boxed{\alpha = \sin^{-1} \left[\frac{V_{gt} \cdot (R_1 + R_2 + R)}{V_m \cdot R} \right]}$$

- **RC half-wave trigger circuit**

$$\boxed{RC \geq \frac{1.3T}{2} \cong \frac{4}{w}}$$

$$\boxed{R \leq \frac{V_s - V_{gt} - V_{d1}}{I_{gt}}}$$

- **RC full-wave trigger circuit**

$$\boxed{RC \geq 50 \frac{T}{2} \cong \frac{157}{\omega}}$$

$$\boxed{R << \frac{V_s - V_{gt}}{I_{gt}}}$$

- **UJT relaxation oscillator**

$$\boxed{T = \frac{1}{f} = RC \ln \left(\frac{1}{1-\eta} \right)}$$

$$\boxed{\alpha = \omega T = \omega RC \ln \left(\frac{1}{1-\eta} \right)}$$

$$\boxed{R_{\max} = \frac{V_{BB} - V_p}{I_p} = \frac{V_{BB} - (\eta V_{BB} + V_D)}{I_p}}$$

$$\boxed{R_{\min} = \frac{V_{BB} - V_v}{I_V}}$$

- Magnitude of resistor R forming a static equalizing circuit
$$R = \frac{n_s V_b - V_s}{(n_s - 1) I_B}$$
- String efficiency =
$$\frac{\text{Actual voltage/current rating of whole string}}{\left[\frac{\text{Individual voltage/current rating of one SCR}}{\text{no. of SCRs in string}} \right]}$$
- Derating factor (DRF):**
$$\text{DRF} = 1 - \text{string efficiency}$$

$$\text{Voltage derating} = 1 - \frac{V_s}{n_s V_b}$$

Typical values of $\frac{dv}{dt}$ are $(20 - 500) \text{ v}/\mu\text{sec}$

Typical range of $\frac{di}{dt} \rightarrow (20 - 500) \text{ A}/\mu\text{sec}$

- Design of snubber circuit**

$$L = \frac{V_s}{(di/dt)_{\max}}$$

$$R_s = \frac{L}{V_s} \left(\frac{dv_a}{dt} \right)_{\max}$$

$$R_s = 2 \xi \sqrt{\frac{L}{C_s}}$$

REFERENCES/FURTHER READING

- Q. Chen and A. Q. Huang, A low-loss gate drive for emitter turn-off thyristor (ETO), *IEEE Trans. Power Electronics*, vol. 27, no. 22, pp. 4827–4831, 2012.
- P. S. Bhimra, *Power Electronics*, Khanna Publications, 5th edition, 2012.
- IEEE Draft Guide for the Application of Thyristor Surge Protective Device Components, IEEE Standards, pp. 1–72, 2012.
- M. Bragard, M. Conrad, H. V. Hoek, and R. W. De Doncker, The integrated emitter turn-off thyristor (IETO)—An innovative thyristor-based high power semiconductor device using MOS assisted turn-off, *IEEE Trans. Industry Appl.*, vol. 47, no. 5, pp. 2175–2182, 2011.
- K. Yue, S. Li, D. Kong, H. You, L. Pang, Q. Zhang, L. Liu, Reverse recovery time characteristics of high power thyristors, *IEEE Int. Conf. High Voltage Engineering and Application (ICHVE)*, pp. 1–4, 2016.
- M. S. Adler, K. W. Owayang, B. J. Baliga, and R. A. Kokosa, The evolution of power device technology, *IEEE Trans. Electronic Devices*, vol. ED-31, no. 11, pp. 1570–1591, 1984.

7. M. H. Rashid, *Power Electronics: Circuits, Devices, and Applications*, Pearson Education, Singapore, Pvt. Ltd., 2004.
8. *SCR Manual*, 6th ed., General Electric Company, New York, 1979.
9. P. T. Krein, *Elements of Power Electronics*, Oxford University Press, New York, 2003.
10. Internet source: stjosephscollegemoolamattom.org.
11. Internet source: www.vssut.ac.in.
12. R. S. Ramshaw, *Power Electronics Semiconductor Switches*, Springer Nature, 1993.
13. B. K. Bose, *Power Electronics and AC Drives*, Prentice Hall, Englewood Cliffs, NJ, 1986.
14. P. T. Krein, *Elements of Power Electronics*, Oxford University Press, New York, 2003.
15. K. Thorborg, *Power Electronics*. Prentice Hall International (UK) Ltd, London, UK, 1988.
16. R. W. Erickson, *Fundamentals of Power Electronics*, Chapman & Hall, New York, 1997.
17. V. R. Moorthi, *Power Electronics Devices, Circuits and Industrial Applications*, Oxford University Press, India, 2010.
18. T. Suntio, T. Messo, and J. Puukko, *Power Electronic Converters*, Wiley-VCH, Verlag GmbH, Germany, 2018.
19. A. M. Trzynadlowski, *Introduction to Modern Power Electronics*, 3rd edn, John Wiley & Sons, Hoboken, NJ 2010.



Taylor & Francis

Taylor & Francis Group

<http://taylorandfrancis.com>

Section II

Power Electronic Converters



Taylor & Francis

Taylor & Francis Group

<http://taylorandfrancis.com>

4 Phase-Controlled Rectifiers

4.1 INTRODUCTION

Phase-controlled rectifiers are power converters that convert AC input voltage to controlled DC output voltage. Thyristors are extensively used in rectifiers. There are various methods of commutation of thyristors:

1. **If supply is AC:** By natural or line commutation, without using any extra commutation circuit, for example, in phase-controlled rectifiers ($AC \rightarrow DC$), AC voltage controllers ($AC \rightarrow$ variable AC), and cycloconverters ($AC \rightarrow AC$).
2. **If supply is DC:**
 - a. By load commutation, if load is under damped in nature, for example, series inverter.
 - b. By forced commutation, which requires an extra commutation circuit, for example, inverters ($DC \rightarrow AC$), choppers ($DC \rightarrow DC$).

Therefore, in phase-controlled rectifiers, thyristors, are turned off by natural or line commutation without using any extra commutation circuit, so they are also called line-commutated converters. Therefore, these are simple, less expensive and hence widely used in industries where controlled DC power is required, such as in:

- Steel-rolling mills, paper mills, printing presses, and textile mills using DC motor drives
- High-voltage direct current (HVDC) transmission system
- Battery charger circuits
- Traction system working on DC
- Uninterrupted power supplies
- Electroplating and electrolysis

4.2 CLASSIFICATIONS

The rectifier circuits are classified as follows:

1. **Based on the controllability of output voltage:**

Uncontrolled rectifiers: Rectifier circuits in which output voltage cannot be controlled. They use only diodes in the circuit. Because it operates in the first quadrant only, it's also called a single-quadrant converter.

Half-controlled (semiconductor) rectifiers: Rectifier circuits in which output voltage can be controlled from zero to positive maximum by

varying the firing angle α from 0° to 180° . But its output voltage polarity cannot be reversed. They use diodes and thyristors in the circuit. They operate in first quadrant only, so they are also called single-quadrant converters.

Fully controlled rectifiers: Rectifier circuits in which output voltage can be controlled from zero to positive maximum and to negative maximum also by varying the firing angle α from 0° to 180° , that is, its output voltage polarity can be reversed by varying the firing angle. They use only thyristors in the circuit. It operates in the first and fourth quadrant, so it is also called a two-quadrant converter.

2. Based on rectification of input waveform:

Half-wave rectifier (HWR): Rectifier circuit that produces DC output voltage corresponding to only a positive half cycle of input AC voltage.

Full-wave rectifier (FWR): Circuit that produces output voltage corresponding to both positive and negative half cycles.

3. Based on the number of phases of input voltage:

Input AC voltage applied to the rectifier may be single phase, three phase, or polyphase. Based on the number of phases, the rectifiers are termed *single phase* or *three phase* or *polyphase rectifiers*.

4. Based on number of pulses in output voltage waveform:

The output voltage waveform consists of pulses (segments) of input AC voltage, and these pulses repeat over one cycle of input voltage.

Depending upon the number of pulses in output voltage waveforms, the rectifiers are classified as:

Single-pulse rectifier: One pulse in output voltage waveform for one cycle of input, for example, $1 - \phi$ HWR.

Two-pulse rectifier: For one cycle of input, two pulses in the output voltage waveform, for example, $1 - \phi$ FWR.

Three-pulse rectifier: For one input cycle, three pulses in the output voltage waveform, for example, $3 - \phi$ HWR.

Six-pulse rectifier: For one input cycle, six pulses in the output voltage waveform, for example, $3 - \phi$ FWR.

5. Based on quadrant operation (V-I characteristics):

The output or load current of rectifier always remains in same direction (positive) because diodes and thyristors used in the rectifier circuit are unidirectional devices. But the polarity of average output voltage can be reversed by varying the firing angle α . If the polarity of average output voltage remains unchanged, (i.e., v_0 always positive, while varying α from 0° to 180°) then V-I characteristics are confined to only one quadrant, and the rectifier is called the *single-quadrant rectifier*, as shown in [Figure 4.1a](#). Example: All uncontrolled rectifiers, half-controlled or semi-converter rectifiers.

If the output voltage polarity reverses, it operates in two-quadrants (I and IV), and the rectifier is called a *two-quadrant rectifier*, as shown in [Figure 4.1b](#). Example: All fully controlled rectifiers or full converters.

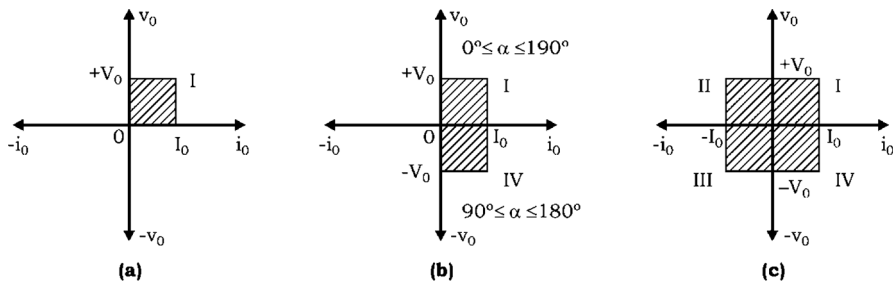


FIGURE 4.1 (a) One-quadrant rectifier, (b) two-quadrant rectifier, and (c) four-quadrant rectifier.

If two full converters are connected in antiparallel, both voltage and current can be reversed and this is called a *four-quadrant converter* or *dual converter*, as shown in Figure 4.1c.

4.3 PERFORMANCE INDICES FOR LINE-COMMUTATED CONVERTER

Rectifiers are also called phase-controlled rectifiers or line-commutated rectifiers. Important external performance parameters of the phase-controlled rectifiers are as follows:

1. Quantities on Output Side:

- a. *The average DC output voltage, V_0*

$$V_0 = \frac{1 \times p}{\text{periodicity}} \int_{\text{Lower limit}}^{\text{Upper limit}} (\text{function}) d \omega t$$

i.e.,

$$V_0 = \frac{1 \times p}{2\pi} \int_{\text{Lower limit}}^{\text{Upper limit}} (V_m \sin \omega t) d \omega t$$

where

lower limit = angle at which output voltage waveform starts

upper limit = angle at which output voltage waveform again becomes zero

p = number of pulse rectifier

- b. *The average DC output current, I_0*

$$I_0 = \frac{V_0}{R}$$

- c. The output DC power, P_0 or $P_{dc} = V_0 I_0$
- d. The root mean square (RMS) output voltage, V_{rms}

$$V_{rms} = \left[\frac{1 \times p}{2\pi} \int_{\text{Lower limit}}^{\text{Upper limit}} (V_m \sin \omega t)^2 d \omega t \right]^{\frac{1}{2}}$$

- e. The RMS output current, I_{rms}

$$I_{rms} = \frac{V_{rms}}{R}$$

- f. The output AC power = $P_{ac} = V_{rms} I_{rms}$
- g. Efficiency of rectification (η): It is defined as

$$\eta = \frac{P_{dc} (= P_0)}{P_{ac}} = \frac{V_0 I_0}{V_{rms} I_{rms}}$$

- h. AC components on output side: The RMS value of the output voltage is due to both DC and AC components, which can be expressed as:

$$V_{ac} = \sqrt{(V_{rms})^2 - (V_0)^2}$$

- i. If V_{ac} decreases, it means good rectifier, and efficiency (η) increases
- j. Form factor (FF) is defined as:

$$FF = \frac{V_{rms}}{V_0}$$

For good rectifier, $FF \cong 1$

- k. Ripple Factor (RF): It is defined as:

$$RF = \frac{V_{ac}}{V_0} = \sqrt{\left(\frac{V_{rms}}{V_0} \right)^2 - 1}$$

2. Quantities on Input Side:

- a. Input Displacement Factor (DF): It is phase-angle difference between the fundamental component and input supply voltage.

$$DF = \cos \phi$$

that is, cosine of displacement angle, where ϕ is the angle between the zero-crossing of input AC voltage and fundamental component of input current.

- b. *Harmonic Factor (HF)*: The amount of harmonic current is defined by harmonic factor (HF), which can be calculated as:

$$HF = \frac{I_h}{I_1}$$

where:

I_h is the harmonic current

I_1 is the fundamental component

The lower the value of the harmonic factor, the better is the quality of the rectifier.

- c. *Input Power Factor (PF)*: It is defined as:

$$PF = \frac{\text{real power}}{\text{apparent power}} = \frac{\text{power delivered to load}}{\text{input VA}}$$

$$= \frac{V_{\text{rms}}}{V_s} \text{ or } \frac{I_1}{I_{\text{rms}}} \cos \phi$$

where power delivered to load = $V_{\text{rms}} \cdot I_{\text{rms}}$

$$\text{input VA} = V_s \cdot I_{\text{rms}}$$

where V_s is the RMS of the source voltage.

Also, $pf = \text{distortion factor} \times \cos \phi$; where $\cos \phi = DF$

- d. *Transformer Utilization Factor*: The extent to which the transformer is utilized is given by the term transformer utilization factor (TUF), which is expressed as:

$$\text{TUF} = \frac{P_0 \text{ or } P_{dc}}{m EI} = \frac{V_o I_o}{EI}$$

where

E = RMS value of transformer phase voltage

I = RMS value of current in transformer phase winding

m = number of phases of transformer

Phase control: The term “phase control” means that by varying the firing angle, the phase relationship between the start of the load current and supply voltage can be controlled (see [Figure 4.2](#)).

Firing angle (α): It is the angle between the instant thyristor would conduct if it were a diode and the instant it is triggered. It can also be defined as the angle measured from the instant that gives the largest average output voltage (at $\omega t = \alpha = 0^\circ$) to the instant it is triggered, as shown in [Figure 4.2](#).

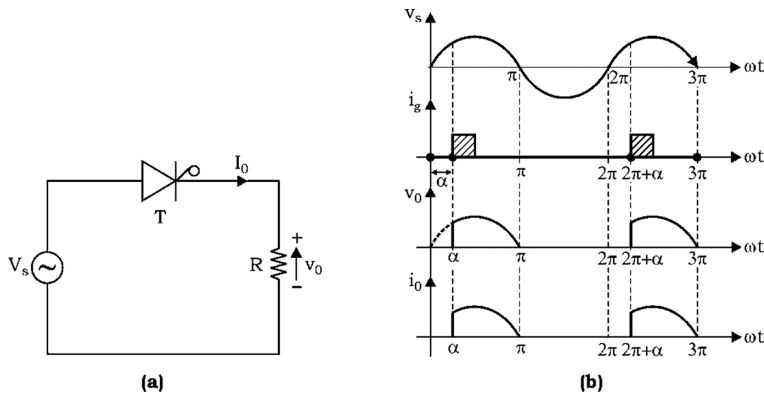


FIGURE 4.2 Principle of phase control: (a) Power circuit diagram and (b) voltage and current waveforms.

4.4 SINGLE-PHASE CONVERTERS

4.4.1 SINGLE-PHASE HALF-WAVE-CONTROLLED RECTIFIER WITH R LOAD

Since, the thyristor conducts only for a positive half cycle, it's called a half-wave rectifier. The power circuit diagram of $1-\phi$ HWR with R load is shown in Figure 4.3a.

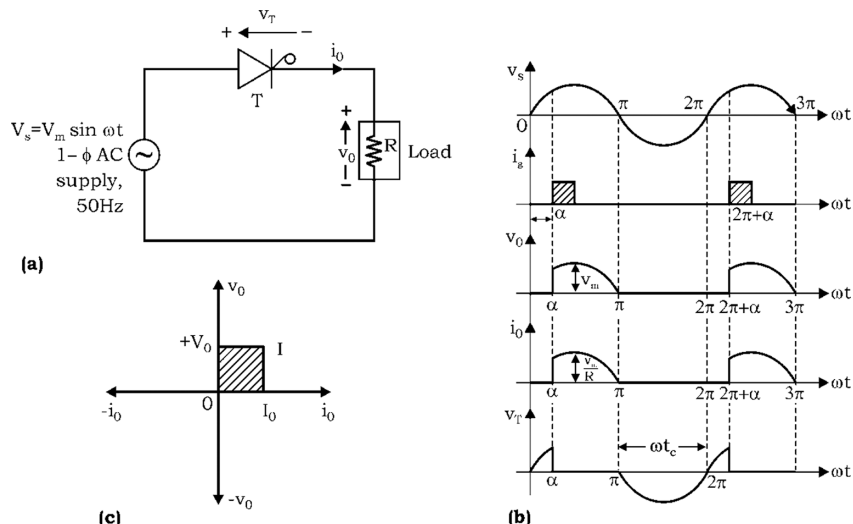


FIGURE 4.3 Single-phase half-wave-controlled rectifier with R load: (a) power circuit diagram, (b) voltage and current waveforms, and (c) quadrant.

Working: During the positive half cycle of input AC supply $v_s (=V_m \sin \omega t)$, the thyristor T is in forward blocking mode (FBM), whereas during the negative half cycles of supply it is in reverse blocking mode (RBM). Thyristor starts conducting when a positive gate pulse is applied to it during the FBM.

Therefore, let at $\omega t = \alpha$, thyristor T is triggered, and it conducts up to π . So, the load gets connected with the source, and load current i_0 in phase with the load voltage v_0 flows through V_s , T , and the load. At $\omega t = \pi$, as the supply voltage becomes zero, the load current also becomes zero, and therefore thyristor T gets turned off at $\omega t = \pi$ due to the natural reversal of supply voltage, that is, the natural or line commutation, as shown in [Figure 4.3b](#). Thyristor T does not conduct from π to 2π since it is reverse biased. Again, at $\omega t = 2\pi + \alpha$, when the thyristor is triggered, it starts conducting, and in this way the cycle repeats. Therefore, by controlling the firing angle, the average output voltage can be controlled that is, as the firing angle increases, the average load voltage decreases.

A single-phase HWR is one that produces only one pulse of load voltage or current during one cycle of source voltage, ([Figure 4.3b](#)). So, it is also called the *single-phase one-pulse rectifier*. The variation of voltage across the thyristor is also shown as v_T in [Figure 4.3b](#). When the thyristor conducts, voltage across it (v_T) is ideally zero, (practically $v_T = 1$ to 1.5 V). But during the off period of the thyristor, voltage across the thyristor (v_T) has the wave shape of supply voltage v_s . Therefore, it can be seen that $v_s = v_0 + v_T$.

Performance Parameters:

- **Circuit turn-off time (t_c):** It is the period during which the thyristor is in reverse blocking mode.
 \therefore From v_T waveform in [Figure 4.3b](#), $\omega t_c = \pi$
 or

$$t_c = \frac{\pi}{\omega} \text{ sec} \quad (4.1)$$

where $\omega = 2\pi f$ and f are the supply frequencies in Hz. For reliable commutation $t_c > t_q$, where t_q is the thyristor turn-off time.

- **Average output voltage, V_0 :**

$$V_0 = \frac{1}{2\pi} \int_{\alpha}^{\pi} V_m \sin \omega t d(\omega t)$$

or

$$= \frac{V_m}{2\pi} [1 - \cos \omega t]_{\alpha}^{\pi}$$

or

$$= \frac{V_m}{2\pi} [-\cos \pi - (-\cos \alpha)]$$

or

$$\boxed{V_o = \frac{V_m}{2\pi} (1 + \cos \alpha)} \quad (4.2)$$

∴ Therefore, by varying the firing angle average, output voltage can be controlled.

- **Average load (or output) current**

$$I_0 = \frac{V_0}{R} = \frac{V_m}{2\pi R} (1 + \cos \alpha) \quad (4.3)$$

- **RMS load (or output) voltage, V_{rms}**

$$V_{\text{rms}} = \left[\frac{1}{2\pi} \int_{\alpha}^{\pi} (V_m \sin \omega t)^2 d(\omega t) \right]^{\frac{1}{2}}$$

or

$$\begin{aligned} &= \left[\frac{V_m^2}{2\pi} \int_{\alpha}^{\pi} \frac{(1 - \cos 2\omega t)^2}{2} d(\omega t) \right]^{\frac{1}{2}} \\ &= \left[\frac{V_m^2}{2\pi} \left[\omega t - \frac{\sin 2\omega t}{2} \right]_{\alpha}^{\pi} \right]^{\frac{1}{2}} \end{aligned}$$

$$\boxed{V_{\text{rms}} = \frac{V_m}{2\sqrt{\pi}} \left[(\pi - \alpha) + \frac{\sin 2\alpha}{2} \right]^{\frac{1}{2}}} \quad (4.4)$$

- **RMS load current**

$$I_{\text{rms}} = \frac{V_{\text{rms}}}{R} \quad (4.5)$$

- **Power delivered to load** = $V_{\text{rms}} \cdot I_{\text{rms}}$ (4.6)

- **Input** = $V_s \cdot I_{\text{rms}}$ (4.7)

- **Input power factor**

$$= \frac{\text{Power delivered to load}}{\text{input VA}}$$

$$= \frac{V_{\text{rms}} I_{\text{rms}}}{V_s I_{\text{rms}}} \quad (4.8a)$$

$$= \frac{V_{\text{rms}}}{V_s}$$

$$= \frac{1}{\sqrt{2}\pi} \left[(\pi - \alpha) + \frac{\sin 2\alpha}{2} \right]^{\frac{1}{2}} \quad (4.8b)$$

- **Peak inverse voltage of thyristor (PIV) = V_m**

Using the above equations and as per definitions given in [Section 4.2](#), other performance parameters, such as rectification efficiency, FF, RF, and TUF can be calculated.

4.4.2 SINGLE-PHASE HALF-WAVE-CONTROLLED RECTIFIER WITH RL LOAD

A single-phase half-wave-controlled rectifier with RL load is shown in [Figure 4.4a](#).

Working: As load is inductive in nature, so the load current i_0 rises gradually, not instantly as in the case of R load. Similarly, when the load disconnects from the source, it falls gradually, as shown in load current i_0 waveform of [Figure 4.4b](#). At $\omega t = \alpha$, thyristor T is triggered, so the load connects with the source. Because the load is inductive in nature, the load current rises gradually.

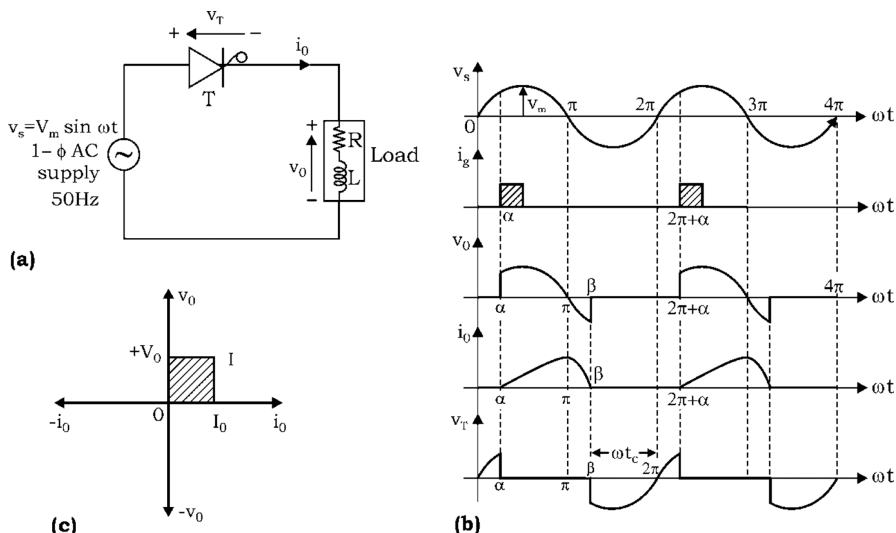


FIGURE 4.4 Single-phase half-wave-controlled rectifier with RL load: (a) power circuit diagram, (b) voltage and current waveforms, and (c) quadrant.

When the thyristor is conducting, voltage across the load is the same as the source voltage, as shown in load voltage v_0 waveform of [Figure 4.4b](#).

At $\omega t = \pi$, supply voltage becomes zero so load voltage v_0 also becomes zero, but load current i_0 does not become zero due to inductive nature of load. Rather, it becomes zero at $\omega t = \beta$, where β is $\pi < \beta \leq 2\pi$ and is called an extinction angle. Therefore, from α to $\pi \rightarrow v_0$ and i_0 are positive and from π to $\beta \rightarrow i_0$ is positive but v_0 is negative. So, at $\omega t = \beta$, when i_0 becomes zero, the thyristor is turned off because it is already reverse biased by the supply voltage. After $\omega t = \beta$, $v_0 = 0$, $i_0 = 0$. At $\omega t = 2\pi + \alpha$, thyristor T is again triggered, so the load connects with the source and therefore the load current i_0 develops as before. As the thyristor conducts from α to β , during this period $v_T = 0$ during which the thyristor does not conduct, then $v_T = v_s$.

Performance Parameters:

- **Circuit turn-off time (t_c):** From v_T waveform of [Figure 4.4b](#):

$$\omega t_c = 2\pi - \beta$$

$$\therefore t_c = \frac{\pi - \beta}{\omega} \text{ sec} \quad (4.9)$$

To achieve reliable commutation t_c must be greater than t_q , that is, $t_c > t_q$.

- **Average output voltage, V_0**

$$V_0 = \frac{1}{2\pi} \int_{\alpha}^{\pi} V_m \sin \omega t d(\omega t)$$

or

$$\begin{aligned} &= \frac{V_m}{2\pi} \left[-\cos \omega t \right]_{\alpha}^{\beta} \\ &= \frac{V_m}{2\pi} \left[\cos \alpha - \cos \beta \right] \end{aligned} \quad (4.10)$$

- **Average load current**

$$I_0 = \frac{V_0}{R} = \frac{V_m}{2\pi R} (\cos \alpha - \cos \beta) \quad (4.11)$$

- **RMS load voltage**

$$V_{\text{rms}} = \frac{V_m}{2\sqrt{\pi}} \left[(\beta - \alpha) - \frac{1}{2} \{ \sin 2\beta - \sin 2\alpha \} \right]^{\frac{1}{2}} \quad (4.12)$$

- **PIV of thyristor, PIV = V_m**

From the preceding equations, other performance parameters of the rectifier can be calculated as per their definitions given in [Section 4.2](#).

Instantaneous value of load current i_0 can be found out as:

The voltage equation for circuit of Figure 4.4a is:

$$V_m \sin \omega t = Ri_o + L \frac{di_0}{dt}$$

The load current i_0 consists of two components,

$$i_0 = i_s + i_t$$

$$i_s = \frac{V_m}{\sqrt{R^2 + X^2}} \sin(\omega t - \phi)$$

where i_s is the steady-state component

$$\phi = \tan^{-1} \frac{X}{R} \quad \& \quad X = \omega L$$

where ϕ is the angle by which the RMS current I_s lags V_s . The transient component i_t can be obtained by using force-free equation:

$$Ri_t + L \frac{di_t}{dt} = 0$$

$$\text{Its solution gives, } i_t = Ae^{-\left(\frac{R}{L}t\right)}$$

$$\therefore i_0 = i_s + i_t \quad (4.13)$$

$$= \frac{V_m}{Z} \sin(\omega t - \phi) + Ae^{-\left(\frac{R}{L}t\right)}$$

where

$$Z = \sqrt{R^2 + X^2}$$

Constant A can be find out by using boundary conditions, that is, at $\omega t = \alpha$, $i_0 = 0$, so from Equation (4.13)

$$\therefore O = \frac{V_m}{Z} \sin(\alpha - \phi) + Ae^{-R\alpha/L\omega}$$

or

$$A = -\frac{V_m}{Z} \sin(\alpha - \phi) e^{-R\alpha/L\omega}$$

Substituting the value of constant A in Equation (4.13) gives

$$i_o = \frac{V_m}{Z} \sin(\omega t - \phi) - \frac{V_m}{Z} \sin(\alpha - \phi) e^{-\left[\frac{R}{\omega L}(\omega t - \alpha)\right]} \quad (4.14)$$

(for $\alpha < \omega t < \beta$)

\therefore Equation (4.14) gives the instantaneous value of load current i_0 .

Effect of inductive load:

1. Average output voltage v_0 reduces.
2. Input PF reduces.
3. Load current i_0 waveforms gets distorted.
4. Load performance deteriorates.

4.4.3 SINGLE-PHASE HALF-WAVE-CONTROLLED RECTIFIER WITH RL LOAD AND FREEWHEELING DIODE (FD)

The waveform of load current i_0 shown in Figure 4.4b can be improved by connecting a freewheeling (or flywheel) diode (FD) across the load, as shown in Figure 4.5a.

Working: At $\omega t = \alpha$, thyristor T is triggered, so the load connects with the source. The load current i_0 starts rising gradually due to the inductive nature of the load, and the load voltage v_0 becomes equal to supply voltage v_s .

At $\omega t = \pi$, supply voltage v_s becomes zero, and so does the load voltage. After $\omega t = \pi$, as the supply voltage v_s tends to reverse, FD becomes forward biased through the conducting thyristor. As a result, i_0 is immediately transferred from thyristor T to FD. At the same time, the supply voltage appears as a reverse voltage for the thyristor, and therefore it gets turned off at $\omega t = \pi$. From π to $2\pi + \alpha$, it is assumed that FD conducts and the load current i_0 does

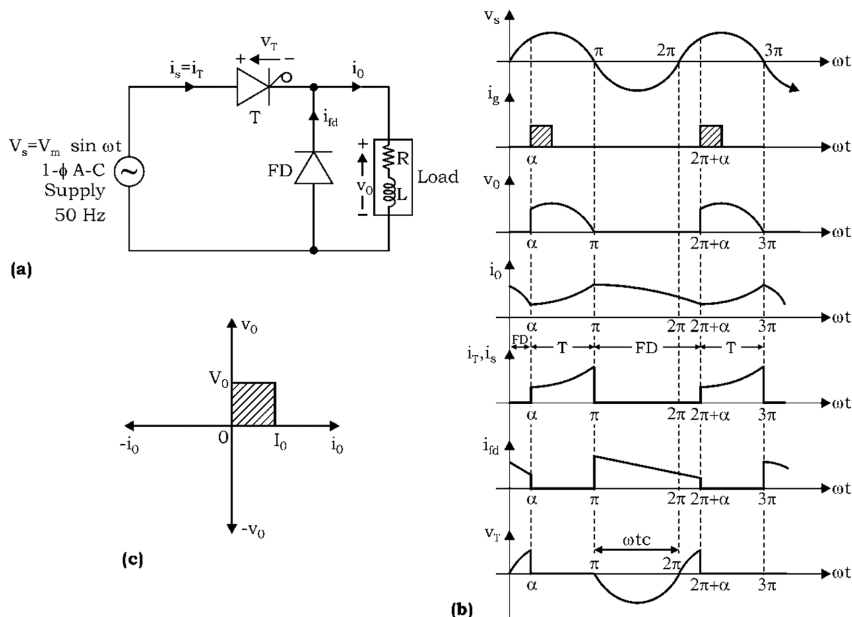


FIGURE 4.5 Single-phase half-wave-controlled rectifier with RL load and freewheeling diode: (a) power circuit diagram, (b) voltage and current waveforms, and (c) quadrant.

not decay to zero until thyristor T is triggered again at $2\pi + \alpha$. During this period, as the FD conducts, it short-circuits the load terminals, and therefore, the load voltage v_0 becomes zero, as shown in [Figure 4.5b](#).

Performance Parameters:

- **Circuit turn-off time (t_c):** From v_T waveform as shown in [Figure 4.5b](#),

$$\omega t_c = 2\pi - \pi$$

or

$$t_c = \frac{\pi}{\omega} \text{ sec} \quad (4.15)$$

- **Average load voltage, V_0** [see [Figure 4.5b](#)] is:

$$\begin{aligned} V_0 &= \frac{1}{2\pi} \int_{\alpha}^{\pi} (V_m \sin \omega t) d \omega t \\ &= \frac{V_m}{2\pi} \left[-\cos \omega t \right]_{\alpha}^{\pi} \end{aligned}$$

or

$$V_0 = \frac{V_m}{2\pi} (1 + \cos \alpha) \quad (4.16)$$

- **Average load current**

$$I_0 = \frac{V_0}{R} = \frac{V_m}{2\pi R} (1 + \cos \alpha) \quad (4.17)$$

- **RMS load voltage**

$$\begin{aligned} V_{\text{rms}} &= \left[\frac{1}{2\pi} \int_{\alpha}^{\pi} (V_m \sin \omega t)^2 d \omega t \right]^{\frac{1}{2}} \\ V_{\text{rms}} &= \frac{V_m}{2\sqrt{\pi}} \left[(\pi - \alpha) + \frac{\sin 2\alpha}{2} \right]^{\frac{1}{2}} \end{aligned} \quad (4.18)$$

Other performance parameters can be found out using above equations.

Advantages of using FD:

1. Average output voltage is increased (i.e., it prevents load voltage v_0 from becoming negative).
2. Input PF is improved.
3. Load current waveform is improved.
4. Load performance becomes better.

4.4.4 SINGLE-PHASE FULL-WAVE-CONTROLLED CONVERTER

Full-wave-controlled converters have two basic configurations:

1. Mid-point type or center-tap type
2. Bridge type

Both types of configurations for single and three phases are shown in [Figure 4.6 \[3–6\]](#).

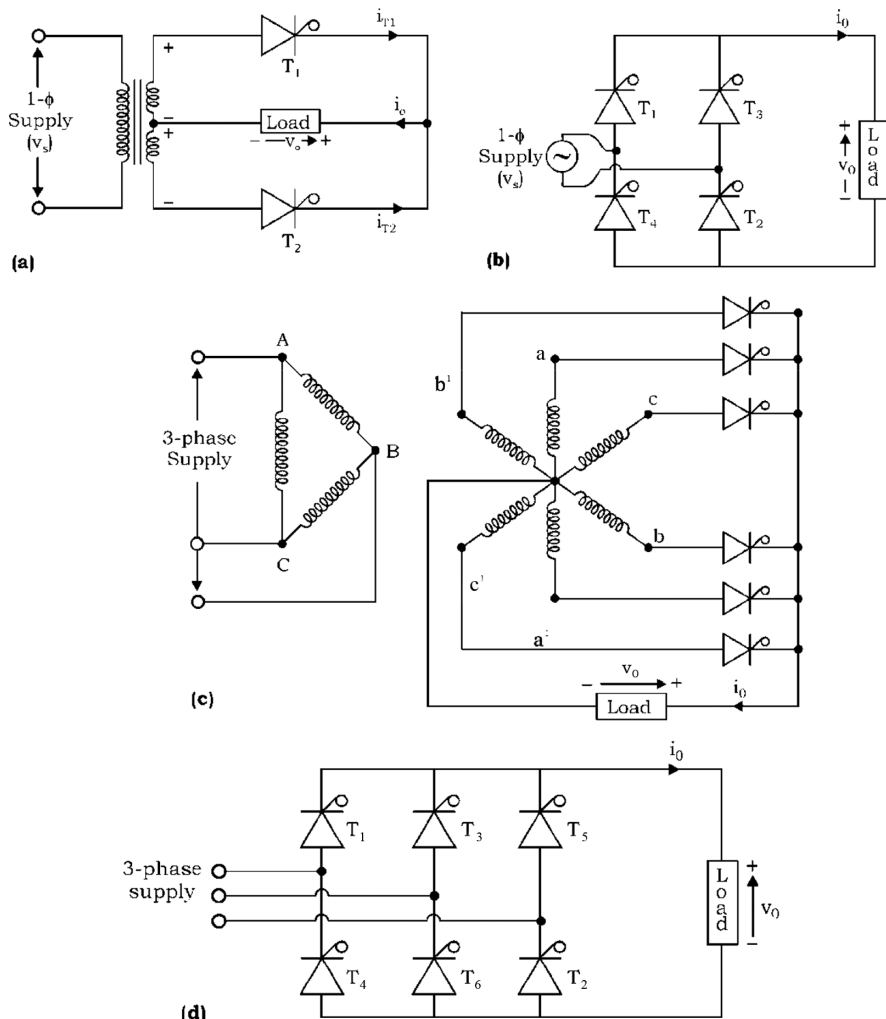


FIGURE 4.6 Various full-wave converter configurations: (a) single-phase midpoint or center-tap-type rectifier, (b) single-phase bridge-type rectifier, (c) three-phase six-pulse midpoint-type rectifier, and (d) three-phase six-pulse bridge-type rectifier.

4.4.4.1 Single-Phase Full-Wave Mid-Point Rectifier with R Load

The power circuit for single-phase full-wave rectifiers using a center-tapped transformer is shown in Figure 4.7a. Equivalent circuits when T_1 and T_2 conducts are shown in Figure 4.7b and c, respectively. Various voltage and current waveforms are shown in Figure 4.7d.

Working: It is assumed that the load current is continuous.¹ During a positive half cycle of AC supply, thyristor T_1 is forward biased, and therefore it conducts from α to π , when triggered at $\omega t = \alpha$. The load current i_o flows from terminal “a” through T_1 , R load to the “n” terminal. The direction of output voltage is from left to right, as shown in equivalent circuit during the

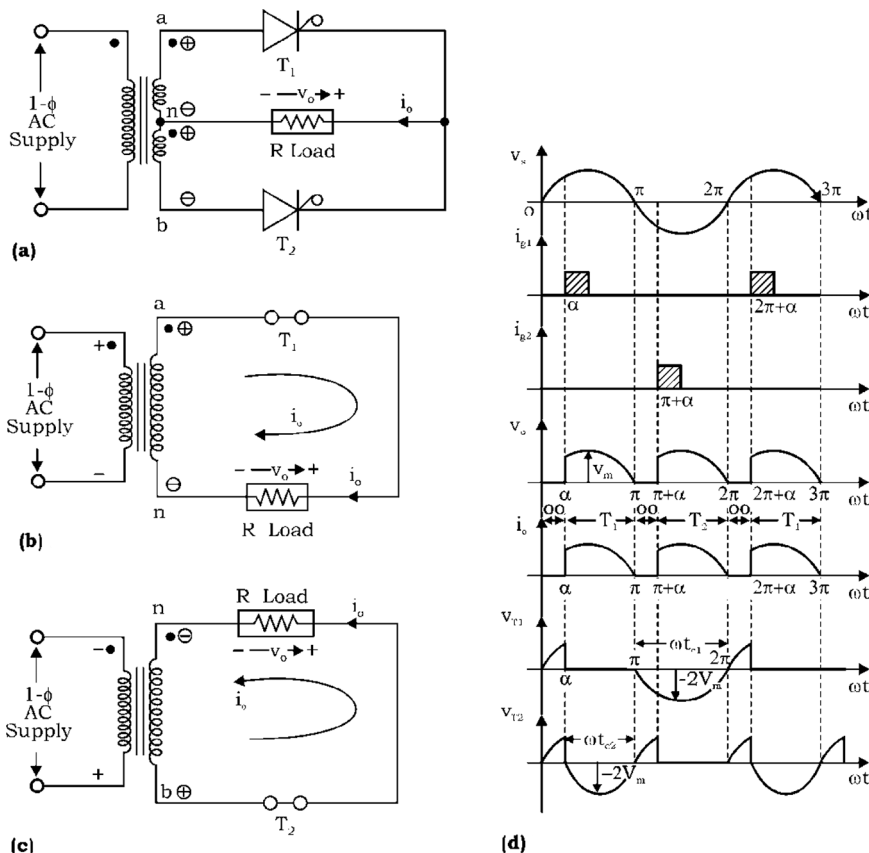


FIGURE 4.7 Single-phase full-wave midpoint-type rectifier with R load: (a) power circuit diagram, (b) equivalent circuit during positive half cycle, (c) equivalent circuit during negative half cycle, and (d) voltage and current waveforms.

¹ **Discontinuous conduction:** It is the condition when the load current becomes zero during each half cycle.

positive half cycle ([Figure 4.7b](#)). Therefore, the direction of load current i_0 is positive, and the load voltage v_0 is also positive. During the negative half cycle of AC supply, thyristor T_2 is forward biased. Therefore, it conducts from $(\pi + \alpha)$ to 2π when triggered at $\omega t = (\pi + \alpha)$. The load current i_0 flows from terminal “ b ” through T_2 , R load to the “ n ” terminal, as shown in the equivalent circuit ([Figure 4.7c](#)). Once again, the direction of the load current i_0 and load voltage v_0 remain the same as in the previous positive half cycle. Thus, the rectifier converts bidirectional AC current into unidirectional DC current.

Performance Parameters:

- **Circuit turn-off time of T_1 and T_2 are the same**
that is,

$$\omega t_{cl} = \omega t_{c2} = 2\pi - \pi$$

$$\therefore t_{cl} = t_{c2} = \frac{\pi}{\omega} \text{ s} \quad (4.19)$$

- **Average output voltage**

$$\begin{aligned} V_0 &= \frac{1 \times 2}{2\pi} \int_{\alpha}^{\pi} (V_m \sin \omega t) d \omega t \\ &= \frac{V_m}{\pi} \left[-\cos \omega t \right]_{\alpha}^{\pi} \end{aligned}$$

$$V_o = \frac{V_m}{\pi} (1 + \cos \alpha) \quad (4.20)$$

- **RMS output voltage**

$$V_{rms} = \left[\frac{1 \times 2}{2\pi} \int_{\alpha}^{\pi} (V_m \sin \omega t)^2 d \omega t \right]^{\frac{1}{2}}$$

$$V_{rms} = \frac{V_m}{\sqrt{2\pi}} \left[(\pi - \alpha) + \frac{\sin 2\alpha}{2} \right]^{\frac{1}{2}} \quad (4.21)$$

- **Peak inverse voltage of thyristors**

$$PIV = 2V_m, [\text{see } [\text{Figure 4.7d}](#)] \quad (4.22)$$

Using the preceding equations and as per definitions given in [Section 4.2](#), other performance parameters can be found out.

4.4.4.2 Single-Phase Full-Wave Bridge-Type-Controlled Rectifier with R Load

The power circuit diagram of a bridge-type rectifier is shown in [Figure 4.8a](#). It has two legs or arms. Each leg consists of two thyristors.

Working: During the positive half cycle, thyristors T_1 and T_2 are forward biased. If they are triggered at the same instant (let at $\omega t = \alpha$), current flows through the path → terminal “a” – T_1 – R load – T_2 – terminals “b” ([Figure 4.8a](#)). The voltage across the load is a segment of the supply voltage.

During the negative half cycle, thyristors T_3 and T_4 are forward biased. When they are triggered at same instant (let at $\omega t = \pi + \alpha$), the current flows through the path → terminal “b” – T_3 – R load – T_4 – terminal “a” ([Figure 4.8a](#)). The voltage across the load is a segment of supply voltage. Various voltage and current waveforms are shown in [Figure 4.8b](#).

Performance Parameters:

- Circuit turn-off time for all thyristors t_c : $\omega t_c = 2\pi - \pi$

$$\therefore t_c = \frac{\pi}{\omega} \text{ sec} \quad (4.23)$$

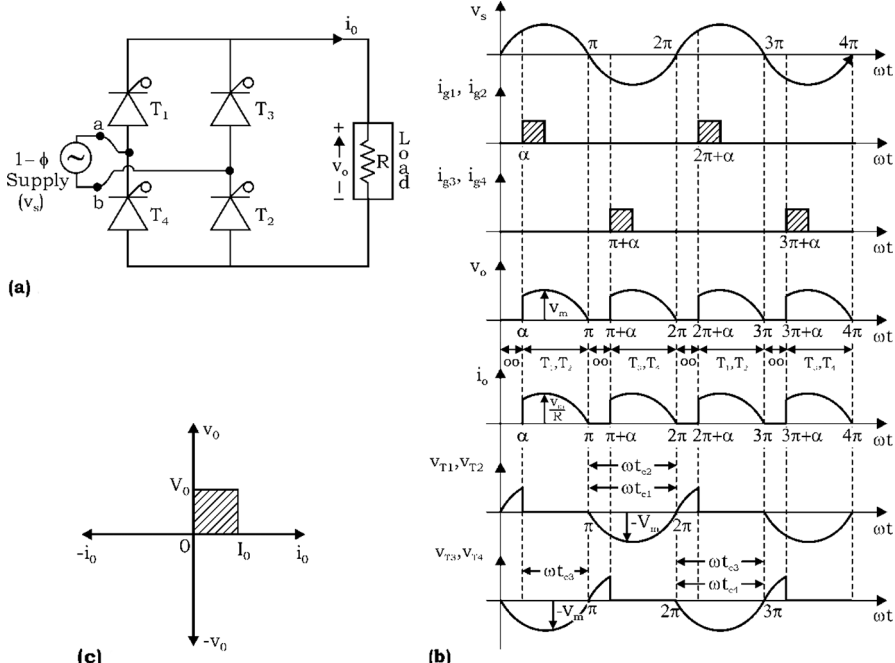


FIGURE 4.8 Single-phase full-wave bridge-type-controlled rectifier with R load: (a) power circuit diagram, (b) various voltage and current waveforms, and (c) quadrant.

- **Average output voltage**

$$V_0 = \frac{1 \times 2}{2\pi} \int_{\alpha}^{\pi} V_m \sin \omega t d \omega t$$

$$V_0 = \frac{V_m}{\pi} (1 + \cos \alpha)$$

- **RMS output voltage**

$$V_{\text{rms}} = \left[\frac{1 \times 2}{2\pi} \int_{\alpha}^{\pi} (V_m \sin \omega t)^2 d \omega t \right]^{\frac{1}{2}} \quad (4.24)$$

$$V_{\text{rms}} = \frac{V_m}{\sqrt{2\pi}} \left[(\pi - \alpha) + \frac{\sin 2\alpha}{2} \right]^{\frac{1}{2}} \quad (4.25)$$

- Peak inverse voltage of all thyristors, $\text{PIV} = V_m$ (4.26)

So, it can be seen and concluded that except the circuit configuration and PIV, other performance parameters and waveforms are the same for center-tapped type and bridge-type converters. Here, the bridge-type converter will be discussed.

4.4.4.3 Single-Phase Full-Wave Bridge-Type-Controlled Rectifier with RL Load

Case I: Continuous conduction:

Power circuit and various voltage and current waveforms for the single-phase full-wave-controlled rectifier are shown in [Figure 4.9](#).

Working: At $\omega t = \alpha$, thyristors T_1 and T_2 are triggered. They conduct from α to $(\pi + \alpha)$ due to inductive nature of the load. At $\omega t = (\pi + \alpha)$, T_3 and T_4 are triggered. The incoming thyristors reverse biased the outgoing thyristors, and therefore T_1 , T_2 get turned off by natural or line commutation at $\omega t = \pi + \alpha$. Thyristors T_3 and T_4 conduct from $(\pi + \alpha)$ to $(2\pi + \alpha)$, and above process repeats.

In the case of the center-tapped type, thyristors T_1 and T_2 conduct alternately, and the waveforms are similar to that of the bridge type (except magnitude of PIV).

Performance Parameters:

- Circuit turn-off time t_c for all thyristors

$$\omega t_c = 2\pi - (\pi + \alpha)$$

$$\therefore t_c = \frac{\pi - \alpha}{\omega} \text{ sec}$$

(4.27)

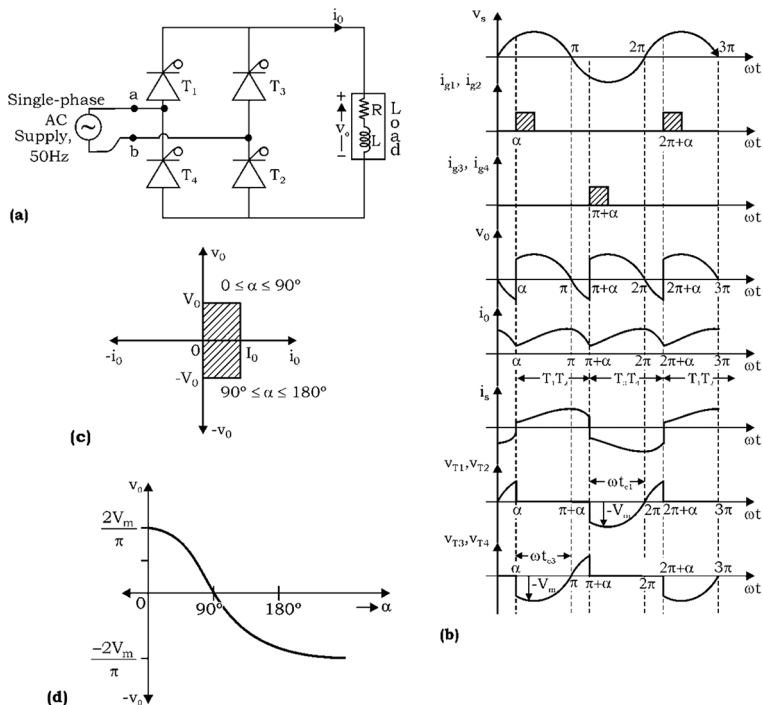


FIGURE 4.9 Single-phase full-wave bridge-type-controlled rectifier with RL load (continuous conduction): (a) power circuit diagram, (b) various voltage and current waveforms, (c) quadrant, and (d) plot between average output voltage and the firing angle.

- PIV
 - Bridge type = V_m
 - Midpoint or center-tapped type = $2V_m$
- Average output voltage

$$V_o = \frac{1 \times 2}{2\pi} \int_{\alpha}^{\pi+\alpha} (V_m \sin \omega t) d \omega t$$

$$= \frac{V_m}{2\pi} \left[-\cos \omega t \right]_{\alpha}^{\pi+\alpha}$$

$$= \frac{V_m}{2\pi} \left[-\cos(\pi + \alpha) - (-\cos \alpha) \right]$$

or

$$\boxed{V_o = \frac{2V_m}{\pi} \cos \alpha} \quad (4.29)$$

With firing angle α between 0° and 90° , the converter acts as a rectifier. The average output voltage and current are positive, so power ($P_0 = V_0 I_0$) is also positive, that is, power flows from the AC side to the DC side. But when firing angle α is between 90° and 180° , the average output voltage is negative. The converter operates as an inverter. The power flows from the DC side to the AC side. This is called ***regeneration***. When the converter operates with firing angle α between 90° and 180° , it is called a ***line-commutated inverter***.

This converter is also called a *fully controlled converter*, since the output can be controlled during the full cycle of input AC supply. Also, by varying its firing angle α , the output voltage polarity can be reversed,

that is, $\alpha = 0^\circ$

$$\alpha = 90^\circ$$

$$\alpha = 180^\circ$$

Therefore, it can be seen that by varying firing angle α from 0° to 180° , the output voltage polarity can be reversed, as shown in [Figure 4.9d](#).

Because i_0 is always positive and v_0 can be positive as well as negative, this results in a two-quadrant operation as shown in [Figure 4.9c](#). So it is also called a **two-quadrant converter**.

Case II: Discontinuous Conduction²:

In practice, the load current may become discontinuous at high values of firing angle α or at low values of load current. The load performance deteriorates if the load current is discontinuous, and therefore it is avoided by using an FD and an external inductor in series with the load.

Working: Various voltage and current waveforms for discontinuous conduction are shown in [Figure 4.10](#). At $\omega t = \alpha$, T_1 and T_2 are triggered, and they conduct up to angle β due to inductive nature of the load. At β , the current reduces to zero. At $\omega t = (\pi + \alpha)$, T_3 and T_4 are triggered, and the above process repeats. From the current i_0 waveform, it can be seen that conduction is discontinuous.

It has two modes of operation:

1. *Conduction period:* $\alpha \leq \omega t \leq \beta$, T_1 and T_2 conduct, $v_0 = v_s$. Also, $(\pi + \alpha) < \omega t < (\pi + \beta)$, T_3 and T_4 conduct, $v_0 = v_s$.
2. *Idle period:* $\beta < \omega t < \pi + \alpha \rightarrow$ no device conducts and so $v_0 = 0$

Performance Parameters:

- Circuit turn-off time for thyristors

$$\therefore \omega t_c = 2\pi - \beta$$

$$t_c = \frac{2\pi - \beta}{\omega} \text{ sec}$$

(4.30)

² **Continuous conduction:** It is a condition when the load current never becomes zero but continuously flows through the silicon-controlled rectifier (SCR)/diode.

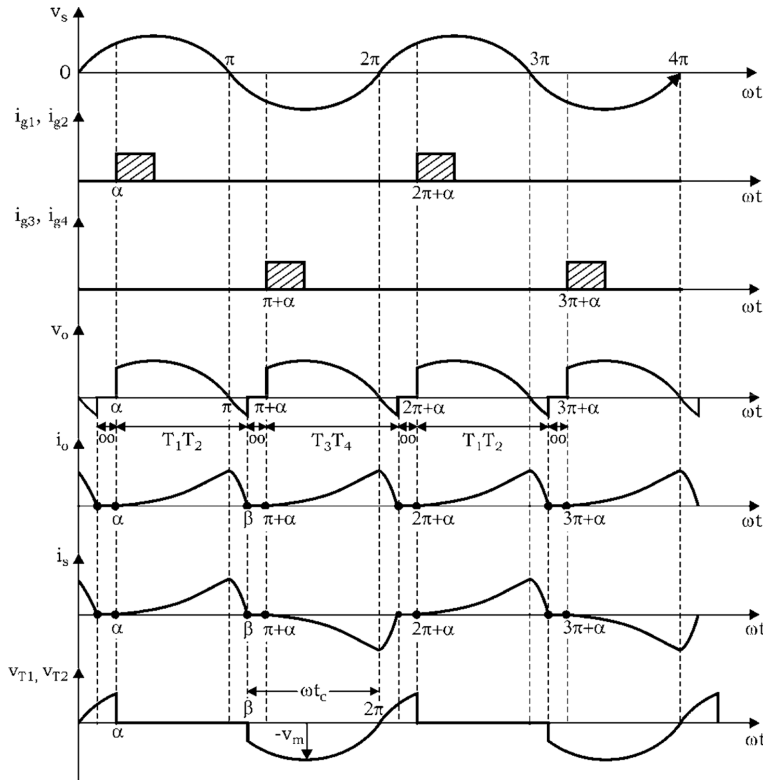


FIGURE 4.10 Various voltage and current waveforms with discontinuous conduction.

- Average output voltage, V_0

$$\begin{aligned}
 V_0 &= \frac{1 \times 2}{2\pi} \int_{\alpha}^{\beta} V_m \sin \omega t \, d\omega t \\
 &= \frac{V_m}{\pi} [-\cos \omega t]_{\alpha}^{\beta} \\
 V_0 &= \frac{V_m}{\pi} (\cos \alpha - \cos \beta) \tag{4.31}
 \end{aligned}$$

Using the preceding equations and as per definitions given in [Section 4.2](#), other performance parameters can be found out.

4.4.5 SINGLE-PHASE HALF-WAVE-CONTROLLED RECTIFIER WITH RLE LOAD

The power circuit diagram of a single-phase half-wave-controlled rectifier with RLE load is shown in [Figure 4.11a](#). The emf E in the load may be due to a battery or a DC motor.

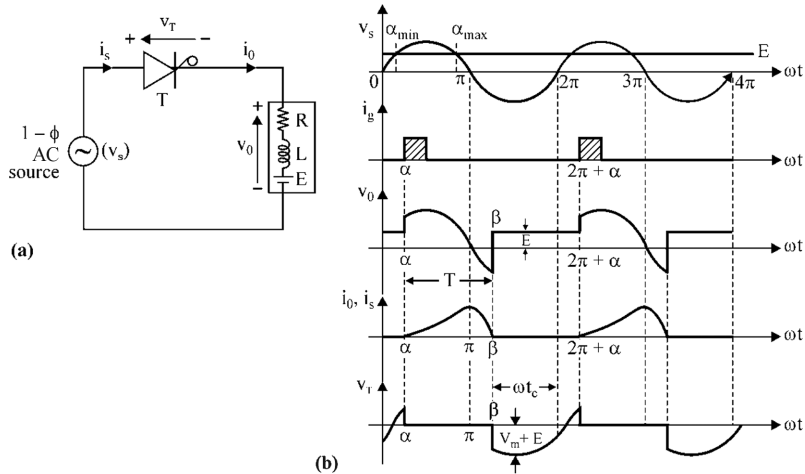


FIGURE 4.11 Single-phase half-wave-controlled rectifier with RLE load: (a) power circuit and (b) voltage and current waveforms.

The minimum and maximum value of the firing angle can be obtained from the relation [see Figure 4.11b].

$$V_m \sin \omega t = E$$

or

$$V_m \sin \alpha_{\min} = E$$

or

$$\alpha_{\min} = \sin^{-1} \left(\frac{E}{V_m} \right) \quad (4.32)$$

Similarly,

$$\alpha_{\max} = \pi - \alpha_{\min} \quad (4.33)$$

It can be seen from the waveforms of Figure 4.11b that thyristor T is in reverse blocking mode during the periods $0 \leq \omega t \leq \alpha_{\min}$ and $\alpha_{\max} \leq \omega t \leq \pi$ as $E > V_m$. Therefore, during these periods, the thyristor is reverse biased and so it will not turn on. It should be noted that while the interval load current i_0 is zero, the load voltage $v_0 = E$, and during the time i_0 is not zero, v_0 follows the supply voltage v_s curve.

For the circuit of Figure 4.11a, Applying Kirchoff's Voltage law (KVL) during the internal $\alpha \leq \omega t \leq \beta$ gives the voltage differential equation as [3,5,6]:

$$V_m \sin \omega t = R i_0 + L \frac{di_0}{dt} + E \quad (4.34)$$

The solution of this equation consists of two components:

1. Steady-state component (i_s)

$$i_{s_1} = \frac{V_m}{Z} \sin(\omega t - \varphi)$$

and

$$i_{s_2} = -(E / R)$$

2. Transient current component (i_t)

$$i_t = A e^{-(R/L)t}$$

Thus, the total current i_0 is given by:

$$i_0 = i_s + i_t \quad (4.35)$$

$$i_0 = \frac{V_m}{Z} \sin(\omega t - \varphi) - \frac{E}{R} + A e^{-(R/L)t} \quad (4.36)$$

Using boundary conditions, that is, at $\omega t = \alpha$, $i_0 = 0$, i.e., at $t = \frac{\alpha}{\omega}$, $i_0 = 0$, we get:

$$i_0 = \frac{V_m}{Z} \sin(\alpha - \varphi) - \frac{E}{R} + A e^{-\frac{(R/L)\alpha}{\omega}}$$

or

$$A = \left[\frac{E}{R} - \frac{V_m}{Z} \sin(\alpha - \varphi) \right] e^{-\frac{Ra}{L\omega}} \quad (4.37)$$

Substituting the value of A in Equation (4.36), we get

$$i_0 = \frac{V_m}{Z} \left[\sin(\omega t - \varphi) - \sin(\alpha - \varphi) e^{-\left[\frac{R}{\omega L}(\omega t - \alpha)\right]} \right] - \frac{E}{R} \left[1 - e^{-\left[\frac{R}{\omega L}(\omega t - \alpha)\right]} \right] \quad (4.38)$$

- The average load current I_0 is given by:

$$\begin{aligned} I_0 &= \frac{1}{2\pi R} \left[\beta (V_m \sin \omega t - E) \phi \omega t \right] \\ &= \frac{1}{2\pi R} [V_m (\cos \lambda - \cos \beta) - E (\beta - \alpha)] \end{aligned} \quad (4.39)$$

- The average load voltage V_0 is given by:

$$V_0 = E + I_0 R \quad (4.40)$$

- **Circuit turn-off time**

$$t_c = \frac{2\pi - \beta}{\omega} \text{ sec.} \quad (4.41)$$

- **PIV as shown in Figure 4.11b** $= V_m + E$ (4.42)

- **From the waveform of voltage, a thyristor V_T as shown in Figure 4.11b:**
At

$\omega t = 0, v_s = 0$, therefore, $V_T = E$

$\omega t = \alpha_{\min}, v_s = E$, therefore, $V_T = 0$

$\omega t = \alpha, v_s = V_m \sin \alpha$, therefore $V_T = V_m \sin \alpha - E$

During

$\alpha \leq \omega t \leq \beta, V_T = 0$

At

$\omega t = \beta, V_T = V_m \sin \beta - E$

4.4.6 SINGLE-PHASE FULL CONVERTER WITH RLE LOAD AND DISCONTINUOUS CONDUCTION

The power circuit diagram for a single-phase full converter (bridge type) is shown in Figure 4.12a. At $\omega t = \alpha$, when the SCR pair T_1T_2 is triggered, the load current begins to build up from zero as shown. At some angle β (extinction angle), the load current decays to zero. Because T_1T_2 are reverse biased after $\omega t = \pi$, this pair is turned off at $\omega t = \beta$ by natural commutation when the load current i_0 becomes zero.

From α to β , output voltage v_0 follows source voltage v_s . From β to $(\pi + \alpha)$, no SCR conducts, so the load voltage $v_0 = E$ as shown in Figure 4.12b.

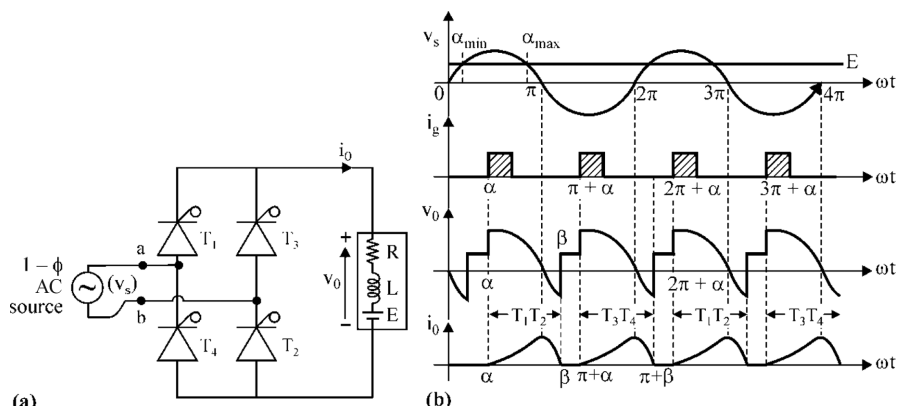


FIGURE 4.12 Single-phase full converter with RLE load and discontinuous conduction:
(a) power circuit diagram and (b) voltage and current waveforms.

At $\omega t = \pi + \alpha$, as pair T_3T_4 is triggered, the load current starts to build up again as before, and load voltage v_0 follows v_s waveform as shown in Figure 4.12b. At $\pi + \beta$, i_0 falls to zero; v_0 becomes equal to E as no SCR conducts. Therefore, it can be observed that there are two modes of operation:

1. Conduction period: $\alpha \leq \omega t \leq \beta$, T_1T_2 conducts and $v_0 = v_s$
Also, $(\pi + \alpha) \leq \omega t \leq (\pi + \beta)$, T_3T_4 conducts and $v_0 = v_s$.
2. Idle period, $\beta \leq \omega t \leq \pi + \alpha$, no SCR conducts, $v_0 = E$

4.5 THREE-PHASE CONVERTERS

The advantages of three-phase converters over single-phase converters are:

1. Provides higher average output voltage.
2. Output ripple frequency is higher as compared to single-phase converters.
Therefore, filtering requirements for smoothing out the load current/voltage are less.
3. Load current is mostly continuous, so the load performance is superior as compared to when single-phase converters are used.

4.5.1 THREE-PHASE HALF-WAVE CONVERTERS WITH RL LOAD

The power circuit diagram of the three-phase half-wave rectifier with RL load is drawn in Figure 4.13a [3–6,10].

The output of this converter has three pulses per cycle of input AC supply. Hence, it is also called a *three-pulse converter*. At any time, the SCR (or thyristor) that has the largest positive voltage at the anode will conduct.

Let the phase voltage be:

$$v_{an} = V_m \sin \omega t; v_{bn} = V_m \sin (\omega t - 120^\circ); \text{ and } v_{cn} = V_m \sin (\omega t + 120^\circ) \quad (4.43)$$

Working: As shown in Figure 4.13a, between points *a* and *b*, the v_{an} phase is the most positive so thyristor T_1 connected to it gets forward biased. Similarly, between points *b* and *c*, T_2 is forward biased and between *c* and *d*, T_3 is forward biased. Therefore, whenever the forward-biased thyristor is triggered, it starts conducting and the load gets connected with source. Because the load is inductive, the load voltage goes to the negative direction. Triggering of one thyristor turns off the outgoing thyristor by *natural commutation*.

When thyristor T_1 is triggered at $\omega t = (\frac{\pi}{6} + \alpha)$, the phase voltage v_{an} appears across the load until thyristor T_2 is triggered at $\omega t = (\frac{5\pi}{6} + \alpha)$. When thyristor T_2 is triggered, thyristor T_1 is reverse biased, because line-to-line voltage v_{ab} ($= v_{an} - v_{bn}$) is negative, and therefore, T_1 is turned off.

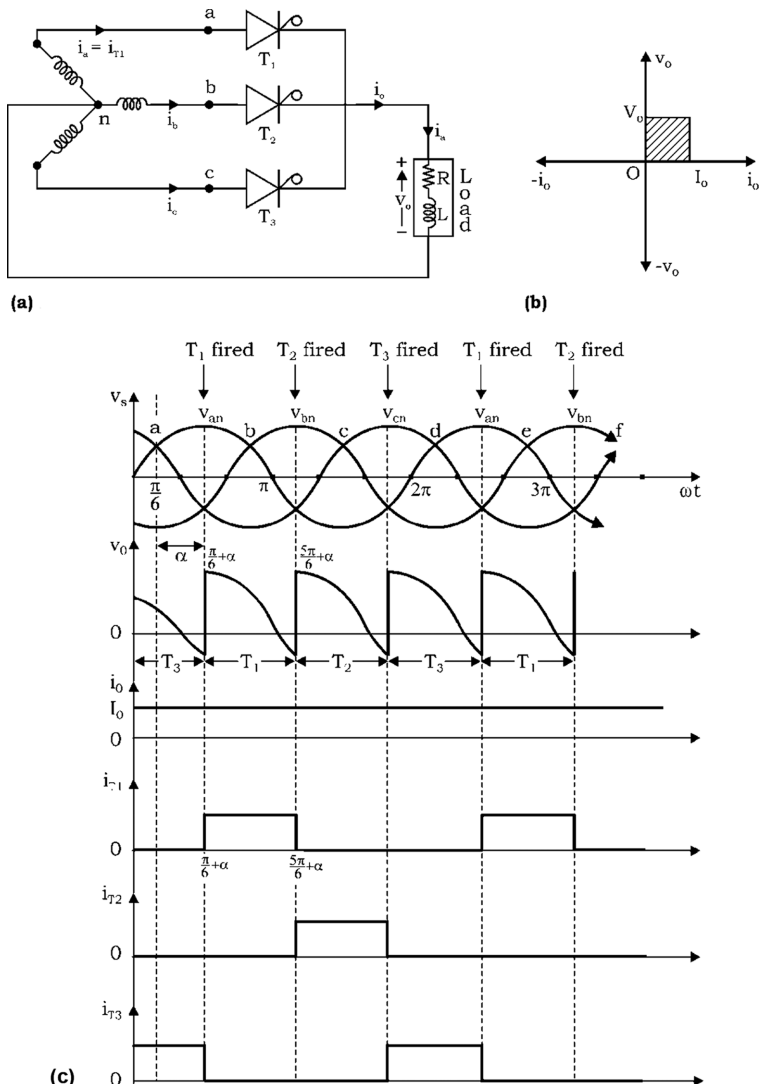


FIGURE 4.13 Three-phase half-wave converter with RL load: (a) power circuit diagram, (b) quadrant (V - I characteristics), and (c) voltage and current waveforms for RL load.

The phase voltage v_{bn} appears across the load until thyristor T_3 is triggered at $\omega t = (\frac{3\pi}{2} + \alpha)$. When T_3 is triggered, T_2 is turned off and v_{cn} appears across the load until T_1 is triggered again at the beginning of next cycle. Figure 4.13b and Figure 4.13c shows the quadrants operation and various voltage and current waveforms for the RL load, respectively.

For R load, if $\alpha > 30^\circ$, for this case the load current becomes discontinuous, and each thyristor gets turned off by self-commutation. The frequency of output ripple voltage is three times the supply frequency. This converter is generally not used in practical systems because the supply current contains DC components.

Performance Parameters:

- The average output voltage for continuous load current:

$$\begin{aligned} V_0 &= \frac{1 \times 3}{2\pi} \int_{\pi/6+\alpha}^{5\pi/6+\alpha} V_m \sin \omega t \, d(\omega t) \\ &= \frac{3V_m}{2\pi} \left[-\cos \alpha \right]_{\frac{\pi}{6}+\alpha}^{\frac{5\pi}{6}+\alpha} \\ &= \frac{3V_m}{2\pi} \left[-\cos \left(\frac{5\pi}{6} + \alpha \right) - \cos \left(\frac{\pi}{6} + \alpha \right) \right] \end{aligned}$$

or

$$V_0 = \frac{3\sqrt{3}V_m}{2\pi} \cos \alpha \quad (4.44)$$

where V_m is the maximum of phase voltage.

The maximum average output voltage, $V_{0\max}$ (at $\alpha = 0^\circ$)

$$V_{0\max} = \frac{3\sqrt{3}V_m}{2\pi} \quad (4.45)$$

- The RMS output voltage is V_{rms} :

$$V_{\text{rms}} = \left[\frac{1 \times 3}{2\pi} \int_{\pi/6+\alpha}^{5\pi/6+\alpha} (V_m \sin \omega t)^2 \, d(\omega t) \right]^{\frac{1}{2}}$$

$$V_{\text{rms}} = \sqrt{3}V_m \left(\frac{1}{6} + \frac{\sqrt{3}}{8\pi} \cos 2\alpha \right)^{\frac{1}{2}} \quad (4.46)$$

- Normalized average output voltage is

$$V_n = \frac{V_0}{V_{0\max}} = \cos \alpha \quad (4.47)$$

For R load and $\alpha \geq \pi/6$: (Discontinuous conduction)

$$V_0 = \frac{1 \times 3}{2\pi} \int_{\pi/6+\alpha}^{\pi} V_m \sin \omega t \, d\omega t$$

$$V_0 = \frac{3V_m}{2\pi} \left[1 + \cos \left(\frac{\pi}{6} + \alpha \right) \right] \quad (4.48)$$

$$V_n = \frac{V_0}{V_{0\max.}} = \frac{1}{\sqrt{3}} \left[1 + \cos \left(\frac{\pi}{6} + \alpha \right) \right] \quad (4.49)$$

$$V_{\text{rms}} = \left[\frac{1 \times 3}{2\pi} \int_{\pi/6+\alpha}^{\pi} (V_m \sin \omega t)^2 \, d\omega t \right]^{\frac{1}{2}}$$

$$V_{\text{rms}} = \sqrt{3}V_m \left[\frac{5}{24} - \frac{\alpha}{4\pi} + \frac{1}{8\pi} \sin \left(\frac{\pi}{3} + 2\alpha \right) \right]^{\frac{1}{2}} \quad (4.50)$$

$$\boxed{\text{The average output current, } I_0 = \frac{V_0}{R}} \quad (4.51)$$

$$\boxed{\text{The rms load current, } I_{\text{rms}} = \frac{V_{\text{rms}}}{R}} \quad (4.52)$$

$$\boxed{\text{The average current of thyristor, } I_A = \frac{I_0}{3}} \quad (4.53)$$

$$\boxed{\text{The RMS current of thyristor, } I_R = \frac{I_{\text{rms}}}{\sqrt{3}}} \quad (4.54)$$

$$\boxed{\text{The rectification efficiency, } \eta = \frac{V_0 I_0}{V_{\text{rms}} I_{\text{rms}}}} \quad (4.55)$$

$$\boxed{\text{Input VA rating, } VI = 3V_s I_s} \quad (4.56)$$

$$\boxed{\text{TUF} = \frac{V_0 I_0}{VI} = \frac{V_0 I_0}{3V_s I_s}} \quad (4.57)$$

$$\boxed{\text{The output power, } P_0 = (I_{\text{rms}})^2 R} \quad (4.58)$$

$$\boxed{\text{The input pf} = \frac{P_0}{VI} = \frac{P_0}{3V_s I_s}} \quad (4.59)$$

4.5.2 THREE-PHASE FULL CONVERTER

The power circuit for the three-phase fully controlled converter consists of six thyristors as shown in [Figure 4.14a](#) [3–6]. The output of this converter has six pulses per cycle of input supply. So, it is also called a *three-phase six-pulse converter*. It has three legs or arms. At a time, two thyristors, that is, one from positive or upper group (T_1, T_3, T_5) and the other from the negative or lower group (T_2, T_4, T_6) conducts.

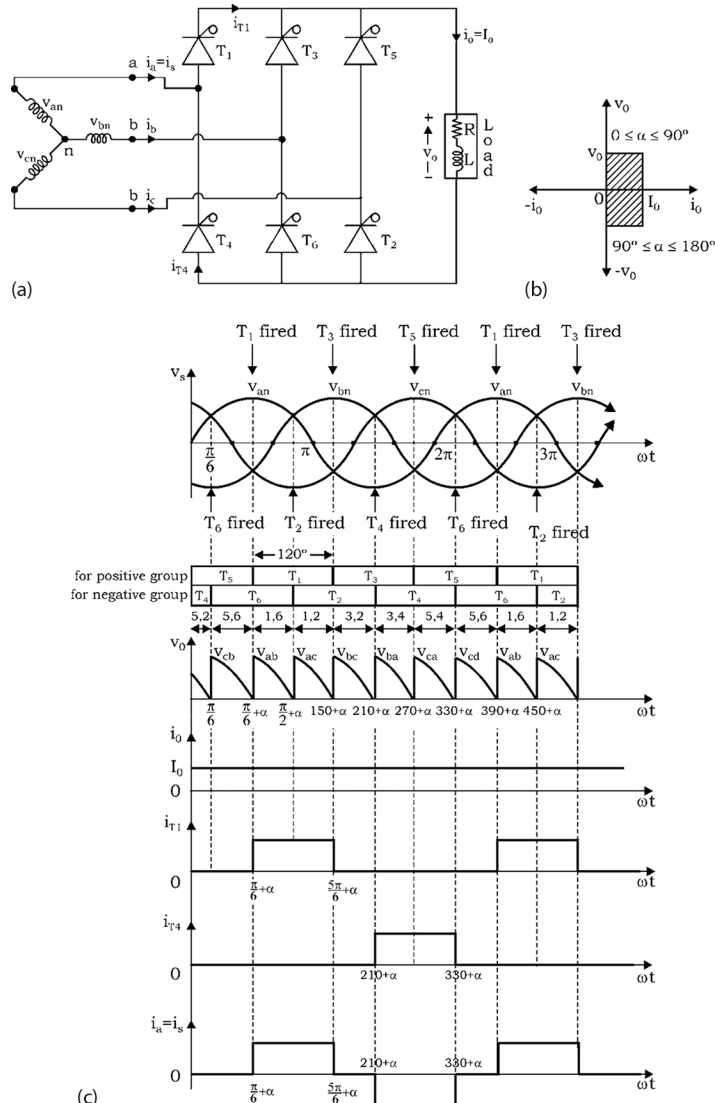


FIGURE 4.14 Three-phase full converter: (a) power circuit diagram, (b) quadrant operation, and (c) voltage and current waveforms for RL load.

Working: To produce six-pulses per cycle, the following key points are ensured while firing the thyristors in the bridge:

1. At a time, two thyristors conduct, that is, one from the positive (or upper) group and the other from the negative (or lower) group.
2. The positive group of thyristors (T_1, T_3, T_5) is fired at an interval of 120° . Similarly, the negative group of thyristors (T_2, T_4, T_6) is also fired after every 120° .
3. Thyristors are fired after every 60° , that is, commutation occurs every 60° , alternatively in positive and negative groups.
4. Each thyristor from both groups conducts for 120° .

Let at $\omega t = (\frac{\pi}{6} + \alpha)$, thyristor T_6 is already conducting, and T_1 is turned on. During interval $(\pi/6 + \alpha) \leq \omega t \leq (\pi/6 + \alpha)$, thyristors T_1 and T_6 conduct, and the line-to-line voltage v_{ab} appears across the load.

At $\omega t = (\frac{\pi}{6} + \alpha)$, T_2 is triggered, and T_6 is reverse biased immediately. So, T_6 is turned off due to natural commutation.

During interval $(\pi/2 + \alpha) \leq \omega t \leq (5\pi/6 + \alpha)$, T_1 and T_2 conduct and the line-to-line voltage v_{ac} appears across the load. In this way, the process repeats. The firing sequence is shown in Figure 4.14c. Waveforms are shown in Figure 4.14b and Figure 4.14c, respectively.

Performance Parameters:

Let the phase voltage be:

$$v_{an} = V_m \sin \omega t; v_{bn} = V_m \sin \left(\omega t - \frac{2\pi}{3} \right); \text{ and } v_{cn} = V_m \sin \left(\omega t + \frac{2\pi}{3} \right) \quad (4.60)$$

then, corresponding line-to-line voltages are:

$$v_{ab} = v_{an} - v_{bn} = \sqrt{3} V_m \sin \left(\omega t + \frac{\pi}{6} \right)$$

$$v_{bc} = v_{bn} - v_{cn} = \sqrt{3} V_m \sin \left(\omega t - \frac{\pi}{2} \right) \quad (4.61)$$

$$v_{ca} = v_{cn} - v_{an} = \sqrt{3} V_m \sin \left(\omega t + \frac{5\pi}{6} \right)$$

- **The average output voltage V_0 :** (see Figure 4.14c, v_0 waveform)

$$V_0 = \frac{1 \times 6}{2\pi} \int_{\pi/6+\alpha}^{\pi/2+\alpha} v_{ab} d(\omega t) \quad (\because p = 6, \text{ as six pulse converter})$$

$$= \frac{3}{\pi} \int_{\pi/6+\alpha}^{\pi/2+\alpha} \sqrt{3} V_m \sin(\omega t + \pi/6) d \omega t$$

$$V_0 = \frac{3\sqrt{3}V_m}{\pi} \cos \alpha \quad (4.62)$$

- The maximum average output voltage, $V_{0\max}$ (at $\alpha = 0^\circ$)

$$V_{0\max} = \frac{3\sqrt{3}V_m}{\pi} \quad (4.63)$$

- The normalized output voltage, V_n :

$$V_n = \frac{V_0}{V_{0\max}} = \cos \alpha \quad (4.64)$$

- RMS output voltage, V_{rms} :

$$V_{\text{rms}} = \left[\frac{1 \times 6}{2\pi} \int_{\pi/6+\alpha}^{\pi/2+\alpha} \left[\sqrt{3} V_m \sin (\omega t + \pi/0) \right]^2 d \omega t \right]^{\frac{1}{2}}$$

$$V_{\text{rms}} = \sqrt{3} V_m \left(\frac{1}{2} + \frac{3\sqrt{3}}{4\pi} \cos 2\alpha \right) \quad (4.65)$$

In this converter, the output ripple frequency is six times the supply frequency, so filtering required is less than that of half-wave converters.

4.6 DUAL CONVERTERS

When two full converters are connected in antiparallel to the same DC load, then such an arrangement is called a dual converter. Dual converters provide four-quadrant operation without any mechanical changeover switch. It has two modes of operation:

1. Noncirculating-current mode
2. Circulating-current mode

Power circuit diagram of noncirculating types of single-phase and three-phase dual converters configurations are shown in [Figure 4.15a](#) and [b](#), respectively. Operation in the I and IV quadrants can be obtained by operating the full converter 1 of [Figure 4.15a](#) and [b](#) [3–6]. With full converter 2 working alone in [Figure 4.15a](#) and [b](#), the polarity of the load voltage as well as direction of the load current, with respect to converter 1, can be reversed. So, full converter 2 can operate in both II and III quadrants. Thus, a dual converter using two full converters can provide four-quadrant operations as shown in [Figure 4.15c](#).

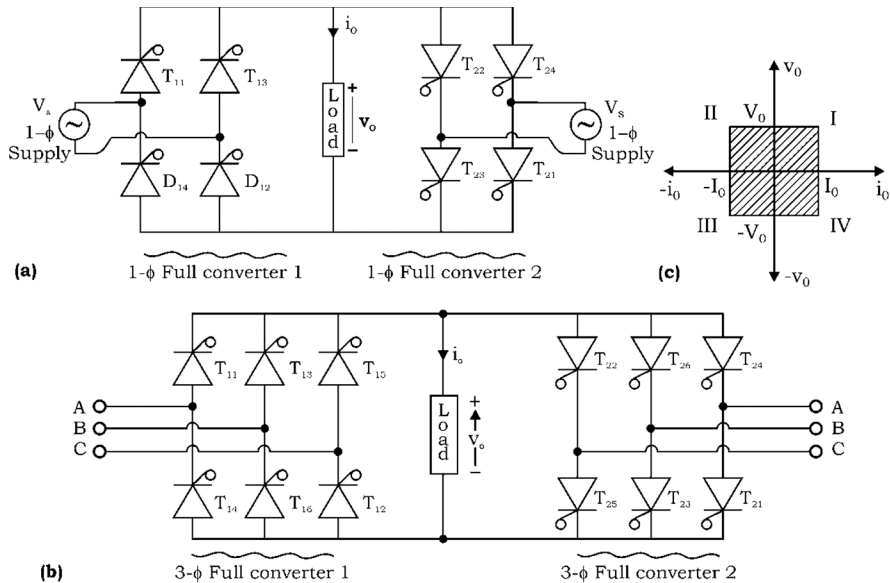


FIGURE 4.15 Noncirculating-type dual converter: (a) single-phase dual converter, (b) three-phase dual converter, and (c) four-quadrant diagram.

4.6.1 IDEAL DUAL CONVERTER

It is assumed that the dual converter consists of two ideal converters. The ideal dual converter is represented by an equivalent circuit, shown in Figure 4.16a. V_{01} and V_{02} are the magnitudes of average output voltages of converters 1 and 2, respectively. D_1 and D_2 indicate the unidirectional flow of current, but the current through the load can flow in either direction.

The firing angles α_1 and α_2 for both the full converters are controlled in such a way that their average output voltages V_{01} and V_{02} are equal in magnitude but opposite

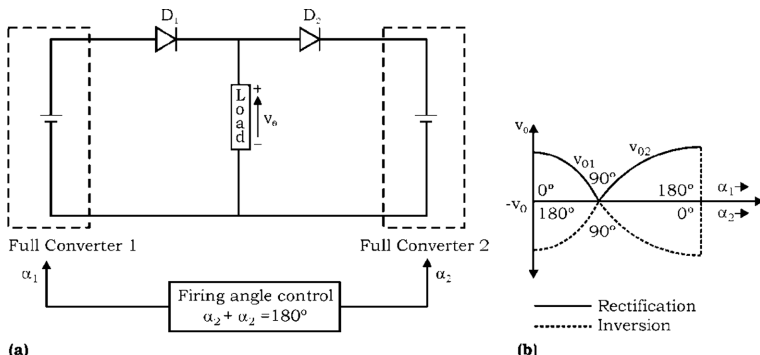


FIGURE 4.16 Ideal dual converter: (a) equivalent circuit of an ideal dual converter and (b) variation of V_0 with α .

in polarity. Thus, when one converter operates as a rectifier, then the other converter operates as an inverter. The average output voltages V_0 for both single-phase and three-phase full converters are:

$$V_{01} = \frac{2V_m}{\pi} \cos \alpha_1 = V_{0 \max} \cos \alpha_1$$

$$V_{02} = \frac{2V_m}{\pi} \cos \alpha_2 = V_{0 \max} \cos \alpha_2 \quad \text{for } 1-\phi \text{ full converter} \quad (4.66)$$

and

$$V_{01} = \frac{3V_{m1}}{\pi} \cos \alpha_1 = V_{0 \max} \cos \alpha_1$$

$$V_{02} = \frac{3V_{m1}}{\pi} \cos \alpha_2 = V_{0 \max} \cos \alpha_2 \quad \text{for } 3-\phi \text{ full converter} \quad (4.67)$$

For an ideal converter,

$$V_0 = V_{01} = -V_{02} \quad (4.68)$$

From Equations (4.66) and (4.67), substitute V_{01} and V_{02} in Equation (4.68) ([Figure 4.16](#)),

$$\therefore V_{0 \max} \cos \alpha_1 = -V_{0 \max} \cos \alpha_2$$

or

$$\cos \alpha_1 = -\cos \alpha_2$$

$$= \cos (180 - \alpha_2)$$

or

$$\alpha_1 = 180 - \alpha_2$$

or

$\alpha_1 + \alpha_2 = 180^\circ$

$$(4.69)$$

From Equations (4.66)–(4.68), the variation of output voltage with the firing angle for two converters are shown in [Figure 4.16b](#) [3–6].

4.6.2 PRACTICAL DUAL CONVERTER

With both the converters in operation, their firing angles are controlled in such a way that $\alpha_1 + \alpha_2 = 180^\circ$. Therefore, one converter will be operating as a rectifier with firing angle α_1 and the other as an inverter with firing angle $(180^\circ - \alpha_1)$. Though their average output voltages are equal, yet their instantaneous voltages v_{01} and v_{02} are out of phase, in a practical dual converter. This results in a voltage difference when the two converters are interconnected, and as a result, a large circulating current flows between the two converters but not through the load. In practical dual converters, this circulating current is limited to a safe value by inserting a reactor between the two converters as shown in [Figure 4.17](#).

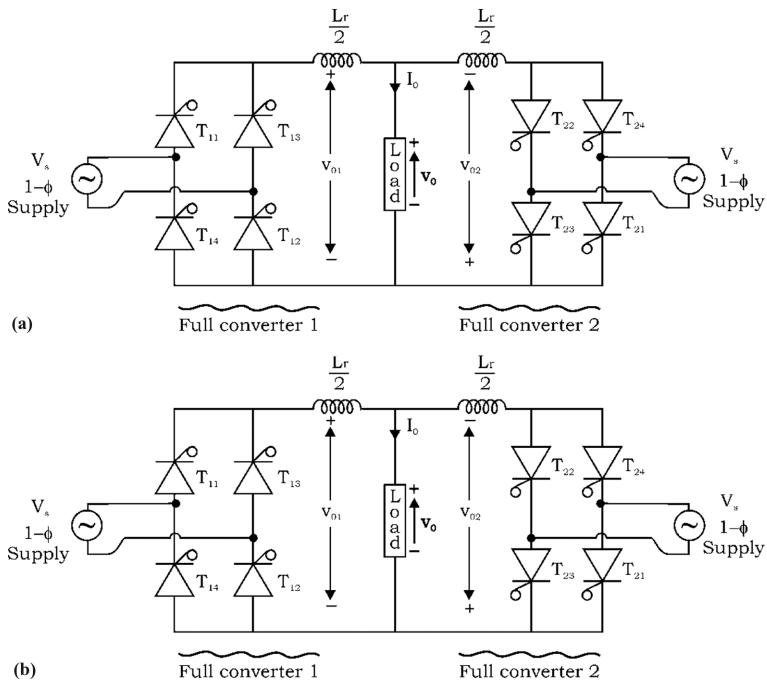


FIGURE 4.17 Circulating current-type dual converter: (a) single-phase dual converter and (b) three-phase dual converter.

A dual converter can be operated in the following two modes:

4.6.2.1 Dual Converter without Circulating Current

In this mode, only one converter operates at a time, and it alone carries the load current. Only this converter receives the firing pulses from the firing control circuit. The other converter is blocked from conduction by removing the firing pulses. The power circuit diagram for the noncirculating-type dual converter is shown in Figure 4.15. No circulating current flows between the two converters. So, the reactor is not required for this mode of dual converters.

Advantages of noncirculating type:

1. No circulating current flows, so less losses, hence high efficiency.
2. No need of reactors.

Disadvantages of noncirculating type:

1. Load current may become discontinuous, which is undesirable.
2. Its operation is slow, because it requires a time delay of 10 to 20 ms in between the operation of two converters.

4.6.2.2 Dual Converter with Circulating Current

In this mode of the dual converter, a reactor is inserted between converter 1 and 2 as shown in [Figure 4.17](#) [3–6]. This reactor L_c limits the magnitude of the circulating current.

In this mode, both converters 1 and 2 operate together in such a way that firing angles $\alpha_1 + \alpha_2 = 180^\circ$. One converter will be operating as a rectifier with firing angle α_1 and the other as an inverter with firing angle $\alpha_2 = (180^\circ - \alpha_1)$. Though their average output voltages V_{01} and V_{02} are equal, their instantaneous output voltages v_{01} and v_{02} are not similar. As a result of it, circulating current flows between two converters.

If the load current is to be reversed, the role of the two converters is interchanged. The normal delay period of 10–20 ms, as required in the noncirculating current mode, is not needed here. Hence, operation becomes faster with this type of dual converter.

Advantages:

1. Operation is faster because the time delay of 10 to 20 ms is not required.
2. Power can flow in either direction because both converters are in operation.
3. Time response for changing from one quadrant operation to other is faster.

Disadvantages:

1. A reactor is required to limit the circulating current, so size and cost increase.
2. Circulating current gives more losses; hence, the efficiency is low.
3. Because converters have to handle load current as well as circulating current, thyristors of high ratings are required.

But despite of these drawbacks, a dual converter with circulating current mode is preferred to obtain a fast response in four-quadrant operations.

4.6.3 SINGLE-PHASE DUAL CONVERTER

If two single-phase full converters are connected back to back (or in antiparallel) to the same load, as shown in [Figure 4.18a](#), both the output voltage and load current flow can be reversed. As shown in [Figure 4.18b](#), it provides four-quadrant operation and is called a single-phase dual converter [3–6].

If α_1 and α_2 are the firing angles (or delay angles) of converters 1 and 2, respectively, the corresponding average output voltages are V_{01} and V_{02} . The firing angles are controlled such that one converter operates as the rectifier and the other as the inverter with the scheme $\alpha_1 + \alpha_2 = 180^\circ$.

The average output voltage for a single-phase full converter is given by:

$$V_0 = \frac{2V_m}{\pi} \cos \alpha \quad (4.70)$$

Therefore, for converter 1,

$$V_{01} = \frac{2V_m}{\pi} \cos \alpha_1 \quad (4.71)$$

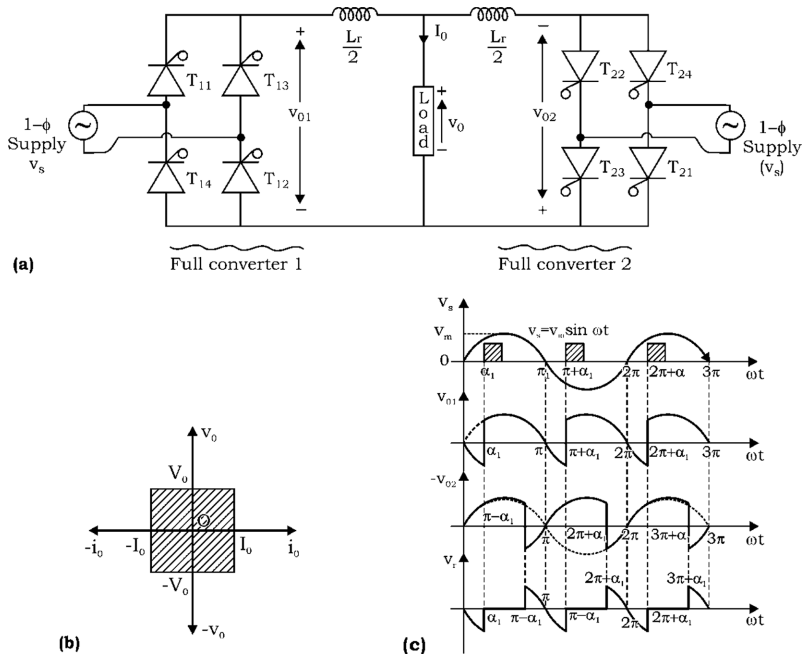


FIGURE 4.18 Single-phase dual converter: (a) single-phase dual converter, (b) quadrant operation, and (c) waveforms.

for converter 2,

$$V_{01} = \frac{2V_m}{\pi} \cos \alpha_2 \quad (4.72)$$

As one converter is rectifying and other is inverting,

$$\therefore V_{01} = -V_{02}$$

Substituting v_{01} and v_{01} from Equations (4.71) and (4.72), we get

$$\therefore \frac{2V_m}{\pi} \cos \alpha_l = -\frac{2V_m}{\pi} \cos \alpha_2$$

or

$$\cos \alpha_1 = -\cos \alpha_2$$

$$= \cos (180 - \alpha_2)$$

or

$$\alpha_1 = 180 - \alpha_2$$

or

$$\boxed{\alpha_1 + \alpha_2 = 180^\circ} \quad (4.73)$$

Because the instantaneous output voltages v_{01} and v_{02} of two converters are not similar, it results in a flow of a large circulating current between the two converters. This current is limited by circulating current reactor L_r .

The reactor voltage v_r is equal to the difference of the instantaneous converter output voltages (v_{01} and v_{02}), that is,

$$v_r = v_{01} - v_{02} \quad (4.74)$$

The variations of reactor voltages v_r , v_{01} , v_{02} , v_s are shown in Figure 4.18c.

Also,

$$v_r = L_r \frac{di_r}{dt} \quad (4.75)$$

where i_r is the circulating current through both converters and reactor L_r .

The circulating current i_r can be found by integrating the instantaneous voltage difference ($v_r = v_{01} - v_{02}$) starting from $\omega t = \pi - \alpha_1$.

$$\begin{aligned} \therefore i_r &= \frac{1}{\omega L_r} \int_{\pi-\alpha_1}^{\omega t} v_r \cdot d(\omega t) = \frac{1}{\omega L_r} \int_{\pi-\alpha_1}^{\omega t} (v_{01} - v_{02}) d(\omega t) \\ &= \frac{V_m}{\omega L_r} \left[\int_{\pi-\alpha_1}^{\omega t} \sin \omega t d(\omega t) - \int_{\pi-\alpha_1}^{\omega t} -\sin \omega t d(\omega t) \right] \end{aligned}$$

(\because As, $v_{01} = V_m \sin \omega t$ and $v_{02} = -V_m \sin \omega t$)

$$\begin{aligned} &= \frac{V_m}{\omega L_r} \left[\int_{\pi-\alpha_1}^{\omega t} \sin \omega t d(\omega t) + \int_{\pi-\alpha_1}^{\omega t} -\sin \omega t d(\omega t) \right] \\ &= \frac{2V_m}{\omega L_r} [-\cos \omega t]_{\pi-\alpha_1}^{\omega t} \end{aligned}$$

or

$$= \frac{2V_m}{\omega L_r} [-\cos \omega t - (-\cos(\pi - \alpha_1))]$$

$$\boxed{i_r = \frac{2V_m}{\omega L_r} (\cos \alpha_1 - \cos \omega t)} \quad (4.76)$$

Therefore, $i_r > 0 \rightarrow \text{for } 0 \leq \alpha_1 \leq \pi/2$

$$i_r > 0 \rightarrow \text{for } \pi/2 \leq \alpha_1 \leq \pi$$

The instantaneous circulating current depends on the delay angle. For $\alpha_1 = 0$, its magnitude becomes minimum when $\omega t = n\pi$, where $n = 0, 2, 4\dots$ and maximum when $\omega t = n\pi$, where $n = 1, 3, 5\dots$ If the peak load current is I_p , one of the converters that controls the power flow may carry a peak current of $(I_p + \frac{4V_m}{\omega L_r})$

In general, for some firing angle α_1 ;

$$I_{r(\max)} = \frac{2V_m}{\omega L_r} (1 - \cos \alpha_1) \quad (4.77)$$

4.6.4 THREE-PHASE DUAL CONVERTERS

[Figure 4.19a](#) shows the power circuit for a three-phase dual converter where two three-phase full converters are connected back to back to the same load. It has been already discussed that due to the instantaneous voltage differences between the output voltages of two full converters, a circulating current flows through the converters. The circulating current is normally limited by a circulating reactor L_r , as shown in [Figure 4.19a](#). The firing angles (or delay angles) α_1 and α_2 of two converters are so controlled that $(\alpha_1 + \alpha_2) = 180^\circ$. [Figure 4.19b](#) shows various waveforms [3–6]. The operation of each converter is identical to that of a three-phase full converter. During interval $(\pi/6 + \alpha_1) \leq \omega t \leq (\pi/2 + \alpha_1)$, line-to-line voltage v_{ab} appears across the output of converter 1, and v_{bc} appears across converter 2.

Let line to neutral (phase) voltages be:

$$\begin{aligned} v_{an} &= V_m \sin \omega t \\ v_{bn} &= V_m \sin \left(\omega t - \frac{2\pi}{3} \right) \\ v_{cn} &= V_m \sin \left(\omega t + \frac{2\pi}{3} \right) \end{aligned} \quad (4.78)$$

then, corresponding line-to-line voltages are

$$\begin{aligned} v_{ab} &= v_{an} - v_{bn} = \sqrt{3}V_m \sin \left(\omega t + \frac{\pi}{6} \right) \\ v_{bc} &= v_{bn} - v_{cn} = \sqrt{3}V_m \sin \left(\omega t - \frac{\pi}{2} \right) \\ v_{ca} &= v_{cn} - v_{an} = \sqrt{3}V_m \sin \left(\omega t + \frac{5\pi}{6} \right) \end{aligned} \quad (4.79)$$

If v_{01} and v_{02} are instantaneous output voltage of converters 1 and 2, respectively, the instantaneous voltage across the reactor L_r during interval $(\pi/6 + \alpha_1) \leq \omega t \leq (\pi/2 + \alpha_1)$ is

$$v_r = v_{01} + v_{02} = v_{ab} - v_{bc}$$

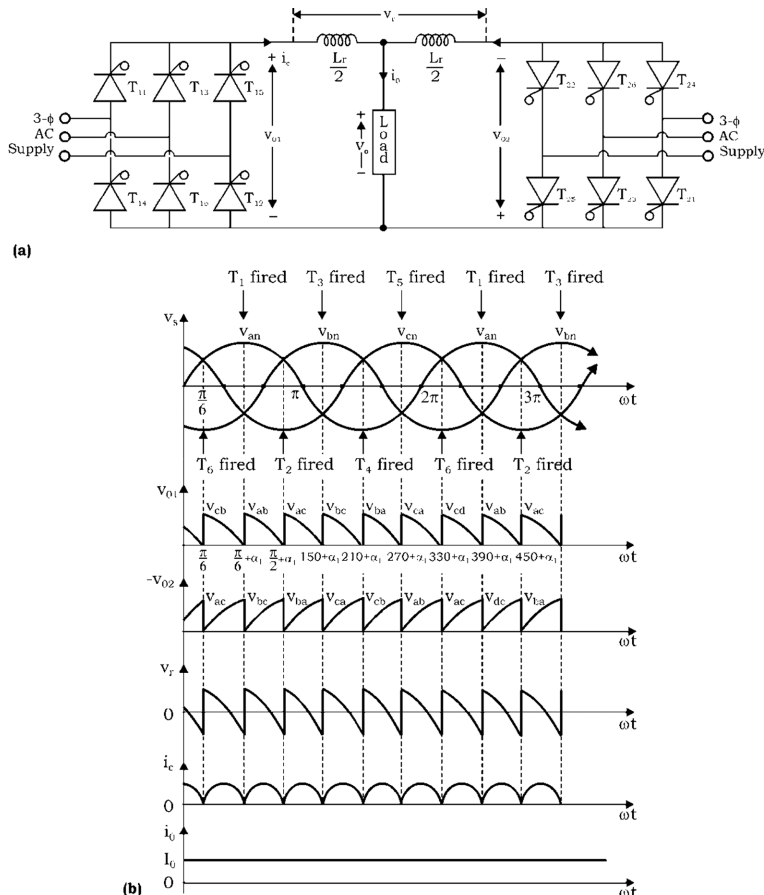


FIGURE 4.19 Three-phase dual converter: (a) power circuit and (b) voltage and current waveforms.

$$= \sqrt{3}V_m \cos(\omega t - \pi / 6) \quad (4.80)$$

The circulating current can be found by integrating reactor voltage V_r :

$$i_r = \frac{1}{\omega L_r} \int_{\frac{\pi}{6} + \alpha_1}^{\omega t} v_r d(\omega t) = \frac{1}{\omega L_r} \int_{\frac{\pi}{6} + \alpha_1}^{\omega t} 3V_m \cos(\omega t - \pi / 6) d\omega t$$

or

$$= \frac{3V_m}{\omega L_r} [\sin(\omega t - \pi / 6) - \sin \alpha_1]$$

The circulating current becomes maximum when $\omega t = \frac{2\pi}{3}$ and $\alpha_1 = 0$. Therefore,

$$(i_r)_{\max} = \frac{3V_m}{\omega L_r} (1 - \sin \alpha_1) \quad (4.81)$$

or

$$(i_r)_{\max} = \frac{\sqrt{3}V_{ml}}{\omega L_r} (1 - \sin \alpha_1) \quad (4.82)$$

where V_{ml} = maximum value of line voltage.

4.7 EFFECT OF SOURCE IMPEDANCE

The two main effects of source impedance on performance of converters are:

1. It causes the outgoing and incoming thyristors to conduct together because the transfer of current from outgoing thyristors to incoming thyristors is not instantaneous; rather, it is gradual.
2. Average output voltage v_o of the converters reduce; therefore, the power factor also reduces.

If the source impedance is purely resistive (i.e., $Z_s = r_s$), then there will be a voltage drop across the source resistance, and the average output voltage of the converter is reduced by an amount $I_0 \cdot r_s$ for a single-phase converter and by $2I_0 \cdot r_s$ for a three-phase converter, where I_0 is the constant DC load current, and r_s is the source resistance per phase.

But if the source impedance is purely inductive, then the transfer of current from the outgoing thyristor to the incoming thyristor will not be instantaneous. As a result, outgoing and incoming thyristors conduct together for a period called the overlap period in seconds or overlap angle (μ) or commutation angle in degrees or radians. During this period, the average output voltage v_o is zero. *In general, the average output voltage v_o gets reduced by an amount*

$$\frac{m\omega L_s \cdot I_0}{2\pi}$$

where m = number of pulse converters, I_0 = load current, and L_s = source inductance.

4.7.1 SINGLE-PHASE FULLY CONTROLLED RECTIFIER WITH SOURCE AND LOAD INDUCTANCE

The operation of a single-phase full converter can be understood by using an equivalent circuit, shown in [Figure 4.20a](#) [3–6].

Working: The load current is assumed constant. When terminal P of the source voltage v_s is positive, load current i_l flows through L_s , T_1 , load, and T_2 as shown in [Figure 4.20b](#). Similarly, when terminal Q of the source

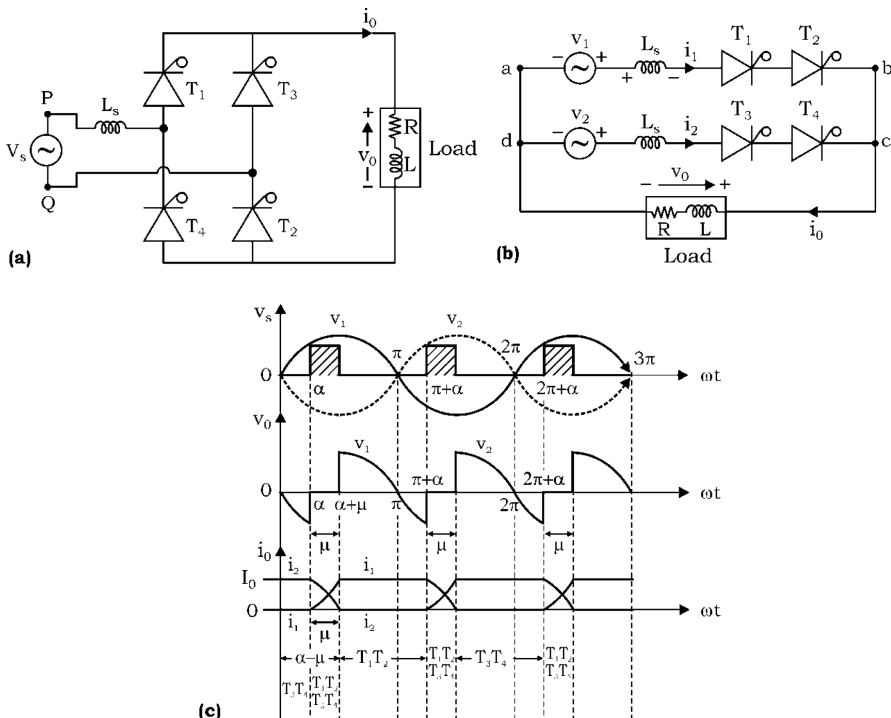


FIGURE 4.20 Single-phase full converter with source and load inductance: (a) single-phase full converter with source and load inductance, (b) equivalent circuits, and (c) waveforms.

voltage v_s is positive, the load current i_2 flows through T_3 , load, T_4 , L_s , and V_s . At $\omega t = \alpha_1$, thyristor T_1 and T_2 are fired. The thyristors T_1 and T_2 conduct up to $\pi + \alpha$, as shown in Figure 4.20c. The current cannot be transferred instantaneously from an already conducting (outgoing thyristor) thyristor T_3 , T_4 to incoming thyristors T_1 , T_2 due to the presence of source inductance, that is, current through outgoing thyristors T_3 and T_4 decreases gradually to zero from its initial value I_0 ; whereas through incoming thyristor T_1 and T_2 , the current rises gradually from zero to a full-load current I_o . The period for which all the incoming and outgoing thyristors (T_1 , T_2 , T_3 , T_4) conducts is called the overlap period or overlap angle (μ).

Analysis: During the overlap angle μ , KVL for loop abcd of Figure 4.20b gives,

$$v_1 - L_s \frac{di_1}{dt} = v_2 - L_s \frac{di_2}{dt}$$

or

$$v_1 - v_2 = L_s \left(\frac{di_1}{dt} - \frac{di_2}{dt} \right)$$

If $v_1 = V_m \sin \omega t$, than $v_2 = -V_m \sin \omega t$

$$\therefore 2V_m \sin \omega t = L_s \left(\frac{di_1}{dt} - \frac{di_2}{dt} \right) \quad (4.83)$$

Since the load current is assumed constant, during the overlap period μ ,

$$i_1 + i_2 = I_0$$

or

$$\frac{di_1}{dt} + \frac{di_2}{dt} = 0 \quad (4.84)$$

From Equation (4.83),

$$\frac{di_1}{dt} - \frac{di_2}{dt} = \frac{2V_m}{L_s} \sin \omega t \quad (4.85)$$

Adding Equations (4.84) and (4.85), we get

$$\frac{di_1}{dt} = \frac{V_m}{L_s} \sin \omega t \quad (4.86)$$

During the overlap period μ (Figure 4.20c), load current i_1 through T_1, T_2 rises from zero to I_0 , that is, at $\omega t = \alpha$, $i_1 = 0$ and at $\omega t = (\alpha + \mu)$, $i_1 = I_0$

$$\therefore \int_0^{I_0} di_1 = \frac{V_m}{L_s} \int_{\alpha/\omega}^{(\alpha+\mu)/\omega} \sin \omega t \, dt$$

or

$$I_0 = \frac{V_m}{\omega L_s} \left[\cos \alpha - \cos (\alpha + \mu) \right] \quad (4.87)$$

During the overlap period μ , because all the thyristors conduct, the output voltage $V_0 = 0$. Therefore, the average output voltage,

$$V_0 = \frac{1 \times 2}{2\pi} \int_{(\alpha+\mu)}^{(\pi+\alpha)} V_m \sin \omega t \, d\omega t$$

or

$$= \frac{V_m}{\pi} \left[-\cos \omega t \right]_{\alpha+\mu}^{\pi+\alpha}$$

$$V_0 = \frac{V_m}{\pi} \left[\cos \alpha + \cos (\alpha + \mu) \right] \quad (4.88)$$

From Equation (4.87),

$$\cos(\alpha + \mu) = \cos\alpha - \frac{\omega L_s}{V_m} I_0$$

Substituting the value of $\cos(\alpha + \mu)$ in Equation (4.88), we get

$$V_0 = \frac{2V_m}{\pi} \cos\alpha - \frac{\omega L_s}{\pi} I_0 \quad (4.89)$$

Therefore, it can be concluded that as the load current or source inductance increases, overlap angle μ increases, and as a result, the average output voltage decreases.

If I_o or L_s increases μ also increases and so V_0 decreases

In general, for the m -pulse converter, a reduction in the average output voltage due to source inductance (i.e., overlap angle μ) is

$$\frac{m\omega L_s \cdot I_0}{2\pi}$$

For example,

- For the two-pulse converter ($m = 2$), voltage drops due to $L_s = \frac{\omega L_s}{\pi} I_0$
- For the six-pulse converter ($m = 6$), voltage drops due to $L_s = \frac{3\omega L_s}{\pi} I_0$

Therefore, the output voltage for the $3 - \phi$ full converter when the source inductance L_s is taken into account,

$$V_0 = \frac{3V_{m1}}{\pi} \cos\alpha - \frac{3\omega L_s}{\pi} I_0 \quad (4.90)$$

or

$$V_o = \frac{3V_{m1}}{\pi} \cos(\alpha + \mu) + \frac{3\omega L_s}{\pi} I_0 \quad (4.91)$$

4.8 SOLVED PROBLEMS

Example 4.1: A single-phase half-wave-controlled rectifier has a purely resistive load of R . Calculate (a) rectification efficiency, (b) the FF, (c) the RF, (d) TUF, and (e) PIV of thyristor T , for delay angles of 45° and 90° .

SOLUTION

For delay angle $\alpha = 45^\circ$: For $1 - \phi$ half-wave-controlled rectifier, the average output voltage V_0 is,

$$V_0 = \frac{V_m}{2\pi} (1 + \cos\alpha)$$

$$\therefore V_0 = \frac{V_m}{2\pi} (1 + \cos 45^\circ) = 0.2718 V_m$$

The average load current,

$$I_0 = \frac{V_0}{R} = \frac{0.2718 V_m}{R}$$

The RMS output voltage,

$$V_{\text{rms}} = \frac{V_m}{2} \left[\frac{1}{\pi} \left(\pi - \alpha + \frac{\sin 2\alpha}{2} \right) \right]^{\frac{1}{2}}$$

$$\therefore V_{\text{rms}} = \frac{V_m}{2} \left[\frac{1}{\pi} \left(\pi - \frac{\pi}{4} + \frac{\sin 90^\circ}{2} \right) \right]^{\frac{1}{2}}$$

$$= \frac{V_m}{2} \left[\frac{3}{4} + 0.5 \right]^{\frac{1}{2}}$$

$$= 0.5590 V_m$$

RMS load current,

$$V_{\text{rms}} = \frac{V_{\text{rms}}}{R} = \frac{0.5590}{R} V_m$$

output DC power,

$$P_0 = V_o I_o = \frac{(0.2718 V_m)^2}{R}$$

output AC power,

$$P_{\text{ac}} = V_{\text{rms}} I_{\text{rms}} = \frac{(0.5590 V_m)^2}{R}$$

Now,

1. Rectification efficiency,

$$\eta = \frac{P_o}{P_{\text{ac}}} = \frac{(0.2718 V_m)^2}{(0.5590 V_m)^2} \times 100 = 48.62\%$$

2. FF,

$$FF = \frac{V_{\text{rms}}}{V_0} = \frac{0.5590 V_m}{0.2718 V_m} = 2.056 \text{ or } 205.66\%$$

3. RF,

$$RF = \frac{V_{\text{ac}}}{V_0} = \sqrt{\frac{V_{\text{rms}}^2 - V_0^2}{V_o}} = \sqrt{\left(\frac{V_{\text{rms}}^2}{V_o} \right)^2 - 1}$$

$$= \sqrt{(2.056)^2 - 1} = \sqrt{(FF)^2 - 1}$$

$$= 1.796 \text{ or } 179.6\%$$

4. RMS voltage of transformer secondary, V_s

$$V_s = \frac{V_m}{\sqrt{2}} = 0.707 V_m$$

RMS value of transformer secondary current is the same as that of load, I_s

$$\therefore I_s = I_{\text{rms}} = \frac{0.5590 V_m}{R}$$

\therefore VA rating of transformer, $VA = V_s I_s = 0.707 V_m \times \frac{0.5590 V_m}{R}$

$$\text{Now, TUF} = \frac{P_0}{V_s I_s} = \frac{(0.2718 V_m)^2}{0.707 V_m \times 0.5590 V_m} = 0.186$$

PF is approximately equal to TUF. Thus, $PF = 0.186$

5. PIV = V_m

For delay angle $\alpha = 90^\circ$: For $1 - \phi$ half-wave-controlled rectifier with R load and delay angle $\alpha = 90^\circ$:

$$V_o = \frac{V_m}{2\pi} (1 + \cos\alpha) = 0.1592 V_m$$

$$I_0 = \frac{V_o}{R} = \frac{0.1572 V_m}{R}$$

$$V_{\text{rms}} = \frac{V_m}{2} \left[\frac{1}{\pi} \left(\pi - \frac{\pi}{2} + \frac{\sin 180^\circ}{2} \right) \right]^{\frac{1}{2}}$$

$$= \frac{V_m}{2} \left[\frac{1}{\pi} \left(\frac{\pi}{2} \right) \right]^{\frac{1}{2}}$$

$$= 0.3536 V_m$$

$$I_{\text{rms}} = \frac{V_{\text{rms}}}{R} = \frac{0.3536 V_m}{R}$$

output DC power,

$$P_0 = V_0 I_0 = \frac{(0.1592 V_m)^2}{R}$$

output AC power, $P_{ac} = V_{\text{rms}} I_{\text{rms}}$

$$= \frac{(0.3536 V_m)^2}{R}$$

Now,

(a) Rectification efficiency,

$$\eta = \frac{P_0}{P_{ac}} = \frac{(0.1592 V_m)^2}{(0.3536 V_m)^2} = 20.27\%$$

(b) FF,

$$FF = \frac{V_{rms}}{V_0} = \frac{0.3536 V_m}{0.1592 V_m} = 2.221 \text{ or } 222.1\%$$

$$(c) RF = \sqrt{(FF)^2 - 1}$$

$$= \sqrt{(2.221)^2 - 1} = 1.983 \text{ or } 198.3\%$$

$$(d) TUF = \frac{P_0}{V_s I_s} = \frac{(0.1592 V_m)^2 / R}{0.707 V_m \times \left(\frac{0.3536 V_m}{R} \right)} = 0.1014$$

PF is approximately equal to TUF. Thus, PF = 0.1014.

(e) PIV = V_m .

Example 4.2: A single-phase 220 V, 1 kW heater is connected across a one-phase, 220-V, 50-Hz supply through an SCR. For firing angle delays of 45° and 90°, calculate the power absorbed in the heater element.

SOLUTION

$$\text{Heater resistance, } R = \frac{V^2}{P} = \frac{(220)^2}{1000} = 48.4 \Omega$$

Because it is a half-wave controlled rectifier, the RMS output voltage is,

$$V_{rms} = \frac{V_m}{2\sqrt{\pi}} \left[(\pi - \alpha) + \frac{1}{2} \sin 2\alpha \right]^{\frac{1}{2}}$$

∴ value of rms voltage for $\alpha = 45^\circ$ is

$$V_{rms} = \frac{\sqrt{2} \cdot 220}{2\sqrt{\pi}} \left[\left(\pi - \frac{\pi}{4} \right) + \frac{1}{2} \sin 90^\circ \right]^{\frac{1}{2}} = 149 \text{ V}$$

∴ Power absorbed by heater element for $\alpha = 45^\circ$ is

$$= 458 \text{ W}$$

For $\alpha = 90^\circ$, RMS voltage is

$$V_{rms} = \frac{\sqrt{2} \cdot 220}{2\sqrt{\pi}} \left[\left(\pi - \frac{\pi}{2} \right) + 0 \right]^{\frac{1}{2}} = 110 \text{ V}$$

∴ Power absorbed for $\alpha = 90^\circ$ is

$$\frac{V_{rms}^2}{R} = \frac{(110)^2}{48.4} = 250 \text{ watt}$$

Example 4.3: A 220-V, 50-Hz, one-pulse SCR-controlled converter is gated at a firing angle of 60° , and the load current extinguishes at an angle of 220° . Determine the circuit turn-off time, average output voltage, and average load current for $R = 7 \Omega$ and $L = 3mH$.

SOLUTION

Since it is a one-pulse SCR-controlled converter, that is, $1 - \phi$ half-wave-controlled rectifier with RL load (discontinuous conduction),

therefore, the circuit turn-off t_c for the SCR is:

$$t_c = \frac{2\pi - \beta}{\omega} = \frac{(360 - 220)\pi}{180 \times 2\pi \times 50} = 7.777 \text{ m-sec.}$$

Average output voltage V_o is:

$$\begin{aligned} V_o &= \frac{V_m}{2\pi} (\cos \alpha - \cos \beta) \\ &= \frac{\sqrt{2} \cdot 220}{2\pi} (\cos 60^\circ - \cos 220^\circ) \\ &= 62.722 \text{ V} \end{aligned}$$

$$\text{Average load current, } I_0 = \frac{V_o}{R} = \frac{62.722}{7} = 8.96 \text{ A}$$

Example 4.4: A single-phase full converter is connected to a 200-V, 50-Hz supply. Assume the load current is continuous and ripple free. The turn ratio of the transformer is unity. (a) Express the input current in a Fourier series; determine HF of input current, DF, and input PF. (b) For the delay angles of $\alpha = 45^\circ$ and 60° , calculate V_o , $V_{n'}$, V_{rms} , HF, DF, and PF.

SOLUTION

- (a) For single-phase full converter, instantaneous input current can be expressed in a Fourier series as

$$i_s(t) = a_o + \sum_{n=1,2,\dots}^{\infty} (a_n \cos n\omega t + b_n \sin n\omega t)$$

where

$$\begin{aligned} a_o &= \frac{1}{2\pi} \int_{\alpha}^{2\pi+\alpha} i_s(t) d(\omega t) = \frac{1}{2\pi} \left[\int_{\alpha}^{\pi+\alpha} I_o d(\omega t) - \int_{\pi+\alpha}^{2\pi+\alpha} I_o d(\omega t) \right] = 0 \\ a_n &= \frac{1}{\pi} \int_{\alpha}^{2\pi+\alpha} i_s(t) \cos n\omega t d(\omega t) \\ &= \frac{1}{\pi} \left[\int_{\alpha}^{\pi+\alpha} I_0 \cos n\omega t d(\omega t) - \int_{\pi+\alpha}^{2\pi+\alpha} I_0 \cos n\omega t d(\omega t) \right] \end{aligned}$$

$$= -\frac{4I_o}{n\pi} \sin n\alpha \quad \text{for } n = 1, 3, 5, \dots$$

$$= 0 \text{ for } n = 2, 4, \dots$$

$$b_n = \frac{1}{\pi} \int_{\alpha}^{2\pi+\alpha} i(t) \sin n\omega t d(\omega t)$$

$$= \frac{1}{\pi} \left[\int_{\alpha}^{\pi+\alpha} I_0 \sin n\omega t d(\omega t) - \int_{\pi+\alpha}^{2\pi+\alpha} I_0 \sin n\omega t d(\omega t) \right]$$

$$= -\frac{4I_o}{n\pi} \cos n\alpha \text{ for } n = 1, 3, 5, \dots$$

$$= 0 \text{ for } n = 2, 4, \dots$$

Because $a_0 = 0$, the input current can be expressed as

$$i_s(t) = \sum_{n=1,3,5}^{\infty} \sqrt{2} I_n \sin(n\omega t + \phi_n)$$

where

$$\phi_n = \tan^{-1} \frac{a_n}{b_n} = -n\alpha \quad (4.92)$$

and ϕ_n is the displacement angle of nth harmonic current. The RMS value of the nth harmonic input current is

$$I_{sn} = \frac{1}{\sqrt{2}} \left(a_n^2 + b_n^2 \right)^{\frac{1}{2}} = \frac{4I_0}{\sqrt{2}n\pi} = \frac{2\sqrt{2} I_0}{n\pi} \quad (4.93)$$

and the RMS value of the fundamental current is

$$I_{s1} = \frac{2\sqrt{2} I_0}{\pi}$$

The RMS value of the input current can be calculated from Equation (4.93) as

$$I_s = \left(\sum_{n=1,3,5}^{\infty} I_{sn}^2 \right)^{\frac{1}{2}}$$

I_s can also be determined directly from

$$I_s = \left[\frac{2}{2\pi} \int_{\alpha}^{\pi+\alpha} I_0^2 d(\omega t) \right]^{\frac{1}{2}} = I_0$$

The HF is found as

$$HF = \left[\left(\frac{I_s}{I_{s1}} \right)^2 - 1 \right]^{\frac{1}{2}} = 0.483 \text{ or } 48.3\%$$

It is also called the total harmonic distortion (THD)
The displacement factor

$$DF = \cos\phi_l = \cos(-\alpha) \quad (4.94)$$

The power factor PF is found as

$$PF = \frac{I_{s1}}{I_s} \cos\phi_l = \frac{I_{s1}}{I_s} \cos(-\alpha) = \frac{2\sqrt{2}}{\pi} \cos\alpha \quad (4.95)$$

(b) For delay angle $\alpha = 45^\circ$:

For $1 - \phi$ full converter with RL load, the average output voltage V_0 is:

$$V_0 = \frac{2V_m}{\pi} \cos\alpha = V_{0m} \cos\alpha$$

$$= \frac{2\sqrt{2} \times 200}{\pi} \cos 45^\circ = 127.39 \text{ V}$$

The normalized average output voltage, V_n is

$$V_n = \frac{V_0}{V_{0m}} = \cos\alpha$$

where, V_{0m} is the maximum average output voltage.

$$\therefore V_n = \cos 45^\circ = 0.707 \text{ pu}$$

The RMS output voltage, $V_{rms} = \frac{V_m}{\sqrt{2}} = V_s = 200 \text{ V}$

The RMS value of the fundamental input current is

$$I_{s1} = \frac{2\sqrt{2} I_0}{\pi} = 0.90078 I_o \text{ and } I_o = I_s$$

$$HF = \left[\left(\frac{I_s}{I_{s1}} \right)^2 - 1 \right]^{\frac{1}{2}}$$

$$= \left[\left(\frac{I_o}{0.90078 I_o} \right)^2 - 1 \right]^{\frac{1}{2}} = 0.4820 \text{ or } 48.20\%$$

$$\phi_l = -\alpha \text{ and } DF = \cos(-\alpha) = 0.707$$

$$PF = \frac{I_{s1}}{I_s} \cos(-\alpha)$$

$$= \frac{0.90078 I_0}{I_0} \cos\left(-\frac{\pi}{4}\right)$$

$$= 0.637 \text{ (lagging)}$$

For delay angle $\alpha = 60^\circ$:

For $1 - \phi$ full converter with RL load, the average output voltage V_0 is

$$\begin{aligned} V_0 &= \frac{2V_m}{\pi} \cos\alpha = V_{om} \cos\alpha \\ &= \frac{2\sqrt{2} \times 200}{\pi} \cos 60^\circ = 180.15 \cos 60^\circ \\ &= 90.078 \text{ V} \end{aligned}$$

$$V_n = \frac{V_0}{V_{om}} \cos\alpha = 0.5 \text{ pu}$$

$$V_{nns} = \frac{V_m}{\sqrt{2}} = V_S = 200 \text{ V}$$

$$I_{s1} = \frac{2\sqrt{2} I_0}{\pi} = 0.90078 I_o$$

$$I_s = I_0$$

$\therefore HF,$

$$HF = \left[\left(\frac{I_s}{I_{s1}} \right)^2 - 1 \right]^{\frac{1}{2}} = 0.4820 \text{ or } 48.20\%$$

$$\phi_l = -\alpha \text{ and } DF = \cos(-\alpha) = \cos = 0.5$$

$$PF = \frac{I_{s1}}{I_s} \cos(-\alpha) = 0.45 \text{ (lagging)}$$

Example 4.5: A single-phase full-bridge converter is connected to the RL load. The input AC voltage is 220 V, 50 Hz. The average load current of 20 A is continuous. For $R = 0.4 \Omega$ and $L = 3 \text{ mH}$. Calculate:

- (a) Firing angle delay α . Sketch the time variations of output voltage and load current for the above rectifier.
- (b) In case the output current is assumed constant, find the input PF for the above case.

SOLUTION

- (a) For $1 - \phi$ full-converter bridge with RL load, the average output voltage V_0 is given as:

$$V_0 = \frac{2V_m}{\pi} \cos\alpha = I_0 R$$

or

$$\frac{2\sqrt{2} \cdot 220}{\pi} \cos\alpha = 20 \times 0.4$$

or

$$\cos\alpha = 0.040369$$

or

$$\alpha = \cos^{-1}(0.040369) = 87.68^\circ$$

For $\alpha = 87.68^\circ$, the power flows from the AC source to the DC load.

Output voltage and load current waveforms for $\alpha = 87.68^\circ$ can be drawn by referring to Figure 4.9b.

- (b) For constant load current, the RMS value of the load current I_{rms} is:

$$I_{rms} = I_0 = 20 \text{ A}$$

$$\therefore V_s \cdot I_{rms} \cos\phi = I_{rms}^2 R$$

$$\text{For } \alpha = 87.68^\circ, \text{ input PF, } \cos\phi = \frac{(20)^2 \times 0.4}{220 \times 10} = 0.073 \text{ (lagging)}$$

Example 4.6:

- (a) A single-phase full converter delivers power to a resistive load R . For AC-source voltage V_s , show that the average output voltage V_o is given by

$$V_o = \frac{V_m}{\pi} (1 + \cos\alpha)$$

Sketch the time variations of the source voltage, output voltage, output current, and voltage across one pair of SCRs. Hence, find from there the circuit turn-off time.

- (b) For the converter of part (a), show that the RMS value of the output current is given by

$$I_{rms} = \frac{V_m}{\sqrt{2}R} \left[\frac{1}{\pi} \left\{ (\pi - \alpha) + \frac{1}{2} \sin 2\alpha \right\} \right]^{\frac{1}{2}}$$

SOLUTION

- (a) Time variations of source voltage, load voltage, and load current are shown in Figure 4.21. At $\omega t = \pi$, $v_0 = v_s = 0$ and for resistive load R ,

$$i_s = \frac{V_s}{R} = 0 \quad \text{and} \quad i_0 = \frac{V_s}{R} = 0$$

Soon after $\omega t = \pi$, supply voltage reverse biases T_1, T_2 ; this pair is therefore turned off. When T_3, T_4 is triggered at $\omega t = \pi + \alpha$, output voltage v_0 becomes equal to v_s up to $\omega t = 2\pi$. No SCR conducts during 0 to α , π to $(\pi + \alpha)$ and so on (Figure 4.21). For the output voltage waveform v_0 , the average output voltage V_o is

$$V_o = \frac{1 \times 2}{2\pi} \int_{\alpha}^{\pi} V_m \sin \omega t \cdot d(\omega t)$$

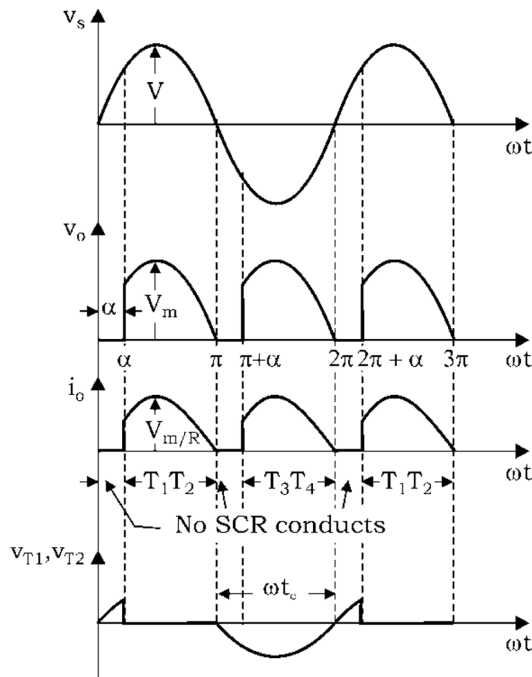


FIGURE 4.21 Various waveforms for Example 4.6.

$$= \frac{V_m}{\pi} (1 + \cos \alpha)$$

- (b) The RMS value of the output current can be obtained from the waveform i_o shown in Figure 4.21.

$$\begin{aligned} I_{\text{rms}} &= \left[\frac{1 \times 2}{2\pi} \int_{\alpha}^{\pi} \left(\frac{V_m}{R} \sin \omega t \right)^2 d(\omega t) \right]^{\frac{1}{2}} \\ &= \frac{V_m}{\sqrt{2}R} \left[\frac{1}{\pi} \int_{\alpha}^{\pi} (1 - \cos 2\omega t) d(\omega t) \right]^{\frac{1}{2}} \\ &= \frac{V_m}{\sqrt{2}R} \left[\frac{1}{\pi} \left\{ (\pi - \alpha) + \frac{1}{2} \sin 2\alpha \right\} \right]^{\frac{1}{2}} \end{aligned}$$

Example 4.7

- (a) A single-phase-controlled bridge rectifier consists of one SCR and three diodes as shown in Figure 4.22. Sketch the output voltage waveform for a firing angle α and hence obtain an expression for the average output

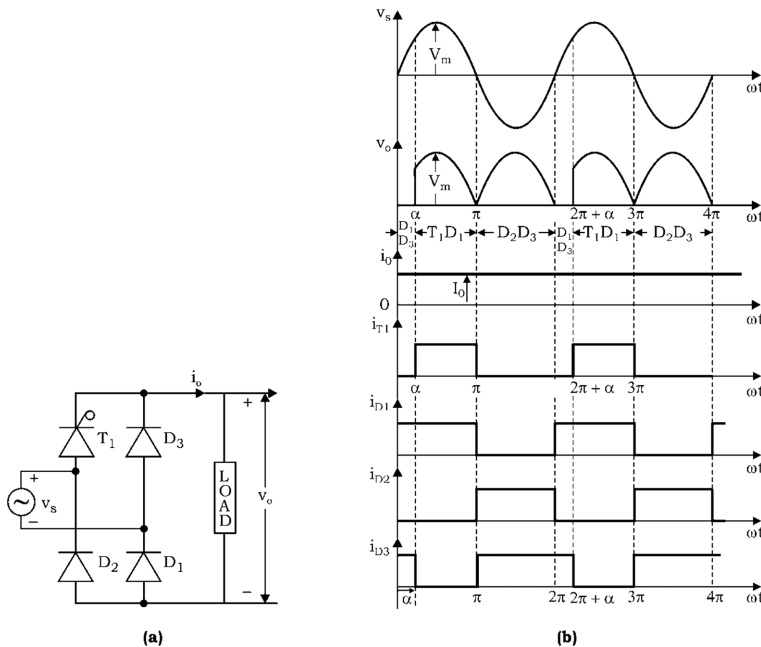


FIGURE 4.22 (a) Circuit diagram for Example 4.7 and (b) various voltage and current waveforms.

voltage. Show the conduction of various components as well. Assume continuous current.

- Draw waveforms of current through T_1 , D_1 , D_2 , and D_3 assuming a constant load current.
- For an AC-source voltage of 220 V, 50 Hz and firing angle of 60° , find the average output current and power delivered to the load if the case load consists of $R = 10 \Omega$, $L = 12 \text{ mH}$.

SOLUTION

- For circuit of Figure 4.19a, the output voltage waveform v_o is shown in Figure 4.22b. The average value of v_o is given by

$$V_0 = \frac{1}{2\pi} \left[\int_{\alpha}^{\pi} V_m \sin \omega t \cdot d(\omega t) - \int_{\pi}^{2\pi} V_m \sin \omega t \cdot d(\omega t) \right]$$

$$= \frac{V_m}{2\pi} [3 + \cos \alpha]$$

- The conduction of various elements shown help in drawing the waveforms for currents through T_1 , D_1 , D_2 , and D_3 . For example, D_3 conducts from $\omega t = 0$ to α , from π to $2\pi + \alpha$, from 3π to $4\pi + \alpha$ and so on; this is shown as i_{D3} in Figure 4.22b.

$$(c) V_0 = \frac{\sqrt{2} \cdot 220}{2 \cdot \pi} (3 + \cos 60^\circ) = 173.40 \text{ V}$$

$$I_0 = \frac{173.40}{10} = 17.34 \text{ A}$$

Power delivered to load,

$$V_0 I_0 = \frac{173.40 \times 17.34}{1000} = 3 \text{ kW}$$

Example 4.8: Find the average value of load current for a single-phase full converter feeding power to the RL load with $R = 7 \Omega$, $L = 7 \text{ mH}$; input voltage of 220 V, 50 Hz for delay angle of 60° . Assume continuous conduction.

In the case where one of the four SCRs gets open circuited due to a fault, determine the new value of the load current. Sketch the waveform for the new output voltage, and indicate the conduction of various SCRs.

SOLUTION

Average output voltage V_0 for $1 - \phi$ full converter is given by:

$$\begin{aligned} V_0 &= \frac{2V_m}{\pi} \cos \alpha = \frac{2\sqrt{2} \cdot 220}{\pi} \cos 60^\circ \\ &= 99.09 \text{ V} \end{aligned}$$

Average value of load current,

$$I_0 = \frac{V_0}{R} = \frac{99.09}{7} = 14.15 \text{ A}$$

Suppose SCR T_4 in Figure 4.9a is damaged and is open circuited. With this, the output voltage waveform v_o is as shown in Figure 4.23. Initially, suppose T_1 , T_2 are conducting from α to $\pi + \alpha$. At $\omega t = \pi + \alpha$, when T_3 , T_4 are gated, only T_3 is turned

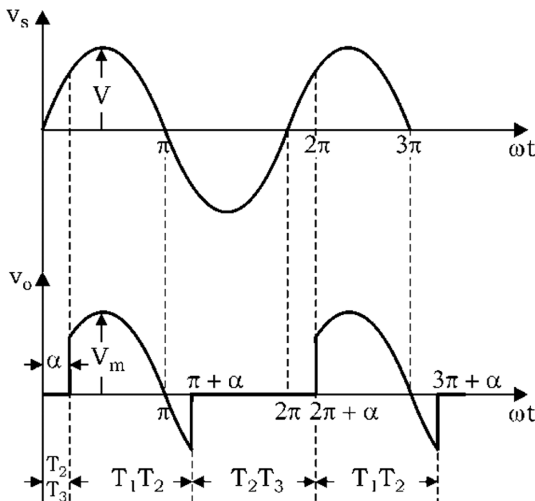


FIGURE 4.23 Various voltage waveforms for Example 4.8.

on, and as a result, the load current freewheels through T_2 , T_3 and therefore v_0 is zero till T_1 , T_2 are triggered again at $\omega t = 2\pi + \alpha$. For this waveform, the average output voltage is given by

$$V_0 = \frac{1 \times 1}{2\pi} \int_{\alpha}^{\pi+\alpha} V_m \sin \omega t \cdot d(\omega t) = \frac{V_m}{\pi} \cos \alpha$$

$$V_o = \frac{\sqrt{2} \cdot 220}{\pi} \cos 60^\circ = 49.54 \text{ V}$$

and average load current, $I_0 = \frac{49.54}{7} = 7.08 \text{ A}$.

It is seen that the load current is reduced with one SCR becomes open circuited. It is also observed that thyristor T_2 remains on.

Example 4.9: A three-phase half-wave converter is operated from a three-phase Y-connected 208-V, 50-Hz supply, and the load resistance is $R = 20 \Omega$. It is required to obtain an average output voltage of 50% of the maximum possible output voltage. Determine (a) delay angle α , (b) RMS and average output currents, (c) average and RMS thyristor currents, (d) rectification efficiency, (e) TUF, and (f) input PF.

SOLUTION

Given: The phase voltage is $V_s = \frac{208}{\sqrt{3}} = 120.1 \text{ V}$
(as Y-connected supply)

$$V_m = \sqrt{2} V_s = 169.83 \text{ V},$$

$$V_n = \frac{V_0}{V_{0m}} = \frac{50\% \text{ of } V_{0m}}{V_{0m}} = 0.5$$

$$R = 20 \Omega.$$

The maximum output voltage of a three-phase half-wave converter is,

$$V_{0m} = \frac{3\sqrt{3} V_m}{2\pi} = 3\sqrt{3} \times \frac{169.83}{2\pi} = 140.45 \text{ V}$$

The average output voltage,

$$V_0 = V_{0m} \times V_n$$

$$= 140.45 \times 0.5 = 70.23 \text{ V}$$

Now:

- (a) For a resistive load, the load current is continuous if $\alpha \leq \frac{\pi}{6}$ and, the equation for normalized average output voltage $v_n (= \frac{V_0}{V_{0m}} = \cos \alpha)$ gives $V_n \geq \cos(\frac{\pi}{6}) = 86.6\%$. With a resistive load and 50% output, the load current is discontinuous.

For a resistive load $\alpha \geq \frac{\pi}{6}$ and average output voltage $V_0 = \frac{3V_m}{2\pi} [1 + \cos(\frac{\pi}{6} + \alpha)]$,

and

$$V_n = \frac{V_o}{V_{om}} = \frac{1}{\sqrt{3}} \left[1 + \cos\left(\frac{\pi}{6} + \alpha\right) \right]$$

$$\therefore 0.5 = \frac{1}{\sqrt{3}} \left[1 + \cos\left(\frac{\pi}{6} + \alpha\right) \right]$$

or

$$\frac{\pi}{6} + \alpha = \cos^{-1}(-0.134)$$

or

$$\alpha = 97.699^\circ - 30^\circ = 67.69^\circ$$

\therefore Delay angle $\alpha = 67.69^\circ$

- (b) The average output current,

$$I_0 = \frac{V_o}{R} = \frac{70.23}{20} = 3.51 \text{ A}$$

The RMS output voltage,

$$V_{rms} = \sqrt{3} V_m \left[\frac{5}{24} - \frac{\alpha}{4\pi} + \frac{1}{8\pi} \sin\left(\frac{\pi}{3} + 2\alpha\right) \right]^{\frac{1}{2}}$$

$$= 94.74 \text{ V}$$

The RMS output current,

$$I_{rms} = \frac{V_{rms}}{R} = 4.74 \text{ A}$$

- (c) The average current of thyristor I_A is:

$$I_A = \frac{I_0}{3} = \frac{3.51}{3} = 1.17 \text{ A}$$

The RMS current of thyristor I_R is

$$I_A = \frac{I_0}{\sqrt{3}} = \frac{3.51}{\sqrt{3}} = 2.74 \text{ A}$$

- (d) The rectification efficiency, $\eta = \frac{V_0 I_0}{V_{rms} I_{rms}}$

$$= \frac{70.23 \times 3.51}{94.74 \times 4.74} \times 100$$

$$= 54.9\%$$

- (e) TUF = $\frac{V_0 I_0}{VI} = \frac{V_0 I_0}{3V_s I_s}$

$$= \frac{70.23 \times 3.51}{3 \times 120.1 \times 2.74} = 0.249 \text{ or } 24.96\%$$

(∴ RMS input line current I_s is same as the thyristor RMS current I_R)

$$(f) \text{ The input } PF = \frac{P_0}{VI} = \frac{I_{\text{rms}}^2 \cdot R}{3V_s I_s} = \frac{(4.74)^2 \times 20}{3 \times 120.1 \times 2.74} = 0.455 \text{ (lagging)}$$

Example 4.10: Repeat Example 4.9 for the three-phase full converter with RL load.

SOLUTION

The phase voltage $V_s = 120.1$, $V_m = V_s = 169.83$, $V_n = 0.5$, and $R = 20 \Omega$. The maximum output voltage $V_{0m} = 3 V_m / \pi = 3 \times 169.83 / \pi = 280.9 \text{ V}$; average output voltage $V_o = 0.5 \times 280.9 = 140.45 \text{ V}$.

$$(a) \text{ We know that normalized average output voltage, } V_n = \frac{V_o}{V_{0m}} = \cos \alpha$$

$$\therefore 0.5 = \cos \alpha$$

or

$$\alpha = \cos^{-1}(0.5) = 60^\circ$$

∴ Delay angle, $\alpha = 60^\circ$

(b) The average output current,

$$I_o = \frac{V_o}{R} = \frac{140.45}{20} = 7.02 \text{ A}$$

The RMS output voltage V_{rms} is,

$$V_{\text{rms}} = \sqrt{3} V_m \left[\frac{1}{2} + \frac{3\sqrt{3}}{4\pi} \cos 2\alpha \right]^{\frac{1}{2}}$$

$$= \sqrt{3} \times 169.83 \left[\frac{1}{2} + \frac{3\sqrt{3}}{4\pi} \cos 120^\circ \right]^{\frac{1}{2}}$$

$$= 159.29 \text{ V}$$

$$I_{\text{rms}} = \frac{V_{\text{rms}}}{R} = \frac{159.29}{20} = 7.96 \text{ A}$$

(c) Average current of a thyristor

$$I_A = \frac{I_o}{3} = \frac{7.02}{3} = 2.34 \text{ A}$$

RMS current of a thyristor

$$I_R = \frac{I_{\text{rms}}}{\sqrt{3}} = \frac{7.96}{\sqrt{3}} = 4.6 \text{ A}$$

(d) The rectification efficiency,

$$\begin{aligned}\eta &= \frac{V_0 I_0}{V_{\text{rms}} I_{\text{rms}}} = \frac{140.45 \times 7.02}{159.29 \times 7.96} \times 100 \\ &= 77.76\%\end{aligned}$$

(e) RMS input line current

$$I_s = I_{\text{rms}} \sqrt{\frac{2}{3}} = 6.5 \text{ A}$$

$$\begin{aligned}\text{TUF} &= \frac{V_0 I_0}{VI} = \frac{V_0 I_0}{3V_s I_s} = \frac{140.45 \times 7.02}{3 \times 120.1 \times 65} \\ &= 0.420\end{aligned}$$

$$(f) \text{ The input PF} = \frac{P_0}{VI} = \frac{I_{\text{rms}}^2 \times R}{3V_s I_s} = 0.54 \text{ (lagging)}$$

Example 4.11: The load current of a three-phase full converter with RL load is continuous with a negligible ripple content. (a) Express the input current in Fourier series, and determine the HF of input current, the DF, and the input PF. (b) If the delay angle is 45° , calculate V_n , HF, DF, and PF.

SOLUTION

(a) The waveform for input current is shown in Figure 4.12c and the instantaneous input current of a phase in Fourier series can be expressed as:

$$i_s(t) = a_o + \sum_{n=1,2,\dots}^{\infty} (a_n \cos n\omega t + b_n \sin n\omega t)$$

where

$$a_0 = \frac{1}{2\pi} \int_0^{2\pi} i_s(t) d(\omega t) = 0$$

$$a_n = \frac{1}{\pi} \int_0^{2\pi} i_s(t) \cos n\omega t d(\omega t)$$

$$= \frac{1}{\pi} \left[\int_{\frac{\pi}{6}+\alpha}^{\frac{5\pi}{6}+\alpha} I_0 \cos n\omega t d(\omega t) - \int_{\frac{7\pi}{6}+\alpha}^{\frac{11\pi}{6}+\alpha} I_0 \sin n\omega t d(\omega t) \right]$$

$$= + \frac{4I_0}{n\pi} \sin \frac{n\pi}{3} \cos n\alpha \text{ for } n = 1, 3, 5, \dots$$

$$= 0 \text{ for } n = 2, 4, 6, \dots$$

$$b_n = \frac{1}{\pi} \int_0^{2\pi} i(t) \sin n\omega t d(\omega t)$$

$$= \frac{1}{\pi} \left[\int_{\frac{\pi}{6}+\alpha}^{\frac{5\pi}{6}+\alpha} I_0 \sin n\omega t d(\omega t) - \int_{\frac{7\pi}{6}+\alpha}^{\frac{11\pi}{6}+\alpha} I_0 \cos n\omega t d(\omega t) \right]$$

$$= - \frac{4I_0}{n\pi} \sin \frac{n\pi}{3} \sin n\alpha \text{ for } n = 1, 3, 5, \dots$$

$$= 0 \text{ for } n = 2, 4, 6, \dots$$

Because $a_0 = 0$ and the triplen harmonic currents (for $n = \text{multiple of 3}$) will be absent in a balanced three-phase supply, the input current can be written as

$$i_s(t) = \sum_{n=1,3,5,\dots}^{\infty} \sqrt{2} I_{sn} \sin(n\omega t + \phi_n) \text{ for } n = 1, 5, 7, 11, 13, \dots$$

where

$$\phi_n = \tan^{-1} \frac{a_n}{b_n} = -n\alpha \quad (4.96)$$

The RMS value of the nth harmonic input current is given by

$$I_{sn} = \frac{1}{\sqrt{2}} (a_n^2 + b_n^2)^{\frac{1}{2}} = \frac{2\sqrt{2}I_0}{n\pi} \sin \frac{n\pi}{3} \quad (4.97)$$

The RMS value of the fundamental current is

$$I_{s1} = \frac{\sqrt{6} I_0}{\pi} = 0.7797 I_0 \quad (4.98)$$

The RMS input current

$$I_s = \left[\frac{2}{2\pi} \int_{\frac{\pi}{6}+\alpha}^{\frac{5\pi}{6}+\alpha} I_0^2 d(\omega t) \right]^{\frac{1}{2}} = I_0 \sqrt{\frac{2}{3}} = 0.8165 I_0 \quad (4.99)$$

$$\text{HF} = \left[\left(\frac{I_s}{I_{s1}} \right)^2 - 1 \right]^{\frac{1}{2}} \left[\left(\frac{\pi}{3} \right)^2 - 1 \right]^{\frac{1}{2}} = 0.3108 \text{ or } 31.08\% \quad (4.100)$$

$$\text{DF} = \cos \phi_l = \cos(-\alpha) \quad (4.101)$$

$$\text{PF} = \frac{I_{s1}}{I_s} \cos(-\alpha) = \frac{3}{\pi} \cos \alpha = 0.9549 \text{ DF} \quad (4.102)$$

(b) For $\alpha = \frac{\pi}{4}$, $V_n = \cos\left(\frac{\pi}{4}\right) = 0.7 \text{ pu}$, HF = 31.08%, DF = $\cos 45^\circ = 0.7$, and PF = 0.68 (lagging).

Example 4.12: A single-phase dual converter is operated from a 200-V, 50-Hz supply, and the load resistance is $R = 20 \Omega$. The circulating inductance is $L_r = 50 \text{ mH}$; delay angles are $\alpha_1 = 50^\circ$ and $\alpha_2 = 130^\circ$. Find the peak circulating current and the peak current of converter 1.

SOLUTION

$\omega = 2\pi \times 50 = 314 \text{ rad/s}$, $\alpha_1 = 50^\circ$, $V_m = \sqrt{2} \times 200 = 282.85 \text{ V}$, $f = 50 \text{ Hz}$, and $L_r = 50 \text{ mH}$. Circulating current will be maximum at $\omega t = 2\pi$.

\therefore for $\omega t = 2\pi$ and $\alpha_1 = 50^\circ$, the peak circulating current

$$I_r(\max) = \frac{2V_m}{\omega L_r} (1 - \cos \alpha_1) = \frac{565.7 \times 1000}{314 \times 50} (1 - \cos 50^\circ) = 12.87 \text{ A}$$

The peak load current is $I_p = 282.85/20 = 14.15 \text{ A}$. The peak current of converter 1 is $= I_p + (I_r)_{\max} (14.15 + 12.87) = 27.01 \text{ A}$.

Example 4.13: A three-phase dual converter, operating in the circulating-current mode has the following data:

Per phase supply voltage = 220 V, $f = 50 \text{ Hz}$, $\alpha_1 = 50^\circ$, current-limiting reactor, $L = 20 \text{ mH}$. Find the peak value of the circulating current.

SOLUTION

The peak value of the circulating current, for firing angle $\alpha_1 = 50^\circ$, is given by equation $(i_r)_{\max} = \frac{\sqrt{3}V_m}{\omega L} [1 - \sin \alpha_1]$

$$\therefore (i_r)_{\max} = \frac{\sqrt{3} \cdot \sqrt{6} \cdot 220}{2\pi \times 50 \times 20 \times 10^{-3}} [1 - \sin 50^\circ] = 37.772 \text{ A.}$$

Example 4.14: A single-phase full converter is supplied from a 220-V, 50-Hz source. The load consists of $R = 8 \Omega$ and a large inductance so as to render the load current constant. For a firing angle delay of 60° , calculate (a) average output voltage (b) average output current (c) average and RMS values of thyristor currents, and (d) the power factor.

SOLUTION

The waveforms for source voltage v_s , load current i_o , load voltage v_o , thyristor current i_{T1} (or i_{T2}), and source current i_s (refer to Figure 4.9a) are drawn in Figure 4.24.

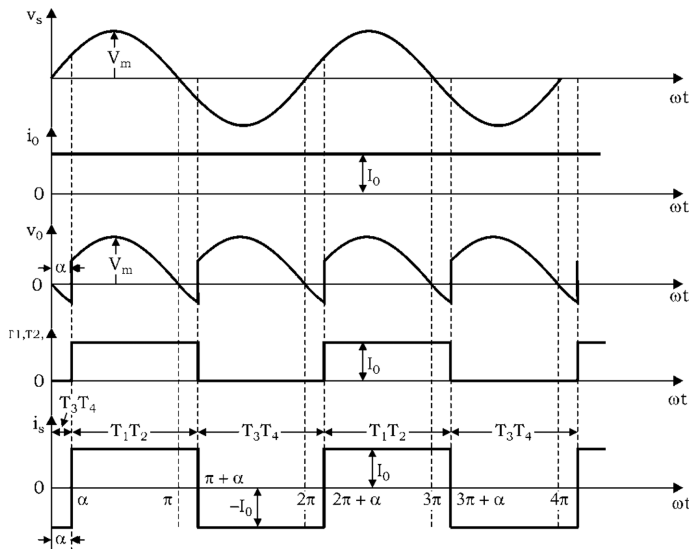


FIGURE 4.24 Various waveforms for Example 4.14.

$$(a) V_o = \frac{2V_m}{\pi} \cos \alpha = \frac{2\sqrt{2} \times 220}{\pi} \cos 60^\circ = 99.085 \text{ V}$$

$$(b) \text{Average output current, } I_0 = \frac{V_0}{R} = \frac{99.085}{8} = 12.38 \text{ A}$$

(c) It is seen from the waveform of thyristor current i_{T1} (or i_{T2}) that its average value is given by $(I_T)_{\text{avg.}} = I_0 \cdot \frac{\pi}{2\pi} = \frac{I_0}{2} = \frac{12.38}{2} = 6.192 \text{ A}$
The RMS value of the thyristor current is

$$(I_T)_{\text{rms}} = \sqrt{I_0^2 \cdot \pi \times \frac{1}{2\pi}} = \frac{I_0}{\sqrt{2}} = \frac{12.38}{\sqrt{2}} = 8.75 \text{ A}$$

$$(d) \text{RMS value of source current, } I_s = \sqrt{I_0^2 \cdot \frac{\pi}{\pi}} = I_0 = 12.38 \text{ A}$$

$$\text{Load power} = V_0 I_0 = 99.085 \times 12.38 \text{ W}$$

$$\text{Input power} = V_s I_s \cos \phi$$

For no loss in the power converter,

$$V_s I_s \cos \phi = V_0 I_0$$

$$\therefore \text{Power factor, } \cos \phi = \frac{99.085 \times 12.38}{220 \times 12.38} = 0.450 \text{ (lagging)}$$

In general, for a one-phase full converter with a ripple-free load current as in this example and with no device drops,
input power = load power
or

$$V_s I_s \cos \phi = V_0 I_0$$

$$\therefore \text{Input pf} = \frac{2V_m}{\pi} \cos \alpha \cdot I_0 \times \frac{1}{V_s I_0}$$

$$= \frac{2\sqrt{2}V_s}{\pi} \cos\alpha \cdot \frac{1}{V_s} = \frac{2\sqrt{2}}{\pi} \cos\alpha$$

For this example, input $Pf = \frac{2\sqrt{2}}{\pi} \cos 60^\circ = 0.450$ (lagging).

Example 4.15: A single-phase HWR feeds a 20Ω resistance. The supply voltage is 220 V. The firing angle is 90° . Find (a) V_0 , I_0 , V_{rms} , I_{rms} (b) P_0 , P_{ac} , rectification efficiency, (c) FF , RF , (d) volt-ampere rating of transformer feeding the rectifier and TUF, and (e) PIV across the thyristor.

SOLUTION

$$V_m = \times 220 = 311.12 \text{ V}$$

(a) For $1 - \phi$ HWR with R load,

$$V_0 = \frac{V_m}{2\pi} (1 + \cos\alpha) = \frac{311.12}{2\pi} (1 + \cos 90^\circ) = 49.52 \text{ V}$$

$$I_0 = \frac{V_0}{R} = \frac{49.52}{20} = 2.48 \text{ A}$$

$$\begin{aligned} V_{rms} &= \frac{V_m}{2\sqrt{\pi}} \left[(\pi - \alpha) + \frac{1}{2} \sin 2\alpha \right]^{\frac{1}{2}} \\ &= \frac{311.12}{2\sqrt{\pi}} \left[\left(\pi - \frac{\pi}{2} \right) + \frac{1}{2} \sin \pi \right]^{\frac{1}{2}} \\ &= 110 \text{ V} \end{aligned}$$

$$I_{rms} = \frac{V_{rms}}{R} = \frac{110}{20} = 5.5 \text{ A}$$

$$(b) \quad P_0 = V_0 I_0 = 49.52 \times 2.48 = 122.8 \text{ W}$$

$$P_{ac} = V_{rms} I_{rms} = 110 \times 5.5 = 605 \text{ W}$$

$$\text{Rectification efficiency} = \frac{P_0}{P_{ac}} = \frac{122.8}{6.5} = 0.202$$

$$(c) \quad \text{Form factor} = \frac{\text{RMS voltage}}{\text{Average voltage}} = \frac{V_{rms}}{V_0} = \frac{110}{49.52} = 2.22$$

$$RF = (FF^2 - 1)^{0.5} = (2.22^2 - 1)^{0.5} = 1.982$$

(d) The transformer secondary current is the same as RMS value of the load current.

$$\text{VA rating of transformer} = 220 \times 5.5 = 1210 \text{ VA}$$

$$\text{Transformer utilization factor} = \frac{122.8}{1210} = 0.1014$$

$$(e) \quad \text{Peak inverse voltage} = V_m = 311.12 \text{ V}$$

Example 4.16: A single-phase center-tapped FWR whose output voltage from center tapping to outside terminal has an RMS value of 150 V. It feeds a load having a resistance of 20 ohms. If the firing angle is 45°, find the average DC voltage, RMS load voltage, average load current, and RMS load current.

SOLUTION

For 1 – ϕ FWR with R load, average output voltage,

$$V_o = \frac{V_m}{\pi} (1 + \cos \alpha) = \frac{\sqrt{2} \times 150}{\pi} (1 + \cos 45^\circ) = 115.25 \text{ V}$$

Average load current

$$I_0 = \frac{V_0}{R} = \frac{115.25}{20} = 5.76 \text{ A}$$

The RMS output voltage,

$$\begin{aligned} V_{rms} &= \frac{V_m}{\sqrt{\pi}} \left[(\pi - \alpha) + \frac{1}{2} \sin 2\alpha \right]^{\frac{1}{2}} \\ &= \frac{\sqrt{2} \times 150}{\sqrt{\pi}} \left[\left(\pi - \frac{\pi}{2} \right) + \frac{1}{2} \sin \frac{\pi}{2} \right]^{\frac{1}{2}} = 143 \text{ V} \\ \text{RMS load current} &= \frac{143}{20} = 7.15 \text{ A} \end{aligned}$$

Example 4.17: A highly inductive load is fed by a full-wave converter with center-tapped transformer. The primary of transformer is fed by a 220-V, 50-Hz supply. The average values of the load voltage and current are 100 V and 10 A. The firing angle is 30°. Find (a) transformer turn ratio, (b) transformer VA rating, (c) PIV for thyristor, and (d) peak and RMS currents of the thyristors. Assume that the forward voltage drop across the thyristor V_T is 1.5 V.

SOLUTION

(a) Let the peak value of voltage across each half of secondary is V_m . Then

$$V_0 = \frac{2V_m}{\pi} \cos \alpha - V_T$$

or

$$100 = \frac{2V_m}{\pi} \cos 30^\circ - 1.5$$

or

$$V_m = 181.38 \text{ V}$$

$$\text{RMS voltage of each half cycle of secondary} = \frac{181.38}{\sqrt{2}} = 128.25 \text{ V}$$

$$\text{Turn ratio of transformer } \frac{22.0}{128.25} = 1.71$$

- (b) Peak current of thyristor = 10 A
Each half of secondary carries 10 A current for 50% of time.

$$\text{RMS value of secondary current} = \sqrt{\frac{10^2}{2}} = 7.07 \text{ A}$$

$$\text{Transformer rating} = 2 \times 128.25 \times 7.07 = 1814 \text{ VA}$$

- (c) PIV = $2V_m = 2 \times 181.38 = 362.76 \text{ V}$
(d) Peak thyristor current = 10 A.

$$\text{RMS value of the thyristor current} = 7.07 \text{ A}$$

Example 4.18: Thyristors having a peak voltage rating of 800 V and average forward current of 40 A are available for building a converter circuit. Find the average power output for (a) single-phase full-wave midpoint converter and (b) single-phase full-bridge converter. Use a safety factor of 2 for both current and voltage ratings.

SOLUTION

- (a) In a midpoint converter (M-2) connection, the peak voltage across the thyristor can be $2V_m$ where V_m is the peak voltage from the midpoint to the outer terminal. Using a safety factor of 2.

$$2V_m = \frac{800}{2}$$

or

$$V_m = 200 \text{ V}$$

Maximum output is obtained if $\alpha = 0$

$$\text{Therefore } V_0 = \frac{V_m}{\pi} (1 + \cos 0) = \frac{2V_m}{\pi} = \frac{2 \times 200}{\pi} = 127.32 \text{ V}$$

$$\text{Current} = \frac{40}{2} = 20 \text{ A}$$

$$\text{Average output power} = 20 \times 127.32 = 2547 \text{ W}$$

- (b) In a bridge converter, the peak voltage across the thyristor is V_m

$$V_m = \frac{800}{2} = 400 \text{ V}$$

For $\alpha = 0$

$$V_0 = \frac{V_m}{\pi} (1 + \cos 0) = \frac{2V_m}{\pi} = \frac{2 \times 400}{\pi} = 254.64 \text{ V}$$

$$\text{Current} = \frac{40}{2} = 20 \text{ A}$$

Average power output = $20 \times 254.64 = 5093 \text{ W}$.

Therefore, it can be concluded that for the same rating of thyristors or devices, the output power obtained in the bridge type is double to that of midpoint type.

Example 4.19: A single-phase dual converter is fed by a 220-V, 50-Hz single-phase system. It feeds a resistive load of 20-ohm resistance. The firing angles are $\alpha_1 = 60^\circ$ and $\alpha_2 = 120^\circ$. The inductance L is 50 mH. Find the peak circulating current and peak current of converter 1.

SOLUTION

$$V_m = \sqrt{2} \times 220 = 311.12 \text{ V}$$

$$\alpha_1 = 60^\circ, \alpha_2 = 120^\circ, \omega = 100\pi$$

$$\omega L_r = 100\pi (50 \times 10^{-3}) = 15.71 \Omega$$

The expression for instantaneous circulating current for $1 - \phi$ dual converter is

$$\begin{aligned} I_r &= \frac{2V_m}{\omega L_r} (\cos \omega t - \cos \alpha_1) \\ &= \frac{2 \times 311.12}{15.71} (\cos \omega t - \cos 60^\circ) \end{aligned}$$

The peak circulating current occurs at $\omega t = 2\pi$

$$(I_r)_{\max} = \text{Peak circulating current} = \frac{2 \times 311.12}{15.71} (1 - 0.5) = 19.80 \text{ A}$$

$$\text{Peak value of load current, } (I_p) = \frac{V_m}{R} = \frac{311.12}{20} = 15.56 \text{ A}$$

The peak current of converter 1 is the sum of the peak load current and peak circulating current.

$$\text{Peak current of converter 1} = I_p + (I_r)_{\max} = 15.56 + 19.80 = 35.36 \text{ A}$$

Example 4.20: A single-phase circulating current dual converter is fed by a 220-V, single-phase 50-Hz AC supply. The firing angles are $\alpha_1 = 30^\circ$ and $\alpha_2 = 150^\circ$. The load resistance is 15 ohms. The peak circulating current is 10.5 A. Find (a) inductance of current limiting reactor and (b) peak current of converter 1.

SOLUTION

$$(a) V_m = \sqrt{2} \times 220 = 311.12 \text{ V}$$

$$\alpha_1 = 30^\circ, \alpha_2 = 150^\circ, \omega = 100\pi$$

Expression for circulating current,

$$I_r = \frac{2V_m}{\omega L_r} [\cos \omega t - \cos \alpha_1]$$

Peak circulating current occurs at $\omega t = 2\pi$.

$$\therefore 10.5 = \frac{2 \times 311.12}{100 \pi L} (\cos 2\pi - \cos 30^\circ)$$

or

$$10.5 = \frac{2 \times 311.12}{100 \pi L} (1 - 0.886)$$

or

$$L_r = \frac{2 \times 311.12 \times 0.134}{100 \pi (10.5)} = 0.0252 \text{ H}$$

$$(b) \text{ Peak load current} = \frac{311.12}{15} = 20.74 \text{ A}$$

Peak current of converter 1 is the sum of peak load current and peak circulating current.

$$\text{Peak current converter 1} = 20.74 + 10.5 = 31.24 \text{ A}$$

Example 4.21: A single-phase circulating current dual converter is fed by a 220-V, single-phase, 50-Hz AC supply. The load is purely resistive. The peak current of converter 1 is 40 A. The firing angles are 45° and 135° , respectively. If peak circulating current is 12.5 A find (a) inductance of current limiting reactor and (b) load resistance.

SOLUTION

$$(a) V_m = \sqrt{2} \times 220 = 311.12 \text{ V}$$

$$\omega = 100\pi, \alpha_1 = 45^\circ, \alpha_2 = 135^\circ$$

The instantaneous circulating current,

$$I_r = \frac{2V_m}{\omega L_r} (\cos \omega t - \cos \alpha_1)$$

Peak circulating current occurs at $\omega t = 2\pi$.

$$\therefore (I_r)_{\max} = \frac{2V_m}{\omega L_r} (\cos 2\pi - \cos \alpha_1)$$

or

$$12.5 = \frac{2 \times 311.12}{100\pi L_r} (\cos 2\pi - \cos 45^\circ)$$

or

$$12.5 = \frac{2 \times 311.12}{100\pi L_r} (1 - 0.707)$$

or

$$L_r = \frac{2 \times 311.12 \times (1 - 0.707)}{100\pi (12.5)} = 0.046 \text{ H}$$

(b) Peak load current = $40 - 12.5 = 27.5 \text{ A}$

$$\text{Peak load current} = \frac{V_m}{R} = \frac{311.12}{R}$$

or

$$R = \frac{311.12}{27.5} \text{ A} = 11.31 \Omega$$

Example 4.22: A three-phase dual converter is fed by a 400-V, 50-Hz supply. The inductance of the current-limiting reactor is 60 mH. Find the circulating current at $\omega t = 0^\circ$, 30° , and 90° . Assume that the firing angle is zero. Also find the maximum value of the circulating current.

SOLUTION

$$V_m = \frac{400\sqrt{2}}{\sqrt{3}} = 326.56 \text{ V}$$

$$\omega L_r = 2\pi (50)(60 \times 10^{-3}) = 18.85 \Omega$$

Instantaneous value of circulating current i_r for $3 - \phi$ dual converter,

$$i_r = \frac{3V_m}{\omega L_r} [\sin(\omega t - 30^\circ) - \sin\alpha_1]$$

$$\text{For } \omega t = 0 \text{ and } \alpha_1 = 0, i_r = \frac{3 \times 326.56}{18.85} [\sin(-30^\circ)] = -25.99 \text{ A}$$

The negative sign indicates the direction of flow of circulating current.

For $\omega t = 30^\circ$ and $\alpha_1 = 0$, $i_r = 0$

For $\omega t = 90^\circ$ and $\alpha_1 = 0$

$$i_r = \frac{3 \times 326.56}{18.85} [\sin(60 - 0)] = 45 \text{ A}$$

The peak value of circulating current occurs at $\omega t = 120^\circ$ and is equal to
 $(i_r)_{\max} = \frac{3 \times 326.56}{18.85} [\sin 90 - 0] = 51.97 \text{ A}$

Example 4.23: A three-phase circulating-current dual converter is fed from a 400-V, 50-Hz AC supply. The peak value of the circulating current is 40 A. If the firing angle is zero, find the inductance of the current-limiting reactor.

SOLUTION

$$V_m = \frac{400\sqrt{2}}{\sqrt{3}} = 326.56 \text{ V}$$

$$\omega L_r = 100\pi L_r, \alpha_1 = 0$$

Instantaneous value of circulating current i_r for 3 - ϕ dual converter,
 $i_r = \frac{3V_m}{\omega L_r} [\sin(\omega t - 30^\circ) - \sin \alpha_1]$

The peak value of the circulating current occurs at $\omega t = 120^\circ$ and is equal to

$$(i_r)_{\max} = \frac{3V_m}{\omega L_r} [\sin(120 - 30^\circ) - \sin \alpha_1]$$

$$\therefore 40 = \frac{3 \times 326.56}{100\pi L} [\sin(120 - 30^\circ) - \sin 0]$$

or

$$40 = \frac{3 \times 326.56}{100\pi L} [\sin 90 - \sin 0]$$

or

$$L = \frac{3 \times 326.56}{100\pi (40)} = 0.077 \text{ H}$$

REVIEW QUESTIONS AND UNSOLVED PROBLEMS

- 4.1 A single-phase half-wave converter is operated from a 120-V, 50-Hz supply. If the load resistive load is $R = 20 \Omega$ and the delay angle is $\alpha = \pi/3$, determine (a) efficiency, (b) FF, (c) RF, (d) transformer utilization factor, and (e) the PIV of the thyristor T_1 .
- 4.2 A single-phase half-wave converter is operated from a 120-V, 50-Hz supply, and the load resistive load is $R = 20 \Omega$. If the average output voltage is 25% of the maximum possible average output voltage, calculate (a) delay angle, (b) RMS and average output currents, (c) average and RMS thyristor currents, and (d) input power factor.

- 4.3 A single-phase half-converter is supplied from a 120-V, 50-Hz supply and a FD is connected across the load. The load consists of series-connected resistance $R = 10 \Omega$; inductance $L = 8 \text{ mH}$. (a) Express the instantaneous output voltage in a Fourier series, and (b) determine the RMS value of the lowest order output harmonic current.
- 4.4 Repeat problem 1 for the single-phase full converter.
- 4.5 Repeat problem 2 for the single-phase full converter.
- 4.6 Repeat problem 3 for the single-phase full converter.
- 4.7 Repeat problem 3 for the three-phase semiconverter.
- 4.8 Repeat problem 2 if the average output voltage is 90% of the maximum possible output voltage.
- 4.9 The three-phase dual converter is operated from a three-phase Y-connected 220-V, 50-Hz supply and the load resistance $R = 10 \Omega$. The circulating inductance $L_r = 5 \text{ mH}$ and the delay angles are $\alpha_1 = 60^\circ$ and $\alpha_2 = 120^\circ$. Calculate the peak circulating current and the peak current of converters.
- 4.10 The single-phase full converter has an RL load having $L = 2 \text{ mH}$, $R = 2 \Omega$. The input voltage is $V = 120 \text{ V}$ at (RMS) 50 Hz. (a) Determine (1) the load current I_0 at $\omega t = \alpha = 30^\circ$, (2) the average thyristor current, (3) the RMS thyristor current, (4) the RMS output current I , and (5) the average output current I_{dc} .
- 4.11 The single-phase full converter has an RL load having $L = 4.5 \text{ mH}$, $R = 1.5 \Omega$. The input voltage is $v_s = 120 \text{ V}$ at (RMS) 60 Hz. (a) Determine (1) the load current I_0 at $\omega t = \alpha = 30^\circ$, (2) the average thyristor current I_A , (3) the RMS thyristor current I_R , (4) the RMS output current I_{rms} , and (5) the average output current I_{dc} .
- 4.12 The holding current of thyristor in the three-phase full converter is $I_H = 200 \text{ mA}$ and the delay time is $2.5 \mu\text{s}$. The converter is supplied from a three-phase Y-connected 208-V, 50-Hz supply and has a load of $L = 10 \text{ mH}$ and $R = 2 \Omega$ ωt is operated with a delay angle of $\alpha = 60^\circ$. Determine the minimum width of the gate pulse width t_G .
- 4.13 What is the effect of source resistance and inductance on the performance of single-phase and three-phase full converters?
- 4.14 Why PF is poor in case of full converters?
- 4.15 What is the effect of load inductance on performance of rectifiers?
- 4.16 What is an FD? How does it improve the performance of rectifiers with an inductive load?
- 4.17 Derive the expression for input PF of a single-phase fully controlled bridge converter with RL load and discontinuous conduction.
- 4.18 Derive expressions for output voltage of a single-phase and three-phase full converter.
- 4.19 Explain practical dual converter.
- 4.20 List the advantage and disadvantage of circulating and noncirculating-type dual converters.

SUMMARY

The controlled rectifiers are used at high power levels for controlled transfer of power between an AC source and the adjustable DC load by controlling the phase angle or delay angle of thyristors. Here, the polarity of DC voltage can be reversed, but the DC current remains unidirectional. This chapter has discussed in detail the various types of rectifiers with the effect of the source and load impedance on the performance of rectifiers.

MAIN FORMULAS OF THE CHAPTER

- Single-phase half-wave-controlled rectifier with R load

$$t_c = \frac{\pi}{\omega} \text{ sec}$$

$$V_0 = \frac{V_m}{2\pi} (1 + \cos\alpha)$$

$$I_0 = \frac{V_0}{R} = \frac{V_m}{2\pi R} (1 + \cos\alpha)$$

$$V_{\text{rms}} = \frac{V_m}{2\sqrt{\pi}} \left[(\pi - \alpha) + \frac{\sin 2\alpha}{2} \right]^{\frac{1}{2}}$$

$$I_{\text{rms}} = \frac{V_{\text{rms}}}{R}$$

$$\text{Input power factor} = \frac{1}{\sqrt{2\pi}} \left[(\pi - \alpha) + \frac{\sin 2\alpha}{2} \right]^{\frac{1}{2}}$$

- Single-phase half-wave-controlled rectifier with RL load

$$t_c = \frac{\pi - \beta}{\omega} \text{ sec}$$

$$v_o = \frac{V_m}{2\pi} [\cos\alpha - \cos\beta]$$

$$I_o = \frac{V_0}{R} = \frac{V_m}{2\pi R} (\cos\alpha - \cos\beta)$$

$$V_{\text{rms}} = \frac{V_m}{2\sqrt{\pi}} \left[(\beta - \alpha) - \frac{1}{2} \{ \sin 2\beta - \sin 2\alpha \} \right]^{\frac{1}{2}}$$

Effect of inductive load:

1. Average output voltage v_0 reduces.
2. Input PF reduces.
3. Load current i_0 waveforms gets distorted.
4. Load performance deteriorates.

- Single-phase half-wave-controlled rectifier with RL load and FD

$$t_c = \frac{\pi}{\omega} \text{ sec}$$

$$V_0 = \frac{V_m}{2\pi} (1 + \cos\alpha)$$

$$I_o = \frac{V_0}{R} = \frac{V_m}{2\pi R} (1 + \cos\alpha)$$

$$V_{\text{rms}} = \frac{V_m}{2\sqrt{\pi}} \left[(\pi - \alpha) + \frac{\sin 2\alpha}{2} \right]^{\frac{1}{2}}$$

Advantages of using FD:

1. Average output voltage is increased (i.e., it prevents load voltage v_0 from becoming negative).
2. Input PF is improved.
3. Load current waveform is improved.
4. Load performance becomes better.

- Single-phase full-wave midpoint rectifier with R load

$$t_{c1} = t_{c2} = \frac{\pi}{\omega} \text{ sec}$$

$$V_0 = \frac{V_m}{\pi} (1 + \cos\alpha)$$

$$V_{\text{rms}} = \frac{V_m}{\sqrt{2\pi}} \left[(\pi - \alpha) + \frac{\sin 2\alpha}{2} \right]^{\frac{1}{2}}$$

- Single-phase full-wave bridge-type-controlled rectifier with RL load

$$t_c = \frac{\pi - \alpha}{\omega} \text{ sec}$$

PIV Bridge type = V_m
 Midpoint or center-tapped type = $2V_m$

$$V_0 = \frac{2V_m}{\pi} \cos\alpha$$

- Three-phase half-wave converters with RL load

$$V_0 = \frac{3\sqrt{3}V_m}{2\pi} \cos\alpha$$

$$V_{0\max} = \frac{3\sqrt{3}V_m}{2\pi}$$

$$V_{\text{rms}} = \sqrt{3}V_m \left(\frac{1}{6} + \frac{\sqrt{3}}{8\pi} \cos 2\alpha \right)^{\frac{1}{2}}$$

$$V_n = \frac{V_0}{V_{0\max}} = \cos \alpha$$

- Three-phase full converter

$$V_0 = \frac{3\sqrt{3}V_m}{\pi} \cos \alpha$$

$$V_{0\max} = \frac{3\sqrt{3}V_m}{\pi}$$

$$V_n = \frac{V_0}{V_{0\max}} = \cos \alpha$$

$$V_{\text{rms}} = \sqrt{3} V_m \left(\frac{1}{2} + \frac{3\sqrt{3}}{4\pi} \cos 2\alpha \right)$$

- Single-phase dual converter

$$\alpha_1 + \alpha_2 = 180^\circ$$

$$i_r = \frac{2V_m}{\omega L_r} (\cos \alpha_1 - \cos \omega t)$$

$$I_{r(\max)} = \frac{2V_m}{\omega L_r} (1 - \cos \alpha_1)$$

- Single-phase fully controlled rectifier with source and load inductance

$$I_0 = \frac{V_m}{\omega L_s} [\cos \alpha - \cos(\alpha + \mu)]$$

$$V_0 = \frac{V_m}{\pi} [\cos \alpha + \cos(\alpha + \mu)]$$

$$V_0 = \frac{2V_m}{\pi} \cos \alpha - \frac{\omega L_s}{\pi} I_0$$

In general, for m -pulse converters, reduction in average output voltage due to source inductance (i.e., overlap angle μ) is $\frac{m\omega L_s I_0}{2\pi}$.

REFERENCES/FURTHER READING

1. N. Mohan, T. M. Undeland, and W. P. Robbins, *Power Electronics: Converters, Applications and Design*, John Wiley & Sons, New York, 1996.
2. B. K. Bose, *Power Electronics and AC Drives*, Prentice Hall, Englewood Cliffs, NJ, 1986.
3. M. H. Rashid, *Power Electronics: Circuits, Devices, and Applications*, Pearson Education, Singapore, 2004.
4. P. T. Krein, *Elements of Power Electronics*, Oxford University Press, New York, 2003.
5. K. Thorborg, *Power Electronics*. Prentice Hall International (U.K) Ltd, London, UK, 1988.
6. P. S. Bhimra, *Power Electronics*, 4th edn, Khanna Publications, New Delhi, 2012.
7. I. Batarsehand A. Harb, *Power Electronics*, Springer Nature, Cham, Switzerland 2018.
8. R. S. Ramshaw, *Power Electronics Semiconductor Switches*, Springer Nature, Boston, MA, 1993.
9. K. M. Smedley and E. Santi, *AC-DC Power Converters*, Wiley, 1999.
10. R. W. Erickson, *Fundamentals of Power Electronics*, Springer, New York, 2001.
11. B. Wu and B. Wu, *High-Power Converters and AC Drives*, John Wiley & Sons, Hoboken, NJ, 2017.
12. R. W. Erickson, *Fundamentals of Power Electronics*, Chapman and Hall, New York, 1997.
13. V. R. Moorthi, *Power Electronics Devices, Circuits and Industrial Applications*, Oxford University Press, New York, 2010.
14. T. Suntio, T. Messo, and J. Puukko, *Power Electronic Converters*, Wiley-VCH, Verlag GmbH, Berlin, Germany, 2018.
15. A. M. Trzynadlowski, *Introduction to Modern Power Electronics*, 3rd edn, John Wiley and Sons, Hoboken, NJ, 2010.
16. M. Trzynadlowski, *Power Electronic Converters and Systems*, Institution of Engineering and Technology, London, UK, 2016.
17. B. M. Wilamowski and J. D. Irwin, *Power Electronics and Motor Drives*, CRC Press, Boca Raton, FL/London, New York, 2011.
18. E. Acha, V. G. Agelidis, O. Anaya-Lara, and T. J. E. Miller, *Power Electronic Control in Electrical Systems*, Oxford, Newnes, UK, 2002.
19. F. Mazda, *Power Electronics Handbook*, Oxford, Newnes, UK, 1997.
20. F. Blaabjerg, *Control of Power Electronic Converters and Systems*, Academic Publishers, New York, 2018.
21. S. N. Manias, *Power Electronics and Motor Drive Systems*, Academic Publishers, London, UK, 2017.



Taylor & Francis

Taylor & Francis Group

<http://taylorandfrancis.com>

5 Semiconverters

5.1 INTRODUCTION

Though semiconverters have inherent freewheeling action, these are generally not utilized. Rather a separate freewheeling diode (FD) is connected across the load. This is because the inherent freewheeling increases the average current rating of the silicon-controlled rectifier (SCR). These are half-controlled converters having limited control on their average DC output voltage. They use a mixture of diodes and thyristors. It is a single or one-quadrant converter as it has one polarity of DC output voltage and current at its output terminals, as shown in [Figure 5.1](#).

5.2 SINGLE-PHASE SEMICONVERTER WITH RL LOAD

It is a half-controlled full-wave rectifier. It is also called a single-phase two-pulse rectifier or one-quadrant converter. It uses a mixture of diodes and thyristors, and there is a limited control over the output DC voltage. The single-phase semiconverter has two configurations as shown in [Figure 5.2](#).

1. **Symmetrical semiconverter:** In this configuration, each arm or leg has one thyristor and one diode. It requires a FD if the load is inductive.
2. **Asymmetrical semiconverter:** In this configuration, one leg has two thyristors and the other leg has two diodes. It does not require an FD if the load is inductive because the two diodes D_1 and D_2 can play the role of the FD.

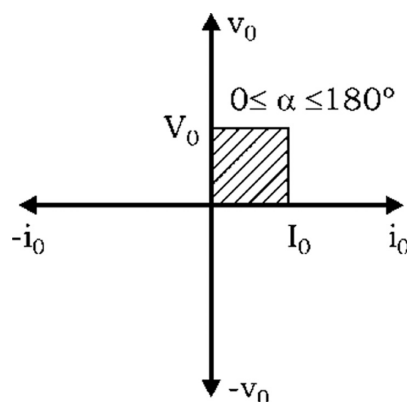


FIGURE 5.1 Quadrant operation of semiconverter.

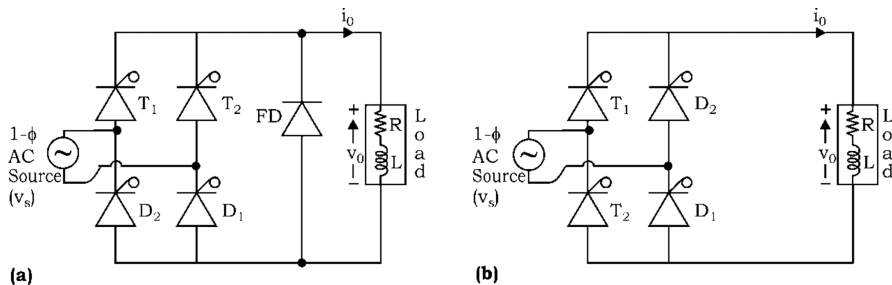


FIGURE 5.2 Single-phase semiconverter configuration: (a) symmetrical-semiconductor configuration and (b) asymmetrical-semiconductor configuration.

Case I: Continuous Conduction:

Power circuit and various voltage and current waveforms for symmetrical $1-\phi$ semiconverter with RL load are shown in [Figure 5.3](#).

Working: During the positive half cycle, thyristor T_1 and diode D_1 are forward biased. If thyristor T_1 is gated, current flow through the path: point a – T_1 – RL load – D_1 – point b, see [Figure 5.3a](#). The voltage across the load is a segment of the supply voltage. T_1 and D_1 conduct from α to π . Soon after $\omega t = \pi$, load voltage v_0 tends to reverse as the AC source voltage v_s also reverses its direction. Just as v_0 tends to reverse (at $\omega t = \pi^+$), FD gets forward biased and therefore starts conducting. The load or output current i_0 is transferred from T_1D_1 to the FD. Therefore, now the FD conducts from π to $\pi + \alpha$. During this period, $v_0 = 0$, because the FD short-circuits the load terminals.

During the negative half cycle, thyristor T_2 and diode D_2 are forward biased. If T_2 is gated, the current flows through the path: point b – T_2 – RL load – D_2 – point a. At $\omega t = 2\pi$, FD is again forward biased, and therefore the load current i_0 is transferred from T_2D_2 to FD as explained earlier, and in this way, the cycle repeats.

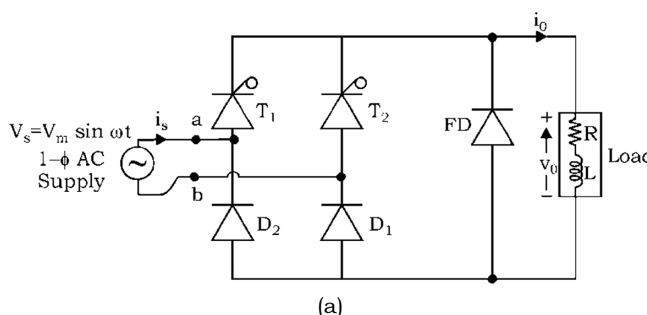


FIGURE 5.3 (a) Power circuit diagram

(Continued)

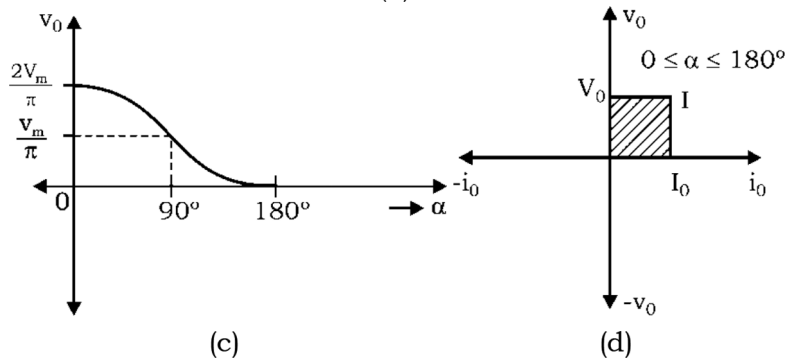
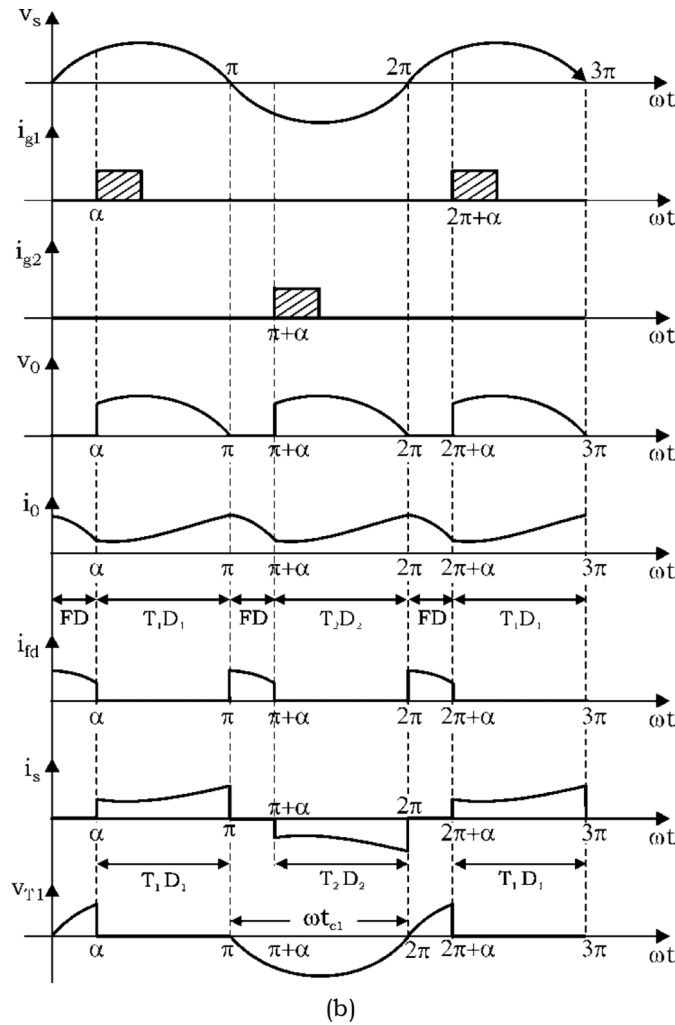


FIGURE 5.3 (Continued) (b) various voltage and current waveforms, (c) a plot between V_0 and α , and (d) quadrant operation.

Performance Parameters:

- The average output voltage,

$$\begin{aligned}
 V_0 &= \frac{1 \times 2}{2\pi} \int_{\alpha}^{\pi} V_m \sin \omega t d(\omega t) \\
 &= \frac{V_m}{\pi} \left[-\cos \omega t \right]_{\alpha}^{\pi} \\
 &\boxed{V_0 = \frac{V_m}{\pi} (1 + \cos \alpha)} \tag{5.1}
 \end{aligned}$$

- The root mean square (RMS) output voltage,

$$\boxed{V_{\text{rms}} = \left[\frac{1 \times 2}{2\pi} \int_{\alpha}^{\pi} (V_m \sin \omega t)^2 d \omega t \right]^{\frac{1}{2}}} \tag{5.2}$$

or

$$\boxed{V_{\text{rms}} = \frac{V_m}{\sqrt{2\pi}} \left[(\pi - \alpha) + \frac{\sin 2\alpha}{2} \right]^{\frac{1}{2}}} \tag{5.2}$$

It is also called a *half-controlled converter* because by varying the firing angle (α) from 0° to 180° , its output voltage polarity cannot be reversed (Figure 5.3c), that is, it has limited control over the level of DC output voltage.

$$\text{As } V_0 = \frac{V_m}{\pi} (1 + \cos \alpha)$$

\therefore when

$$\alpha = 0^\circ, V_0 = \frac{2V_m}{\pi}$$

$$\alpha = 90^\circ, V_0 = \frac{V_m}{\pi}$$

$$\alpha = 180^\circ, V_0 = 0$$

Therefore, if a graph is plotted between average output voltage (V_0) and firing angle (α), then it can be seen that output voltage can be controlled from zero to maximum positive only by varying the firing angle from 0° to 180° .

Therefore, the single-phase semiconverter is also called the *single-quadrant converter* because it can be operated in the first quadrant only, as shown in Figure 5.3d. (As i_0 = always positive and V_0 = positive, when α is varied from 0° to 180°).

Case II: Discontinuous Conduction:

Working: From α to π , T_1D_1 conducts and so $v_0 = v_s$ and i_0 increases gradually due to inductive nature of load.

At $\omega t = \pi$, the FD gets forward biased, so i_0 is transferred from T_1D_1 to FD. Therefore, from π to β , FD conducts. During this period, $i_0 = i_{fd}$, and $v_0 = 0$. At $\omega t = \beta$, load current i_0 becomes zero so the FD gets turned off. From β to $(\pi + \alpha)$ no device conducts. So $i_0 = 0$, $v_0 = 0$. At $\omega t = (\pi + \alpha)$, T_2 is triggered; therefore, T_2D_2 conducts from $(\pi + \alpha)$ to 2π . So the load voltage $v_0 = v_s$ and i_0 increases gradually because the load is inductive in nature. Again, at $\omega t = 2\pi$, FD gets forward biased, and in this way the cycle repeats. Various voltage and current waveforms for discontinuous conduction are shown in Figure 5.4 [4,5,8,18].

Therefore, it can be observed that it has three modes:

1. *Conduction period*, $\alpha < \omega t < \pi$: T_1D_1 conducts and $v_0 = v_s$
For $(\pi + \alpha) < \omega t < 2\pi$: T_2D_2 conducts and $v_0 = v_s$
2. *Freewheeling period*, $\pi < \omega t < \beta$: FD conducts; and $i_{fd} = i_0$, $v_0 = 0$
For $2\pi < \omega t < \pi + \alpha$: FD conducts and $i_{fd} = i_0$, $v_0 = 0$
3. *Idle period*, $\beta < \omega t < \pi + \alpha$: no device conducts, therefore $i_0 = 0$, $v_0 = 0$

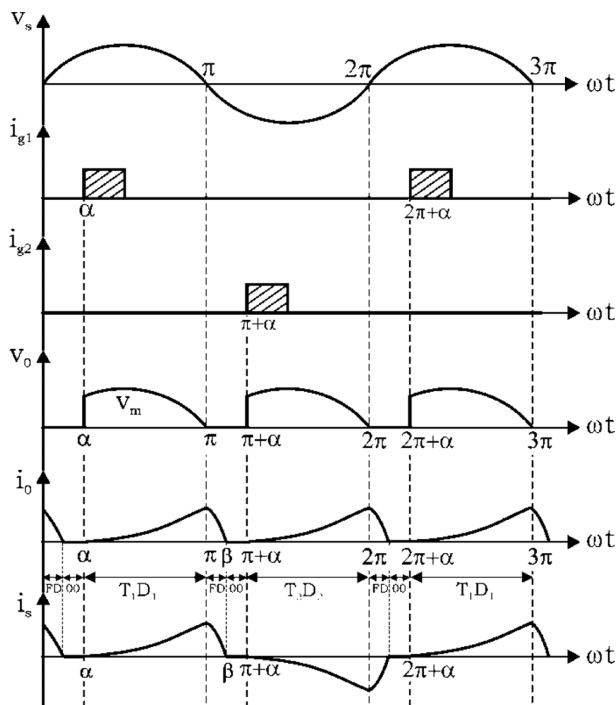


FIGURE 5.4 Various voltage and current waveforms (discontinuous conduction).

Performance Parameters:

- Average output voltage,

$$V_0 = \frac{1 \times 2}{2\pi} \int_{\alpha}^{\pi} V_m \sin \omega t d(\omega t)$$

$$= \frac{V_m}{\pi} [-\cos \omega t]_{\alpha}^{\pi}$$

$$V_o = \frac{V_m}{\pi} (1 + \cos \alpha)$$

(5.3)

Other performance parameters can be found out by using the above equations and as per definitions given in [Section 4.2](#) of the previous chapter.

With RL E Load:

The power circuit and various voltage and current waveforms for single-phase semiconverters are given in [Figure 5.5](#). At $\omega t = \alpha$, when T_1 is triggered, the load current builds up from zero and rises to the maximum and then decays to zero at b , which is greater than π .

From α to π , T_1D_1 conducts and $v_0 = v_s$. At $\omega t = \pi$, as v_s tends to become negative, the FD is forward biased and starts conducting the load current. When the FD conducts from π to β , $v_0 = 0$. From β to $\pi + \alpha$, no component

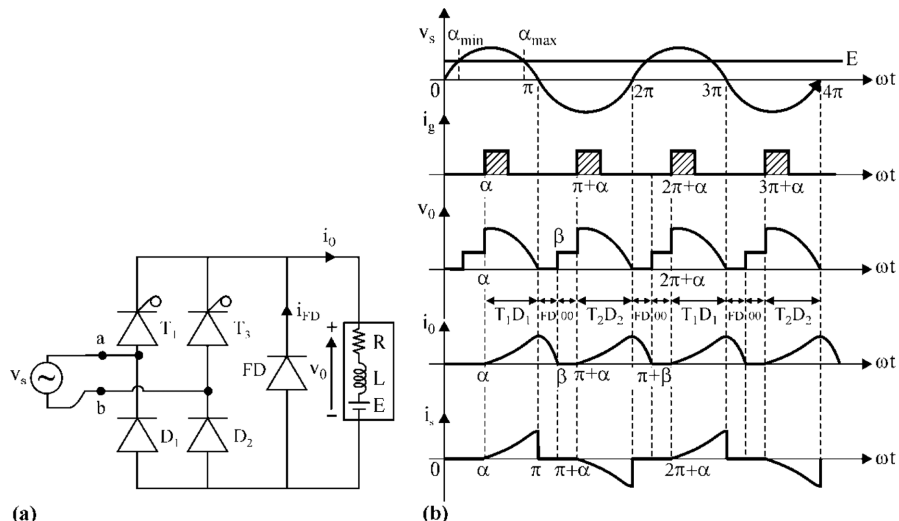


FIGURE 5.5 Power circuit diagram and various waveforms: (a) power circuit waveforms and (b) voltage and current waveforms.

in the circuit conducts, so $v_0 = E$ and $i_0 = 0$ as shown in Figure 5.5b. During the period from β to $\pi + \alpha$, as load current is zero, so it makes the load current discontinuous.

When T_2 is triggered at $\pi + \alpha$, load current i_0 builds as shown in the waveforms. At $\omega t = 2\pi$, the FD is forward biased and starts conducting till $\pi + \beta$. During the time the FD conducts, $v_0 = 0$. From $\pi + \beta$ to $2\pi + \alpha$, no component in the circuit conducts, and so $v_0 = E$. At $2\pi + \alpha$, T_1 is triggered again, and the above sequence repeats.

From the preceding discussion and waveforms, it can be observed that it has three modes [4,5,8,18]:

(a) *Conduction period:*

$\alpha < \omega t < \pi$, $T_1 D_1$ conducts and $v_0 = v_s$

for $\pi + \alpha < \omega t < 2\pi$, $T_2 D_2$ conducts and $v_0 = v_s$

(b) *Freewheeling period:*

$\pi < \omega t < \beta$, FD conducts, $i_{fd} = i_0$, $v_0 = 0$

for $2\pi < \omega t < \pi + \beta$, FD conducts, $i_{fd} = i_0$, $v_0 = 0$

(c) *Idle period:*

$\beta < \omega t < \pi + \alpha$, no component conducts $i_0 = 0$, $v_0 = E$

- The average load current I_0 is given by:

$$\begin{aligned} I_0 &= \frac{1}{\pi R} \int_{\alpha}^{\beta} (V_m \sin \omega t - E) d\omega t \\ &= \frac{V_m}{\pi R} (\cos \alpha - \cos \beta) - \frac{E}{\pi R} (\beta - \alpha) \end{aligned} \quad (5.4)$$

- Average output voltage V_0 :

$$V_0 = E + I_0 R \quad (5.5)$$

Also

$$\begin{aligned} V_0 &= \frac{1}{\pi} \left[\int_{\alpha}^{\pi} V_m \sin \omega t d\omega t + E(\pi + \alpha - \beta) \right] \\ &= \frac{V_m}{\pi} (1 + \cos \alpha) + \frac{E}{\pi} (\pi + \alpha - \beta) \end{aligned} \quad (5.6)$$

or

$$V_0 = \frac{V_m}{\pi} (1 + \cos \lambda) + E \left(1 - \frac{\gamma}{\pi} \right) \quad (5.7)$$

where γ = conduction angle = $\beta - \alpha$

5.3 THREE-PHASE SEMICONVERTER WITH RL LOAD

Power circuit for three-phase semiconverter with RL load is drawn in Figure 5.6a [4,5,8,18].

The output voltage across the load terminals is controlled by varying the firing angle of thyristors T_1 , T_2 and T_3 . The diodes D_1 , D_2 and D_3 provide the return path for the current.

Working: In a $3-\phi$ phase semiconverter, thyristors are fired at an interval of 120° in a proper sequence. It has a *unique feature of working as a six-pulse converter for $\alpha < 60^\circ$ and as a three-pulse converter for $\alpha \geq 60^\circ$* .

For $\alpha = 0^\circ$: Thyristors T_1 , T_2 , and T_3 behave like diodes and output voltage of semiconverter is symmetrical six-pulses per cycle as shown in Figure 5.6c. The FD does not come into play.

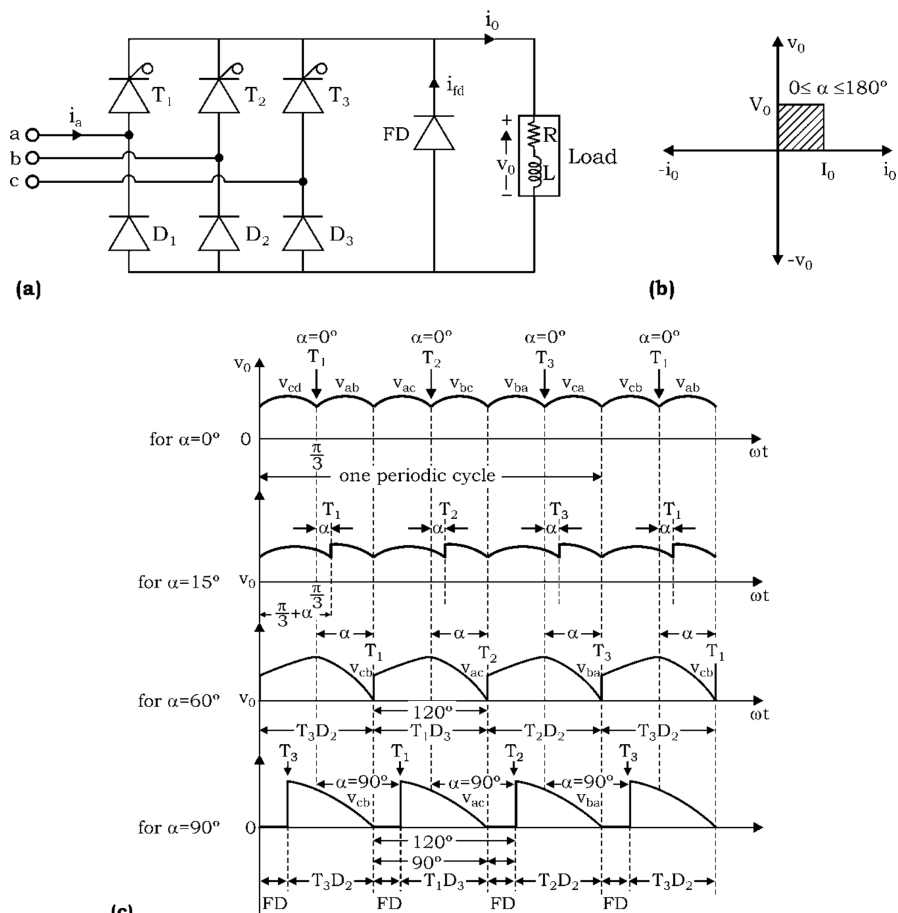


FIGURE 5.6 Three-phase semiconverter with RL load: (a) power circuit, (b) quadrant, and (c) voltage waveforms.

For $\alpha = 15^\circ$: The firing of T_1 , T_2 and T_3 is delayed but return diodes D_1 , D_2 , D_3 remain unaffected so that only alternate pulses are affected. The FD does not come into play. Each diode and thyristor conducts for 120° .

For $\alpha = 60^\circ$: Thyristors are so fired that the current returns through one diode during each 120° conduction period. The FD does not come into play, [see Figure 5.6c].

For $\alpha = 90^\circ$: The output voltage v_0 is discontinuous. Here the FD becomes forward biased at $\omega t = 120^\circ$, 240° , 360° . Therefore, for each periodic cycle of 120° , output voltage v_0 is equal to a line voltage for only 90° and for the remaining 30° , when the FD conducts, v_0 is zero. So, for $\alpha = 90^\circ$, the conduction angle of thyristors and diodes is less than 120° for every output pulse, that is, the conduction angle for both positive and negative group elements (T and D) is 90° and for the remaining 30° , current completes its path through the FD, as shown in Figure 5.6c [4,5,8,18].

For $\alpha = 120^\circ$: For each periodic cycle of 120° , load voltage v_0 has two components (if load is RL):

1. When the thyristor is fired, the thyristor and diode conduct for 60° only.
2. As v_0 reaches zero and tends to become negative, the FD becomes forward biased and so starts conducting, and therefore output voltage $v_0 = 0$.

As in the $3-\phi$ semiconverter, each periodic cycle of output voltage has a periodicity of 120° . So the average output voltage is only calculated over 120° .

For $\alpha < 60^\circ$, the average output voltage:

$$V_0 = \frac{1 \times 3}{2\pi} \int_{-(\pi/6-\alpha)}^{(\pi/6+\alpha)} V_{m1} \sin \omega t \, d\omega t$$

$$V_0 = \frac{3V_{m1}}{2\pi} (1 + \cos \alpha) \quad (5.8)$$

For $\alpha \geq 60^\circ$, the average output voltage:

$$V_0 = \frac{1 \times 3}{2\pi} \int_{\alpha}^{\pi} V_{m1} \sin \omega t \, d\omega t$$

$$V_0 = \frac{3V_{m1}}{2\pi} (1 + \cos \alpha) \quad (5.9)$$

5.4 POWER FACTOR IMPROVEMENT

The power factor (PF) of phase-controlled converters depends on delay angle, and is low, especially when the output voltage is less than the maximum, that is, when the firing angle (α) is large. These converters generate harmonics into the supply. The poor PF operation is a major concern in variable speed drives and in high-power applications. The various techniques to improve the PF in phase-controlled converters are [4,5,8,18]:

1. Phase-angle control (PAC)
2. Semiconverter operation of full converters
3. Asymmetrical firings

But in forced-commutated converters, each thyristor is provided with its own commutation circuit and therefore can be commutated at any desired instant. Forced commutation helps in improving the input PF and reduce the harmonics level. The various control schemes that improve the PF of forced commutated converters are:

1. Extinction angle control (EAC)
2. Symmetrical angle control (SAC)
3. Pulse-width modulation (PWM) control

5.4.1 EXTINCTION ANGLE CONTROL (EAC)

Figure 5.7a shows a single-phase semiconverter, where S_1 and S_2 are two switches [4,5,8,18]. The two switches can be SCRs, gate turn-offs (GTOs) or insulated-gate bipolar transistors (IGBTs).

In this control, switch S_1 is triggered at $\omega t = 0$ and is commutated by force commutation at $\omega t = (\pi - \beta)$. Switch S_2 is triggered at $\omega t = \pi$ and is commutated at $\omega t = (2\pi - \beta)$. The output voltage is controlled by varying the extinction angle β . Various voltage and current waveforms are shown in Figure 5.7b [4,5,8,18]. Waveforms depict that fundamental component of input current leads input voltage and the displacement factor, PF, is leading.

The average output voltage can be derived as:

$$\begin{aligned}
 V_0 &= \frac{1 \times 2}{2\pi} \int_0^{(\pi-\beta)} v_s d(\omega t) = \frac{1 \times 2}{2\pi} \int_0^{(\pi-\beta)} V_m \sin \omega t d(\omega t) \\
 &= \frac{V_m}{\pi} [-\cos \omega t]_0^{\pi-\beta} \\
 &\boxed{V_0 = \frac{V_m}{\pi} (1 + \cos \beta)} \quad (5.10)
 \end{aligned}$$

Therefore, average output voltage V_0 can be varied from $\frac{2V_m}{\pi}$ to zero by varying the extinction angle β from 0 to π .

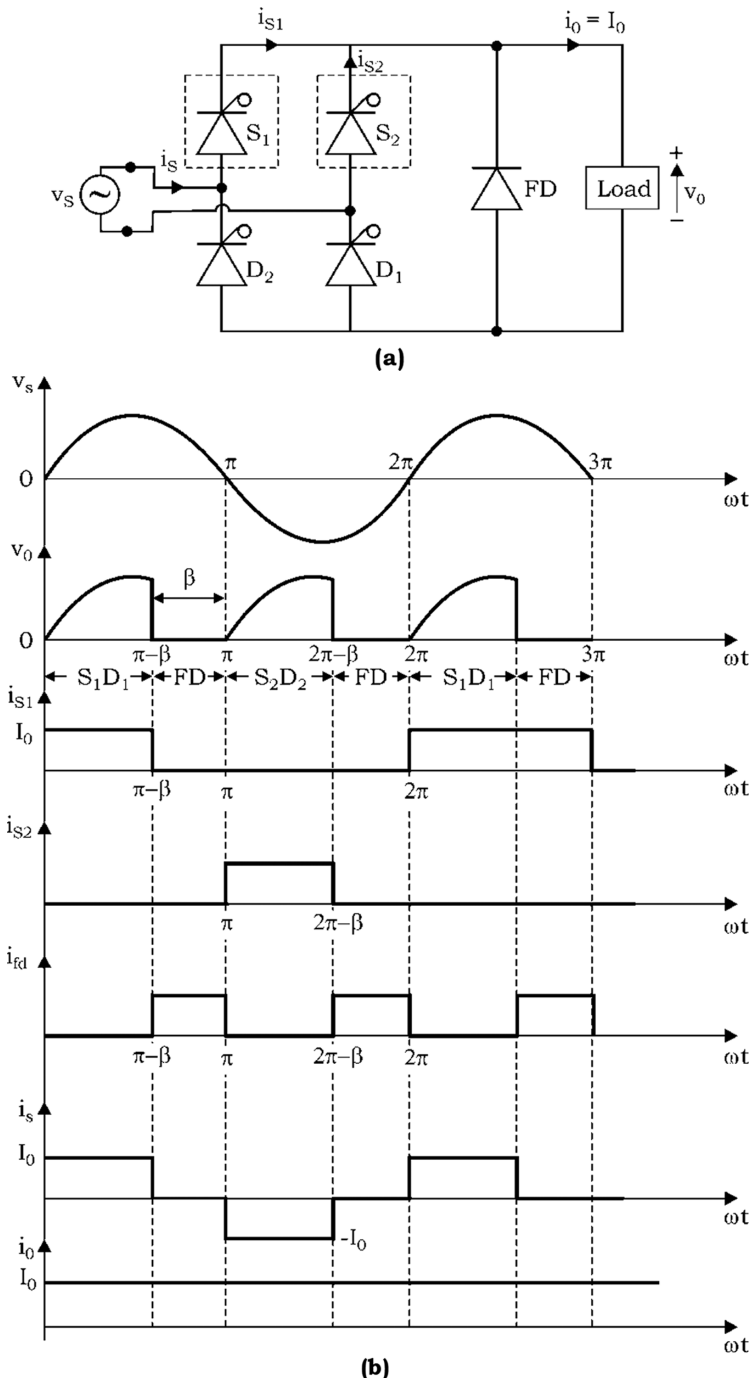


FIGURE 5.7 (a) Power circuit employing forced commutation, and (b) voltage and current waveforms.

The expression for RMS output voltage V_{rms} can be derived as:

$$V_{\text{rms}} = \left[\frac{1 \times 2}{2\pi} \int_0^{(\pi-\beta)} (V_m \sin \omega t)^2 d\omega t \right]^{\frac{1}{2}}$$

$$V_{\text{rms}} = \frac{V_m}{\sqrt{2}} \left[\frac{1}{\pi} \left(\pi - \beta + \frac{\sin 2\beta}{2} \right) \right]^{\frac{1}{2}} \quad (5.11)$$

The performance of this converter with EAC is similar to those with phase-angle control, except the PF (and displacement factor) is leading. In the case of phase-angle control, the PF is lagging.

The RMS supply current I_s can be derived as:

$$I_s = \left[\frac{1 \times 2}{2\pi} \int_0^{\beta} I_0^2 d\omega t \right]^{\frac{1}{2}}$$

$$I_s = \sqrt{\frac{\beta}{\pi}} I_0 \quad (5.12)$$

5.4.2 SYMMETRICAL ANGLE CONTROL (SAC)

Figure 5.8a presents various voltage and current waveforms for the SAC scheme for a single-phase semiconverter [4,5,8,18]. SAC allows only one quadrant operation.

Working: Under this control, switch S_1 is triggered at $\omega t = \frac{(\pi-\gamma)}{2}$ and is commutated at $\omega t = \frac{(\pi+\gamma)}{2}$. Switch S_2 is triggered at $\omega t = \frac{(3\pi-\gamma)}{2}$ and commutated at $\omega t = \frac{(3\pi+\gamma)}{2}$. The output voltage is controlled by varying the conduction angle (γ). The gate pulses are generated by comparing half sine waves with a DC signal, as shown in Figure 5.8b [4,5,8,18]. Waveforms depict that supply current pulse is placed symmetrically with respect to the supply voltage peak, and therefore, the fundamental component of the input current is in phase with the supply voltage and displacement factor is unity. Therefore, the PF is improved.

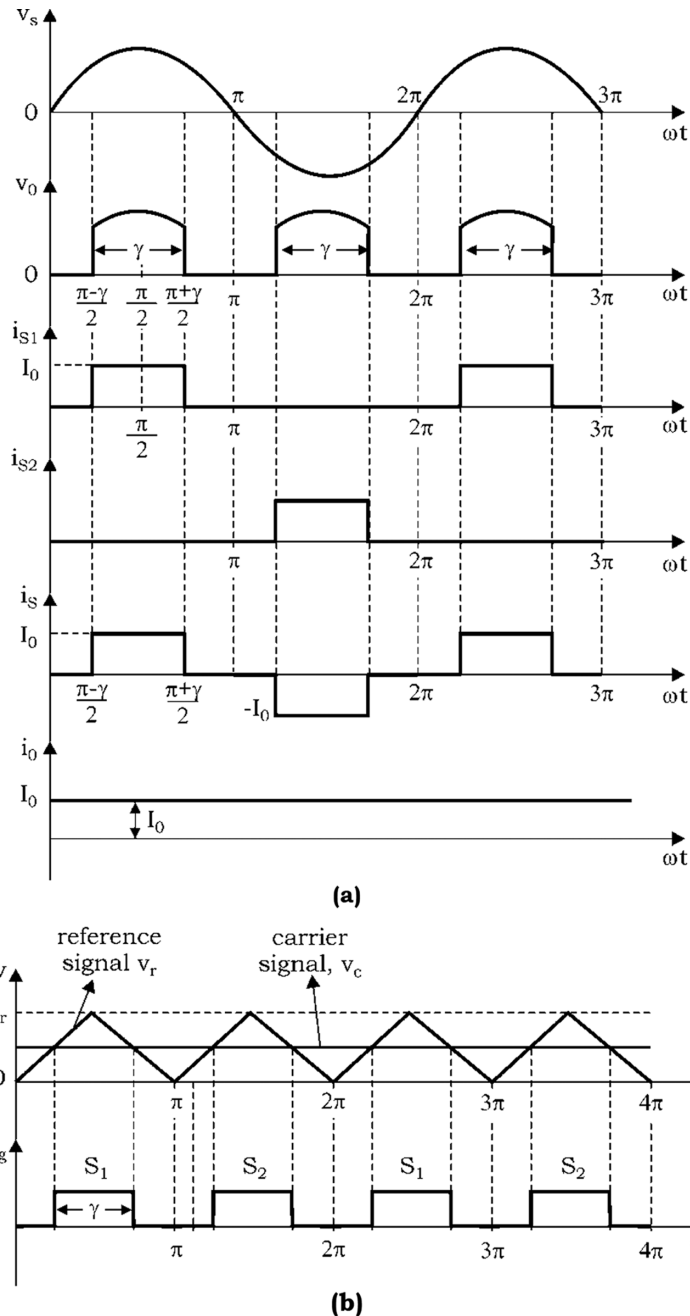


FIGURE 5.8 Symmetrical angle control: (a) voltage and current waveforms and (b) gate-pulse generation for SAC.

The average output voltage V_0 can be derived as:

$$V_0 = \frac{1 \times 2}{2\pi} \int_{\left(\frac{\pi-\gamma}{2}\right)}^{\left(\frac{\pi+\gamma}{2}\right)} V_m \sin \omega t d(\omega t) \quad (5.13)$$

$$\boxed{V_0 = \frac{2V_m}{\pi} \sin\left(\frac{\gamma}{2}\right)}$$

Therefore, V_0 can be varied from $\frac{2V_m}{\pi}$ to zero by varying conduction angle γ from π to zero.

The expression for RMS output voltage V_{rms} can be obtained as [4,5,8,18]:

$$V_{\text{rms}} = \left[\frac{1 \times 2}{2\pi} \int_{\left(\frac{\pi-\gamma}{2}\right)}^{\left(\frac{\pi+\gamma}{2}\right)} (V_m \sin \omega t)^2 d \omega t \right]^{\frac{1}{2}}$$

or

$$\boxed{V_{\text{rms}} = \frac{V_m}{\sqrt{2}} \left[\frac{1}{\pi} \gamma + \sin \gamma \right]^{\frac{1}{2}}} \quad (5.14)$$

$$\text{Displacement angle is } \phi_n = \tan^{-1} 0 = 0^\circ \quad (5.15)$$

$$\text{Displacement factor } DF = \cos \phi_l = \cos 0 = 1 \quad (5.16)$$

5.4.3 PULSE WIDTH MODULATION CONTROL

In the case of PAC, EAC, and SAC, the supply current has only one pulse per half cycle, and therefore the lowest order harmonics is third, which is very difficult to filter out. The lower-order harmonics can be eliminated if the supply current has more than one pulse per half cycle.

But contrary in PWM control, the converter switches are turned on/off several times during a half cycle to have more pulses per half cycle as shown in Figure 5.9a [4,5,8,18]. Here, the output voltage is controlled by varying the width of pulses.

The gate signals are generated by comparing a triangular wave with a DC signal, as shown in Figure 5.9b. The lower-order harmonics can be eliminated by selecting the number of pulses per half cycle.

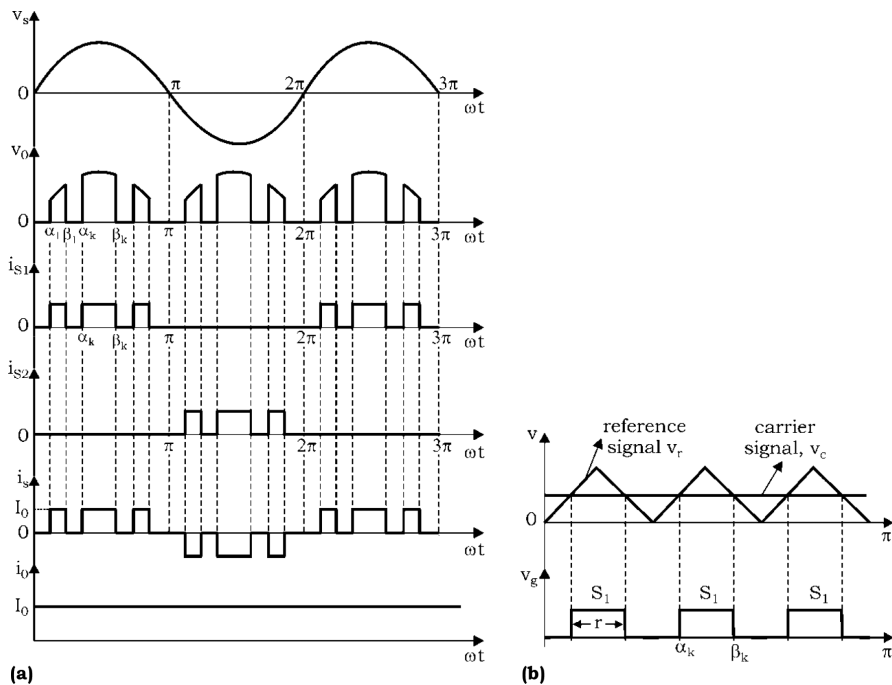


FIGURE 5.9 PWM control: (a) voltage and current waveforms and (b) gate-pulse generation for PWM control.

The average output voltage V_0 is given by:

$$V_0 = \frac{1 \times 2}{2\pi} \int_0^{\pi} V_m \sin \omega t \cdot d \omega t$$

$$= \frac{V_m}{\pi} \sum_{k=1}^p \int_{\alpha_k}^{\beta_k} \sin \omega t \cdot d \omega t$$

$$V_o = \frac{V_m}{\pi} \sum_{k=1}^p (\cos \alpha_k - \cos \beta_k) \quad (5.17)$$

where p = no. of pulse per half cycle.

$$\text{Displacement angle, } \phi_n = 0^\circ \quad (5.18)$$

$$\text{Displacement factor (DF)} = \cos \phi_l = \cos 0 = 1 \quad (5.19)$$

5.4.4 SINUSOIDAL PULSE WIDTH MODULATION CONTROL

There are different methods of varying the width of pulses and the most common one is the sinusoidal pulse-width modulation (SPWM). In SPWM control, as shown in [Figure 5.10](#), the firing signals (gate signals) for the switches are obtained by comparing a triangular reference wave (v_r) of amplitude (A_r) and frequency (f_r) with a rectified sinusoidal carrier wave (v_c) of amplitude (A_c) and frequency $2f_s$ [4,5,8,18]. The rectified sinusoidal wave is in phase with the supply phase voltage and has twice the supply frequency (f_s). The output voltage (i.e., width of pulses) is varied by changing the amplitude (A_c) or the modulation index (M) from 0 to 1. The modulation index can be defined as:

$$M = \frac{A_c}{A_r} \quad (5.20)$$

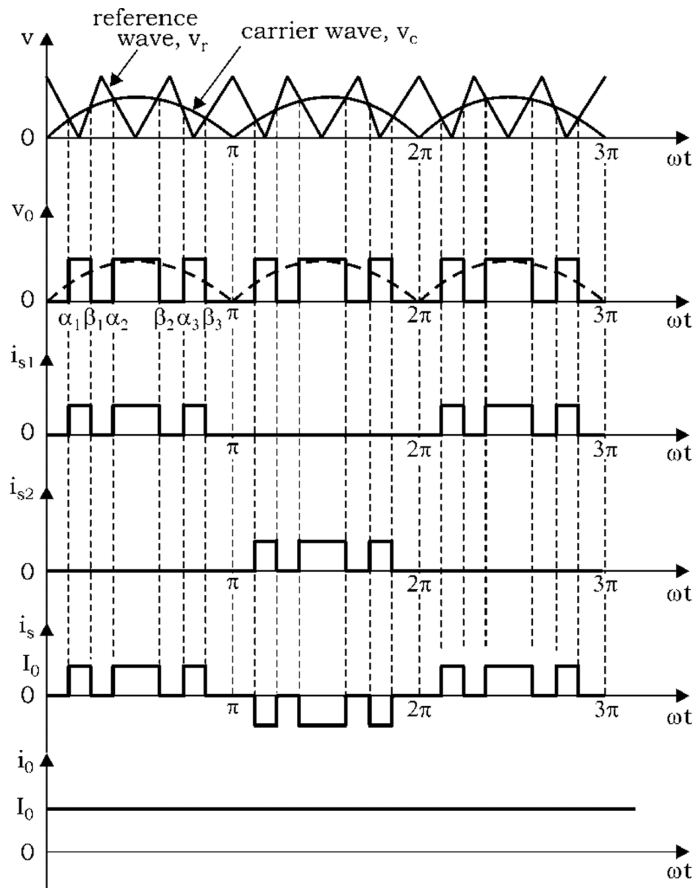


FIGURE 5.10 Sinusoidal PWM control.

In a sinusoidal PWM control, the displacement factor is unity, and the PF is improved. The lower-order harmonics are eliminated or reduced. For example: with four-pulses per half cycle, the lowest-order harmonic is 5th, with six-pulses per half cycle, the lowest-order harmonic is 7th.

5.5 INVERSION OPERATION

When phase-controlled full converters or line-commutated full converters are operated with a firing angle greater than 90° , then this operation of full converter is known as *inverter operation or inversion operation*. With the firing angle is greater than 90° , the average output voltage of converter V_0 becomes negative as shown in [Figure 5.11a](#) [4,5,8,18]. Therefore, the power is fed back to the AC supply.

Such an operation is used in the regenerative braking operation of a DC motor, where E is the back emf. Such an operation provides 4th-quadrant operation, as shown in [Figure 5.11b](#). When the full converter operates with a firing angle greater than 90° , that is, $\alpha > 90^\circ$, it is also called a line-commutated inverter.

5.6 SOLVED PROBLEMS

Example 5.1: A single-phase semiconverter is supplied from a 220-V, 50-Hz supply. Assume the load current I_0 to be continuous, and it is ripple free. The transformer turn ratio is unity. (a) Express input current in a Fourier series; find the input current HF, DF, and input PF. (b) for the delay angle $\alpha = \frac{\pi}{4}$ and $\frac{\pi}{2}$, calculate V_0 , V_{rms} , H_F , D_F , and PF .

SOLUTION

- (a) The instantaneous input current can be expressed in a Fourier series as [4,5,8,18]:

$$i_s(t) = a_0 + \sum_{n=1,2,\dots}^{\infty} (A_n \cos n\omega t + B_n \sin n\omega t) \quad (5.21)$$

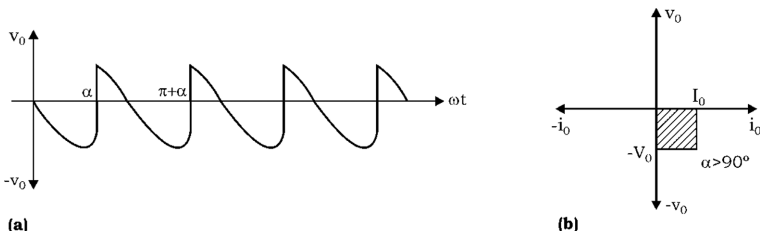


FIGURE 5.11 Inversion operation: (a) output voltage waveform for $1 - \phi$ full converter (RLE load) with $\alpha > 90^\circ$ and (b) quadrant.

where

$$a_0 = \frac{1}{2\pi} \int_{-\alpha}^{2\pi} i_s(t) d(\omega t) = \frac{1}{2\pi} \left[\int_{-\alpha}^{\pi} l_0 d(\omega t) - \int_{\pi+\alpha}^{2\pi} l_0 d(\omega t) \right] = 0$$

$$a_n = \frac{1}{\pi} \int_0^{2\pi} i_s(t) \cos n\omega t d(\omega t)$$

$$= \frac{1}{\pi} \left[\int_{-\alpha}^{\pi} l_0 \cos n\omega t d(\omega t) - \int_{\pi+\alpha}^{2\pi} l_0 \cos n\omega t d(\omega t) \right]$$

$$= -\frac{2l_0}{n\pi} \sin n\alpha \quad \text{for } n = 1, 3, 5, \dots$$

$$= 0 \quad \text{for } n = 2, 4, 6, \dots$$

$$b_n = \frac{1}{\pi} \int_0^{2\pi} i_s(t) \sin n\omega t d(\omega t)$$

$$= \frac{1}{\pi} \left[\int_{-\alpha}^{\pi} l_0 \sin n\omega t d(\omega t) - \int_{\pi+\alpha}^{2\pi} l_0 \sin n\omega t d(\omega t) \right]$$

$$= \frac{2l_0}{n\pi} (1 + \cos n\alpha)$$

$$\quad \text{for } n = 1, 3, 5, \dots$$

$$= 0 \quad \text{for } n = 2, 4, 6, \dots$$

Because $a_0 = 0$, Equation (5.21) can be expressed as

$$i_s(t) = \sum_{n=1,3,5}^{\infty} \sqrt{2} I_{sn} \sin(n\omega t + \phi_n) \quad (5.22)$$

where

$$\phi_n = \tan^{-1} \frac{a_n}{b_n} = -\frac{n\alpha}{2} \quad (5.23)$$

The RMS value of the n th harmonic component of the input current is derived as

$$I_{sn} = \frac{1}{\sqrt{2}} (a_n^2 + b_n^2)^{\frac{1}{2}} = \frac{2\sqrt{2} I_0}{n\pi} \cos \frac{n\alpha}{2} \quad (5.24)$$

From Equation (5.24), the RMS value of the fundamental current is

$$I_{s1} = \frac{2\sqrt{2} I_0}{\pi} \cos \frac{\alpha}{2}$$

The RMS input current can be calculated from Equation (5.24) as

$$I_s = \left(\sum_{n=1,2,\dots}^{\infty} I_{sn} \right)^{\frac{1}{2}}$$

I_s can also be determined directly from

$$I_s = \left[\frac{2}{2\pi} \int_{\alpha}^{\pi} I_0^2 d(\omega t) \right]^{\frac{1}{2}} = I_0 \left(1 - \frac{\alpha}{\pi} \right)^{\frac{1}{2}}$$

$$HF = \left[\left(\frac{I_s}{I_{s1}} \right)^2 - 1 \right]^{\frac{1}{2}}$$

or

$$HF = \left[\frac{\pi(\pi - \alpha)}{4(1 + \cos\alpha)} - 1 \right]^{\frac{1}{2}} \quad (5.25)$$

$$DF = \cos\phi$$

or

$$DF = \cos\phi_l = \cos\left(-\frac{\alpha}{2}\right) \quad (5.26)$$

or

$$PF = \frac{I_{s1}}{I_s} \cos\phi$$

$$PF = \frac{I_{s1}}{I_s} \cos \frac{\alpha}{2} = \frac{\sqrt{2}(1 + \cos\alpha)}{\left[\pi(\pi - \alpha)\right]^{\frac{1}{2}}} \quad (5.27)$$

(b) For delay angle $\alpha = \frac{\pi}{4}$:

$$\text{Given } \alpha = \frac{\pi}{4}, V_m = \sqrt{2} \times 220 = 311.2 \text{ V}$$

For 1- ϕ semiconverter:

$$\text{The average output voltage, } V_0 = \frac{V_m}{\pi} (1 + \cos \alpha)$$

$$= \frac{\sqrt{2} \times 220}{\pi} (1 + \cos 45^\circ)$$

$$= 169.06 \text{ V}$$

The normalized average output voltage, V_n

$$V_n = \frac{V_0}{V_{om}} = 0.5 (1 + \cos \alpha)$$

$$= 0.5 (1 + \cos 45^\circ) = 0.854 \text{ p.u.}$$

where V_{om} is maximum average output voltage $\left(\frac{2V_m}{\pi} \right)$

$$\text{The RMS output voltage, } V_{rms} = \frac{V_m}{\sqrt{2}} \left[\frac{1}{\pi} \left(\pi - \alpha + \frac{\sin 2\alpha}{2} \right) \right]^{\frac{1}{2}}$$

$$= \frac{311.2}{\sqrt{2}} \left[\frac{1}{\pi} \left(\pi - \frac{\pi}{4} + \frac{1}{2} \right) \right]^{\frac{1}{2}}$$

$$= \frac{311.2}{\sqrt{2}} \left[\frac{1}{\pi} \left(\frac{3}{4} \pi + \frac{1}{2} \right) \right]^{\frac{1}{2}}$$

$$= 209.82 \text{ V}$$

The RMS value of fundamental current,

$$I_{s1} = \frac{2\sqrt{2}I_o}{\pi} \cos \left(\frac{\alpha}{2} \right)$$

$$= \frac{2\sqrt{2}I_o}{\pi} \cos \frac{\pi}{8} = 0.832 I_o$$

$$\begin{aligned}
 \text{The RMS input current, } I_s &= I_0 \left(1 - \frac{\alpha}{\pi} \right)^{\frac{1}{2}} \\
 &= I_0 \left(1 - \frac{1}{4} \right)^{\frac{1}{2}} = 0.866 I_0 \\
 \therefore HF &= \left[\left(\frac{I_s}{I_{s1}} \right)^2 - 1 \right]^{\frac{1}{2}} \\
 &= \left[\left(\frac{0.866 I_0}{0.832 I_0} \right)^2 - 1 \right]^{\frac{1}{2}} = 0.288 \text{ or } 28.8\% \\
 \therefore DF \cos \phi &= \cos \left(-\frac{\pi}{8} \right) = 0.924
 \end{aligned}$$

$$PF = \frac{I_{s1}}{I_s} \cos \frac{\alpha}{2} = \frac{0.832 I_0}{0.866 I_0} \cos \frac{\pi}{8} = 0.89 \text{ (lagging)}$$

For delay angle $\alpha = \frac{\pi}{2}$:

$$\text{Given: } \alpha = \frac{\pi}{2}, V_m = \sqrt{2} \times 220 = 311.2 \text{ V}$$

For $1-\phi$ semiconverter,

$$\begin{aligned}
 V_o &= \frac{V_m}{\pi} (1 + \cos \alpha) = \frac{311.2}{\pi} (1 + \cos 90^\circ) \\
 &= 99.05 \text{ V}
 \end{aligned}$$

$$V_n = 0.5 (1 + \cos 90^\circ) = 0.5 \text{ p.u.}$$

$$V_{rms} = \frac{311.2}{\sqrt{2}} \left[\frac{1}{\pi} \left(\pi - \frac{\pi}{2} + \frac{\sin \pi}{2} \right) \right]^{\frac{1}{2}}$$

$$= 155.6 \text{ V}$$

$$I_{s1} = \frac{2\sqrt{2} I_0}{\pi} \cos \frac{\pi}{4} = 0.6366 I_0$$

$$I_s = I_0 \left(1 - \frac{1}{2} \right)^{\frac{1}{2}} = 0.707 I_0$$

$$\therefore HF = \left[\left(\frac{I_s}{I_{s1}} \right)^2 - 1 \right]^{\frac{1}{2}} = 0.4835 \text{ or } 48.35\%$$

$$\phi_l = -\frac{\pi}{4}$$

and

$$DF = \cos\left(-\frac{\pi}{4}\right) = 0.707$$

$$PF = \frac{I_{s1}}{I_s} \cos\frac{\pi}{4} = 0.6366 \text{ (lagging)}$$

Example 5.2: A three-phase semiconverter is supplied from a Y-connected 208-V, 50-Hz supply and load resistance is $R = 20 \Omega$. It is required to obtain an average output voltage of 50% of the maximum possible output voltage, calculate (a) delay angle α , (b) RMS and average output currents, (c) average and RMS thyristor currents, (d) rectification efficiency, (e) TUF, and (f) input PF.

SOLUTION

Given: Because the system is Y connected, the phase voltage is

$$V_s = \frac{208}{\sqrt{3}} = 120.1 \text{ V}$$

$$V_m = \sqrt{2} V_s = 169.83 \text{ V}$$

$$V_n = 0.5$$

$$R = 20 \Omega$$

The maximum output voltage of the three-phase semiconverter is,

$$V_{0m} = \frac{3\sqrt{3} V_m}{\pi} = 3\sqrt{3} \times \frac{169.83}{\pi}$$

$$= 280.9 \text{ V}$$

The average output voltage, $V_0 = V_{0m} \times V_n = 280.9 \times 0.5 = 140.5 \text{ V}$

- (a) Now with resistive load and 50% output, the output voltage is discontinuous. The normalized average output voltage, V_n is:

$$V_n = \frac{V_0}{V_{0m}} = 0.5(1 + \cos\alpha)$$

or

$$0.5 = 0.5(1 + \cos\alpha)$$

or

$$\alpha = 90^\circ$$

- (b) The average output current, $I_0 = \frac{V_0}{R} = \frac{140.5}{20} = 7.03 \text{ A}$
 The RMS output voltage for a 3- ϕ semiconverter,

$$\begin{aligned} V_{\text{rms}} &= \sqrt{3} V_m \left[\frac{3}{4\pi} \left(\pi - \alpha + \frac{1}{2} \sin 2\alpha \right) \right]^{\frac{1}{2}} \\ &= \sqrt{3} \times 169.83 \left[\frac{3}{4\pi} \left(\pi - \frac{\pi}{2} + 0.5 \sin 2 \times 90^\circ \right) \right]^{\frac{1}{2}} \\ &= 180.13 \text{ V} \end{aligned}$$

$$\therefore \text{The RMS load current, } I_{\text{rms}} = \frac{V_{\text{rms}}}{R} = \frac{180.13}{20} = 9.01 \text{ A}$$

- (c) The average current of thyristor, $I_A = \frac{I_0}{3} = \frac{7.03}{3} = 2.35 \text{ A}$
 The RMS current of a thyristor, $I_R = \frac{I_{\text{rms}}}{\sqrt{3}} = \frac{9.01}{\sqrt{3}} = 5.21 \text{ A}$

- (d) The rectification efficiency, η

$$\begin{aligned} \eta &= \frac{V_0 I_0}{V_{\text{rms}} I_{\text{rms}}} = \frac{140.5 \times 7.03}{180.13 \times 9.01} \times 100 \\ &= 60.86\% \end{aligned}$$

- (e) As a thyristor conducts for 120° , the RMS input line current is

$$I_s = I_{\text{rms}} \sqrt{\frac{2}{3}}$$

$$= 7.35 \text{ A}$$

The input VA rating, $VI = 3V_s I_s = 3 \times 120.1 \times 7.35 = 2650.5$ VA

$$\text{Now, TUF} = \frac{V_0 I_0}{VI} = \frac{V_0 I_0}{3V_s I_s} = \frac{140.5 \times 7.03}{3 \times 120.1 \times 7.35}$$

$$= 0.372 \text{ or } 37.2\%$$

$$(f) \text{ The input } PF = \frac{P_0}{VI} = \frac{I_{\text{rms}}^2 \times R}{2650.5} = 0.612 \text{ (lagging)}$$

Example 5.3: A three-phase full converter is fed from a three-phase 220-V, 50-Hz supply. The load current is continuous and ripple-free. If the average load current $I_0 = 180$ A and commutating inductance $L_s = 0.2$ mH, find the overlap angle when (a) $\alpha = 15^\circ$, (b) $\alpha = 30^\circ$, and (c) $\alpha = 60^\circ$.

SOLUTION

$$V_m = \sqrt{2} \times 220 / \sqrt{3} = 179.63 \text{ V}$$

and

$$V_{0m} = 3\sqrt{3} V_m / \pi = 297.11 \text{ V.}$$

$$\text{The average output voltage } V_0(\alpha) = \frac{3\sqrt{3} V_m}{\pi} \cos \alpha$$

$$= V_{0m} \cos \alpha$$

$$= 297.11 \cos \alpha$$

and average output voltage with overlap, $V_0(\alpha + \mu) = V_{0m} \cos(\alpha + \mu)$
 $= 297.11 \cos(\alpha + \mu)$

For a three-phase converter, the average voltage reduction due to commutating inductance L_s ,

$$6I_0 L_s = V_0(\alpha) - V_0(\alpha + \mu)$$

$$6 \times 50 \times 180 \times 0.2 \times 10^{-3} = 297.11 [\cos \alpha - \cos(\alpha + \mu)]$$

- (a) For $\alpha = 15^\circ$, $\mu = 6.62^\circ$;
- (b) For $\alpha = 30^\circ$, $\mu = 3.93^\circ$;
- (c) For $\alpha = 60^\circ$, $\mu = 2.37^\circ$;
- (d) For $\alpha = 75^\circ$, $\mu = 2.14^\circ$.

Example 5.4: If single-phase semiconverter is supplied from 220-V, 50-Hz supply. Find V_o , V_{rms} and form factor for firing angle $\frac{\pi}{2}$?

SOLUTION

$$\sqrt{2} \times 220 = 311.12 \text{ V}$$

For a 1- ϕ semiconverter, average output voltage,

$$V_o = \frac{V_m}{\pi} (1 + \cos \alpha)$$

$$= \frac{311.12}{\pi} (1 + \cos 90^\circ) = 99.05 \text{ V}$$

The RMS output voltage,

$$V_{rms} = \frac{V_m}{\sqrt{2}} \left[\frac{1}{\pi} \left(\pi - \alpha + \frac{\sin 2\alpha}{2} \right) \right]^{\frac{1}{2}}$$

$$= \frac{311.12}{\sqrt{2}} \left[\frac{1}{\pi} \left(\pi - \frac{\pi}{2} + \frac{\sin \pi}{2} \right) \right]^{\frac{1}{2}}$$

$$= \frac{311.12}{\sqrt{2}} \left[\frac{1}{\pi} \left(\frac{\pi}{2} \right) \right]^{\frac{1}{2}}$$

$$= 155.56 \text{ V.}$$

$$\text{Form Factor} = \frac{V_{rms}}{V_o} = \frac{155.56}{99.05} = 1.57 \text{ or } 157\%$$

Example 5.5: A three-phase full converter is fed by a 400-V, three-phase, 50-Hz mains. If the average load current is 200 A, source inductance is 0.2 mH per phase. Find the overlap angle if the firing angle is (a) 20°, (b) 30°, and (c) 60°.

SOLUTION

Peak value of line-to-neutral voltage, $V_m = \frac{\sqrt{2} \times 400}{\sqrt{3}} = 326.56 \text{ V}$. For a 3- ϕ full converter, the average voltage reduction due to source inductance,

$$V_x = \frac{3\omega L_s I_0}{\pi} = \frac{3 \times 2\pi \times 50 \times 0.2 \times 10^{-3}}{\pi} \times 200 = 12 \text{ V}$$

$$V_{0m} = \frac{3\sqrt{3} V_m}{\pi} = \frac{3\sqrt{3} (326.56)}{\pi} = 540.1 \text{ V}$$

(a) For $\alpha = 20^\circ$, $V_{0m} \cos(\alpha + \mu) = V_{0m} \cos\alpha - V_x$

$$\therefore 540.1 \cos(20^\circ + \mu) = 540.1 \cos 20^\circ - 12$$

or

$$\cos(20^\circ + \mu) = 0.917$$

or

$$20^\circ + \mu = \cos^{-1}(0.917) = 23.5^\circ$$

or

$$\mu = 3.5^\circ$$

(b) $\alpha = 30^\circ$, $V_{0m} \cos(\alpha + \mu) = V_{0m} \cos\alpha - V_x$

$$\therefore 540.1 \cos(30^\circ + \mu) = 540.1 \cos 30^\circ - 12$$

or

$$\cos(30^\circ + \mu) \mu = \frac{455.79}{540.1}$$

$$\mu = 2.46^\circ$$

For $\alpha = 60^\circ$, $V_{0m} \cos(\alpha + \mu) = V_{0m} \cos\alpha - V_x$

$$\therefore 540.1 \cos(60^\circ + \mu) = 540.1 \cos 60^\circ - 12$$

or

$$\cos(60^\circ + \mu) = 0.4777$$

or

$$\mu = 1.465^\circ$$

Example 5.6:

- (a) A three-phase semiconverter feeds power to a resistive load of 10Ω . For a firing angle delay of 30° , the load takes 5 kW . Determine the magnitude per phase input supply voltage.
- (b) Repeat part (a) in the case where the load current is made ripple-free by connecting an inductor in series with the load.

SOLUTION

We know that for $\alpha < 30^\circ$, the output voltage is continuous. For a resistive load, output current is also continuous. For a $3-\phi$ semiconverter, the RMS value of the output voltage is given by

$$(a) \quad V_{\text{rms}} = \left[\frac{1 \times 3}{2\pi} \left\{ \int_{-\left(\frac{\pi}{6}-\alpha\right)}^{\frac{\pi}{6}} V_{m1}^2 \cos^2 \omega t d(\omega t) + \int_{\frac{\pi}{6}}^{\left(\frac{\pi}{6}+\alpha\right)} V_{m1}^2 \cos^2 \omega t d(\omega t) \right\} \right]^{\frac{1}{2}}$$

or

$$V_{\text{rms}}^2 = \frac{3V_{m1}^2}{4\pi} \left[\left| \omega t + \frac{\sin 2\omega t}{2} \right|_{-\frac{\pi}{6}+\alpha}^{-\frac{\pi}{6}} + \left| \omega t + \frac{\sin 2\omega t}{2} \right|_{-\frac{\pi}{6}}^{\frac{\pi}{6}+\alpha} \right]$$

or

$$V_{\text{rms}} = \frac{V_{m1}}{2} \sqrt{\frac{3}{\pi}} \left[\frac{2\pi}{3} + \frac{\sqrt{3}}{2} (1 + \cos 2\alpha) \right]^{\frac{1}{2}},$$

$$\text{As } P = \frac{V_{\text{rms}}^2}{R}, V_{\text{rms}}^2 = P \times R$$

$$\therefore \text{for } \alpha = 30^\circ, \frac{2V_s^2}{4} \frac{3}{\pi} \left[\frac{2\pi}{3} + \frac{\sqrt{3}}{2} (1 + \cos 60^\circ) \right] = 5000 \times 10$$

or

$$V_s = 175.67 \text{ V and } V_{ph} = 101.43 \text{ V}$$

(b) For constant load current, $I_{\text{rms}} = \text{average load current, } I_0$

$$\therefore P = \frac{V_{\text{rms}}^2}{R}$$

or

$$\left[\frac{3V_{m1}}{2\pi} (1 + \cos 30^\circ) \right]^2 \frac{1}{10} = 5000 \text{ W}$$

or

$$V_s = \sqrt{50000} \times \frac{\sqrt{2}\pi}{3 \times 1.866} = 177.44 \text{ V and } V_{ph} = 102.45 \text{ V}$$

Example 5.7: A single-phase full converter is fed from a AC source with 220-V and 50-Hz. If the load resistance $R = 8\Omega$ and the source has an inductance of 1.5 mH. For a firing angle delay of 60° find (a) average output voltage, (b) angle of overlap, and (c) PF.

SOLUTION

(a) Average output voltage for $1-\phi$ full converter with overlap is,

$$\begin{aligned} V_o &= \frac{2V_m}{\pi} \cos \alpha - \frac{\omega L_s}{\pi} I_0 \\ &= \frac{2\sqrt{2} \times 220}{\pi} \cos 60^\circ - \frac{2\pi \times 50 \times 1.5 \times 10^{-3}}{\pi} \times 12.38 \\ &= 97.29 \text{V} \end{aligned}$$

(b) Also, the average output voltage V_o of $1-\phi$ full converter with overlap is,

$$\text{where } I_0 = V_o/R = (2Vm/\pi) \cos \alpha = 12.38 \text{A}$$

$$\therefore V_o = \frac{2V_m}{\pi} \cos(\alpha + \mu) + \frac{\omega L_s}{\pi} I_0$$

or

$$97.29 = \frac{\sqrt{2} \times 220}{\pi} \cos(\alpha + \mu) + \frac{2\pi \times 50 \times 1.5 \times 12.38}{1000 \times \pi}$$

$$\alpha + \mu = \cos^{-1} \left(\frac{95.433\pi}{2\sqrt{2} \times 220} \right) = 61.21^\circ$$

$$\therefore \mu = 1.22^\circ$$

\therefore overlap angle in degree = 1.22°

$$(c) \text{ Power factor} = \frac{V_o I_0}{V_s I_s} = \frac{97.29 \times 12.38}{220 \times 12.38} = 0.45 \text{ (lagging).}$$

Example 5.8: A three-phase full converter bridge is connected to a supply voltage of 220 V per phase and a frequency of 50 Hz. The source inductance is 3 mH. The load current on the DC side is constant at 18 A. If the load consists of a DC voltage source of 400 V having an internal resistance of 0.5 Ω, then calculate:

- (a) Firing angle delay and
- (b) Overlap angle in degrees.

SOLUTION

(a) Converter output voltage $V_o = E + I_0 R$

$$= 400 + 18 \times 0.5 = 409 \text{ V}$$

The average output voltage of a $3-\phi$ full converter bridge with overlap is:

$$V_0 = \frac{3V_{m1}}{\pi} \cos\alpha - \frac{3\omega L_s}{\pi} I_0$$

$$\therefore 409 = \frac{3\sqrt{6} \times 220}{\pi} \cos\alpha - \frac{3(2\pi \times 50)3}{1000 \times \pi} \times 18$$

or $\alpha = 34.33^\circ$

(b) Also, the average output voltage V_0 of a $3-\phi$ full-converter with overlap is:

$$V_0 = \frac{3V_{m1}}{\pi} \cos(\alpha + \mu) + \frac{3\omega L_s}{\pi} I_0$$

$$\therefore 409 = \frac{3\sqrt{6} \times 220}{\pi} \cos(\alpha - \mu) + \frac{3(2\pi \times 50)3}{1000 \times \pi} \times 18$$

or

$$\alpha + \mu = \cos^{-1}\left(\frac{392.8 \times \pi}{3\sqrt{6} \times 220}\right) = 40.28^\circ$$

$$\therefore \mu = 40.28^\circ - 34.33^\circ = 5.95^\circ$$

\therefore Overlap angle in degrees = 5.95°

Example 5.9: A single-phase symmetrical semiconverter, is fed from a 220-V, 50-Hz source. The load consists of $R = 20 \Omega$ and a large inductance. For a delay angle of 45° , find (a) average output voltage, (b) average output current, (c) average and RMS values of thyristor currents, (d) average and RMS values of diode currents, (e) input PF, and (f) circuit turn-off time.

SOLUTION

The waveforms for voltages and currents are sketched in [Figure 5.12](#).

When forward-biased thyristor T_1 is triggered at firing angle α , T_1D_1 starts conducting the constant current I_0 . Soon after $\omega t = \pi$, as supply voltage tends to go negative, diode D_2 becomes forward biased through D_1 . Therefore, from $\omega t = \pi$, the load current begins to freewheel through T_1D_2 . Thyristor T_2 becomes forward biased after $\omega t = \pi$. At $\omega t = \pi + \alpha$, when T_2 is turned on, current I_0 begins to flow

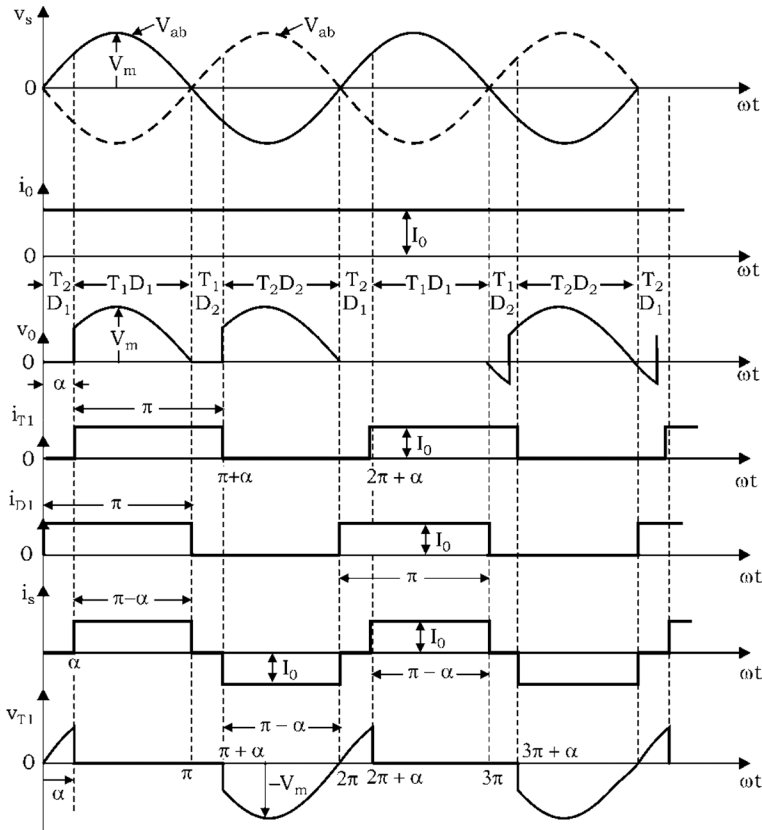


FIGURE 5.12 Semiconverter waveforms for voltages and currents.

through T_2D_2 as shown in Figure 5.13. Soon after $\omega t = 2\pi$, as the supply voltage tends to go positive, diode D_1 becomes forward biased through D_2 . As a result, current flows through T_2D_1 till T_1 is turned on at $\omega t = 2\pi + \alpha$ and so on.

The waveform of output voltage V_0 shows that average value of output voltage is:

$$V_0 = \frac{V_m}{\pi} (1 + \cos \alpha)$$

(a) Average value of output voltage

$$V_0 = \frac{\sqrt{2} \cdot 220}{\pi} (1 + \cos 45^\circ) = 169.15 \text{ V}$$

(b) $V_0 = I_0 R$

$$169.15 = I_0 \times 20$$

Average value of output current

$$I_0 = \frac{169.15}{20} = 8.45 \text{ A}$$

- (c) It is seen from the waveforms of thyristor current i_{T1} and diode current i_{D1} that both conduct for π radians for any value of firing delay angle. On account of this, the circuit of Figure 5.13 [4,5,8,18] is sometimes called a symmetrical configuration for a single-phase semiconverter.

The average value of the thyristor current

$$(I_T)_{\text{avg.}} = I_0 \frac{\pi}{2\pi} = \frac{I_0}{2} = \frac{8.45}{2} = 4.225 \text{ A}$$

RMS value of the thyristor current

$$(I_T)_{\text{rms}} = \sqrt{I_0^2 \frac{\pi}{2\pi}} = \frac{I_0}{\sqrt{2}} = \frac{8.45}{\sqrt{2}} = 5.97 \text{ A}$$

- (d) \therefore Average value of diode current = 4.225 A

RMS value of the diode current = 5.97 A

- (e) RMS value of source current

$$(I_s)_{\text{rms}} = \sqrt{I_0^2 \frac{\pi - \alpha}{\pi}} = I_0 \sqrt{\frac{\pi - \alpha}{\pi}}$$

$$= 8.45 \sqrt{\frac{\pi - \frac{\pi}{4}}{\pi}} = 7.32 \text{ A}$$

RMS value of load current $I_{\text{rms}} = I_0 = 8.45 \text{ A}$.

$$I_{\text{rms}}^2 \times R = (8.45)^2 \times 20$$

Also $220 \times 7.32 \times \cos \phi =$ Power delivered to load

$$\therefore \text{Input pf} = \frac{(8.45)^2 \times 20}{220 \times 7.32} = 0.88 \text{ (lagging)}$$

- (f) It is seen from the waveform of v_{T1} that circuit turn-off time is

$$t_c = \frac{\pi - \alpha}{\omega} = \frac{\pi - \frac{\pi}{4}}{2\pi \times 50} \times 1000 \text{ ms} = 7.5 \text{ ms}$$

Example 5.10: A single-phase full converter is operated with SAC. The load current is continuous and ripple-free. (a) Express the input current of converter in Fourier series, and find the HF of input current, DF, and input PF, (b) If the conduction angle is $\beta = \frac{\pi}{4}$ and the peak input voltage is $V_m = 169.83$ V, calculate V_o , V_{rms} , HF, DF, and PF.

SOLUTION

- (a) The waveform for input current is shown in Figure 5.7a and the instantaneous input current can be expressed in Fourier series as [4,5,8,18]:

$$i_s(t) = a_0 + \sum_{n=1,2,\dots}^{\infty} (A_n \cos n\omega t + B_n \sin n\omega t)$$

where

$$a_0 = \frac{1}{2\pi} \left[\int_{\frac{\pi-\beta}{2}}^{\frac{\pi+\beta}{2}} I_0 d(\omega t) - \int_{\frac{(3\pi-\beta)}{2}}^{\frac{(3\pi+\beta)}{2}} I_0 d(\omega t) \right] = 0$$

$$a_n = \frac{I}{\pi} \int_0^{2\pi} i_s(t) \cos n\omega t d(\omega t) = 0$$

$$b_n = \frac{1}{\pi} \int_0^{2\pi} i_s(t) \sin n\omega t d(\omega t) = \frac{4I_0}{n\pi} \sin \frac{n\beta}{2} \quad \text{for } n = 1, 3, \dots$$

$$= 0 \text{ for } n = 2, 4, \dots$$

Because $a_0 = 0$, the input current can be written as

$$i_s(t) = \sum_{n=1,3,5,\dots}^{\infty} \sqrt{2} I_{sn} \sin(n\omega t + \phi_n) \quad (5.28)$$

where

$$\phi_n = \tan^{-1} \frac{a_n}{b_n} = 0 \quad (5.29)$$

The RMS value of the n th harmonic input current is given as

$$I_{sn} = \frac{1}{\sqrt{2}} (a_n^2 + b_n^2)^{\frac{1}{2}} = \frac{2\sqrt{2}I_0}{n\pi} \sin \frac{n\beta}{2} \quad (5.30)$$

The RMS value of the fundamental current is

$$I_{s1} = \frac{2\sqrt{2}I_0}{\pi} \sin \frac{\beta}{2} \quad (5.31)$$

The RMS input current is found as

$$I_s = I_0 \sqrt{\frac{\beta}{\pi}} \quad (5.32)$$

$$HF = \left[\left(\frac{I_s}{I_{s1}} \right)^2 - 1 \right]^{\frac{1}{2}} = \left[\frac{\pi\beta}{4(1-\cos\beta)} - 1 \right]^{\frac{1}{2}} \quad (5.33)$$

$$DF = \cos\phi_l = 1 \quad (5.34)$$

$$PF = \left(\frac{I_{s1}}{I_s} \right) DF = \frac{2\sqrt{2}}{\sqrt{\beta\pi}} \sin \frac{\beta}{2} \quad (5.35)$$

- (b) For $\beta = \frac{\pi}{4}$, and $DF = 1.0$. With symmetrical angle control, average output voltage

$$V_0 = \frac{2V_m}{\pi} \sin \frac{\beta}{2}$$

or

$$V_0 = \left(2 \times \frac{169.83}{\pi} \right) \sin \frac{\pi}{8} = 41.4 \text{ V}$$

The RMS output voltage,

$$V_{rms} = \frac{V_m}{\sqrt{2}} \left[\frac{1}{\pi} (\beta + \sin \beta) \right]^{\frac{1}{2}}$$

or

$$V_{rms} = \frac{169.83}{\sqrt{2}} \left(\frac{\beta + \sin \beta}{\pi} \right)^{\frac{1}{2}} = 82.79 \text{ V}$$

From Equation (5.27), $I_{s1} = \frac{2\sqrt{2}I_0}{\pi} \sin \frac{\beta}{2}$

or

$$I_{s1} = I_0 \left(\frac{2\sqrt{2}}{\pi} \right) \sin \frac{\pi}{8} = 0.345 I_0$$

From Equation (5.28), $I_s = I_0 \sqrt{\frac{\beta}{\pi}} = 0.5 I_0$

$$HF = \left[\left(\frac{I_s}{I_{sl}} \right)^2 - 1 \right]^{\frac{1}{2}} = \left[\left(\frac{0.5 I_0}{0.345 I_0} \right)^2 - 1 \right]^{\frac{1}{2}} = 1049 \text{ or } 104.9\%$$

$$\therefore PF = \frac{I_{sl}}{I_s} = 0.69 \text{ (lagging)}$$

Example 5.11: A three-phase semiconverter connected with a 220-V, 50-Hz source charges a battery whose emf is 180 V with internal resistance of 0.4Ω . On account of inductance connected in series with the battery, the charging current is constant at 18 A. Determine the firing angle delay and the RMS value of the supply current.

SOLUTION

The battery terminal voltage is $V_0 = E + I_0 R$

$$V_0 = 118 + 18 \times 0.4 = 187.2 \text{ V}$$

But

$$V_0 = \frac{3V_m}{2\pi} (1 + \cos\alpha) = 187.2 \text{ V}$$

$$\therefore \alpha = \cos^{-1} \left[\frac{187.2 \times 2\pi}{3\sqrt{2} \times 220} - 1 \right] = 74.96^\circ$$

For firing angle $\alpha > 60^\circ$, each SCR conducts for $180^\circ - \alpha$. So, in this example, each SCR conducts for $(180 - 74.96) = 105.04^\circ$. For constant load current of $I_0 = 18 \text{ A}$, supply current i_A is of square wave of amplitude 18 A. As i_A flows for 105.04° over every half cycle of 180° , the RMS value of the supply current I_s is given by

$$I_s = \left[\frac{1}{\pi} (18)^2 \frac{105.04 \times \pi}{180} \right]^{\frac{1}{2}} = 18 \sqrt{\frac{105.04}{180}} = 13.75 \text{ A}$$

$$\text{Power delivered to load} = V_0 I_0 = 187.2 \times 18 = 3370 \text{ W}$$

$$\therefore \text{Input supply pf} = \frac{3370}{\sqrt{3} \times 220 \times 13.75} = 0.6431 \text{ (lagging).}$$

REVIEW QUESTIONS AND UNSOLVED PROBLEMS

- 5.1 A single-phase semiconverter is supplied from a 120-V, 50-Hz supply. The load current is continuous ripple-free. The transformer turns ratio is unity. For a delay angle of $\alpha = \pi/3$, calculate (a) harmonic factor of input current, (b) displacement factor, and (c) input PF.

- 5.2 Repeat Problem 5.1 for the three-phase semiconverter.
- 5.3 The single-phase semiconverter is supplied from a 120-V, 50-Hz supply. The load consists of series-connected resistance $R = 12 \Omega$, inductance $L = 8 \text{ mH}$
(a) Express the output voltage in a Fourier series and
(b) Calculate the RMS value of the lowest-order output harmonic current.
- 5.4 The single-phase semiconverter has an RL load of $L = 2 \text{ mH}$, $R = 2 \Omega$. The input voltage is $V_s = 120 \text{ V}$ (RMS) at 50 Hz: (a) Determine the load current I_0 , at $\omega t = 0$, and the load current I_1 at $\omega t = \alpha = 30^\circ$, (b) average thyristor current I_A , (c) RMS thyristor, current I_R , (d) RMS output current I_{rms} , and (e) average output current I_{dc} .
- 5.5 The single-phase semiconverter is operated from a 120-V, 50-Hz supply and uses an EAC. The load current is continuous and ripple-free. If the extinction angle is $\beta = \pi/3$, calculate (a) the outputs V_{dc} and V_{rms} (b) the harmonic factor of input current, (c) the displacement factor, and (d) the input PF.
- 5.6 Repeat Problem 5.5 for the three-phase semiconverter.
- 5.7 Repeat Problem 5.6 if SAC is used.
- 5.8 Repeat Problem 5.7 if EAC is used.
- 5.9 The single-phase semiconverter is operated with a sinusoidal PWM control and is supplied from a 130-V, 50-Hz supply. The load current with an average value of I_0 is continuous with negligible ripple content. There are five pulses per half cycle, and the pulses are $\alpha_1 = 7.93^\circ$, $\delta_1 = 5.82^\circ$; $\alpha_2 = 30^\circ$, $\delta_2 = 16.25^\circ$; $\alpha_3 = 52.07^\circ$, $\delta_3 = 127.93^\circ$; $\alpha_4 = 133.75^\circ$, $\delta_4 = 16.25^\circ$, and $\alpha_5 = 166.25^\circ$, $\delta_5 = 5.82^\circ$. Calculate (a) the V_{dc} , and V_{rms} , (b) the harmonic factor of input current, (c) the displacement factor, and (d) the input PF.
- 5.10 A three-phase semiconverter is operated from a three-phase Y-connected 220-V, 50-Hz supply. The load current is continuous and has negligible ripple. The average load current is $I_0 = 250 \text{ A}$ and commutating inductance per phase is $L_r = 0.5 \text{ mH}$. Determine the overlap angle if (a) $\alpha = \pi/6$, and (b) $\alpha = \pi/3$.
- 5.11 Repeat Problem 5.10 if $L = 0$.
- 5.12 Explain why the input PF of the semiconverter is better than full converter.
- 5.13 Why are semiconverter called half-controlled rectifiers?
- 5.14 List various PF improvement techniques.
- 5.15 Draw the power circuit diagram for symmetrical and asymmetrical single-phase semiconverters.

SUMMARY

The half-controlled rectifiers or semiconverters are used at high power levels for controlled transfer of power between an AC source and the adjustable DC load by controlling phase angle or delay angle of thyristors. Their input PF is better as compared to full converters due to their inherent freewheeling action. Because the polarity of DC voltage cannot be reversed, these converters operate in the first quadrant only. This chapter has discussed in detail the various types of semiconverters with the effect of source and load impedance on their performance.

MAIN FORMULAS OF THE CHAPTER

- Single-phase semiconverter with RL load (*continuous conduction*)

$$V_0 = \frac{V_m}{\pi} (1 + \cos \alpha)$$

$$V_{\text{rms}} = \frac{V_m}{\sqrt{2\pi}} \left[(\pi - \alpha) + \frac{\sin 2\alpha}{2} \right]^{\frac{1}{2}}$$

- Three-phase semiconverter with RL load

$$\text{For } \alpha < 60^\circ, V_0 = \frac{3V_{m1}}{2\pi} (1 + \cos \alpha)$$

$$\text{For } \alpha \geq 60^\circ, V_0 = \frac{3V_{m1}}{2\pi} (1 + \cos \alpha)$$

- EAC

$$V_0 = \frac{V_m}{\pi} (1 + \cos \beta)$$

$$V_{\text{rms}} = \frac{V_m}{\sqrt{2}} \left[\frac{1}{\pi} \left(\pi - \beta + \frac{\sin 2\beta}{2} \right) \right]^{\frac{1}{2}}$$

$$I_s = \sqrt{\frac{\beta}{\pi}} I_0$$

- SAC

$$V_0 = \frac{2V_m}{\pi} \sin\left(\frac{\gamma}{2}\right)$$

$$V_{\text{rms}} = \frac{V_m}{\sqrt{2}} \left[\frac{1}{\pi} \gamma + \sin \gamma \right]^{\frac{1}{2}}$$

Displacement angle is $\phi_n = \tan^{-1} 0 = 0^\circ$

Displacement factor $DF = \cos \phi_1 = \cos 0 = 1$

- **PWM control**

$$V_0 = \frac{V_m}{\pi} \sum_{k=1}^p (\cos \alpha_k - \cos \beta_k)$$

Displacement angle, $\phi_n = 0^\circ$

Displacement factor (DF) = $\cos \phi_l = \cos 0 = 1$

- **Sinusoidal PWM control**

$$M = \frac{A_c}{A_r}$$

- **For single-phase semiconverter**

$$HF = \left[\frac{\pi(\pi - \alpha)}{4(1 + \cos \alpha)} - 1 \right]^{\frac{1}{2}}$$

$$DF = \cos \phi_l = \cos \left(-\frac{\alpha}{2} \right)$$

$$PF = \frac{I_{s1}}{I_s} \cos \frac{\alpha}{2} = \frac{\sqrt{2}(1 + \cos \alpha)}{\left[\pi(\pi - \alpha) \right]_2^{\frac{1}{2}}}$$

- **For single-phase full converter**

$$HF = \left[\left(\frac{I_s}{I_{s1}} \right)^2 - 1 \right]^{\frac{1}{2}} = \left[\frac{\pi \beta}{4(1 - \cos \beta)} - 1 \right]^{\frac{1}{2}}$$

$$DF = \cos \phi_l = 1$$

$$PF = \left(\frac{I_{s1}}{I_s} \right) DF = \frac{2\sqrt{2}}{\sqrt{\beta \pi}} \sin \frac{\beta}{2}$$

REFERENCES/FURTHER READING

1. B. C. Kharbas, P.F. improvement technique in SPC, *IET-UK International Conference Information and Communication Technology in Electrical Sciences (ICTES)*, Chennai, India, 2007.
2. K. Basu, A. K. Sahoo, V. Chandrasekaran, and N. Mohan, Grid-side AC line filter design of a current source rectifier with analytical estimation of input current ripple, *IEEE Transactions on Power Electronics*, vol. 29, no. 12, pp. 6394–6405, 2014.
3. N. Mohan, T. M. Undeland, and W. P. Robbins, *Power Electronics: Converters, Applications and Design*, John Wiley & Sons, Hoboken, NJ, 1996.
4. B. K. Bose, *Power Electronics and AC Drives*, Prentice Hall, Englewood Cliffs, NJ, 1986.
5. M. H. Rashid, *Power Electronics: Circuits, Devices, and Applications*, Pearson Education, Singapore, 2004.
6. P. T. Krein, *Elements of Power Electronics*, Oxford University Press, New York, 2003.
7. K. Thorborg, *Power Electronics*, Prentice Hall International (U.K) Ltd, London, UK, 1988.
8. P. S. Bhimra, *Power Electronics*, 4th edn, Khanna Publications, New Delhi, 2012.
9. I. Batarseh and A. Harb, *Power Electronics*, Springer Nature, Cham, Switzerland, 2018.
10. R. S. Ramshaw, *Power Electronics Semiconductor Switches*, Springer Nature, Boston, MA, 1993.
11. K. M. Smedley and E. Santi, *AC-DC Power Converters*, Wiley, New York, 1999.
12. B. L. Dokić and B. Blanusa, *Power Electronics: Converters and Regulator*, 3rd edn, Springer-Verlag, Berlin, Germany, 2015.
13. R. W. Erickson, *Fundamentals of Power Electronics*, Springer, New York, 2001.
14. B. Wu and B. Wu, *High-Power Converters and AC Drives*, John Wiley & Sons, Hoboken, NJ, 2017.
15. R. W. Erickson, *Fundamentals of Power Electronics*, Chapman and Hall, New York, 1997.
16. V. R. Moorthi, *Power Electronics Devices, Circuits and Industrial Applications*, Oxford University Press, New York, 2010.
17. T. Suntio, T. Messo, and J. Puukko, *Power Electronic Converters*, Wiley-VCH, Verlag GmbH, Berlin, Germany, 2018.
18. A. M. Trzynadlowski, *Introduction to Modern Power Electronics*, 3rd edn, John Wiley & Sons, 2010.
19. M. Trzynadlowski, *Power Electronic Converters and Systems*, Institution of Engineering and Technology, London, UK, 2016.
20. B. M. Wilamowski and J. D. Irwin, *Power Electronics and Motor Drives*, CRC Press, 2011.
21. E. Acha, V. G. Agelidis, O. Anaya-Lara, and T. J. E. Miller, *Power Electronic Control in Electrical Systems*, Newnes, Oxford, UK, 2002.
22. F. Mazda, *Power Electronics Handbook*, Newnes, Oxford, UK, 1997.
23. F. Blaabjerg, *Control of Power Electronic Converters and Systems*, Academic Publishers, New York, 2018.
24. S. N. Manias, *Power Electronics and Motor Drive Systems*, Academic Publishers, London, UK, 2017.

6 Chopper

6.1 INTRODUCTION

Choppers are the switching converters, which convert unregulated DC input voltage into a controlled DC output at a desired voltage with little power loss. Nowadays, DC-to-DC conversion is becoming very important in different electronic circuit applications. There are many circuits which use DC power at several different voltage levels, such as in battery-operated systems. Duty ratio control or the pulse-width modulation (PWM) is effectively used to control these converters. Various applications where variable DC power (chopper) is required are trolley cars, marine hoists, battery-operated vehicles, battery charging, subway cars, mine haulers etc. Chopper system provides smooth control, high efficiency, and fast response. The power semiconductor devices used for a chopper circuit can be power bipolar junction transistor (BJT), power metal-oxide semiconductor field-effect transistor (MOSFET), gate turn-off (GTO), or forced-commutated thyristor.

6.2 CHOPPER CLASSIFICATIONS

DC choppers can be classified as:

- **According to the input/output voltage levels**
 1. *Step-down chopper*: The output voltage is less than the input voltage, that is, $V_0 < V_s$.
 2. *Step-up chopper*: The output voltage is greater than the input voltage, that is, $V_0 > V_s$.
- **According to the directions of output voltage and current**
 1. *Class A (type A) chopper*
 2. *Class B (type B) chopper*
 3. *Class C (type C) chopper*
 4. *Class D (type D) chopper*
 5. *Class E (type E) chopper*

The voltage and current directions for above classes are shown in [Figure 6.1](#).

- **According to circuit operation**
 1. *One-quadrant chopper*: The output voltage and current both are positive (Class A and Class B).
 2. *Two-quadrant chopper*: The output voltage is positive and current can be positive or negative (Class C), or the output current is positive, and the voltage can be positive or negative (Class D).
 3. *Four-quadrant chopper*: The output voltage and current both can be positive or negative (Class E).

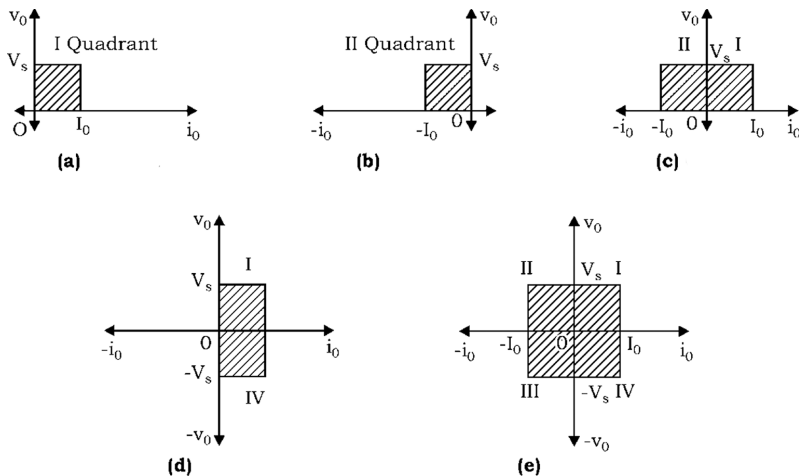


FIGURE 6.1 Voltage and current direction for various classes of choppers: (a) Class A, (b) Class B, (c) Class C, (d) Class D, and (e) Class E.

- **According to commutation method**

1. *Voltage-commutated choppers*
2. *Current-commutated choppers*
3. *Load-commutated choppers*

6.3 PRINCIPLE OF CHOPPER OPERATION

DC-to-DC converter (chopper) is a high-speed on/off semiconductor switch that connects the source with the load and disconnects the load from the source at a very fast speed. In this way, a chopped load voltage as shown in Figure 6.2a is obtained from a constant/fixed DC supply.

In Figure 6.2b, the chopper is represented by a switch inside a rectangular. It includes a power semiconductor device along with circuitry used for controlling the on and off periods of the device.

When the chopper is on, then the load voltage V_0 becomes equal to source voltage V_s , and load current i_0 increases from I_{\min} to I_{\max} .

When the chopper is off, then the load current flows through a freewheeling diode (FD) and so load terminals are short-circuited by the FD. Therefore, the load voltage V_0 becomes zero and load current i_0 decreases from I_{\max} to I_{\min} . In this way, by turning on and off the chopper, a chopped DC output voltage is produced. Here, the load current is taken as continuous.*

From Figure 6.2b, the average load voltage V_0 is given by:

$$V_0 = \frac{1}{T} \int_0^{T_{on}} V_s \, dt$$

* Continuous conduction means the load current never becomes zero during the operation.

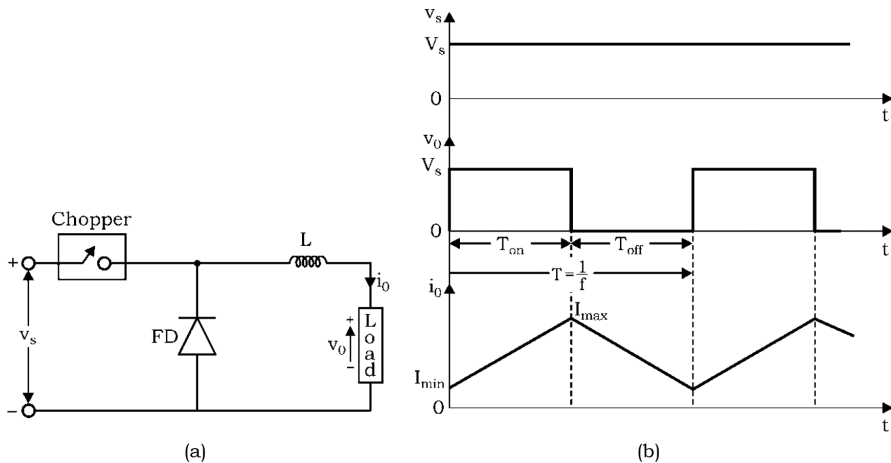


FIGURE 6.2 (a) Chopper circuit, and (b) voltage and current waveforms.

$$= \frac{V_s}{T} [t]_0^{T_{on}}$$

$$= \frac{V_s}{T} [T_{on} - 0]$$

$V_0 = \frac{T_{on}}{T} V_s = \delta V_s$

(6.1)

$V_0 = f T_{on} V_s$

(6.2)

where

T_{on} is the on-period of the chopper,

T_{off} is the off period of the chopper,

$T = T_{on} + T_{off}$ = chopping period

$\delta = \frac{T_{on}}{T}$ = duty cycle or duty ratio

$f = \frac{1}{T}$ = chopper frequency

Therefore, from Equation (6.2), it can be seen that the load voltage can be controlled by varying the duty cycle (δ), and also the load voltage is independent of the load current.

6.4 CONTROL STRATEGIES

As seen from Equation (6.1), that average value of output voltage V_0 can be controlled by controlling the duty cycle (δ), that is, by turning on and off the semiconductor switch periodically [1,3,4,23,24]. Two control strategies are used to control the duty cycle:

1. Time ratio control (TRC):
 - a. Constant frequency system
 - b. Variable frequency system
2. Current limit control (CLC)

6.4.1 TIME RATIO CONTROL

In TRC control, the value of T_{on}/T is varied, which is affected by two ways:

1. *Constant frequency system*: In this control, T_{on} period is varied by keeping total time T or chopping frequency f constant, as shown in [Figure 6.3](#). As T_{on} period is varied, so it is also called PWM control.
2. *Variable frequency system*: In this control, the chopping frequency f (or chopping period T) is varied by either keeping T_{on} period as constant or T_{off} period as constant, as shown in [Figure 6.4](#). Because the total time period T or frequency f is varied, it is also called the frequency modulation control.

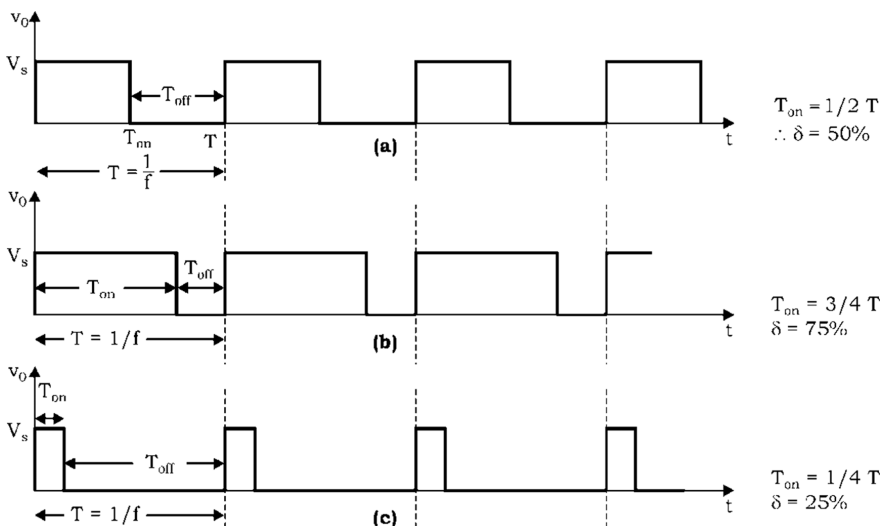


FIGURE 6.3 Principle of constant frequency system.

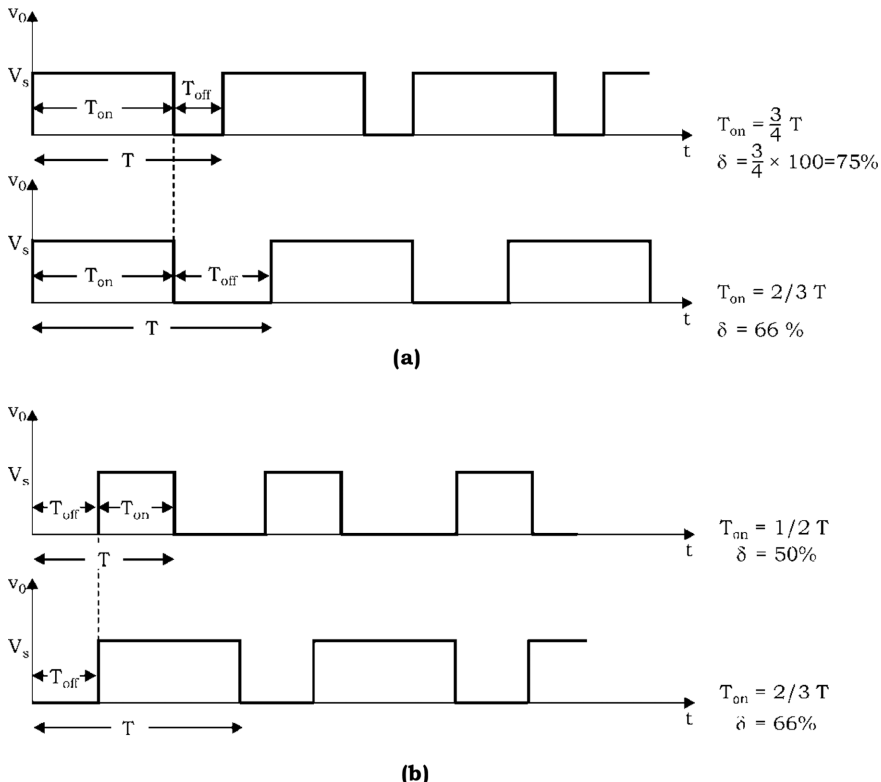


FIGURE 6.4 Principle of variable frequency system: (a) T_{on} kept constant but $T = 1/f$ is varied and (b) T_{off} kept constant but $T = 1/f$ is varied.

Frequency modulation control has some disadvantages as compared to PWM control, which are given as:

1. Because the chopping frequency has to be varied over a wide range in frequency modulation control, the filter design for such a wide frequency variation becomes difficult and expensive.
2. Large T_{off} period in frequency modulation may result into discontinuous.* conduction, which is undesirable.
3. More possibility of interference with signals and telephone lines in frequency modulation control due to wide frequency variation.

Therefore, a generally constant frequency system (PWM) is preferred.

* Discontinuous conductions: where the load current become zero in every cycle.

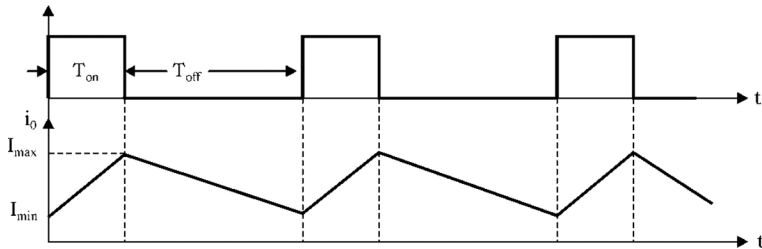


FIGURE 6.5 Current limit control.

6.4.2 CURRENT LIMIT CONTROL

In this type of control strategy, the chopper is switched on and off in such a way that the current in the load is maintained between two limits. When the current exceeds the upper limit, the chopper is switched off. During the off period, the load current freewheels through the FD, and therefore it decreases. When it reaches the lower limits, the chopper is switched on, and therefore the load current increases. It is used only when the load has energy storage elements. [Figure 6.5](#) illustrates the CLC.

6.5 STEP UP/DOWN CHOPPER

A chopper can also be used both in step-up and step-down mode by continuously varying its duty cycle (δ). The principle of operation is illustrated in [Figure 6.6](#). As shown, output-voltage polarity is opposite to that of input voltage V_s .

When the chopper is on, the supply current flows through the path $V_s+ \rightarrow \text{CH} \rightarrow L \rightarrow V_s-$, and inductor L stores the energy during on period T_{on} .

When the chopper is off, the inductor current tends to decrease, and as a result, the polarity of the emf induced in L is reversed as shown in [Figure 6.6](#). Thus, the energy stored by indicator L discharges in the load through the path $L_+ - \text{Load} - D - L_-$, as shown in [Figure 6.6](#).

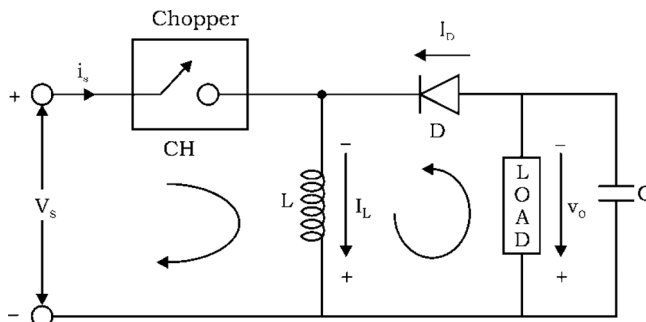


FIGURE 6.6 Step up/down chopper.

During T_{on} , energy stored in L is given by:

$$E_i = V_s I_s T_{on} \quad (6.3)$$

During T_{off} , energy fed to load is

$$E_0 = v_0 I_s T_{off} \quad (6.4)$$

for a lossless system, in the steady state:

input energy E_i = output energy E_0

$$\therefore V_s I_s T_{on} = V_0 I_s T_{off}$$

or

$$V_0 = V_s \frac{T_{on}}{T_{off}}$$

or

$$V_0 = V_s \frac{T_{on}}{T - T_{on}} = V_s \frac{\frac{1}{\frac{T}{T_{on}} - \frac{T_{on}}{T_{on}}}}{1}$$

Substitute $\frac{T_{on}}{T} = \delta$, we get

$$V_0 = V_s \frac{1}{1/\delta - 1}$$

or

$$V_0 = V_s \frac{\delta}{1 - \delta}$$

(6.5)

For $0 < \delta < 0.5$ —step-down chopper operation
and for $0.5 < \delta < 1$ —step-up chopper operation

6.6 CHOPPER CONFIGURATIONS

Choppers may be classified according to the number of quadrants of $V_0 - I_0$ diagram in [Figures 6.1](#) and [6.7](#), which they are capable of operating [1–24]. So, they are classified as Class A, Class B, Class C, Class D, and Class E choppers.

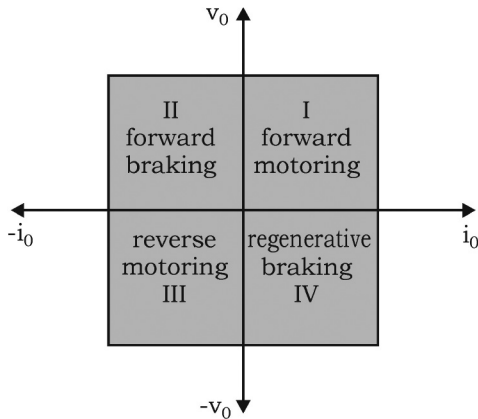


FIGURE 6.7 Polarities of output voltage and current.

6.6.1 FIRST-QUADRANT OR TYPE-A CHOPPER

The power circuit diagram for this chopper is shown in [Figure 6.8a](#). When chopper CH_1 is on, load current i_0 flows through path $-\text{CH}_1\text{-load}$. So, load voltage is $V_0 = V_s$ and load current is $i_0 = \text{positive}$ (in the direction of arrow).

When the chopper is turned off, then load current i_0 freewheels through the FD. So, load voltage, $v_0 = 0$ and load current, i_0 is the positive (in direction of arrow). Therefore, the load voltage and load current, that is, v_0 and i_0 are always positive, giving the first-quadrant operation as shown in [Figure 6.8b](#). It is also called a step-down chopper as $V_0 < V_s$, that is, power flows from the source to the load.

6.6.2 SECOND-QUADRANT OR TYPE-B CHOPPER

The power circuit diagram for this type of chopper is shown in [Figure 6.9a](#).

When CH_2 is on, load voltage E drives current i_0 through L and CH_2 . Inductor L stores energy during T_{on} period of CH_2 , so i_0 is the negative (as flow in opposite direction of arrow) and $V_0 = 0$.

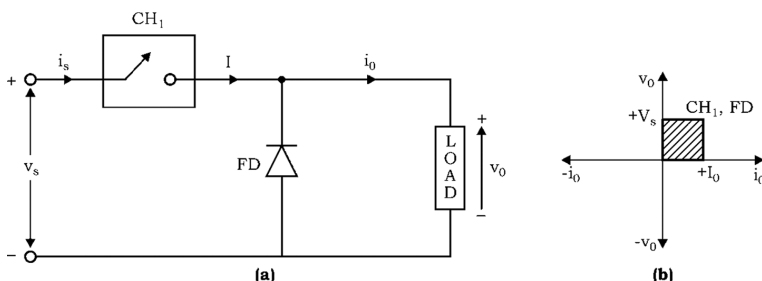


FIGURE 6.8 First quadrant or Type A, or Class A chopper. (a) Power circuit diagram (b) Quadrant diagram.

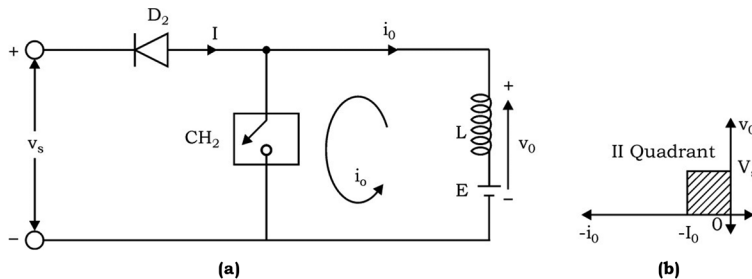
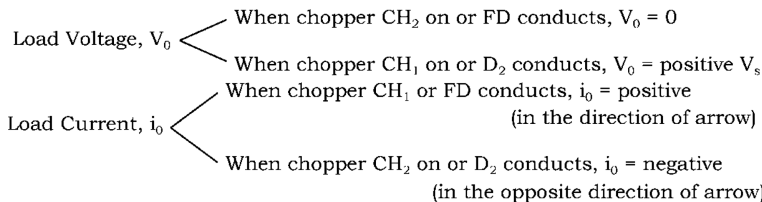


FIGURE 6.9 Second quadrant or Type-B or Class-B chopper: (a) circuit diagram (b) $v_0 - i_0$ characteristic.

When CH_2 is turned off, $V_0 = (E + L \frac{di_0}{dt})$ exceeds source voltage V_s . So, D_2 becomes forward biased (FB) and starts conducting. Therefore, power flows from load to source, so i_0 is negative. Since v_0 is always positive and i_0 is negative, this chopper operates in the second quadrant, as shown in $v_0 - i_0$ characteristics (Figure 6.9b).

6.6.3 TWO-QUADRANT TYPE-A CHOPPER OR TYPE-C CHOPPER

This type of chopper is obtained by connecting Type-A and Type-B chopper in parallel as shown in Figure 6.10a.



Therefore, it can be seen that for Type C chopper, the load voltage v_0 is always positive, but the load current can be positive as well as negative. So, the first- and second-quadrant operation can be achieved by properly operating the devices, as illustrated in Figure 6.10b.

6.6.4 TWO-QUADRANT TYPE-B CHOPPER OR TYPE-D CHOPPER

The power circuit diagram of Type-D chopper is shown in Figure 6.11a. When CH_1 and CH_2 conduct, load voltage V_0 and load current I_0 are positive. But when Diodes

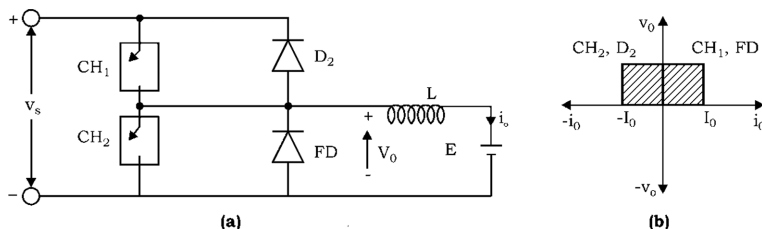


FIGURE 6.10 Class C or Type C chopper. (a) Circuit diagram (b) $v_0 - i_0$ characteristic.

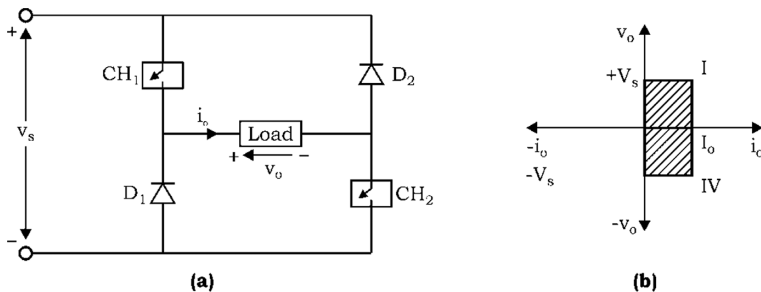


FIGURE 6.11 Class D or Type-D chopper. (a) Power circuit diagram and (b) quadrant diagram.

D_1 and D_2 conduct a load, voltage V_o is negative, but the load current remains positive, as shown in Figure 6.11.

So, the load current is always positive (i.e., in direction of the arrow), but the load voltage can be positive as well as negative. Therefore, power flow is reversible, resulting into I- and IV-quadrant operation, as illustrated in Figure 6.11b.

6.6.5 FOUR-QUADRANT CHOPPER OR TYPE-E CHOPPER

The power circuit diagram for Type-E chopper is shown in Figure 6.12a. It consists of four semiconductor switches CH_1 to CH_4 and four diodes D_1 to D_4 in antiparallel. It can

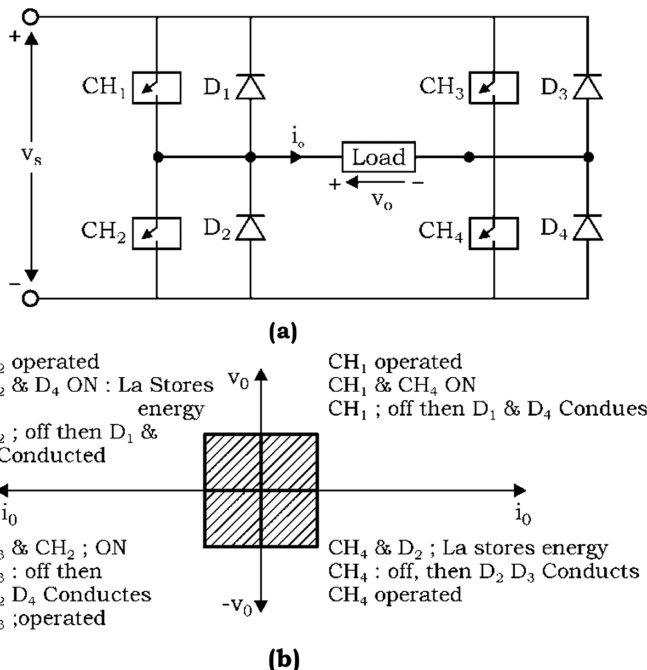


FIGURE 6.12 Type E chopper: (a) circuit diagram and (b) $v_o - i_o$ characteristics.

be operated in any of the four quadrants by properly turning on and off the choppers (CH_1 to CH_4). The devices conducting in four quadrants are indicated in Figure 6.12b.

6.7 ANALYSIS OF TYPE-A (STEP-DOWN) CHOPPER

6.7.1 WITH RESISTIVE LOAD

For resistive load, the load current waveform is similar to the load voltage waveform, and there is no role of the FD as shown in Figure 6.13.

- The average output voltage, V_0 is:

$$V_0 = \frac{T_{on}}{T_{on} + T_{off}} V_s = \frac{T_{on}}{T} V_s = \delta V_s \quad (6.6)$$

- Average output current,

$$I_0 = \frac{V_0}{R} = \frac{T_{on}}{T} \frac{V_s}{R} = \delta \frac{V_s}{R} \quad (6.7)$$

- For resistive load, the FD does not have a role.
- Root mean square (RMS) output voltage,

$$V_{rms} = \left[\frac{1}{T} \int_0^{T_{on}} (V_s)^2 dt \right]^{1/2} = \sqrt{\delta} V_s \quad (6.8)$$

- Average thyristor current (chopper) = $\frac{T_{on}}{T} \cdot \frac{V_s}{R} = \delta \frac{V_s}{R}$

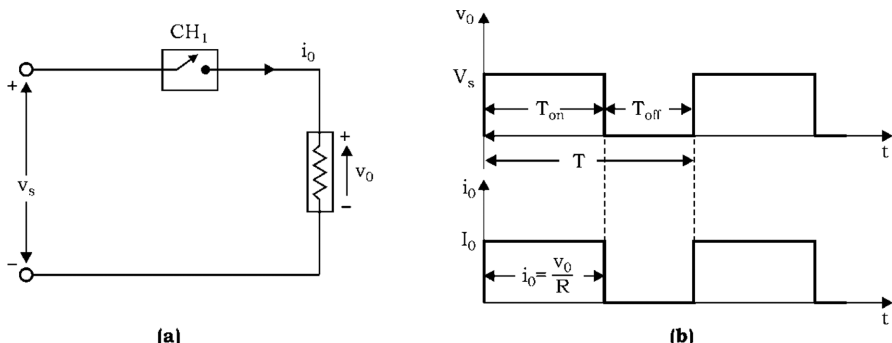


FIGURE 6.13 Type A or step-down chopper with R load: (a) circuit diagram and (b) voltage and current waveforms.

- RMS thyristor current (chopper) = $\sqrt{\delta} \frac{V_s}{R}$ (6.10)

- Power output,

$$P_0 = \frac{V_{\text{rms}}^2}{R} = \frac{\delta V_s^2}{R} \quad (6.11)$$

- If losses are neglected, the input power is equal to the output power. Therefore

average thyristor current = average load current = average source current

$$= \frac{V_0}{R} = \frac{\delta V_s}{R} \quad (6.12)$$

- Effective input resistance of chopper (R_i) = $\frac{\text{input voltage}}{\text{average input current}}$

$$= \frac{V_s}{\delta V_s / R} = \frac{R}{\delta} \quad (6.13)$$

6.7.2 WITH RLE LOAD

Power circuit diagram along with its load voltage and current waveforms for continuous and discontinuous conduction are shown in [Figure 6.14 \[3,4,23\]](#).

When CH_1 is on, the equivalent circuit is as shown in [Figure 6.14d](#). For this mode of operation, the differential equation governing its performance is:

$$V_s = Ri + L \frac{di}{dt} + E \quad \text{for } 0 < t < T_{on} \quad (6.14)$$

When CH_1 is off, the load current continues flowing through the FD and the equivalent circuit is shown in [Figure 6.14e](#). The differential equation for this circuit is:

$$0 = Ri + L + E \frac{di}{dt} \quad \text{for } T_{on} < t < T \quad (6.15)$$

Initial value of current is I_{\min} for Equation (6.14) and I_{\max} for Equation (6.15). So, Laplace transform of Equations (6.14) and (6.15) are:

$$RI(s) + L[sI(s) - I_{\min}] = \frac{V_s - E}{s} \quad (6.16)$$

and

$$RI(s) + L[sI(s) - I_{\max}] - \frac{E}{s} = 0 \quad (6.17)$$

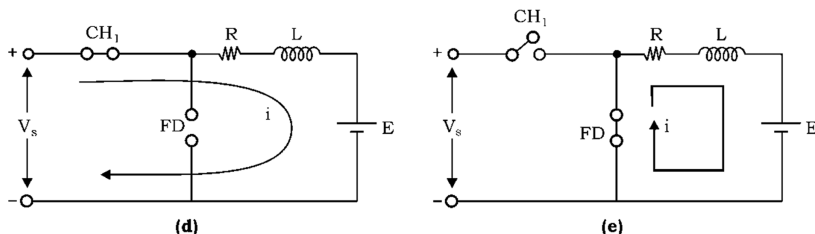
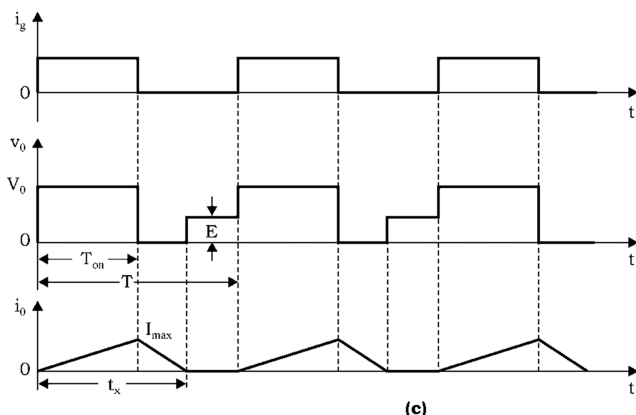
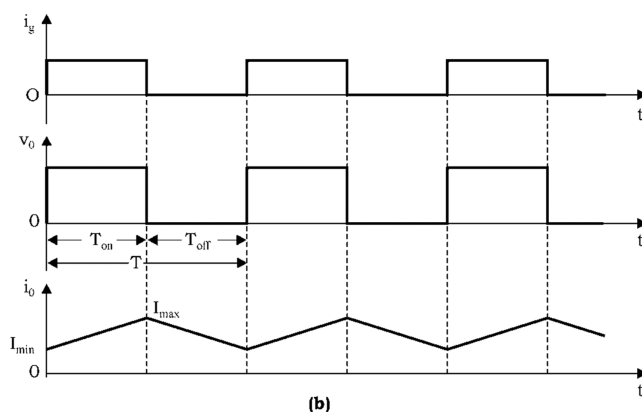
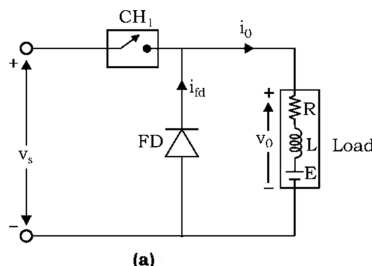


FIGURE 6.14 Type-A chopper with RLE load and its equivalent circuit: (a) circuit diagram, (b) waveforms: continuous condition, (c) waveforms: discontinuous condition, (d) when chopper CH_1 is on, and (e) when chopper CH_1 is off.

From Equation (6.16), $I(s) = \frac{V_s - E}{s(R + L_s)} + \frac{L \cdot I_{\min}}{R + L_s} = \frac{V_s - E}{L_s \left(s + \frac{R}{L} \right)} + \frac{I_{\min}}{\left(s + \frac{R}{L} \right)}$

Laplace inverse of above expression is

$$i(t) = \frac{V_s - E}{R} \left(1 - e^{-\frac{R}{L}t} \right) + I_{\min} e^{\frac{-R}{L}t} \quad \text{for } 0 \leq t \leq T_{on} \quad (6.18)$$

Similarly, the time domain expression for current from Equation (6.17) is

$$i(t') = \frac{-E}{R} \left(1 - e^{\frac{-R}{L}t'} \right) + I_{\max} e^{\frac{-R}{L}t'} \quad \text{for } T_{on} \leq t \leq T \quad (6.19)$$

where $t' = t - T_{on}$

Using boundary conditions in Equation (6.18), at $t = T_{on}$, $i(t) = I_{\max}$

$$\therefore I_{\max} = \frac{V_s - E}{R} \left(1 - e^{\frac{-T_{on}}{T_a}} \right) + I_{\min} e^{\frac{-T_{on}}{T_a}} \quad (6.20)$$

Similarly, in Equation (6.19), at $t' = T_{off} = T - T_{on}$, $i(t') = I_{\min}$

$$\therefore I_{\min} = \frac{-E}{R} \left(1 - e^{\frac{-(T-T_{on})}{T_a}} \right) + I_{\max} e^{\frac{-(T-T_{on})}{T_a}} \quad (6.21)$$

where $T_a = \frac{L}{R}$

Solving Equations (6.20) and (6.21) for I_{\max} and I_{\min} , we get

$$I_{\max} = \frac{V_s}{R} \left[\frac{1 - e^{-T_{on}/T_a}}{1 - e^{-T/T_a}} \right] - \frac{E}{R} \quad (6.22)$$

Substitute I_{\max} from Equation (6.22) in (6.21), we get

$$I_{\min} = \frac{V_s}{R} \left[\frac{e^{T_{on}/T_a} - 1}{e^{T/T_a} - 1} \right] - \frac{E}{R} \quad (6.23)$$

In the case where chopper CH₁ conducts continuously, then $T_{on} = T$ and therefore, from Equations (6.22) and (6.23),

$$I_{\max} = I_{\min} = \frac{V_s - E}{R} \quad (6.24)$$

6.7.2.1 Steady-State Ripple

Load current pulsates between I_{\min} and I_{\max} . So, the ripple current [$I_{\max} - I_{\min}$] can be obtained from Equations (6.22) and (6.23) [3,4].

$$\begin{aligned}
 I_{\max} - I_{\min} &= \frac{V_s}{R} \left[\frac{1 - e^{-T_{on}/T_a}}{1 - e^{-T/T_a}} - \frac{e^{T_{on}/T_a} - 1}{e^{T/T_a} - 1} \right] \\
 &= \frac{V_s}{R} \left[\frac{1 - e^{-T_{on}/T_a}}{1 - e^{-T/T_a}} - \frac{(1 - e^{-T_{on}/T_a})e^{T_{on}/T}}{(-e^{-T/T_a})e^{T/T_a}} \right] \\
 &= \frac{V_s}{R} \left[\frac{(1 - e^{-T_{on}/T_a}) - (1 - e^{-T_{on}/T_a})e^{(T_{on}-T)/T_a}}{1 - e^{-T/T_a}} \right] \\
 &= \frac{V_s}{R} \left[\frac{(1 - e^{-T_{on}/T_a})(1 - e^{-T_{off}/T_a})}{1 - e^{-T/T_a}} \right]
 \end{aligned} \tag{6.25}$$

$$\begin{aligned}
 \text{per unit ripple current} &= \frac{I_{\max} - I_{\min}}{V_s / R} \\
 &= \frac{(1 - e^{-T_{on}/T_a}) - (1 - e^{-T_{off}/T_a})}{1 - e^{-T/T_a}}
 \end{aligned} \tag{6.26}$$

It should be noted that per unit ripple current in load current is maximum when the duty cycle is 0.5.

Per unit ripple current is maximum at $\delta = 0.5$

6.7.2.2 Limits of Continuous Conduction

The limit of continuous conduction is reached when I_{\min} in Equation (6.23) goes to zero. The value of duty cycle δ at the limit of continuous conduction is obtained by equating I_{\min} in Equation (6.23) to zero.

$$\therefore I_{\min} = \frac{V_s}{R} \left[\frac{e^{T_{on}/T_a} - 1}{e^{T/T_a} - 1} \right] - \frac{E}{R} = 0$$

or

$$\frac{e^{T_{on}/T_a} - 1}{e^{T/T_a} - 1} = \frac{E}{V_s} = k$$

or

$$e^{T_{on}/T_a} = 1 + k (e^{T/T_a} - 1)$$

or

$$\delta' = \frac{T_{on}}{T} = \frac{T_a}{T} \ln \left[1 + k(e^{T/T_a} - 1) \right] \quad (6.27)$$

For given V_s , E , T , and T_a , if the duty cycle is δ' as given by Equation (6.27), then the current is just continuous. If the actual duty cycle δ is less than δ' , then the load current is discontinuous.

$\delta < \delta'$ —discontinuous conduction
$\delta > \delta'$ —continuous conduction

6.7.2.3 Computation of Extinction Time (t_x)

Due to large T_{off} , the load current may become discontinuous. The time t_x , called extinction time, can be calculated as [3,4,18]:

In Equation (6.20), put $I_{\min} = 0$ at $t = t_x$, which gives

$$I_{\max} = \frac{V_s - E}{R} \left(1 - e^{-\frac{T_{on}}{T_a}} \right) \quad (6.28)$$

Substituting this value of I_{\max} in Equation (6.19) at $t' = t_x - T_{on}$ gives $i(t') = 0$ as

$$0 = \frac{-E}{R} \left[1 - e^{-\frac{(t_x - T_{on})}{T_a}} \right] + \frac{V_s - E}{R} \left[1 - e^{-\frac{T_{on}}{T_a}} \right] e^{-\frac{(t_x - T_{on})}{T_a}}$$

or

$$e^{\frac{(t_x - T_{on})}{T_a}} - 1 = \frac{V_s - E}{E} \left(1 - e^{-\frac{T_{on}}{T_a}} \right)$$

This gives the extinction time t_x as:

$$t_x = T_{on} + T_a \ln \left[1 + \frac{V_s - E}{E} \left(1 - e^{-\frac{T_{on}}{T_a}} \right) \right] \quad (6.29)$$

The average output voltage for the discontinuous conduction mode is:

$$\begin{aligned} V_0 &= \frac{1}{T} \int_0^T V_s dt \\ &= \frac{1}{T} \left[\int_0^{T_{on}} V_s dt + \int_{T_{on}}^{t_x} 0 dt + \int_{t_x}^T E dt \right] \\ &= V_s \frac{T_{on}}{T} + \frac{E}{T} (T - t_x) \end{aligned}$$

or

$$V_0 = \delta V_s + \left(1 - \frac{t_x}{T}\right) E \quad (6.30)$$

6.7.2.4 AC Ripple Voltage (V_r)

It is defined as:

$$V_r = \sqrt{V_{\text{rms}}^2 - V_0^2}$$

where

$$V_{\text{rms}} = \sqrt{\delta} V_s \text{ and } V_0 = \delta V_s$$

$$\therefore V_r = V_s \sqrt{\delta - \delta^2} \quad (6.31)$$

6.7.2.5 Ripple Factor (RF)

It is defined as the ratio of AC ripple voltage to average output voltage.

$$\therefore \text{RF} = \frac{V_r}{V_0} = \sqrt{\frac{1-\delta}{\delta}} = \sqrt{\frac{1}{\delta} - 1} \quad (6.32)$$

6.8 COMMUTATION OF CHOPPER

The chopper consists of a main power semiconductor device along with its turn-on and turn-off mechanisms. In low-power chopper circuits, power transistors, GTOs, etc. are being used widely because they do not require extra-forced commutation circuits for their turn off. But for high-power applications, thyristors are in common use and require extra-forced commutation circuits. A forced-commutation circuit consists of a commutating inductor and capacitor.

There are various ways of turning off a chopper. All these methods differ from one another in the manner in which commutation is achieved. On this basis, these are broadly classified as [1–24]:

1. Forced commutation
 - a. Voltage commutation
 - b. Current commutation
2. Load commutation

1. Forced commutation:

In forced commutation, the commutating inductor and capacitor, which do not carry load current continuously, are used to turn off the thyristor. Forced commutation can be achieved in two ways:

- Voltage commutation:* In this method of forced commutation, the conducting main thyristor is commutated by the application of a pulse of large reverse voltage, which is applied by switching the precharged capacitor. Due to a sudden application of the large capacitor reverse voltage across the thyristor, the anode current is reduced to zero, and then the presence of reverse voltage across the thyristor further helps in completion of its turn-off processes. Because the main thyristor is commutated by the application of pulse of reverse voltage, it is called voltage commutation.
- Current commutation:* In this method of forced commutation, the main thyristor is commutated (turned off) by the application of an external pulse of current (generated by precharged capacitor C) greater than load current is passed to flow in the opposite or reverse direction to the main thyristor. When an external current pulse becomes equal to the load current, the net current through the main thyristor becomes zero, and the device is turned off. Because the commutation of the main thyristor occurs due to an external pulse of current, it is called current commutation.

2. Load commutation:

In this method of commutation, a conducting thyristor is turned off due to the underdamped nature of the load or by transferring the load current from one device to another.

6.8.1 VOLTAGE-COMMUTATED CHOPPER (CLASSICAL CHOPPER OR PARALLEL CAPACITOR TURN-OFF CHOPPER)

The power circuit diagram of a voltage-commutated chopper consists of a main thyristor T_1 and commutation circuit consisting of auxiliary thyristor (AT), commutating capacitor C , diode D , and commutating inductor L , as shown in [Figure 6.15](#) [3,4]. The FD is connected across the RLE type load. Initially, capacitor C is charged to a voltage V_s with upper plate positive and lower negative, as shown in [Figure 6.15](#).

Capacitor C is precharged to a voltage V_s through charging resistor R_C by closing switch S . It can also be charged by triggering the auxiliary thyristor AT through the load. The directions marked in the circuit diagram are taken as positive. It is assumed that load current is constant. The chopper operation can be explained with the help of following modes [3,4]:

Mode I: ($0 < t < t_1$): The main thyristor T_1 is triggered at $t = 0$, so the load gets connected to source V_s . During this mode, there are two current paths as shown in [Figure 6.16a](#):

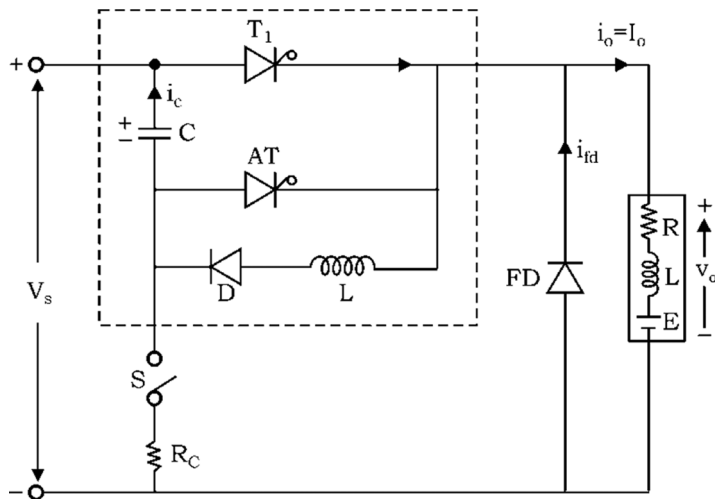


FIGURE 6.15 Voltage-commutated chopper.

One Path—load current I_0 flowing through path V_{S^+} — T_1 —load— V_{S^-}

Second Path—commutation current or capacitor current i_c flowing through oscillatory circuit formed by C , T_1 , L , and D . Commutating or capacitor or oscillatory current i_c flows sinusoidal with mathematical expression

$$i_c = V_s \sqrt{\frac{C}{L}} \sin \omega_0 t$$

$$= I_{cp} \sin \omega_0 t \quad (6.33)$$

where

$$I_{cp} = V_s \sqrt{\frac{C}{L}} = \text{peak value of } i_c$$

and

$$\omega_0 = \text{resonant frequency} = \frac{1}{\sqrt{LC}}$$

whereas the capacitor voltage changes sinusoidal from $t = 0$ to $t = t_1$

$$v_c = \frac{1}{C} \int i_c dt = V_0 \cos \omega_0 t \quad (6.34)$$

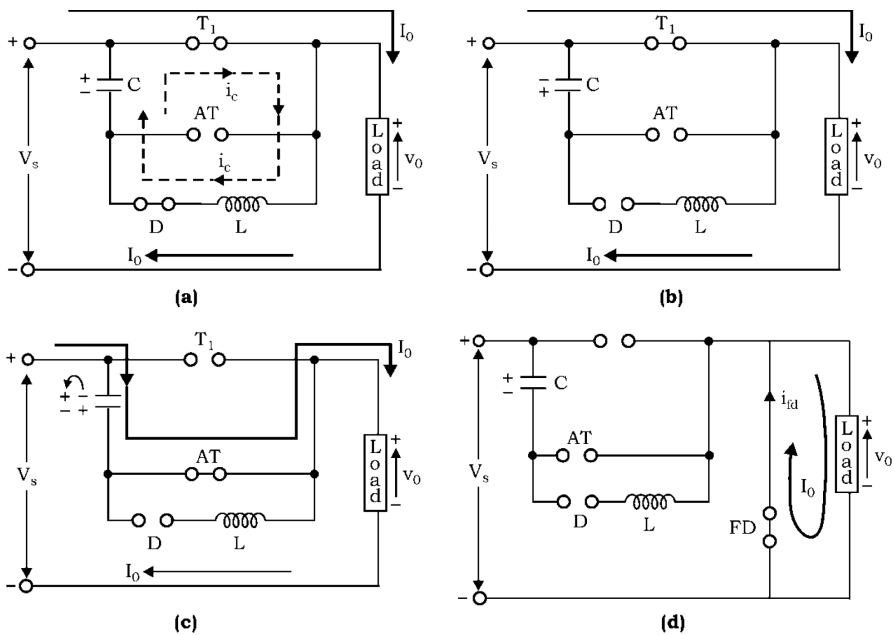


FIGURE 6.16 Equivalent circuit of voltage-commutated chopper during various modes of working: (a) Mode I: $0 < t < t_1$, (b) Mode II: $t_1 < t < t_2$, (c) Mode III: $t_2 < t < t_3$, and (d) Mode IV: $t_3 < t < T$.

During this mode, current flowing through T_1 is

$$i_{T_1} = I_0 + i_c \quad (6.35)$$

So, at end of *Mode I*, $i_c = 0$, $i_{T_1} = I_0$, $v_c = -V_s$, $i_D = 0$, $V_{AT} = V_s$, $v_0 = V_s$, as shown in Figure 6.17. The equivalent circuit of the chopper during this mode is drawn in Figure 6.16a.

Mode II: ($t_1 < t < t_2$): During this mode, only the load current flows through V_s-T_1 -load. So, conditions existing at the end of *Mode I* are continuous, as shown in Figure 6.17, i.e., $i_c = 0$, $i_{T_1} = I_0$, $v_c = -V_s$, $i_D = 0$, $V_{AT} = V_s$, $v_0 = V_s$.

Mode III: ($t_2 < t < t_3$): Now, when main thyristor T_1 is to be turned off, auxiliary thyristor AT is fired. With the turning-on of auxiliary thyristor AT at time $t = t_2$, capacitor voltage ($-V_s$) appears as reverse voltage across T_1 , and therefore main thyristor T_1 gets turned off. It is called a voltage-commutated chopper because the capacitor voltage does the required job of commutation.

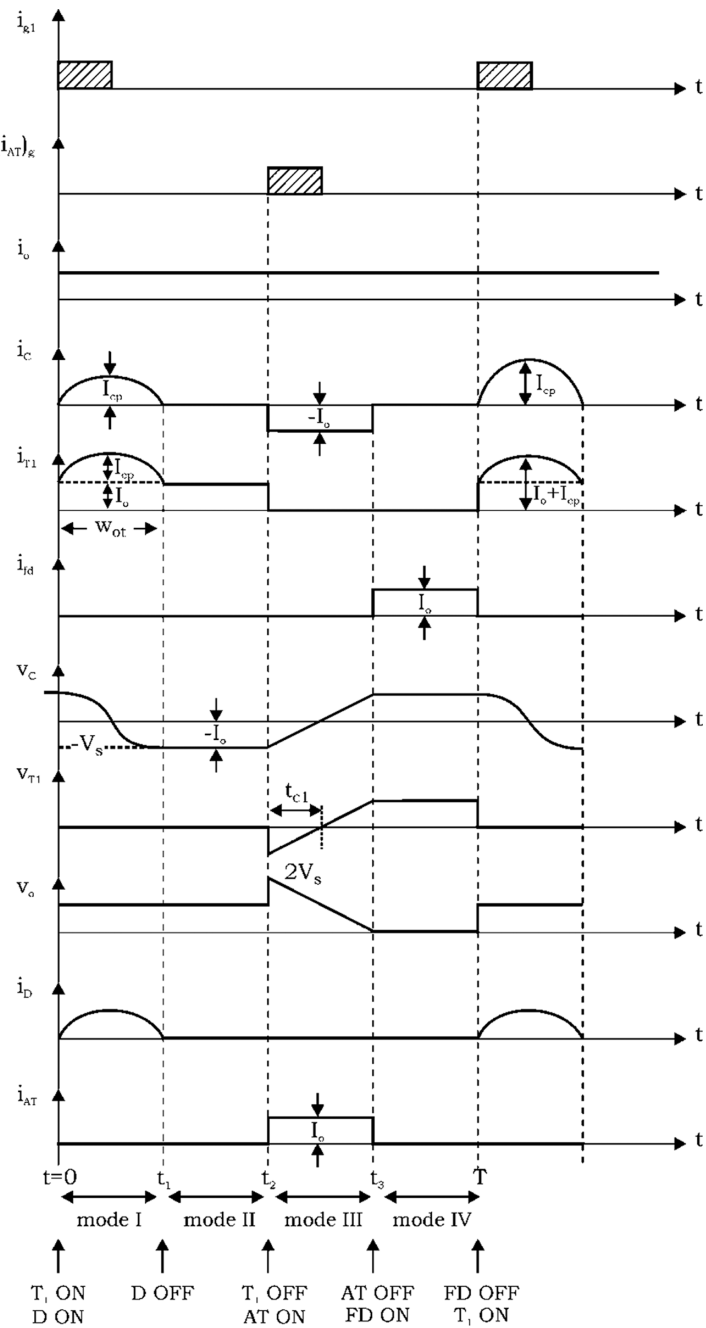


FIGURE 6.17 Voltage and current waveforms for voltage-commutated chopper.

Now the load current flows through V_{S^+} –C–AT–load– V_{S^-} . So, at time $t = t_2$, load voltage, ($v_0 = V_s + v_c (=V_s)$, becomes $2V_s$; see v_0 waveform of [Figure 6.17](#). But load voltage v_0 decreases linearly as the capacitor now charges linearly (as constant I_0 flowing) in opposite direction. When v_c charges to a voltage V_s with upper plate positive, then the net load voltage becomes:
 $v_0 = +V_s - v_c = +V_s - V_s = 0$ and load current also becomes zero. Therefore, auxiliary thyristor AT gets turned off naturally.

So, during this mode, $i_c = -I_0$, $i_{T_1} = 0$, $v_c = v_{T_1}$ (charges linearly from $-V_s$ to $+V_s$), $V_{AT} = 0$, V_0 decreases linearly from $2V_s$ to zero and $i_{AT} = I_0$.

Mode IV: ($t_3 < t < T$): At $t = t_3$ (at the end of Mode III) $i_c = 0$, $i_{T_1} = 0$, $v_c = +V_s = V_{T_1}$, $v_0 = 0$, $i_{AT} = 0$.

Because the capacitor is slightly overcharged at t_3 , the FD becomes FB. Therefore, the load current during this mode freewheels through load and FD, as shown in [Figure 6.16d](#). During this mode, $i_c = 0$, $i_{T_1} = 0$, $I_{fd} = I_0$, $V_{T_1} = V_s$, $v_c = V_s$, $v_0 = 0$, $i_{AT} = 0$. Now, at $t = T$, the main thyristor is triggered again, and in this way the cycle repeats.

Advantage: The circuit is simple.

Disadvantage: (i) Starting circuit to precharge the capacitor is required, (ii) load voltage at once rises to $2V_s$ at the instant of commutation of main thyristor is initiated.

Design Considerations:

The values of commutating capacitor C and inductor L can be designed as [3,4]:
Commutating capacitor C:

Its value depends on *circuit turn-off* time t_c of main thyristor T_1 . During time t_c , capacitor voltage charges linearly from $(-V_s)$ to zero as constant load current I_0 flows.

$$\therefore i_c = C \frac{dv}{dt}$$

$$\therefore I_0 = C \frac{0 - (-V_s)}{t_c}$$

or

$$C = \frac{t_c \cdot I_0}{V_s}$$

(6.36)

For reliable commutation, it must be ensured that circuit turn-off time (t_c) must be greater than the thyristor turn-off time (t_q), that is,

$$t_c = t_q + \Delta t$$

$$\therefore i_c = C \frac{dv}{dt} \quad (6.37)$$

where

$$\Delta t \approx t_q \text{ (can be taken equal to } t_q)$$

Commutating Inductor L:

Its value can be designed from the consideration of oscillatory current (i_c) established when the main thyristor T_1 is turned on, that is,

$$v_c = \frac{1}{C} \int i_c dt$$

$$i_c = V_s \sqrt{\frac{C}{L}} \sin \omega_0 t = I_{CP} \sin \omega_0 t$$

where

$$\omega_0 = \frac{1}{\sqrt{CL}} = \text{resonant frequency}$$

$$I_{CP} = \text{Peak capacitor current} = V_s \sqrt{\frac{C}{L}}$$

As main thyristor T_1 handles load current I_0 as well as I_{CP} , so I_{CP} should not be too large. Therefore, I_{CP} can be taken equal or less than load current I_0 , or

$$V_s \sqrt{\frac{C}{L}} \leq I_0$$

or

$$L \geq \left(\frac{V_s}{I_0} \right)^2 C$$

(6.38)

$$\text{Peak current through } T_1, (I_{TT})_{\max} = I_0 + I_{CP} \quad (6.39)$$

$$\text{Peak voltage across } T_1 \text{ and AT} = (V_{TT})_{\max} = (V_{AT})_{\max} = \pm V_s \quad (6.40)$$

$$\text{Peak current through AT} = (I_{AT})_{\max} = I_o = \frac{CV_s}{t_c} \quad (6.41)$$

$$\text{Peak voltage across FD, } (V_{FD})_{\max} = 2V_s \quad (6.42)$$

$$\text{Peak diode current, } (I_D)_{\max} = V_s \sqrt{\frac{C}{L}} = I_{CP} \quad (6.43)$$

6.8.2 CURRENT-COMMUTATED CHOPPER

The power circuit diagram for a current-commutated chopper consists of a main thyristor T_1 , auxiliary thyristor AT, C , L , D_1 and D_2 , FD, and charging resistor R_c , see Figure 6.18 [3,4,24].

It is assumed that the load current is constant and capacitor C is precharged to a voltage V_s with upper plate positive and lower negative, through charging resistor R_c . The directions marked for voltage and current are taken as positive. The whole commutation process is explained using following modes of operation:

Mode 1 ($0 < t < t_1$): Main thyristor T_1 is fired at $t = 0$. Therefore, load gets connected with source V_s and so load voltage $v_0 = V_s$ and load current $i_0 = I_0$, as shown in Figure 6.20a–c. Equivalent circuit of chopper during this mode is drawn in Figure 6.19a.

Mode 2 ($t_1 < t < t_2$): Initiation of turn-off process begins with the triggering of auxiliary thyristor AT. Let at time $t = t_1$, AT is triggered to commute main thyristor T_1 . As a result, an oscillatory current $i_c = -\frac{V_s}{\omega_0 L} \sin \omega_0 t = V_s \sqrt{\frac{C}{L}} \sin \omega_0 t = I_{cp} \sin \omega_0 t$ starts flowing in circuit consisting of C , AT, and L , as shown in the equivalent circuit, see Figure 6.19b. This i_c current flows for a period $t = \frac{\pi}{\omega_0} = \pi \sqrt{LC}$ and so during this period, capacitor C charges co-sinusoidal to a voltage $v_c = -V_s$, with upper plate negative and lower positive (see Figure 6.19b).

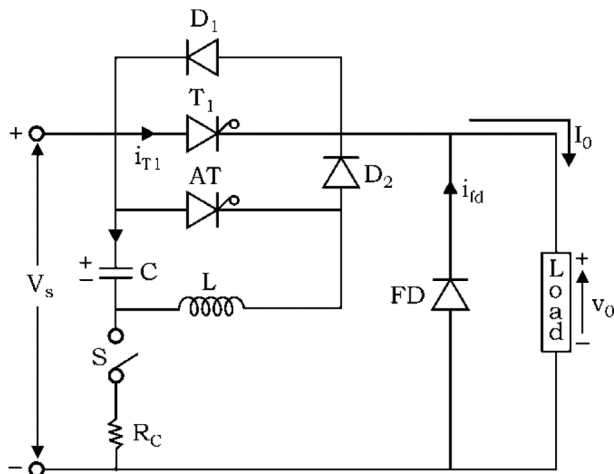


FIGURE 6.18 Power circuit diagram of current-commutated chopper.

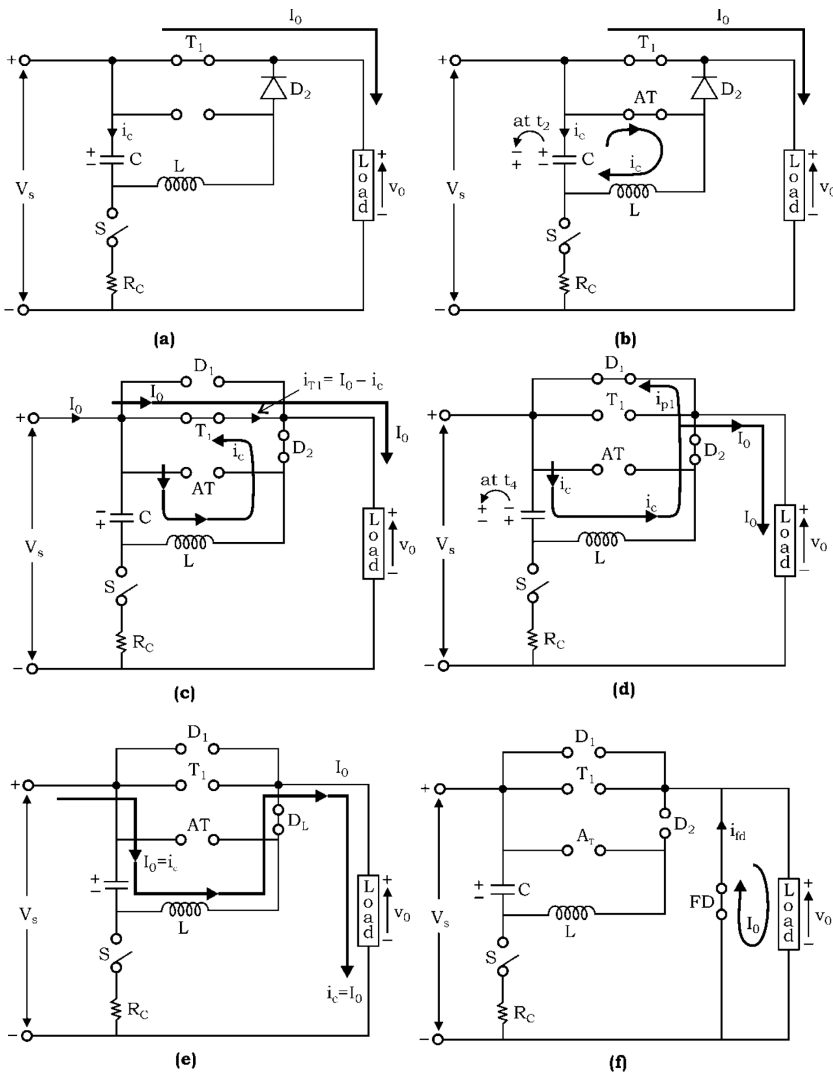


FIGURE 6.19 Equivalent circuit of current-commutated chopper during various modes of working: (a) Mode 1: $0 < t < t_1$, (b) Mode 2: $t_1 < t < t_2$, (c) Mode 3: $(t_2 < t < t_3)$, (d) Mode 4: $(t_3 < t < t_4)$, (e) Mode 5: $(t_4 < t < t_5)$, and (f) Mode 6: $(t_5 < t < t_6)$.

During this mode, $i_0 = I_0$, $v_0 = V_s$, $i_c = I_{cp} \sin \omega_0 t$, $v_c = -V_s$, $v_{T_1} = 0$, $v_{AT} = 0$.

As i_c current becomes zero at $t = t_2$, auxiliary thyristor AT gets turned off naturally.

Mode 3 ($t_2 < t < t_3$): As auxiliary thyristor AT is turned off at t_2 , so now oscillatory current i_c flows through C , L , D_2 and T_1 as shown in equivalent circuit of Figure 6.19c. Current i_c does not flow through D_1 because it is reverse biased due to a voltage drop across conducting thyristor T_1 . Now, the net current through the main thyristor T_1 , $iT_1 = I_0 - i_c$. At $t = t_3$, i_c current rises

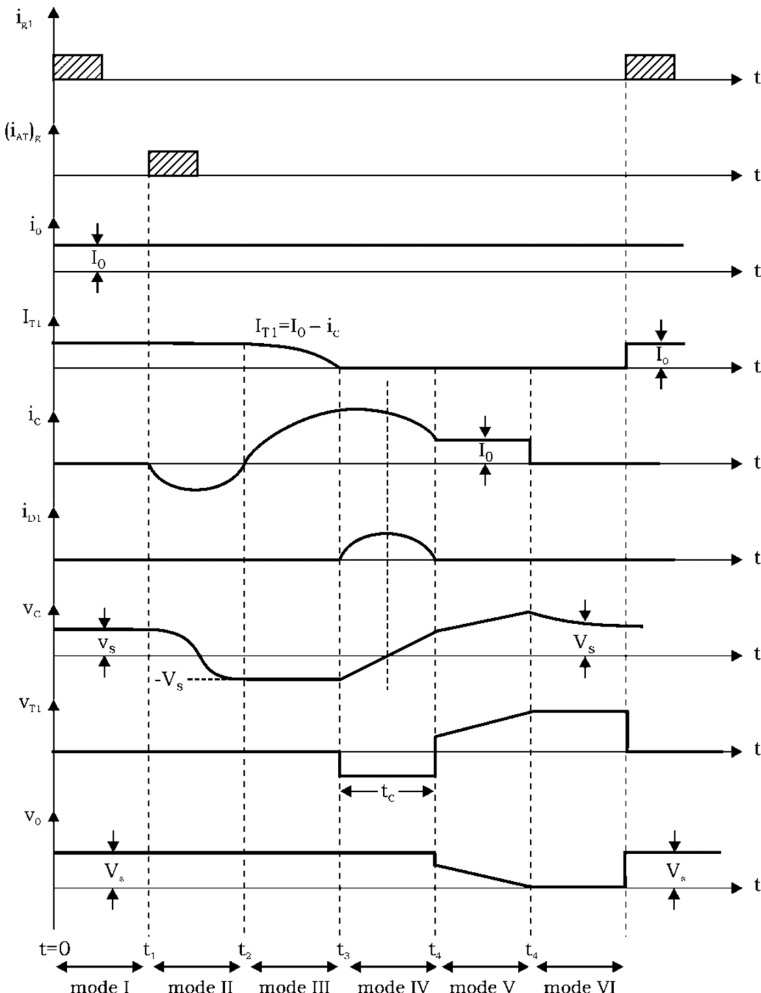


FIGURE 6.20 Voltage and current waveforms for current-commutated chopper.

to I_0 so i_{T_1} becomes zero as a result main thyristor T_1 gets turned off at $t = t_3$. Because the oscillator current through T_1 turns it off, it is called a current-commutated chopper.

Mode 4 ($t_3 < t < t_4$): As T_1 is turned-off at $t = t_3$, i_c becomes more than I_0 . So, after t_3 , i_c supplies current I_0 to load and excess current $iD_1 = i_c - I_0$ conducts through diode D_1 as shown in an equivalent circuit of Figure 6.20d. At t_4 in case $v_c > v_s$, the FD conducts; otherwise, Mode 5 would follow.

Mode 5 ($t_4 < t < t_5$): At $t = t_4$, current i_c reduces to zero, so i_{D_1} becomes zero and therefore diode D_1 gets turned off.

After t_4 , a constant current equal to I_0 flows through source V_s , C , L , D_2 , and load. So capacitor C gets charged linearly to a voltage V_s at t_5 and during this mode $i_c = I_0$.

Mode 6 ($t_5 < t < t_6$): at $t = t_6$, as capacitor is overcharged so FD becomes FB, and therefore load current I_0 starts to conduct through the FD. As a result, the load voltage becomes zero at t_5 and in this way the cycle repeats.

Design Considerations:

The conditions governing the design of L and C are [1,3,4]:

1. I_{CP} must be more than maximum possible load current I_0 to ensure reliable commutation of main thyristor. The oscillatory current is given by:

$$i_c = V_s \sqrt{\frac{C}{L}} \sin \omega_0 t = I_{\text{CP}} \sin \omega_0 t$$

$$\therefore I_{\text{CP}} = V_s \sqrt{\frac{C}{L}} > I_0$$

or

$$V_s \times \sqrt{\frac{C}{L}} = xI_0$$

(6.44)

where $x > 1$ and generally in the range $1.4 < x < 3$.

2. t_c (circuit turn-off time) $> t_q$ (thyristor turn-off time), that is,

$$t_c = t_q + \Delta t$$

$$t_c = \frac{1}{\omega_0} \left[\pi - 2 \sin^{-1} \left(\frac{I_0}{I_{\text{CP}}} \right) \right] \quad (6.45)$$

$$L = \frac{V_s \cdot t_c}{xI_0 [\pi - 2 \sin^{-1}(1/x)]} \quad (6.46)$$

$$C = \frac{xI_0 \cdot t_c}{V_s [\pi - 2 \sin^{-1}(1/x)]} \quad (6.47)$$

$$\text{Peak capacitor voltage } (V_C)_{\text{max}} = V_s + I_0 \sqrt{\frac{L}{C}} \quad (6.48)$$

$$\text{Turn-off time for main thyristor, } t_{c1} = [\pi - \sin^{-1}(1/x)] \sqrt{LC} \quad (6.49)$$

$$\text{Peak commuting current, } I_{\text{CP}} = xI_0 = V_s \sqrt{\frac{C}{L}} \quad (6.50)$$

6.8.3 LOAD-COMMUTATED CHOPPER

The power circuit diagram of the load-commutated chopper is shown in Figure 6.21 [1,3,4]. It consists of four thyristors T_1-T_4 and one commuting capacitor C .

For the conduction of the load current, $T_1 T_2$ acts as one pair and $T_3 T_4$ as second pair alternately. Initially, the capacitor is charged to a voltage V_s with the upper plate negative and lower positive as shown in Figure 6.21. It is assumed that the load current is constant. Various current and voltage waveforms of load-commutated chopper are shown in Figure 6.22. The working of this chopper is explained with the help of various modes of operation:

Mode 1: ($0 < t < t_1$): At $t = 0$, thyristor T_1 and T_2 are triggered, so the load gets connected to source V_s , and circuit consists of V_s , T_1 , C , T_2 and load (see Figure 6.23a). The load voltage at once becomes $2V_s$, i.e. $v_0 = V_s + v_c = 2V_s$. As constant load current I_0 flows through the capacitor C , so it charges linearly from V_s at $t = 0$ to $-V_s$ at $t = t_1$.

At $t = 0$, when T_1 and T_2 are turned on, T_3 and T_4 are reverse biased by capacitor voltage, that is, at $t = 0$, $v_{T_3} = v_{T_4} = -v_s$, but at $t = t_1$, $v_c = -V_s$ so, $v_{T_3} = v_{T_4} = V_s$, that is, T_3 and T_4 become FB at t_1 .

Mode 2: ($t_1 < t < t_2$): At $t = t_1$, capacitor C is slightly overcharged, due to which the FD becomes FB and the load current is transferred from T_1 , T_2 to FD. So, now load current I_0 freewheels through the FD, as shown in equivalent circuit of Figure 6.23b. During this mode: $v_c = -V_s$, $v_0 = 0$, (as the FD conducts), $i_c = 0$, $i_{fd} = I_0$, $i_{T_1} = i_{T_2} = 0$, $v_{T_3} = v_{T_4} = V_s$.

Mode 3: ($t_2 < t < t_3$): At $t = t_2$, thyristor pair T_3 and T_4 are triggered, so load voltage at once again becomes $v_0 = V_s + v_c = 2V_s$ and, thyristor pair $T_1 T_2$ get reverse biased by capacitor voltage v_c , so turned off at t_2 . Load current I_0 now flow through V_s , T_4 , C , T_3 and load. So, capacitor charges linearly from $-V_s$ at t_2 to V_s at t_3 , as shown in Figure 6.23c. Therefore, load voltage falls to zero at t_3 . During this mode, $i_c = -I_0$, $i_{T_3} = i_{T_4} = I_0$, $v_{T_1} = v_{T_2} = -V_s$ at t_2 and V_s at t_3 , that is, $T_1 T_2$ becomes FB at t_3 .

Mode 4: At t_3 , capacitor C is overcharged, so FD becomes FB, and therefore after t_3 , the load current I_0 freewheels through the FD and load, similarly like Mode 2.

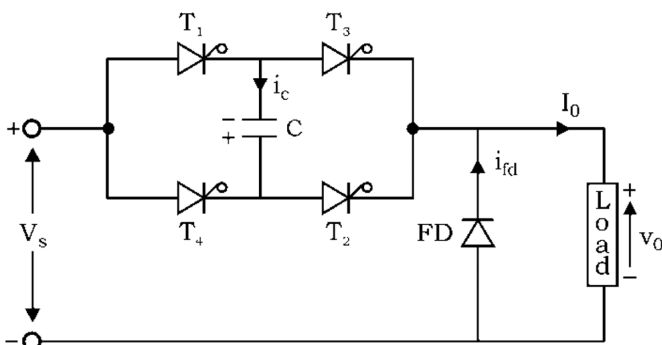


FIGURE 6.21 Power circuit diagram.

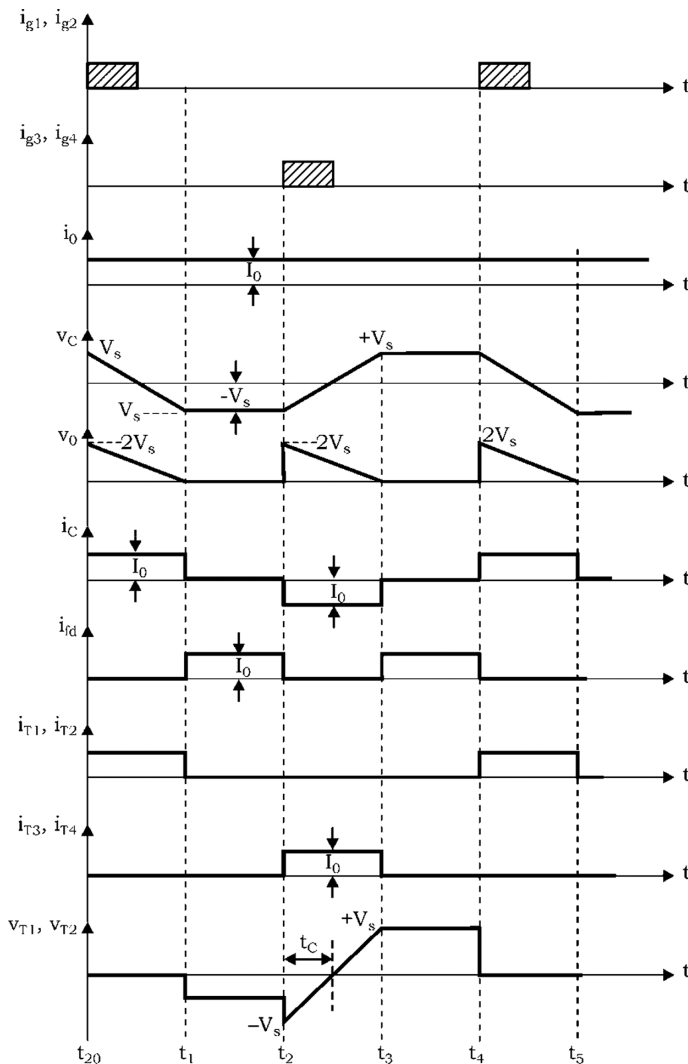


FIGURE 6.22 Current and voltage waveforms for load-commutated chopper.

In this way, again T_1 T_2 are turned on at t_4 and the cycle repeats.

Design Considerations:

The value of commutating capacitor and circuit turn-off time for each thyristor is designed and calculated as:

Commutating Capacitor:

For constant load current I_0 , v_c charges linearly from $-V_s$ to V_s in time T_{on} , that is, total change in voltage is $2V_s$ during time T_{on} .

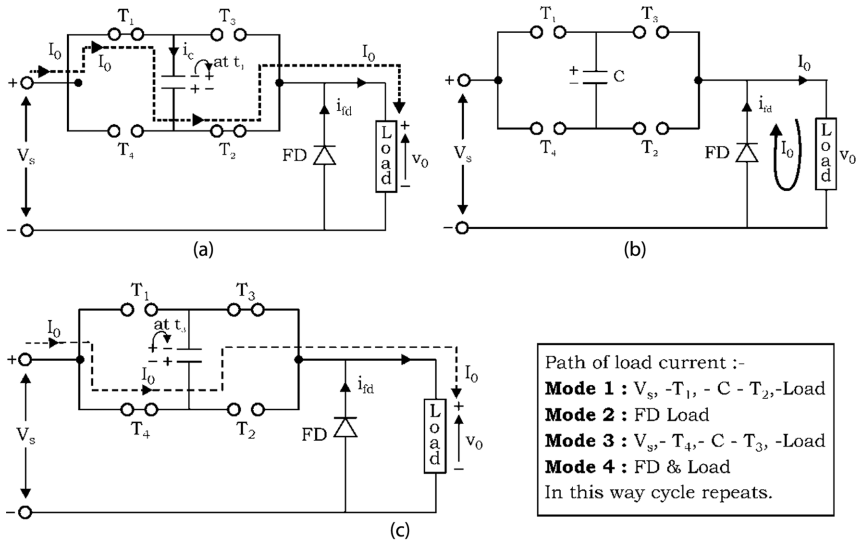


FIGURE 6.23 Equivalent circuit during various modes of working: (a) Mode 1: $0 < t < t_1$, (b) Mode 2: $t_1 < t < t_2$, and (c) Mode 3: $t_2 < t < t_3$.

$$i_c = C \frac{dv}{dt}$$

$$\therefore I_0 = C \frac{2V_s}{T_{on}}$$

or

$$C = \frac{I_0 \cdot T_{on}}{2V_s} \quad (6.51)$$

output voltage,

$$V_0 = \frac{1}{2}(2V_s)T_{on} \cdot \frac{1}{T} = V_s \cdot T_{on} f \quad (6.52)$$

Putting $T_{on} = \frac{2V_s \cdot C}{I_0}$ in Equation (6.52), we get

$$V_0 = V_s \cdot f \cdot \frac{2CV_s}{I_0} = \frac{2V_s^2 \cdot C \cdot f}{I_0} \quad (6.53)$$

Minimum chopping period, $T_{min} = T_{on}$

\therefore Maximum chopping frequency, $f_{\max.} = \frac{1}{T_{\min}} = \frac{1}{T_{on}}$
 From Equation (6.51),

$$\boxed{C = \frac{I_0}{2V_s} \cdot \frac{1}{f_{\max.}}} \quad (6.54)$$

Circuit turn-off time for each thyristor

$$t_c = \frac{1}{2} T_{on} = \frac{1}{2} C \frac{2V_s}{I_0}$$

$$\boxed{t_c = \frac{CV_s}{I_0}} \quad (6.55)$$

6.9 SWITCHED-MODE REGULATORS

DC converters can be used as switched-mode regulators to convert an unregulated DC voltage to a regulated DC output voltage. The regulation is achieved by a PWM at a fixed frequency and the switching device is normally BJT, MOSFET, or IGBT. The following switched-mode regulators are used in regulated switch-mode DC power supplies [1,3,7,9,24]:

1. Buck (step-down) converter
 2. Boost (step-up) converter
 3. Buck-boost (step-down/up) converter
 4. Cuk converter
1. *Buck (step-down) converter:*

The power circuit diagram of the buck converter is shown in [Figure 6.24a](#).

It produces output voltage V_0 less than DC input voltage V_s .

By varying the duty ratio, $(\delta = \frac{T_{on}}{T})$, the average output voltage V_0 can be controlled.

Voltage and current waveforms for continuous conduction are shown in [Figure 6.24b](#).

Working: As shown in [Figure 6.24b](#), when power transistor T_1 is switched on at time $t = 0$, the load gets connected with the source and load current flows through the path V_s, L, C and load. Therefore, inductor stored energy $(\frac{1}{2}LI^2)$ during T_{on} period and therefore inductor current i_L rises.

Now, let at instant, $t = T_{on}$, power transistor T_1 is switched off, so the load gets disconnected with the source. During the off period, inductor current flows through L, C , load, and FD. Therefore, stored energy by the inductor during T_{on} period is dissipated to the load through the FD. So, inductor current i_L decreases.

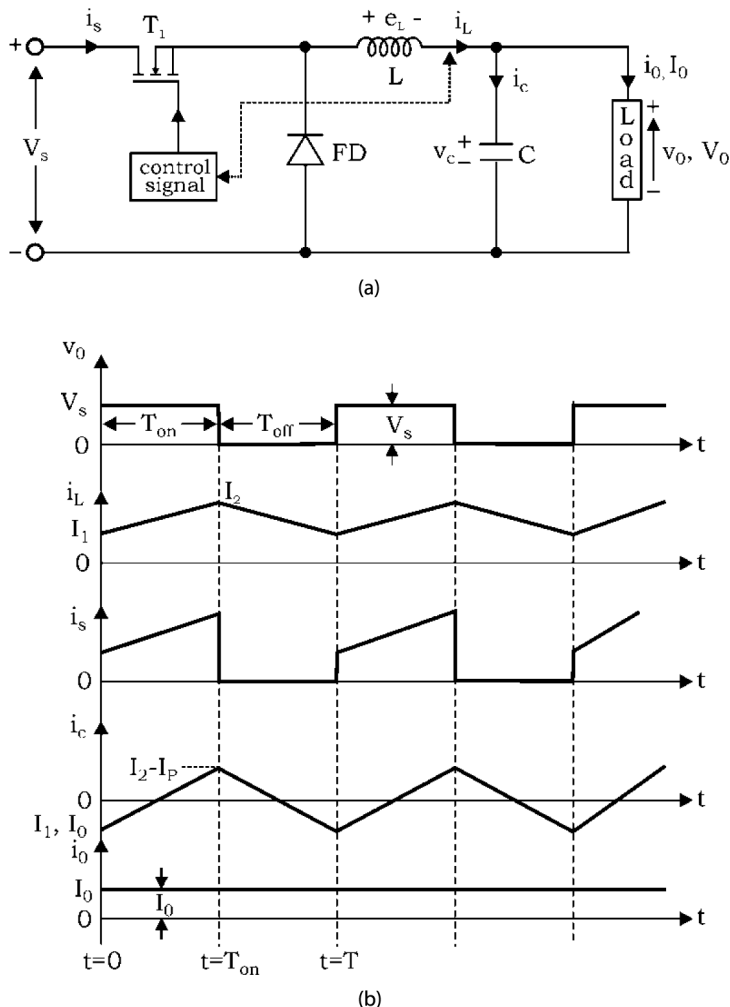


FIGURE 6.24 (a) Buck (step-down) converter, and (b) voltage and current waveforms of the buck converter.

Mathematical Analysis:

Voltage across inductor L is given by:

$$e_L = L \frac{di}{dt}$$

During T_{on} period, inductor current rises from I_1 to I_2

$$\therefore V_s - V_0 = L \left(\frac{I_2 - I_1}{T_{on}} \right) \quad (6.56)$$

Let $\Delta I = I_2 - I_1$ = peak-to-peak ripple current of L

$$\therefore V_s - V_0 = \frac{L \cdot \Delta I}{T_{on}} \quad (6.57)$$

or

$$T_{on} = \frac{L \cdot \Delta I}{V_s - V_0} \quad (6.58)$$

During T_{off} period, inductor current falls from I_2 to I_1

$$\therefore -V_0 = -L \frac{\Delta I}{T_{off}} \quad (6.59)$$

or

$$T_{off} = + \frac{L \cdot \Delta I}{V_0} \quad (6.60)$$

Equating the values of ΔI in Equations (6.58) and (6.60)

$$\Delta I = \frac{(V_s - V_0)}{L} T_{on} = \frac{T_{off} \cdot V_0}{L}$$

$$\therefore V_s T_{on} - V_0 T_{on} = T_{off} V_0$$

$$V_s T_{on} = T_{off} V_0 + V_0 T_{on}$$

$$V_s T_{on} = V_0 (T_{off} + T_{on})$$

$$\therefore V_s T_{on} = V_0 T$$

$$\therefore \boxed{V_0 = \frac{T_{on}}{T} V_s = \delta V_s} \quad (6.61)$$

where

$$\delta = \frac{T_{on}}{T} = \text{duty ratio or duty cycle}$$

and

$$T = T_{on} + T_{off}$$

Assuming lossless system, $V_s I_s = V_0 I_0 = \delta V_s \cdot I_0$

Therefore, average input current is given by

$$\boxed{I_s = \delta \cdot I_0} \quad (6.62)$$

Switching period T is given as:

$$T = T_{on} + T_{off}$$

Substituting the values of T_{on} and T_{off} from Equations (6.58) and (6.60), we get

$$T = \frac{L \Delta I}{V_s - V_0} + \frac{L \cdot \Delta I}{V_0}$$

or

$$T = \frac{1}{f} = \frac{\Delta I \cdot L \cdot V_s}{V_0(V_s - V_0)} \quad (6.63)$$

From Equation (6.63), the peak-to-peak ripple current (ΔI) is

$$\Delta I = \frac{V_0(V_s - V_0) \cdot T}{L \cdot V_s} \quad (6.64)$$

or

$$\Delta I = \frac{V_0(V_s/V_s - V_0/V_s) \cdot T}{L \cdot V_s/V_s}$$

or

$$\boxed{\Delta I = \frac{\delta \cdot V_s(1-\delta)}{f \cdot L}} \quad (6.65)$$

Peak-to-peak ripple voltage of capacitor is

or

$$\Delta V_c = V_c - V_{c(t=0)}$$

$$= \frac{1}{C} \int i_c dt = \frac{1}{C} \int_0^{\frac{T}{2}} \frac{\Delta I}{4} dt$$

$$\boxed{\Delta V_c = \frac{\Delta I}{8f \cdot C}} \quad (6.66)$$

Merits:

- It is simple because it requires only one transistor T_1 .
- It has high efficiency (>92%).

Demerits:

- Only first-quadrant operation is possible as $v_0 = \text{positive}$, and $i_0 = \text{positive}$.

2. Boost (step-up) converter:

The power circuit diagram of the boost converter using power MOSFET is shown in [Figure 6.25a](#). Its output voltage V_0 is greater than input DC voltage V_s .

Working: When power transistor is on, inductor L is connected to supply V_s . Inductor stores energy during T_{on} period. The load is not connected with the source in this period, as shown in equivalent circuit of [Figure 6.25b](#).

When the power transistor is off, the load receives energy from the inductor as well as from the input V_s . Now, the current flows through L , D , C , and load as shown in [Figure 6.25c](#). The associated voltage and current waveforms are shown in [Figure 6.25d](#).

Mathematical Analysis:

During T_{on} period, inductor current rises from I_1 to I_2

$$\therefore V_s = L \frac{(I_2 - I_1)}{T_{on}} = L \frac{\Delta I}{T_{on}} \quad (6.67)$$

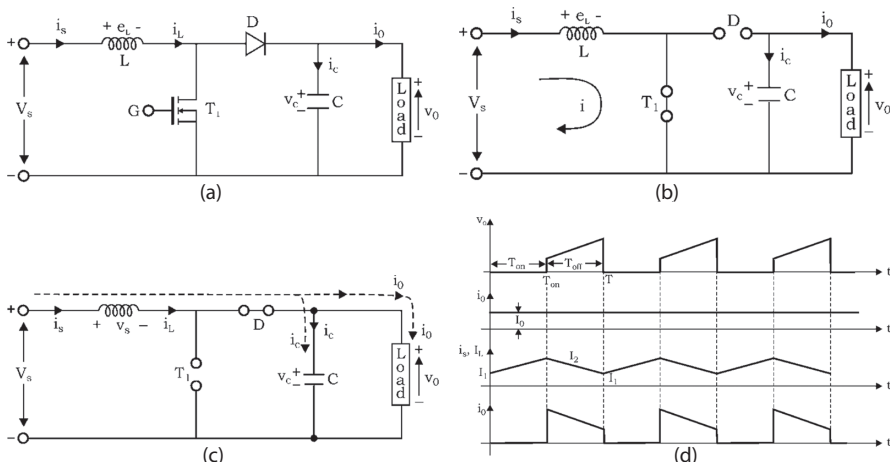


FIGURE 6.25 Boost converter: (a) power circuit diagram, (b) equivalent circuit when T_1 is on, (c) equivalent circuit when T_1 is off, and (d) voltage and current waveforms of boost (step-up) converter.

or

$$T_{on} = \frac{\Delta I \cdot L}{V_s} \quad (6.68)$$

During T_{off} period, inductor current i_L falls from I_2 to I_1

$$\therefore V_s - V_0 = -L \cdot \frac{\Delta I}{T_{off}} \quad (6.69)$$

or

$$V_s - V_0 = -L \cdot \frac{\Delta I}{T_{off}} \quad (6.70)$$

From Equations (6.67) and (6.69), the peak-to-peak ripple current of inductor L can be written as

$$\Delta I = \frac{V_s T_{on}}{L} = \frac{(V_0 - V_s) T_{off}}{L} \quad (6.71)$$

Substitute $T_{on} = \delta T$ and $T_{off} = (1-\delta)T$, gives average output voltage V_0 ,

$$V_0 = V_s \frac{T}{T_{off}} = \frac{V_s}{1-\delta} \quad (6.72)$$

Assuming lossless system, $P_i = P_0$

$$\therefore V_s I_s = V_0 I_0 = \frac{V_s I_0}{(1-\delta)}$$

\therefore Average input current, I_s

$$I_s = \frac{I_0}{1-\delta} \quad (6.73)$$

Switching period T can be obtained as

$$T = \frac{1}{f} = T_{on} + T_{off}$$

$$= \frac{\Delta I \cdot L}{V_s} + \frac{\Delta I \cdot L}{(V_0 - V_s)}$$

$$T = \frac{\Delta I \cdot L \cdot V_0}{V_s (V_0 - V_s)} \quad (6.74)$$

and from Equation (6.74), the peak-to-peak ripple current,

$$\boxed{\Delta I = \frac{V_s(V_0 - V_s)}{f.LV_0}} \quad (6.75)$$

or

$$\Delta I = \frac{V_s(\delta - 1)}{f.L.\delta} \quad (6.76)$$

Peak-to-peak capacitor ripple voltage, ΔV_C

$$\boxed{\Delta V_c = \frac{I_0\delta}{f.C}} \quad (6.77)$$

3. Buck-boost converter:

This regulator provides an output voltage that may be less than or greater than the input voltage, hence the name “buck-boost.” Here, the polarity of output voltage is opposite to that of input voltage. This regulator is also known as an *inverting regulator*. The power circuit diagram for a buck-boost converter is shown in [Figure 6.26a \[3,7,9\]](#).

Working: The circuit operation can be divided into two modes:

Mode 1: When power MOSFET Q is switched on, the supply current i_s flows through the path, as shown in equivalent circuit of [Figure 6.26b](#). Diode D is reverse biased.

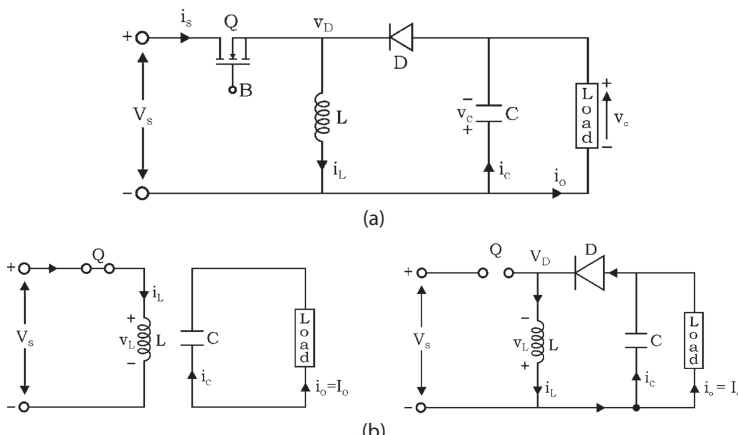


FIGURE 6.26 Buck-boost converter: (a) power circuit diagram, (b) equivalent circuits during Modes 1 and 2. (Continued)

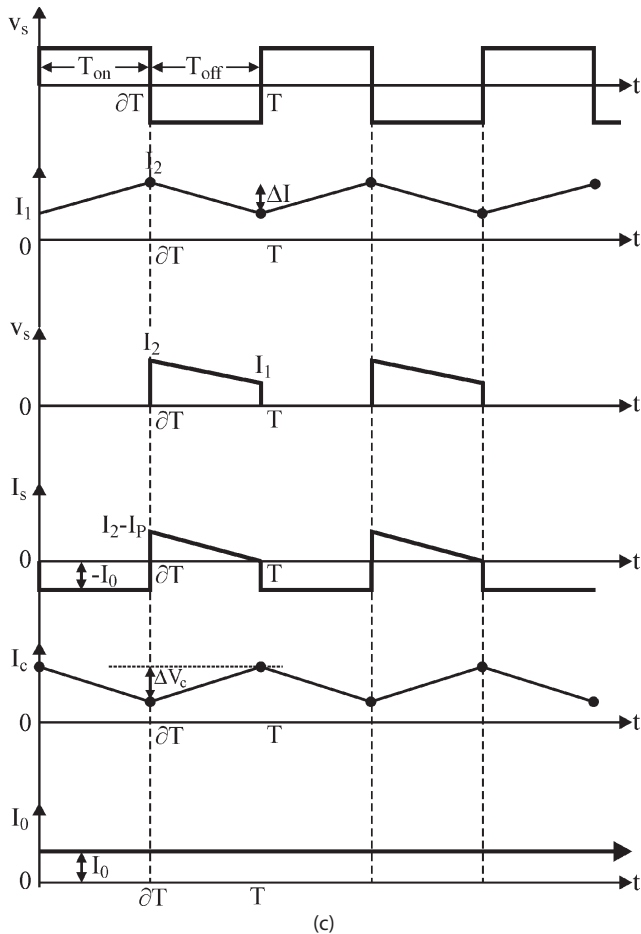


FIGURE 6.26 (Continued) Buck-boost converter: (c) various waveforms.

Mode 2: During this mode, power MOSFET Q is switched off. The current that was flowing through inductor L would flow through the L–C–D–load. The inductor current decreases. As the inductor current tends to decrease, the polarity of the emf induced in L is reversed as shown in equivalent circuits. Thus, the energy stored in inductor L is transferred to the load through the path L₊–Load–D–L₋ as shown in equivalent circuit [Figure 6.26b] of Mode 2. The various voltage and current waveforms are shown in Figure 6.26c.

Mathematical analysis: Let inductor current i_L rise linearly from I_1 to I_2 during T_{on} time.

$$V_s = L \cdot \frac{I_2 - I_1}{T_{on}} = L \cdot \frac{\Delta I}{T_{on}} \quad (6.78)$$

or

$$T_{on} = \frac{\Delta I \cdot L}{V_s} \quad (6.79)$$

During T_{off} time, the inductor current reduces linearly from I_2 to I_1 .

$$\therefore V_0 = -L \cdot \frac{\Delta I}{T_{off}} \quad (6.80)$$

or

$$T_{off} = \frac{-\Delta I \cdot L}{V_0} \quad (6.81)$$

where peak-to-peak ripple current of inductor is given by

$$\Delta I = I_2 - I_1$$

From Equations (6.78) and (6.80), we can write

$$\Delta I = \frac{V_s \cdot T_{on}}{L} = \frac{-V_0 \cdot T_{off}}{L}$$

or

$$V_0 = -V_s \cdot \frac{T_{on}}{T_{off}} = -V_s \frac{T_{on}/T}{T_{off}/T}$$

$$= \frac{-\delta \cdot V_s}{(T - T_{on})/T}$$

or

$V_0 = -V_s \cdot \frac{\delta}{(1-\delta)}$

(6.82)

For a lossless system,

$$V_s \cdot I_s = -V_0 \cdot I_0$$

$$= V_s \left(\frac{\delta}{1-\delta} \right) I_0$$

So, average input current is given by

$I_s = \left(\frac{\delta}{1-\delta} \right) I_0$

(6.83)

The switching period, T can be calculated as

$$T = 1/f = T_{on} + T_{off}$$

substituting values of T_{on} and T_{off} from Equations (6.79) and (6.81)

$$T = \frac{\Delta I \cdot L}{V_s} - \frac{\Delta I \cdot L}{V_0}$$

or

$$T = \frac{\Delta I L (V_0 - V_s)}{V_s V_0}$$

(6.84)

Also, from Equation (6.84), peak-to-peak ripple current can be written as

$$\Delta I = \frac{T \cdot V_s V_0}{L (V_0 - V_s)}$$

or

$$\Delta I = \frac{V_s \cdot \delta}{f \cdot L}$$

(6.85)

During T_{on} period, when power MOSFET Q is on, the filter capacitance C supplies the load current. So, average discharging current of capacitor is $I_c = I_0$. Also, peak-to-peak ripple voltage ΔV_c of capacitor is

$$\Delta V_c = \frac{1}{C} \int_0^{T_{on}} I_c dt = \frac{1}{C} \int_0^{T_{on}} I_0 dt = \frac{I_0 T_{on}}{C} \quad (6.86)$$

Substituting the value of T_{on} from Equation (6.79) in Equation (6.86), we get

$$\Delta V_c = \frac{I_0 \cdot V_0}{(V_0 - V_s) f \cdot C}$$

or

$$\Delta V_c = \frac{I_0 \cdot \delta}{f \cdot C}$$

(6.87)

From Equation (6.82), it is clear that the buck-boost converter provides output voltage polarity reversal without a transformer.

4. Cuk regulator:

Similar to the buck-boost regulator, the Cuk regulator also provides an output voltage that is less than or greater than the input voltage, but the output polarity is opposite to that of the input voltage. Figure 6.27a shows the power circuit diagram of a Cuk converter, after the name of the inverter [3,7,9]. The key difference between buck-boost regulator and Cuk regulator is that a capacitor, rather than an inductor, is used for energy storage.

When the input voltage is turned on and transistor T is switched off, diode D is FB and capacitor C is charged through L_1 , D_1 and the input supply V_s . Its circuit operation can be explained using two modes:

Mode 1: When transistor T is turned on at $t = 0$, the current through inductor L_1 rises. At the same time, the voltage of capacitor C_1 reverse biases diode D and turns it off. The capacitor C_1 discharges its energy to the circuit formed by C_1 , C_2 , load, and L_2 . The equivalent circuit during this mode is shown in Figure 6.27b.

Mode 2: It begins when transistor T is switched off at $t = t_1$. The capacitor C_1 is charged from the input supply, and the energy stored in the inductor L_2 is transferred to the load. The capacitor C_1 is the medium for transferring

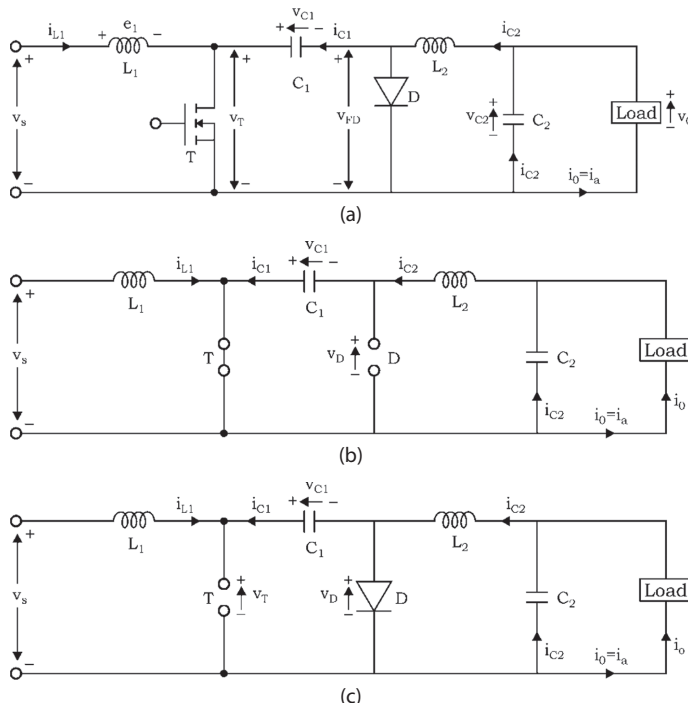


FIGURE 6.27 Cuk regulator: (a) power circuit diagram, (b) equivalent circuit during Mode 1 when T is switched on, (c) equivalent circuit during Mode 2 when T is switched-off.

(Continued)

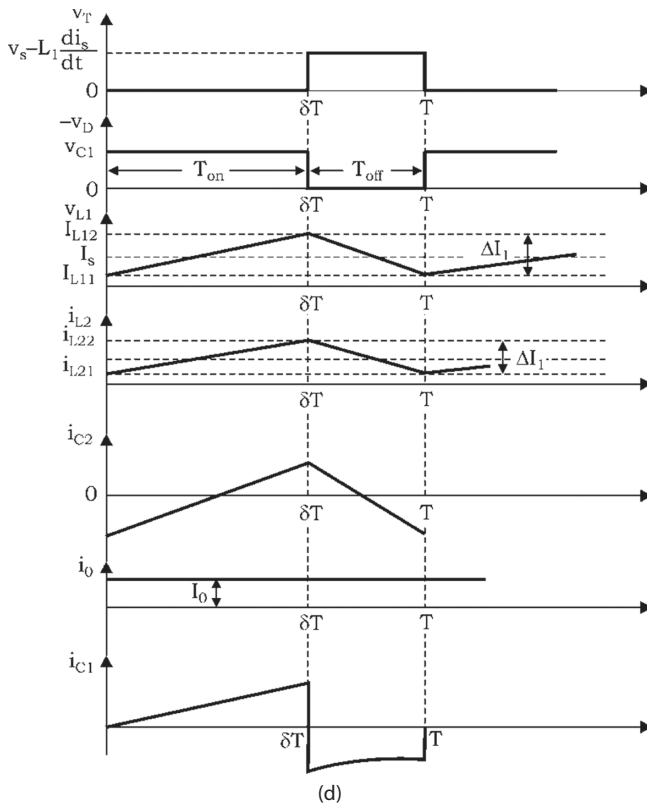


FIGURE 6.27 (Continued) Cuk regulator: (d) voltage and current waveforms.

the energy from source to the load. Equivalent circuit during this mode is shown in Figure 6.27c. The various voltage and current waveforms are shown in Figure 6.27d.

During T_{on} time, current through inductor L_1 , i_{L_1} rises from i_{L11} to i_{L12} .

$$V_s = L_1 \frac{i_{L12} - i_{L11}}{T_{on}} = L_1 \frac{\Delta I_1}{V_s} \quad (6.88)$$

or

$$T_{on} = \frac{\Delta I_1 \cdot L_1}{V_s} \quad (6.89)$$

During T_{off} time, current through inductor L_1 , i_{L_1} reduces linearly from I_{L12} to I_{L11} due to the charged capacitor C_1 .

$$\therefore V_s - v_{C1} = -L_1 \frac{\Delta I_1}{T_{off}} \quad (6.90)$$

or

$$T_{off} = \frac{-\Delta I_1 \cdot L_2}{V_s - v_{C1}} \quad (6.91)$$

where, v_{C1} is the average value of capacitor C_1 and

$$\Delta I_l = I_{L12} - I_{L11}$$

From Equations (6.88) and (6.90), we can write

$$\Delta I_1 = \frac{V_s \cdot T_{on}}{L_1} = \frac{-(V_s - v_{C1})}{L_1} T_{off}$$

or

$$V_s (T_{on} + T_{off}) = v_{C1} T_{off}$$

or

$$v_{C1} = \frac{V_s \cdot T}{T_{off}} = \frac{V_s}{1-\delta}$$

(6.92)

Similarly, we can also write,

$$v_{C1} = \frac{-V_0}{\delta}$$

(6.93)

Therefore, average output voltage V_0 can be calculated by equating the Equations (6.92) and (6.93) as,

$$v_{C1} = \frac{V_s}{1-\delta} = \frac{-V_0}{\delta}$$

or

$$V_0 = \frac{-\delta \cdot V_s}{1-\delta}$$

(6.94)

for a lossless system,

$$V_s \cdot I_s = -V_0 \cdot I_0 = \frac{\delta V_s}{1-\alpha} I_0$$

\therefore Average input current,

$$I_s = \frac{\delta \cdot I_0}{1 - \delta} \quad (6.95)$$

The switching period T can be calculated as

$$T = \frac{1}{f} = T_{on} + T_{off}$$

Substituting the values of T_{on} and T_{off} from Equations (6.89) and (6.91), we get

$$T = \frac{-\Delta I_1 \cdot L_1 \cdot v_{C1}}{V_s (V_s - v_{C1})} \quad (6.96)$$

From Equation (6.96), the peak-to-peak ripple current of inductor L_1 becomes

$$\Delta I_1 = \frac{-V_s \cdot (V_s - v_{C1})}{f \cdot L_1 \cdot v_{C1}}$$

or

$$\Delta I_1 = \frac{V_s \cdot \delta}{f \cdot L_1} \quad (6.97)$$

Peak-to-peak ripple voltage of capacitor C_1 is

$$\Delta v_{C1} = \frac{1}{C_1} \int_0^{T_{off}} I_{C1} dt = \frac{1}{C_1} \int_0^{T_{off}} I_s dt = \frac{I_s \cdot T_{off}}{C_1} \quad (6.98)$$

Substituting the value of T_{off} in Equation (6.98), we get

$$\Delta v_{C1} = \frac{I_s \cdot (1 - \delta)}{f \cdot C_1} \quad (6.99)$$

Similarly, the peak-to-peak ripple current of inductor L_2 becomes

$$\Delta I_2 = \frac{\delta \cdot V_s}{f \cdot L_2} \quad (6.100)$$

and the peak-to-peak ripple voltage of capacitor C_2 is,

$$\Delta v_{C2} = \frac{\delta \cdot V_s}{8C_2 L_2 f^2} \quad (6.101)$$

6.10 SOLVED PROBLEMS

Example 6.1: For type-A chopper, DC input voltage = 220V, load resistance = 20Ω . Take a voltage drop of 1.5V across chopper when it is on. For a duty cycle of 0.5, determine

- a. average and RMS values of output voltage and
- b. chopper efficiency.

SOLUTION

- a. When chopper is on, output voltage is $(V_s - 1.5)$ V and during the time chopper is off, output voltage is zero.

$$\therefore \text{Average output voltage} = \frac{(V_s - 1.5)T_{on}}{T} = \delta(V_s - 1.5)$$

$$= 0.5(220 - 1.5) = 109 \text{ V}$$

$$\text{RMS value of output voltage } V_{rms} = \left[(V_s - 1.5)^2 \cdot \frac{T_{on}}{T} \right]^{\frac{1}{2}} = \sqrt{\delta}(V_s - 1.5)$$

$$= \sqrt{0.5}(220 - 1.5) = 154.50 \text{ V}$$

- b. Power output or power delivered to load,

$$P_0 = \frac{V_{rms}^2}{R} = \frac{(154.50)^2}{20} = 1193.51 \text{ W}$$

$$\text{Power input to chopper, } P_i = V_s I_0 = 220 \times \frac{109}{20} = 1199 \text{ W}$$

$$\text{Chopper efficiency} = \frac{P_0}{P_i} \times 100 = \frac{1193.51}{1199} \times 100 = 99.54\%$$

Example 6.2: Calculate the pulse width of a step-up chopper if it has input voltage of 230 V; output voltage of 690 V; non-conducting time of the thyristor-chopper is $100 \mu\text{s}$.

In the case where the pulse width is halved for constant frequency operation, find the new output voltage.

SOLUTION

For step up chopper output voltage is,

$$V_0 = \frac{V_s}{1 - \delta}$$

$$\therefore 690 = 230 = \frac{1}{1-\delta}$$

or

$$\delta = \frac{2}{3} = \frac{T_{on}}{T}$$

$$\therefore T_{on} = \frac{2}{3}T \text{ and } T_{off} = T - T_{on} = \frac{1}{3}T = 100 \mu\text{s} \text{ (given)}$$

$$\therefore T = 300 \mu\text{s} \text{ and } T_{on} = \frac{2}{3} \times 300 = 200 \mu\text{s}$$

When pulse width (T_{on}) is halved, $T_{on} = \frac{1}{2} \times 200 = 100 \mu\text{s}$ for constant frequency operation,

$$T = 300 \mu\text{s}; T_{off} = T - T_{on} = 300 - 100 = 200 \mu\text{s}$$

$$\text{Therefore, New } \delta = \frac{T_{on}}{T} = \frac{100}{300} = \frac{1}{3}$$

$$\therefore \text{New output voltage, } V_0 = 230 \frac{\frac{1}{1-\frac{1}{3}}}{1-\frac{1}{3}} = 345 \text{ V}$$

Example 6.3: For type-A chopper, feeding on RLE load, obtain maximum value of average current rating for the thyristor in case load current remains constant.

SOLUTION

For constant load current I_0 , the current waveform for thyristor current i_T is as shown in Figure 6.28. Here

$$I_0 = \frac{V_0 - E}{R}$$

The average thyristor current I_T is given by

$$\begin{aligned} I_T &= I_0 \frac{T_{on}}{T} = \frac{V_0 - E}{R} \cdot \delta \\ &= \frac{\delta V_s - E}{R} \cdot \delta = \frac{\delta^2 V_s - \delta E}{R} \end{aligned} \quad (6.102)$$

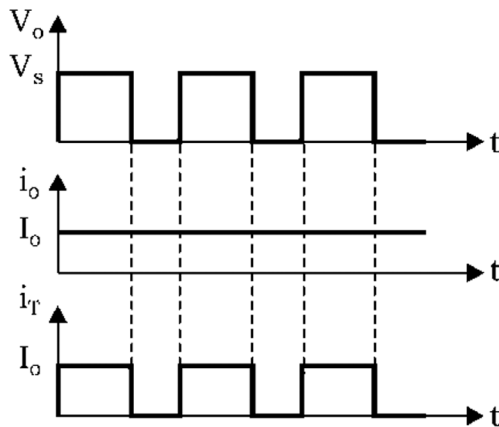


FIGURE 6.28 Circuit diagram for Example 6.3.

This will give a maximum value when

$$= \frac{dI_T}{d\delta} = \frac{2\delta V_s - E}{R} = 0$$

and from this,

$$\delta = \frac{E}{2V_s} \quad (6.103)$$

Therefore, the maximum value of average thyristor current is obtained by substituting the value of δ from Equation (6.103) in Equation (6.102).

$$I_{T,\max} = \frac{E}{2V_s R} \cdot \left(\frac{E}{2V_s} \cdot V_s - E \right) = \frac{E^2}{4V_s R}$$

Example 6.4: The DC converter (type-A chopper) has a resistance load of $R = 15\Omega$ and the input voltage is $V_s = 220$ V. When the converter switch remains on, its voltage drop is $v_{ch} = 1$ V, and the chopping frequency is $f = 1$ kHz. If the duty cycle is 50%, find (a) the average output voltage V_o (b) the RMS output voltage V_{rms} , (c) the converter efficiency, (d) the effective input resistance R_i of the converter, and (e) the RMS value of the fundamental component of output harmonic voltage.

SOLUTION

Given: $V_s = 220$ V, $\delta = 0.5$, $R = 20\Omega$, $v_{ch} = 1$ V, $f = 1$ kHz.

When the chopper is on, output voltage is $(V_s - 1)$ V and during the time chopper is off, output voltage is zero.

a. The average output voltage, $V_0 = \frac{T_{on}}{T} V_s = \delta V_s$

$$\therefore V_0 = 0.5 (220 - 1) = 109.5 \text{ V}$$

b. The RMS output voltage, $V_{rms} = \sqrt{\delta} V_s$

$$= \sqrt{0.5} (220 - 1)$$

$$= 154.85 \text{ V}$$

c. The output power or power delivered to load,

$$P_0 = \frac{V_{rms}^2}{R} = \frac{(154.85)^2}{20} = 1198.92 \Omega$$

Power input to chopper (or DC converter),

$$P_i = V_s \times I_0 = V_s \times \frac{V_0}{R}$$

$$= 220 \times \frac{109.5}{20}$$

$$= 1204.5 \text{ W}$$

\therefore The DC converter efficiency $= \frac{P_0}{P_i} = \frac{1198.92}{1204.5} \times 100$

$$= 99.53\%$$

d. The effective input resistance R_i of the converter is $= \frac{R}{\delta} = \frac{20}{0.5} = 40 \Omega$

e. The output voltage can be expressed in a Fourier series as

$$v_0(t) = \delta V_s + \frac{V_s}{n\pi} \sum_{n=1}^{\infty} \sin 2n\pi\delta \cos 2n\pi ft + \frac{V_s}{n\pi} \sum_{n=1}^{\infty} (1 - \cos 2\pi\delta) \sin 2n\pi ft$$

The fundamental component (for $n = 1$) of output voltage harmonic can be determined from above equations:

$$v_1(t) = \frac{V_s}{\pi} [\sin 2\pi\delta \cos 2\pi ft + (1 - \cos 2\pi\delta) \sin 2\pi ft]$$

$$= \frac{220 \times 20}{\pi} \sin(2\pi \times 1000 t) = 140.06 \sin(6283.2 t)$$

and its rms value is $V_1 = 140.06/\sqrt{2} = 99.04 \text{ V}$

Example 6.5: A step-down DC converter has a load resistance $r = 0.4\Omega$, input voltage $V_s = 550$ V, and battery voltage $E = 0$ V. The average load current $I_0 = 200$ A, and chopping frequency $f = 250$ Hz. Determine the load inductance L , which would limit the maximum load ripple current to 10% of I_0 .

SOLUTION

Given: $V_s = 550$ V, $R = 0.4 \Omega$, $f = 250$ Hz, $T = 1/f = 0.004$ s, $\Delta i = 200 \times 0.1 = 20$ A. The average output voltage $V_0 = \delta V_s = RI_0$. The voltage across the inductor is given by

$$L \frac{di}{dt} = V_s - RI_0 = V_s - \delta V_s = V_s(1 - \delta)$$

If the load current is assumed to rise linearly, $dt = t_l = \delta T$ and $di = \Delta i$

$$\Delta i = \frac{V_s(1 - \delta)}{L} \delta T$$

For the worst-case ripple conditions,

$$\frac{d(\Delta i)}{d\delta} = 0$$

This gives $\delta = 0.5$ and

$$\Delta i L = 20 \times L = 550 (1 - 0.5) \times 0.5 \times 0.004$$

and the required value of inductance is $L = 27.5$ mH.

Example 6.6: In the continuous conduction mode of type-A chopper, show that per unit ripple in the load current is maximum when duty cycle is equal to 0.5.

SOLUTION

The ripple current ΔI for type A chopper is

$$\Delta I = I_{\max} - I_{\min} = \frac{V_s}{R} \left[\frac{(1 - e^{\delta T/T_a}) (1 - e^{-(1-\delta)T/T_a})}{1 - e^{-T/T_a}} \right] \quad (6.104)$$

Also per-unit ripple in load current is

$$\frac{\Delta I}{V_s/R} = \frac{(1 - e^{-\delta T/T_a} - e^{-(1-\delta)T/T_a} + e^{-T/T_a})}{1 - e^{-T/T_a}} \quad (6.105)$$

For obtaining the values of duty cycle for which the ripple in current is maximum, differentiate Equation (6.104) or (6.105) with respect to δ and equate to zero.

$$\therefore \frac{d\left(\frac{\Delta I}{V_s/R}\right)}{d\delta} = \frac{(1-e^{-T/T_a}) \left[0 - e^{-\delta T/T_a} \cdot \left(-\frac{T}{T_a} \right) - e^{-(1-\delta)T/T_a} \cdot \frac{T}{T_a + 0} \right]}{(1-e^{-T/T_a})^2}$$

or

$$\frac{T}{T_a} \cdot -e^{-\delta T/T_a} - \frac{T}{T_a} \cdot e^{-(1-\delta)T/T_a} = 0$$

or

$$e^{-\delta T/T_a} = e^{-(1-\delta)T/T_a}$$

or

$$\frac{\delta T}{T_a} = (1-\delta) \frac{T}{T_a}$$

$$\therefore \delta = (1-\delta) \text{ or } \delta = \frac{1}{2} = 0.5.$$

This shows that for duty cycle equal to 0.5, the ripple in the load current is maximum.

Example 6.7: A DC chopper has input voltage of 220 V and output voltage of 150 V. Load resistance is 20 Ω . Find (a) duty cycle, (b) average and RMS load currents, (c) RMS thyristor current, (d) average input current, (e) effective input resistance.

SOLUTION

a. $\delta = \frac{V_0}{V_s} = \frac{150}{220} = 0.68$

b. Average load current, $I_0 = \frac{V_0}{R} = \frac{150}{20} = 7.5 \text{ A}$

c. RMS load current, $I_{\text{rms}} = \frac{\sqrt{\delta} V_s}{R} = \frac{\sqrt{0.68} \times 220}{20} = 9.07 \text{ A}$

d. RMS thyristor current = RMS load current = 9.07 A

e. Average input current = average load current = 7.5 A

f. Effective input resistance, $R_i = \frac{R}{\delta} = \frac{20}{0.68} = 30 \Omega$

Example 6.8: Determine the periods of conduction and blocking in each cycle of a DC chopper if input voltage is 220 V and output voltage is 150 V. It is operating at a frequency of 1 kHz.

SOLUTION

$$T = \frac{1}{f} = 1 \times 10^{-3} \text{ sec}$$

$$V_0 = V_s \frac{T_{on}}{T}$$

or

$$T_{on} = \frac{V_0 T}{V_s} = \frac{150 \times 1 \times 10^{-3}}{220} = 0.68 \text{ ms}$$

$$T_{off} = T - T_{on} = 1 \times 10^{-3} - 0.68 \times 10^{-3} = 0.32 \text{ ms}$$

Example 6.9: An RLE load is fed from a 400-V DC source through a chopper circuit. If $R = 0$, $L = 0.8 \text{ H}$ and duty cycle of chopper is 0.4. Find the chopping frequency to limit the amplitude of load current excursion of 20 A.

SOLUTION

An RLE load signifies a load having resistance, inductance, and a motor (E stands for back emf of motor).

$$\delta = \frac{T_{on}}{T_{on} + T_{off}} = 0.4$$

$$V_0 = \delta V_s = 0.4 \times 400 = 160 \text{ V}$$

The difference between V_s and V_0 is responsible for the setting of flux by the inductance

$$\therefore 400 - 160 = L \frac{di}{dt} = L \frac{\Delta i}{\Delta t}$$

$$L = 0.8 \text{ H}, \Delta i = 20 \text{ A}, \Delta T = T_{on}$$

$$T_{on} = \frac{L \Delta i}{240} = \frac{0.8 \times 20}{240} = 66.67 \text{ ms}$$

$$T = T_{on} + T_{off} = \frac{T_{on}}{\delta} = \frac{66.67 \times 10^{-3}}{0.4} = 166.68 \text{ ms}$$

$$\text{Chopper frequency } f = \frac{1}{T} = \frac{1}{166.68 \times 10^3} = 6 \text{ pulses/s}$$

Example 6.10: Determine the load inductance so that maximum ripple in load current is 20% of average load current for a chopper having input voltage of 220 V; chopping frequency is 300 Hz, and average load current is 40 A. It feeds an RL load having $R = 8 \Omega$. Find load inductance so that maximum ripple in load current is 20% of average load current.

SOLUTION

$$V_s = 220 \text{ V}, E = 0, R = 8 \Omega, f = 300 \text{ Hz}$$

$$I_{\max} - I_{\min} = 0.2 (\text{average load current}) = 0.2 \times 40 = 8 \text{ A}$$

$$\text{Maximum ripple } (I_{\max} - I_{\min})_{\max} = \frac{V_s}{4fL}$$

$$\therefore 8 = \frac{220}{4 \times 300 \times L} \text{ or } L = 23 \times 10^{-3} \text{ H}$$

Example 6.11: A DC motor has an armature resistance of 0.5Ω and an armature inductance of 14 mH . It is fed from a 220-V DC source through a chopper. Back emf of motor is constant at 100 V. Minimum load current is 10 A. The thyristor turns off after 3 ms. Find (a) current at the instant of turn-off of thyristor, (b) 6 ms after turn-off of thyristor.

SOLUTION

a. Instantaneous value of current i is given by:

$$\begin{aligned} i &= \frac{V_s - E}{R} \left(1 - e^{-Rt/L}\right) + I_{\min} e^{-Rt/L} \\ &= \frac{220 - 100}{0.5} \left(1 - e^{-(0.5 \times 3 \times 10^{-3})/(14 \times 10^{-3})}\right) + 10 e^{-(0.5 \times 3 \times 10^{-3})/(14 \times 10^{-3})} \\ &= 24.38 + 8.98 = 33.36 \text{ A} \end{aligned}$$

b. After turn-off of thyristor, the current freewheels through the load. So, current at the instant of 6 ms after turn-off of thyristor

$$i = 33.36 e^{-(0.5 \times 6 \times 10^{-3})/(14 \times 10^{-3})} = 26.93 \text{ A}$$

Example 6.12: For type-A chopper circuit, source voltage $V_s = 220 \text{ V}$, chopping period $T = 2000 \mu\text{s}$, on-period = $800 \mu\text{s}$, load circuit parameters: $R = 2 \Omega$, $L = 8 \text{ mH}$ and $E = 30 \text{ V}$.

- a. Find whether load current is continuous or not.
- b. Determine the value of average output current.
- c. Determine the maximum and minimum values of steady-state output current.
- d. Sketch the time variations of gate signal i_g , load voltage v_o , load current i_o , thyristor current i_T , FD current i_{fd} and voltage across thyristor v_T .
- e. Find RMS values of the first, second, and third harmonics of load current.
- f. Determine the average value of supply current.
- g. Determine input power, the power absorbed by the load counter emf, and the power loss in the resistor.

SOLUTION

Given: $V_s = 220 \text{ V}$, $T = 2000 \mu\text{s}$, $T_{on} = 800 \mu\text{s}$, $R = 2 \Omega$, $L = 8 \mu\text{H}$, $E = 30 \text{ V}$

$$\text{a. } T_a = \frac{L}{R} = \frac{8 \times 10^{-3}}{2} = 4 \times 10^{-3} \text{ s}$$

$$\frac{T_a}{T} = \frac{4 \times 10^{-3}}{2000 \times 10^{-6}} = 2$$

$$\frac{T}{T_a} = 0.5; \quad m = \frac{E}{V_s} = \frac{30}{220} = 0.13$$

$$\delta = \frac{T_{on}}{T} = \frac{800}{2000} = 0.4, \frac{T_{on}}{T_a} = \frac{800}{4000} = 0.2$$

If actual duty cycle δ is less than δ' , then the load current would be discontinuous.

Where,

$$\delta' = \frac{T_a}{T} \ln \left[1 + m \left(e^{T/T_a} - 1 \right) \right]$$

$$\therefore \delta' = 2 \ln \left[1 + 0.13 \left(e^{0.5} - 1 \right) \right] = 0.1619$$

As actual duty cycle $\delta (=0.4)$ is more than δ' , so load current is continuous.

- b. Average output current, $I_0 = \frac{\delta V_s - E}{R} = \frac{0.4 \times 220 - 30}{2} = 29 \text{ A}$
- c. Maximum value of steady-state output current,

$$I_{\max} = \frac{220}{2} \left[\frac{1 - e^{-0.2}}{1 - e^{-0.5}} \right] - \frac{30}{2} = 35.68 \text{ A}$$

Minimum value of steady-state output current,

$$I_{\min} = \frac{220}{2} \left[\frac{e^{0.2} - 1}{e^{0.5} - 1} \right] - \frac{30}{2} = 22.54 \text{ A}$$

d. The various waveforms are sketched in [Figure 6.29](#).

e. The RMS value of n th harmonic voltage is $v_n = \frac{2V_s}{n\pi} \sin n\pi\delta$

\therefore RMS value of first harmonic voltage is, $v_1 = \frac{2V_s}{\pi} \sin \pi\delta$

$$V_1 = \frac{2V_s}{\sqrt{2}\pi} \sin(\pi \times 0.4) = \frac{2 \times 220}{\sqrt{2}\pi} \sin 72^\circ = 94.187 \text{ V}$$

Here chopping frequency, $f = \frac{1}{T} = \frac{10^6}{2000} = 500 \text{ Hz}$

$$\therefore Z_1 = \sqrt{R^2 + (\omega L)^2}$$

$$= \sqrt{2^2 + (2\pi \times 500 \times 8 \times 10^{-3})^2} = 25.212 \Omega$$

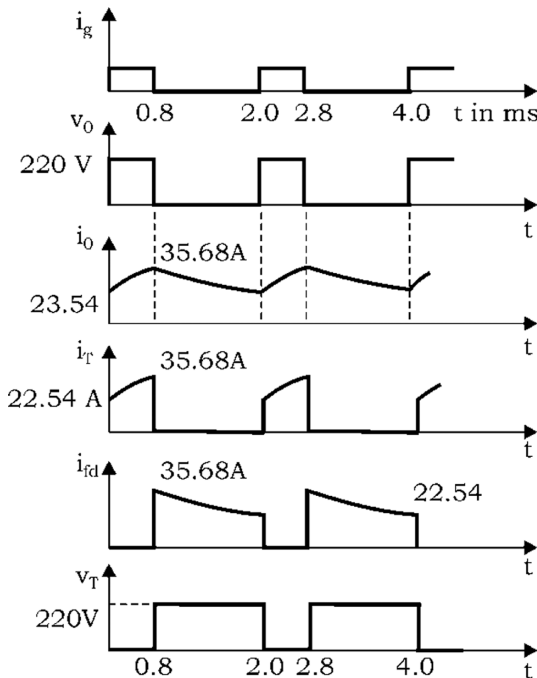


FIGURE 6.29 Various waveforms for Example 6.12.

$$\therefore I_1 = \frac{V_1}{Z_1} = \frac{94.187}{25.212} = 3.735 \text{ A}$$

$$\begin{aligned}\text{Similarly, } I_2 &= \frac{2 \times 220}{2 \cdot \sqrt{2} \cdot \pi} [\sin 144^\circ] \times \frac{1}{\sqrt{2^2 + (2\pi \times 500 \times 2 \times 8 \times 10^{-3})^2}} \\ &= 0.579 \text{ A}\end{aligned}$$

$$\begin{aligned}I_3 &= \frac{2 \times 220}{3 \cdot \sqrt{2} \cdot \pi} [\sin 216^\circ] \times \frac{1}{\sqrt{2^2 + (2\pi \times 1500 \times 8 \times 10^{-3})^2}} \\ &= -0.2573 \text{ A}\end{aligned}$$

f. Average supply current $I_{\text{TAV}} = \frac{\delta(V_s - E)}{R} - \frac{L}{RT}(I_{\max} - I_{\min})$

$$I_{\text{TAV}} = \frac{0.4(220 - 30)}{2} - \frac{8 \times 10^3 (35.68 - 22.54)}{2 \times 2000 \times 10^6}$$

$$= 38 - 26.28 = 11.72 \text{ A}$$

g. Input power = $V_s \times$ average supply current

$$= 220 \times 11.72 = 2578.4 \text{ W}$$

Power absorbed by load emf = $E \times$ average load current

$$= 30 \times 29 = 870 \text{ watts}$$

Power loss in resistor $R = 2578.4 - 870 = 1708.4 \text{ W}$

Example 6.13: For type-A chopper, source voltage $V_s = 220 \text{ V}$, chopping frequency $f = 500 \text{ Hz}$, $T_{on} = 800 \mu\text{s}$, $R = 2\Omega$, $L = 2 \text{ mH}$ and $E = 75 \text{ V}$.

- a. Determine whether load current is continuous or not.
- b. Calculate the values of average output voltage and average output current.
- c. Compute the maximum and minimum values of steady-state output current.
- d. Sketch the time variations of gate signal i_g , load current i_0 , load voltage v_0 , thyristor current i_T , FD current i_{fd} , and voltage across thyristor v_T .

SOLUTION

$$\text{Here } T_a = \frac{L}{R} = \frac{2 \times 10^{-3}}{2} = 10^{-3} \text{ s}$$

$$T = \frac{1}{f} = \frac{1}{500} = 2000 \mu\text{s}$$

$$\frac{T_a}{T} = f T_a = 500 \times 10^3 = 0.5, \frac{T}{T_a} = \frac{1}{f T_a} = 2,$$

$$m = \frac{E}{V_s} = \frac{75}{220} = 0.340$$

$$\delta = \frac{T_{on}}{T} = f \cdot T_{on} = 500 \times 800 \times 10^{-6} = 0.4,$$

$$\frac{T_{on}}{T_a} = 0.8$$

a. Now, $\delta' = \frac{T_a}{T} \ln \left[1 + m(e^{T/T_a} - 1) \right]$

$$= 0.5 \ln [1 + 0.34(e^2 - 1)] \\ = 0.577$$

As actual duty cycle $\delta (= 0.4)$ is less than δ' , so the load current is discontinuous.

b. As conduction is discontinuous, so the extinction time

$$t_x = T_{on} + T_a \ln \left[1 + \frac{V_s - E}{E} \left(1 - e^{-\frac{T_{on}}{T_a}} \right) \right]$$

$$\therefore t_x = 800 \times 10^{-6} + 1 \times 10^{-3} \ln \left[1 + \frac{220 - 75}{75} \left(1 - e^{-0.8} \right) \right]$$

$$= 1.55702 \times 10^{-3} \text{ s}$$

The average output current voltage,

$$V_0 = \delta V_s + \left(1 - \frac{t_x}{T} \right) E$$

$$\therefore V_0 = 0.4 \times 220 + \left(1 - \frac{1.55702 \times 10^{-3}}{2 \times 10^{-3}} \right) \times 75$$

$$= 104.62 \text{ V}$$

The average output current

$$I_0 = \frac{V_s - E}{R}$$

$$\therefore I_0 = \frac{104.62 - 75}{2} = 14.80 \text{ A}$$

c. As the load current is discontinuous, therefore $I_{\min} = 0$. The maximum value of current is

$$I_{\max} = \frac{V_s - E}{R} \left(1 - e^{-T_{on}/T_d}\right)$$

$$I_{\max} = \frac{220 - 75}{2} \left(1 - e^{-0.8}\right) = 39.92 \text{ A}$$

d. The time variations of various waveforms are sketched in [Figure 6.30](#).

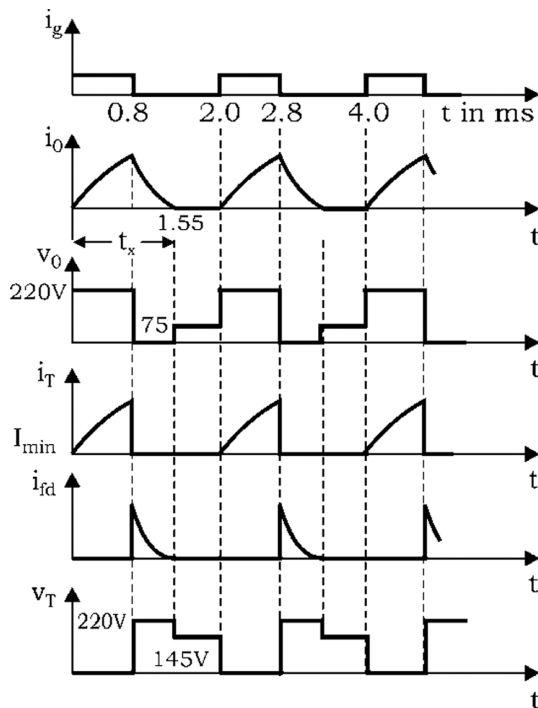


FIGURE 6.30 Various waveforms for Example 6.13.

Example 6.14: An RLE load is operating in a chopper circuit from a 400-V DC source. For the load, $L = 0.08 \text{ H}$ and $R = 0$. For a duty cycle of 0.3, find the chopping frequency to limit the amplitude of load current excursion to 12 A.

Solution

The average output, $V_0 = \delta V_s$

As the average value of voltage drop across L is zero,

$$\therefore E = V_0 = \delta V_s = 0.3 \times 400 = 120 \text{ V}$$

During T_{on} , $(V_s - E)$ appears across inductance L as shown in Figure 6.31.

\therefore During T_{on} , volt-time area applied to inductance

$$= (400 - 120) T_{on} = 280 T_{on} \text{ Volt-sec}$$

Also, during T_{on} , the current through L rises from I_{\min} to I_{\max} so, volt-time area across L during this current change is given by

$$\int_0^{T_{on}} v_L dt = \int_0^{T_{on}} L \frac{di}{dt} dt = \int_{I_{\min}}^{I_{\max}} L di = (I_{\max} - I_{\min}) = L \Delta I$$

These two volt-time areas during T_{on} must be equal.

$$\therefore 280 T_{on} = L \Delta I$$

or

$$T_{on} = \frac{0.08 \times 12}{280} = 3.42 \text{ ms}$$

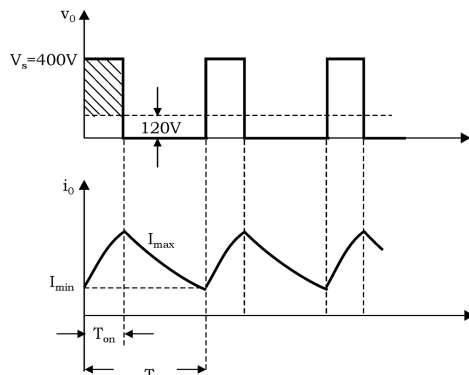
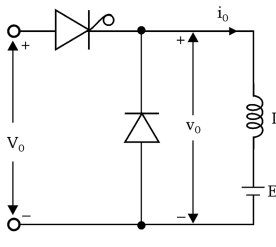


FIGURE 6.31 Circuit diagram and various waveforms for Example 6.14.

$$\text{Thus, chopping frequency, } f = \frac{1}{T} = \frac{\delta}{T_{on}} = \frac{0.3}{1.5 \times 10^{-3}} = 200 \text{ Hz}$$

Example 6.15: A DC motor having total circuit resistance of 3Ω and an inductance of 2 mH is used for a rapid transit system is fed through a DC chopper. What external inductance should be inserted in series with the armature so as to limit the per unit ripple in armature current to 20% for a duty cycle ratio of 0.5, if the chopping frequency is 1 kHz ?

SOLUTION

Per unit ripple in current is given by:

$$\text{p.u. ripple current} = \frac{I_{\max} - I_{\min}}{V_s / R} = \left[\frac{(1 - e^{-\delta T/T_a}) (1 - e^{-(1-\delta)T/T_a})}{1 - e^{-T/T_a}} \right]$$

Let $\frac{T}{T_a} = x$. Here $\delta = 0.5$ and p.u. ripple $= \frac{20}{100} = 0.2$. Substitution of these values in the above expression gives

$$0.2 = \frac{(1 - e^{-0.5x}) (1 - e^{-0.5x})}{1 - e^{-x}} = \frac{(1 - e^{-0.5x}) (1 - e^{-0.5x})}{(1 - e^{-0.5x})(1 + e^{-0.5x})} = \frac{1 - e^{-0.5x}}{1 + e^{-0.5x}}$$

or

$$0.2 = \frac{1-y}{1+y} \text{ where } y = e^{-0.5x}$$

or

$$y = \frac{0.8}{1.2} = e^{-0.5x}$$

or

$$e^{0.5x} = \frac{1.2}{0.8} = 1.5 \text{ or } x = \frac{T}{T_a} = 0.8109$$

$$\therefore T_a = \frac{T}{0.8109} = \frac{1}{0.8109 f} = \frac{1}{0.8109 \times 1000}$$

or

$$L = RT_a = \frac{3}{0.8109 \times 1000} \\ = 3.7 \text{ mH}$$

Therefore, external inductance that should be inserted $= 3.7 - 2 = 1.7 \text{ mH}$

Example 6.16: A voltage-commutated chopper has the following parameters:

$V_s = 220 \text{ V}$, load circuit parameters, $R = 0.5 \Omega$, $L = 3 \text{ mH}$, $E = 40 \text{ V}$.

Commutation circuit parameters:

$L = 25 \mu\text{H}$, and $C = 60 \mu\text{F}$, $T_{on} = 700 \mu\text{ sec}$, $T = 2000 \mu\text{s}$.

For a constant load current of 100 A, determine the following:

- Effective on period.
- Peak currents through main thyristor T_1 and auxiliary thyristor AT.
- Turn-off time for T_1 and AT.
- Total commutation interval.
- Capacitor voltage 150 μs after AT is triggered.
- Time needed to recharge the capacitor to voltage V_s .

SOLUTION

- a. The effective-on period, T'_{on}

$$= T_{on} + \frac{2V_s}{I_0} C = 700 \times 10^{-6} + \frac{2 \times 220}{100} \times 60 \times 10^{-6} = 964 \mu\text{s}$$

- b. Peak current through main thyristor T_1 , $(i_{T_1})_{\max} = I_0 + V_s \cdot \sqrt{\frac{C}{L}}$

$$= 100 + 220 \sqrt{\frac{60}{25}} = 440.82 \text{ A}$$

Since load current is given as constant at 100 A, peak current through AT is 100 A.

- c. Turn-off time for T_1 is

$$t_c = \frac{CV_s}{I_0} = \frac{60 \times 10^{-6} \times 220}{100} = 132 \mu\text{s}$$

Turn-off time for thyristor AT is

$$\begin{aligned} i_{c1} &= \frac{\pi}{2} \sqrt{LC} = \frac{\pi}{2} \sqrt{25 \times 60} \times 10^{-6} \\ &= 60.84 \mu\text{s} \end{aligned}$$

d. Total commutation interval

$$= 2t_c = 2 \times 132 = 264 \mu\text{s}$$

e. Capacitor voltage before AT is triggered is equal to $(-V_s)$. After AT is triggered, capacitor begins to charge from $(-V_s)$. Therefore, capacitor voltage, after AT is triggered, is given by:

$$v_C = \frac{I_0 \cdot t}{C} - V_s$$

Where t is the time measured from the instant AT is triggered

$$\therefore v_C = \frac{100 \times 150 \times 10^{-6}}{60 \times 10^{-6}} - 220 \\ = 30 \text{ V}$$

f. Time needed to recharge from $(-V_s)$ to V_s is given by

$$\frac{(\text{Total change in voltage}) (\text{Capacitance})}{\text{Load current}}$$

$$= \frac{[V_s - (-V_s)] C}{I_0} = \frac{2 \times 220 \times 60}{100} = 264 \mu\text{s}$$

Example 6.17: For an impulse-commutated chopper feeding inductive load, if source voltage is 220 V DC, chopping frequency is 500 Hz, Turn-off time for main thyristor is 20 μs and requires a constant current of 250 A. Peak current through main thyristor is limited to 1.6 times the constant load current. Take a factor of safety 2 for the main thyristor, find the values of (a) commutating components C and L and (b) the minimum and maximum output voltage.

SOLUTION

a. Load current $I_0 = 250 \text{ A}$, $V_s = 220 \text{ V}$

For a factor of safety 2, the commutation circuit turn-off time for main thyristor

$$t_c = 2 \times 20 = 40 \mu\text{s}$$

The value of commutating capacitor C is given by, $C = \frac{t_c \cdot I_0}{V_s}$

$$\therefore C = \frac{40 \times 10^{-6} \times 250}{220} = 45.46 \mu\text{F}$$

Peak current through main thyristor, is

$$(i_{T_1})_{\max} = 1.6I_0 = I_0 + V_s \sqrt{\frac{C}{L}} \quad \text{or} \quad 220 \sqrt{\frac{C}{L}} = 0.6 \times I_0$$

$$L = \left(\frac{220}{0.6 \times 250} \right)^2 \times 45.46 = 97.78 \mu\text{H}$$

b. Minimum value of duty cycle δ_{\min} is

$$\delta_{\min} = \pi f \sqrt{LC} = \pi \times 500 \sqrt{97.78 \times 45.46} \times 10^{-6} = 0.104$$

Minimum value of output voltage, $(V_0)_{\min}$ is

$$(V_0)_{\min} = V_s(\delta_{\min} + 2t_c)$$

$$= 220(0.104 + 2 \times 500 \times 40 \times 10^{-6}) = 31.68 \text{ V}$$

Maximum value of output voltage is $(V_0)_{\max} = 220 \text{ V}$

Example 6.18:

- a. A current-commutated chopper has following parameters: The source voltage is 220 V DC; main SCR turn-off time is 25 μs , and peak commutating current is twice the maximum possible load current. For a maximum load current of 150 A, calculate
 - i. the value of the commutating inductor and capacitor,
 - ii. maximum capacitor voltage and
 - iii. the peak-commutating current.
- b. Repeat part (a), in case peak commutating current is thrice the maximum possible load current. Compare the results obtained in parts (a) and (b).

SOLUTION

a. $x = 2, t_q = 25 \mu\text{s}$

$$t_c = t_q + \Delta t.$$

Taking $\Delta t = 25 \mu\text{s}$, $t_c = (25 + 25) \mu\text{s} = 50 \mu\text{s}$

i. The value of commutating inductor L is given by,

$$L = \frac{V_s \cdot t_c}{x I_0 \left[\pi - 2 \sin^{-1} \left(\frac{1}{x} \right) \right]}$$

$$\therefore L = \frac{220 \times 50 \times 10^{-6}}{2 \times 150 \left[\pi - 2 \sin^{-1} \left(\frac{1}{2} \right) \right]} = 17.507 \mu\text{H}$$

The value of commutating capacitor C is,

$$C = \frac{x I_0 \cdot t_c}{V_s \left[\pi - 2 \sin^{-1} \left(\frac{1}{x} \right) \right]}$$

$$\therefore C = \frac{2 \times 150 \times 50 \times 10^{-6}}{220 \left[\pi - 2 \sin^{-1} \left(\frac{1}{2} \right) \right]} = 32.56 \mu\text{F}$$

ii. Peak capacitor voltage, $V_{cp} = V_s + I_0 \sqrt{\frac{L}{C}}$

$$\therefore V_{cp} = 220 + 150 \sqrt{\frac{17.507}{32.56}} = 330 \text{ V}$$

iii. Peak commutating current,

$$I_{cp} = x I_0 = 2 \times 150 = 300 \text{ A}$$

b. i. Here $x = 3$,

$$\therefore L = \frac{220 \times 50 \times 10^{-6}}{3 \times 150 \left[\pi - 2 \sin^{-1} \left(\frac{1}{3} \right) \right]} = \frac{11000 \times 10^{-6}}{450 [\pi - 0.22\pi]} = 9.98 \mu\text{H}$$

$$C = \frac{3 \times 150 \times 50 \times 10^{-6}}{220 \left[\pi - 2 \sin^{-1} \left(\frac{1}{3} \right) \right]} = \frac{22500 \times 10^{-6}}{220 [\pi - 0.22\pi]} = 41.74 \mu\text{F}$$

ii. Peak capacitor voltage,

$$V_{cp} = 220 + 150 \sqrt{\frac{9.98}{41.74}} = 293.35 \text{ V}$$

iii. Peak commutating current,

$$I_{cp} = 3 \times 150 = 450 \text{ A}$$

From above, it is revealed that with increase IN x , value of inductor L is reduced whereas value of capacitor C is increased, the peak capacitor voltage reduces but the peak commutating current increases.

Example 6.19: A current-commutated chopper is fed from a DC source of 220 V. Its commutating components are $L = 25 \mu\text{H}$ and $C = 55 \mu\text{F}$. If load current of 200 A is assumed constant during the commutation process, then compute the following:

- Turn-off time of main thyristor
- Total commutation interval.
- Turn-off time of auxiliary thyristor

SOLUTION

- a. Peak commuting current, I_{cp} is

$$I_{cp} = V_s \sqrt{\frac{C}{L}} = 220 \sqrt{\frac{55}{25}} = 326.31 \text{ A}$$

$$\therefore x = \frac{I_{cp}}{I_0} = \frac{326.31}{200} = 1.63$$

$$\text{Turn-off time of main SCR, } t_c = \left[\pi - 2 \sin^{-1} \left(\frac{1}{x} \right) \right] \sqrt{LC}$$

$$\therefore t_c = \left[\pi - 2 \sin^{-1} (1/1.63) \right] \sqrt{25 \times 55 \times 10^{-12}} = 67.51 \mu\text{s}$$

$$\text{b. } \theta_1 = \sin^{-1} \left(\frac{I_0}{I_{cp}} \right) = \sin^{-1} \left(\frac{200}{326.31} \right) = 37.8^\circ$$

$$\text{Total commutation interval, } = \left(\frac{5\pi}{2} - \theta_1 \right) \sqrt{LC} + CV_s \frac{1 - \cos \theta_1}{I_0}$$

$$\left(\frac{5\pi}{2} - \frac{37.8 \times \pi}{180} \right) \sqrt{1375} \times 10^{-6} + 55 \times 10^{-6} \times 220 \frac{1 - \cos 33.8^\circ}{200}$$

$$= 266.77 \times 10^{-6} + 12.695 \times 10^{-6} = 279.465 \mu\text{s}$$

$$\text{c. Turn-off time of auxiliary thyristor} = \frac{\pi - \theta_1}{\omega_1} = (\pi - \theta_1) \sqrt{LC}$$

$$\left(\pi - \frac{37.8 \times \pi}{180} \right) \sqrt{1375} \times 10^{-6} = 92.031 \mu\text{s}$$

Example 6.20: A buck regulator has an input voltage of $V_s = 15$ V. The required average output voltage is $V_0 = 7$ V at $R = 500\Omega$, and the peak-to-peak output ripple voltage is 30 mV. The switching frequency is 30 kHz. If the peak-to-peak ripple current of inductor is limited to 0.8 A, determine (a) the duty cycle δ , (b) the filter inductance L , (c) the filter capacitor C , and (d) the critical values of L and C .

SOLUTION

$V_s = 15$ V, $\Delta V_C = 30$ mV, $\Delta I = 0.8$ A, $f = 30$ kHz, and $V_0 = 7$ V

- Average output voltage, $V_0 = \delta V_s$ and $\delta = V_0/V_s = 7/15 = 0.47 = 47\%$
- Peak-to-peak ripple current,

$$\Delta I = \frac{V_0(V_s - V_0)}{fL V_s}$$

$$\therefore L = \frac{V_0(V_s - V_0)}{\Delta I \cdot f \cdot V_s}$$

$$\therefore L = \frac{7(15 - 7)}{0.8 \times 30,000 \times 15} = 155.56 \mu\text{H}$$

- Peak-to-peak ripple voltage of the capacitor,

$$\Delta V_C = \frac{\Delta I}{8fC}$$

$$\therefore C = \frac{\Delta I}{8f\Delta V_C}$$

$$= \frac{0.8}{8 \times 30 \times 10^{-3} \times 30,000} = 111.12 \mu\text{H}$$

- Critical value of inductor,

$$L_C = \frac{(1-\delta)R}{2f} = \frac{(1-0.47) \times 500}{2 \times 30 \times 10^3} = 4.42 \text{ mH}$$

Critical value of capacitor,

$$C_C = \frac{1-\delta}{16Lf^2} = \frac{1-0.47}{16 \times 4.42 \times 10^{-3} \times (30 \times 10^3)^2}$$

$$= \frac{0.53}{63648 \times 10^{-3}} = 0.008 \mu\text{H}$$

Example 6.21: A boost regulator has an input voltage of $V_s = 7$ V. The average output voltage $V_0 = 15$ V and the average load current $I_0 = 0.8$ A. The switching frequency is 30 kHz. If $L = 150 \mu\text{H}$ and $C = 220 \mu\text{F}$, determine (a) the duty cycle δ , (b) the ripple current of inductor ΔI , (c) the peak current of inductor I_2 , (d) the ripple voltage of filter capacitor ΔV_C , and (e) the critical values of L and C .

SOLUTION

$V_s = 7$ V, $V_0 = 15$ V, $f = 30$ kHz, $L = 150 \mu\text{H}$, $C = 220 \mu\text{F}$ and $I_0 = 0.8$ A

a. Average output voltage, $V_0 = \frac{V_s}{1-\delta}$

$$\therefore 15 = 7/(1 - \delta) \text{ or } \delta = 0.5334 = 53.34\%$$

b. Peak-to-peak ripple current,

$$\Delta I = \frac{V_s(V_0 - V_s)}{fL V_0}$$

$$\therefore \Delta I = \frac{7 \times (15 - 7)}{30,000 \times 150 \times 10^{-6} \times 15} = 0.83 \text{ A}$$

c. Average input current, $I_s = \frac{I_0}{1-\delta}$

$$\begin{aligned}\therefore I_s &= \frac{0.8}{1 - 0.83} \\ &= 4.7 \text{ A}\end{aligned}$$

So, the peak inductor current,

$$I_2 = I_s + \frac{\Delta I}{2} = 4.7 + \frac{0.83}{2} = 5.11 \text{ A}$$

d. Peak-to-peak ripple voltage of capacitor, $\Delta V_C = \frac{I_0 \delta}{fC}$

$$\therefore \Delta V_C = \frac{0.8 \times 0.5334}{30,000 \times 220 \times 10^{-6}} = 64.65 \text{ mV}$$

e. $R = \frac{V_0}{I_0} = \frac{15}{0.8} = 18.75 \Omega$

Critical value of inductor,

$$L_C = \frac{(1 - \delta) \delta R}{2f} = \frac{(1 - 0.5334) \times 0.5334 \times 18.75}{2 \times 30 \times 10^{-3}} = 77.78 \mu\text{H}$$

Critical value of capacitor,

$$C_C = \frac{\delta}{2fR} = \frac{0.5334}{2 \times 30 \times 10^3 \times 18.75} = 0.47 \mu\text{F}$$

Example 6.22: A buck-boost regulator has an input voltage of $V_s = 15 \text{ V}$. The duty cycle $\delta = 0.30$ and the switching frequency is 30 kHz . The inductance $L = 150 \mu\text{H}$ and filter capacitance $C = 220 \mu\text{F}$. The average load current $I_0 = 1.5 \text{ A}$. Determine (a) the average output voltage, V_0 ; (b) the peak-to-peak output voltage ripple, ΔV_C ; (c) the peak-to-peak ripple current of inductor, ΔI ; (d) the peak current of the transistor, I_p ; and (e) the critical values of L and C .

SOLUTION

$V_s = 15 \text{ V}$, $\delta = 0.3$, $I_0 = 1.5 \text{ A}$, $f = 30 \text{ kHz}$, $L = 150 \mu\text{H}$, $C = 220 \mu\text{F}$

a. Average output voltage of buck-boost regulator,

$$\begin{aligned} V_0 &= -\frac{\delta V_s}{1-\delta} \\ &= -\frac{0.3 \times 15}{1-0.3} \\ &= -6.43 \text{ V} \end{aligned}$$

b. Peak-to-peak output ripple voltage of capacitor,

$$\begin{aligned} \Delta V_C &= \frac{\delta I_0}{fC} \\ \therefore \Delta V_C &= \frac{0.3 \times 1.5}{30,000 \times 220 \times 10^{-6}} = 68.18 \text{ mV} \end{aligned}$$

c. The peak-to-peak inductor ripple current, $\Delta I = \frac{\delta V_s}{fL}$

$$\therefore \Delta I = \frac{0.3 \times 15}{30,000 \times 150 \times 10^{-6}} = 1.0 \text{ A}$$

d. Average input current, $I_s = \frac{\delta I_0}{1-\delta} = \frac{0.3 \times 1.5}{1-0.3} = 0.643 \text{ A}$

Because I_s is the average of duration δT , so the peak-to-peak current of transistor is

$$I_p = \frac{I_s}{\delta} + \frac{\Delta I}{2} = \frac{0.643}{0.3} + \frac{1}{2} = 2.65 \text{ A}$$

e. $R = \frac{-V_0}{I_0} = \frac{6.43}{1.5} = 4.29 \Omega$

Critical value of inductor, $L_C = \frac{(1 - \delta) R}{2f} = \frac{(1 - 0.3) \times 4.29}{2 \times 30 \times 10^3} = 50 \mu\text{H}$

Critical value of capacitor, $C_C = \frac{\delta}{2fR} = \frac{0.3}{2 \times 30 \times 10^3 \times 4.29} = 1.17 \mu\text{F}$

Example 6.23: The input voltage of a Cuk converter is $V_s = 15 \text{ V}$. The duty cycle $\delta = 0.30$ and the switching frequency is 30 kHz . The filter inductance is $L_2 = 150 \mu\text{H}$ and filter capacitance $C_2 = 220 \mu\text{F}$. The energy transfer capacitance is $C_1 = 200 \mu\text{F}$ and inductance $L_1 = 180 \mu\text{H}$. The average load current is $I_0 = 1.5 \text{ A}$. Determine (a) the average output V_0 ; (b) the average input current I_s ; (c) the peak-to-peak ripple current of inductor L_1 , ΔI_1 ; (d) the peak-to-peak ripple voltage of capacitor C_1 , ΔV_{C1} ; (e) the peak-to-peak ripple current of inductor L_2 , ΔI_2 ; (f) the peak-to-peak ripple voltage of capacitor C_2 , ΔV_{C2} ; and (g) the peak current of the transistor I_p .

SOLUTION

$V_s = 15 \text{ V}$, $\delta = 0.3$, $I_0 = 1.5 \text{ A}$, $f = 30 \text{ kHz}$, $L_1 = 180 \mu\text{H}$, $C_1 = 200 \mu\text{F}$, $L_2 = 150 \mu\text{H}$, and $C_2 = 220 \mu\text{F}$.

a. The average output voltage for Cuk regulator, $V_0 = \frac{-\delta V_s}{1 - \delta}$

$$= \frac{-0.3 \times 15}{1 - 0.3} = -6.43 \text{ V}$$

b. The average input current, $I_s = \frac{\delta I_0}{1 - \delta}$

$$= \frac{0.3 \times 15}{1 - 0.3} = 0.642 \text{ A}$$

c. Peak-to-peak ripple current of inductor L_1 , ΔI_1 ,

$$\Delta I_1 = \frac{\delta V_s}{f L_1} = \frac{0.3 \times 15}{30,000 \times 180 \times 10^{-6}} = 0.84 \text{ A}$$

d. Peak-to-peak ripple voltage of capacitor C_1 , ΔV_{C1} ,

$$\Delta V_{C1} = \frac{I_s (1 - \delta)}{f C_1} = \frac{0.642 (1 - 0.3)}{30,000 \times 200 \times 10^{-6}} = 74.9 \text{ mV}$$

e. Peak-to-peak ripple current of inductor L_2 , ΔI_2

$$\Delta I_2 = \frac{\delta V_s}{f L_1} = \frac{0.3 \times 15}{30,000 \times 150 \times 10^{-6}} = 1.0 \text{ A}$$

f. Peak-to-peak ripple voltage of capacitor C_2 , ΔV_{c2}

$$\Delta V_{c2} = \frac{\Delta I_2}{8fC_2} = \frac{1.0}{8 \times 30,000 \times 220 \times 10^{-6}} = 18.94 \text{ mV}$$

g. The average voltage across the diode can be found from

$$V_{0m} = -\delta V_{c1} = -V_0 \delta \frac{1}{-\delta} = V_0$$

For a lossless circuit, $I_{L_2} V_{0m} = V_0 I_0$ and the average value of the current in inductor L_2 is

$$I_{L_2} = \frac{I_0 V_0}{V_{om}} = I_0 = 1.5 \text{ A}$$

Therefore, the peak current of transistor is

$$I_p = I_s + \frac{\Delta I_1}{2} + I_{L_2} + \frac{\Delta I_2}{2} = 0.64 + \frac{0.84}{2} + 1.5 + \frac{1.0}{2} = 3.06 \text{ A}$$

Example 6.24:

a. For an ideal type-A chopper feeding RLE load, show that:

$$I_{\text{TAV}} = \frac{\delta(V_s - E)}{R} - \frac{L}{RT} (I_{\max} - I_{\min}).$$

b. Also, derive an expression for the average current in the FD for a continuous load current.

c. Prove that average value of load current I_0 is given by

$$I_0 = \frac{V_0 - E}{R}$$

SOLUTION

For type-A chopper, various waveforms are shown in [Figure 6.32](#).

a. When the chopper is on, the voltage equation is given by

$$Ri_T + L \frac{di_T}{dt} + E = V_s$$

or

$$Ri_T \cdot dt + L \frac{di_T}{dt} dt = (V_s - E) dt.$$

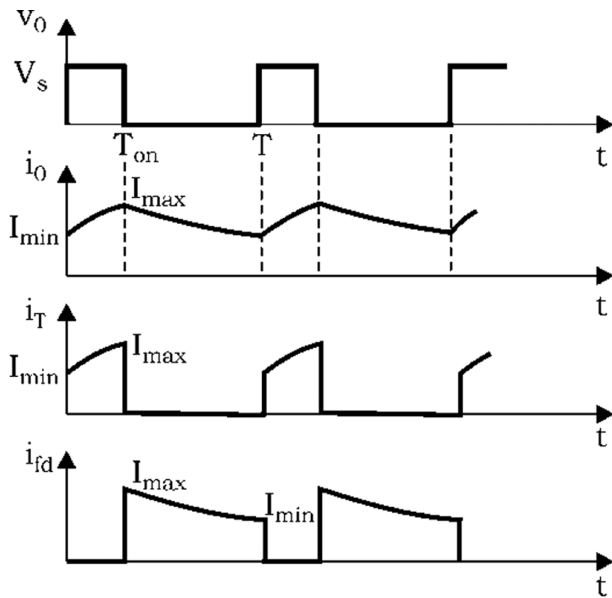


FIGURE 6.32 Various waveforms for Example 6.25.

Its average value, [Figure 6.32](#), is

$$R \cdot \frac{1}{T} \int_0^{T_{on}} i_T \cdot dt + \frac{1}{T} \int_0^{T_{on}} L \frac{di_T}{dt} dt = \frac{(V_s - E)}{T} \int_0^{T_{on}} dt$$

$$R I_{TAV} + \frac{1}{T} \int_{I_{min}}^{I_{max}} L di_T = (V_s - E) \frac{T_{on}}{T}$$

or

$$R I_{TAV} + \frac{L}{T} (I_{max} - I_{min}) = (V_s - E) \delta$$

or

$$I_{TAV} = \frac{\delta (V_s - E)}{R} - \frac{L}{RT} (I_{max} - I_{min}) \quad (6.106)$$

- b. When the FD conducts, the load voltage is zero. The voltage equation is given by

$$R i_{fd} + L \frac{di_{fd}}{dt} + E = 0$$

Its average value for [Figure 6.32](#), is

$$R \cdot \frac{1}{T} \int_{T_{on}}^T i_{fd} \cdot dt + L \frac{1}{T} \int_{T_{on}}^T \frac{di_{fd}}{dt} dt + E \frac{1}{T} \int_{T_{on}}^T dt = 0$$

or

$$R \cdot I_{fd} + \frac{L}{T} \int_{I_{min}}^{I_{max}} di_{fd} = -E \frac{T - T_{on}}{T}$$

or

$$R I_{fd} + \frac{L}{T} (I_{min} - I_{max}) = -E (1 - \delta)$$

$$\therefore I_{fd} = \frac{L (I_{max} - I_{min})}{TR} - \frac{E (1 - \delta)}{R} \quad (6.107)$$

- c. Average load current over a complete cycle can be obtained by adding I_{TAV} and I_{fd} from Equations (6.106) and (6.107), respectively.

$$\therefore I_0 = \frac{\delta (V_s - E)}{R} - \frac{L}{RT} (I_{max} - I_{min}) + \frac{L}{RT} (I_{max} - I_{min}) - \frac{E (1 - \delta)}{R}$$

$$= \frac{\delta V_s - E}{R} = \frac{V_0 - E}{R}. \text{ This is the required result.}$$

Example 6.25: A voltage-commutated chopper feeds power to a battery-powered electric vehicle. The battery voltage is 80 V, starting current is 80 A, and thyristor turn-off time is 25 μ s. Calculate the values of commutating capacitor C and inductor L .

SOLUTION

Let circuit turn-off time $t_c = t_q + \Delta t = 25 + 25 = 50 \mu$ s for reliable turn-off of T_1 and AT. Let I_0 is the maximum load current that the commutation circuitry must be able to commutate.

$$\text{Commutating capacitor } C = \frac{(t_q + \Delta t) I_0}{V_s} = \frac{t_c I_0}{V_s}$$

$$\therefore C = \frac{50 \times 80 \times 10^{-6}}{80} = 50 \mu\text{F}$$

Value of commutating inductor can be designed by, $L \geq \left(\frac{V_s}{I_0} \right)^2 C$

$$L \geq \left(\frac{80}{80} \right)^2 \times 50 \times 10^{-6} = 50 \mu\text{H}$$

Also, the value of $L = \left(\frac{2t_{c1}}{\pi} \right)^2 \cdot \frac{1}{C}$

$$\therefore L = \left(\frac{2 \times 50 \times 10^{-6}}{\pi} \right)^2 \times \frac{1}{50 \times 10^{-6}} = 20.26 \mu\text{H}$$

There are two values of L . Low value of L increases the peak value of capacitor current. So higher value of $L = 50 \mu\text{H}$ should be chosen.

REVIEW QUESTIONS AND UNSOLVED PROBLEMS

- 6.1 a. What is a DC chopper? Describe the various types of chopper configurations with appropriate diagrams wherever necessary.
 b. A DC battery is charged from a constant DC source of 220 V through a chopper. The DC battery is to be charged from its internal emf of 90 V to 122 V. The battery has internal resistance of 2Ω . For a constant charging current of 10 A, compute the range of the duty cycle.
- 6.2 For a type-A chopper, express the following variables in terms of V_s , R , I_0 , and duty cycle δ in case load inductance causes the load current I_0 to remain constant at a value $I_0 = V_0/R$. Here, V_s is the source voltage.
 a. Average output voltage and current
 b. Output current at the instant of commutation
 c. Average and RMS values of FD current
 d. RMS value of the output voltage
 e. Average and RMS values of thyristor current
 Sketch the time variations of gate signal i_g , output voltage v_0 , output current i_0 , thyristor current i_T , and FD current i_{fd} .
- 6.3 Draw the power circuit diagram for a type-A chopper. Show load voltage waveforms for (i) $\delta = 0.4$ and (ii) $\delta = 0.7$. For both these duty cycles, calculate:
 a. the average and RMS values of output voltage in terms of source voltage V_s
 b. the output power in case of resistive load R
 c. the RFs
- 6.4 a. A chopper controls power given to an RL load. For $T/T_a = Q$, derive an expression for the value of duty cycle δ below which the per unit value of minimum load current falls below x per unit for V_s/R .
 b. A chopper has the following data:
 $T = 1000 \mu\text{s}$, $R = 2 \Omega$, $L = 5 \text{ mH}$.
 Find the duty cycle α so that per unit value of minimum load current does not fall below (i) 0.1 and (ii) 0.3 of V_s/R .

- 6.5 a. A chopper, fed from a 220-V DC source, is working at a frequency of 50 Hz and is connected to an RL load of $R = 5 \Omega$ and $L = 1\text{mH}$. Determine the value of duty cycle at which the minimum load current will be (i) 5 A, (ii) 5 A, (iii) 25 A, and (iv) 30 A.
- b. For the values of δ obtained in (a), calculate the corresponding values of maximum currents and the RFs.
- 6.6 a. Describe the principle of a step-up chopper. Derive an expression for the average output voltage in terms of input DC voltage and the duty cycle. State the assumptions made.
- b. A step-up chopper has output voltage of two to four times the input voltage. For a chopping frequency of 2,000 Hz, determine the range of off periods for the gate signal.
- 6.7 For type-A chopper connected to RLE load, write the basic voltage equations and derive the expressions for the maximum and minimum values of load current in terms of source voltage V_s , R , E , etc.

Hence, show that the expression for per unit ripple in the load current is given by

$$\frac{(1 - e^{-\delta T/T_a}) (1 - e^{-(1-\delta)T/T_a})}{(1 - e^{-T/T_a})}$$

where T is the chopping period, δ is the duty cycle and $T_a = L/R$ and T is the chopping period.

- 6.8 A type-A chopper feeds, RLE load. For low value of T_{on} , limit of continuous conduction is reached when load current during $T_{on} < t < T$ falls to zero. Derive an expression for this load current from basic voltage equations, and hence obtain from that the duty cycle δ' at the limit of continuous conduction is given by

$$\delta' = \frac{T_a}{T} \ln \left[1 + \frac{E}{V_s} (e^{T/T_a} - 1) \right]$$

where V_s is the source voltage, $T_a = L/R$, and T is the chopping period.

- 6.9 A DC converter has a resistive load, $R = 20 \Omega$ and input voltage, $V_s = 220 \text{ V}$. When the converter remains on, its voltage drop is $V_{ch} = 1.5 \text{ V}$ and chopping frequency is $f = 10 \text{ kHz}$. If the duty cycle is 80% determine (a) the average output voltage V_0 , (b) the RMS output voltage V_{rms} , (c) the converter efficiency, (d) the effective input resistance R_i , and (e) the RMS value of the fundamental component of harmonics on the output voltage.
- 6.10 A DC converter is feeding an RL load with $V_s = 220 \text{ V}$, $R = 20 \Omega$, $L = 15.5 \text{ mH}$, $f = 5 \text{ kHz}$, and $E = 20 \text{ V}$. Calculate (a) the minimum instantaneous load current I_1 , (b) the peak instantaneous load current I_2 , (c) the maximum peak-to-peak

ripple current in the load, (d) the average load current I_0 , (e) the RMS load current I_0 , (f) the effective input resistance R_i , and (g) the RMS value of converter current I_R .

- 6.11 A DC converter has load resistance, $R = 0.2 \Omega$; input voltage $V_s = 220$ V; battery voltage, $E = 10$ V. The average load current, $I_a = 200$ A, and the chopping frequency is $f = 200$ Hz ($T = 5$ ms). Use the average output voltage to calculate the value of load inductance L , which would limit the maximum load ripple current to 5% of I_0 .
- 6.12 The DC converter is used to control power flow from a DC voltage, $V_s = 110$ V to a battery voltage, $E = 220$ V. The power transferred to the battery is 30 kW. The current ripple of the inductor is negligible. Determine (a) the duty cycle δ , (b) the effective load resistance R_{eq} , and (c) the average input current I_s .
- 6.13 An RL load is controlled by a converter. If load resistance $R = 0.25 \Omega$, inductance $L = 20$ mH, supply voltage $V_s = 600$, battery voltage $E = 150$ V, and chopping frequency $f = 250$ Hz, determine the minimum and maximum load current, the peak-to-peak load ripple current, and average load current for $\delta = 0.1$ to 0.9 with a step of 0.1.
- 6.14 The step-up converter has $R = 10 \Omega$, $L = 6.5$ mH, $E = 5$ V, and $\delta = 0.5$. Find I_1 , I_2 , and ΔI .
- 6.15 The buck regulator has an input voltage, $V_s = 15$ V. The required average output voltage $V_s = 5$ V and the peak-to-peak output ripple voltage is 10 mV. The switching frequency is 20 kHz. The peak-to-peak ripple current of inductor is limited to 0.5 A. Determine (a) the duty cycle δ , (b) the filter inductance L , (c) the filter capacitor C , and (d) the critical values of L and C .
- 6.16 The boost regulator has an input voltage, $V_s = 6$ V. The average output voltage, $V_a = 15$ V and average load current, $I_a = 0.5$ A. The switching frequency is 20 kHz. If $L = 250 \mu\text{H}$ and $C = 440 \mu\text{F}$, determine (a) the duty cycle δ , (b) the ripple current of inductor, ΔI , (c) the peak current of inductor, I_2 , (d) the ripple voltage of filter capacitor, ΔV_c , and (e) the critical values of L and C .
- 6.17 The buck-boost regulator has an input voltage, $V_s = 12$ V. The duty cycle $\delta = 0.6$, and the switching frequency is 25 kHz. For the inductance, $L = 250$ mH and for filter capacitance, $C = 220 \mu\text{F}$. For the average load current, $I_0 = 1.5$ A. Determine (a) the average output voltage V_a , (b) the peak-to-peak output ripple voltage ΔV_c , (c) the peak-to-peak ripple current of inductor ΔI , (d) the peak current of the transistor I_p , and (e) the critical values of L and C .
- 6.18 The Cuk regulator has an input voltage, $V_s = 15$ V. The duty cycle is $\delta = 0.4$ and the switching frequency is 25 kHz. The filter inductance is $L_2 = 350 \mu\text{H}$ and filter capacitance is $C_2 = 220 \mu\text{F}$. The energy transfer capacitance is $C_1 = 400 \mu\text{F}$ and inductance is $L_1 = 250 \mu\text{H}$. The average load current is $I_0 = 1.25$ A. Determine (a) the average output voltage V_a , (b) the average input current I_s , (c) the peak-to-peak ripple current of inductor L_1 , ΔI_1 , (d) the peak-to-peak ripple voltage of capacitor C_1 , ΔV_{c1} , (e) the peak-to-peak ripple current of inductor L_2 , ΔI_2 , (f) the peak-to-peak ripple voltage of capacitor C_2 , ΔV_{c2} , and (g) the peak current of the transistor I_p .

- 6.19 In Problem 6.18 for the Cuk regulator, find the critical values of L_1 , C_1 , L_2 , and C_2 .
- 6.20 The buck converter has a DC input voltage $V_s = 110$ V, average load voltage $V_0 = 80$ V, and average load current $I_0 = 20$ A. The chopping frequency is $f = 10$ kHz. The peak-to-peak ripples are 5% for load voltage 25% for load current, and 10% to, filter L_e , current. (a) Determine the values of L_e , L , and C_e .
- 6.21 A DC regulator is operated at a duty cycle of $\delta = 0.4$. The load resistance is $R = 150 \Omega$, the inductor resistance is $r_L = 1 \Omega$, and the resistance of the filter capacitor is 0.2Ω . Determine the voltage gain for the (a) buck converter, (b) boost converter, and (c) buck-boost converter.

SUMMARY

This chapter has studied in detail various converter topologies for DC-to-DC conversion. It can be seen that DC-to-DC converters can be operated in all the quadrants, which is not possible for the AC-to-DC converters. In certain applications, such as for DC-motor drive needs, the energy flows in two directions, that is, output current to be either positive or negative, which can be achieved using type-C choppers and buck-boost converters. These converters are widely used for various types of DC power supplies. These are also very common in telecommunication systems and battery-operated systems.

MAIN FORMULAS OF THE CHAPTER

- **For step-down chopper**

$$V_0 = \frac{T_{on}}{T} V_s = \delta V_s$$

$$V_0 = f T_{on} V_s$$

$$I_{\max} = \frac{V_s}{R} \left[\frac{1 - e^{-T_{on}/T_a}}{1 - e^{-T/T_a}} \right] - \frac{E}{R}$$

$$I_{\min} = \frac{V_s}{R} \left[\frac{e^{T_{on}/T_a} - 1}{e^{T/T_a} - 1} \right] - \frac{E}{R}$$

$$\text{Steady State Ripple} = \frac{V_s}{R} \left[\frac{(1 - e^{-T_{on}/T_a})(1 - e^{-T_{off}/T_a})}{1 - e^{-T/T_a}} \right]$$

Limits of Continuous Conduction

$$\delta' = \frac{T_{on}}{T} = \frac{T_a}{T} \ln \left[1 + k(e^{T/T_a} - 1) \right]$$

$$t_x = T_{on} + T_a \ln \left[1 + \frac{V_s - E}{E} \left(1 - e^{-\frac{T_{on}}{T_a}} \right) \right]$$

During discontinuous conduction

$$V_0 = \delta V_s + \left(1 - \frac{t_x}{T} \right) E$$

$$V_r = V_s \sqrt{\delta - \delta^2}$$

$$RF = \frac{V_r}{V_0} = \sqrt{\frac{1-\delta}{\delta}} = \sqrt{\frac{1}{\delta} - 1}$$

- **For step up/down chopper**

$$V_0 = V_s \frac{\delta}{1-\delta}$$

- **Voltage-commutated chopper**

Commutating capacitor

$$C = \frac{t_c I_0}{V_s}$$

Commutating inductor

$$L \geq \left(\frac{V_s}{I_0} \right)^2 C$$

- **Current-commutated chopper**

$$C = \frac{x I_0 t_c}{V_s [\pi - 2 \sin^{-1}(1/x)]}$$

$$L = \frac{V_s t_c}{x I_0 [\pi - 2 \sin^{-1}(1/x)]}$$

- **Load-commutated chopper**

$$C = \frac{I_0 \cdot T_{on}}{2V_s}$$

$$t_c = \frac{CV_s}{I_0}$$

- **Buck (step-down) converter**

$$V_0 = \frac{T_{on}}{T} V_s = \delta V_s$$

$$I_s = \delta \cdot I_0$$

$$\Delta I = \frac{\delta \cdot V_s (1 - \delta)}{f \cdot L}$$

$$\Delta V_c = \frac{\Delta I}{8f \cdot C}$$

- **Boost (step-up) converter**

$$V_0 = V_s \frac{T}{T_{off}} = \frac{V_s}{1 - \delta}$$

$$I_s = \frac{I_0}{1 - \delta}$$

$$\Delta I = \frac{V_s (V_0 - V_s)}{f \cdot L V_0}$$

$$\Delta V_c = \frac{I_0 \cdot \delta}{f \cdot C}$$

- **Buck-boost converter**

$$V_0 = -V_s \cdot \frac{\delta}{(1 - \delta)}$$

$$I_s = \left(\frac{\delta}{1 - \delta} \right) I_0$$

$$\Delta I = \frac{V_s \cdot \delta}{f \cdot L}$$

$$\Delta V_C = \frac{I_0 \cdot \delta}{f \cdot C}$$

- **Cuk regulator**

$$V_0 = \frac{-\delta \cdot V_s}{1 - \delta}$$

$$I_s = \frac{\delta \cdot I_0}{1 - \delta}$$

$$\Delta I_1 = \frac{V_s \cdot \delta}{f \cdot L_1}$$

$$\Delta v_{C1} = \frac{I_s \cdot (1 - \delta)}{f \cdot C_1}$$

$$\Delta v_{C2} = \frac{\delta \cdot V_s}{8C_2L_2f^2}$$

REFERENCES/FURTHER READING

1. P. T. Krein, *Elements of Power Electronics*, Oxford University Press, New York, 2003.
2. K. Thorborg, *Power Electronics*. Prentice Hall International, London, UK, 1988.
3. P. S. Bhimra, *Power Electronics*, 5th ed., Khanna Publications, New Delhi, India, 2012.
4. I. Batarseh, A. Harb. *Power Electronics*, Springer Nature, Cham, Switzerland, 2018.
5. K. R. Ramela, V. Suresh Kumar, Simulation of ride through capability of adjustable speed drive for type A and type B voltage sags and well using Buck-Boost converter, *Int. Conf. Recent Advancements in Electrical, Electronics and Control Engineering*, IEEE, 2011.
6. S. K. Rathor, A. Patel, S. Patel, J. Patel. Closed loop buck-boost converter using RTW, *Int. Conf. Electrical, Electronics, and Optimization Techniques (ICEEOT)*, IEEE, 2016.
7. B. K. Bose, *Power Electronics and AC Drives*, Prentice Hall, Englewood Cliffs, NJ, 1986.
8. G. W. Wester, R. D. Middlebrook, Low frequency characterization of dc-dc converters, *IEEE Trans. Aero. Elect. Sys*, vol. AES-9, no. 3, pp. 376–385, 1973.
9. M. H. Rashid, *Power Electronics: Circuits, Devices, and Applications*, Pearson Education, Singapore, 2004.
10. G. C. Chryssis, *High-Frequency Switching Power Supplies*, 2nd edn, McGraw-Hill, New York, 1989.
11. D. M. Mitchell, *DC-DC Switching Regulator Analysis*. McGraw-Hill, New York, 1988.

12. S. Sreekanth, C. Moses Alvin. A comparative and analytical study of DC/DC converter in incremental MPPT, *International Conference on Circuits, Power and Computing Technologies (ICCPCT)*, IEEE, 2014.
13. B. Choi, *Pulse Width Modulated DC-to-DC Power Conversion*, IEEE Press, Wiley, 2013.
14. D. O. Neacsu, *Switching Power Converters: Medium and High Power Electronics and Motor Drives*, CRC Press, Boca Raton, FL, 2014.
15. E. C. D. Santos Jr., E. R. C. Da Silva, *Advanced Power Electronics Converters*, IEEE Press, Wiley, 2015.
16. M. K. Kazimierczuk, *Pulse-Width Modulated DC–DC Power Converters*, Wiley, Chichester, UK, 2016.
17. T. Suntio, T. Messo, J. Puukko, *Power Electronic Converters*, Wiley-VCH, Verlag GmbH, Germany, 2018.
18. V. Vodovozov, R. Jansikene, *Power Electronic Converters*, TUT, Tallinn, Estonia, 2006.
19. R. W. Erickson, *Fundamentals of Power Electronics*, Chapman & Hall, New York, 1997.
20. P. C. Sen, *Principles of Electric Machines and Power Electronics*, John Wiley & Sons, Hoboken, NJ, 2010.
21. V. R. Moorthi, *Power Electronics Devices, Circuits and Industrial Applications*, Oxford University Press, New Delhi, India, 2010.
22. S. N. Manias, *Power Electronics and Motor Drive Systems*, Academic Publishers, Amsterdam, the Netherlands, 2017.
23. F. Mazda, *Power Electronics Handbook*, Newnes, Oxford, 1997.
24. B. M. Wilamowski, J. D. Irwin, *Power Electronics and Motor Drives*, CRC Press, Boca Raton, FL, 2011.



Taylor & Francis

Taylor & Francis Group

<http://taylorandfrancis.com>

7 DC-to-AC Converter Inverter

7.1 INTRODUCTION

The DC-to-AC converter, which is also termed an *inverter*, converts DC power into AC power at a desired output voltage and frequency. The term *inverter* generally refers to the voltage source rather than current source, that is, it converts energy from a battery or any other fixed DC voltage into AC form whose both magnitude and frequency can be controlled. When thyristors [or silicon-controlled rectifiers (SCRs)] are used as semiconductor device in the inverter, then forced commutation techniques are required for their turn off. This makes the inverter costlier and bulky. Therefore, thyristor-based inverters are used only in high-power applications. For low- and medium-power applications, devices such as the power bipolar junction transistor (BJT), metal-oxide semiconductor field-effect transistor (MOSFET), insulated-gate bipolar transistor (IGBT), and gate turn-off (GTO) are used [1–22]. This chapter discusses in detail the voltage and current source inverters with single- and three-phase AC outputs along with different voltage-control techniques. It also explains the different pulse-width modulation schemes.

Various applications of inverters are:

- Adjustable speed AC drive
- Uninterruptible power supplies (UPS)
- Induction heating
- High-voltage direct current (HVDC) transmission lines

7.2 CLASSIFICATIONS

Inverters can be classified as:

1. **Line-Commuted Inverters:** Inverters that require an existing AC supply at output terminal for their commutation. Their output AC voltage level and frequency cannot be changed.
2. **Force-Commuted Inverter:** Inverters whose output AC voltage level and frequency can be changed as per requirement. These require forced commutation for their turn-off, for example, series inverter, auxiliary commutated inverter, parallel inverter, complementary-commutated inverter.
3. **Voltage Source Inverters (VSI):** Inverters in which the DC source has small impedance.
4. **Current Source Inverter (CSI):** Inverts in which the DC source has high impedance.

5. **Square Wave Inverters:** Such inverters produce a square-wave AC voltage of a constant magnitude. The output voltage of this type of inverter can only be varied by controlling the input DC voltage.
6. **Pulse-Width Modulation (PWM) Inverters:** In these, output has one or more pulses in each half cycle, and by varying the width of pulses, the output voltage is controlled.

7.3 PERFORMANCE PARAMETERS OF INVERTERS

Ideally, an inverter should give a sinusoidal voltage at its output. But the output of practical inverters is non-sinusoidal and contains harmonics. The quality of an inverter is evaluated in terms of the following performance parameters [1–7]:

1. **Harmonic Factor of n th Harmonic (HF $_n$):** A harmonic factor is a measure of the individual harmonic contribution in the output voltage of an inverter. It is defined as:

$$HF_n = \frac{V_n}{V_1} \quad (7.1)$$

where

V_n = root mean square (RMS) value of the n th harmonic component.

V_1 = RMS value of the fundamental component of the output voltage.

2. **Total Harmonic Distortion (THD):** A total harmonic distortion is a measure of closeness in shape between a waveform and its fundamental component. It is defined as the ratio of the RMS value of the total harmonic component of the output voltage and the RMS value of the fundamental component, that is,

$$THD = \frac{\sqrt{\sum_{n=2,3,\dots}^{\infty} V_n^2}}{V_1} = \frac{\sqrt{V_{rms}^2 - V_1^2}}{V_1} \quad (7.2)$$

where V_{rms} is the RMS value of output voltage.

3. **Distortion Factor (DF):** A DF indicates the amount of harmonics (or harmonic distortions) that remains in the output voltage waveform. It is a measure of effectiveness in reducing unwanted harmonics. It is defined as:

$$THD = \frac{\sqrt{\sum_{n=2,3,\dots}^{\infty} \left(\frac{V_n}{n}\right)^2}}{V_1} \quad (7.3)$$

The DF of an individual (or n th) harmonic component is defined as:

$$DF_n = \frac{V_n}{V_1 n^2} \quad (7.4)$$

- 4. Lowest-Order Harmonic (LOH):** The LOH is that harmonic component whose frequency is closest to the fundamental one, and its amplitude is greater than or equal to 3% of the fundamental component.

7.4 VOLTAGE SOURCE INVERTERS

If thyristors are used in voltage source inverters (VSIs), then forced commutation is required. But, if GTOs, power MOSFETs, and power IGBTs are used, then self-commutation with base or gate drive signals is used for their turn on/turn off.

7.4.1 SINGLE-PHASE VOLTAGE SOURCE INVERTERS

Single-phase bridge inverters have two configurations [2–4,6,7]:

1. Single-phase half-bridge inverter.
2. Single-phase full-bridge inverter.

1. Single-phase half-bridge inverter: Power circuit and various waveforms for single-phase half-bridge configuration are shown in [Figure 7.1a](#) and [b](#). For period $0 < t < T/2$, thyristor T_1 conducts, and the load is connected to the upper voltage source $V_s/2$. Therefore, output voltage becomes $V_s/2$. At $t = T/2$, thyristor T_1 is turned off by force commutation, and at same instant thyristor T_2 is triggered. During the period $T/2 < t < T$, thyristor T_2 conducts and output voltage becomes $-V_s/2$ due to lower voltage source $V_s/2$. Therefore, from [Figure 7.1b](#) it can be seen that output voltage is an alternating voltage waveform of amplitude $V_s/2$ and frequency $1/T$ Hz. Frequency of inverter output AC voltage can be changed by varying the periodic time T .

Demerits of half-bridge configuration:

- a. It requires a three-wire DC supply.
- b. Output voltage magnitude is $V_s/2$ only.

2. Single-phase full-bridge inverter: Power circuit diagram of full-bridge configuration with various waveforms are shown in [Figure 7.2](#) [2–4,6,7]. When thyristors T_1, T_2 conduct, the load voltage becomes $+V_s$, and when thyristors T_3, T_4 conduct, load voltage becomes $-V_s$ as shown in equivalent circuit diagrams, [Figure 7.2c](#) and [7.2d](#). Frequency of the inverter output AC voltage can be changed by varying the periodic time T .

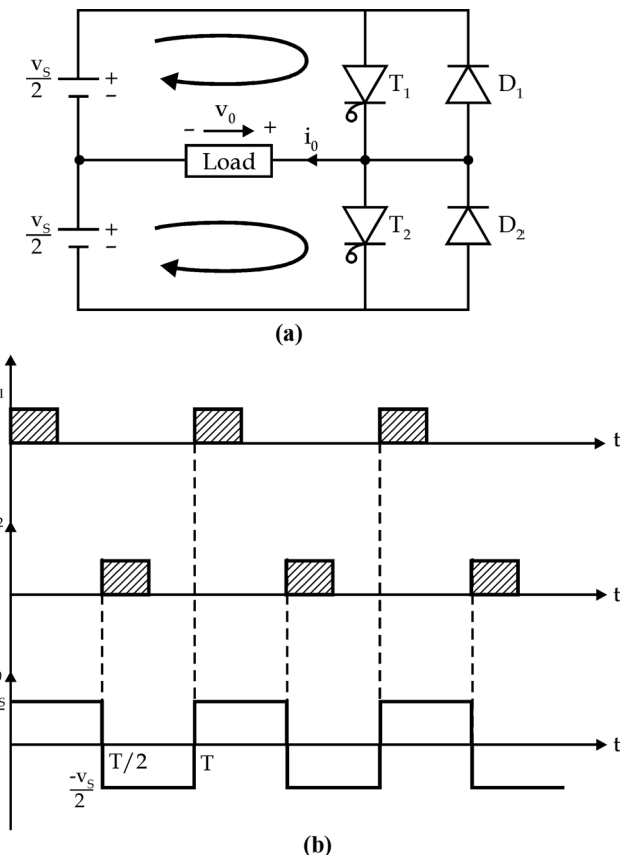


FIGURE 7.1 Single-phase half-bridge inverter: (a) power circuit diagram and (b) various waveforms.

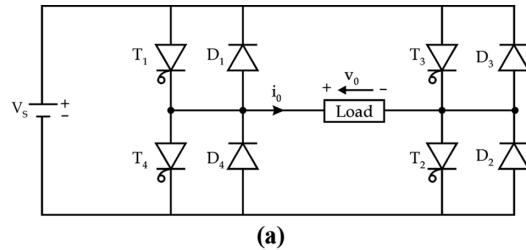
Therefore,

$$v_0 = +V_S \text{ and } i_0 = +I_0 \quad \text{for } 0 < t < T/2$$

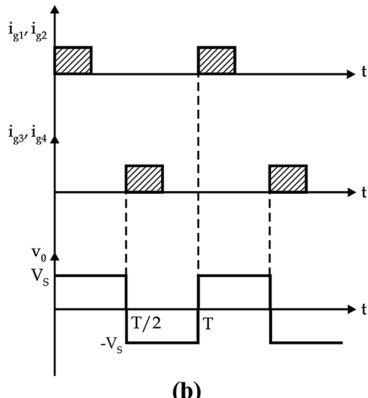
$$v_0 = -V_S \text{ and } i_0 = -I_0 \quad \text{for } T/2 < t < T$$

It should be noted that in VSIs, the load voltage waveforms do not depend on the nature of load, but the load current depends on the nature of load. For the different load, the load current waveforms for the full-bridge inverter are shown in Figure 7.3a-d [2-4,6,7].

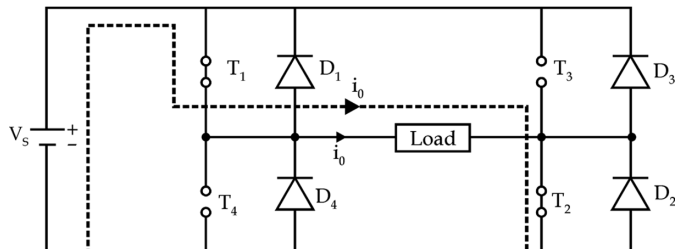
With R load: For resistive load R, load current i_0 is identical with load voltage waveform v_0 and diodes D_1-D_4 connected in antiparallel with thyristors (called feedback diodes) are not required, see Figure 7.3a.



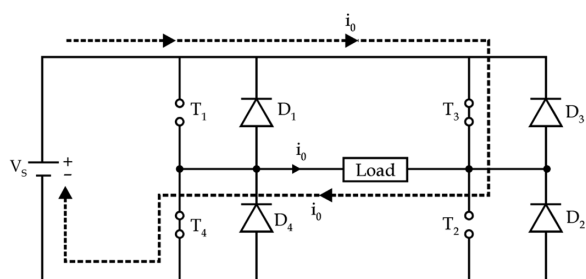
(a)



(b)



(c)



(d)

FIGURE 7.2 Single-phase full-bridge inverter: (a) power circuit diagram, (b) various waveforms, (c) equivalent circuit when T_1 T_2 conducts, and (d) equivalent circuit when T_3 T_4 conducts.

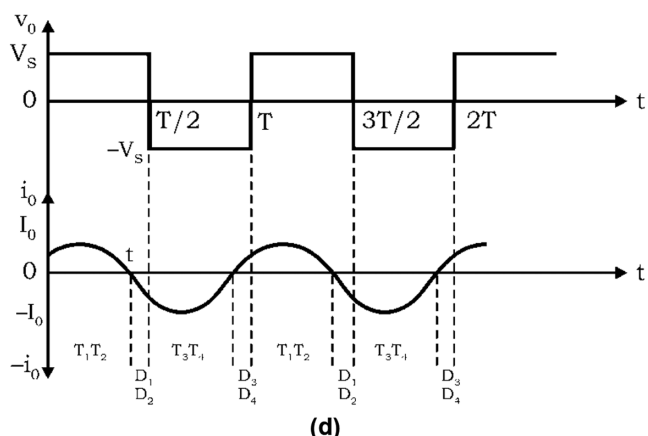
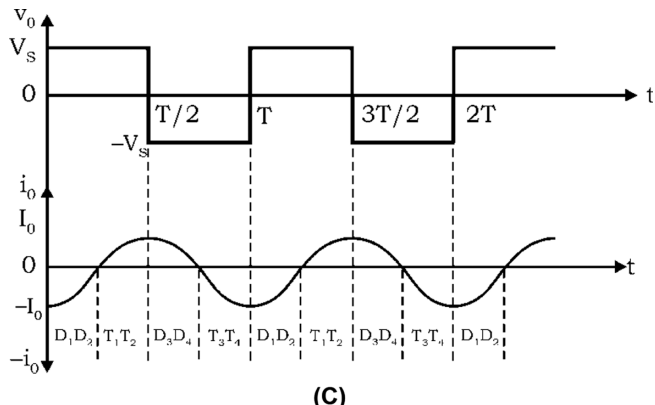
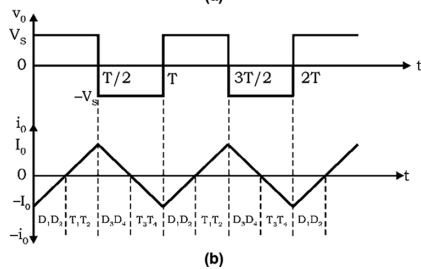
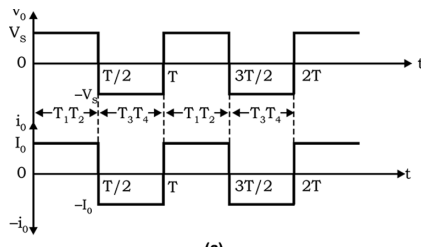


FIGURE 7.3 Load voltage and current waveforms for single-phase full-bridge inverter:
(a) resistive load, (b) RL load, (c) RLC overdamped load, and (d) RLC underdamped load.

7.4.1.1 With RL and RLC Overdamped Loads

For inductive loads, load current will not be in phase with voltage v_0 , and therefore, feedback diodes D_1-D_4 are required to allow the current to flow when the main thyristors are turned off. The load current waveforms for RL and RLC overdamped loads are shown in [Figure 7.3b](#) and [c](#), respectively. Before $T = 0$, thyristors T_3, T_4 are conducting, and therefore load current i_0 was $-I_0$, as shown in [Figure 7.3b](#) and [c](#). Though thyristors T_3, T_4 are turned off by forced commutation at $t = 0$, due to the inductive nature of the load, current i_0 cannot change its direction immediately. As a result, diodes D_1, D_2 start conducting after $t = 0$ and allow i_0 to flow against the supply voltage V_S , and therefore, $v_0 = +V_S$ and $i_0 = \text{negative}$, as shown. Though T_1, T_2 are gated at $t = 0$, these SCRs get turned on when load current i_0 through D_1, D_2 falls to zero. Therefore, now $v_0 = +V_S$, $i_0 = \text{positive}$ as shown.

At $t = T/2$; thyristors T_1, T_2 are turned off by forced commutation, and since the load current cannot reverse immediately, diodes D_3, D_4 conduct. Therefore $v_0 = -V_S$ and $i_0 = \text{positive}$, as shown. Though thyristors T_3, T_4 are gated at $t = T/2$, but will not turn on because these are reverse biased due to voltage drop across diodes D_3, D_4 . So, T_3, T_4 are turned on when current in diodes D_3, D_4 becomes zero, as shown. In this way, the cycle repeats.

7.4.1.2 With RLC Underdamped Load

The load current i_0 for RLC underdamped load is shown in [Figure 7.3d](#). After $t = 0$, load current flows through T_1, T_2 . Because i_0 through T_1, T_2 reduces to zero at t_1 , these SCRs are turned off before T_3, T_4 are triggered. As T_1, T_2 stop conducting, current through the load reverses and is now carried by diodes D_1, D_2 because T_3, T_4 are not yet gated. The diodes D_1, D_2 are connected in antiparallel to T_1, T_2 so voltage drop across these diodes appears as reverse biased across T_1, T_2 . If the duration of this reverse bias is more than the SCR turn-off time t_q , that is, if $(T/2 - t_1) > t_q$; then SCRs T_1, T_2 will get turned off naturally, and therefore no extra commutation circuit is required. Such method of commutation is known as *load commutation*.

7.4.1.3 Fourier Analysis of Single-Phase Inverter Output Voltage

The output or load voltage waveforms of the voltage source inverter do not depend on the nature of load. Voltage waveforms of [Figures 7.1b](#) and [7.2b](#) can be resolved in Fourier series as [\[2–4,6,7\]](#):

$$v_0 = \sum_{n=1,3,5,\dots}^{\infty} \frac{2V_S}{n\pi} \sin n\omega t \dots \text{ for } 1-\phi \text{ half bridge inverter} \quad (7.5)$$

$$v_0 = \sum_{n=1,3,5,\dots}^{\infty} \frac{4V_S}{n\pi} \sin n\omega t \dots \text{ for } 1-\phi \text{ full bridge inverter} \quad (7.6)$$

where

n = order of harmonics

ω = frequency of output voltage in rad/s

The load current i_0 for full-bridge inverter can be expressed as:

$$i_0 = \sum_{n=1,3,5,\dots}^{\infty} \frac{4V_s}{n\pi \cdot Z_n} \sin(n\omega t - \varphi_n) \quad (7.7)$$

where

Z_n = load impedance at frequency nf

$$= \left[R^2 + \left(n\omega L - \frac{1}{n\omega C} \right)^2 \right]^{\frac{1}{2}} \quad (7.8)$$

$$\phi_n = \text{phase angle} = \tan^{-1} \frac{\left(n\omega L - \frac{1}{n\omega C} \right)}{R} \quad (7.9)$$

$$\text{The fundamental load power } P_{01} = I_{01}^2 R = V_{01} I_{01} \cos \varphi_1 \quad (7.10)$$

At time of commutation:

If load current $I_0 > 0$, forced commutation is required.

If load current $I_0 < 0$, no forced commutation is required.

7.4.2 THREE-PHASE VSI BRIDGE INVERTER

Three-phase bridge inverters are more common than single-phase inverters for providing adjustable frequency power to industrial loads. The power circuit diagram for three-phase VSI consists of six thyristors as shown in Figure 7.4a. The three-phase load may be delta or star-connected as shown in Figure 7.4b and c, respectively [2–4,6,7].

On the basis of period of conduction of each thyristor, three-phase bridge inverters can be classified as 180° conduction mode or 120° conduction mode inverter.

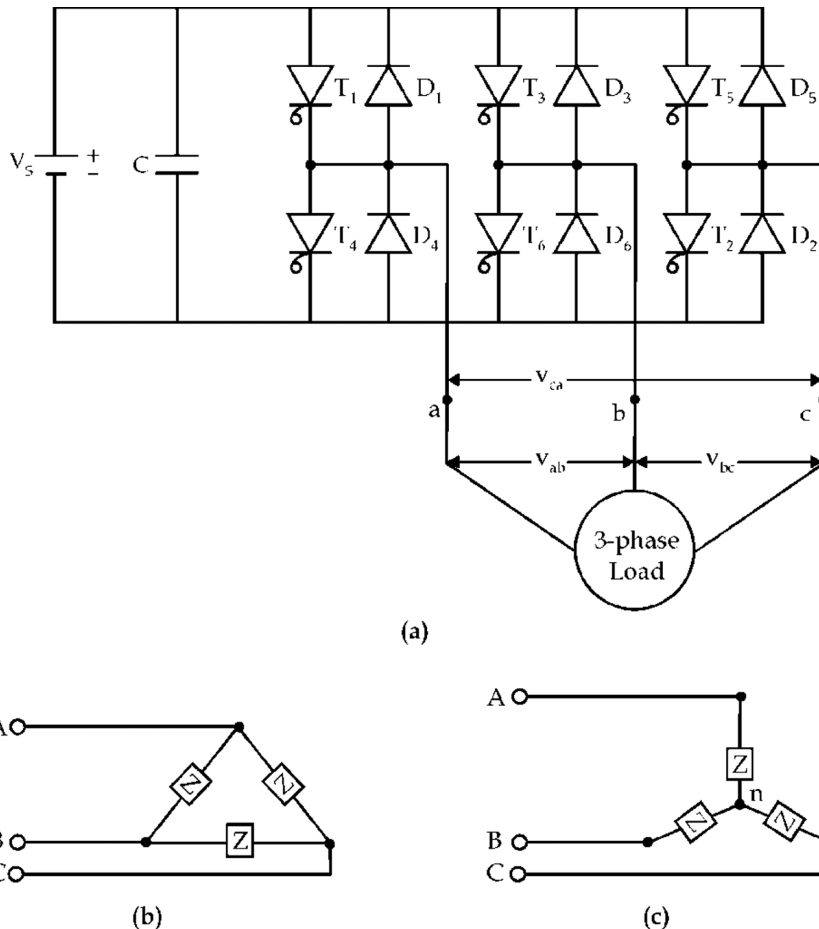


FIGURE 7.4 Three-phase VSI bridge inverter: (a) power circuit, (b) delta-connected load, and (c) star-connected load.

7.4.2.1 Three-Phase 180-degree Mode VSI

In this, each thyristor conducts for a period of 180° of a cycle, so it's called a 180-degree conduction-mode inverter. The following points must be ensured while making firing table (shown in Figure 7.5):

1. Each thyristor conducts for 180° of a cycle.
2. In each group, that is, upper or lower group, thyristors are fired after every 120° , that is, if T_1 is fired at 0° , then T_3 will be fired at 120° and T_5 at 240° .
3. In each leg, thyristors are fired after every 180° , that is, if T_1 is fired at 0° , then T_4 will be fired at 180° .

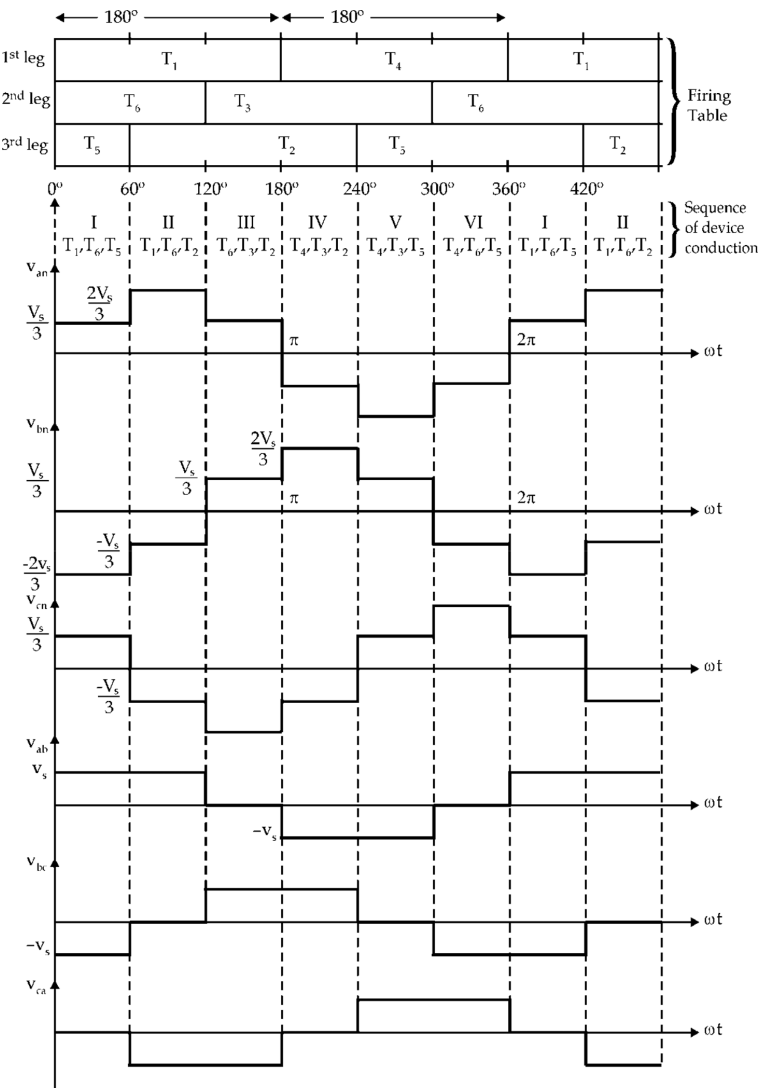


FIGURE 7.5 Firing table and voltage waveforms for 180°-mode three-phase VSI.

Therefore, it can be seen that:

1. At a time, three thyristors conduct, that is, two from upper group and one from lower group or one from upper group and two from lower group.
2. Thyristors are triggered in sequence of their numbers after every 60°.

One control cycle (360°) is divided into six steps, each of 60° interval. So, it is also called a *six-step bridge inverter*.

During Step I ($0^\circ < \omega t < 60^\circ$): Thyristors T_1 , T_6 , and T_5 conduct as shown in equivalent circuit (Figure 7.6a).

$$\text{Therefore, current, } i_l = \frac{V_s}{Z + \frac{Z}{2}} = \frac{2}{3} \frac{V_s}{Z}$$

The line-to-neutral voltages are:

$$v_{an} = v_{cn} = i_l \frac{Z}{2} = \frac{V_s}{3}$$

$$v_{nb} = i_l Z = \frac{2V_s}{3}$$

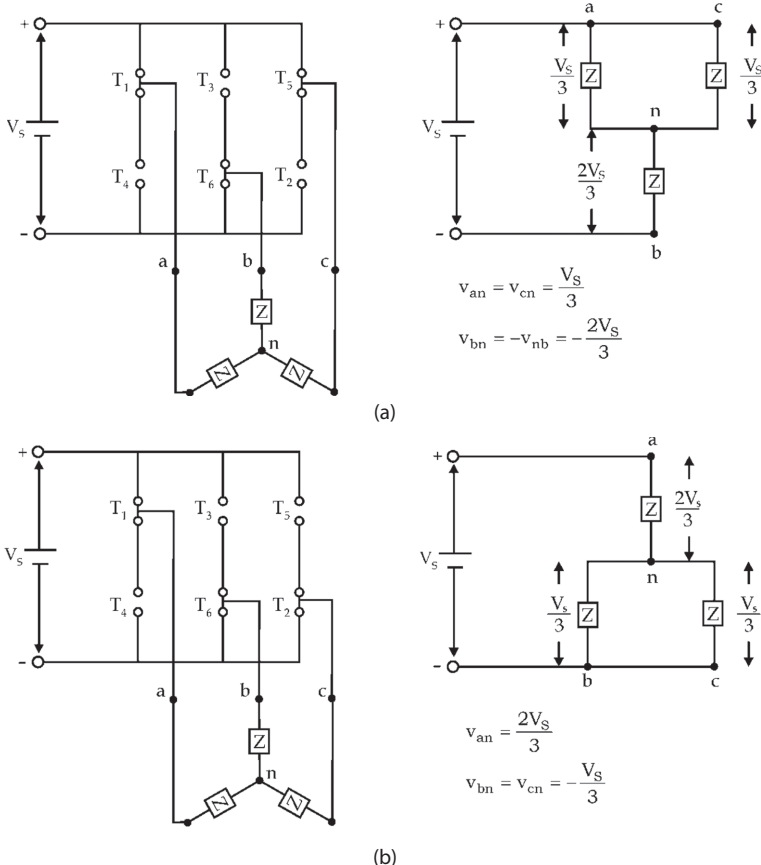


FIGURE 7.6 Equivalent circuit during (a) Step I (0° – 60°); T_1 , T_6 , T_5 conducts; and (b) Step II (60° – 120°); T_1 , T_6 , T_2 conducts.

$$\therefore v_{bn} = -v_{nb} = -\frac{2V_S}{3}$$

The line voltage $v_{ab} = -v_{an} - v_{bn} = \frac{V_S}{3} - \left(\frac{2V_S}{3} \right) = V_S$

$$v_{bc} = v_{bn} - v_{cn} = -\frac{2V_S}{3} - \left(\frac{V_S}{3} \right) = -V_S$$

$$v_{ca} = v_{cn} - v_{an} = \frac{V_S}{3} - \left(\frac{V_S}{3} \right) = 0$$

The above line to neutral voltages (phase voltages) v_{an} , v_{bn} , v_{cn} and line voltages v_{ab} , v_{bc} , v_{ca} are drawn in [Figure 7.5](#) for Step I.

During Step II: During this step, thyristors T_1 , T_6 , and T_2 conduct as shown in equivalent circuit ([Figure 7.6b](#)).

Therefore, current, $i_2 = \frac{2}{3} \frac{V_S}{Z}$

So, phase voltages $v_{an} = i_2 Z = \frac{2V_S}{3}$

$$v_{nb} = v_{nc} = i_2 \frac{Z}{2} = \frac{V_S}{3}$$

$$v_{bn} = v_{cn} = -\frac{V_S}{3}$$

or

The line voltages, $v_{ab} = v_{an} - v_{bn} = \frac{2V_S}{3} - \left(-\frac{V_S}{3} \right) = +V_S$

$$v_{bc} = v_{bn} - v_{cn} = -\frac{V_S}{3} - \left(-\frac{V_S}{3} \right) = 0$$

$$v_{ca} = v_{cn} - v_{an} = -\frac{V_S}{3} - \left(\frac{2V_S}{3} \right) = -V_S$$

The above phase voltages and line voltages are drawn in [Figure 7.5](#) for Step II.

Similarly, analysis for Steps III–VI can be done, and corresponding line and phase voltages can be drawn as shown in [Figure 7.5](#).

The function of antiparallel connected diodes (or feedback diodes) D_1 to D_6 is to allow the flow of currents through them when load is inductive in nature. The output line voltages can be expressed by the following Fourier series as [1–7]:

$$v_{ab} = \sum_{n=1,3,5,\dots}^{\infty} \frac{4V_s}{n\pi} \cos \frac{n\pi}{6} \sin n \left(\omega t + \frac{\pi}{6} \right) \quad (7.11)$$

$$v_{bc} = \sum_{n=1,3,5,\dots}^{\infty} \frac{4V_s}{n\pi} \cos \frac{n\pi}{6} \sin n \left(\omega t - \frac{\pi}{2} \right) \quad (7.12)$$

$$v_{ca} = \sum_{n=1,3,5,\dots}^{\infty} \frac{4V_s}{n\pi} \cos \frac{n\pi}{6} \sin n \left(\omega t + \frac{5\pi}{6} \right) \quad (7.13)$$

For $n = 3 \cos \frac{3\pi}{6} = 0$, therefore, all triplen harmonics are absent from the line voltages.

$$V_L = \sqrt{3}V_p \text{ and } I_L = I_p$$

$$V_L = V_p \text{ and } I_L = \sqrt{3}I_p$$

The RMS value of n th component of line voltage:

$$V_{Ln} = \frac{1}{\sqrt{2}} \frac{4V_s}{n\pi} \cos \frac{n\pi}{6} \quad (7.14)$$

The RMS value of fundamental ($n = 1$) line voltage:

$$V_{L1} = \frac{1}{\sqrt{2}} \frac{4V_s}{\pi} \cos \frac{\pi}{6} = 0.78V_s \quad (7.15)$$

From waveforms of line voltage v_{ab} in Figure 7.5, it is seen that line voltage is V_s from 0° to 120° . So, the RMS value of line voltage V_L is:

$$V_L = \left[\frac{1 \times 2}{2\pi} \int_0^{\frac{2\pi}{3}} V_s^2 d(\omega t) \right]^{\frac{1}{2}} = \sqrt{\frac{2}{3}} V_s = 0.81V_s \quad (7.16)$$

The RMS value of phase voltage V_p :

$$V_p = \frac{V_L}{\sqrt{3}} = \frac{\sqrt{2}}{3} V_S = 0.47 V_S \quad (7.17)$$

The RMS value of fundamental phase voltage:

$$V_{p1} = \frac{2V_S}{\sqrt{2}\pi} = 0.45V_S = \frac{V_{L1}}{\sqrt{3}} \quad (7.18)$$

The output power of the inverter:

$$P_L = \frac{3V_p^2}{R} = \frac{3}{R} \left(\frac{\sqrt{2}}{3} V_S \right)^2 = \frac{2V_S^2}{3R} \quad (7.19)$$

The RMS value of the thyristor current:

$$I_{\text{Thyristor(rms)}} = \frac{I_p}{\sqrt{2}} = \frac{V_p/R}{\sqrt{2}} = \frac{V_S}{3R} \quad (7.20)$$

7.4.2.2 Three-Phase 120-degree Mode VSI

The power circuit diagram for 180-degree mode and 120-degree mode VSIs are same, as shown in [Figure 7.4a](#). In this mode, each thyristor conducts for 120°, so it's called a 120-degree conduction-mode bridge inverter. The following points must be ensured while making firing table (as shown in [Figure 7.7](#)):

1. Each thyristor conducts for 120° of a cycle.
2. In each group (i.e., upper or lower group), thyristors are fired after every 120°, that is, if T_1 is fired at $\omega t = 0^\circ$, then T_3 will be fired at $\omega t = 120^\circ$, and T_5 at $\omega t = 240^\circ$.
3. In each leg, thyristors are fired after every 180°, that is, if T_1 is fired at $\omega t = 0^\circ$, then T_4 at $\omega t = 180^\circ$.

Therefore, it can be seen that ([Figure 7.7](#)):

1. At a time, two thyristors conduct, that is, one from upper group and one from lower group.
2. Thyristors are triggered in sequence of their numbers after every 60°.

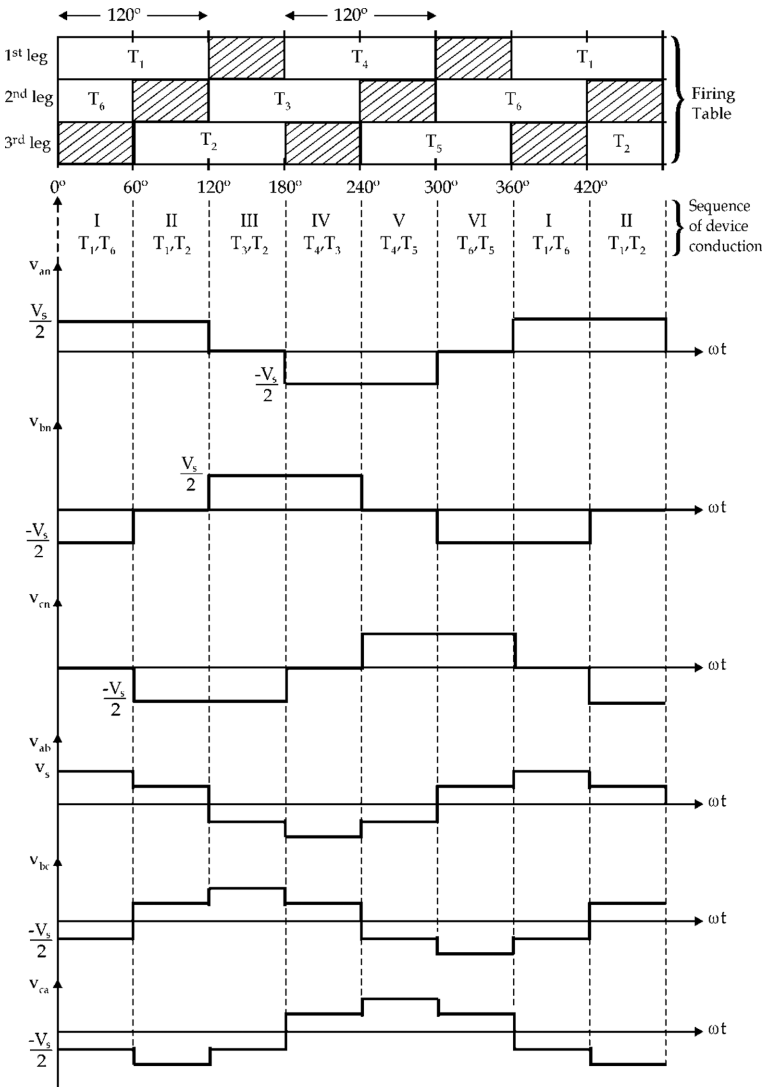


FIGURE 7.7 Firing table and voltage waveforms for 120°-mode three-phase VSI.

It is also a *six-step bridge inverter*.

Step I ($0 < \omega t < 60^\circ$): As can be seen from the firing table that during this mode, thyristors T_1 and T_6 conduct. Equivalent circuit during this step is drawn in [Figure 7.8a](#).

Therefore, the line to neutral voltages or phase voltages, from [Figure 7.8a](#) are:

$$v_{an} = \frac{V_s}{2}, v_{bn} = -\frac{V_s}{2}, v_{cn} = 0$$

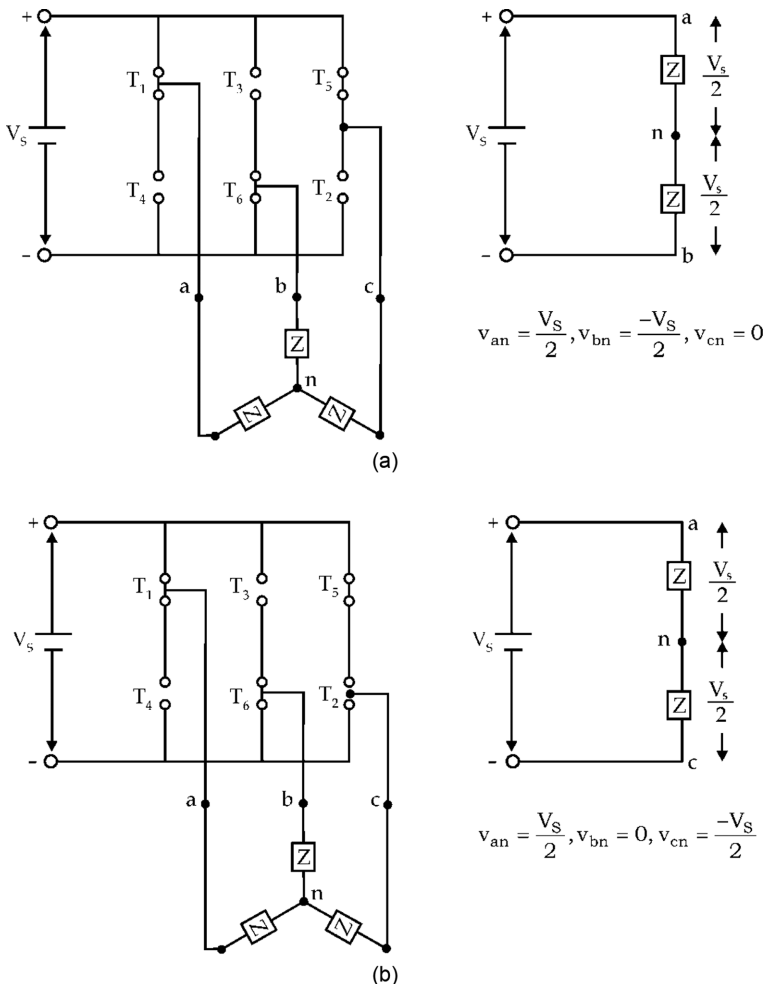


FIGURE 7.8 Equivalent circuit during (a) Step I (0° – 60°); T_1 , T_6 conducts; and (b) Step II (60° – 120°); T_1 and T_2 conducts.

and the line voltages during this step are:

$$v_{ab} = v_{an} - v_{bn} = \frac{V_s}{2} - \left(-\frac{V_s}{2} \right) = +V_s$$

$$v_{bc} = v_{bn} - v_{cn} = -\frac{V_s}{2} - (0) = -\frac{V_s}{2}$$

$$v_{ca} = v_{cn} - v_{an} = 0 - \left(\frac{V_s}{2} \right) = -\frac{V_s}{2}$$

The above phase voltages and line voltages are drawn as shown in Figure 7.7 during step-I.

Step II ($60^\circ < \omega t < 120^\circ$): During this step, thyristors T_1 and T_2 conduct (see firing table, Figure 7.7). Therefore, an equivalent circuit can be drawn as shown in Figure 7.8b.

From Figure 7.8b, it can be noted that the phase voltages are:

$$v_{an} = \frac{V_S}{2}, v_{bn} = 0, v_{cn} = -\frac{V_S}{2}$$

and the line voltages are:

$$v_{ab} = v_{an} - v_{bn} = \frac{V_S}{2} - (0) = \frac{V_S}{2}$$

$$v_{bc} = v_{bn} - v_{cn} = 0 - \left(-\frac{V_S}{2}\right) = \frac{V_S}{2}$$

$$v_{ca} = v_{cn} - v_{an} = -\frac{V_S}{2} - \left(\frac{V_S}{2}\right) = -V_S$$

The above phase voltages and line voltages can be drawn as shown in Figure 7.7 for Step II. Similarly, the analysis can be made for Steps III–VI, and the corresponding phase and line voltages can be drawn as shown in Figure 7.7.

The output voltages can be expressed in Fourier series as:

$$v_{an} = \sum_{n=1,3,5,\dots}^{\infty} \frac{2V_S}{n\pi} \cos \frac{n\pi}{6} \sin n \left(\omega t + \frac{\pi}{6} \right) \quad (7.21)$$

$$v_{bn} = \sum_{n=1,3,5,\dots}^{\infty} \frac{2V_S}{n\pi} \cos \frac{n\pi}{6} \sin n \left(\omega t - \frac{\pi}{2} \right) \quad (7.22)$$

$$v_{cn} = \sum_{n=1,3,5,\dots}^{\infty} \frac{2V_S}{n\pi} \cos \frac{n\pi}{6} \sin n \left(\omega t + \frac{5\pi}{6} \right) \quad (7.23)$$

The RMS value of fundamental phase voltage:

$$V_{p1} = \frac{2V_S}{\sqrt{2\pi}} \cos \frac{\pi}{6} = \frac{\sqrt{3}V_S}{\sqrt{2\pi}} = 0.39V_S \quad (7.24)$$

The RMS value of fundamental line voltage:

$$V_{L1} = \sqrt{3}V_p = \frac{3V_s}{\sqrt{2}\pi} = 0.675 V_s \quad (7.25)$$

(.: as load is assumed star connected)

The RMS value of phase voltage:

$$V_p = \left[\frac{1}{\pi} \int_0^{\frac{2\pi}{3}} \left(\frac{V_s}{2} \right)^2 .d\omega t \right]^{\frac{1}{2}} = \sqrt{\frac{2}{3}} \frac{V_s}{2} = \frac{V_s}{\sqrt{6}} = 0.408 V_s \quad (7.26)$$

The RMS value of line voltage:

$$V_L = \sqrt{3}V_p = 0.707 V_s \quad (7.27)$$

The output power of the inverter:

$$P_L = 3 \frac{V_p^2}{R} = \frac{V_s^2}{2R} \quad (7.28)$$

The RMS value of the thyristor current:

$$I_{\text{Thyristor(rms)}} = \frac{I_p}{\sqrt{2}} = \frac{V_p/R}{\sqrt{2}} = \frac{V_s}{2\sqrt{3}R} \quad (7.29)$$

7.4.2.3 Merits and Demerits of 180°- and 120°-Mode VSIs

The merits and demerits of both the modes are as follows [2–4,6,7]:

1. In the 180°-mode inverter, there is no delay between switching on and switching off of the thyristors in the same leg or arm. So, it may result into short-circuiting of the DC source due to conduction of thyristors of same leg together. This problem is overcome in the 120°-mode by providing a time lag of 60° between turn-on and turn-off of two thyristors of same leg. This results in reliable and safe operation of the inverter.
2. In the 120°-mode inverter, potentials of only two output terminals connected to the DC source are defined at any time of cycle. The potential of the third terminal is not well defined. So, the analysis of the performance of this inverter becomes complicated. But in the 180°-mode inverter, potentials of all the three output terminals are well defined. So, analysis becomes easy.
3. In the 120°-mode inverter, there is poor utilization of thyristor devices for the same load condition as compared to the 180°-mode inverter.

Therefore, the 180°-mode is preferred, and it is generally used in three-phase inverters.

7.5 CURRENT SOURCE INVERTERS

In the CSIs, the input current is constant but adjustable. The amplitude of output current from the CSI is independent of the load, but the magnitude of output voltage and its waveform is dependent upon the nature of load. A CSI converts the input DC current to an AC current, and the frequency of the AC current depends upon the rate of triggering the SCRs. The amplitude of the AC output current can be adjusted by controlling the magnitude of the DC input current. Because power semiconductors in a CSI have to withstand reverse voltage, devices like GTOs, power transistors, power MOSFETS, and power BJTs cannot be used in CSIs [2–4,6,7].

7.5.1 SINGLE-PHASE CSI

A basic thyristor-based single-phase CSI is shown in Figure 7.9 [2–4,6,7]. Capacitors are used here as a commuting device. Working of this inverter can be explained using following points:

- Initially, T_1 and T_2 are conducting, and the capacitors are charged with the polarities, as shown. The positive load current is flowing through T_1 , D_1 , load, D_2 , and T_2 .
- To turn off the conducting thyristors T_1 and T_2 , the other two thyristors T_3 and T_4 , are triggered.
- When these thyristors (T_3 and T_4) start conducting, the capacitor voltage v_{C1} and v_{C2} appears as reverse voltage across the thyristors T_1 and T_2 , respectively. So, thyristors T_1 and T_2 get turned off.

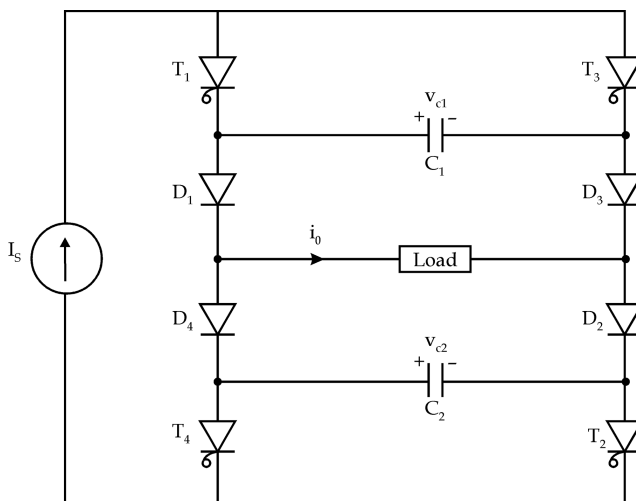


FIGURE 7.9 Single-phase CSI.

4. Now, the load current flows through T_3 , C_1 , D_1 , load, D_2 , C_2 , and T_4 . So, the polarity of the capacitors reverses due to the charging current in the reverse direction, that is, the right plate of capacitors C_1 and C_2 become positive, and the left plate becomes negative. When the capacitor voltage becomes equal to the load voltage, the load current becomes zero, and the diodes D_1 and D_2 get turned off.
5. The load current now flows in the reverse direction through T_3 , D_3 , load, D_4 , and T_4 .
6. Similarly, when the thyristors T_1 and T_2 are triggered, the capacitor voltage v_{C1} , v_{C2} turn off T_2 and T_4 in a similar fashion. In this way, the cycle repeats and output AC voltage of the desired frequency is obtained.

7.5.2 THREE-PHASE CSI

A basic three-phase CSI, feeding a star-connected resistive load, is shown in Figure 7.10a [2–4,6,7]. Diodes are used in series with each switch to handle reverse voltage, which should be avoided to appear across the power semiconductor-based switches. The switches are turned on in the sequence of their numbers, with an interval of 60° , and each switch conducts for 120° duration.

At a time two switches conduct, that is, one from the upper group (T_1 , T_3 , T_5) and other from the lower group (T_4 , T_6 , T_2). The load current of a particular phase is $+I_s$ when upper switch of the corresponding arm conducts, and it is $-I_s$ when the lower switch conducts, as shown in Figure 7.10b.

Advantages of CSI:

1. It has inherent short-circuit fault protection because the input is a controlled-current source, so the current does not rise to a dangerously high level during the fault, so, it is more reliable.
2. It requires a simple commutation circuit, that is, only capacitors.
3. It does not require any feedback diode.
4. It may use a converter-grade SCR, which is cheaper than inverter-grade SCR.
5. It has inherent four-quadrant operation capability due to converter-inverter combination.

Disadvantages of CSI:

1. It suffers from stability problems at light loads.
2. It suffers from operating problems at high frequency.
3. Its response is sluggish.

Applications of CSI:

Various applications of CSI are:

1. Speed control of AC motors
2. Lagging VAr compensation
3. Solar photovoltaic utility systems
4. Synchronous motor starting

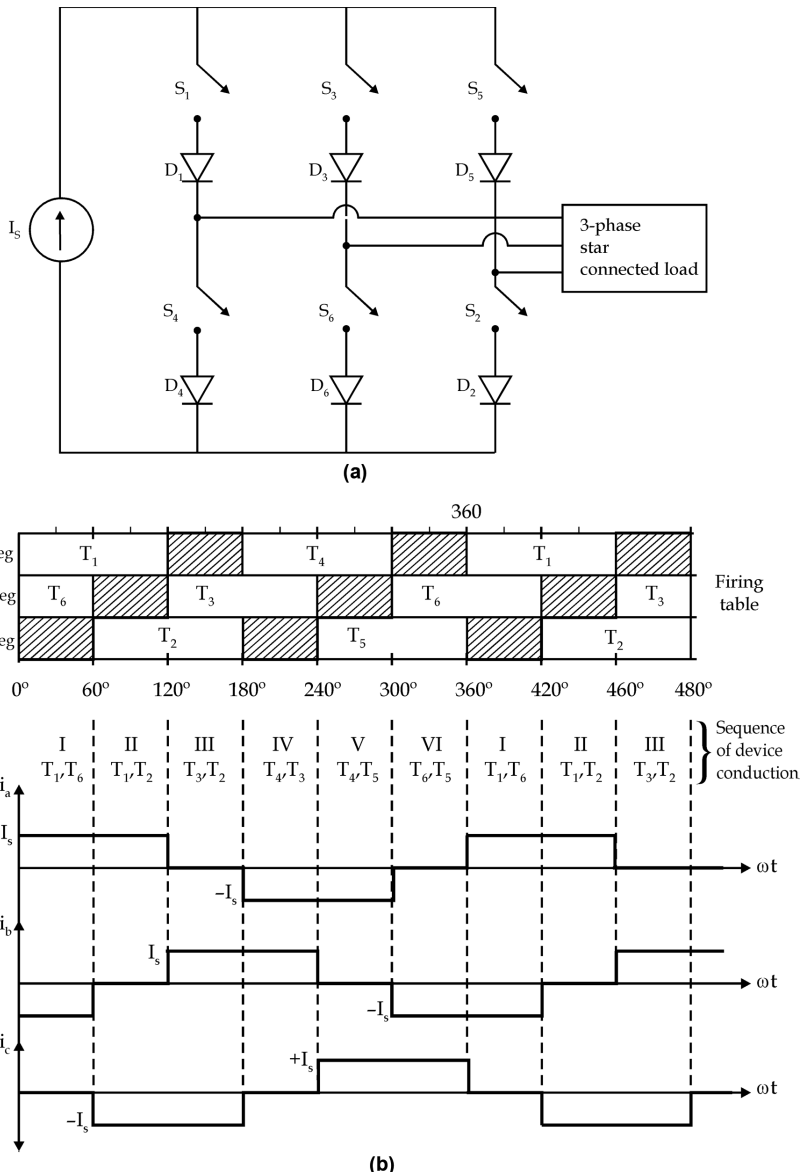


FIGURE 7.10 Three-phase CSI: (a) power circuit diagram and (b) firing table and output currents.

7.6 CSI VERSUS VSI

1. Input of CSI is a constant DC current source, whereas in case of VSI, it is a constant DC voltage source.
2. CSIs do not require feedback diodes, whereas VSIs require feedback diodes if the load is inductive or capacitive in nature.

3. In CSIs, the semiconductor device can be thyristor only, whereas in VSIs, power transistor, power IGBTs, power MOSFETs, or GTOs can also be used.
4. In case of CSI, output current is independent of nature of load, but load voltage depends on load. Whereas in the case of VSIs, load voltage is independent of nature of load, but load current depends on load.

7.7 VOLTAGE CONTROL OF SINGLE-PHASE INVERTERS

Voltage control of inverter is required to [2–4,6,7]:

1. Survive with the variations in the input DC voltage
2. Counteract the voltage regulation of the inverter switches and transformer
3. Allow adjustable voltage to the load

Certain loads, such as the variable-frequency Induction Motor (IM) drive, need simultaneous control of frequency and voltage. The frequency of inverter output can be controlled by varying the conduction period of switches. Voltage control may be achieved by any of the following techniques:

1. Control of input DC voltage
2. External control of inverter AC output voltage
3. Internal control of inverter

7.7.1 CONTROL OF INPUT DC VOLTAGE

Various schemes may be used to control the input DC voltage to achieve the controlled output voltage of the inverter as shown in Figure 7.11 [2–4,6,7]. As shown, if the power source is DC, then control of input DC voltage can be obtained using chopper as presented in Figure 7.11a.

If the source is AC, then control of input DC voltage can be obtained using an AC voltage controller followed by uncontrolled rectifier as shown in Figure 7.11b. However, this scheme suffers low efficiency with poor input power factor (PF). Another scheme is presented in Figure 7.11c where variable DC voltage is obtained using a controlled rectifier. The efficiency of the system is better but with poor input PF and low-frequency harmonics. The drawbacks of the scheme shown in Figure 7.11c are removed in the system shown in Figure 7.11d where uncontrolled rectifiers with high-frequency DC-to-DC converters are used.

7.7.2 EXTERNAL CONTROL OF AC OUTPUT VOLTAGE

The constant AC output voltage from an inverter may be controlled using an AC voltage regulator (AC phase control) but at the cost of large harmonic content in the output voltage. Therefore, this method is employed only for low-power applications.

For high-power applications, two square-wave inverters may be connected in series to obtain variable AC voltage, as shown in Figure 7.12 [2–4,6,7], where it

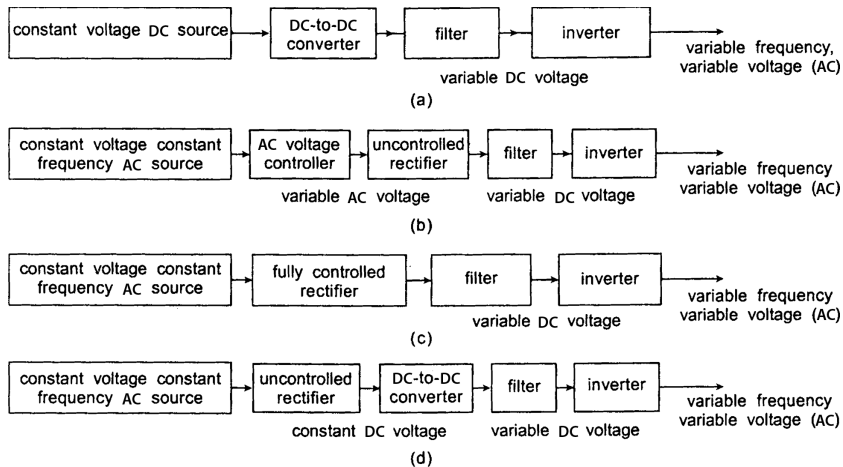


FIGURE 7.11 Inverter voltage control by control of DC input voltage.

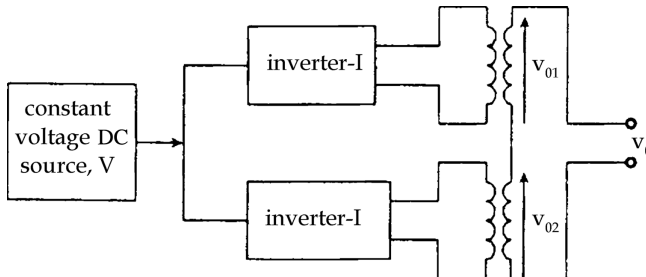


FIGURE 7.12 Series-connected inverters.

can be seen that the output of both the inverters are supplied to the primaries of the two transformers, whose secondary windings are connected in series. The resultant output voltage (v_0) has a constant magnitude 2 V (double the peak of v_{01} and v_{02}) of variable pulse width.

7.7.3 INTERNAL CONTROL OF INVERTERS

In this technique, the voltage control of the inverter is obtained by varying the pulse width of the output modulated wave. This scheme is most popular, efficient, and economical because this not only provides controlled output voltage but also eliminates the lower-order harmonics. The selection of a suitable PWM technique depends on the range of voltage control and performance. The different PWM techniques are discussed in the next section.

7.8 PULSE-WIDTH MODULATION

PWM is widely used in industrial inverters to control the output voltage and to reduce or eliminate the lower-order harmonics. It is the most efficient and economical method because it does not require any extra hardware to achieve these objectives. The commonly used PWM techniques are [1–7]:

1. Single PWM
2. Multiple PWM
3. Sinusoidal PWM

7.8.1 SINGLE PULSE-WIDTH MODULATION

In this PWM technique, there is only one pulse per half cycle, and the width of the pulse is varied to control the inverter output voltage. The gating signals are generated by comparing a rectangular reference signal of amplitude A_r with a triangular carrier-wave of amplitude A_c . The frequency of the reference signal determines the fundamental frequency of output voltage. Generation of gating signals and output voltage of single-phase full-bridge inverters are shown in [Figure 7.13](#) [2–4,6,7].

The ratio of amplitude of reference wave A_r to amplitude of carrier wave A_c is the control variable and is called the amplitude modulation index (M).

$$M = \frac{A_r}{A_c} \quad (7.30)$$

The RMS output voltage can be derived from voltage v_0 waveform in [Figure 7.11b](#).

$$V_0 = \left[\frac{1 \times 2}{2\pi} \int_{\frac{(\pi-\delta)}{2}}^{\frac{(\pi+\delta)}{2}} V_s^2 d\omega t \right]^{\frac{1}{2}}$$

or

$$V_0 = V_s \sqrt{\frac{\sigma}{\pi}} \quad (7.31)$$

Therefore, by varying A_r from 0 to A_c , the pulse width δ can be varied from 0° to 180° , and so the RMS output voltage V_0 , is from 0 to V_s . The output voltage can be expressed in Fourier series as:

$$v_0 = \sum_{n=1,3,5,\dots}^{\infty} \frac{4V_s}{n\pi} \sin \frac{n\delta}{2} \sin n\omega t \quad (7.32)$$

Due to the symmetry of the output voltage, the even harmonics (for $n = 2, 4, 6\dots$) are absent.

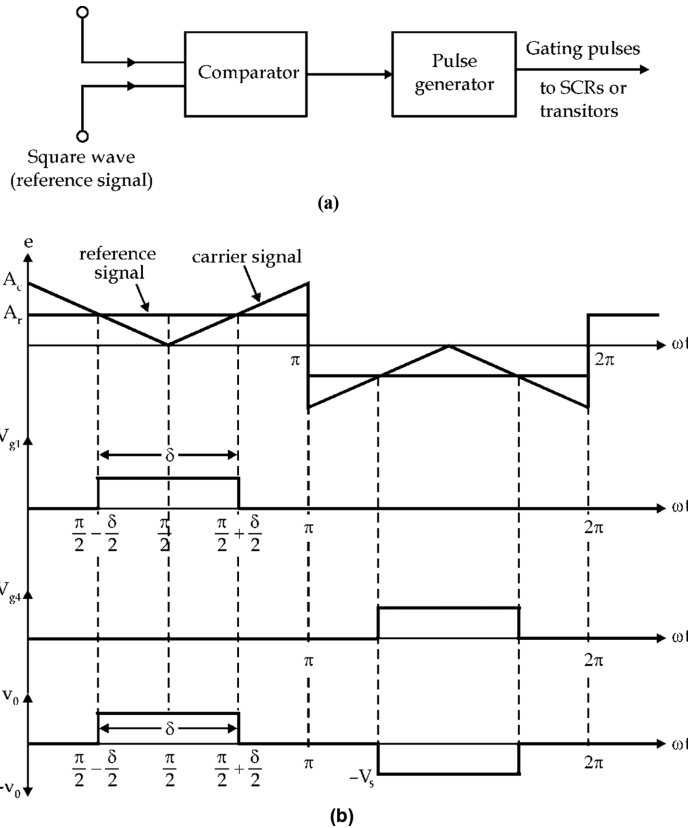


FIGURE 7.13 Single PWM: (a) control circuit for generation of gating signals and (b) gating signals and voltage waveforms.

7.8.2 MULTIPLE PULSE-WIDTH MODULATION

In this PWM technique, there are two or more than two pulses per half cycle, and the width of pulse is varied to control the inverter output voltage. By using several pulses in each half cycle of output voltage, harmonic content is reduced. Here, pulses are of equal width and are at an equidistance. The generation of gating signals for turning on and off the thyristors or transistors are obtained by comparing a reference signal with a triangular carrier wave, as shown in Figure 7.14 [2–4,6,7]. The frequency of reference signal sets the output frequency f_0 , and the carrier frequency f_c determines the number of pulses per half cycle (p).

The modulation index controls the output voltage and this type of modulation is called as uniform pulse width modulation (UPWM). The number of pulses per half cycle can be obtained by:

$$P = \frac{f_c}{2f_0} = \frac{M_f}{2} \quad (7.33)$$

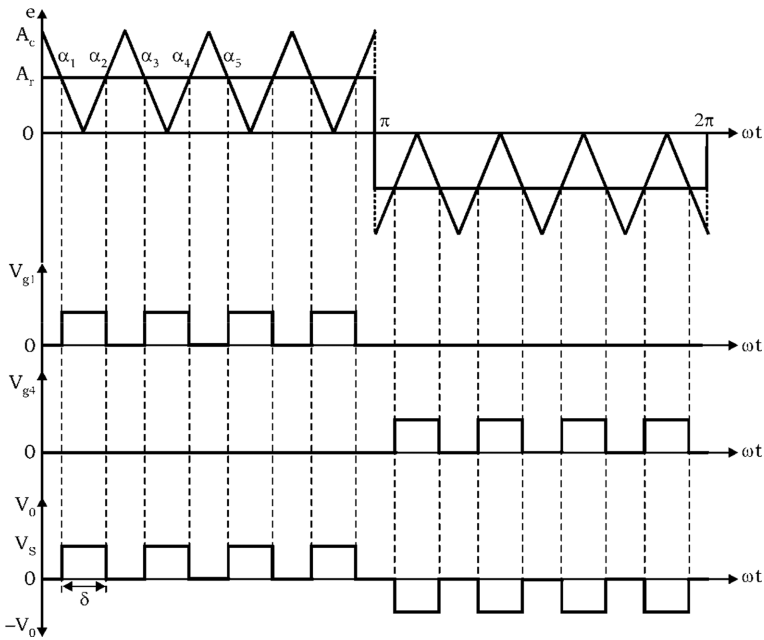


FIGURE 7.14 Multiple PWM.

where $M_f = \frac{f_c}{f_0}$, is called the frequency modulation ratio.

The RMS output voltage can be derived as:

$$V_0 = \left[\frac{2p}{2\pi} \int_{\frac{(\pi/p-\delta)}{2}}^{\frac{(\pi/p+\delta)}{2}} V_s^2 d\omega t \right]^{\frac{1}{2}}$$

or

$$V_0 = V_s \sqrt{\frac{p\delta}{\pi}} \quad (7.34)$$

7.8.3 SINUSOIDAL PULSE-WIDTH MODULATION

In this method of modulation, several pulses per half cycle are used such as in the case of multiple PWM. But in this, the pulse widths are not equal; rather, it is a sinusoidal function of the angle positions of the pulse in a cycle as shown in Figure 7.15 [2–4,6,7]. The distortion factor and lower-order harmonics are greatly reduced in this technique.

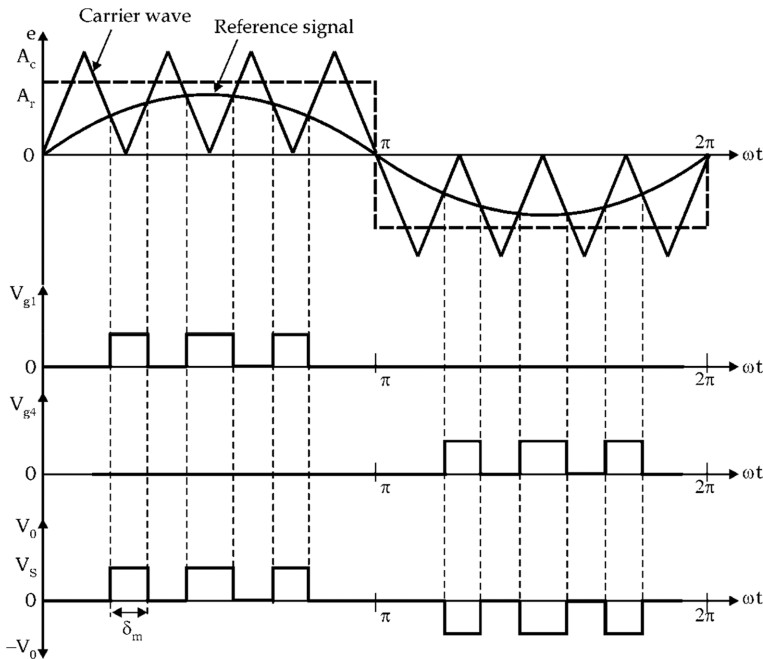


FIGURE 7.15 Sinusoidal PWM.

The gating signals shown in Figure 7.15 are generated by comparing a sinusoidal reference signal with a triangular carrier wave of frequency f_c . The frequency of reference signal f_r determines the inverter output frequency f_0 , and its peak amplitude A_r controls the modulation index M , and so the RMS output voltage V_0 .

The RMS output voltage for n th pulse:

$$V_0 = V_s \left(\sum_{n=1}^{12p} \frac{\delta_m}{\pi} \right)^{\frac{1}{2}} \quad (7.35)$$

7.9 ADVANCED MODULATION TECHNIQUES

The sinusoidal PWM, which is most commonly used, suffers from drawbacks, such as low fundamental output voltage. The other techniques that offer improved performances are [2–4,6,7]:

- Trapezoidal modulation
- Staircase modulation
- Stepped modulation
- Harmonic injection modulation
- Delta modulation

7.9.1 TRAPEZOIDAL MODULATION

To achieve trapezoidal modulation, gating signals are generated by comparing a triangular carrier wave with modulated trapezoidal wave as shown in Figure 7.16 [2–4,6,7].

If σ is called the triangular factor, then trapezoidal wave can be obtained from a triangular wave by limiting its magnitude to $\pm A_r$, which is related to the peak value $A_r(\max)$ by:

$$A_r = \sigma A_{r(\max)}$$

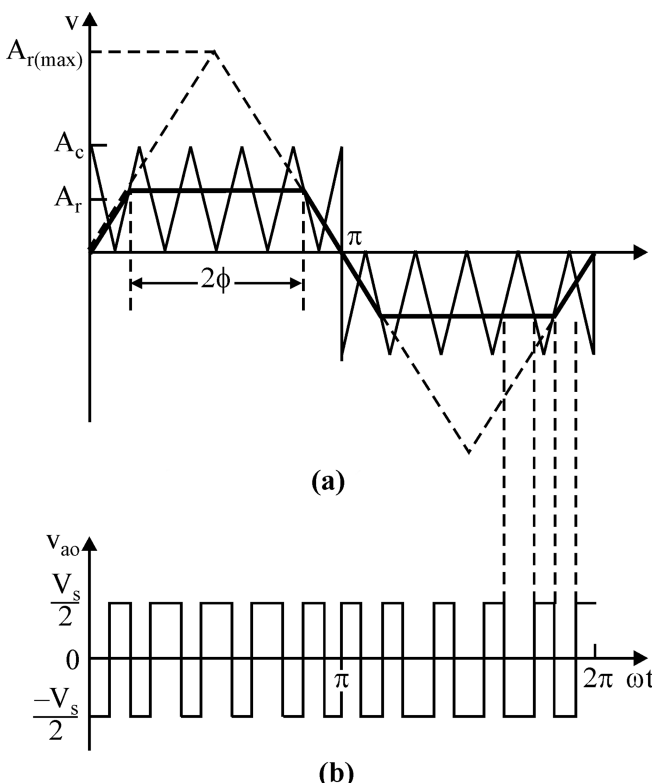


FIGURE 7.16 Trapezoidal modulation: (a) gate-signal generation and (b) output voltage. (From Bose, B.K., *Power Electronics and AC Drives*, Prentice Hall, Englewood Cliffs, NJ, 1986; Rashid, M.H., *Power Electronics: Circuits, Devices, and Applications*, Pearson Education, Singapore, 2004; Bhimra, P.S., *Power Electronics*, 4th edn, Khanna publications, New Delhi, 2012; Krein, P.T., *Elements of Power Electronics*, Oxford University Press, New York, 2003; Thorborg, K., *Power Electronics*, Prentice Hall International, London, UK, 1988.)

The modulation index M is:

$$M = \frac{A_r}{A_c} = \frac{\sigma A_{r(\max)}}{A_c} \text{ for } 0 \leq M \leq 1 \quad (7.36)$$

The angle of the flat portion of the trapezoidal wave is given by:

$$2\phi = (1 - \sigma)\pi$$

This type of modulation increases the peak fundamental output voltage up to 1.05 V_s , but the output contains lower order harmonics [1–3].

7.9.2 STAIRCASE MODULATION

In this technique, the modulating signal is a staircase wave as shown in Figure 7.17 [2–4,6,7]. The quality of output voltage depends on the number of steps and the modulation ratio. The elimination of particular harmonics depends on the levels of the selected stairs. Such technique is generally utilized and recommended for more than 15 pulses in one cycle. It provides good quality output voltage with fundamental value of up to 0.94 V_s .

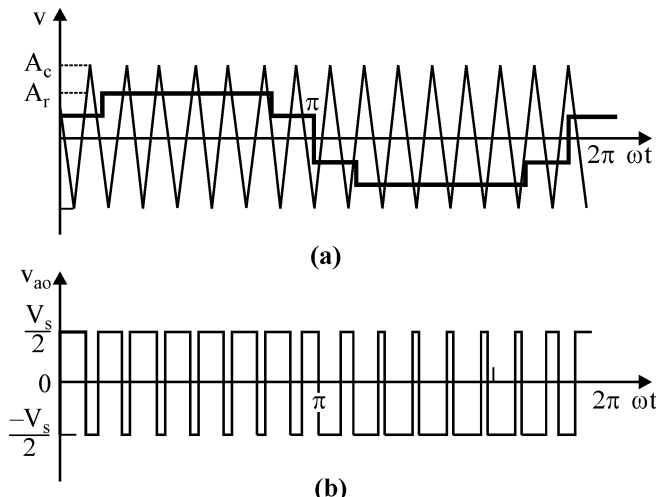


FIGURE 7.17 Staircase modulation: (a) gate-signal generation and (b) output voltage. (From Bose, B.K., *Power Electronics and AC Drives*, Prentice Hall, Englewood Cliffs, NJ, 1986; Rashid, M.H., *Power Electronics: Circuits, Devices, and Applications*, Pearson Education, Singapore, 2004; Bhimra, P.S., *Power Electronics*, 4th edn, Khanna publications, New Delhi, 2012; Krein, P.T., *Elements of Power Electronics*, Oxford University Press, New York, 2003; Thorborg, K., *Power Electronics*, Prentice Hall International, London, UK, 1988.)

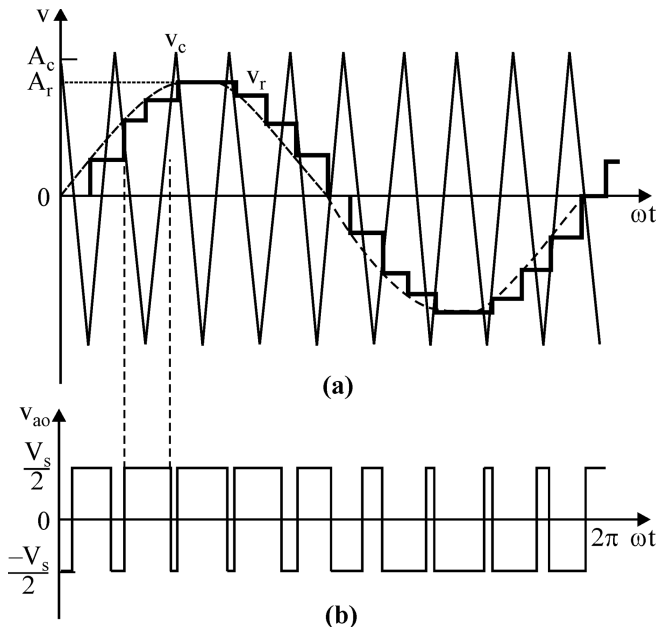


FIGURE 7.18 Stepped modulation: (a) gate-signal generation and (b) output voltage. (From Bose, B.K., *Power Electronics and AC Drives*, Prentice Hall, Englewood Cliffs, NJ, 1986; Rashid, M.H., *Power Electronics: Circuits, Devices, and Applications*, Pearson Education, Singapore, 2004; Bhimra, P.S., *Power Electronics*, 4th edn, Khanna publications, New Delhi, 2012; Krein, P.T., *Elements of Power Electronics*, Oxford University Press, New York, 2003; Thorborg, K., *Power Electronics*, Prentice Hall International, London, UK, 1988.)

7.9.3 STEPPED MODULATION

In this technique, the modulating signal is a stepped wave as shown in Figure 7.18 [2–7]. As compared to normal PWM control, it gives higher output amplitude with low distortion. Elimination of particular harmonics and control of voltage is achieved by controlling the intervals individually.

7.9.4 HARMONIC-INJECTED MODULATION

In this technique, modulating signal is generated by injecting the selected harmonics to the sine wave as shown Figure 7.19 [1–3]. As compared to normal PWM control, it gives higher output amplitude with low distortion. The modulating signal is generally composed of

$$v_r = 1.15 \sin \omega t + 0.27 \sin 3\omega t - 0.029 \sin 9\omega t \quad (7.37)$$

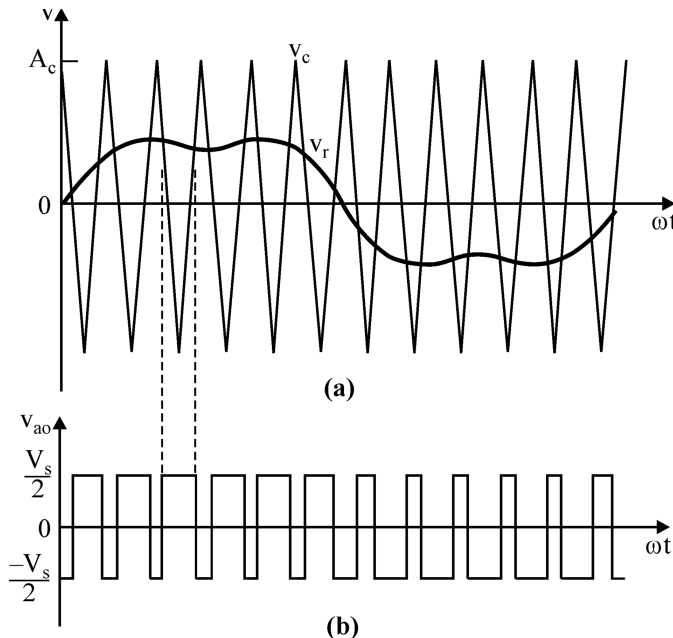


FIGURE 7.19 Selected harmonic injection modulation: (a) gate-signal generation and (b) output voltage. (From Bose, B.K., *Power Electronics and AC Drives*, Prentice Hall, Englewood Cliffs, NJ, 1986; Rashid, M.H., *Power Electronics: Circuits, Devices, and Applications*, Pearson Education, Singapore, 2004; Bhimra, P.S., *Power Electronics*, 4th edn, Khanna publications, New Delhi, 2012; Krein, P.T., *Elements of Power Electronics*, Oxford University Press, New York, 2003; Thorborg, K., *Power Electronics*, Prentice Hall International, London, UK, 1988.)

The quality of output voltage of three-phase inverter is not affected from the injection of 3 n th harmonics as it does not have triplen harmonics. The magnitude of voltage V_r is given by:

$$V_r = 1.15 \sin \omega t + 0.19 \sin 3 \omega t \quad (7.38)$$

7.9.5 DELTA MODULATION

In this modulation, a triangular wave oscillates within a defined window as shown in Figure 7.20 [1–3]. It is also called as hysteresis modulation as the switching function is generated from triangular wave vertices. The importance of this technique is that it can control the ratio of voltage to frequency, which is required in various applications like control of AC motors.

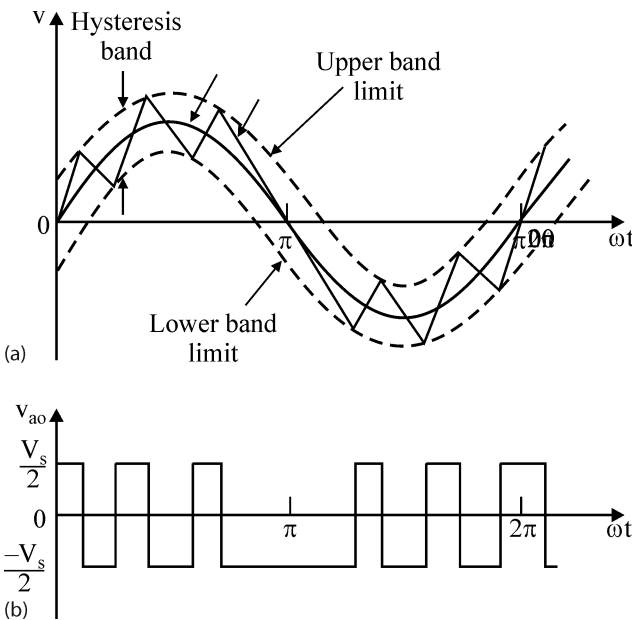


FIGURE 7.20 Delta modulation: (a) Gate signal generation and (b) output voltage. (From Bose, B.K., *Power Electronics and AC Drives*, Prentice Hall, Englewood Cliffs, NJ, 1986; Rashid, M.H., *Power Electronics: Circuits, Devices, and Applications*, Pearson Education, Singapore, 2004; Bhimra, P.S., *Power Electronics*, 4th edn, Khanna publications, New Delhi, 2012; Krein, P.T., *Elements of Power Electronics*, Oxford University Press, New York, 2003; Thorborg, K., *Power Electronics*, Prentice Hall International, London, UK, 1988.)

7.10 SPACE VECTOR MODULATION

Space vector PWM is very flexible in selecting vectors for both control of input current and output voltage, even under unbalanced conditions. In this, reference voltage vector (V_r) is approximated using a switching pattern to generate the average output of the inverter in a switching period (T_s) which is same as that of reference voltage vector (V_r) in same period. This technique is used to achieve reduced total harmonic distortion (THD), switching losses and wide range of modulation with simple and easy computational calculation and implementation [2–6]. Fourier analysis is used to determine the harmonic content of any waveform.

In space vector PWM method, the reference voltage vector (V_r) is approximated using the eight switching vectors namely $V_0, V_1, V_2, V_3, V_4, V_5, V_6, V_7$ as shown in Figure 7.21. In α - β frame, there are six sectors in space vector diagram, where each sector is equally divided by 60° as shown. Each sector is divided equally by 60° . Basic active vectors are V_1, V_2, V_3, V_4, V_5 , and V_6 , while V_0 and V_7 are zero vectors.

7.10.1 IMPLEMENTATION OF SPACE VECTOR PWM

The space vector PWM can be implemented using the following steps:

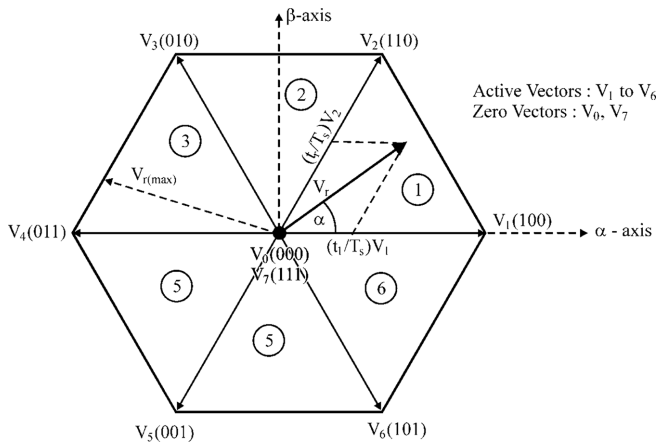


FIGURE 7.21 Space vector diagram with sectors and vectors.

Step-1: Determination of V_α and V_β

Let us assume supply voltage as

$$V_a = V_m \sin(\omega t)$$

$$V_b = V_m \sin(\omega t - 120^\circ)$$

$$V_c = V_m \sin(\omega t + 120^\circ) \quad (7.39)$$

where, V_m is the peak amplitude in volts and ω as angular frequency in rad/sec.

The voltage equation in *abc reference frame* are transformed into stationary $\alpha\beta$ *reference frame* using Park's transformation. The $\alpha\beta$ and *abc reference frame* are shown in [Figure 7.22](#). Thus, V_α and V_β can be written as,

$$\begin{bmatrix} V_\alpha \\ V_\beta \end{bmatrix} = \begin{bmatrix} 1 & -\frac{1}{2} & -\frac{1}{2} \\ 0 & \frac{\sqrt{3}}{2} & -\frac{\sqrt{3}}{2} \end{bmatrix} \begin{bmatrix} V_a \\ V_b \\ V_c \end{bmatrix} \Rightarrow \begin{aligned} V_\alpha &= \frac{3}{2} V_m \sin(\omega t) \\ V_\beta &= \frac{3}{2} V_m \cos(\omega t) \end{aligned} \quad (7.40)$$

Step-2: Calculate reference voltage vector (V_r) and angle (α)

From the above equations, V_r and angle (α) can be calculated as:

$$V_r = \sqrt{V_\alpha^2 + V_\beta^2}$$

$$\alpha = \tan^{-1} \left(\frac{V_\alpha}{V_\beta} \right) \quad (7.41)$$

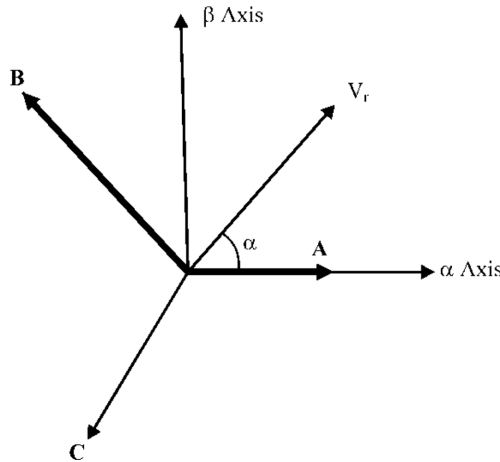


FIGURE 7.22 $\alpha\beta$ and abc reference frame.

Step-3: Determination of time duration t_1 , t_2 , and t_0

In Sector-1 as per Figure 7.21, V_1 , V_2 are active voltage vectors and V_0 , V_7 are zero vectors. Also, V_r makes an angle α with respect to V_1 . This reference voltage V_r can be calculated using the Figure 7.22. T_s is the sampling time interval where output voltage of inverter is constant. The time t_1 and t_2 are switching duration of vectors V_1 and V_2 . Similarly, the time t_0 is the switching duration of both vectors V_0 and V_7 . These times duration (t_1 , t_2 , and t_0) can be calculated as:

$$t_1 = \sqrt{3}T_s \left(\frac{V_r}{V_{dc}} \right) \sin\left(\frac{\pi}{3} - \alpha\right)$$

$$t_2 = \sqrt{3}T_s \left(\frac{V_r}{V_{dc}} \right) \sin(\alpha)$$

$$t_0 = T_s - t_1 - t_2 \quad (7.42)$$

Step-4: Calculation of switching time of each switches (S1 to S6)

Based on the calculation of time duration (t_1 , t_2 , and t_0), the switching patterns for each switch in Sector-1 is depicted in Figure 7.23. Similarly, Figures 7.24 to Figure 7.26 depict the switching pattern for each switch in Sectors-2, 3, and 4 [2–4]. The switching patterns for other sectors can be drawn with the help of Table 7.1. Table 7.1 presents the six sectors and the time calculation of each upper and lower group switches.

The sequence and the segments of the three-phase output voltage during two sampling periods are shown in Figure 7.27, where it can be seen that time intervals of the zero or null vectors (V_0 , V_7) are equally distributed [2–4].

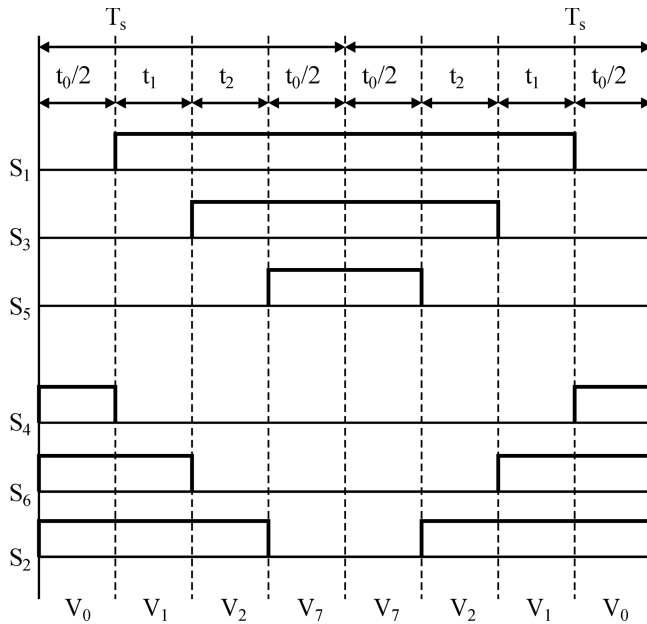


FIGURE 7.23 Switching pattern in Sector-1.

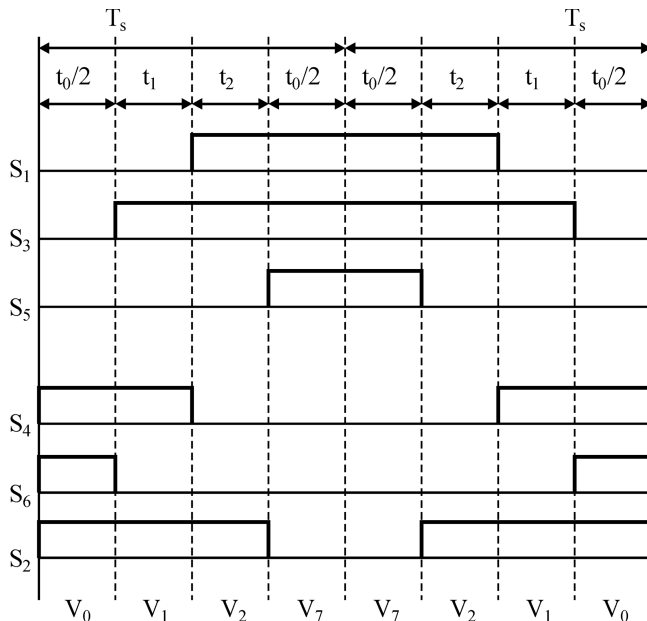


FIGURE 7.24 Switching pattern in Sector-2.

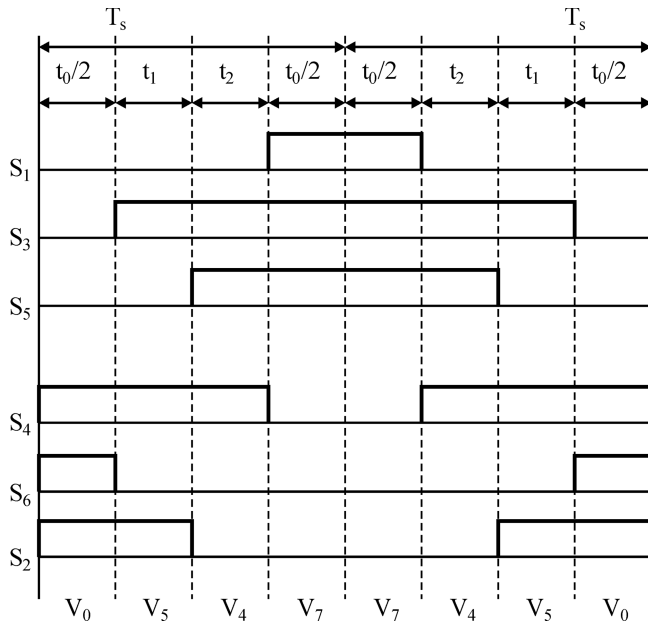


FIGURE 7.25 Switching pattern in Sector-3.

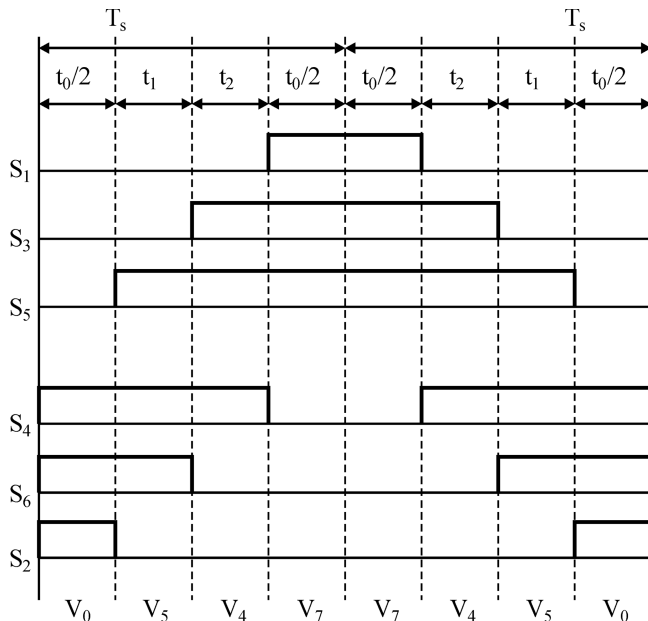


FIGURE 7.26 Switching pattern in Sector-4.

TABLE 7.1
Switching Time Calculation of Each Section Switch (VSI)

Sectors	Upper Group Switches (S_1, S_3, S_5)	Lower Group Switches (S_4, S_6, S_2)
1	$S_1 = t_1 + t_2 + t_0/2$ $S_3 = t_2 + t_0/2$ $S_5 = t_0/2$	$S_4 = t_0/2$ $S_6 = t_1 + t_0/2$ $S_2 = t_1 + t_2 + t_0/2$
2	$S_1 = t_2 + t_0/2$ $S_3 = t_1 + t_2 + t_0/2$ $S_5 = t_0/2$	$S_4 = t_1 + t_0/2$ $S_6 = t_0/2$ $S_2 = t_1 + t_2 + t_0/2$
3	$S_1 = t_0/2$ $S_3 = t_1 + t_2 + t_0/2$ $S_5 = t_2 + t_0/2$	$S_4 = t_1 + t_2 + t_0/2$ $S_6 = t_0/2$ $S_2 = t_1 + t_0/2$
4	$S_1 = t_0/2$ $S_3 = t_2 + t_0/2$ $S_5 = t_1 + t_2 + t_0/2$	$S_4 = t_1 + t_2 + t_0/2$ $S_6 = t_1 + t_0/2$ $S_2 = t_0/2$
5	$S_1 = t_2 + t_0/2$ $S_3 = t_0/2$ $S_5 = t_1 + t_2 + t_0/2$	$S_4 = t_1 + t_0/2$ $S_6 = t_1 + t_2 + t_0/2$ $S_2 = t_0/2$
6	$S_1 = t_1 + t_2 + t_0/2$ $S_3 = t_0/2$ $S_1 = t_1 + t_0/2$	$S_4 = t_0/2$ $S_6 = t_1 + t_2 + t_0/2$ $S_2 = t_2 + t_0/2$

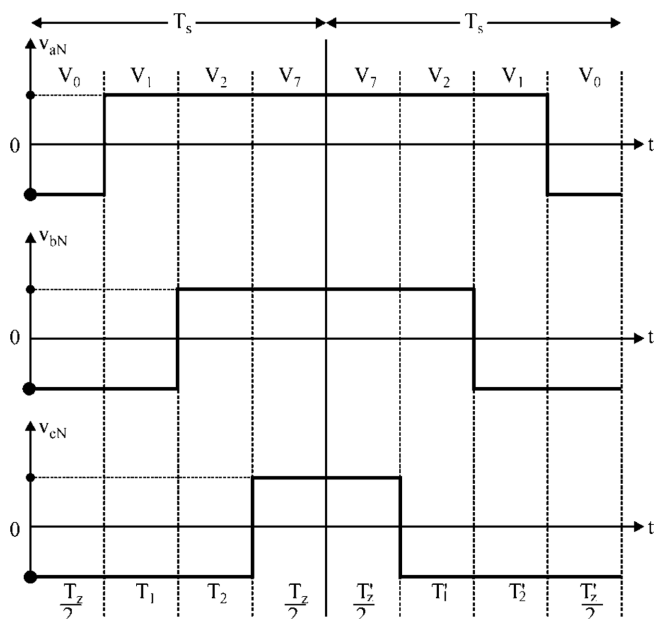


FIGURE 7.27 Pattern of space vector modulation.

7.11 HARMONIC REDUCTION

There are certain harmonics which are undesirable as they cause some particular harmful effects such as interferences, oscillations, harmonic torque and heating in motors etc. Also, control of the output voltage of inverters needs variation of pulse widths as well as the number of pulses per half cycle generated by modulation techniques [2–4,6]. The different ways through which the harmonics can be reduced or eliminated from the output of inverters are pinpointed as:

1. By proper selection of phase displacement angle (α)

The output voltage of inverter is expressed as:

$$v_{ab} = \sum_{n=1,3,5,\dots}^{\infty} \frac{4V_s}{n\pi} \sin \frac{n\alpha}{2} \cos n \left(\omega t - \frac{\alpha}{2} \right)$$

The n th harmonic can be eliminated as, if $\cos n\alpha = 0$

or

$$\text{phase displacement angle } \alpha = \frac{90}{n} \quad (7.43)$$

The *third* harmonic can be eliminated if the phase displacement angle $\alpha = \frac{90}{3} = 30^\circ$. Similarly, *fifth* harmonic can be eliminated if the phase displacement angle $\alpha = \frac{90}{5} = 18^\circ$.

2. By introducing a pair of symmetrically placed bipolar voltage notches
3. Using uni-polar output voltage notches
4. Using 60-degree modulation technique
5. By connecting the output voltage of two or more inverters in series using a transformer

7.12 SOLVED PROBLEMS

Example 7.1: A single-phase, half-bridge inverter feeds a resistive load, $R = 10 \Omega$. If the source voltage is 240 V, determine

- the RMS value of fundamental component of output voltage,
- the output power,
- the peak off-state voltage across each semiconductor switch,
- the lowest-order harmonic and the corresponding harmonic factor, and
- the RMS and average values of currents through semiconductor switches.

SOLUTION

The magnitude of square-wave output voltage for the half-bridge inverter,

$$V_L = \frac{240}{2} = 120 \text{ V}$$

The output voltage may be expressed in Fourier series, using Equation (7.5) as

$$\begin{aligned} v_0(t) &= \sum_{n=1,3,5,\dots}^{\infty} \frac{2V_s}{n\pi} \sin(n\omega t) \\ &= \frac{2 \times 240}{\pi} \sum_{n=1,3,5,\dots}^{\infty} \frac{\sin(n\omega t)}{n} \\ &= 152.87 \left[\sin(\omega t) + \frac{\sin(3\omega t)}{3} + \frac{\sin(5\omega t)}{5} + \dots \right] \end{aligned}$$

Now, we get the following:

- (a) The RMS value of fundamental component of the output voltage,
 $V_1 = 152.79/\sqrt{2} = 108.04 \text{ V}$
- (b) The output power is given by $P_0 = V_0^2/R$
 where V_0 is the RMS value of the output voltage. For the square-wave output, $V_0 = V_L = 120 \text{ V}$. Therefore, $P_0 = 120^2/10 = 1440 \text{ W}$
- (c) The peak voltage that appears across each semiconductor switch is

$$2V_L = 2 \times 120 = 240 \text{ V}$$

- (d) The lowest-order harmonic is the third harmonic, which has an RMS value equal to $V_3 = 152.79/(3\sqrt{2}) = 36.01 \text{ V}$. The corresponding harmonic factor is

$$HF_3 = \frac{V_3}{V_1} = \frac{36.01}{108.04} = 0.333$$

- (e) The output current has a square-wave shape with magnitude $12/10 = 1.2 \text{ A}$. In the positive half cycle, the load current flows through the switch S_1 , and in the negative half cycle, the switch S_2 carries the load current.
 The average switch current may be obtained as

$$I_{s(\text{avg})} = \frac{1}{T} \int_0^{T/2} 12dt = \frac{12(T/2)}{T} = 6 \text{ A}$$

The RMS switch current is given by

$$I_{s(\text{rms})} = \left[\frac{1}{T} \int_0^{T/2} (12)^2 dt \right]^{\frac{1}{2}} = \left[\frac{1}{T} \times (12)^2 \times \frac{T}{2} \right]^{\frac{1}{2}} = \frac{12}{\sqrt{2}} = 8.48 \text{ A}$$

Example 7.2: A single-phase, half-bridge inverter with total source voltage, $V = 500 \text{ V}$, feeds an RL load with $R = 20 \Omega$, and $L = 0.1 \text{ H}$. If the frequency of the output voltage is 50 Hz , determine

- (a) the output current at the end of first cycle,
- (b) the expression of steady-state output current for both the half cycles and
- (c) the THD of load current.

SOLUTION

For the half-bridge inverter the magnitude of the square-wave voltage waveform $V_L = V/2 = 250 \text{ V}$. The time constant of the RL load $\tau = L/R = 0.1/20 = 0.005 \text{ s}$. Time period of the output voltage $T = 1/50 = 0.02 \text{ s}$.

- (a) At $t = 0$, the RL load is subjected to a step function with magnitude V_L . The voltage equation is given by

$$V_L = Ri_o(t) + L \frac{di(t)}{dt}$$

$$i_o(t) = \frac{V_L}{R} \left[1 - \exp\left(-\frac{t}{\tau}\right) \right] + I_o \exp\left(-\frac{t}{\tau}\right)$$

where I_o is the current at $t = 0$, which is zero in the present case. Putting in the values, we get

$$i_o(t) = \frac{250}{20} \left[1 - \exp\left(-\frac{t}{0.005}\right) \right] = 12.5(1 - e^{-200t}) \text{ A}$$

At half time period, that is, $t = T/2 = 0.01 \text{ s}$,

$$i_o = 12.5(1 - e^{-2}) = 10.81 \text{ A}$$

For the next half cycle, the load voltage reverses and the load current is given by

$$i_o(t') = -12.5[1 - \exp(-200t)] + 10.81 \exp(-200t')$$

where $t' = t - (T/2)$. At the end of the first cycle,

$$t' = 0.02 - \frac{0.02}{2} = 0.01 \text{ s}$$

$$\text{Then } i_o = -12.5[1 - \exp(-2)] + 10.81 \exp(-2) = -9.345 \text{ A}$$

- (b) The steady-state load current for the positive half cycle can be obtained, as

$$i_o = \frac{V_L}{R} \left[1 - \frac{2}{1 + e^{-T/(2\tau)}} e^{-t/\tau} \right]$$

$$= \frac{250}{20} \left[1 - \frac{2}{1+e^{-2}} e^{-200t} \right]$$

$$= 12.5(1 - 1.76 e^{-200t})$$

For the negative half cycle, the load current is given by

$$i_o = 12.5(1 - 1.76 e^{-200(t-0.01)})$$

(c) The RMS value of the n th harmonic component is given by

$$I_n = \frac{4V_L}{n\pi\sqrt{2}\sqrt{R^2 + (n\omega L)^2}} = \frac{225.08}{n\sqrt{400 + 986.96n^2}}, n = 1, 3, 5, \dots$$

Putting different values of n , we get

$$I_1 = 6.044, I_3 = 0.7785, I_5 = 0.2845, I_7 = 0.1455, I_9 = 0.088, I_{11} = 0.0585, \dots$$

The THD for the load current may be obtained as

$$THD_i = \frac{\sqrt{I_3^2 + I_5^2 + I_7^2 + I_9^2 + I_{11}^2 + \dots}}{I_1} = 0.1403 \text{ or } 14.03\%$$

Note: THD_i is 14.03%, which is far less than THD_v which is 48.34%. This is because of the higher impedance offered by the inductance to the high-frequency harmonics, which are filtered out.

Example 7.3: The full-bridge inverter of Figure 7.2a has a source voltage, $V = 220$ V. The inverter supplies an RLC load with $R = 5 \Omega$, $L = 10$ mH, and $C = 26 \mu F$. The frequency of operation of inverter is 400 Hz. Calculate:

- (a) the RMS load current at fundamental frequency,
- (b) the RMS value of load current,
- (c) the THD in the load current,
- (d) the power output, and
- (e) the average supply current.

SOLUTION

Given $V_L = 220$ V, $R = 5 \Omega$, $L = 10$ mH, $C = 26 \mu F$, $f = 400$ Hz. The inductive reactance for the fundamental voltage,

$$X_L = 2\pi fL = 2 \times \pi \times 400 \times 10 \times 10^{-3} = 25.13 \Omega$$

The capacitive reactance for the fundamental voltage,

$$X_C = \frac{1}{2\pi fC} = \frac{1}{2\pi \times 400 \times 26 \times 10^{-6}} = 15.3 \Omega$$

Impedance offered to n th harmonic component,

$$Z_n = \sqrt{R^2 + \left(nX_L - \frac{X_C}{n} \right)^2}$$

Putting different values of n , impedance offered to different harmonic components are

$$Z_1 = \sqrt{5^2 + (25.13 - 15.3)^2} = 11.03 \Omega$$

$$Z_3 = \sqrt{25 + \left(3 \times 25.13 - \frac{15.3}{3} \right)^2} = 70.47 \Omega$$

Similarly,

$$Z_5 = 122.690 \Omega, Z_7 = 173.79 \Omega, Z_9 = 224.52 \Omega$$

From, the RMS value of the n th harmonic component of the output voltage is given by

$$V_n = \frac{0.9V_L}{n} = \frac{0.9 \times 220}{n} = \frac{198}{n}$$

The RMS value of the n th harmonic component of the current is given by

$$I_n = \frac{V_n}{Z_n} = \frac{198}{nZ_n} \quad (7.44)$$

- (a) The RMS value of the fundamental component of the load current

$$I_1 = \frac{198}{1 \times 11.03} = 17.95 \text{ A}$$

- (b) Putting the values of n and Z_n in Equation (7.44), RMS values of the different harmonic components may be obtained as $I_3 = 0.94 \text{ A}$, $I_5 = 0.32 \text{ A}$, $I_7 = 0.16 \text{ A}$, $I_9 = 0.1 \text{ A}$,...

The RMS value of the load current

$$I = \sqrt{I_1^2 + I_3^2 + I_5^2 + I_7^2 + I_9^2 + \dots}$$

$$= \sqrt{17.95^2 + 0.94^2 + 0.32^2 + 0.16^2 + 0.1^2 + \dots}$$

$$= 17.98 \text{ A}$$

(c) THD in the load current

$$\text{THD}_i = \frac{\sqrt{I^2 - I_1^2}}{I_1} = \frac{\sqrt{17.98^2 - 17.95^2}}{17.95} = 0.0578 = 5.78\%$$

(d) The power output

$$P_0 = I^2 R = (17.98)^2 \times 5 = 1.616 \text{ kW}$$

(e) The average supply current

$$I_{av} = \frac{P_0}{V} = \frac{1616}{220} = 7.35 \text{ A}$$

Example 7.4: A single PWM inverter feeds an RL load with $R = 10 \Omega$ and $L = 20 \text{ mH}$. If the source voltage is 120 V, find out the THD in the load current. The width of each pulse is 120° and the output frequency is 50 Hz.

SOLUTION

The RMS value of the n th harmonic component of the output voltage is given by

$$V_n = \frac{4V}{\sqrt{2n\pi}} \sin \frac{nW}{2}$$

Here $V = 120$ and $W = 2\pi/3$. Therefore,

$$V_n = \frac{4 \times 120}{\sqrt{2n\pi}} \sin \frac{n\pi}{3} = \frac{108.04}{n} \sin \frac{n\pi}{3}$$

The impedance offered to the n th harmonic current is given by

$$Z_n = \sqrt{R^2 + (n\omega L)^2} = \sqrt{10^2 + n^2(2\pi \times 50 \times 20 \times 10^{-3})^2} = \sqrt{100 + 39.478n^2}$$

The RMS value of the n th harmonic current

$$I_n = \frac{V_n}{Z_n} = \frac{108.04}{n\sqrt{100 + 39.478n^2}} \sin \frac{n\pi}{3}$$

Putting different values of n , we get $I_1 = 7.922 \text{ A}$, $I_3 = 0$, $I_5 = 0.5675 \text{ A}$, $I_7 = 0.2963 \text{ A}$, $I_9 = 0$, $I_{11} = 0.1218 \text{ A}$, $I_{13} = 0.0814 \text{ A}$. Then

$$\text{THD}_i = \frac{\sqrt{I_3^2 + I_5^2 + I_7^2 + I_9^2 + I_{11}^2 + I_{13}^2}}{I_1} = \frac{0.4323}{7.922} = 0.0545 = 5.45\%$$

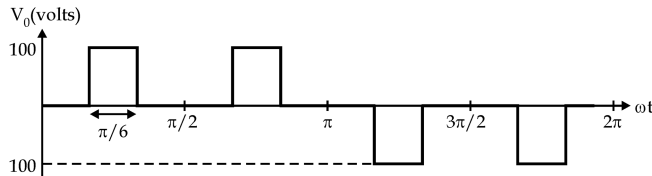


FIGURE 7.28 Output voltage uniform PWM inverter Example 7.5.

Example 7.5: The output voltage of a uniform PWM inverter is shown in Figure 7.28. Find out the RMS value of the output voltage, fundamental component of the output voltage, and THD.

SOLUTION

- (a) The RMS value of output voltage

$$V_0 = \left[\frac{100^2 (\pi / 6)}{(\pi / 2)} \right]^{\frac{1}{2}} = 100 \sqrt{\frac{1}{3}} = 57.735 \text{ V}$$

- (b) The waveform possesses odd- and half-wave symmetry. Hence, only odd b -components will be present in the Fourier series, which are given by

$$b_n = \frac{4}{\pi} \int_0^{\pi/2} v_0(t) \sin(n\omega t) d(\omega t) = \frac{4}{\pi} \left[\int_{30^\circ}^{60^\circ} 100 \sin(n\omega t) d(\omega t) \right]$$

and

$$b_1 = \frac{400}{\pi} [-\cos \omega t]_{30^\circ}^{60^\circ} = \frac{400}{\pi} (-\cos 60^\circ + \cos 30^\circ) = 46.604$$

The RMS value of fundamental component

$$V_1 = \frac{46.604}{\sqrt{2}} = 32.953 \text{ V}$$

$$(c) \text{ THD} = \frac{\sqrt{V_0^2 - V_1^2}}{V_1} = 1.4385 = 143.85\%$$

Example 7.6: A single-phase full-bridge inverter controls the power in a resistive load. The nominal value of input DC voltage is $V_s = 220 \text{ V}$, and a uniform PWM with five pulses per half cycle is used. For the required control, the width of each pulse is 30° . (a) Determine the RMS voltage of the load. (b) If the DC supply increases by 10%, determine the pulse width to maintain the same load power. If the maximum possible pulse width is 35° , determine the minimum allowable limit of the DC input source.

SOLUTION

- (a) $V_s = 220 \text{ V}$, $p = 5$ and, $\delta = 30^\circ$

$$V_0 = 220\sqrt{5 \times 30 / 180} = 200.8 \text{ V}$$

- (b) $V_s = 1.1 \times 220 = 242 \text{ V}$. $242\sqrt{5\delta/180} = 200.8$ and this gives the required value of pulse width, $\delta = 24.75^\circ$.

To maintain the output voltage of 200.8 V at the maximum possible pulse width of $\delta = 35^\circ$, the input voltage can be found from $200.8 = V_s \sqrt{5 \times 35 / 180}$, and this yields the minimum allowable input voltage, $V_s = 203.64 \text{ V}$.

Example 7.7: A three-phase bridge inverter is fed from a 600-V DC source. The inverter is operated in 180° conduction mode, and it is supplying a purely resistive, star-connected load with $R = 15 \Omega/\text{phase}$. Determine

- (a) the RMS value of the load current,
- (b) the RMS value of the switch current,
- (c) the power delivered to the load, and
- (d) the average source current.

SOLUTION

- (a) The RMS value of the per-phase load voltage is given by

$$V_{ph} = \frac{\sqrt{2}}{3}V = \frac{\sqrt{2}}{3} \times 600 = 282.84 \text{ V}$$

Therefore, the RMS value of the load current per phase

$$I_{ph} = \frac{V_{ph}}{R} = \frac{282.84}{15} = 18.85 \text{ A}$$

- (b) The RMS value of the current through the switch

$$I_{\text{switch(rms)}} = \frac{V}{3R} = \frac{600}{3 \times 15} = 13.33 \text{ A}$$

- (c) Power delivered to the load

$$P_L = 3 \frac{V_{ph}^2}{R} = 3 \times \frac{282.84^2}{15} = 15999 \text{ W or } 16 \text{ kW}$$

- (d) Power delivered by the source = $V_L I_{av} = P_L$, where, I_{av} is the average source current. Therefore,

$$I_{av} = \frac{P_L}{V_L} = \frac{15999}{600} = 26.66 \text{ A}$$

Example 7.8: A single-phase bridge inverter is connected to a series connected RLC load with $R = 4 \Omega$ and $\omega L = 10 \Omega$. Given that periodic time $T = 0.1 \text{ ms}$, the thyristor turn-off time $10 \mu\text{s}$. Take the circuit turn-off time as $2 t_q$. Determine the value of C for which SCRs have load commutation.

SOLUTION

The magnitude of C should be such that the RLC load becomes underdamped, that is, the load current must lead the load voltage by an angle θ as shown in Figure 7.29. From this phasor diagram:

$$\tan \theta = \frac{X_C - X_L}{R}$$

Here, $X_C > X_L$ as the current is leading the voltage. Now (θ/ω) must be at least equal to circuit turn-off time, that is, $2 \times 10 = 20 \mu\text{s}$

$$\therefore \frac{\theta}{\omega} = 20 \times 10^{-6} \text{ s}$$

Now

$$f = \frac{10^3}{0.1} = 10^4 \text{ Hz}$$

$$\theta = 2\pi \times 10^4 \times 20 \times 10^{-6} = 1.256 \text{ rad} = 72^\circ$$

$$\therefore \tan 72^\circ = \frac{X_C - 10}{4}$$

or

$$X_C = 22.3107 = \frac{1}{2\pi \times 10^4 \times C}$$

or

$$C = 0.72 \mu\text{F}$$

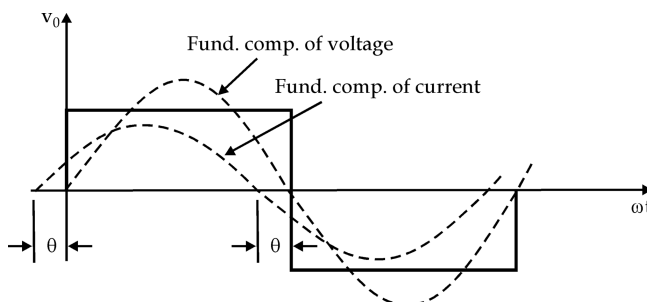


FIGURE 7.29 Output voltage single-phase bridge inverter of Example 7.8.

Example 7.9: A single-phase half-bridge inverter has load $R = 4 \Omega$. and DC source voltage

$$\frac{V_s}{\pi} = 110 \text{ V}$$

- (a) Sketch the waveforms for v_o , i_o , load current i_{01} , currents through thyristor 1 and diode 1, and voltage across thyristor T_1 . Harmonics other than fundamental component are neglected. Indicate the devices that conduct during different intervals of one cycle.
- (b) Find the power delivered to load due to fundamental current.
- (c) Check whether forced commutation is required.

SOLUTION

- (a) The fundamental component ($n = 1$) of output voltage, from Equation (7.5), is

$$v_{01} = \frac{2V_s}{\pi} \sin \omega t$$

The RMS value of this voltage,

$$V_{01} = \frac{2 \times 220}{\pi \cdot \sqrt{2}} = 99.08 \text{ A}$$

and the RMS load current,

$$I_{01} = \frac{V_{01}}{R} = \frac{99.08}{4} = 22.78 \text{ A}$$

The fundamental frequency component of load current is

$$i_{01} = 22.78\sqrt{2} \sin \omega t$$

The waveforms for the various voltages and currents are shown in **Figure 7.30**. For resistive load, feedback diodes do not come into conduction; therefore, i_{D1} is zero. When T_1 conducts, $v_{T1} = 0$. When T_2 conducts, $v_{T2} = V_s$ as shown.

- (b) Power delivered to load = $I_{01}^2 R = (22.78)^2 \times 4 = 2075.72 \text{ W}$
When T_1 is conducting, power to load is delivered by upper source $\frac{V_s}{2}$ and when T_2 is on, lower source delivers power to load.
Power delivered by each source = $\frac{V_s}{2} \cdot I_s$

$$\text{Here, } I_s = \frac{1}{2\pi} \int_0^\pi \sqrt{2} i_{01} \sin \omega t \cdot d(\omega t)$$

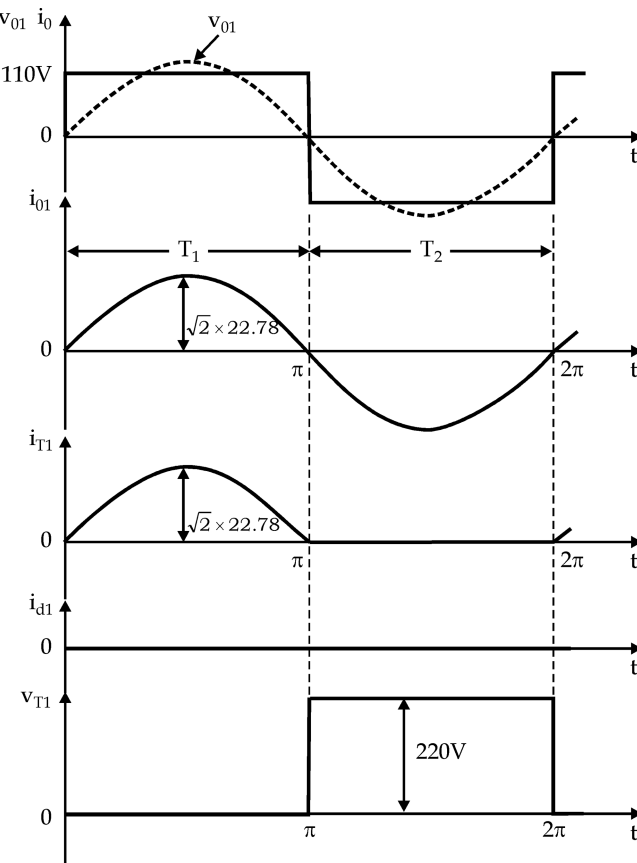


FIGURE 7.30 Various waveforms for Example 7.9.

Power delivered by each source

$$= 110 \times 10.26 = 1128.58 \text{ W}$$

Power delivered by both the sources

$$= 2 \times 1128.58 \cong 2258 \text{ W}$$

- (c) Because the load is resistive, the diodes do not conduct, and therefore forced commutation is essential.

Example 7.10: For a single-phase full-bridge inverter, $V_s = 220 \text{ V dc}$, $T = 1 \text{ ms}$. The load consists of RLC in series with $R = 1 \Omega$, $\omega L = 6 \Omega$ and $1/\omega C = 7$.

- (a) Sketch the different waveforms.
 (b) Find the power delivered to load to the fundamental component.
 (c) Check whether forced commutation is required or not. Take thyristor turn-off time as 100 μ s and 150 μ s.

SOLUTION

- (a) The load voltage waveform v_0 and its fundamental component v_{01} are shown in Figure 7.31.

The RMS value of load voltage is

$$V_{01} = \frac{4V_s}{\pi\sqrt{2}} = \frac{4 \times 220}{\pi\sqrt{2}} = 198.17 \text{ V}$$

The RMS value of current, $i_{01} = \frac{V_{01}}{Z_1}$

$$= \frac{V_{01}}{\left[R^2 + \left(\omega L - \frac{1}{\omega C} \right)^2 \right]^{1/2}}$$

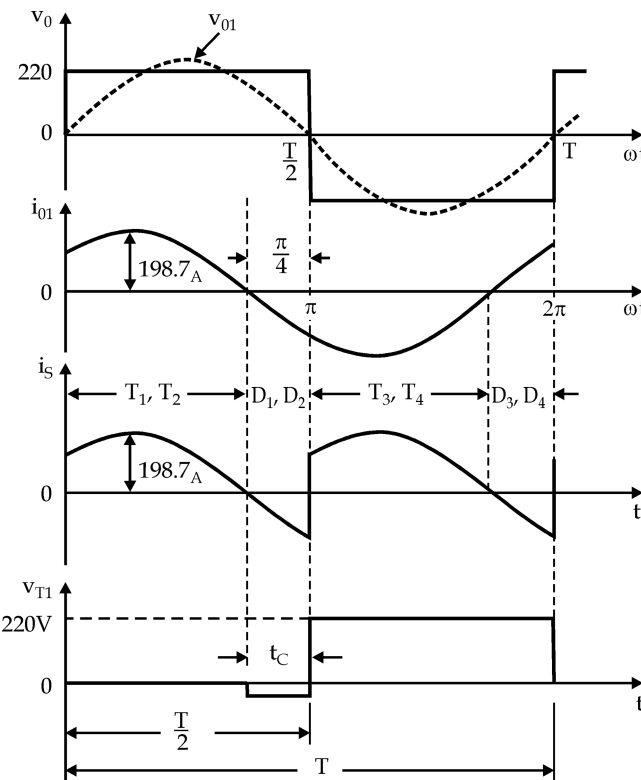


FIGURE 7.31 Various waveforms for Example 7.10.

$$= \frac{198.17}{\left[1^2 + (-1)^2\right]^{1/2}} = \frac{198.17}{\sqrt{2}} = 140.13 \text{ A}$$

$$\varphi_1 \tan^{-1} \frac{X_L - X_C}{R} = \tan^{-1}(-1)$$

$$= -45^\circ$$

The fundamental component of current i_{01} as a function of time is

$$i_{01} = \sqrt{2} I_{01} \sin(\omega t - \varphi_1)$$

$$= \sqrt{2} \frac{198.7}{\sqrt{2}} \sin(\omega t + 45^\circ)$$

$$= 198.7 \sin(\omega t + 45^\circ)$$

$$(b) \text{ Power delivered to load} = I_{01}^2 R = \left(\frac{198.7}{\sqrt{2}} \right)^2 \times 1 = 19.7 \text{ kW}$$

This must be equal to the power P_S delivered by the source.

$$\therefore P_S = V_S I_S W$$

where I_S = average value of fundamental component of source current

$$= \frac{1}{\pi} \int_0^\pi \sqrt{2} I_{01} \sin(\omega t + 45^\circ) d(\omega t)$$

$$= \frac{198.7}{\pi} [-\cos(\omega t + 45^\circ)]_0^\pi = \frac{198.7}{\pi} [2 \cos 45^\circ] = 89.5 \text{ A}$$

$$P_s = 220 \times 89.5 = 19.6 \text{ kW}$$

- (c) **Figure 7.31** reveals that v_{T1} is negative for some time before T_3, T_4 are triggered. Thus, circuit turn-off time can be obtained from

$$\text{or } \omega t_c = \theta = \tan^{-1} \frac{X_L - X_C}{R} = 45^\circ = \frac{\pi}{4}$$

$$\text{or } t_c = \frac{1}{4} \cdot \frac{T}{2} = 0.125 \text{ ms} = 125 \mu\text{s}$$

As voltage drop in diodes, D_1, D_2 reverse biases T_1, T_2 for 125 μs , which is more than the thyristor turn-off time of 100 μs , so no forced commutation is required. But if the thyristor turn-off time is 150 μs , then force commutation will be required.

Example 7.11: A single-phase full-bridge inverter is connected to an RLC load of $R = 4 \Omega$, $L = 35 \text{ mH}$ and $C = 155 \text{ mF}$. The DC input voltage is 230 V, and the output frequency is 50 Hz.

- Find an expression for load current up to a fifth harmonic.
- Calculator RMS value of fundamental load current.
- Calculate the power absorbed by the load and the fundamental power.
- Calculate the conduction time of thyristors and diodes if only fundamental component were considered.
- For what values of thyristor turn-off time will load commutation will occur?

SOLUTION

- (a) From Equation (7.6), an expression for output voltage is

$$\begin{aligned} v_0 &= \frac{4V_s}{\pi} \sin \omega t + \frac{4V_s}{3\pi} \sin 3 \omega t + \frac{4V_s}{5\pi} \sin 5 \omega t \\ &= \frac{4 \times 230}{\pi} \left[\sin \omega t + \frac{1}{3} \sin 3 \omega t + \frac{1}{5} \sin 5 \omega t \right] \\ &= 292.85 \sin 314t + 97.62 \sin(3 \times 214t) + 58.57 \sin(5 \times 314t) \end{aligned}$$

Load impedance at frequency $n.f.$ is

$$\begin{aligned} Z_n &= 4 + j \left(2\pi \times 50 \times 35 \times 10^{-3} \times n - \frac{10^6}{2\pi \times 50 \times 155 \times n} \right) \\ &= 4 + j \left(11n - \frac{20.54}{n} \right) \Omega \end{aligned}$$

$$\therefore Z_1 = \sqrt{4^2 + (11 - 20.54)^2} = 10.345 \Omega$$

and

$$\varphi_1 = \tan^{-1} \left(\frac{11 - 20.54}{4} \right) = -67.25^\circ$$

$$Z_3 = \sqrt{4^2 \left(11 \times 3 - \frac{20.54}{3} \right)^2} = 26.46 \Omega$$

and

$$\varphi_3 = \tan^{-1} \left[\frac{33 - 20.54 / 3}{4} \right] = 81.3^\circ$$

Similarly, $Z_5 = 51.05 \Omega$ and $\varphi_5 = 85.5^\circ$

Load current from Equation (7.7) is given by

$$\begin{aligned} i_0 &= \frac{292.85}{10.345} \sin(\omega t + 67.25^\circ) + \frac{97.62}{26.46} \sin(2\omega t - 81.3^\circ) + \frac{58.57}{5105} \sin(5\omega t - 85.5^\circ) \\ &= 28.31 \sin(314t + 67.25^\circ) + 3.689 \sin(3 \times 314t - 81.3^\circ) \\ &\quad + 1.1473 \sin(5 \times 314t - 85.5^\circ) \end{aligned}$$

$$(b) I_{01} = \frac{I_{m1}}{\sqrt{2}} = \frac{28.31}{\sqrt{2}} = 20.02 \text{ A}$$

$$(c) I_m = \sqrt{28.31^2 + 3.689^2 + 1.1473^2} = 28.572 \text{ A}$$

$$\text{RMS load current} = \frac{28.572}{\sqrt{2}} = 20.207 \text{ A}$$

$$\text{Load power} = (20.207)^2 \times 4 = 1633.3 \text{ W}$$

$$(d) i_{01} = 28.31 \sin(314t + 67.25^\circ)$$

This current leads the fundamental voltage component by 67.25° . This means that diode conducts for 67.25° , and thyristor for $180^\circ - 67.25^\circ = 112.75^\circ$.

\therefore Conduction time for thyristors

$$= \frac{112.75 \times \pi}{180 \times 314} = 6.267 \text{ ms}$$

$$\text{Conduction time for diodes} = \frac{67.25 \times \pi}{180 \times 314} = 3.738 \text{ ms},$$

- (e) Therefore, in case thyristor turn-off time is less than 3.738 ms, load commutation will occur, and no forced commutation will be required under the assumption of no harmonics.

Example 7.12: A three-phase bridge inverter connects the star-connected resistive load of 10 W per phase with a 440-V DC source. Calculate the RMS value of the load current, thyristor current, and load power for both 180° mode and 120° mode.

SOLUTION

Waveforms of phase-load current and thyristor current are as shown in Figure 7.32. (a) for 180° -mode operation and in Figure 7.32 (b) for 120° -mode operation.

- (a) **180° mode:** Upper waveform of Figure 7.32a shows that the RMS value of per-phase load current I_{rms} is given by

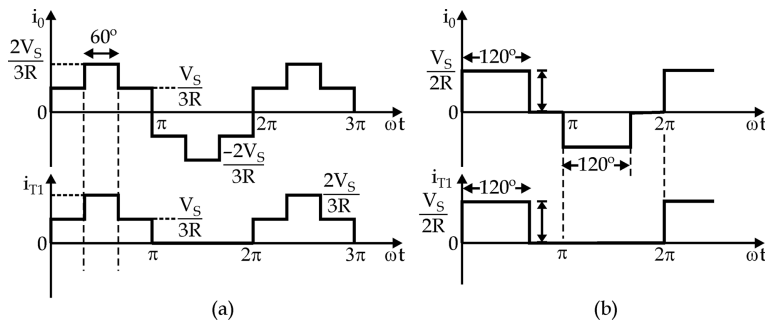


FIGURE 7.32 Various waveforms for Example 7.12: (a) 180° mode and (b) 120° mode.

$$I_{\text{rms}} = \left[\frac{1}{\pi} \left\{ \frac{V_s^2}{3R} \frac{\pi}{3} + \left(\frac{2V_s}{3R} \right)^2 \times \frac{\pi}{3} + \left(\frac{V_s}{3R} \right)^2 \frac{\pi}{3} \right\} \right]^{1/2}$$

$$= \left[\left(\frac{440}{3 \times 10} \right)^2 \times \frac{2}{3} + \left(\frac{2 \times 440}{3 \times 10} \right)^2 \times \frac{1}{3} \right]^{1/2}$$

$$= (143.41 + 286.82)^{1/2}$$

$$= 20.75 \text{ A}$$

RMS value of thyristor current is

$$I_{T1} = \left[\frac{1}{2\pi} \left\{ \left(\frac{440}{3 \times 10} \right)^2 \times \frac{2\pi}{3} + \left(\frac{2 \times 440}{3 \times 10} \right)^2 \times \frac{\pi}{3} \right\} \right]^{1/2}$$

$$= (71.70 + 143.40)^{1/2}$$

$$= 14.67 \text{ A}$$

Power delivered to load

$$= 3I_{rms}^2 R = 3(20.75)^2 \times 10 = 12.9 \text{ kW}$$

(b) **120° mode:** Upper waveform in Figure 7.32b gives RMS value of per-phase load current I_{rms} as under:

$$I_{rms} = \left[\frac{1}{\pi} \left(\frac{440}{2 \times 10} \right)^2 \times \frac{2\pi}{3} \right]^{1/2} = 17.96 \text{ A}$$

$$\text{Load power} = 3I_{\text{rms}}^2 R$$

$$= 3 \times (17.96)^2 \times 10 = 9677 \text{ W}$$

RMS value of thyristor current,

$$I_{T1} = \left[\frac{1}{2\pi} \left(\frac{440}{2 \times 10} \right)^2 \times \frac{2\pi}{3} \right]^{1/2} = 12.70 \text{ A}$$

Example 7.13: Single-phase full-bridge inverter connecting the 230-V DC source with a load consisting of $R = 10 \Omega$ and $L = 0.03 \text{ H}$. Calculate the power delivered to load when inverter operates at 50 Hz with (a) square-wave output (b) single-pulse modulated wave output with an on-period of 0.5 of a cycle, and (c) two symmetrically spaced pulses per half cycle with an on-period of 0.5 of a cycle.

SOLUTION

(a) Square-wave output: RMS value of fundamental voltage is

$$V_{01} = \frac{4V_s}{\pi \sqrt{2}} = \frac{4 \times 230}{\pi \sqrt{2}} = 207.10 \text{ V}$$

Load impedance at fundamental frequency is

$$Z_1 = [10^2 + (2\pi \times 50 \times 0.03)^2]^{1/2} = 13.7414 \Omega$$

$$I_{01} = \frac{207.10}{13.7414} = 15.0712 \text{ A}$$

$$V_{03} = \frac{4 \times 230}{3 \times \pi \times r \sqrt{2}} = 69.035 \text{ V}$$

and

$$Z_3 = \sqrt{10^2 + (2\pi \times 50 \times 3 \times 0.03)^2} = 29.9906 \Omega$$

$$I_{03} = \frac{69.035}{29.9906} = 2.302 \text{ A}$$

$$\text{Similarly, } I_{05} = \frac{920}{5 \times \pi \times \sqrt{2}} \times \frac{1}{\sqrt{10^2 + (2\pi \times 50 \times 5 \times 0.03)^2}} = 0.8598 \text{ A}$$

$$I_{07} = \frac{920}{7 \times \pi \times \sqrt{2}} \times \frac{1}{\sqrt{10^2 + (2\pi \times 50 \times 7 \times 0.03)^2}} = 0.4434 \text{ A}$$

RMS value of resultant load current,

$$I_{07} = \frac{920}{7 \times \pi \times \sqrt{2}} \times \frac{1}{\sqrt{10^2 + (2\pi \times 50 \times 7 \times 0.03)^2}} = 0.4434 \text{ A}$$

$$\text{Power delivered to load} = I_0 = \left[I_{01}^2 + I_{03}^2 + I_{05}^2 + I_{07}^2 \right]^{1/2}$$

$$\text{Power delivered to load} = I_0^2 R$$

$$= [15.0712^2 + 2.302^2 + 0.8598^2 + 0.4434^2] \times 10$$

$$= 2333.76 \text{ W}$$

- (b) *Single-pulse modulates wave output:* For single-pulse modulated wave or quasi-square wave where pulse width, $2d = 0.5 \times 180^\circ = 90^\circ$ or $d = 45^\circ$. RMS value of fundamental voltage is

$$V_{01} = \frac{4V_s}{\pi \cdot \sqrt{2}} \sin d = \frac{4 \times 230}{\pi \cdot \sqrt{2}} \sin 45^\circ = 146.423 \text{ V}$$

$$I_{01} = \frac{146.423}{13.7414} = 10.6556 \text{ A}$$

$$V_{03} = \frac{4 \times 230}{3 \times \pi \times \sqrt{2}} \sin 3 \times 45^\circ = 48.8075 \text{ V}$$

$$I_{03} = \frac{48.8075}{29.9906} = 1.6274 \text{ A}$$

$$\text{Similarly, } I_{05} = \frac{4 \times 230}{5 \times \pi \times \sqrt{2}} \sin(5 \times 45^\circ) \times \frac{1}{48.17324} = -0.6079 \text{ A}$$

$$I_{07} = \frac{4 \times 230}{7 \times \pi \times \sqrt{2}} \sin(7 \times 45^\circ) \times \frac{1}{66.727} = -0.3135 \text{ A}$$

$$\text{Power delivered to load} = [10.6556^2 + 1.6274^2 + 0.6079^2 + 0.3135^2] \times 10$$

$$= 1166.58 \text{ W}$$

- (c) *For two symmetrically spaced pulses per half cycle.* For this $2d = 0.5 \times 180 = 90^\circ$ or $d = 45^\circ$ and $\gamma = \frac{180-90}{3} + \frac{45}{2} = 52.5^\circ$. RMS value of fundamental voltage is

$$V_{01} = \frac{8V_s}{\pi \cdot \sqrt{2}} \sin \gamma \sin \frac{d}{2} = \frac{8 \times 230}{\pi \cdot \sqrt{2}} \sin 52.5^\circ \sin \frac{45}{2} = 125.755 \text{ V}$$

$$I_{01} = \frac{125.755}{13.7414} = 9.1515 \text{ A}$$

$$V_{03} = \frac{8 \times 230}{3 \times \pi \times \sqrt{2}} \sin(52.5 \times 3) \cdot \sin\left(\frac{45}{2} \times 3\right) = 48.815 \text{ V}$$

$$I_{03} = \frac{48.815}{29.9906} = 1.6277 \text{ A}$$

$$I_{05} = \frac{8 \times 230}{5 \times \pi \times \sqrt{2}} \sin(52.5 \times 5) \sin(22.5 \times 5) \times \frac{1}{48.17324} = 1.575 \text{ A}$$

$$I_{07} = \frac{8 \times 230}{7 \times \pi \times \sqrt{2}} \sin(52.5 \times 7) \sin(22.5 \times 7) \times \frac{1}{66.727} = 0.0443 \text{ A}$$

$$\begin{aligned} \text{Power delivered to load} &= [9.1515^2 + 1.6277^2 + 1.575^2 + 0.0443^2] \times 10 \\ &= 888.82 \text{ W} \end{aligned}$$

REVIEW QUESTIONS AND UNSOLVED PROBLEMS

- 7.1 (a) Define inverter along with its various industrial applications.
 (b) Explain the operation of line-commutated inverters.
 (c) What are the differences between line-commutated and force-commutated inverters?
- 7.2 (a) Describe the working of a single-phase half-bridge inverter. What is its main drawback? Explain how this drawback is overcome.
 (b) What is the purpose of connecting diodes in antiparallel with thyristors in inverter circuits? Explain how these diodes come into play.
- 7.3 Draw the load voltage and load current waveforms for single-phase full-bridge inverter with (a) R (b) RL or RLC overdamped, and (c) RLC underdamped. Explain the nature of these waveforms.
- 7.4 For a single-phase full-bridge inverter, $V_s = 220 \text{ V dc}$, $T = 1 \text{ ms}$. The load consists of RLC in series with $R = 2 \Omega$, $\omega L = 8 \Omega$, $1/\omega C = 7 \Omega$.
 (a) Draw various waveforms. Also find the RMS value of the fundamental component of load current.
 (b) Find the power delivered to load due to fundamental component.
 (c) Check whether forced commutation is required or not.
- 7.5 Write Fourier series expression for the output voltages and currents of single-phase half-bridge and full-bridge inverters.
- 7.6 (a) A single-phase full-bridge inverter is connected to a DC source of V_s . Resolve the output voltage wave shape into Fourier series.
 (b) A single-phase full-bridge inverter delivers power to RLC load with $R = 2 \Omega$ and $XL = 10 \Omega$. The bridge operates with a periodicity of 0.3 ms. Calculate the value of C so that load commutation is achieved by the

thyristors. Turn-off time for thyristors is 12 μs . Factor of safety is 1.5. Assume the load current to contain only the fundamental component.

- 7.7 A single-phase full-bridge inverter feeds power at 50 Hz to RLC load with $R = 5 \Omega$, $L = 0.3 \text{ H}$ and $C = 50 \mu\text{F}$. The DC input voltage is 220 V DC.
 - (a) Find an expression for load current up to the fifth harmonic.
 - (b) Calculate the power absorbed by the load and the fundamental power.
 - (c) Calculate the RMS and peak currents of each thyristor.
- 7.8 Explain the working of a three-phase bridge inverter with an appropriate circuit diagram. Draw phase and line voltage waveforms on the assumption that each thyristor conducts for 180° and the resistive load is star connected.
- 7.9 Repeat Problem 7.7 in case each thyristor conducts for 120° .
- 7.10 Repeat Problem 7.7 in case the load is delta connected.
- 7.11 A star-connected load of 28Ω per phase is fed from 440-V DC source through a three-phase bridge inverter. For both (a) 180° mode and (b) 120° mode, determine:
 - (i) RMS value of load current
 - (ii) RMS value of thyristor current
 - (iii) Load power
- 7.12 What is the need for controlling the voltage at the output terminals of an inverter?
- 7.13 What is PWM? List the various PWM techniques.
- 7.14 Explain various methods of harmonic reductions in detail?

SUMMARY

In practice, the term *inverter* is a circuit used for DC-to-AC conversion, that is, transfer for energy from a DC source to an AC current source. The PWM schemes effectively controls the magnitude and frequency of the output voltage along with the reduction in harmonics.

MAIN FORMULAS OF THE CHAPTER

$$HF_n = \frac{V_n}{V_1}$$

$$\text{THD} = \frac{\sqrt{\sum_{n=2,3,\dots}^{\infty} V_n^2}}{V_1} = \frac{\sqrt{V_{rms}^2 - V_1^2}}{V_1}$$

$$\text{THD} = \frac{\sqrt{\sum_{n=2,3,\dots}^{\infty} \left(\frac{V_n}{n}\right)^2}}{V_1}$$

$$DF_n = \frac{V_n}{V_i n^2}$$

- Single PWM

$$V_0 = V_s \sqrt{\frac{\sigma}{\pi}}$$

- Multiple PWM

$$V_0 = V_s \sqrt{\frac{p\delta}{\pi}}$$

- Sinusoidal PWM

$$V_0 = V_s \left(\sum_{m=1}^{2p} \frac{\delta_m}{\pi} \right)^{\frac{1}{2}}$$

REFERENCES/FURTHER READING

1. J. Holtz, Pulse width modulation—A survey, *IEEE Trans. Industrial Electronics*, vol. 39, no. 5, pp. 410–420, 1992.
2. B. K. Bose, *Power Electronics and AC Drives*, Prentice Hall, Englewood Cliffs, NJ, 1986.
3. M. H. Rashid, *Power Electronics: Circuits, Devices, and Applications*, Pearson Education, Singapore, 2004.
4. P. S. Bhimra, *Power Electronics*, 4th edn, Khanna Publications, New Delhi, India, 2012.
5. G. C. Chryssis, *High-Frequency Switching Power Supplies*, 2nd edn, McGraw-Hill, New York, 1989.
6. P. T. Krein, *Elements of Power Electronics*, Oxford University Press, New York, 2003.
7. K. Thorborg, *Power Electronics*, Prentice Hall International, London, UK, 1988.
8. Internet source ijsetr.org.
9. S. N. Manias, *Inverters (DC–AC Converters)*, Elsevier BV, Taiwan, 2017.
10. I. Batarseh and A. Harb, *Power Electronics*, Springer Nature, Cham, Switzerland, 2018.
11. A. Tiwari and A. Khatik, Comparative analysis of switching techniques for three phase induction motor drive, *International Conference Information, Communication, Instrumentation and Control (ICICIC)*, 2017.
12. T. Banerjee, J. N. Bera, S. Chowdhuri, and G. Sarkar, A comparative study between different modulations techniques used in field-oriented control induction motor drive, *2nd International Conference Control, Instrumentation, Energy and Communication (CIEC)*, Kolkata, West Bengal, India, 2016.
13. T. Suntio, T. Messo, and J. Puukko, *Power Electronic Converters*, Wiley-VCH, Verlag GmbH, Germany, 2018.
14. V. Vodovozov and R. Jansikene, *Power Electronic Converters*, TUT, Tallinn, 2006.
15. R. W. Erickson, *Fundamentals of Power Electronics*, Chapman & Hall, New York, 1997.
16. P. C. Sen, *Principles of Electric Machines and Power Electronics*, John Wiley and Sons, Hoboken, NJ, 2010.

17. V. R. Moorthi, *Power Electronics Devices, Circuits and Industrial Applications*, Oxford University Press, New York, 2010.
18. S. N. Manias, *Power Electronics and Motor Drive Systems*, Academic Publishers, Taiwan, 2017.
19. F. Mazda, *Power Electronics Handbook*, Newnes, Burlington, MA, 1997.
20. B. M. Wilamowski and J. D. Irwin, *Power Electronics and Motor Drives*, CRC Press, New York, 2011.
21. D. O. Neacsu, *Switching Power Converters: Medium and High Power Electronics and Motor Drives*, CRC Press, Boca Raton, FL, 2014.
22. E. C. D. Santos Jr. and E. R. C. Da Silva, *Advanced Power Electronics Converters*, IEEE Press, Wiley, Hoboken, NJ, 2015.



Taylor & Francis

Taylor & Francis Group

<http://taylorandfrancis.com>

8 AC Voltage Controllers

8.1 INTRODUCTION

AC voltage controllers (or AC regulators) are AC-to-AC converters that convert fixed alternating voltage to variable alternating voltage at constant frequency. In these, relatively cheap converter-grade silicon-controlled rectifiers (SCRs) and TRIACS are used as switching devices as shown in [Figure 8.1](#). Because these devices are line commutated, there is no need for separate commutation circuits. The main disadvantage of AC voltage controllers is the introduction of objectionable harmonics in the supply current and load voltage [1–5]. However, because of their simplicity, AC voltage controllers are preferred for domestic and industrial heating and lighting loads, which are not affected by harmonics. There are two methods of voltage control:

1. On-off control or integral cycle control
2. Phase control

8.2 PRINCIPLE OF ON-OFF CONTROL

In this control, load is connected to the source for an integral number of cycles and then disconnected from the source for further number of integral cycles, as explained in [Figure 8.2](#) for a single-phase voltage controller with resistive load. That is why this method of voltage control is also called *integral cycle control* (ICC) [3,5,6].

Gate pulses trigger the thyristors T_1 , T_2 at zero-voltage crossings of the supply voltage. The source is connected to the load for $n = 2$ cycles. When gate pulses are withdrawn, the load remains disconnected from the source for $m = 1$ cycle. In this way, the process of turning on and turning off are repeated to control the load power, that is, by varying the number of n and m cycles, AC output voltage can be varied and controlled as per the required application. On-off control or ICC is also known as *burst firing, zero-voltage switching, cycle selection*.

Advantage of on-off control

1. It does not cause fluctuations in performance of the system.

Disadvantage of on-off control

2. It introduces subharmonics in the line current.

Applications of on-off control

3. Such control is used in heating applications, such as a furnace.

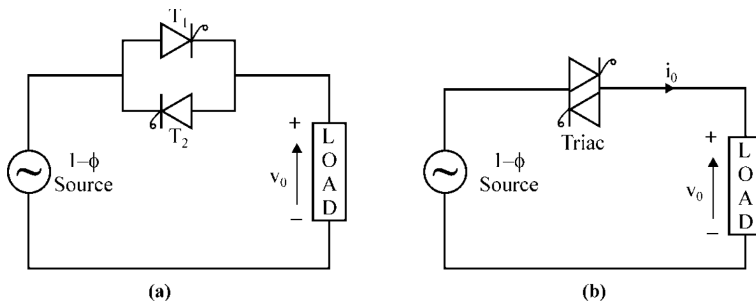


FIGURE 8.1 Power circuit diagram of single-phase AC voltage controller: (a) power circuit diagram using SCRs and (b) various waveform power circuit diagram using TRIAC.

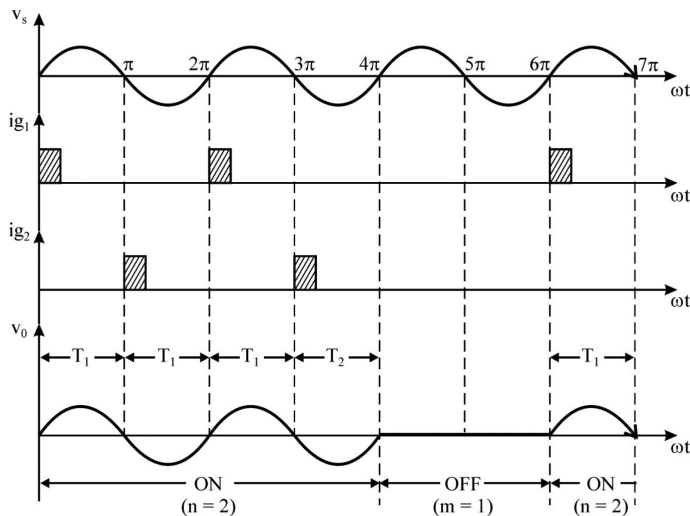


FIGURE 8.2 Output voltage control of single-phase AC voltage controller using on-off control or ICC.

Mathematical Analysis

If the load is connected to the source for n number of cycles and disconnected for m number of cycles, then

- **Root mean square (RMS) value of output voltage,**

$$V_{or} = \left[\frac{n}{2\pi(n+m)} \int_0^{2\pi} (V_m \sin \omega t)^2 d\omega t \right]^{\frac{1}{2}}$$

$$= \left[\frac{nm_m^2}{4\pi(n+m)} \int_0^{2\pi} (1 - \cos 2\omega t) d\omega t \right]^{\frac{1}{2}}$$

or

$$V_{or} = \frac{V_m}{\sqrt{2}} \sqrt{\frac{n}{n+m}} = V_s \sqrt{\frac{n}{n+m}}$$

$$V_{or} = V_s \sqrt{K} \quad (8.1)$$

where

V_s = RMS value of source voltage

$$K = \frac{n}{n+m} = \text{duty cycle of AC voltage controller}$$

- **RMS load current,**

$$I_{or} = \frac{V_{or}}{R} \quad (8.2)$$

- **Power delivered to load**

$$= \frac{V_{or}^2}{R} = \frac{V_s^2}{R} \left(\frac{n}{n+m} \right) = \frac{KV_s^2}{R} \quad (8.3)$$

- **RMS value of input current,**

$$I_s = \text{RMS value of load current} \quad (8.4)$$

- **Input VA = $V_s I_s$** (RMS value of source current)

$$= V_s \cdot I_s = V_s \cdot = V_s \cdot \frac{V_{or}}{R} \quad (8.5)$$

- **Input power factor (PF),**

$$\begin{aligned} \text{PF} &= \frac{\text{Output power}}{\text{Input power}} = \frac{\text{Power delivered to load}}{\text{Input VA}} \\ &= \left(\frac{V_{or}^2}{R} \right) \cdot \frac{R}{V_s \cdot V_{or}} \end{aligned} \quad (8.6)$$

or

$$\text{PF} = \frac{V_{or}}{V_s} = \sqrt{K}$$

- **Average value of thyristor current, (I_T)**

$$(I_T)_{avg} = \frac{n}{2\pi(n+m)} \int_0^\pi I_m \cdot \sin \omega t \cdot d\omega t$$

or

$$(I_T)_{avg} = \frac{K \cdot I_m}{\pi} \quad (8.7)$$

- RMS value of thyristor current, $(I_T)_{\text{rms}}$

$$(I_T)_{\text{rms}} = \left[\frac{n}{2\pi(n+m)} \int_0^\pi (I_m \sin \omega t)^2 \cdot d\omega t \right]^{\frac{1}{2}}$$

or

$$(I_T)_{\text{rms}} = \frac{I_m \sqrt{k}}{2} \quad (8.8)$$

From Equation (8.1), it is clear that output voltage can be controlled in steps only. Therefore, a smooth and fine voltage variation is not possible. For increasing the resolution of steps, the total numbers of control cycles ($n + m$) are to be increased, which cause large fluctuations in the output voltage. This is the main hurdle in the adoption of on-off technique. If on and off periods (n and m) are reduced to overcome this demerit, it limits the controllability.

8.3 PRINCIPLE OF PHASE CONTROL

In case of on-off control or ICC method, the output voltage is controlled by opening and closing the switch for one or several cycles of the AC input voltage. While in the case of phase-controlled switching, the output voltage is controllable by opening and closing the switch within a cycle as shown in Figure 8.3 for circuits shown in Figure 8.2a for resistive load [2,3,5].

In ICC control, the load is disconnected from the source in steps of the half cycles, but, in the case of phase control, the disconnection of the load from the source is

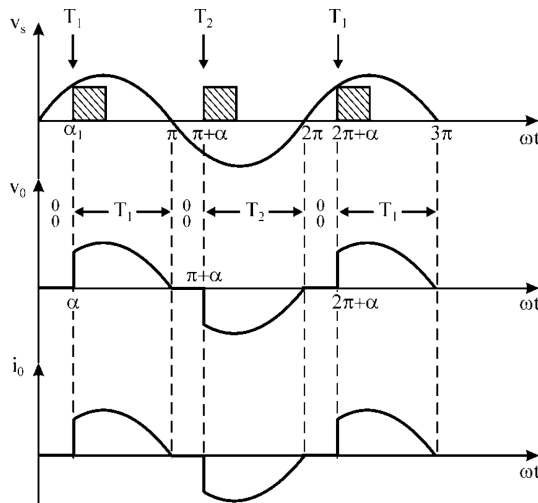


FIGURE 8.3 Output voltage control by phase-controlled method.

maintained within each cycle; therefore, a fine output control is possible. The power circuit configuration of on-off control differs in no way from those for phase control, but the trigger circuits are different.

Advantages of phase control

1. More fine output control of voltage is possible.
2. No transformer is necessary, so the size, weight, and cost are small and efficiency is very high.

8.4 SINGLE-PHASE AC VOLTAGE CONTROLLERS

Figure 8.4 shows various possible configurations of single-phase full-wave AC voltage controllers [2,3,5]. Here, either two thyristors (SCRs), one TRIAC, one SCR with a diode bridge, or a bridge with two SCRs and two diodes can be used as a switch.

8.4.1 SINGLE-PHASE FULL-WAVE AC VOLTAGE CONTROLLER WITH RESISTIVE LOAD

Power circuit and various waveforms for single-phase full-wave AC voltage controller with resistive loads are shown in Figure 8.5 [2,3,5]. Here, the principle of AC phase control is applied in both the half cycles. Thyristors T_1 and T_2 are in the forward-blocking mode during positive and negative half cycles of input supply, respectively.

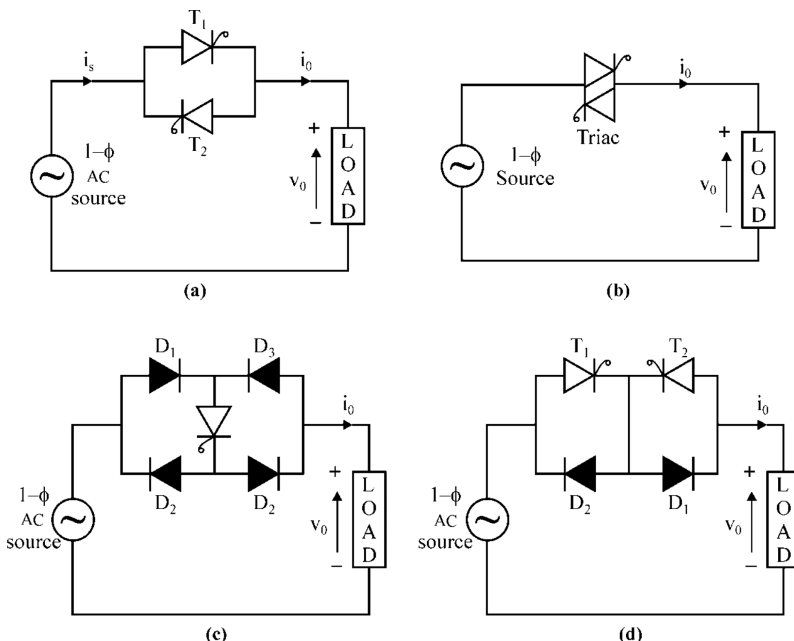


FIGURE 8.4 (a-d) Various circuit configurations for single-phase full-wave AC voltage controllers.

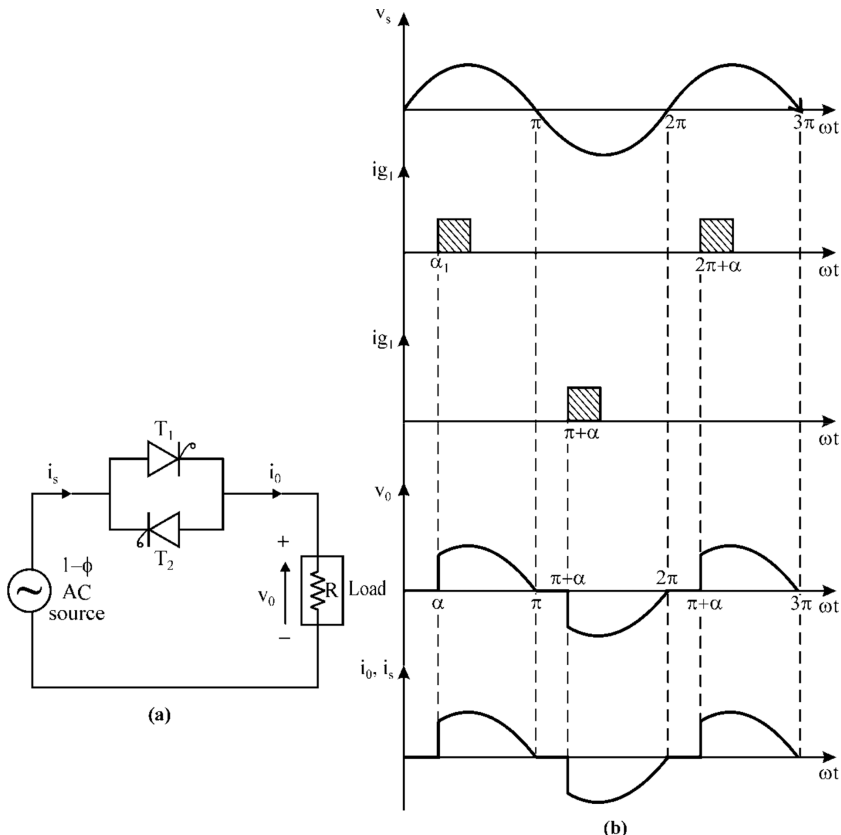


FIGURE 8.5 Single-phase AC voltage controller with R load (a) power circuit diagram, and (b) various waveform.

During a positive half cycle, T_1 is triggered at a firing angle α . So, it starts conducting, and the source voltage is applied to the load from α to π as shown in Figure 8.5b. At π , as supply voltage v_s becomes zero, so the load voltage v_0 and current i_0 also fall to zero because the load is resistive. Just after π , T_1 is reverse biased and therefore gets turned off by natural or line commutation.

During a negative half cycle, T_2 is triggered at $(\pi + \alpha)$. It conducts from $(\pi + \alpha)$ to 2π . Soon after 2π , T_2 is reverse biased, and so it gets turned off. In this way, the cycle repeats. It can be seen from the waveform of Figure 8.5b that the output voltage is symmetrical in both the half cycles.

- The RMS value of output voltage, V_{or}

$$V_{or} = \left[\frac{1}{\pi} \int_{\alpha}^{\pi} (V_m \sin \omega t)^2 \cdot d\omega t \right]^{\frac{1}{2}}$$

or

$$V_{or} = \frac{V_m}{\sqrt{2}} \left[\frac{1}{\pi} \left\{ (\pi - \alpha) + \frac{1}{2} \sin 2\alpha \right\} \right]^{\frac{1}{2}} \quad (8.9)$$

- The RMS load current, I_{or}

$$I_{or} = \frac{V_{or}}{R} = \text{RMS value of source current} \quad (8.10)$$

$$\text{Power delivered to load} = I_{or}^2 R = \frac{V_{or}^2}{R} \quad (8.11)$$

- The PF:

$$\text{PF} = \frac{V_{or}}{V_s} = \left\{ \frac{1}{\pi} \left[(\pi - \alpha) + \frac{1}{2} \sin 2\alpha \right] \right\}^{\frac{1}{2}} \quad (8.12)$$

8.4.2 SINGLE-PHASE FULL-WAVE AC VOLTAGE CONTROLLER WITH RL LOAD

The power circuit diagram and various waveforms of single-phase AC voltage controllers with RL load are shown in [Figure 8.6](#).

Working operation with an RL load is the same as that with an R load, except the difference that, due to the inductive nature of the load, the load voltage and current are not in phase. Due to the inductive load, the load current i_0 rises and decays gradually, so it does not reduce to zero at $\omega t = \pi$; rather reduces to zero at $\omega t = \beta$, where $\beta > \pi$ as shown in waveforms of [Figure 8.6b](#). Here also, thyristors are turned off by natural or line commutation.

If $\alpha \leq \phi$, where ϕ is PF angle or impedance angle of RL load, and $\phi = \tan^{-1} \left(\frac{\omega L}{R} \right)$, then the control becomes ineffective, and so the output voltage remains same as that of the input sinusoidal voltage ($v_0 = v_s$). But if $\alpha \geq \phi$, then commutation of thyristor takes place at extinction angle β , where the load or thyristor current becomes zero as shown in [Figure 8.6b](#).

- The expression for instantaneous load current i_0 can be obtained as [2,3,5]

During period $\alpha < \omega t < \beta$, when thyristor T_1 is on, the voltage equation for the circuit of [Figure 8.6a](#) is

$$v_s = V_m \sin \omega t = R i_0 + L \frac{di_0}{dt}$$

Its solution is of the form

$$i_0 = \frac{V_m}{Z} \sin(\omega t - \varphi) + A e^{-(R/L)t} \quad (8.13)$$

where $Z = \sqrt{R^2 + (\omega L)^2}$

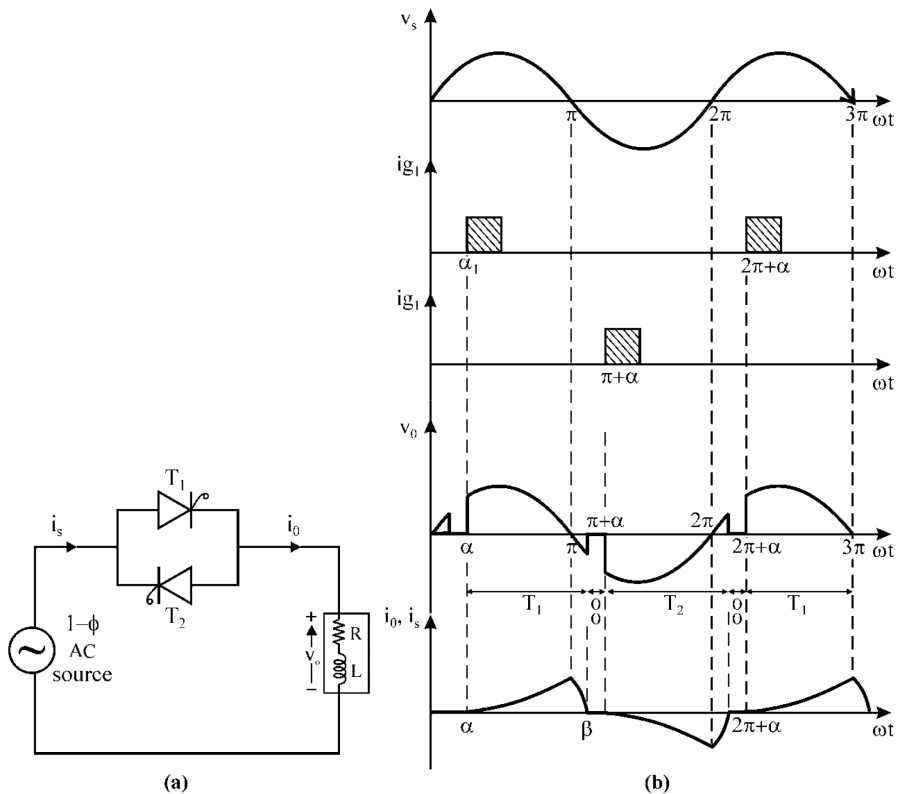


FIGURE 8.6 1- ϕ AC voltage controller with RL load: (a) power circuit diagram and (b) various waveform.

$$\varphi = \tan^{-1} \left(\frac{\omega L}{R} \right) \quad (8.14)$$

Constant A can be obtained using initial boundary conditions, that is, at $\omega t = \alpha, i_0 = 0$.

Therefore,

$$0 = \frac{V_m}{Z} \sin(\alpha - \varphi) + A e^{-\frac{R\alpha}{L\omega}}$$

or

$$A = \frac{-V_m}{Z} \sin(\alpha - \varphi) e^{\frac{R\alpha}{L\omega}}$$

Substitution of this value of A in Equation (8.13) gives i_0 as

$$i_0 = \frac{V_m}{Z} \left[\sin(\omega t - \varphi) - \sin(\alpha - \varphi) \exp \left\{ \frac{R}{L} \left(\frac{\alpha}{\omega} - t \right) \right\} \right] \quad (8.15)$$

The value of β can be found by solving the above equation for $i_0(\beta) = 0$, which gives

$$\sin(\beta - \varphi) = \sin(\alpha - \varphi) \cdot \exp\left[\frac{R}{L}\left(\frac{\alpha - \beta}{\omega}\right)\right] \quad (8.16)$$

and the conduction angle γ during which current flows from angle α to angle β is given by

$$\gamma = \beta - \alpha \quad (8.17)$$

8.4.3 SINGLE-PHASE FULL-WAVE AC VOLTAGE CONTROLLER WITH PURELY INDUCTIVE LOAD

The power circuit diagram and various waveforms of a transistor-controlled reactor (TCR) or AC voltage controller with purely inductive load are shown in Figure 8.7 [2,3,5]. For a purely inductive load, $\phi = 90^\circ$. Therefore, the output voltage control is only effective during $\pi/2 \leq \alpha \leq \pi$ for which v_0 varies from V_{or} to 0.

- The expression for load current is given by:

$$\begin{aligned} i_0(\omega t) &= \frac{V_m}{\omega L} \left[\sin\left(\omega t - \frac{\pi}{2}\right) - \sin\left(\alpha - \frac{\pi}{2}\right) \exp\left(\frac{\alpha - \omega t}{\tan(\pi/2)}\right) \right] \\ &= \frac{V_m}{\omega L} (\cos \alpha - \cos \omega t) \end{aligned} \quad (8.18)$$

The value of β can be found as

$$i_0(\beta) = 0 = \cos \alpha - \cos \beta$$

this gives,

$$\beta = 2\pi - \alpha \quad (8.19)$$

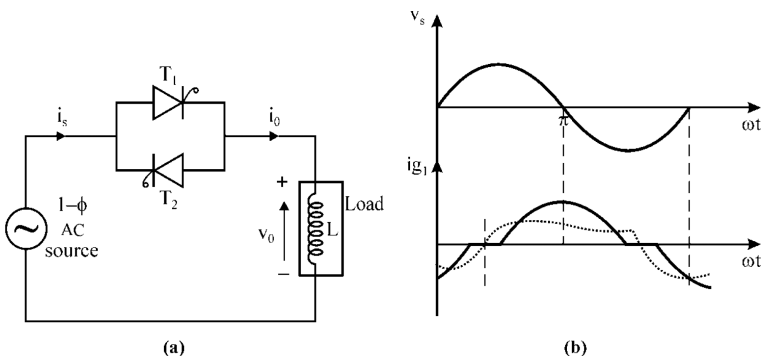


FIGURE 8.7 Single-phase AC voltage controller with L load or TCR: (a) power circuit diagram and (b) voltage and current waveform of TCR or L load.

8.5 THREE-PHASE FULL-WAVE AC VOLTAGE CONTROLLERS

Three phase controllers of bidirectional nature are preferred over unidirectional controllers for AC drives due to lower harmonic contents. Various configurations for three-phase AC voltage controllers are shown in [Figure 8.8](#) [2,3,5].

8.6 SOLVED PROBLEMS

Example 8.1: For a delay angle of 120° , find the RMS load current, RMS thyristor current, and input PF for single-phase full-wave AC voltage controller delivering power to resistive load of 5 W. The input AC voltage is 230 V at 50 Hz.

SOLUTION

RMS load voltage is given by

$$\begin{aligned}V_{or} &= V_s \left[\frac{1}{\pi} \left\{ (\pi - \alpha) + \frac{\sin 2\alpha}{2} \right\} \right]^{1/2} \\&= 230 \left[\left(\frac{1}{\pi} \right) \left\{ \frac{\pi}{3} - \frac{0.866}{2} \right\} \right]^{1/2} \\&= 101.69 \text{ V}\end{aligned}$$

RMS load current is given by

$$\begin{aligned}I_{or} &= V_{or}/R \\&= 101.69/5 \\&= 20.34 \text{ A}\end{aligned}$$

$$\text{RMS thyristor current} = I_{or}/\sqrt{2} = 20.34/\sqrt{2} = 14.38 \text{ A}$$

Input PF is given by

$$\begin{aligned}\text{PF} &= \left[\frac{1}{\pi} \left\{ (\pi - \alpha) + \frac{1}{2} \sin 2\alpha \right\} \right]^{1/2} \\&= \left[\frac{1}{\pi} \left\{ \frac{\pi}{3} - \frac{0.866}{2} \right\} \right]^{1/2} \\&= 0.442 \text{ lag}\end{aligned}$$

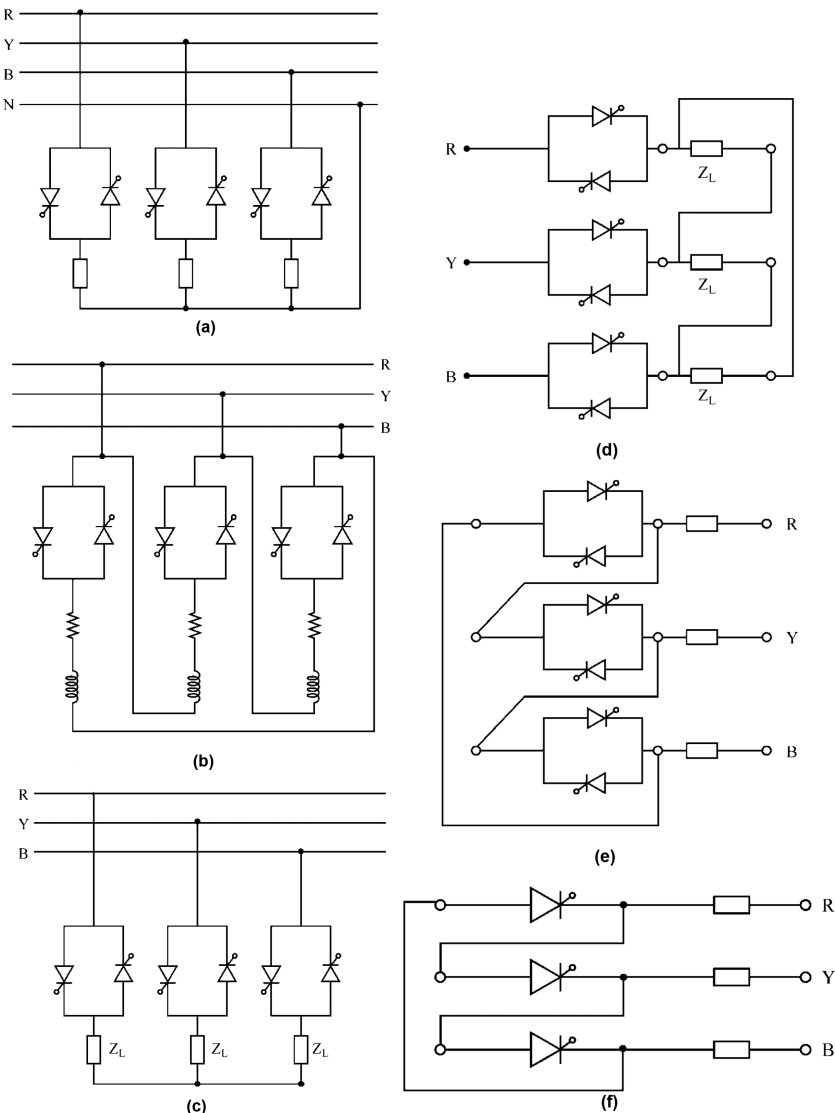


FIGURE 8.8 Three-phase AC voltage controller: (a) three-phase four-wire voltage controller, (b) delta-connected voltage controller, (c) symmetrical three-phase three-wire voltage controller, (d) three-wire voltage controller feeding a delta-connected load, (e) three-phase delta controller, and (f) three-phase half-wave delta controller.

Example 8.2: An AC voltage regulator operating from 230 V, 50 Hz delivers power to 10Ω load using ICC. If it conducts for 18 cycles and remains off for 32 cycles. Find

- RMS value of output voltage, V_{or}
- Power output to the load

- (c) Power input to the regulator
- (d) Input PF
- (e) Average and RMS values of SCR current (neglect losses).

SOLUTION

Duty ratio,

$$k = \frac{18}{18+32} = 0.36$$

- (a) RMS value of the output voltage,

$$V_{or} = 230\sqrt{0.36} = 138 \text{ V}$$

- (b) Power output to the load,

$$\frac{V_{or}^2}{R_L} = \frac{138^2}{10} = 1904.4 \text{ W}$$

- (c) Power input to the regulator

$$= 1904.4 \text{ W as losses are neglected.}$$

- (d) Input PF,

$$\frac{\text{Real power}}{\text{Apparent power}} = \frac{1904.4}{230 I_{or}}$$

But

$$I_{or} = \frac{V_{or}}{R_L} = \frac{138}{10} = 13.8 \text{ A}$$

Substituting for I_{or} the input PF = 0.6 lag

$$(e) I_m = \frac{230\sqrt{2}}{10} = 32.522 \text{ A}$$

$$\text{RMS value of thyristor current} = \frac{I_m\sqrt{k}}{2} = \frac{32.522 \times 0.6}{2} = 9.756 \text{ A}$$

$$\text{Average value of thyristor current} = \frac{k I_m}{\pi} = 3.727 \text{ A}$$

Example 8.3: A single-phase AC voltage controller supplied from 230 V, 50 Hz AC input is connected to a resistive load of 10 Ω. Find the RMS load voltage, RMS load current, power input, and load PF for a delay angle of 90°.

SOLUTION

RMS load voltage,

$$V_{or} = V_s \left[\frac{1}{\pi} \left\{ (\pi - \alpha) + \frac{\sin 2\alpha}{2} \right\} \right]^{1/2}$$

$$= 230 \left[\frac{1}{\pi} \left\{ \left(\pi - \frac{\pi}{2} \right) + \frac{1}{2} \sin \frac{2\pi}{2} \right\} \right]^{1/2}$$

$$= \frac{230}{\sqrt{2}} = 162.66 \text{ V}$$

RMS load current,

$$I_{or} = \frac{V_{or}}{R} = \frac{162.66}{10} = 16.26 \text{ A}$$

$$\text{Power input to load} = 16.26^2 \times 10 = 2644 \text{ W}$$

Load PF,

$$\text{PF} = \frac{V_{or} I_{or}}{V_s I_{or}} = \frac{V_{or}}{V_s} = \frac{162.66}{230} = 0.7$$

Example 8.4: A single-phase AC chopper supplied from 230 V, 50 Hz AC input and is connected to a resistive load of 30Ω . Find the RMS load voltage and RMS load current for a firing angle of 45° .

SOLUTION

$$\text{PF} = \frac{V_{or} I_{or}}{V_s I_{or}} = \frac{V_{or}}{V_s} = \frac{162.66}{230} = 0.7$$

$$= 230 \left[\frac{1}{\pi} \left\{ \frac{3\pi}{4} + \frac{1}{2} \right\} \right]^{1/2}$$

$$= 219.3 \text{ V}$$

$$I_{or} = \frac{219.3}{30} = 7.31 \text{ A}$$

Example 8.5: A single-phase AC voltage controller is supplied from 230 V, 50 Hz AC input. It is connected to an inductive load with a resistance of 10Ω and load impedance angle of 45° . Determine the maximum load voltage, maximum load current, and range of delay angle for which the load voltage does not change.

SOLUTION

Load impedance angle or load phase angle, $\phi = 45^\circ$

Maximum RMS load voltage can only be the supply voltage; hence, it is 230 V.

$$\tan \varphi = \frac{X_L}{R} = 1$$

$$\therefore R = X_L = 10 \text{ W}$$

$$Z = 10\sqrt{2} \Omega$$

Maximum RMS load current, $I_{\max} = \frac{230}{10\sqrt{2}} = 23 \times 0.707 = 16.261 \text{ A (rms)}$
 Range of delay angle = 0° to 45°

Example 8.6: A TRIAC-based AC voltage controller is used to control resistance heating in the phase-angle control mode. Find the firing angle delay when the load power is 50% of its maximum value.

$$\left[\frac{1}{\pi} \left\{ (\pi - \alpha) + \frac{\sin 2\alpha}{2} \right\} \right] = \frac{50}{100} = \frac{1}{2}$$

$$1 - \frac{\alpha}{\pi} + \frac{\sin 2\alpha}{2\pi} = \frac{1}{2}$$

By inspection, $\alpha = \pi/2$

Example 8.7: A single-phase voltage controller supplied from 230 V, 50 Hz AC input controls the power input to a load circuit consisting of $R = 3 \Omega$ and $\omega L = 4 \Omega$, calculate

- (a) Control range of firing angle,
- (b) Maximum value of RMS load current,
- (c) Maximum power input to the load,
- (d) Maximum PF, and
- (e) Maximum value of average and RMS thyristor current.

SOLUTION

- (a) Control range of firing angle: ϕ to π
 Load phase angle $\phi = \tan^{-1} \frac{\omega L}{R} = \tan^{-1} \frac{4}{3} = 1.333 = 53.13^\circ$
- (b) The maximum value of load current i_0 occurs when $\alpha = 53.13^\circ$. But at this value of firing angle, the controller behaves as if the load is directly connected to the AC source.
 \therefore The maximum value of RMS load current $= \frac{230}{\sqrt{R^2 + \omega^2 L^2}} = \frac{230}{\sqrt{3^2 + 4^2}} = 46 \text{ A}$
- (c) Maximum power input to the load $= I_0^2 R = 6348 \text{ W}$
- (d) Maximum PF $= \frac{6348}{230 \times 46} = 0.6 = \cos \phi$
- (e) Maximum value of thyristor current, $I_{th \text{ rms}} = \frac{i_0}{\sqrt{2}} = \frac{46}{1.414} = 32.527 \text{ A}$
 Average value of SCR current, $I_{th \text{ rms}} = \frac{I_{th \text{ rms}}}{1.57} = 20.707 \text{ A}$

Example 8.8 A single-phase voltage controller is supplied from 230 V, 50 Hz AC input for controlling the power flow into a load circuit consisting of $R = 3\Omega$ and $\omega L = 4\Omega$. Determine the control range of the firing angle, maximum value of RMS load current, power and PF, maximum values of average and RMS thyristor currents, maximum possible value of di/dt , and the conduction angle for $\alpha = 0^\circ$ and $\alpha = 120^\circ$ assuming a gate pulse of duration π radian.

SOLUTION

- (a) For controlling the load, the minimum value of firing angle $\alpha = \text{load phase angle}$, $\phi = \tan^{-1} \frac{\omega L}{R} = \tan^{-1} \frac{4}{3} = 53.13^\circ$. The maximum possible value of α is 180° .
- (b) The maximum value of the RMS load current i_0 occurs when $\alpha = \phi = 53.13^\circ$. But at this value of firing angle, the controller behaves as if load is directly connected to the AC source. Therefore, the maximum value of the RMS load current is

$$i_0 = \frac{230}{\sqrt{R^2 + (\omega L)^2}} = \frac{230}{\sqrt{3^2 + 4^2}} = 46 \text{ A}$$

- (c) Maximum power = $i_0^2 R = 46^2 \times 3 = 6348 \text{ W}$

$$\text{PF} = \frac{i_0^2 R}{V_s i_0} = \frac{46 \times 3}{230} = 0.6$$

- (d) Average thyristor current is maximum when $\alpha = \phi$ and conduction angle $\gamma = \pi$.

$$\begin{aligned} I_{TAVM} &= \frac{1}{2\pi} \int_{\alpha}^{\alpha+\pi} \frac{V_m}{Z} \sin(\omega t - \phi) d(\omega t) \\ &= \frac{V_m}{2Z} = \frac{\sqrt{2} \times 230}{\pi \times \sqrt{3^2 + 4^2}} = 32.527 \text{ A} \end{aligned}$$

- (e) Maximum value of $\frac{di_0}{dt}$ occurs when $\alpha = \phi$

$$\frac{di_0}{dt} = \frac{\omega V_m}{Z} \cos(\omega t - \phi) - 0$$

Its value is maximum when $\cos(\omega t - \phi) = 1$

$$\therefore \left(\frac{di_0}{dt} \right)_{\max} = \frac{\sqrt{2} \cdot 230 \cdot 2\pi \times 50}{5} = 2.0437 \times 10^4 \text{ A/s}$$

- (f) For $\alpha = 0^\circ$, the conduction angle γ is 180° . For $\alpha = 120^\circ$ and $\phi = 53.13^\circ$ gives a conduction angle of about 95° .

REVIEW QUESTIONS

- 8.1 List two methods of voltage control employed in AC voltage controllers.
- 8.2 Write the expression for the output voltage of AC voltage controller employing ICC.
- 8.3 Draw the circuit of a bidirectional switch using a common cathode.
- 8.4 Sketch the circuit of single-phase AC chopper that uses common cathode-connected SCRs.
- 8.5 What is the control range of the firing angle of single-phase bidirectional controller supplying an RL load?
- 8.6 What is the load angle in connection with an RL load?
- 8.7 Mention the advantages and disadvantages of AC voltage controllers.
- 8.8 List the applications of AC voltage controllers.
- 8.9 For the single-phase AC voltage controller, discuss how single-pulse gating is not suitable, and show that high-frequency carrier gating overcomes the problems due to single-frequency gating.
- 8.10 Explain the reason for using inverse parallel-connected SCRs in preference to TRIAC in the AC voltage controllers feeding highly inductive loads.
- 8.11 Explain the operation of a solid-state tap changer using antiparallel SCRs. How can this be used as an AC voltage stabilizer?
- 8.12 Write short notes on AC voltage regulators using thyristors.
- 8.13 Discuss the operation of a single-phase AC voltage controller with an inductive load. Draw the relevant voltage waveforms.
- 8.14 Draw the power circuitry for a single-phase AC voltage controller using a thyristor and explain its operation for a resistive load. Also derive an expression for RMS load voltage.
- 8.15 Prove that the form-factor of SCR current of an AC chopper feeding resistance load is $\frac{\sqrt{\pi}}{(1+\cos\alpha)} \left[(\pi - \alpha) + \frac{\sin 2\alpha}{2} \right]^{1/2}$ where α is the firing angle.
- 8.16 Investigate the operation of a single-phase AC voltage controller supplying RL load when the firing angle α is
 1. Less than the load angle ϕ
 2. Equal to load angle ϕ
 3. Greater than the load angle ϕ

SUMMARY

This chapter has studied in detail the principles of different AC voltage controllers along with their controls. It can be seen that two types of control strategies, that is, phase control and ICC, can be effectively used to control the power flow in AC voltage controllers. Few main applications of such converters are for industrial and domestic heating, lighting control, starting of induction motors, motion control of AC drives, etc. AC voltage controllers have replaced the use of magnetic amplifiers, reactors, auto transformers, etc. for these applications due to faster control, high efficiency, less maintenance, and being compact in size.

MAIN FORMULAS OF THE CHAPTER

- Single-phase AC voltage controller with ICC

$$V_{or} = \frac{V_m}{\sqrt{2}} \sqrt{\frac{n}{n+m}} = V_s \sqrt{\frac{n}{n+m}}$$

$$I_{or} = \frac{V_{or}}{R}$$

$$\text{Power delivered to load} = \frac{V_{or}^2}{R} = \frac{V_s^2}{R} \left(\frac{n}{n+m} \right) = \frac{KV_s^2}{R}$$

$$PF = \frac{V_{or}}{V_s} = \sqrt{K}$$

$$(I_T)_{avg} = \frac{K \cdot I_m}{\pi}$$

$$(I_T)_{rms} = \frac{I_m \sqrt{k}}{2}$$

REFERENCES/FURTHER READING

1. B. K. Bose, *Power Electronics and AC Drives*, Prentice Hall, Englewood Cliffs, NJ, 1986.
2. A. Chattopadhyay, *AC-AC converters*. In: M. H. Rashid (Ed.), *Power Electronics Handbook*, Academic Press, London, 2007.
3. M. H. Rashid, *Power Electronics: Circuits, Devices, and Applications*, Pearson Education, Singapore, 2004.
4. P. T. Krein, *Elements of Power Electronics*, Oxford University Press, New York, 2003.
5. P. S. Bhimra, *Power Electronics*, 5th edn, Khanna Publications, New Delhi, India, 2012.
6. K. Thorborg, *Power Electronics*. Prentice Hall International, London, UK, 1988.
7. A. Imran, S. Nehal, and M. Dey, Introducing antiparallel back-to-back connected thyristor for speed control of three phase induction motor, *International Conference on Electrical, Computer and Communication Engineering (ECCE), IEEE*, 2017.
8. S. N. Manias, *AC Voltage Controllers and Thyristor-Based Static VAR Compensators*, Elsevier, Amsterdam, the Netherlands, 2017.
9. E. A. Qasmi, W. Sun, J. Soomro, M. U. Tahir, and F. A. Chachar, Power quality analysis of phase controlled bidirectional and unidirectional AC voltage controllers and their impacts on input power system, *2nd International Conference on Computing, Mathematics and Engineering Technologies (iCoMET), IEEE*, 2019.
10. F. L. Luo, *Traditional AC/AC Converters*, Industrial Electronics, Boca Raton, FL, 2012.
11. R. W. Erickson, *Fundamentals of Power Electronics*, Chapman & Hall, New York, 1997.
12. V. R. Moorthi, *Power Electronics Devices, Circuits and Industrial Applications*, Oxford University Press, Oxford, 2010.

13. T. Suntio, T. Messo, and J. Puukko, *Power Electronic Converters*, Wiley-VCH, Verlag GmbH, Germany, 2018.
14. A. M. Trzynadlowski, *Introduction to Modern Power Electronics*, 3rd edn, John Wiley & Sons, New York, 2010.
15. A. M. Trzynadlowski, *Power Electronic Converters and Systems*, Institution of Engineering and Technology, London, UK, 2016.
16. B. M. Wilamowski and J. D. Irwin, *Power Electronics and Motor Drives*, CRC Press, Boca Raton, FL, 2011.
17. E. Acha, V. G. Agelidis, O. Anaya-Lara, and T. J. E. Miller, *Power Electronic Control in Electrical Systems*, Newnes, Oxford, 2002.
18. F. Mazda, *Power Electronics Handbook*, Newnes, Oxford, 1997.
19. F. Blaabjerg, *Control of Power Electronic Converters and Systems*, Academic Publishers, London, UK, 2018.
20. S. N. Manias, *Power Electronics and Motor Drive Systems*, Academic Publishers, London, UK, 2017.

9 Cycloconverter

9.1 INTRODUCTION

The cycloconverter is a one-stage frequency changer that converts AC power at one input frequency to output AC power at different frequency. Cycloconverters are widely used in various applications, such as induction heating; slip-power recovery scherbius drives; static VAr generation and variable-speed constant frequency (VSCF) power generation for aircraft or shipboards; and speed control of high-power AC drives in cement, ball mills, and rolling mills [1–22].

9.2 CLASSIFICATIONS

1. **On the basis of its operation:**
 - a. Step-up cycloconverter, that is, $f_o > f_i$.
 - b. Step-down cycloconverter, that is, $f_o < f_i$.
2. **On the basis of configuration:**
 - a. Midpoint-type cycloconverter
 - b. Bridge-type cycloconverter

9.3 PRINCIPLE OF OPERATION OF SINGLE-PHASE TO SINGLE-PHASE CYCLOCONVERTER

Basic principle of operation and working of single-phase to single-phase step-up as well as step-down cycloconverter is explained as follows [4–8].

9.3.1 SINGLE-PHASE TO SINGLE-PHASE STEP-UP CYCLOCONVERTER

The power circuit diagram for single-phase to single-phase midpoint and bridge-type cycloconverters is drawn in [Figure 9.1](#) [4,5,8,10]. The step-up cycloconverter requires *forced commutation* for turning off the thyristors.

9.3.1.1 Midpoint Cycloconverter

The power circuit consists of four thyristors and transformer with midtap on the secondary winding. Two of these thyristors P_1, P_2 are for the positive group, and the other two N_1, N_2 are for the negative group as shown in [Figure 9.1a](#). Directions of voltage and current marked in the figure are taken as positive.

During the positive half cycle, terminal “*a*” is positive with respect to terminal “*b*,” and so thyristors P_1 and N_2 are in a forward-blocking mode from $\omega t = 0$ to $\omega t = \pi$. Therefore, at $\omega t = 0$, thyristor P_1 is triggered, so the load gets connected with a supply, and the load voltage v_0 follows the positive envelope of the supply voltage

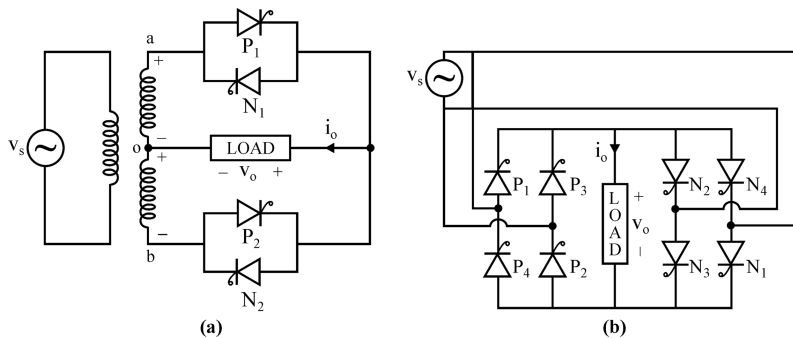


FIGURE 9.1 Single-phase to single-phase cycloconverter: (a) midpoint type and (b) bridge type.

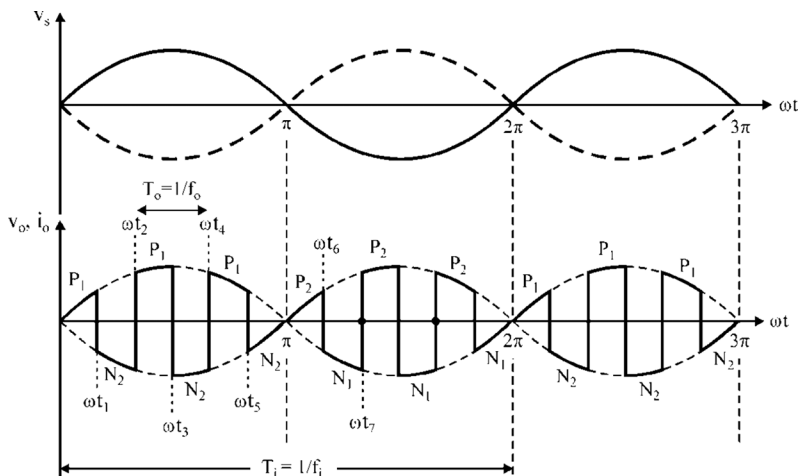


FIGURE 9.2 Waveforms for step-up cycloconverter (midpoint type).

as shown in [Figure 9.2](#). At instant ωt_1 , thyristor P_1 is force commutated, and the forward-biased thyristor N_2 is triggered so that load voltage v_0 now follows the negative envelope of the supply voltage as shown in [Figure 9.2](#). At ωt_2 , thyristor N_2 is force commutated, and P_1 is triggered again. So the load voltage v_0 is now positive and follows the positive envelope of the supply voltage as shown. In this way, thyristor P_1 and N_2 are turned on and off during the positive half cycle.

During the negative half cycle, terminal “*b*” is positive with respect to terminal “*a*,” and so thyristors P_2 and N_1 are in a forward-blocking mode from $\omega t = \pi$ to $\omega t = 2\pi$. Therefore, at $\omega t = \pi$, thyristor N_2 is forced commutated, and the forward-biased thyristor P_2 is triggered. So, the load voltage becomes positive and follows the positive envelope of the supply voltage as shown. At ωt_6 , thyristor P_2 is force commutated, and the forward-biased thyristor N_1 is triggered. So, the load voltage becomes negative and follows the negative envelope of the supply voltage as shown in [Figure 9.2](#).

It can also be seen that when positive-group silicon-controlled rectifiers (SCRs) conduct, the load voltage follows a positive envelope of the supply voltage, and when negative-group SCRs conduct, it follows a negative envelope of the supply voltage. In this way, SCRs P_1 and N_2 conduct for a positive half cycle of the supply and P_2, N_1 in the negative half cycle of the supply. These are therefore switched on alternately between positive and negative envelopes at a high frequency. As a result, output AC voltage of frequency f_o higher than the input supply frequency f_i is obtained.

In Figure 9.2, f_i is the input supply frequency, and f_o is the output frequency. As can be seen from the waveform that output frequency is $f_o = 6f_i$, that is, the step-up operation is achieved. Therefore, it should be noted that frequency of output voltage f_o depends on the rate of triggering of positive- and negative-group SCRs alternately in each half cycle of the supply.

9.3.1.2 Bridge-Type Cycloconverter

The power circuit for single-phase to single-phase bridge-type cycloconverters consists of eight thyristors, that is, four for the positive group (P_1 to P_4) and four for the negative group (N_1 to N_4) as shown in Figure 9.1b.

As can be seen from the Figure 9.1b, during the positive half cycle of the supply voltage, thyristor pairs P_1, P_2 and N_1, N_2 are in the forward-blocking mode. When forward-biased thyristors P_1, P_2 are triggered together at $\omega t = 0$, the load voltage is positive and follows the positive envelope of the supply voltage as shown in Figure 9.3. At ωt_1 , thyristor pair P_1, P_2 is force commutated, and the forward-biased pair N_1, N_2 is triggered. So, now the load voltage is negative and follows a negative envelope of the supply voltage as shown. At ωt_2 , pair N_1, N_2 is force commutated, and pair P_1, P_2 is triggered. So, the load voltage becomes positive and follows the positive envelope of the supply voltage.

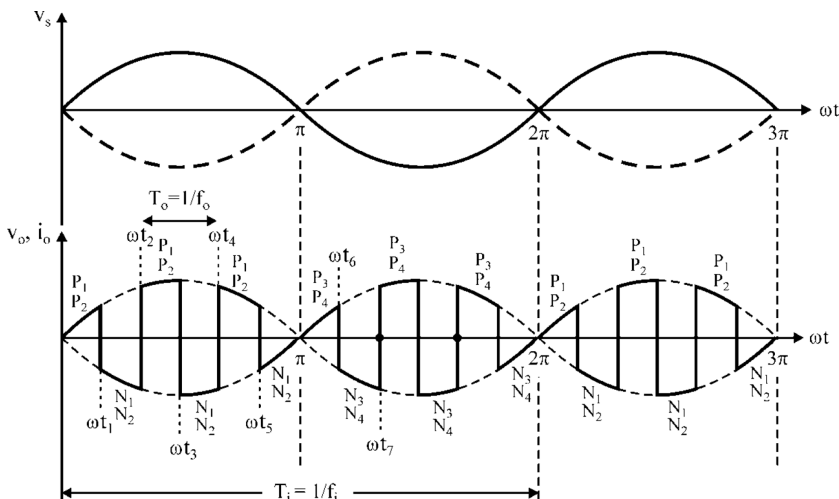


FIGURE 9.3 Waveforms for step-up cycloconverter (bridge type).

During the negative half cycle, thyristor pairs P_3, P_4 and N_3, N_4 are in the forward-blocking mode. Therefore, these pairs are turned on and force commutated during the negative half cycle as shown in [Figure 9.3](#). In this way, a high-frequency turning-on and force commutation of pairs P_1P_2, N_1N_2 and pairs P_3P_4, N_3N_4 give output voltage of frequency greater than input supply frequency.

9.3.2 SINGLE-PHASE TO SINGLE-PHASE STEP-DOWN CYCLOCONVERTER

In a step-down cycloconverter, the frequency of output voltage f_o is less than the input supply frequency f_i , that is, $f_o < f_i$. It also does not require forced commutation for turning off the thyristors. Rather, thyristors are turned off by line or natural or class F commutation, which is provided by an AC supply. The power circuit diagram for midpoint-type and bridge-type step-down cycloconverters is shown in [Figure 9.1a](#) and [b](#), respectively.

9.3.2.1 Bridge-Type Cycloconverter

The load is assumed to consist of R and L in series.

Case (a): Discontinuous load current:

From [Figure 9.1b](#), it can be seen that during the positive half cycles of AC supply, thyristor pairs P_1P_2 and N_1N_2 are in the forward-blocking mode and during negative half cycles of AC supply, thyristor pairs P_3P_4 and N_3N_4 are in the forward-blocking mode.

So, at $\omega t = \alpha$, the forward-biased SCR pair P_1P_2 is triggered. With this, load current i_o starts building up gradually (due to the inductive load) in the positive direction, and load voltage v_o follows the supply voltage waveform as shown in [Figure 9.4](#). Load current i_o becomes zero at $\omega t = \beta$ (where $\pi < \beta < \pi + \alpha$) due to inductive nature of load. Thyristor pair P_1P_2 is thus naturally commutated at $\omega t = \beta$.

After half a cycle, that is, during a negative half cycle, the forward-biased SCR pair P_3P_4 is triggered at $\omega t = \pi + \alpha$. The load current i_o again builds up in the positive direction from zero as shown in [Figure 9.4](#). At $\omega t = \pi + \beta$, the load current decays to zero, and SCR pair P_3P_4 is naturally commutated. At $\omega t = 2\pi + \alpha$, SCR pair P_1P_2 is triggered again. After three positive half cycles of load voltage and load current, thyristor pair N_3N_4 is triggered at $\omega t = 3\pi + \alpha$. When pair N_3N_4 conducts, the load current direction is reversed and it builds up gradually in the negative direction as shown in [Figure 9.4](#). In the next half cycle (i.e., positive cycle of AC supply), the forward-biased pair N_1N_2 is triggered at $\omega t = 4\pi + \alpha$. Now, i_o again builds up gradually in negative direction, and it decays to zero before SCR pair N_3N_4 in sequence is triggered again.

In this way, three negative half cycles of load voltage and load current, equal to the number of three positive half cycles, are generated. Now, SCR pair P_1P_2 is triggered again at $\omega t = 6\pi + \alpha$ to fabricate further three positive half cycles of load voltage, and in this way, the operation repeats.

In [Figure 9.4](#), average output voltage and current waves are also shown by dotted lines. It can also be seen from [Figure 9.4](#) that the frequency of output voltage and current is $f_0 = \frac{f_i}{3}$, that is, step-down operation is achieved.

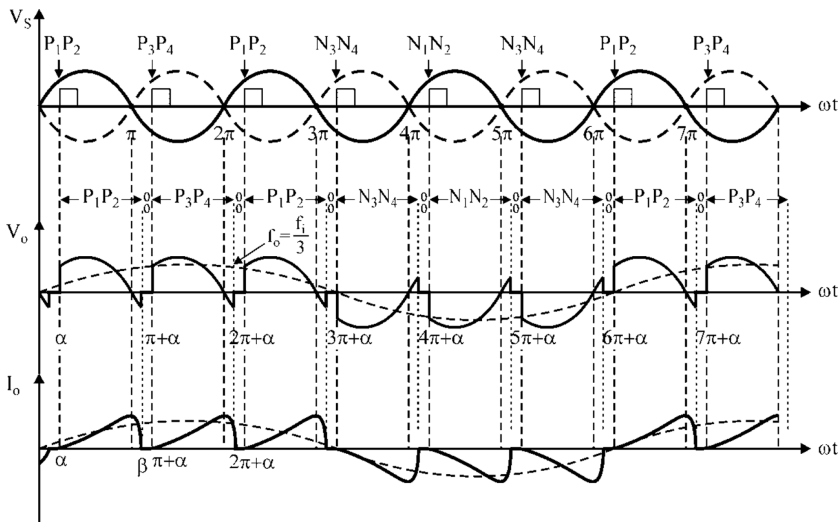


FIGURE 9.4 Voltage and current waveforms (bridge type) for step-down cycloconverter with discontinuous conduction.

Case (b): Continuous load current:

As we know that during the positive half cycles of AC supply, SCR pair P_1P_2 and N_1N_2 are in the forward-blocking mode, and during the negative half cycles, SCR pairs P_3P_4 and N_3N_4 are in the forward-blocking mode.

At $\omega t = \alpha$, SCR pair P_1P_2 is triggered, and so positive output voltage appears across the load, and the load current starts building up gradually due to inductive nature of load as shown in Figure 9.5. At $\omega t = \pi$, supply voltage and load voltage are zero. Because the load current is assumed continuous, the SCR pair P_3P_4 is triggered in sequence at $\omega t = (\pi + \alpha)$, a reverse voltage appears across P_1P_2 , and it is therefore turned off at $\omega t = \pi + \alpha$ by natural commutation. When P_1P_2 is commutated, load current has built up to a value equal to AA (see Figure 9.5). With the turning-on of P_3P_4 at $\omega t = \pi + \alpha$, output voltage is again positive as it was with P_1P_2 on. As a consequence, the load current builds up further than AA as shown in Figure 9.5.

At $\omega t = (2\pi + \alpha)$, when P_1P_2 is again triggered, the SCR pair P_3P_4 is naturally commutated, and the load current through P_1P_2 builds up beyond AB as shown. At the end of three positive half cycles of output voltage, the load current is AC.

Now, the SCR pair N_3N_4 is triggered at $\omega t = (3\pi + \alpha)$, the load voltage becomes negative, and the load current i_0 decreases from positive AC to negative AP as shown in Figure 9.5. Now SCR pair N_3N_4 is commutated, and pair N_1N_2 is triggered at $\omega t = (4\pi + \alpha)$. Load current i_0 becomes more negative than AP at $(5\pi + \alpha)$. For three negative half cycles of output voltage, current i_0 is shown in Figure 9.5.

The positive group of voltage waves and current waves consists of three pulses, and the same is true for negative group of waves. The output frequency is $f_0 = \frac{f_1}{3}$, that is, the step-down operation is achieved as shown in Figure 9.5.

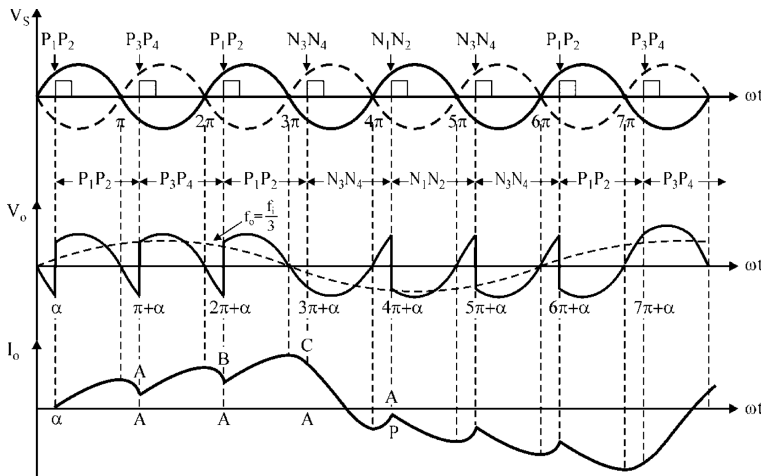


FIGURE 9.5 Voltage and current waveforms for step-down cycloconverter (bridge type) with continuous load current.

9.3.2.2 Midpoint Cycloconverter

The operation of midpoint-type cycloconverter shown in Figure 9.1a can be easily explained for both discontinuous and, continuous load currents. The voltage and current waveforms would be same as shown in Figure 9.4 for a discontinuous load current, the same as in Figure 9.5 for continuous load current. For a midpoint type, during the positive half cycles, SCR P_1 and N_2 are in the forward-blocking mode and during negative half cycles, SCR P_2 and N_1 are in the forward-blocking mode. So, replace P_1P_2 by P_1 , P_3P_4 by P_2 , N_1N_2 by N_2 and N_3N_4 by N_1 for a midpoint-type operation.

9.4 THREE-PHASE TO SINGLE-PHASE CYCLOCONVERTERS

Many industrial applications using AC motors require sinusoidal AC voltages as input. Single-phase to single-phase cycloconverters are seldom used in single-phase induction motor control because they can supply only non-sinusoidal output voltage. Alternatively, a very nearly sinusoidal output voltage can be fabricated from three-phase input voltage waves by means of three-phase to single-phase cycloconverters. A three-phase to three-phase cycloconverter can also be derived from three, three-phase to single-phase cycloconverters, as would be described later in this subsection.

A three-phase to single-phase cycloconverter is shown in Figure 9.6 [4,5,8,10]. The positive group converter P is a three-phase half-wave-controlled rectifier that can conduct load current that flows downward toward the neutral. Similarly, negative group converter N is also a three-phase half-wave-controlled rectifier, which conducts the load current in the reverse.

The reactor is sometimes necessarily used to limit the circulating current common to P and N converters. The low-frequency load voltage is fabricated by P and N converters making use of three-phase input supply. This is achieved by varying

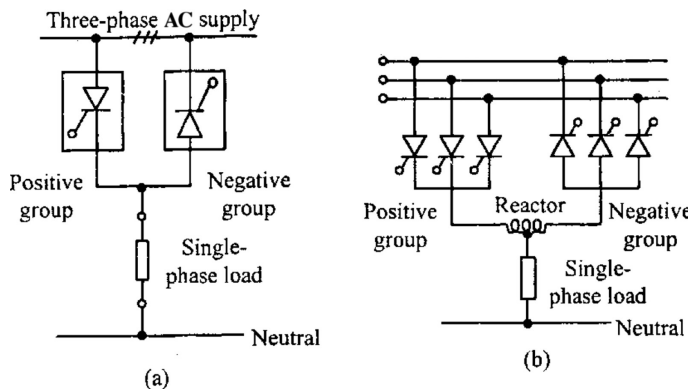


FIGURE 9.6 (a) Three-phase to (b) single-phase cycloconverter.

progressively the firing angle of three thyristors of a three-phase half-wave circuit. It is well known that the average direct output voltage (V_d) is given by

$$V_d = V_{do} \cos \alpha \quad (9.1)$$

where α is the firing angle or delay angle, and V_{do} is the maximum output voltage with zero firing delay. This only means that the variation of α will produce a sine wave output whose instantaneous values change with the firing angle in proportion to average direct voltage.

Assume that the rectifier firing angle is slowly varied as shown in Figure 9.7 [4,5,8,10]. In Figure 9.7, the firing angle at A is 90° , and the mean output voltage is zero. At B, the firing angle is somewhat less than 90° , at C the firing angle is still further reduced than it is at B, and so on. In this manner, a continuously decreasing delay in firing angle is introduced at C, D, E, F, and at G. The firing angle is zero where the mean output voltage, given by $v_o = V_{do} \cos \alpha$, is maximum. After point G, the firing angle is progressively increased at points H, I, J, K, L, and M. At M, the firing angle is again 90° , and the value of mean output voltage is zero. The firing circuit is suitably designed to introduce progressive firing angle delay as discussed.

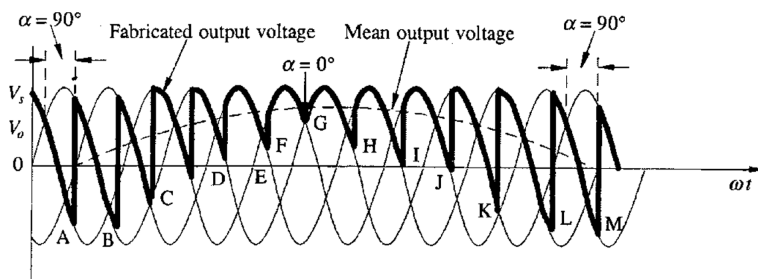


FIGURE 9.7 Synthesis of sinusoidal output voltage (three-phase to single-phase cycloconverter).

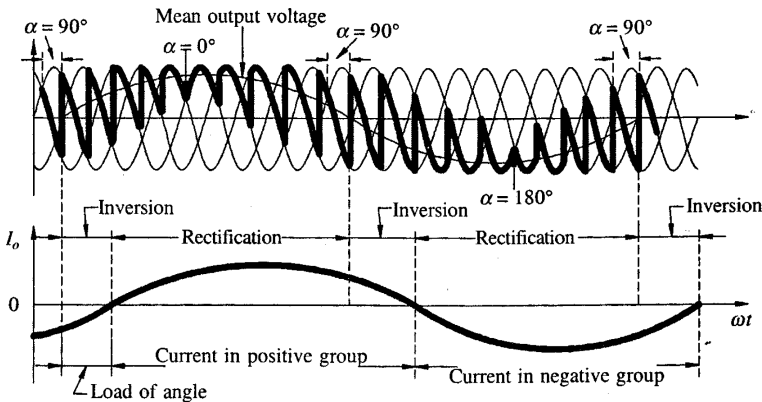


FIGURE 9.8 Voltage and current waveforms of a three-phase half-wave cycloconverter.

In Figure 9.7, the single-phase output voltage fabricated from three-phase input voltage is shown by a thick curve. The mean output voltage wave is obtained by joining points pertaining to average voltage values. It is seen from Figure 9.7 that the fabricated output voltage given by a thick curve can be resolved into fundamental frequency output voltage plus several other harmonic components. The load inductance can, however, filter out the high-frequency unwanted harmonics. Figure 9.7 reveals that for one half-cycle of fundamental frequency output voltage (marked mean output voltage in this figure), there are eight half cycles of supply frequency voltage. This shows that output frequency $f_o = (\frac{1}{8})f_s$, where f_s is the supply frequency. The output frequency can be varied by varying the number of input waves chosen for synthesizing the output voltage, which in fact means the rate of variation of the firing angle. To summarize, to obtain a positive half cycle of low-frequency output voltage, the firing angle is varied from 90° to 0° . The corresponding negative half cycle is obtained when the firing angle varies from 90° to 180° and back to 90° . This is illustrated in Figure 9.8 [4,5,8,10].

9.5 THREE-PHASE TO THREE-PHASE CYCLOCONVERTERS

When a three-phase low-frequency output is required, three sets of phase-controlled three-phase to single-phase cycloconverters with a phase displacement of 120° between their outputs are connected, as shown in Figure 9.9.

With a balanced load, the neutral connection is no longer necessary and may be omitted. The simplest arrangement using three-phase half-wave circuits is shown in Figure 9.9 [4,5,8,10]. This circuit requires 18 thyristors.

Three-Phase to Three-Phase Cycloconverter in Bridge Configuration

This six-pulse three-phase to three-phase cycloconverter employs 36 thyristors as shown in Figure 9.10. Each phase group consists of a three-phase dual converter with two intergroup reactors (IGRs). The load phases are as shown star-connected in the Figure 9.10 [4,5,8,10].

In this arrangement, as individual phase groups are isolated from each other on the input side, the interconnection of load phases in star and delta is possible.

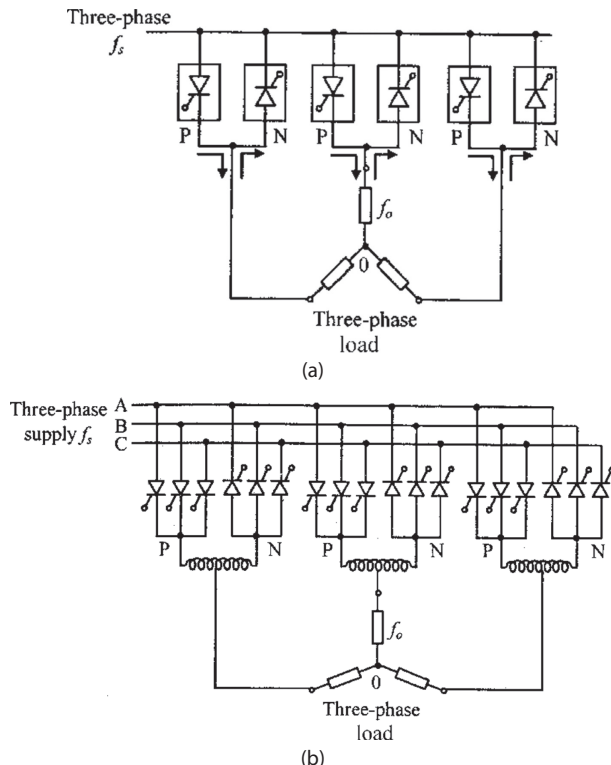


FIGURE 9.9 Three-phase to three-phase cycloconverter (midpoint type): (a) schematic diagram and (b) basic circuit arrangements.

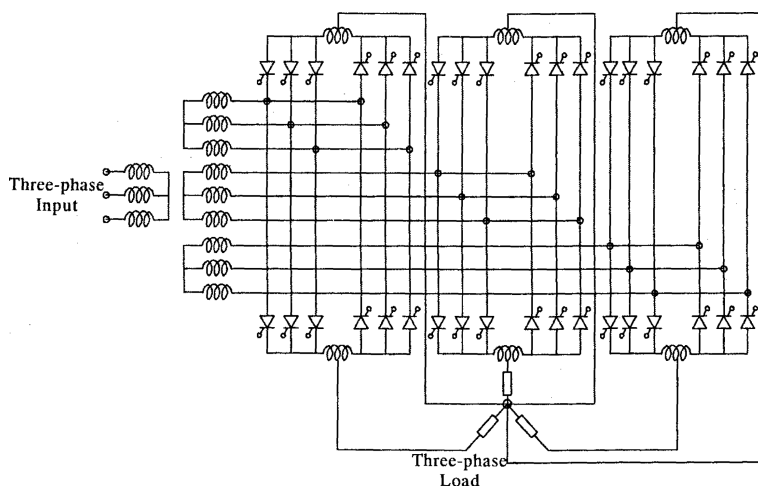


FIGURE 9.10 Three-phase bridge-type cycloconverter using 36 thyristors.

The magnitude of the output voltage in a three-phase bridge circuit is double of that in the three-phase half-wave arrangement. The VA rating of a bridge circuit is also double of three-phase half-wave circuits, provided the voltage and current ratings of the thyristors of these two circuits are identical. The three-phase bridge circuit gives a smooth variation of output voltage and is suitable for the control of large industrial drives though the control and the firing circuits are complex and expensive.

9.6 OUTPUT VOLTAGE EQUATION FOR THE CYCLOCONVERTER

In general, for m -phase half-wave converter, each phase conducts for $2\pi/m$ radians in one cycle of 2π radians, as shown in Figure 9.11 [4,5,8,10].

The instantaneous phase voltage,

$$v = V_m \cos \omega t = \sqrt{2} V_{ph} \cos \omega t \quad (9.2)$$

where V_{ph} = root mean square (RMS) value of per phase supply voltage. From Figure 9.11, it can be seen that conduction takes place from $-\frac{\pi}{m}$ to $\frac{\pi}{m}$ for $\alpha=0^\circ$. For any firing angle α , the conduction is from $(-\frac{\pi}{m} + \alpha)$ to $(\frac{\pi}{m} + \alpha)$. So, average output voltage [4,5,8]

$$V_0 = \frac{m}{2\pi} \int_{(-\frac{\pi}{m} + \alpha)}^{\left(\frac{\pi}{m} + \alpha\right)} V_m \cos \omega t \cdot d\omega t$$

or

$$V_0 = V_m \left[\left(\frac{m}{\pi} \right) \sin \frac{\pi}{m} \right] \cos \alpha \quad (9.3)$$

If V_{rms} is the fundamental RMS value of per phase output voltage of cycloconverter, the peak output voltage for zero firing angle is,

$$\sqrt{2}V_{rms} = V_0 = \sqrt{2}V_{ph} \left(\frac{m}{\pi} \right) \sin \frac{\pi}{m}$$

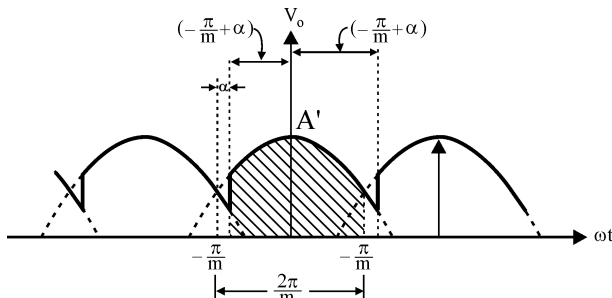


FIGURE 9.11 Output voltage waveform for m -phase half-wave converter with firing angle.

or

$$V_{rms} = V_{Ph} \left(\frac{m}{\pi} \right) \sin \left(\frac{\pi}{m} \right) \quad (9.4)$$

Practically, the firing angle α_p of positive group cannot be reduced to zero, and firing angle α_n of negative group can never be equal to 180° because of commutation overlap and thyristor turn-off time. As a result, $\alpha_p \neq 0$ but must have some finite value. Let this minimum value of firing angle for positive group be α_{min} . For this firing angle, the maximum output voltage per phase is

$$(V_0)_{max} = V_m \left(\frac{m}{\pi} \right) \sin \left(\frac{\pi}{m} \right) \cos \alpha_{min} \quad (9.5)$$

So, the expression for the fundamental RMS phase value of the output voltage of a cycloconverter is

$$V_{rms} = r \left[V_{Ph} \left(\frac{m}{\pi} \right) \sin \left(\frac{\pi}{m} \right) \right] \quad (9.6)$$

where $r = \cos \alpha_{min}$ and is called the *voltage reduction factor*.

As $\alpha_{min} > 0$, so “r” is always less than unity.

9.7 REDUCTION OF OUTPUT HARMONICS

It can be noticed from [Figures 9.4](#) and [9.5](#) that the output voltage is not purely sinusoidal due to the presence of harmonics [4,5,8]. Also, the input power factor (PF) depends on the delay angle of thyristors and is poor, especially at the low output voltage range.

The output voltage of cycloconverters is basically made up of segments of input voltages, and the average value of a segment depends on the delay angle for that segment. The harmonics on the output voltage can be minimized if the delay angles of segments are varied in such a way that the average values of segments correspond to the variations of desired sinusoidal output voltage. Also, the average output voltage of a segment is a cosine function of delay angle. The delay angles for segments can be generated by comparing a cosine signal at source frequency ($v_c = \sqrt{2} V_s \cos \omega_s t$) with an ideal sinusoidal reference voltage at the output frequency ($v_r = \sqrt{2} V_o \cos \omega_0 t$).

The maximum average voltage of a segment (which occurs for $\alpha_p = 0$) should be equal to the peak value of output voltage:

$$V_p = \frac{2\sqrt{2}V_s}{\pi} = \sqrt{2}V_o$$

which gives the RMS value of output voltage as

$$V_0 = \frac{2V_s}{\pi} = \frac{2V_p}{\pi}$$

9.8 SOLVED PROBLEMS

Example 9.1: A three-phase to one-phase cycloconverter employs three-phase-positive and negative-group converters. Each converter is supplied from a delta/star transformer with per phase turn ratio of 2: 1. The supply voltage is 400 V, 50 Hz. The RL load has $R = 2\Omega$ and at low output frequency, $\omega_0 L = 1.5 \Omega$. In order to account for communication overlap and thyristor turn-off time, the firing angle in the inversion mode should not exceed 160°. Calculate

- (a) Value of the fundamental RMS output voltage,
- (b) RMS output current, and
- (c) Output power.

SOLUTION

(a) Given: input voltage to transformer = 400 V per phase

Therefore, input voltage to converter (per phase), $V_{ph} = \frac{400}{2} = 200$ V

Also, the voltage reduction factor, $r = \cos(180 - 160) = \cos 20^\circ$

For a three-phase pulse device, $m = 3$, the RMS value of fundamental voltage is

$$V_{or} = \cos 20 \left[200 \left(\frac{3}{\pi} \right) \cdot \sin \frac{\pi}{3} \right] = 155.424 \text{ V}$$

$$(b) \text{ RMS output current} = \frac{155.424}{\sqrt{2^2 + 1.5^2}} \left| -6 \tan^{-1} \frac{1.5}{20} \right.$$

$$I_{or} = 62.17 \left| -36.87^\circ \right. \text{ Amps.}$$

$$(c) \text{ Output power } I_{or}^2 \cdot R = (62.17)^2 \times 2 = 7730.22 \text{ W}$$

Example 9.2: Repeat Example 9.1 in case three-phase to one-phase cycloconverter uses a six-phase bridge converter.

SOLUTION

(a) Per phase input voltage to converter = 200 V

Line voltage input to bridge converter = $200\sqrt{3}$ V

Voltage reduction factor, $r = \cos 20^\circ$

For six-phase device, $m = 6$. From Equation (9.6), the RMS value of output voltage is

$$V_{or} = \cos 20 \left[200\sqrt{3} \left(\frac{6}{\pi} \right) \sin \frac{\pi}{6} \right] = 310.84 \text{ V}$$

It shows that output voltage in a six-pulse bridge converter using 36 thyristors is double to that of three-pulse half-wave converter using 18 thyristors.

$$(b) \text{ RMS output current} = \frac{3.1084}{\sqrt{2^2 + 1.5^2}} \left[-\tan^{-1} \frac{1.5}{2} \right]$$

$$= 124.34 \angle -36.87^\circ \text{ Amps}$$

$$(c) \text{ RMS output power} = (124.34)^2 \times 2 = 30920.88 \text{ W.}$$

This shows that output power handled by a six-pulse bridge converter is four times the power handled by a three-phase converter.

REVIEW QUESTIONS UNSOLVED PROBLEMS

- 9.1 Mention the advantages of cycloconverter over an inverter.
- 9.2 What are the advantages and the disadvantages of cycloconverters?
- 9.3 Mention two applications of cycloconverters.
- 9.4 What is a cycloconverter? Give the merits and demerits of cycloconverters when compared to converter-inverter combination.
- 9.5 Explain the operation of a single-phase to single-phase cycloconverter feeding an R load.
- 9.6 Explain the operation of any one of the three-phase cycloconverters. Draw and explain the trigger circuit of the cycloconverter.
- 9.7 Explain the motor control using a cycloconverter.
- 9.8 Explain the working principle of a single-phase bridge-type step-down cycloconverter feeding an RL load.
- 9.9 Explain the principle of working of a three-phase to single-phase cycloconverter.
- 9.10 Show that the fundamental RMS value of per phase output voltage of a low frequency for an m pulse cycloconverter is given by $V_{or} = V_{ph} \left(\frac{m}{\pi} \right) \sin \left(\frac{\pi}{m} \right)$. Hence, express V_{or} in terms of voltage reducing factor, r .
- 9.11 A three-phase to single-phase cycloconverter employs three-phase-positive and negative-group converters. Each converter is supplied from a delta/star transformer with per phase turn ratio of 2:1. The supply voltage is 4,000 V, 50 Hz. The RL load has $R = 5 \Omega$ and at low output frequency, $\omega_0 L = 2.5 \Omega$. In order to account for communication overlap and thyristor turn-off time, the firing angle in the inversion mode should not exceed 150° . Compute
 1. The value of the fundamental RMS output voltage,
 2. RMS output current, and
 3. Output power.
- 9.12 Explain the operation of a single-phase to single-phase step-up midpoint-type cycloconverter feeding an R load.
- 9.13 Explain the operation of a single-phase to single-phase step-down midpoint-type cycloconverter feeding an R load.
- 9.14 Explain reduction of output harmonics in a cycloconverter.
- 9.15 Explain the three-phase bridge-type cycloconverter with circuit diagrams.

SUMMARY

This chapter has studied in detail the principle of operation of different step-up and step-down cycloconverters, such as single-phase to single-phase, three-phase to single-phase, and three-phase to three-phase cycloconverters. Various applications of cycloconverters include induction heating, motion control of AC drives, power supply in aircrafts and shipboards, static VAr compensators, etc.

MAIN FORMULAS OF THE CHAPTER

$$V_{\text{rms}} = V_{Ph} \left(\frac{m}{\pi} \right) \sin \left(\frac{\pi}{m} \right)$$

$$(V_0)_{\text{max}} = V_m \left(\frac{m}{\pi} \right) \sin \left(\frac{\pi}{m} \right) \cos \alpha_{\min}$$

$$V_{\text{rms}} = r \left[V_{Ph} \left(\frac{m}{\pi} \right) \sin \left(\frac{\pi}{m} \right) \right]$$

REFERENCES/FURTHER READING

1. E. Babaei, A new PWM based control method for forced commutated cycloconverters, *Energy Conversion and Management*, vol. 53, no. 1, pp. 305–313, 2012.
2. F. L. Luo, *Traditional AC/AC Converters*, Industrial Electronics, Boca Raton, FL, 2012.
3. J. S. Vinodhini, R. S. R. Babu, J. A. Glenn. Single-phase to single-phase step-down cycloconverter for electric traction applications, *International Conference on Electrical, Electronics, and Optimization Techniques (ICEEOT), IEEE*, 2016.
4. B. K. Bose, *Power Electronics and AC Drives*, Prentice Hall, Englewood Cliffs, NJ, 1986.
5. M. H. Rashid, *Power Electronics: Circuits, Devices, and Applications*, Pearson Education, Singapore, 2004.
6. P. T. Krein, *Elements of Power Electronics*, Oxford University Press, New York, 2003.
7. K. Thorborg, *Power Electronics*, Prentice Hall International, London, UK, 1988.
8. P. S. Bhimra, *Power Electronics*, 5th Khanna Publications, New Delhi, India, 2012.
9. Internet source: www.actapress.com
10. A. Chattopadhyay, *AC-AC converters, Power Electronics Handbook*, 2007.
11. E. Babaei, A. A. Heris, PWM-based control strategy for forced commutated cycloconverters, *IEEE Symposium on Industrial Electronics and Applications*, October 4–6, Kuala Lumpur, Malaysia, 2009.
12. S. Jeevananthan, Novel single-phase to single-phase cycloconversion strategies: Mathematical and simulation studies, *Int. J. Power Energy Systems*, vol. 27, no. 4, 2007.
13. R. W. Erickson, *Fundamentals of Power Electronics*, Chapman & Hall, New York, 1997.
14. V. R. Moorthi, *Power Electronics Devices, Circuits and Industrial Applications*, Oxford University Press, Oxford, UK, 2010.
15. T. Suntio, T. Messo, J. Puukko, *Power Electronic Converters*, Wiley-VCH, Verlag GmbH, Germany, 2018.
16. A. M. Trzynadlowski, *Introduction to Modern Power Electronics*, 3rd edn, John Wiley & Sons, Hoboken, NJ, 2010.

17. M. Trzynadlowski, *Power Electronic Converters and Systems*, Institution of Engineering and Technology, London, UK, 2016.
18. B. M. Wilamowski, J. D. Irwin, *Power Electronics and Motor Drives*, CRC Press, Boca Raton, FL, 2011.
19. E. Acha, V. G. Agelidis, O. Anaya-Lara, T. J. E. Miller, *Power Electronic Control in Electrical Systems*, Newnes, Oxford, 2002.
20. F. Mazda, *Power Electronics Handbook*, Newnes, Oxford, 1997.
21. F. Blaabjerg, *Control of Power Electronic Converters and Systems*, Academic Publishers, London, UK, 2018.
22. S. N. Manias, *Power Electronics and Motor Drive Systems*, Academic Publishers, London, UK, 2017.



Taylor & Francis

Taylor & Francis Group

<http://taylorandfrancis.com>

10 Switched-Mode Power Supplies

10.1 INTRODUCTION

The following requirements are often needed from the power supplies widely used for industrial applications [1–7]:

1. Isolation of output load from the input source
2. Regulated output within specified limits for changes in input and output side
3. Multiple isolated outputs with different voltage and current ratings
4. Reduced size and weight with high-power density
5. Controlled direction of power flow
6. High efficiency
7. Low total harmonic distortion (THD) in output waveforms

Traditionally, linear power supplies have been used, but advancement in semiconductor technology has led to switching power supplies, which are smaller in size and lighter in weight with improved efficiency as compared to linear power supplies. The behavior of the linear power supply is identical to the switching power supply when viewed as a black box with input and output terminals. The basic difference is that a continuous load current is regulated by the linear supply to maintain constant load voltage, whereas the switching power supply regulates the constant current flow by chopping the input voltage and the duty cycle.

The use of linear and switching power supplies depends on the need of the application, that is, cost and electrical requirement. Both have distinct merits in particular areas of applications. [Table 10.1](#) presents the comparison between both types of power supplies.

10.2 BASIC WORKING OF SWITCHED-MODE POWER SUPPLY

The forward-mode and the flyback-mode regulators are the two basic types of switched-mode power regulators, which make the foundation of all the pulse-width modulation (PWM) switching regulators. All the switching mode power regulators have four basic components, i.e.,

1. A power switch to create PWM waveform. It may be a power transistor or power metal-oxide semiconductor field-effect transistor (MOSFET)
2. A diode
3. A series inductor
4. A capacitor

TABLE 10.1
Comparison of Linear and Switching Power Supply

S. No.	Linear Power Supply	Switching Power Supply
(i)	Simple in design.	Complex in design.
(ii)	Quiet operation with load-handling capability.	Considerable noise is generated on its input and output.
(iii)	Component and manufacturing costs are lesser.	Component and manufacturing costs are higher.
(iv)	Limited range of applications, that is, used as step-down regulator only with one output terminals.	Range of applications is not limited, that is can be operated as step-up or step-down regulator with multiple isolated output terminals.
(v)	Efficiency is average, that is, 40%–70%.	Efficiency is high, that is 70%–95%.
(vi)	Large size with high cost at large output power levels.	Small size with low cost at large output power levels.
(vii)	Preferred for low power, board level regulators, that is for circuits needing quiet supply, such as analog and audio circuits.	Preferred where high supply efficiency is needed and dissipation of heat is problematic, such as battery-powered applications.

10.2.1 FORWARD-MODE-TYPE SWITCHING REGULATOR

The power circuit of a forward-mode-type switching regulator consisting of a power switch, a diode, series inductor, and capacitor is shown in [Figure 10.1a](#). There may be a transformer for step-up or down of the input voltage as in the case of transformer-isolated forward regulators. The role of a series inductor, capacitor, and diode is to make an energy storage reservoir so as to maintain the load current and voltage during the entire off time of the power switch.

The working operation of forward type switching mode regulator can be explained using following two modes of operation:

Mode 1: When power switch is ON

During this mode, the load current flows through the path: input source—inductor—load—input source, as shown in [Figure 10.1b](#). Diode (D) is reversed biased, and the inductor stores energy during this mode.

Mode 2: When power switch is OFF

When power switch is turned off, the load current follows the flows: diode (D)—inductor (L)—load—diode, as shown in [Figure 10.1c](#). In this mode, energy stored by the inductor is delivered to the load.

Because the forward current always flows through the inductor, these are *termed forward-switching-mode regulators*. The amount of energy being delivered to load is controlled by the duty cycle (δ).

The average output voltage can be expressed as:

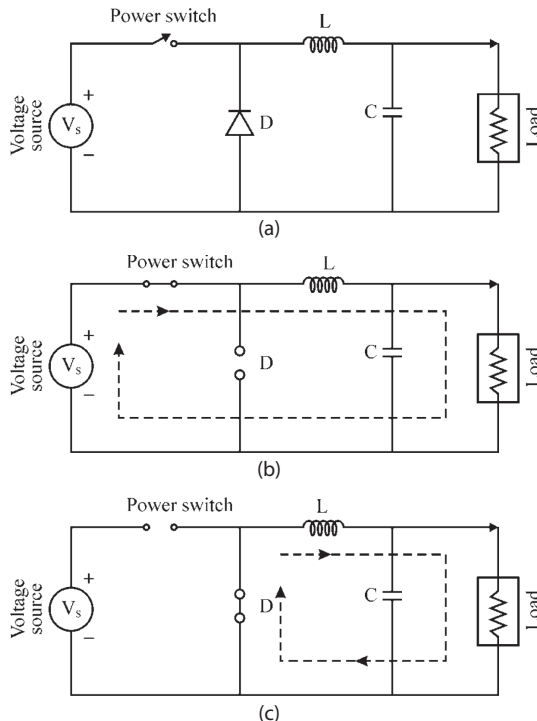


FIGURE 10.1 Forward-mode-type switching regulator: (a) power circuit diagram, (b) equivalent circuit diagram when power switch is on, and (c) equivalent circuit diagram when power switch is off.

$$V_0 = \frac{T_{on}}{T} V_s = \delta V_s \quad (10.1)$$

where δ is the duty cycle or duty ratio. Its range is $0 \leq \delta \leq 1$.

10.2.2 FLYBACK-MODE-TYPE SWITCHING REGULATOR

The power circuit of the flyback-mode-type switching regulator is shown in [Figure 10.2a](#). This type of regulator also consists of a power switch, a diode, series inductor, and capacitor.

The operation of the flyback regulator can be explained using following two modes of operation:

Mode 1: When power switch is ON

When power switch is turned on, the current flows through the inductor, and it stores the energy with polarity as shown in the equivalent circuit of [Figure 10.2b](#). Diode (D) is reverse biased.

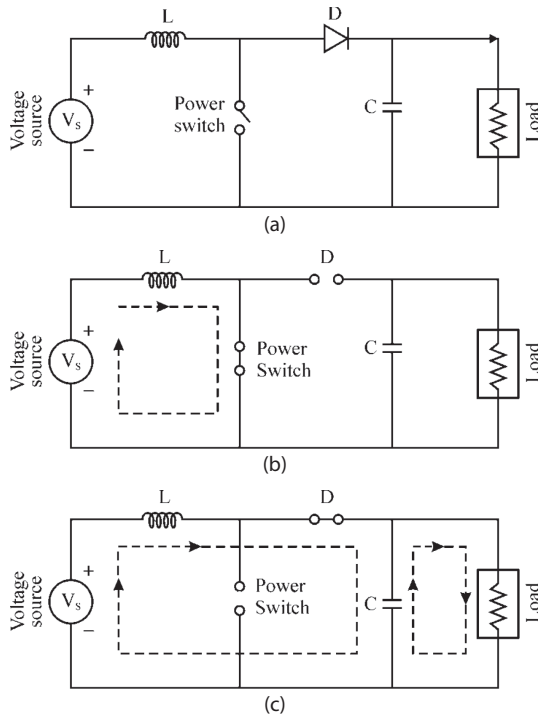


FIGURE 10.2 Flyback-mode-type switching regulator: (a) power circuit diagram, (b) equivalent circuit diagram when power switch is on, and (c) equivalent circuit diagram when power switch is off.

Mode 2: When power switch is OFF

When power switch is turned off, the voltage across the inductor ($v_L = L \frac{di}{dt}$) reverses (flies back) because the current through the inductor cannot change instantaneously. As a result, diode (D) gets turned on, and thus energy stored by the inductor is dumped into the capacitor, as shown in Figure 10.2c, that is,

$$v_C = V_s + v_L \quad (10.2)$$

$$v_C = V_s + L \frac{di}{dt} \quad (10.3)$$

Therefore, it can be seen that the inductor voltage *flies back* above the input voltage, and the voltage across capacitor is higher than the input voltage; hence, these are termed *flyback switching-mode regulators*.

The average output voltage can be expressed as:

$$V_0 = V_s \left(1 + \frac{T_{on}}{T_{off}} \right) \quad (10.4)$$

10.3 SWITCHED-MODE POWER SUPPLY (SMPS)

The SMPSs or regulators can be classified as:

- Flyback SMPS
- Push-pull SMPS
- Half-bridge SMPS
- Full-bridge SMPS

10.3.1 FLYBACK SWITCHED-MODE POWER SUPPLY

The power circuit of the flyback SMPS consists of a power MOSFET (M1), diode (D), capacitor C1, transformer for isolation purpose, and load, as shown in [Figure 10.3a](#). The working of the flyback regulator can be explained using two modes of operation:

Mode 1: When power MOSFET M1 is ON

When power MOSFET M1 is turned on, supply voltage (V_s) is applied to the primary winding of the transformer, that is,

$$v_1 = V_s; v_2 = \frac{N_2}{N_1} V_s; v_C = V_0; \text{ and } i_D = 0 \quad (10.5)$$

The magnetizing current (i_m) rises linearly from I_{\min} to I_{\max} at $t = T_{\text{on}}$

$$i_m = I_{\min} + \frac{V_s}{L} t \quad (10.6)$$

As shown in equivalent circuit of [Figure 10.3b](#), the voltage across secondary winding of the transformer (v_2) reverse biases the diode (D).

Mode 2: When power MOSFET M1 is OFF

When power MOSFET M1 is turned off, then since the current through the winding of the transformer that is highly inductive cannot change instantly, therefore, the voltage of opposite polarity is induced in the primary and the secondary windings of the transformer, as shown in [Figure 10.3c](#). As a result, diode (D) becomes forward biased, and the energy stored in the transformer core is delivered to the load and the capacitor. Various voltage and current waveforms are shown in [Figure 10.3d](#). The magnetizing current (i_m) reduces linearly from I_{\max} to I_{\min} at $t = T$.

Also,

$$v_2 = -V_0; v_1 = -\frac{N_1}{N_2} V_0 \quad (10.7)$$

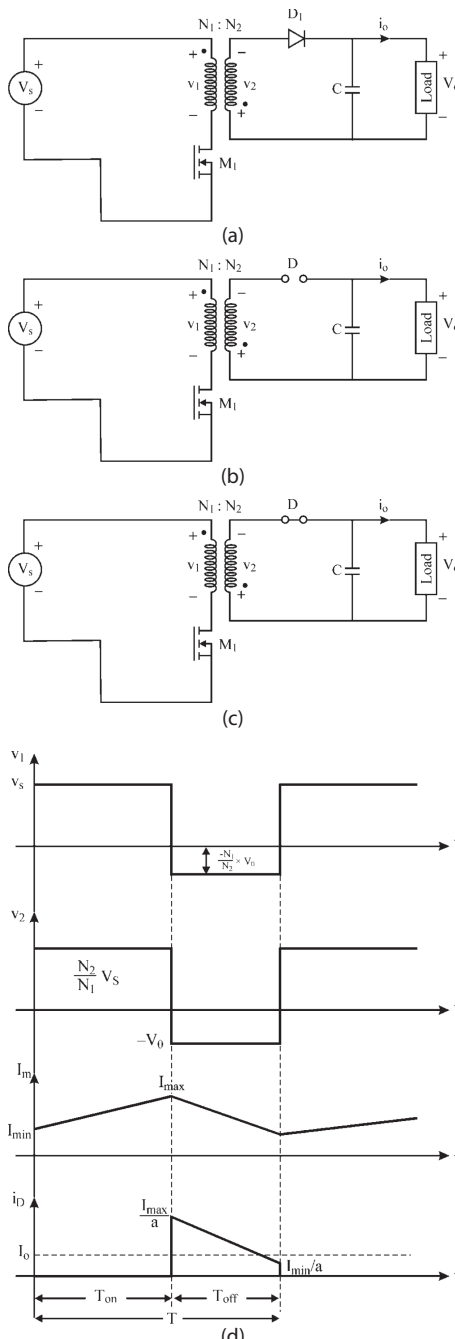


FIGURE 10.3 Flyback SMPS: (a) power circuit diagram, (b) equivalent circuit diagram when power switch is on, (c) equivalent circuit diagram when power switch is off, and (d) various voltage and current waveforms.

Load voltage,

$$V_0 = \left(\frac{\delta}{1-\delta} \right) a V_s \quad (10.8)$$

where $a = N_2/N_1$ is the transformer turn ratio.

10.3.2 PUSH-PULL SWITCHED-MODE POWER SUPPLY

The power circuit of the push-pull SMPS consists of two power MOSFETs (M1 and M2), two diodes (D1 and D2), inductor (L), capacitor C1, and a transformer with midtaps on both primary and secondary sides, as shown in Figure 10.4. The working of the push-pull regulator can be explained using two modes of operation:

Mode 1: When power MOSFET M1 is ON

When power MOSFET M1 is turned on, supply voltage (V_s) is applied to the lower half of the primary winding of the transformer due to which voltage v_2 is induced in both the upper and the lower half of the secondary winding, and therefore output voltage is obtained. Various quantities during this mode can be expressed as:

$$v_1 = V_s; v_2 = \frac{N_2}{N_1} V_s; \text{ and load voltage, } V_0 = \frac{N_2}{N_1} V_s = a V_s \quad (10.9)$$

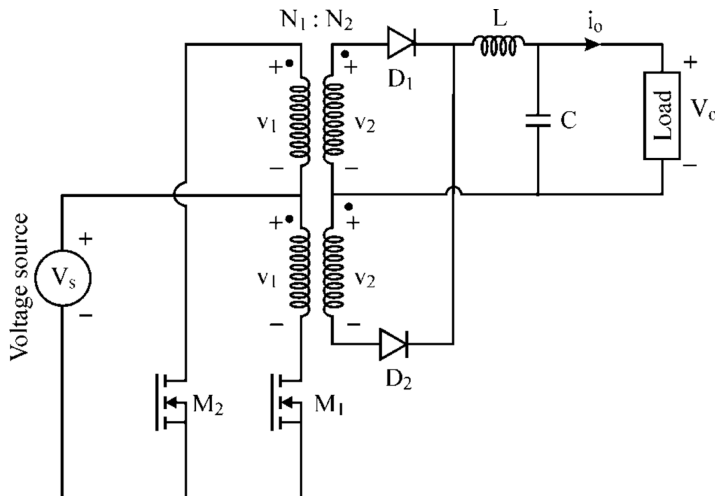


FIGURE 10.4 Push-pull SMPS.

Mode 2: When power MOSFET M2 is ON

When power MOSFET M2 is turned on, the supply voltage ($-V_S$) is applied to the upper half of the primary winding of the transformer due to which voltage v_2 is induced in both the primary and the secondary windings of the transformer, that is,

$$v_1 = -V_S; \text{ and } v_2 = -\frac{N_2}{N_1} V_S = -aV_S \quad (10.10)$$

The diode D2 becomes forward biased due to reverse voltage v_2 , and hence the output load voltage is obtained as:

$$\text{Load voltage, } V_0 = \frac{N_2}{N_1} V_S = aV_S \quad (10.11)$$

From the preceding discussion, it can be seen that voltage across the primary winding changes from $+V_S$ (when M1 is ON) to $-V_S$ (when M2 is ON). When any of the power MOSFET is off, then voltage across their terminals is $2V_S$, and therefore this type of SMPS is suitable for only low-voltage applications.

10.3.3 HALF-BRIDGE SWITCHED-MODE POWER SUPPLY

The power circuit of the half-bridge SMPS consists of two power MOSFETs (M1 and M2), two diodes (D1 and D2), filter circuits of inductor (L) and capacitor (C), two capacitors (C1 and C2), and a transformer with midtaps on secondary sides, as shown in [Figure 10.5](#).

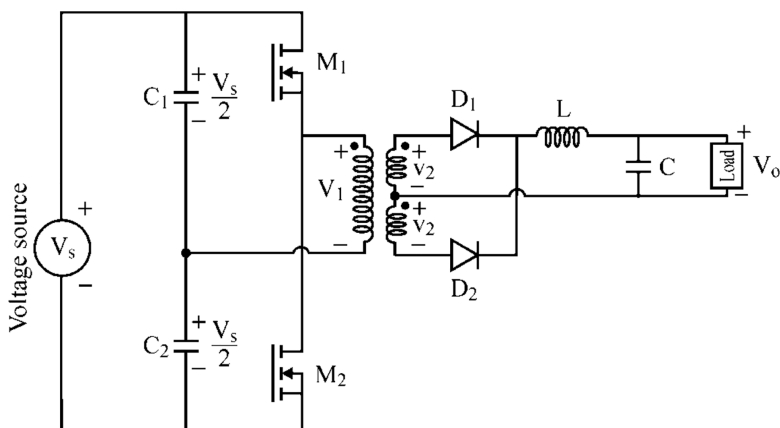


FIGURE 10.5 Half-bridge SMPS.

The working of the half-bridge regulator can be explained using two modes of operation:

Mode 1: When power MOSFET M1 is ON

When power MOSFET M1 is turned on, then the voltage of capacitor C1 appears across primary winding of the transformer, and as a result, voltage v_2 is induced in the secondary winding. The diode D1 becomes forward biased, that is,

$$v_1 = \frac{V_S}{2}; \text{ and } v_2 = \frac{N_2}{N_1} \frac{V_S}{2} = \frac{aV_S}{2} \quad (10.12)$$

Mode 2: When power MOSFET M2 is ON

When power MOSFET M2 is turned on, a reverse voltage of $V_S/2$ appears across primary winding of the transformer due to capacitor C2. As a result, voltage v_2 is induced in the secondary winding of the transformer, and therefore diode D2 becomes forward biased, that is,

$$v_1 = -\frac{V_S}{2}; \text{ and } v_2 = -\frac{N_2}{N_1} \frac{V_S}{2} = -\frac{aV_S}{2} \quad (10.13)$$

It can be seen that the voltage across the primary winding of the transformer changes from $-V_S/2$ to $+V_S/2$. The average output voltage can be expressed as:

$$V_0 = \left(\frac{N_2}{N_1} \right) \left(\frac{V_S}{2} \right) = 0.5aV_S \quad (10.14)$$

When any of the power MOSFET is off, then the voltage across their terminals is V_S , and therefore this type of SMPS is suitable for high-voltage applications.

10.3.4 FULL-BRIDGE SWITCHED-MODE POWER SUPPLY

The power circuit of the full-bridge SMPS consists of four power MOSFETs (M1, M2, M3, and M4), two diodes (D1 and D2), inductor (L), and capacitor (C) as filter circuits, and a transformer with midtaps on the secondary winding, as shown in [Figure 10.6](#).

The working of the full-bridge regulator can be explained using two modes of operation:

Mode 1: When power MOSFET M1 and M2 are ON

When power MOSFETs M1 and M2 are turned on, then voltage v_1 and v_2 appears across the primary and secondary windings of the transformer, respectively. As a result, diode D1 becomes forward biased, and output across the load is obtained, that is,

$$v_1 = V_S; v_2 = \frac{N_2}{N_1} V_S = aV_S \quad (10.15)$$

$$V_0 = v_2 = aV_S \quad (10.16)$$

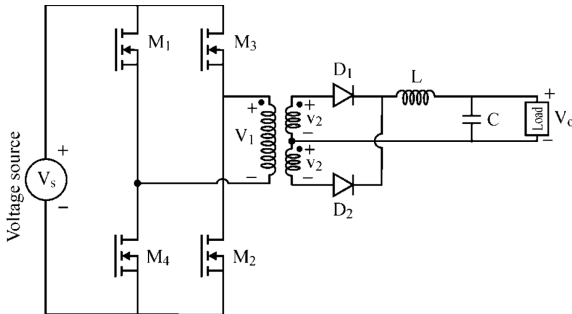


FIGURE 10.6 Full-bridge SMPS.

Mode 2: When power MOSFETs M3 and M4 are ON

When power MOSFETs M3 and M4 are turned on, then a reverse voltage of magnitude V_s appears across the primary and secondary windings of the transformer. As a result, diode D2 becomes forward biased, and output is obtained, that is,

$$v_1 = -V_s; \quad v_2 = -\frac{N_2}{N_1} V_s = -aV_s \quad (10.17)$$

$$V_0 = v_2 = aV_s \quad (10.18)$$

When any of the power MOSFETs is off, then voltage across their terminals is V_s , that is, this SMPS operates with minimum current and voltage stress on the power semiconductor devices. Therefore, such SMPSs are very popular and demanding for high-power applications, particularly above 750 W. When compared with the half-bridge, the full-bridge uses four power switches instead of two, and therefore, two more gate drivers and secondary windings are needed in the pulse transformer for the gate circuit. For the same output power, the maximum current of a full bridge is half that of the half bridge, while the output power is twice that of a half bridge with the same input voltage and current.

10.4 RESONANT DC POWER SUPPLIES

The resonant pulse inverters are generally used where variation in the DC output voltage is not wide. The frequency of the inverter, which may be the same as the resonant frequency, is too high with almost sinusoidal output voltage. Due to resonant oscillation, the transformer core is always reset, and there are no saturation problems of the DC current. The power circuit diagram of the half-bridge and full-bridge configurations of the resonant inverters is shown in [Figure 10.7](#) [2,4,7]. Here,

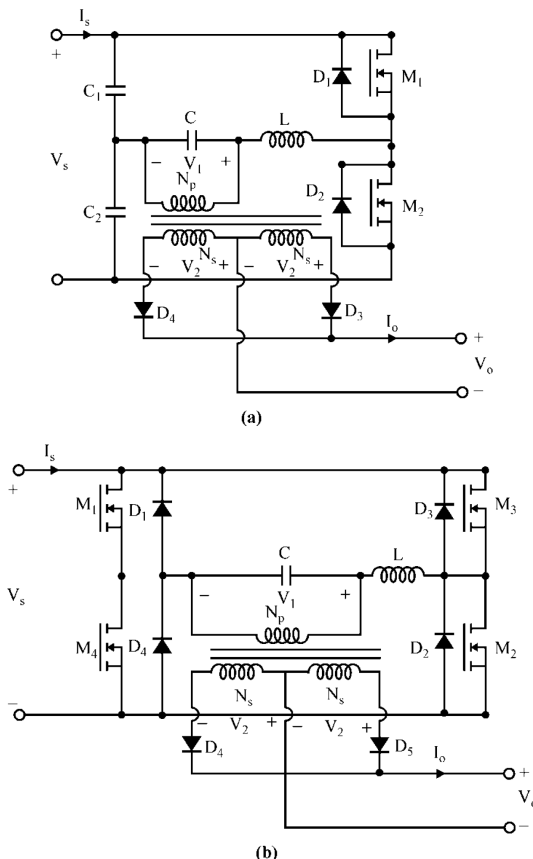


FIGURE 10.7 Resonant DC power supplies: (a) half-bridge and (b) full-bridge inverter. (From Rashid, M.H., *Power Electronics: Circuits, Devices, and Applications*, Pearson Education, Singapore, 2004.)

it must be noted that the sizes of the transformer and output filter are reduced due to their operation at high frequency.

10.5 BIDIRECTIONAL DC POWER SUPPLIES

In different applications, such as battery charging and discharging, it is generally preferred to have bidirectional power flow capability. A bidirectional power supply is shown in [Figure 10.8](#) [2,4,7]. The direction of the power flow depends on the magnitudes of load voltage, supply voltage, and the turn ratio of the transformer. The inverter can either be operated in the inversion mode if $V_o < aVs$ or in the rectifier mode if $V_o > aVs$. The bidirectional converters allow the inductive current to flow in either direction continuous conduction of current.

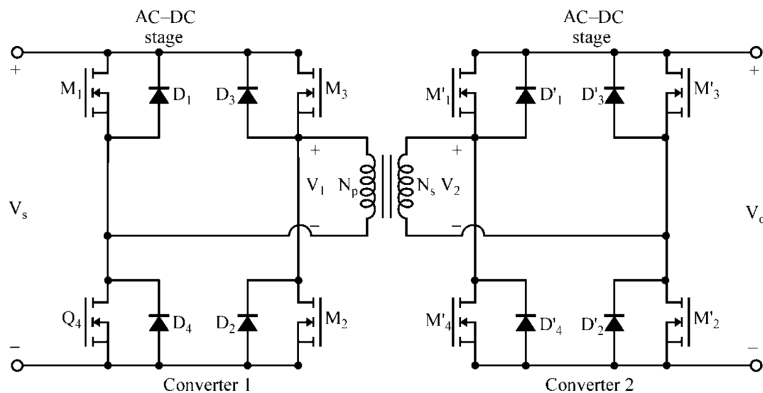


FIGURE 10.8 Bidirectional DC power supplies. (From Rashid, M.H., *Power Electronics: Circuits, Devices, and Applications*, Pearson Education, Singapore, 2004.)

REVIEW QUESTIONS

- 10.1 Why are SMPSs in demand?
- 10.2 What are the advantages and disadvantages of linear and SMPSs?
- 10.3 List the different types of SMPSs.
- 10.4 What is the basic difference in forward and flyback-type SMPSs?
- 10.5 List the main components used in any SMPS.
- 10.6 Explain in detail with equivalent circuits the working of the flyback SMPS with suitable mathematical equations and waveforms.
- 10.7 Repeat Question 10.6 for the push-pull-type SMPS.
- 10.8 Make a detailed comparison between half-bridge and full-bridge-type configurations of SMPS?
- 10.9 Write short notes on resonant DC power supplies.
- 10.10 Write short notes on bidirectional power supplies.

SUMMARY

This chapter has studied the concept and principle of operation of different SMPSs, resonant DC power supplies, and bidirectional power supplies. Due to factors such as increased switching speeds, low cost, low-power dissipation, higher current, and voltage ratings the switching power supplies have emerged significantly.

MAIN FORMULAS OF THE CHAPTER

- **Flyback SMPS**

$$\text{Load voltage, } V_0 = \left(\frac{\delta}{1-\delta} \right) a V_s$$

where $a = \frac{N_2}{N_1}$ is the transformer turn ratio

- **Push-Pull SMPS**

$$V_0 = \frac{N_2}{N_1} V_S = aV_S$$

- **Half-Bridge SMPS**

$$V_0 = \left(\frac{N_2}{N_1} \right) \left(\frac{V_S}{2} \right) = 0.5aV_S$$

- **Full-Bridge SMPS**

$$V_0 = v_2 = aV_S.$$

REFERENCES/FURTHER READING

1. N. Mohan, T. M. Undeland, and W. P. Robbins, *Power Electronics: Converters, Applications and Design*, John Wiley & Sons, Singapore, 1996.
2. B. K. Bose, *Power Electronics and AC drives*, Prentice Hall, Englewood Cliffs, NJ, 1986.
3. K. K. Sum, *Switched Mode Power Conversion-Basic Theory and Design*, Marcel Dekker, New York, 1984.
4. M. H. Rashid, *Power Electronics: Circuits, Devices, and Applications*, Pearson Education, Singapore, 2004.
5. P. T. Krein, *Elements of Power Electronics*, Oxford University Press, New York, 2003.
6. K. Thorborg, *Power Electronics*, Prentice Hall International, London, UK, 1988.
7. P.S. Bhimra, *Power Electronics*, 15th ed, Khanna Publications, New Delhi, India, 2012.
8. A. Emadi, A. Nasiri, S. B. Bekiarov, *Uninterruptible Power Supplies and Active Filters*, CRC Press, Boca Raton, FL, 2005.
9. A. Emadi, *Handbook of Automotive Power Electronics and Motor Drives*, CRC Press, Chicago, IL, 2005.
10. A. M. Trzynadlowski, *Introduction to Modern Power Electronics*, 3rd edn., John Wiley & Sons, 2010.
11. A. M. Trzynadlowski, *Power Electronic Converters and Systems*, Institution of Engineering and Technology, London, UK, 2016.
12. B. M. Wilamowski, J. D. Irwin, *Power Electronics and Motor Drives*, CRC Press, Boca Raton, FL, 2011.
13. B. Choi, *Pulse Width Modulated DC-to-DC Power Conversion*, IEEE Press, Wiley, 2013.
14. D. O. Neacsu, *Switching Power Converters: Medium and High Power Electronics and Motor Drives*, CRC Press, Boca Raton, FL, 2014.
15. A. I. Pressman, *Switching Power Supply Design*, McGraw-Hill, New York, 1998.
16. K. C. Wu, *Switch-Mode Power Converters-Design and Analysis*, Elsevier Academic Press, Boston, MA, 2006.
17. B. R. Nair, P. C. Sen. A novel power MOSFET switching-mode power supply, *International Journal of Electronics*, 59(2), 141–151, 2007.
18. M. Rajeev. An input current shaper with boost and flyback converter using integrated magnetics, *The Fifth International Conference on Power Electronics and Drive Systems 2003 PEDS 2003 PEDS-03*, IEEE, Singapore, 2003.



Taylor & Francis

Taylor & Francis Group

<http://taylorandfrancis.com>

11 Multipulse Converter

11.1 INTRODUCTION

The demand for modern technological development in the field of power electronics needs a high-quality power supply and reliability. Hence, power converters are the heart of all power-processing units, including renewal energy converters, industrial, telecommunications, defense, and aerospace applications. The power converters, especially the front-end AC-DC converters are widely used. Hence, AC-DC converters should be able to provide high-quality power to the utility under all circumstances. The diode-based AC-DC converters have a lot of disadvantages, such as power-quality problems in terms of ripple in output due to harmonics injection and distortion voltage, which cause a poor power factor. The active front-end converters or multipulse converters (MPC) are becoming popular nowadays due to improved power quality and simple control.

11.2 MULTIPULSE CONVERTER

The MPCs have been developed for reducing harmonics of AC-DC conversion. It feeds the load from a few kilowatts to several megawatts with unidirectional and bidirectional power flow. These MPCs have different configurations to reduce magnetics and circuit integration with a different topology. There are many MPC topologies available in the literature, such as pulse multiplication, phase staggering, and varying connections, such as the *T* connection, double star and extended delta, zigzag, fork, polygon, active-interphase reactors, optimum interphase reactor-pulse doubling circuits, and reduced-rating autotransformers. Several circuit configurations of MPCs have been explored to meet the demands of vast varying applications while maintaining good power quality at AC mains and output DC loads. The classification of the MPC is given in [Figure 11.1](#).

11.2.1 UNIDIRECTIONAL AC-DC CONVERTERS

If the power flow direction is unidirectional, then that converter is known as a unidirectional AC-DC converter. [Figure 11.2](#) shows the AC-DC three-phase unidirectional converter with diodes, transformers, and other additional components. It is further subclassified into different numbers of pulses based on its advantages, such as cost, reliability, and power-quality considerations.

11.2.1.1 12-Pulse AC-DC Converters

The 12-pulse unidirectional AC-DC converters consist of an isolated multiwinding transformer and diode-bridge rectifiers. The voltage difference between input and output is nearly zero. The choice of rectifier connection is designed according to the secondary connection of the transformer. There are many MPC topologies available in the

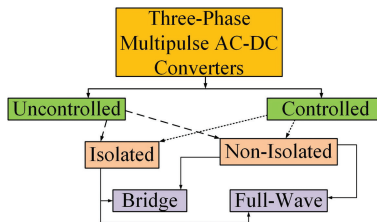


FIGURE 11.1 Types of a three-phase multiphase AC-DC converters. (From Behera, R.K., *Notes on Power Electronics and Drives*, IIT Patna, Bihta, Bihar, 2010.)

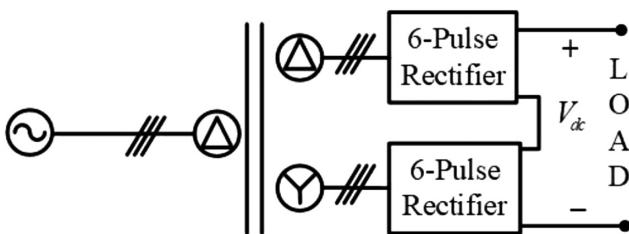


FIGURE 11.2 Block diagram of 12-pulse converter. (From Behera, R.K., *Notes on Power Electronics and Drives*, IIT Patna, Bihta, Bihar, 2010.)

literature. However, T-connection, double star and extended delta, zigzag, fork, polygon, active interphase reactors, and optimum interphase reactors pulse doubling circuits are very popular in industrial applications. Figure 11.2 shows a 12-pulse full-wave AC-DC unidirectional converter using an isolated transformer with delta primary and two secondary with one star, and other one is delta for a 30° phase shift. The secondary of the transformer is feeding to the rectifiers, and both the rectifiers are connected in series.

11.2.1.2 18-Pulse AC-DC Converters

The 18-pulse AC-DC converters have improved performance and have less ripples in AC mains current, and voltage, and thereby low total harmonic distortion (THD). Figure 11.3 shows the block diagram of the 18-pulse AC-DC converter. The primary is star connected, and the secondary windings are zigzag-star-zigzag connected to give supply to 18 diodes to the load circuit. There are several pioneering circuits of non-isolated 18-pulse AC-DC converters developed to get prominent performance in THD. According to required specifications, there are two types of topologies available, such as isolated and non-isolated.

11.2.1.3 24-Pulse AC-DC Converters

The conventional 12-pulse controlled rectifier has inherent harmonics in its input current and output voltage. These harmonics can be reduced by using filters, but these filters are bulky and have significant loss. However, some applications need precise power-quality specifications, and it is advisable to use a 24-pulse AC-DC converter. Because it gives less ripples in its DC output and pure sinusoidal current in the AC

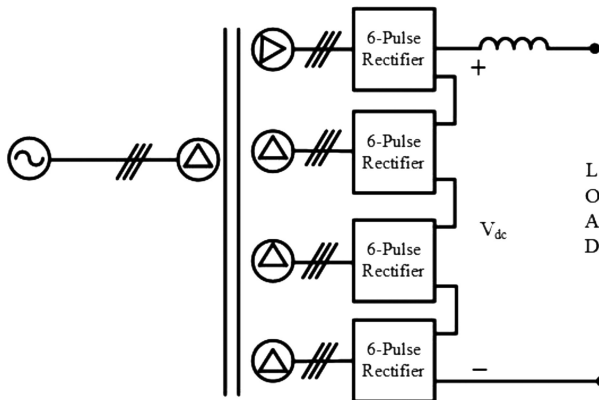


FIGURE 11.3 Block diagram of 18-pulse AC-DC converter. (From Behera, R.K., *Notes on Power Electronics and Drives*, IIT Patna, Bihta, Bihar, 2010.)

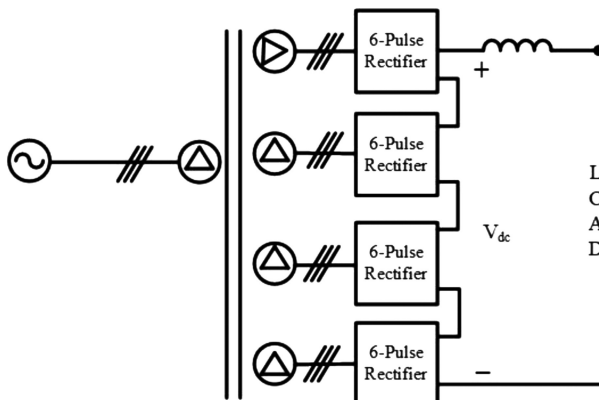


FIGURE 11.4 Block diagram of 24-pulse AC-DC converter. (From Behera, R.K., *Notes on Power Electronics and Drives*, IIT Patna, Bihta, Bihar, 2010.)

mains. The block diagram of 24-pulse AC-DC converter is shown in Figure 11.4. It consists of a delta-connected primary, and the secondary has a phase-shifted delta that feeds to four six-pulse rectifiers connected in cascade.

11.3 MULTILEVEL INVERTERS

For the past three decades, multilevel voltage source inverter (VSI) technology has been developed rapidly around power electronics. It is a promised power conversion device in the medium voltage range (4.6–13.8 kV) application without the requirement of a step-up transformer. It may operate with a higher voltage level by using a step-up transformer. Multilevel voltage source converter (VSC) technology has been utilized in various industrial applications, such as the traction system and variable

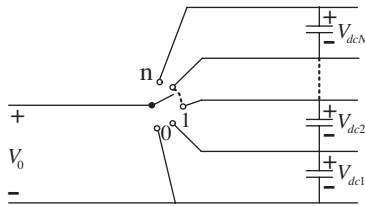


FIGURE 11.5 Equivalent circuit representation of multilevel VSI. (From Behera, R.K. and Das, S.P., A utility high performance multilevel inverter fed induction motor drive system for traction and industrial applications, PhD Thesis, Indian Institute of Technology Kanpur, India, February 2009.)

speed drives. Besides that, it has also found applications in AC power supplies, reactive power compensations, and in enabling the use of renewable energy sources.

The basic idea to implement the multilevel converter is shown in Figure 11.5. The switch showing “0” to “n” means the number of switches that connected in series to the DC link voltage. The output voltage depends on the switch to turn on across the DC link voltage. In order to generate a adverse input voltage, the reference output signal must be linked to the distinct sections of the capacitor string.

Both industries and universities have introduced several state-of-the-art multilevel VSCs over the last two decades. The three major multilevel topologies are

1. Cascaded H-bridge multilevel inverter (CHBMI)
2. Neutral point clamped (NPC) or diode-clamped inverter
3. Flying capacitor or floating capacitor or capacitor-clamped inverter

11.3.1 CASCADED H-BRIDGE MULTILEVEL INVERTER

The H-bridge inverter is shown in Figure 11.6. The H-bridge can produce three discrete levels of voltage waveforms— $+V_{dc}$, 0, and $-V_{dc}$ —where V_{dc} is the DC link

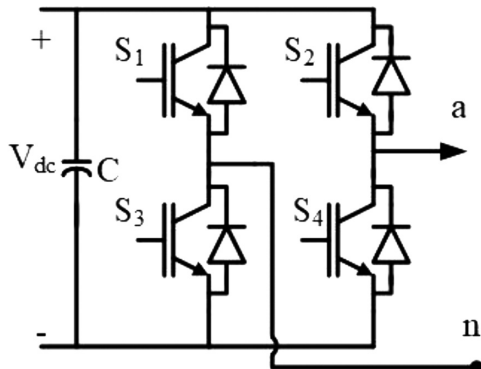


FIGURE 11.6 Full bridge or H-bridge VSI. (From Behera, R.K. and Das, S.P., A utility high performance multilevel inverter fed induction motor drive system for traction and industrial applications, PhD Thesis, Indian Institute of Technology Kanpur, India, February 2009.)

voltage. Therefore, the H-bridge inverter can form by connecting series with several H-bridges to produce more levels in its output waveform. This type of configuration is called the cascaded H-bridge multilevel inverter.

The single-phase m -level cascaded inverter is shown in [Figure 11.7](#). The DC source has been connected to each single-phase H-bridge inverter. Every VSI stage can produce three distinct levels of voltage outputs: $+V_{dc}$, 0, and $-V_{dc}$. To achieve this, the DC is connected to the AC output by distinct switching possibilities of S_1 , S_2 , S_3 , and S_4 . To get $+V_{dc}$, the switches S_1 and S_4 need to be turned on, whereas $-V_{dc}$ can be achieved by turning on the switches S_2 and S_3 . To get the 0, either turn on the upper two switches (S_1 and S_2) or lower two switches (S_3 and S_4).

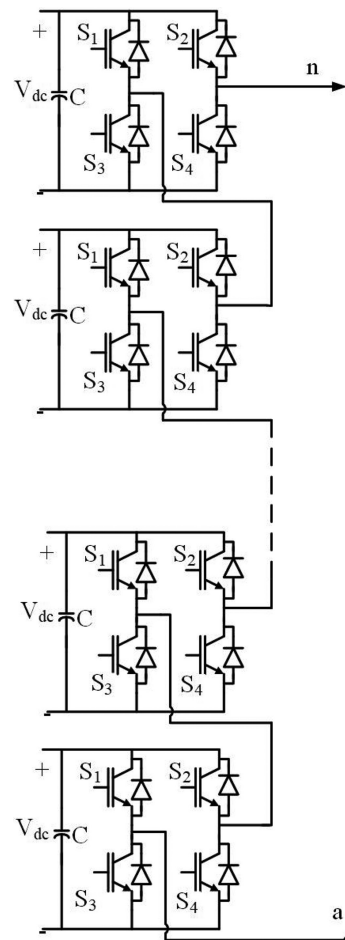


FIGURE 11.7 Single-phase topology of a multilevel-cascaded H-bridge VSI. (From Behera, R.K. and Das, S.P., A utility high performance multilevel inverter fed induction motor drive system for traction and industrial applications, PhD Thesis, Indian Institute of Technology Kanpur, India, February 2009.)

The outputs of each cascade-connected full-bridge inverters are connected in sequence, such that the synthesized voltage waveform is the sum total of the cascaded VSI outputs. Therefore, the output phase voltage level “m” in a cascaded VSI is defined by

$$m = 2s + 1 \quad (11.1)$$

where s is the number of separate dc sources. The phase voltage for 5-level H-bridge is given as follows

$$v_{an} = v_{a1} + v_{a2} + v_{a3} + v_{a4} + v_{a5} \quad (11.2)$$

11.3.2 NEUTRAL POINT-CLAMPED MULTILEVEL INVERTER

The NPC or diode-clamped inverter is the most popular multilevel topology in industry and traction applications. [Figure 11.8](#) shows a three-phase three-level (TPTL) NPC topology. The TPTL-NPC has two pairs of series switches (top and bottom) adjacent to two line capacitors. The capacitor midpoint is connected with the cathode of bottom and anode of the top diode. The cathode of the top and anode of the bottom diode is linked to the center of the top and bottom switch pairs respectively, as shown in [Figure 11.8](#). The primary DC voltage in this instance is split into two components. If location n is deemed to be the ground reference, the feasible three-phase voltage inputs are indicated as $-V_{dc}/2$, 0, or $V_{dc}/2$. The line-line voltages of two legs with common DC capacitors are as V_{dc} , $V_{dc}/2$, 0, $-V_{dc}/2$, $-V_{dc}$. The switching states and possible output voltage for the TPTL-NPC inverter are given in [Table 11.1](#). From

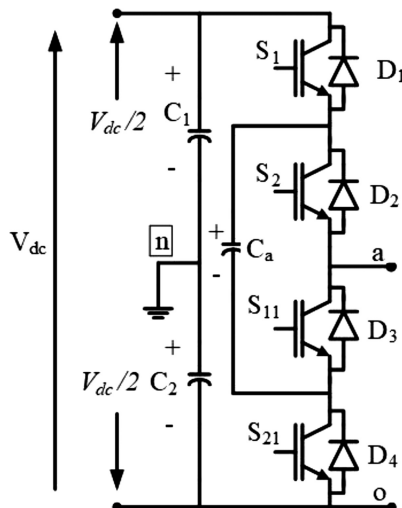


FIGURE 11.8 TPTL-NPC MLI topology. (From Behera, R.K. and Das, S.P., A utility high performance multilevel inverter fed induction motor drive system for traction and industrial applications, PhD Thesis, Indian Institute of Technology Kanpur, India, February 2009.)

TABLE 11.1
The Switching States and Their
Corresponding Output Voltages in
TPTL-NPC MLI

S_1	S_2	S_{11}	S_{21}	V_{an}
1	1	0	1	$\frac{V_{dc}}{2}$
1	0	0	1	0
0	0	1	1	$-\frac{V_{dc}}{2}$

Table 11.1, it is observed that the switches (S_1, S_{11}) and (S_2, S_{21}) are complementary to each other. Similarly, switching states exist in all three stages to generate matching three-level voltage outputs to distinguish the conventional two-level to three-level, and the key components are D_{11} and D_{22} . Both diodes clamp the switching voltage to half the voltage of the DC-bus stage. When both switches S_1 and S_2 turn on, the voltage across a and n is $\frac{V_{dc}}{2}$, that is, $V_{an} = \frac{V_{dc}}{2}$.

The three-level topology shown in [Figure 11.8](#) can be further extended to a higher-level inverter configuration.

11.3.3 FLYING CAPACITOR MULTILEVEL INVERTER (FCMLI)

The FCMLI design is comparable to the NPC-inverter, except that it employs capacitors rather than clamping diodes. [Figure 11.9](#) shows the topology of the three-level flying capacitor (FC) inverter. The extra voltage level and clamping is accomplished with capacitors that “float” to the corresponding DC source. These floating capacitors are referred to as “flying capacitors” and therefore, it is known as FC topology. The switch pairs (S_1, S_{11}) and (S_2, S_{21}) are complementary to each other. It is important to note that the complementary pair of a top switch is positioned differently in the bottom of the leg in FC topology. The capacitors are regulated at a voltage of $V_{dc}/2$. The FC is operated or switched in such a way that the flying capacitors voltage is maintained at $V_{dc}/2$. This is achieved by proper modulation schemes. By doing so, the voltage stress across inverter switch devices keeps limited to $V_{dc}/2$. The FC voltage balance is accomplished by the use of the auxiliary switching state for the same voltage at the inverter supply. The switching states for three-level voltage outputs per phase are mentioned in [Table 11.2](#). One can understand from this table that for producing “0” voltage level, it possesses two different switch states, that is, turn on S_1, S_2 together, the output $+V_{dc}/2$ without changing the state of C_a which is represented by the NC state of the FC in [Table 11.2](#). Similarly, turn off S_1, S_2 together outputs $-V_{dc}/2$ with the NC state of C_a . For the remaining switching states, either S_1 -on S_2 -off or vice versa will result in zero output voltage with the state of the capacitor charging and discharging, respectively. The THL-FC inverter voltage is generally specified for any initial state of the FC voltage as,

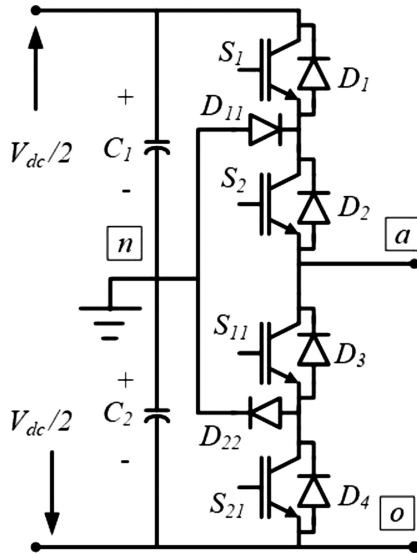


FIGURE 11.9 Three-phase three-level topology of FCMLI. (From Behera, R.K. and Das, S.P., A utility high performance multilevel inverter fed induction motor drive system for traction and industrial applications, PhD Thesis, Indian Institute of Technology Kanpur, India, February 2009.)

$$V_{an} = S_1(V_{dc} - V_{fa}) + S_2 V_{fa} - \frac{V_{dc}}{2} \quad (11.3)$$

Based on Equation (11.3), **Table 11.2** shows the switch combinations to synthesize the output voltage V_{an} of phase a to n , where S_1 and S_2 are either one or zero depending on switching instant.

TABLE 11.2
Switching States and Their
Corresponding Output Voltages for
Three-Level FCMLI

S_1	S_2	V_{an}	C_a
ON	ON	$+\frac{V_{dc}}{2}$	(NC)
ON	OFF	0	(+)
OFF	ON	0	(-)
OFF	OFF	$-\frac{V_{dc}}{2}$	(NC)

Note: NC means no change, + means charging,
- means discharge.

11.4 POWER CONVERTER SWITCHING TECHNIQUES

11.4.1 HYSTERESIS CURRENT CONTROL OF INVERTERS

The performance of the inverter largely depends upon current control techniques. The hysteresis current-control technique has many advantages, such as control of the instantaneous current waveform, peak-current protection, overload rejection, extremely good dynamic response, and compensation of effects due to load parameter changes.

Linear and nonlinear controllers are used to control the power converters. The linear controllers have good steady-state performance and fewer harmonic content with the fixed switching frequency (SF). Although it does not have a good dynamic response and robustness to the system, its performance can be affected by a change in parameters, such as filter capacitor and an inductor connected to the system. On the other side, the nonlinear controller has a fast, dynamic response and robustness toward the change in a parameter of the system. The response of the nonlinear controllers is not affected by the change in load dynamics, such as filter capacitor and inductors connected to the system. Varying the SF and complex hardware implementation are the major disadvantages of nonlinear controllers.

The study of hysteresis current controller for single-phase inverter as shown in Figure 11.10 can be considered as one of the basic nonlinear controllers. It has four switches S_1, S_4 in a leg and S_2, S_3 in another leg of the inverter, and it is connected to an inductor and the load resistance.

We get bipolar output voltage at the output of the inverter for single-band hysteresis current control (SBHCC). To obtain the switching-frequency equation, the equivalent circuit diagram of the single-phase inverter is considered as shown in Figures 11.11 and 11.12.

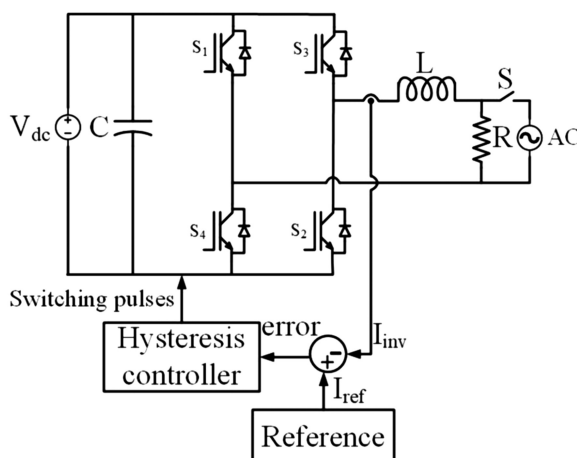


FIGURE 11.10 Hysteresis scheme in single-phase full-bridge inverter. (From Kumar, J. and Behera, R.K., Hysteresis current controllers for grid connected inverter: Review and experimental implementation, in *Proceedings of PEDES'18*, December 18–21, 2018, IIT Madras, Chennai, India, pp. 1–6.)

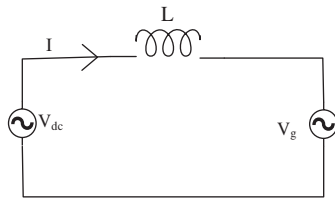


FIGURE 11.11 Equivalent circuit diagram of the inverter as an ideal condition. (From Kumar, J. and Behera, R.K., Hysteresis current controllers for grid connected inverter: Review and experimental implementation, in *Proceedings of PEDES'18*, December 18–21, 2018, IIT Madras, Chennai, India, pp. 1–6.)

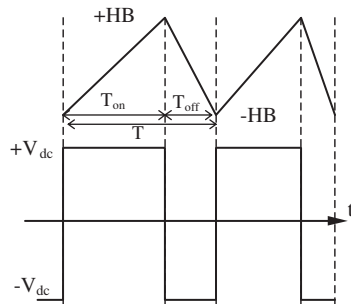


FIGURE 11.12 Single-band hysteresis control voltage generation logic. (From Kumar, J. and Behera, R.K., Hysteresis current controllers for grid connected inverter: Review and experimental implementation, in *Proceedings of PEDES'18*, December 18–21, 2018, IIT Madras, Chennai, India, pp. 1–6.)

When S_1 and S_2 are on,

$$L \frac{di_e}{dt} = V_{dc} - V_g \quad (11.4)$$

When S_3 and S_4 are on,

$$L \frac{di_e}{dt} = V_{dc} + V_g \quad (11.5)$$

Then the on period can be written as in Equation (11.6), and the off period can be written as in Equation (11.7). Thus, the total time can be calculated as in Equation (11.8).

$$T_{on} = \frac{2HB \times L}{V_{dc} - V_g} \quad (11.6)$$

$$T_{off} = \frac{2HB \times L}{V_{dc} + V_g} \quad (11.7)$$

$$T = T_{\text{on}} + T_{\text{off}} = \frac{4HB \times L \times V_{dc}}{V_{dc}^2 - V_g^2} \quad (11.8)$$

$$f_{s_{SB}} = \frac{\left(V_{dc}^2 - V_g^2\right)}{4V_{dc} \times L \times HB} \quad (11.9)$$

The maximum frequency is obtained when the voltage crossing is zero, that is, $V_g = 0$. The output voltage of the inverter is sinusoidal in nature; thus, SF changes at a fixed band during a complete cycle from 0 to V_{dc} . [Figure 11.13](#) shows the single-band hysteresis controller.

$$f_{\max} = \frac{V_{dc}}{4L \times HB} \quad (11.10)$$

11.4.2 PULSE-WIDTH MODULATION (PWM) TECHNIQUES

In the PWM technique, the two waveforms called *carrier* and *reference* are generally compared with each other to get the desired switching pulses. For the sinusoidal pulse-width modulation (SPWM) technique, the carrier frequency f_c of the amplitude of A_c is continuously compared with reference signal frequency f_r of amplitude A_r . If the $A_r > A_c$, then the active device connected to that switch is on. If the $A_r < A_c$, then the active device connected to that carrier is switched off.

The ratio of the amplitude of reference to the carrier signal is called the modulation index (m_a) of the modulating signal, and the ratio of carrier signal frequency to the reference signal frequency is called frequency modulation index (m_f), where

$$m_a = \frac{A_r}{A_c} \text{ and } m_f = \frac{f_c}{f_r}$$

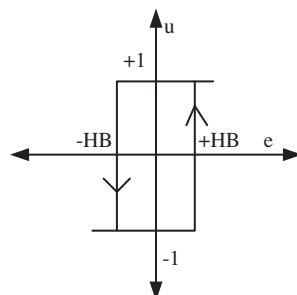


FIGURE 11.13 Single-band hysteresis controller. (From Behera, R.K. and Das, S.P., A utility high performance multilevel inverter fed induction motor drive system for traction and industrial applications, PhD Thesis, Indian Institute of Technology Kanpur, Uttar Pradesh, India, February 2009.)

The following PWM techniques are discussed:

1. SPWM
2. Phase-opposition sinusoidal PWM (POSPWM)
3. In-phase sinusoidal PWM (IPSPWM)
4. Third-harmonic injection SPWM (THISPWM)
5. Space vector pulse width modulation (SVPWM)

11.4.2.1 Sinusoidal PWM

The SPWM MATLAB/Simulink implementation is shown in [Figure 11.14](#) with modulation index 0.8, and the corresponding pulse generation is shown in [Figure 11.15](#).

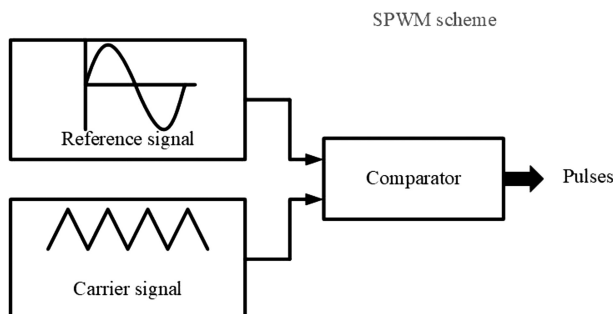


FIGURE 11.14 MATLAB/Simulink diagram of SPWM method. (From Behera, R.K. and Das, S.P., A utility high performance multilevel inverter fed induction motor drive system for traction and industrial applications, PhD Thesis, Indian Institute of Technology Kanpur, Uttar Pradesh, India, February 2009.)

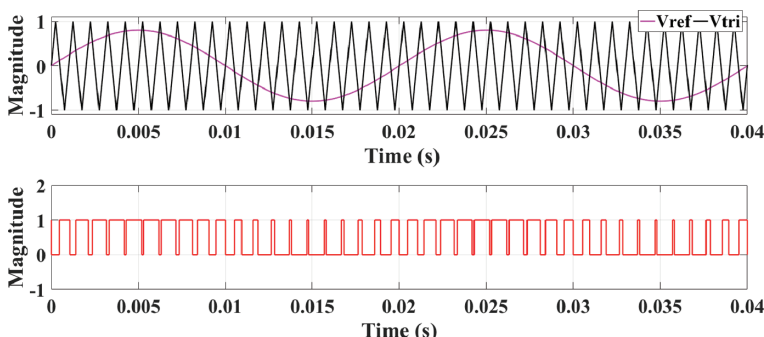


FIGURE 11.15 Switching pulses of SPWM method. (From Behera, R.K. and Das, S.P., A utility high performance multilevel inverter fed induction motor drive system for traction and industrial applications, PhD Thesis, Indian Institute of Technology Kanpur, Uttar Pradesh, India, February 2009.)

11.4.2.2 Phase-Opposition Sinusoidal PWM

The POSPWM switching method and the pulses are shown in Figures 11.16 and 11.17. Two carrier signals are compared with a single reference wave to get the switching pulses, whenever the reference is greater than the carrier. These carrier pulses are phase-opposite with each other.

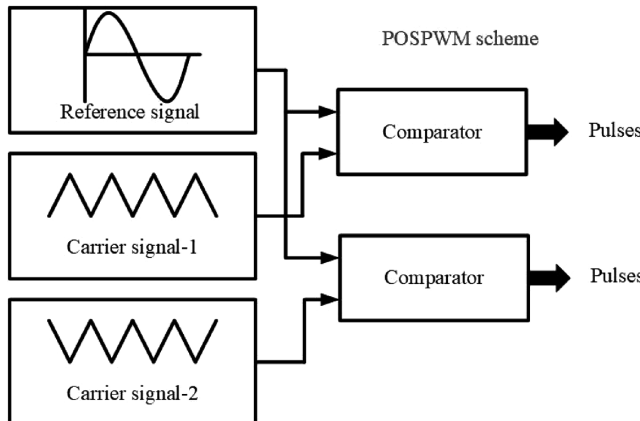


FIGURE 11.16 MATLAB/Simulink diagram of POSPWM method. (From Behera, R.K. and Das, S.P., A utility high performance multilevel inverter fed induction motor drive system for traction and industrial applications, PhD Thesis, Indian Institute of Technology Kanpur, Uttar Pradesh, India, February 2009.)

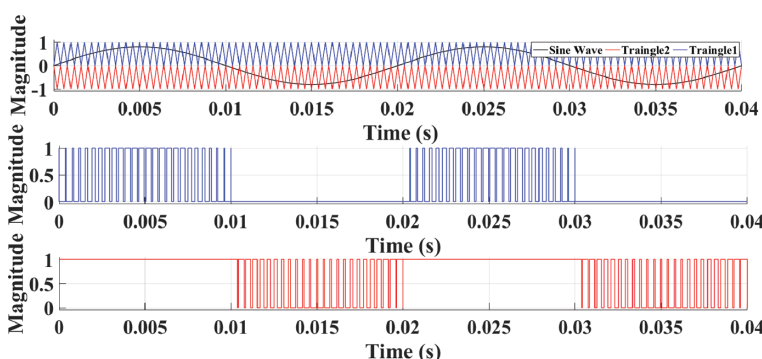


FIGURE 11.17 Switching pulses of POSPWM method. (From Behera, R.K. and Das, S.P., A utility high performance multilevel inverter fed induction motor drive system for traction and industrial applications, PhD Thesis, Indian Institute of Technology Kanpur, Uttar Pradesh, India, February 2009.)

11.4.2.3 In-Phase Sinusoidal PWM

The IPSPWM switching method and the pulses are represented in Figures 11.18 and 11.19. Two carrier signals are compared with a single reference wave to get the pulses, whenever the reference is greater than the carrier. These carrier pulses are in-phase with each other.

11.4.2.4 Third-Harmonic Injection Sinusoidal PWM (THISPWM)

The output using the SPWM technique is limited to $0.5 V_{dc}$. To enhance the output voltage using carrier-based SPWM, a third harmonic injected in the fundamental

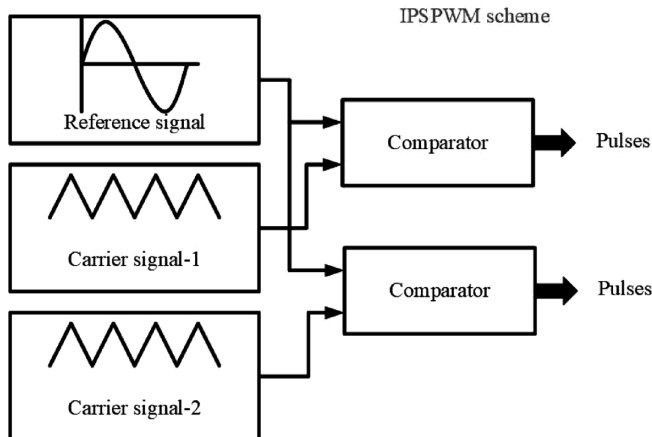


FIGURE 11.18 MATLAB/Simulink diagram of IPSPWM method. (From Behera, R.K. and Das, S.P., A utility high performance multilevel inverter fed induction motor drive system for traction and industrial applications, PhD Thesis, Indian Institute of Technology Kanpur, Uttar Pradesh, India, February 2009.)

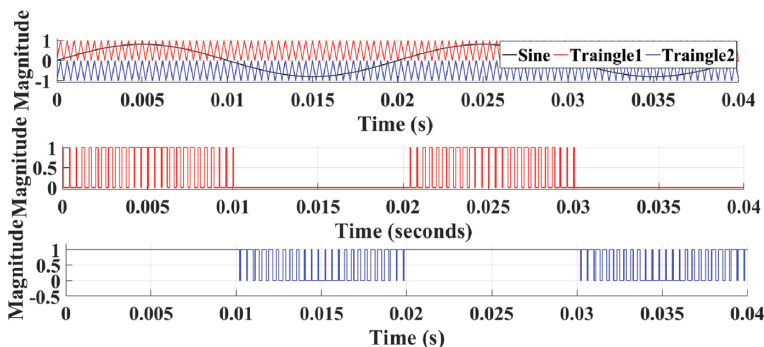


FIGURE 11.19 Switching pulses of IPSPWM method. (From Behera, R.K. and Das, S.P., A utility high performance multilevel inverter fed induction motor drive system for traction and industrial applications, PhD Thesis, Indian Institute of Technology Kanpur, Uttar Pradesh, India, February 2009.)

sine wave has been done. The addition of an appropriate third harmonic in the reference-modulating signal reduces the peak of the resultant reference signal as shown in [Figure 11.20](#), which increases the output voltage from $0.5 V_{dc}$. The injected third harmonics cancel out each other and does not appear in the output phase voltages as shown in [Figure 11.21](#).

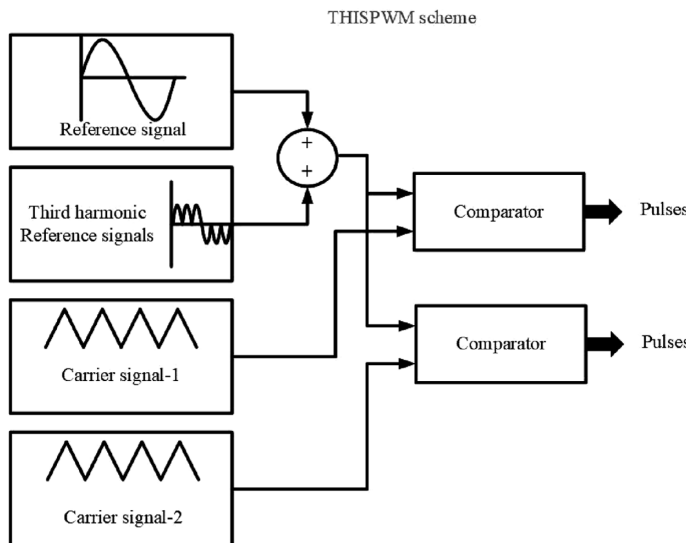


FIGURE 11.20 MATLAB/Simulink diagram of THISPWM method. (From Behera, R.K. and Das, S.P., A utility high performance multilevel inverter fed induction motor drive system for traction and industrial applications, PhD Thesis, Indian Institute of Technology Kanpur, Uttar Pradesh, India, February 2009.)

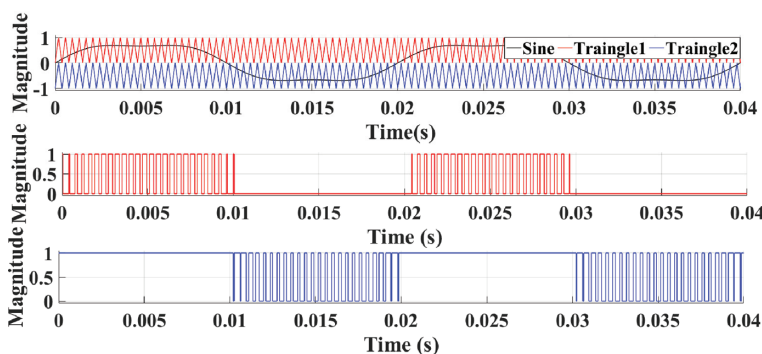


FIGURE 11.21 Switching pulses of THISPWM method. (From Behera, R.K. and Das, S.P., A utility high performance multilevel inverter fed induction motor drive system for traction and industrial applications, PhD Thesis, Indian Institute of Technology Kanpur, Uttar Pradesh, India, February 2009.)

11.4.2.5 Three-Phase Two-Level SVPWM

Modulation of space vectors is a prime method of modulating the inverter output voltages in real time and for digital control. [Figure 11.22](#) shows the three-phase two-level voltage-source inverter.

[Table 11.3](#) gives the information of switching states of the inverter. Switching state “P” shows that the upper switch in the inverter leg is on and the pole voltage (V_{AO} , V_{BO} , V_{CO}) is positive ($V_{dc}/2$) while “O” suggests that the inverter pole voltage is ($-V_{dc}/2$) owing to the conduction of the lower switch.

In the two-level inverter, there are eight (2^3) possible switching combinations that exist, and these switching states with their space vector and vector magnitude are listed in [Table 11.4](#). The relationship between the space vectors and the switching states, related to the two-level inverter, is shown in [Figure 11.23](#) for a balanced inverter operation

$$V_{AO}(t) + V_{BO}(t) + V_{CO}(t) = 0 \quad (11.11)$$

where V_{AO} , V_{BO} , and V_{CO} are the instantaneous phase (pole) voltages. To transform three-phase variables into two-phase variables, only two voltage vectors are enough, and from a balanced condition another voltage vector can be found.

$$\begin{bmatrix} v_\alpha(t) \\ v_\beta(t) \end{bmatrix} = \frac{2}{3} \begin{bmatrix} 1 & \frac{1}{2} & \frac{1}{2} \\ 0 & \sqrt{3} & \frac{\sqrt{3}}{2} \end{bmatrix} \begin{bmatrix} V_{AO}(t) \\ V_{BO}(t) \\ V_{CO}(t) \end{bmatrix} \quad (11.12)$$

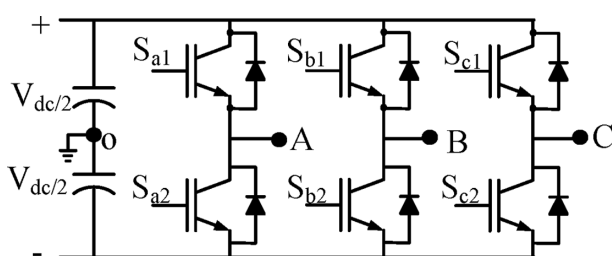


FIGURE 11.22 Three-phase two-level VSI. (From Behera, R.K. and Das, S.P., A utility high performance multilevel inverter fed induction motor drive system for traction and industrial applications, PhD Thesis, Indian Institute of Technology Kanpur, Uttar Pradesh, India, February 2009.)

TABLE 11.3
Switching States Definition

Switching State	Leg A			Leg B			Leg C		
	S_{a1}	S_{a2}	v_{AO}	S_{b1}	S_{b2}	v_{BO}	S_{c1}	S_{c2}	v_{CO}
P	On	Off	$(V_{dc})/2$	On	Off	$(V_{dc})/2$	On	Off	$(V_{dc})/2$
O	Off	On	$-(V_{dc})/2$	Off	On	$-(V_{dc})/2$	Off	On	$-(V_{dc})/2$

TABLE 11.4
Space Vector, Switching States, and On-State Switches

Space Vector	Switching State	On-State Switch	Vector Magnitude
V_o	[PPP]	S_{a1}, S_{b1}, S_{c1}	$\vec{V}_o = 0$
V_7	[OOO]	S_{a2}, S_{b2}, S_{c2}	
V_1	[POO]	S_{a1}, S_{b2}, S_{c2}	$\vec{V}_1 = \frac{2}{3}V_{dc}e^{j0}$
V_2	[PPO]	S_{a1}, S_{b1}, S_{c2}	$\vec{V}_2 = \frac{2}{3}V_{dc}e^{j\frac{\pi}{3}}$
V_3	[OPO]	S_{a2}, S_{b1}, S_{c2}	$\vec{V}_3 = \frac{2}{3}V_{dc}e^{j\frac{2\pi}{3}}$
V_4	[OPP]	S_{a2}, S_{b1}, S_{c1}	$\vec{V}_4 = \frac{2}{3}V_{dc}e^{j\frac{3\pi}{3}}$
V_5	[OOP]	S_{a2}, S_{b2}, S_{c1}	$\vec{V}_5 = \frac{2}{3}V_{dc}e^{j\frac{4\pi}{3}}$
V_6	[POP]	S_{a1}, S_{b2}, S_{c1}	$\vec{V}_6 = \frac{2}{3}V_{dc}e^{j\frac{5\pi}{3}}$

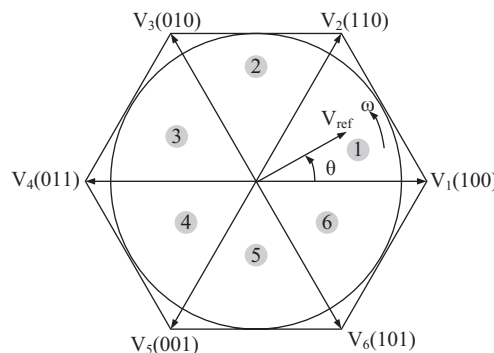


FIGURE 11.23 Space vector diagram for two-level inverter. (From Wu, B., *High-Power Converters and AC Drives*, IEEE Press, Wiley, Piscataway, NJ, 2nd edn., 2017.)

A space vector can be generally composed of stationary reference frame voltage equations,

$$\vec{V}(t) = V_\alpha(t) + jV_\beta(t) \quad (11.13)$$

$$\vec{V}(t) = \frac{2}{3} \left[v_{AO}(t)e^{j0} + v_{BO}(t)e^{j\frac{2\pi}{3}} + v_{CO}(t)e^{j\frac{4\pi}{3}} \right] \quad (11.14)$$

where $e^{jx} = \cos x + j \sin x$ and $x = 0, \frac{2\pi}{3}$ or $\frac{4\pi}{3}$. The produced phase voltages for the effective switching state [POO] can be represented as

$$v_{AO}(t) = \frac{2}{3}V_{dc}, v_{BO}(t) = -\frac{1}{3}V_{dc}, v_{CO}(t) = -\frac{1}{3}V_{dc} \quad (11.15)$$

Substitute Equation (11.15) into Equation (11.14), and then the obtained space vector for the switching state [POO] is

$$\vec{V}_1 = \frac{2}{3}V_{dc}e^{j0} \quad (11.16)$$

Following the above procedure, all six active vectors can be obtained

$$\vec{V}_k = \frac{2}{3}V_{dc}e^{\frac{j(k-1)\pi}{3}}, k = 1, 2, \dots, 6 \quad (11.17)$$

Table 11.4 represents the relation between the space vector and corresponding switching states. In **Figure 11.23**, the space vector diagram with reference vector \vec{V}_{ref} rotates with ω , and the other vectors (zero and active vectors) do not rotate.

$$\omega = 2\pi f \quad (11.18)$$

The angular displacement between \vec{V}_{ref} and the α axis of the stationary reference frame can be obtained by

$$\theta(t) = \int_0^t \omega(t) dt + \theta(0) \quad (11.19)$$

1. Dwell-Time Calculations

The dwell time can be calculated based on volt-second balancing principle given in Equation (11.20), which describes the product of the reference voltage \vec{V}_{ref} and sample period T_s equals the addition of the voltage multiplied by the time interval between the selected position vectors.

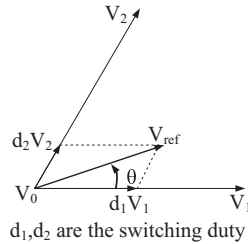


FIGURE 11.24 \vec{V}_{ref} is synthesized by \vec{V}_1 , \vec{V}_2 , and \vec{V}_0 . (From Wu, B., *High-Power Converters and AC Drives*, IEEE Press, Wiley, Piscataway, NJ, 2nd edn., 2017.)

To calculate the dwell times, let us consider the sector one of the input space vector as shown in Figure 11.24 and the volt-second balance equation given by

$$\vec{V}_{\text{ref}} \cdot T_s = \vec{V}_1 \cdot T_a + \vec{V}_2 \cdot T_b + \vec{V}_o \cdot T_o \quad (11.20)$$

$$T_s = T_a + T_b + T_o \quad (11.21)$$

where T_a , T_b , and T_o are dwell times for the vectors \vec{V}_1 , \vec{V}_2 , and \vec{V}_o , respectively. The space vectors in Equation (11.20) can be expressed as

$$\vec{V}_{\text{ref}} = \vec{V}_{\text{ref}} \cdot e^{j\theta} \quad V_1 = \frac{2}{3} V_{dc}, V_2 = \frac{2}{3} V_{dc} \cdot e^{j\frac{\pi}{3}}, V_o = 0 \quad (11.22)$$

Substitute Equation (11.22) into Equation (11.20) and split the resultant equations into real and imaginary components in the $\alpha - \beta$ plane, then we have

$$\begin{aligned} \vec{V}_{\text{ref}} (\cos(\theta) \cdot T_s + j \sin(\theta) \cdot T_s) &= \vec{V}_1 \cdot T_a + \vec{V}_2 \cdot T_b + \vec{V}_o \cdot T_o \\ \vec{V}_{\text{ref}} \cos(\theta) \cdot T_s &= \frac{2}{3} V_{dc} \cdot T_a + \frac{1}{3} V_{dc} \cdot T_b \\ j \sin(\theta) \cdot T_s &= \frac{1}{\sqrt{3}} V_{dc} \cdot T_b \end{aligned} \quad (11.23)$$

Solving Equations (11.24) and (11.22) together we will get

$$T_a = \frac{\sqrt{3} \cdot \vec{V}_{\text{ref}} \cdot T_s}{V_{dc}} \cdot \sin\left(\frac{\pi}{3} - \theta\right)$$

$$T_b = \frac{\sqrt{3} \cdot \vec{V}_{\text{ref}} \cdot T_s}{V_{dc}} \cdot \sin(\theta) \text{ for } 0 \leq \theta < \frac{\pi}{3}$$

$$T_o = T_s - (T_a + T_b) \quad (11.24)$$

Equation (11.25) yields dwell time when the reference space vector (v_{ref}) falls in sector I. It can also be used when v_{ref} is in other sectors, provided that a finding new θ' , which is a multiple of $\frac{\pi}{3}$, is subtracted from original angular displacement θ such that the modified angle θ' falls into the range between zero and $\frac{\pi}{3}$.

$$\theta' = \theta - (k-1) \frac{\pi}{3} \text{ for } 0 \leq \theta' < \frac{\pi}{3} \quad (11.25)$$

where $k = 1, 2, \dots, 6$ for Sectors I, II, ..., VI, respectively. Equation (11.25) can be rewritten in terms of the modulation index,

$$T_a = m_a T_s \sin\left(\frac{\pi}{3} - \theta\right)$$

$$T_b = m_a T_s \sin(\theta)$$

$$T_o = T_s - (T_a + T_b) \quad (11.26)$$

where m_a is the modulation index

$$m_a = \frac{\sqrt{3} \vec{V}_{\text{ref}}}{V_{dc}} \quad (11.27)$$

The maximum magnitude of the reference vector, which forms the largest circle within the hexagon, is shown in Figure 11.25. The hexagon formed by six active vectors having a length of $\frac{2}{3} V_{dc}$, $v_{\text{ref,max}}$ can be found as

$$v_{\text{ref,max}} = \frac{2}{3} V_{dc} \times \frac{\sqrt{3}}{2} = \frac{V_{dc}}{\sqrt{3}} \quad (11.28)$$

Substituting Equation (11.28) into Equation (11.27) gives the maximum modulation index $m_{a,\text{max}} = 1$, from which the modulation index range for the SVPWM scheme is

$$0 \leq m_a \leq 1 \quad (11.29)$$

The maximum fundamental line-to-line voltage root mean square (RMS) produced by the Space Vector Modulation (SVM) scheme can be calculated by

$$V_{\text{max,SVM}} = \frac{\sqrt{3} V_{\text{ref,max}}}{\sqrt{2}} = 0.707 V_{dc} \quad (11.30)$$

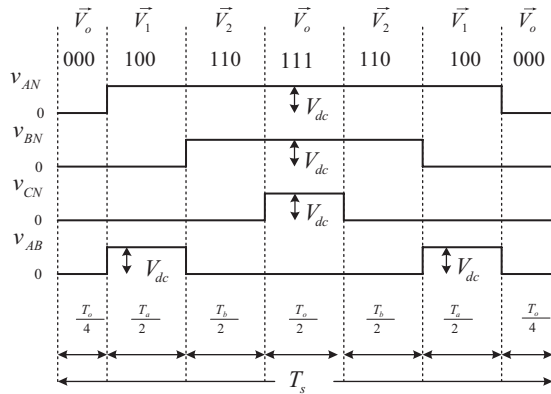


FIGURE 11.25 Seven-segment switching sequence for v_{ref} in Sector I. (From Wu, B., *High-Power Converters and AC Drives*, IEEE Press, Wiley, Piscataway, NJ, 2nd edn., 2017.)

2. Switching Sequence:

- a. To change from one switching state to the next switching state, there should be only two switches involved in the same inverter leg, one being on and other being off.
 - b. There should be a minimum number of switching taking place when the reference space vector moves from one sector to another sector.

The seven-segment switching sequence and output voltage waveforms for Sector 1 for a reference space vector V_{ref} is shown in Figure 11.25. The sampling time T_s is divided into seven segments as tabulated in Table 11.5, which are equal to the total sampling time T_s .

Every switch of an inverter turns on and off once in a sample time. The SF f_{sw} of the device is equal to the sampling frequency f_{sp} . Therefore, the $f_{sw} = f_{sp} = 1/T_s$.

TABLE 11.5
Switching Sequence for Three-Phase Two-Level SVPWM

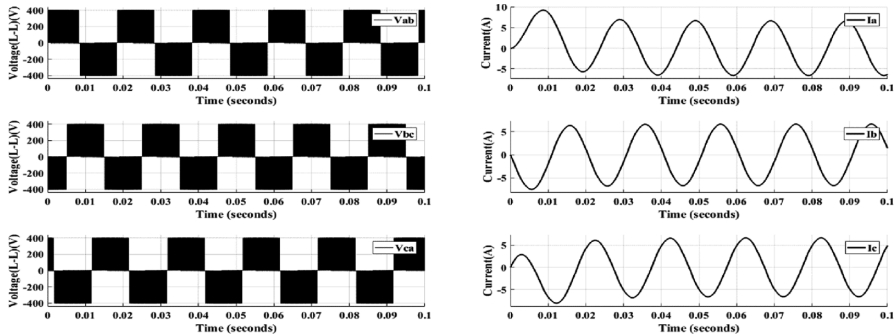


FIGURE 11.26 Inverter output waveforms produced by SVPWM scheme with $f_{sw} = 5$ kHz, $f = 50$ Hz, and $m_a = 0.8$. (From Behera, R.K. and Das, S.P., Space vector modulation for a three-level NPC ac–dc converter system: An experimental investigation, *Proceedings of IEEE-ICPCES 2010, MNNIT, Allahabad, India, November 29–December 01, 2010.*)

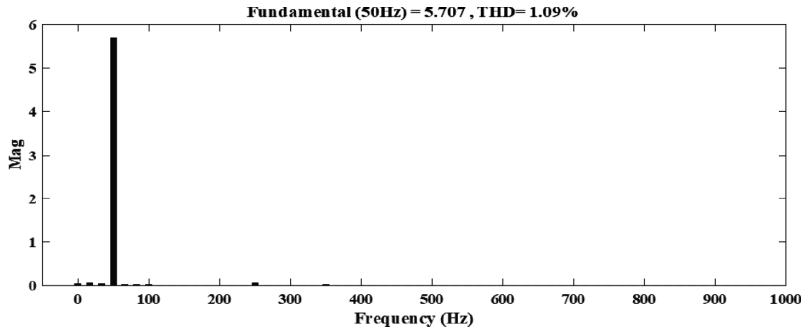


FIGURE 11.27 Simulated THD waveform of the three-phase two-level inverter output line current with $f_{sw} = 5$ kHz, $f = 50$ Hz, and $m_a = 0.8$. (From Behera, R.K. and Das, S.P., Space vector modulation for a three-level NPC ac–dc converter system: An experimental investigation, *Proceedings of IEEE-ICPCES 2010, MNNIT, Allahabad, India, November 29–December 01, 2010.*)

3. Simulation Results:

The simulation results provided with the SF of $f_{sw} = 5$ kHz and fundamental frequency $f = 50$ Hz and the modulation index $m_a = 0.8$ with a three-phase resistive-inductive ($R = 10 \Omega$, $L = 100 \text{ mH}$) load. The line-voltage and line-current of the inverter output as well as current THD are shown in Figures 11.26 and 11.27.

11.5 RESONANT CONVERTERS

The researchers are interested in designing resonant converters, due to increased demand for high-power density power supplies in aerospace, defense, and telecommunications. These can operate at a high-switching frequencies (SFs) and without harmful effects from PWM converters. In these applications, there are few

constraints upon the size, volume, and weight of converters to enable them to accommodate greater payloads. A great effort has been made in the development of soft switching operations by utilizing transformer magnetizing and leakage inductors as two resonant elements. It is possible to design the converter with a lesser number of discrete component counts and lower cost. The voltage and current regulation in the resonant converter are achieved by frequency modulation. Hence, the input to the output voltage gain of the converter is not derived from the conventional inductor volt-second balance, such as the traditional PWM converter.

In the conventional PWM switched-mode power supply (SMPS), the switches are turned on at full current to the full voltage across the switches. Similarly, the switches have fully turned-off voltage from the full current. Such switching is classified as hard switching. The losses during the hard switching period are considerable. Further, because of the parasitic capacitance and inductance of the switching circuit, the turned-off voltage and turned-on current are more than full. [Figure 11.28](#) shows diode-clamped inductive load. [Figure 11.29](#) shows its switching waveforms and switching trajectory. The switching loss for the switching waveform in [Figure 11.29](#) is given by,

$$\text{Switching loss} = \left\{ \frac{1}{2} \times V_g \times I_l \times t_r \times f_s \right\} + \left\{ \frac{1}{2} \times V_g \times I_l \times t_f \times f_s \right\} \quad (11.31)$$

where V_g = source voltage, I_l = load current, t_r = rise time, f_s = switching frequency, and t_f = fall time.

From Equation (11.31), it can be observed that the losses due to switching are proportional to the f_s (SF). [Figure 11.30](#) shows the typical switching trajectory when parasitic effects are present.

To protect the devices from the switching stresses of high off-state voltages and high on-state current, snubber circuits are used. Snubber circuits are of two types: turn-off snubber and turn-on snubber. The turn-off snubber uses a resistor, capacitor, and diode. During turn off, capacitor C effectively comes across the device and limits the rate of rising of voltage. Thus, overvoltages during the turn-off process are snubbed. The device turn-off loss is also reduced. When properly sized, the snubber

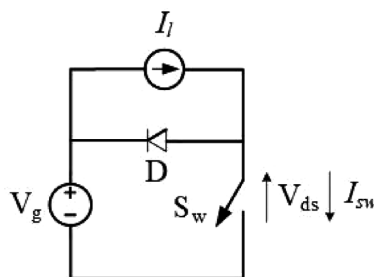


FIGURE 11.28 Circuit diagram of diode-clamped inductive load. (From Behera, R.K., *Notes on Power Electronics and Drives*, IIT Patna, Bihar, India, 2010.)

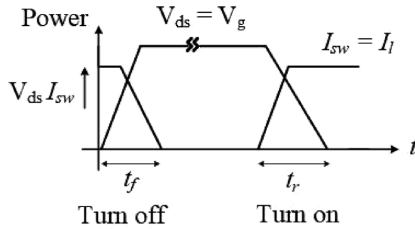


FIGURE 11.29 Switching waveforms and switching trajectory. (From Behera, R.K., *Notes on Power Electronics and Drives*, IIT Patna, Bihar, India, 2010.)

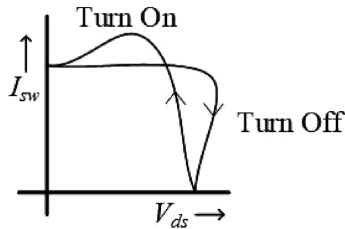


FIGURE 11.30 Effects of parasitics on switching trajectory. (From Vorperian, V., Analysis of resonant converters, PhD Thesis, California Institute of Technology, Pasadena, CA, May 1984.)

may also marginally reduce the overall losses. [Figure 11.31](#) shows the diode-clamped inductive load with turn-off snubber. The switching trajectory with the snubber circuit is shown in [Figure 11.32](#).

11.5.1 SOFT-SWITCHING TOPOLOGIES

Although the snubber circuit reduces the loss during one switching transition, during the other switching transition, the energy stored in snubber L or C will be dissipated in the snubber resistor. Hence, the snubber circuit will contribute to additional losses. Further snubber circuits are not so useful if the switching transition frequency is above 200 kHz, because the energy associated with the switching transition is more. Hence, soft-switching techniques are used to achieve lossless switching to obtain good efficiency at the high-SF.

In zero-voltage switching (ZVS) just before turn-on, the device voltage is zero, thus eliminating the turn-on losses. In zero-current switching (ZCS), the device current is zero just before the turn off, thus eliminating the turn-off losses. The following are the features of soft switching:

1. Soft switching converters can be switched at high frequency (HF).
2. HF switching reduces the converter size.

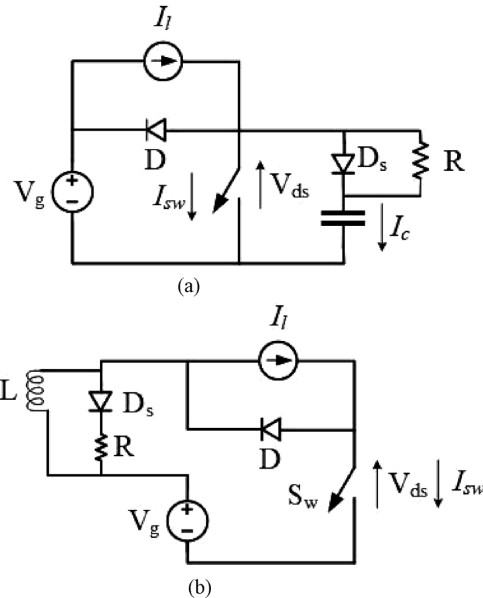


FIGURE 11.31 Circuit diagram of the clamped inductive circuit with (a) turn-off snubber, and (b) turn-on snubber. (From Behera, R.K., *Notes on Power Electronics and Drives*, IIT Patna, Bihar, India, 2010.)

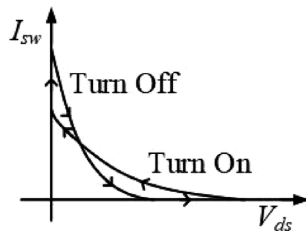


FIGURE 11.32 Switching trajectory with snubber circuit. (From Behera, R.K., *Notes on Power Electronics and Drives*, IIT Patna, Bihar, India, 2010.)

3. The switching process is not abrupt, so it emits less electromagnetic interference (EMI).
4. The energy stored in the parasitic can be recovered fully.

Figure 11.33 shows the soft-switching trajectory.

11.5.1.1 Resonant Load Converters

Resonant load converters employ a resonant circuit for power conversion. They exhibit ZVS/ZCS property. ZVS is to be achieved if the soft SF is greater than the resonant frequency (RF). ZCS is to be achieved if the SF is lesser than the RF.

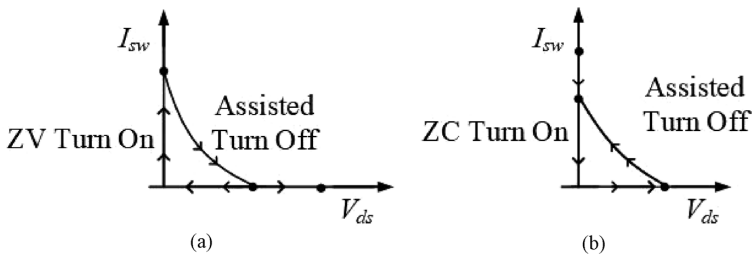


FIGURE 11.33 Soft-switching trajectory: (a) ZVS trajectory and (b) ZCS trajectory. (From Behera, R.K., *Notes on Power Electronics and Drives*, IIT Patna, Bihar, India, 2010.)

Output voltage control in such converters is achieved through the control of the SF. Resonant load converters are classified into series-loaded resonant converters and parallel-loaded resonant converters. Figure 11.34 shows the series-loaded resonant converter, and Figure 11.35 shows the parallel-loaded resonant converter.

Figure 11.36 shows the typical switch voltage and switch-current waveforms for a series resonant converter under ZVS condition. During the turn on, the device current is negative. This indicates that during the turn on, the switch achieves ZVS.

11.5.1.2 Resonant Switch Converters

Resonant switch converters are also called quasi-resonant converters that achieve ZVS or ZCS by using resonant switches. Resonant switches consist of a switch and resonant elements (L_r and C_r). They are classified based on a switch current (half

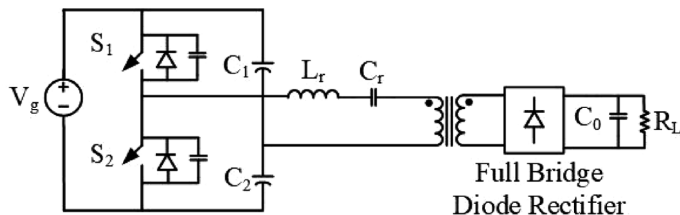


FIGURE 11.34 Series-loaded resonant converter. (From Behera, R.K., *Notes on Power Electronics and Drives*, IIT Patna, Bihar, India, 2010.)

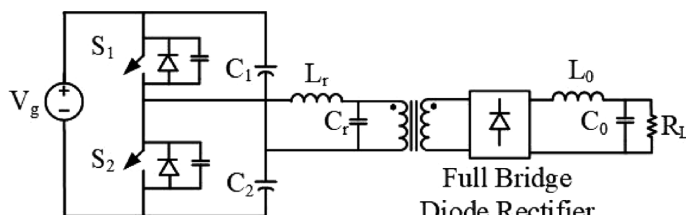


FIGURE 11.35 Parallel-loaded resonant converter. (From Behera, R.K., *Notes on Power Electronics and Drives*, IIT Patna, Bihar, India, 2010.)

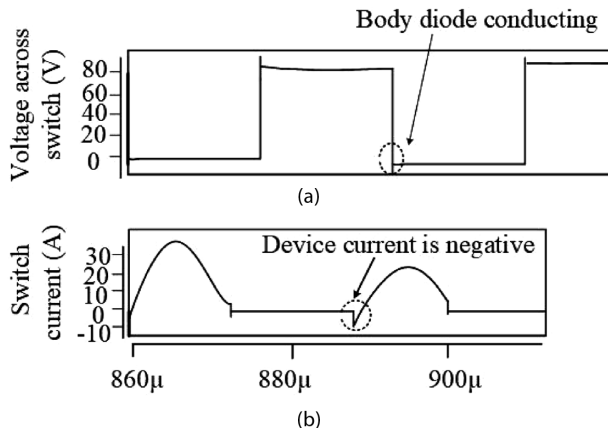


FIGURE 11.36 (a) Typical switch voltage and (b) switch current waveforms. (From Behera, R.K., *Notes on Power Electronics and Drives*, IIT Patna, Bihar, India, 2010.)

wave and full wave) type of resonant switches (M type or L type) and soft-switching techniques (ZVS or ZCS). Figure 11.37 shows the full-wave quasi-resonant buck converter.

11.5.1.3 Flyback Converter

For output voltage and power below 10 kV and 100 W, the conventional flyback topology suits well. It has an inherent overcurrent protection for the primary switching device, independent of what happens on the load side. When the switching device shown in Figure 11.38 is on, the output diode (D) is reverse biased, and a short-circuit on the load side does not affect the current flow on the primary side.

Another advantage is the output filter (C) is it requires only a capacitor filter, avoiding high-voltage inductors. Flyback converters find typical use for the energy storage capacitor charging in high-energy pulse applications, such as lasers, lamp flashers, and low-power cathode ray tube monitors.

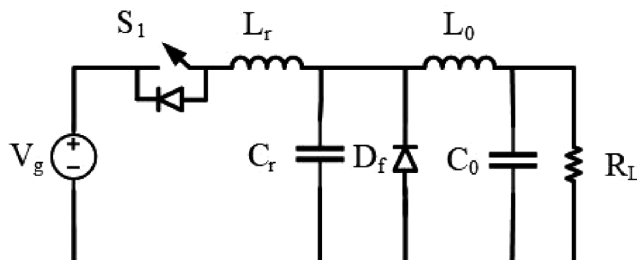


FIGURE 11.37 Quasi-resonant ZCS full-wave buck converter. (From Behera, R.K., *Notes on Power Electronics and Drives*, IIT Patna, Bihar, India, 2010.)

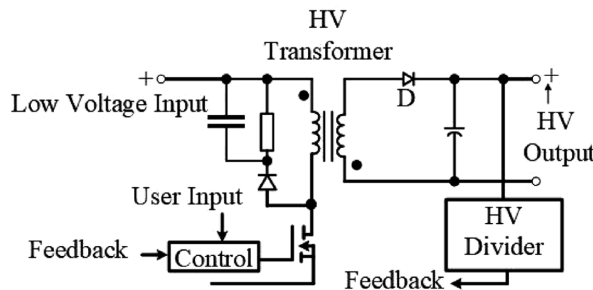


FIGURE 11.38 Flyback HV SMPC. (From Behera, R.K., *Notes on Power Electronics and Drives*, IIT Patna, Bihar, India, 2010.)

11.5.1.4 Switched Mode Power Conversion (SMPC) with Regulated DC Source

One of the widely used methods is to have an uncontrolled inverter generating the HF AC to feed the HV transformer. HV output regulation is achieved by regulating the DC source using a front-end converter. Figure 11.39 shows the block diagram of the scheme. The rectified line voltage is stepped down to a lower DC level by the buck converter. The control circuit ensures that the output of the buck regulator is at the level required to maintain a constant output HV. The uncontrolled inverter switches at a constant frequency with a 50% duty ratio. It makes use of the HV transformer parasitics to make the switch transition resonant (resulting in soft switching). Since only the input DC level is varied, the soft-switching region is large. The disadvantage is the necessity for an extra converter at the front end. Lower efficiency, reduced reliability, and larger size are the shortcomings.

11.5.1.5 Phase-Shift Bridge

The phase-shifted bridge or resonant transition converter, shown in Figure 11.40, combines the low conduction loss of the general PWM converters and the low switching-loss characteristic to resonant or quasi-resonant converters. The leakage inductance of the HV transformer and the device output capacitance resonant during

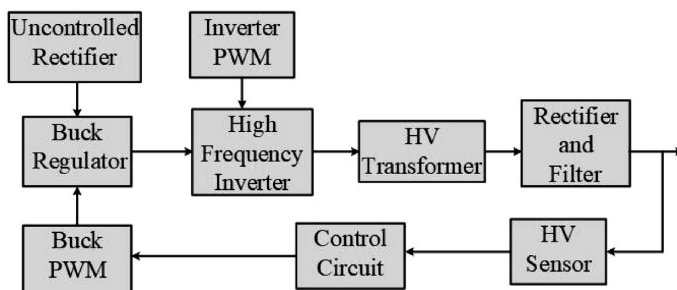


FIGURE 11.39 HV power supply with regulated DC input. (From Behera, R.K., *Notes on Power Electronics and Drives*, IIT Patna, Bihar, India, 2010.)

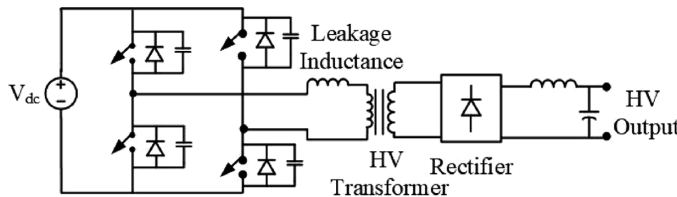


FIGURE 11.40 Resonant transition converter. (From Behera, R.K., *Notes on Power Electronics and Drives*, IIT Patna, Bihar, India, 2010.)

switch transition results in the soft switching. Once the device starts conducting, the output capacitor plays no role, and the circuit current peak is limited. However, the leakage inductance associated with the HV transformer is quite large, thereby, affecting the transformer power. Another disadvantage is the need for HV filter inductors.

The output rectifier diodes are hard switches. Parasitic HV transformer capacitance is isolated from the inverter devices, but it still must be charged and discharged every cycle, thereby reducing the effective duty ratio.

11.5.1.6 Parallel Resonant Converter

A frequency-controlled parallel resonant converter (PRC) is shown in Figure 11.41 in a half-bridge topology. The PRC has its load connected across the resonant capacitor. It acts as a voltage source with low impedance output. An Inductor-capacitor (LC) output filter is required at the output. PRC with a capacitive output filter has been described in the literature with confliction claims on its feasibility. The PRC effectively absorbs both the HV transformer leakage inductance and the parasitic capacitance. Soft switching of inverter devices is possible.

The characteristic gain curves for a frequency-controlled PRC are given in Figure 11.42. It is seen that the converter voltage gain can be greater than unity (without HV transformer). At or near resonance, the gain is a function of the load and can rise to very large values at low loads. Also, the converter is controllable at light loads.

The main disadvantage is that the current in the primary is relatively independent of the load. The PRC can be made efficient at a particular load; however, the efficiency cannot be maintained for a varying load or varying input voltage. In the

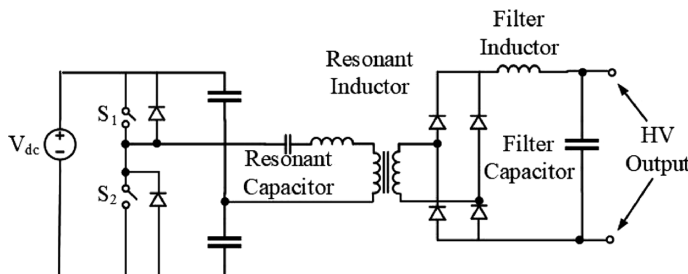


FIGURE 11.41 The half-bridge parallel-resonant converter. (From Behera, R.K., *Notes on Power Electronics and Drives*, IIT Patna, Bihar, India, 2010.)

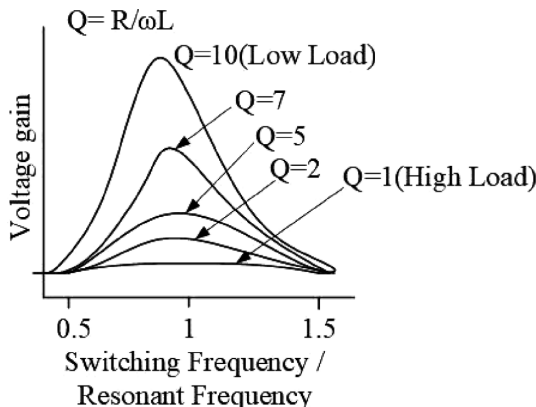


FIGURE 11.42 Gain characteristics of a frequency-controlled parallel resonant converter. (From Behera, R.K., *Notes on Power Electronics and Drives*, IIT Patna, Bihar, India, 2010.)

PRC, the resonant capacitor voltage is rectified and filtered. The high-voltage (HV) rectifier is subject to switching stress.

11.5.1.7 Multielement Resonant Converters

The basic series resonant converter (SRC) and PRC topologies can be modified by adding more reactive components in the tank. The reason is to combine the advantages offered by the SRC and PRC topologies. The LLC type, as shown in Figure 11.43, is obtained by adding an extra inductor across the resonant capacitor. It improves the light-load operating characteristics. The load range extends from no load to full load with a small variation of SF.

The LLC type, also known as the series-parallel hybrid converter, is a modification to the SRC by adding an extra resonant capacitor across the HV transformer. By proper selection of the series and parallel capacitors (C_s , C_p), the low-load operating characteristic of a PRC and low-circulating current of SRC can be achieved. The LLC type also takes care of the parasitic capacitance across the HV transformer. Multielement converters are complex to analyze and more difficult to control.

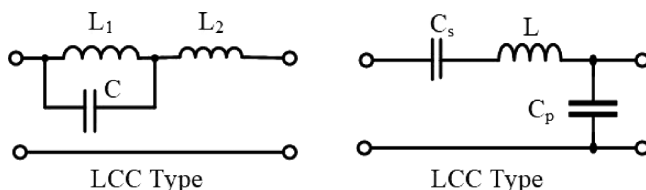


FIGURE 11.43 Tank circuit of two types of multielement resonant converters. (From Behera, R.K., *Notes on Power Electronics and Drives*, IIT Patna, Bihar, India, 2010.)

11.6 DUAL ACTIVE-BRIDGE CONVERTER

High-frequency (HF) link-power conversion technology based on power electronics plays an important role in modern power management systems based on solar photovoltaic, fuel cell, wind, and other form of renewable energy sources. There are different bidirectional and isolated DC-DC converters studied with an HV port (ranging from 240 to 450 V), a low-voltage (LV) port (11 to 16 V), and a rated power of 1–2 kW. The block diagram of different components of an isolated and bidirectional DC-DC converter is shown in Figure 11.44. There are two ports: Port 1 and Port 2. Port 1 defines for HV, and Port 2 is the LV side. In Port 1, a filter, DC-AC converter, resonant HF network, and primary side of HF transformer are connected. For Port 2, the secondary side of the HF transformer, HF network, AC-DC converter, and a filter are connected.

The single-phase dual active bridge (DAB) full-stage conversion configuration shown in Figure 11.45 is regarded as the most promised option due to elevated

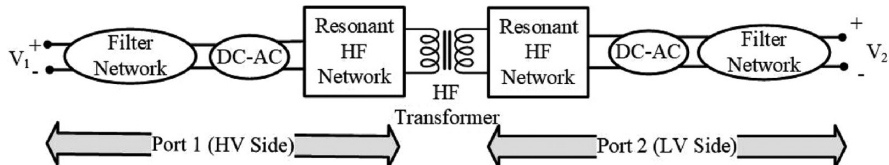


FIGURE 11.44 Block diagram of dual active-bridge converter. (From Behera, R.K. and Ojo, O., “Design of all solar micro-grid,” BASE Report on Indo-US and DST Forum, *BASE Research Report*, 2015.)

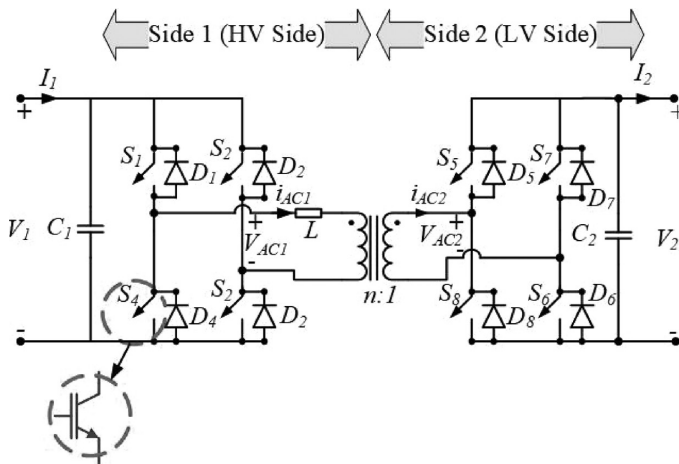


FIGURE 11.45 Single-phase dual active-bridge (DAB) converter. (From Behera, R.K. and Ojo, O., “Design of all solar micro-grid,” BASE Report on Indo-US and DST Forum, *BASE Research Report*, 2015.)

converter effectiveness and higher-power density. This is owing to the small amount of inductors and the use of capacitive filters on the HV side and on the LV side. **Figure 11.45** demonstrates a full-bridge integrated DC-DC converter, where V_1 and V_2 are the voltage of input and output, and n is the transformer transformation ratio. Two H-bridge converters are connected to an HF transformer. A square wave AC voltage with a 50% duty ratio to the main winding of the HF-transformer is provided on the first H-bridge. This bridge comprises of four frequently insulated-gate bipolar transistors (IGBTs) with power semiconductor switches S_1 , S_2 , S_3 , and S_4 for energy devices and metal-oxide semiconductor field-effect transistors (MOSFETs) for low-power application. Port 2 is linked to secondary winding of the HF transformer and operated in full mode with the phase-shift control in Port 2 with four power semiconductor switches S_5 , S_6 , S_7 , and S_8 . This DC-DC converter can work in a two-way configuration. The H-bridge in Port 1 and Port 2, based on the power flow path, may therefore be regarded as main or secondary. By reflecting the transformer on one side and by contemplating the transformer magnetizing inductance much bigger than the leakage inductance, the assessment of the DAB transformer is made easier. Therefore, two effective H-bridges connected with transformer leakage inductance L are the DAB converter. The simplified lossless model of DAB is shown in **Figure 11.46**.

The voltage sources V_{AC1} and V_{AC2} thus generate or receive the respective instantaneous powers

$$\begin{aligned} p_1(t) &= V_{AC1}(t) \cdot i_L(t) \\ p_2(t) &= nV_{AC2}(t) \cdot i_L(t) \end{aligned} \quad (11.32)$$

The average power over one switching cycle T_s , $T_s = 1/f_s$, is finally calculated with

$$P_1 = \frac{1}{T_s} \int_{t_0}^{t_0+T_s} p_1(t) dt$$

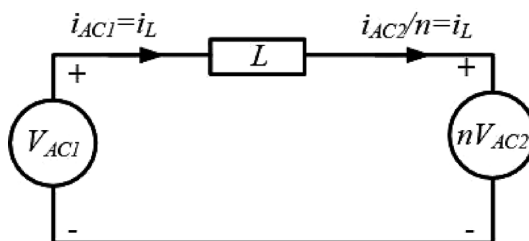


FIGURE 11.46 Lossless model of DAB. (From Behera, R.K. and Ojo, O., "Design of all solar micro-grid," BASE Report on Indo-US and DST Forum, *BASE Research Report*, 2015.)

$$P_2 = \frac{1}{T_s} \int_{t_0}^{t_0+T_s} p_2(t) dt \quad (11.33)$$

The supplied power is

$$P_1 = nV_1\bar{I} = \frac{nV_1V_2}{2f_sL} D(1-D) \quad (11.34)$$

Assume fixed load,

$$P_0 = \frac{V_2^2}{R_L} \quad (11.35)$$

Considered to be a lossless DAB converter, the load voltage is given as

$$V_2 = \frac{V_1}{2f_sL} R_L D(1-D) \quad (11.36)$$

Load current can be written as

$$I_2 = \frac{V_1}{2f_sL} D(1-D) \quad (11.37)$$

The output power can be written as

$$P_0 = \left(\frac{V_1}{2f_sL} \right)^2 R_L D^2 (1-D)^2 \quad (11.38)$$

11.7 THREE-PHASE AC-AC MATRIX CONVERTER

Most of these apps involve a quicker vibrant output than manufacturing drives with elevated inertia, and therefore no reaction rates are required. The matrix converter (MC) is a dynamically tightly coupled input/output device, and it is difficult to develop the general scheme and especially control the design without an extra energy-buffer component. Two synchronous devices that target applications have been addressed—regulated three-phase distribution of voltage and mitigation of voltage sag.

The MC is a single-stage converter without any intermediate bulk-energy storage element, except small AC filters connected at the input side to eliminate switching ripples. The AC-AC MC can be commonly classified into the direct matrix converter (DMC) and the indirect matrix converter (IMC). The IMC uses a fictitious

DC-link (but without DC storage elements) with two stages of conversion. However, the classical DMC uses direct conversion of power without any intermediate stages. The DMC function is performed in two modes: as a voltage-source matrix converter (VSMC) and a current-source matrix converter (CSMC). Generally, the DMC has an assortment of $m \times n$ bidirectional power switches to link, directly, an m -phase voltage source to an n -phase load.

The MC has the following advantages over traditional rectifier–inverter based variable frequency drives.

1. Sinusoidal input and output waveforms, with minimal higher-order harmonics and no subharmonics
2. Bidirectional energy flow capability
3. Minimal energy storage requirements (minimal-size reactive components), which may increase the efficiency and the lifetime of the converter
4. Controllable input power factor

The design of MCs began with Venturini and Alesina [18] in the mid-1980s proposing fundamental operating concepts. The most popular setup of this matrix converter is the three-phase to three-phase VSMC form mentioned in the literature.

The simplified power-circuit topology of a three phase AC-AC DMC is shown in Figure 11.47. The MC has three input phases and three output phases, with each phase having three bidirectional power switches connected in series. Each bidirectional power switch is consisting of two antiparallel IGBTs and diodes. MC input is powered from three-phase voltage sources via LC filters and linked to a three-phase

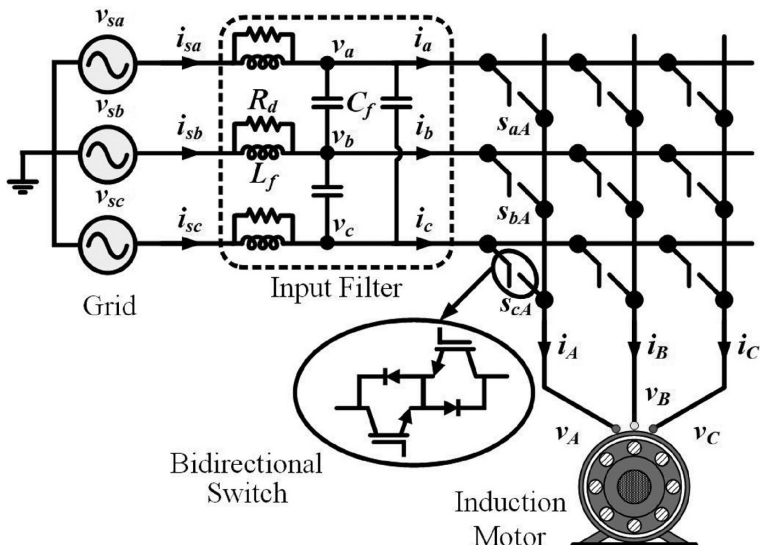


FIGURE 11.47 Simplified three-to-three-phase direct matrix converter topology. (From Muduli, U. and Behera, R.K., Matrix converter fed induction motor drive, *Registration Report*, April 2019.)

induction motor in all three production stages. In general, the LC origin filter is necessary to minimize the HF elements in load flows and decrease the effect of load-system disturbances. LC is inversely proportionate to the changing frequency of the matrix converter.

The input and output supply voltages have three phases with 120° -phase displacement between each phase.

11.7.1 THREE-PHASE TO THREE-PHASE DMC MODELING

The converter-changing behavior produces discontinuous waveforms for the input voltage. If the inductive loads are connected on the output side, the waveforms are continuous. To analyze the modulation strategies, a DMC model with following assumptions is considered.

- All the bidirectional switches are ideal in nature.
- The frequency of operation is considerably greater than the frequencies of entry and supply energy.
- The average voltages at the input side of the DMC are constant over a switching cycle interval T_{sw} .

Under these assumptions, the higher-frequency components present in input/output currents, and voltages can be neglected. Hence, the average output voltages can be described from the switching model of the DMC as:

$$\begin{bmatrix} v_{oA} \\ v_{oB} \\ v_{oC} \end{bmatrix} = \begin{bmatrix} S_{aA} & S_{bA} & S_{cA} \\ S_{aB} & S_{bB} & S_{cB} \\ S_{aC} & S_{bC} & S_{cC} \end{bmatrix} \begin{bmatrix} v_a \\ v_b \\ v_c \end{bmatrix} = [S] \begin{bmatrix} v_i \end{bmatrix} \quad (11.39)$$

where:

$[S]$ is the switching transfer matrix

$\begin{bmatrix} v_i \end{bmatrix} = [v_{ia}, v_{ib}, v_{ic}]^t$ is input-phase voltage vector

$\begin{bmatrix} v_o \end{bmatrix} = [v_{oA}, v_{oB}, v_{oC}]^t$ is the output-phase voltage vector

The subscripts $j \in \{a, b, c\}$ and $k \in \{A, B, C\}$ correspond to the input and output phases, respectively. Since, the MC is supplied by the voltage source, the input stages must not be short-circuited, and due to inductive loads, output stages shall not remain open-circuited. The representation of constraints as per [Figure 11.48](#) can be expressed mathematically as:

$$S_{ak} + S_{bk} + S_{ck} = 1 \quad (11.40)$$

The switching function of a single switch is defined as follows:

$$s_{jk} = \begin{cases} 1, & \text{switch } S_{jk} \text{ turn-on} \\ 0, & \text{switch } S_{jk} \text{ turn-off} \end{cases} \quad (11.41)$$

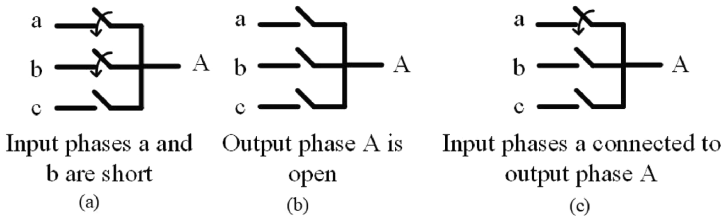


FIGURE 11.48 Possible connection configurations for any input/output phases: (a) input phases “a” and “b” are short, (b) output phase A is open, and (c) input phase “a” connected to output phase A. (From Muduli, U. and Behera, R.K., Matrix converter fed induction motor drive, *Registration Report*, April 2019.)

The problem of defining the duty-cycle matrix that satisfies input-output-voltage relationships in Equation (11.39) is the needed instantaneous input power factor and the constraint condition in Equation (11.40) can be formulated for determining any modulation strategy for the matrix conversion device over each cycle period.

Discontinuous input currents can be built when limitations in Equation (11.41) and immediate energy equilibrium is applied on the input and output sides of an optimal MC. Capacitors and inductors must be present on the output side to guarantee ongoing configuration stresses and waveform currents, alternatively. The power balance equation can be written as

$$p_i = p_o \quad (11.42)$$

$$[i_i]^t [v_i] = [i_o]^t [v_o] \quad (11.43)$$

by applying Equation (11.39),

$$[i_i]^t [v_i] = [i_o]^t [S] [v_i] \quad (11.44)$$

which implies that

$$[i_i] = \begin{bmatrix} i_a \\ i_b \\ i_c \end{bmatrix} = \begin{bmatrix} S_{aA} & S_{aB} & S_{aC} \\ S_{bA} & S_{bB} & S_{bC} \\ S_{cA} & S_{cB} & S_{cC} \end{bmatrix} \begin{bmatrix} i_A \\ i_B \\ i_C \end{bmatrix} = [S]^t [i_o] \quad (11.45)$$

11.7.2 SPACE VECTOR PWM

A direct AC-to-AC converter is used in powered varying speed drives for varying voltage and varying source frequencies. For MCs, the significant task of the SVPWM is to produce the necessary voltages while regulating the input currents or the power factor. The MC has one limit, because the highest accessible yield voltage in its linear modulation range is restricted to 86.6% of the original voltage. In essence, there are three MC power PWM systems. These include the PWM centered on the

carrier, PWM space vector, and PWM techniques for specific harmonic extraction. The carrier-based PWM techniques can be used with advantages for inverter systems: (1) the control of the common-mode voltage and (2) the control of complex topologies for inverters such as multilevel inverters. A useful tool for a healthy three-phase output is the space vector modulation technique. However, its execution algorithm is quite hard, especially when the PWM performance is improved by common-mode controls. The MC operating frequency comes from two switching functions from the PWM converter and the modulation of the inverter. This technique has the benefit of having a well-established PWM space vector technique for the VSI modulation of the MC. While several calculations are necessary. The carriers of PWM were able to regulate the output power factor, peak-usage voltage, and modulate under uneven load voltage. As a prevalent manufacturing exercise, the SVPWM possesses flexible and many excellent features. However, more calculations and charts are needed to switch models according to the input current and output voltage sectors. Implementation is unintuitive because gating pulses are produced from the wait times calculated by the efficient time vectors.

In the space vector-modulation technique for control of MCs, the modulation process is fictitiously divided in two steps: rectification and inversion. In the first step, the three-phase full-wave rectification is applied to obtain maximal voltage gain. Hence, the input voltage of the fictitious inverter is the envelope of the three-phase full-wave rectified input line voltages. The three-phase-balanced input phase voltages, line voltages, and the envelope voltage shown are in [Figure 11.49](#), respectively. In the inversion process, the output voltages are obtained using space-vector modulation to assure low-harmonic distortion. Since the same switches have to perform both rectification and inversion, a detailed analysis of switching configurations has been carried out. In addition, the constraints imposed by the source and the load are considered for better reliability.

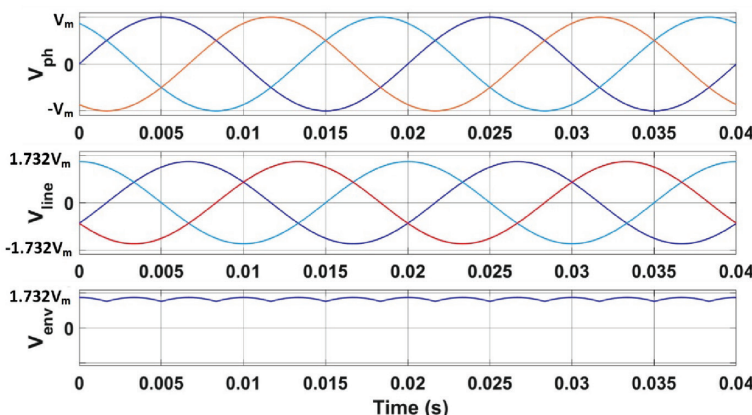


FIGURE 11.49 Input phase voltages, input line voltages, and envelope voltage. (From Muduli, U. and Behera, R.K., Matrix converter fed induction motor drive, *Registration Report*, April 2019.)

The space vector algorithm is based on the representation of the three-phase input current and three-phase output line voltages on the space vector plane. For a three-to-three-phase matrix converter, total $9(3 \times 3)$ bidirectional switches have been used. With this number of switches, the total combination of switching is 2^{15} . Considering the aforementioned constraints in Section 11.6.1, there are 3^3 , that is, 27, different switching combinations that allow any output phase to be connected to any input phase. However, there are 93 active switching combinations that have been identified and discussed as follows.

For each switching combination, the input and output line voltage space vector are expressed as

$$\vec{v}_i = \frac{2}{3} (v_{ab} + a_i v_{bc} + a_i^2 v_{ca}) = V_i e^{j\beta_i}, a_i = e^{\frac{j2\pi}{3}}$$

$$\vec{v}_o = \frac{2}{3} (v_{AB} + a_o v_{BC} + a_o^2 v_{CD}) = V_o e^{j\beta_o}, a_o = e^{\frac{j2\pi}{3}} \quad (11.46)$$

Similarly, the input and output line current space vectors are defined for each switching configuration,

$$\vec{i}_i = \frac{2}{3} (i_a + a_i i_b + a_i^2 i_c) = I_i e^{j\alpha_i}, a_i = e^{\frac{j2\pi}{3}}$$

$$\vec{i}_o = \frac{2}{3} (i_A + a_o i_B + a_o^2 i_C) = I_o e^{j\alpha_o}, a_o = e^{\frac{j2\pi}{3}} \quad (11.47)$$

The possible switching groups are symbolized as $\{p, q, r\}$, where p, q , and r interpret the number of output phases of MCs connected to input phases a, b , and c , respectively. Analyzing [Table 11.6](#), the switch configuration may be categorized as one of the three groups.

Group 1:3 combinations, such as $\{3,0,0\}$, $\{0,3,0\}$, $\{0,0,3\}$, where the “zero vectors” are called, giving the null output voltage and input current vectors.

In these combinations, all three output phases are connected to the same input phase.

Group 2:6 combinations, such as $\{1,1,1\}$, where the “synchronous signals” are designated in which each output phase is attached to a distinct input stage. The output voltage and input current vectors have variable directions in this case and cannot be used to synthesize the reference vectors properly.

Group 3:18 combinations, such as $\{2,1,0\}$, $\{1,2,0\}$, $\{0,2,1\}$, $\{0,1,2\}$, $\{1,0,2\}$, $\{2,0,1\}$, where the magnitude of those vectors depends on instantaneous values of input line-to-line voltages and output line currents, and the magnitude of the input voltage and the output current is defined as “active vectors.” Two output lines are linked in this situation to the same input line.

TABLE 11.6
Vectors Corresponding to Output Voltages and Input Currents ($m = \frac{2}{\sqrt{3}}$)

	Vector	A	B	C	V_{AB}	V_{BC}	$ V_O $	β_o	I_a	I_b	I_c	$ I_i $	α_i
Active Vector													
1+	a	b	b	ab	0	-ab	mV_{ab}	30°	I_A	$-I_A$	0	ml_A	-30°
1-	b	a	a	-ab	0	ab	mV_{ab}	-150°	$-I_A$	I_A	0	ml_A	150°
2+	b	c	c	bc	0	-bc	mV_{bc}	30°	0	I_A	$-I_A$	ml_A	90°
2-	c	b	b	-bc	0	bc	mV_{bc}	-150°	0	$-I_A$	I_A	ml_A	-90°
3+	c	a	a	ca	0	-ca	mV_{ca}	30°	$-I_A$	0	I_A	ml_A	-150°
3-	a	c	c	-ca	0	ca	mV_{ca}	-150°	I_A	0	$-I_A$	ml_A	30°
4+	b	a	b	-ab	ab	0	mV_{ab}	150°	I_B	$-I_B$	0	ml_B	-30°
4-	a	b	a	ab	-ab	0	mV_{ab}	-30°	$-I_B$	I_B	0	ml_B	150°
5+	c	b	c	-bc	bc	0	mV_{bc}	150°	0	I_B	$-I_B$	ml_B	90°
5-	b	c	b	bc	-bc	0	mV_{bc}	-30°	0	$-I_B$	I_B	ml_B	-90°
6+	a	c	a	-ca	ca	0	mV_{ca}	150°	$-I_B$	0	I_B	ml_B	-150°
6-	c	a	c	ca	-ca	0	mV_{ca}	-30°	I_B	0	$-I_B$	ml_B	30°
7+	b	b	a	0	-ab	ab	mV_{ab}	-90°	I_C	$-I_C$	0	ml_C	-30°
7-	a	a	b	0	ab	-ab	mV_{ab}	90°	$-I_C$	I_C	0	ml_C	150°
8+	c	c	b	0	-bc	bc	mV_{bc}	-90°	0	I_C	$-I_C$	ml_C	90°
8-	b	b	c	0	bc	-bc	mV_{bc}	90°	0	$-I_C$	I_C	ml_C	-90°
9+	a	a	c	0	-ca	ca	mV_{ca}	-90°	$-I_C$	0	I_C	ml_C	-150°
9-	c	c	a	0	ca	-ca	mV_{ca}	90°	I_C	0	$-I_C$	ml_C	30°
Zero Vector	O_1	a	a	0	0	0	0	0°	0	0	0	0	0°
O_2	b	b	b	0	0	0	0	0°	0	0	0	0	0°
O_3	c	c	c	0	0	0	0	0°	0	0	0	0	0°

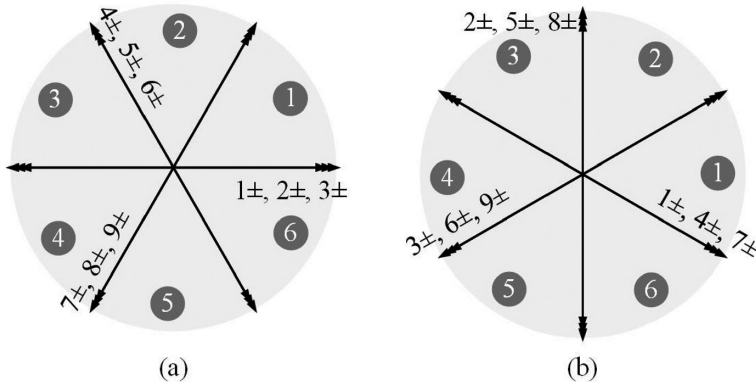


FIGURE 11.50 Graphical representation of space vector and corresponding sectors for (a) output line voltage, and (b) input phase current. (From Muduli, U. and Behera, R.K., Matrix converter fed induction motor drive, *Registration Report*, April 2019.)

Figure 11.50 shows output voltage and current input vectors of 18 effective configurations. This figure also describes the system for dividing the complex space vector plane into sectors. SO refers to the sector that contains the voltage vector output, and Si refers to that sector comprising the matrix input current. The configurations in each sub-group produce a space voltage and current vectors in a defined direction, which change every 120°. The amplitude and polarity of the space vectors along the defined direction depend on which of the line-to-line voltages is used.

The stationary vector time essentially represents the duty cycle time (in-state or off-state time) of the selected switches over a modulation scheme sample period. The dwell time calculation is based on the concept of “volt-second balancing.” Duty cycles for Sector 1 can be evaluated as (Figure 11.51)

$$\begin{bmatrix} d_{7-} \\ d_{0+} \\ d_{1+} \\ d_{3-} \end{bmatrix} = \frac{m_a}{\sin\left(\frac{\pi}{3}\right)\cos\Phi_i} \begin{bmatrix} \sin\delta_o \sin\left(\frac{\pi}{3} - \delta_i\right) \\ \sin\delta_o \sin\delta_i \\ \sin\left(\frac{\pi}{3} - \delta_o\right) \sin\left(\frac{\pi}{3} - \delta_i\right) \\ \sin\left(\frac{\pi}{3} - \delta_o\right) \sin\delta_i \end{bmatrix} \quad (11.48)$$

where $0 \leq \beta_o^* \leq \frac{\pi}{5}$, $\delta_o = \beta_o^*$, $-\frac{\pi}{6} \leq \alpha_i \leq \frac{\pi}{6}$, $\delta_i = \alpha_i + \frac{\pi}{6}$ and $0 \leq \delta_i \leq \frac{\pi}{3}$. Φ_i is the required input power-factor angle. Note that the value of the on-time ratio (duty cycle) should be positive. Furthermore, the sum of the ratios must be lower than or equal to unity. By adding duty cycles in Equation (11.49), with the aforementioned constraints, one can write

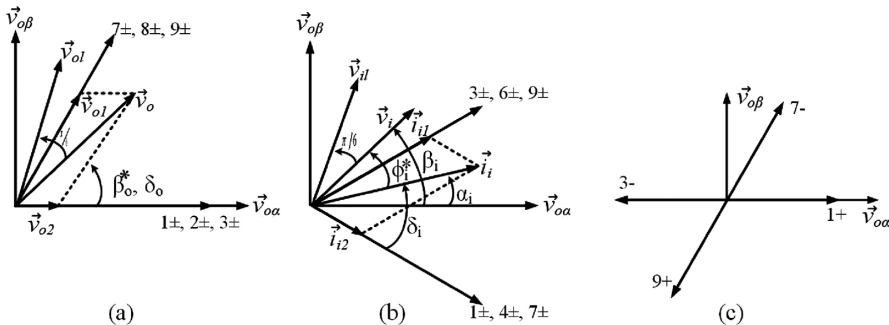


FIGURE 11.51 (a) Output voltage vector decomposition, (b) input current vector decomposition, and (c) optimum voltage vector selection for Sector 1. (From Muduli, U. and Behera, R.K., Matrix converter fed induction motor drive, *Registration Report*, April 2019.)

$$\delta_{M7-} + \delta_{M9+} + \delta_{M1+} + \delta_{M3-} \leq 1 \quad (11.49)$$

The maximum value of the voltage transfer ratio can be determined as $m_a = 0.866$ for a three-phase to three-phase MC. Once the input current vector and output voltage vector are known from the phase angle, the SVPWM is to be implemented with eight active space vectors (except zero vectors). The eight-space vectors are used until the angular sector is changed or will change. A symmetrical switching waveform should be used for one of the zero space vectors in each switching cycle. In order to minimize the number of switch switches, the resulting sequences of nine space vectors (four active vectors and one zero).

Concerning the α_i or β_o^* values considered in Figure 11.50, the available space vectors and their sequence of switching are listed in Table 11.7. Assuming the input and output reference vectors in Sector 1, the switching sequence can be represented as $1+, 7-, 9+, 3-, O_3$. The duty cycles corresponding to selected switching sequence are $\delta_{1+}, \delta_{7-}, \delta_{9+}, \delta_{3-}$, and δ_0 . Here, δ_0 can be represented as

$$\delta_0 = 1 - (\delta_{7-} + \delta_{9+} + \delta_{1+} + \delta_{3-}) \quad (11.50)$$

The sequence of application of space vectors can be defined such that the number of switching in one sampling period is minimum. To obtain a symmetrical switching, at first, a zero vector is applied, followed by eight active vectors in half of the sampling instance T_{svm} . The mirror image of the switching sequence can be obtained in the second half of the sampling period. This can be achieved by using a dual side reference signal of sample time T_{svm} . It should be noted that, only five commutations are required in each half of the sampling period. Once the configurations are selected and sequenced, the on-time ratios of each configuration are calculated using Equation (11.48).

TABLE 11.7
Switching-State Selection for SVPWM in Different Sectors

		Output Voltage Sector								
		1 or 4		2 or 5		3 or 6				
Input Current Sector	1 or 4	1+	7-	9+	9+	3-	2+	2+	8-	7+
	2 or 5	3-	O ₃		8-	O ₂		1-	O ₁	
	3 or 6	4+	7-	9+	9+	6-	5+	5+	8-	7+
	4 or 1	6-	O ₃		8-	O ₂		4-	O ₁	
	5 or 2	4+	1-	3+	3+	6-	5+	5+	2-	1+
	6 or 3	6-	O ₃		2-	O ₂		4-	O ₁	
	1 or 4	7+	1-	3+	3+	9-	8+	8+	2-	1+
	2 or 5	9-	O ₃		2-	O ₂		7-	O ₁	
	3 or 6	7+	4-	6+	6+	9-	8+	8+	5-	4+
	4 or 1	9-	O ₃		5-	O ₂		7-	O ₁	
	5 or 2	1+	4-	6+	6+	3-	2+	2+	5-	4+
	6 or 3	3-	O ₃		5-	O ₂		1-	O ₁	

11.7.3 COMMUTATION METHODS IN DMC

The commutation must always be regulated actively. At the same time, there must be no two bidirectional switches “on.” This results in the contribution of the capacitive load short-circuit and the inductive load open-circuit. The accessible matrix converters have distinct kinds of commutation, and this is clarified in the following sections.

11.7.4 DEADTIME COMMUTATION

The inverter uses this sort of commutation switching technique. This suggests freewheel current is stacked during deadtime to throw against parallel diodes. The deadtime commutation switching technique is ineffective for the case of the MC. This results in the load side open-circuit, and hence the switches have forced spike. Snubber clamping equipment is supplied to prevent this. This is a way to the load current during the dead time, and therefore it is hard to develop a snubber circuit.

11.7.5 CURRENT COMMUTATION BASED ON MULTIPLE STEPS

This kind of commutation utilizes bidirectional switches. These are solid in current replacement and comply with the fundamental principles. It can control the course of the current. This procedure is basic if there should be an occurrence of controlled output current direction. This commutation strategy depends on the prior knowledge of output current direction. This current direction can be hard to dependably decide and permit

current levels in high-power drives. To maintain a strategic distance from this issue, a procedure of utilizing the voltage over the bidirectional change to decide the current direction has been created. This procedure gives reliable current commutation utilizing a smart-gate drive circuit, which controls the switching of the IGBTs and recognizes the direction of current flow inside the bidirectional switch cell. On the same output leg, the prior knowledge of current direction calculated by the effective gate drive is carried on to all other gate drivers. All gate drivers, thus, add to a safe commutation switching. MATLAB simulation takes account of the problem of commutation in the MC.

11.7.6 SIMULATION RESULTS

The performance of the MC has been simulated in MATLAB/Simulink environment. The three-phase induction motor is considered as a load with stator resistance 4.565 Ω , rotor resistance 9.86 Ω , stator/rotor inductances 41.22 mH, mutual inductance 821.7 mH, moment of inertia 0.078 kg-m², and damping constant 0.001. The sampling time of the Simulink model is taken as 10 μ s. Figure 11.52a represents the line voltage at the output of the MC. From this waveform, it can be noticed that output line voltage follows the input line voltage envelope as mentioned previously.

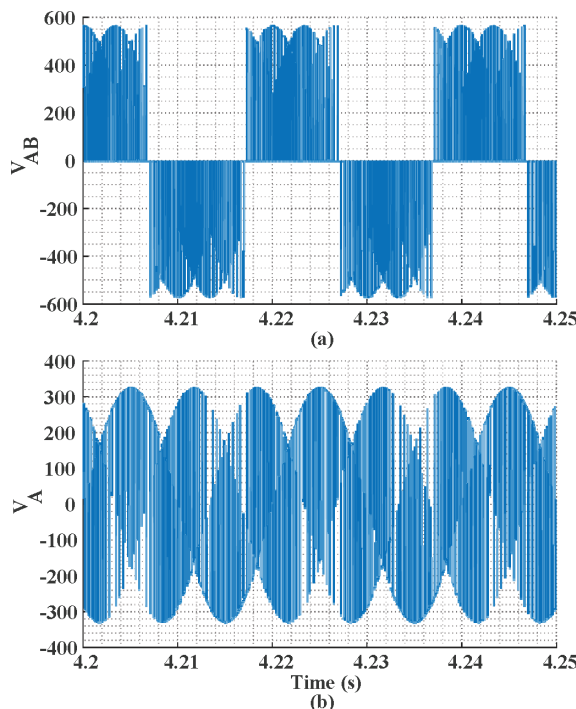


FIGURE 11.52 (a) Output line voltage and (b) output phase voltage of 3×3 -phase DMC. (From Muduli, U. and Behera, R.K., Matrix converter fed induction motor drive, *Registration Report*, April 2019.)

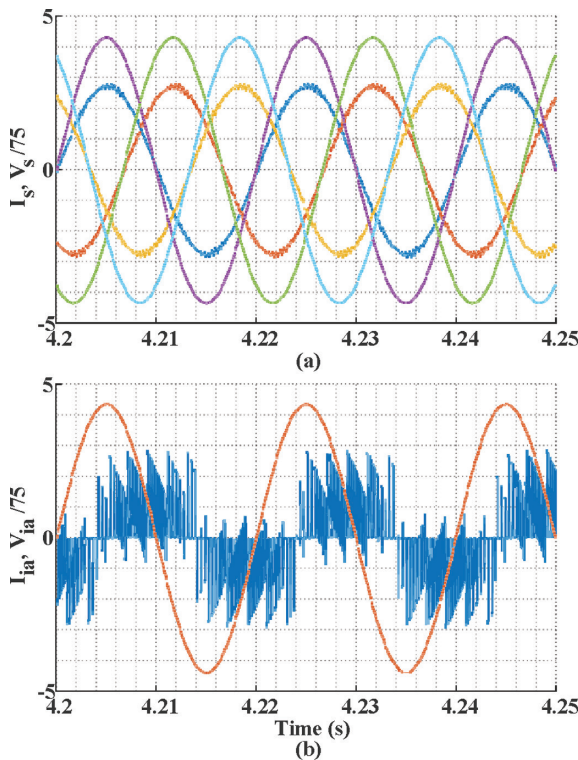


FIGURE 11.53 (a) Source voltage and current and (b) input voltage and current of 3×3 -phase DMC. (From Muduli, U. and Behera, R.K., Matrix converter fed induction motor drive, *Registration Report*, April 2019.)

Figure 11.52b shows the output phase voltage of Phase A, which includes the common-mode voltage. By analyzing the output voltage waveform of the MC with its counterpart voltage source inverter, it can be concluded that the percentage of THD present in output voltage in case of the MC is less than VSI. The objective of the MC is to get the required phase difference between source voltage and current, which can be analyzed from Figure 11.53. Here, a unity power factor is achieved at the point of common coupling, that is, a phase difference of zero is obtained.

REVIEW QUESTIONS

Multipulse Converter

- 11.1 What is the multipulse converter? Briefly describe the advantages of multipulse converter.
- 11.2 Differentiate between the controlled and uncontrolled rectifier. Write down the benefits of the isolated and nonisolated converter.

- 11.3 Mention different types of multipulse converter with a circuit diagram.
- 11.4 What is the frequency of the lowest-order harmonics in a 12-pulse AC-DC converter?
- 11.5 What is the frequency of the lowest-order harmonics in an 18-pulse AC-DC converter?
- 11.6 What is the frequency of the lowest-order harmonics in a 24-pulse AC-DC converter?

Multilevel Converter

- 11.1 What is the multilevel converter? Write down the advantages of multilevel converter over a two-level converter.
- 11.2 Compare the performance of different multilevel converters.
- 11.3 Differentiate between an NPC converter and capacitor-clamped converter.
- 11.4 Which factor decides the number of levels in an output phase voltage for the cascaded H-bridge converter? Write down the relation between them.
- 11.5 What are the main advantages of the cascaded H-bridge converter over other multilevel converters?
- 11.6 Briefly describe the operation principle of the three-phase cascaded H-bridge converter.
- 11.7 Briefly describe the operation principle of the three-phase NPC converter.
- 11.8 Briefly describe the operation principle of the three-phase capacitor clamped converter.

Control Methods

- 11.1 What is the closed-loop control methods used for the power electronic converter?
- 11.2 Describe the operation principle of a hysteresis current controller.
- 11.3 Differentiate between single-band and multiband hysteresis controller.
- 11.4 Describe the purpose of a three-level hysteresis controller for the application of a multilevel converter.
- 11.5 Compare the performance of a hysteresis controller with a PWM-based controller.
- 11.6 What is the modulation index?
- 11.7 Describe the performance of the sinusoidal PWM controller for a converter.
- 11.8 Differentiate between the in-phase and phase-opposed sinusoidal PWM controller.
- 11.9 What are the advantages of third-harmonic-injection sinusoidal PWM?
- 11.10 What are the main advantages of space vector-modulated PWM controller?
- 11.11 Describe the operation of a space vector modulated PWM controller for the three-phase two-level converter.
- 11.12 What is dwell time? Derive the relations for a dwell time of the three-phase two-level converter.
- 11.13 Describe the operation of a space vector modulated PWM controller for a three-phase three-level converter.
- 11.14 Derive the relations for a dwell time of the three-phase three-level converter.

Resonant Converter

- 11.1 What is the principle of the series resonant converter?
- 11.2 Differentiate between series and parallel resonant converters.
- 11.3 What is the principle of the flyback converter?
- 11.4 What are the effects of series loading on the series-resonant converter?
- 11.5 What are the effects of parallel loading on the series-resonant converter?
- 11.6 What is the zero-voltage switching?
- 11.7 What are the zero-current switchings?

Dual Active-Bridge Converter

- 11.1 What are the operation modes in a dual active-bridge converter?
- 11.2 Explain the operation principle of the dual active-bridge converter with a circuit diagram.
- 11.3 Describe different switching strategies of the dual active-bridge converter.

SUMMARY

In this chapter, different kinds of multipulse converter structures for AC-DC converters, and how they help in reducing the harmonics, are discussed. Detailed multilevel PWM VSCs for high-power drive applications are discussed. The operating principles, relevant characteristics, established modulation methods, and latest developments of these converters show that all described topologies, such as neutral point clamped, cascaded H-bridge, and flying capacitor multilevel converters are presented. Well-known modulation PWMs for industrial application and hysteresis current control techniques for VSCs are discussed. The generation of HV presents a unique challenge, and are magnified when HF switching, a high degree of safety, reliability, and functionality are specified along with the requirement to minimize the cost of size. Choosing the proper converter topology and designing it to meet the specification is critical. The series-resonant converter with phase modulation control is seen to be best suited for HV DC generation, for a varying load. The advantages commanded by it are a good compromise over the other topologies for HV DC generation. The operation of the DAB converter is discussed, and the working of MC technology has been presented. The MC requires an input filter to reduce the switching-frequency harmonics. The size of the MC is increased if this input filter is not properly designed, and that is a disadvantage. At the same time, it is concluded that the MC is a good alternative to the conventional AC-DC-AC topologies with better voltage THD_v and current THD_i. It is also possible to get the desired phase angle and harmonic label at the source side of the converter.

REFERENCES/FURTHER READING

1. B. Singh, S. Gairola, B.N. Singh, A. Chandra, K. Al-Haddad, Multipulse AC-DC converters for improving power quality: A review, *IEEE Trans. Power Electron.*, vol. 23, no. 1, pp. 260–281, 2008.
2. R. K. Behera and S. P. Das, *A Utility Friendly High Performance Multilevel Inverter Fed Induction Motor Drive System for Traction and Industrial Applications*, PhD Thesis, Indian Institute of Technology Kanpur, Uttar Pradesh, India, February 2009.

3. B. Wu, *High-Power Converters and AC Drives*, 2nd edn., IEEE Press, Wiley, Piscataway, NJ, 2017.
4. J. Rodriguez, J. S. Lai, and F. Z. Peng, Multilevel inverters: Survey of topologies, controls, and applications, *IEEE Trans. Ind. Appl.*, vol. 49, no. 4, pp. 724–738, 2002.
5. J. S. Lai, and F. Z. Peng, Multilevel converters—A new breed of power converters, *IEEE Trans. Ind. Appl.*, vol. 32, pp. 509–517, 1996.
6. L. M. Tolbert, F. Z. Peng, and T. Habetler, Multilevel converters for large electric drives, *IEEE Trans. Ind. Appl.*, vol. 35, pp. 36–44, 1999.
7. R. K. Behera, *Notes on Power Electronics and Drives*, IIT Patna, India, 2010.
8. M. F. Escalante, J. C. Vannier, and A. Arzande, Flying capacitor multilevel inverters and DTC motor drive applications, *IEEE Trans. Ind. Electron.*, vol. 49, no. 4, pp. 809–815, 2002.
9. V. Vorperian, Analysis of resonant converters, PhD Thesis, California Institute of Technology, Pasadena, CA, May 1984.
10. R. Steigerwald, A comparison of half-bridge resonant converter topologies, *IEEE Trans. Power Electr.*, vol. 3, no. 2, pp. 174–182, 1988.
11. R. Oruganti, F. C. Lee, Resonant power processors, part I—State plane analysis, *IEEE Trans. Ind. Appl.*, vol. IA-21, no. 6, pp. 1453–1460, 1985.
12. R. E. Tarter, *Solid-State Power Conversion Handbook*, John Wiley & Sons, New York, 1993.
13. S. D. Johnson, A. F. Witulski, R. W. Erickson, Comparison of resonant topologies in high-voltage DC applications, *IEEE Trans. Aerosp. Electron. Syst.*, vol. 24, no. 3, pp. 263–273, 1988.
14. S. Bifaretti, P. Zanchetta, A. Watson, L. Tarisciotti, and J. C. Clare, Advanced power electronic conversion and control system for universal and flexible power management, *IEEE Trans. Smart Grid*, vol. 2, no. 2, pp. 231–243, 2011.
15. J. Rocabert, A. Luna, F. Blaabjerg, and P. Rodriguez, Control of power converters in AC microgrids, *IEEE Trans. Power Electron.*, vol. 27, no. 11, pp. 4734–4749, 2012.
16. G. Pepermans, J. Driesen, D. Haeseldonckx, R. Belmans, and W. D'haeseleer, Distributed generation: Definition, benefits and issues, *Energy Policy*, vol. 33, no. 6, pp. 787–798, 2005.
17. R. K. Behera, and O. Ojo, Design of All Solar Micro-grid, BASE Report on Indo-US and DST Forum, BASE Research Report 2015, India.
18. M. Venturini and A. Alesina, The generalised transformer: A new bidirectional, sinusoidal waveform frequency converter with continuously adjustable input power factor, *IEEE Annu. Power Electron. Spec. Conf.*, vol. 1980, pp. 242–252, 1980.
19. P. W. Wheeler, J. Rodriguez, J. C. Clare, L. Empringham, and A. Weinstein, Matrix converters: A technology review, *IEEE Trans. Ind. Electron.*, vol. 49, no. 2, pp. 276–288, 2002.
20. D. Casadei, A. Member, G. Serra, and A. Tani, The use of matrix converters in direct torque control of induction machines, *IEEE Trans. Ind. Electron.*, vol. 48, no. 6, pp. 1057–1064, 2001.
21. F. Gao and M. R. Iravani, Dynamic model of a space vector modulated matrix converter, *IEEE Trans. Power Delivery*, vol. 22, no. 3, pp. 1696–1705, 2007.
22. M. Y. Lee, P. Wheeler, and C. Klumpner, Space-vector modulated multilevel matrix converter, *IEEE Trans. Ind. Electron.*, vol. 57, no. 10, pp. 3385–3394, 2010.
23. A. Dasgupta and P. Sensarma, Filter design of direct matrix converter for synchronous applications, *IEEE Trans. Ind. Electron.*, vol. 61, no. 12, pp. 6483–6493, 2014.
24. X. Huang, A. Goodman, C. Gerada, Y. Fang, and Q. Lu, A single sided matrix converter drive for a brushless DC motor in aerospace applications, *IEEE Trans. Ind. Electron.*, vol. 59, no. 9, pp. 3542–3552, 2012.

25. U. Muduli, and R. K. Behra, Matrix converter fed variable speed drive system, *Registration Seminar Report*, IIT Patna, India, April 2019.
26. S. M. Ahmed, H. Abu-Rub, Z. Salam, and A. Kouzou, Space vector PWM technique for a novel three-to-seven phase matrix converter, *IECON Proceedings of the (Industrial Electronics Conferences)*, Vienna, Austria, vol. 1, pp. 4949–4954, 2013.
27. D. Orser and N. Mohan, A Matrix converter ride-through configuration using input filter capacitors as an energy exchange mechanism, *IEEE Trans. Power Electron.*, vol. 30, no. 8, pp. 4377–4385, 2015.
28. M. A. Sayed and A. Iqbal, Pulse width modulation technique for a three-to-five phase matrix converter with reduced commutations, *IET Power Electron.*, vol. 9, no. 3, pp. 466–475, 2016.
29. M. Ali, A. Iqbal, M. R. Khan, M. Ayyub, and M. A. Anees, Generalized theory and analysis of scalar modulation techniques for a m x n matrix converter, *IEEE Trans. Power Electron.*, vol. 32, no. 6, pp. 4864–4877, 2016.
30. A. Iqbal, S. M. Ahmed, and H. Abu-Rub, Space vector PWM technique for a three-to-five-phase matrix converter, *IEEE Trans. Ind. Appl.*, vol. 48, no. 2, pp. 697–707, 2012.
31. H. Wang et al., Topology and modulation scheme of a three-level third-harmonic injection indirect matrix converter, *IEEE Trans. Ind. Electron.*, vol. 64, no. 10, pp. 7612–7622, 2017.
32. S. S. Sebtahmadi, H. Pirasteh, S. H. Aghay Kaboli, A. Radan, and S. Mekhilef, A 12-sector space vector switching scheme for performance improvement of matrix-converter-based DTC of IM drive, *IEEE Trans. Power Electron.*, vol. 30, no. 7, pp. 3804–3817, 2015.
33. M. Imayavaramban, A. V. Krishna Chaithanya, and B. G. Fernandes, Analysis and mathematical modelling of matrix converter for adjustable speed AC drives, *IEEE PES Power System Conference and Exposition*, Atlanta, GA, pp. 1113–1120, 2006.
34. J. Kumar and R. K. Behera, Hysteresis current controllers for grid connected inverter: Review and experimental implementation, in *Proceedings of PEDES'18*, December 18–21, 2018, IIT Madras, India, pp. 1–6.
35. R. K. Behera, S. P. Das, and O. Ojo, Analysis and experimental investigation of CM voltage mitigation of a high performance Induction Motor drive, *Proceedings of PEDES'12*, Bangalore, India, December 16–19, 2012, pp. 1–6.
36. R. K. Behera and S. P. Das, Space vector modulation for a three-level NPC ac-dc converter system: An experimental investigation, *Proceedings of IEEE-ICPCES 2010*, MNNIT, Allahabad, India, November 29–December 1, 2010.
37. U. Muduli and R. K. Behera, Matrix converter fed induction motor drive, *Registration Report*, April 2019.

Section III

Electrical Drives



Taylor & Francis

Taylor & Francis Group

<http://taylorandfrancis.com>

12 Introduction of Electrical Drives

12.1 ELECTRIC DRIVES CONCEPTS

In modern industrial undertakings, the equipment used for production consists of a prime mover, energy transmission system, and actual equipment to perform the desired job, as shown in the block diagram of [Figure 12.1](#).

The function of the prime mover and energy transmission system is to provide motion to operate the actual equipment. The most economical prime mover is an electric motor. It is clean, efficient, and flexible to operate. It works under its own inherent operating characteristics. However, in many applications some desirable characteristics are obtained by use of control equipment. The control equipment used with the electric motor is based on solid-state control techniques. A technically feasible and economically viable combination of the electric motor, the control equipment and energy transmission mechanism are called electric drives [1–3,6,8,9]. The combination of drive and load is called a drive system. Elements of the electric drive system are shown in [Figure 12.2](#).

The basic elements of any electric drive system are as follows [1–12]:

1. Load: The load is the equipment designed to accomplish the given task. It can be fan, pump, washing machine, train, trolley, lift, robot, machine tools, and mechanical machine in the industry. These are specified by their ratings and torque-speed characteristics.
2. Motor: A motor has the desired and compatible speed characteristics of the load selected. The rating of the selected motor should be the same as that of the load.
3. Power Source: Usually AC or DC supply is available. When a DC motor is the choice and the available supply is AC, it is rectified.
4. Power Modulator: It performs one or more of the following functions:
 - a. It modulates the available power from the source to drive the motor to give torque-speed characteristics required by the load.
 - b. During transient operations such as starting, braking, and speed reversal, it restricts the source and motor currents within the permissible limits. This will prevent the excessive current drawn from the source, which may overload the supply system and cause a voltage dip.

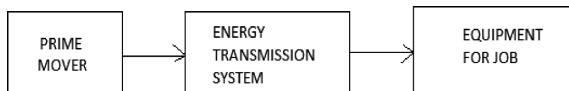


FIGURE 12.1 Block diagram.

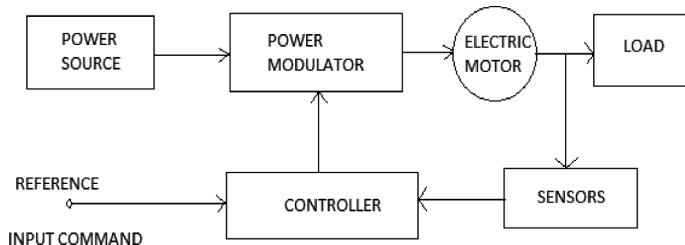


FIGURE 12.2 Electric drive system.

- c. It converts the form of source of energy to the form of energy required by the motor.
- d. The mode of operation such as motoring or regenerative braking is selected.
- 5. Sensors: It senses the parameters such as motor current and speed. It may be required for protection or a closed-loop electric drive.
- 6. Controller: The desired control characteristics are obtained by use of a controller. It operates at much lower voltage and power levels. It operates the power modulator to give the desired performance. It may also generate commands to protect the power modulator and electric motor.
- 7. Input Command: It is a reference signal. It adjusts the operating point of the drive. It forms an input to the control unit.

There is a large variety of industrial loads. To meet the specific requirements of the load, the important components of an electrical drive are the electrical motor, power modulator, source, and controller.

12.1.1 ELECTRICAL MOTORS

The main component of an electrical drive is the electrical motor. The commonly used electric motors are:

1. *DC motors*: There can be the shunt, series, compound, and permanent magnet type.
2. *Induction motors*: These can be a squirrel cage and wound rotor motor. Linear motors are also being developed for direct linear drives.
3. *Synchronous motors*: There can be wound field and permanent magnet, brushless DC motor, stepper motors, and switched-reluctance motors.

Based on speed, these drives can be:

1. *Constant-speed drives*: Induction motors and synchronous motors are basically constant-speed drives.
2. *Variable-speed drives*: DC drives are economically variable-speed drives with the development of power transistors, insulated-gate bipolar transistors (IGBTs), and gate turn-offs (GTOs); the variable speed operation of induction motors has become competitive.

Due to the presence of brushes and commutators in DC motors, as compared to induction motors, they have higher cost weight, volume, and inertia for the same rating. They also have a short life and high maintenance. They are unsuitable for an explosive environment, higher voltage, speed, and power ratings. Squirrel cage motors are more economical. The permanent magnet motors are economical for short ratings. Brushless DC motors are suitable as variable-speed drives, and stepper motors are popular as position control and reluctance motor drives for speed control.

12.1.2 POWER MODULATOR

Usually the power modulators can be converters, variable impedances, and switching circuits.

1. *Converter*: A power converter is used when the supply is AC and the drive is DC or vice versa. There can be fixed voltage DC or fixed voltage and fixed frequency AC. Some of the commonly employed converters are:

- a. *AC-to-DC Converters*: It is shown in [Figure 12.3](#). AC is rectified to get DC fixed voltage.

These converters can be fully controlled thyristor rectifiers or half-controlled thyristor rectifiers. To have variable DC voltage, AC input is made variable by the use of a tap-changing transformer; alternatively, the rectified DC is made variable by use of a chopper. A variable DC supply can also be obtained by use of an induction motor coupled to a DC generator. The use of two machines is uneconomical and less efficient. It can operate in one quadrant only while controllers employing devices belonging to the thyristor family operate in all the four quadrants.

- b. *AC Regulators*: They employ autotransformers or transformers with tap to give variable AC output voltage. Thyristor voltage controllers are also used to give variable output AC voltage.

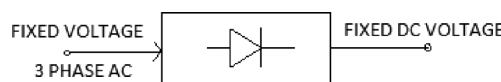


FIGURE 12.3 AC-DC converter.

- c. *DC-to-DC Converters*: To get variable DC output voltage, the input fixed DC voltage is provided with a chopper. Output voltage can be varied steplessly by controlling the duty rates of the choppers.
 - d. *DC-to-AC Converters*: Inverters are employed to obtain a variable frequency supply from a fixed DC supply. Stepped-wave inverters are designed to act as a voltage source inverter (VSI) or current source inverter (CSI). To control the speed of the AC motor, a constant flux is required in the air gap. This requires V/f control. So along with variable voltage, the corresponding variation in frequency is also achieved. These inverters produce large harmonics. To reduce harmonics, pulse-width modulator (PWM)-controlled inverters are used.
 - e. *AC-to-AC Converters*: Cycloconverters are used to obtain variable AC voltage and variable frequency from fixed voltage and fixed-frequency supply. They are built by the use of devices from the thyristor family. Output frequency is restricted to 40% of the supply frequency to minimize the harmonics effect in output voltage and source current.
2. **Variable Impedances**: Variable resistors are used to start the DC motors. It can be used for small AC motors. Variable resistors are controlled manually or automatically with contactors. For stepless control, semicontactors are used in parallel with fixed resistors. To get stepless variation of resistance in high-power applications, liquid rheostats called slip regulators are used. Variable inductors are employed to limit the starting current of AC motors.
3. **Switching Circuits**: Switching circuits are employed to meet one or more of the following:
- a. Change motor connections for its quadrant operation
 - b. Change motor circuit parameters in discrete steps for auto-starting and braking control
 - c. Operate drives according to the specified sequence
 - d. Provide interlocking and prevent mal-operation
 - e. Disconnect motor from the supply under abnormal operating conditions

Switching operations are performed by use of electromagnetic relays or thyristorized relays. To implement complicated sequencing and interlocking operations, programmable logic controllers (PLCs) are provided.

12.1.3 SOURCES

Low-power drives are fed from single-phase sources. Most of the industrial drives use three-phase sources. For electric traction 25 kV, a single-phase supply is used. Most of the commercial drives are fed directly from a 50-Hz source. In aircraft, a high power-to-weight ratio is an important requirement. In aircraft, a 400-Hz AC supply is generated and supplied to motors to achieve a high power-to-weight ratio. Some drives, such as lift tractions, are fed from a battery. For energy conservation, solar-power drives are used in space and water-pumping operations.

12.1.4 CONTROLLER

Depending upon the specifications of the load, the controller is used with a power modulator. When semiconductor converters are used, the controller consists of firing circuits employing linear and digital integrated circuits (ICs) and transistors. A microprocessor is used for sophisticated control.

12.1.5 LOAD TORQUES

They are of two types: one provides passive torque and other provides active torque.

Passive torque: It is due to friction or shear and deformation in elastic bodies, such as fans, pumps, and lathes. It always opposes the motion and retards the rotation of the electrical motor. With the change of direction of motion, the sense of passive torque changes. As in a lift, the friction torque is added to the useful torque when it is going up, while it is subtracted from the useful torque when the lift is going down.

Active torque: This torque is due to gravitational force or deformation in elastic bodies. Active torques are due to gravitational pull. When an electric locomotive operates in gradients then active torque is produced. This torque is also developed during compression or release of springs and other elastic bodies. The active torque is closely connected to the potential energy. For example, when a load moves upward or a spring is compressed, the stored potential energy increases, and the developed active torque opposes the action that is taking place. In this case, the active torque is directed against the upward movement or compression. In the other case, when the load is moving downward or the spring is released, the stored potential energy decreases. The active torque associated with it aids the action. Therefore, it is observed that the active torque continues to act in the same direction, even after the direction of the drive has been reversed.

12.2 ADVANTAGES OF ELECTRICAL DRIVES

Various advantages of electrical drives are as follows [1–3,6,8,9]:

1. High efficiency: The efficiency of the electric motor is very high. It has low no load losses and considerable short-time overload capability.
2. Flexible operation: They can be made in a variety of designs to make them compatible with the load.
3. Longer life: They have a longer life as compared to mechanical prime movers. They also have less noise, lower maintenance requirement, and cleaner operation.
4. Flexible-control characteristics: Their steady state and dynamic characteristics can be made compatible to the load characteristics.

5. New semiconductor devices with the development of semiconductor technology: Devices such as IGBTs, GTOs, linear and digital ICs, and microcontrollers have made the control of drives more flexible. It is possible to reshape the characteristics of electrical drives to almost meet the requirements of the load in an optimum manner. Torque and speed from one mode to another mode can be controlled steplessly.
6. Optimal control with the implementation of optimal-control strategies: Electrical drives are operated to give high dynamic performance, high efficiency, or to minimize a desired performance index.
7. Automotive electric drives can be provided with an automatic fault-detection system.
8. Adjustable: They are adaptable to various operative conditions, such as explosive and radioactive environment, vertical mountings, and submerged in water. They do not pollute the environment.
9. Four-quadrant drive: The electrical drive can be economically operated in all four quadrants.
10. Instant start: Electrical motors require no warm-up time. They can be just started by a push button. They can be fully loaded immediately.
11. Braking: Electrical braking gives smooth deceleration and increased life of the equipment where regenerative braking is possible, and considerable energy saving takes place.
12. Advantages of electrical energy: The electrical drives work on electrical energy. Electrical energy has a number of advantages, such as economic and flexible generation and transmission. Conversion of electrical energy to mechanical energy and vice versa is more efficient and economical.
13. Electrical link: It can provide a flexible link between mechanical energy to mechanical energy. For example, in a diesel electric locomotive, the mechanical energy produced by the diesel engine is converted into electrical energy by a generator coupled to it. The electrical energy is then utilized economically by the electrical motor at the angle of the locomotive.

12.3 CHARACTERISTICS OF AN ELECTRICAL DRIVE

It depends upon the following factors:

1. Steady-state characteristics: The desired torque speed characteristics, speed regulation and range, efficiency, duty cycle, speed fluctuation and quadrant operation.
2. Transient state characteristics: The values of acceleration and deceleration, starting, speed control, braking and reversing characteristics.
3. Sources: AC or DC sources, its capacity, amplitude of voltage and its fluctuations power factors and harmonics, their effect on load, acceptability to regenerated power.
4. Economics: Cost of maintenance, running and capital cost.
5. Environment and location: Space and weight limitation.
6. Reliability: A space vehicle requires highest reliability.

12.4 CLASSIFICATIONS

In general the electric drives may be classified as follows [1–3,6,8,9]:

1. *Individual Drive System:* An electrical motor is used to transmit motion to various parts or mechanism of single equipment. A commonly used individual drive is a mono block or a tube well to lift water to the desired height. In a lathe, an individual drive is used to rotate the spindle to move the feed. With the help of gears, it imparts motion to the lubricating and cooling pumps of the lathe. In many applications, the individual drive is an electric motor that forms the integral part of the equipment. In an electric fan, the blades to circulate air are bolted to the body of the electric motor. In this case, energy is transmitted to the various parts by gears and pulleys, so there may be power loss.
2. *Group Drive System:* It consists of a large, single electrical motor to actuate several mechanisms or machines by means of one or more live shafts supported on it. The live shafts may be fitted with multistep pulleys and belts to drive machines with varying speeds. It is also called a live-shaft drive system.

When there are a number of mechanisms or machines to be driven by live shafts, pulleys, and belts, the group drive is economical since the large motor is less costly as compared to the large number of small motors of equivalent power. The use of the group drive has become obsolete due to the following disadvantages:

- Any fault in the drive motor makes all the driven equipment come to a standstill.
- In transmitting energy to various mechanisms, a lot of energy is wasted. This reduces the efficiency of the system.
- Layout of the different machines is not flexible. All the machines are to be located to be approachable by the driven live shaft.
- A group drive requires the use of belts and pulleys, so it gives an untidy appearance.
- It is less safe to operate.
- It has a larger-sized motor and connected mechanism of noise.
- During maintenance of the main motor, no production can be done. This results in a loss of product.

3. *Multimotor Drive System:* In this system, individual motors are provided to actuate different parts of the driven mechanism. In a traveling crane, three motors are employed: one motor to hoists, the second to provide long travel motion, and the third motor is used for cross-travel motion. In rolling mills, paper mills, rotary printing machines, and metal-working machines where large numbers of operations are to be performed, multimotor drives are used. Each operation is driven by a separate electrical motor.

The applications of individual drives and multimotor drives have made the automation in production processes possible. The automation has considerably increased the production of essential consumer products. Partial or complete automation in an industry provides an optimal use of resources. It increases the reliability and safety of operation.

12.5 QUADRANT OPERATION OF THE DRIVE

In general, both active and passive load torques are present in a drive system. The electrical motor driving the load may have to operate in the mode of motoring, generating, or braking. Suitable conventions are followed to represent torque and speed of an electric drive. The speed of an electrical motor is positive in the forward direction. Electric drives operating in only one direction, the normal speed, is their forward speed. In electrical drives used for up and down motion, the upward motion is the forward motion. In reversible drives, the forward speed is positive, and the reverse speed is the negative speed. The motor torque is positive, when it produces acceleration or the rate of change of speed in the forward (positive) direction is positive. Torque of the electrical motor is negative when it produces deceleration.

An electrical motor operates in two modes:

1. *Motoring mode*: It converts electrical energy into mechanical energy to support its motion.
2. *Braking mode*: It acts as a generator to convert mechanical energy into electrical energy. Therefore, it opposes the motion. An electrical motor can provide motoring and braking operations in both forward and backward or reverse directions.

12.5.1 ONE QUADRANT

Based on the above sign conventions of torque and speed, the electrical motor can be operated in various quadrants as shown in [Figure 12.4 \[1–3,6,8,9\]](#). Power developed by the electrical motor is the product of speed and torque ($W_m \times T_m$).

In Quadrant I, both speed and torque have a positive sign. Their product is positive to give positive power. The machine works as a motor to supply mechanical energy. In Quadrant II, the torque is negative while the speed is positive. This will

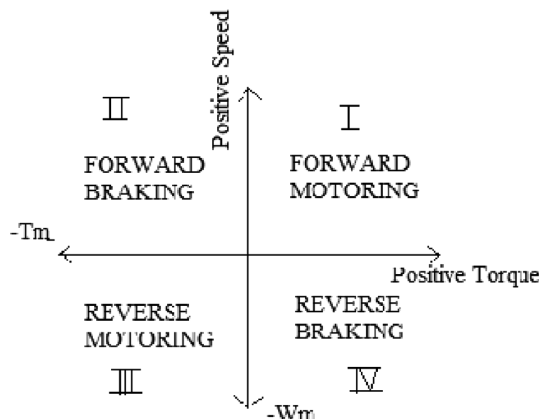


FIGURE 12.4 Four-quadrant operation of the electric motor.

give negative power. Hence, the machine works under braking to oppose the motion. Therefore, operation in Quadrant II is called the forward braking because the speed is in the forward or positive direction.

In Quadrant IV, the torque is positive while the speed becomes negative. This will give negative power to break the drive in the reverse direction. It is called reverse braking. Usually one quadrant drive operates in Quadrant I. The electrical motor provides positive torque and positive speed only.

12.5.2 Two QUADRANTS

When the electrical motor has only torque in the positive direction, but the speed can be reversed, it is called operating in two quadrants, that is, Quadrants I and IV. Usually, a reversible electrical drive operates in Quadrants I and III, that is, in formed motoring and reverse motoring.

12.6 FOUR-QUADRANT OPERATION OF ELECTRICAL DRIVES

Four-quadrant operation of an electrical drive can be best understood by considering an electrical motor driving a hoist as shown in [Figure 12.5 \[1–3,6,8,9\]](#). The direction of motor and load torques and the direction of speed are marked by arrows. A hoist consists of a rope wound on a drum, which is coupled to the shaft of the electrical motor. One end of this rope is tied to an empty cage, which is used to transport man or materials from one level to the other. A counterweight is placed on the other end of the rope. The weight of the counterweight should be higher than that of the empty cage, but it should be lower than that of the fully loaded cage.

The forwarded direction of the motor speed will be the one that gives upward motion to the cage. According to the convention, the positive load torque is opposite

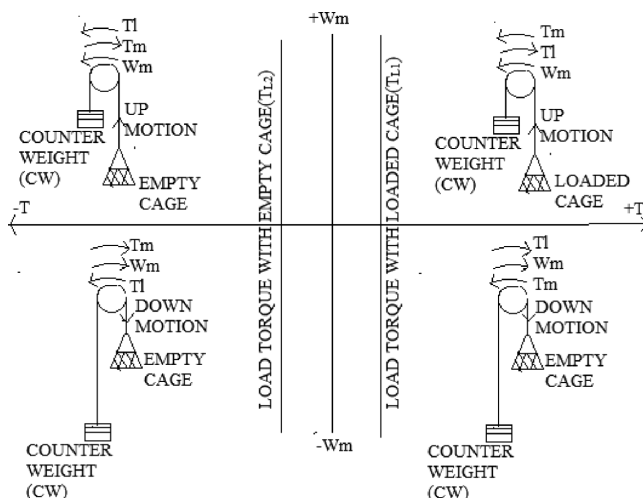


FIGURE 12.5 Four-quadrant operation of a hoist drive.

in sign to the positive motor torque. However, it is convenient to plot it on the same axes. Load torque so drawn will be negative to the actual motor torque.

In this case, the hoist has a low speed having negligible friction and windage torques as compared to the gravitational torque. Gravitational torque is always of the same sign, as it is acting downward. Load torque T_{L1} in Quadrants I and IV is of the same sign. The weight of the loaded cage is more than that of the counterweight. The load torque T_{L2} in Quadrants II and III is of the same sign. The weight of empty cage is less than that of the counterweight, so the sign of T_{L2} torque is negative of the sign of torque T_{L1} .

In Quadrant I, the loaded cage moves upward, and the direction of the motor is anticlockwise, which is the positive direction. This motion will be obtained when the motor develops the positive torque in the anticlockwise direction equal to load torque T_{L1} . The developed torque is positive, and the speed is positive; therefore, it is a case of forward motoring as explained earlier.

Quadrant IV operation is obtained when the loaded cage is lowered to give reverse direction to the motor, and the speed will be negative w_m . Since the weight of the loaded cage is more than that of the counterweight, it is able to come down by itself. So the electrical motor must produce a positive torque $T_m = T_{L2}$ in the anticlockwise direction. Since both power and speed are negative, it is a case of reverse braking, as explained earlier.

Quadrant III operation is obtained when the empty cage moves upward. Since the counterweight is higher than the weight of the empty cage, it will move upward under the load torque. To limit the speed, the electrical motor must produce torque in the clockwise direction. Its value should be equal to T_{L2} . Since the speed is positive, but the motor torque is negative, it is a case of a forward-braking operation.

Quadrant III operation is obtained when the empty cage is lowered. Since the empty cage has less weight than that of the counterweight, the motor must produce torque in the clockwise direction, and $T_m = t_{L2}$. Since the speed is negative and the motor torque is also negative, the power is positive. It is a case of reverse motoring.

12.7 CONSTANT-TORQUE DRIVE

A drive running at nearly fixed speed is called a constant speed or single-speed drive. A drive operating at a discrete speed setting is called a multispeed drive. Drives having stepless change of speed and multispeed drives are called variable-speed drives.

A variable-speed drive is called a constant-torque drive when its maximum torque setting does not change with a change in speed setting. The corresponding mode or region of operation is called the constant-torque mode. It may be pointed out here that the term constant torque refers to the maximum torque capability of the drive and not its actual output torque. The actual torque of the electrical motor may vary from no load to full load conditions. The speed torque curve of a dry friction load is shown in [Figure 12.6](#).

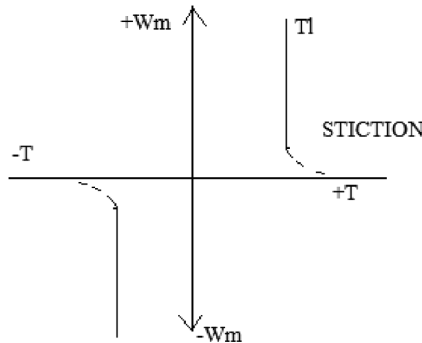


FIGURE 12.6 Speed torque curve of a dry friction load.

In this type, the load presents to the motor a passive torque independent of the speed. It requires an extra torque even at a zero speed; in power applications, it is called the breakaway torque, and in control system it is called stiction due to the sticking friction. Since torque is the product of the flux and current, for the constant flux machines it is a constant-current drive.

12.8 CONSTANT-POWER DRIVE

The power is the product of angular speed and torque, that is, $P = W \times T$. So for constant power, the speed should be inversely proportional to the torque, that is, the torque speed characteristics should be soft. In a DC series motor, $w \propto E/I$ and $T \propto I^2$. So for constant power, WT will be constant, and $W \propto 1/T$.

The examples of the loads demanding constant power are lathes, boring machines, milling machines, and steel-mill coilers. Its characteristic is shown in [Figure 12.7](#).

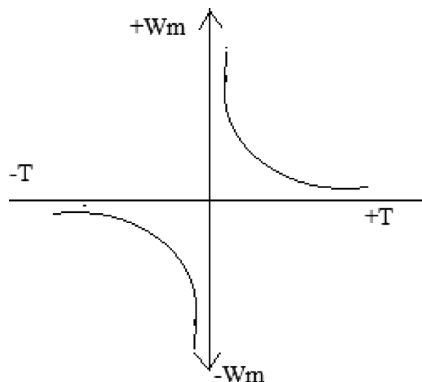


FIGURE 12.7 Speed torque curve of a constant power load.

12.9 NATURE AND COMPONENTS OF LOAD

The nature of load depends upon their torque-speed characteristics [1–12]. It can be a constant torque load when the load does not vary with speed. It is a passive load called dry friction. Due to stiction, it requires some extra torque near the zero speed. In control engineering, viscous friction plays a significant role. This force, or torque, loading varies with speed. These characteristics are represented by eddy-current brakes.

12.9.1 FAN-TYPE LOAD

In this type of load, the load torque varies as the square of the speed. It is given by a fan or blower pump.

Centrifugal pumps, propellers in ships or airplanes, have such type of characteristics. The power $P = T_L w$ when the load operates on a constant power, then its torque-speed characteristics are represented as $T_L \propto 1/w$, or it is a hyperbolic characteristic.

These load characteristics are associated with loads of lathe, boring machines, milling machines, steel-mill coilers, and similar loads. In any system application, the load torque may consist of any one, or combination, of the above torques in varying proportion.

12.9.2 LOAD TORQUE AS A FUNCTION OF POSITION

In practice, the load torque not only depends upon the speed but also on the nature of path traced by the load during its movement. For example, when an electric train moves up a gradient or on a curved path, the load torque depends upon the magnitude of the gradient or the radius of the curvature of the track. When a train of weight of W moves up, then the force resisting the motor F_G for small gradient is given by

$$F_G = W \sin \alpha \sim W \alpha = WG / 1000 \text{ kg}$$

where G is the rise in meters in the track distance of 1,000 m. When the radius of curvature of track is R in meters, then the tractive force required to overcome the curve resistance will be $F_c = 700 W/R \text{ kg}$.

12.9.3 HOISTING LOAD

In hoists when the tail ropes or balancing ropes are not used, then the torque load consists of weight of two cages and that of the lifting ropes or cables. The weight of the rope depends upon the position of the two cages. When Cage 1 is at the bottom-most position and it is being lifted up, then the entire weight of the rope is also to be moved up. When both cages are at same height, that is, $h = 0$, then the weight of the rope to be lifted up becomes zero. When Cage 1 moves farther up and is at a

higher position than Cage 2, the position of the rope acts in such a way so as to aid the upward motion of the Cage 1. When Cage 1 reaches the top-most position, the whole weight of the rope aids the upward movement. If the total weight in kilograms is W_{rope} , h is the desired height to which the cage is to be moved upward in meters, then for any position at height x from the bottom, the force due to the rope resisting the upward motion will be F_R given by:

$$F_R = W_{\text{ROPE}} \left(1 - \frac{2x}{h} \right)$$

For high values of h , the weight of the rope is higher. It may be considerably higher than the weight of the load to be lifted upward. The above force affects the performance of the hoist drive when the tail rope movement of the two cages are obtained. Such a load torque, which is a function of the path traced, is obtained in the planning machine when the moving table is at a particular position. In a different position, when the cutter has come out of the job, the magnitude of the load torque decreases sharply.

12.9.4 LOAD TORQUE AS A FUNCTION OF ANGLE OF SHAFT DISPLACEMENT

In drive systems having a crankshaft—as in reciprocating pumps, compressors, weaving loom, rocking pumps in petroleum industry, frame saws, and drives of steering ships—the load torque is of the position θ of the crank. The load torque is of the form $T_L = f(\theta)$. The angular position θ itself varies with time.

Such a load characteristic can be resolved into two components: one of the constant magnitude T_{AUG} and other a variable T'_L . It changes periodically in magnitude, which depends upon the angular position of the shaft. Such a torque can be represented by Fourier series as

$$T'_L = \sum_{n=0}^m T_l' \sin(n\theta + \varphi_n)$$

When there are small changes in speed, $\theta = (Wa + \Delta W)t$, then the variable portion of the load torque will be

$$T'_L = \sum_{n=0}^m T_l' \sin[(nWat + \varphi_n) + n\Delta wt]$$

The term $n\Delta wt$ is very small and can be ignored. Therefore, for small variations in the angle for the equilibrium position, the load torque varying with the angular position of displacement of shaft can be represented by one varying periodically with time.

12.9.5 LOAD TORQUES VARYING WITH TIME

Most of the load torques vary with time. In applications, these torque variations can be periodic and repetitive. One cycle of the variation is called a duty cycle. These load torques can be classified as follows:

Continuous Constant Load: These loads operate for a long time under the same conditions. The magnitude of the load torque remains constant and parallel to the time axis for a very long period. Some examples of such loads are centrifugal pumps, fans, and paper-making machines.

Continuous Variable Loads: These loads vary with time and are continuous. Some examples are metal-cutting lathes and mine hoists; its power time diagram is shown in [Figure 12.8](#).

Pulsating Loads: These loads come on the motor in pulses. The power-time diagram of the textile loom is shown in [Figure 12.9](#). Other examples are reciprocating pumps and compressor frame saws and similar machines having crank shafts.

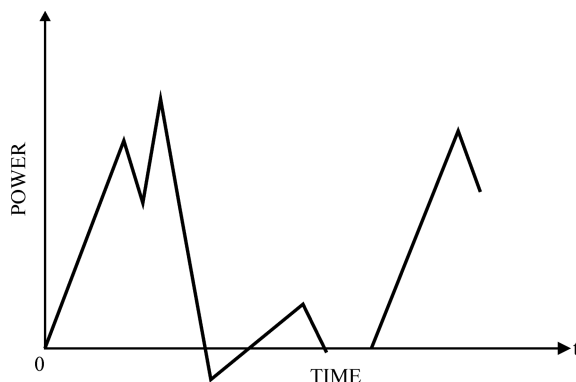


FIGURE 12.8 Mine hoist power time curve.

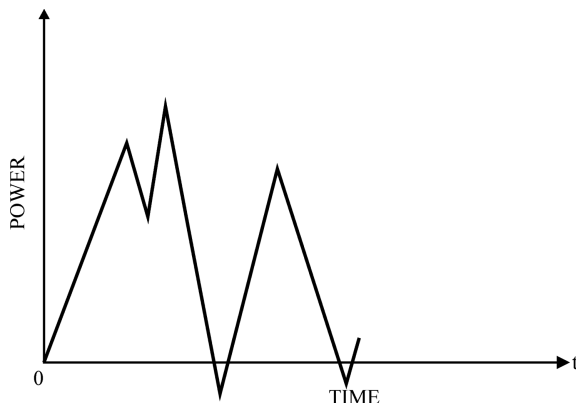


FIGURE 12.9 Textile loom load.

Impact Loads: These torques are due to apparent regular and repetitive load peaks or pulses. These occur in rolling mills, presses, shearing machines, forging hammers, and drivers using flywheels for load equalization.

Short-Time Intermittent Loads: The loads which occurs intermittently and that too for short time. Almost all forms of cranes and hoist mechanisms, excavates, and rolling trains produce such types of load torques.

Short-Time Loads: These loads are of a short time duration. Some examples are motor generator sets to charge batteries and servo-drives in remote applications to control the clamping rods of drilling machines.

Some machines, such as stone crushers and ball mills, have loads that cannot be specified as any one of the above. These loads have small peaks and may be characterized as impact loads. But these loads are continuously varying, so they may be classified as such. Moreover, it is difficult to distinguish between a pulsating load and impact load, as both are periodic in nature. Therefore, it is better to express them as a sum of sinusoidal waves of different amplitude, frequency, and phase like the Fourier series.

Some load torques vary with speed of time, such as the fan load, which has torque proportional to the square of the speed, and it is a continuous constant load. The load torque of a crane does not depend upon the speed, but its nature is short-time intermittent. Rocking pumps used in petroleum industries have a load that varies with the angular position of the shaft. It can also be classified as pulsating loads.

12.10 COMBINED MOTOR LOAD DYNAMICS

The rotational system representing the motor load combination is shown in **Figure 12.10**.

When the moment of inertia of drive system is J , then the motor developed torque T_m is related to the load torque T_L at rotational speed ω related as

$$T_M = T_L + Jd\omega/dt$$

From the equation, the acceleration will be

$$\frac{d\omega}{dt} = (T_M - T_L) / J$$

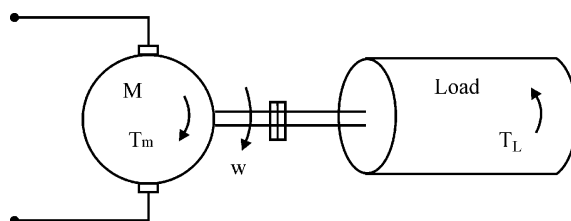


FIGURE 12.10 Motor load drive system.

Depending upon the developed torque as compared to the load torque, the following conditions are possible:

1. When the developed torque $T_M > T_L$, then $\frac{d\omega}{dt}$ will be positive. This will accelerate the drive. The drive will accelerate to reach the rated speed.
2. When $T_M = T_L$, then $\frac{d\omega}{dt} = 0$ the motor will not have any change in speed. The drive will run at constant speed.
3. When $T_M < T_L$, then $d\omega/dt$ will be negative. The drive will decelerate and may come to rest.

This condition is true only when load torque T_L is due to a passive load. In case of an active load, the reverse may occur, as in the case of a winch hoist load when the motor is switched on to hoist up, while it is coming down due to its own weight, until the direction of rotation changes, for $T_M > T_L$.

Deceleration takes place instead of acceleration. When the motor is switched on to move the winch up for $T_M < T_L$, the load will continue to come down, and the motor will accelerate and not decelerate as per the preceding conditions.

The inertia torque $J \frac{d\omega}{dt}$ is also called the dynamic torque. It is present only when the speed of the drive ω varies during transient conditions. During acceleration of the drive, the insertion torque is directed against the motion. During braking, it maintains the motion of the drive. So inertia torque in magnitude and sign is the algebraic sum of the motor and load torques. Depending upon the region of operation, the torque developed in the motor will be $\pm T_M$. The active load torque will be $-T_L$. So in general, the dynamic equation of the motion during the transient operation will be

$$\pm T_M = \pm T_L + J \frac{d\omega}{dt}$$

This equation of the motor determines the dynamics of variations of torque current and speed with respect to time during the transient operation of the drive system.

12.11 EQUIVALENT SYSTEM

In practice, different loads requiring different speeds are connected to the shaft of the motor. The different speeds of the various loads are obtained by the use of speed-changing mechanisms, such as gears and belts. For a drive system, it is always desirable to select a suitable motor. To obtain this objective, all the load torques and inertia torques are all referred to the output shaft of the motor. This is achieved through the principle of conservation of energy.

12.11.1 EQUIVALENT LOAD TORQUE REFERRED TO THE MOTOR

Let the load torque at speed W_L be T_L . It is connected to the motor at speed W_M with an efficiency of transmission η . The equivalent load torque referred to the shaft of the motor T_{eq} will be

$$\eta T_{eq} W_M = T_L W_L$$

$$\text{or } T_{eq} = (W_L / W_M) \frac{T_L}{\eta}$$

For gear ratio $W_m/W_1 = g$ and equivalent motor torque will be $T_{eq} = \frac{T_L}{\eta g}$

When the load is connected to the shaft of the motor through number of gears.

As shown in Figure 12.11, the various gear ratios are $g_1, g_2 \dots g_n$ and efficiency are $\eta_1, \eta_2 \dots \eta_n$, respectively.

The equivalent load torque referring to the shaft of the motor will be

$$T_{eq} = T_L \times \left(\frac{1}{g_1 g_2 \dots g_n} \right) \times \left(\frac{1}{\eta_1 \eta_2 \dots \eta_n} \right)$$

12.11.2 EQUIVALENT MOMENT OF INERTIA

The equivalent moment of inertia J_{eq} is obtained on the basis of equating the total amount of kinetic energy stored in the moving parts and referring to the given shaft remains same. Let the moment of inertia of moving parts be $J_m, J_1, J_2 \dots J_n$ with their respective angular speeds as $w_m, W_1, W_2 \dots w_n$. In this case, the equivalent moment of inertia referring to the motor shaft will be

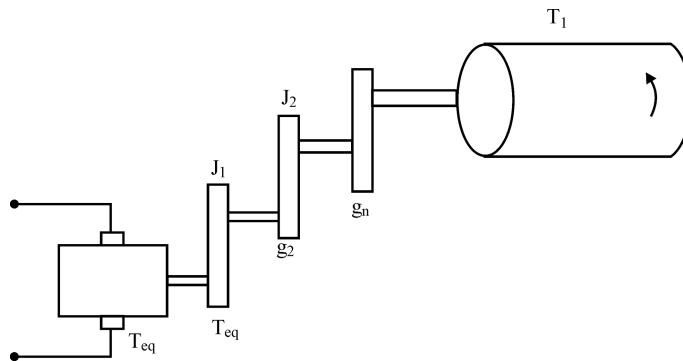


FIGURE 12.11 Gear ratios.

$$\frac{J_{eq} Wm^2}{2} = J_m \frac{Wm^2}{2} + J_1 \frac{W1^2}{2} + J_2 \frac{W2^2}{2} + \dots + J_n \frac{Wn^2}{2}$$

so

$$\begin{aligned} J_{eq} &= J_m + J_1 \left(\frac{W1}{Wm} \right)^2 + J_2 \left(\frac{W2}{Wm} \right)^2 + \dots + J_n \left(\frac{Wn}{Wm} \right)^2 \\ &= J_m + \frac{J1}{gn^2} + \frac{J2}{(gn g1)^2} + \dots + \frac{J3}{(gn g1 \dots gn)^2} \end{aligned}$$

12.11.3 RELATING TRANSLATION MOTION TO ROTATIONAL MOTOR

In loads such as hoists, cranes, and shaping machines, some of the moving parts rotate, and the remaining parts have a translational motion. One such drive is shown in [Figure 12.12](#).

In this case, the moving mass m of weight W moves upward with a speed of V m/s. It is converted to a motor shaft of angular velocity Wm rad/s. The resisting force Fr developed by the load due to gravitational pull at an efficiency of transmission η will give the referred torque T_{eq} of the load on the shaft of the motor

$$T_{eq} = \frac{Fr v}{Wm\eta}$$

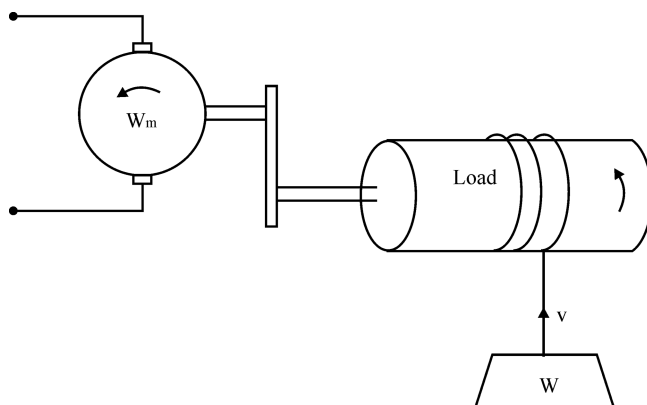


FIGURE 12.12 Hoist load drive system.

The moment of inertia J_{eq} will be obtained by law of conservation of energy as

$$J_{eq} \frac{Wm^2}{2} = \frac{Wv^2}{2}$$

$$J_{eq} = m \left(\frac{v}{Wm} \right)^2 = \frac{1}{g} \left(\frac{v}{Wm} \right)^2$$

where g = acceleration due to gravity

12.12 PRACTICAL DETERMINATION OF MOMENT OF INERTIA

To analyze the dynamic performance of the drive system, it is necessary to know the moment of inertia of the system. If dimensions of all the parts of the rotating masses are known, it can be obtained analytically. The best way to obtain the value of moment of inertia is to perform the retardation test [1–3,6,8,9].

12.12.1 RETARDATION TEST

In this test, the motor is run up to a speed slightly higher than the rated speed. At a higher speed, the supply to the motor is cut off before switching off the power supplied to the motor is noted, corresponding to various speeds. After switching off the supply, the oscillographic record of the motor speed as function of time is recorded. These records are drawn on a graph paper as shown in Figure 12.13 [1,3,6,8,9].

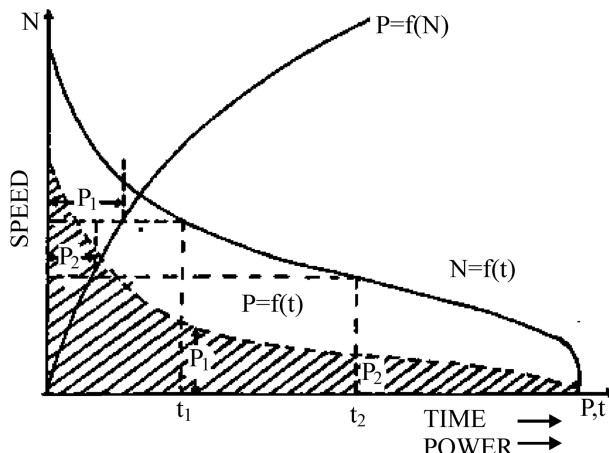


FIGURE 12.13 Results of retardation test.

When the supply energy is cut off, the rotational system continues to rotate because of initial K.E. stored in the drive system. However, this energy is used to overcome the rotational losses in the system. So it slows down, and finally it stops the power consumed to overcome rotational losses. P is given by

P = rate of change of K.E.

$$= \frac{d}{dt} \left(\frac{1}{2} J w^2 \right) = J w \cdot \frac{dw}{dt}$$

For $w = \frac{2\pi N}{60}$

$$P = \frac{4\pi^2}{3600} (J N) \frac{dN}{dt}$$

From the plotted result in graph, the value of P and $\frac{dN}{dt}$ is obtained for rated speed N .

This will give $J = \frac{P \cdot 3600}{4\pi^2 N \frac{dN}{dt}}$

This will give an approximate value of J to obtain a more accurate value of J , the machine is run at varying speeds, and corresponding to each speed the rotational losses are determined. These are plotted as $P = f(N)$ on the same graph. This is done at $N = 0$, $t = t_2$, $n = N_2$ and $P = P_2$. The area under the curve $P = f(t)$ and time is the K.E. used to make up for the rotational losses. In rotational masses, that occurs during retardation

so $J \frac{w^2}{2} = \text{Area } A$

$$J = \frac{2(\text{Area } A) \cdot 3600}{(2\pi N)^2} = \frac{1800(\text{Area } A)}{(\pi N)^2}$$

12.13 RATING OF ELECTRICAL DRIVES

In a drive system, the size and rating of a motor depends upon the following factors [1,3,6,8]:

12.13.1 HEATING AFFECTS ALL MACHINES DURING RUNNING PRODUCE LOSSES

This energy is converted into heat energy, and the heat energy heats up the machine. The cooling of the machine is provided to cool the machine, and the results limit the temperature rise within the permissible limits of temperature rise for the insulating materials provided by ISS:1271. ISS:4722 gives the limit of temperature rise for the various parts of the rotating electrical machine. Heating and cooling curves are obtained from the following heat-balance equation of the drive

$$Gh \cdot d\theta + s\theta e \cdot dt = p \cdot dt$$

where the weight of the active part of the drive motor = G in kg

Specific heat in J/kg/ $^{\circ}$ K = h

Small incremental temperature = $d\theta$ in time dt

Cooling surface area in m^2 S

Rise in temperature = θ

Emissivity or specific heat dissipated surface and ambient temperature of the

cooling medium heat time constant of second = T_h

Cooling time constant in second = T_c

Losses producing heat in watts = p

The differential from the heat-balance equation can be expressed as

$$\frac{d\theta}{dt} + \theta \frac{Se}{Gh} = \frac{p}{Gh}$$

$$\theta = \frac{p}{Se} \left[1 - e^{-\left(\frac{Se}{Gh}\right)t} \right]$$

For the initial temperature rise to be zero at $t = 0$ when $t = \infty$, the $\theta = \theta_m$ will be the final maximum temperature rise, and its value will be $\theta_m = \frac{p}{se}$

Denoting $\frac{Gh}{Se} = T_h$ = heating time constant the heating rise curve will be

$$\theta = \theta_m \left[1 - e^{-\left(\frac{t}{T_h}\right)} \right]$$

When $t = T_h$, then $\theta = 0.632 \theta_m$. This value of θ determines the value of the time constant of the drive motor.

Good ventilation leads to small time constant because T_h is inversely proportional to emissary, which is large, so for an open machine of rating 10 to 20 kW, the value of T_h is 0.5 hour. A medium-size machine in the range of 500–800 kW has T_h in the same range of 2–2.5 hours. The large machine or totally enclosed machine has a very large time constant.

During cooling, $p = 0$, and the heat balance equation will be

$$\frac{d\theta}{dt} + \frac{\theta}{T_c} = 0$$

This gives the solution from the initial temperature of θ_m as

$$\theta = \theta_m e^{\frac{-t}{T_c}}$$

12.13.2 LOADING CONDITIONS

The electrical motor used to drive the mechanical load develops electromagnetic torque T_m of such a magnitude as to counterbalance the actual load torque T_l . Also, it overcomes the torque required to overcome various losses of the system and in transmission of torque T_{loss} so the torque equation will be

$$T_m = T_l + T_{\text{loss}} + T_{\text{dyn}}$$

where T_{dyn} = torque due to inertia of system.

Based on the loading conditions, the rating of the electrical drive motor is selected.

12.13.3 LOAD INERTIA

When an electric motor drives loads of heavy inertia and has a large number of starts in the given time, the principal loads on the electrical motor are the acceleration and the braking of the rotating masses of the mechanical system. The load torque acting on the shaft of the motor is negligible. The rating of electrical motors for such a drive system depends on the torque required during acceleration and braking. The power rating required for the motor will be the product of the rating torque T and the maximum speed of the motor W_{max} . In practice, these loads have permissible speeds of rotation, torque, and acceleration. Consider a triangular speed-time curve as shown in [Figure 12.14](#).

The drive motor accelerates up to the rated speed, and then immediately it decelerates to complete stoppage.

$$\text{Torque } T = J \frac{d\omega}{dt}$$

$$\text{Power rating } P = Tw_{\text{max}}$$

Sometime in the drives used for excavation and traction, the speed-time curve is trapezoidal, as shown in [Figure 12.15](#).

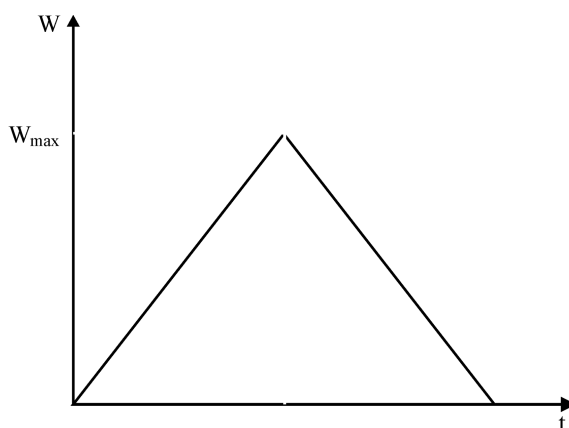


FIGURE 12.14 Triangular speed-time curve.

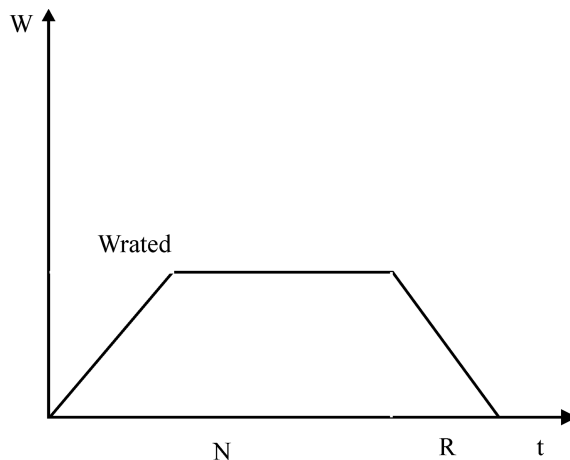


FIGURE 12.15 Trapezoidal speed-time curve.

The period of steady-state motion is a period of constant load. The equivalent rating of such an electrical motor will be $P_{eq} = P \sqrt{\frac{N}{N+R}}$ where N = time for which the motor is on, and R = time for which motor is off.

12.13.4 ENVIRONMENTAL FACTORS

The environment plays a key role in the rating of the electrical motor, as the temperature rise is of importance. The cooling of the machine depends upon the value of ambient temperature. At the North Pole, the ambient temperature is -80°C . So a 100-kW electric motor can safely drive a continuous load of 200 kW because the heat energy generated by the losses in the motor may not be sufficient to overheat the electric motor at the North Pole, rather than at the equator. As the motor is used at altitudes, the cooling effect becomes less as compared to that at sea level. However, up to a height of 1,000 m above sea level, this effect is of air. However, at heights above 1,000 m, the rating of the motor is decreased.

Totally enclosed machines have little less rating as compared to their equivalent size in open and well-ventilated motors.

12.14 SELECTION OF ELECTRICAL DRIVES

In the selection of an electrical motor for a particular application, the following features are considered [2,6,8,15,17,19]:

1. *Speed regulation:* Regulation is the ability of the drive to maintain a particular speed under varying conditions of load. It is the total percent change in speed from no load to full load.

2. *Speed range:* It is the range of speed of the drive, which defines the lowest speed at which the drive can be operated to the maximum speed of the drive under a rated continuous load. To specify the low speed, it must be assured that at low speed the motor is properly cooled, and its regulation is within limits. For example, a 10:1 range of the drive at continuous rated load is 1/10th of the maximum speed at which it can be operated on a rated continuous load.
3. *Adjustable minimum speed:* The minimum speed that can be obtained by adjusting the drive controller.
4. *Adjustable maximum speed:* The maximum speed that can be obtained by adjusting the drive controller.
5. *Speed sensing:* The counterelectromotive force (CEMF) voltage generated by a DC motor is proportional to the speed of the rotation of drive. This voltage is detected and compared with a reference speed voltage. The error so obtained is amplified and fed to the controller. Alternatively, a DC or AC technogenerator is used to generate voltage for comparing in a feedback loop. This technique is also used for remote speed control.
6. *Jogging control:* It is used to operate the drive at a very low speed during setting up operations. It is designed to run the drive with a push button in the down position, or it is designed to run the drive continuously at very low speeds for threading operations.
7. *Reversibility:* It implies that the drive control has contacts that are operated to reverse the direction of drive motor.
8. *Regenerative braking:* It is a means of extracting mechanical inertial energy to be fed back to supply as electrical energy during the braking operation.
9. *Dynamic braking:* It is a means of operating the motor as a generator during braking and dissipating its electrical energy in some resistive load.
10. *Torque limit:* In the drive controller, circuits are incorporated to limit the motor torque during the periods of acceleration or overloads. These circuits are used to obtain timed acceleration of high-inertia loads to protect the motor and control equipment from overcurrent and to prevent the drive from becoming unstable.
11. *Constant torque drive:* The drive system has the inherent capability to supply the rated torque over the given range.
12. *Constant-power drive:* The drive system has the inherent capability to supply the rated power, that is, the product of speed and torque over a given speed range. The size of the motor and the control equipment is specified according to the product of highest torque and the lowest speed.
13. *Current limit acceleration control:* In this type of control, the maximum allowable armature current is set within limits. Depending upon the load, this control will limit the acceleration during the period of starting.
14. *Time-delay acceleration control:* This control is achieved by employing electronic delay circuits to delay the full application of the reference signal. In this control, when the speed setting is changed abruptly, the rate at which the drive speed changes automatically is independent of the change in the

speed-setting element. With this feature, the acceleration of the drive is controlled during the starting and running period as well.

15. *Torque regulation:* The value of output torque is limited by limiting the value of current in the armature. The range of torque required to maintain the constant set speed is called torque regulation.

12.14.1 DRIVE CONSIDERATIONS

The problem of selecting a variable-speed drive for a particular application is choosing an economical system that can provide the required speed range and speed regulation with the desired accuracy and speed of response. With the development of solid-state devices, the emphasis is on selecting brushless drives. For precise speed control, the closed-loop feedback circuits are adopted. A balance sheet between the DC motor and squirrel cage induction motor is presented in **Table 12.1**.

Modern static drives using static frequency converters coupled with squirrel cage motor, permanent magnet synchronous motor, or reluctance motor can provide accuracy up to 0.001%. Such drives have found widespread application in the paper-making, textile, and synthetic fiber industries. It is also becoming popular in the various process industries, where exact speed coordination is essential in order to maintain the quality of the product. In these industries, the system reliability is vital because failure in any system element will lead to substantial loss in production. Such high reliability can be ensured by solid-state and brushless DC drives.

Further applications such as reeling drives requiring constant power can be arranged by the use of a DC link inverter in a closed-loop control system. Environmental considerations not permitting rubbing contact with the inherent risk of sparking need solid-state brushless AC drives.

TABLE 12.1
Comparison of Squirrel Cage Induction Motor and DC Motor

Squirrel Cage Induction Motor	DC Motor
1 No brush and commutator wear. Commutation problems are also absent.	Brush, commutator, and problem of commutation limit its voltage and power ratings.
2 Power-to-weight ratio large.	Power-to-weight ratio low.
3 Voltage control to control its speed is not recommended.	Speed control by the method of armature voltage control is economical and widely used.
4 Low cost of construction.	High cost of construction.
5 Frequency variation in stator supply is used to control its speed effectively. The cost of static frequency converter is usually high.	Frequency control is not used with DC motor.
6 Digital and microprocessor controls are possible to produce exact speed ratio with accuracy and stability of the drive.	Digital and microprocessor controls are not economical due to brushes and commutator.

The waveform obtained from the inverter contains large number of harmonics, which increases the losses in the motor. In practice, such motors are derated by 10% as compared to their normal sine-wave excitation. Provision may also have to be made for forced cooling.

12.15 GUIDES FOR SELECTION OF ELECTRICAL MOTORS

Table 12.2 presents the basic guidelines for the selection of the electric motors.

TABLE 12.2
Application of Electric Motor in Electric Drives

S. No	Application	Special Features Required	Type of the Electrical Motor
1	Domestic appliances like sewing machines, mixers, vacuum cleaners	Simple speed control workable on AC and DC supply	Universal motor
2	Domestic refrigerators air conditioners and compressors	Good starting torque	Single phase capacitor motor with D.O.L starter
3	Lift	Smooth uniform acceleration, frequent starts and stops, noiseless running	High torque induction motors
4	Line shafts, load conveyors, and pulp grinders	On-load starting torque required twice the full load torque	High torque induction motors
5	Circular saws, chipper flour mills, rubber mills, crushers, and drives beater without flywheels	High peak load is 062.5 times the rated load with frequent start and stops	High torque induction motors
6	Punch presser, power presses, and drives with flywheels	High peak loads high starting torque	High-slip and high-torque induction motor
7	Centrifugal pumps and fans	Starting with closed value, starting torque 45% of rated	Standard squirrel cage induction motor
8	Cranes and hoists	Heavy starting torque, frequent starts and stops	High-torque induction motor
9	Reciprocating pumps	Starting with the closed values	Slip-ring induction motor
10	Reciprocating compressors	Start with partial load	Slip-ring induction motor
11	Blowers	Start with closed values	Induction motor
12	Hot rolling steel mills	Wide range of speed, automatic control, reversal of direction	Double armature twin drive, variable speed drive with integral control

(Continued)

TABLE 12.2 (Continued)**Application of Electric Motor in Electric Drives**

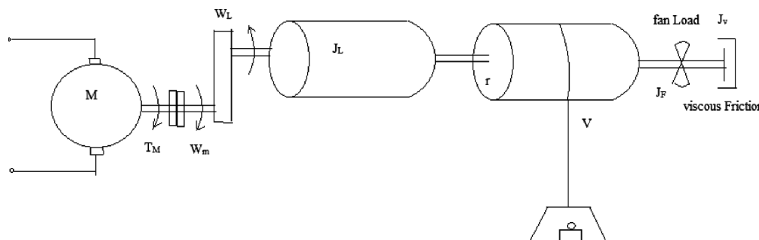
S. No	Application	Special Features Required	Type of the Electrical Motor
13	Reverse cold rolling mills	Armature inertia more than that of rolls, reversible coolers	Coiler motors having two or three armatures
14	Kiln drives	Variable speed	Twin motor drive
15	Crusher drives	Starting 1.6 times the rated torque, withstand fan due to big boulders	Totally enclosed fan cooled
16	Spinning motors	High starting torque, smooth accelerator	4/6 or 6/8 pole motors
17	Loom motors card motors	High starting torque frequent starts and stops	Totally enclosed fan cooled
18	Paper machine drive	Adjustable steel 10:1	Separately excited DC motor, solid-state drives
19	Small ships	Medium power	DC or slip-ring induction motor
20	Large ships	Large power	Synchronous or slip-ring motors
21	Numerical-controlled machines	Fast response, reverse duty cycle, low vibrations	Brush less DC drives, inverter-fed induction motors
22	Traction motors	High starting torque at high speed, good speed control	DC reverse motor, thyristor DC motors

12.16 SOLVED PROBLEMS

Example 12.1: A drive system is shown in Figure 12.16. It consists of a drive motor, a single gear system, an inertia torque hoist load, viscous friction, and a fan load. Calculate the equivalent moment of inertia referred to the motor. Hence, or otherwise, write the equation of motion of the drive system.

SOLUTION

To obtain the values referred to the shaft of the motor, the law of conservation of energy is employed. The equivalent values are denoted by primes.

**FIGURE 12.16** Drive system for Example 12.1.

Inertia torque: equating kinetic energy to obtain

$$(J_L W_L^2) / 2 = (J_L' W_M^2) / 2$$

$$\text{or } J_L' = J_L (W_L / W_M)^2$$

Hoist load: kinetic energy stored by the weight W moving at a speed of v m/s will be $Wv^2/2$ g

$$\text{This will give } J_{LH} = (w/g)(v/w_L)^2$$

In terms of equivalent value, it will be

$$J_{LH}' = J_{LH} (W_L / W_M)^2 = (w/g)(v/w_M)^2$$

It will also produce a constant load torque of $TLH = Wr$

From load: equivalent moment of inertia of fan load and viscous friction is $J_f + J_v$. It is referred to the motor shaft and will be $= (J_f + J_v) \left(\frac{wl}{Wm} \right)^2$

The torque produced by the fan load and viscous friction will be proportional to the speed² and speed, respectively. These values will be $K_1 W_l^2$, and $K_2 W_l$, respectively.

Equivalent torque will be

$$T_f' = T_f \left(\frac{wl}{Wm} \right) = K_1 \left(\frac{wl}{Wm} \right)^2 Wm^2$$

and due to the viscous friction will be

$$T_v' = T_v \left(\frac{wl}{Wm} \right) = K_2 \left(\frac{wl}{Wm} \right)^2 Wm^2$$

If there is dry friction also, it will be a constant load torque of magnitude T_d if it will give an equivalent torque as

$T_d' = \left(\frac{wl}{Wm} \right)$. In combining all these, the equivalent moment of inertia referred to the shaft of the motor will be

$$J_{eq} = J_1 \left(\frac{wl}{Wm} \right)^2 + \frac{W}{g} \left(\frac{v}{Wm} \right)^2 + (J_f + J_v) \left(\frac{wl}{Wm} \right)^2$$

When $\frac{wl}{Wm} = G$, the gear ratio, the equation of the motor will be

$$T_m = J_1 G^2 + \frac{W}{g} \left(\frac{v}{Wm} \right)^2 W r G + T_d G + K_1 G^2 W_m^2 + K_2 G^2 W_m$$

Example 12.2: The retardation test performed on an electrical motor has the following values at 600 rpm: power $P = 2000 \text{ W}$, $\frac{dN}{dt} = 6 \text{ rpm/s}$. Calculate the value of the moment of inertia of the motor.

SOLUTION

$$\text{Moment of inertia } J = \frac{P \cdot 3600}{4\pi^2 N \frac{dN}{dt}}$$

$$J = \frac{2000 \times 3600}{4\pi^2 \times 600 \times 10}$$

$$30.4 \text{ kg}\cdot\text{m}^2$$

Example 12.3: The enclosure of a 10-kW motor has a cooling surface area of 2.2 m^2 . The weight of the motor is 500 kg. It has specific heat of the motor is 500 kg and emissivity of $12 \text{ W/m}^2/\text{k}$. While running on a full load, the motor generates a loss of 1 kW. Calculate the value of the heating time constant and the final rise in temperature of the motor.

SOLUTION

$$\text{Heating time constant } T_h = \frac{Gh}{se} = \frac{500 \times 700}{2 \cdot 2 \times 12} = 132578 = 3.68 \text{ hours}$$

$$\text{Final temperature rise } = \frac{W}{Se} = \frac{1000}{2 \cdot 2 \times 12} = 37.9^\circ\text{C}$$

Example 12.4: A 25-kW motor is running continuously for 10 min on, followed by 2 min off. Calculate the value of its equivalent rating.

SOLUTION

$$P_{eq} = 25 \sqrt{\frac{10}{10+2}} \\ = 22.8 \text{ KW}$$

REVIEW QUESTIONS

- 12.1 Describe the significance of electrical drives in modern industrial undertaking.
- 12.2 Explain the basic concepts of an electrical drive system.
- 12.3 State the advantages of an electrical drive over other available forms of drives.
- 12.4 Give an overview of electrical motors that are suitable to be used in a drive system.

- 12.5 Discuss with examples the classification of electrical drive.
- 12.6 Describe two types of load torques connected to electrical motors in drive systems.
- 12.7 Explain with hoist load, the four-quadrant operation of an electrical drive.
- 12.8 Distinguish between constant torque drive and constant power drive. Draw the characteristics of each drive.
- 12.9 Distinguish between the friction torque, fan-type load, and constant power load. Draw then T-W characteristics
- 12.10 How do the weights of the rope affect the torque in hoisting loads?
- 12.11 Explain some load torque that varies with time.
- 12.12 A motor is driving through a gear the following loads: inertia load, fan load, and viscous friction load. Obtain the equation of motion of this drive system.
- 12.13 With the help of a sketch, describe various forces acting in the crankshaft mechanism. Derive its equation of motion.
- 12.14 How is a retardation test performed to determine the moment of inertia of motion?
- 12.15 Determine the moment of inertia of a drive system.
- 12.16 Discuss the factors that determine the rating of the motor in an electrical drive system.
- 12.17 Discuss the heating effect in electrical motor.
- 12.18 Draw and explain the heating and cooling curve of an electrical machine. Hence, determine the value of heating and cooling time constants.
- 12.19 Explain the criteria commonly used to select an electrical motor for a drive system.

UNSOLVED PROBLEMS

- 12.1 A 100-ton train moves on a curvature of 1,000 m. Calculate the value of tractive force required to overcome this curve resistance.
- 12.2 A 10-kg weight is moving up with a speed of 10 m/s. It is driven by a motor of rotational speed 5.6 rad/s. Calculate the value of its equivalent inertia.
- 12.3 The linear torque speed characteristics of a drive motor is $T_m = 3w + 6$ driving a fan load of torque $T_L = 2w^2 + 4$. Calculate
 1. The value of its equilibrium speed. Comment upon the stability of this speed.
 2. The value of the speed at which it will give maximum acceleration and the value of this maximum acceleration
- 12.4 The cooling surface of a 12.5-kW motor is cylindrical type of length 1.2 m and diameter 800 mm. The weight of the motor is 600 kg. It has the specific heat of 700 J/kg/°C and emissivity of 12 W/m²/°C. It has a full-load efficiency of 90%. Calculate the value of the heating time constant and time temperature rise.

- 12.5 The linear torque-speed characteristics of a drive motor can be described as $T_m = A_w + B$. It drives a load having parabolic characteristics as $T_l = Cw^2 + D$. A , B , C , and D are all position constants, and the total inertia of the drive is J .
1. For the drive system to start, obtain the relation between the A , B , C , and D position constant.
 2. Calculate the value of speed at which the drive operates in equilibrium.
 3. When the drive is running at speed obtained in 2, will the drive be stable?
 4. Calculate the value of initial acceleration of the drive when $A = 3$, $B = 6$, $C = 2$, $D = 4$, and $J = 1$.
 5. Calculate the value of maximum acceleration of the drive when $A = 3$, $B = 6$, $C = 2$, $D = 4$, and $J = 1$.

SUMMARY

This chapter deals with the basic concepts of the electric drive. Each component of the electric drive is explained. Emphasis is also given on the load component, which is a deciding factor to select a suitable rating for the electric drive. For understanding of the complete chapter, some solved and unsolved problems are given at the end of this chapter.

REFERENCES

1. B. K. Bose, *Power Electronics and AC drives*, Prentice Hall, Englewood Cliffs, NJ, 1986.
2. M. H. Rashid, *Power Electronics: Circuits, Devices, and Applications*, Pearson Education, Singapore, 2004.
3. N. Mohan, T. M. Undeland, and W. P. Robbins, *Power Electronics: Converters, Applications and Design*, John Wiley & Sons, Hoboken, NJ, 1996.
4. P. T. Krein, *Elements of Power Electronics*, Oxford University Press, New York, 2003.
5. K. Thorborg, *Power Electronics*. Prentice Hall International, London, UK, 1988.
6. P.S. Bhimra, *Power Electronics*, 5th edn, Khanna Publications, New Delhi, India, 2012.
7. I. Batarseh, and A. Harb, *Power Electronics*, Springer Nature, Cham, Switzerland, 2018.
8. G. K. Dubey, *Fundamentals of Electrical Drives*, Alpha Science International Limited, Pangbourne, UK, 2001.
9. Robert W. Erickson, *Fundamentals of Power Electronics*, Springer, New York, 2001.
10. B. Wu, and Bin Wu, *High-Power Converters and AC Drives*, John Wiley & Sons, Hoboken, NJ, 2017.
11. V. R. Moorthi, *Power Electronics Devices, Circuits and Industrial Applications*, Oxford University Press, Oxford, UK, 2010.
12. T. Suntio, T. Messo, and J. Puukko, *Power Electronic Converters*, Wiley-VCH, Verlag GmbH, Weinheim, Germany, 2018.
13. A. M. Trzynadlowski, *Introduction to Modern Power Electronics*, 3rd edn, John Wiley & Sons, New York, 2010.

14. M. Trzynadlowski, *Power Electronic Converters and Systems*, Institution of Engineering and Technology, London, UK, 2016.
15. B. M. Wilamowski, and J. D. Irwin, *Power Electronics and Motor Drives*, CRC Press, Boca Raton, FL, 2011.
16. E. Acha, V. G. Agelidis, O. Anaya-Lara, and T. J. E. Miller, *Power Electronic Control in Electrical Systems*, Oxford, UK, 2002.
17. F. Mazda, *Power Electronics Handbook*, Oxford, UK, 1997.
18. F. Blaabjerg, *Control of Power Electronic Converters and Systems*, Academic Publishers, London, UK, 2018.
19. S. N. Manias, *Power Electronics and Motor Drive Systems*, Academic Publishers, London, UK, 2017.

13 Control of DC Motor Drives

13.1 INTRODUCTION

The electric drive is a system used for motion control. [Figure 13.1](#) shows the block diagram of an electric drive. It has three main parts:

1. *Electric Motors*: It may be DC motors, such as shunt, series, compound, and permanent magnet; induction motors, such as squirrel cage, wound rotor; synchronous motors, brushless DC motors, stepper motors, or switched-reluctance motors.
2. *Power modulators*: These modulate the electrical energy of the source as per the requirement of the motor used, such as:
 - *For DC drive*—rectifier ($AC \rightarrow DC$) or chopper ($DC \rightarrow DC$) may be used as power modulators.
 - *For AC drive*—inverter ($DC \rightarrow AC$), cycloconverter ($AC \rightarrow DC$), AC voltage controller ($AC \rightarrow AC$) may be used as power modulators.
3. *Load*: It is machinery designed to perform a given task, such as fans, pumps, robots, washing machines, and trains.

Example of electric drive: Single-phase induction motor drives like ceiling fans. It has a single-phase induction motor as the electric motor, voltage regulator as the power modulator, and blades as the agency converting mechanical energy into wind/air.

In the past, DC drives found their applications for the speed and position control only, but nowadays these drives are also in use, which require a low initial cost with excellent performance [[1–5,10](#)].

13.2 BASICS OF DC MACHINES

The basic DC machine equations are:

$$V_a = E + I_a R_a \quad (13.1)$$

$$E = K_a \phi \omega_m \quad (13.2)$$

$$T = K_a \phi I_a \quad (13.3)$$

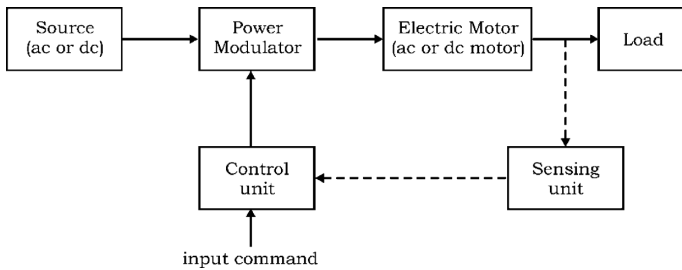


FIGURE 13.1 Block diagram of an electric drive.

From Equations (13.1) and (13.2):

$$\omega_m = \frac{E}{K_a\phi} = \frac{V_a}{K_a\phi} - \frac{I_a R_a}{K_a\phi} \quad (13.4)$$

Substituting the value of armature current I_a from Equation (13.3) in Equation (13.4), we get:

$$\boxed{\omega_m = \frac{V_a}{K_a\phi} - \frac{TR_a}{(K_a\phi)^2}} \quad (13.5)$$

where:

V_a is the armature DC input supply

E is the back emf

I_a is the armature current

R_a is the armature resistance

ϕ is the field flux per pole

ω_m is the speed of DC motor in rad/s

K_a is the motor constant

T is the motor torque in N/m

13.2.1 SHUNT AND SEPARATELY EXCITED DC MOTORS

The power circuit diagrams of separately excited and shunt DC motors are shown in [Figure 13.2a](#) and [b](#). In both motors, the flux can be assumed constant if field current is constant, that is, the armature supply voltage (in case of shunt motor) and field supply voltage (in case of separately excited) are kept constant.

Let,

$$K_a\phi = K \text{ (constant)} \quad (13.6)$$

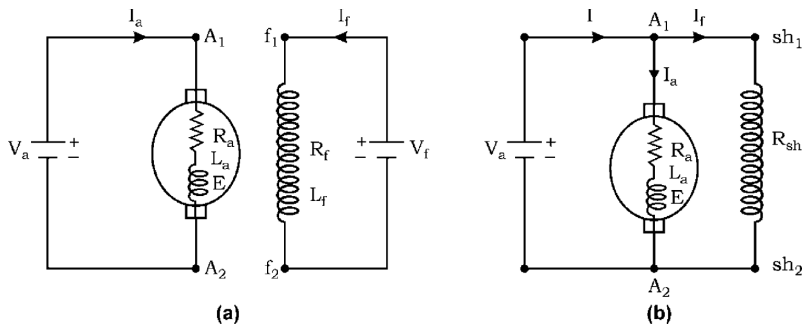


FIGURE 13.2 Power circuit diagrams: (a) separately excited DC motor and (b) DC shunt motor.

Then, from Equations (13.2) to (13.6), we can write:

$$T = K I_a \quad (13.7)$$

$$E = K \omega_m \quad (13.8)$$

$$\omega_m = \frac{V_a}{K} - \frac{R_a T}{K^2} \quad (13.9)$$

From the preceding equations, the speed-torque and torque-current characteristics of both the motors can be drawn, as shown in [Figure 13.3](#).

13.2.2 DC SERIES MOTOR

In the DC series motor, the flux is a function of armature current. It can be assumed that ϕ is proportional to I_a . Therefore,

$$\phi = K_f I_a \quad (13.10)$$

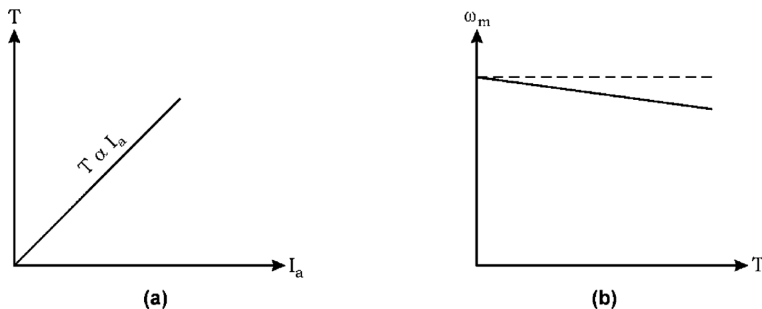


FIGURE 13.3 Various characteristics of separately excited and shunt DC motor: (a) torque-current curve and (b) speed-torque curves.

Also,

$$V_a = E + I_a (R_a + R_{se}) \quad (13.11)$$

Substituting the preceding Equations in Equations (13.12) to (13.15), we get:

$$E = K_a K_f I_a \omega_m \dots \quad (13.12)$$

$$T = K_a K_f I_a^2 \quad (13.13)$$

$$\omega_m = \frac{V_a}{K} - \frac{R_a T}{K^2} \quad (13.14)$$

or

$$\omega_m = \frac{V_a}{\sqrt{-K_a K_f}} \frac{1}{\sqrt{T}} - \frac{(R_a + R_{se})}{K_a K_f} \quad (13.15)$$

From the preceding equations, the torque-current and speed-torque characteristics of the DC series motor can be drawn, as shown in [Figure 13.4](#).

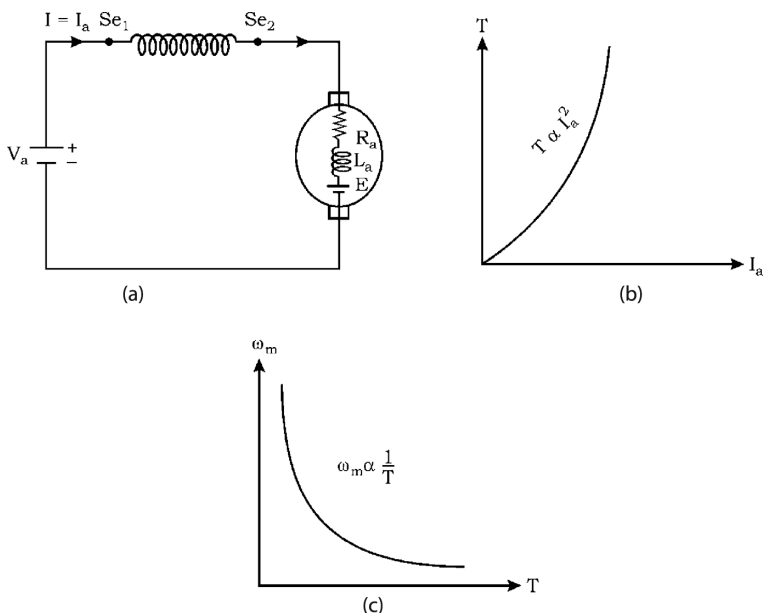


FIGURE 13.4 DC series motor: (a) Power circuit diagram, (b) torque-current curve, and (c) speed torque curve.

13.3 EFFECT OF CHANGE IN SUPPLY VOLTAGE ON CHARACTERISTICS OF DC MOTORS

When a sudden change in supply voltage occurs, it is assumed that instantaneously the motor speed does not change because of mechanical inertia of the drive and that the magnetic field flux remains unchanged due to electromagnetic inertia [1–3,10]. So, the armature current $I_a = V/R_a - E/R_a$ due to DC change depends upon the change in E .

13.3.1 SEPARATELY EXCITED DC MOTOR

In the case of a separately excited DC motor, the field flux remains constant. Let the voltage changes from V to $V + \Delta V$ and current changes from I_a to $I_a + \Delta I_a$, so

$$I_a + \Delta I_a = \frac{V + \Delta V - E}{R_a}$$

$$\frac{\Delta I_a}{I_a} = \frac{\Delta V}{I_a R_a} = \frac{\Delta V}{V - E}$$

13.3.2 DC SERIES MOTOR

When the supply voltage V increases to $+ \Delta V$, the armature current increases, and this will increase the series field winding current and thereby the series field flux increases. This will cause voltage E to change to $E + \Delta E$. So, the armature current will be again brought to the initial value. Therefore, the DC series motor is less sensitive to sudden change in supply voltage.

13.4 EFFECT OF CHANGE IN LOAD TORQUE

In the case of the separately excited and DC shunt motor, the field flux is fairly constant, so the torque is directly proportional to the armature current. When the load torque changes, there should be a corresponding change in the magnitude of the armature current.

In the case of the DC series motor, the torque equation is

$$T = Kt\phi I_a$$

Differentiating it gives $dT = Kt(\phi dI_a + I_a d\phi)$

Dividing it by $T = Kt\phi I_a$ to get

$$\frac{dT}{T} = \frac{dI_a}{I_a} + \frac{d\phi}{\phi}$$

For a small deviation, this equation will be

$$\Delta T / T = \frac{\Delta I_a}{I_a} + \frac{\Delta \phi}{\phi}$$

In the DC series motors considering small changes $\frac{\Delta I_a}{I_a} = \frac{\Delta \varphi}{\varphi}$

$$\text{so } \frac{\Delta I_a}{I_a} = \Delta T / (2 \times T)$$

So, when load torque changes by 2%, the current changes by 1% while in short motors $\Delta \varphi = 0$, so

$$\frac{\Delta I_a}{I_a} = \Delta T / T$$

This shows that the changes in current in case of DC shunt motor are more as compared to dc series motor.

13.5 SPEED CONTROL OF DC MOTORS

We know that expression for speed of the DC motor is given by Equation (13.5); therefore, according to preceding equation, speed can be controlled by controlling three variables: armature voltage, field flux, and armature resistance. So, there are three methods of speed control [10]:

1. Armature voltage control
2. Field flux control
3. Armature resistance control

The armature voltage control method is usually preferred because of its high efficiency with good transient response and excellent speed regulation. But it has the demerit that it can provide speed control only below the base or rated speed because armature voltage can't be allowed to exceed the rated value. On the other hand, the field-flux control method is used to control the speeds above the base speed.

In armature resistance control, speed is varied by wasting power in form of heat across armature resistance and the external resistors, so it is a highly inefficient method to control the speed of the DC motor, and therefore rarely used for intermittent load applications. Variable armature DC voltage for speed control can be obtained by phase-controlled rectifiers if the supply is AC and by chopper control if the supply is DC.

13.6 PHASE-CONTROLLED RECTIFIER CONTROL OF DC MOTOR

Phase-controlled rectifiers are used to get variable DC voltage from an AC source of fixed voltage. Controlled rectifier-fed DC drives can be operated in I and IV quadrants, that is, the forward motoring and regenerative braking operation can be achieved. It is because thyristors are capable of conducting current only in one direction (being unidirectional devices). All full converters (or fully controlled) provide I- and IV-quadrant operations, whereas semiconverters (or half controlled) provide only I-quadrant operation.

13.6.1 SINGLE-PHASE FULLY CONTROLLED RECTIFIER CONTROL OF DC SEPARATELY EXCITED MOTOR DRIVE

The power circuit diagram for this drive is shown in Figure 13.5a. When field control is required, then field winding is energized from a controlled rectifier; otherwise, an uncontrolled rectifier is generally used. In a cycle of AC source voltage, T_1, T_2 are triggered at α and T_3, T_4 at $(\pi + \alpha)$. Motor terminal voltage V_a and current I_a waveforms for continuous and discontinuous conduction modes are shown in Figure 13.5b and c, respectively.

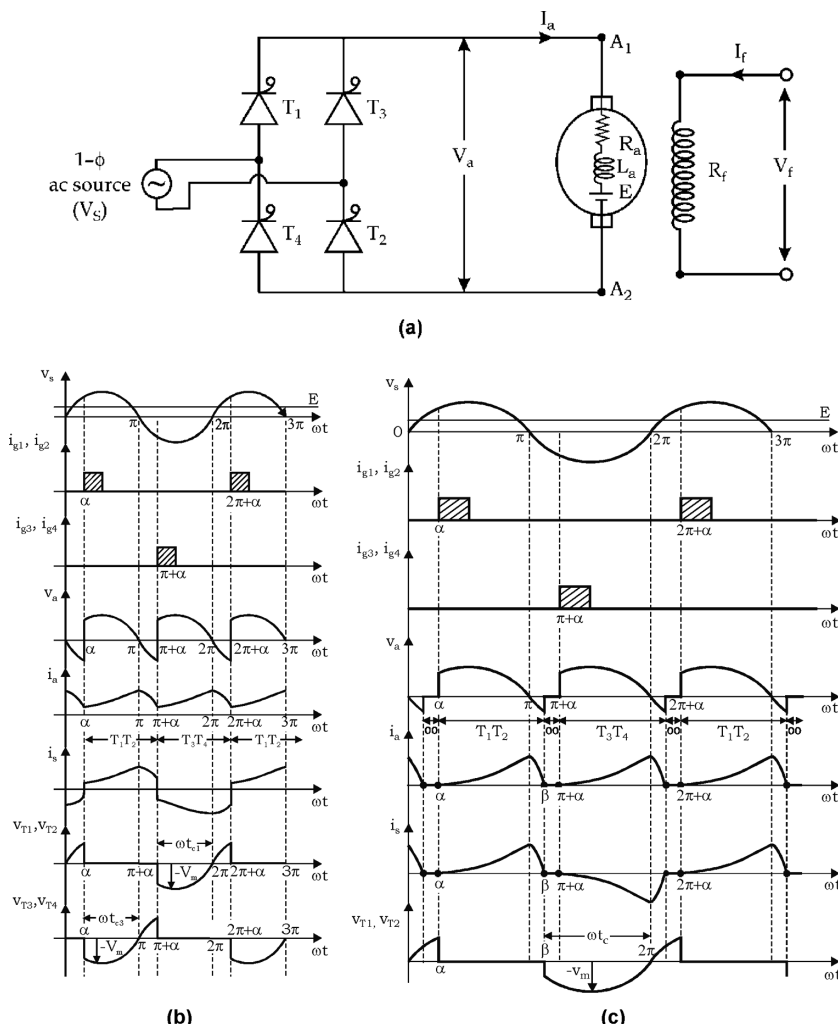


FIGURE 13.5 Single-phase fully-controlled rectifier-fed DC separately excited motor drive:
(a) power circuit diagram, and (c) discontinuous conduction.

From the voltage waveform of [Figure 13.5b](#), the average motor terminal voltage V_a , which is the input to the armature, can be derived as:

$$\begin{aligned} V_a &= \frac{1 \times 2}{2\pi} \int_{\alpha}^{\pi+\alpha} V_m \sin \omega t \, d\omega t \\ &= \frac{V_m}{\pi} [-\cos \omega t]_{\alpha}^{\pi+\alpha} \end{aligned}$$

or

$$V_a = \frac{2V_m}{\pi} \cos \alpha \quad (13.16)$$

If

$$\alpha = 0^\circ, \quad V_a = \frac{+2V_m}{\pi}$$

$$\alpha = 90^\circ, \quad V_a = 0$$

$$\alpha = 180^\circ, \quad V_a = \frac{-2V_m}{\pi}$$

So, it can be seen that by varying the firing angle α from 0° to 180° , polarity of voltage V_a can be changed. Therefore, such a drive can be operated in I and IV quadrants, that is, forward motoring (Quadrant I) and regenerative braking (Quadrant IV) operation can be achieved, as shown in [Figure 13.6a](#). It is also called a *two-quadrant drive*.

Substituting the value of V_a from Equation (13.16) in Equation (13.9), we get:

$$\omega_m = \frac{(2V_m / \pi)}{K} \cos \alpha - \frac{TR_a}{K^2} \quad (13.17)$$

From Equation (13.17), the speed-torque characteristic of the single-phase-controlled rectifier-fed separately excited DC motor can be drawn as shown in [Figure 13.6b](#) [1–3,6,10].

For discontinuous conduction, we substitute voltage V_a as:

$$V_a = \frac{V_m (\cos \alpha - \cos \beta) + (\pi + \alpha - \beta) E}{\pi} \quad (13.18)$$

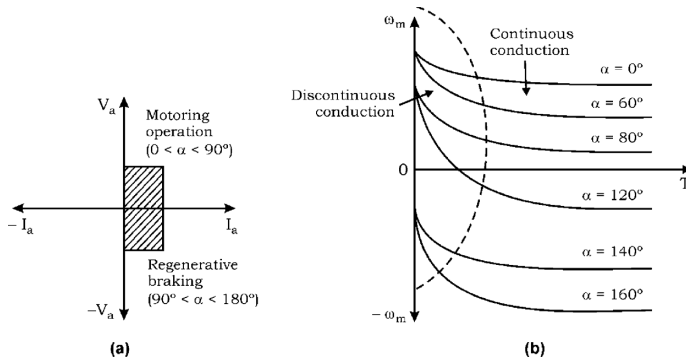


FIGURE 13.6 (a) V_a - I_a plane (quadrant operation) and (b) speed-torque characteristics.

13.6.2 SINGLE-PHASE HALF-CONTROLLED RECTIFIER (OR SEMICONVERTER) CONTROL OF DC SEPARATELY EXCITED MOTOR DRIVE

The power circuit diagram for this drive is shown in Figure 13.7a. In a cycle of AC source voltage, T_1 is triggered at α and T_2 at $(\pi + \alpha)$. Motor terminal voltage (V_a) and armature current (I_a) waveforms for continuous and discontinuous conduction modes are shown in Figure 13.7b and c.

From the voltage waveform of Figure 13.7b and c, the average motor terminal voltage V_a , which is the input to the armature can be derived as:

For continuous conduction,

$$V_a = \frac{1 \times 2}{2\pi} \int_{\alpha}^{\pi} V_m \sin \omega t \cdot d\omega t$$

or

$$\boxed{V_a = \frac{V_m}{\pi} (1 + \cos \alpha)} \quad (13.19)$$

For discontinuous conduction,

$$V_a = \frac{1 \times 2}{2\pi} \left[\int_{\alpha}^{\pi} V_m \sin \omega t \cdot d\omega t + \int_{\beta}^{\pi+\alpha} E \cdot d\omega t \right]$$

or

$$\boxed{V_a = \frac{V_m (1 + \cos \alpha) + (\pi + \alpha - \beta) E}{\pi}} \quad (13.20)$$

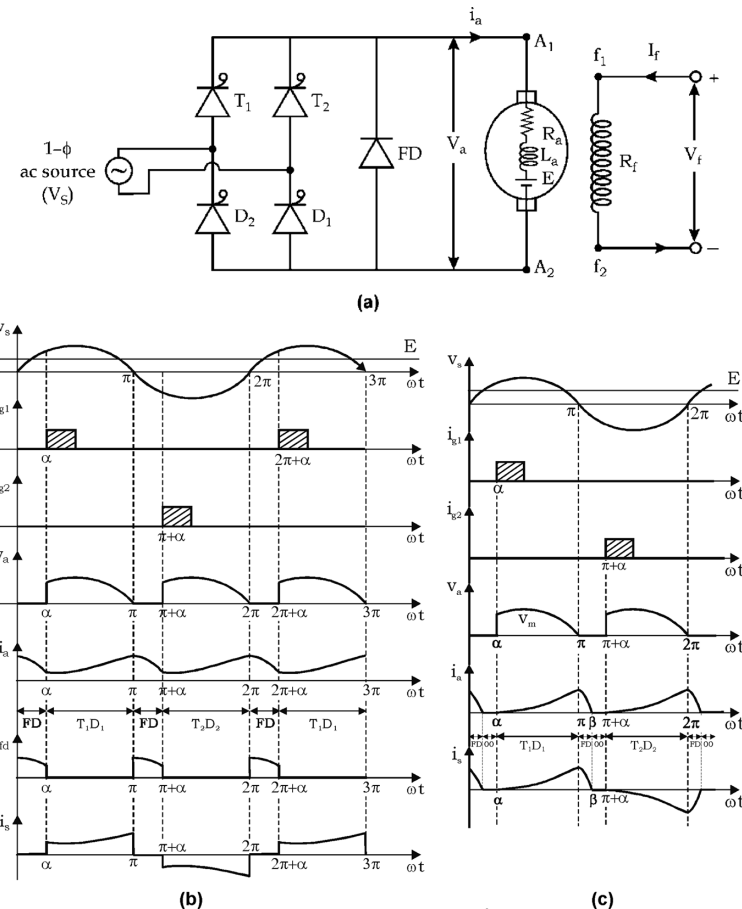


FIGURE 13.7 Single-phase half-controlled rectifier-fed separately excited DC motor:
(a) power circuit diagram, (b) continuous conduction, and (c) discontinuous conduction.

From Equation (13.19), if $\alpha = 0^\circ$, $V_a = \frac{2V_m}{\pi}$

$$\alpha = 90^\circ, \quad V_a = \frac{V_m}{\pi}$$

$$\alpha = 180^\circ, \quad V_a = 0$$

Therefore, it can be seen that by varying the firing angle α from 0° to 180° , the polarity of voltage V_a remains positive only, so resulting into Quadrant I, that is, forward-motoring operation only, as shown in Figure 13.8a.

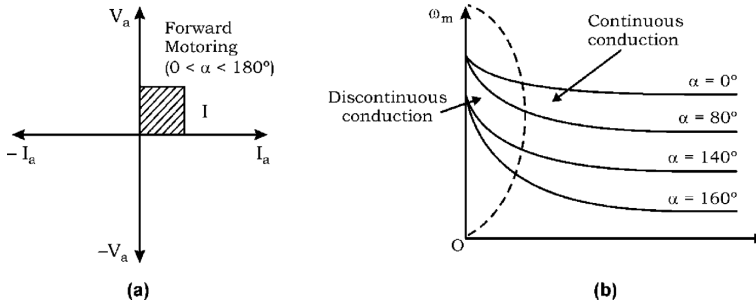


FIGURE 13.8 (a) V_a - I_a plane (quadrant operation) and (b) speed-torque characteristics.

For the separately excited DC motor, substituting the value of voltage V_a from Equation (13.19) in Equation (13.9), we get:

$$\boxed{\omega_m = \frac{V_m}{\pi K} (1 + \cos \alpha) - \frac{TR_a}{K^2}} \quad (13.21)$$

From Equation (13.21), the speed-torque characteristics of the single-phase half-controlled rectifier-fed separately excited DC motor can be drawn as shown in Figure 13.8b. Therefore, it can be seen that this drive operates in Quadrant I only, giving forward-motoring operation. So it is also called as a *single-quadrant drive*.

13.6.3 THREE-PHASE FULLY CONTROLLED RECTIFIER CONTROL OF DC SEPARATELY EXCITED MOTOR DRIVE

Power circuit diagram of three-phase fully controlled rectifier-fed separately excited DC motor drive is shown in Figure 13.9.

Thyristors are fired in the sequence of their numbers after every 60° , and each thyristor conducts for 120° . At a time, two thyristors conduct, that is, one from the upper group (1, 3, 5) and the other from the lower group (2, 4, 6).

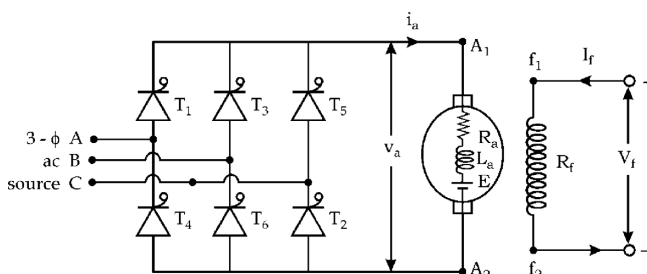


FIGURE 13.9 Power circuit diagram of three-phase fully controlled rectifier-fed separately excited DC motor drive.

In three-phase rectifier-fed drives, the discontinuous conduction occurs in a very narrow region due to its operation at higher ripple frequency, which can be ignored.

The average motor terminal voltage V_a can be derived as:

$$V_a = \frac{1 \times 6}{2\pi} \int_{\left(\frac{\pi}{3} + \alpha\right)}^{\left(\frac{2\pi}{3} + \alpha\right)} V_m \sin \omega t \cdot d\omega t$$

or

$$V_a = \frac{3V_m}{\pi} \cos \alpha \quad (13.22)$$

From Equation (13.22), if

$$\alpha = 0^\circ, \quad V_a = \frac{+3V_m}{\pi}$$

$$\alpha = 180^\circ, \quad V_a = \frac{-3V_m}{\pi}$$

$$\alpha = 90^\circ, \quad V_a = 0$$

So, it can be seen that by varying the firing angle α from 0° to 180° , the polarity of motor terminal voltage V_a can be reversed. Therefore, this drive operates in Quadrant I (forward motoring) and Quadrant IV (regenerative braking), as shown in Figure 13.10a. It is also called a *two-quadrant drive*.

For the DC separately excited motor, we knew that:

$$\omega_m = \frac{V_a}{K} - \frac{TR_a}{K^2}$$

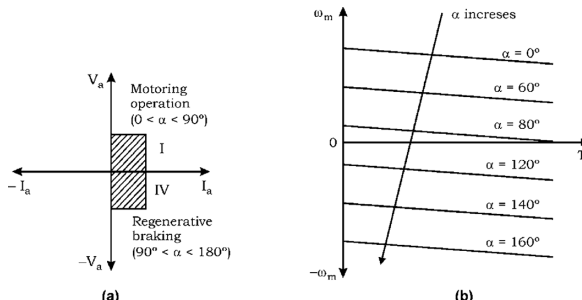


FIGURE 13.10 Three-phase fully controlled rectifier-fed separately excited DC motor drive: (a) $V_a - I_a$ plane and (b) speed-torque characteristics.

Substituting the value of voltage V_a from Equation (13.22), we get:

$$\boxed{\omega_m = \frac{(3V_m / \pi)}{K} \cos \alpha - \frac{TR_a}{K^2}} \quad (13.23)$$

From preceding equation, speed-torque curves for the three-phase fully controlled rectifier-fed separately excited DC motor drive can be drawn, as shown in Figure 13.10b.

13.6.4 THREE-PHASE HALF-CONTROLLED RECTIFIER CONTROL OF SEPARATELY EXCITED DC MOTOR

The power circuit diagram for the three-phase half-controlled or semiconverter-fed separately excited DC motor is shown in Figure 13.11a.

The motor terminal voltage for this drive under continuous conduction is given by:

$$V_a = \frac{3V_m}{2\pi} (1 + \cos \alpha) \quad (13.24)$$

For the DC separately excited motor,

$$\omega_m = \frac{V_a}{K} - \frac{TR_a}{K^2}$$

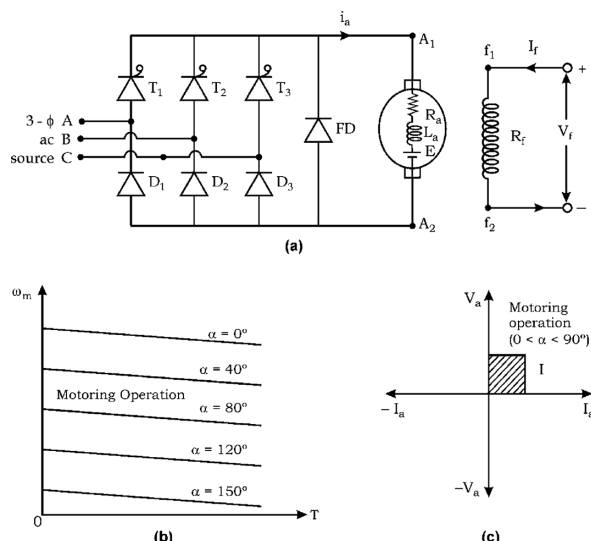


FIGURE 13.11 Three-phase half-controlled rectifier-fed of separately excited DC motor drive: (a) power circuit diagram, (b) V_a – I_a plane, and (c) speed-torque characteristics.

Substituting the value of voltage V_a from Equation (13.24), we get:

$$\omega_m = \frac{3V_m}{2\pi K} (1 + \cos \alpha) - \frac{TR_a}{K^2} \quad (13.25)$$

Using the preceding equation, speed-torque curves for the 3- ϕ half-controlled rectifier-fed separately excited DC motor can be drawn, as shown in Figure 13.11b. It can be seen that this drive operates only in Quadrant I, that is, speed control during the forward-motoring operation can be achieved by varying the firing angle from 0° to 180° , as shown in Figure 13.11c [1–3,6,10].

13.7 CHOPPER CONTROL OF DC MOTOR

Choppers are used to get variable DC voltage from a DC source of fixed voltage. Self-commutated devices such as metal-oxide semiconductor field-effect transistors (MOSFETs), insulated-gate bipolar transistors (IGBTs), and gate turn-offs (GTOs) are preferred over thyristors for building choppers because they can be turned off by a small control signal and do not require an extra commutation circuit [1–19]. Also, they can be operated at a higher frequency, which results in a reduction in the ripple current and elimination of discontinuous conduction.

Using chopper control, DC motors can be operated in any of the four quadrants or their combinations, which is not possible in the case of phase-controlled rectifier control.

13.7.1 CHOPPER CONTROL OF SEPARATELY EXCITED DC MOTORS

Only Motoring Operation: A power circuit diagram of a chopper-controlled separately excited DC motor during only the motoring operation (Quadrant I) is shown in Figure 13.12a.

Chopper (Class A) is operated periodically with period T and remains on for a duration T_{on} . When the chopper is on, motor terminal voltage (V_a) becomes V_s , and when the chopper is off, voltage V_a becomes zero, as shown in Figure 13.12b.

From the waveforms of motor terminal voltage (V_a) and current (I_a), it can be seen that both V_a and I_a are positive in direction, resulting in Quadrant-I operation (forward motoring), as shown in Figure 13.12c.

From the voltage waveform of Figure 13.12b, the average motor-terminal voltage (V_a) can be derived as:

$$V_a = \frac{1}{T} \int_0^{T_{on}} V_s dt = \delta V_s \quad (13.26)$$

where δ is called duty ratio or duty cycle and

$$\delta = \frac{T_{on}}{T} \quad (13.27)$$

For the separately excited DC motor, we knew that:

$$V_a = E + I_a R_a$$

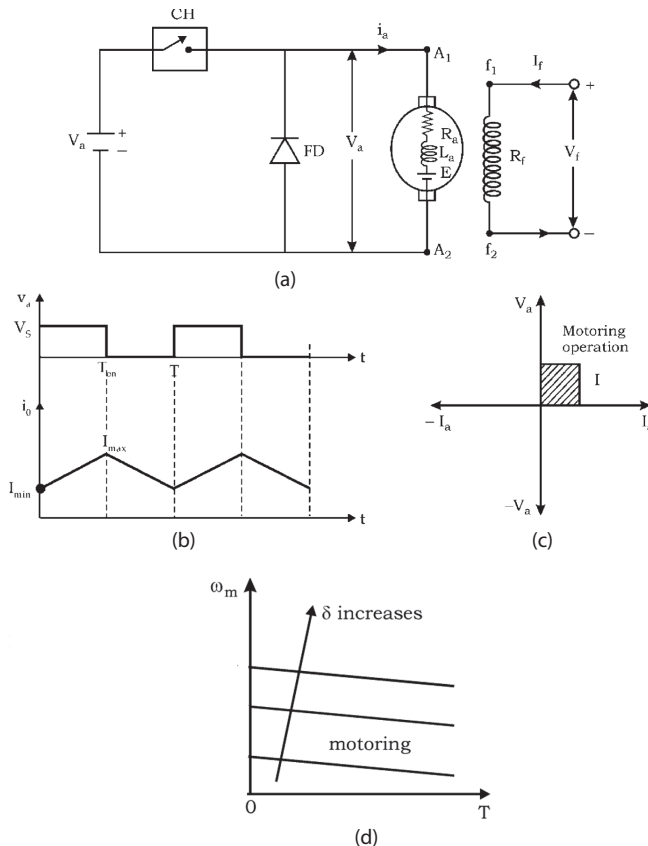


FIGURE 13.12 Only motoring control of separately excited motor using a chopper: (a) power circuit diagram, (b) various waveforms, and (c) V_a - I_a plane, (d) Speed-torque curves during only motoring operation.

or

$$I_a = \frac{V_a - E}{R_a} \quad (13.28)$$

Substituting Equation (13.26) in Equation (13.28), we get

$$I_a = \frac{\delta V_s - E}{R_a} \quad (13.29)$$

$$\text{Also, } \omega_m = \frac{V_a}{K} - \frac{TR_a}{K^2}$$

or

$$\boxed{\omega_m = \frac{\delta V_s}{K} - \frac{TR_a}{K^2}} \quad (13.30)$$

From Equation (13.30), the speed-torque characteristic for chopper control of the separately excited motor during only the motoring operation can be drawn, as shown in [Figure 13.12d](#).

Only Regenerative Braking: The Class B chopper is used to operate the drive in Quadrant II (regenerative braking operation) as shown in [Figure 13.13a](#). The chopper is operated periodically with a period T and on-period of T_{on} . When the chopper is on, motor terminal voltage V_a becomes zero, and when chopper is off, voltage V_a becomes V_s , as shown in [Figure 13.13b](#).

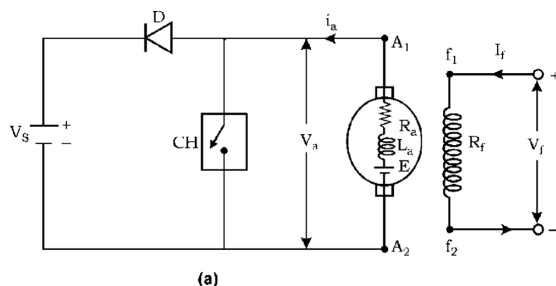
During the off-period of the chopper, stored electromagnetic energy and energy supplied by the machine (now working as generator due to the braking operation) is fed to the source. Therefore, this drive operates in Quadrant II, giving regenerative braking.

Here, the duty cycle

$$\delta = \frac{T - T_{on}}{T} = \frac{T_{off}}{T} \quad (13.31)$$

Average motor terminal voltage V_a is derived as:

$$V_a = \frac{1}{T} \int_{T_{on}}^T V_s dt = \delta V_s \quad (13.32)$$



(a)

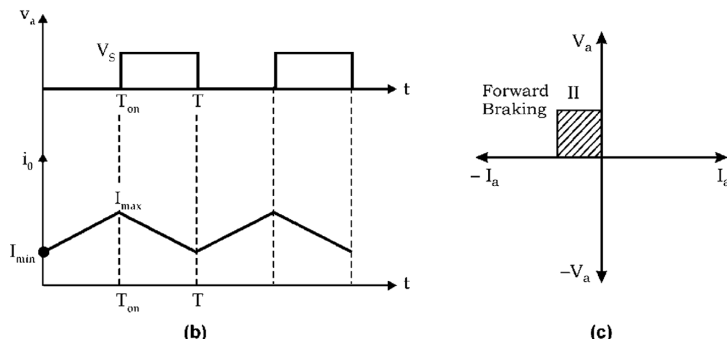


FIGURE 13.13 Only regenerative braking operation of separately excited motor by chopper control: (a) power circuit diagram, (b) various waveforms, and (c) $V_a - I_a$ plane.

Motor armature current I_a :

$$I_a = \frac{E - \delta V_s}{R_a} \quad (13.33)$$

Since I_a has reversed, then

$$T = -KI_a \quad (13.34)$$

$$\omega_m = \frac{\delta V_s}{K} + \frac{TR_a}{K^2} \quad (13.35)$$

Combined Motoring and Regenerative Braking: The Class C chopper can be used to provide combined forward motoring (Quadrant I) and forward regenerative braking (Quadrant II) operations, as shown in Figure 13.14a.

For the motoring operation, Chopper-1 is controlled, and for the braking operation Chopper-2 is controlled. The shifting of control from Chopper-1 to Chopper-2 shifts operation from motoring to braking and vice versa. Motor terminal voltage (v_a) and current (i_a) are shown in Figure 13.14b.

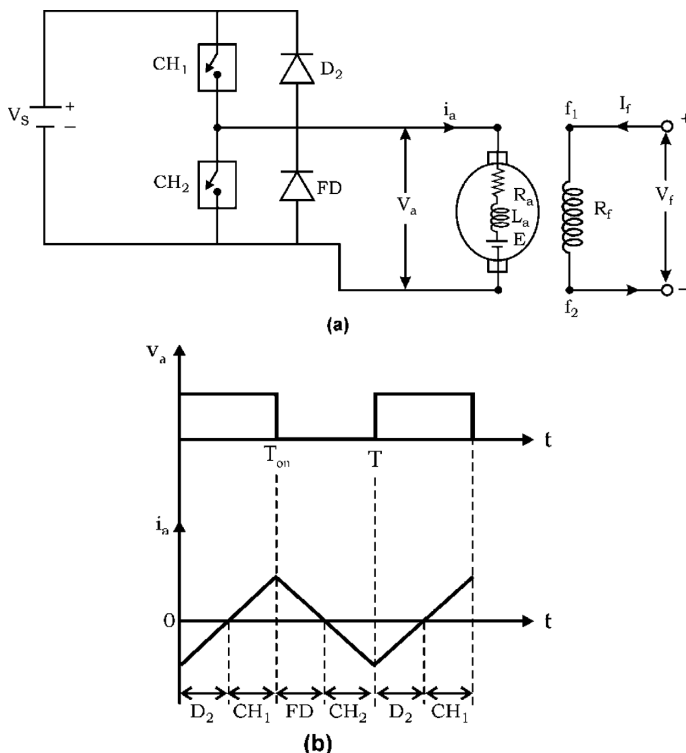


FIGURE 13.14 Combined motoring and braking operation using chopper control: (a) power circuit diagram and (b) various waveforms.

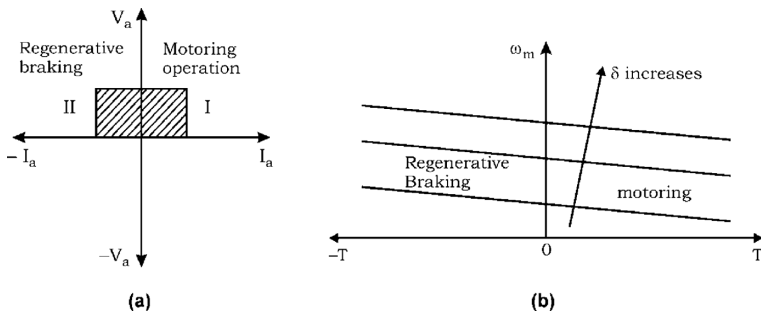


FIGURE 13.15 Combined motoring and braking operation using chopper control: (a) $V_a - I_a$ plane and (b) speed-torque curves.

From motor terminal voltage (v_a) waveform,

$$V_a = \delta V_s \quad (13.36)$$

and

$$I_a = \frac{\delta V_s - E}{R_a} \quad (13.37)$$

For motoring operation, I_a = positive, $\delta > \frac{E}{V_s}$

For regenerative braking operation, I_a = negative, $\delta > \frac{E}{V_s}$

Transition from motoring to braking and vice versa occurs at $\delta = \frac{E}{V_s}$. This drive operates in two quadrants as shown in Figure 13.15a, and the nature of the torque characteristic is shown in Figure 13.15b.

Only dynamic braking: During the off-period of the chopper, energies generated by the machine and stored in inductance L_a are dissipated in braking resistance R_B , R_a and diode D . In this way, the chopper controls the magnitude of energy dissipated in R_B (Figure 13.16).

The energy consumed (E) by the braking resistor during a cycle of chopper operation can be expressed as:

$$E = I_a^2 R_B (T - T_{on}) \quad (13.38)$$

Average power consumed by R_B :

$$P = \frac{E}{T} = I_a^2 R_B (1 - \delta) \quad (13.39)$$

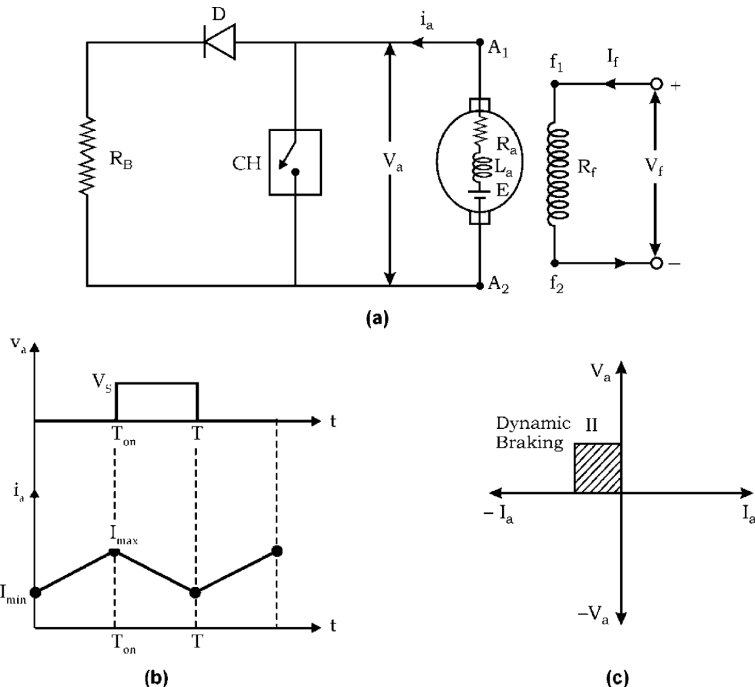


FIGURE 13.16 Dynamic braking of separately excited motor by chopper control: (a) power circuit diagram, (b) various waveforms, and (c) $V_a - I_a$ plane.

\therefore Effective value of R_B :

$$R'_B = \frac{P}{I_a^2} = R_B(1-\delta) \quad (13.40)$$

where

$$\delta = \frac{T_{on}}{T} \quad (13.41)$$

Equation (13.40) shows that the effective value of the braking resistor can be varied steplessly from 0 to R_B by varying the duty cycle (δ) from 1 to 0.

Note: Basic machine equations, characteristics, and analysis during speed control of the DC shunt motor is similar to separately excited DC motor except the circuit diagram of motors.

13.7.2 CHOPPER CONTROL OF DC SERIES MOTOR

Only Motoring Operation: The power circuit diagram for chopper control of the DC series motor for only the motoring operation is shown in Figure 13.17a [1–6,10,12].

Motor terminal voltage (v_a) and current (i_a) waveforms are the same as shown in Figure 13.12b. But here, back emf (e) is not constant; rather, it varies with armature current (i_a). The nature of speed torque curves is shown in Figure 13.17b.

Braking Operation: The power circuit diagram during braking of the DC series motor using chopper control is shown in Figure 13.18a and b. During braking operation, the series motor works as a self-excited series generator. Therefore, to assist residual magnetism, field current should flow in the same direction, that is, from Se_1 terminal to Se_2 terminal as shown.

This is achieved by reversing the field terminals w.r.t. armature when changing from motoring to braking operation. Waveforms of voltage V_a and current I_a are the same as that of Figure 13.13b for regenerative braking and also for dynamic braking (Figure 13.16b). The nature of the speed-torque curve during the braking operation is shown in Figure 13.17b.

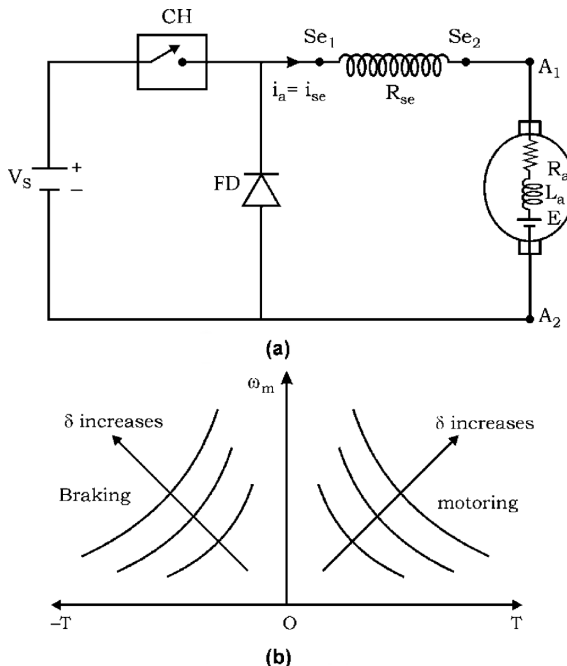


FIGURE 13.17 Chopper control of DC series motor: (a) power circuit diagram and (b) speed-torque curves.

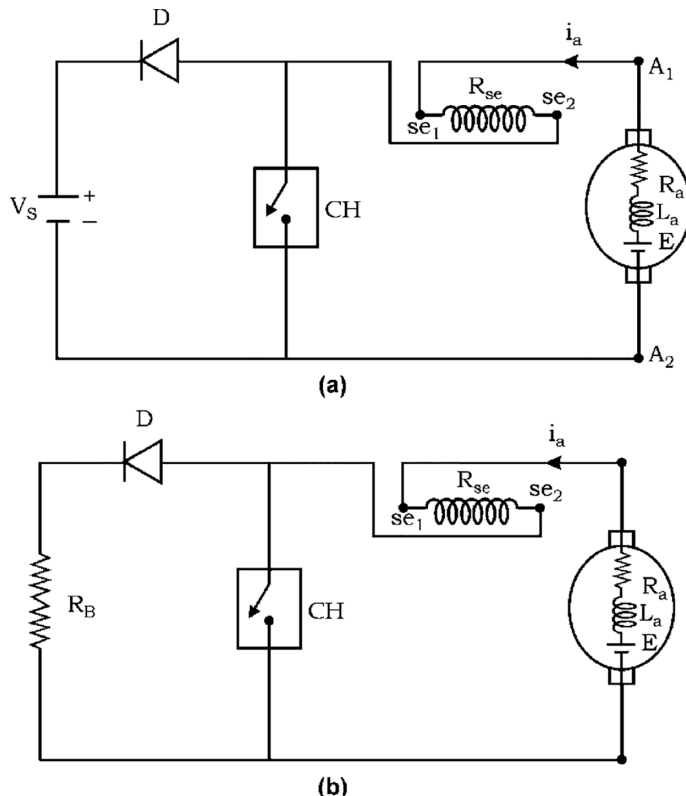


FIGURE 13.18 DC series motor during different braking operations using chopper control: (a) power circuit diagram during regenerative braking and (b) power circuit diagram during dynamic braking.

13.8 SOLVED PROBLEMS

Example 13.1: A 220-V, 500-A, 600-rpm separately excited DC motor has armature and field resistance of 0.02 and 10 Ω, respectively. The load torque is expressed by the expression $T_L = 2000 - 2N$, N-m, where N is the speed in rpm. Calculate the motor terminal voltage and the armature current when the speed is 450 rpm.

SOLUTION

At 450 rpm, $T_L = 2000 - 2 \times 450 = 1100$ N-m

At rated operation $E_1 = 220 - 500 \times 0.02 = 210$ V

$$\text{Rated torque} = \frac{E_1 I_{a1}}{\omega_m 1} = \frac{210 \times 500}{600 \times 2\pi/60} = 1671 \text{ N-m}$$

$$\text{For a torque of } 1100 \text{ N-m, } I_{a2} = \frac{1100}{1671} \times 500 = 329 \text{ A}$$

$$\text{At } 450 \text{ rpm, } E_2 = \frac{450}{600} \times 210 = 157.5$$

$$V = E_2 + I_{a2}R_a = 157.5 + 329 \times 0.02 = 164 \text{ V}$$

Example 13.2: A two-pole separately excited DC motor has the ratings of 220 V, 100 A, and 750 rpm. Resistance of the armature is 0.1 Ω. The motor has two field coils that are normally connected in parallel. It is used to drive a load whose torque is expressed as $T_L = 500 - 0.3 N$, where N is the motor speed in rpm. Calculate the motor armature current and speed when the armature voltage is reduced to 110 V.

SOLUTION

$$\text{At rated operation, } E_1 = 220 - 100 \times 0.1 = 210 \text{ V}$$

$$\omega_{m1} = 750 / 60 \times 2\pi = 250 / 25\pi = 2.674 \text{ rad/s}$$

$$K_e \phi_l = K = 2.674$$

Let the motor speed and current be N_2 and I_{a2} , respectively.

$$E_2 = K\omega_{m2} = 2.674 \times N_2 \times 2\pi / 60 = 0.28N_2$$

$$V = E_2 + I_{a2}R_a$$

or

$$110 = 0.28N_2 + 0.1I_{a2} \quad (13.42)$$

Since $T = T_L$

$$KI_a = 500 - 0.3N$$

or

$$2.67I_{a2} = 500 - 0.3N_2$$

or

$$500 = 0.3N_2 + 2.67I_{a2} \quad (13.43)$$

Simultaneous solution of Equations (13.42) and (13.43) gives

$$I_{a2} = 148.9 \text{ A and } N_2 = 339.7 \text{ rpm}$$

Example 13.3: A 200-V, 875-rpm, 150-A separately excited DC motor that is energized from a single-phase two-quadrant rectifier with an AC source voltage of 220 V and 50 Hz has an armature resistance of 0.06 Ω. Assuming continuous conduction, calculate:

- i. Firing angle for rated motor torque and 750 rpm.
- ii. Firing angle for rated motor torque and (-500) rpm.
- iii. Motor speed for $\alpha = 160^\circ$ and rated torque.

SOLUTION

At rated operation $E = 200 - 150 \times 0.06 = 191 \text{ V}$

- i. E at 750 rpm,

$$E = (700/875) \times 191 = 163.7 \text{ V}$$

$$V_a = E + I_a R_a = 163.7 + (150 \times 0.06) = 172.7 \text{ V}$$

Now $(2V_m/\pi) \cos \alpha = V_a$
or $\cos \alpha = 0.872$ or $\alpha = 29.3^\circ$

- ii. At -500 rpm

$$E = (-500/875) \times 191 = -109 \text{ V}$$

Since $V_a = E + I_a R_a$

$$V_a = -109 + (150 \times 0.06) = -100 \text{ V}$$

Now $(2V_m/\pi) \cos \alpha = V_a$
or $\cos \alpha = -0.5$ or $\alpha = 120^\circ$

- iii. At $\alpha = 160^\circ$

$$V_a = (2V_m/\pi) \cos \alpha = -186 \text{ V}$$

Since $V_a = E + I_a R_a$

$$-186 = E + (150 \times 0.06)$$

or $E = -195 \text{ V}$

$$\text{Speed} = (-195/191) \times 875 = -893.2 \text{ rpm}$$

REVIEW QUESTIONS AND UNSOLVED PROBLEMS

- 13.1 Make a detailed transient analysis of the separately excited motor with armature and field control.
- 13.2 Derive and explain the energy losses during transient operation in detail.
- 13.3 What is load equalization? Explain in detail.

- 13.4 Design and simulate a single-phase fully controlled rectifier-fed DC separately excited motor drive using MATLAB/Simulink, for a motoring and braking operation.
- 13.5 Design and simulate a Class C chopper-fed DC separately excited motor drive using MATLAB/Simulink for a motoring and braking operation.
- 13.6 Explain with circuit diagrams and waveforms types of electrical braking in a DC motor drive.
- 13.7 Explain the two-pulse-controlled rectifier-fed DC separately excited motor drive, along with a circuit diagram and waveforms.
- 13.8 Explain in detail with related circuit diagram and waveforms the dynamic braking of the DC shunt motor drive. Also, list its merit and demerit.
- 13.9 A 230-V, 960-rpm, and 150-A separately excited DC motor has an armature resistance of 0.03 ohms. The motor is fed from a Class C chopper. The source has a voltage of 230 V. Calculate maximum permissible motor speeds obtainable without field weakening and power fed to the source if the maximum duty ratio of the chopper is limited to 0.95, and maximum permissible motor current is twice the rated.
- 13.10 Explain, why Quadrant IV operation is not possible with rectifier control of a DC series motor drive.
- 13.11 A 230-V, 875-rpm, 200-A separately excited DC motor has an armature resistance of 0.03Ω . It is fed from a single-phase half-controlled rectifier with an AC source voltage of 220 V, 50 Hz. Assuming continuous conduction, calculate the firing angle for rated motor torque and 750 rpm.

SUMMARY

The DC motor drives are highly suitable for the servo-drive applications because electromagnetic torque is directly proportional to the field flux and armature current. Also, its speed can be controlled beyond its rated value, without exceeding the input voltage. However, the use of DC motors for control and position applications have been replaced by AC motor drives due to various demerits with the DC motor, such as periodic maintenance, not suitable for all environments.

REFERENCES/FURTHER READING

1. B. K. Bose, *Power Electronics and AC Drives*, Prentice Hall, Englewood Cliffs, NJ, 1986.
2. M. H. Rashid, *Power Electronics: Circuits, Devices, and Applications*, Pearson Education, Singapore, 2004.
3. N. Mohan, T. M. Undeland, and W. P. Robbins, *Power Electronics: Converters, Applications and Design*, John Wiley & Sons, Hoboken, NJ, 1996.
4. P. T. Krein, *Elements of Power Electronics*, Oxford University Press, New York, 2003.
5. K. Thorborg, *Power Electronics*. Prentice Hall International, London, UK, 1988.
6. P. S. Bhimra, *Power Electronics*, 5th ed., Khanna Publications, New Delhi, India, 2012.
7. I. Batarseh, and A. Harb, *Power Electronics*, Springer Nature, Cham, Switzerland, 2018.

8. K. M. Smedley and E. Santi, *AC-DC Power Converters*, Wiley, Hoboken, NJ, 1999.
9. R. W. Erickson, *Fundamentals of Power Electronics*, Springer, New York, 2001.
10. G. K. Dubey, *Fundamentals of Electrical Drives*, Alpha Science International Limited, Pangbourne, UK, 2001.
11. V. R. Moorthi, *Power Electronics Devices, Circuits and Industrial Applications*, Oxford University Press, Oxford, UK, 2010.
12. T. Suntio, T. Messo, and J. Puukko, *Power Electronic Converters*, Wiley-VCH, Verlag GmbH, Weinheim, Germany, 2018.
13. A. M. Trzynadlowski, *Introduction to Modern Power Electronics*, 3rd ed., John Wiley & Sons, Hoboken, NJ, 2010.
14. M. Trzynadlowski, *Power Electronic Converters and Systems*, Institution of Engineering and Technology, London, UK, 2016.
15. B. M. Wilamowski and J. D. Irwin, *Power Electronics and Motor Drives*, CRC Press, Boca Raton, FL, 2011.
16. E. Acha, V. G. Agelidis, O. Anaya-Lara, and T. J. E. Miller, *Power Electronic Control in Electrical Systems*, Newnes, Oxford, UK, 2002.
17. F. Mazda, *Power Electronics Handbook*, Newnes, Oxford, UK, 1997.
18. F. Blaabjerg, *Control of Power Electronic Converters and Systems*, Academic Publishers, London, UK, 2018.
19. S. N. Manias, *Power Electronics and Motor Drive Systems*, Academic Publishers, Amsterdam, the Netherlands, 2017.



Taylor & Francis

Taylor & Francis Group

<http://taylorandfrancis.com>

14 Control of Induction Motor Drives

14.1 INTRODUCTION

Three-phase induction motors are of two types: squirrel cage and wound rotor. In squirrel cage, the rotor consists of longitudinal conductor bars shorted by circular connectors at the two ends. In the wound-rotor motor, the rotor also has a balanced three-phase-distributed winding having the same poles as the stator winding. However, in both, the stator carries a three-phase-balanced distributed winding.

Induction motors have been used in the past mainly in applications requiring a constant speed because conventional methods of their speed control have either been expensive or highly inefficient. Variable-speed applications have been dominated by DC drives. Availability of thyristors, power transistors, and gate turn-offs (GTOs) has allowed the development of variable-speed induction-motor power drives. The main drawback of DC motors is the presence of commutators and brushes, which require frequent maintenance and make them unsuitable for explosive and dirty environments.

On the other hand, induction motors particularly squirrel cage are rugged, cheaper, lighter, smaller, more efficient, require lower maintenance, and can operate in dirty and explosive environments. Although variable-speed induction-motor drives are generally expensive than DC drives, they are used in a number of applications, such as fans, blowers, cranes, conveyance, and traction because of the advantages of induction motors [1–19]. Other dominant applications are underground and underwater installations, and explosive and dirty environments.

14.2 BASICS OF THE INDUCTION MOTOR

The per-phase equivalent circuit of a three-phase induction motor is shown in [Figure 14.1a](#) and shows the stator referred values of rotor resistance R_r and rotor reactance X_r .

Slip is defined by:

$$s = \frac{\omega_{ms} - \omega_m}{\omega_{ms}} \quad (14.1)$$

where ω_m and ω_{ms} are rotor and synchronous speeds, respectively.

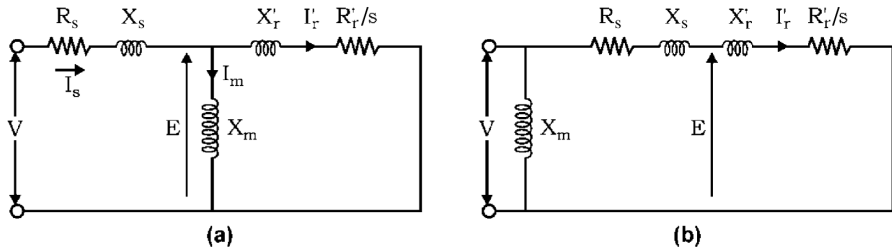


FIGURE 14.1 Per-phase stator referred equivalent circuits of an induction motor:
(a) Per-phase equivalent circuit and (b) simplified per-phase equivalent circuit.

Further,

$$\omega_{ms} = \frac{4\pi f}{p} \text{ rad/sec} \quad (14.2)$$

where f and p are supply frequency and number of poles, respectively.

Since, the stator impedance drop is generally negligible compared to the terminal voltage V , the equivalent circuit can be simplified to that shown in Figure 14.1b.

Also from Equation (14.1),

$$\omega_m = \omega_{ms} (1 - s) \quad (14.3)$$

From Figure 14.1b

$$\bar{I}'_r = \frac{V}{\left(R_s + \frac{R'_r}{s} \right) + j(X_s + X_r)} \quad (14.4)$$

Speed-torque and speed-rotor current characteristics of the induction motor are shown in Figure 14.2 [1–3, 6, 12].

Power transferred to the rotor (or air-gap power):

$$P_g = 3I'^2 R'_r / s \quad (14.5)$$

Rotor copper loss is:

$$P_{cu} = 3I'^2 R'_r / s \quad (14.6)$$

Electrical power converted into mechanical power:

$$P_m = P_g - P_{cu} = 3I'^2 R'_r \left(\frac{1-s}{s} \right) \quad (14.7)$$

Torque developed by the motor:

$$T = P_m / \omega_m \quad (14.8)$$

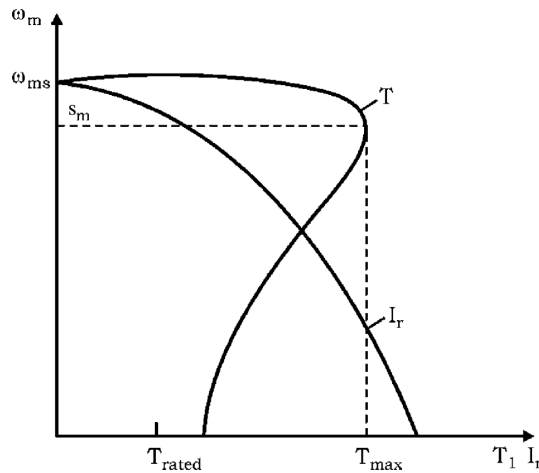


FIGURE 14.2 Speed torque and speed rotor current characteristics of an induction motor.

Substituting from Equations (14.3) and (14.7) yields:

$$T = \frac{3}{\omega_{ms}} I_r'^2 \frac{R'_r}{s} \quad (14.9)$$

Substituting from Equation (14.4) gives

$$T = \frac{3}{\omega_{ms}} \left[\frac{V^2 R'_s / s}{\left(R_s + \frac{R'_r}{s} \right) + j(X_s + X'_r)} \right] \quad (14.10)$$

A comparison of Equations (14.5) and (14.9) suggests that

$$T = P_g / \omega_{ms} \quad (14.11)$$

Motor output torque at the shaft is obtained by deducting friction, windage, and core-loss torques from the developed torque. The developed torque is a function of slip only [Equation (14.10)]. Differentiating T in Equation (14.10) with respect to s and equating to zero gives the slip for maximum torque:

$$s_m = \pm \frac{R'_r}{\sqrt{R_s^2 + (X_s + X'_r)^2}} \quad (14.12)$$

Substituting from Equation (14.10) into (14.12) yields an expression for maximum torque:

$$T_{\max} = \frac{3}{2\omega_{ms}} \left[\frac{V^2}{R_s \pm \sqrt{R_s^2 + (X_s + X'_r)^2}} \right] \quad (14.13)$$

Maximum torque, also known as breakdown torque, is independent of rotor resistance, but slip at maximum torque s_m is directly proportional to rotor resistance.

14.3 MODELING AND CHARACTERISTICS OF INDUCTION DRIVES

The equivalent circuit for three-phase induction is shown in [Figure 14.3](#).

All the parameters represented in the equivalent circuit are referred to as stator. The various power relations at slip (s) are:

1. Input power to the rotor $= 3I_r^2 \frac{R_r}{s}$ W
2. Rotor copper loss $= 3I_r^2 R_r$
3. Mechanical power output $= 3I_r^2 \frac{R_r}{s} (1-s)$ W
4. The developed power $P = T \cdot \omega_r$
5. $T = \frac{3}{\omega_s} I_r^2 \frac{R_r}{s}$ Nm
6. $I_R = \frac{V_s}{\sqrt{(R_s + R_r/s)^2 + (X_r + X_s)^2}}$ A
7. $T = \frac{3}{\omega_s} \frac{V_s^2}{(R_s + \frac{R_r}{s})^2 + X^2}$

The typical torque speed characteristics are drawn in [Figure 14.4](#).

One curve is formed for the forward direction of rotation, and the other is identical for the reverse direction of rotation. During the forward motoring, the main characteristics are in Quadrant I. On extension, it moves to Quadrant IV. It indicates

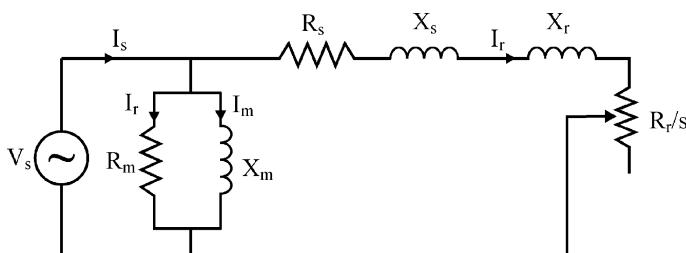


FIGURE 14.3 Equivalent circuit of a three-phase induction motor.

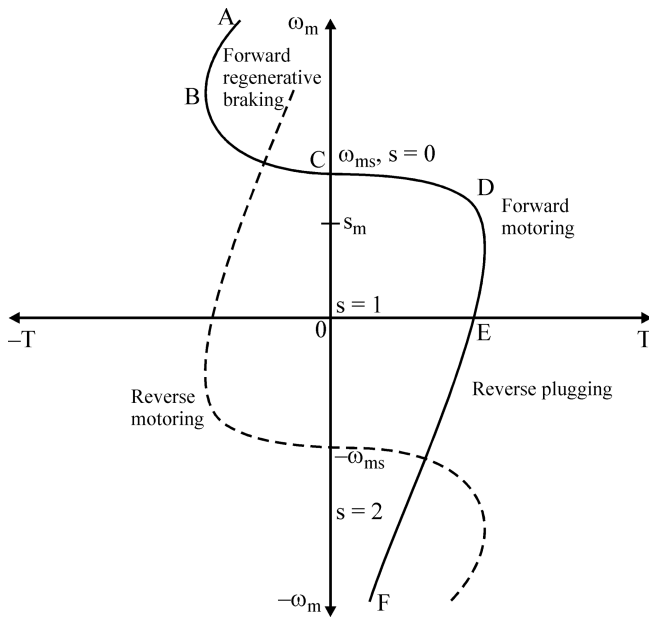


FIGURE 14.4 Speed-torque characteristics of an induction motor.

that for positive torque, the speed is negative. It is a case of regenerative action. It is possible only when the required reactive power for excitation is supplied to the motor from their main supply.

The maximum torque will occur at a slip $s_{\max} = \pm R_R / \sqrt{R_s^2 + X^2}$

This will give maximum torque as:

$$T_{\max} = V_s^2 / 2 \left[R_s^2 \pm \sqrt{R_s^2 + X^2} \right] \quad (14.14)$$

This torque expression is independent of value of rotor resistance. Because $R_s^2 - \sqrt{R_s^2 + X^2}$ is less than $R_s^2 + \sqrt{R_s^2 + X^2}$, the torque developed in the generating mode will be more than that in the motoring mode.

The starting torque will be at $s = 1$, and its value will be

$$T_{ST} = \frac{3}{\omega_s} \frac{V_s^2}{(R_s + R_r)^2 + X^2} \text{ Nm} \quad (14.15)$$

And current will be

$$I_{ST} = \frac{V_s^2}{\sqrt{(R_s + R_r)^2 + X^2}} \text{ A} \quad (14.16)$$

These equations show that low value of X gives a larger torque, and a large value of x gives a lower value of torque. The torque ratio will be

$$\frac{T}{T_{\max}} = \frac{2(R_s + R_r)^2 + X^2}{(R_s + R_r / s)^2 + X^2} \frac{R_r}{s} \quad (14.17)$$

When the effect of the stator resistance R_s is neglected, then the above values will become

$$s_{\max} = \pm \frac{R_r}{X} \quad (14.18)$$

and

$$\begin{aligned} T_{\max} &= \frac{\frac{2R_r}{X}}{\frac{R_r^2}{s^2} + x^2} \\ &= \frac{\frac{2R_r^2}{s s_{\max}}}{\frac{R_r^2}{s^2} + R_r^2 (s_{\max} T)^2} \\ &= \frac{2}{\frac{s}{s_{\max} T} + \frac{s_{\max} T}{s}} \end{aligned} \quad (14.19)$$

14.4 NO-LOAD CURRENT OF A THREE-PHASE MOTOR

The value of no-load current, I_0 , depends on the magnitude of the magnetizing current of the induction motor. It is determined experimentally when the motor is on no load or disconnected from the load and given supply [1,2,6,12]. In actual practice, the no-load current will be more if it is started with the attached equipment. In large totally enclosed motors and motors having large air gaps, the value of I_0 is high. The value of the no-load current greatly affects the performance of the induction motor [1–3,6,12]. As the rating increases, the ratio of I_0/I_{fl} decreases. This ratio increases with a decrease in speed.

14.5 STARTING PERFORMANCE OF THE THREE-PHASE INDUCTION MOTOR

The torque expression can be written for any slip as $T_s = 3I_r^2 \frac{R_r}{s\omega_s}$

At starting, $s = 1$, so

$$T_{st} = 3I_{rst}^2 \frac{R_{rst}}{\omega_s} \quad (14.20)$$

At full load slip of s_f , the torque

$$T_{sf} = 3 I_{rf\ell}^2 \frac{R_{rf\ell}}{s_f \omega_s} \quad (14.21)$$

$$\frac{T_{st}}{T_{fl}} = \left(\frac{I_{rst}}{I_{rf\ell}} \right) 2 \left(\frac{R_{rst}}{R_{rf\ell}} \right) s_f \quad (14.22)$$

The ratio of stator currents at full load and starting does not differ much from the ratio of corresponding rotor currents [1-3,12]. So in terms of stator values

$$\frac{I_{rst}}{I_{rf\ell}} = 0.9 \left(\frac{I_{sst}}{I_{sfl}} \right) \quad (14.23)$$

Usually $R_{rst} = 1.2 R_{rf\ell}$, so the torque ratio will be

$$\frac{T_{st}}{T_{fl}} = \left(\frac{I_{sst}}{I_{sfl}} \right)^2 s_f \quad (14.24)$$

These expressions are true for normal motors.

14.6 MODIFYING TORQUE-SPEED CHARACTERISTICS OF THE THREE-PHASE INDUCTION MOTORS

Depending upon the torque equation, the characteristics of the three-phase induction motor can be modified as follows [1-3,6,12].

14.6.1 VARYING THE SUPPLY VOLTAGE

All the machine parameters remaining constant, for any value of the slip the torque is directly proportional to square of the voltage applied to the stator. The torque-speed characteristics according to the voltage applied to the stator are shown in Figure 14.5.

The characteristics show that the maximum value of torque for each voltage occurs at the same slip given by

$$s_{max,t} = \frac{R_r}{X}$$

Further in the stable region of operation for the same torque the variation in speed is small. So this method is suitable when a small variation in speed is desired.

14.6.2 CONSTANT V/f CONTROL

A three-phase induction is a constant-flux machine. To keep flux constant, the ratio is kept constant; in this case, speed will be proportional to the frequency. For the

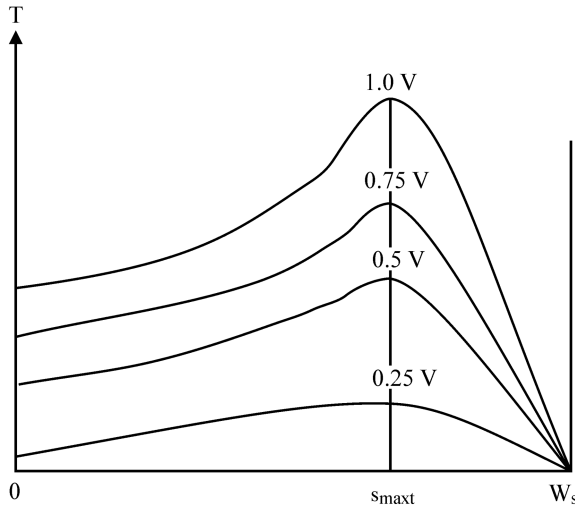


FIGURE 14.5 Effect of varying stator voltage.

rated frequency f_r of the supply, let the operating frequency be $f = \alpha f_r$. Then the corresponding synchronous speed will be αw_s . The applied voltage for constant-flux operation will be αV_s . In such a case, the torque equation will be

$$T = \frac{1}{\omega_s} \frac{2V_s^2 R_r / \alpha s}{\left(\frac{R_s}{\alpha} + \frac{R_r}{\alpha s} \right)^2 + X^2}$$

This torque equation shows that the effect of varying V/f as constant value α is to increase the resistances of stator and rotor by a factor $1/\alpha$. The starting torque as

$$T_{st} = \frac{3}{\omega_s} \frac{V_s^2 R_r / \alpha s}{\left(\frac{R_s}{\alpha} + \frac{R_r}{\alpha s} \right)^2 + X^2}$$

The value of maximum torque will be

$$T_{max} = \frac{3}{\omega_s} \frac{V_s^2}{\left(\frac{R_s}{\alpha} \pm \sqrt{\left(\frac{R_r}{\alpha} \right)^2 + X^2} \right)}$$

The corresponding value of slip will be

$$s_{max} = \frac{\frac{R_s}{\alpha}}{\sqrt{\left(\frac{R_s}{\alpha} \right)^2 + X^2}}$$

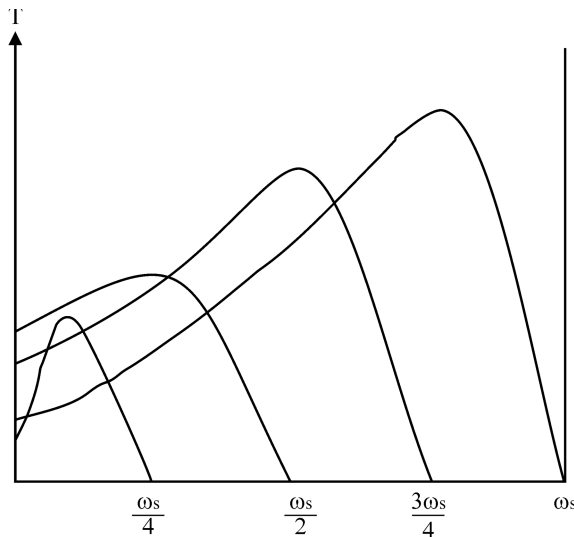


FIGURE 14.6 $V/f = \text{constant}$ control.

These characteristics are shown in Figure 14.6. The slip at which maximum torque occurs increases as the frequency of supply is decreased. It is associated with a degree in the value of maximum torque. The value of starting torque increases with a decrease in frequency up to a limit and beyond that it decreases with further decrease in frequency. The reduction in the developed torque is due to apparent increase in resistances R/α , and also there is a slight decrease in the air-gap flux. The decrease in flux is due to a drop in impedance of the stator. This can be compensated by slightly increasing v/f as α becomes small. However, this will increase in the magnetizing current, which is drawn from the supply.

14.6.3 ADDING IMPEDANCE IN THE STATOR CIRCUIT

When a resistance or inductance is added in the stator circuit, the voltage available at the stator terminals of the induction motor decrease. This will decrease the developed torque. For some values of the starting torque by addition of R , X , or residual voltage, the modified torque speed characteristics are shown in Figure 14.7.

This method of control will give better power factor with R , but losses will increase. When X is added, the losses are lesser, but the power factor is poor.

14.6.4 ADDING RESISTANCE IN THE ROTOR CIRCUIT

When balanced resistors are connected to the three slip rings of a slip-ring induction motor the torque-speed characteristics can be modified as shown in Figure 14.8.

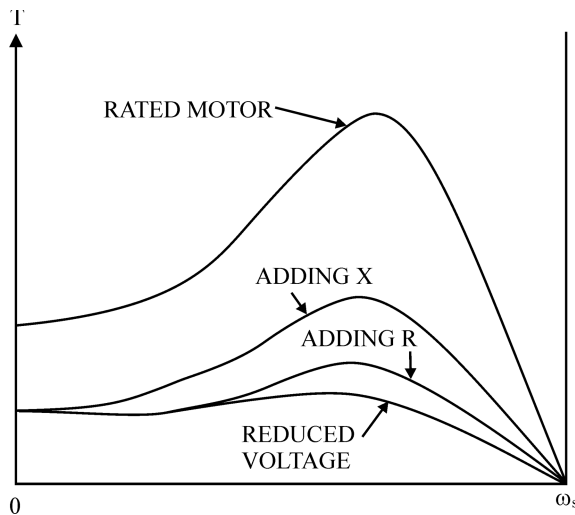


FIGURE 14.7 Adding impedance in a stator circuit.

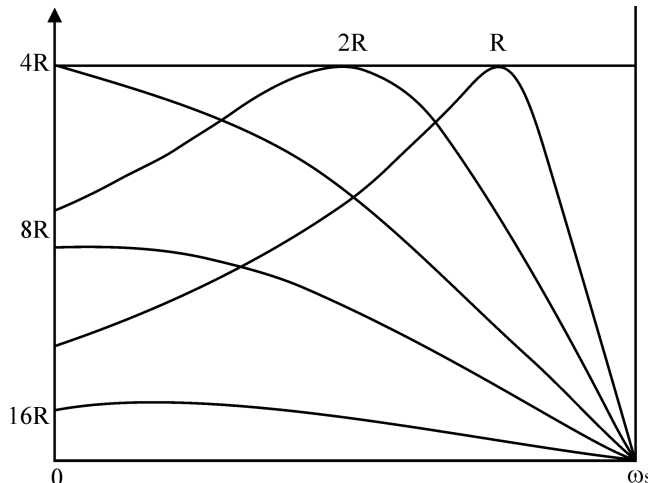


FIGURE 14.8 Adding resistance in a rotor circuit.

These characteristics show that the maximum value of torque is the same for all values of rotor resistance, because the maximum torque occurs when $X = \text{resistance of the rotor circuit}$. It is also observed that the maximum torque may occur at starting when the above relation is satisfied for $s = 1$. If the resistance is further increased, the value of the starting current will decrease, and it may lower the value of the starting torque.

14.6.5 VOLTAGE INJECTION—THE ROTOR CIRCUIT

When the effect of stator impedance drop is neglected, the voltage E_r is induced in the rotor circuit at standstill. At slip s , its value will be sE_r . Neglecting the effect of rotor reactance, the current in rotor I_r will be approximately equal to $I_r = sE_r/R_r$

Now when E_j voltage per phase is injected at the slip rings, the current in the rotor circuit at s_j will be

$$I_{r2} = \frac{s_i E_r - E_j}{R_r}$$

This will give $s_i = s + (E_j / E_r)$

Now if voltage is injected 180° out of phase with induced emf in the ratio, then

$$s_i = s - (E_j / E_r)$$

In such a case, the slip may become negative also, that it becomes above the synchronous speed. These characteristics are shown in [Figure 14.9](#).

In order to inject the appropriate voltage in the rotor circuit, it must be ensured that the frequency of the injected voltage is the same as that of the induced voltage. This is achieved in modern drives by use of solid-state frequency converters or cycloconverters.

14.6.6 POLE-CHANGING DRIVE

The squirrel-cage induction motor has a rotor winding adjustable for any number of poles. So the stator winding can be connected for varying number of poles. Since the speed of an induction motor is a function of a number of poles for a fixed frequency of supply, by varying the direction, the connection of current can be reversed, and that will reverse the polarity of the pole.

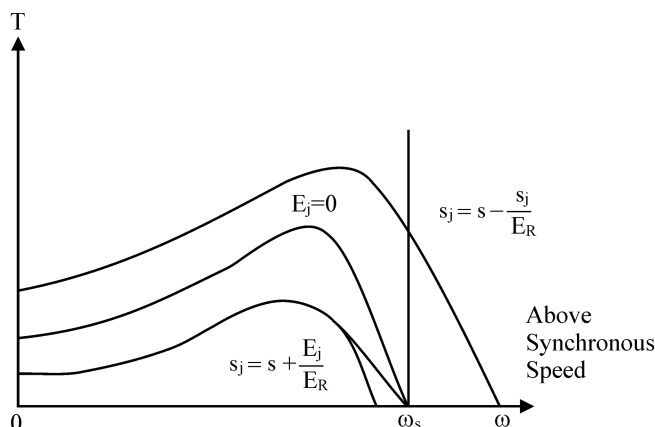


FIGURE 14.9 Effect of voltage injection in a rotor circuit.

14.6.7 POLE-AMPLITUDE MODULATION

The pole-amplitude modulation makes use of the principle of several pole combinations to be economically obtained with a single winding and without any increase in frame size. In this case, the mmf of a p' pole pair air-gap field is modulated to yield two superimposed fields as $(p'-k)$ and $(p'+k)$, where k is an integer. By suitable arrangement of three-phase connections, only the desired emf is retained; the term *modulation* implies the current in parts of the winding.

14.7 TRANSIENT STABILITY

The transient stability of the drive system is considered from the initial and final condition of the speed-torque characteristics of the motor and the load. In this consideration, the inertia torque and time duration between the initial and final condition are ignored [1–3,12]. The transient study is performed to estimate the performance of the drive with respect to its stability of motion. When load changes slowly and steadily, the drive motor can be loaded up to its maximum capacity of torque and power. The induction motor can be safely loaded up to pull out torque only.

The transient process is quite fast, and pullout torque of the induction motor may not be the permissible limit of load torque because the inertia torque of the rotating masses plays a significant role. It aids in the motor torque during a decrease in speed and opposes when the speed increases. Therefore, the steady-state stability criteria outlined above does not hold true during transient conditions. However, the transient stability of an electrical drive during the design and operation helps in the optimal use of equipment. In the case of drives having flywheels, the size of the flywheel can be decreased when transient stability is considered. But in practice, it is done only partially, the transient stability limit is always kept as a reserve capacity to meet the sudden load changes.

14.8 BRAKING OF THE INDUCTION MOTOR

During braking operation, any motor (AC or DC) works as a generator and thus produces a negative torque. Various merits of electrical braking over mechanical brakes are quick-and-smooth stops; accurate stops without involving mechanical parts; no wear and tear of mechanical parts; and use of energy generated due to the braking operation.

Various types of braking in induction motors are:

1. Regenerative braking
2. Plugging or reverse-voltage braking
3. Dynamic or rheostatic braking

14.8.1 REGENERATIVE BRAKING

In this type of braking, the induction motor works as an induction generator and thus converts mechanical energy into electrical energy, which is stored in the supply side using some energy storing devices. For this braking, it is essential that the motor speed (N_r) must be greater than the synchronous speed (N_s). When the induction motor runs

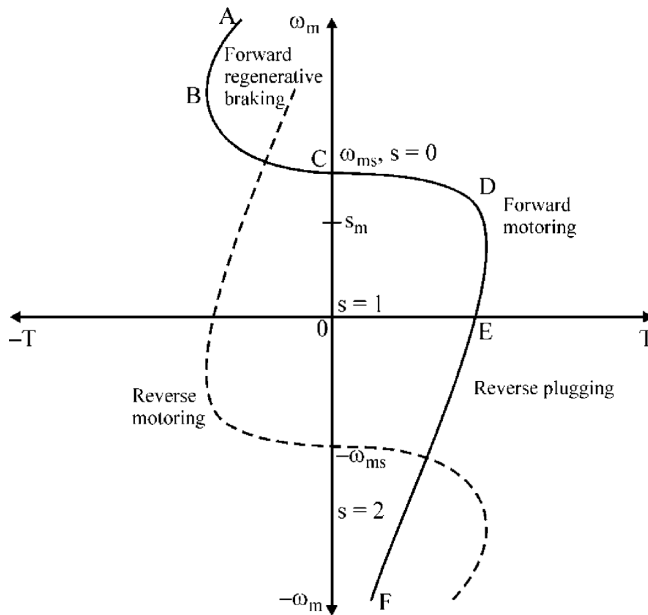


FIGURE 14.10 Speed-torque curves of an induction motor drive.

greater than the synchronous speed, then the relative speed between the rotor and rotating field is negative. Therefore, the direction of the rotor-induced voltage and currents are in the opposite direction to that of the motoring operation. Also, the stator current is in the opposite direction. Therefore, the power flows from the motor to the source, and thus it works as a generator. [Figure 14.10](#) illustrates the speed-torque curves [2,12].

The developed braking torque can be expressed as:

$$T_{\text{braking}} = -T = -\frac{3}{\omega_{ms}} \left[\frac{V_s^2}{\left(R_{Th} + \frac{R_\gamma^1}{s} \right)^2 + (X_s + X_\gamma^1)^2} \right] \frac{R_\gamma^1}{s} N - m \quad (14.25)$$

For regenerative braking

$$\frac{R_\gamma^1}{s_m} = \sqrt{R_{Th}^2 + (X_\gamma^1 + X_{Th})^2} \quad (14.26)$$

The maximum braking torque can be expressed as:

$$T_{\max} = \frac{3}{2\omega_{ms}} \left[\frac{V_{TH}^2}{R_{Th} - \sqrt{R_{Th}^2 + (X_{Th} + X_\gamma^1)^2}} \right] \quad (14.27)$$

The braking torque, braking speeds, and the regenerated power are higher than the corresponding motoring torque, motoring speed, and motoring power for same magnitude of slip.

14.8.2 PLUGGING

For the induction motor to operate in the plugging mode, the slip must be greater than 1. This is obtained when the rotor moves in the reverse direction. The portion EF in the speed-torque curve of Figure 14.10 shows the plugging operation of the induction motor. The motor torque is positive because the relative speed between the rotating field and rotor is positive. The inductor motor draws power from the source. This is a highly inefficient method of braking because both the generated power and the power supplied from the source are dissipated in the form of heat across the motor circuit resistance. The plugging braking can be achieved by changing the phase sequence of the motor terminal voltage by interchanging the connections of any two motor terminals. In this, the motor torque is not zero at zero speed, and therefore, the motor should be disconnected from the source at or near to zero speed when braked for stopping. Therefore, an additional device will be needed to detect zero speed and disconnect the motor from the source. Hence, this type of braking is not suitable for stopping.

14.8.3 DYNAMIC BRAKING

In this type of braking, the inductor motor is disconnected from the AC source and connected to DC supply as shown in Figure 14.11. The equivalent circuit of inductor motor during DC dynamic braking is shown in Figure 14.12 [1–3,6,12].

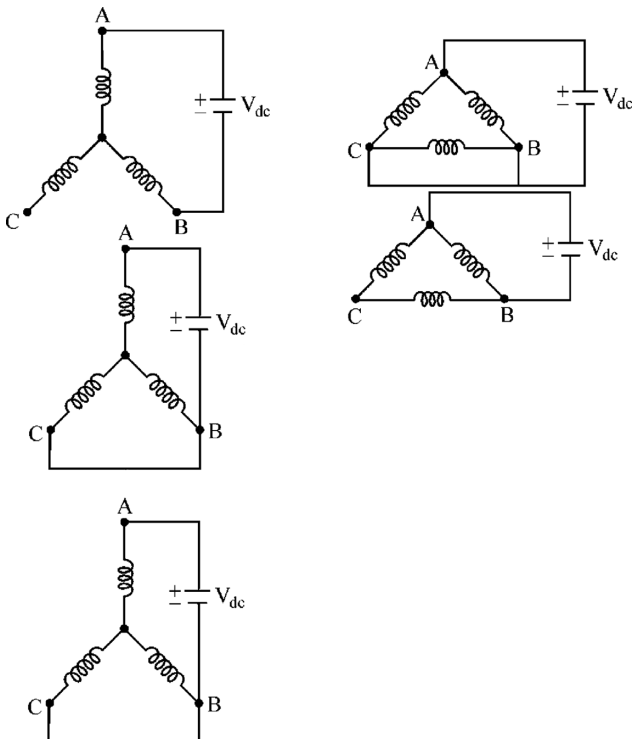


FIGURE 14.11 Circuits of an induction motor drive during DC dynamic braking.

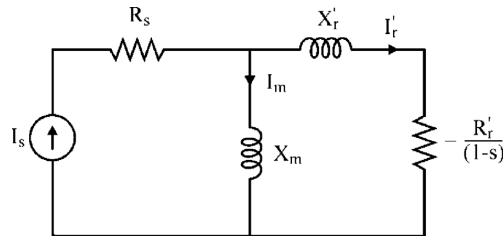


FIGURE 14.12 Equivalent circuit of an induction motor drive during DC dynamic braking.

14.9 SPEED CONTROL OF THREE-PHASE INDUCTION MOTORS

Various methods of speed control generally used in power semiconductor-controlled induction-motor drives are:

1. Stator voltage control
2. Variable frequency control
3. Rotor resistance control
4. Injecting voltage in rotor circuit

14.9.1 STATOR VOLTAGE CONTROL METHOD

Torque developed by the induction motor is proportional to the square of the terminal voltage. So, torque-speed curves retain their shapes but shrink or grow as a square of the voltage. Because terminal voltage cannot be applied greater than the rated value, this method of speed control is used to control speeds below the rated speeds. This method is suitable for applications where torque demand reduces with speed as shown in [Figure 14.13 \[1,2,12\]](#), which finds it suitable for fan and pump-type drives.

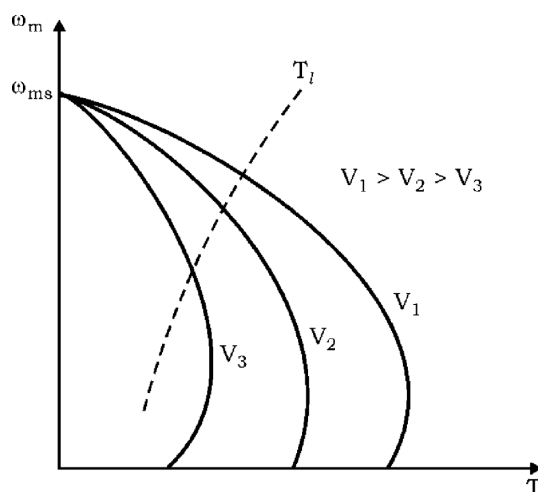


FIGURE 14.13 Stator voltage control.

If stator copper loss, core loss, and friction losses are ignored, then motor efficiency η is given by:

$$\eta = P_m / P_g = (1 - s) \quad (14.28)$$

The preceding equation shows that efficiency falls with a decrease in speed. The speed control is therefore obtained by dissipating a portion of the rotor input power in rotor resistance. Thus, not only is the efficiency low but the power dissipation occurs in the rotor itself, which may overheat the rotor. Therefore, this drive is used in fan and pump drives of low power ratings and for narrow speed range.

Variable AC voltage for speed control is obtained using AC voltage controllers, shown in Figure 14.14 [1–3,6,12]. Domestic fan motors, which are always single-phase, are controlled by a TRIAC as shown in Figure 14.14a.

Speed control is obtained by varying the firing angle of the TRIAC. Industrial fans and pumps of high ratings are driven by three-phase motors, so thyristor-based three-phase voltage controllers are used for speed control by varying the firing angle. For low power ratings, antiparallel-connected thyristors can be replaced by a TRIAC. These AC voltage controllers provide stepless control of voltage from its zero value.

14.9.2 VARIABLE-FREQUENCY CONTROL METHOD

From Equation (14.2), it can be seen that the synchronous speed ω_{ms} is directly proportional to the frequency of supply voltage, so synchronous speed and motor speed ω_m can be controlled below and above the normal full-load speed by changing the supply frequency [1–3,6,12]. We know that the voltage induced in stator (E) is directly proportional to supply frequency f and air-gap flux ϕ ,

that is,

$$E \propto f\phi \quad (14.29)$$

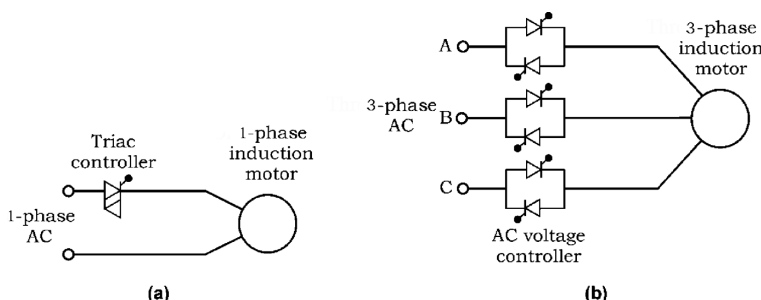


FIGURE 14.14 Stator voltage control by AC voltage controllers: (a) Single phase TRIAC controller based IM drive and (b) three phase IM drive.

If the stator drop is neglected, then $E \cong V$
 where V is the motor terminal voltage.
 Therefore

$$V \propto f\phi \quad (14.30)$$

Any reduction in frequency f , without a change in voltage V causes an increase in flux ϕ , which results in saturation of the motor. It also results in a high magnetization current, increased coreless, stator copper loss, and produce noise.

So, the variable frequency controlled below the rated frequency is carried out by reducing voltage V along with frequency f in such a manner that flux is maintained constant, that is, (V/f) ratio is constant. Above the rated frequency, the motor is operated at constant voltage because of limitations imposed by stator insulation or by supply voltage limitation.

Let,

$$'a' = \frac{f_o}{f_{rated}} = \frac{\text{Operating frequency}}{\text{rated frequency}} \quad (14.31)$$

where ' a ' is called the per unit frequency.

Case-I: Operation below rated frequency ($a < 1$):

It is preferred to operate the motor at a constant flux, which is possible if the magnetizing current I_m is maintained constant.

$$I_m = \frac{E_{rated}}{X_m} = \frac{E_{rated}}{f_{rated}} \cdot \frac{1}{2\pi L_m} \quad (14.32)$$

When the motor is operated at frequency f , then:

$$I_m = \frac{E}{aX_m} = \frac{E}{af_{rated}} \cdot \frac{1}{2\pi L_m} \quad (14.33)$$

So, from Equations (14.32) and (14.33), I_m will be constant when:

$$E = aE_{rated} \quad (14.34)$$

So, flux will remain constant if emf change is in the same ratio as the frequency, that is, when the (E/f) ratio is maintained constant.

Torque expression is given by:

$$T = \frac{3}{\omega_s} \left[\frac{V_1^2 \left(\frac{R'_2}{s} \right)}{\left[R_l + \frac{R'_2}{s} \right]^2 + \left[X_1 + X'_2 \right]^2} \right] \quad (14.35)$$

Therefore, for constant (E/f) ratio operation, the synchronous speed becomes ($a\omega_s$), applied voltage becomes (aV), and all reactance becomes (aX). Substituting these in the preceding torque expression, we get:

$$T = \frac{3}{\omega_s} \frac{V_t^2 \left(\frac{R_2'}{as} \right)}{\left[\frac{R_1}{a} + \frac{R_2'}{as} \right]^2 + \left[X_1 + X_2' \right]^2} \quad (14.36)$$

So, both the expressions of torque are the same except all resistances have become larger by ($1/a$). For the starting torque, put $s = 1$ in Equation (14.35). The maximum torque can be given by:

$$T_{\max} = \frac{3}{\omega_s} \frac{0.5 V_{\text{rated}}^2}{\left[\frac{R_1}{a} + \sqrt{\left(\frac{R_1}{a} \right)^2 + \left(X_1 + X_2' \right)^2} \right]} \quad (14.37)$$

and slip at maximum torque $s_{\max,T}$ is given by:

$$s_{\max,T} = \pm \frac{\left(\frac{R_2'}{a} \right)}{\sqrt{\left(\frac{R_1}{a} \right)^2 + \left(X_1 + X_2' \right)^2}} \quad (14.38)$$

Slip at which the maximum torque occurs becomes larger as the operating frequency decreases or per unit frequency “ a ” decreases, as shown in Figure 14.15. The operation of the machine at a constant flux requires a closed-loop control of flux. When the operating point changes, the closed-loop control adjusts the motor voltage to maintain a constant flux.

Case-II: Operation above rated frequency ($a > 1$)

Operation at a frequency higher than the rated frequency takes place at constant terminal voltage V_{rated} . Since terminal voltage is maintained constant, flux decreases as per unit frequency a increases. Therefore, the motor operates in a field-weakening mode. Various torque expressions for this case can be given by:

$$T = \frac{3}{a\omega_s} \left[\frac{V_{\text{rated}}^2 \left(\frac{R_2'}{s} \right)}{\left(R_1 + \frac{R_2'}{s} \right)^2 + a^2 \left(X_1 + X_2' \right)^2} \right] \quad (14.39)$$

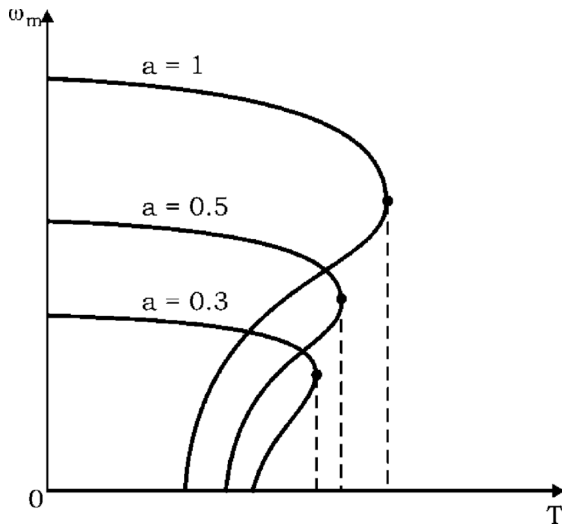


FIGURE 14.15 Operation below rated frequency ($a < 1$).

$$T_{\max} = \frac{3}{a\omega_s} \left[\frac{0.5 V_{\text{rated}}^2}{R_l + \sqrt{(R_l)^2 + a^2 (X_1 + X_2')^2}} \right] \quad (14.40)$$

Therefore, it can be seen that breakdown torque decreases with an increase in frequency and speed, as shown in [Figure 14.16a](#).

The block diagram of the variable-frequency speed-control scheme is shown in [Figure 14.16b](#) [6,12], where the motor is fed from a variable-frequency variable-source (VFVS). The VFVS can be a voltage-source inverter or a cycloconverter.

Advantage and disadvantage of variable-frequency control: It provides good running and transient performance because of the following features:

1. Speed control and braking operation are available from zero speed to above-rated speed.
2. During transient, operation can be carried out at maximum torque with reduced current giving good response.
3. Copper losses are low, and therefore efficiency and power factor are high.
4. Drop in speed from no load to full load is small.
5. It allows variable-speed drive to be obtained from squirrel-cage induction motor, which has many advantages.
6. Overall cost of variable-frequency induction-motor drive is high.

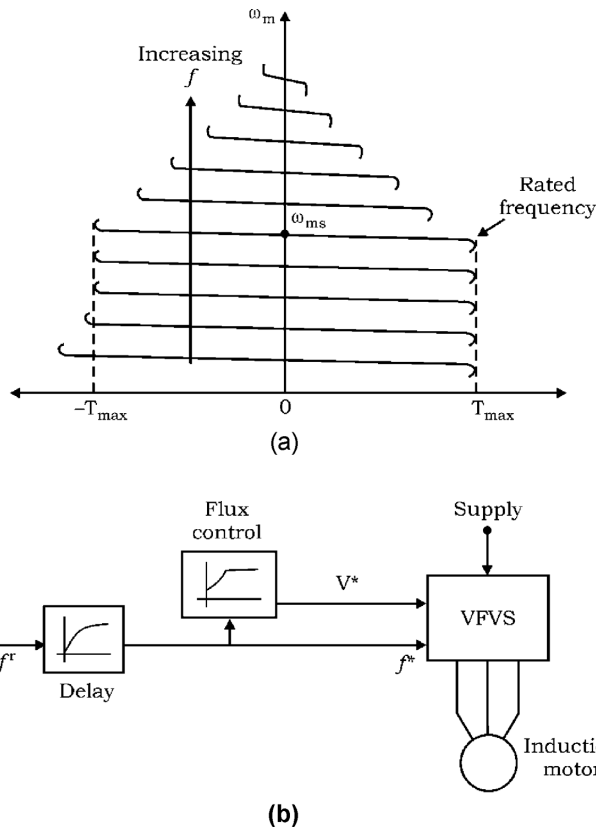


FIGURE 14.16 Variable-frequency control method: (a) Speed-torque characteristics and (b) block diagram.

14.9.3 ROTOR-RESISTANCE CONTROL

This method of speed control is used only for wound-rotor-type induction motors. In these motors, rotor winding is designed with low resistance so as to have low full-load slip with high running efficiency. The external resistors are connected in series with the rotor winding to have improved starting performance. The speed-torque and speed-rotor current characteristics of this motor with rotor-resistance control are shown in Figure 14.17.

It can be seen that for a given load torque, as the rotor resistance increases, the motor speed reduces. But the no-load speed remains unaffected, with variations in rotor resistance.

We know that:

$$\text{Rotor copper loss} = sP_g = 3(I'_r)^2 R'_r \quad (14.41)$$

where sP_g is called as the *slip power*.

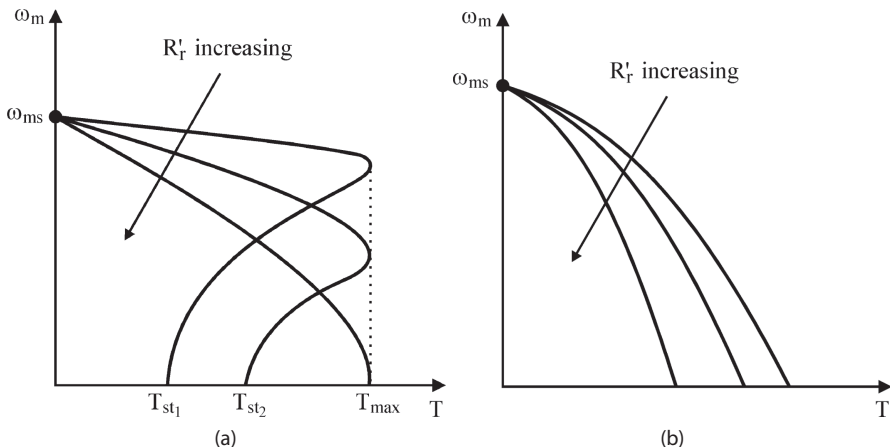


FIGURE 14.17 Characteristics of induction motor drive during rotor-resistance control method.

The motor efficiency is expressed as:

$$\eta = \frac{P_m}{P_g} = (1 - s) \quad (14.42)$$

Equations (14.41) and (14.42) illustrate that with the decrease in motor speed or increase in slip, the rotor copper losses increase while the motor efficiency decreases. Therefore, this method of speed control is a highly inefficient method of speed control. But it has the merit of providing a constant torque operation with a high torque-to-current ratio.

14.9.4 INJECTION OF VOLTAGE IN THE ROTOR CIRCUIT

The equivalent circuit of a wound-rotor-type inductor motor with injected voltage of $V_r \angle \phi_r$ volts per phase is shown in Figure 14.18 [1–3,6,12].

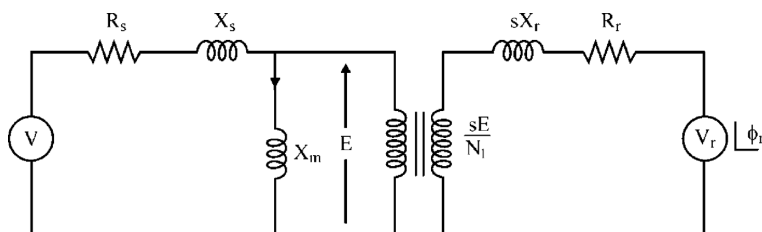


FIGURE 14.18 Equivalent circuit of induction motor drive with rotor-injected voltage control method.

Various mathematical expressions for this control method can be expressed as:

$$T = \frac{P_g}{\omega_{ms}} \quad (14.43)$$

The mechanical power,

$$\begin{aligned} P_m &= T\omega_m \\ &= \frac{P_g}{\omega_{ms}}\omega_m \\ &= \frac{P_g}{\omega_{ms}} = (1-s) \omega_{ms} \\ &= (1-s) P_g \end{aligned} \quad (14.44)$$

The rotor circuit electrical power can be expressed as:

$$\begin{aligned} P_e &= P_g - P_m \\ &= P_g - (1-s) P_g \\ &= sP_g \end{aligned} \quad (14.45)$$

Also,

$$P_e = \text{rotor copper loss } (P_{cr}) + \text{power absorbed by } V_r(P_r)$$

that is,

$$P_e = P_{cr} + P_r = sP_g \quad (14.46)$$

$$\text{Total input power, } P_m = \text{stator copper loss } (P_{cs}) + P_g$$

$$\text{where } P_g = sP_g + (1-s) P_g$$

or

$$= \text{Slip power} + P_m \quad (14.47)$$

and

$$\text{Slip power, } sp_g = \text{rotor copper loss}(P_{cr}) + P_r \quad (14.48)$$

Substituting Equation (14.48) in (14.47), we get

$$P_g = P_{cr} + P_r + P_m$$

or

$$P_m = P_g - P_r - P_{cr} \quad (14.49)$$

or

$$T\omega_m = T\omega_{ms} - P_r - P_{cr}$$

or

$$\omega_m = \omega_{ms} - \frac{P_r + P_{cr}}{T} \quad (14.50)$$

14.10 SLIP POWER CONTROL USING POWER SEMICONDUCTOR CONVERTER

In this method, the speed of wound-rotor induction motor is controlled by regulating the slip power (sP_g). Here, rotor resistance control and injection of voltage in rotor circuits are implemented using power converters. Various methods where slip power control is achieved are:

- (a) Static rotor resistance control
- (b) Static scherbius control
- (c) Static Kramer control

14.10.1 STATIC ROTOR-RESISTANCE CONTROL

In this control, rotor resistance of the wound-rotor induction motor is varied by using the chopper statically instead of mechanically. This method gives stepless and smooth variation of the motor speed. [Figure 14.19](#) presents the static rotor-resistance control method, where it can be seen that the effective value of resistance R is varied from R to 0 by varying the conductor period of semiconductor switch (S) [12].

The filter inductor L_d is used to minimize the ripple in current I_d , which in turn results in low harmonic content in the rotor and reduced copper losses. Generally, a power transistor or gate turn-off (GTO) is used as a semiconductor switch.

The energy absorbed by resistor R during a period of switch (S) is:

$$E_R = I_d^2 R(T_{off})$$

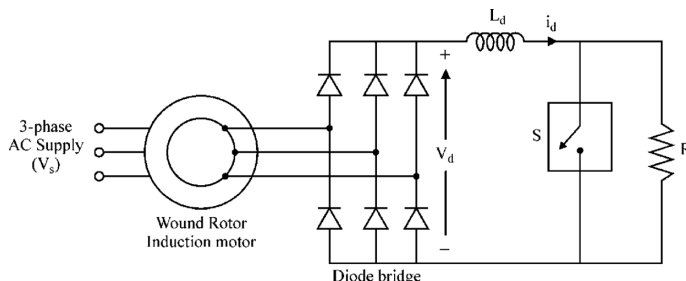


FIGURE 14.19 Static rotor-resistance control method of wound-rotor induction-motor drive.

or

$$E_R = I_d^2 R(T - T_{on}) \quad (14.51)$$

The average power absorbed by resistor R during a period T is:

$$P_R = \frac{1}{T} [I_d^2 R(T - T_{on})]$$

or

$$P_R = I_d^2 R \left(1 - \frac{T_{on}}{T}\right)$$

or

$$P_R = I_d^2 R(1 - \delta) \quad (14.52)$$

where δ is the duty ratio of the switch

$$\delta = \frac{T_{on}}{T} \quad (14.53)$$

Therefore, the effective value of resistance R is:

$$R^l = (1 - \delta)R \quad (14.54)$$

The total resistance across the diode bridge is:

$$R_e = R_d + R_l$$

or

$$R_e = R_d + (1 - \delta)R \quad (14.55)$$

The per-phase power consumed by resistance R_e :

$$P_e = \frac{1}{3} I_d^2 [R_d + (1 - \delta)R] \quad (14.56)$$

where:

$$I_d = \frac{\sqrt{3}}{\sqrt{2}} I_{rms} \quad (14.57)$$

where I_{rms} is the root mean square (RMS) value of rotor phase current.

Substituting the value of I_d in Equation (14.56), we get:

$$P_e = 0.5 [R_d + (1 - \delta)R] I_{rms}^2 \quad (14.58)$$

So, the effective per-phase value of resistance R_e is:

$$R_e^l = 0.5 [R_d + (1 - \delta)R] \quad (14.59)$$

The equivalent circuit of the wound-rotor induction motor with static rotor-resistance control can be derived from the fundamental equivalent circuit. The power transferred across the air gap is expressed as:

$$P_g = 3E I_r^1 \cos \theta_r \quad (14.60)$$

where θ_r is the phase angle between E and I_r^1

The total power consumed in the rotor circuit under this control method is:

$$P_g^1 = 3 I_{\text{rms}}^2 (R_r + R_e^1) + P_m \quad (14.61)$$

Also,

$$I_r = 3 \frac{I_{\text{rms}}}{\pi} \quad (14.62)$$

From Equations (14.61) and (14.62),

$$P_g^1 = \frac{\pi^2}{9} I_r^1 (R_r + R_e^1) + P_m. \quad (14.63)$$

The equivalent circuit must satisfy the condition:

$$P_g = P_g^1$$

Therefore,

$$3EI_r^1 \cos \theta_r = \frac{\pi^2}{9} I_r^2 (R_r + R_e^1) + P_m \quad (14.64)$$

For this drive,

$$sP_{g1} = 3I_r^2 (R_r + R_e^1) \quad (14.65)$$

$$P_m = P_{g1} - sP_{g1}$$

or

$$P_m = P_{g1} - sP_{g1}$$

or

$$P_m = (1-s)P_{g1}$$

$$P_m = 3I_r^2 (R_r + R_e^1) \frac{(1-s)}{s} \quad (14.66)$$

Substituting the magnitude of P_m from Equation (14.66) into Equation (14.64), we get:

$$\begin{aligned} E I_r^1 \theta_r &= \left[\left(\frac{\pi^2}{9} - 1 \right) (R_r + R_e^1) + \frac{(R_r + R_e^1)}{s} \right] I_r^2 \\ &= \left(R_h + \frac{R_f}{s} \right) I_r^2 \end{aligned} \quad (14.67)$$

where

$$R_h = \left(\frac{\pi^2}{9} - 1 \right) (R_l + R_e^l) \quad (14.68)$$

$$R_f = (R_l + R_e^l) \quad (14.69)$$

Referring to stator side,

$$E I_r^l \cos \theta_r = \left(R_h^l + \frac{R_f^l}{s} \right) I_r^{l2} \quad (14.70)$$

where:

$$R_h^l = N_1^2 R_h$$

$$R_f^l = N_1^2 R_f$$

where N_1 is the stator to rotor turn ratio.

$$I_r^l = \frac{V}{\left(R_s + R_h^l + \frac{R_f^l}{s} \right) + j(x_s + x_r^l)} \quad (14.71)$$

$$T = \frac{3}{\omega_{ms}} I_r^{l2} \left(\frac{R_f^l}{s} \right) \text{ N-m} \quad (14.72)$$

or

$$T = \frac{3}{\omega_{ms}} \left[\frac{V^2}{\left(R_s + R_h^l + \frac{R_f^l}{s} \right)^2 + (x_s + x_r^l)^2} \right] \times \frac{R_f^l}{s} \quad (14.73)$$

The equivalent circuit of a wound-rotor induction-motor drive with static rotor-resistance control method and the speed-torque curves for different values of duty cycle (δ) can be drawn as shown in Figures 14.20 and 14.21, respectively [12]. From the curve, it can be seen that for a given torque, speed reduces with the duty cycle.

Advantage of Static Rotor-Resistance Control Method

- Stepless and smooth control
- Less maintenance
- Fast response
- Compact size

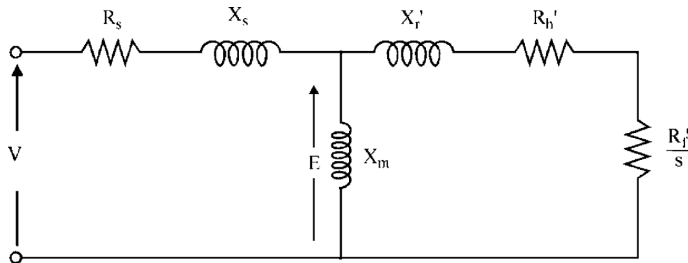


FIGURE 14.20 Equivalent circuit of wound-rotor induction-motor drive with static rotor-resistance control method.

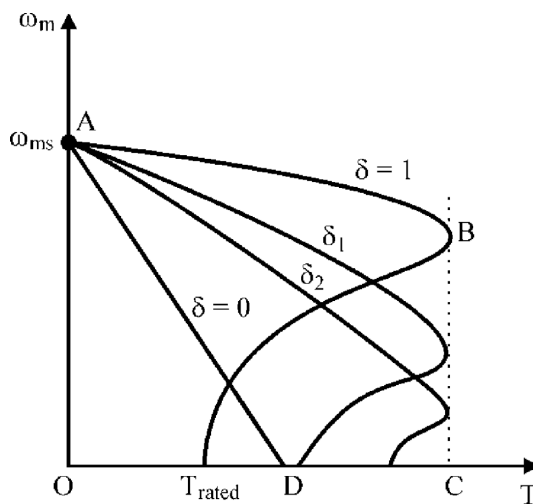


FIGURE 14.21 Speed-torque curves for wound-rotor induction-motor drive for different values of duty cycles.

- Longer life
- Simple closed-loop control

Disadvantage

- Derating of motor by 0.95

14.10.2 STATIC SCHERBIUS DRIVE

Scherbius suggested the slip-power recovery scheme where slip power (sP_g) was fed back to the AC mains instead of wasting it across the rotor resistance, and hence it is termed as static Scherbius drive as shown in [Figure 14.22 \[3,12\]](#).

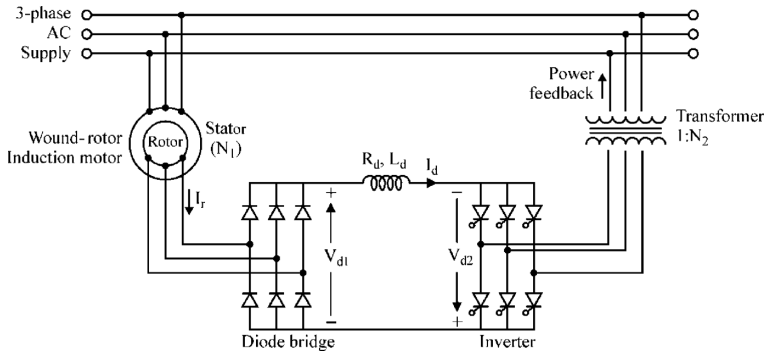


FIGURE 14.22 Static Scherbius drive.

As can be seen from the circuit diagram, the diode bridge converts some part of the rotor AC power into the DC, which further is converted into AC by the inverter and fed back to the AC supply through the transformer. The filter inductor L_d is used to reduce the ripples, which helps in maintaining the low harmonic copper losses. The supersynchronous speed control can be achieved by replacing the diode bridge and inverter by the cycloconverter.

Neglecting the stator and rotor drops, the output voltage of the diode bridge is expressed as:

$$V_{d1} = \frac{3\sqrt{6}}{\pi} \frac{sV}{N_1} \quad (14.74)$$

and

$$V_{d2} = \frac{3\sqrt{6}}{\pi} \frac{V}{N_2} \cos \alpha \quad (14.75)$$

where

V is the stator phase voltage

N_1 is the stator-to-rotor turn ratio

N_2 is the turn ratio of transformer-line side to inverter side

α is the firing angle of the inverter

Neglecting the losses in the inductor (L_d), then:

$$V_{d1} + V_{d2} = 0$$

$$\text{Therefore, } \frac{3\sqrt{6}}{\pi} \frac{sV}{N_1} + \frac{3\sqrt{6}V}{\pi N_2} \cos \alpha = 0$$

or

$$s = -\frac{N_1}{N_2} \cos \alpha$$

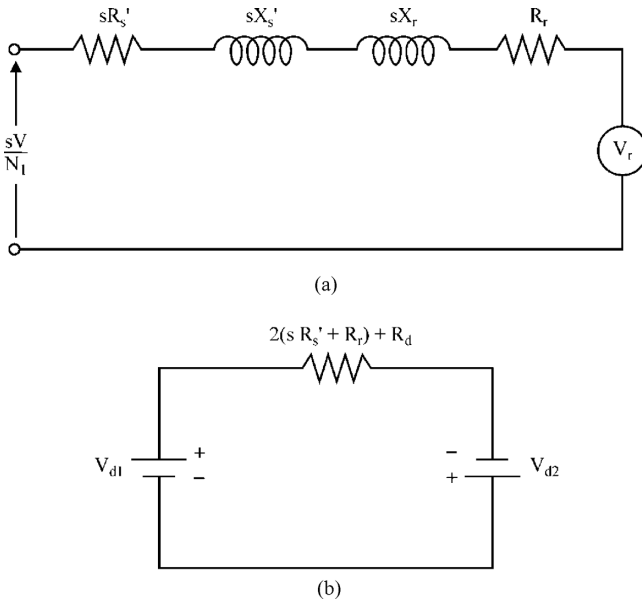


FIGURE 14.23 Equivalent circuit of motor and drive with Static Scherbius drive: (a) equivalent circuit of motor when referred to rotor and (b) equivalent circuit of drive.

or

$$s = -N \cos \alpha \quad (14.76)$$

where $N = \frac{N_1}{N_2}$

Figure 14.23 shows the equivalent circuit of the wound-rotor induction motor with static Scherbius control when referred to the rotor side.

The performance parameters of this drive can be expressed as below:

The DC link current I_d can be obtained from the equivalent circuit of the drive of Figure 14.23b:

$$I_d = \frac{V_{d1} + V_{d2}}{2(sR_s^1 + R_r) + R_d} \quad (14.77)$$

Substituting the magnitude of V_{d1} and V_{d2} , we get:

$$I_d = \frac{3}{\pi} \sqrt{6} V \left[\frac{s}{N_1} + \frac{\cos \alpha}{N_2} \right] \quad (14.78)$$

Ignoring the rotor copper losses,

$$sP_g = V_{d2} I_d$$

or

$$P_g = \frac{V_{d2} I_d}{s} \quad (14.79)$$

The developed torque can be obtained as:

$$T = \frac{P_g}{\omega_{ms}} \quad (14.80)$$

or

$$T = \frac{V_d I_d}{s \omega_{ms}} \quad (14.81)$$

The preceding equation shows that static Scherbius drive provides constant torque control. The speed-torque curves for this drive can be drawn as shown in Figure 14.24 for different values for firing angles.

Advantages of the static Scherbius drive

- High efficiency
- Low cost
- Provide constant torque control
- Simple control
- Running cost is lower

Drawback

- Unable to provide braking operation
- Poor pf
- Initial cost is higher

Applications

- Fan and pump drives
- Medium- and high-power applications

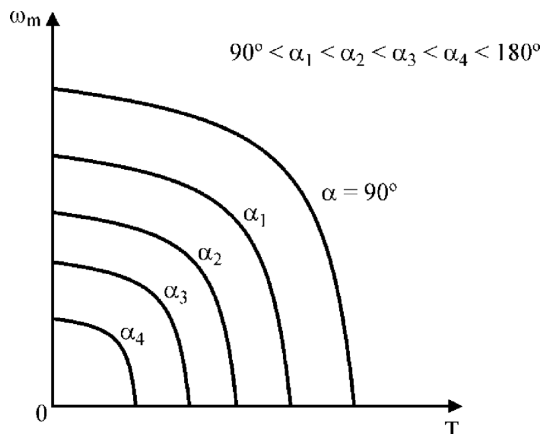


FIGURE 14.24 Speed-torque curves at different values of firing angles.

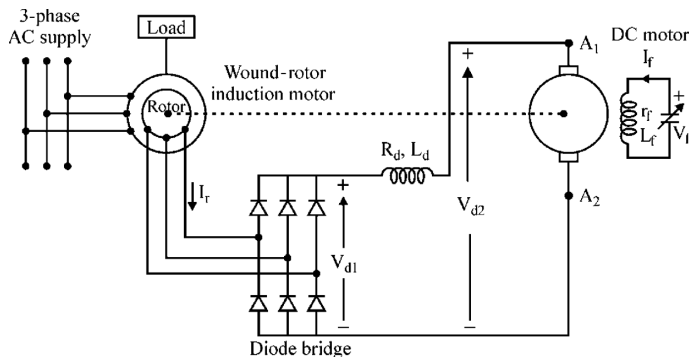


FIGURE 14.25 Static Kramer drive.

14.10.3 STATIC KRAMER DRIVE

Kramer suggested that slip power can be used for the speed control by converting this power into mechanical power of an auxiliary motor (DC or synchronous motor) coupled mechanically with the shaft of the induction motor, as shown in Figure 14.25 [2,3,12]. As shown, the slip power (sP_g) is converted into DC using the diode bridge. This DC power is then fed to the armature of the DC motor, which is coupled with the shaft of the induction motor whose speed has to be controlled. The speed of the induction motor is controlled by controlling the field and the induced voltage of the DC motor as shown in the diagram. The supersynchronous speed control can be achieved by replacing the diode bridge with a six-pulse fully controlled rectifier. As compared to the static Scherbius drive, it has better pf and lower harmonic content. Also, the problems due to feedback of the power back to line are also eliminated.

Presently, static Kramer drive is rarely used due to several problems associated with the DC motors. Instead of this, the modified Kramer drive is employed where the DC motor is replaced by a synchronous motor fed by a load-commutated inverter.

14.11 SOLVED EXAMPLES

Example 14.1: A three-phase induction motor at rated supply voltage and speed has a maximum torque of 2.5 times the full-load torque. It has a starting torque of 1.5 times the full-load torque. Neglect the effect of stator resistance and rotational losses. The rotor resistance remains constant during the above working. Calculate the values of slip at:

1. Full load
2. At maximum torque

$$\frac{T}{T_{\max}} = \frac{\frac{s}{s_{\max T}} + \frac{s_{\max T}}{s}}{2}$$

We know that at starting, the slip $s = 1$ substituting this in above

$$\frac{2.5T_f}{1.5T_f} = \frac{\frac{s_1}{s_{maxT}} + \frac{s_{maxT}}{s_1}}{2}$$

$$\text{or } s_{maxT}^2 - \frac{10}{3}s_{maxT} + 1 = 0$$

This gives $s_{maxT} = 3$ or $1/3$

The greater value is for the braking operation.

So $s_{maxT} = 1/3$

$$\text{Again } \frac{T_{max}}{T_f} = \frac{\frac{1}{3s_f} + \frac{3s_f}{1}}{2}$$

$$\text{or } \frac{1}{3s_f} + \frac{3s_f}{1} = 5$$

$$\text{or } s_f^2 - 10s_f + \frac{1}{9} = 0$$

this gives $s_f = 3.3$ or 0.033

So a possible value of slip is 3.3% . The other value of slip can be discarded.

Example 14.2: The maximum torque in a three-phase induction motor occurs at 20% slip. Calculate the ratio of the starting current with that of a full-load current at 4% slip.

SOLUTION

When the effect of resistance of the stator is neglected, the current at slip s will be

$$I_s = \frac{V}{\sqrt{(R_r/s)^2 + X^2}}$$

The starting current will be

$$I_{st} = \frac{V}{\sqrt{R_r^2 + X^2}}, \quad \frac{I_{st}}{I_s} = \frac{\sqrt{(R_r/s)^2 + X^2}}{\sqrt{R_r^2 + X^2}}$$

For maximum torque, $R_r = s_{maxT}X$

$$\frac{I_{st}}{I_s} = \frac{\sqrt{(s_{maxT}/s)^2 + 1^2}}{\sqrt{s_{maxT}^2 + 1^2}}$$

$$\frac{I_{st}}{I_s} = \frac{\sqrt{(s_{maxT})^2 + s^2}}{\sqrt{s^2(s_{maxT}^2 + 1^2)}}$$

Substituting $s_{maxT} = 0.2$ and $s = 0.04$

$$\frac{I_{st}}{I_s} = \frac{\sqrt{0.2^2 + 0.04^2}}{\sqrt{0.04^2(0.2^2 + 1^2)}} = 5$$

Example 14.3: A three-phase induction motor runs on a rated load, when the slip is 4% and applied voltage is 400 V. It has a slip of 20% at maximum value of torque developed. Calculate the value of slip when the voltage applied to the stator is 300 V. The load torque remains constant.

SOLUTION

The torque T at slip is given by the expression

$$T = \frac{2T_{\max}s \cdot s_{\max T}}{s^2 + s_{\max T}^2}$$

When voltage is reduced to x times the rated voltage, the torque will be reduced by x^2 times, that is,

$$T_x = x^2 T = \frac{2x^2 T_{\max}s \cdot s_{\max T}}{s^2 + s_{\max T}^2}$$

Let the load torque be a function of speed, that is,

$$K_L = K(SPEED)^n = K(1-s)^n$$

Let the slip at the new applied voltage be s_2 , then

$$T = T_L \text{ and } T_L = T_{L2}$$

From these equations

$$\frac{2T_{\max}s \cdot s_{\max T}}{s^2 + s_{\max T}^2} = K(1-s)^n$$

and

$$\frac{2T_{\max}s_2 \cdot s_{\max T}}{s_2^2 + s_{\max T}^2} = K(1-s_2)^n$$

Dividing these equations we obtain

$$\frac{x^2 s_2}{(1-s_2)^n (s_2^2 + s_{\max T}^2)} = \frac{s}{(1-s^2)^n (s^2 + s_{\max T}^2)}$$

In the given problem, $s = 0.4$, $s_{\max T} = 0.2$, $x = 300/400 = 0.75$, and $n = 0$ due to the constant-load torque. Substituting these values we obtain

$$\frac{0.75^2 s_2}{(s_2^2 + 0.2^2)} = \frac{0.04}{(0.04^2 + 0.04)}$$

On simplifying it will be

$$s_2^2 - 0.585s_2 + 0.04 = 0$$

This will give $s_2 = 0.506, 0.079$

$s_2 = 0.079$ will be a stable value, being less than $s_{\max T}$

Example 14.4: The per-unit constants of a three-phase 50-Hz induction motor are $R_s = R_r = 0.02 \Omega$ and $X_s = X_r = 0.1 \Omega$. The motor is operating with constant volts per hertz control when its supply frequency and magnitude of the voltage is made half. Calculate the values of the ratio of the

- i. Maximum value of the torque at new values as compared to that at the rated values
- ii. Starting torque at new values as compared to that at the rated values

SOLUTION

i. The maximum value of torque at the rated value will be

$$T_{\max 1} = \frac{3}{W_s} \frac{V_s^2}{2[R_s + \sqrt{R_s^2 + X^2}]}$$

At half values

$$T_{\max 2} = \frac{3}{W_s/2} \frac{\left(\frac{V_s}{2}\right)^2}{2[R_s + \sqrt{R_s^2 + \left(\frac{X}{4}\right)^2}]}$$

$$\text{The ratio } \frac{T_{\max 2}}{T_{\max 1}} = \frac{[R_s + \sqrt{R_s^2 + X^2}]}{2[R_s + \sqrt{R_s^2 + \left(\frac{X}{4}\right)^2}]} = \frac{[0.02 + \sqrt{0.02^2 + 0.2^2}]}{2[0.02 + \sqrt{0.0004^2 + (0.01)^2}]} = 0.906$$

ii. The starting torque at the rated value will be

$$T_{ST1} = \frac{3V_s^2 R_R}{W_s \left[(R_s + R_R)^2 + X^2 \right]}$$

$$\text{At starting values } T_{ST2} = \frac{3\left(\frac{V_s}{2}\right)^2 R_R}{W_s/2 \left[(R_s + R_R)^2 + \left(\frac{X}{4}\right)^2 \right]}$$

$$\text{The ratio } \frac{T_{ST2}}{T_{ST1}} = \frac{\left[(R_s + R_R)^2 + X^2 \right]}{\left[(R_s + R_R)^2 + \left(\frac{X}{4}\right)^2 \right]} = \frac{\left[(0.04)^2 + 0.2^2 \right]}{2\left[(0.04)^2 + (0.01)^2 \right]} = 1.79$$

Example 14.5: A three-phase, 400-V, 50-Hz, 100-kW, 12-pole, 480-rpm *slip-ring induction motor has both stator and rotor windings as connected in star. The ratio of the stator to rotor turns is 1.2:1. The resistance per phase of the rotor winding is 0.02 Ω. At full-rated speed, the rotor drives a fan load torque that requires 100 kW. The fan load has torque as a function of square of the speed. Calculate the value of resistance to be inserted in the rotor circuit to run the fan load at 350 rpm. Neglect the impedance in the stator circuit and rotation at losses of the motor.*

SOLUTION

$$\text{Synchronous speed of the motor} = 120 \times 50 / 12 = 500 \text{ rpm}$$

$$\text{Slip at full load} = (500 - 480) / 500 = 0.04$$

$$\text{Torque at full load} = \frac{100 \times 1000 \times 60}{2\pi \times 480} = 1989 \text{ Nm}$$

$$\text{Rotor resistance referred to the stator} = 0.02 \times 1.2^2 = 0.0288 \Omega$$

$$T = \frac{3V_s^2 R_r}{\omega_s s \left[\left(\frac{R_r}{s} \right)^2 + X^2 \right]} = 1989$$

$$\Rightarrow 1989 = \frac{3 \left(\frac{400}{\sqrt{3}} \right)^2 \times 0.0288}{2\pi \times \frac{500}{60} \times 0.04 \left[\left(\frac{0.0288}{0.04} \right)^2 + X^2 \right]} \Rightarrow X^2 = \frac{4568}{(2.1 \times 1989)} - 0.5184 = 0.5756$$

$$\Rightarrow X = 0.76 \Omega$$

$$\text{Slip at 350 rpm} = \frac{500 - 350}{500} = 0.3$$

Let the slip rotor resistance be R_{r_2} .

The torque will be

$$\frac{T_1}{T_2} = \left(\frac{N_1}{N_2} \right)^2 = \left(\frac{480}{350} \right)^2 = \frac{s_2 \left[\left(\frac{R_{r_2}}{s_2} \right)^2 + X^2 \right] R_r}{s_1 \left[\left(\frac{R_r}{s_1} \right)^2 + X^2 \right] R_{r_2}} = \frac{0.03 \left[\left(\frac{R_{r_2}}{0.03} \right)^2 + 0.5756 \right] 0.0288}{0.04 \left[\left(\frac{0.0288}{0.04} \right)^2 + 0.5756 \right] R_{r_2}} = 1.88$$

$$\Rightarrow R_{r_2}^2 - 0.86R_{r_2} + 0.052 = 0$$

This will give $R_{r_2} = 0.8 \Omega$ or 0.06Ω

The second answer is less than the original rotor resistance, so it is ignored. The external resistance to be added in each slip ring to obtain the speed of 350 rpm will be $\frac{0.8 - 0.0288}{1.2^2} = 0.54 \Omega$.

REVIEW AND UNSOLVED QUESTIONS

- 14.1 Mention the advantages of the squirrel-cage induction motor over DC motors.
- 14.2 A 440-V, 50-Hz, six-pole, star-connected induction motor has the following parameters per phase referred to the stator: $R_s = R_r' = 0.4 \Omega$, and $X_s = X_r' = 1.0 \Omega$, $X_m = 50 \Omega$, normal full-load slip = 0.04. Determine (i) motor current, torque, and efficiency at normal full-load slip, (ii) maximum torque, and (iii) speed at which the maximum torque occurs.
- 14.3 Derive an equivalent circuit and torque expression for a delta-connected induction motor.
- 14.4 What are the effects of a non-sinusoidal supply on a squirrel-cage induction motor?
- 14.5 When operating in regenerative braking mode, the induction motor slip should not be allowed to exceed the breakdown slip. Why?
- 14.6 Why is it necessary to disconnect the induction motor from the supply when the speed reaches close to zero during the plugging operation?
- 14.7 Why is an external resistance inserted into the rotor circuit of a wound-rotor induction motor during the plugging operation?
- 14.8 Derive an equivalent circuit for the DC dynamic braking of an induction motor.
- 14.9 What are the important features of the DC dynamic braking in relation to other methods of braking of induction motors?
- 14.10 Why is the V/f ratio maintained constant for the variable-frequency control of the induction motor for speeds below the base speed?
- 14.11 Why is the terminal voltage maintained constant for variable-frequency control of the induction motor for speeds above the base speed?
- 14.12 Why is the variable-frequency control of the induction motor more efficient than the stator-voltage control?

SUMMARY

AC drives have several advantages over DC drives, such as being cheaper, 30% lighter, and low maintenance. However, AC drives need complex and advanced control techniques. These require controls of voltage, frequency, and current for several domestic and industrial applications. The power converters, AC voltage controllers, cycloconverters, and inverters are used to control the voltage, frequency, and current to meet the drive requirements.

REFERENCES

1. B. K. Bose, *Power Electronics and AC Drives*, Prentice Hall, Englewood Cliffs, NJ, 1986.
2. M. H. Rashid, *Power Electronics: Circuits, Devices, and Applications*, Pearson Education, Singapore, 2004.
3. N. Mohan, T. M. Undeland, and W. P. Robbins, *Power Electronics: Converters, Applications and Design*, John Wiley & Sons, Hoboken, NJ, 1996.
4. P. T. Krein, *Elements of Power Electronics*, Oxford University Press, New York, 2003.

5. K. Thorborg, *Power Electronics*, Prentice Hall International, London, UK, 1988.
6. P. S. Bhimra, *Power Electronics*, 5th edn., Khanna Publications, New Delhi, India, 2012.
7. I. Batarseh and A. Harb, *Power Electronics*, Springer Nature, Cham, Switzerland, 2018.
8. K. M. Smedley and E. Santi, *AC-DC Power Converters*, Wiley, Hoboken, NJ, 1999.
9. R. W. Erickson, *Fundamentals of Power Electronics*, Springer, New York, 2001.
10. B. Wu, *High-Power Converters and AC Drives*, John Wiley & Sons, Hoboken, NJ, 2017.
11. V. R. Moorthi, *Power Electronics Devices, Circuits and Industrial Applications*, Oxford University Press, Oxford, UK, 2010.
12. G. K. Dubey, *Fundamentals of Electrical Drives*, Alpha Science International Limited, Pangbourne, UK, 2001.
13. A. M. Trzynadlowski, *Introduction to Modern Power Electronics*, 3rd edn., John Wiley & Sons, Hoboken, NJ, 2010.
14. M. Trzynadlowski, *Power Electronic Converters and Systems*, Institution of Engineering and Technology, London, UK, 2016.
15. B. M. Wilamowski and J. D. Irwin, *Power Electronics and Motor Drives*, CRC Press, Boca Raton, FL, 2011.
16. E. Acha, V. G. Agelidis, O. Anaya-Lara, and T. J. E. Miller, *Power Electronic Control in Electrical Systems*, Newnes, Oxford, UK, 2002.
17. F. Mazda, *Power Electronics Handbook*, Newnes, Oxford, UK, 1997.
18. F. Blaabjerg, *Control of Power Electronic Converters and Systems*, Academic Publishers, London, UK, 2018.
19. S. N. Manias, *Power Electronics and Motor Drive Systems*, Academic Publishers, Amsterdam, the Netherlands, 2017.



Taylor & Francis

Taylor & Francis Group

<http://taylorandfrancis.com>

15 FPGA-Based Fuzzy-Logic Control of DTC for Matrix-Converter-Fed Induction-Motor Drives

15.1 INTRODUCTION

The use of the electric motor has increased tremendously due to its simple construction, low cost, and easy maintenance with good reliability. Worldwide, it consumes around 45% of the total consumption of electricity. The three-phase induction motor (IM) is very popular and commonly used in various applications in around 60% of the total domestic and industrial loads. It almost accounts for 70% of the total electricity consumption. DC motors are also used but have the disadvantages of brushes and commutators, which need timely maintenance and replacement [1,2].

Variable-speed drives (VSDs) are generally used to control the speed with high efficiency and performance. These drives make extensive use of different controllers and switching techniques. The pulse-width modulation (PWM) and space vector pulse-width modulation (SVPWM) switching techniques are used to control and regulate the frequency and output voltage of the drive. These switching techniques have the ability to reduce the harmonic content, low switching losses, and produce more output power with satisfactory performance. To reduce complex online computation, artificial neural network (ANN)-, adaptive neuro fuzzy inference system (ANFIS)-, and fuzzy logic controller (FLC)-based SVPWM are also used [3–13]. The power modulator of the drive consists of controlled semiconductor devices, such as the insulated-gate bipolar transistor (IGBT) and metal-oxide semiconductor field-effect transistor (MOSFET), which are capable of controlling the parameters of the motor.

15.2 VARIOUS CONTROLLERS FOR INDUCTION MOTOR DRIVES

Apart from the conventional controllers (proportional integral derivative [PID], proportional integral [PD], and proportional integral [PI]), the microcontrollers, digital signal processors (DSPs), field-programmable gate arrays (FPGAs), dSPACE and other integrated circuits are used as controller platforms to design the IM controllers to regulate the motor variables such as flux, voltage, torque, and speed with quick response [3–13]. Among different types of conventional controllers, the PID controller is the widely used controller due to its easy design being more efficient, cheaper, and simple in structure. These conventional controllers have major drawbacks, such as performance sensitivity to variations in system parameters, and so

TABLE 15.1
Comparison of Different Controller Schemes for Three-Phase IM Drive

S. No.	Parameter	Conventional Controller	ANN Controller	FLC Controller	ANFIS Controller
1.	Structure	Simple	Normal	Simple	Complex
2.	Design	Easy	Moderate	Easy	Moderate
3.	Requirement of mathematical modeling	Yes	No	No	No
4.	Performance	Good	Good	Strong	Good
5.	Needs a learning step	No	Yes	No	Yes

with fixed-gain controllers, it may not provide the required speed performance, which generally results in overshoot/undershoot in speed response.

In order to overcome these challenges, ANN, ANFIS, and FLC controllers have been used for motion control of the IM drive. ANN and ANFIS are used as intelligent controllers to estimate the parameters, to detect faults, and estimate the speed and torque of the IM drive [8–12]. Fuzzy-logic controllers are used to improve *v/f* control and improve dynamic response of induction motor. Table 15.1 presents the comparative performance among conventional and artificial intelligence (AI)-based controllers for the three-phase induction motor drive.

The main advantage of FLC when compared to the conventional controller is that no mathematical model is required for the controller design. Fuzzy logic has been successfully used to control complex systems where precise modeling is difficult or impossible.

15.3 INTEGRATED CIRCUITS FOR IM DRIVES

Integrated circuits such as microcontrollers, DSPs, FPGAs, and the dSPACE are widely used to implement control systems experimentally for IM drives [1,10–13]. The detailed comparison among different integrated circuits for IM drives is presented in Table 15.2.

TABLE 15.2
Comparison of Different Integrated Circuits

S. No.	Parameter	Microcontrollers	DSPs	FPGAs	dSPACE
1.	Cost	Low	Low	High	High
2.	Processor	Medium	Fast	Fast	Fast
3.	Operation	Standalone	Standalone	Require PC	Require PC
4.	Memory	Low	High	High	High
5.	Compatibility with MATLAB	Few versions only	All versions	All versions	All versions

An FPGA consists of an array of logic blocks or configurable logic blocks (CLB) that can be programmed and connected to achieve different designs. Presently available commercial FPGAs make extensive use of logic blocks, which are based on transistor pairs, basic small gates (two-input NANDs and exclusive-ORs), multiplexers, look-up tables, and wide fan-in AND-OR structures. Reprogramming of FPGAs is achieved through electrically programmable switches using one of three main technologies, that is, static RAM (SRAM), antifuse, and floating gate. The design process of an FPGA consists of three main stages:

1. Logic design and simulation
2. Placement, routing, and connectivity check
3. Programming

There are three main advantages of an FPGA over a microprocessor chip for controller designing:

1. It operates faster than a microprocessor chip.
2. The new FPGAs support the hardware that is upwards of one million gates, and this increases the program capacity of the FPGAs.
3. Additional functionality and user interface controls can be incorporated into the FPGA, which minimizes the requirements for additional external components.

15.4 DETAILS OF IM DRIVE UNDER INVESTIGATION

Figure 15.1 illustrates the block diagram of the fuzzy-logic controller-based direct-torque control (DTC) matrix converter (MC)-fed IM drive. The control system is implemented using the Altium nanoboard 3000, which is mainly based on Xilinx Spartan XC3S1400an-FGG676 FPGA using MATLAB/Simulink. The actual motor

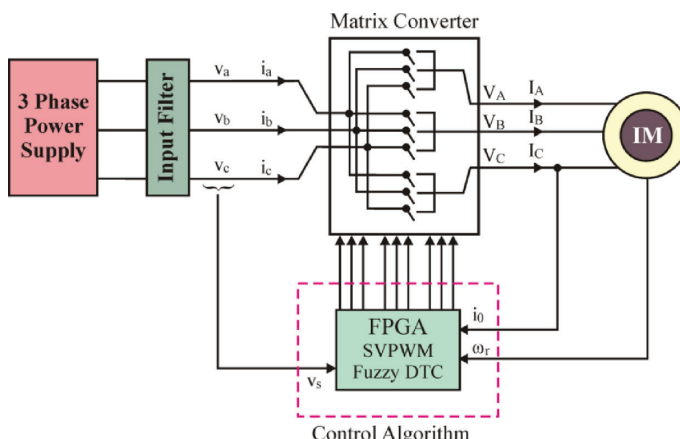


FIGURE 15.1 Block diagram of developed FLC-based DTC-controlled MC-fed IM drive.

currents are measured by current sensors and fed back to the FPGA board through the A/D channels. The rotor position is sensed by an optical incremental encoder and is fed back to the FPGA board through the encoder interface. The outputs of the FPGA board are SVPWM logic signals, which are sent to the MC switches through driver circuitry.

15.4.1 DIRECT-TORQUE CONTROL FOR MATRIX-CONVERTER-FED INDUCTION-MOTOR DRIVE

The DTC scheme controls the stator flux and electromagnetic torque independently at the same time. For the MC, the DTC is developed from the conventional DTC for the voltage source inverter (VSI). There are six switching configurations for any selected VSI output vector, and these six switching configurations can be applied to the MC to generate the same output voltage vector, as shown in Figure 15.2a, and six input current vectors for every sector having different directions as shown in Figure 15.2b.

The possible switching configurations (SCs) in a 3×3 MC are 27. Out of these, in first six configurations, each output phase is connected to a different input phase. In the next 18 configurations, the two output phases among three are shorted, and in the final three configurations the three output phases are short-circuited. Twenty-one out of these 27 configurations are useful. The switching configurations of the MC and look-up table for selecting output vector are shown in Tables 15.3 and 15.4, respectively.

Figure 15.3 shows the block diagram of the DTC scheme for the MC. A two-level hysteresis comparator is used for flux error, and for electromagnetic torque error, a three-level hysteresis comparator is used because the DTC scheme allows the motor to run in all four quadrants.

Further, when the input current is lying in Sector 1, the SC +1 is applied when the average value of $\sin \phi_i$ has to be increased, and when the average value of $\sin \phi_i$ is to be decreased, SC -3 is applied. Table 15.5 presents the SCs for the DTC MC.

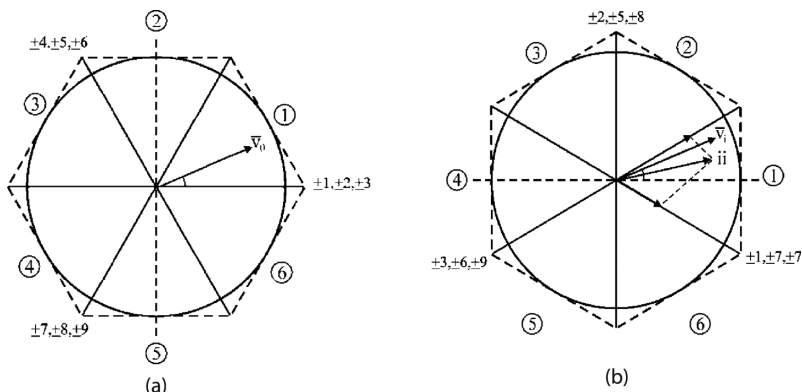


FIGURE 15.2 (a) Output voltage vector and (b) input current vector.

TABLE 15.3
Switching Configuration of the Matrix Converter

Switching Configuration	A B C	V_o	α_{vo}	I_i	β_{in}
+1	a b b	$2/3v_{ab}$	0	$2/\sqrt{3} i_A$	$-\pi/6$
-1	b a a	$-2/3v_{ab}$	0	$-2/\sqrt{3} i_A$	$-\pi/6$
+2	b c c	$2/3v_{bc}$	0	$2/\sqrt{3} i_A$	$\pi/2$
-2	c b b	$-2/3v_{bc}$	0	$-2/\sqrt{3} i_A$	$\pi/2$
+3	c a a	$2/3v_{ca}$	0	$2/\sqrt{3} i_A$	$7\pi/6$
-3	a c c	$-2/3v_{ca}$	0	$-2/\sqrt{3} i_A$	$7\pi/6$
+4	b a b	$2/3v_{ab}$	$2\pi/3$	$2/\sqrt{3} i_B$	$-\pi/6$
-4	b a a	$-2/3v_{ab}$	$2\pi/3$	$-2/\sqrt{3} i_B$	$-\pi/6$
+5	b c b	$2/3v_{bc}$	$2\pi/3$	$2/\sqrt{3} i_B$	$\pi/2$
-5	c b c	$-2/3v_{bc}$	$2\pi/3$	$-2/\sqrt{3} i_B$	$\pi/2$
+6	a c a	$2/3v_{ca}$	$2\pi/3$	$2/\sqrt{3} i_B$	$7\pi/6$
-6	c a c	$-2/3v_{ca}$	$2\pi/3$	$-2/\sqrt{3} i_B$	$7\pi/6$
+7	b b a	$2/3v_{ab}$	$4\pi/3$	$2/\sqrt{3} i_C$	$-\pi/6$
-7	a a b	$-2/3v_{ab}$	$4\pi/3$	$-2/\sqrt{3} i_C$	$-\pi/6$
+8	c c b	$2/3v_{bc}$	$4\pi/3$	$2/\sqrt{3} i_C$	$\pi/2$
-8	b b c	$-2/3v_{bc}$	$4\pi/3$	$-2/\sqrt{3} i_C$	$\pi/2$
+9	a a c	$2/3v_{ca}$	$4\pi/3$	$2/\sqrt{3} i_C$	$7\pi/6$
-9	c c a	$-2/3v_{ca}$	$4\pi/3$	$-2/\sqrt{3} i_C$	$7\pi/6$
0 _a	a a a	0	—	0	—
0 _b	b b b	0	—	0	—
0 _c	c c c	0	—	0	—

TABLE 15.4
Look-Up Table for Selecting Output Vector

Sector of Stator Flux	I	II	III	IV	V	VI
$C_{Flux} = -1$	$C_{Torque} = -1$	V_2	V_3	V_4	V_5	V_6
	$C_{Torque} = 0$	V_7	V_0	V_7	V_0	V_7
	$C_{Torque} = 1$	V_6	V_1	V_2	V_3	V_4
$C_{Flux} = 1$	$C_{Torque} = -1$	V_3	V_4	V_5	V_6	V_1
	$C_{Torque} = 0$	V_0	V_7	V_0	V_7	V_0
	$C_{Torque} = 1$	V_5	V_6	V_1	V_2	V_4

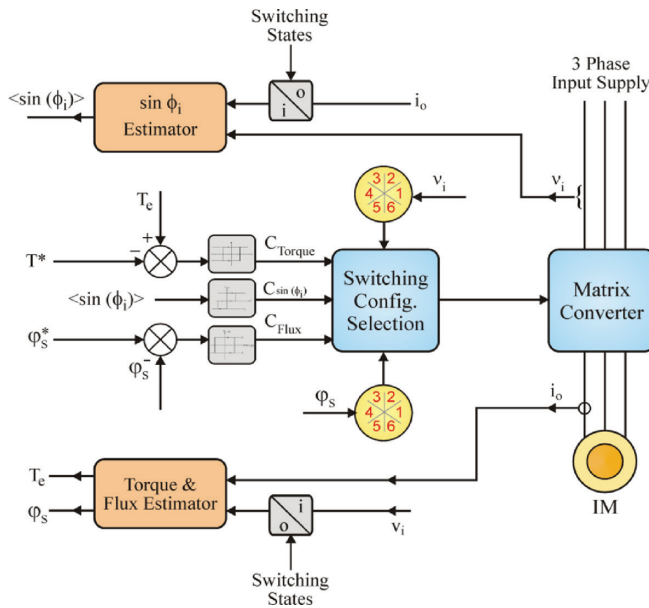


FIGURE 15.3 Block diagram of the DTC scheme for the MC-fed IM drive.

TABLE 15.5
Switching Configurations for DTC-Controlled Matrix Converter

Sectors of Input

Voltage Vector	I	II	III	IV	V	VI
$C_{\sin(\phi)}$	+1	-1	+1	-1	+1	-1
Output Vector (Inverter Stage of MC)	V_1	-3	+1	+2	-3	-1
V_2	+9	-7	-8	+9	+7	-8
V_3	-6	+4	+5	-6	-4	+5
V_4	+3	-1	-2	+3	+1	-2
V_5	-9	+7	+8	-9	-7	+8
V_6	+6	-4	-5	+6	+4	-5

15.4.2 ESTIMATION OF FLUX AND ELECTROMAGNETIC TORQUE

The stator flux linkage can be estimated by integrating the stator voltage:

$$\varphi_s = \int (v_s - i_s R_s) dt \quad (15.1)$$

$$\varphi_{ds} = \int (v_{ds} - i_{ds} R_s) dt \quad (15.2)$$

$$\varphi_{qs} = \int (v_{qs} - i_{qs} R_s) dt \quad (15.3)$$

$$\varphi_s = \sqrt{\varphi_{ds}^2 + \varphi_{qs}^2} \quad (15.4)$$

In high-power motors, the stator resistance is very small as compare to the inductance because the IM is an inductive load; therefore, the voltage drop on stator resistance is neglected. For a short period of Δt , the preceding equation can be written as:

$$\Delta\varphi_s = V_s \Delta t \quad (15.5)$$

It is seen from the preceding equation that by selecting the appropriate voltage vector, the stator flux can be controlled directly. The electromagnetic torque can be estimated using the stator flux linkage and motor current vector.

$$T_e = \left(\frac{3}{2}\right) \left(\frac{P}{2}\right) (\varphi_{ds} i_{qs} - \varphi_{qs} i_{ds}) \quad (15.6)$$

$$T_e = \left(\frac{3}{2}\right) \left(\frac{P}{2}\right) \frac{L_m}{L_r L_s} |\varphi_r| |\varphi_s| \sin \lambda \quad (15.7)$$

where λ is difference between stator flux and rotor flux angle. The screenshot of the simulation in MATLAB of the developed system is shown in [Figure 15.4](#).

15.4.3 DEVELOPMENT OF DEVELOPED FUZZY-LOGIC CONTROLLER

The DTC method is simple to implement, and it gives a fast response. In addition to these advantages, there are some drawbacks of the DTC scheme, for example, higher electromagnetic torque and stator flux ripples. This problem in DTC occurs because none of the switching vectors produce the exact voltage, which is required to desire change in flux and torque. The fuzzy-logic-based DTC developed here overcomes these drawbacks. The Mamdani-type fuzzy-logic controller is used to adjust the torque hysteresis band to reduce the ripples in the torque. The general structure of the fuzzy-logic controller is shown in [Figure 15.5](#). The design of the fuzzy-logic controller is achieved by observing the results of the conventional method of DTC. The block diagram of the developed fuzzy-logic controller is shown in [Figure 15.6](#).

The fuzzy-logic controller controls the lower and upper limits of the torque hysteresis band results, and the torque ripples are minimized in the developed scheme. The fuzzy-logic controller has two inputs: one is change in torque (ΔT_e) and another is change in stator current (ΔI_s). There are five membership functions for input (ΔT_e), and for another input change in stator current (ΔI_s) there are five membership functions.

The flux linkage of stator is directly proportional to the stator current. Here, the difference between the present and previous sample estimated motor electromagnetic torque (ΔT_e) and the difference between the present and previous sample of

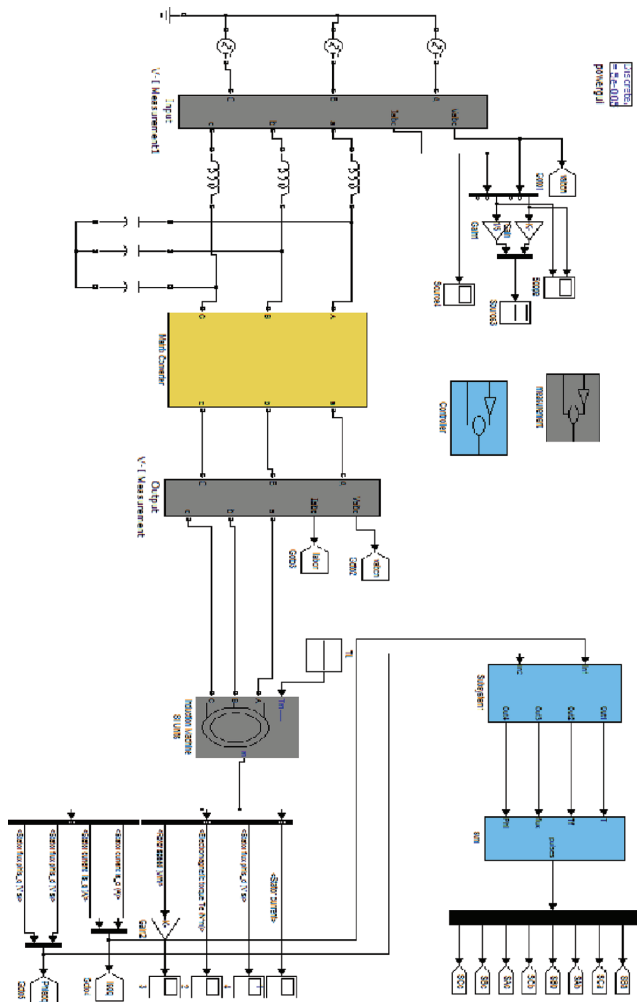


FIGURE 15.4 Simulink block diagram of the developed FLC-based DTC-controlled MC-fed IM drive.

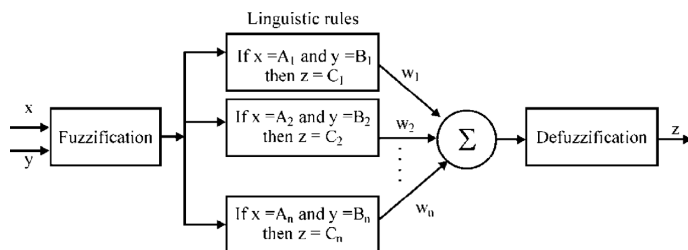


FIGURE 15.5 General structure of Fuzzy logic controller considering x and y as inputs and z is output.



FIGURE 15.6 Schematic diagram of developed FLC.

stator current (ΔI_s) are taken as the inputs of the fuzzy-logic controller. These variations in estimated motor electromagnetic torque and stator current can be defined as:

$$\Delta T_e = T_e[n] - T_e[n-1] \quad (15.8)$$

$$\Delta I_s = I_s[n] - I_s[n-1] \quad (15.9)$$

The five membership functions for input ΔT_e are: negative large (NL), negative small (NS), zero (ZO), positive small (PS), and positive large (PL) as shown in [Figure 15.7a](#). The membership function of the input stator current error (ΔI_s) is represented by five fuzzy sets: NL, NS, ZO, PS, PL as shown in [Figure 15.7b](#). The membership functions of the output are shown in [Figure 15.7c](#). The fuzzy sets and the respective membership function for the input variables are given in [Table 15.6](#). The fuzzy sets and the respective membership function for the output variable is given in [Tables 15.7](#) and [15.8](#).

It can be observed from the fundamental torque equation of the IM that the ripples in the speed of the motor can be reduced directly by reducing the ripples in electromagnetic torque. The change in torque hysteresis band is considered as the output of the fuzzy-logic controller. Therefore, the upper band and lower band of torque hysteresis controller are adjusted with output of the fuzzy-logic controller in such a way that the ripples in electromagnetic torque becomes minimum, which further minimizes the ripples in the motor speed to get the smooth speed of the IM.

15.4.4 CONTROL IMPLEMENTATION ON THE FPGA BOARD

The hardware implementation of the developed controller is done using the Altium nanoboard 3000, which is mainly based on Xilinx Spartan XC3S1400an-FGG676 FPGA. In the experimental design process of the controller, the model of the developed controller is designed in MATLAB/Simulink using XSG (Xilinx System Generator) block set and converted in (VHSIC-HDL) Very High Speed Integrated Circuit Hardware Description Language (VHDL) code using Xilinx software, because the FPGA board is compatible with VHDL code. The experimental block diagram of the developed system is shown in [Figure 15.3](#), and a snapshot of real-time setup is shown in [Figure 15.8](#).

VHDL code is loaded in the FPGA board using Altium designer software. Altium designer software also provides communication between the FPGA board and computer for controlling command and analysis of performances. The results were recorded using the RS232, USB 2.0 and an oscilloscope. The harmonics spectrums in transient conditions have also been experimentally recorded with the help

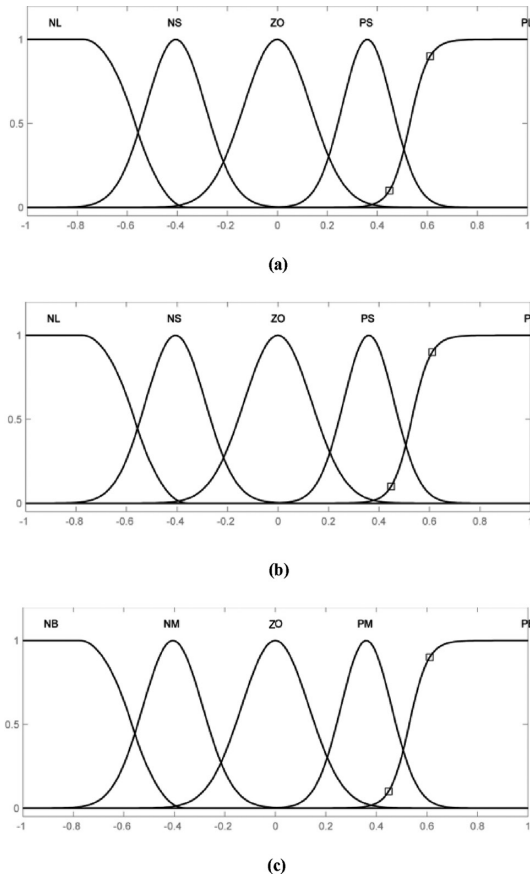


FIGURE 15.7 Membership function for fuzzy-logic controls: (a) input variables ΔT_e , (b) input variables (ΔI_s) , and (c) output variables ΔC_{TH} .

TABLE 15.6
Fuzzy Sets and the Respective Membership Function for the Input Variables

Fuzzy Set or Label	Set Description	Ranges	Membership Function
NL (negative large)	Error is large in the negative direction	-1.0 to -1.0 -1.0 to -0.4	Gaussian
NS (negative small)	Error is small in the negative direction	-0.7 to -0.4 -0.4 to 0.0	Gaussian
ZO (zero)	Error is approximately zero	-0.4 to 0.0 0.0 to 0.4	Gaussian
PS (positive small)	Error is small in the positive direction	0.0 to 0.4 0.4 to 0.7	Gaussian
PL (positive large)	Error is large in the positive direction	0.4 to 1 1 to 1	Gaussian

TABLE 15.7
Fuzzy Sets and the Respective Membership Function for the Output Variable (ΔC_{TH})

Fuzzy Set or Label	Ranges	Membership Function
NB (negative big)	-1.0 to -1.0 -1.0 to -0.4	Gaussian
NM (negative medium)	-0.7 to -0.4 -0.4 to 0.0	Gaussian
ZZ (zero)	-0.4 to 0.0 0.0 to 0.4	Gaussian
PM (positive medium)	0.0 to 0.4 0.4 to 0.7	Gaussian
PB (positive big)	0.4 to 1 1 to 1	Gaussian

TABLE 15.8
Fuzzy Rule Table for Output

ΔI_s	ΔT_e	NL	NS	Z0	PS	PL
NL	NB	NB	NB	ZZ	PM	PB
NS	NB	NM	NM	ZZ	PM	PB
Z0	NB	NM	NM	ZZ	PM	PB
PS	NB	NM	NM	ZZ	PM	PB
PL	NB	NM	NM	ZZ	PB	PB

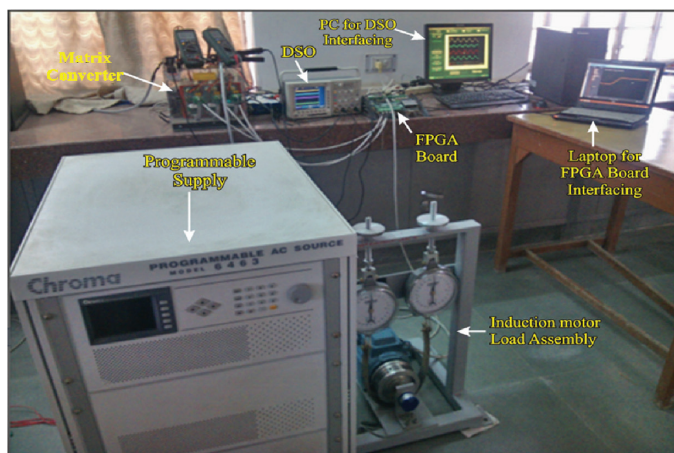


FIGURE 15.8 Experimental setup for hardware implementation.

of an fast Fourier transform (FFT) analyzer facility of the storage oscilloscope. The four-step commutation technique, which is commonly used, is implemented in the FPGA using a finite-state machine. On the basis of the datasheet and characteristics of the power semiconductor device used in the direct MC, the delay time between each step is considered as $1.5 \mu\text{s}$.

15.5 SIMULATION RESULTS OF PERFORMANCE COMPARISON BETWEEN DEVELOPED FUZZY-LOGIC DTC-CONTROLLER-BASED IM DRIVE AND CONVENTIONAL DTC-BASED IM DRIVE

The developed fuzzy-logic DTC (FLDTC)-based MC-fed IM drive is simulated in MATLAB/Simulink using an IGBT-based MC and sampling time of $2 \mu\text{s}$. The input-phase voltage of the MC is taken a 230 V, and the frequency of the input is 50 Hz. The reference speed is considered 100 rad/sec.

15.5.1 RESPONSE OF THE SYSTEM AT CONSTANT REFERENCE SPEED 100 RAD/s AND NO-LOAD CONDITION

The desired speed is considered 100 rad/sec and load torque is taken at 0 N-m to test the steady-state performance of the developed system at no load, and the comparison is shown between the conventional DTC and the developed FLDTC-based IM drive. [Figure 15.9](#) shows the simulated starting speed performance of the drive with and without fuzzy-logic control. It is observed from [Figure 15.10](#) that the developed FLDTC-based system reaches its steady-state condition in 0.18 s, while the conventional DTC-based system settles down in 0.21 s.

The developed controller yields a faster response. The maximum variation in speed is 1.2 rad/s in the case of the conventional DTC, whereas the maximum variation in speed is 0.8 rad/s in the developed system. The variations in speed is less in the developed FLDTC-based IM drive, resulting lower vibrations in the motor. The rotor-flux response is shown in [Figure 15.11](#).

The electromagnetic torque and speed of the IM are compared in the case of the developed controller and conventional controller in [Figure 15.12](#). It is seen that the response of the system with the developed controller is fast.

15.5.2 RESPONSE OF THE SYSTEM WITH REFERENCE SPEED REVERSAL AT NO-LOAD CONDITION

In this case, the speed reversal is initiated at 0.5 s at the no-load condition. The speed decreases until zero speed is reached, and it starts in the reverse direction and settles down to the desired speed 80 rad/s in the reverse direction. The speed performance of the drive with the conventional DTC-based controller and with the developed FLDTC-based IM drive is shown in [Figure 15.13](#). The large magnitudes of the currents are produced during speed reversal in order to produce large electromagnetic torque. It can be seen from [Figure 15.13](#) that the desired speed achieved

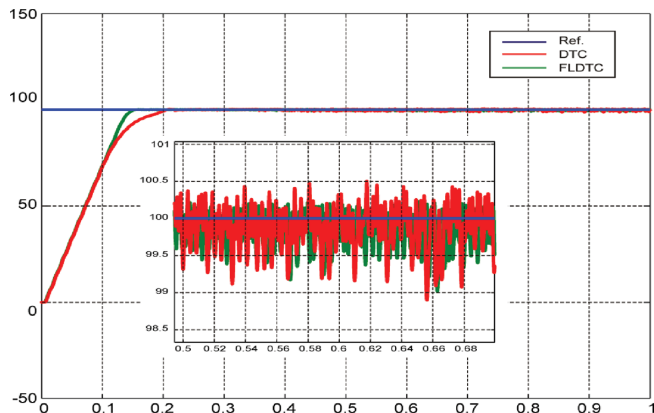


FIGURE 15.9 Simulated speed response of IM drive with developed FLDTC controller and conventional DTC controller without fuzzy logic at constant reference speed at no-load condition.

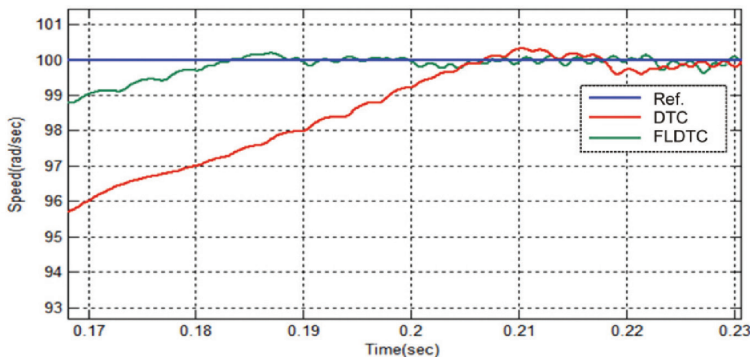


FIGURE 15.10 Simulated starting-speed response of IM drive with developed FLDTC controller and conventional DTC controller without fuzzy logic at constant reference speed at no-load condition.

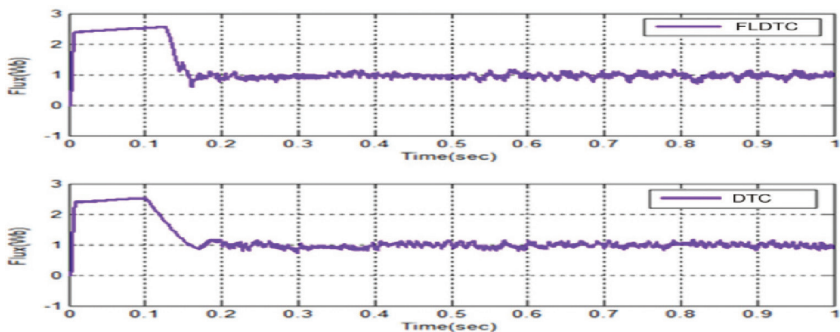


FIGURE 15.11 Simulated flux response of with and without fuzzy-logic-control-based IM drive at constant reference speed and no load.

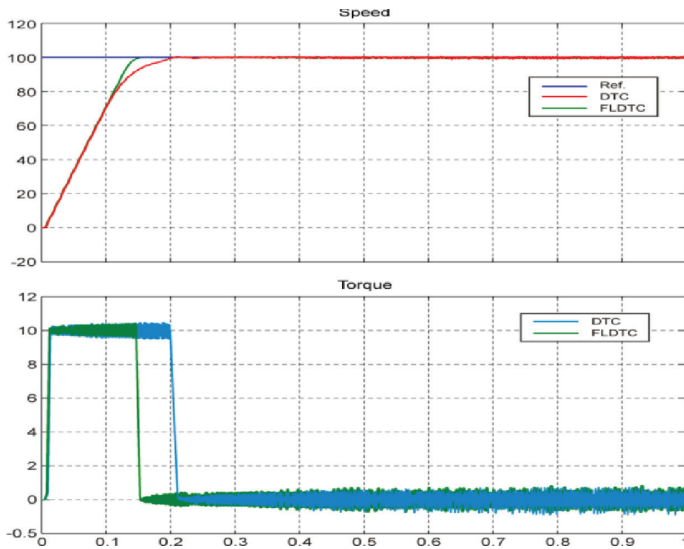


FIGURE 15.12 Comparison of speed and electromagnetic torque of IM with developed controller and conventional controller.

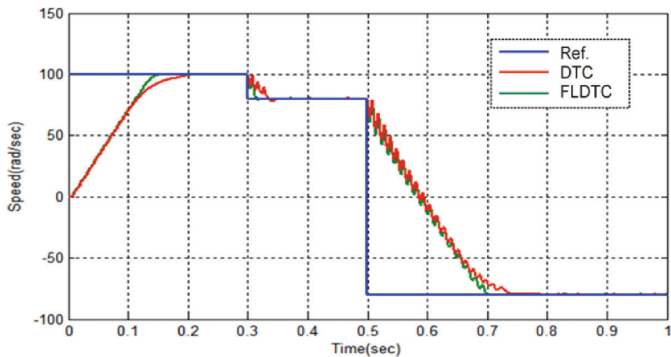


FIGURE 15.13 Simulated speed response of with and without fuzzy-controller-based IM drive at reference speed reversal and no-load condition.

with conventional DTC-based controller is at 0.72 s, whereas the motor achieves the desired speed at 0.7 s with a developed FLDTC-based controller.

The performance of the drive with the developed controller is better than the conventional controller because the time of speed reversal is less with the developed controller. The comparative rotor flux and electromagnetic torque response during 0.5 s to 0.7 s at the speed reversal are shown in Figures 15.14 and 15.15, respectively.

The total harmonic distortion (THD) in the stator current using the conventional DTC-based controller is 11.5%, whereas the THD using the developed FLDTC-based controller is 2.1%. The developed FLDTC-based controller yields the better performance as compare to the conventional as shown in Table 15.9.

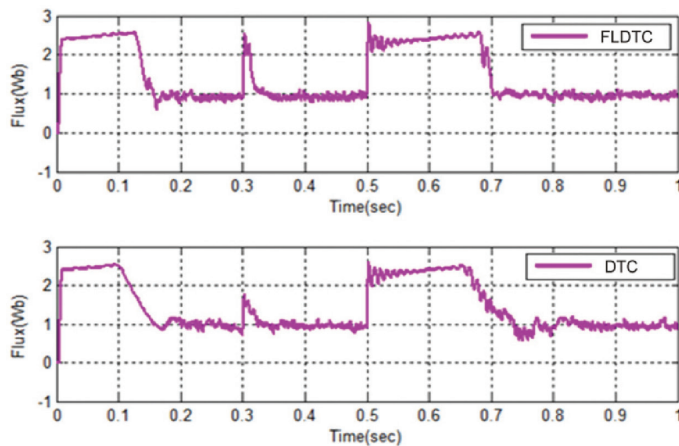


FIGURE 15.14 Simulated flux response of IM with conventional DTC and with developed controller in the case of speed reversal at no-load condition.

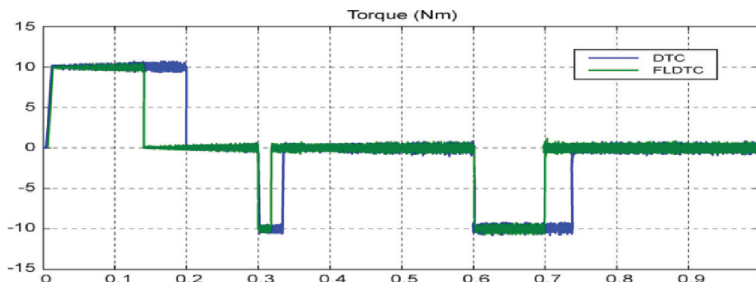


FIGURE 15.15 Simulated electromagnetic torque response of IM drive with developed controller and with conventional DTC in the case of speed reversal at no-load condition.

TABLE 15.9

Summary of the Simulated Response with Fuzzy-Logic Controller and Conventional Controller-based IM Drive

Measured Value	Developed FLDTC-Based IM Drive	Conventional DTC-Based IM Drive
Settling time(s) at starting and no-load condition	0.17	0.2
Settling time(s) at step change in speed and no-load condition	0.05	0.07
Speed fluctuations (rad/s) while change in speed at 1 N-m load	0.5	3
Speed variation (rad/s) while change in load	0.1	5

15.6 EXPERIMENTAL RESULTS OF DEVELOPED FLDTC-BASED MC-FED IM DRIVE

The developed fuzzy-logic controls for the DTC of the MC-fed IM drive has been validated through detailed experimentation under different conditions. Some of the cases are discussed as follows.

15.6.1 RESPONSE OF THE DRIVE WITH CONSTANT REFERENCE SPEED (500 RPM) AT NO-LOAD CONDITION

The starting performance of the FLDTC-based IM drive is taken at 500 rpm reference speed and no-load condition. The speed of the IM settles down in very small time duration and tracks the actual speed using a developed control scheme as shown in [Figure 15.16](#). The stator current of the IM during starting is shown in [Figure 15.17](#), where it is observed that the stator current during starting is high, and it decreases as the speed of the IM is settled down to the desired speed. The experimental waveforms of the input supply-line voltage (V_s), input supply-phase current (I_s), MC output-line voltage (V_o), and output phase current (I_o) are shown in [Figure 15.18](#).

15.6.2 STABILITY ANALYSIS OF THE DEVELOPED SYSTEM

The response of the system, in terms of stability, has been analyzed for different values of the voltage transfer ratio (q). The results obtained are presented in [Figures 15.19–15.24](#). As can be seen, voltage and current waveforms are practically sinusoidal and have small ripples. The waveform of the load current is also sinusoidal except initial large oscillations. The behavior of the system has been tested for sudden change in load and frequency. The harmonic components are practically negligible. A power-quality analyzer has been connected to the input side of the MC drive in order to determine the input power. Here, it can be validated that operation of the MC at the rated motor torque is excellent with sinusoidal input/output currents and negligible low-frequency harmonics. The measured THD of the input current is in the range of 2.1%–2.4%, while the input voltage THD is 1.1%.

15.6.3 HARMONIC ANALYSIS

In this section, the harmonic analysis is done in the case of the steady state as well as transient conditions to test the performance of the MC in terms of input-current quality. It is shown with the results that the developed FLDTC-based controller effectively improves the input current waveform. Also, the experimental results show better performance in steady-state conditions.

It can be seen from the FFT analysis from [Figures 15.25](#) to [15.27](#) that there are some fifth and seventh-order harmonics in the output voltage. There also exists switching-frequency harmonics of 4.2 kHz. [Figures 15.28–15.30](#) show the harmonic spectrum of the input/output current and voltage, which reveals practically very few ripples. It can be seen that the experimental results show good performance in steady-state as well as transient conditions. Results show that with the

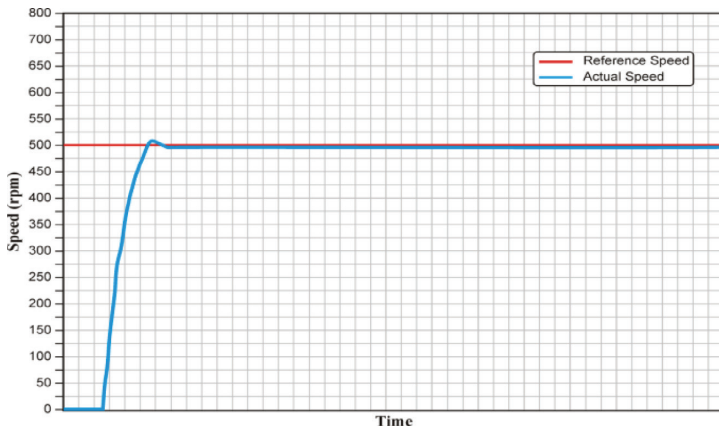


FIGURE 15.16 Speed response of IM using developed FLDTC-based controller with constant reference speed and at no load.

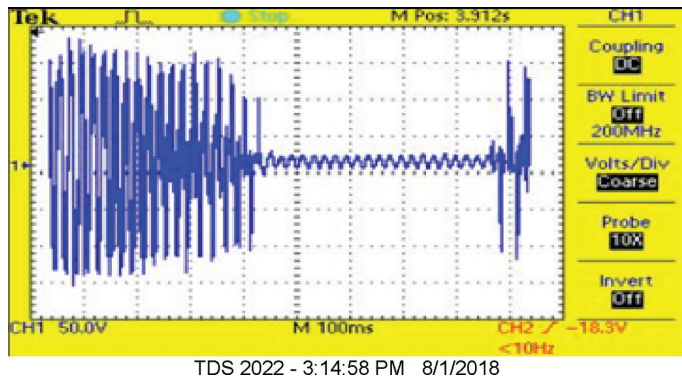


FIGURE 15.17 Stator current of the IM.

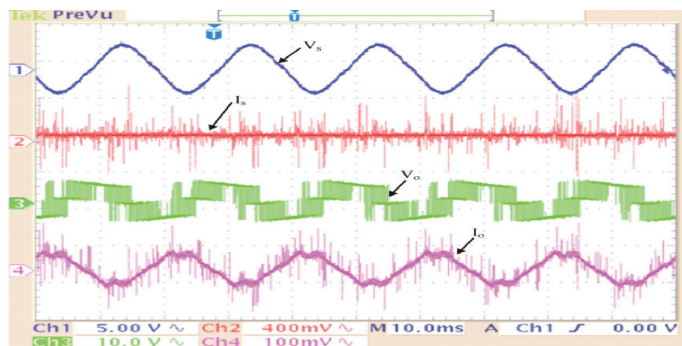
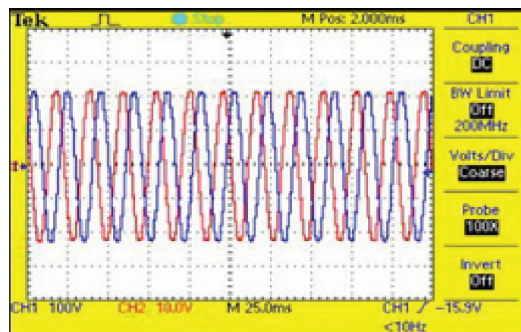
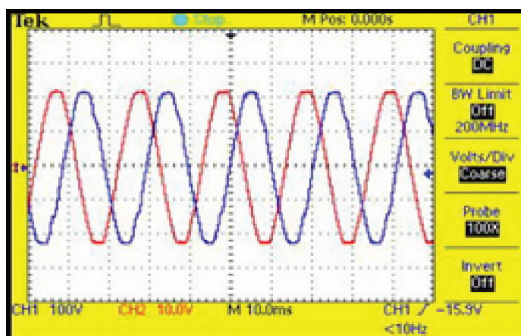


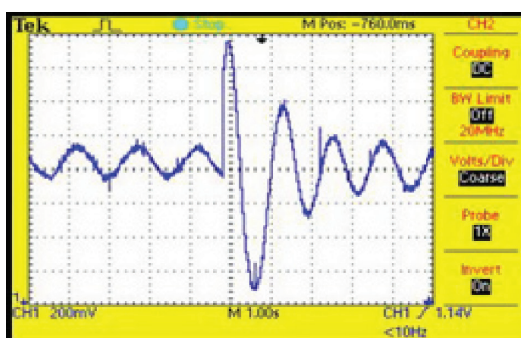
FIGURE 15.18 Experimental response of developed IM drive parameters with constant reference speed and no-load condition. (CH1: Supply Input Voltage, CH2: Supply Input Current, CH3: MC Output Voltage, CH4: MC Output Current)



TDS 2022 - 11:35:43 AM 8/4/2018

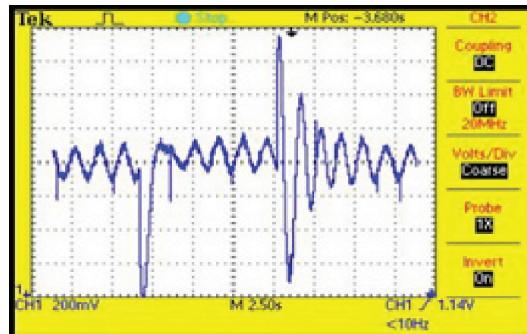
FIGURE 15.19 o/p voltage, $q = 0.2$.

TDS 2022 - 11:33:41 AM 8/4/2018

FIGURE 15.20 i/p grid voltage, $q = 0.25$.

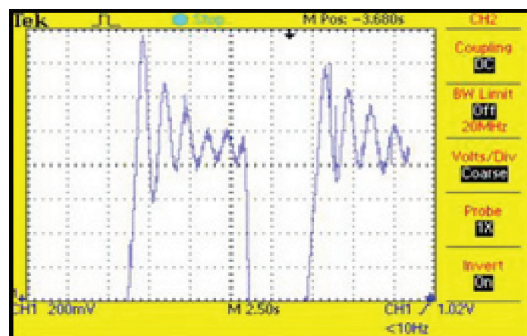
TDS 2022 - 1:22:23 PM 8/4/2018

FIGURE 15.21 Transients at step load $q = 0.35$.



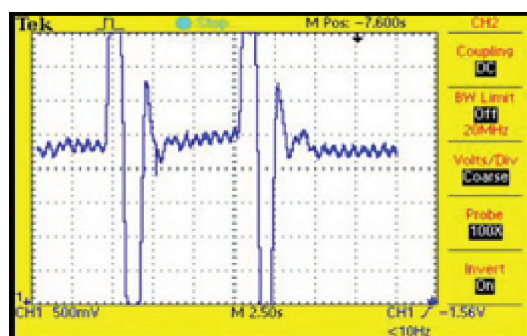
TDS 2022 - 1:20:02 PM 8/4/2018

FIGURE 15.22 Transients at frequent step load $q = 0.36$.



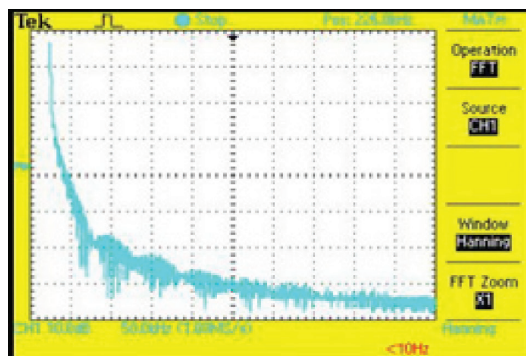
TDS 2022 - 1:13:22 PM 8/4/2018

FIGURE 15.23 Transients at frequent step load $q = 0.45$.



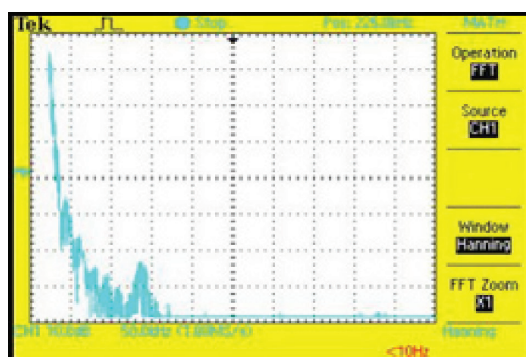
TDS 2022 - 12:33:29 PM 8/4/2018

FIGURE 15.24 Transients at frequent step load $q = 0.50$.



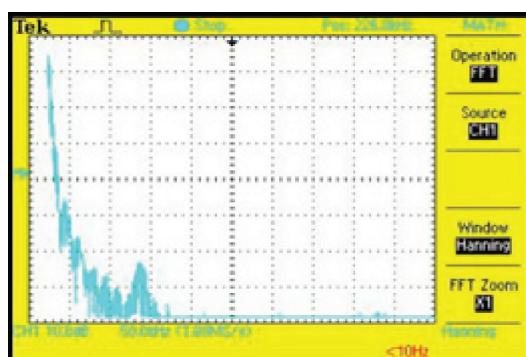
TDS 2022 - 12:25:37 PM 8/6/2018

FIGURE 15.25 FFT of *i/p* current.



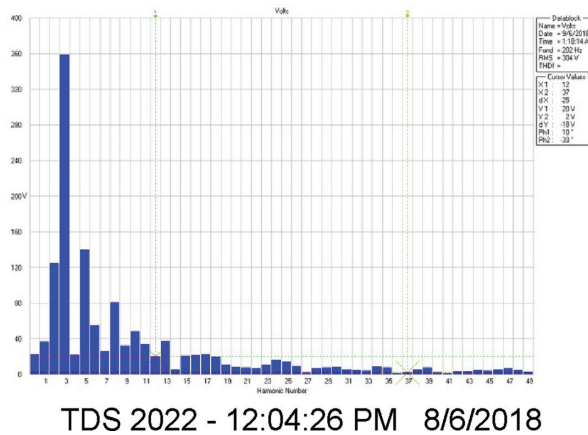
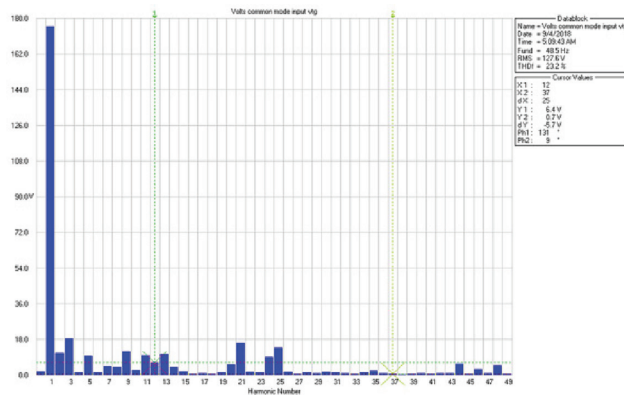
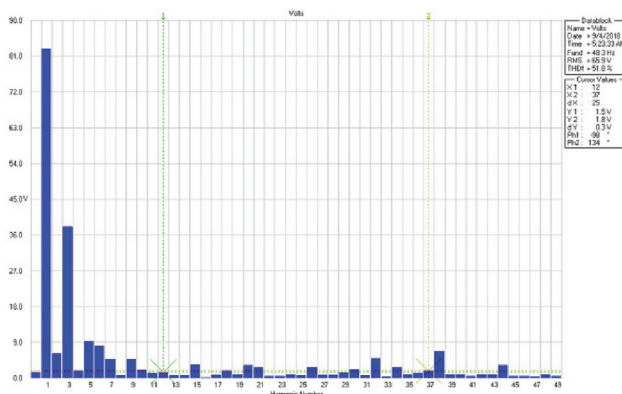
TDS 2022 - 2:09:08 PM 8/4/2018

FIGURE 15.26 FFT of *o/p* current.



TDS 2022 - 12:04:26 PM 8/4/2018

FIGURE 15.27 FFT of *o/p* voltage.

**FIGURE 15.28** Harmonic spectrum current (*i/p*).**FIGURE 15.29** Harmonic spectrum voltage (*o/p*).**FIGURE 15.30** Harmonic spectrum input (*i/p*).

developed method, the input current ripple is suppressed effectively from input current THD of 11.9%–2.3%. The experimental results show the good performance in both the steady-state and transient conditions.

SUMMARY

This chapter has explained the development of FLDTC-based controller on an FPGA board for the MC-fed IM drive to achieve superior performance under different conditions with reduced harmonics. The MC is selected because it enables three-phase AC to AC conversion without any intermediate energy storage in the power circuit, which makes it most suitable for high-energy density applications, such as motion control of AC motors. The advantage of the MC with the advantage of DTC can be achieved using the developed method.

The main drawback of the DTC scheme is higher ripples in electromagnetic torque. These ripples are significantly reduced using a novel FLDTC-based controller in order to reduce the vibrations in rotor during running conditions. Also, the fuzzy-logic controller significantly reduces the ripple contents in the input current and output voltage, resulting in less harmonics in line current, and the output voltage waveform is near to sinusoidal. The controller provides a fast, dynamic response and stability to the system during steady-state as well as transient conditions.

REFERENCES/FURTHER READING

1. B. K. Bose, *Power Electronics and AC Drives*, Prentice Hall, Englewood Cliffs, NJ, 1986.
2. M. H. Rashid, *Power Electronics: Circuits, Devices, and Applications*, Pearson Education, Singapore, 2004.
3. B. K. Bose, Scalar decoupled control of induction motor, *IEEE Trans. Ind. Appl.*, vol. IA-20, no. 1, pp. 216–225, 1984.
4. B. Robyns, F. Berthereau, J. P. Hautier, and H. Buyse, A fuzzy-logic-based multimodal field orientation in an indirect FOC of an induction motor, *IEEE Trans. Ind. Electron.*, vol. 47, no. 2, pp. 380–388, 2000.
5. I. Takahashi, and T. Noguchi, A new quick-response and high efficiency control strategy of an induction motor, *IEEE Trans. Ind. Appl.*, vol. IA-22, pp. 820–827, 1986.
6. M. Depenbrok, Direct self-control (DSC) of inverter fed induction machine, *IEEE Trans. Power Electron.*, vol. 3, pp. 420–429, 1988.
7. D. Casadei, G. Serra and A. Tani, The use of matrix converters in direct torque control of induction machine, *IEEE Trans. Ind. Electron.*, vol. 48, no. 6, pp. 1057–1064, 2001.
8. O. Hemakesavulu, C. Ganesh and M. Manasa, Simulation of fuzzy logic controller based matrix converter DTC-SVM method for induction motor, *Int. J. Comput. Eng. Appl.*, vol. 7, no. 3, pp. 98–110, 2014.
9. V. N. Naik, and A. Panda, A three-level fuzzy-2 DTC of induction motor drive using SVPWM, *IEEE Trans. Ind. Electron.*, vol. 63, pp. 1467–1479, 2016.
10. N. V. Naik, and S. P. Singh, A comparative analytical performance of F2DTC and PIDTC of induction motor using DSPACE-1104, *IEEE Trans. Ind. Electron.*, vol. 62, pp. 7350–7359, 2015.
11. S. Gdaim, A. Mtibaa, and M. F. Mimouni, Design and experimental implementation of DTC of an induction machine based on fuzzy logic control on FPGA, *IEEE Trans. Fuzzy Syst.*, vol. 23, no. 3, pp. 644–655, 2015.

12. C. Liu, R. Ma, H. Bai, F. Gechter, and F. Gao, A new approach for FPGA based real-time simulation of power electronic system with no simulation latency in subsystem partitioning, *Int. J. Electr. Power Energy Syst.*, vol. 99, pp. 650–658, 2018.
13. R. Arulmozhiyaly, and K. Baskaran, Implementation of a fuzzy PI Controller for speed control of induction motors using FPGA, *J. Power Electron.*, vol. 10, pp. 65–57, 2010.
14. G. Yougui, Z. Jianlin, C. Caixue, Direct torque control for induction machine based on AC-AC matrix converter, *7th International Conference on Power Electronics*, 2007.
15. M. Cirstea, Modern control systems design using CAD techniques, *Neural and Fuzzy Logic Control of Drives and Power Systems*, Elsevier, Amsterdam, the Netherlands, 2002.
16. F. Liu, C. Klumpner, F. Blaabjerg, A robust method to improve stability in matrix converters, *IEEE 35th Annual Power Electronics Specialists Conference*, 2004.
17. H. Sudheer, S. F. Kodad, B. Sarvesh, Improvements in direct torque control of induction motor for wide range of speed operation using fuzzy logic, *J. Electr. Syst. Inform. Technol.*, vol. 5, pp. 813–828, 2018.
18. G. Qiangang, L. Yaohua, M. Yanjing, L. Weiguo, Modeling and simulation study on matrix converter fed induction motor drive system implemented by direct torque control, *International Conference on Electrical Machines and Systems, IEEE*, Nanjing, China, 2005.
19. M. N. Uddin, Z. R. Huang, A. B. M. Siddique Hossain, Development and implementation of a simplified self-tuned neuro-fuzzy-based IM drive, *IEEE Trans. Industry Applications Conf.* Orlando, FL, 2011.



Taylor & Francis

Taylor & Francis Group

<http://taylorandfrancis.com>

16 Control of Synchronous and Special Motor Drives

16.1 INTRODUCTION

During the overexcitation mode, the synchronous motor works with improved power factor and its use as an asynchronous condenser makes it an economical drive in spite of its high cost. The manufacturing of induction motors is limited up to 20 mW and 1,500 rpm. Beyond this rating, the only answer is the use of synchronous motors. These are available up to a rating of 110 mW and 3,000 rpm. The torque-speed characteristic of a synchronous motor is to give constant torque at a fixed speed determined by the number of its poles and supply frequency. As a constant-speed drive, synchronous motors are widely used in pumps, crushers, and large compressors [1–24]. Medium-sized synchronous drives are applicable in the paper and cement industries.

16.2 BASICS OF THE SYNCHRONOUS MOTOR

The air-gap flux rotating at synchronous speed (ω_{ms}) is produced when the armature of the motor is energized by a balanced three-phase source of frequency (ω), that is,

$$\omega_{ms} = \frac{2}{p} \omega = \frac{4\pi f}{p} \text{ rad/s} \quad (16.1)$$

where p is the number of poles, and f is the supply frequency.

The equivalent circuit of the motor can be drawn as shown in [Figure 16.1](#).

The power input to the motor is

$$P_{in} = 3VI_s \cos \phi \quad (16.2)$$

where ϕ is the phase angle between V and I_s .

Ignoring the stator losses, and since no power is transferred to the rotor, all the air-gap power is converted into mechanical power.

$$P_m = 3VI_s \cos \phi \quad (16.3)$$

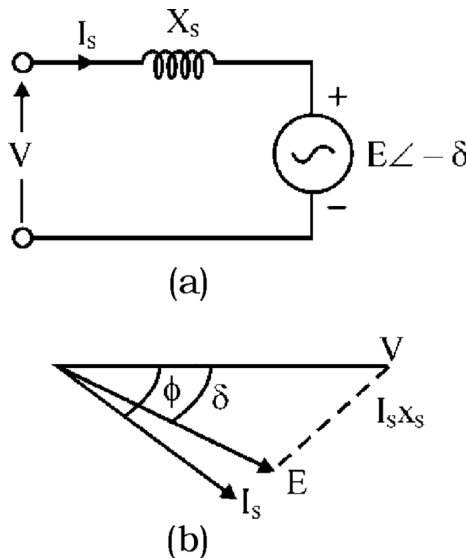


FIGURE 16.1 Synchronous motor: (a) simplified equivalent circuit of synchronous motor and (b) phasor diagram.

From [Figure 16.1](#), the magnitude of the stator current I_s can be expressed as

$$I_s = \frac{V\angle 0 - E\angle -\delta}{jX_s}$$

or

$$I_s = \frac{V\angle -90^\circ}{X_s} - \frac{E\angle -(90^\circ + \delta)}{X_s}$$

or

$$I_s \cos \phi = \frac{E}{X_s} \sin \delta \quad (16.4)$$

where

X_s is the synchronous reactance

E is the excitation emf

δ is the power or torque angle.

From Equations (16.1) and (16.4), we get

$$P_m = \frac{3VE}{X_s} \sin \delta \quad (16.5)$$

When the synchronous motor is excited, the field produced by the DC winding on the rotor interacts with the air-gap flux to produce the torque [1,2,6,13,19]. The air-gap flux and the rotor field rotate at the same speed. Therefore, torque is expressed as:

$$T = \frac{P_m}{\omega_{ms}}$$

$$T = \frac{3}{\omega_{ms}} \frac{VE}{X_s} \sin \delta \quad (16.6)$$

From Equations (16.5) and (16.6), it can be seen that for a given field excitation E is constant and mechanical power P_m and developed torque T are proportional to $\sin \delta$. The speed-torque characteristic with constant frequency supply is shown in Figure 16.2 [1–8,13,19].

From speed-torque and torque-angle curves, it can be seen that the motoring operation is achieved when δ is positive and E lags V , whereas the braking operation is achieved when δ is negative and E leads V .

The maximum torque or power known as pull-out torque (T_{\max}) or pull-out power is obtained at $\delta = \pm 90^\circ$ as shown in Figure 16.2.

$$T_{\max} = \frac{3}{\omega_{ms}} \frac{VE}{X_s} \quad (16.7)$$

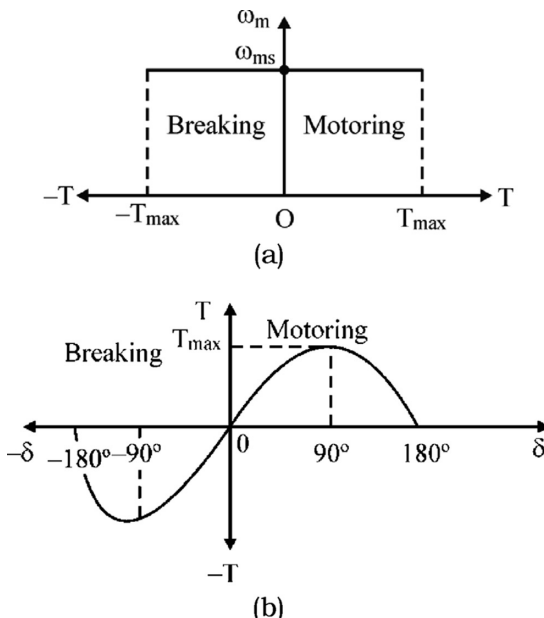


FIGURE 16.2 Speed-torque and torque-angle characteristics of synchronous motor: (a) speed-torque characteristics and (b) torque-angle characteristics.

16.3 SPEED CONTROL OF THE SYNCHRONOUS MOTOR

The speed of the synchronous motor can be controlled by varying the supply frequency. With this variable-frequency control, the synchronous motor can be operated in the following two modes:

1. True synchronous mode
2. Self-controlled mode or self-synchronous mode

16.3.1 TRUE SYNCHRONOUS MODE

In this mode, the supply frequency is controlled from an independent oscillator. Here, the frequency is gradually changed from the initial speed to the desired value. The rotor speed tracks the changes in the synchronous speed. The rotor pulls into step, once the synchronous speed or frequency reaches the desired speed. The speed-torque characteristic of the synchronous motor with variable-frequency control is shown in [Figure 16.3 \[6,13–17\]](#). Due to hunting and stability issues, this mode of control is only used for multiple synchronous reactances and Magnet synchronous motor (MSM) drives, that is, paper mills, textile mills, spinning mills, etc.

16.3.2 SELF-CONTROLLED MODE

In this mode, the supply frequency is varied in proportion to the rotor speed so that the rotating field, due to the stator, rotates at the same speed as the motor or its field. In this control, synchronous frequency tracks the frequency of the induced voltage. Sensors called *rotor position sensors* are mounted on the stator to track the rotor position. The supply frequency tracks the frequency of signals generated by sensors whose frequency is proportional to the rotor speed. [Figure 16.4](#) shows the power circuit diagram of a self-controlled synchronous-motor drive using load-commutated thyristor inverters and cycloconverters.

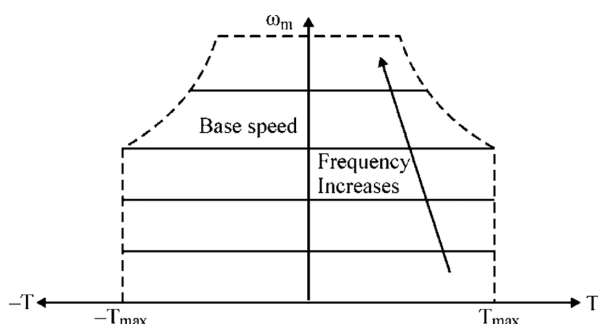


FIGURE 16.3 Speed-torque characteristics of synchronous motor with variable-frequency control.

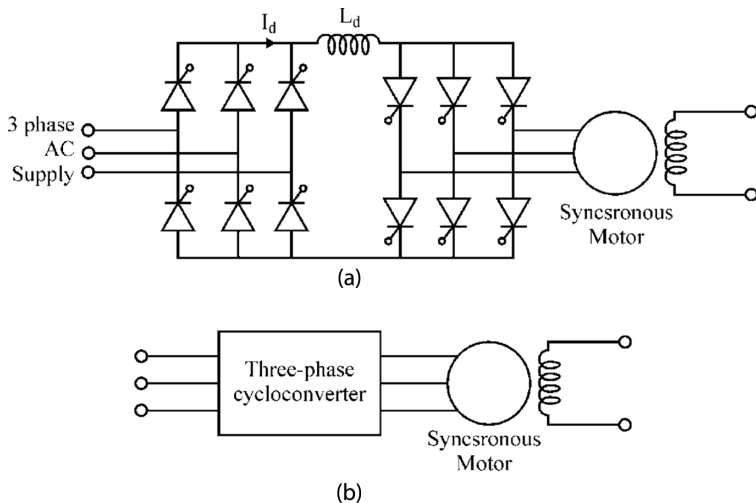


FIGURE 16.4 Self-controlled synchronous motor drive: (a) speed control using load-commutated thyristor inverter and (b) speed control using cycloconverter.

16.4 STEPPER MOTOR

A stepper motor is an electromechanical device that actuates a train of step-angular movements in response to a train of input pulses on a one-to-one basis. This means that the motor moves one step for one input pulse. It is a digital-controlled motor, and the rotational speed is determined by the frequency of the applied pulses, and therefore, the speed of response is very high (10,000 full steps per second).

This motor can be rotated in either direction—clockwise or counterclockwise—by changing the sequence of pulses of the drive circuit to its stator windings. The basic feature of the stepper motor is that when it is energized it will move and come to rest after a few steps in strict accordance with the provided digital input commands. So, the stepper motor can control the velocity, direction, and distance of the load. The error that can be introduced in the system where the stepper motor is used is a small percentage of one step and is noncumulative, irrespective of the distance traveled. Moreover, the stepper motor is inherently reliable. Various applications of the stepper motor are [2,3,6,20–24]:

1. In the field of numerical control of machines, such as milling machines, lathes, and robotics
2. Computer peripherals, for example, disc drives, X-Y plotters, printers, and paper readers
3. Electronic clocks and watches
4. Photo printing machines and cameras
5. Solar-panel positioning systems

On the basis of construction and performance characteristics, stepper motors can be divided into three types:

1. Variable-reluctance stepper motor
2. Permanent-magnet stepper motor
3. Hybrid stepper motor

All three types of stepper motors are discussed in following sections [2,3,6,20–24].

16.5 VARIABLE-RELUCTANCE MOTOR

The variable-reluctance motor has a number of stator and rotor-salient poles, that is, both stator and rotor poles have projections. The rotor is made of laminated soft steel and does not have permanent magnets (PMs) or windings, but the stator poles have concentrated windings.

There is a definite relationship between the number of stator and rotor poles. The number of rotor poles is determined by the required step angle. The number of stator poles may be 6, 8, or 12, and the number of corresponding rotor teeth is 4, 6, and 8, for three-phase motors. The step angle is related with the stator and rotor poles as

$$\theta_S = \frac{N_S - N_R}{N_S \cdot N_R} \times 360^\circ \quad (16.8)$$

where:

N_s = number of stator poles

N_R = number of rotor teeth

θ_S = step angle

Also, the number of stator poles is the product of the number of phases and number of poles per phase, that is,

$$N_s = m \times N_P = N_R + N_P \quad (16.9)$$

where N_P = number of stator poles per phase

The relationship between the number of phases or step sequences, rotor teeth, and steps per revolution can be expressed as:

$$\text{Step / Revolution} = m \times N_R = \frac{360}{\theta_S} \quad (16.10)$$

For example, if the number of stator poles is $N_s = 12$ and the number of phases or step sequence is 3, the number of rotor teeth should be 8, and the step angle θ_Σ will be 15° according to Equation (16.8). The number of steps per revolution will be $3 \times 8 = 24$, from Equation (16.10).

The stator has 12 poles having three-phase winding, and the rotor has 8 teeth. When one of the stator coils is energized, the rotor teeth will align with the energized

stator poles, which are located 90° apart around the stator. This means, that they will move to a position of minimum reluctance.

If the coils of Phase A are energized, rotor teeth marked 1 will align themselves with the energized poles. The poles that are not energized will provide a return magnetic path. If the windings of Phase B are energized next and Phase A is deenergized, the rotor teeth marked 2 will align with the stator poles under Phase B and be locked there, thereby the rotor will turn counterclockwise by one step. Similarly, if Phase C is energized next, then rotor teeth marked 1 will align with poles under Phase C, and the rotor moves another step counterclockwise. Therefore, the operation of the variable-reluctance stepper motor is based on the minimum reluctance principle, that is, the rotor will always try to align its poles with the position that provides minimum reluctance for the magnetic circuit.

16.5.1 SINGLE-STACK VARIABLE-RELUCTANCE STEPPER MOTOR

These are normally of the variable-reluctance type with no excitation in the rotor as shown in [Figure 16.5 \[2,3,6,20–24\]](#). The motor can be stepped clockwise or counterclockwise by energizing the phase winding. The step angle, which is defined as the angle moved by the rotor for each change in excitation sequence, is given by:

$$\theta_s = \frac{360^\circ}{NP} \quad (16.11)$$

where:

N = no. of phases

P = no. of poles of stator

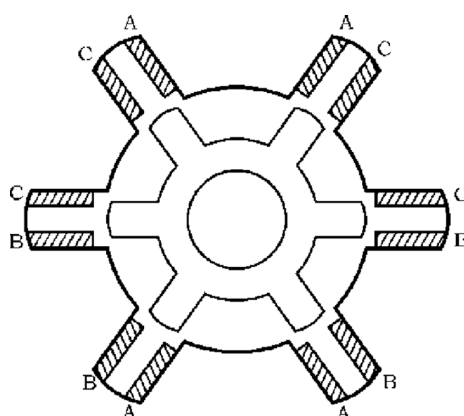


FIGURE 16.5 Cross-section of single-stack variable-reluctance motor.

16.5.2 MULTISTACK VARIABLE-RELUCTANCE STEPPER MOTOR

In this type, stator windings are stacked along the shaft. Each stack section has the same number of poles in the stator and the rotor. The step size of this motor is:

$$\theta_s = \frac{360^\circ}{NP} \quad (16.12)$$

where:

N = number of phases in stator

p = number of stator and rotor poles in each stack

Here, more excitation sequences are available when the stator winding is energized, and the rotor poles of that section tend to align with those defined by the stator excitation.

Advantages of Variable-Reluctance Motor

1. It has simple rotor with no windings or magnets, and so it has low cost and high speed.
2. It does not have a magnetic saturation problem at high temperature.
3. It has independent phases.

Therefore, variable- or switched-reluctance motors of more than 100 HP with a maximum speed of 25,000 rpm are available in the market.

16.6 PERMANENT-MAGNET MOTORS

The PM stepper motor consists of a rotor made of permanent magnetic material such as alnico surrounded by a number of stator poles carrying windings. The simplest stepper motor consists of two-phase stator windings producing two poles as shown in Figure 16.6 [2,3,6,20–24]. A bipolar PM stepper motor has a single winding for each phase, and the current must be reversed to reverse the stator field. But unipolar motors

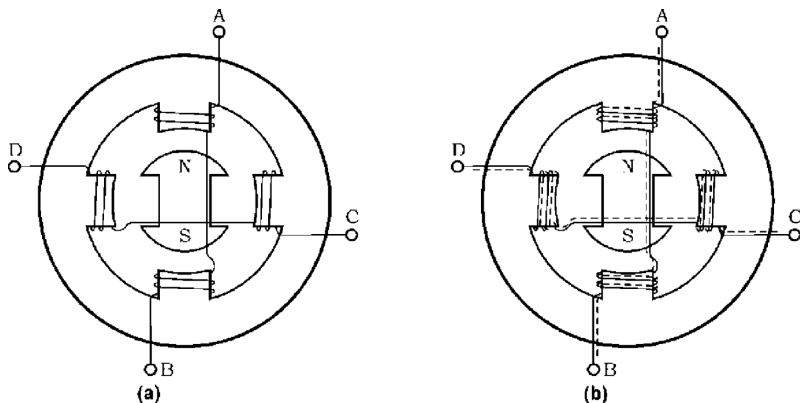


FIGURE 16.6 PM motors: (a) bipolar type and (b) bifilar type.

have two windings that are wound in opposite directions for each phase so that the field can be reversed with a single polarity drive. Therefore, the drive circuit for the unipolar motors is simple. The PM stepper motors are mostly used in low-power applications.

16.7 HYBRID STEPPER MOTOR

A hybrid stepper motor has an axially oriented PM that is sandwiched between the two sections of the stator and rotor, as shown in Figure 16.7 [2,3,6,20–22]. The magnet flux distributes radially through the two stator and rotor sections. Stator windings are excited with bipolar currents, as opposed to the unipolar currents in the variable-reluctance motors. The magnetic flux produced by the stator windings passes through each stator and rotor sections and air gap. But it does not pass through the rotor magnet.

The rotor magnet causes the stator and rotor teeth to settle at the minimum reluctance position. The motor can be stepped forward or backward by energizing windings in sequence $A\bar{B} \rightarrow AB \rightarrow \bar{A}\bar{B} \rightarrow \bar{A}B$ or $A\bar{B} \rightarrow \bar{A}\bar{B} \rightarrow \bar{A}B \rightarrow A\bar{B}$, respectively, where the overbar indicates the polarity of currents in Phases A and B.

The stepping angle (θ_s) of a hybrid stepper motor is given by

$$\theta_s = \frac{90^\circ}{p} \quad (16.13)$$

where p is the number of rotor poles.

The angular velocity (ω) of the rotor is determined by the step angle and the pulse frequency. It is given by:

$$\omega = \frac{2\pi f \times \text{step angle}}{360} \text{ rad/s} \quad (16.14)$$

$$= \frac{2\pi f}{\text{step angle}} \text{ rad/s} \quad (16.15)$$

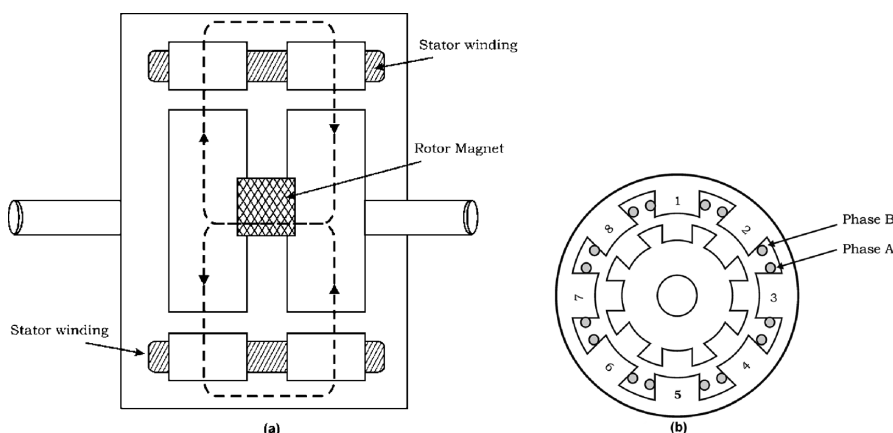


FIGURE 16.7 Hybrid motor: (a) axial section and (b) cross section.

where:

f = applied pulses per second

step angle = angle per step of rotation in degrees

16.8 DRIVE CIRCUITS FOR STEPPER MOTORS

There are two types of drive circuits used for stepper motors [2,3,6,20–24]:

1. Unipolar drive circuit
2. Bipolar drive circuit

The unipolar drive is suitable for variable-reluctance stepper motors where the developed torque is determined by the magnitude of the current, not by its polarity.

1. **Unipolar drive circuits:** The simplest unipolar drive circuits, one for each winding, are shown in Figure 16.4a.

The transistor Q is turned on to energize the winding, with a current that is limited either by the winding resistance or by hysteresis or pulse-width modulation (PWM) current controllers. The freewheeling diode allows the winding current a circulating path when the transistor Q is turned off.

The drive circuit of Figure 16.8a is a basic one. A better drive circuit is shown in Figure 16.8b, which includes a Zener diode in the freewheeling path. In this, a PWM is also included in the gate-driving circuit. The PWM allows a higher DC supply voltage to be used, and so it reduces the rise time of the current. The diode allows a fast fall time for the current when the transistor Q is turned off by dissipating the trapped energy of the winding.

2. **Bipolar drive circuits:** The bipolar drive allows the motor windings to be driven with bidirectional currents. The most popular four-transistor bridge drive circuit, one for each winding, is shown in Figure 16.9.

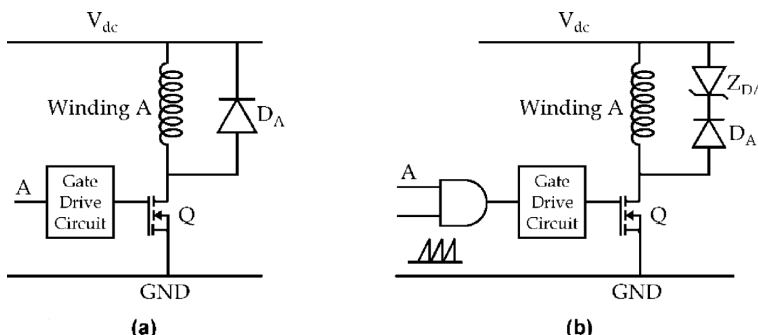


FIGURE 16.8 Unipolar drive circuit: (a) basic unipolar drive and (b) unipolar drive with PWM.

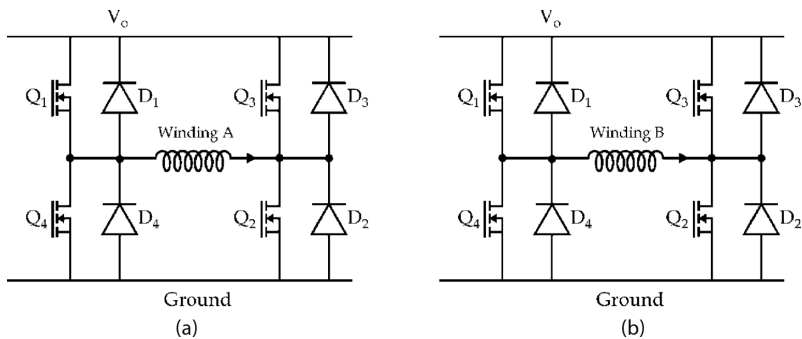


FIGURE 16.9 Bipolar drive circuit: (a) Winding A and (b) Winding B.

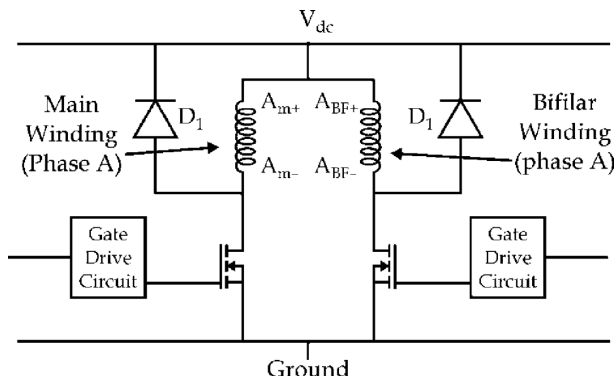


FIGURE 16.10 Drive circuit for bifilar-wound motor.

This circuit provides the required rise and fall times of the winding by properly selecting the DC supply voltage V_0 , the PWM, and the current controller gains.

Hybrid stepper motors with bifilar windings also uses simpler unipolar drive circuits as shown in [Figure 16.10](#) [2,3,6,20–22]. These motors have two tightly coupled windings for each phase.

UNSOLVED PROBLEMS

- 16.1 What is the difference between an induction motor and synchronous motor?
- 16.2 Derive the equivalent circuit of the three-phase synchronous motor.
- 16.3 Write the basic torque equation for the three-phase synchronous motor.
- 16.4 What are the different modes of speed control of the synchronous motor.
- 16.5 Explain the self-controlled mode of the speed control of the synchronous motor.
- 16.6 Draw the phasor diagram of the three-phase synchronous motor.

- 16.7 Draw the speed-torque and torque-angle curves for the three-phase synchronous motor.
- 16.8 Draw the speed-torque curve for the synchronous motor with variable-frequency control.
- 16.9 What is a true synchronous mode?
- 16.10 What are stepper motors? How many types of stepper motors are there?
- 16.11 Describe the construction of a PM stepper motor. Describe both the unipolar and bipolar types.
- 16.12 What are the advantages of the hybrid stepper motor?
- 16.13 What is a variable-reluctance stepper motor? Explain in detail its principle of operation.

SUMMARY

Two developments in the synchronous motors have contributed to the development of synchronous motor drives in the market, that is, *first*, the replacement of conventional field excitation in the rotor of synchronous motors by the PM excitation, and *second*, the replacement of the mechanical commutator with the electronic commutator in the form of the inverter due to the advancement in power semiconductor technology. Synchronous motors are constant-speed AC motors whose speed is controlled by varying the voltage, frequency, and current using different power modulators.

REFERENCES

1. B. K. Bose, *Power Electronics and AC Drives*, Prentice Hall, Englewood Cliffs, NJ, 1986.
2. M. H. Rashid, *Power Electronics: Circuits, Devices, and Applications*, Pearson Education (Singapore) Pvt. Ltd., Singapore, 2004.
3. N. Mohan, T. M. Undeland, and W. P. Robbins, *Power Electronics: Converters, Applications and Design*, John Wiley & Sons, New York, 1996.
4. P. T. Krein, *Elements of Power Electronics*, Oxford University Press, New York, 2003.
5. K. Thorborg, *Power Electronics*. Prentice Hall International (UK) Ltd, London, UK, 1988.
6. P. S. Bhimra, *Power Electronics*, 4th edn, Khanna Publications, New Delhi, 2012.
7. I. Batarseh and A. Harb, *Power Electronics*, Springer Nature, Cham, Switzerland, 2018.
8. K. M. Smedley and E. Santi, *AC-DC Power Converters*, Wiley, Hoboken, NJ, 1999.
9. R. W. Erickson, *Fundamentals of Power Electronics*, Springer, Hoboken, NJ, 2001.
10. B. Wu and B. Wu, *High-Power Converters and AC Drives*, John Wiley & Sons, Hoboken, NJ, 2017.
11. V. R. Moorthi, *Power Electronics Devices, Circuits and Industrial Applications*, Oxford University Press, New York, 2010.
12. T. Suntio, T. Messo, and J. Puukko, *Power Electronic Converters*, Wiley-VCH, Verlag GmbH, Germany, 2018.
13. A. M. Trzynadlowski, *Introduction to Modern Power Electronics*, 3rd edn, John Wiley & Sons, Hoboken, NJ, 2010.
14. M. Trzynadlowski, *Power Electronic Converters and Systems*, Institution of Engineering and Technology, London, UK, 2016.
15. B. M. Wilamowski and J. D. Irwin, *Power Electronics and Motor Drives*, CRC Press, New York, 2011.

16. E. Acha, V.G. Agelidis, O. Anaya-Lara, and T. J. E. Miller, *Power Electronic Control in Electrical Systems*, Newnes, Oxford, UK, 2002.
17. F. Mazda, *Power Electronics Handbook*, Newnes, Oxford, UK, 1997.
18. F. Blaabjerg, *Control of Power Electronic Converters and Systems*, Academic Publishers, India, 2018.
19. S. N. Manias, *Power Electronics and Motor Drive Systems*, Academic Publishers, Palo Alto, CA, 2017.
20. V. V. Athani, *Stepper Motors: Fundamentals, Applications and Design*, New Age publication, New Delhi, India, 1997.
21. M. Y. Tarnini, Fast and cheap stepper motor drive, *International Conference on Renewable Energy Research and Applications (ICRERA)*, San Diego, CA, pp. 689–693, 2015.
22. B. Aranjo, P. K. Soori, and P. Talukder, Stepper motor drives for robotic applications, *IEEE International Power Engineering and Optimization Conference*, Melaka, Malaysia, pp. 361–366, 2012.
23. R. Innes, Industrial applications of stepper control systems, *IEE Colloquium on Stepper Motors and Their Control*, London, UK, pp. 5/1–5/3, 1994.
24. C. K. Lai, J. S. Ciou, and C. C. Tsai, FPGA-based stepper motor vector control system design, *International Automatic Control Conference (CACS)*, Taiwan, pp. 1–5, 2017.



Taylor & Francis

Taylor & Francis Group

<http://taylorandfrancis.com>

Section IV

*Advanced Power Electronics
Applications*



Taylor & Francis

Taylor & Francis Group

<http://taylorandfrancis.com>

17 Electric/Hybrid Electric Vehicles

17.1 INTRODUCTION

In the last few decades, the oil consumption of the transportation sector has grown more rapidly as compared to any other sector. The emission of gases from the internal combustion engine (ICE) causes environmental problems, such as greenhouse effects. To curb these harmful gases, government agencies have established stringent principles for the release and consumption of fuel. Battery-powered electric vehicles (BEVs) are the best choice. But BEVs have some limitations, such as high cost, limited driving range, and long charging time of the battery.

To overcome these problems, hybrid electric vehicles (HEVs) were developed, which have both the advantages of BEVs and ICE vehicles. The HEV consists of a conventional propulsion system, battery storage system, and an electric propulsion system. When HEVs are run in electric mode, then zero emission is possible because it is propelled by an electric motor (EM). The other form of HEV is the plug-in HEVs (P-HEVs). In this topology, the battery can be recharged by plugging into an electrical grid.

The other form of zero-emission vehicle (ZEV) is fuel-cell vehicles (FCVs). It uses hydrogen and air to generate power. This power is either used to drive the vehicle to store the energy in the battery or supercapacitors. FCVs emit only water vapors. However, FCVs have some drawbacks, such as (1) high cost and short life cycle of fuel cells, (2) onboard hydrogen storage system, and (3) hydrogen refilling station needed.

17.2 POWER-TRAIN ARCHITECTURES

17.2.1 MAJOR CHARACTERISTICS OF BEVs, HEVs, AND FCVs

The comparison of BEVs, HEVs, and FCVs is shown in [Table 17.1](#). Various works have been reported with detailed analysis to measure the global energy consumption of these types of vehicles. It is found that BEVs and HEVs are the most economical in terms of fuel consumption as compared to ICE vehicles. Moreover, using BEVs and HEVs reduces the greenhouse gas emissions, but in the case of FCVs, the results are not so obvious because they are dependent on hydrogen gas.

1. *Series-Parallel HEVs:* A series-parallel HEV is shown in [Figure 17.1](#).

In [Figure 17.1](#), electric motor 1 (EM1) and the transmission shaft are connected to the planetary ring gear set (R), whereas the ICE is connected to the carrier (C), and electric motor 2 (EM2) is connected to the sun gear (S). BAT is the battery power fed through voltage source inverters (VSI 1

TABLE 17.1
Features of BEV, HEV, and FCV

Characteristics	BEV	HEV	FCV
Propulsion	• EM drives	• EM drives and ICE	• EM drives
Energy storage subsystem (ESS)	• Battery • Supercapacitor	• Battery • Supercapacitor • Fossil or alternative fuels	• Hydrogen tank • Battery/ supercapacitor needed to enhance power density
Energy source and infrastructure	• Electrical grid charging facilities	• Gasoline stations • Electrical grid charging facilities (for plug-in hybrid)	• Hydrogen • Hydrogen production and transportation infrastructure
Characteristics	• Zero local emission • High-energy efficiency • Independent of fossil fuel • Fairly short range • High primary price • Commercially available	• Low local emission • High fuel economy • Long driving range • Dependence on fossil fuel • Higher cost than ICE vehicles • Commercially available	• Zero low local emission • High-energy efficiency • Independent of fossil fuel (if not using gasoline to produce) • High cost • Under development • Fuel cell cost, life cycle, and reliability
Major issues	• Battery sizing and management • Charging facilities • High cost • Battery lifetime	• Battery sizing and management • Control optimization and management of multiple energy sources	• Hydrogen production and distribution infrastructure • High cost

and VSI 2). This design is shown such that it allows the other conventional structure (i.e., series and parallel HEVs, ICE vehicles, and BEVs) to be realized. By means of a DC voltage bus and the planetary gear set, a series-parallel HEV can operate as either a series HEV or a parallel HEV in terms of energy flow. Due to planetary gear, the speed of the ICE is dependent on the average of the speeds of EM1 and EM2. The EM1 speed depends on vehicle speed, and the EM2 speed can be chosen to modify the ICE speed. Hence, the ICE can operate in an optimal region by controlling the EM2 speed.

2. *Series HEVs:* In series HEVs, all the traction power is fed from a DC bus. There is no mechanical connection between ICE and the traction load. Since there is no connection between the EM1 and the ICE, a series HEV can be attained from the series-parallel hybrid structure. A simple gear is connected between the ICE and the EM2.

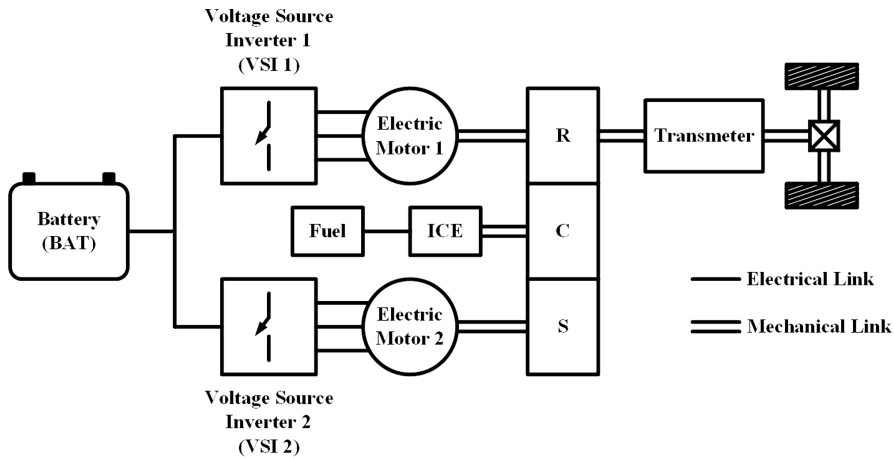


FIGURE 17.1 Series-parallel HEV with planetary gear. (From Chan, C.C., The state of the art of electric, hybrid, and fuel cell vehicles, *Proceedings of the IEEE*, 95, 704–718, 2007.)

3. *Parallel HEVs*: A parallel HEV is obtained when EM2 is removed from the series-parallel hybrid architecture. In this type of configuration, the traction power is supplied either by the ICE, or by only EM1, or by using both EM1 and ICE together. EM1 can only be used to charge the battery when the vehicle is in regeneration mode or if the output power of the ICE is higher than the drive wheel power; extra power can store power from the ICE. This parallel HEV architecture requires only two motors: the ICE and the EM1, and it is more efficient than series HEV.
4. *ICE Vehicles*: An ICE vehicle is obtained when only the ICE powertrain remains and EM1 and EM2 are removed. ICE vehicles have a decent range of driving and smaller refueling time, but it contributes to environmental pollution.
5. *BEVs*: In BEVs, only EM1 remains in the power train from the series-parallel hybrid architecture. Zero emission is achieved because it is propelled only by battery or other electrical energy sources. The drawbacks of BEVs are that they have high initial cost and short driving range.
6. *FCVs*: FCVs are similar to the BEV because they can also be equipped with batteries or supercapacitors. In this type of architecture, the fuel cell functions as an electrical source, which uses hydrogen and either powers the machine or charges the battery.

17.2.2 DIFFERENT FUNCTIONS OF THE VARIOUS HEV ARCHITECTURES

The prior HEV architectures provide various functionality levels. These levels are differentiated by the ratio of power between the ICE and EMs.

TABLE 17.2
Different Functions of the Various HEV Architectures

	Micro HEV	Mild HEV	Full HEV	Plug-in HEV
Series-Parallel	—	—	X	X
Series	—	—	X	X
Parallel	X	X	X	—

1. *Microhybrid*: Microhybrid vehicles use the EM as a starter alternator, and the ICE insures the propulsion of the vehicle. Because of the fast dynamics of EMs, microhybrid HEVs can be stopped immediately and again start instantly using the EM.
2. *Mild Hybrid*: In addition to the features of microhybrid vehicles, in mild hybrid vehicles, the EM is used to boost the ICE during acceleration or braking by applying additional torque.
3. *Full Hybrid*: Full hybrid vehicles are equipped with a fully electric traction system. This means that the vehicle can run only by the EM. When such a vehicle is propelled by the electric system, it becomes a ZEV. However, the propulsion of the vehicle can also be propelled by the ICE or by both the ICE and EM.
4. *Plug-in Hybrid*: In P-HEVs, batteries can be externally charged by using an electrical grid. In few cases, the battery can be charged from the ICE to extend the vehicle driving range. This type of P-HEV is also called a “range extend EV.”

HEV architectures have various levels of functionality. As shown in [Table 17.2](#), some architecture is for certain HEV functions.

17.3 DRIVETRAIN ANALYSIS

17.3.1 BEV DRIVETRAIN TOPOLOGY

A purely electrical drive system mainly substitutes the ICE and the multiple transmission systems with an all-electric system. An elementary configuration of a BEV is as shown in [Figure 17.2](#). It consists of battery pack, inverter, traction motor, and ultra-capacitor.

17.3.2 SERIES HEV DRIVETRAIN TOPOLOGY

A series hybrid vehicle is essentially an electric vehicle (EV) with an onboard battery charger. Usually an ICE is used to run the generator and charge the onboard batteries, as shown in [Figure 17.3](#). The ICE is switched on when the state of charge (SOC) of the battery is small. When the battery has a desired peak SOC, the ICE turns off again.

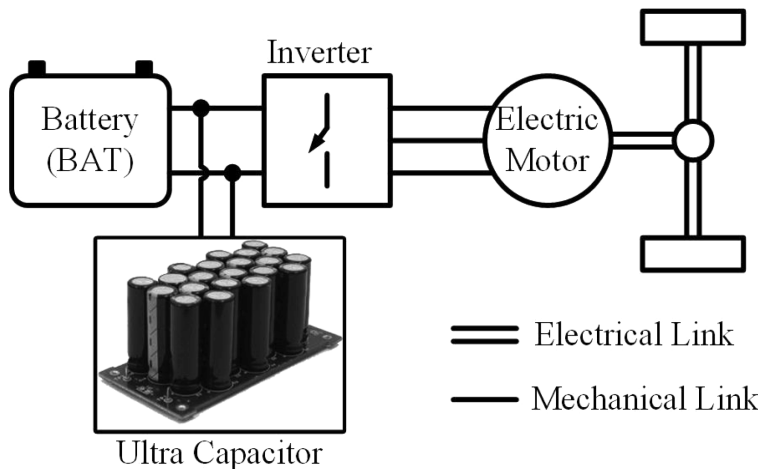


FIGURE 17.2 Topological arrangement for an EV drivetrain. (From Eshani, M. et al., *Modern Electric, Hybrid Electric, and Fuel Cell Vehicles*, 2nd ed., CRC Press, New York, 2009.)

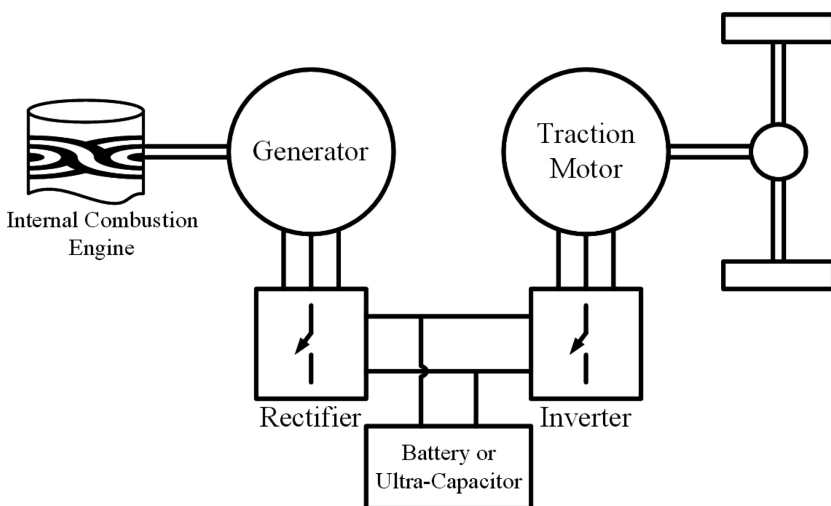


FIGURE 17.3 Typical layout of a series HEV drivetrain. (From Eshani, M. et al., *Modern Electric, Hybrid Electric, and Fuel Cell Vehicles*, 2nd ed., CRC Press, New York, 2009.)

The benefit of the HEV series setup is that the ICE operates mostly at its optimum balance of speed and torque, resulting in low fuel consumption and high performance.

17.3.3 PARALLEL HEV DRIVETRAIN TOPOLOGY

In parallel HEV, both the ICE and traction motors are linked mechanically to the transmission line. A schematic diagram of the parallel hybrid is shown in Figure 17.4. The vehicle can be powered by the ICE, or the electric motor, or together. There are

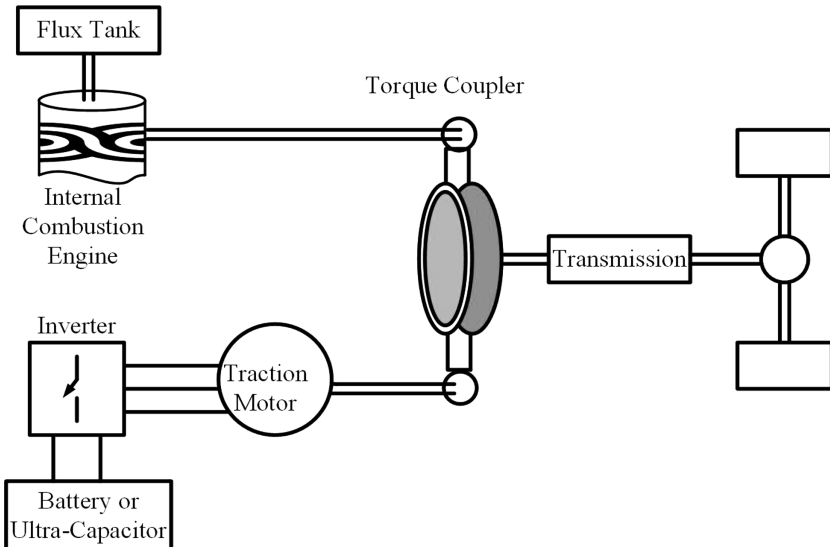


FIGURE 17.4 Schematic of a parallel HEV drivetrain configuration. (From Eshani, M. et al., *Modern Electric, Hybrid Electric, and Fuel Cell Vehicles*, 2nd ed., CRC Press, New York, 2009.)

different methods of using the ICE and the traction motor in parallel HEV configuration. One way is to use the motor at low speeds and the ICE at higher speeds. The traction motor can work as a generator and charge the battery when only the ICE is operating.

17.3.4 SERIES-PARALLEL HEV DRIVETRAIN TOPOLOGY

The series-parallel HEV is a combination of the series and parallel hybrids. The generator and the electric motor are mechanically linked together compared to the setup of the series configuration and the extra generator compared to the parallel hybrid as shown in [Figure 17.5](#). This configuration has both the advantages of parallel and series HEV configuration.

17.3.5 FCV DRIVETRAIN TOPOLOGY

The goal of continuing fuel-cell technology development programs is to create a fuel-cell engine that will offer benefits to standard vehicles and BEVs. A schematic of a fuel-cell-based propulsion system is shown in [Figure 17.6](#).

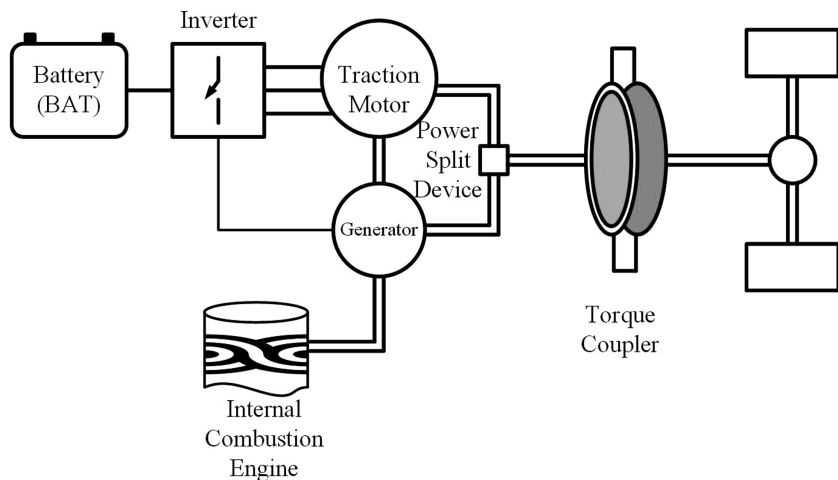


FIGURE 17.5 Typical drivetrain configuration of a series–parallel combined HEV. (From Eshani, M. et al., *Modern Electric, Hybrid Electric, and Fuel Cell Vehicles*, 2nd ed., CRC Press, New York, 2009.)

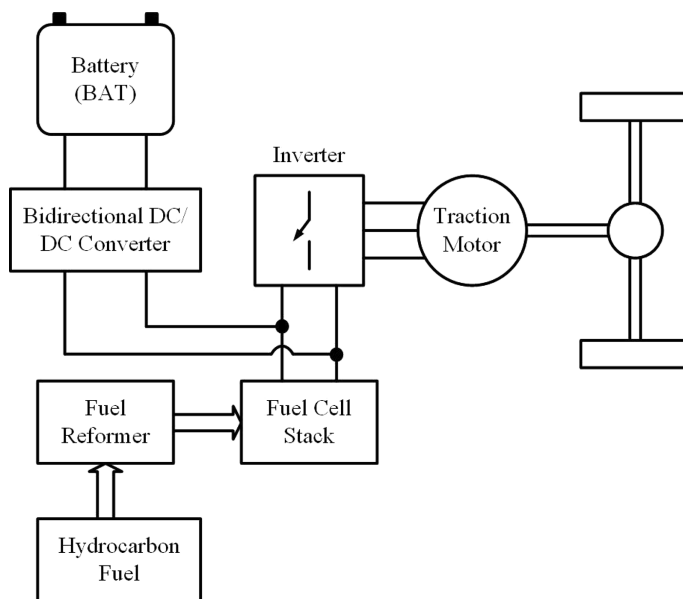


FIGURE 17.6 Typical topological arrangement of a hybrid fuel-cell vehicle drivetrain. (From Eshani, M. et al., *Modern Electric, Hybrid Electric, and Fuel Cell Vehicles*, 2nd ed., CRC Press, New York, 2009.)

17.4 VIBRATION AND VEHICLE DYNAMICS

17.4.1 VIBRATION

Bearing currents in EV motor drives are caused by common mode voltage. Bearing currents cause bearing failure and hence severe vibrations. There are four types of bearing currents: capacitive-bearing currents, electric discharge machining currents, circulating bearing currents, and rotor ground currents. Capacitive-bearing currents are of the order of 5–10 mA; hence, it is neglected, but the rest are prominent. The vibration can be reduced by reducing the common mode voltage using advanced modulation techniques.

17.4.2 VEHICLE DYNAMICS

To model EVs, all the forces that influence the dynamics of the vehicle must be identified, and the torque generated by the forces on the vehicle must be determined. It is essential to understand each force when the vehicle is stopped or in motion. There are many forces acting on the vehicle body and driving wheel. The major forces affecting vehicle dynamics are static friction, rolling resistance, traction or braking force, and aerodynamic drag force. A model of an EV used to determine the normal reaction on the front and rear wheels is shown in [Figure 17.7](#).

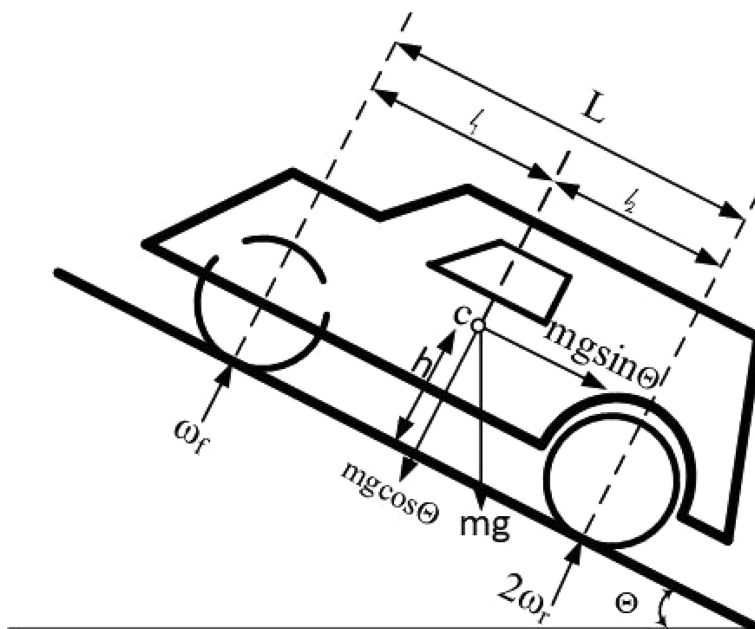


FIGURE 17.7 Free body diagram of three-wheeler. (From Jones, W.D., Take this car and plug it [plug-in hybrid vehicles], *IEEE Spectrum*, 42, 10–13, 2005.)

$$\omega_f = \frac{mgl_2 \cos\theta - mgh \sin\theta}{L} \quad (17.1)$$

$$\omega_r = \frac{mgl_1 \cos\theta + mgh \sin\theta}{2L} \quad (17.2)$$

At maximum inclination angle, the braking force is proportional to the normal force. Therefore,

$$F_{x2} = f_r \omega_r \quad (17.3)$$

where F_{x2} is the braking force applied on the wheel.

Applying Newton's second law of motion on the vehicle and assuming that the forces on all wheels are equal, the rolling condition $a = \alpha R$.

The net mechanical torque offered by the vehicle is

$$T_e = \alpha \left[I_\omega + \frac{mR^2}{3} \right] + \frac{R}{3} [mg \sin\theta + F_d] \quad (17.4)$$

where:

α is the angular acceleration of wheel

I_ω is the wheel moment of inertia

m is the mass of vehicle

R is the radius of wheel

g is the gravitational acceleration

θ is the slope of road

F_d is the drag force

Mathematical modeling of the brushless DC (BLDC) motor is carried out. **Figure 17.8** shows the basic block diagram of the BLDC motor and mechanical load. The major construction difference between the BLDC and DC motor is that

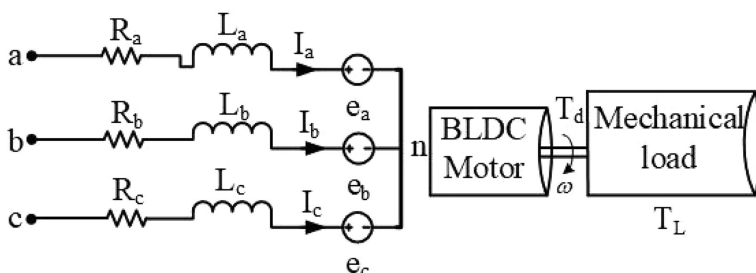


FIGURE 17.8 Three-phase BLDC motor equivalent circuit and mechanical model. (From Jones, W.D., Take this car and plug it [plug-in hybrid vehicles], *IEEE Spectrum*, 42, 10–13, 2005.)

the BLDC motor has phase winding at the stator side, and the rotor contains a permanent magnet, but in the DC motor, the rotor has armature winding and stator holds a permanent magnet.

For simplicity, the electrical model of one phase can be represented as stator winding, phase k ($k = a, b$ or c) is given by Equation (17.5).

$$v_{kn}(t) = i_k R_k + L_k \frac{di_k(t)}{dt} + e_k(t) \quad (17.5)$$

where:

$V_{kn}(t)$ is the instantaneous k -phase voltage

$i_k(t)$ is the instantaneous k -phase current

$e_k(t)$ is the instantaneous k -phase back-emf voltage

R_k is the k -phase resistance

L_k is the k -phase inductance

On the other hand, the mechanical model of the BLDC motor is given in Equation (17.6).

$$T_d(t) = J \frac{d\omega}{dt} + b\omega(t) + T_L(t) \quad (17.6)$$

where:

$\omega(t)$ is the rotor angular velocity

B is the viscous friction

J is the moment of inertia

T_L is the load torque

The total torque produced by the motor is a summation of the torque produced by each phase:

$$T_d(t) = \sum_{k=a,b,c} T_{d,k}(t) \quad (17.7)$$

The production of torque and back-emf voltage of each phase is calculated as

$$T_{d,k}(t) = i_k(t) \cdot k_{T,k}(\theta) \quad (17.8)$$

$$e_k(t) = k_{v,k}(\theta) \cdot \omega_e(t) \quad (17.9)$$

where:

The torque constant $k_{T,k}(\theta)$ can be assumed equivalent to back emf voltage constant $k_{v,k}(\theta)$.

The angular velocity ω_e is the product of rotor angular velocity, and the multiplication factor depends on the number of poles.

17.5 POWER CONVERTER FOR ELECTRIC/HYBRID ELECTRIC VEHICLES

17.5.1 CONFIGURATIONS OF ENGINE-BASED HEV

Two different types of energy management systems for the engine-based HEV are shown in [Figure 17.9](#). It has electric generator to generate DC bus voltage to power the inverter-motor drive, also charge the battery during cruising, deceleration, and regenerative braking. The configuration shown in [Figure 17.9a](#) does not include a bidirectional DC-DC converter. It consists of a high-voltage battery, which is equivalent to the output of the generator that supplies the rated voltage to the inverter-motor drive. The other configuration is shown in [Figure 17.9b](#). It comprises a bidirectional DC-DC converter that controls the flow of energy between the battery and DC bus. The first type of configuration is more attractive because it uses a smaller number of components, but performance-wise, the second configuration is better.

17.5.2 CONFIGURATIONS OF FCV

The FCV can also be configured with or without a bidirectional DC-DC converter. [Figure 17.10a](#) shows the configuration of FCV without the bidirectional DC-DC converter, whereas [Figure 17.10b](#) shows the FCV configuration with DC-DC converter.

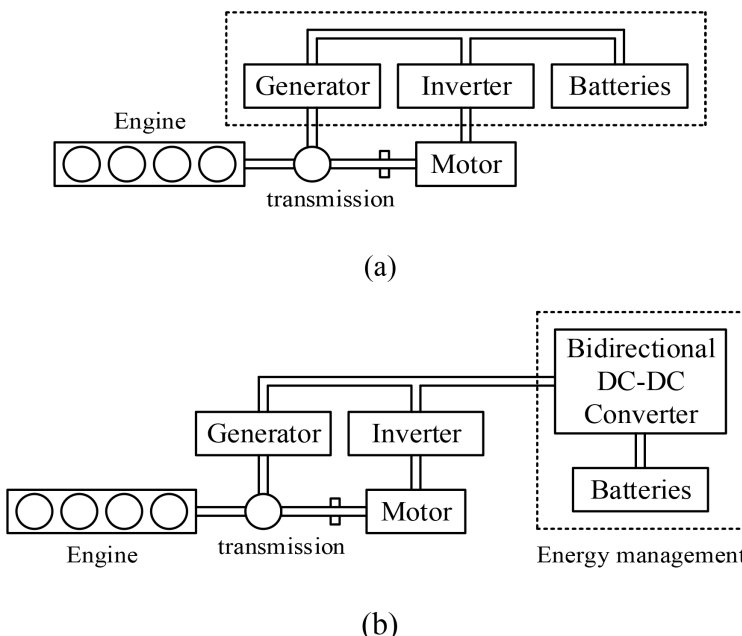


FIGURE 17.9 Energy management systems of an engine-based HEV: (a) without DC-DC converter and (b) with DC-DC converter. (From Wirasingha, S.G. et al., Plug-in hybrid electric vehicle developments in the US: Trends, barriers, and economic feasibility, in *Proceedings of the IEEE-VPPC*, Harbin, China, 2008, pp. 1–8.)

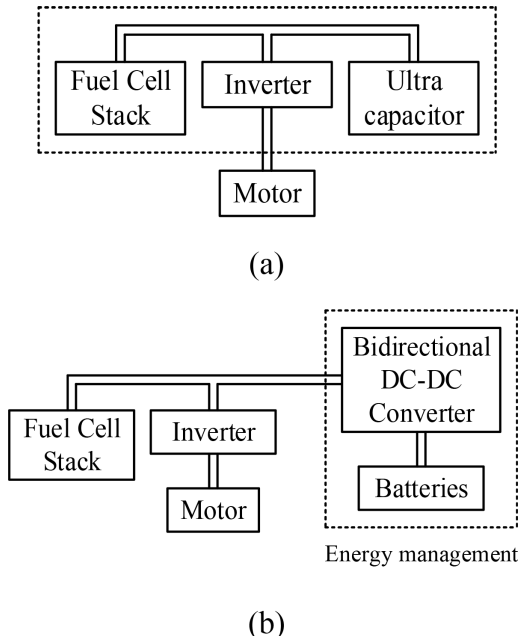


FIGURE 17.10 Energy management systems of an engine-based FCV: (a) without DC–DC converter and (b) with DC–DC converter. (From Wirasingha, S.G. et al., Plug-in hybrid electric vehicle developments in the US: Trends, barriers, and economic feasibility, in *Proceedings of the IEEE-VPPC*, Harbin, China, 2008, pp. 1–8.)

17.5.3 BASIC BIDIRECTIONAL DC-DC CONVERTERS

The nonisolated bidirectional DC–DC converter can be categorized into: (1) buck, (2) boost, and (3) buck-boost type. The inductive energy storage element is placed on the high-voltage (HV) side of the buck type converter and on the low-voltage (LV) side of the boost type converter. The circuit in Figure 17.11a shows an HV fuel cell supplemented with an LV battery, and 17.11b shows an LV fuel cell supplemented with an HV battery. They both represent a boost-type nonisolated bidirectional DC–DC converter.

As it is shown in Figure 17.11a, the DC-link voltage is higher than LV side (V_{in}) and there are two modes of operation. In the battery-charging operation, switch S_1 and diode of S_2 are operated, and it is unidirectional buck converter. In charging, the battery is powered from the HV bus. In the discharging operation, switch S_2 and diode of S_1 are operative. The power is transferred from LV to HV. Figure 17.12 shows a buck-type bidirectional converter for high-power HEV or FCV traction-motor drive applications. HV is needed for higher torque and speed in a traction-motor drive.

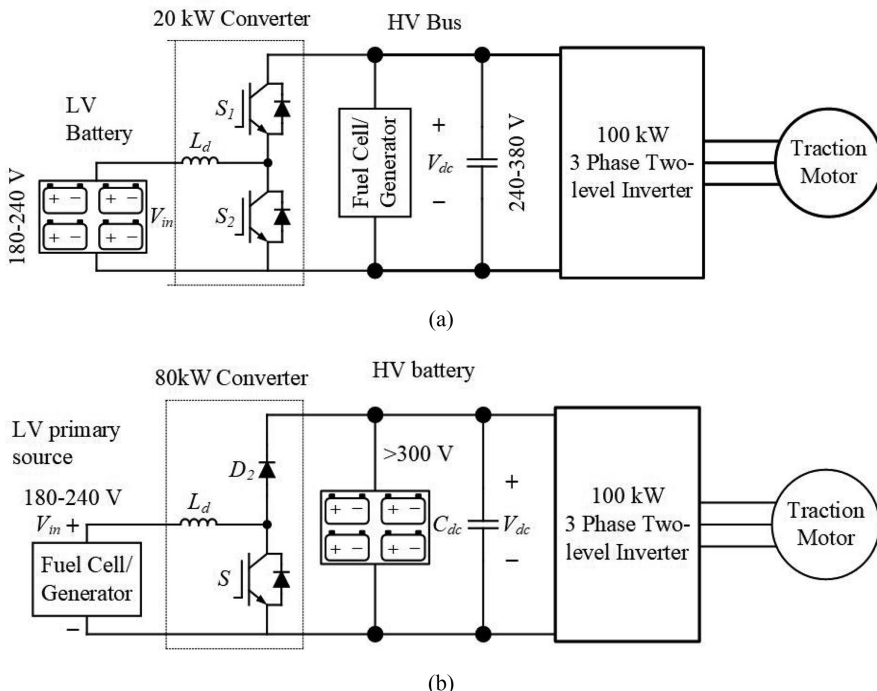


FIGURE 17.11 Power converter sizing for (a) HV fuel-cell supplemented with LV battery and (b) LV fuel cell supplemented with HV battery. (From Wirasingha, S.G. et al., Plug-in hybrid electric vehicle developments in the US: Trends, barriers, and economic feasibility, in *Proceedings of the IEEE-VPPC*, Harbin, China, 2008, pp. 1-8.)

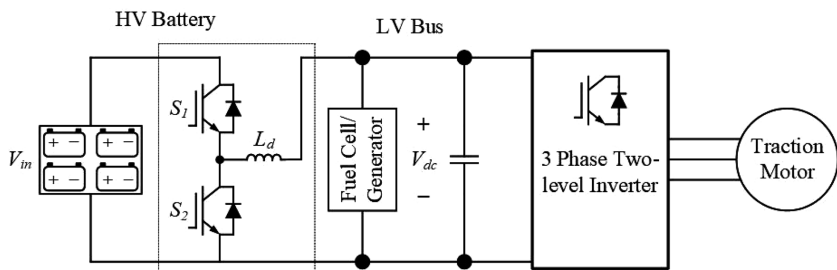


FIGURE 17.12 Buck-type bidirectional converter for high-power HEV or FCV traction motor drive applications. (From Wirasingha, S.G. et al., Plug-in hybrid electric vehicle developments in the US: Trends, barriers, and economic feasibility, in *Proceedings of the IEEE-VPPC*, Harbin, China, 2008, pp. 1-8.)

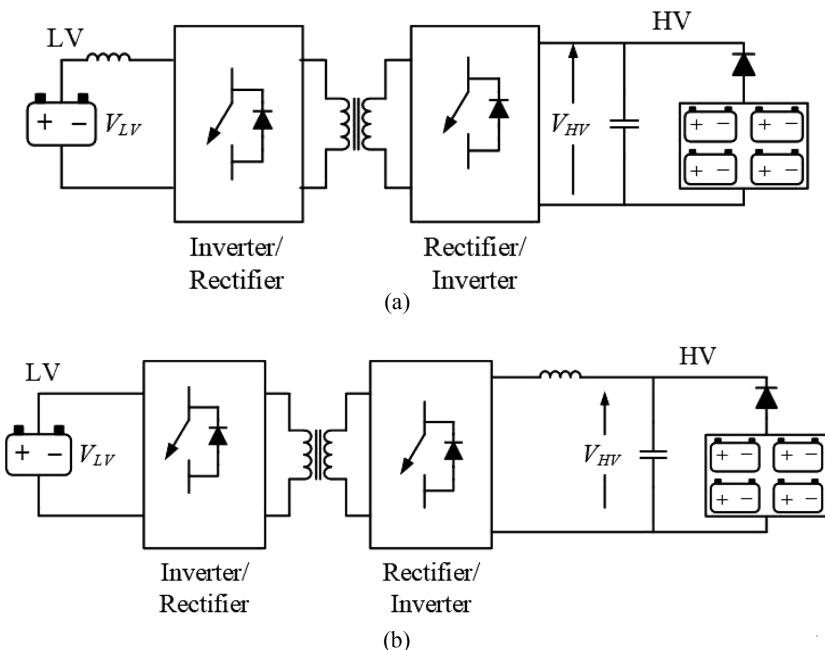


FIGURE 17.13 Basic isolated bidirectional DC-DC converter configurations: (a) LV current source and HV voltage source and (b) LV voltage source and HV current source. (From Wirasingha, S.G. et al., Plug-in hybrid electric vehicle developments in the US: Trends, barriers, and economic feasibility, in *Proceedings of the IEEE-VPPC*, Harbin, China, 2008, pp. 1–8.)

Generally, transformers are used for isolation in DC-DC converter circuits. This increases the loss and cost of the converter. The isolation is required when: (1) the ratio of HV and LV is high, and the device cannot handle HV and high current simultaneously; and (2) LV and HV sides cannot be grounded together. Figure 17.13 shows two basic configurations of the isolated bidirectional DC-DC converter. Figure 17.13a shows a LV current source and HV voltage source, and Figure 17.13b shows a LV voltage source and HV current source. It is possible to operate each side of the DC-DC bidirectional converter as an inverter or rectifier. In the inverter mode, the current conducts through switches, whereas in rectification mode, the diode conducts.

17.5.4 ISOLATED BIDIRECTIONAL DC-DC CONVERTERS

Figure 17.14 shows the circuit diagram using an L-type current source converter for the LV side. It is smaller in size as compared to traditional half-bridge converter because of split inductor. Figure 17.15 shows the bidirectional DC-DC converter. The LV side has a full-bridge current source converter, whereas the HV side has a full-bridge voltage source converter.

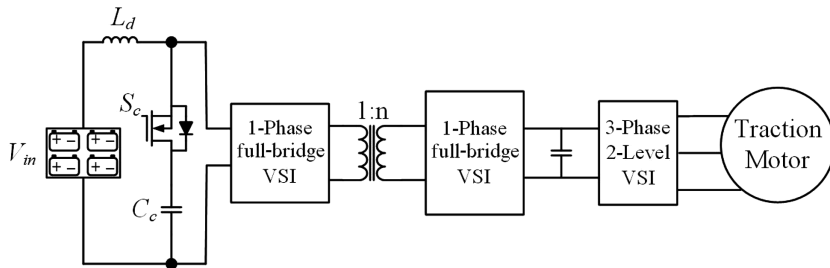


FIGURE 17.14 Bidirectional DC-DC converter with full-bridge current source converter for LV side and full-bridge voltage source converter for HV side. (From Wirasingha, S.G. et al., Plug-in hybrid electric vehicle developments in the US: Trends, barriers, and economic feasibility, in *Proceedings of the IEEE-VPPC*, Harbin, China, 2008, pp. 1–8.)

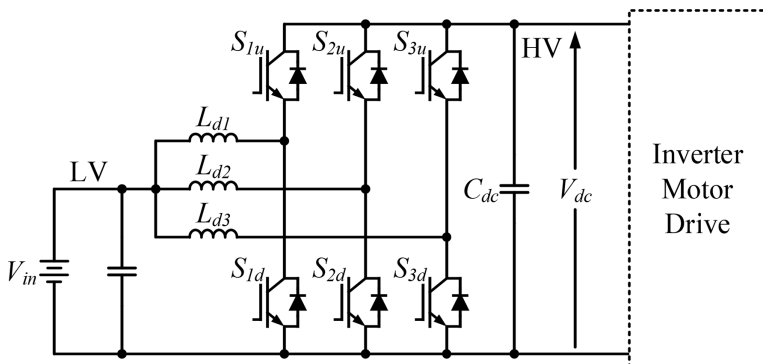


FIGURE 17.15 Three-phase nonisolated bidirectional DC-DC converter. (From Wirasingha, S.G. et al., Plug-in hybrid electric vehicle developments in the US: Trends, barriers, and economic feasibility, in *Proceedings of the IEEE-VPPC*, Harbin, China, 2008, pp. 1–8.)

17.5.5 MULTIPHASE BIDIRECTIONAL DC-DC CONVERTERS

A single converter needs numerous equipment in parallel for high-power applications. As indicated in the previous design case, it is required to have multiple phase legs to reduce voltage or current stress, and thus have higher efficiency. Figure 17.15 shows a three-phase bidirectional DC-DC converter.

It is also possible to design the isolated bidirectional DC-DC converter with multiphase interleaving. Figure 17.16 shows a three-phase converter for both the LV and HV sides. The three-phase leg configuration can be extended to six phase legs with the same three transformers for higher-power applications.

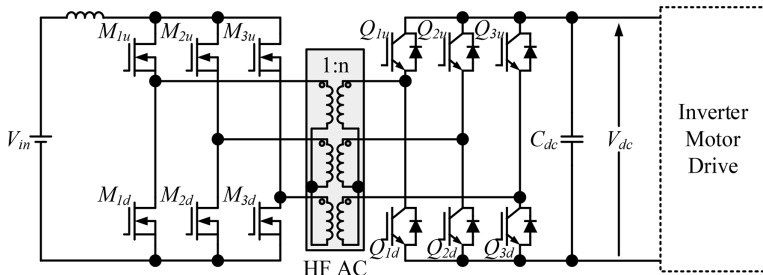


FIGURE 17.16 Three-phase isolated bidirectional DC–DC converter. (From Wirasingha, S.G. et al., Plug-in hybrid electric vehicle developments in the US: Trends, barriers, and economic feasibility, in *Proceedings of the IEEE-VPPC*, Harbin, China, 2008, pp. 1–8.)

17.6 VEHICULAR POWER ELECTRONICS

17.6.1 POWER CONVERTERS FOR DC MOTOR DRIVES

Low-cost EVs such as motorcycles use DC motor drives. The DC-link voltages are 24–48 V, and the power rating is 1–3 kW. A two-quadrant zero-voltage-switching multi-resonant (2Q-ZVS-MR) converter has been applied to DC motor drives as shown in Figure 17.17.

17.6.2 POWER CONVERTERS FOR AC MOTOR DRIVES

Power-converter topology for the AC motor drive is shown in Figure 17.18. AC motor drives should have the following features: high power, density, efficiency, require less maintenance. They should also have the capability of backward power flow. The DC-link voltages are in the range of 240–480 V, and power is in the range of 10–80 kW.

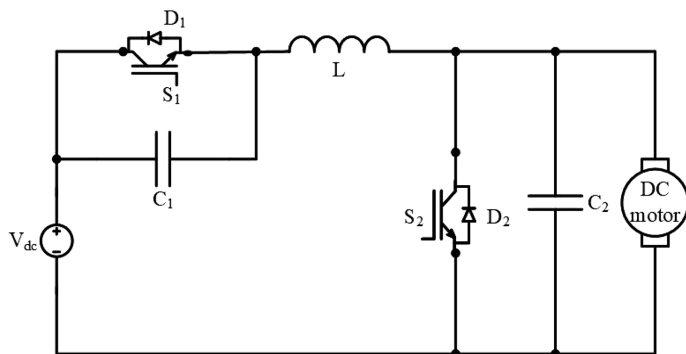


FIGURE 17.17 2Q-ZVS-MR converter for DC motor drives. (From Ceraolo, M. et al., *IEEE Trans. Veh. Technol.*, 57, 1433–1441, 2008.)

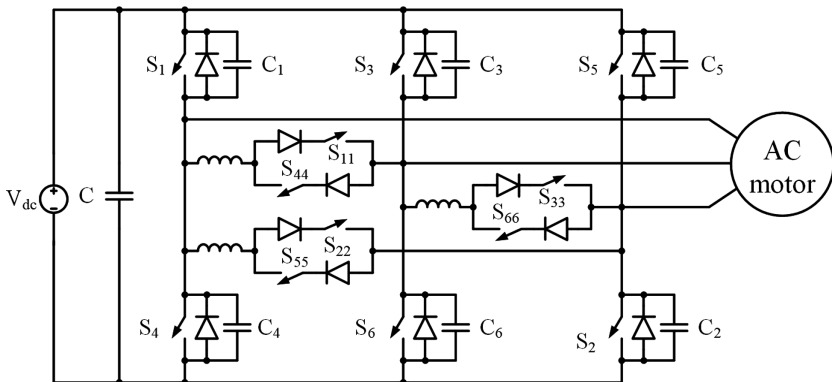


FIGURE 17.18 Delta-configured ARS inverter for AC motor drives. (From Ceraolo, M. et al., *IEEE Trans. Veh. Technol.*, 57, 1433–1441, 2008.)

The soft-switching inverters used in AC motor drive can be categorized as the resonant DC-link types and resonant AC pole types. Many improved soft-switching topologies have been developed. These are (1) quasi-resonant DC-link inverter, (2) series-resonant DC-link inverter, (3) parallel resonant DC-link inverter, and (4) synchronized resonant DC-link inverter. The resonant AC-pole types include the (1) resonant pole inverter, (2) auxiliary-resonant commutated pole inverter, (3) auxiliary resonant snubber (ARS) inverter, (4) zero-voltage transition (ZVT) inverter, and (5) zero-current transition (ZCT) inverter. Among them, the ARS inverter has been actively developed for electric propulsion.

17.7 SELECTION OF MOTOR DRIVES FOR ELECTRIC/HYBRID ELECTRIC VEHICLES

Selection of traction motors for hybrid-propulsion systems is a very significant and requires particular attention. In reality, the most suitable electrical propulsion system for HEVs and EVs is still being investigated. Efficiency, reliability, and price are the main characteristics. Selection of electric-propulsion systems for HEVs depends on three factors: driver expectation, vehicle constraint, and energy source. It is therefore a difficult job to select the most suitable electrical propulsion system for an HEV.

From an industrial point of view, the DC motor, induction motor (IM), permanent magnet (PM) synchronous engine, and switched reluctance motor (SRM) are the main kinds of electric motors used for both HEVs and EVs.

The major requirements of HEVs electric propulsion are summarized as follows:

1. High instantaneous power density.
2. High torque at low starting and climbing speeds while high power at high cruising speeds
3. A very wide speed range, including constant-torque and constant-power regions

4. A fast torque response
5. A high efficiency over the wide speed and torque range
6. A high efficiency for regenerative braking
7. A high reliability and robustness for various vehicle-operating conditions
8. A reasonable cost

[Figure 17.19](#) shows the normal features of an electric motor used in EVs or HEVs. In the constant-torque region, the electric motor delivers a constant torque (rated torque) over the entire speed range till the motor reaches the base speed. After the motor reaches the rated speed, the torque decreases proportionally with speed and enters in a constant-power region and delivers (rated power) output. In the constant-power region, the torque decreases proportionally with the square of the speed.

17.7.1 COMPARATIVE STUDY

17.7.1.1 DC Motor (DC)

DC motors have been prominent in electric propulsion because their torque-speed controls are simple. However, the drawbacks of DC motor drives are that they are bulky, have low efficiency, low reliability, and require regular maintenance due to the presence of commutator brush.

17.7.1.2 Induction Motor

Because of their reliability, roughness, low maintenance, low price, and capacity to function in hostile settings, cage IMs are commonly recognized as the most

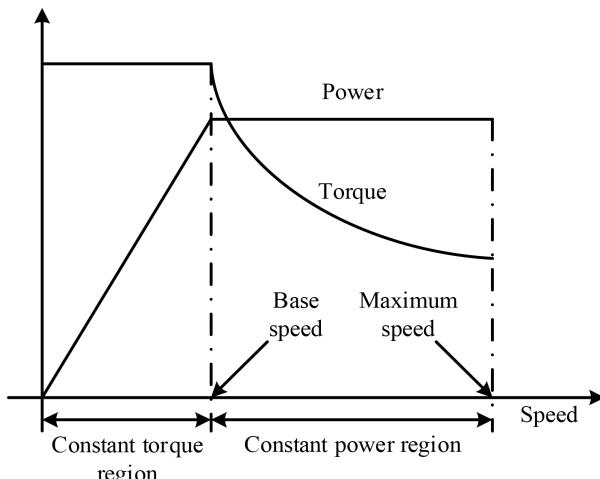


FIGURE 17.19 HEV typical characteristics of Electric traction. (From Ehsani, M. et al., *Modern Electric, Hybrid Electric, and Fuel Cell Vehicles: Fundamentals, Theory, and Design*, CRC Press, Boca Raton, FL, 2004.)

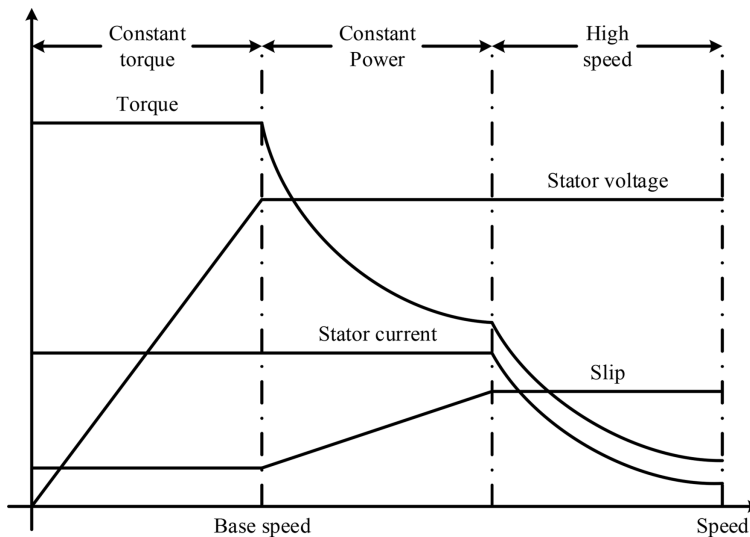


FIGURE 17.20 IM characteristics. (From Ehsani, M. et al., *Modern Electric, Hybrid Electric, and Fuel Cell Vehicles: Fundamentals, Theory, and Design*, CRC Press, Boca Raton, FL, 2004.)

prospective candidate for HEV electrical propulsion. They are especially suitable for industrial and traction drives. Figure 17.20 shows the typical characteristics of an IM drive. IM can be controlled like a DC motor by using field-oriented control, which can decouple its torque control from field control. Extended field range operation with a constant power above the base speed can be achieved by flux weakening. Few disadvantages of IM are predominantly high loss, low efficiency, low power factor, and low inverter usage factor, which are more severe for high speed and large motor.

17.7.1.3 Synchronous Motor (PM Brushless Motor)

PM brushless motors are close competitors with IMs for the electric propulsion of HEVs. In fact, they are accepted by recognized automakers for their HEVs. The advantages of PM brushless motors are: (1) low weight and volume for a given output power (high-power density), (2) higher efficiency, and (3) effective heat dissipation in the environment.

Few drawbacks are that it has a short constant-power region due to their rather limited field weakening capability, as shown in Figure 17.21a. To increase the speed range and enhance the efficiency of brushless PM motors, the power converter's conductive angle can be regulated above the base speed. Figure 17.21b demonstrates the torque-speed profile of a brushless PM motor with conduction angle control.

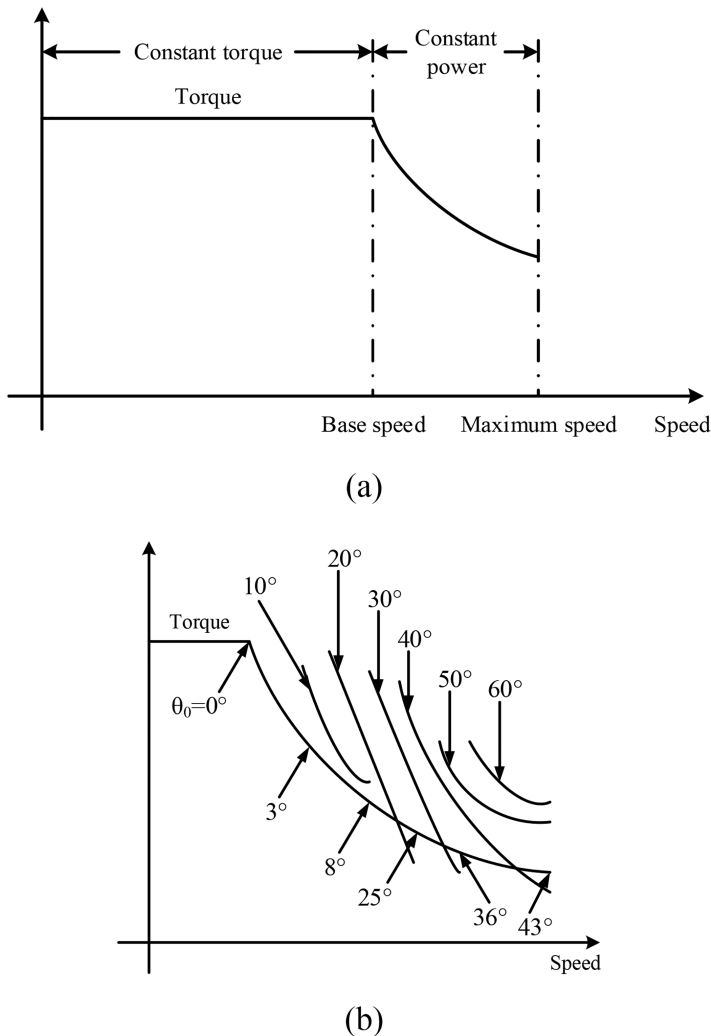


FIGURE 17.21 Torque-speed characteristics of a PM brushless drive: (a) typical characteristic and (b) with conduction-angle control. (From Ehsani, M. et al., *Modern Electric, Hybrid Electric, and Fuel Cell Vehicles: Fundamentals, Theory, and Design*, CRC Press, Boca Raton, FL, 2004.)

17.7.1.4 Switched Reluctance Motor (SRM)

SRMs are gaining a lot of interest, and the potential for HEV application is acknowledged. The advantages of SRM are: (1) simple and robust construction, (2) fault-tolerant operation, (3) simple control, (4) extremely long constant-power range, and (5) good torque-speed characteristics as shown in [Figure 17.22](#). The disadvantages of SRM are acoustic noise generation, more torque ripple, and special converter topology.

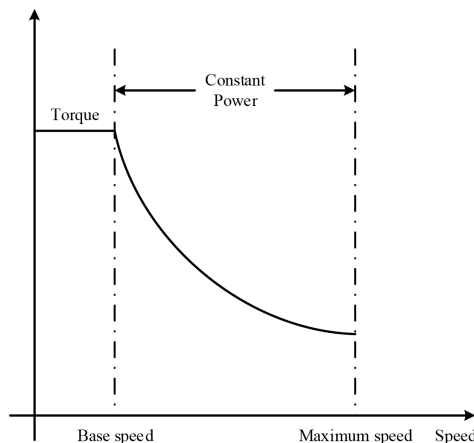


FIGURE 17.22 Typical torque-speed characteristic of an SRM. (From Ehsani, M. et al., *Modern Electric, Hybrid Electric, and Fuel Cell Vehicles: Fundamentals, Theory, and Design*, CRC Press, Boca Raton, FL, 2004.)

17.8 SOLAR AND FUEL CELL DRIVES

Solar photovoltaic (SPV) technology directly converts solar energy into electricity. It has few advantages such as no moving parts, no noise, no emissions, and long lifetime. Hence, it has large industrial potential. SPVs are a sustainable energy source. Harvesting energy from the sun is most easy today with the help of solar arrays. Generally, the photovoltaic (PV) cell characteristic is nonlinear, and it converts the energy for utility interface. The cost of solar panels is on higher side, so the maximum power should be extracted for any irradiation. The solar cells are classified as

- Monocrystalline silicon cells
- Polycrystalline silicon cells
- Amorphous silicon cells

The monocrystalline silicon cell is made of pure silicon (single crystal), and it has efficiency approximately 14%–17%. Liquid silicon is used as raw material in polycrystalline solar cells, and polycrystalline silicon was obtained followed by the solidification process, with an efficiency of 13%–15%. Amorphous silicon cell is acquired by putting silicon film on the substrate such as a glass plate, and it has efficiency of 5%–7%.

17.9 PV ARRAY FORMATIONS

A solar cell is basically a p-n junction fabricated in a thin wafer of semiconductor. It works on the photovoltaic effect, in which the electromagnetic radiation of solar energy is converted to electricity through PV effect. Some electron-hole pairs that are proportional to irradiation are created by photons that have energy higher than the band-gap energy. A PV panel's equivalent circuit is as shown in [Figure 17.23](#).

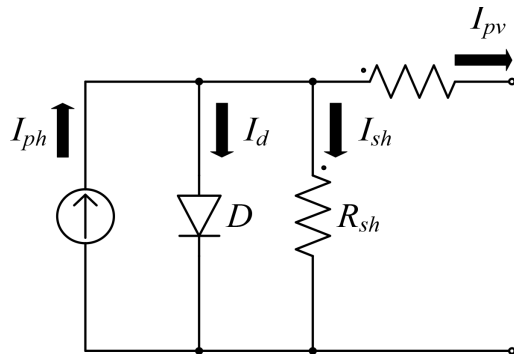


FIGURE 17.23 Equivalent circuit of a PV module. (From Solanki, C.S., *Solar Photovoltaics—Fundamentals, Technologies and Applications*, PHI India, New Delhi, India, 2015.)

The current source I_{ph} is the photocurrent of the cell. R_{sh} and R_s are the cell's shunt and series resistance. The PV cells are connected in series to form a PV module and that module is connected in series-parallel to make arrays. Mathematical modeling of a PV panel can be described by the following equations. Module photo current:

$$I_{ph} = [I_{scr} + K_i(T - 298)] \times \frac{G}{1000} \quad (17.10)$$

Module reverse saturation current (I_{rs})

$$I_{rs} = \left[\frac{I_{scr}}{e^{\left(\frac{q \times V_{oc}}{N_s k A T} \right)} - 1} \right] \quad (17.11)$$

The module saturation current I_s varies with cell temperature, which is given by

$$I_s = I_{rs} \left[\frac{T}{T_r} \right]^3 \exp \left[q \times \frac{E_{go}}{B \times k} \times \left(\frac{1}{T_r} - \frac{1}{T} \right) \right] \quad (17.12)$$

The current output of PV module is

$$I_{pv} = N_p \times I_{ph} - N_p \times I_o \left[\exp \left(q \times \frac{V_{pv} + I_{pv} R_s}{N_s A k T} \right) - 1 \right] \quad (17.13)$$

where:

V_{pv} is the output voltage of a PV module (V)

I_{pv} is the output current of a PV module (A)

T_r is the reference temperature = 298 K

T is the module operating temperature in Kelvin

I_{ph} is the light generated current in a PV module (A)

I_s is the PV module saturation current (A)

A is the ideality factor

k is Boltzmann constant = 1.3805×10^{-23} J/K

q is electron charge = 1.6×10^{-19} C

R_s is the series resistance of a PV module

I_{scr} is the PV module short-circuit current at 250°C and 1000 W/m^2

K_i is the short-circuit current temperature coefficient

G is the PV module illumination in W/m^2

E_{go} is the band gap for silicon

N_s is the number of cells connected in series

N_p is the number of cells connected in parallel

The modeling of the PV array is the same as the PV cells. To obtain the required power, voltage, and current, the PV modules are connected in series and parallel.

Figure 17.24 shows a photovoltaic array, which consists of multiple modules, connected in parallel and series. The value of equivalent resistance in series and resistance in parallel of the PV array are:

$$R_{s,\text{equ}} = R_s \times \frac{N_s}{N_p} \quad (17.14)$$

$$R_{p,\text{equ}} = R_p \times \frac{N_s}{N_p} \quad (17.15)$$

The PV array current can be modeled as

$$I_{pv} = N_p \times I_{ph} - N_p \times I_o \left[\exp \left(q \times \frac{V_{pv} + I_{pv} R_s \left(\frac{N_s}{N_p} \right)}{AkTN_s} \right) - 1 \right] \quad (17.16)$$

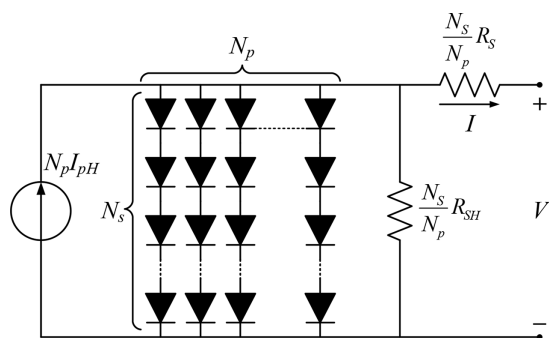


FIGURE 17.24 Equivalent circuit of a PV module. (From Solanki, C.S., *Solar Photovoltaics—Fundamentals, Technologies and Applications*, PHI India, New Delhi, India, 2015.)

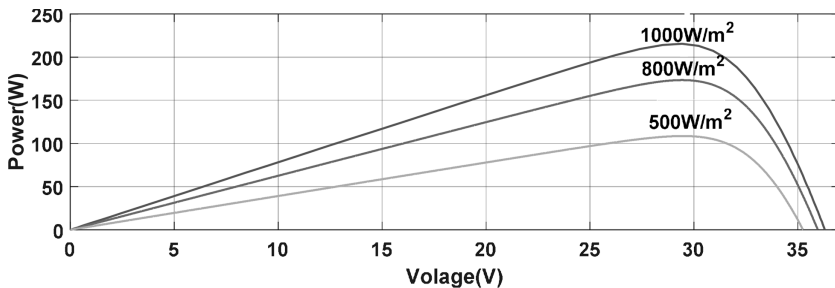


FIGURE 17.25 P-V curve of a solar array. (From Kumar, J. and Behera, R.K., Solar powered motor drive, Registration Report, January 2019.)

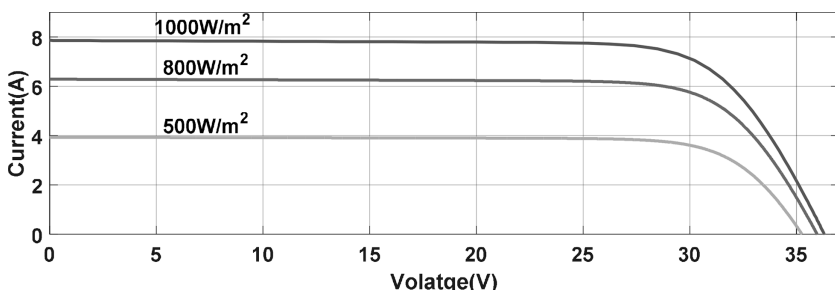


FIGURE 17.26 I-V curve of a solar array. (From Kumar, J. and Behera, R.K., Solar powered motor drive, Registration Report, January 2019.)

Figures 17.25 and 17.26 show the I-V curves and P-V curves of a PV strings with different isolation.

17.10 SOLAR-POWERED VARIABLE-SPEED DRIVE

The solar-powered variable-speed drive consists of a solar panel, MPPT charge controller, battery, power converter with motor controller, and a motor. Solar panels produce a variable energy over the day, and it is called fluctuating energy flow. It may damage the motor due to variable power flow. The protection system should be developed along with the motor drive control. Now the solar-based motor drive is very popular, and some of its applications are given below.

17.10.1 SOLAR-BASED ELECTRIC VEHICLES

Mainly, solar energy is used in EV for charging purpose. Generally, the battery of the EV is connected through a solar charger and also plugged into a grid. It will be helpful for fast charging and during the rainy season. There are various types of solar-powered EVs based on the DC motor, BLDC motor, permanent magnet synchronous motor (PMSM), and IM reported in the literature. However, a general block diagram

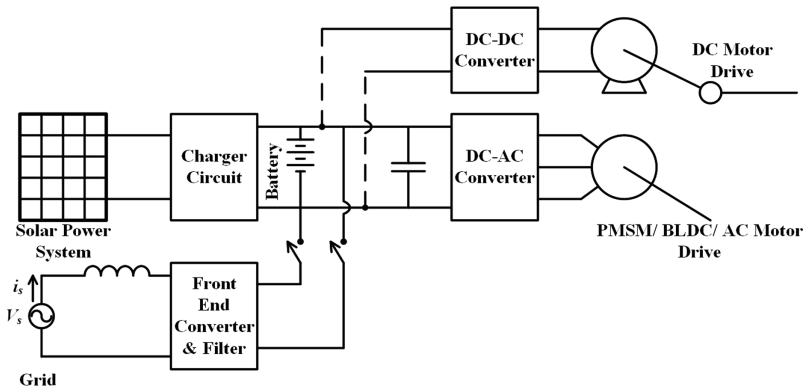


FIGURE 17.27 Block diagram of a solar-based EV. (From Behera, R.K. and Das, S.P., A utility friendly high-performance multilevel inverter fed induction motor drive system for traction and industrial applications, Ph. D Thesis, Indian Institute of Technology Kanpur, Uttar Pradesh, India, 2009.)

of the solar-based EV is shown in [Figure 17.27](#). From [Figure 17.27](#), if the DC motor is used in an EV, the DC-DC converter will be used, and if the EV motor is a PMSM or BLDC motor or AC motor used, the DC-AC converter will be used.

17.10.2 SOLAR-BASED PUMP DRIVE

The solar-based water-pumping system consists of a solar array, DC-DC converter, inverter, and motor drive. Mainly, the DC-DC converter is used to step up or step down the DC-link voltage. There are few topologies available with a solar- and grid-integrated hybrid-pumping system. A general block diagram of the solar pumping system is shown in [Figure 17.28](#). From [Figure 17.28](#), if the DC motor is used for

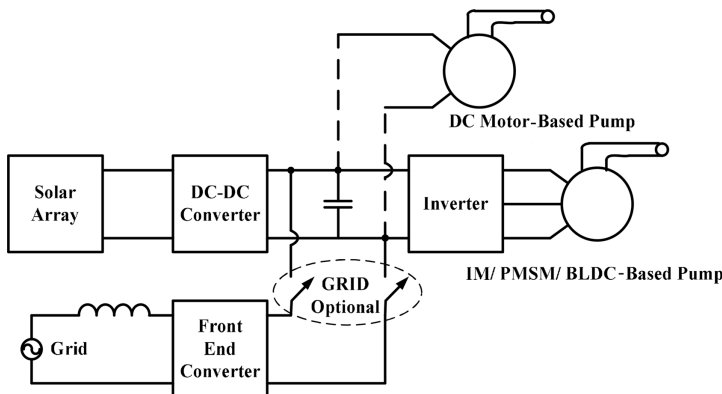


FIGURE 17.28 Block diagram of solar pumping system. (From Ehsani, M. et al., *Modern Electric, Hybrid Electric, and Fuel Cell Vehicles: Fundamentals, Theory, and Design*, CRC Press, Boca Raton, FL, 2004.)

pumping drives, a DC-DC converter is appropriate, and if the pumping motor is PMSM or BLDC motor or AC motor, the DC-AC converter is the suitable choice.

17.11 FUEL-CELL-POWERED ELECTRICAL DRIVES

Fuel-cell technology converts the chemical energy from a fuel to produce electricity. Chemical energy continuously flows. The typical fuel cell has two electrodes and an electrolyte. One electrode is called an anode, and the other is the cathode. The process of electric-current production is shown in [Figure 17.29](#).

There are various types of fuel cell mentioned below:

- Proton exchange membrane
- Direct methanol
- Alkaline
- Phosphoric acid
- Molten carbonate
- Solid oxide

Fuel-cell-based energy conversion technology takes place through an electrochemical process. Hence, it is a clean, quiet, and high-efficient process. The fuel-cell technology is a stable power source because, till fuel is available, it will operate. Therefore, the various applications are in space craft, remote weather station, large park, and rural. In this chapter, different applications on the drive technology are discussed.

Due to many advantages, fuel-cell technology became one of the popular propulsion systems for EVs. It is very useful in other applications, such as onboard power generation and stationary power generation. A suitable power converter such as the step-up or step-down DC-DC converter is used between fuel cell stacks and with the matching voltage of the battery. A DC-AC converter is used to generate variable voltage and variable frequency, and it drives the propulsion motor. In general, the fuel cell is connected to battery storage or ultracapacitor and is used for supplementary power requirement during starting and other dynamic conditions. A general block diagram of fuel-cell-powered electric drives system is shown in [Figure 17.30](#).

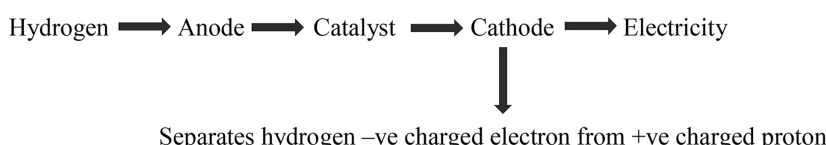


FIGURE 17.29 Fuel-cell current production process. (From Ehsani, M. et al., *Modern Electric, Hybrid Electric, and Fuel Cell Vehicles: Fundamentals, Theory, and Design*, CRC Press, Boca Raton, FL, 2004.)

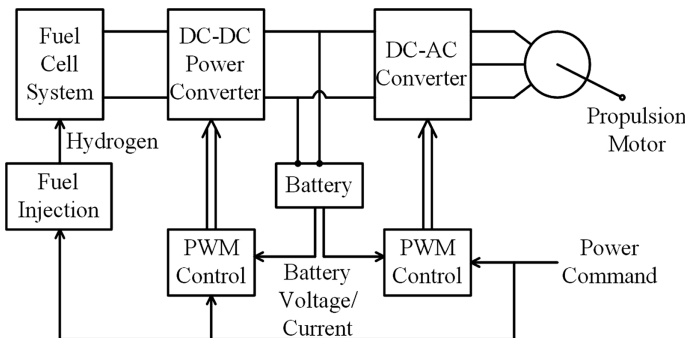


FIGURE 17.30 Block diagram of fuel-cell-powered electric drive system. (From Ehsani, M. et al., *Modern Electric, Hybrid Electric, and Fuel Cell Vehicles: Fundamentals, Theory, and Design*, CRC Press, Boca Raton, FL, 2004.)

17.12 SOLVED PROBLEMS

Example 17.1: Calculate the tractive power for accelerating the vehicle from zero speed to 60 km/hr in 5 s. The data for the EV is given as: mass of vehicle = 1200 kg, tire-rolling resistance coefficient = 0.01, air density = 1.205 kg/m³, aerodynamic drag coefficient = 0.3, vehicle frontal area = 2 m², vehicle base speed = 30 km/hr, and vehicle rotational inertial factor = 1.5.

SOLUTION

Tractive power is given as

$$P_t = \frac{\delta M}{2t_a} (V_f^2 + V_b^2) + \frac{2}{3} Mg f_r + \rho_a C_D A_f V_f^3$$

$$\delta = 1.25, M = 1200 \text{ kg}, t_a = 5 \text{ s}, V_f = 60 \text{ km/hr}, V_b = 30 \text{ km/hr}, g = 9.8 \text{ m/s}^2, f_r = 0.01, \rho_a = 1.205 \text{ kg/m}^3, C_D = 0.3, A_f = 2 \text{ m}^2$$

Substituting all the values in preceding equation we get tractive power, $P_t = 55.46327 \text{ kW}$.

Example 17.2: The speed of a DC motor is controlled by a DC-DC converter. The DC supply voltage is 80 V. The armature circuit resistance is $R_a = 0.3 \Omega$, and armature inductance is $L_a = 8 \text{ mH}$. The motor constant $K_a = 0.07 \text{ V/rpm}$. The motor drives a constant torque load requiring an average armature current of 20 A. Assuming that the motor current is continuous, compute (a) the range of speed control, and (b) range of duty cycle.

SOLUTION

The average value of armature voltage is given by

$$V_a = I_a R_a + E_b$$

Minimum speed is zero at which $E_b = 0$

$$V_a = I_a R_a = 20 \times 0.3 = 6 \text{ V}$$

The duty ratio is given by

$$D = \frac{6}{80} = 0.075$$

Maximum speed corresponds to $D = 1$, at which $V_a = V_{dc} = 80 \text{ V}$

The back emf at maximum speed is

$$E_b = V_a - I_a R_a = 80 - (20 \times 0.3) = 74 \text{ V}$$

The maximum speed is

$$N_{\max} = \frac{74}{0.07} = 1057.14 \text{ rpm}$$

Hence, the range of speed control is 0–1057.14 rpm.

REVIEW QUESTIONS AND UNSOLVED PROBLEMS

- 17.1 How are EVs classified? Describe each of them briefly.
- 17.2 What are the different powertrain architectures for the HEV? Describe each one of them using a block diagram.
- 17.3 What are the different HEV architectures?
- 17.4 Describe the converters used for HEV, EV, and fuel-cell vehicles.
- 17.5 What are bidirectional converters? Describe each using a block diagram.
- 17.6 What are the requirements for traction motor characteristics?
- 17.7 Explain the typical torque-speed curve for the electric traction motor.
- 17.8 The tractive power of a motor is 50 hp. Calculate the time required by the vehicle to accelerate from zero speed to 60 km/hr. The data for the EV is given as: mass of vehicle = 1200 kg, tire-rolling resistance coefficient = 0.01, air density = 1.205 kg/m³, aerodynamic drag coefficient = 0.3, vehicle frontal area = 2m², vehicle base speed = 30 km/hr, and vehicle rotational inertial factor = 1.5.
- 17.9 The vehicle road load characteristic on a level road is $T_{TR} = 24.7 + 0.0051 \omega_{wh}^2$. The IM torque-speed relationship in the linear region is given by $Te = K_{IM}(40 - \omega_m)$, including the gear ratio of the transmission system. The rated torque of 40 Nm is available at a speed of 35 rad/s. Find the steady-state operating point of the vehicle.
- 17.10 A DC motor used in an EV is powered from a 200 V source. The motor rotates at 2,000 rpm at no load and at 1,800 rpm at half load. What is the motor speed at full load?

- 17.11 A three-phase controlled rectifier is supplying a DC motor with $K = 1 \text{ V-s}$ and $R_a = 1 \Omega$. The rectifier is supplied from a source of 208 V source: (1) Calculate the maximum no-load speed of the DC motor, (2) The motor now is producing torque of 20 N-m. What is the maximum speed the motor can achieve? and (3) The motor is now connected as a generator, with a countertorque of 20 N-m at 1,500 rpm. What should be the delay angle and AC current?

SUMMARY

In this chapter, fundamentals of electric/hybrid electric vehicles and their drive technology are discussed. These includes drivetrain analysis, vibration and vehicle dynamics, power converters, vehicular power electronics, and selection of motor drives for electric/hybrid electric vehicles. The general solar-powered electric drive is briefly discussed. A brief discussion of the fuel cell with its motor drive is carried out.

REFERENCES/FURTHER READING

1. C. C. Chan, The state of the art of electric, hybrid, and fuel cell vehicles, *Proc. IEEE*, vol. 95, no. 4, pp. 704–718, 2007.
2. International Energy Agency Implementing Agreement on Hybrid and Electric Vehicles, Outlook for hybrid and electric vehicles, IA-HEV Outlook, June 2008. Available: http://www.ieahhev.org/pdfs/iahev_outlook_2008.pdf.
3. S. M. Lukic and A. Emadi, Charging ahead, *IEEE Ind. Electron. Mag.*, vol. 2, no. 4, pp. 22–31, 2008.
4. M. Eshani, Y. Gao, S. E. Gay, and A. Emadi, *Modern Electric, Hybrid Electric, and Fuel Cell Vehicles*, 2nd ed., CRC Press, New York, 2009.
5. W. D. Jones, Take this car and plug it [plug-in hybrid vehicles], *IEEE Spectr.*, vol. 42, no. 7, pp. 10–13, 2005.
6. S. G. Wirasingha, N. Schofield, and A. Emadi, Plug-in hybrid electric vehicle developments in the US: Trends, barriers, and economic feasibility, in *Proc. IEEE-VPPC*, Harbin, China, September 2008, pp. 1–8.
7. J. S. Lai and D. J. Nelson, Energy management power converters in hybrid electric and fuel cell vehicles, *Proc. IEEE*, vol. 95, no. 4, pp. 766–777, 2007.
8. N. Brinkman, M. Wang, T. Weber, and T. Darlington, Well-to-wheels analysis of advanced fuel/vehicle systems: A North American study of energy use, greenhouse gas emissions, and criteria pollutant emissions, Argonne National Laboratory, Argonne, IL. Available: www.transportation.anl.gov/
9. S. S. Williamson and A. Emadi, Comparative assessment of hybrid electric and fuel cell vehicles based on comprehensive well-to-wheels efficiency analysis, *IEEE Trans. Veh. Technol.*, vol. 54, no. 3, pp. 856–862, 2005.
10. J. Kessels, Energy management for automotive power net, PhD Dissertation, Technische Universiteit Eindhoven, Eindhoven, the Netherlands, February 2007.
11. M. Ceraolo, A. Di Donato, and G. Franceschi, A general approach to energy optimization of Hybrid Electric Vehicles, *IEEE Trans. Veh. Technol.*, vol. 57, no. 3, pp. 1433–1441, 2008.

12. A. A. Ferreira, J. A. Pomilio, G. Spiazzi, and L. de Araujo Silva, Energy management fuzzy logic supervisory for electric vehicle power supplies system, *IEEE Trans. Power Electron.*, vol. 23, no. 1, pp. 107–115, 2008.
13. D. Hissel, D. Candusso, and F. Harel, Fuzzy-clustering durability diagnosis of polymer electrolyte fuel cell dedicated to transportation applications, *IEEE Trans. Veh. Technol.*, vol. 56, pp. 2414–2420, 2007.
14. R. Sepe, C. Morrison, J. M. Miller, and A. Gale, High efficiency operation of a Hybrid Electric Vehicle starter/generator over road profile, in *Conf. Rec. IEEE IAS Annu. Meeting*, September/October 2000, vol. 2, pp. 921–925.
15. M. Ehsani, Y. Gao, S. E. Gay, and A. Emadi, *Modern Electric, Hybrid Electric, and Fuel Cell Vehicles: Fundamentals, Theory, and Design*. CRC Press, Boca Raton, FL, December 2004.
16. K. K. Afzidi, R. D. Tabors, and J. G. Kassakian, Alternative electrical distribution system architectures for automobiles, in *Proceedings of the IEEE Workshop Power Electronics in Transportation*, Dearborn, MI, 1994, pp. 33–38.
17. A. Sciarretta, M. Back, and L. Guzzella, Optimal control of parallel hybrid electric vehicles, *IEEE Trans. Contr. Syst. Technol.*, vol. 12, no. 3, pp. 352–363, 2004.
18. A. R. Gale, and M. W. Degner, Voltage trade-off evaluation for electric and hybrid electric vehicle applications, in *Proceedings of the IEEE Workshop Power Electronics in Transportation*, Auburn Hills, MI, October 2002, pp. 11–15.
19. S. Delprat, J. Lauber, T. M. Guerra, and J. Rimaux, Control of a parallel hybrid power train: Optimal control, *IEEE Trans. Veh. Technol.*, vol. 53, no. 3, pp. 872–881, 2004.
20. C. C. Lin, H. Peng, J. W. Grizzle, and J. M. Kang, Power management strategy for a parallel hybrid electric truck, *IEEE Trans. Contr. Syst. Technol.*, vol. 11, no. 6, pp. 839–849, 2003.
21. X. He, and J. W. Hodgson, Modeling and simulation for hybrid electric vehicles—part I: Modeling, *IEEE Trans. Intell. Transport. Syst.*, vol. 3, no. 4, pp. 235–243, 2002.
22. K. Rajashekara, J. Fattic, and H. Husted, Comparative study of new on-board power generation technologies for automotive applications, in *Proceedings of the IEEE Workshop Power Electronics in Transportation*, Auburn Hills, MI, October 2002, pp. 3–10.
23. J. Moreno, M. E. Ortuzar, and J. W. Dixon, Energy management system for a hybrid electric vehicle, using ultra capacitors and neural networks, *IEEE Trans. Ind. Electron.*, vol. 52, no. 2, pp. 614–623, 2006.
24. C. Musardo, G. Rizzoni, and B. Staccia, A-ECMS: An adaptive algorithm for hybrid electric vehicle energy management, in *Proceedings of the IEEE CDC-ECC*, Seville, Spain, December 2005, pp. 1816–1823.
25. Y. Gao, and M. Ehsani, Parametric design of the traction motor and energy storage for series hybrid off-road and military vehicles, *IEEE Trans. Power Electron.*, vol. 21, no. 3, pp. 749–756, 2006.
26. P. Atwood, S. Gurski, D. J. Nelson, and K. B. Wipke, Degree of hybridization modeling of a fuel cell hybrid electric sport utility vehicle, *SAE Trans. J. Engines*, vol. 110, pp. 93–100.
27. T. Matsumoto, N. Watanabe, H. Sugiura, and T. Ishikawa, Development of fuel-cell hybrid vehicle, *Presented at the Proceedings of 2002 SAE Congress, Fuel Cell Power for Transportation*, Detroit, MI, March 2002.
28. F. Caricchi, F. Crescimbini, and A. Di Napoli, 20 kW water-cooled prototype of a buck-boost bidirectional dc–dc converter topology for electrical vehicle motor drives, in *Proceedings of the APEC*, Dallas, TX, March 1995, pp. 887–892.
29. F. Caricchi, F. Crescimbini, F. Giulii-Capponi, and L. Solero, Study of bidirectional buck-boost converter topologies for application in electrical vehicle motor drives, in *Proceedings of the APEC*, Anaheim, CA, February 1998, pp. 287–293.

30. M. W. Ellis, M. R. von Spakovsky, and D. J. Nelson, Fuel cell systems: Efficient, scalable energy conversion for the 21st century, *Proc. IEEE*, vol. 89, no. 12, pp. 1808–1818, 2001.
31. G. Kulp, and D. J. Nelson, A comparison of two fuel cell air compression systems at low load, *SAE Trans., J. Passenger Cars: Electron. Electr. Syst.*, vol. 110, pp. 660–669.
32. S. Gurski, and D. J. Nelson, Cold start fuel economy and power limitations for a PEM fuel cell vehicle, in *Proceedings of the 2003 SAE Congr., Fuel Cell Power for Transportation 2003*, Detroit, MI, March 2003, pp. 111–118.
33. J. Lai and K. Stanton, *Power Electronics Assessment-Vehicle System and Subsystem Interactions with Power Electronics*, Oak Ridge National Lab, DOE Freedom CAR Program Rep., June 2004.
34. J. Chen, D. Maksimovic, and R. Erickson, Analysis and design of a low-stress buck-boost converter for universal-input PFC applications, *IEEE Trans. Power Electron.*, vol. 21, no. 2, pp. 320–329, 2006.
35. J. Chen, D. Maksimovic, and R. Erickson, Buck-boost PWM converters having two independently controlled switches, in *Proceedings of the PESC*, Vancouver, BC, June 2001, pp. 736–741.
36. P. Midya, L. E. Connell, and K. R. Haddad, Buck or boost power converter, U.S. Patent 6 348 781, February 19, 2002.
37. D. M. Dwelley, and T. W. Barcelo, Control circuit and method for maintaining high efficiency in a buck-boost switching regulator, U.S. Patent 6 166 527, September 12, 2000.
38. P. Bainciarelli, Buck-boost dc–dc switching power conversion, U.S. Patent 6 788 033, September 7, 2004.
39. R. W. De Doncker, D. M. Divan, and M. H. Kheraluwala, A three-phase soft-switched high power density dc-to-dc converter for high power applications, *IEEE Trans. Ind. Appl.*, vol. 27, no. 1, pp. 63–73, 1991.
40. H. Xu, X. Wen, E. Qiao, X. Guo, and L. Kong, High power interleaved boost converter in fuel cell hybrid electric vehicle, in *Proceedings of the IEEE IEMDC*, San Antonio, TX, May 2005, pp. 1814–1819.
41. X. Huang, X. Wang, T. Nergaard, J. S. Lai, X. Xu, and L. Zhu, Parasitic ringing and design issues of digitally controlled high power interleaved boost converters, *IEEE Trans. Power Electron.*, vol. 19, no. 5, pp. 1341–1352, 2004.
42. D. P. Urciuoli, and C. W. Tipton, Development of a 90 kW bi-directional dc–dc converter for power dense applications, in *Proceedings of the IEEE APEC*, Dallas, TX, March 2006, pp. 1375–1378.
43. J. Zhang, R. Y. Kim, and J.-S. Lai, High-power density design of a soft-switching high-power bidirectional dc–dc converter, in *Proceedings of the IEEE PESC*, Jeju, Korea, June 2006, pp. 2119–2125.
44. D. S. Oliveira, Jr., and I. Barbi, A three-phase ZVS PWM DC/DC converter with asymmetrical duty cycle for high power applications, in *Proceedings of the IEEE PESC*, Acapulco, Mexico, June 2003, pp. 616–621.
45. C. Liu, A. Johnson, and J.-S. Lai, A novel three-phase high-power soft-switched dc–dc converter for low-voltage fuel cell applications, *IEEE Trans. Ind. Appl.*, vol. 41, no. 6, pp. 1691–1697, 2005.
46. C. Liu, A. Johnson, and J. S. Lai, Modeling and control of a novel six-leg three-phase high-power converter for low-voltage fuel cell applications, *IEEE Trans. Power Electron.*, vol. 21, no. 5, pp. 1292–1300, 2006.
47. J. S. Lai, A high-performance V6 converter for fuel cell power conditioning system, in *Proceedings of the IEEE Conference on Vehicle Power and Propulsion*, Chicago, IL, September 2005, pp. 624–630.

48. Z. Rahman et al., An investigation of electric motor drive characteristics for EV and HEV propulsion systems, *Presented at the SAE Technical Paper Series*, Paper # 2000-01-3062.
49. L. Eudy et al., Overview of advanced technology transportation, 2004 Update, National Renewable Energy Laboratory, Golden, CO, DOE/GO-102004-1849, August 2004.
50. C. C. Chan, The state of the art of electric and hybrid vehicles, *Proc. IEEE*, vol. 90, no. 2, pp. 247–275, 2002.
51. C. C. Chan et al., An overview of power electronics in electric vehicles, *IEEE Trans. Ind. Electron.*, vol. 44, no. 1, pp. 3–13, 1997.
52. M. Zeraoulia, M. E. H. Benbouzid, and D. Diallo, Electric motor drive selection issues for HEV propulsion systems: A comparative study, in *IEEE Transactions on Vehicular Technology*, vol. 55, no. 6, pp. 1756–1764, 2006.
53. J. Lai, and D. J. Nelson, Energy management power converters in hybrid electric and fuel cell vehicles, in *Proceedings of the IEEE*, vol. 95, no. 4, pp. 766–777, 2007.
54. A. Emadi, S. S. Williamson, and A. Khaligh, Power electronics intensive solutions for advanced electric, hybrid electric, and fuel cell vehicular power systems, in *IEEE Transactions on Power Electronics*, vol. 21, no. 3, pp. 567–577, 2006.
55. C. C. Chan, A. Bouscayrol, and K. Chen, Electric, hybrid, and fuel-cell vehicles: Architectures and modeling, in *IEEE Transactions on Vehicular Technology*, vol. 59, no. 2, pp. 589–598, 2010.
56. K. T. Chau, and Z. Wang, Overview of power electronic drives for electric vehicles, *HAIT J. Sci. Eng. B*, vol. 2, no. 5–6, pp. 737–761, 2005.
57. S. Payami, R. K Behera, A. Iqbal, and R. Al-ammani, Common mode voltage and vibration mitigation of a five-phase three-level NPC inverter fed induction motor drive system, *IEEE J. Emerging Selected Top. Power Electron.*, vol. 3, no. 2, pp. 349–361, 2015.
58. R. K. Behera, R. Kumar, S. M. Bellala, and P. Raviteja, Analysis of electric vehicle stability effectiveness on wheel force with BLDC motor drive, *Proceedings of the IEEE 1st International Conference on Industrial Electronics for Sustainable Energy Systems (IESES)*, January 30–February 2, 2018, Hamilton, New Zealand.
59. A. Emadi, *Handbook of Automotive Power Electronics and Motor Drives*, CRC Press, NW, Boca Raton, FL, 2005.
60. A. Emadi, *Advanced Electric Drive Vehicles*, CRC Press, Boca Raton, FL, 2015.
61. B. M. Wilamowski, J. D. Irwin, Power electronics and motor drives, Ch. 33, CRC Press, Boca Raton, FL, 2011.
62. H. Abu-Rub, M. Malinowski, K. Al-Haddad, *Power Electronics for Renewable Energy Systems, Transportation and Industrial Applications*, Ch 13, IEEE Press, Wiley, 2014.
63. C. S. Solanki, *Solar Photovoltaics—Fundamentals, Technologies and Applications*, PHI India, New Delhi, India, 2015.
64. A. Khaligh, and Z. Li, Battery, Ultracapacitor, fuel cell, and hybrid energy storage systems for electric, hybrid electric, fuel cell, and plug-in hybrid electric vehicles: State of the art, *IEEE Vehicular Technol.*, vol. 59, no. 6, 2010, pp. 2806–2814.
65. R. K Behera, and S. P. Das, A utility friendly high performance multilevel inverter fed induction motor drive system for traction and industrial applications, PhD Thesis, Indian Institute of Technology Kanpur, Uttar Pradesh, India, February 2009.
66. J. Kumar, and R. K. Behera, Solar powered motor drive, *Registration Report*, IIT Patna Library Repository, India, January 2019.

18 Power Electronics Applications in Power Systems

18.1 INTRODUCTION

Power electronics play a significant part in the transmission and use of electric power, thanks to its ability to maintain a high level of effectiveness and flexibility in the control system. Moreover, the implementation of the electronic power in all possible electrical engineering sectors is eventually essential because energy conservation has become the standard of the day. The emergence of contemporary self-commuted systems, such as gate turn-offs thyristor (GTOs), insulated-gate bipolar transistors (IGBTs), and MOS-controlled thyristors (MCTs) further strengthened their utility. It is expected that by the turn of this millennium, the bulk of electric power produced will flow through power electronic switches.

18.2 GENERAL ASPECTS OF DC TRANSMISSION

There are two types of energy transfer schemes available for transmission of energy from source to power by AC at power frequencies of 50 or 60 Hz and DC at 0 Hz. Both energy transmissions use a steady frequency, but the AC power transmission has theoretical and conceptual constraints as:

1. The electric power transmission for long distance with power frequency is not an easy task.
2. The stability is critical for a lengthy transmission line length. Additional equipment is needed to enhance stability.
3. The entire system must be synchronized with the same frequency.
4. The AC power transmission capacity is restricted by several factors.
5. The use of underground/undersea cables will lead to massive capacitance currents flow. Hence, it will increase losses in the transmission line.

The classical DC power transmission has many advantages, which makes DC transmission attractive over AC power transmission. The advantages of DC power transmission are as follows:

1. The DC power transmission requires a smaller number of conductors as compared to three-phase AC power transmission.
2. In DC power transmission, there is no skin effect. Therefore, the cross-section area of entire conductor is fully utilized.

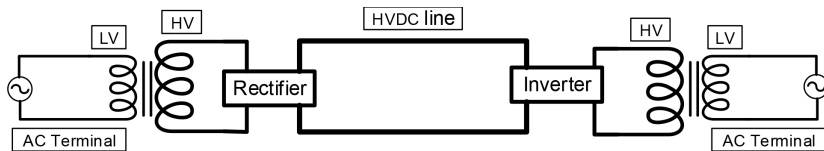


FIGURE 18.1 DC power transmission systems. (From Behera, R. K., *HVDC and FACTS Class Notes*, IIT Patna, 2016.)

3. The DC effective resistance of the conductor is less as compared to the AC system.
4. In the DC power transmission, the effect of capacitance, inductance, and phase-angle displacement on the transmission line is negligible.
5. The absence of inductance makes the voltage drop less as compared to the AC power transmission. So, the DC power transmission has better voltage regulation.
6. The problem associated with synchronizing and stability is higher in AC power transmission as compared to the DC power transmission.
7. The interference with communication circuits and corona effect has the least effects in DC power transmissions.

The classical DC power transmission system is shown in [Figure 18.1](#). The 50~60 Hz frequency-based AC sources feed the utility grid through step-up transformers and power converter, a transmission line, and again a step-down transformer and power converter for converting AC at station. Therefore, the electric power source and utility grid works at power frequency, but the DC transmission line operates at zero frequency.

Apart from many advantages of the DC power transmission it also has some disadvantages which are as follows:

1. Transformers in the DC transmission system cannot change the voltage levels.
2. In the DC transmission system, the power converters generate the current and voltage harmonics at substations and need large reactive power for compensation. So, expensive power filters and reactive power support should be connected.
3. Generally, it is tough to build high-voltage DC circuit breakers due to zero current breaking and arcing.

18.3 CONVERTER CIRCUITS AND THEIR ANALYSIS

The DC power transmission is done with the help of converters. Apart from rectifiers and inverters, several other converter components are used in the DC converters stations, which are shown in [Figure 18.2](#). There are two converter stations at both ends of the transmission line. The AC-DC rectifier and DC-AC inverters are the main converters used in the DC power transmission. These converters are used with high

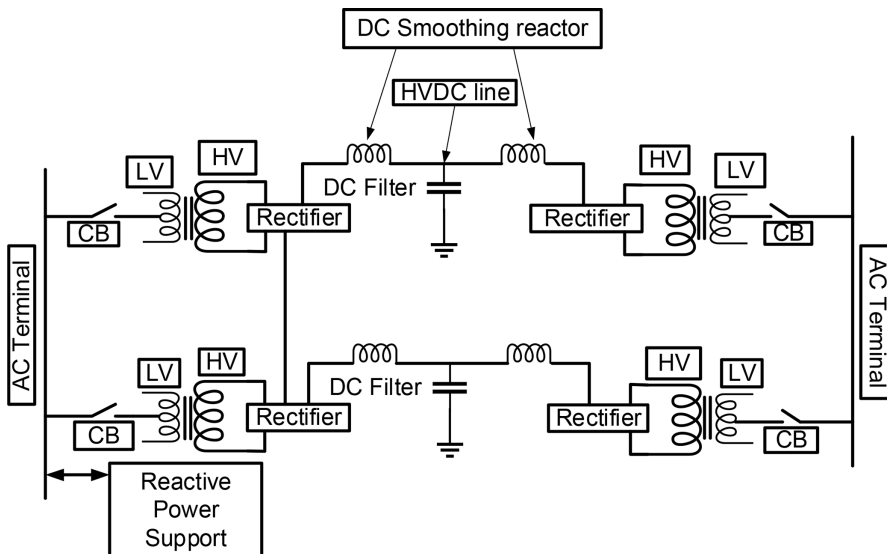


FIGURE 18.2 DC power-stations converter components. (From Behera, R. K., *HVDC and FACTS Class Notes*, IIT Patna, 2016.)

current and voltage capability of power electronics switch devices. The smoothing reactor is simply an inductor used in series with the pole. The smoothing reactors are used to avoid commutation failures occurring in converters, reduce harmonics, and avoid discontinuation of the current. The shunt capacitors are used for providing the reactive power. This is due to the fact that the reactive power used by the converters can be more than 50% of the total transferred active power. The circuit breakers are a key component for clearing the fault in the transformer and also used to disconnect the DC link.

18.4 HIGH VOLTAGE DC TRANSMISSION

Depending on the location, type, and purpose of use, there are several configurations and types of high-voltage direct current (HVDC) transmission systems. The main types of connections in HVDC electricity transmission system are:

- Monopolar
- Bipolar
- Back-to-Back
- Multiterminal
- Tripolar HVDC configuration

The monopolar HVDC structure consists of a single conductor and two converter stations. The earth or sea is used as a return path, and sometimes metallic return is used. It has many disadvantages and generally not in use.

The bipolar HVDC structure has two conductors. It has one positive, and other negative conductor is connected with respect to the earth. There are two converters, and each converter midpoint electrode is earthed. If one converter or structure fails, it behaves like a monopolar link, and half of the system will work. Generally, the homopolar HVDC structure has same polarity, and it has negative polarity. It is always earthed or has a metallic return path.

18.5 MECHANISM OF ACTIVE AND REACTIVE POWER FLOW CONTROL

The power flow in the transmission line is discussed with the help of Figure 18.3. The power flow consists of active power (P) and reactive power (Q). The source voltage and current are written as v_s and i_s , respectively. The instantaneous power (p) is from the voltage source to the load.

$$p = v_s i_s \quad \text{whereas} \quad \begin{cases} v_s = V_m \cos \omega t \\ i_s = I_m \cos(\omega t - \phi) \end{cases} \quad (18.1)$$

$$\begin{aligned} p &= \frac{V_m I_m}{2} \{ \cos \phi - \cos(2\omega t - \phi) \} \\ &= VI \cos \phi (1 + \cos 2\omega t) + VI \sin \phi \cdot \sin 2\omega t \end{aligned} \quad (18.2)$$

where V and I are the root mean square (RMS) values of v_s and i_s , respectively. The instantaneous power consists of active and reactive power, which is clear from Equation (18.2). The total average power (S) is simplified from Equation (18.2):

$$S = \bar{V} \hat{I}^* = P + jQ = VI \cos \phi + j VI \sin \phi$$

whereas P = active power (W), and Q = reactive power (VAR).

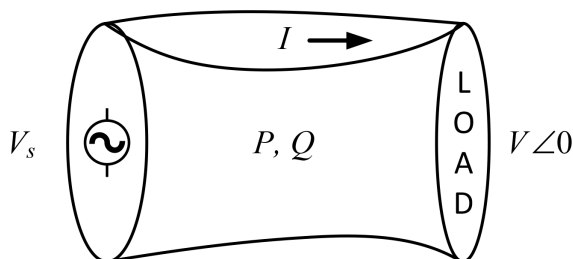


FIGURE 18.3 Power flow control in a transmission line. (From Behera, R. K., *HVDC and FACTS Class Notes*, IIT Patna, 2016.)

18.6 BASIC FACTS CONTROLLERS: SVC, TCR, TSC, STATCOM, TCSC, UPFC

The energy system is subjected to several transients, such as voltage sags, swells, and flickers. These transients would influence the voltage at the distribution level. Excessive reactive load power would enhance the generating capacities of power stations and reduce transmission losses on lines. Therefore, the reactive power supply at load ends is crucial. Flexible AC transmission system (FACTS) and custom energy products such as the static synchronous compensator (STATCOM), and the dynamic voltage restorer (DVR) address power quality solution issues with appropriate control strategies and concepts, as a result of which FACTS provide feasible solutions to the following problems:

- Improves the transmission efficiency
- Improves the transient stability limit
- Improves system damping
- Mitigates subsynchronous resonance
- Voltage instability recovery
- Improves HVDC terminal efficiency

The FACTS controllers (or the FACTS devices), by considerably improving the transmission ability of the current transmission corridors, are essentially avoided or delayed by the building of new transmission systems. In comparison to installation of new transmission lines, the service time of FACTS technology is considerably reduced, and this makes technology quite appealing.

1. Thyristor-based FACTS controllers
 - Static VAR compensator (SVC)
 - Thyristor-controlled series compensator (TCSC)
2. Voltage source converter (VSC)-based controllers
 - Static synchronous compensator (STATCOM)
 - Static synchronous series compensator (SSSC)
 - Unified power flow controller (UPFC)

18.6.1 STATIC VAR COMPENSATOR

In general, SVCs consist of standard reactive power shunt elements (reactors and capacitors), which are controlled to provide rapid and variable reactive power. They can be grouped into two basic categories: thyristor-controlled reactor (TCR) and thyristor-switched capacitor (TSC).

18.6.2 THYRISTOR-CONTROLLED REACTOR (TCR)

The TCR consists of a two antiparallel phase-controlled thyristors with a series reactor. A TCR can be designed for a single-phase or three-phase power system. A single-phase TCR is shown in [Figure 18.4](#). In this TCR structure, the

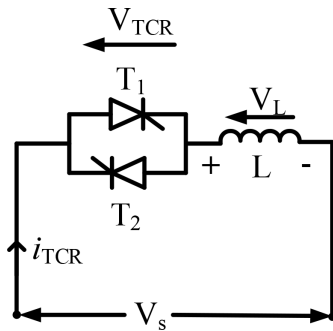


FIGURE 18.4 Single-phase TCR. (From Behera, R. K., *HVDC and FACTS Class Notes*, IIT Patna, 2016.)

reactor current is varied by varying firing angles of the thyristor according to the requirement of varied reactive power needed in the power system. This structure is used when the transmission system is lightly loaded. The TCR current can be written as

$$i_{TCR}(t) = \frac{V_m}{\omega L} (\cos \alpha - \cos \omega t) \quad (18.3)$$

18.6.3 THYRISTOR-SWITCHED CAPACITOR (TSC)

The TSC consists of a two antiparallel phase-controlled thyristors with a series capacitor. A TSC can be designed for a single-phase or three-phase power system. A single-phase TSC is shown in Figure 18.5. A small inductor is connected in series to control the inrush current. In this TSC structure, the capacitor voltage is varied by varying firing angles of the thyristor according to the requirement of varied reactive

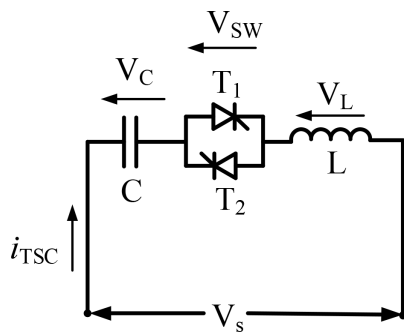


FIGURE 18.5 Single-phase TSC. (From Behera, R. K., *HVDC and FACTS Class Notes*, IIT Patna, 2016.)

power needed in the power system. This structure is used when the transmission system is highly loaded. The TSC current can be written as

$$v = V_m \sin \omega t \quad (18.4)$$

$$i(t) = V_m \frac{n^2}{n^2 - 1} \omega C \cos \omega t$$

$$\text{where } n = \frac{1}{\sqrt{\omega^2 LC}} = \sqrt{\frac{X_c}{X_L}}$$

The amplitude of the voltage across the capacitor is

$$V_c = \frac{n^2}{n^2 - 1} V \quad (18.5)$$

Apart from TSC and TCR, further attempts were made primarily for dynamic compensation of reactive power with the intention of minimizing standby losses and providing increased operating flexibility. This includes fixed capacitor with thyristor-controlled reactor (FC-TCR), thyristor-switched capacitor-thyristor-controlled reactor (TSC-TCR)-type compensators. But still the dynamic response, limited control range, and dependency on the point of common coupling (PCC) voltage make the thyristor family less attractive as compared with the newly emerged technology, called “switching-converter-type VAR compensators.”

18.6.4 STATIC SYNCHRONOUS COMPENSATOR

The STATCOM comprises of a voltage source inverter configured with fully controlled semiconductor switches. On the AC side, it is connected to the PCC terminals through a synchronous link reactor X_s that links the voltage sources at both ends. X_s also filters the switching harmonic generated by the inverter switching. The basic block diagram of the voltage-sourced STATCOM is shown in [Figure 18.6](#). Generally, electrical loads generate and absorb the reactive power. STATCOM caters continue reactive support to the PCC or load and stabilizes the grid.

STATCOM supplies the required harmonic and reactive component of the load and the compensation points. It also supplies both real and reactive power to the PCC. The VSC has to absorb necessary active power from the source so that DC link voltage is maintained constant. The adjustment of the phase shift between both the converter output voltage and the AC system voltage can also regulate the actual power exchange between the converter and the AC system. In other words, the VSC can supply the AC system with actual power from its DC energy storage when the converter output voltage is used to drive the AC system voltage.

[Figure 18.7](#) depicts a typical V-I characteristic of a STATCOM. It can be seen that the STATCOM can deliver both capacitive and inductive compensation power.

18.6.5 TCSC

A TCSC is the series-controlled capacitive reactant that offers continuous monitoring of the reactive energy of the AC line across a broad range and consists of a series of

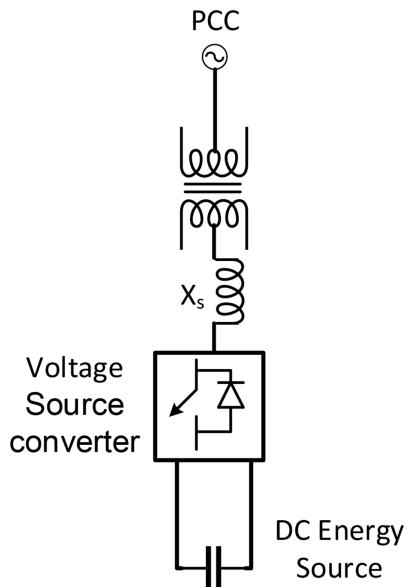


FIGURE 18.6 STATCOM structure. (From Behera, R. K., *HVDC and FACTS Class Notes*, IIT Patna, 2016.)

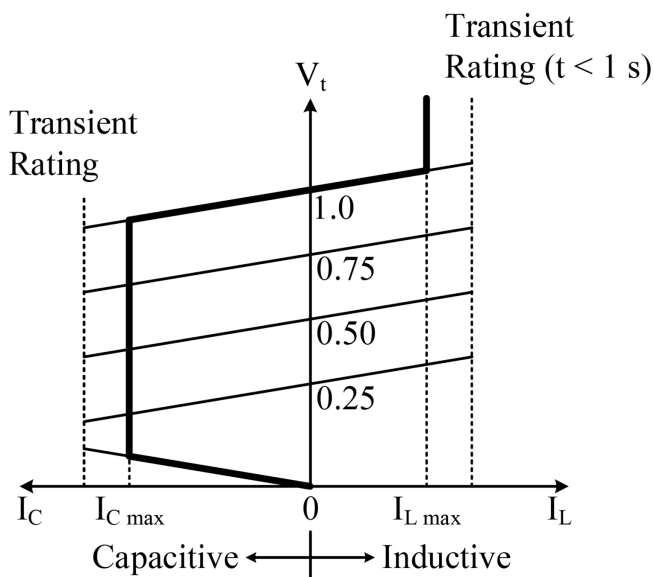


FIGURE 18.7 Voltage-current characteristic of STATCOM. (From Behera, R. K., *HVDC and FACTS Class Notes*, IIT Patna, 2016.)

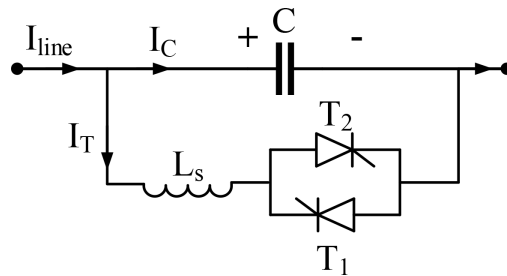


FIGURE 18.8 Basic TCSC modules. (From Behera, R. K., *HVDC and FACTS Class Notes*, IIT Patna, 2016.)

condensers shunted by a thyristor-controlled reactor for a smooth capacitance variable reaction. The concept of a compensating varying sequence is merely to boost the basic frequency voltage through a fixed condenser by changing the firing angle α appropriately. TCSC is very helpful in suppression of subsynchronous oscillations. At subsynchronous frequencies, the TCSC shows an inherently resistive-inductive reactance, which effectively damps the subsynchronous oscillations. The basic conceptual TCSC module is shown in Figure 18.8.

18.6.6 UPFC

The UPFC, which can be controlled autonomously by both real power and reactive power in a transmission line at an extremely fast rate, offers voltage regulations, serial compensation, and phase shift.

Figure 18.9 shows the block diagram of the UPFC, which consists of two VSCs coupled via a common DC terminal. The VSC-1, in the shunt of the line, is connected to the line using the coupling transformer, and the VSC-2 is in series with the transfer line via a series transformer. A common capacitor bank provides the DC voltage of the two converters. The serial transformer is regulated to inject a V_{pq} voltage into a line sequence that can range from 0 to $V_{pq\max}$. Moreover, phase angles for the phasor V_{pq} can vary independently from 0° to 360° . In this manner, the series converter exchanges real and reactive power for the transmission line. The real power generation/absorption is produced through the DC link capacitor while the internal reactive power is produced/absorbed by the series converter. The linked shunt VSC-1 is used primarily to provide the VSC-2's real power requirement, derived from the transmission line. The DC-link voltage is continuously maintained by the shunt converter. The aggregate real energy derived from the AC system is therefore equivalent to the losses of both converters and their coupling transformers. The UPFC control system can select either one or a mixture of above three functions as a control object. Furthermore, the shunt converter acts as a STATCOM and separately controls the terminal voltage of the connected bus by generating the required reactive power. Figure 18.10 shows concurrent performance of each of the three power flow control functions.

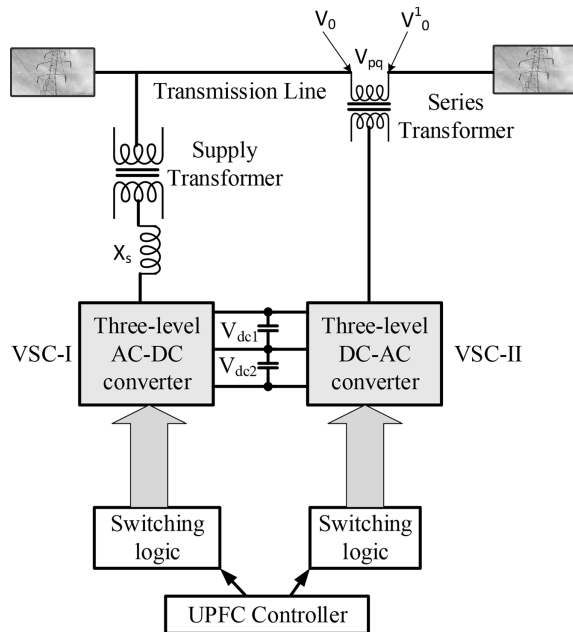


FIGURE 18.9 UPFC implementation with two three-level voltage-source converters. (From Behera, R. K., *HVDC and FACTS Class Notes*, IIT Patna, 2016.)

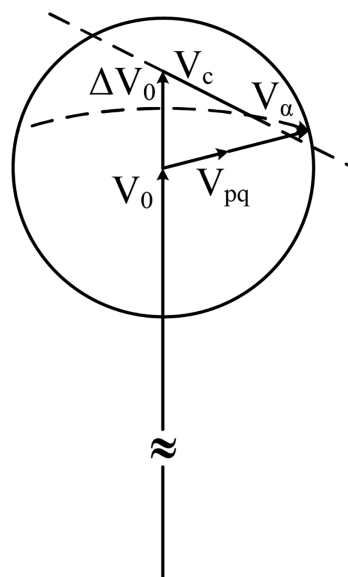


FIGURE 18.10 Phasor diagram of controlling terminal voltage, line impedance, and phase angle. (From Behera, R. K., *HVDC and FACTS Class Notes*, IIT Patna, 2016.)

18.7 MODELING OF FACTS CONTROLLERS

Modeling of the FACTS controller system can be carried out to find the dynamic response system. There are two types of modeling: large signal and small signal. These modeling types give detailed systems mathematical expressions that will be used for simulation study. There are few assumptions outlined:

1. Supply voltage and load are considered balanced.
2. All the components are ideal.
3. All parameters are well known.

Filter and STATCOM modeling is provided in the subsequent sections.

18.7.1 FILTER MODELING

The filters will introduce some gain as well as phase displacement. Figure 18.11 shows the single-phase circuit of a series-compensated distribution system.

The voltage source inverter (VSI) is supported by a DC source and is connected to the system through an Inductor-capacitor (LC)-filter and a series injection transformer. The injection transformer is assumed to be lossless and having turns ratio of $a = V_p/V_s$, where V_p is the primary voltage (inverter side), and V_s is the secondary voltage (high-voltage side). The transformer has a leakage inductance of L_T . The LC filter consists of a series inductor with inductance L_f and resistance R_f and a shunt capacitor with capacitance C_f .

The reference voltage on the primary side of the series injection transformer (v_{inj}^*) is given by,

$$v_{inj}^* = a(v_l^* - v_t) + \frac{L_T}{a} \frac{di_s}{dt} \quad (18.6)$$

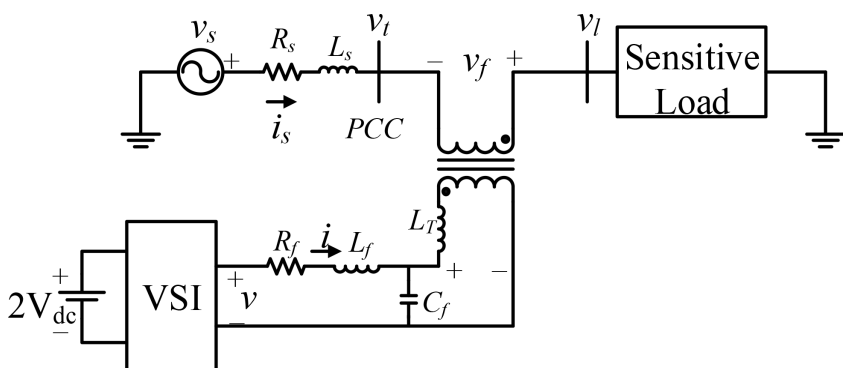


FIGURE 18.11 Single-phase circuit of series compensator with LC filter. (From Behera, R. K., *HVDC and FACTS Class Notes*, IIT Patna, 2016.)

The inverter current i^* can be calculated as,

$$i^* = \frac{i_s}{a} + C_f \frac{dv_{inj}^*}{dt} \quad (18.7)$$

From Equations (18.6) and (18.7) we get,

$$v^* = v_{inj}^* + R_f i^* + L_f \frac{di^*}{dt} \quad (18.8)$$

v^* is the reference voltage for the inverter.

18.7.2 STATCOM MODELING

A simple STATCOM with a connected linear load is shown in Figure 18.12. This STATCOM controls the PCC voltage (v_t). The compensated system consists of the VSI connected through interface inductor (L_T) and has some internal resistance (R_T). Load is a linear load of resistance (R_L) and inductor (L_L). Choosing state vector $x^T = [i_{sh} \ i_{cf} \ v_t \ i_l]$ and considering terminal voltage as output, the state space representation can be written as

$$\dot{x} = Ax + b_1 v_s + b_2 u \quad (18.9)$$

$$v_t = cx \quad (18.10)$$

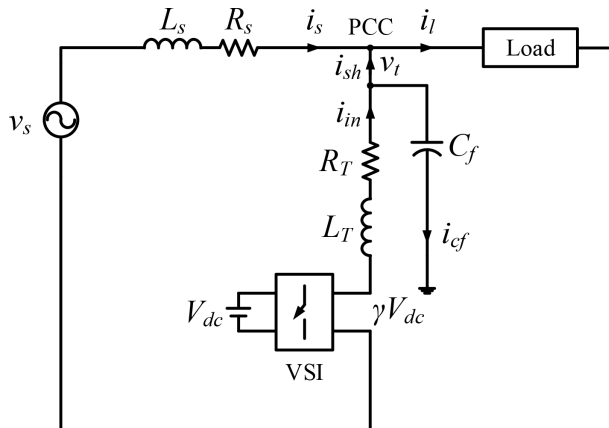


FIGURE 18.12 STATCOM with linear load. (From Behera, R. K., *HVDC and FACTS Class Notes*, IIT Patna, 2016.)

where

$$A = \begin{bmatrix} -\frac{R_s}{L_s} & 0 & \left(\frac{1}{L_s} + \frac{1}{L_L}\right) & \left(\frac{R_s}{L_s} - \frac{R_L}{L_L}\right) \\ \left(\frac{R_s}{L_s} - \frac{R_T}{L_T}\right) & -\frac{R_T}{L_T} & -\left(\frac{1}{L_s} + \frac{1}{L_L} + \frac{1}{L_T}\right) & \left(-\frac{R_s}{L_s} + \frac{R_L}{L_L}\right) \\ 0 & \frac{1}{C_f} & 0 & 0 \\ 0 & 0 & \frac{1}{L_L} & -\frac{R_L}{L_L} \end{bmatrix}, b_1 = \begin{bmatrix} -\frac{1}{L_s} \\ \frac{1}{L_s} \\ 0 \\ 0 \end{bmatrix}, b_2 = \begin{bmatrix} 0 \\ \frac{V_{dc}}{L_T} \\ 0 \\ 0 \end{bmatrix}$$

$$c = [0 \ 0 \ 1 \ 0]$$

18.8 SYSTEM DYNAMIC PERFORMANCE IMPROVEMENT WITH FACTS CONTROLLERS

The use of a solid-state switching converter in the dynamic impedance compensation system is extremely effective in transmission system. An SSSC is a VSI solid-state impedance compensator that injects a variable sinusoidal voltage magnitude in a series of transmission lines. This injected voltage is nearly quadrature by the line current. The loss in the VSI is compensated by a small amount of the injected voltage. The injected voltage in quadrature with the current line gives rise to an inductance or capacitive reactance in series. [Figure 18.13](#) indicates a single line circuit with

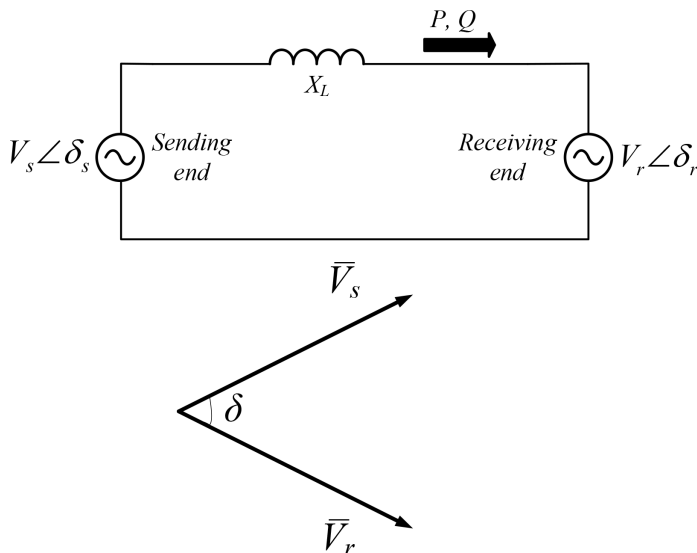


FIGURE 18.13 Elementary power transmission system. (From Hingorani, N. G., and Gyugyi, L., *Understanding FACTS*, IEEE Press, Wiley Interscience, New York, 2000.)

an inductive reactance of a transmission line, X_L , connecting a sending-end voltage source, \hat{V}_s , and a receiving-end voltage source, \hat{V}_r , respectively. The following expressions give the real and reactive power (P and Q) flow at the receiving-end voltage source:

$$P = \frac{V_s V_r}{X_L} \sin(\delta_s - \delta_r) = \frac{V^2}{X_L} \sin \delta \quad (18.11)$$

$$Q = \frac{V_s V_r}{X_L} (1 - \cos(\delta_s - \delta_r)) = \frac{V^2}{X_L} (1 - \cos \delta) \quad (18.12)$$

where V_s and V_r are the magnitudes of source and receiving end voltage, and δ_s and δ_r are the phase angles of the voltage sources \hat{V}_s and \hat{V}_r , respectively. For simplicity, $V = V_s = V_r$ and the difference between the phase angles is $\delta = \delta_s - \delta_r$. SSSC can offer a compensatory reactance of X_q , (both inductive and capacitive) in series with the transmission line inductive reactance, X . Consequently, the power flow expressions in Equation (18.11) become

$$P_q = \frac{V^2}{X_{eff}} \sin \delta = \frac{V^2}{X_L (1 - X_q / X_L)} \sin \delta \quad (18.13)$$

and

$$Q_q = \frac{V^2}{X_{eff}} (1 - \cos \delta) = \frac{V^2}{X_L (1 - X_q / X_L)} (1 - \cos \delta) \quad (18.14)$$

where X_{eff} is the efficient reactance of the transmission line between two ends. X_q is defined as a negative compensating reactance when the SSSC is operating in an inductive mode and positive when the SSSC is operating in a capacitive mode. [Figure 18.14](#) shows a power transmission system with an SSSC operating in both inductive and capacitive mode and related phasor diagram.

From Equations (18.13) and (18.11), the expressions for the normalized power flow in the transmission line and the normalized effective reactance of the transmission line can be written as

$$P_q / P = Q_q / Q = 1 / (1 - X_q / X_L) \quad (18.15)$$

$$X_{eff} / X_L = 1 - X_q / X_L \quad (18.16)$$

The impacts of the offset reactance, X_q , on standardized transmission line power flows and on normalized efficient transmission line reactance are illustrated in [Figure 18.15](#). When the emulated reactance is inductive, the power flow, P_q and Q_q , decreases and the effective reactance, X_{eff} , increases as the reactance compensation, $-X_q/X_L$, increases. When the emulated reactance is capacitive, the power flow, P_q and Q_q , increases and the effective reactance, X_{eff} , decreases as the reactance compensation, X_q/X_L , increases.

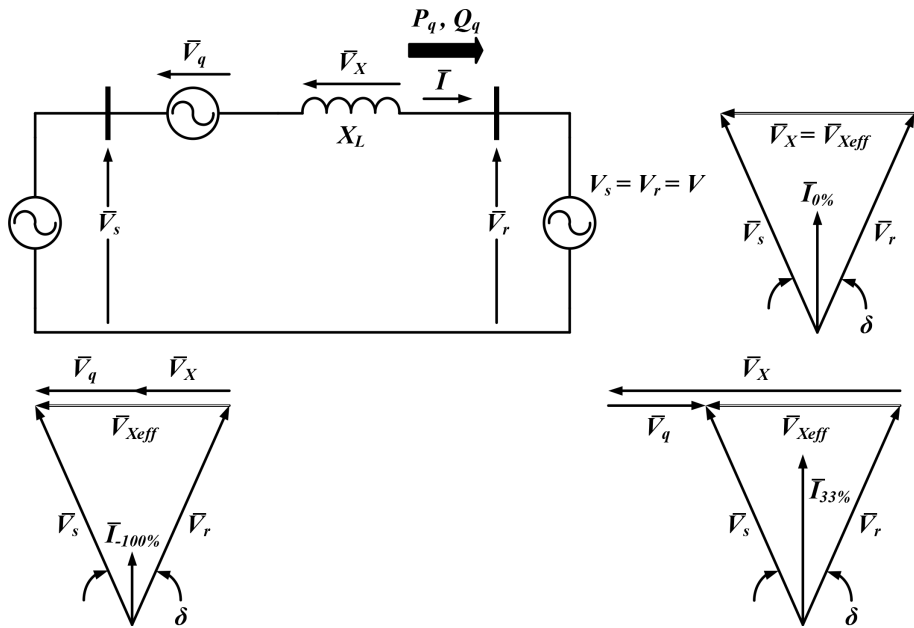


FIGURE 18.14 SSSC operated in inductive and capacitive modes and associated phasor diagrams. (From Hingorani, N. G., and Gyugyi, L., *Understanding FACTS*, IEEE Press, Wiley Interscience, New York, 2000.)

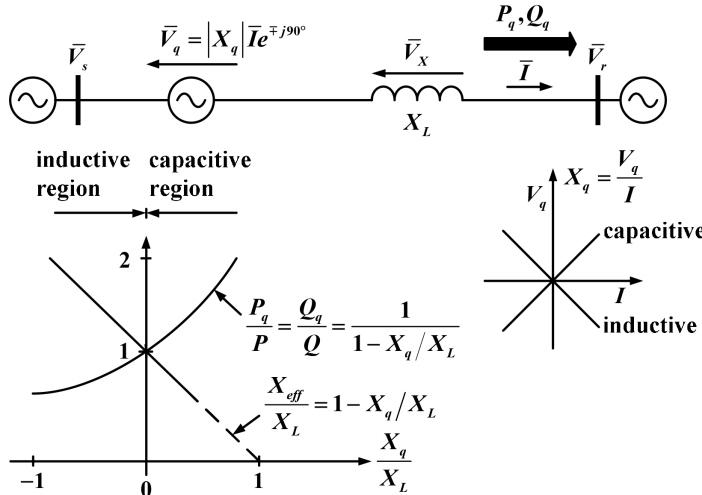


FIGURE 18.15 Effect of compensating reactance on power flow and effective reactance. (From Hingorani, N. G., and Gyugyi, L., *Understanding FACTS*, IEEE Press, Wiley Interscience, New York, 2000.)

18.9 INTERLINE POWER FLOW CONTROLLER (IPFC)

The IPFC provides compensation to multiple power transmission lines in a substation. It has the capability to control both the real and reactive power among transmission lines. It is a series compensating device for controlling injected-voltage magnitude and phase angle according to grid code standards. It consists of two or more SSSC devices connected to a common DC link, and it is shown in Figure 18.16. Figure 18.17 shows the simplified diagram of the IPFC control system. It consists of two back-to-back inverters connected between two transmission lines TR1 and TR2. It injects voltage with the help of two synchronous voltage sources of V_{1pq} and V_{2pq} to the transmission line TR1 of power P_{1pq} and TR2 of power P_{2pq} .

$$P_{12} = P_{1pq} = -P_{2pq} \quad (18.17)$$

V_{1S} and V_{2S} are the sending end voltages of TR1 and TR2, and V_{1R} and V_{2R} are the receiving end voltages of TR1 and TR2 respectively. X_1 and X_2 are the reactances of TR1 and TR2.

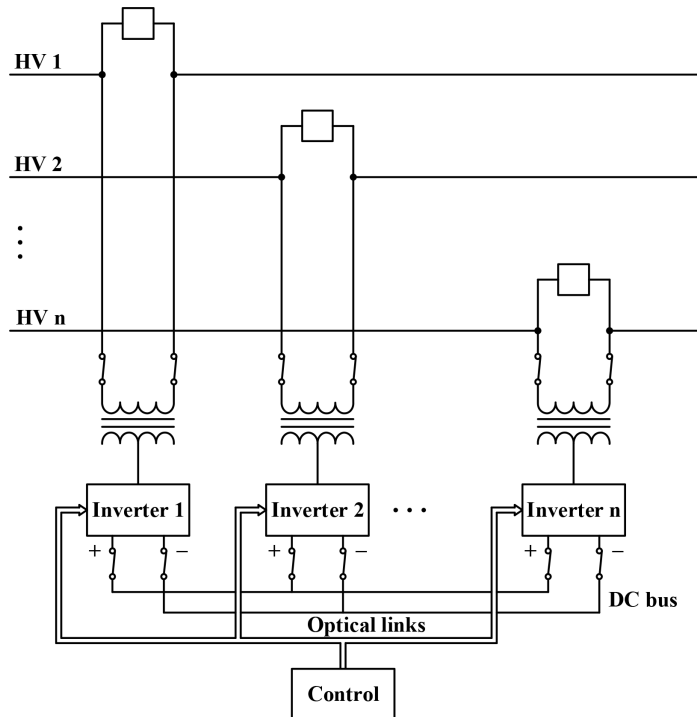


FIGURE 18.16 n -inverter based interline power flow controller. (From Hingorani, N. G., and Gyugyi, L., *Understanding FACTS*, IEEE Press, Wiley Interscience, New York, 2000.)

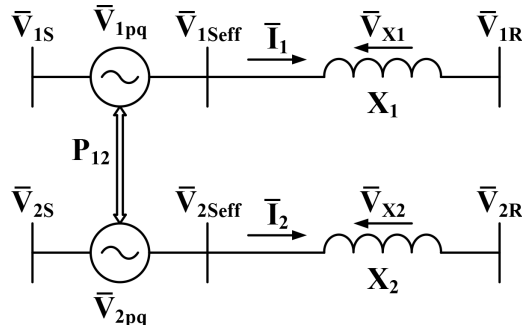


FIGURE 18.17 Basic two-inverter interline power-flow controller. (From Hingorani, N. G., and Gyugyi, L., *Understanding FACTS*, IEEE Press, Wiley Interscience, New York, 2000.)

18.10 UNIFIED POWER QUALITY CONDITIONERS (UPQC)

The integration of both series and shunt active filters (AFs) is a new device called the unified power quality conditioner. The UPQC has the following functions shared by the series AF and the shunt AF. The series AF provides dynamic restoration of PCC voltage by compensating voltage sags, low-frequency voltage-flicker compensation, and load-voltage balancing by neutralizing the nonpositive sequence voltage components. However, the shunt AF provides the reactive power compensation, harmonic current elimination from supply line, negative-sequence current compensation, and DC link voltage regulation between both AFs. These functions are traditionally defined in the literature. But depending upon the control algorithm and system requirement, some of the functions can be exchanged between the series and shunt converters.

The UPQC can be broadly classified with respect to angle of voltage injection by the series AF in two categories, namely, UPQC-Q and UPQC-P. The schematic block diagram of (right shunt) UPQC-Q is shown in Figure 18.18. The UPQC consists

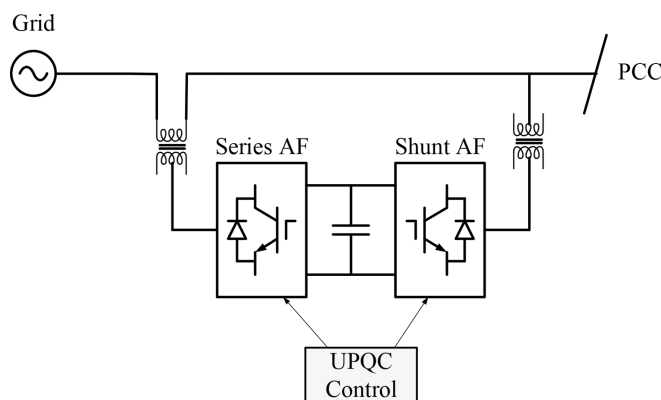


FIGURE 18.18 General structure of UPQC. (From Behera, R. K., *HVDC and FACTS Class Notes*, IIT Patna, 2016.)

of two three-phase or single-phase voltage source inverters connected in cascade through a common DC link capacitor. The series AF and the shunt AF are series- and shunt-connected VSIs, respectively. For UPQC-Q, the angle of injection is 90° leading the post-sag source voltage, whereas in UPQC-P, the voltage is injected in phase with the post-sag source voltage.

18.11 POWER ELECTRONICS IN POWER GENERATION

Large power generating stations are situated in the remote location of India, and high-voltage transmission systems are utilized to transport the bulk amount of power from the generating station to the distribution centers. However, these transmission systems are controlled and monitored at the control center to regulate for the system frequency, voltage, and power quality according to grid stands. The modern power system consists of conventional generating sources, distributed generations (DGs) and renewal energy sources, with the connected DGs, such as wind, solar PV, and the fuel cell. So, renewable integration with the existing transmission system became one of the most challenging objectives for monitoring and control. Hence, the power electronics converter and its controller became one of the attractive solutions for renewable power integration with the existing power grid. For all kinds of renewable energy sources, power electronics converters (PECs) are the main power-converting devices. The PEC has a power source, connected load, power electronics converter, and control unit as shown in Figure 18.19. PECs have good efficiency, reliable, low-voltage ride through (LVRT) capability, and at the same time, it can support reactive power injection to maintain voltage and frequency of the grid.

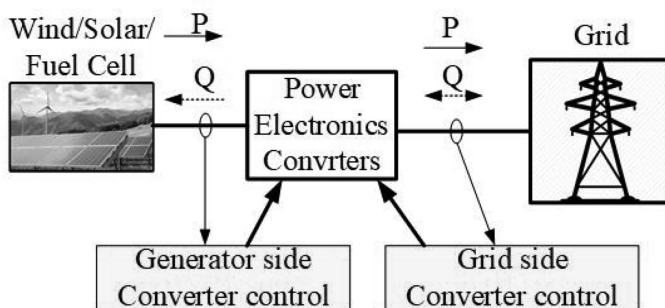


FIGURE 18.19 Renewable energy-generation system demands when integrated with the grid. (From Behera, R. K., *HVDC and FACTS Class Notes*, IIT Patna, 2016.)

REVIEW QUESTIONS

- 18.1 What are basic principles of shunt compensation? In an ideal shunt compensation system, show that the active power transfer $P = \frac{2V^2}{X} \sin \frac{\delta}{2}$, where $V_s = V_r = V$ and reactive power $Q = \frac{2V^2}{X} (1 - \cos \frac{\delta}{2})$; all the symbols are as per discussed in class. Draw the active and reactive power versus load-angle plot and compare results with the uncompensated system.
- 18.2 What is TCSC? Write the details of operation, characteristics, control components and associated waveforms, and control components.
- 18.3 Write briefly about transient stability improvement using equal area criteria with series, shunt, and phase-angle regulation.
- 18.4 What are the problems associated with the AC transmission system? Write advantages and disadvantages of the HVDC system.
- 18.5 What are multifunctional FACTS controllers?
- 18.6 What are different types of HVDC links?
- 18.7 What are SVC and STATCOM?

SUMMARY

This chapter gives a general introduction of power electronics application to power systems. This includes the HVDC transmission system, power flow modeling, and FACTS controllers in power systems such as SVC, STATCOM, TCSC, and UPFC and related to the field of active power filters. Modeling of FACTS controllers and performance improvement in the transmission system is designed. IPFC and power-quality conditioners are discussed.

REFERENCES/FURTHER READING

1. K. R. Padiyar, *HVDC Power Transmission Systems*, New Age International, Publishers, New Delhi, India, 2010.
2. <https://www.electrical4u.com/high-voltage-direct-current-transmission/> 2019.
3. R. K. Varma, *Elements of FACTS Controllers*, IEEE PES T&D, New Orleans, LA, 2010, pp. 1–6.
4. L. Gyugyi, Dynamic compensation of AC transmission lines by solid-state synchronous voltage sources, *IEEE Transactions on Power Delivery*, vol. 9, no. 2, pp. 904–911, 1994.
5. K. K. Sen, SSSC-static synchronous series compensator: Theory, modeling, and application, *IEEE Transactions on Power Delivery*, vol. 13, no. 1, pp. 241–246, 1998.
6. L. Gyugyi, K. K. Sen and C. D. Schauder, The interline power flow controller concept: A new approach to power flow management in transmission systems, *IEEE Transactions on Power Delivery*, vol. 14, no. 3, pp. 1115–1123, 1999.
7. M. T. Hagh and M. Sabahi, A single phase unified power quality conditioner (UPQC), *IEEE International Conference on Power System Technology (POWERCON)*, Wollongong, Australia, 2016, pp. 1–4.

8. H. Fujita and H. Akagi, The unified power quality conditioner: The integration of series- and shunt-active filters, *IEEE Trans. Power Electron.*, vol. 13, no. 2, pp. 315–322, 1998.
9. D. Graovac, V. Katic and A. Rufer, Power quality compensation using universal power quality conditioning system, *IEEE Power Eng. Rev.*, vol. 20, no. 12, pp. 58–60, 2000.
10. F. Blaabjerg, F. Iov, R. Teodorescu and Z. Chen, Power electronics in renewable energy systems, *12th International Power Electronics and Motion Control Conference*, Portoroz, 2006, pp. 1–17.
11. J. P. Lyons, V. Vlatkovic, Power electronics and alternative energy generation, *2004 IEEE 35th Annual Power Electronics Specialists Conference (IEEE Cat. No.04CH37551)*, Aachen, Germany, 2004, vol. 1, pp. 16–21.
12. F. Blaabjerg, K. Ma and Y. Yang, Power electronics—The key technology for renewable energy systems, *Ninth International Conference on Ecological Vehicles and Renewable Energies (EVER)*, IEEE, Monte-Carlo, 2014, pp. 1–11.
13. R. K. Behera, *HVDC and FACTS Class Notes*, IIT Patna, 2016.
14. N. G. Hingorani and L. Gyugyi, *Understanding FACTS*, IEEE Press, Wiley Interscience, New York, 2000.
15. Y. H. Song and A. T. Johns, *Flexible AC Transmission Systems (FACTS)*, IEEE Press, London, UK.
16. R. Gupta and A. Ghosh, *Characterization and Design of Inverter Switching Control for Distribution System Compensation*, PhD Thesis, Indian Institute of Technology Kanpur, 2007.
17. Y. Y. Kolhatkar and S. P. Das, *Design and Implementation of an Optimum Unified Power Quality Conditioner with Minimum VA Loading*, PhD Thesis, Indian Institute of Technology Kanpur, 2007.

19 Power Electronics Application in Renewable Energy (Wind and PV) System Integration

19.1 INTRODUCTION

Modern society requires significant amount of energy to survive under the current way of living. Over the past centuries, the limited amount of fossil fuel diverges research focus on renewable energy resources. The intermittent nature of renewable resources poses many challenges in integration with the grid. Thus, to regulate the voltage, frequency, and output power, power electronics converters are required. Depending upon the available renewable energy resources, DC/DC converters, DC/AC converters, and AC/DC converters can be used. Power converters for renewable energy integration have high complexities with grid-connected or standalone systems for efficiently managing the power flow and staying synchronized with the grid. Power converters for renewable energy sources require some desirable characteristics and attributes such as:

1. *High efficiency*: Converters should have a negligible amount of power loss during conversion process.
2. *Optimal power utilization*: For utilization of the maximum amount of power generated from renewable energy sources, it should operate on the maximum power extraction point. Thus, a control algorithm such as maximum power point tracking (MPPT) is required.
3. *Synchronization and high reliability*: The converters should have a synchronization capability to the grid in order to ensure high efficiency and reliability.
4. *Bidirectional power flow*: For renewable sources with the battery storage system, a bidirectional flow of power is required.
5. *Communication*: Intelligent functioning of power electronics converters depends on their capability of communication system. Hence, the power flow between different renewable resources and the grid should be optimized during normal operation and faulted condition.
6. *Fault tolerance*: A smart grid has the ability to avoid failures among the nodes to recover from local failures, and fault tolerance capability is required. This capability can be managed by the power converters by incorporating monitoring, communication, and reconfiguration systems.

7. There are several other attributes renewable energy resources used for supporting the existing grid system and for local microgrid systems. The focus of this chapter is on wind turbine (WT) and photovoltaic (PV) renewable resources.

19.2 GRID-CONNECTED CONVERTERS—KEY ELEMENT FOR GRID INTEGRATION OF WT AND PV SYSTEMS

Power electronics plays a very crucial role in grid-connected converters (GCC) for integration of renewable energies to the utility grid or distributed generation (DG) systems. After recent evolution in power electronics, the development of fast semiconductor devices, which are capable of handling high-switching frequencies at high power, have changed the structure of renewable energy sources of grid integration. Another important factor for grid integration of WT and PV systems is the real-time processors, which can handle the implementation of complex controller algorithms. The general control structure of renewable energy to grid integration is shown in [Figure 19.1](#).

Renewable energy sources integrated to AC grid systems should operate in both islanded and grid-connected mode to transfer the active and reactive power. To transfer the power, a robust controller is required, which can operate in both the steady-state and dynamic condition. Even under fault conditions and dynamic change in the load parameter, the controller should operate efficiently, such that power should transfer from WT and PV to the grid/DG system. There are many key elements for grid integration of the WT and PV system on the basis of performance, reliability, protection, and stability, for example,

1. Development of maximum power point tracking (MPPT) algorithm
2. Active and reactive power transfer at constant DC-link voltage control
3. Grid synchronization algorithm
4. Control of transition modes from off-grid to grid-tie and vice versa

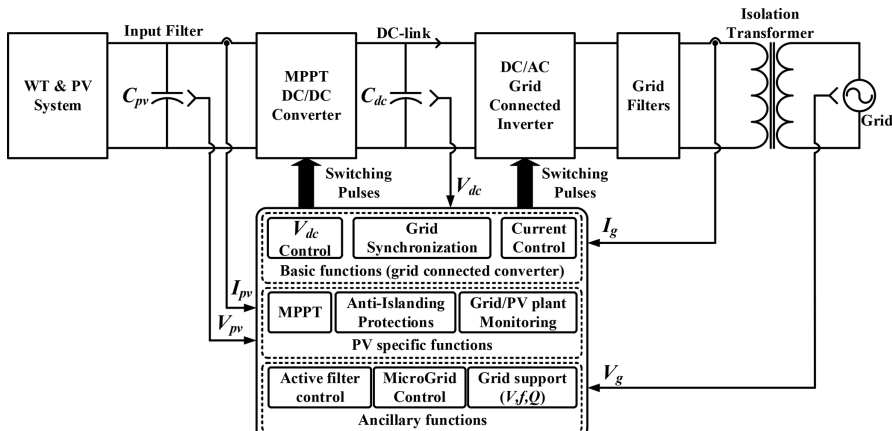


FIGURE 19.1 Basic control structure for a grid-integrated WT and PV system.

5. Islanding detection algorithm and protection system
6. Stringent current control to maintain power quality
7. Filter design and damping technique to minimize the effect of resonance

19.3 POWER ELECTRONICS CONVERTERS FOR RENEWABLE ENERGY INTEGRATION

For integration of renewable energy sources with grid or local load, power electronics converters are required. These converters are mainly DC/DC converters, DC/AC converters, and AC/DC converters used for interfacing, boosting up voltage, and extracting the maximum amount of power from renewable energy resources. In some cases where a storage system is utilized, a separate bidirectional converter is required to integrate with the grid system. Thus, GCCs for renewable energies are basically divided into different groups in WT and PV systems and it is based on converter topology with different power ratings. In variable-speed WTs, the converter topology is subsequently described.

19.3.1 VARIABLE-SPEED DOUBLE-FED INDUCTION GENERATOR (DFIG)

In the DFIG, the rotor winding is connected to the grid via a power converter, while the stator winding is directly connected to the grid as shown in [Figure 19.2](#). Thus, this converter decouples the mechanical and electrical frequencies and it makes variable-speed operation feasible and can vary the electrical rotor frequency. These converters are smaller as compared to full-power converters and losses are low.

19.3.2 VARIABLE-SPEED FULL-POWER CONVERTER

In this concept, the energy from generator is rectified, and after that it is converted to AC and fed to the grid as shown in [Figure 19.3](#). The majority of WTs are multipole synchronous generators. The generating side three-phase power converter works as

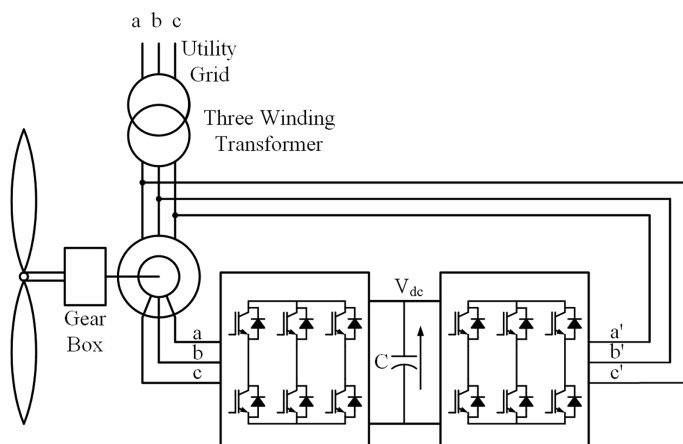


FIGURE 19.2 WT converter topology for DFIG.

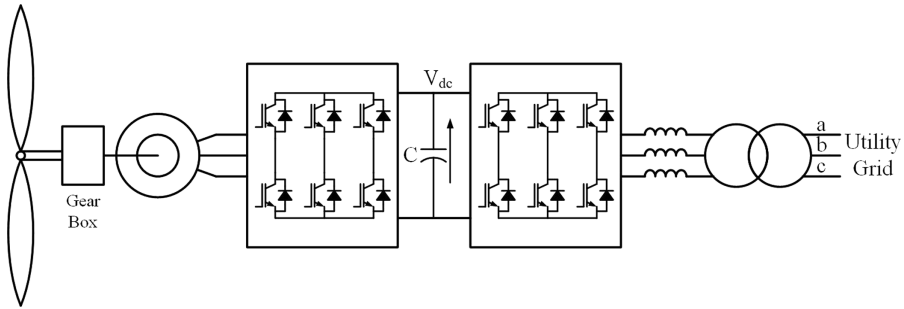


FIGURE 19.3 Full-power converter-based topology for WT.

a driver controlling the generated torque, using a vector control strategy. The grid-side three-phase converter transfers wind energy into the grid and can control the active and reactive powers delivered to grid. The converter can also control the total harmonic distortion (THD) with acceptable limits, thus improving the power quality injected into the grid. The DC link acts as energy storage device to capture the energy from the wind and store as a charge in the capacitor.

Figure 19.4 shows the PV system with several configurations for integrating the PV module to grid are as follows:

1. *AC module configuration:* The configuration shown in Figure 19.4a has a DC/AC converter in each module. These converters have automatic control that performs the MPPT control at the modular level. This topology has a PV module integrated converter that operates like plug-and-play system.

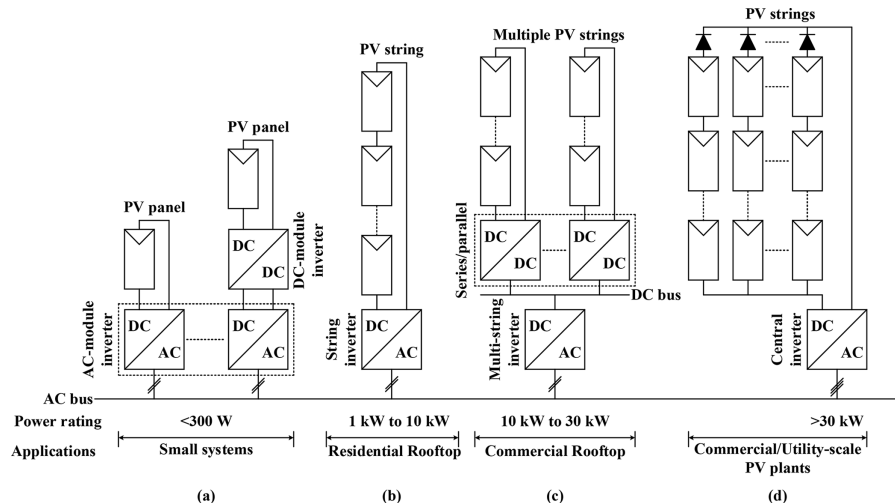


FIGURE 19.4 PV system topologies: (a) AC module configuration, (b) string configuration, (c) multistring configuration, and (d) central inverter configuration.

But in comparison with other configurations, these are more expensive and difficult to maintain when the power of the plant increases. Thus, it is applicable for residential rooftop PV systems.

2. *String configuration:* In string configuration, each string is connected to a DC/AC inverter as shown in [Figure 19.4b](#). If the string voltage is not an appropriate value, then a boost converter or transformer can be used. The string inverter is very popular for small and medium-scale PV systems.
3. *Multistring configuration:* [Figure 19.4c](#) shows an improved version of the string configuration, which have the advantages of string and centralized configurations. Each DC/DC converter can implement the MPPT for the string. This configuration has a flexible design and can improve the overall PV system efficiency.
4. *Centralized configuration:* It is used in PV systems that have nominal power ratings higher than 10 kW as shown in [Figure 19.4d](#). In this configuration, the whole PV array is connected to the grid through a single inverter. Each string has a blocking diode to prevent the energy reversion during the night.

19.3.3 BOOST CONVERTER

Boost converter as shown in [Figure 19.5](#) is used to linearize the PV source and extract maximum power by appropriately varying the duty cycle. The MPPT algorithm is used to ensure that output impedance is exactly same as input impedance irrespective of the load condition. Generally, the boost converter is used as a voltage regulator to convert varying DC voltage into constant DC voltage. The aim is to extract maximum power at any irradiance level; hence, output voltage does not remain constant with any change in irradiance or temperature.

In continuous conduction mode, a continuous inductor current ensures the continuous power flow between the PV source and the load. For the continuous conduction mode, inductor and capacitor values can be calculated by following equations:

$$L = \frac{V_{pv}(V_{dc} - V_{pv})}{\Delta I_{pv} f_s V_{dc}}. \quad (19.1)$$

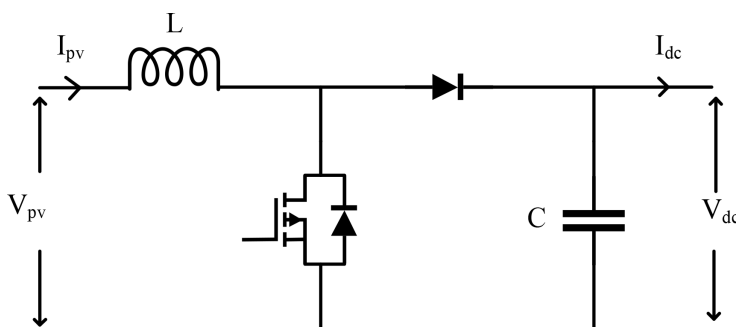


FIGURE 19.5 Circuit diagram of boost converter.

Current ripple factor (CRF) is the ratio between the input current ripple and output current. For a good estimation of the inductor value, the CRF should bound within 30%,

$$C \geq \frac{I_{dc}D}{f_s \Delta V_{dc}} \quad (19.2)$$

where ΔV_{dc} is the output voltage ripple, which is usually considered as 5% of the output voltage, which yields $\Delta V_{dc}/V_{dc} = 5\%$.

The boost converter control system essentially adjusts the duty cycle to achieve the desired input–output voltage ratio imposed by the MPPT algorithm reference and the DC-link voltage reference. In the steady-state, the boost controller should settle the duty cycle of the boost converter D , fulfilling the voltage conversion condition as

$$V_{dc} = \frac{V_{pv}}{1 - D} \quad (19.3)$$

19.4 PHOTOVOLTAIC INVERTER STRUCTURE

Different types of power converters are needed to perform the required function in the microgrid connected with a renewable energy such as PV and wind. The aim of this chapter primarily focuses on some specific H-bridge converters connected to the AC grid. A typical H-bridge-based boosting PV converter is shown in Figure 19.6. It consists of a high-frequency transformer to boost the voltage up to the desired value with isolation. The boost factor of the isolated full-bridge DC/DC converter can be controlled by shifting the switching phase between the two legs.

Figure 19.7 shows the circuit diagram of two-stage boost H-bridge inverter topology. The boost DC/DC converter connected between the PV and full-bridge inverter is used to provide the desired DC-link voltage value. The full-bridge inverter is used to integrate the system with a utility grid and local load. An isolation transformer is used after the full-bridge inverter to provide the necessary isolation between the PV system and grid.

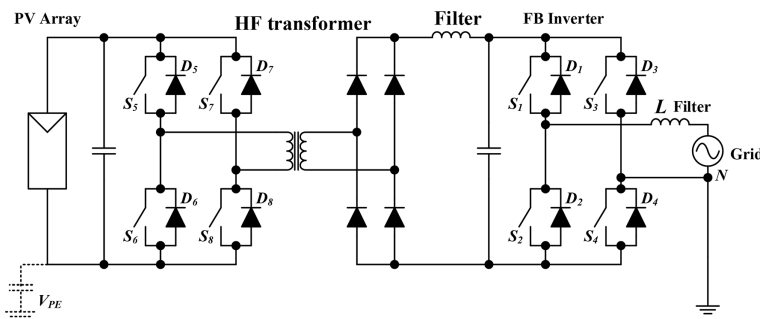


FIGURE 19.6 H-bridge-based boosting PV converter with isolation.

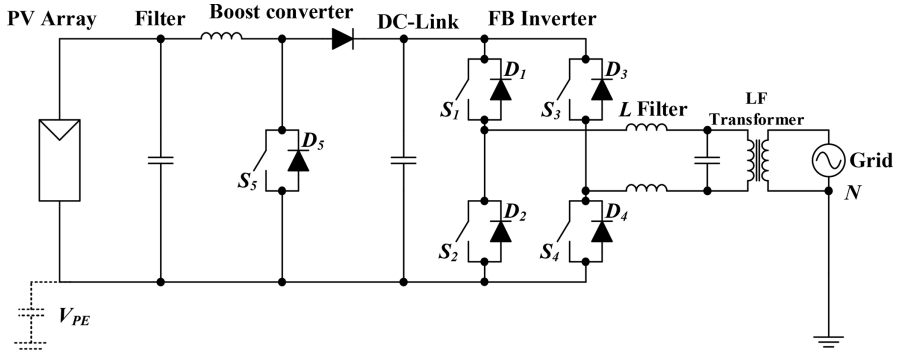


FIGURE 19.7 Two-stage boost H-bridge inverter topology.

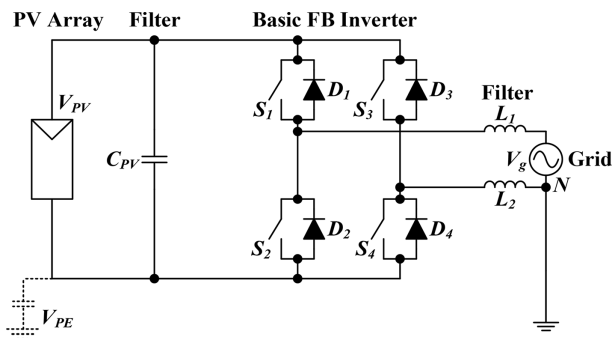


FIGURE 19.8 Circuit diagram of single-stage H-bridge inverter topology.

The single-stage H-bridge inverter topology as shown in [Figure 19.8](#) consists of a PV panel directly connected to the full-bridge inverter. The control algorithm of the inverter performs both MPPT and active power flow into the grid. Switching harmonics can be filtered out by the help of inductors for grid integration. The modulation techniques used for switching the H-bridge inverter can be classified into three main categories: bipolar, unipolar, and hybrid modulation. In the bipolar modulation technique, the switches are on in diagonal, such that a unipolar output voltage with no zero-output voltage state can be obtained across the output of the H-bridge inverter. In the unipolar modulation technique, each leg of an inverter is switched by 180° out of phase sinusoidal signals. Thus, two zero output voltage states are possible: $S_1, S_3 = ON$ and $S_2, S_4 = ON$. The output voltage obtained across the H-bridge inverter is unipolar in nature. In the hybrid modulation technique, one leg is switched at high frequency and another leg switched at grid frequency. The two zero output voltage states are $S_1, S_2 = ON$ and $S_3, S_4 = ON$ and voltage across the inverter is unipolar in nature.

[Figure 19.9](#) shows H5 SMA single-phase solar PV inverter topology. It has a similar topology to the H-bridge inverter with an extra switch just before the H-bridge

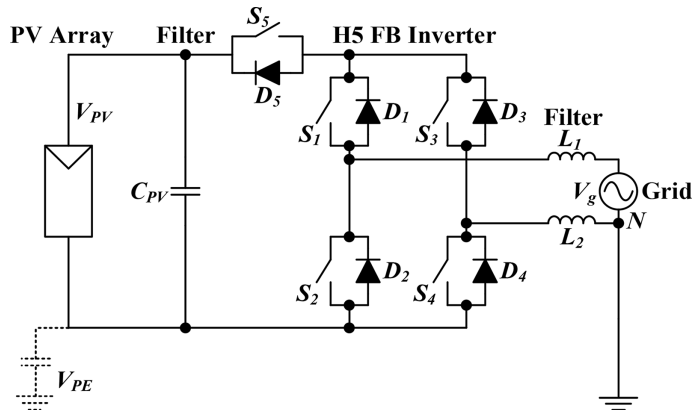


FIGURE 19.9 Circuit diagram of H5 SMA single-phase solar PV inverter topology.

at the positive bus of the DC link. The extra switch S_5 prevents the reactive power exchange between L_1 , L_2 , and C_{PV} during the zero-voltage state. It also isolates the PV array from the grid during the zero-voltage state. This configuration eliminates the high-frequency content of V_{PE} . The switches S_1 , S_3 operate at grid frequency, and at high frequency the switches S_5 and S_4 , S_2 are operated. Thus, when $S_5 = OFF$ and S_1 , $S_3 = ON$ two zero-output voltage states are possible. Thus, this topology is suitable for use in transformerless PV applications due to low leakage current, high efficiency, and low Electromagnetic interference (EMI).

The high efficiency and reliable inverter concept HERIC PV inverter topology has high efficiency and safety by reducing the leakage ground current when the inverter is connected to the national grid without using a transformer. The HERIC inverter shown in Figure 19.10 consists of an H-bridge inverter with AC bypass

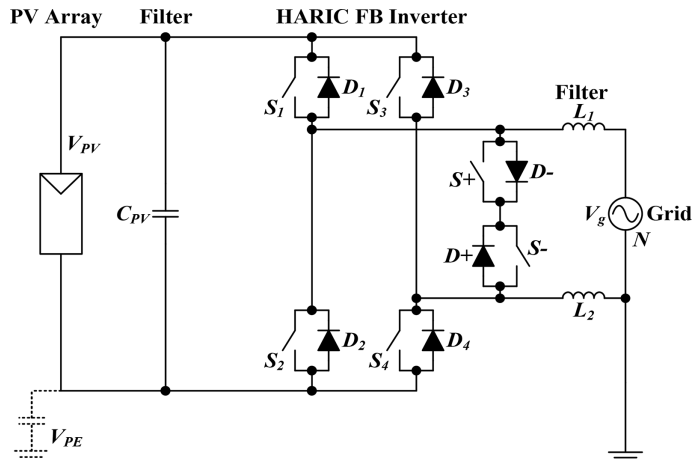


FIGURE 19.10 Circuit diagram of HERIC single-phase solar PV inverter topology.

switches, which has the same function as the fifth switch of the H5 inverter topology. The bypass switch provides isolation between the PV module and grid. It also prevents the reactive power exchange between L and C_{pv} during the zero-voltage state.

In Figure 19.10, the switches S_1, S_4 and S_2, S_3 are switched at high frequency, and S^+ and S^- at grid frequency. Thus, two zero-output voltage states are possible when $S^+ = \text{on}$ and $S^- = \text{on}$ (providing the bridge switched off). This topology is very suitable for use in transformerless PV applications due to high efficiency, low leakage current, and EMI. This topology is currently commercialized by Sunways in the AT series (2.7–5 kW) with reported European efficiency of 95% and maximum efficiency of 95.6%. Due to the structure of PV panels, the leakage capacitance between the PV panels output terminals and ground reaches a significant value. In order to save using isolation transformers, the conventional half-bridge neutral point clamped (NPC) topology is popular in PV inverter applications. As shown in Figure 19.11, the zero voltage can be achieved by clamping the output to the grounded middle point of the DC bus using D^+ or D^- depending on the sign of the output current. The voltage V_{PE} is clamped to $V_{PV}/2$, so that leakage current cannot be generated through C_{PE} . The NPC half-bridge topology has three output voltage levels and efficient performance. During the positive half cycle of the grid voltage, S_2 switches at grid frequency, and S_1 switches at the switching frequency. Therefore, the dead time between S_1 and S_2 can be set to zero by using pulse-width modulation (PWM) strategy. Switches S_3 and S_4 operate complementarily to S_1 and S_2 , respectively. For operation in the unity power factor, S_1 and S_3 switch in opposition during $V_g > 0, I_g < 0$, and S_2 and S_4 during $V_g < 0, I_g > 0$. The NPC half-bridge topology offers advantages

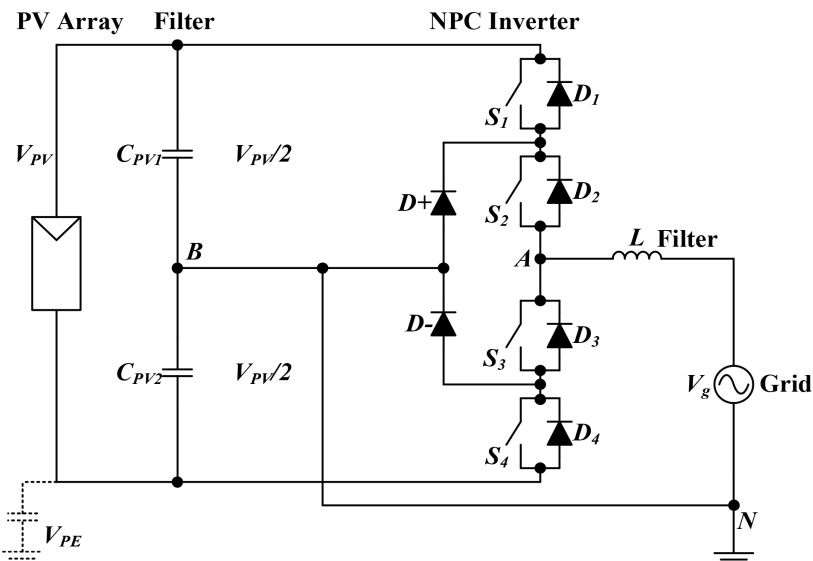


FIGURE 19.11 Circuit diagram of NPC H-bridge inverter topology.

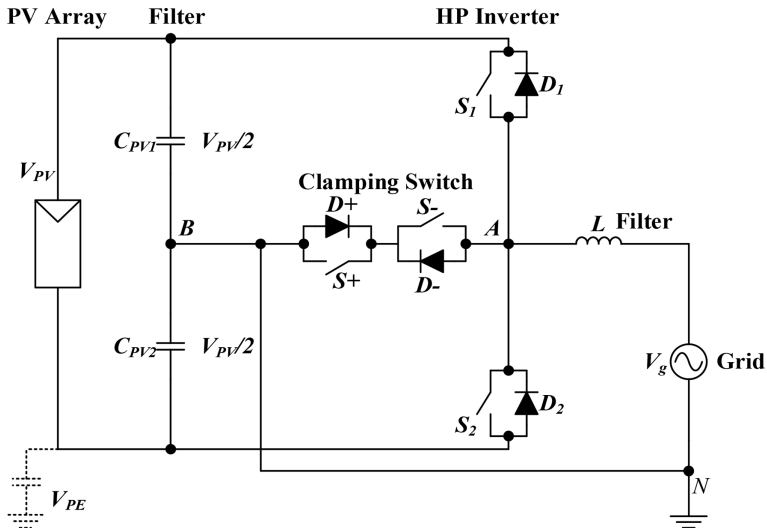


FIGURE 19.12 Circuit diagram of conergy NPC inverter topology.

such as lower core losses, reduced switching losses, very low leakage current, and EMI. The major drawback of this topology is the use of two extra diodes, unbalanced switching losses, and requirement of double-voltage input in comparison with the full bridge.

Figure 19.12 shows a conergy NPC inverter topology, which consists of a classical half-bridge NPC inverter with output clamped to the neutral point B using a bidirectional switch. Zero output voltage can be achieved by clamping the output to the grounded middle point of the DC bus using S^+ or S^- depending on the sign of the current. During the positive half cycle, S_1 and S^+ switch at switching frequency and are complementarily with each other. Similarly, S_2 and S^- operate during the negative half cycle. In the whole process of the work period, the voltage between DC ground B and AC neutral point A is clamped to $-V_{pv}/2$; thus, no common mode current is generated. The unequal distribution of losses is compensated by a double conduction loss of S^+ and S^- . The conergy NPC inverter topology offers advantages of lower core losses, reduced switching losses, higher efficiency, very low leakage current, and low EMI. The drawbacks of this topology require double-voltage input in comparison with full bridge, and a voltage rating of S_1 and S_2 is double in comparison with the outer switches in the NPC.

19.5 GRID CONVERTER STRUCTURE FOR WIND TURBINE SYSTEM

Power converter topologies play a crucial role in power generation from WT systems. The desirable characteristics of converters are reliability, minimum maintenance, physical size/weight, and power loss. The AC/AC conversion of power in

WTs can be direct or indirect. In the indirect case, a DC – link is connected in between an AC/DC and DC/AC converter, which is needed to maintain a constant voltage for conversion of power, while in the direct case, the DC link is not required. The indirect conversion provides decoupling between the grid and generator, which compensates nonsymmetry and solves power-quality issues. It requires energy storage for the DC link, thus reducing the lifetime and increasing expenses. However, the storage battery for the DC link and decoupling between the grid and generator side have advantages over the direct-conversion technique during low-voltage ride-through and for acquiring inertia in power transfer from the generator to the grid.

19.5.1 SINGLE-CELL (VSC OR CSC)

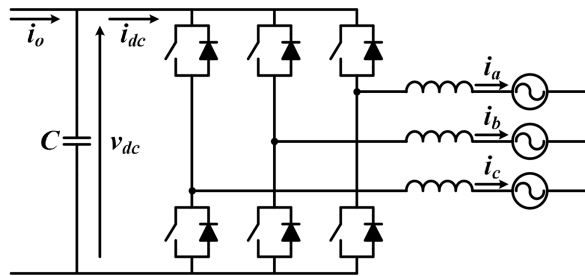
For WTs, the grid side converter topologies can be classified into a voltage source converter (VSC) as shown in [Figure 19.13a](#) and a current source converter (CSC) as shown in [Figure 19.13b](#) and [19.13c](#), respectively. By the inception of research in WT converter topologies, a third option is considered by Z-source converter topology on the DC side as an impedance network with a capacitor and inductors. Based on the direction of power flow, it is named a rectifier or inverter, or if power flows in both directions, it called as a bidirectional converter. They can be classified as phase-controlled by natural commutation synchronized with grid voltage or PWM using forced commutation. Grid-side converters in distributed power generation work as inverters, but with the advancement in research, bidirectional power converters can play a crucial role with dual-direction flow of power, which eliminates the use of an extra convertor to precharge the DC link.

19.5.2 MEDIUM-POWER CONVERTER

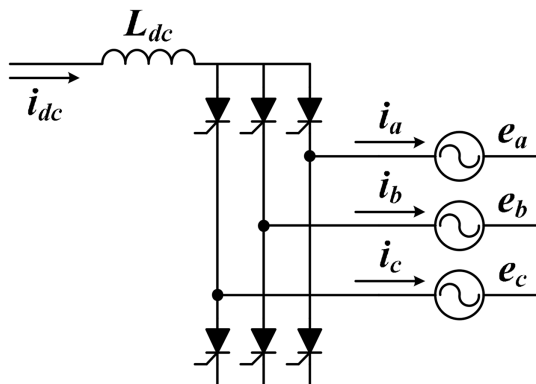
In WT systems, for medium power, 2 MW capacity is the more prominent because at this power level a design trade-off can be considered using single-cell topology with six switches forming a bridge. This solution can also work in low-wind conditions in the case of a doubly-fed induction generator. [Figure 19.14](#) shows a proven technology employing power devices consisting of a two-level back-to-back voltage source inverter (VSI), but power loss (switching and conduction loss) may limit the uses for the high-power system. [Figure 19.15](#) shows an alternative power-converter topology called a two-level back-to-back current source inverter (CSI).

19.5.3 HIGH-POWER CONVERTER

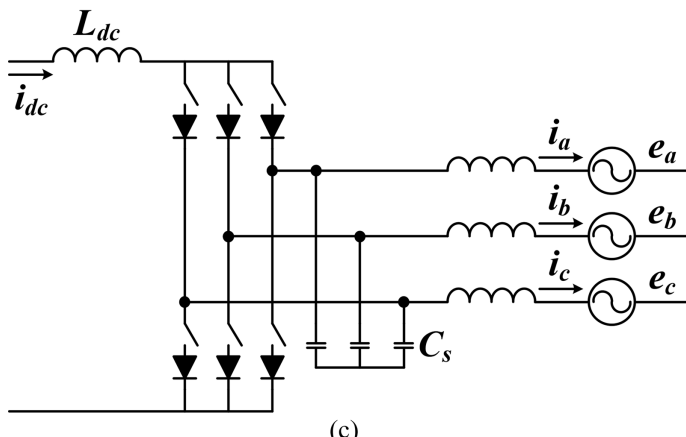
For high-power systems, more than 2 MW, [Figure 19.16](#) shows a multilevel system. This system consists of a three-level VSC that allows a lower rating of semiconductor devices for converters and fed low-harmonic distortion to the grid, which reduces the size due to low switching losses and smaller grid filter requirement.



(a)



(b)



(c)

FIGURE 19.13 Grid converter for indirect-type conversion: (a) forced-commutated VSI, (b) phase-controlled line-commutated converter, and (c) forced-commutated CSI.

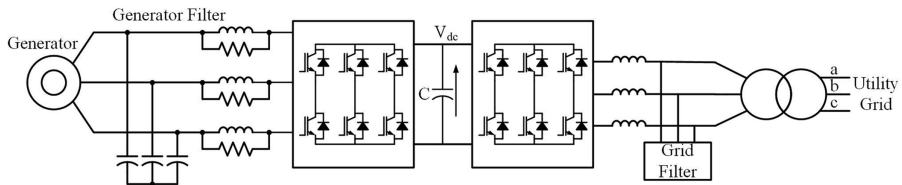


FIGURE 19.14 Circuit diagram showing two-level back-to-back PWM VSI.

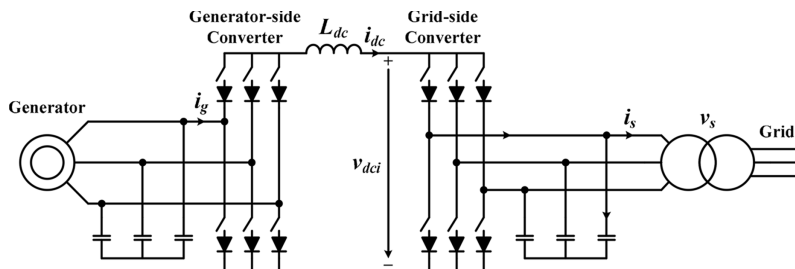


FIGURE 19.15 Circuit diagram showing two-level back-to-back PWM CSI.

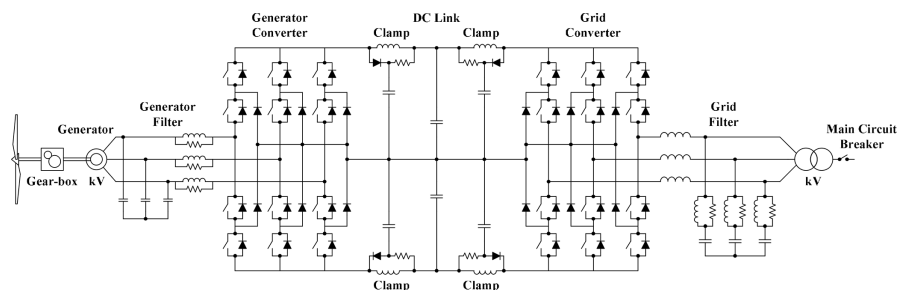


FIGURE 19.16 Circuit diagram showing three-level back-to-back PWM VSI.

A major disadvantage of this topology is high conduction loss due to a higher number of switching devices in series and need of complex control method to balance the DC-link capacitors.

Figure 19.17 shows a six-phase generator connected with the back-to-back converter in parallel and interleaved on the grid side to fed power. Figure 19.18 shows synchronous generator producing high DC voltage through n-leg diode bridge. The DC voltage generated used to fed power to the grid by parallel-connected back-to-back converters interleaved on the grid side.

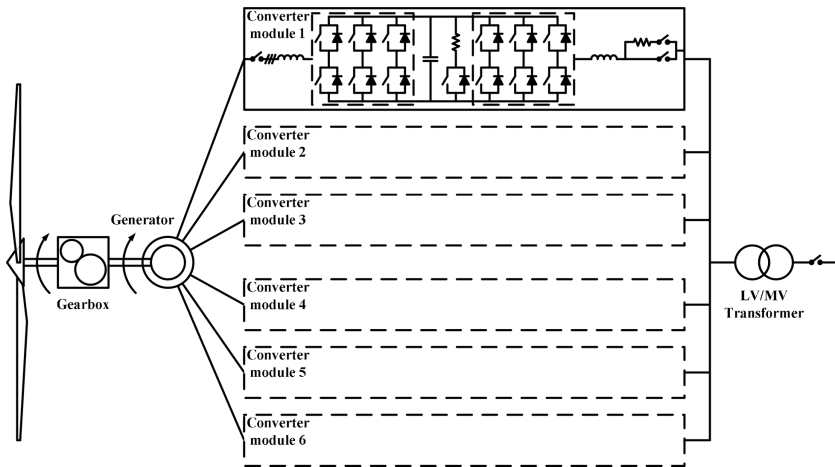


FIGURE 19.17 Six-phase generator topology connected with back-to-back converters in parallel and interleaved on the grid side.

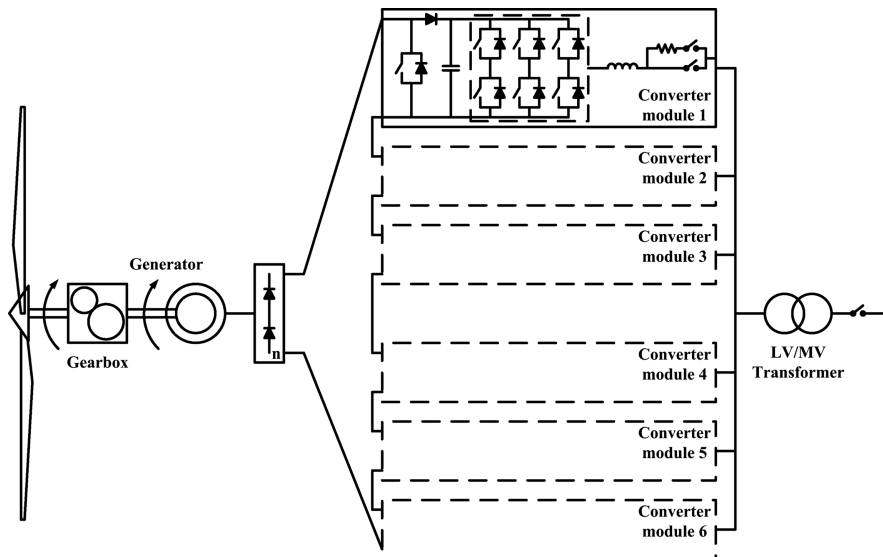


FIGURE 19.18 Synchronous generator topology connected to n -leg diode bridge in series with several converters connected in parallel and interleaved on the grid side.

19.6 GRID REQUIREMENTS FOR PHOTOVOLTAIC AND WIND TURBINE SYSTEMS

Previously, wind turbine generators (WTGs) were allowed to disconnect from the grid during fault. With the penetration of more renewable sources in the distribution network, there is an increased demand that WTs should remain connected to power

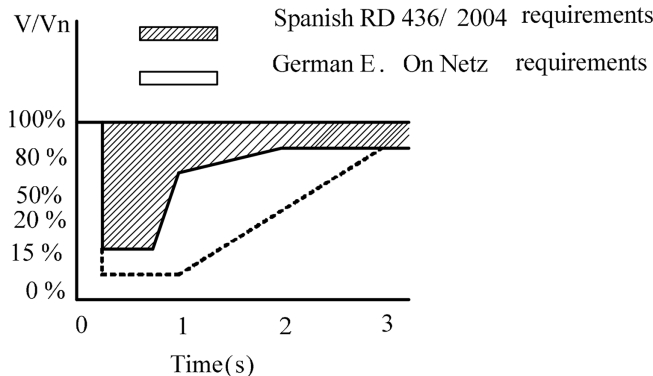


FIGURE 19.19 Fault ride-through requirements for wind farms.

system during fault and disturbance to support the grid. Thus, Figure 19.19 shows a wind-farm transmission grid code released in the Spanish Royal Decree. During fault, low voltage ride-through (LVRT) requirements for WTGs connected to the Spanish Royal Decree transmission system are specified in WF1.4.1 of the Wind Farm Transmission Grid Code Provisions. A wind farm shall remain connected to the transmission system during voltage dips on any or all phases, where the transmission system voltage measured at the HV terminals of the grid-connected transformer remains above the heavy black line shown in Figure 19.19.

The following parameters are required for designing the inverters for PV and WT systems:

- Voltage harmonic levels. Maximum THD in output voltage should be less than 8%.
- Maximum voltage unbalance should be 3% for three-phase inverters.
- Maximum voltage amplitude variations should be less than $\pm 10\%$.
- Maximum grid frequency variations should be $\pm 1\%$.
- Voltage dip duration <1 s, deep <60%.

19.7 GRID SYNCHRONIZATION USING A PHASE-LOCKED LOOP

A phase locked loop (PLL) as shown in Figure 19.20 is a closed-loop feedback system in which an oscillator is used to control the time of some external periodical signal.

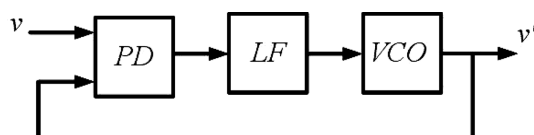


FIGURE 19.20 Basic structure of a PLL.

19.7.1 BASIC STRUCTURE OF A PHASE-LOCKED LOOP

The basic structure of a PLL is shown in [Figure 19.20](#), and it consists of three fundamental blocks:

- *Phase detector (PD)*: This block generates an error signal proportional to the phase difference between the input signal and the signal generated by the voltage-controlled oscillator (VCO) of the PLL. Depending on the type of PD, high-frequency AC components appear together with the DC phase-angle difference signal.
- *Loop filter (LF)*: This block presents a low-pass filtering characteristic to attenuate the high-frequency AC components obtained from the PD output. Typically, this block is constituted by a first-order low-pass filter or a proportional-integral (*PI*) controller.
- *Voltage-controlled oscillator*: This block generates at its output AC signal whose frequency is shifted with respect to a given central frequency. It is a function of the input voltage provided by the LF.

19.7.2 BASIC EQUATIONS OF PLL

The input signal applied to this system is

$$v = V \sin(\omega t + \phi) \quad (19.4)$$

and signal generated by the VCO is given by

$$v' = \cos(\omega' t + \phi') \quad (19.5)$$

The phase error signal from the multiplier PD output can be written as

$$E_{pd} = V k_{pd} \sin(\omega t + \phi) \cos(\omega' t + \phi') \quad (19.6)$$

$$= \frac{V k_{pd}}{2} [\sin((\omega - \omega')t + (\phi - \phi')) + \sin((\omega + \omega')t + (\phi + \phi'))] \quad (19.7)$$

Since, the LF cancelled out the high-frequency components, only the low-frequency term of error signal from PD will be considered for further analysis. Thus, the error signal from PD is considered as

$$\bar{E}_{pd} = \frac{V k_{pd}}{2} \sin((\omega - \omega')t + (\phi - \phi')) \quad (19.8)$$

Considering the VCO is well tuned to the input frequency, that is, with $\omega \approx \omega'$, the DC component of the phase error signal is given by

$$\bar{E}_{pd} = \frac{V k_{pd}}{2} \sin(\phi - \phi') \quad (19.9)$$

Phase error is very small, i.e.

$$\sin(\phi - \phi') \approx \sin(\theta - \theta') \approx (\theta - \theta') \quad (19.10)$$

Phase error signal is

$$\bar{E}_{pd} = \frac{V k_{pd}}{2} (\theta - \theta') \quad (19.11)$$

19.7.3 LINEARIZED SMALL-SIGNAL MODEL OF A PLL

Figure 19.21 shows the block diagram of small-signal mode of an elementary PLL. The following expressions can be obtained for the signals of PLL

$$\text{Phase detector } E_{pd}(s) = \frac{V}{2} (\theta(s) - \theta'(s)) \quad (19.12)$$

$$\text{Loop filter } V_{lf}(s) = K_p \left(1 + \frac{1}{T_i s} \right) E_{pd}(s) \quad (19.13)$$

$$\text{Controlled oscillator } \theta'(s) = \frac{1}{s} V_{lf}(s) \quad (19.14)$$

Open-loop phase transfer function is

$$F_{OL}(s) = PD(s) \cdot LF(s) \cdot VCO(s) = K_{in} \frac{k_p \left(1 + \frac{1}{T_i s} \right)}{s} = \frac{k_p s + \frac{k_p}{T_i}}{s^2} \quad (19.15)$$

Closed-loop phase transfer function is

$$H_\theta(s) = \frac{k_p s + \frac{k_p}{T_i}}{s^2 + k_p s + \frac{k_p}{T_i}} \quad (19.16)$$

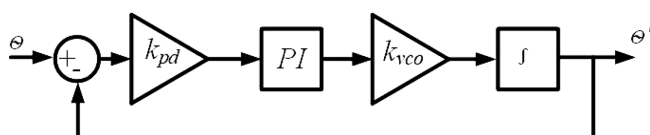


FIGURE 19.21 Small signal mode of an elementary PLL.

Closed-loop error transfer function is

$$E_\theta(s) = 1 - H_\theta(s) = \frac{s^2}{s^2 + k_p s + \frac{k_p}{T_i}} \quad (19.17)$$

Second-order transfer functions can be written in a normalized way as

$$H_\theta(s) = \frac{2\zeta\omega_n s + \omega_n^2}{s^2 + 2\zeta\omega_n s + \omega_n^2} \quad (19.18)$$

$$E_\theta(s) = \frac{s^2}{s^2 + 2\zeta\omega_n s + \omega_n^2} \quad (19.19)$$

where $w_n = \sqrt{\frac{k_p}{T_i}}$ and $\zeta = \frac{\sqrt{k_p T_i}}{2}$

The settling time is measured as the start time to the time in which the system stays within 1% of the steady-state response of a particular second-order system when subjected to the step input signal.

$$t_s = 4.6\tau \quad (19.20)$$

$$\tau = \frac{1}{\zeta\omega_n} \quad (19.21)$$

The tuning parameters of the PI controller of the PLL is

$$K_p = 2\zeta\omega_n = \frac{9.2}{t_s} \quad (19.22)$$

$$T_i = \frac{2\zeta}{\omega_n} = \frac{t_s \zeta^2}{2.3} \quad (19.23)$$

19.7.4 PLL BASED ON $T/4$ TRANSPORT DELAY

The simplest way to generate the quadrature signal is the $T/4$ transport delay technique, where T is the fundamental grid frequency time period. The quadrature signal generator (QSG) is shown in Figure 19.22.

QSG based on transport delay shows better performance for purely sinusoidal input voltage waveforms at the rated grid frequency. If grid voltage frequency shows

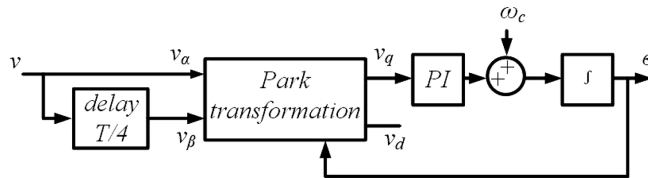


FIGURE 19.22 PLL based on $T/4$ transport delay.

deviation from the rated value, the output signals of the QSG will not be perfectly orthogonal, which impose an error in the PLL synchronization.

19.7.5 PLL BASED ON THE INVERSE PARK TRANSFORM

The phase-quadrature single-phase input signal can be achieved by introducing a filter in the loop consisting of Park transformations, as shown in [Figure 19.23](#).

$$\begin{bmatrix} v_{(\alpha\beta)} \end{bmatrix} = \begin{bmatrix} \cos(\theta') & -\sin(\theta') \\ \sin(\theta') & \cos(\theta') \end{bmatrix} \begin{bmatrix} v_d \\ v_q \end{bmatrix} \quad (19.24)$$

$$\begin{bmatrix} v_{(dq)} \end{bmatrix} = \frac{1}{2} \begin{pmatrix} (e^{j\omega't} + e^{-j\omega't}) & -j(e^{j\omega't} - e^{-j\omega't}) \\ j(e^{j\omega't} - e^{-j\omega't}) & (e^{j\omega't} + e^{-j\omega't}) \end{pmatrix} \begin{bmatrix} v_\alpha \\ v_\beta \end{bmatrix} \quad (19.25)$$

By applying the Laplace transform

$$\begin{bmatrix} V_d(s) \\ V_q(s) \end{bmatrix} = \frac{1}{2} \begin{pmatrix} (V_\alpha(s+j\omega') + V_\alpha(s-j\omega')) & -j(V_\beta'(s+j\omega') - V_\beta'(s-j\omega')) \\ j(V_\alpha(s+j\omega') - V_\alpha(s-j\omega')) & (V_\beta'(s+j\omega') + V_\beta'(s-j\omega')) \end{pmatrix} \quad (19.26)$$

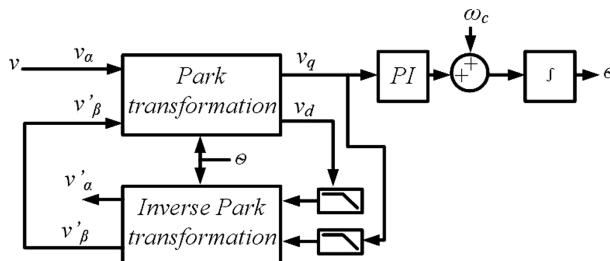


FIGURE 19.23 PLL based on the inverse Park transform.

At the input of the inverse Park transform, the applied signal is

$$\begin{bmatrix} \bar{V}_d(s) \\ \bar{V}_q(s) \end{bmatrix} = \frac{\omega_f}{s + \omega_f} \begin{bmatrix} V_d(s) \\ V_q(s) \end{bmatrix} \quad (19.27)$$

where it is assumed that low-pass filter (*LPF*) is a first-order low-pass filter having a cut-off frequency ω_f .

The Euler formula of the inverse Park transform can be written as

$$\begin{bmatrix} v'_{(\alpha\beta)} \\ v'_\beta \end{bmatrix} = \frac{1}{2} \begin{pmatrix} (e^{j\omega't} + e^{-j\omega't}) & j(e^{j\omega't} - e^{-j\omega't}) \\ -j(e^{j\omega't} - e^{-j\omega't}) & (e^{j\omega't} + e^{-j\omega't}) \end{pmatrix} \begin{bmatrix} \bar{v}_d \\ \bar{v}_q \end{bmatrix} \quad (19.28)$$

which is given in a complex frequency domain

$$\begin{bmatrix} V'_\alpha \\ V'_\beta \end{bmatrix} = \frac{1}{2} \begin{pmatrix} (\bar{V}_d(s + j\omega') + \bar{V}_d(s - j\omega')) & j(\bar{V}_q(s + j\omega') - \bar{V}_q(s - j\omega')) \\ -j(\bar{V}_d(s + j\omega') - \bar{V}_d(s - j\omega')) & (\bar{V}_q(s + j\omega') + \bar{V}_q(s - j\omega')) \end{pmatrix} \quad (19.29)$$

By solving the equation, we get

$$\frac{v'_\beta}{v'_\alpha}(s) = \frac{k\omega'^2}{s^2 + ks\omega' + \omega'^2} \quad (19.30)$$

$$k = \frac{\omega_f}{\omega'} \quad (19.31)$$

$$\frac{v'_\alpha}{v'_\alpha}(s) = \frac{sk\omega'}{s^2 + ks\omega' + \omega'^2} \quad (19.32)$$

The quadrature signals generated by the QSG based on the inverse Park transform are shown in Figure 19.24. Figures 19.25 and 19.26 show the *dq* reference frame

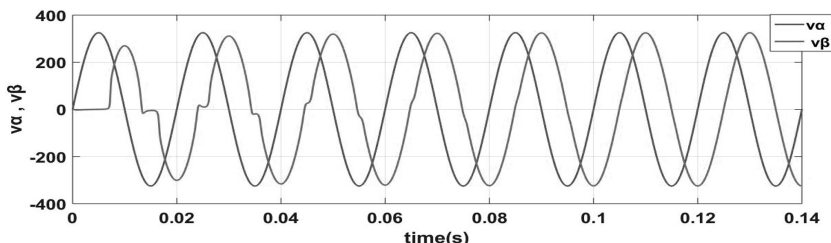


FIGURE 19.24 Quadrature signal generator based on the inverse Park transform.

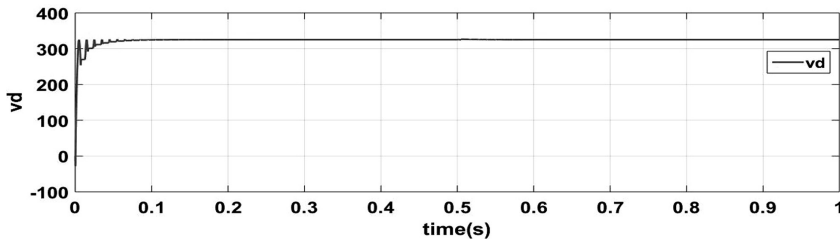


FIGURE 19.25 Direct signal in the synchronous reference frame.

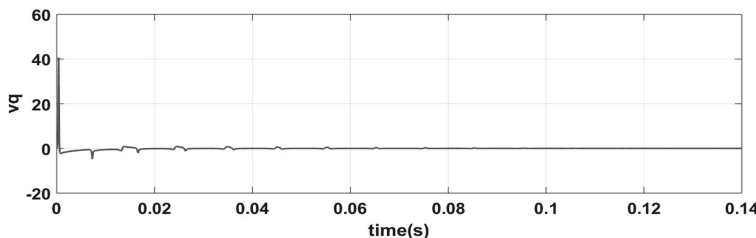


FIGURE 19.26 Quadrature signal in the synchronous reference frame.

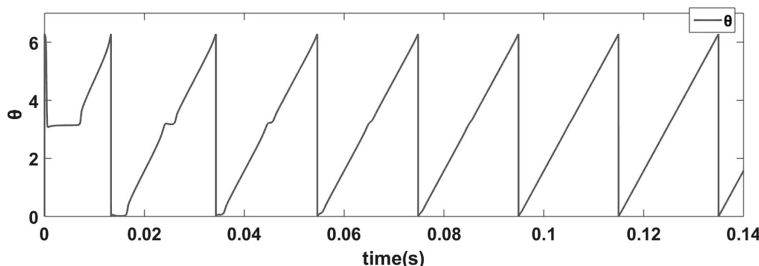


FIGURE 19.27 Phase angle for response of the inverse Park transform PLL.

signal and the v_d signals match the amplitude of the input voltage in the steady-state. Also, by the action of the PI controller of the LF, the v_q signal is made equal to zero. In Figure 19.27, the phase angle detected by the PLL is at setting time of 100 ms with ξ is $1/\sqrt{2}$.

19.7.6 SECOND-ORDER GENERALIZED INTEGRATOR

Figure 19.28 shows the QSG based on second-order adaptive filtering structure, where the adaptive filter (AF) is

$$AF(s) = \frac{s}{s + \omega'^2} \quad (19.33)$$

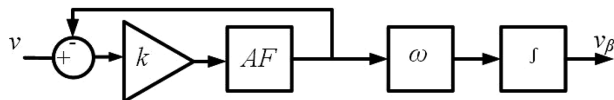


FIGURE 19.28 QSG based on a second-order *AF*.

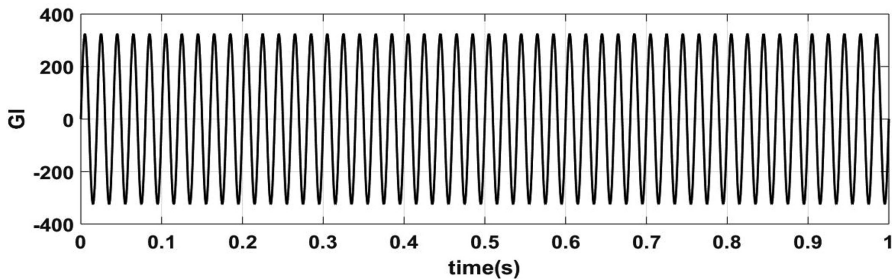


FIGURE 19.29 Response of the GI with unitary step input.

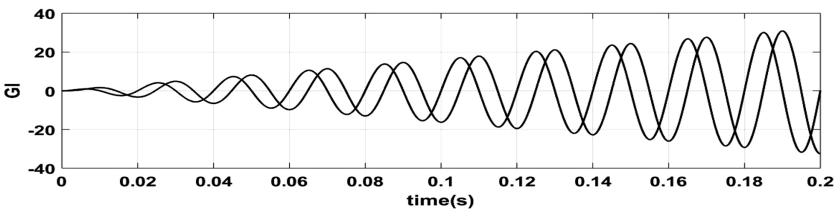


FIGURE 19.30 Response of the GI with unitary sine/cosine input.

Figure 19.28 shows the response of an *AF* block with $\omega = 2\pi \cdot 50$ rad/s applied to its input. The response of the system is defined by the transfer function with two imaginary complex poles placed at $\pm j\omega'$. Figures 19.29 and 19.30 shows the response of the *AF* block in the case of applying both sine and cosine signals with frequency to its input.

The Laplace transforms of the sine and cosine functions are

$$L[\sin(\omega' t)] = \frac{\omega'}{s^2 + \omega'^2} \quad (19.34)$$

$$L[\cos(\omega' t)] = \frac{s}{s^2 + \omega'^2} \quad (19.35)$$

The time response of the system preceding equation with sinusoidal input is given by

$$L^{-1}\left(\frac{\omega'}{s^2 + \omega'^2} \frac{s}{s^2 + \omega'^2}\right) = \frac{1}{2}t \sin(\omega' t) \quad (19.36)$$

$$L^{-1}\left(\frac{s}{s^2 + \omega'^2} \frac{s}{s^2 + \omega'^2}\right) = \frac{1}{2} \left[\frac{\sin(\omega' t)}{\omega'} + t \cos(\omega' t) \right] \quad (19.37)$$

The system with the transfer function AF does not act as an optimal amplitude integrator for the sinusoidal input signal. It depends on the phase angle of the input signal. The output of an AF system contains a steady-state error. The generalized integrator (GI) transfer function offers an infinite gain allowing the cancelation of any steady-state error at resonance frequencies with sinusoidal signals.

Figure 19.31 shows a second-order AF based on efficient implementation of the GI. The GI structure is used for synchronization and grid monitoring. The characteristic transfer functions of the adaptive filter are

$$GI(s) = \frac{v'}{k\varepsilon_v}(s) = \frac{s}{s^2 + \omega'^2} \quad (19.38)$$

$$D(s) = \frac{v'}{v}(s) = \frac{ks}{s^2 + ks + \omega'^2} \quad (19.39)$$

$$Q(s) = \frac{qv'}{v}(s) = \frac{k\omega'^2}{s^2 + ks + \omega'^2} \quad (19.40)$$

The basic transfer function of GI and AF are identical. In GI sine and cosine functions are not used, which reduces the computation at time and quantization noise into the discrete system. In **Figure 19.32**, an adaptive filtering structure generates orthogonal output signals, v' and qv' . The transfer function $D(s)$ indicates the band-pass filter, and $Q(s)$ is a low-pass filter. These transfer functions depend on gain k and the center frequency of the filter. In the case of PLL, it becomes complex to design.

The preceding problem can be overcome by modifying the flow diagram of the AF system. Thus, it is called the second-order generalized integrator (SOGI) to differentiate it from the conventional GI.

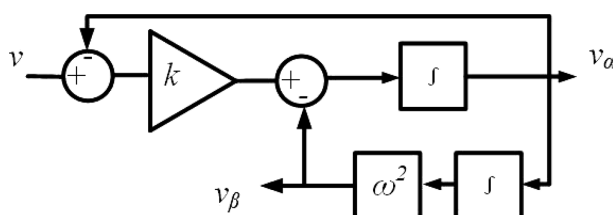


FIGURE 19.31 Second-order AF based on a GI.

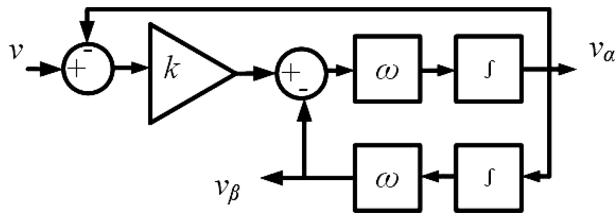


FIGURE 19.32 Second order AF based SOGI.

The transfer function of the AF structure based on the SOGI shown in Figure 19.32 are given by

$$\text{SOGI}(s) = \frac{v'}{k\varepsilon_v}(s) = \frac{\omega' s}{s^2 + \omega'^2} \quad (19.41)$$

$$D(s) = \frac{v'}{v}(s) = \frac{k\omega' s}{s^2 + k\omega' s + \omega'^2} \quad (19.42)$$

$$Q(s) = \frac{qv'}{v}(s) = \frac{k\omega'^2}{s^2 + k\omega' s + \omega'^2} \quad (19.43)$$

The transfer functions of SOGI-based AF is not a function of the center frequency but only depends on gain k . When the center frequency ω' of the filter matches the input frequency ω , the amplitude of in-quadrature signals v' and qv' matches the amplitude of input signal v .

$$v' = -\frac{V}{\sqrt{1-(k/2)^2}} \sin\left(\omega\sqrt{1-(k/2)^2}t\right) e^{-\frac{k\omega}{2}t} + V \sin(\omega t) \quad (19.44)$$

$$qv' = -\frac{V}{\sqrt{1-(k/2)^2}} \cos\left(\omega\sqrt{1-(k/2)^2}t\right) e^{-\frac{k\omega}{2}t} - V \cos(\omega t) \quad (19.45)$$

The setting time for a second-order system can be roughly estimated by $t_s = 4.6\tau$. Since $\tau = 2/k\omega'$ and the gain for a given setting time is $k = 9.2/t_s\omega'$. Figure 19.33 shows the waveforms of in-quadrature signals v' , and qv' matches the amplitude of the input signal with a parameter of $k = \sqrt{2}$ and $\omega = 2\pi.50$ rad/s.

19.7.7 SOGI-QSG

Figure 19.35 shows the response of the SOGI-PLL in Figure 19.34. A single-phase input signal of $230 V_{\text{rms}}$ and 50 Hz frequency is applied. The gain of SOGI-QSG is set to $k = \sqrt{2}$ at a setting time of 20 ms for the AF. LF parameters are calculated to achieve the settling time for PLL.

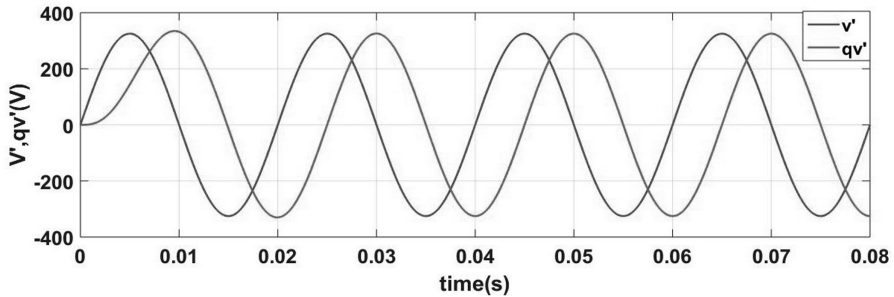


FIGURE 19.33 Response of the SOGI-QSG.

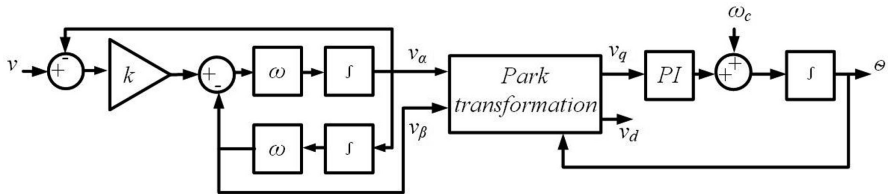


FIGURE 19.34 SOGI-based PLL (SOGI-PLL).

Figure 19.35 shows the quadrature signals generated by the SOGI-QSG, and the transient response is extended until the grid frequency is tuned. Figures 19.36 and 19.37 show the output variables of the Park transformation, and signal v_d matches the amplitude of input voltage, whereas signal v_q is settled to zero in the steady state by the action of PLL. Figure 19.38 shows the phase angle is detected by the PLL at a setting time of 20 ms, and the damping factor ξ is $1/\sqrt{2}$.

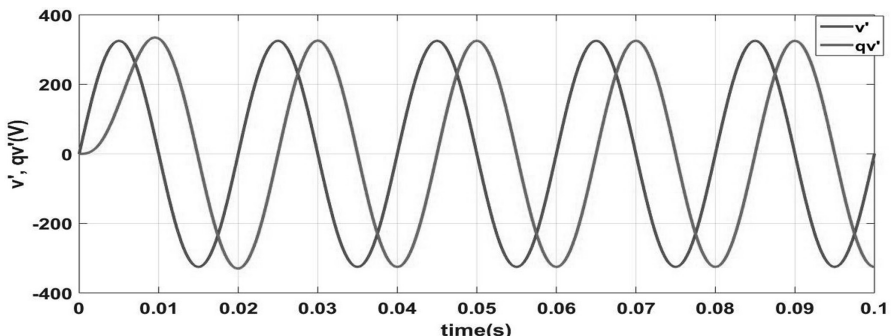


FIGURE 19.35 Response of the SOGI-PLL for in-quadrature signals generated by the SOGI-QSG.

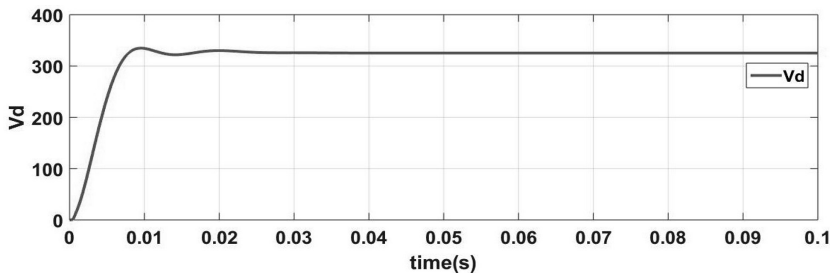


FIGURE 19.36 Response of the SOGI-PLL for direct signal in the synchronous reference frame.

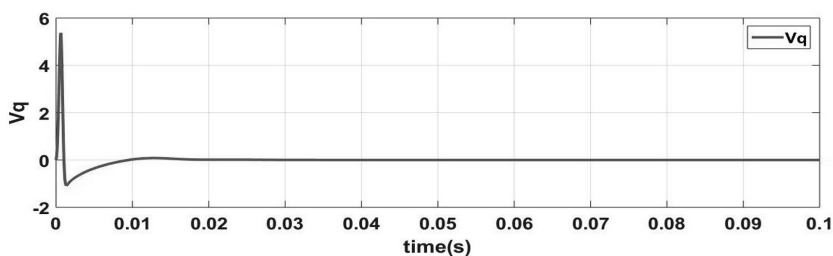


FIGURE 19.37 Response of the SOGI-PLL for quadrature signal in the synchronous reference frame.

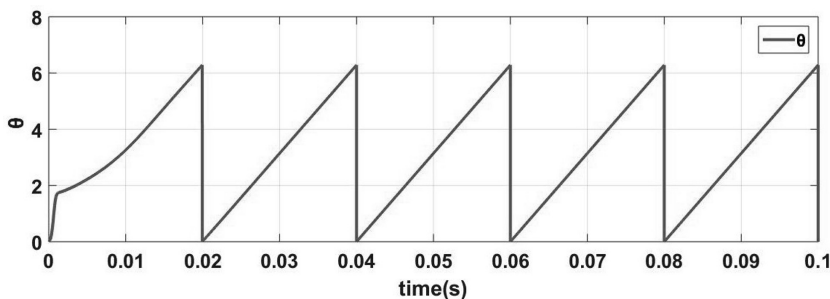


FIGURE 19.38 Response of the SOGI-PLL for detected phase angle.

19.8 CONTROL OF GRID CONVERTER UNDER GRID FAULT

Ideally, the grid voltage should form a perfect sinusoidal waveform with constant frequency and amplitude. However, grid-connected PV/wind-power system causes the voltage deviation from the ideal voltage due to mismatch between generation and demand that causes power-frequency deviation, whereas sudden loading, load disconnection, and losses cause deviations in the voltage amplitude. Commonly, the power system networks have strong grids for the transmission power that controls the voltage amplitude within a narrow band, whereas distribution grids are weaker and are associated with greater deviations in the voltage amplitude.

19.9 DESIGN OF GRID FILTERS

The output of the VSI is voltage generated through the PWM scheme, which contains a fundamental frequency component and higher-order harmonics components around $m \cdot f_s$, where f_s is the switching frequency of the inverter and $m = 1, 2, 3, \dots$ is a multiplication factor. To alleviate the harmonics in grid, current filters are required between VSIs and the grid. The grid-connected filters are low-pass filters that only allow fundamental frequencies to pass. Filters are basically classified as:

1. *L-filters*: The L-filter shown in Figure 19.39 consists of an inductor (L_i) connected in series. It is a first-order filter. Using this filter, the grid-connected inverter (GCI) must have a high-switching frequency and high inductance to sufficiently attenuate the harmonics. The attenuation provided by L-filter is -20 db/dec. The Laplace transform of the L-filter is given by Equation (19.46).

$$\frac{i_i(s)}{V_{dc}(s)} = \frac{1}{L_i s + r_i} \quad (19.46)$$

2. *LC-filters*: As shown in Figure 19.40, it consists of a series inductance (L_i) followed by capacitor (C), with internal resistance r_i and load resistance R . For the LC-filter, the plant model is a second-order system, it has good current ripple attenuation of -40 db/dec even in small inductance value, and it can operate at a low-switching frequency. The resonant frequency of the filter depends on the grid impedance; therefore, it is not suitable for GCI.

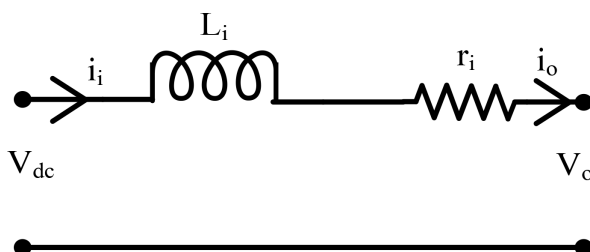


FIGURE 19.39 L-filter configuration.

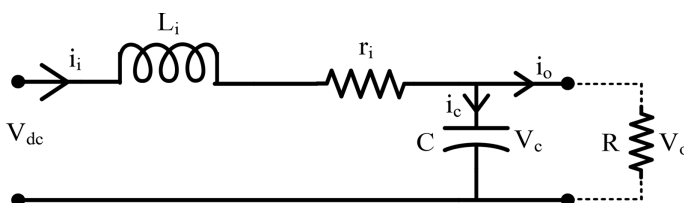


FIGURE 19.40 LC-filter configuration.

The Laplace transform of the LC-filter is given by Equation (19.47), and the resonance frequency is given by Equation (19.48):

$$\frac{Y}{u} = \frac{V_o}{V_{dc}} = \frac{\frac{1}{L_i C}}{s^2 + \left(\frac{r_i}{L_i} + \frac{1}{R C} \right) s + \left(\frac{r_i}{R L_i C} + \frac{1}{L_i C} \right)} \quad (19.47)$$

$$f_o = \frac{1}{2\pi\sqrt{LC}} \quad (19.48)$$

3. LCL-filters: As shown in Figure 19.41, the LCL filter consists of a two-series inductance called an inverter-side inductance (L_i), and grid-side inductance (L_g), and a shunt capacitor connected in between, with internal corresponding resistances r_i and r_g . For LCL-filters, the plant model is a third-order system. It has highest attenuation factor of -60 db/dec, so it requires small inductance values. The capacitor should be designed as small as possible to suppress the current harmonics caused by grid distortion, but excessive reduction is unpractical. It has unstable dynamic behavior due to the undesired resonance caused by zero impedance at a certain frequency in GCI. It is difficult to control and increase the complexity of the controller design. The Laplace transform of the LCL-filter is given by Equation (19.49), and the resonance frequency is given by Equation (19.50).

$$\begin{aligned} \frac{Y}{u} &= \frac{i_g(s)}{V_{dc}(s)} \\ &= \frac{\frac{1}{L_i L_g C}}{s^3 + \left(\frac{r_g}{L_g} + \frac{r_i}{L_i} \right) s^2 + \left(\frac{1}{L_g C} + \frac{r_i r_g}{L_i L_g} + \frac{1}{L_i C} \right) s + \left(\frac{r_i}{L_i L_g C} + \frac{r_g}{L_i L_g C} \right)} \end{aligned} \quad (19.49)$$

$$f_{res} = \frac{1}{2\pi} \sqrt{\frac{L_i + L_g}{L_i L_g C}} \quad (19.50)$$

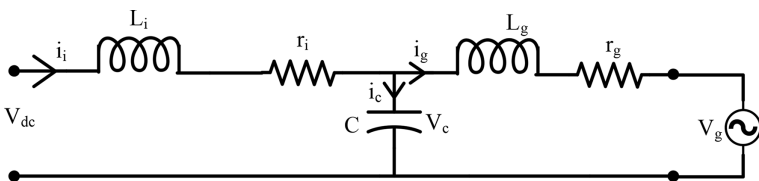


FIGURE 19.41 LCL-filter configuration.

In order to correctly tune the LCL-filter at resonance frequency, the inverter-side inductor and grid-side inductor should bring the current under the standards of the grid code. The inverter-side inductance is designed to limit the current ripple, and the grid-side inductance is designed to suppress the harmonics. Thus, the proper design of the filter depends on:

1. Minimum voltage drop across the filter
2. Minimum stored energy in the filter
3. Minimum reactive power produced by the LCL-filter capacitor
4. Robust to external parameter variation such as grid impedance
5. Minimum damping loss
6. Proper attenuation of switching frequency component to ensure high-quality grid current

19.10 SOLVED PROBLEMS

Example 19.1: In a boost converter, the duty ratio is adjusted to regulate the output voltage V_{dc} at 48 V. The input voltage varies in a wide range from 12 to 24 V. The maximum power output is 500 W. Calculate the maximum value of L that can be used. Assume switching frequency of 50 kHz.

SOLUTION

Given data

$$V_{dc} = 48 \text{ V}, f_s = 50 \text{ kHz}$$

$$I_{dc,\max} = \frac{P_{dc}}{V_{dc}} = \frac{500}{48} = 10.42 \text{ A}$$

For given input range of V_{pv} of 12–24 V,

$$V_{dc} = \frac{V_{pv}}{1-D}$$

Duty ratio (D) is in a range of 0.75 to 0.5.

The average value of output current at the edge of continuous conduction (I_{oB}) is

$$I_{oB} = \frac{V_{dc}}{2Lf_s} D_{\max} (1 - D_{\max})^2$$

So I_{oB} is equated to $I_{o,\max}$ of 10.42 A

$$L = \frac{48}{2 \times 50 \times 10^3 \times 10.42} \times 0.75(1 - 0.75)^2 = 2.16 \mu\text{H}$$

If $L = 2.16 \mu\text{H}$ is used, the converter operation will be the edge of the continuous conduction mode, and if $L < 2.16 \mu\text{H}$ is used, the converter operation will be in the discontinuous conduction mode.

REVIEW QUESTIONS

- 19.1 What are renewable energy sources?
- 19.2 Why are power electronics converters required for extracting power from renewable sources?
- 19.3 What are the desirable characteristics of power electronics converters for renewable energy sources?
- 19.4 What are the basic types of power electronics converters applicable for renewable energy sources?
- 19.5 What are the basic key elements of controllers required for integration of WT and PV to the utility grid?
- 19.6 What are the different configurations of converters required for WT integration with the utility grid?
- 19.7 What are the types of configurations for integrating the PV module to the utility grid?
- 19.8 What is the difference between a centralized inverter and a string inverter?
- 19.9 What is a boost converter?
- 19.10 Why is a boost converter required for PV integration with the grid?
- 19.11 What is a PV inverter?
- 19.12 What is PLL?
- 19.13 What is the role of PLL in grid synchronization?
- 19.14 What is the basic structure of PLL?
- 19.15 Why is the orthogonal signal generator required in single-phase PLL?
- 19.16 Define the grid filter.
- 19.17 What is resonance frequency?
- 19.18 What are the factors on which the design of a filter depends?
- 19.19 What is the difference between an L, LC, and LCL filter?
- 19.20 Why is an LCL filter mostly preferred for grid integration?
- 19.21 An emergency power supply of 2.5 kVA, 230 V, 50 Hz is fed by 48 V battery bank. The circuit diagram of the system consists of a battery bank in series with a DC/DC boost converter, a DC bus with filter capacitor, DC/AC single-phase converter, and a step-up transformer whose output is connected to LC filter. The duty cycle of DC/DC converter varies to compensate the voltage decrease in the battery. The DC bus voltage is regulated at 100 V.
 - a. Calculate the expected range of duty (D) for the DC/DC converter, assuming that the system will shut down when the battery voltage drops to 80% of its rated value to prevent deep discharge.
 - b. Considering the input current of the DC/AC converter to be pure DC, calculate the DC bus capacitor filter value so that the ripple is limited to 10% of DC voltage. The switching frequency of the converter is 10 kHz.
- 19.22 A battery bank of 48 V is used to feed an emergency power supply of 2.5 kVA, 230 V, 50 Hz. The system consists of battery bank in series with a DC/DC boost converter, DC bus with filter capacitor, AC/DC single-phase converter, and a step-up transformer whose output is connected to LC filter. The DC/AC inverter is controlled with SPWM (10 kHz) at modulating factor ($m_a = 1$). The DC bus voltage is regulated at 100 V.

- a. Calculate the required turns ratio of the transformer.
 - b. Calculate the resonant frequency of the LC filter connected at the output of transformer so that magnitude of dominant harmonic across load is limited to 10% of the fundamental component.
- 19.23 Design the components and controller parameters of the AC/DC converter with given specifications of input voltage 1432 V at 50 Hz, output voltage 2,800 V (DC), and switching frequency 660 Hz. The rated power of the converter is 1,400 kW, and its efficiency is 98%.
- 19.24 A series set of solar panels delivers a total DC voltage of 350 V to 450 V, and a current of 1 to 5 A. A PWM inverter is used to connect the panels to a 240 V, 50 Hz load: (a) Draw the complete solar system including inverter circuit, which meets the desired functions; (b) Assume the inverter operates with a unipolar PWM. What range of modulation index will be needed to get the desired voltage range to match the load? (c) If the switching devices are required to work with a switching frequency of $f_{sw} = 2.45$ kHz, what would be the frequency modulation index? (d) Calculate the above (b) and (c), if the inverter operates with bipolar PWM; and (e) Draw the output voltages for unipolar and bipolar with proper labeling.

SUMMARY

In this chapter, key elements required for grid integration of the WT and PV systems are explained. For extracting power from renewable resources, power electronics converters play a crucial role. However, due to the stringent demand of the existing grid, the converters are required to follow certain control features. For extracting maximum power, a brief explanation of the MPPT algorithm and DC/DC is provided. Also, the development of smart, high-efficient, robust inverter topologies are explained. The importance of the filter and its utilization for integration with utility grid is discussed, which helps in proper selection of the filter design.

REFERENCES/FURTHER READING

1. J. M. Carrasco, L. G. Franquelo, J. T. Bialasiewicz, E. Galván, R. C. P. Guisado, M. Á. M. Prats, J. I. León, and N. M.-Alfonso, Power-electronic systems for the grid integration of renewable energy sources: A survey, *IEEE Trans. Ind. Electron.*, vol. 53, no. 4, pp. 1002–1016, 2006.
2. D. E. Olivares, A. M. Sani, A. H. Etemadi, C. A. Cañizares, R. Iravani, M. Kazerani, A. H. Hajimiragha et al., Trends in microgrid control, *IEEE Trans. Smart Grid*, vol. 5, no. 4, pp. 1905–1919, 2014.
3. E. R. Cadaval, G. Spagnuolo, L. G. Franquelo, C. A. R. Paja, T. U. Suntio, and A. E. M. Xiao, Grid-connected photovoltaic generation plants: Components and operation, *IEEE Ind. Electron. Mag.*, vol. 7, no. 3, pp. 6–20, 2013.
4. S. Kouro, J. I. Leon, D. Vinnikov, and L. G. Franquelo, Grid-connected photovoltaic systems: An overview of recent research and emerging PV converter technology, *IEEE Ind. Electron. Mag.*, vol. 9, no. 1, pp. 47–61, 2015.
5. Y. Yang and F. Blaabjerg, Overview of single-phase grid-connected photovoltaic systems, *Electr. Pow. Compo. Sys.*, vol. 43, pp. 1352–1363, 2015.

6. F. Blaabjerg, R. Teodorescu, M. Liserre, and A. V. Timbus, Overview of control and grid synchronization for distributed power generation systems, *IEEE Trans. Ind. Electron.*, vol. 53, no. 5, pp. 1398–1409, 2006.
7. A. Timbus, M. Liserre, R. Teodorescu, P. Rodriguez, and F. Blaabjerg, Evaluation of current controllers for distributed power generation systems, *IEEE Trans. Pow. Electron.*, vol. 24, no. 3, pp. 654–664, 2009.
8. T. Esram and P. L. Chapman, Comparison of photovoltaic array maximum power point tracking techniques, *IEEE Trans. Energy Convers.*, vol. 22, no. 2, pp. 439–449, 2007.
9. B. Subudhi and R. Pradhan, A comparative study on maximum power point tracking techniques for photovoltaic power systems, *IEEE Trans. Sustain. Energy*, vol. 4, no. 1, pp. 89–98, 2013.
10. M. Calais, V. G. Agelidis, and M. Meinhardt, Multilevel converters for single-phase grid connected photovoltaic systems: An overview, *Sol. Energy*, vol. 66, no. 5, 1999, pp. 325–335.
11. L. Ma, T. Kerekes, P. Rodriguez, X. Jin, R. Teodorescu, and M. Liserre, A new PWM strategy for grid-connected half-bridge active NPC converters with losses distribution balancing mechanism, *IEEE Trans. Pow. Electron.*, vol. 30, no. 9, pp. 5331–5340, 2015.
12. S. Jayalath and M. Hanif, Generalized LCL-filter design algorithm for grid-connected voltage-source inverter, *IEEE Trans. Ind. Electron.*, vol. 64, no. 3, pp. 1905–1915, 2017.
13. R. Teodorescu, M. Liserre, and P. Rodríguez, *Grid Converters for Photovoltaic and Wind Power System*, John Wiley & Sons, New Delhi, India, 2011.
14. M. Karimi-Ghartemani, S. A. Khajehoddin, P. K. Jain, and A. Bakhshai, Derivation and design of in-loop filters in phase-locked loop systems, *IEEE Trans. Instrum. Meas.*, vol. 61, no. 4, pp. 930–940, 2012.
15. V. Kaura and V. Blasko, Operation of a phase locked loop system under distorted utility conditions, *IEEE Trans. Ind. Appl.*, vol. 33, no. 1, pp. 58–63, 1997.
16. A. Mohammad, N. Marwali, and M. Dai, *Integration of Green and Renewable Energy in Electric, Power Systems*, John Wiley & Sons, Hoboken, NJ, 2010.
17. A. M. Trzynadlowski, *Introduction to Modern Power Electronics*, Ch. 9, 3rd edn, John Wiley & Sons, Hoboken, NJ, 2010.
18. M. Trzynadlowski, *Power Electronic Converters and Systems*, Ch. 12–13, Institution of Engineering and Technology, London, UK, 2016.
19. G. M. Masters, *Renewable and Efficient Electric Power Systems*, IEEE Press, Wiley, 2013.
20. T. O. Kowalska, F. Blaabjerg, and J. Rodríguez, *Advanced and Intelligent Control in Power Electronics and Drives*, Springer, Cham, Switzerland, 2014.
21. N. Femia, G. Petrone, G. Spagnuolo, and M. Vitelli, *Power Electronics and Control Techniques for Maximum Energy Harvesting in Photovoltaic Systems*, CRC Press, Boca Raton, FL, 2013.
22. R. Teodorescu, M. Liserre, and P. Rodriguez, *Grid Converters for Photovoltaic and Wind Power Systems*, John Wiley & Sons, Chichester, UK, 2011.

20 Distributed Generation and Microgrids

20.1 INTRODUCTION

The converters are the essential power electronics tools for converting AC power to DC and vice versa. The AC and DC power come from the nonrenewable or renewable energy resources. The nonrenewable energy resources, such as thermal, nuclear, and gas power plants are centralized. Whereas, distributed generation (DG) are typically small-scale renewable energy resources, such as solar power, wind power, batteries, biogas, and biomass. The DG systems are decentralized systems with a capability of <10 MW and located close to the load.

Microgrid (MG) is a combination of DG resources and interconnected loads within clearly defined electrical boundaries that acts as a single controllable object with respect to the grid. The MG can be connected and disconnected from the grid to permit it for both islanded mode and grid-connected mode of operation. As shown in [Figure 20.1](#), an MG can consist of different DG resources, converters, and different loads. These MGs are categorized as low voltage (<1 kV), medium voltage (<40 kV), and high voltage (>40 kV) by means of power electronic converters. A bidirectional converter is used for charging the battery or feeding power to DC distribution systems. DC distributions are used by the hybrid electric vehicle (HEV) battery charging and different industrial loads. However, AC distributions are widely used in the household, industries, and home appliances. The MG generally has many advantages, such as:

1. Utilizes DG resources, which has almost zero emissions and freely available
2. Cost of the transmission and distribution system can be reduced because the MG is able to supply the local demand
3. Setup can reduce the cost per unit of energy
4. Area can sustain a normal power supply during natural blackouts, disasters, etc.
5. Reliability and quality of power received by a purchaser are improved by setting up a, MG.

The DG used in the MG can supply power to the grid and also meet the local load demands.

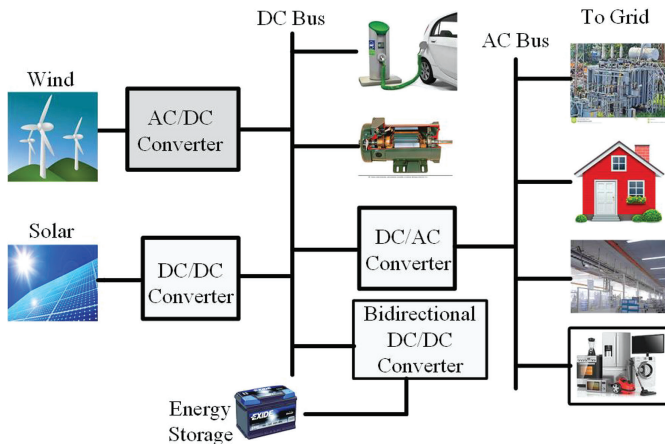


FIGURE 20.1 Typical microgrid. (From Behera, R.K., Report on microgrid structure, control and design, IIT Patna, Bihar, India, 2018.)

20.2 DG AND MG COMPONENTS

The main MG components are as follows:

1. DG
2. Loads
3. Storage devices
4. Control units
5. Point of common coupling (PCC)

The DG is an integral and main component of the MG, which is also discussed in [Section 20.1](#). Storage devices include batteries, ultracapacitors, and flywheels. The storage device can perform several operations, such as voltage and frequency regulation, power-quality enhancement, provide backup power for the system, and cost optimization. The optimal charging and discharging needs additional control units. Generally, for battery charging, the bidirectional battery charger control circuit is required to charge the battery optimally. Control units consist of the control of converters either operating in the grid connected or in islanded mode. In grid-connected mode, grid frequency and phase calculation are important. In both modes, control of the fast inner-current loop is used to regulate the grid current. The DC link voltage is controlled using outer-voltage loop control, which is slow as compared to inner-current control loop. The basic aim of the controller design of current and voltage loop is to make the system stable while in dynamic conditions. The PCC is a common point where multiple electrical loads are connected, and as per the IEEE-519 Standard, this common point should be accessible to both the customer and utility for direct measurement.

20.3 MICROSOURCES AND LOADS

In the MG, the selection of DG availability is the key point for power utilities. The renewable energy microsource includes photovoltaic (PV) systems, wind energy, hydroelectric, biomass, and geothermal. The PV and wind energy are the major microsources, which are available throughout the geographical region.

The loads in the MG are key components. To design the robust MG system, all the system loads are classified into three groups: Tier-1, Tier-2, and Tier-3.

1. *Tier-1 (critical loads)*: These are the loads that should not be interrupted for any reason. These are the most critical loads within the MG. Hospitals, nursing facilities, dispatch centers, etc. are typical examples.
2. *Tier-2*: Generally, these loads are shed for the short term to reduce load peaks. Sometimes these loads are also used to permit the starting of an additional generation. Examples of these category loads are air conditioning, heating, ventilation, washer, and dryers.
3. *Tier-3*: These loads are shed in an emergency only to shield the stability of the MG system and to prevent a blackout. Examples of these category loads are residential clients and commercial amenities with back-up generation.

20.4 POWER ELECTRONICS INTERFACE

The power electronics converters commonly used in MGs are DC-DC converters and DC-AC converters (inverters). The power electronics interfacing consists of different power electronics converters, ancillary services, monitoring and control units, DGs, load control, power conditioning units, interfacing circuits, and filters. The MG system is very reliable, due to the power converters interfacing amongst different DGs units, AC buses, DC buses, and the surrounding power systems. So, two types of interfacing are discussed: DC-bus and AC-bus interfacing.

20.4.1 DC-BUS INTERFACE

The DC-DC converter is an essential component in interfacing DG systems to the DC links. The DC power coming from the PV system has to be stepped up to meet the required DC bus. For this purpose, the high-voltage gain DC-DC converter or boost converter is used. In the case of available AC power fed from the wind system, first it should be converted into DC power using a rectifier circuit. If this DC voltage does not meet the requirement of DC-bus voltage, then again, a DC-DC converter is essential.

The overall goal is to control the output DC-link power. For this purpose, DC-link voltage control techniques are used as shown in [Figure 20.2](#). The DC-link voltage is regulated using a feedforward voltage-control loop. A fast-inner current-control loop is cascaded with the slower outer voltage-control loop, and the controller can simply be a proportional-integral (*PI*) controller.

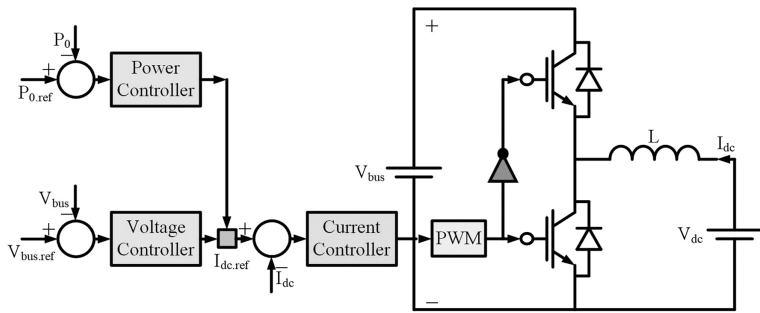


FIGURE 20.2 Control schemes for DC-bus link interface. (From Behera, R.K., Report on microgrid structure, control and design, IIT Patna, Bihar, India, 2018.)

20.4.2 AC-BUS INTERFACE

The inverter circuit is commonly used for converting DC power to AC power. High-voltage AC voltage is directly interfaced with the AC bus, and if the available AC voltage is low, then a rectifier circuit followed by boost converter cascaded with voltage source inverter (VSI) is used. The AC bus interface can also be operated in grid-connected and islanded mode. In islanded mode, the main intention is to control the frequency and magnitude of the output voltage of the VSI. However, in the grid-connected mode, the active and reactive power is controlled.

The AC voltage regulation scheme involves two cascaded control loops as shown in [Figure 20.3](#). The required AC voltage magnitude depends upon V_{qref} . The inner-current control loop independently regulates the d -axis and q -axis components of the inverter output current, in the rotating reference frame. This control scheme is for islanding-mode control schemes. However, in the grid-connected operation, the phase-locked loop (PLL) is commonly used for synchronization.

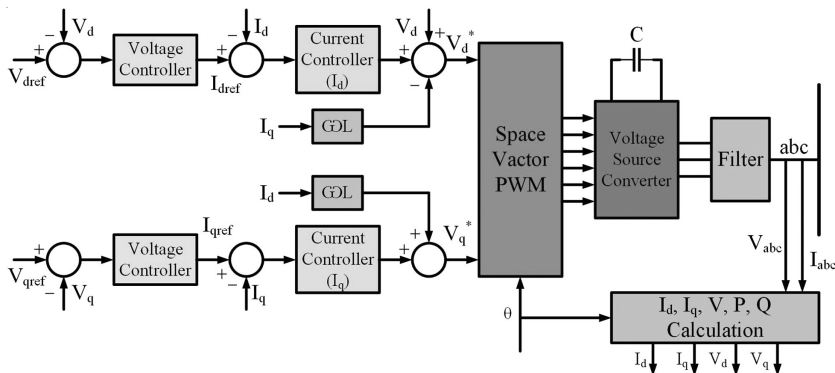


FIGURE 20.3 Control schemes for AC-bus link interface. (From Behera, R.K., Report on microgrid structure, control and design, IIT Patna, Bihar, India, 2018.)

20.5 ARCHITECTURE (DC/AC/HYBRID) OF MICROGRIDS AND STORAGE SYSTEMS

The DC and AC distribution systems are widely used throughout the globe. The DG systems are used for these distribution systems. The MG architectures are based on the distribution system context. The architecture used in the MGs is different, such as the DC, AC, and hybrid MG. These architectures are used depending upon the available DG systems and requirements.

20.5.1 DC MICROGRID

The DC source is commonly available from the PV, ultracapacitors, battery, etc. as shown in [Figure 20.4](#). For the DC MG, available AC power from wind power is converted into DC with the help of converter interfacing. Studies show that approximately 30% of AC-generated DGs are interfaced with power converters to convert into DC distribution systems, and the amount of losses in this process is approximately 10%–25%. Therefore, power electronics DC-DC converters interfacing for DC MG application is a smart choice in terms of reduced conversion stage, increased efficiency, and increased power quality.

20.5.2 AC MICROGRID

AC distribution systems are a commonly used structure of the MG implementation. The established AC structure, such as transformers, protection devices, and distribution systems, are commonly utilized in the AC MG. The AC distribution system is stabilized, and due to easier implementation, the AC MG is a reliable system. The general structure of the AC MG is shown in [Figure 20.5](#). From [Figure 20.5](#), it is clear that the DC supplying DG systems are first converted to AC power using inverters. However, for control of AC-link voltage, sometimes two-stage converters are used for AC-supply DG systems. This architecture also has a feature for selecting critical loads, noncritical loads, or particular DGs with the help of switches and circuit breakers.

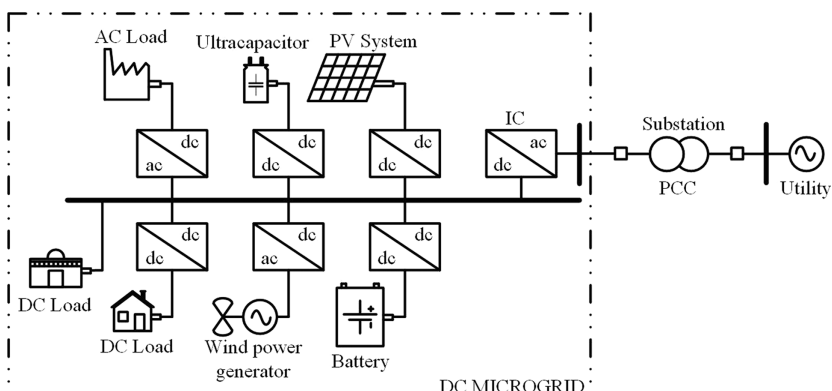


FIGURE 20.4 DC MG architecture. (From Behera, R.K., Report on microgrid structure, control and design, IIT Patna, Bihar, India, 2018.)

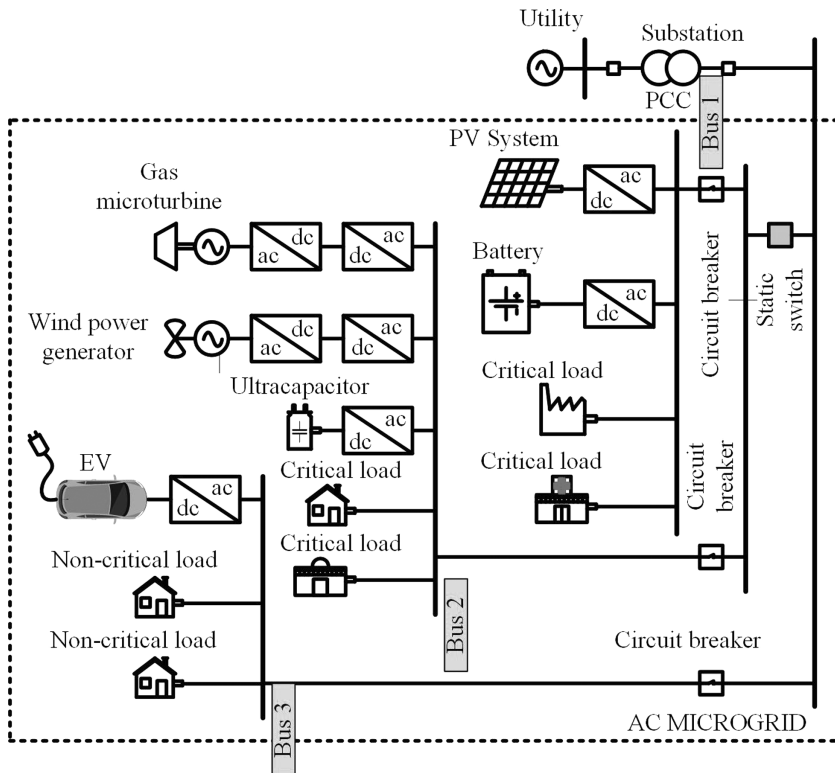


FIGURE 20.5 AC MG architecture. (From Behera, R.K., Report on microgrid structure, control and design, IIT Patna, Bihar, India, 2018.)

The main advantage of the AC MG is the availability of the existing electrical grid. However, complex power electronics converters are required to synchronize DGs with the AC utility grid. This leads to reduction of reliability and efficiency of the overall system.

20.5.3 HYBRID MICROGRID

The advantage of both AC and DC MGs are integration with hybrid MGs as shown in [Figure 20.6](#). This hybrid MG allows the installation of sensible loads in the DC bus and more robust installed in the AC bus.

The reliability of the hybrid architecture is quite low as compared to AC MG architecture due to the main interface converter. The major challenges of the hybrid MG are control of both bus voltages, and power management is complex.

Further, the hybrid MG is classified in two groups: coupled AC configuration and decoupled AC configuration. In coupled AC configuration, the AC bus is coupled directly with the utility grid as shown in [Figure 20.6](#). However, if additional DC-AC or AC-DC converters are used to couple the utility grid, then this category of coupling is known as decoupled AC configuration.

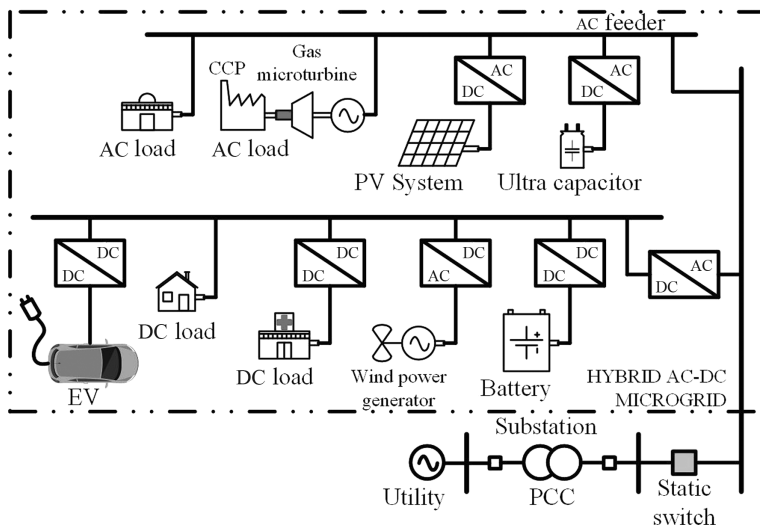


FIGURE 20.6 Hybrid MG architecture. (From Behera, R.K., Report on microgrid structure, control and design, IIT Patna, Bihar, India, 2018.)

20.5.4 STORAGE SYSTEM

The energy storage systems used in MGs are flywheels, batteries, super (or ultra) capacitors, compressed air, superconducting magnetic energy storage, thermal energy storage, and pumped hydroelectric. The main purpose of storage systems is to compensate the unbalance between the DGs and the loads to ensure the quality of the supply during utility grid connection or in islanding mode. The energy storage devices also provide the power balance during the load changes or system disturbances.

20.6 INTEGRATION ISSUES OF DISTRIBUTED GENERATION AND SYNCHRONIZATION

Integration of different DGs system into the distribution grid leads to operational, control, planning, and protection challenges. The synchronization with utility grids is also a major concern with the MG.

20.6.1 INTEGRATION ISSUES

The large-scale integration in the distribution grid directly affects the grid scheduling and has a significant impact on the operation of the distribution grid. The parameters that depend upon the connection of the DG are as follows [10]:

1. Power quality
2. Voltage control
3. Fault level
4. Protection systems
5. Grid losses

All these quantities directly depend upon the type of DG used and type of networks. These DG are directly connected with the distributed grid or via converters. In both cases, grid losses, voltage control, and power flow are affected. The utility grid contributes a large short-circuit current generated by the utility grid, which also causes an increase of the fault level and affects the protection scheme.

20.6.2 GRID SYNCHRONIZATION

The power electronics converter operates according to the sensed grid parameters (magnitude, phase, and frequency). Synchronization of grid parameters is an important task for grid stability and proper functioning. Grid synchronization is performed using PLL. As, the name suggests, the main work of the PLL is to lock the phase of the sensed voltage or current. A PLL is a closed-loop system. In this PLL, an internal oscillator is controlled to keep periodical signal by using the feedback loop as shown in [Figure 20.7](#).

The PLL involves the phase detector, loop filter, and voltage-controlled oscillator. The system descriptions are as follows:

- *Phase detector (PD):* The PD is used to detect the phase of the signal. The PD compares the input signal and the reference signal, which generates the proportional output signal. This output signal of PD is a high-frequency sinusoidal component that appears with the DC phase-angle difference signal.
- *Loop filter (LF):* The main work of the LF is to provide a low-pass filtering characteristic to attenuate the output signal of the PD. Moreover, the LF block constitutes a PI controller or first-order low-pass filter.
- *Voltage-controlled oscillator (VCO):* The VCO generates the oscillated AC signal whose oscillation frequency is controlled by the output of the LF signal.

The mathematical analysis of linearized small signal model is as follows:

The PLL components are given in a frequency domain, and the measuring phase signal is θ . The small signal model of the basic PLL is given in [Figure 20.8](#).

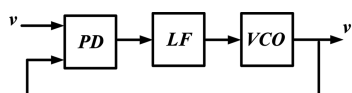


FIGURE 20.7 Basic structure of a PLL. (From Behera, R.K., Report on microgrid structure, control and design, IIT Patna, Bihar, India, 2018.)

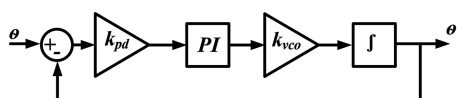


FIGURE 20.8 Small-signal model of a basic PLL. (From Behera, R.K., Report on microgrid structure, control and design, IIT Patna, Bihar, India, 2018.)

$$\text{Phase detector } E_{pd}(s) = \frac{V}{2}(\theta(s) - \theta'(s)) \quad (20.1)$$

$$\text{Loop filter } V_{lf}(s) = K_p \left(1 + \frac{1}{T_i s} \right) E_{pd}(s) \quad (20.2)$$

$$\text{Controlled oscillator } \theta'(s) = \frac{1}{s} V_{lf}(s) \quad (20.3)$$

The open-loop phase-transfer function is calculated as

$$F_{OL}(s) = PD(s) \cdot LF(s) \cdot VCO(s) = K_{in} \frac{k_p \left(1 + \frac{1}{T_i s} \right)}{s} = \frac{k_p s + \frac{k_p}{T_i}}{s^2} \quad (20.4)$$

The closed-loop transfer function is written as

$$H_\theta(s) = \frac{k_p s + \frac{k_p}{T_i}}{s^2 + k_p s + \frac{k_p}{T_i}} \quad (20.5)$$

The error transfer function is given as

$$E_\theta(s) = 1 - H_\theta(s) = \frac{s^2}{s^2 + k_p s + \frac{k_p}{T_i}} \quad (20.6)$$

The second-order transfer functions can also be written as

$$H_\theta(s) = \frac{2\zeta w_n s + w_n^2}{s^2 + 2\zeta w_n s + w_n^2} \quad (20.7)$$

$$E_\theta(s) = \frac{s^2}{s^2 + 2\zeta w_n s + w_n^2}$$

where

$$w_n = \sqrt{\frac{K_p}{T_i}} \text{ and } \zeta = \frac{\sqrt{K_p T_i}}{2}$$

Settling time is given as

$$t_s = 4.6\tau$$

$$\tau = \frac{1}{\zeta w_n}$$

the parameters of the PI controller are given as

$$K_p = 2\zeta w_n = \frac{9.2}{t_s}$$

$$T_i = \frac{2\zeta}{w_n} = \frac{t_s \zeta^2}{2.3}$$

20.7 INTERCONNECTION OF POWER ELECTRONICS CONVERTERS WITH MEDIUM-VOLTAGE GRID

The power electronics converters are interconnected with DGs, loads and switches, or circuit breakers. The key role of interconnected power electronics converters with a medium-voltage grid is given as:

1. Interconnection insures the exchange and control of power.
2. Interconnection allows a controlled connection with grid and without grid (islanding mode).
3. It insures the isolation of the MG from the grid perturbations.
4. The reconfigurable power electronic converter structure gives more flexible and multiple-function capability when the grid is interconnected.

The DG role increases, which increases the power flow from a low-voltage grid to a medium-voltage grid. The bidirectional power flow also assures the voltage and power control of the grid-connected systems. The interconnected system also controls or limits the energy exchange with the distribution grid.

20.8 STABILITY ASPECTS IN MICROGRIDS

The stability issues in the MG are an important aspect for reliability, cost, operation, and safety. The major stability issues may come from different aspects, such as cascading of power electronics converters, different DGs, control parameters, protection systems, dynamic loading, grid utilities issues, islanding, and during normal operations. The stability issues can lead to failure of the MGs. In order to analyze the major cause of the instability in MG, its strategies to limit the instability are discussed in following subsections.

20.8.1 MAJOR STABILITY ISSUES IN THE MICROGRID

The major stability issues are categorized in terms of voltage stability, small-signal stability, and large-signal stability (transient stability). The voltage stability occurs due to the reactive power limit or current limiters, loads dynamics caused by induction motors, undervoltage load shedding, tap changers, and voltage regulators.

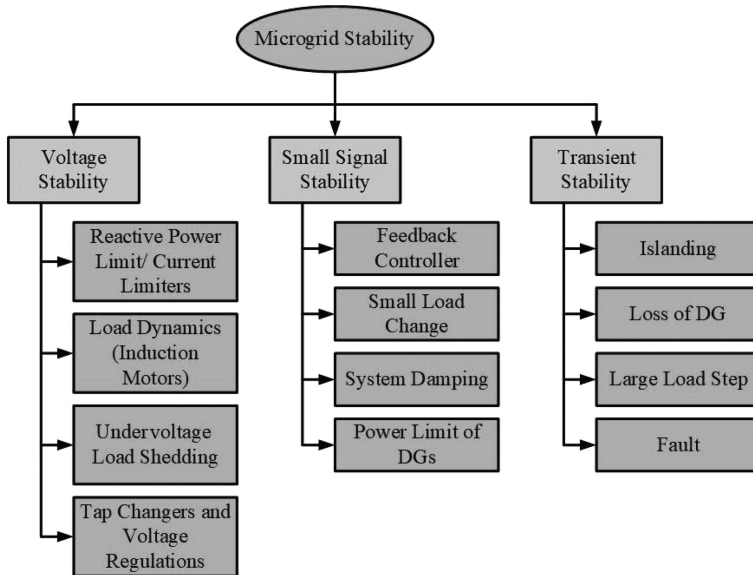


FIGURE 20.9 Major stability issues in different aspects of the MG. (From Majumder, R., *IEEE Trans. Power Systems*, 28, 3243–3252, 2013.)

Major stability issues are shown in the Figure 20.9. The small-signal stability problems come from feedback controller, small load changes, system damping, and power limits of DGs. The controller design is a key component to maintaining the stability. However, in the islanding condition, large load changes and different faults conditions will result in transient stability problems. These stability issues should be resolved within the permissible cycle. Failure to do this can lead to severe damage of protection devices or system failure.

20.8.2 STABILITY IMPROVEMENT IN MICROGRID

The major stability issues shown in Figure 20.9 should be limited within a few cycles. The methods of improving stabilities are shown in Figure 20.10. The instability due to voltage is limited by proper designing of the reactive power compensation, load shedding, use of suitable current limiter for DGs, and effective voltage regulation. The small-signal stability issues generally dominate in MG system. The small-signal analysis of a MG ensures the robust system operation after a small disturbance. The small-signal stability problems are limited by designing robust control loops for the power electronics converters, coordinate control of DG systems, using stabilizers for DGs, and effective energy management systems.

The transient instability is very harmful for the operating system, and this instability occurs due to large disturbances. The transient stability is improved by proper control of storage (e.g., battery), using load-shedding methods, sensitive protection

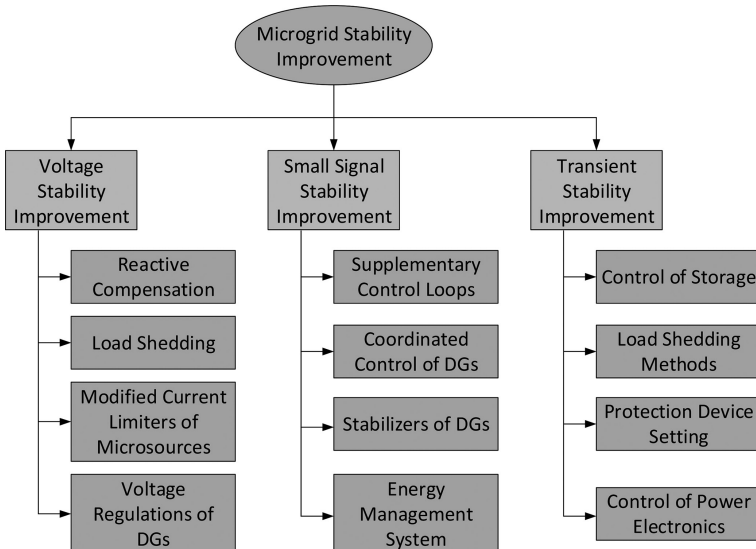


FIGURE 20.10 Major methods used for stability improvement in the MG. (From Majumder, R., *IEEE Trans. Power Systems*, 28, 3243–3252, 2013.)

settings for protection devices, and robust power electronics control design, which can sustain the large signal dynamics.

20.9 ISLANDING TECHNIQUES

Islanding is a condition in which the MG is detached from the main grid, which consists of different DG units and loads. The islanding is required when maintenance or fault occurs in the grid-connected MG. During islanding, the critical/emergency loads are supplied through the uninterrupted power supply, even in the case of grid failure. The DG units can supply the critical/emergency loads until the main grid is resynchronized with the DG units. In the DG unit-based utility-grid-connected MG, the islanding may cause many problems, such as safety concerns, damage to consumer appliances, and inverter damage. The DGs essentially sense islanding and immediately stop feeding the power to the utility grid. This is known as islanding technique or anti-islanding. The islanding detection techniques are mainly categorized into active and passive methods.

20.9.1 ACTIVE ISLANDING DETECTION

The active islanding detection is used for the detection of grid failure. In this detection scheme, an external injected perturbation signal is applied to the system for checking whether the external perturbation has changed or not. The used injected signal is an active signal, such as phase, frequency, active/reactive power, or current.

The active islanding detection is carried out for impedance measurement, negative sequence injection, slip-mode frequency shift, etc. Due to this perturbation, the power balance between the load power and DG power is broken. The main drawback of this islanding detection technique is that due to perturbation, the power quality and output power generation is reduced.

20.9.2 PASSIVE ISLANDING DETECTION

The passive detection mainly includes the transient behavior occurring on the grid. So, this method depends on the system parameters, for example, power, frequency, voltage, and harmonic distortion. These system parameters cause the power electronics converters to regulate the output power. The main measurement for passive islanding detection is carried out for under/overfrequency detection, voltage-phase jump detection, under/overvoltage detection, and harmonics detections. In passive islanding detection, the under/overfrequency and under/overvoltage detection are popular islanding techniques due to effective and easy implementation. Moreover, this detection scheme is easier as compared to active islanding detection. Due to these reasons, the majority of the power electronics converters use passive islanding detection to identify faults.

20.10 POWER ELECTRONICS IN SMART-GRID APPLICATIONS

A smart grid is fundamentally a smart power grid of tomorrow that will integrate power electronics devices and converters, computers, communication, cyber technologies, and information technologies. But the MG presently used can be outdated, inefficient, fault-intolerant, unreliable, and more inclined to cyberattacks. The main objective of smart grids is to have high-energy efficiency of the system, higher system securities, optimum resource utilized, higher reliable, economical, and easier electricity distributed to consumers.

The power electronics systems are probably the utmost vital component in a smart grid for achieving the higher-power density, high efficiency, quick control ability, and reliability. The power electronics converters are used for the power conversion of DC-to-AC, DC-to-DC, AC-to-DC, AC-to-AC in smart-grid applications. The power electronics controller is also a key part of the smart grid. The main parts used in the smart grid are advanced power semiconductors devices, high-voltage DC (HVDC) system, multilevel converters, flexible AC transmission system (FACTS), static VAR compensators (SVCs), uninterruptible power system (UPS), DGs, energy storage systems, application of artificial intelligence (AI) techniques, and smart-grid simulation and control [18–21].

The components of the smart grid are shown in the [Figure 20.11](#). It consists of DGs, energy storage systems, advanced converters, HVDC systems, FACTS devices, etc. The control, protection, and monitoring of the grid is a key part, which includes load curve estimation, generation prediction, wide monitoring and estimation, advanced metering systems, and real-time simulations. Most of the devices, control, and monitoring equipment used in a smart grid are based on the semiconductor electronics.

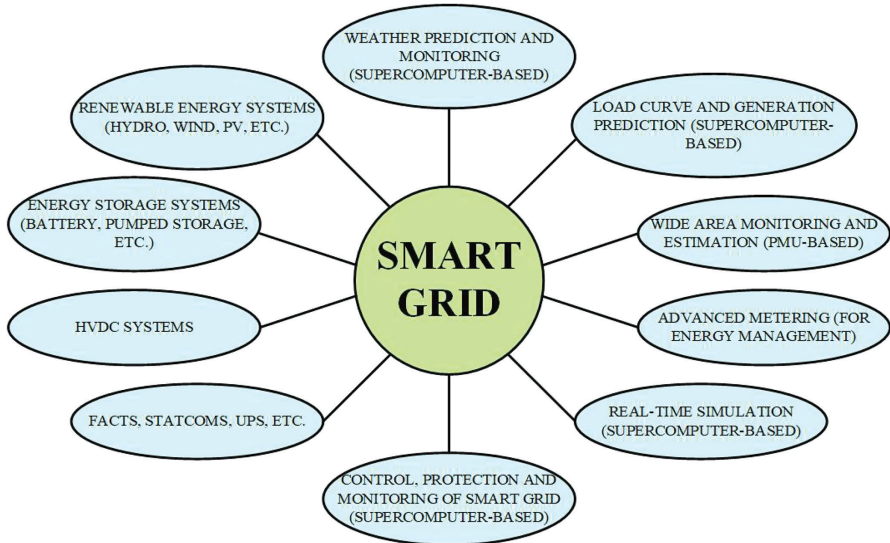


FIGURE 20.11 Smart-grid concept. (From Behera, R.K., Report on microgrid structure, control and design, IIT Patna, Bihar, India, 2018.)

20.11 VEHICLE-TO-GRID INTERCONNECTION

Electric vehicles (EVs) offer a technological advantage of vehicle-to-grid (V2G). A V2G has the ability of a vehicle to make flow of power into the MG or distribution network. The V2G helps build the available distributed energy storage system. There are two main connections that are required to implement V2G:

1. Power connection for transmission of electrical energy to and from the EVs
2. Control and logic connection to give the feedback signals when power is needed, and in the direction, power needs to be sent.

The V2G can enhance the performance of a grid in terms of system efficiency, stability, reliability, and generation dispatch. The EVs can serve as a distributed storage device and a load. When EVs are connected to the MG, the battery of the EVs, can deliver power to a grid at peak hours of load and thus improve the reliability of a system. An EV having the capability of V2G application can have features including:

- Support of reactive power
- Current harmonics filtering
- Active power regulation
- Load balancing by valley fillings
- Reducing of utility operating cost and overall service
- Peak load shaving

- Improved load factors
- Tracking of variable renewable energy resources (RERs)
- Reduced emissions
- Generate revenue

The EVs have adequate power electronics systems and charger controllers having smart connections to the grid. In this scenario, the EVs act as a stored energy resource. Smart communication between the grid and EVs, smart connection to grid, and smart metering are essential for V2G operation. **Figure 20.12** shows the overall components of the V2G system, flow of power by V2G system, and its requirements.

The V2G system consists of charging systems, battery pack, EV, utility grid, RERs, aggregator, and independent system operator (ISO). The communication for the V2G consists of bidirectional and unidirectional. Moreover, it consists of the communications to check battery condition and response of different commands, control of smart metering, and communication between ISO and EV. The EVs consist of energy back-up capacity for further utilizing the energy injection in grid, supply to grid, and providing storage. In emergency situations, EVs act as a power source at the distribution side.

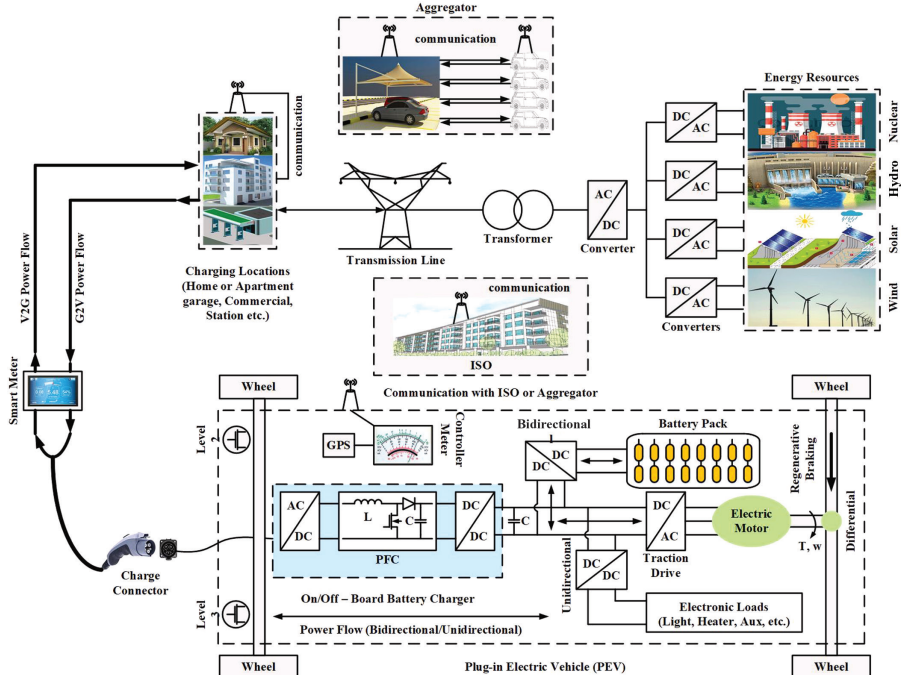


FIGURE 20.12 V2G systems, power flow, and its components. (From Habib, S. et al., *J. Power Sources*, 277, 205–214, 2015.)

20.12 GRID-TO-VEHICLE

The EVs battery-charging process is called grid-to-vehicle (G2V). The flow of energy from grid to battery must be regulated to preserve the power quality in the MG/power grids. Most of the EV charging can take place at household premises overnight in a garage where the EV can be plugged in. EV charging depends on the state-of-charge (SOC) characteristics and may be charged off-board or on-board. Generally, the charger can be divided into three categories, which depend upon charging time, such as:

- *Fast chargers:* Fast charge is essential for higher-power battery pack; usually it takes less than 30 minutes to fully charge. The fast chargers are situated in service stations.
 - *Normal chargers:* Normal chargers are typically placed in parking premises. The normal charges typically take about 4 hours.
 - *Slow chargers:* Slow charges are generally used at the household. The charging duration typically takes about 8 hours to fully charge the battery.

Two types of power flow are conceivable between the grid and EVs, as shown in Figure 20.13. The unidirectional battery chargers can charge the EV but cannot inject energy to the grid. The battery chargers are generally DC-DC converters used with diode bridge and filter. Sometimes high-frequency isolation transformers can also be employed when isolation is necessary. The bidirectional charger has two stages: (1) a bidirectional DC-DC converter for battery current regulation, and (2) grid-connected bidirectional AC-DC converter that implements a power factor. The battery chargers can use the isolated or nonisolated circuit. In charging mode of operation, the sinusoidal current is drawn from the grid with a defined phase angle to control the active and reactive power of the G2V system. When operating in discharge mode of operation, the current returns in a similar sinusoidal form. Moreover, a bidirectional battery charger supports the V2G mode of operation and power stabilization.

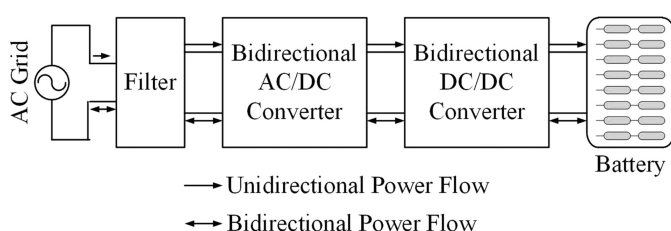


FIGURE 20.13 General unidirectional and bidirectional topology. (From Behera, R.K., Report on microgrid structure, control and design, IIT Patna, Bihar, India, 2018.)

REVIEW QUESTIONS

- 20.1. What is the difference between the nanogrid, microgrid, and smart grid?
- 20.2. What are the components of DG and MG?
- 20.3. How are loads classified in the MG?
- 20.4. Discuss the AC, DC, and hybrid MG architecture of the MG system.
- 20.5. What are the uses of AC- and DC-bus interface in the MG?
- 20.6. What does PLL mean? Why it is important for grid synchronization?
- 20.7. Discuss the small-signal model of the basic PLL.
- 20.8. What are stability problems in a MG system?
- 20.9. What is islanding? What are the different approaches used for islanding?
- 20.10. What does V2G and G2V in a smart grid mean?

SUMMARY

This chapter has addressed the main issue of DG and MG technology including their components, microsources, and loads. It has also discussed that the MG is an electric distribution system comprising distributed energy resources and loads, which can work in controlled, coordinated, and connected to the utility grid or islanded mode. Various classes of microsources, for example, PV modules, small wind turbines, and mini-hydro, and the system loads are classified in three groups: Tier-1, Tier-2, and Tier-3. The power electronics interface with DC and AC bus with its control structure is discussed. Three kinds of MG structures, such as AC MG, DC MG, and hybrid MG architecture with storage, are discussed. MG integration, stability issues, synchronization, and its interconnection with power electronics converters are explained for both grids connected and islanding mode. Few power electronics converters are discussed for smart-grid applications. This chapter has also discussed an overview of V2G and G2V interconnection technology with the MG.

REFERENCES/FURTHER READING

1. N. Hatziargyriou, H. Asano, R. Iravani, and C. Marnay, Microgrids, *IEEE Power Energy Mag.*, vol. 5, no. 4, pp. 78–94, 2007.
2. R. H. Lasseter, Microgrids, *IEEE Power Engineering Society Winter Meeting*, New York, vol. 1, pp. 305–308, 2002.
3. S. Kakran and S. Chanana, Smart operations of smart grids integrated with distributed generation: A review, *Renew. Sust. Energy Rev.*, vol. 81, Part 1, pp. 524–535, 2018.
4. R. C. Dugan and T. E. McDermott, Distributed generation, *IEEE Ind. Appl. Mag.*, vol. 8, no. 2, pp. 19–25, 2002.
5. M. Vaziri, S. Vadhma, T. Oneal, and M. Johnson, Distributed generation issues, and standards, *IEEE International Conference Information Reuse & Integration*, Las Vegas, NV, pp. 439–443, 2011.
6. B. Moran, Microgrid load management and control strategies, *IEEE/PES Transmission and Distribution Conference and Exposition (T&D)*, Dallas, TX, pp. 1–4, 2016.
7. H. A. Gabbar, *Smart Energy Grid Engineering*, Elsevier, San Diego, CA, 2016.

8. A. M. R. Lede, M. G. Molina, M. Martinez, and P. E. Mercado, Microgrid architectures for distributed generation: A brief review, *IEEE PES Innovative Smart Grid Technologies Conference Latin America (ISGT Latin America)*, Quito, pp. 1–6, 2017.
9. E. J. Coster, J. M. A. Myrzik, B. Kruimer, and W. L. Kling, Integration issues of distributed generation in distribution grids, *Proc. IEEE*, vol. 99, no. 1, pp. 28–39, 2011.
10. T. Ackermann and V. Knyazkin, Interaction of distributed generation and the distribution network: Operation aspects, *Proc. PES T&D Conf.*, Asia Pacific, vol. 2, pp. 1357–1362, 2002.
11. R. Teodorescu, M. Liserre, and P. Rodríguez, *Grid Converters for Photovoltaic and Wind Power Systems*, John Wiley & Sons, Chichester, UK, 2011.
12. R. Majumder, Some aspects of stability in microgrids, *IEEE Trans. Power Systems*, vol. 28, no. 3, pp. 3243–3252, 2013.
13. A. Khamis, H. Shareef, E. Bizkevelci, and T. Khatib, A review of islanding detection techniques for renewable distributed generation systems, *Renew. Sustain. Energy Rev.*, vol. 28, pp. 483–493, 2013.
14. Sung-II Jang and Kwang-Ho Kim, An islanding detection method for distributed generations using voltage unbalance and total harmonic distortion of current, *IEEE Trans. Power Delivery*, vol. 19, no. 2, pp. 745–752, 2004.
15. B. K. Bose, Power electronics, smart grid, and renewable energy systems, *Proc. IEEE*, vol. 105, no. 11, pp. 2011–2018, 2017.
16. A. Banerji, D. Sen, A. K. Bera, D. Ray, D. Paul, A. Bhakat, and S. K. Biswas, Microgrid: A review, *IEEE Global Humanitarian Technology Conference: South Asia Satellite (GHTC-SAS)*, 2013.
17. R. C. Bansal, *Power System Protection in Smart Grid Environment*, CRC Press, New York, 2019.
18. Z. Jiang, Power electronics interfaces for hybrid DC and AC-linked microgrids, *IEEE 6th International Power Electronics and Motion Control Conference*, 2009.
19. R. Singh and M. Kirar, Transient stability analysis and improvement in microgrid, *International Conference on Electrical Power and Energy Systems (ICEPES)*, 2016.
20. Z. Shuai, Y. Sun, Z. J. Shen, W. Tian, C. Tu, Y. Li, and X. Yin, Microgrid stability: Classification and a review, *Renew. Sustain. Energy Reviews*, vol. 58, pp. 167–179, 2016.
21. R. C. Bansal (Ed.), *Handbook of Distributed Generation: Electric Power Technologies, Economics and Environmental Impacts*, Springer, Cham, Switzerland, 2017.
22. A. F. Zobaa and R. C. Bansal (Ed.), *Handbook of Renewable Energy Technology*, World Scientific Publishers, Singapore, 2011.
23. T. Adefarati and R. C. Bansal, Integration of renewable distributed generators into the distribution system: A review, *IET-Renew. Power Gener.*, vol. 10, no. 7, pp. 873–884, 2016.
24. P. T. Manditereza and R. C. Bansal, Renewable distributed generation: The hidden challenges—a review from the protection perspective, *Renew. Sustain. Energy Rev.*, vol. 58, pp. 1457–1465, 2016.
25. P. T. Manditereza and R. C. Bansal, Review of technical issues influencing the decoupling DG converter design from the distribution system protection strategy, *IET-Renew. Power Gener.*, vol. 12, no. 10, pp. 1091–1100, 2018.
26. S. Habib, M. Kamran, and U. Rashid, Impact analysis of vehicle-to-grid technology and charging strategies of electric vehicles on distribution networks, *J Power Sources*, 277, pp. 205–214, 2015.
27. R. K. Behera, Report on microgrid structure, control and design, IIT Patna, 2018.
28. M. Yilmaz and P. T. Krein, Review of battery charger topologies, charging power levels, and infrastructure for plug-in electric and hybrid vehicles, *IEEE Trans. Power Electron.*, vol. 28, no. 5, pp. 2151–2169, 2013.

29. J. G. Pinto, V. Monteiro, H. Gonçalves, B. Exposto, D. Pedrosa, C. Couto, and J. L. Afonso, Bidirectional battery charger with grid-to-vehicle, vehicle-to-grid and vehicle-to-home technologies, *IEEE IECON Industrial Electronics Conference*, pp. 5934–5939, Vienna, Austria, November 2013.
30. R. G. Gago, S. F. Pinto, and J. F. Silva, G2V and V2G electric vehicle charger for smart grids, *IEEE International Smart Cities Conference (ISC2)*, 2016.
31. F. Blaabjerg, *Control of Power Electronic Converters and Systems*, Ch. 18, Academic Publishers, London, UK, 2018.



Taylor & Francis

Taylor & Francis Group

<http://taylorandfrancis.com>

21 Wireless Power Transfer

21.1 INTRODUCTION

Nowadays, the wireless power transfer (WPT) system is becoming very popular due to portable electronics loads, electric vehicles (EVs), artificial biomedical devices, and other applications. Recent developments in WPT technologies, such as the resonant-based coupled inductor system, magnetic induction system, and microwave systems, are more prominent. There is a wide range of applications for the WPT systems, especially portable electronics loads.

21.2 WIRELESS CHARGING LANDSCAPE

Initially, Nikola Tesla developed the WPT system in the year 1893. Over the years, growth of WPT technology has been impressive and looking forward to design some efficient techniques to send power without any conductor. To date, wires are used to connect pieces of equipment and the grid and to transmit large amounts of power. The major development of WPT technologies are low-power magnetic inductions for small distances. The WPT system consists of two components, a transmitter, and a receiver with loads connected. If the distance between the transmitter and receiver is small range varying from a few centimeters to a few meters, WPT technologies such as inductive coupling and resonant coupling are used. It is demonstrated that resonant coupling has many advantages such as tolerance transmitter and receiver misalignment.

21.3 WIRELESS POWER TRANSFER MODEL

The WPT takes place between transmitter and receiver when they are aligned with each other and coupled. Different types of inductive WPT schemes are reported in the literature are shown in [Figure 21.1](#).

21.3.1 Two-Coil Structures

Two-coil inductive WPT consists of a single transmitter and single receiver with a common coupling link. There are various two-coil structures reported in the literature based on coupling distance. They are short-distance WPT systems varying from 10 cm to a few meters. The two-coil structure is very simple to implement, and it should be aligned with each other. The coils should be properly and symmetrically placed in the base for proper support. Otherwise, distorted output voltage will be generated.

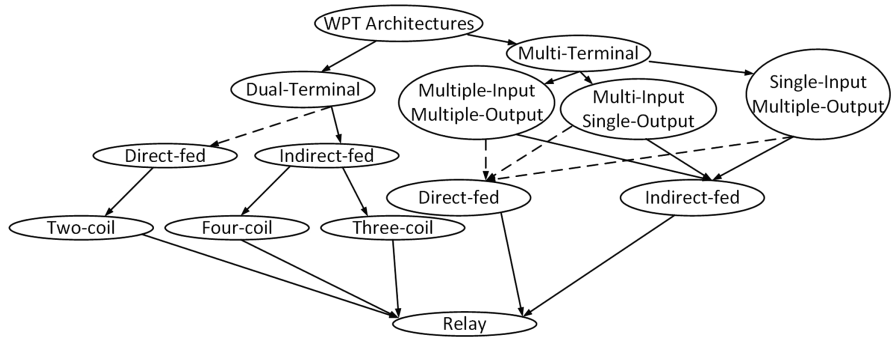


FIGURE 21.1 Types of inductive WPT schemes. (From Eteng, A. A. et al., *Renew. Sust. Energ. Rev.*, 77, 2017, 486–505.)

21.3.2 DIRECT-FED (DF) COILS

DF links are short-range WPT systems consisting of two magnetically coupled coils, a transmitter, and a receiver. Efficiency and power-transfer range can be improved by proper tuning of the coils. Figure 21.2 shows the two-coil WPT system. M_{12} is the mutual inductance of combined coil of receiver and transmitter with $k_{12} = \frac{M_{12}}{\sqrt{L_1 L_2}}$.

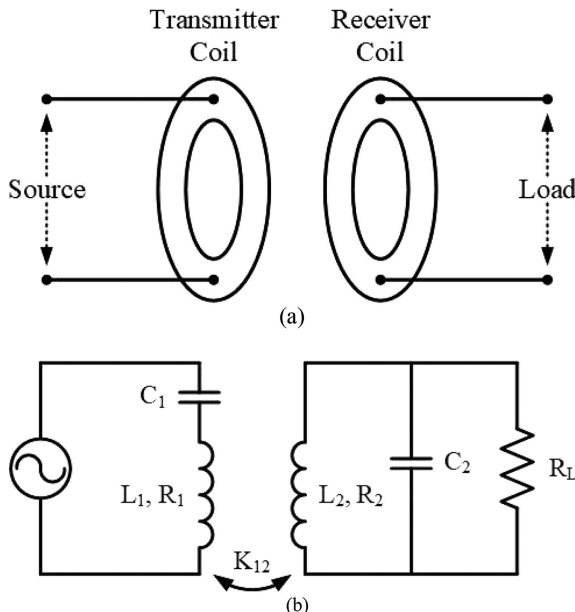


FIGURE 21.2 DF two-coil WPT system: (a) block model and (b) circuit model. (From Behera, R. K., and Kumari, M., *Wireless Power Transfer Via Magnetic Resonance*, Internship Report, IIT Patna, 2013.)

21.4 MAGNETIC RESONANCE WPT SYSTEM

The magnetic resonance link is a self-resonating WPT system for mid-range energy transmission. The resonance takes place between scattered inductance and capacitance. Four-coil magnetic resonance link consists of a transmitter and receiver coils as shown in [Figure 21.3](#). The coupling is established magnetically with a related power source and load circuits. However, the three-coil magnetic resonance link WPT system is shown in [Figure 21.4](#) is connected electrically with the transmitter or receiver coil.

21.4.1 MULTITERMINAL WPT SYSTEM

Multiterminal circuits have many transmitters and many receivers. These circuits work together for transferring energy wirelessly in an interactive way among themselves. The single-input multiple-output (SIMO) circuit normally comprises of one transmitter coil coupled with several receiver coils simultaneously as shown in [Figure 21.5](#). Multi-input single-output (MISO) link topologies, consist of an array of multiple transmitter coils, which are usually in interaction with a single receiver coil, as shown in [Figure 21.6](#). MISO structures are often employed to energize dynamic receivers. Multiple-input multiple-output (MIMO) structures extend the dual-terminal WPT concept to multi-node WPT networks as shown in [Figure 21.7](#).

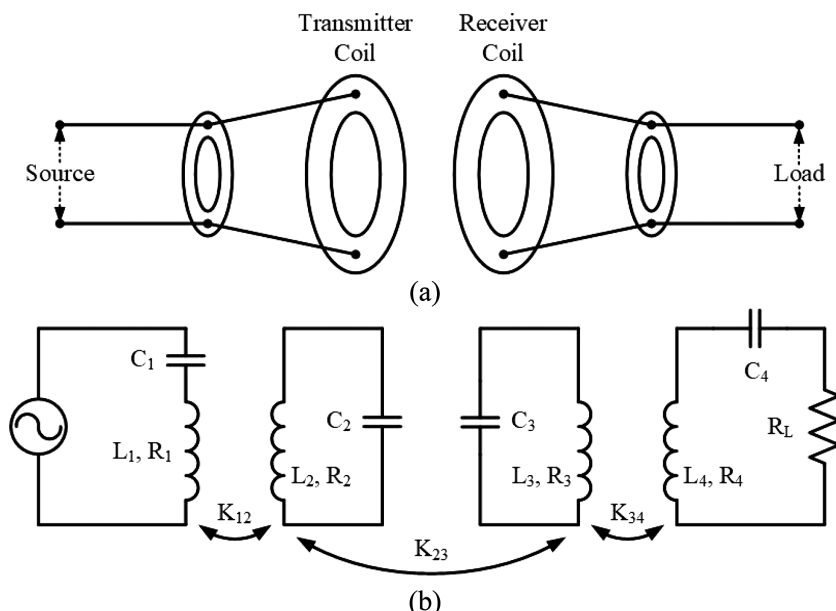


FIGURE 21.3 Magnetic-resonance-link-based four-coil WPT system: (a) block model and (b) circuit model. (From Behera, R. K., and Kumari, M., *Wireless Power Transfer Via Magnetic Resonance*, Internship Report, IIT Patna, 2013.)

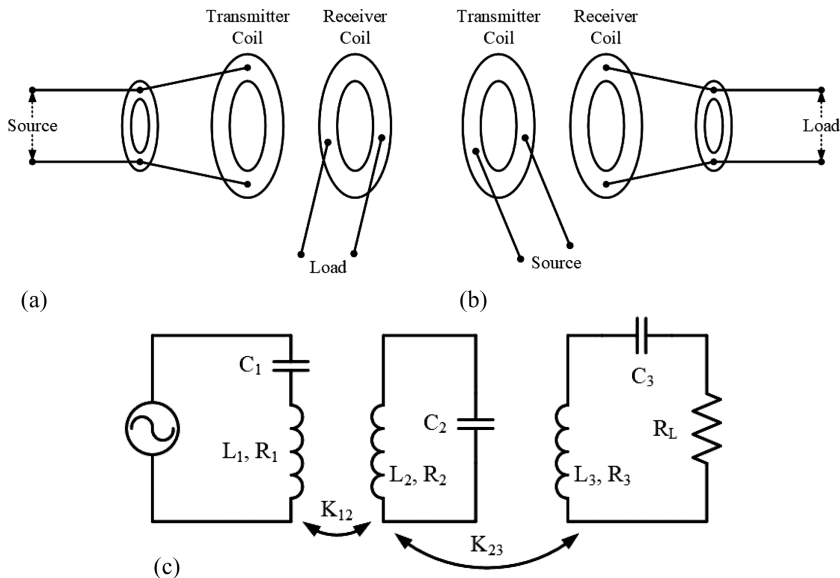


FIGURE 21.4 Magnetic resonance three-coil WPT system: (a) block model of transmitter, (b) block model of receiver, and (c) circuit model. (From Behera, R. K., and Kumari, M., *Wireless Power Transfer Via Magnetic Resonance*, Internship Report, IIT Patna, 2013.)

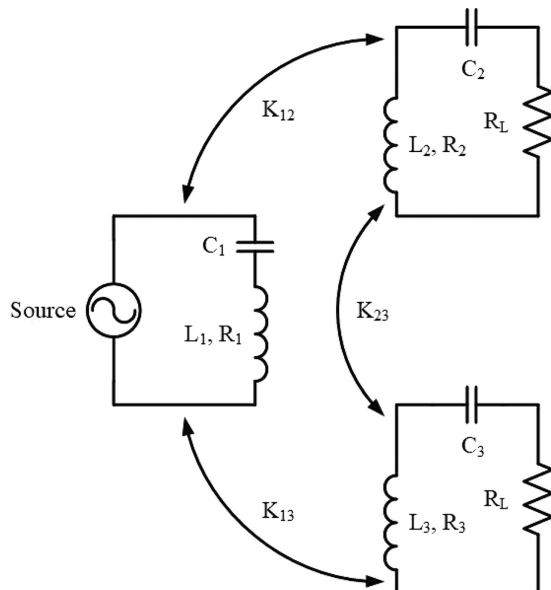


FIGURE 21.5 A three-coil SIMO-link topology. (From Eteng, A. A. et al., *Renew. Sust. Energ. Rev.*, 77, 2017, 486–505.)

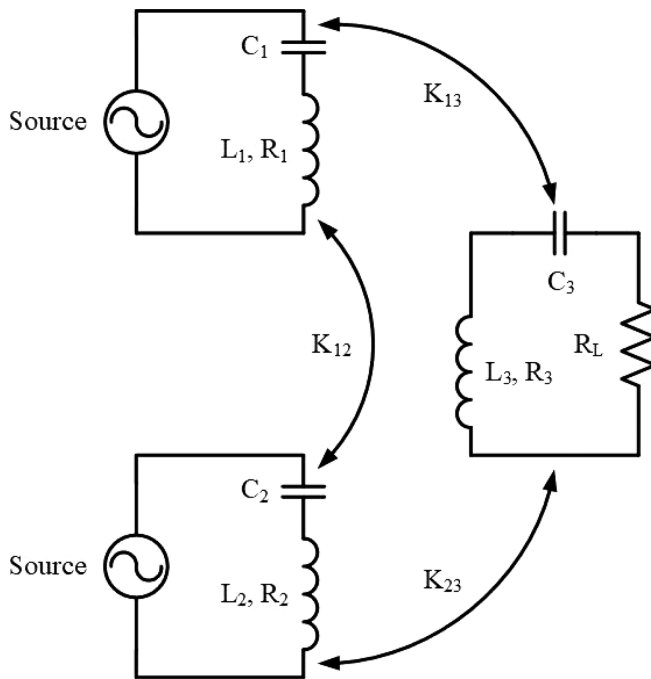


FIGURE 21.6 A three-coil MISO transcutaneous energy transfer link. (From Eteng, A. A. et al., *Renew. Sust. Energ. Rev.*, 77, 2017, 486–505.)

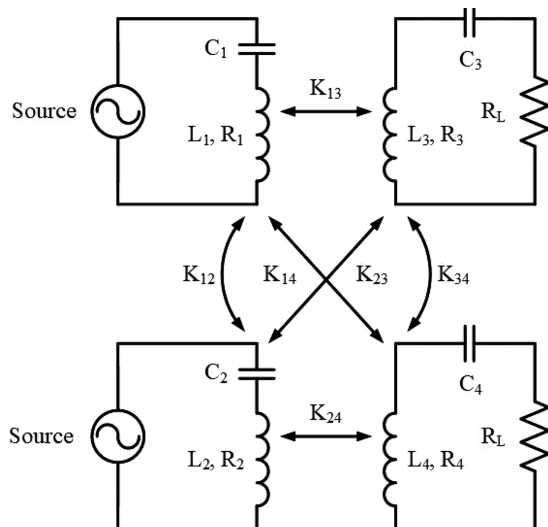


FIGURE 21.7 A four-coil MIMO-link circuit. (From Eteng, A. A. et al., *Renew. Sust. Energ. Rev.*, 77, 2017, 486–505.)

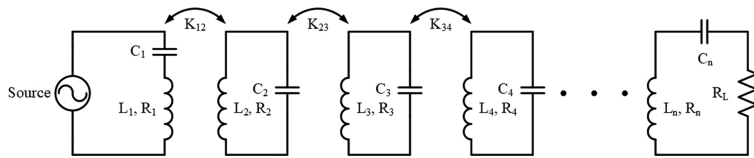


FIGURE 21.8 A circuit model of an n -coil relay link. (From Eteng, A. A. et al., *Renew. Sust. Energ. Rev.*, 77, 2017, 486–505.)

21.4.2 DUAL AND MULTITERMINAL LINKS

A relay circuit consists of dual and multiterminal link circuits. These circuits have transmitters and receiver coils, and they are coupled to each other magnetically over in-between resonating coils as shown in Figure 21.8.

21.5 INDUCTIVE WIRELESS POWER TRANSFER (IWPT)

A simplified inductive coupling circuit is shown in Figure 21.9. It has a capacitor, an inductor, and a resistor in the transmitter and receiver coil.

The series impedances of primary and secondary circuits can be written as:

$$\begin{aligned} Z_1 &= R_1 + j \left(\omega L_1 - \frac{1}{\omega C_1} \right) \\ Z_2 &= R_2 + j \left(\omega L_2 - \frac{1}{\omega C_2} \right) \end{aligned} \quad (21.1)$$

The transfer function of the coupled system can be written as

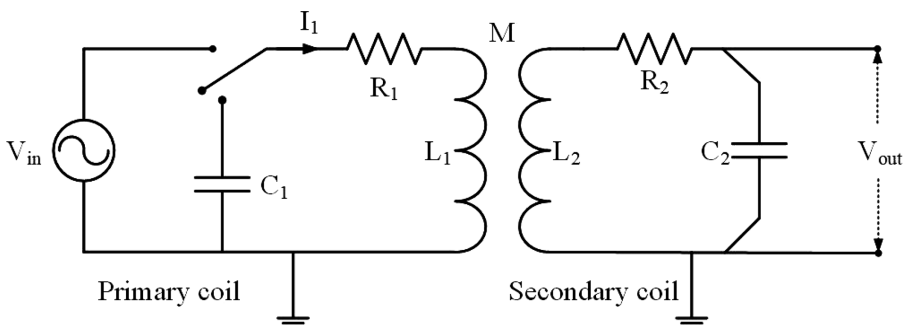


FIGURE 21.9 Simplified IWPT circuit. (From Goyal, R. K. et al., *Wireless Power Transfer System*, BT Project report, IIT Patna, 2013.)

$$\frac{V_{out}}{V_{in}} = -\sqrt{\frac{L_2}{L_1}} \frac{s^2 \omega_2^2 k}{(1-k^2)s^4 + \left(\frac{\omega_1}{Q_1} + \frac{\omega_2}{Q_2}\right)s^3 + \left(\omega_2^2 + \omega_1^2 + \frac{\omega_1 \omega_2}{Q_1 Q_2}\right)s^2 + \omega_1 \omega_2 \left(\frac{\omega_2}{Q_1} + \frac{\omega_1}{Q_2}\right)s + \omega_1^2 \omega_2^2} \quad (21.2)$$

where $M = k\sqrt{L_1 L_2}$, $\omega_i = \frac{1}{\sqrt{L_i C_i}}$ and $Q_i = \frac{\omega_i L_i}{R_i}$

As soon as the primary and secondary circuits resonating frequency is matched, $\omega_1 = \omega_2 = \omega$, the output power depends on the coupling coefficient, k . Hence,

$$\frac{V_{out}}{V_{in}} = \frac{-1}{\alpha} \sqrt{\frac{L_2}{L_1}} \frac{k}{\left(k^2 + \frac{1}{Q_1 Q_2} - \left(1 - \frac{1}{\alpha^2}\right)^2 + j\left(1 - \frac{1}{\alpha^2}\right)\left(\frac{1}{Q_1} + \frac{1}{Q_2}\right)\right)} \quad (21.3)$$

where $s = j\omega$, $\alpha = \omega/\omega_n$ and $\omega_1 = \omega_2 = \omega = \omega_n$

Now Equation (21.3) can be reduced to

$$\frac{V_{out}}{V_{in}} = \frac{-1}{\alpha^2} \sqrt{\frac{Q_2 R_2}{Q_1 R_1}} \frac{k}{\left(k^2 + \frac{1}{Q_1 Q_2} - \left(1 - \frac{1}{\alpha^2}\right)^2 + j\left(1 - \frac{1}{\alpha^2}\right)\left(\frac{1}{Q_1} + \frac{1}{Q_2}\right)\right)} \quad (21.4)$$

when $\alpha = 1$, corresponding to a system resonating at ω_n , Equation (21.4) becomes

$$\frac{V_{out}}{V_{in}} = -\sqrt{\frac{L_2}{L_1}} \frac{k}{\left(k^2 + \frac{1}{Q_1 Q_2}\right)} = -\sqrt{\frac{Q_2 R_2}{Q_1 R_1}} \frac{k}{\left(k^2 + \frac{1}{Q_1 Q_2}\right)} \quad (21.5)$$

The maximum voltage gain with respect to k can be written as

$$k_{crit} = \frac{1}{\sqrt{Q_1 Q_2}} \frac{V_{out}}{V_{in_crit}} = -\sqrt{\frac{L_2}{L_1}} \frac{\sqrt{Q_1 Q_2}}{2} = -\frac{Q_2}{2} \sqrt{\frac{R_2}{R_1}} = -\frac{\omega_n L_2}{\sqrt{R_1 R_2}} \quad (21.6)$$

21.6 TECHNOLOGY OVERVIEW AND CONCEPTS OF WIRELESS CHARGING SYSTEM

Today there are two popular WPT infrastructures in EV applications, such as radiative wireless charging and nonradiative wireless charging technology. Radiative WPT technology is based on radiation of electromagnetic waves. Nonradiative WPT technology is based on the coupling of the magnetic field between two coils or three coils designed in a short distance with the magnetic field of electromagnetic wave attenuation. There are three kinds of wireless charging systems that are subsequently discussed.

21.6.1 INDUCTIVE-COUPLING-BASED WIRELESS CHARGING SYSTEM

In an inductive-coupling-based wireless charging system, the energy is transferred between two coils. The two coils are primary and secondary terminals. Inductive-based power transfer takes place between the primary as a transmitter and the secondary as a receiver with changeable magnetic-field intensity. The power is induced in the secondary coil, and it should be optimally tuned in order to achieve higher efficiency. This type of WPT operates in the kilohertz range.

21.6.2 MAGNETIC-RESONANCE-BASED WIRELESS CHARGING SYSTEM

Magnetic-resonance-based wireless charging consists of two coils, and the energy is transferred based on the resonance principle. Both the coils are designed to operate at equal resonant frequency. In this type of charging, the system can achieve high efficiency due to low leakage, and there may be many resonating receivers and transmitter coils.

21.6.3 MICROWAVE-BASED WIRELESS CHARGING SYSTEM

Microwave-based wireless charging station transmits radio waves from the outer space. The radio wave travels at the speed of light in line-of-sight. The frequency range of the microwave varies from 300 MHz to 300 GHz. The power transfer can take place with infrared and X-rays.

21.7 ANALYSIS OF THREE RESONATING COUPLED COILS

The three-coil resonating circuit is shown in Figure 21.10. Assuming coupling between the first and third coil is ignored. Coil 1 and 2 and coil 2 and 3 is linked magnetically by coupling coefficients K_{12} and K_{23} respectively. The drive loop is excited by a source with finite output impedance R_{source} . A simple loop is modeled with an inductor (L_1) and parasitic resistance R_1 . A capacitor (C_1) is added in the loop so that desired frequency can be obtained at resonance. The intermediate coil consists of a multturn air core spiral inductor (L_2) with parasitic resistance (R_2). The receiver coil with its self-capacitance C_3 inductors L_1 and L_2 are connected with coupling coefficient k_{12} , and

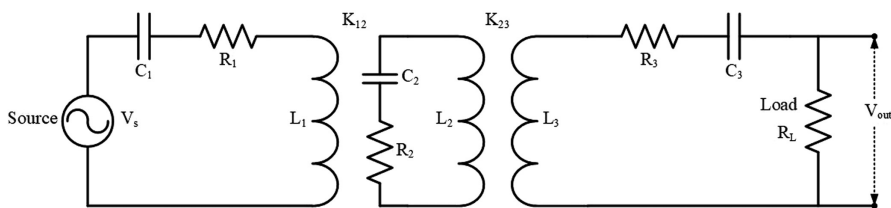


FIGURE 21.10 Circuit of three-coil resonating WPT system. (From Behera, R. K., and Kumari, M., *Wireless Power Transfer Via Magnetic Resonance*, Internship Report, IIT Patna, 2013.)

inductors L_3 and L_2 are connected with coupling coefficient k_{23} . The intermediate coil is shorted. The coupling between the first and third coil is ignored.

From KVL equation,

$$I_1 \left(R_{\text{source}} + R_l + j \left(\omega L_1 - \frac{1}{\omega C_1} \right) \right) + j\omega (I_2 M_{12}) = V_s \quad (21.7)$$

$$I_2 \left(R_2 + j \left(\omega L_2 - \frac{1}{\omega C_2} \right) \right) + j\omega (I_2 M_{12} - I_3 M_{23}) = 0 \quad (21.8)$$

$$I_3 \left(R_3 + j \left(\omega L_3 - \frac{1}{\omega C_3} \right) \right) + j\omega I_3 M_{23} = 0 \quad (21.9)$$

Rewriting equations using series impedances is given by

$$R_{\text{source}} + R_l + j\omega L_1 + \frac{1}{j\omega C_1} = Z_1$$

$$R_2 + j\omega L_2 + \frac{1}{j\omega C_2} = Z_2$$

$$R_{\text{load}} + R_3 + j\omega L_3 + \frac{1}{j\omega C_3} = Z_3$$

So, the Equations (21.7)–(21.9) can be modified as:

$$I_1 Z_1 + s I_1 M_{12} = V_s \quad (21.10)$$

$$I_2 Z_2 + s(I_2 M_{12} - I_3 M_{23}) = 0 \quad (21.11)$$

$$I_3 Z_3 + s I_3 M_{23} = 0 \quad (21.12)$$

Rearranging and solving for I_2 and I_3 , we get

$$I_3 = \frac{s I_2 M_{23}}{Z_3} \quad (21.13)$$

$$I_2 = -\frac{s I_1 M_{12} Z_3}{Z_2 Z_3 - (s M_{23})^2} \quad (21.14)$$

Now,

$$V_{out} = -I_3 R_{load} = -\frac{s I_2 M_{23} R_{load}}{Z_3} \quad (21.15)$$

$$\frac{V_{out}}{V_s} = -\frac{s^2 I_1 M_{12} M_{23} R_{load}}{(Z_2 Z_3 - s^2 M_{23}^2)} \frac{V_{out}}{V_s} = \frac{-s^2 M_{12} M_{23} R_{load}}{\left(Z_2 Z_3 - (s M_{23})^2 \right) \left((Z_1 Z_2 Z_3 - Z_3 (s M_{12}))^2 - Z_1 (s M_{23})^2 \right)} \quad (21.16)$$

$$\frac{V_{out}}{V_s} = \frac{-s^2 M_{12} M_{23} R_{load}}{s^4 (M_{23}^2 M_{12}^2 Z_3 + M_{23}^4 Z_1) - s^2 (M_{12}^2 Z_2 Z_3^2 + M_{23}^2 Z_1 Z_2 Z_3 + M_{23}^2 Z_1 Z_2 Z_3) + Z_1 Z_2^2 Z_3^2} \quad (21.17)$$

We know

$$M_{12} = K_{12} \sqrt{L_1 L_2} \text{ and } M_{23} = K_{23} \sqrt{L_3 L_2}$$

$$\frac{V_{out}}{V_s} = \frac{-s^2 K_{12} K_{23} R_{load} L_2 \sqrt{L_1 L_3}}{s^4 (K_{23}^2 K_{12}^2 Z_3 L_1 L_2^2 L_3 + M_{23}^4 Z_1) - s^2 (K_{12}^2 L_1 L_2 Z_2 Z_3^2 + K_{23}^2 L_2 L_3 Z_1 Z_2 Z_3 + K_{23}^2 L_3 L_2 Z_1 Z_2 Z_3) + Z_1 Z_2^2 Z_3^2} \quad (21.18)$$

The power transfer efficiency (PTE) in the three-coil WPT system is calculated by reflecting the resistive component in each loop from the load back toward the primary loop. Using one stage at a time, PTE denoted by “ n ” can be derived for this system as well. The coupling between the first and third coil is avoided in this derivation due to the larger distance between them.

$Q_i = \omega L_i / R_i$ are the unloaded quality factors of each i th coil, where L_i are inductances and R_i are parasitic resistances of i th coil.

$$n_{total} = n_{12} n_{23} \quad (21.19)$$

$$n_{12} = \frac{K_{12}^2 Q_1 Q_2}{1 + K_{12}^2 Q_1 Q_2 + K_{23}^2 Q_3 Q_{3L}} \quad (21.20)$$

$$n_{23} = \left(\frac{K_{23}^2 Q_2 Q_{3L}}{1 + K_{23}^2 Q_2 Q_{3L}} \right) \left(\frac{Q_{3L}}{Q_L} \right) \quad (21.21)$$

$$n = \left(\frac{K_{12}^2 Q_1 Q_2}{1 + K_{12}^2 Q_1 Q_2 + K_{23}^2 Q_3 Q_{3L}} \right) \left(\frac{K_{23}^2 Q_2 Q_{3L}}{1 + K_{23}^2 Q_2 Q_{3L}} \right) \left(\frac{Q_{3L}}{Q_L} \right) \quad (21.22)$$

where $Q_{3L} = \omega L_3 / (R_3 + R_{\text{load}})$

Thus, in this case, PTE depends on the coupling coefficient of both the pairs of coils and the quality factor of the coils.

21.8 WIRELESS POWER TRANSFER IN ONLINE ELECTRIC VEHICLE

A general contactless EV charging system contains numerous steps to charge an EV contactless. Initially, the main AC power is converted to a DC with the help of an AC-DC converter, and it should be utility friendly with unity power-factor. Now, using a DC-AC converter, DC voltage is converted to a high-frequency AC voltage, and it drives the transmitting coil. A compensation network is provided for improving the performance of the system. Seeing the insulation failure of the primary side coil, a high-frequency isolated transformer is inserted in between the DC-AC inverter and primary side coil for additional protection and shielding.

The high-frequency current circulates in the transmitting coil, and it results varying magnetic field in the primary. This induces alternating voltage on the receiving coil. Power-transfer capability and efficiency in the secondary coil can be improved when it is operated at resonance. Finally, AC power is converted to DC to charge the battery. [Figure 21.11](#) shows general block diagram of the contactless EV charging system.

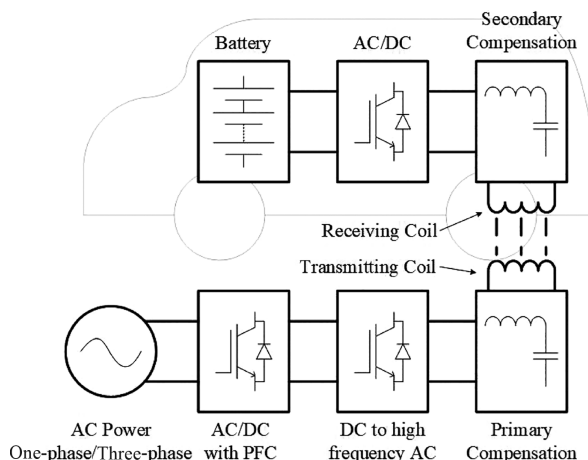


FIGURE 21.11 Block diagram of contactless EV charging system. (From Mi, C., and Abul Masrur, M., *Wireless Power Transfer for Electric Vehicle Applications*, Wiley, 2017.)

21.9 HARDWARE DESIGN OF WIRELESS POWER TRANSMITTER AND RECEIVER

The solenoid-based WPT system is designed with one primary coil as a transmitter and a secondary coil as a receiver. Applying the voltage across the primary will induce voltage in the secondary transmitter coil due to the varying magnetic field. Generally, the secondary has more turns as compared to the primary. The experimental arrangement is shown in [Figure 21.12](#).

A flat spiral coil with inner radius R_{in} and outer radius R_{out} is designed such that R_{in}/R_{out} is almost equal to one. It has magnetic-field lines parallel to the axis of spiral. Two spiral coils are designed: one for the transmitter coil and another for the receiver coil, as shown in [Figure 21.13](#).

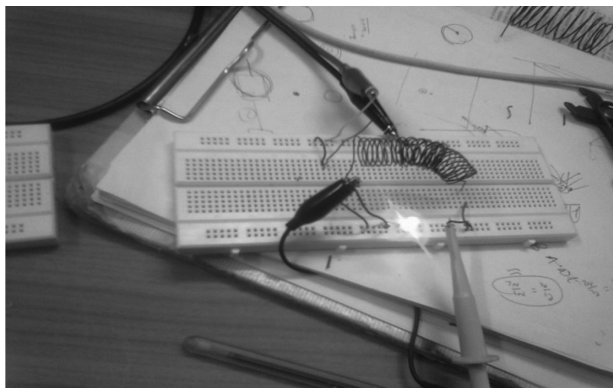


FIGURE 21.12 Solenoid-based design of WPT. (From Goyal, R. K. et al., *Wireless Power Transfer System*, BT Project report, IIT Patna, 2013.)

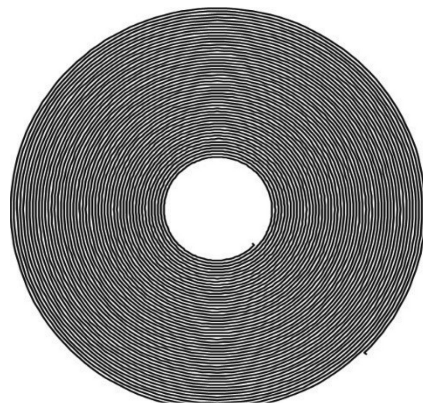


FIGURE 21.13 Spiral-based WPT design. (From Goyal, R. K. et al., *Wireless Power Transfer System*, BT Project report, IIT Patna, 2013.)

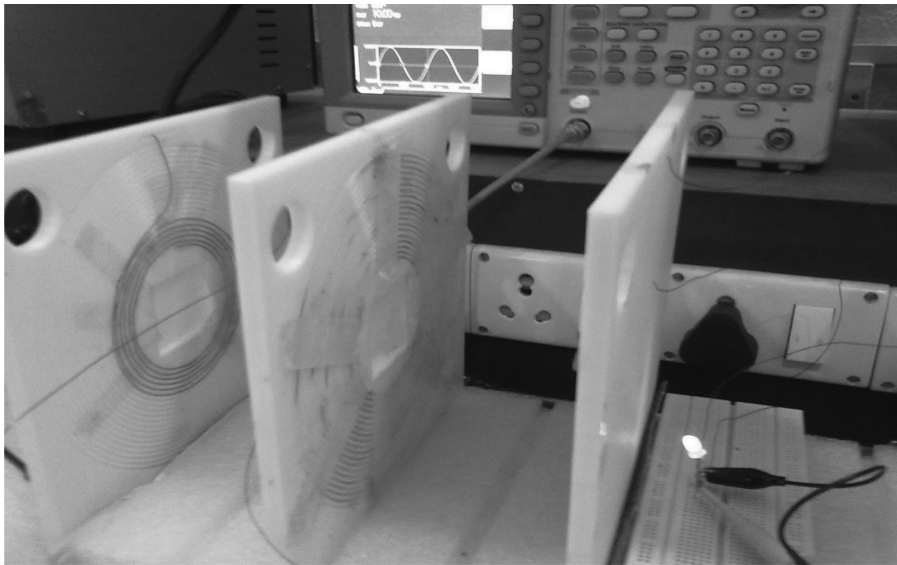


FIGURE 21.14 Experimental setup. (From Behera, R. K., and Kumari, M., *Wireless Power Transfer Via Magnetic Resonance*, Internship Report, IIT Patna, 2013.)

The spiral-coil-based WPT system has a transmitter of 7 turns and a receiver of 20 turns. This transmitter and receiver are placed axially in a straight line like a step-up air core transformer as shown in [Figure 21.14](#), and it shows that the LED is connected on the secondary side.

At 2.52 MHz, the receiver coil induces maximum voltage. Under this condition, the output voltage is shown in [Figure 21.15](#) at input frequency of 1.6 MHz at a distance of 15 cm between the transmitter and receiver.

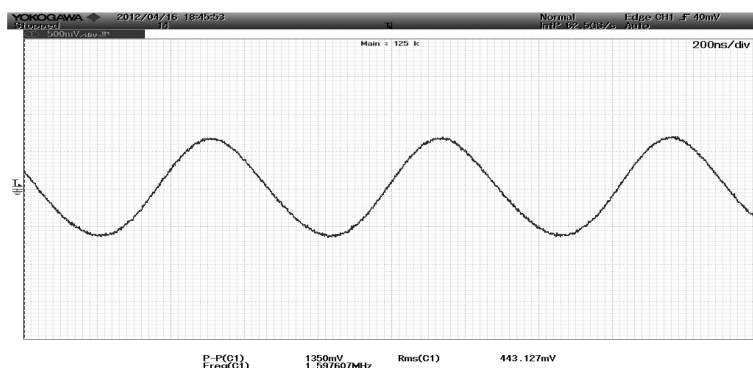


FIGURE 21.15 Output voltage at resonating frequency at 1.6 MHz. (From Behera, R. K., and Kumari, M., *Wireless Power Transfer Via Magnetic Resonance*, Internship Report, IIT Patna, 2013.)

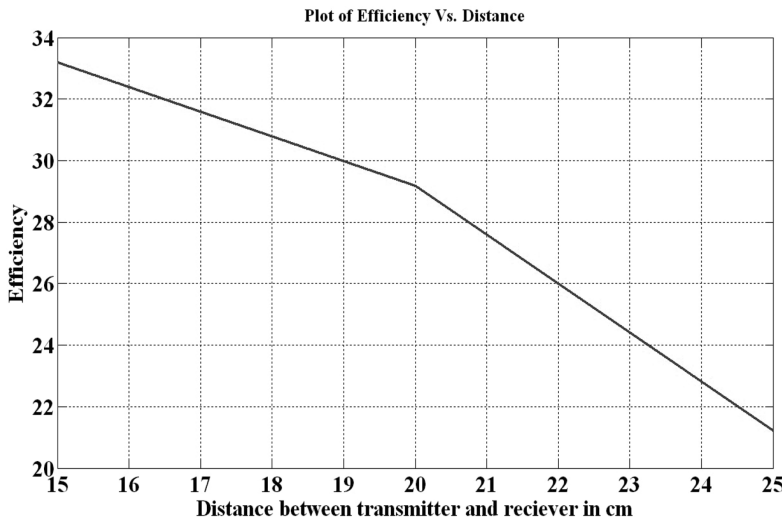


FIGURE 21.16 Efficiency vs. distance. (From Goyal, R. K. et al., *Wireless Power Transfer System*, BT Project report, IIT Patna, 2013.)

The WPT system has maximum efficiency occurring at 33.18%. Figure 21.16 shows the plot of efficiency versus distance between the transmitter and receiver coil. It is observed that power transmitted is inversely proportional to the distance between the transmitter and receiver.

REVIEW QUESTIONS

- 21.1. What is the two-coil WPT structure?
- 21.2. What is the inductive WPT system? Discuss briefly with suitable circuit diagram.
- 21.3. What is the three-coil resonating WPT system?

SUMMARY

Recently, WPT became popular due to a large number of portable electronics. The analysis of inductive coupling and the resonant-based coupled inductor system has been discussed. Analysis of two and three coil WPT system is discussed. Experimental design is briefly discussed.

REFERENCES/FURTHER READING

1. A. A. Eteng, S. K. Abdul Rahim, C. Y. Leow S. Jayaprakasam, and B. W. Chew, Low-power near-field magnetic wireless energy transfer links: A review of architectures and design approaches, *Renew. Sust. Energ. Rev.*, vol. 77, pp. 486–505, 2017.
2. K. B. SaiKiran, M. Kumari, O. Ojo, and R. K. Behera, AtifIqbal, analysis and experimental verification of three-coil inductive resonant coupled wireless power transfer system, *Proceedings of National Power Electronics Conferences (NPEC'17)*, College of Engineering Pune, India, 18–20 December, 2017.

3. R. K. Behera, and M. Kumari, *Wireless Power Transfer Via Magnetic Resonance*, Internship Report, IIT Patna, 2013.
4. R. K. Goyal, U. Gautam, and R. K. Behera, *Wireless Power Transfer System*, BT Project Report, IIT Patna, 2013.
5. S. Li, and C. C. Mi, Wireless power transfer for electric vehicle applications, *IEEE J. Em. Sel. Top. Power Electron.*, vol. 3, no. 1, 2015.
6. X. Lu, P. Wang, D. Niyato, D. I. Kim, and Z. Han, Wireless charging technologies: Fundamentals, standards, and network applications, *IEEE Commun. Surveys Tuts.*, vol. 18, no. 2, pp. 1413–1452, 2016.
7. S. Li, and C. C. Mi, Wireless power transfer for electric vehicle applications, *IEEE J. Em. Sel. Top. Power Electron.*, vol. 3, no. 1, 2015.
8. L. Yang, Q. X. Yang, H. Y. Chen, X. Zhang, and L. Jin, Basic study on improving power of wireless power transfer via magnetic resonance coupling, *Adv. Mater. Res.*, vol. 459, pp. 445–449, 2012.
9. C. Mi, M. Abul Masrur, *Wireless Power Transfer for Electric Vehicle Applications*, Wiley, Hoboken, NJ, 2017.
10. J. R. Smith. Ed., *Wirelessly Powered Sensor Networks and Computational RFID*, Springer, the Netherlands, 2013.



Taylor & Francis

Taylor & Francis Group

<http://taylorandfrancis.com>

Appendix

MATLAB Application in Power Electronic Systems

A.1 INTRODUCTION

MATLAB (MATrix LABoratory) is a high-performance language for technical computing. It integrates computation, visualization, and programming in an easy-to-use environment where problems and solutions are expressed in familiar mathematical notation. Typical uses include:

- Math and computation
- Algorithm development
- Data acquisition modeling
- Simulation and prototyping
- Data analysis, exploration, and visualization
- Scientific and engineering graphics
- Application development, including graphical user-interface building

MATLAB is an interactive system whose basic data element is an array that does not require dimensioning. This allows one to solve many technical computing problems, especially those with matrix and vector formulations, in a fraction of the time it would take to write a program in a scalar non-interactive language such as C or Fortran.

MATLAB is a special-purpose computer program optimized to perform engineering and scientific calculations. It started life as a program designed to perform matrix mathematics, but over the years it has grown into a flexible computing system capable of solving essentially any technical problem.

The MATLAB program implements the MATLAB programming language and provides an extensive library of predefined functions that make technical programming tasks easier and more efficient.

MATLAB is huge program, with an incredibly rich variety of functions. Even the basic version of MATLAB without any toolkits is much richer than other technical programming languages. There are more than 1,000 functions in the basic MATLAB product alone, and toolkits extend this capability with many more functions in various specialties.

A.2 THE ADVANTAGES OF MATLAB

MATLAB has many advantages compared with conventional computer languages for technical problem solving. Among them are the following:

1. **Ease of Use:** MATLAB is an interpreted language, like many versions of Basic. Like Basic, it is very easy to use. The program can be used as a scratch pad to evaluate expressions typed at the command line, or it can be used to execute large prewritten programs. Programs may be easily written and modified with the built-in development environment and debugged with the MATLAB debugger. Because the language is so easy to use, it is ideal for the rapid prototyping of new programs.
2. **Platform Independence:** MATLAB is supported on many different computer systems, providing a large measure of platform independence. Programs written on any platform will run on all the other platforms, and data files written on any platform may be read transparently on any other platform. As a result, programs written in MATLAB can migrate to new platforms when the user's needs change.
3. **Predefined Functions:** MATLAB comes complete with an extensive library of predefined functions that provide tested and prepackaged solutions to many basic technical tasks. There are hundreds of functions built into the MATLAB language making jobs much easier.

In addition to the large library of functions built into the basic MATLAB language, many special-purpose toolboxes are available to help standard complex problems in specific areas. For example, a user can buy standards toolboxes to solve problems in single processing, control systems and communications, image processing, and neural networks, among many others. There is also an extensive collection of free user-contributed MATLAB programs that are shared through the MATLAB website.

4. **Device-Independent Plotting:** Unlike most other computer languages, MATLAB has many integral plotting and imaging commands. The plots and images can be displayed on any graphical output device supported by the computer on which MATLAB is running. This capability makes MATLAB an outstanding tool for visualizing technical data.
5. **Graphical User Interface:** MATLAB includes tools that allow a programmer to interactively construct a graphical user interface (GUI). With this capability, the programmer can design sophisticated data analysis programs that can be operated by relatively inexperienced users.
6. **MATLAB Compiler:** MATLAB's flexibility and platform independence is achieved by compiling MATLAB programs into a device-independent p-code, and then interpreting the p-code instructions at run time. This approach is similar to that used by Microsoft's Visual Basic language.

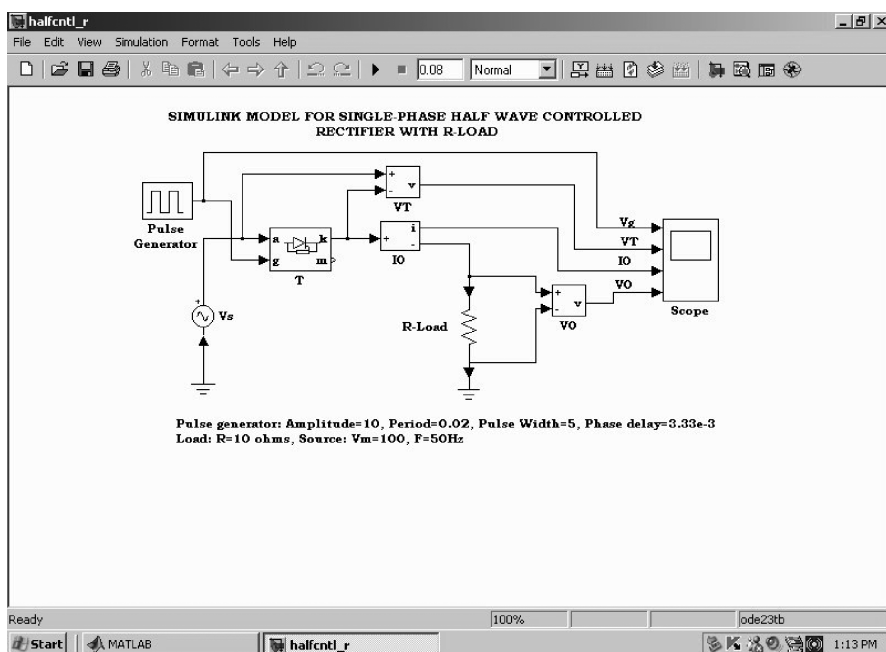
Unfortunately, the resulting programs can sometimes execute slowly because the MATLAB code is interpreted rather than compiled.

MATLAB features a family of add-on application-specific solutions called toolboxes. Very important to most users of MATLAB, toolboxes allow you to learn and apply specialized technology. Toolboxes are comprehensive collections of MATLAB functions (M-files) that extend the MATLAB environment to solve particular classes of problems. Areas in which toolboxes are available include signal processing, control systems, neural networks, fuzzy logic, wavelets, simulation, and many others.

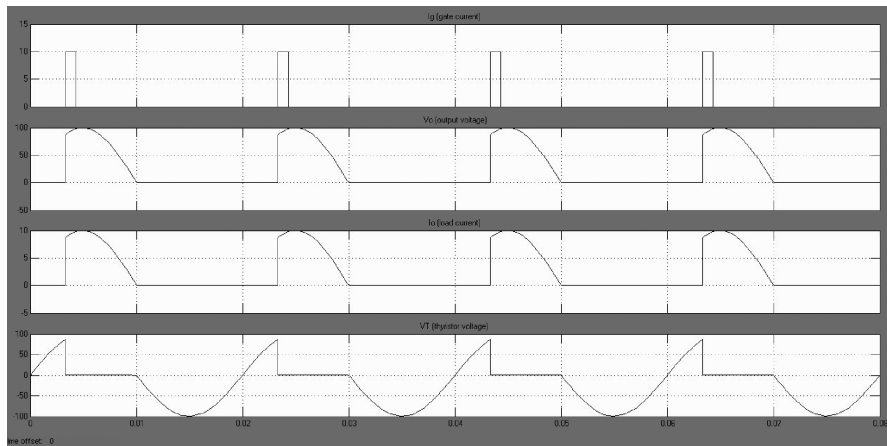
The underdrawn models are designed in MATLAB/Simulink by dragging the various required components from the Simulink library to .mdl file. The model is framed in the .mdl file. Then various components are interconnected as per circuit diagram. Various parameters of many blocks/ components can be changed as per our design by double clicking the block. Then results can be seen by clicking the scope. Various parameters of scope can also be changed as per requirement.

A.3 SIMULATION OF VARIOUS POWER ELECTRONIC CIRCUITS

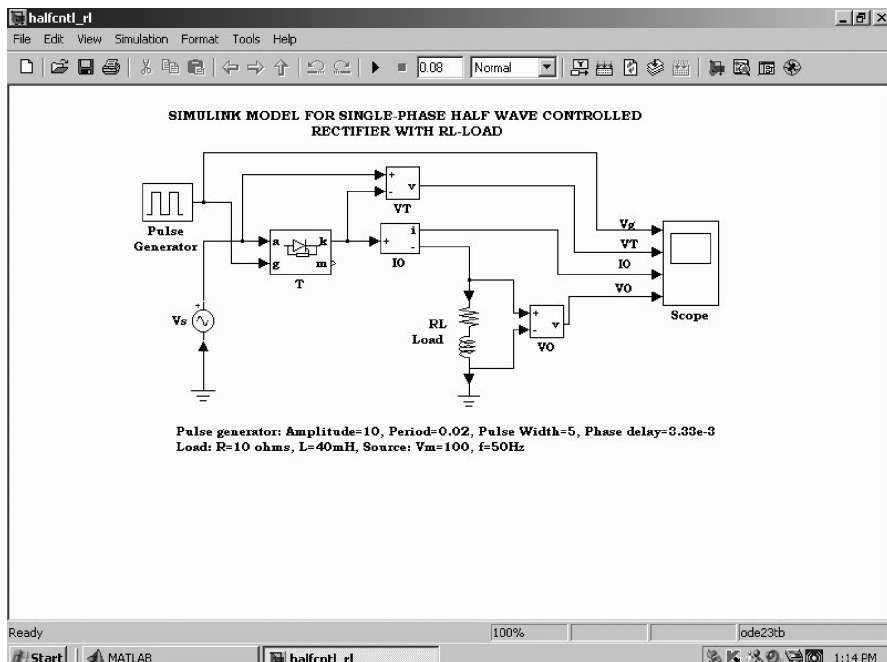
Example A.3.1: To design and simulate single-phase half-wave-controlled rectifier with R-load using MATLAB Simulink



Voltage and current waveforms:



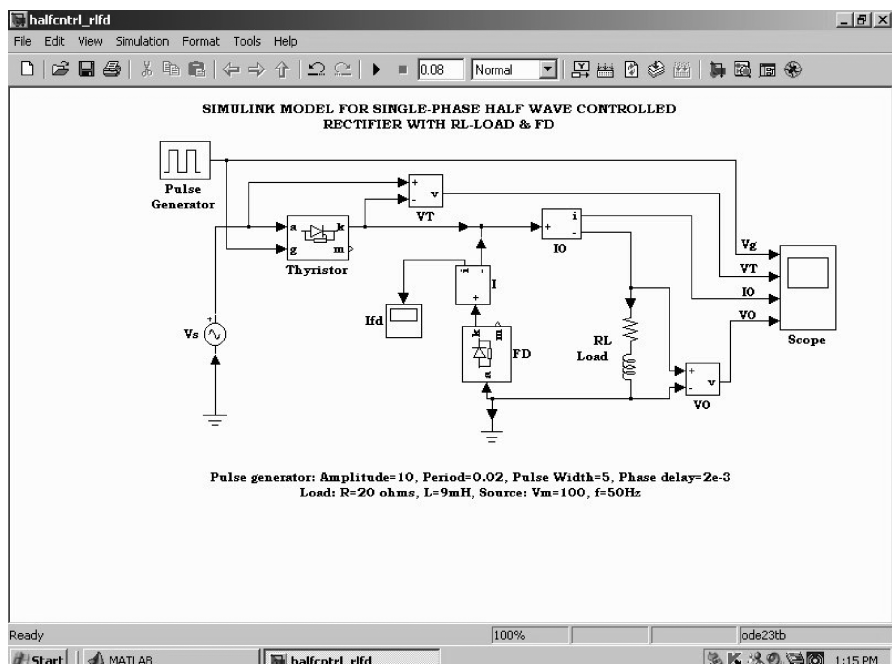
Example A.3.2: To design and simulate single-phase half-wave-controlled rectifier with RL-load using MATLAB Simulink



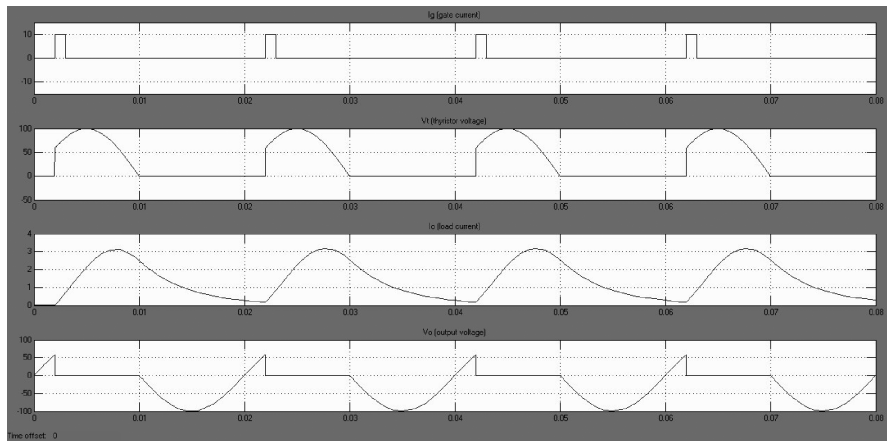
Voltage and current waveforms:



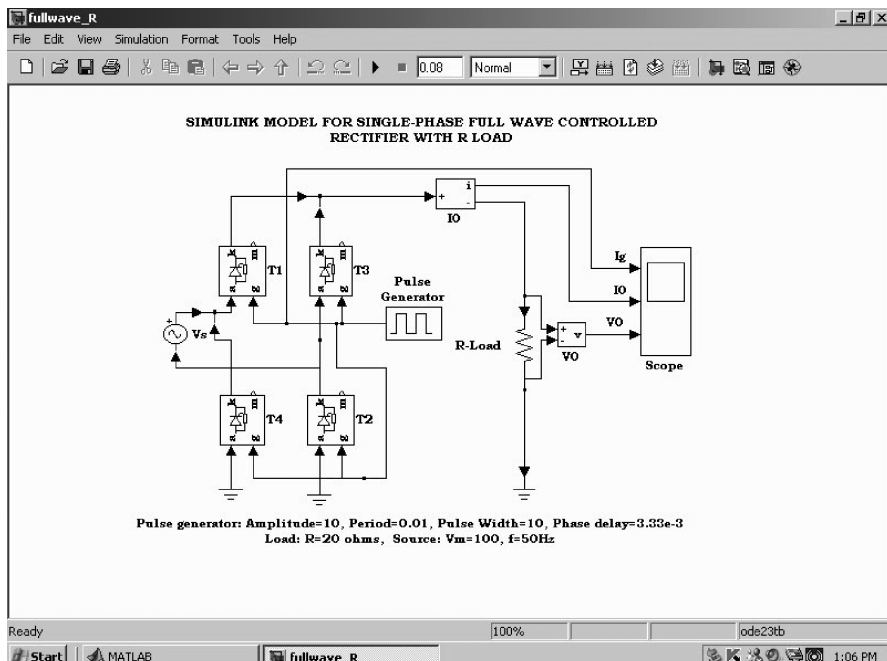
Example A.3.3: To design and simulate single-phase half-wave-controlled rectifier with RL-load and freewheeling diode (FD) using MATLAB Simulink



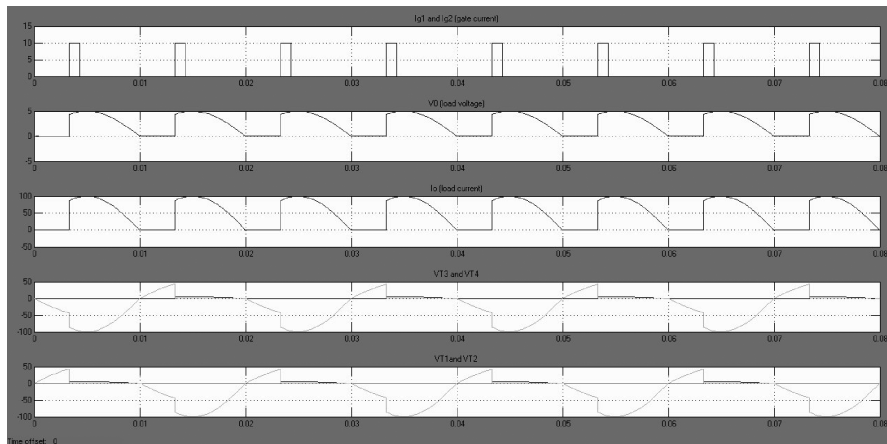
Voltage and current waveforms:



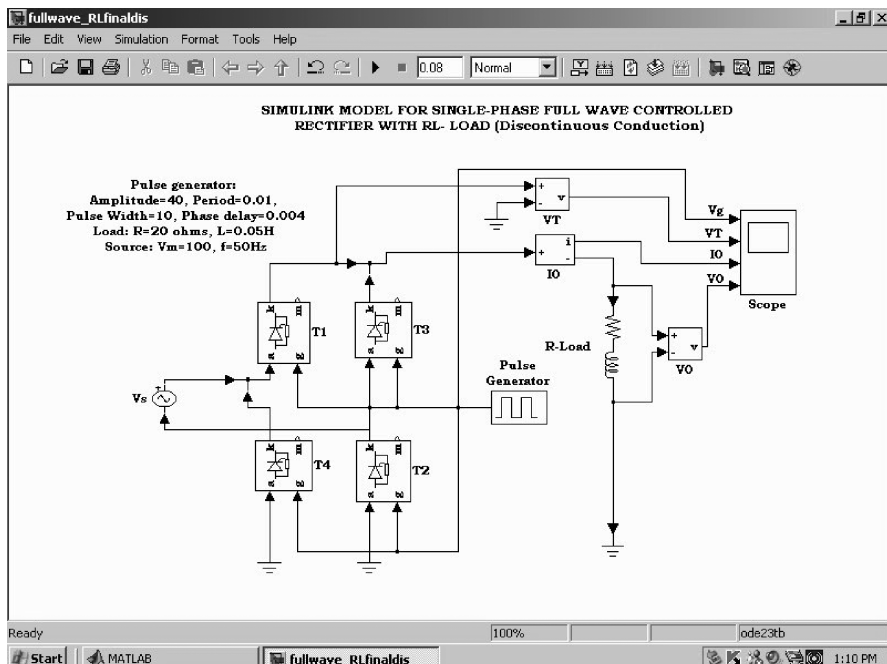
Example A.3.4: To design and simulate single-phase full-wave-controlled rectifier with R-load using MATLAB Simulink



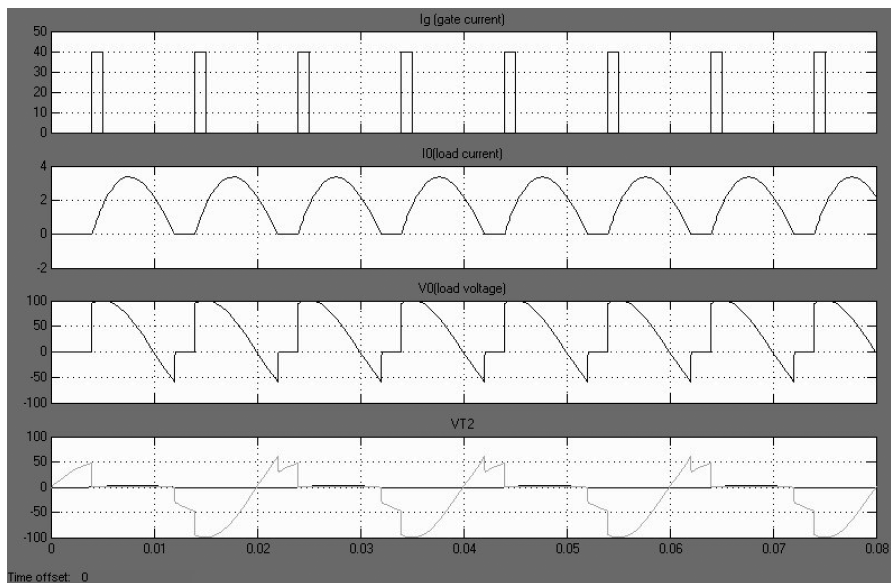
Voltage and current waveforms:



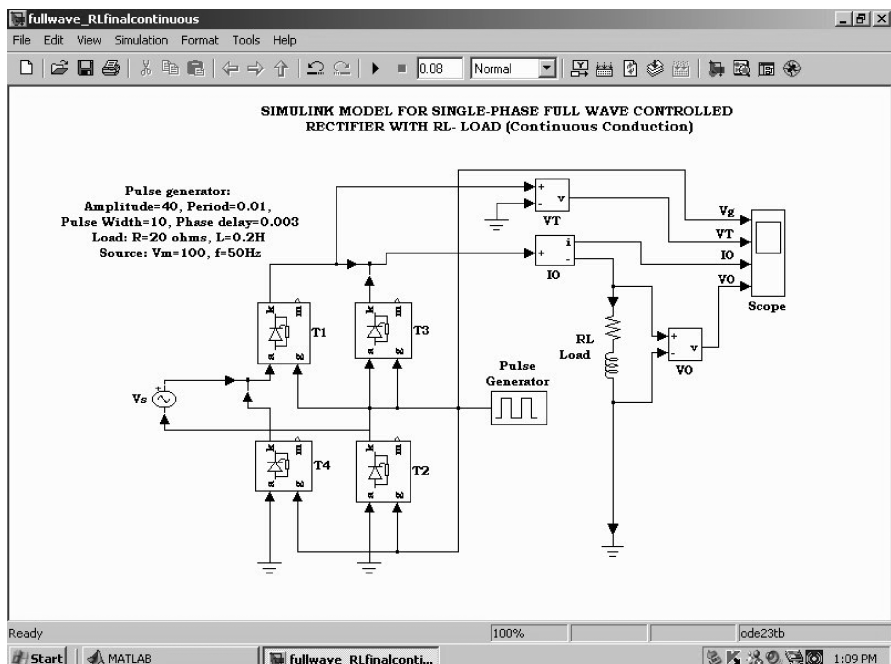
Example A.3.5: To design and simulate single-phase full-wave-controlled rectifier (bridge type) with RL-load (discontinuous conduction) using MATLAB Simulink



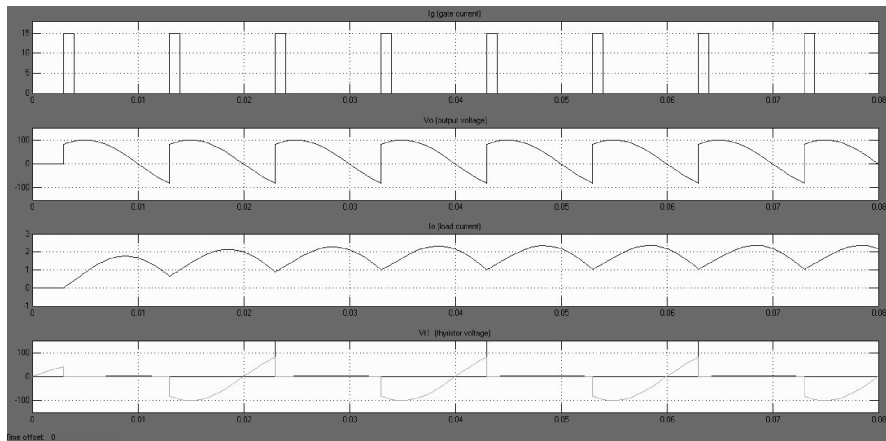
Voltage and current waveforms:



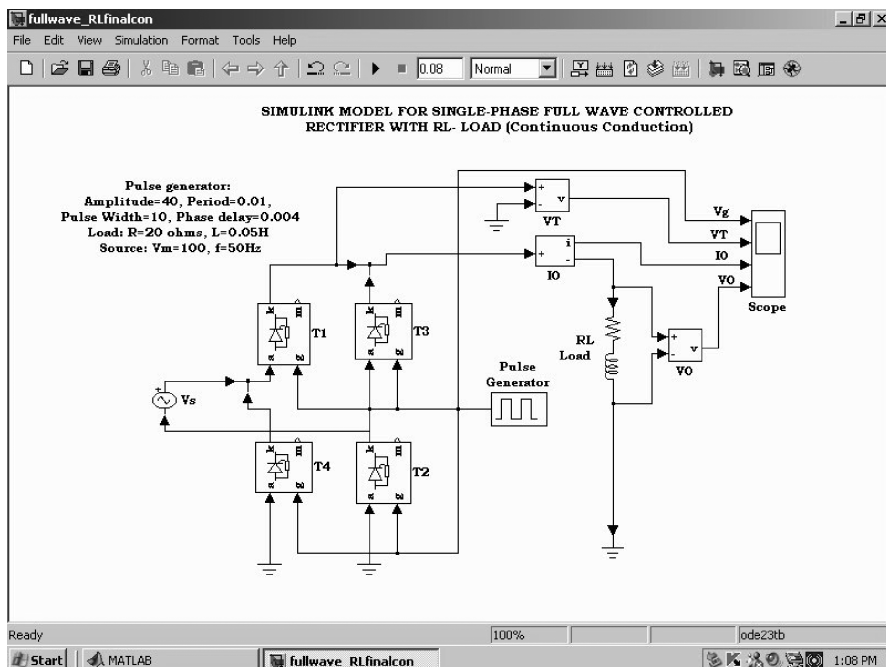
Example A.3.6: To design and simulate single-phase full-wave-controlled rectifier (bridge type) with RL-load (continuous conduction) using MATLAB Simulink



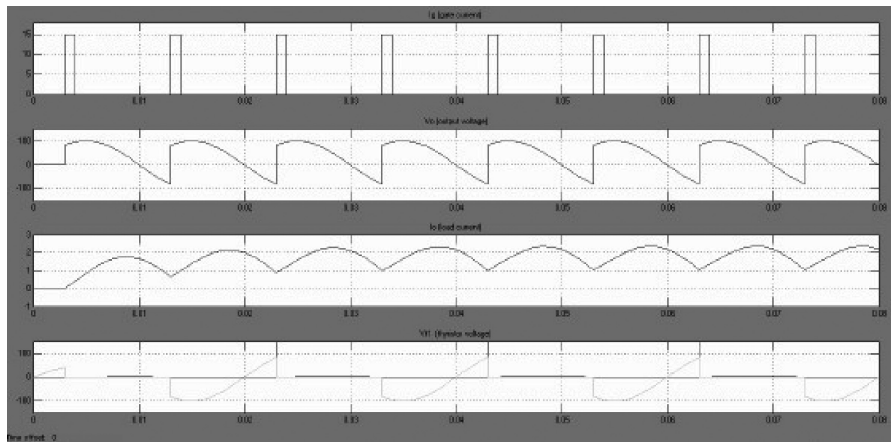
Voltage and current waveforms:



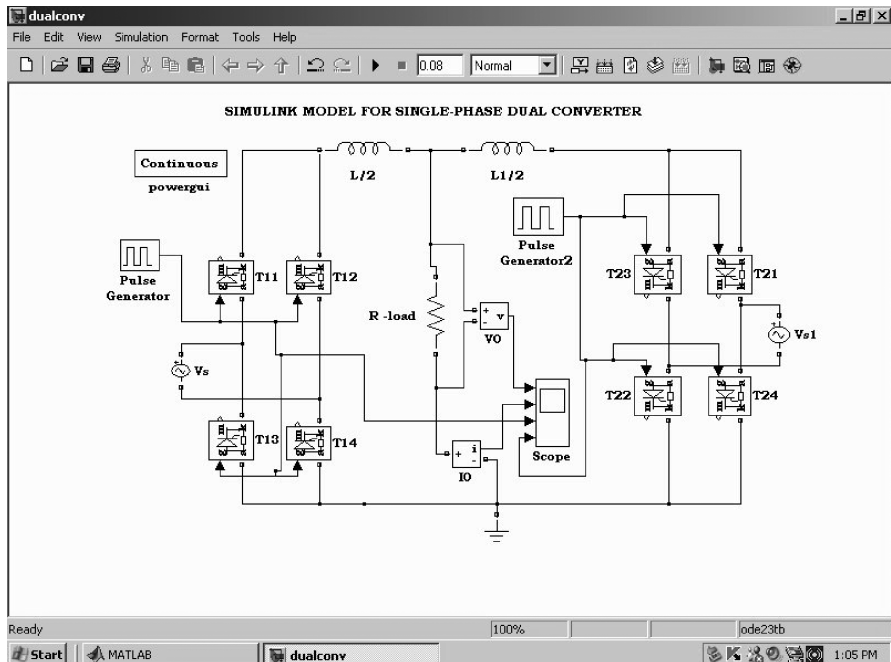
Example A.3.7: To design and simulate single-phase full-wave-controlled rectifier (bridge type) with RL-load (continuous conduction) using MATLAB Simulink



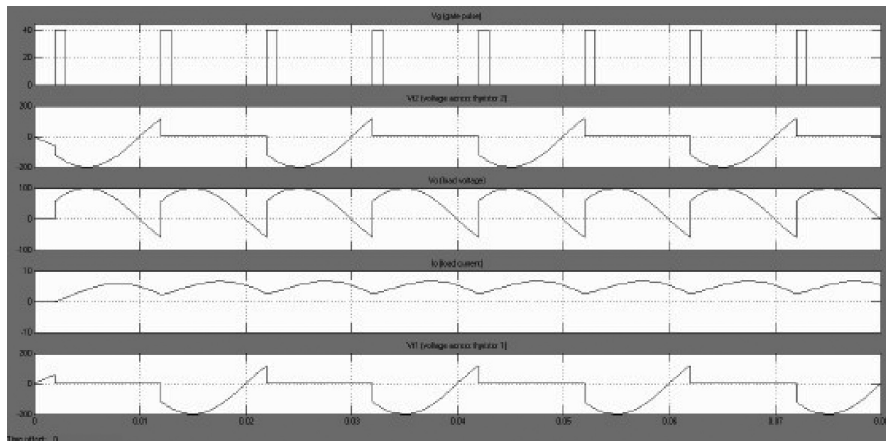
Voltage and current waveforms:



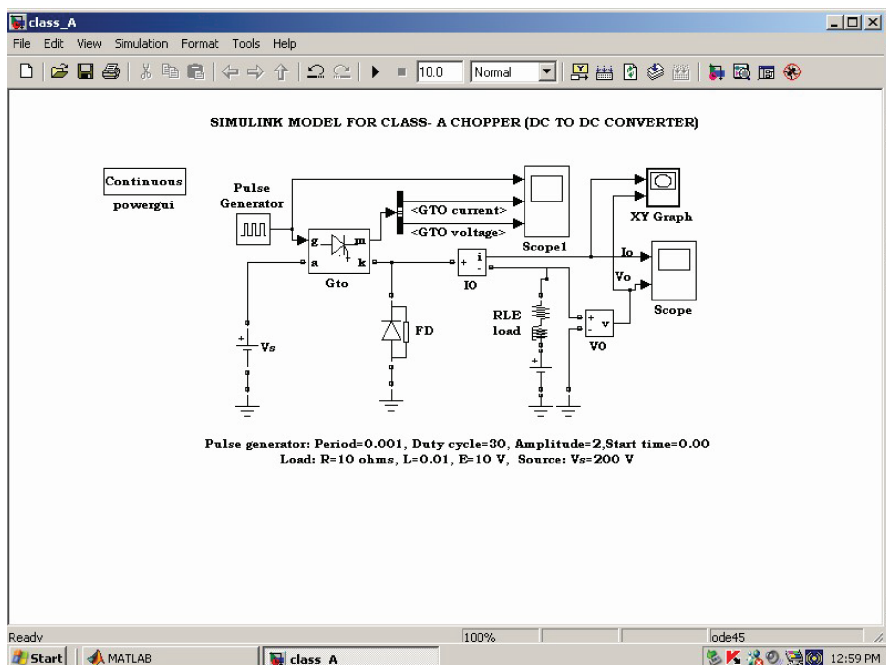
Example A.3.8: To design and simulate single-phase full-wave dual converter with R-load using MATLAB Simulink



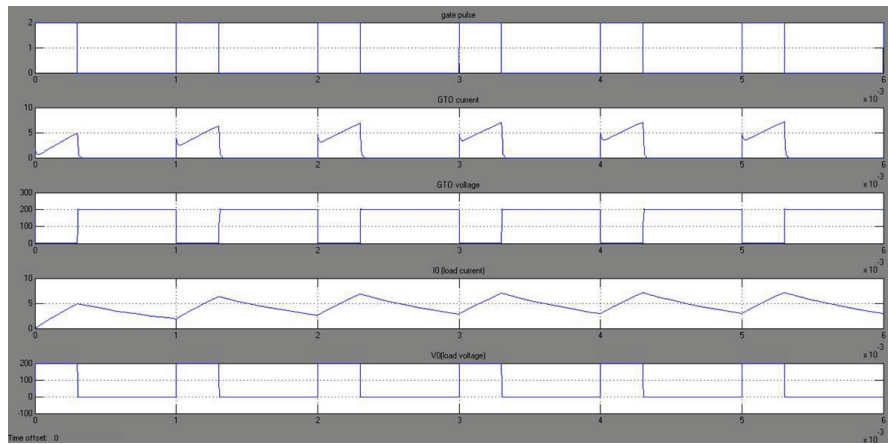
Voltage and current waveforms:



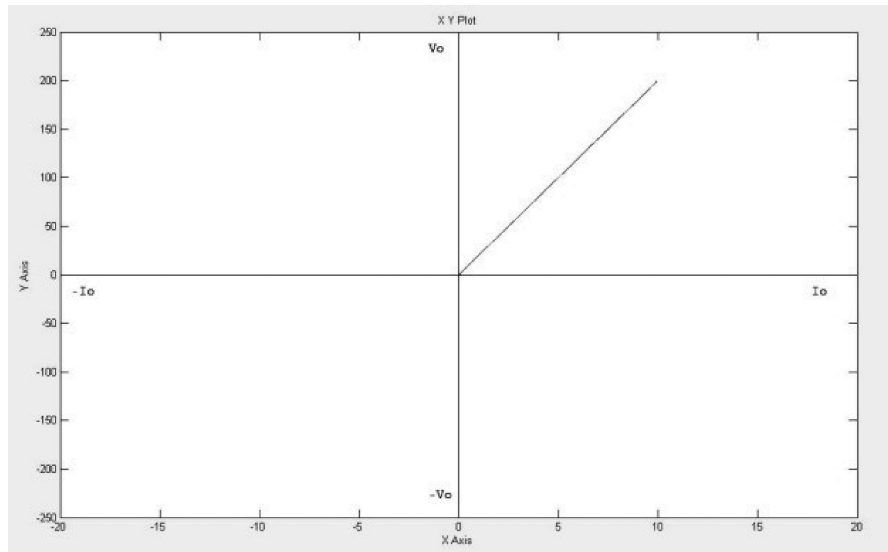
Example A.3.9: To design and simulate Class A chopper with RLE-load using MATLAB Simulink

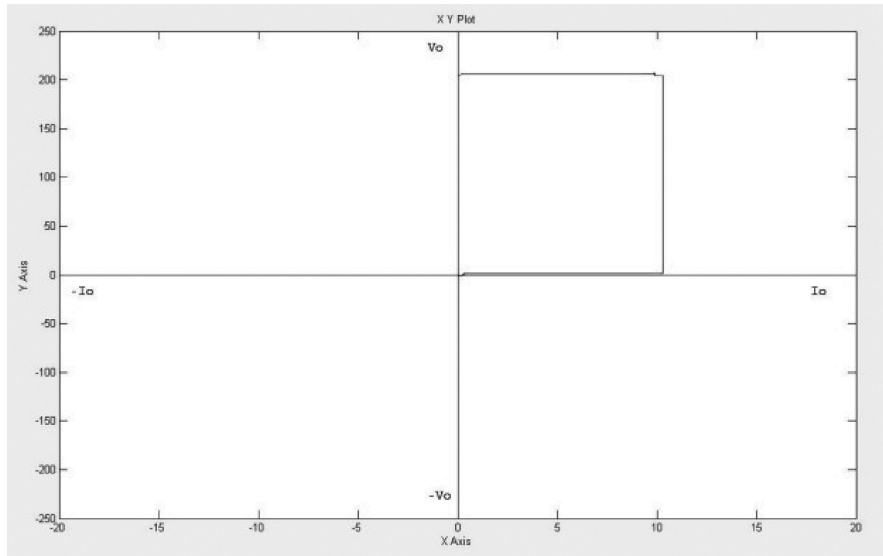


Voltage and current waveforms:

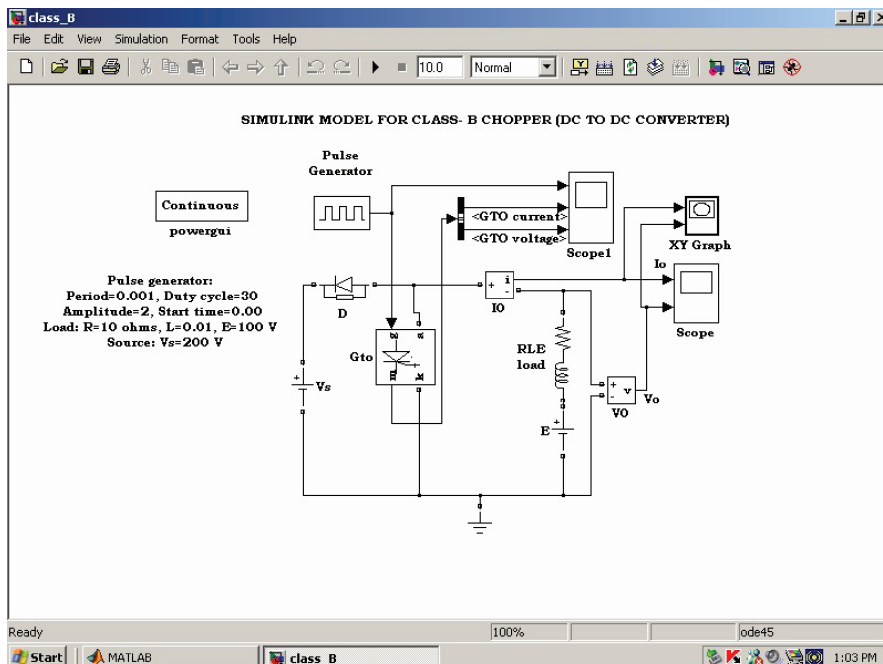


V-I characteristics:

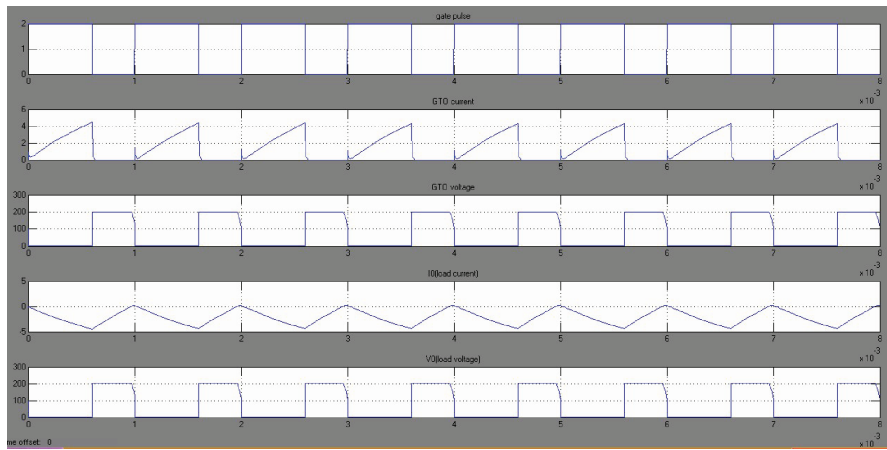




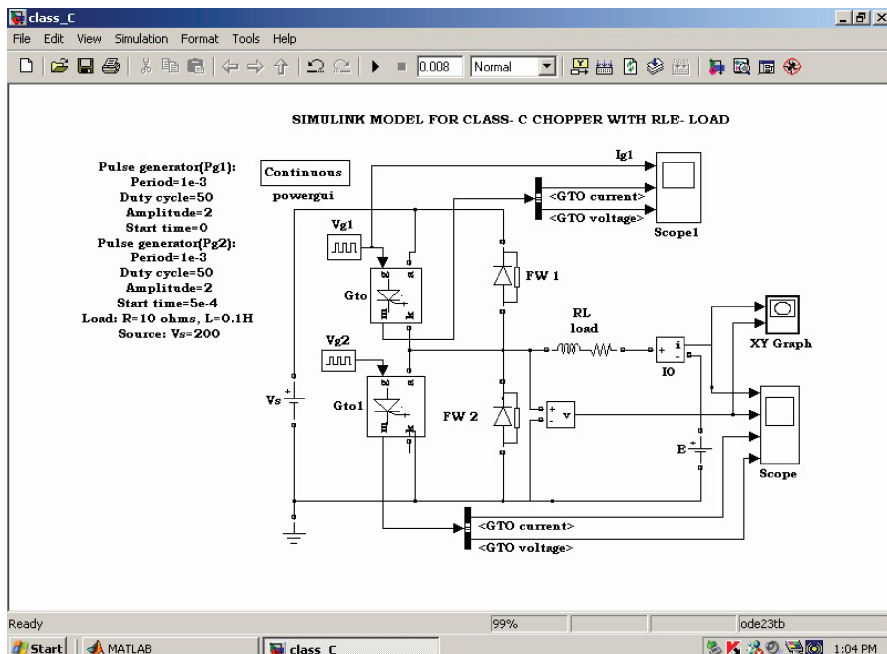
Example A.3.10: To design and simulate Class B chopper with RLE-load using MATLAB Simulink



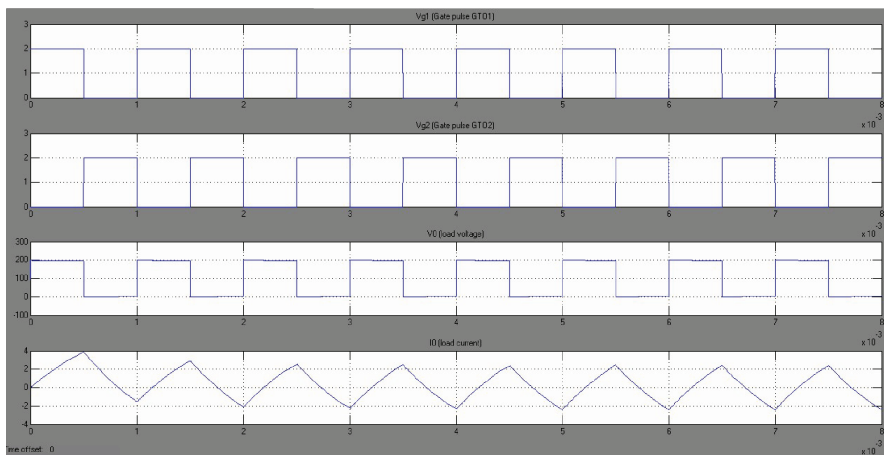
Voltage and current waveforms:



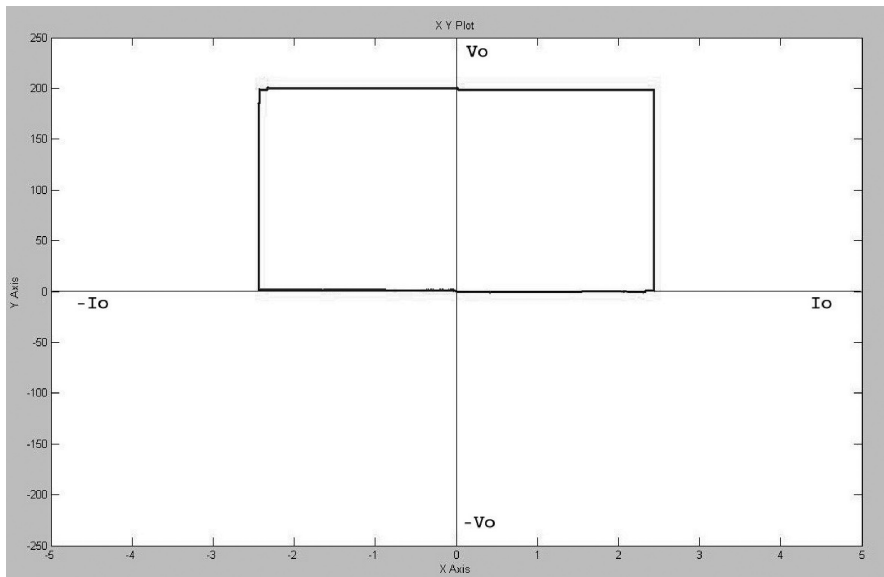
Example A.3.11: To design and simulate class C chopper with RLE-load using MATLAB Simulink



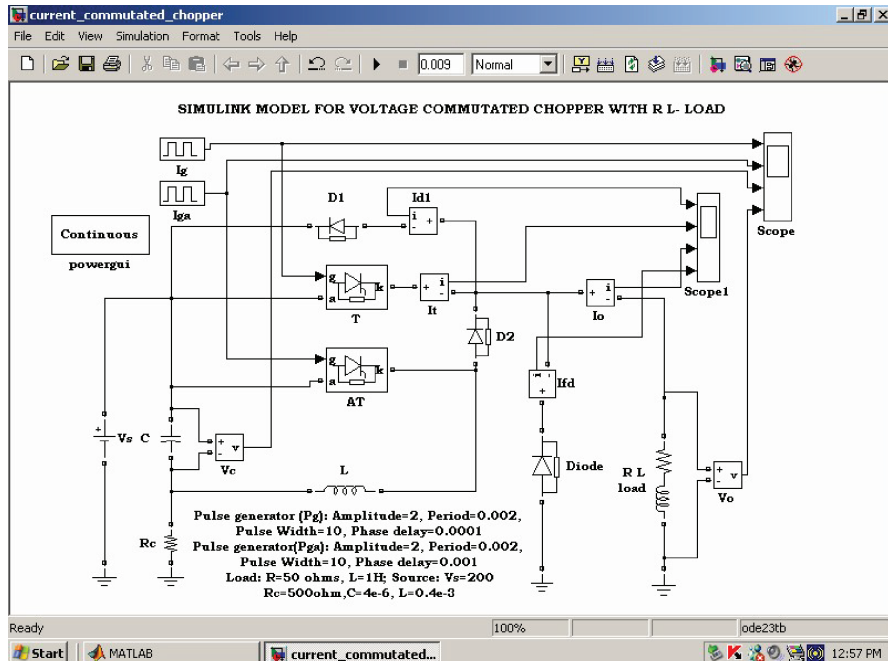
Voltage and current waveforms:



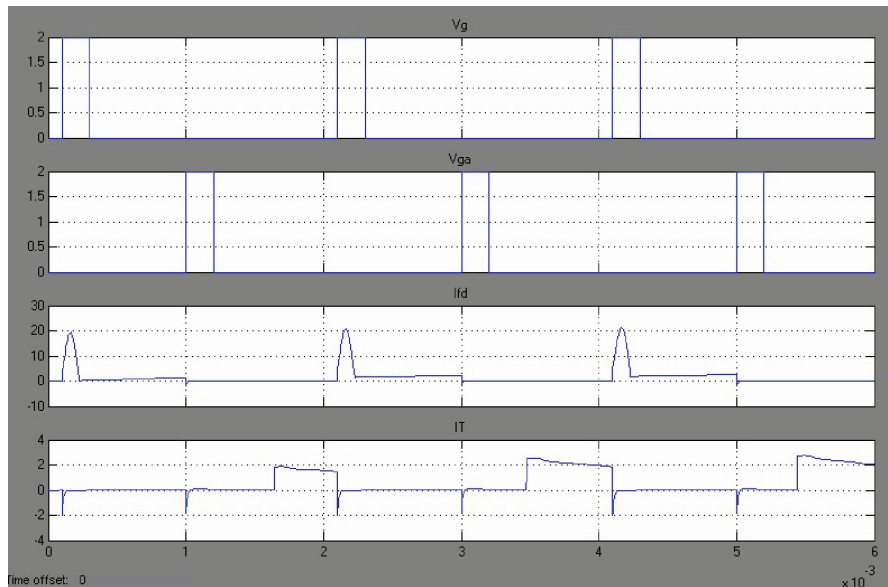
V-I characteristics:

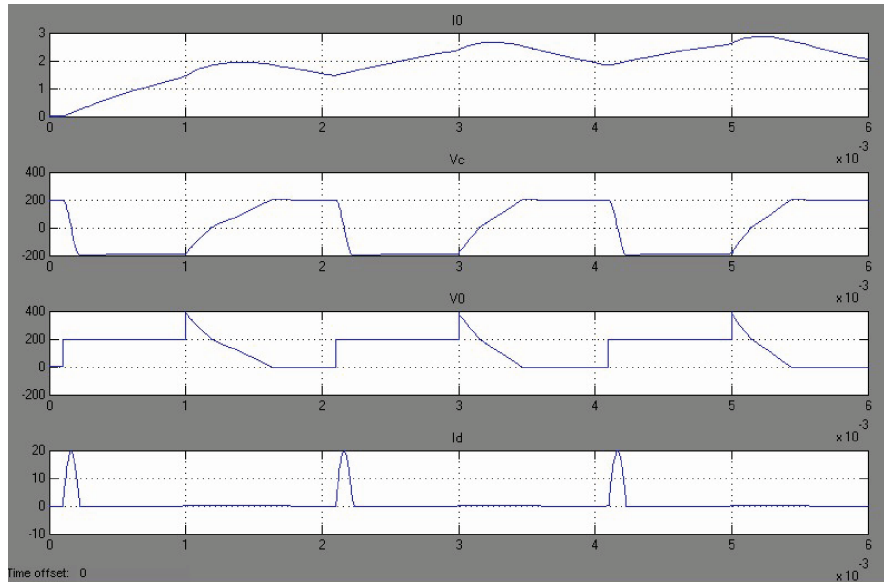


Example A.3.12: To design and simulate voltage-commutated chopper with RLE-load using MATLAB Simulink

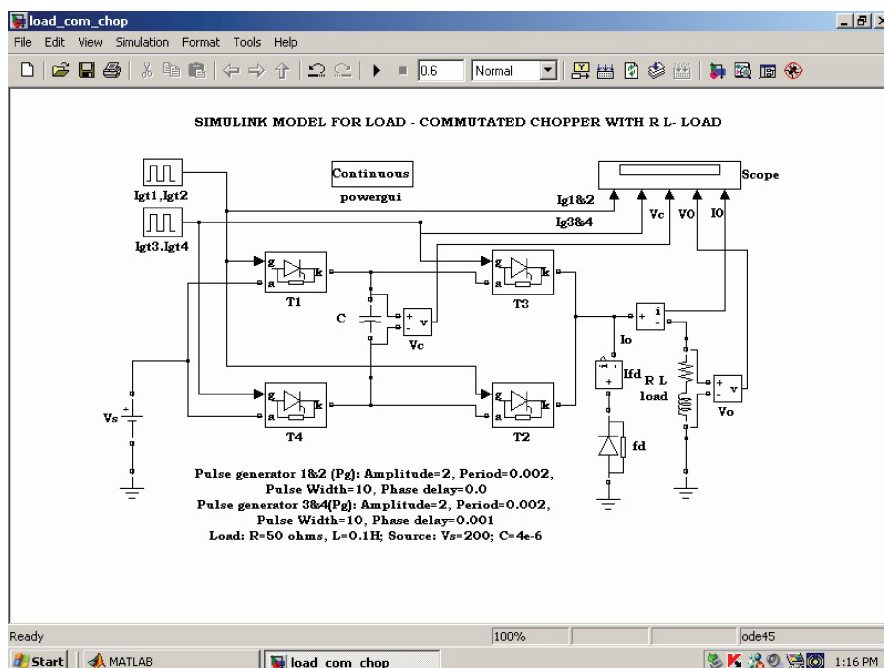


Voltage and current waveforms:

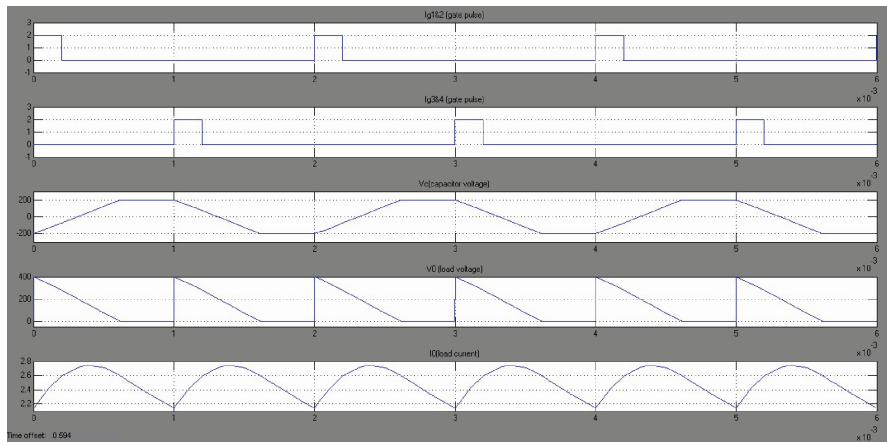




Example A.3.13: To design and simulate load-commutated chopper with RLE-load using MATLAB Simulink

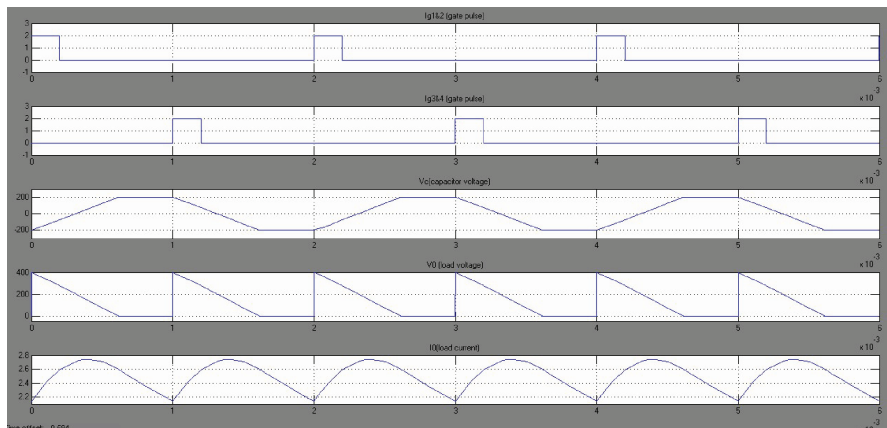


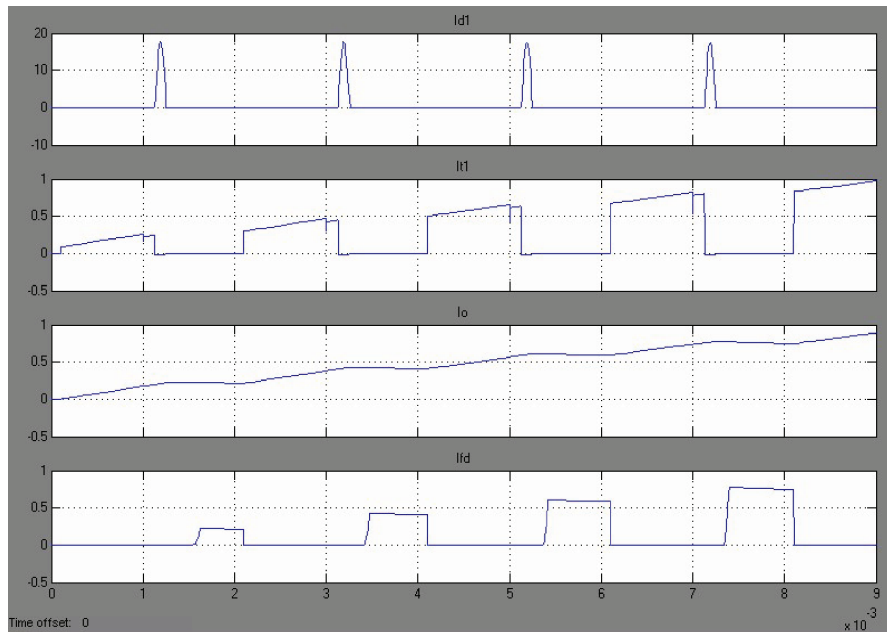
Voltage and current waveforms:



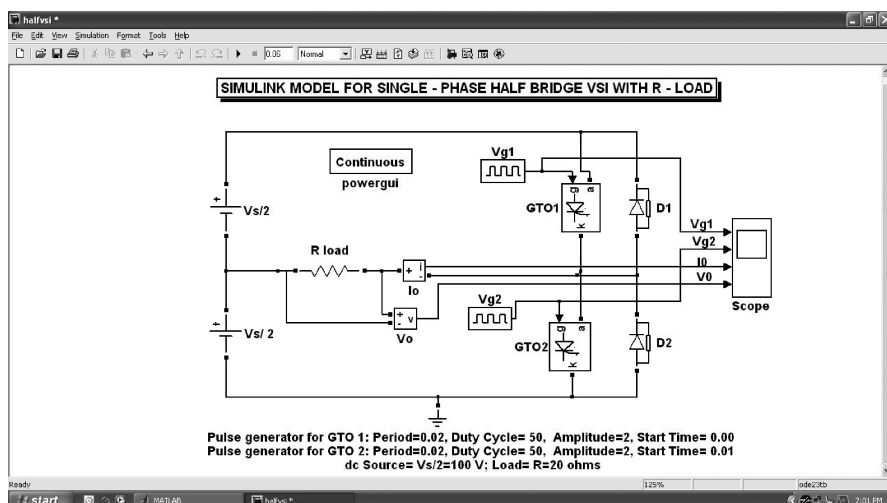
Example A.3.14: To design and simulate current-commutated chopper with RLE-load using MATLAB Simulink

Voltage and current waveforms:

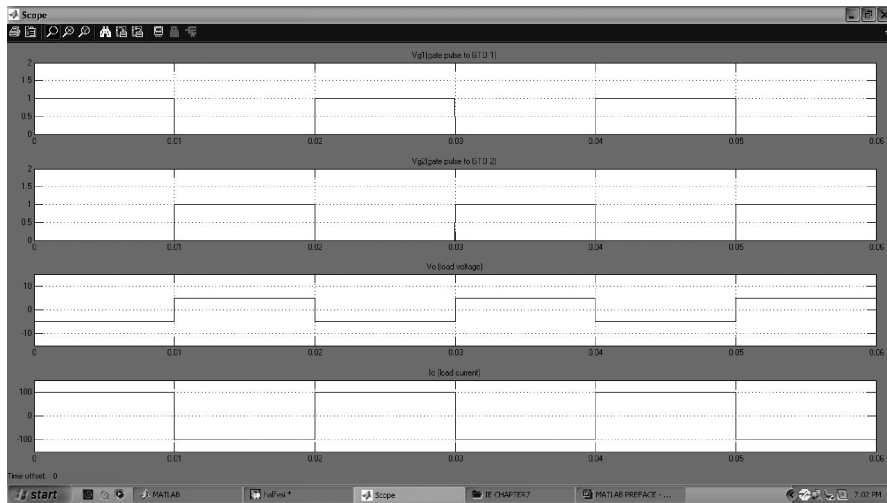




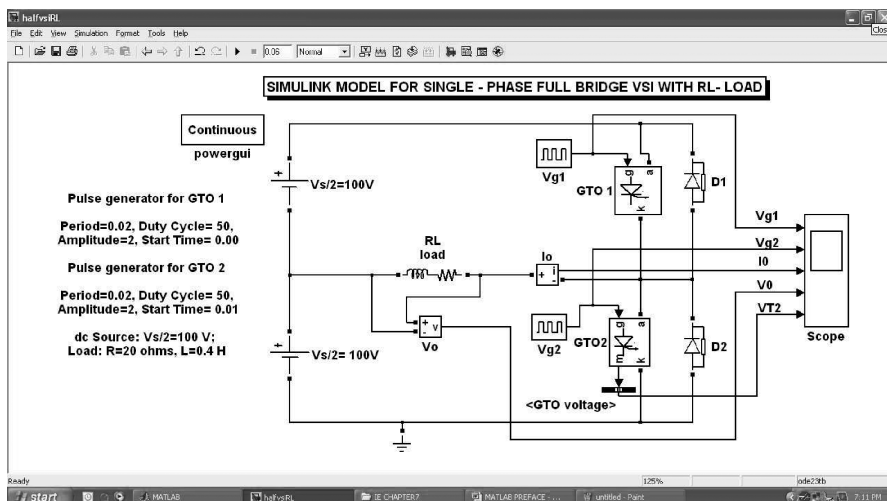
Example A.3.15: To design and simulate single-phase half-bridge voltage source inverter with resistive load



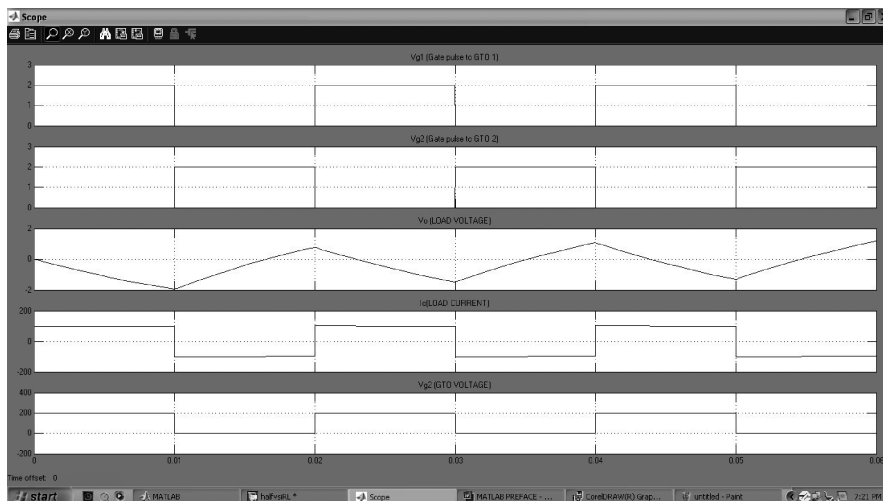
Voltage and current waveforms:



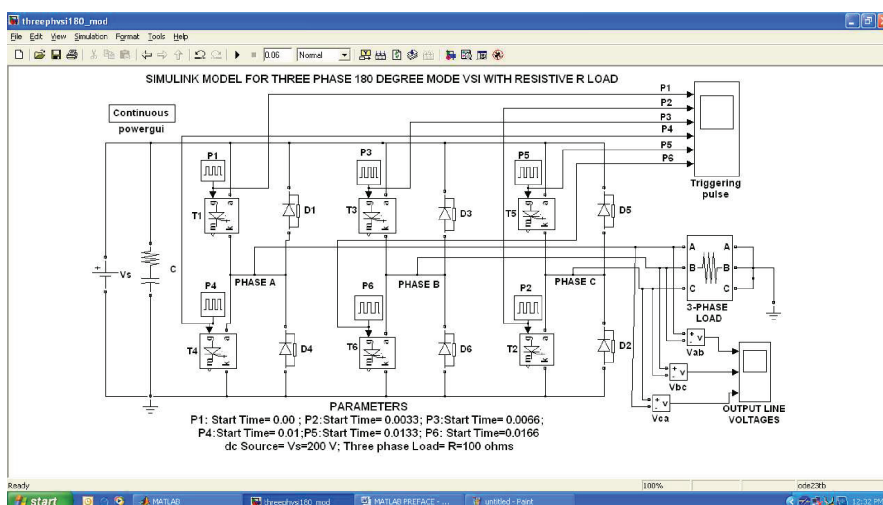
Example A.3.16: To design and simulate single-phase full-bridge voltage source inverter with RL-load



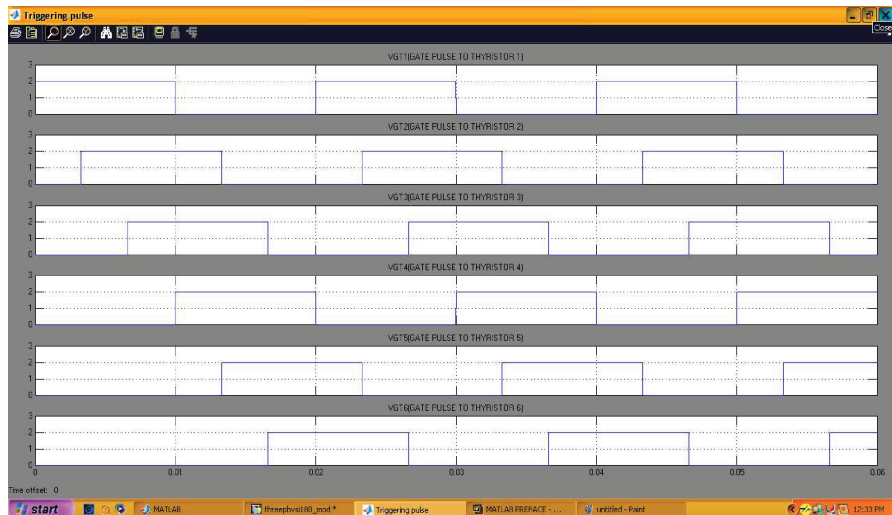
Voltage and current waveforms:



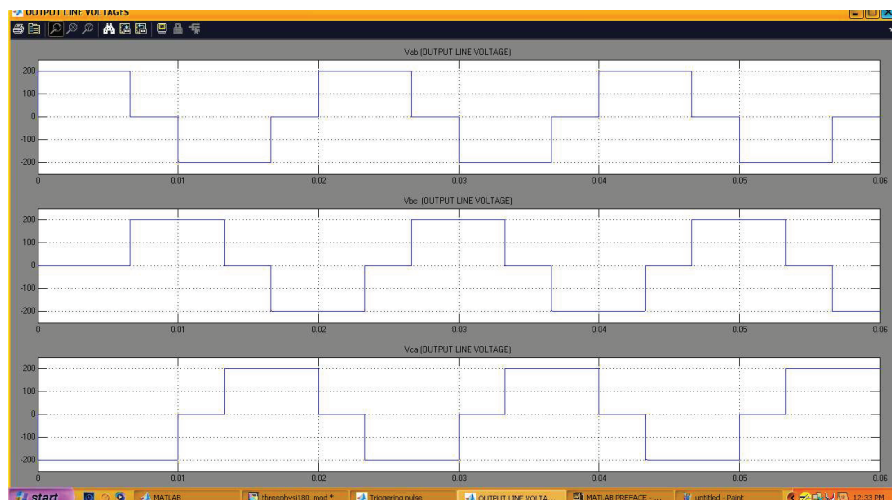
Example A.3.17: To design and simulate three-phase 180-degree-mode voltage source inverter with resistive load



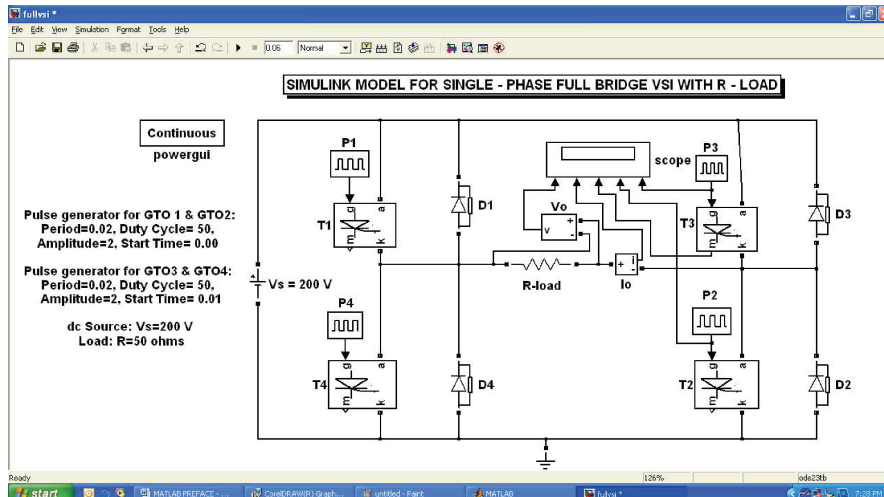
Voltage and current waveforms:



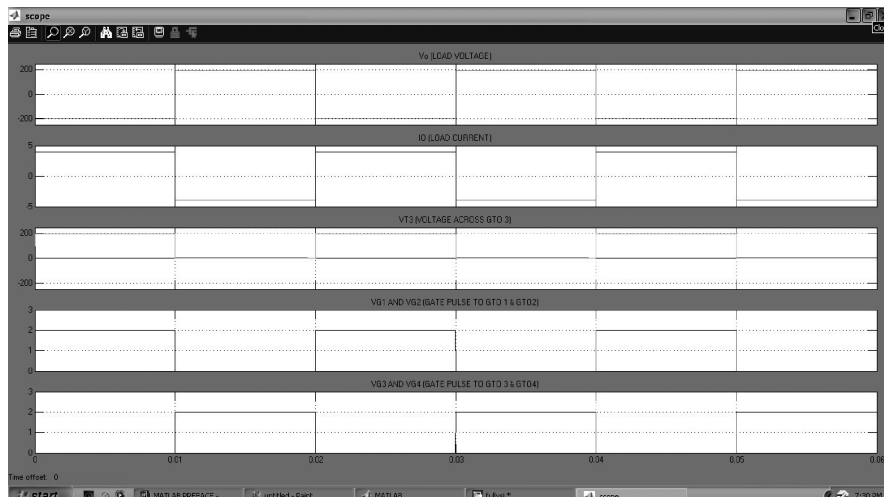
Voltage and current waveforms:



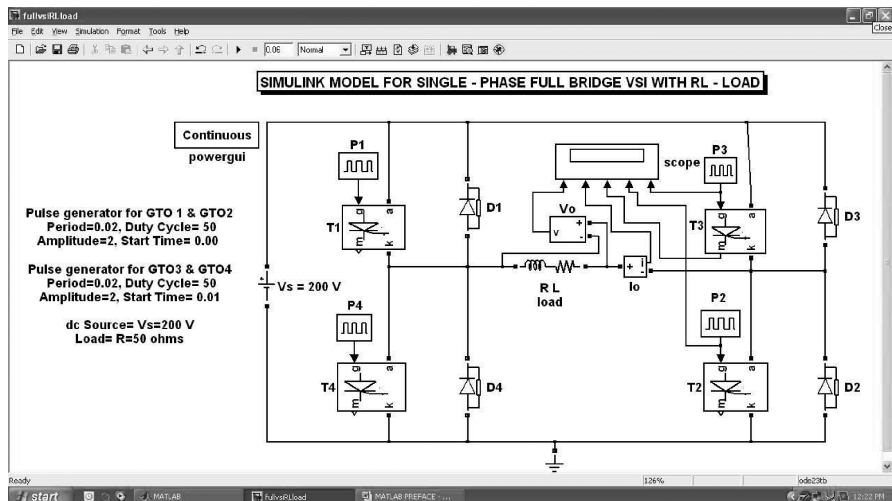
Example A.3.18: To design and simulate single-phase full-bridge voltage source inverter with resistive load



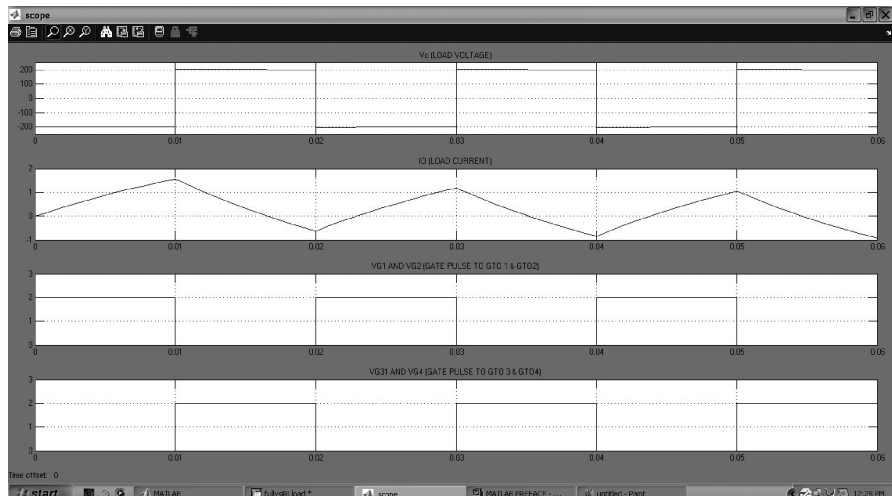
Voltage and current waveforms:



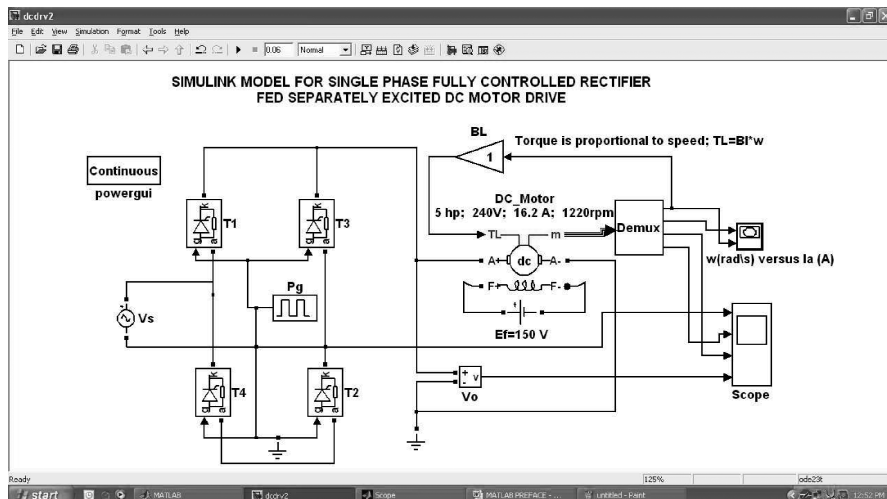
Example A.3.19: To design and simulate single-phase full-bridge voltage source inverter with RL-load



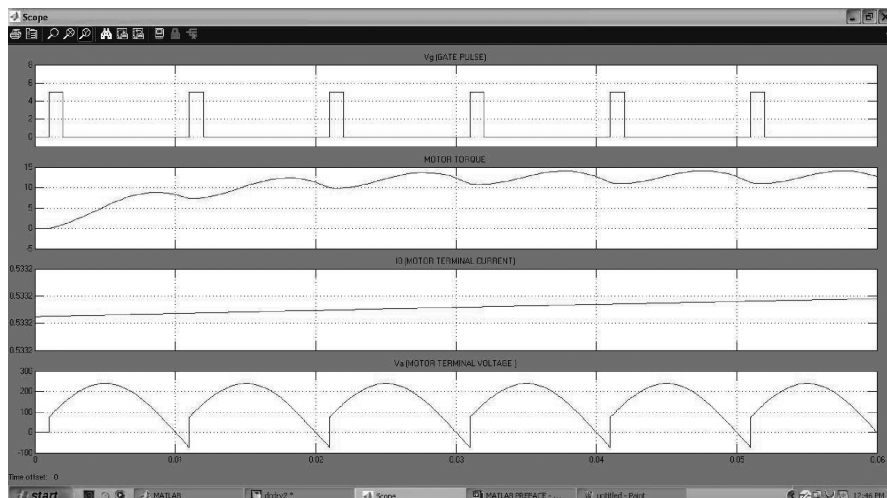
Voltage and current waveforms:



Example A.3.20: To design and simulate single-phase fully controlled rectifier-fed separately excited DC motor drive



Voltage and current waveforms:



A.4 M-FILES FOR ADVANCED POWER ELECTRONICS

Example A.4.1: To calculate average value of a full-wave-rectified sine waveform

SOLUTION

```
% Program to calculate average value of a full wave rectified sine
waveform
% Enter the value of peak voltage
disp('Typical value for peak voltage is 220 V')
Vm=input('Enter Peak voltage in Volts>');
T = pi;
theta = linspace(0, T, 1024);
v = Vm*sin(theta);
V0 = 1/T*trapz(theta, v)
```

Test: Use MATLAB to calculate the average value of a full-wave-rectified sine waveform that has peak values of 220 V, 180 V, 120 V, 75 V?

For $V_m = 220$ V, average value is $V_0 = 140.0562$ V
 For $V_m = 180$ V, average value is $V_0 = 114.5915$ V
 For $V_m = 120$ V, average value is $V_0 = 76.3943$ V
 For $V_m = 75$ V, average value is $V_0 = 47.7464$ V

Example A.4.2: To calculate the RMS value of a full-wave-rectified sine waveform

SOLUTION

```
% Program to calculate the rms value of a full wave rectified sine
% waveform
% Enter the value of peak voltage
disp('Typical value for peak voltage is 220 V')
Vm=input('Enter Peak voltage in Volts>');
T = pi;
theta = linspace(0, T, 1024);
v = Vm*sin(theta);
Vrms = sqrt(1/T*trapz(theta, v.^2))
```

Test: Use MATLAB to calculate the RMS value of a full-wave-rectified sine waveform that has a peak value of 220 V?

For $V_m = 220$ V, RMS value is $V_{rms} = 155.5635$ V

Example A.4.3: To calculate the apparent power, power factor, and average power for given load

SOLUTION

```
% Program to calculate the apparent power, pf, avg power for given load
% Enter the rms ac voltage, reactance, resistance
disp('Typical value for rms voltage is 220 V')
Vs=input('Enter rms voltage in Volts>');
X=input('Enter Load reactance in ohms>');
R=input('Enter Load Resistance in Ohms>');
ZL = R+ j*X;
R = real(ZL);
X = imag(ZL);
magZ = abs(ZL);
Is = Vs/magZ
S = Vs*Is
phi = atan(X/R);
pf = cos(phi)
P = Vs*Is*pf
```

Test: Find the apparent power, power factor, and average power of a load impedance

$Z = 10 + j20$ ohms supplied by a 220 V AC supply?

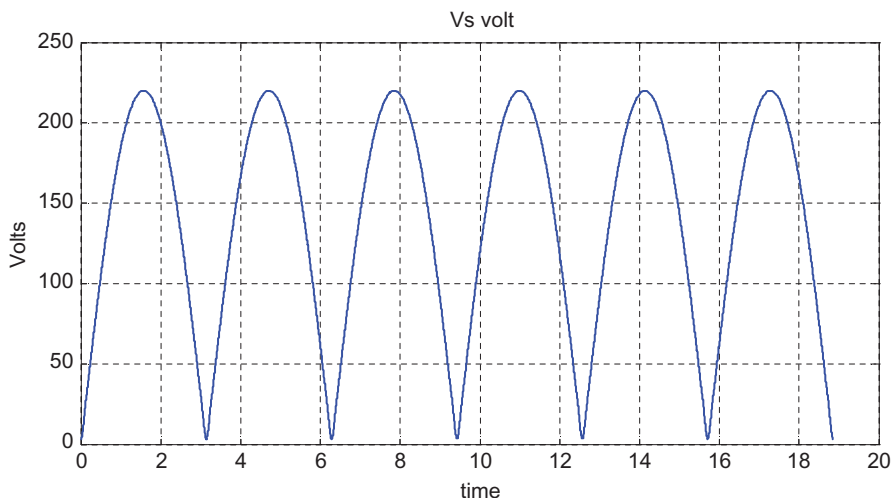
For RMS AC voltage = 220 V, $R = 10$ ohms, $X = 20$ ohms, $I_s = 9.8387$ A,
 $S = 2.1645e + 003$, $pf = 0.4472$, $P = 968.0000$

Example A.4.4: To plot six cycles of a full-wave-rectified sine wave

SOLUTION

```
% Program to plot six cycles of a full-wave rectified sine wave
% Enter the peak voltage, frequency
disp('Typical value for peak voltage is 220 V')
peakV=input('Enter Peak voltage in Volts>');
disp('Typical value for line frequency is 50 Hz')
freq=input('Enter line frequency in Hz>');
N = 1024;
th = linspace(0, pi, 1024);
n = 2:2:40;
vth = 2*Vm/pi + 4*Vm./(pi*(1 - n.^2))*cos(n'*th);
x = linspace(0, 6*pi, 6*N);
Vs = vth'*ones(1, 6);
plot(x, Vs(:)), grid
```

For $V_m = 220$ V, $f = 50$ Hz, six cycles of a full-wave-rectified sine wave are as:

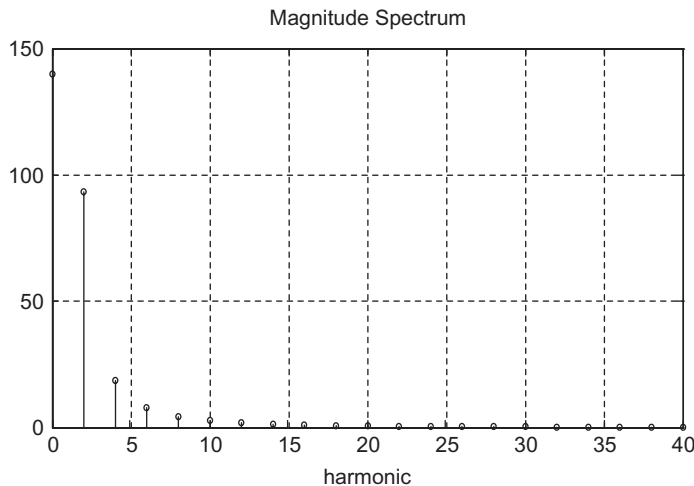


Example A.4.5: Program to plot the magnitude spectrum of a full-wave-rectified sine wave

SOLUTION

```
% Program to plot the magnitude spectrum of a full-wave rectified
sine wave
% Enter the peak voltage, frequency
Vm=input('Enter Peak voltage in Volts>');
freq=input('Enter line frequency in Hz>');
n = [2:2:40];
Vh = [2*Vm/pi abs(4*Vm/pi*1./(1 - n.^2))];
stem([0 n], Vh, 'k'), grid
title('Magnitude Spectrum')
xlabel('harmonic')
```

For $V_m = 220$ V, $f = 50$ Hz, magnitude spectrum of a FW-rectified sine wave is as follows:



Example A.4.6: To compute various performance parameters for half-wave (HW)-controlled rectifier with R-load

SOLUTION

```
%Program to compute various performance parameters for half-wave
%controlled rectifier with R load
% Enter the rms voltage, frequency, resistor R and Vak
rmsV=input('Enter rms voltage in Volts>');
freq=input('Enter line frequency in Hz>');
R=input('Enter Load Resistance in Ohms>');
Vak =input('Enter forward voltage drop across thyristor in volt>');
a=input('Enter Firing angle within range 0 to 180 in deg>');
tpi = 2*pi;
Vm = Vs*sqrt(2);
a = a*pi/180;
th = linspace(a, pi, 1024);
Ith = Vm/R*sin(th);
Is = sqrt(1/tpi*trapz(th, Ith.^2));
a1 = 2/tpi*trapz(th, Ith.*cos(th));
b1 = 2/tpi*trapz(th, Ith.*sin(th));
Is1 = sqrt((a1^2 + b1^2)/2);
S = Vs*Is
P = Vm*b1/2
Q = -Vm*a1/2
D = Vs*sqrt(Is^2 - Is1^2)
pf = P/S
ph1 = atan(a1/b1);
DPF = cos(ph1)
DF = Is1/Is
Pscr = Vak*Vm/(2*pi*R)*(1 + cos(a))
eta = P/(P + Pscr)
```

Test: A HW-controlled rectifier is supplied by a 160 V AC, 50-Hz source and has a load resistance of 10 ohms. Calculate the apparent power; real, reactive, and distortive power; power factor; displacement factor; and distortion factor for a delay angle of 60 degrees. Also calculate the thyristor dissipation for $V_{ak} = 2$ V and circuit efficiency?

SOLUTION

$S = 3.0697e + 003$, $P = 1.9469e + 003$, $Q = 577.7316$, $D = 2.3019e + 003$,
 $pf = 0.6342$, $DPF = 0.9587$, $DF = 0.6616$, $Pscr = 14.8552$, $\eta = 0.9924$

Example A.4.7: To compute various performance parameters for half-wave-controlled rectifier with R-L-load

```
%Program to compute various performance parameters for HW controlled
rectifier with R-L load
% Enter the peak voltage, frequency, inductance L in mH and resistor R
Vs=input('Enter rms voltage in Volts>');
f=input('Enter line frequency in Hz>');
X=input('Enter Load reactance X in ohms>');
R=input('Enter Load Resistance R in Ohms>');
a=input('Enter Firing angle within range 0 to 180 in deg>');
T = 2*pi;
Vm = Vs*sqrt(2);
q = X/R;
phi = atan(q);
a = a*pi/180;
B = beta_solv(a, q);
thc = B - a;
th = linspace(a, B, 1024);
Ith = Vm/R*cos(phi)*(sin(th - phi) - sin(a - phi)*exp(-(th - a)/q));
Is = sqrt(1/T*trapz(th, Ith.^2));
ap = a - phi;
bp = B - phi;
Io = Vm/(2*pi*R)*cos(phi)*(cos(ap) - cos(bp) - q*sin(ap)*(1 - exp
(-thc/q)));
S = Vs*Is
P = (Is^2)*R
pf = P/S
```

Function for beta solver of the above example:

```
% beta = beta_solv(a, q)
function beta = beta_solv(a, q)
phi = atan(q);
LHS = 1;
beta = pi;
inc = pi/4;
while(abs(LHS) > 1E-6),
    LHS = exp(a/q)*sin(a - phi) - exp(beta/q)*sin(beta - phi);
    if LHS < 0,
        beta = beta + inc;
    else
        beta = beta - inc;
        inc = inc/2;
        beta = beta + inc;
    end
end
```

Example A.4.8: To compute the power computations for FW-controlled-rectifier with R-load

Test: A full-wave (FW)-controlled rectifier is supplied by a 170 V AC, 50-Hz source and has a load resistance of 10 ohms. Calculate the apparent power; real, reactive, and distortive power; power factor; displacement factor; and distortion factor for a delay angle of 60 degrees. Also calculate the thyristor dissipation for $V_{ak} = 1$ V and circuit efficiency?

SOLUTION

$$S = 2.5922e + 003, P = 2.3250e + 003, Q = 689.9357, D = 915.2112 \\ pf = 0.8969, DPF = 0.9587, DF = 0.9356, \eta = 0.9902$$

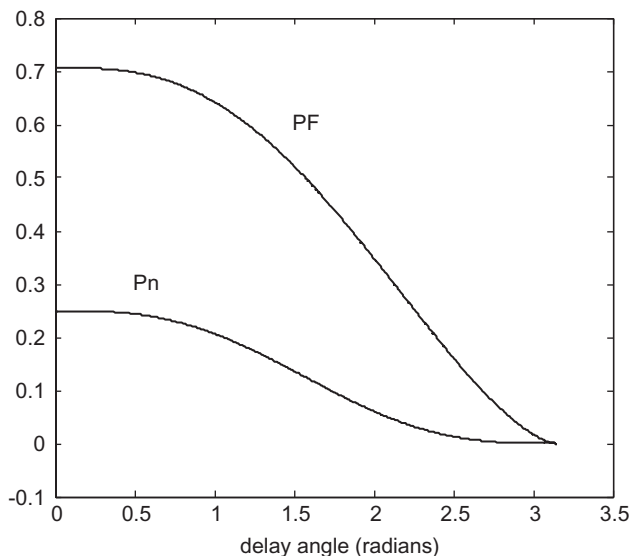
```
%Program to compute the power computations for FW controlled
rectifier with R load
% Enter the rms voltage, frequency, resistor R and Vak
Vs=input('Enter rms voltage in Volts>');
freq=input('Enter line frequency in Hz>');
R=input('Enter Load Resistance in Ohms>');
Vak =input('Enter forward voltage drop across thyristor in volt>');
a=input('Enter Firing angle within range 0 to 180 in deg>');
Vf = 0.9;
Vm = Vs*sqrt(2);
a = a*pi/180;
th = linspace(a, pi, 1024);
Ith = Vm/R*sin(th);
Is = sqrt(1/pi*trapz(th, Ith.^2));
a1 = 2/pi*trapz(th, Ith.*cos(th));
b1 = 2/pi*trapz(th, Ith.*sin(th));
Is1 = sqrt((a1^2 + b1^2)/2);
S = Vs*Is
P = Vm*b1/2
Q = -Vm*a1/2
D = Vs*sqrt(Is^2 - Is1^2)
pf = P/S
ph1 = atan(a1/b1);
DPF = cos(ph1)
DF = Is1/Is
Pscr = Vak*Vm/(2*pi*R)*(1 + cos(a));
Pdio = Vf*Vm/(2*pi*R)*(1 + cos(a));
eta = P/(P + 4*Pscr)
```

Example A.4.9: To simulate the normalized average power of half-wave-controlled rectifier along with power factor

SOLUTION

```
%Program to simulate the normalized average power of half-wave controlled rectifier along with power factor
tpi = 2*pi;
a = linspace(0, pi, 1024);
pf = sqrt(0.5 - a/tpi + 0.5/tpi*sin(2*a));
Pn = 0.5*pf.^2;
plot(a, Pn, 'k', a, pf, 'k')
xlabel('delay angle (radians)')
text(1.5, 0.6, 'PF')
text(0.5, 0.3, 'Pn')
```

Test: The plot of normalized average power of half-wave-controlled rectifier along with power factor is:



Example A.4.10: To calculate and plot the inductor current response of the given circuit

SOLUTION

```
% Program to calculate and plot the inductor current response of the
given circuit
% Enter the source voltage Vs, Rs, L, C, Rb, and Vb
Vs=input('Enter source voltage in Volts>');
Vb=input('Enter Vb in Volts>');
Rs=input('Enter Rs in ohms>');
L=input('Enter inductance in mH>');
C=input('Enter C in uF >');
Rb=input('Enter Rb in ohms>');
global A B u
mH = 1E-3;
uF = 1E-6;
RC = Rb*C;
A = [-Rs/L -1/L; 1/C -1/RC];
B = [1/L 0; 0 1/RC];
u = [Vs; Vb];
X0 = [0; 0];
[t, X] = ode23('ckta', [0 0.1], X0);
IL = X(:, 1);
plot(t, IL), grid
xlabel('Time (seconds)')
```

Function file for the above example:

```
% Function file for Example 24
function dX = ckta(t, X)
global A B u
dX = A*X + B*u;
```

Example A.4.11: Program to simulate the single-phase full-wave (full-converter)-controlled rectifier

SOLUTION

```
% Program to simulate the single-phase full-
wave(full-converter)controlled rectifier
% Simulation at a specified firing angle
% Enter the peak voltage, frequency, inductance L in mH
and resistor R
disp('Typical value for peak voltage is 220 V')
peakV=input('Enter Peak voltage in Volts>');
disp('Typical value for line frequency is 50 Hz')
freq=input('Enter line frequency in Hz>');
disp('Typical value for Load inductance is 28.8 mH')
L=input('Enter Load inductance in mH');
disp('Typical value for Load Resistance is 10.0 Ohms')
R=input('Enter Load Resistance in Ohms>');
disp('Typical value for Firing angle is 30.0 degree')
```

```
fangDeg=input('Enter Firing angle within range  
0 to 180 in deg>');  
fangRad=fangDeg/180.0*pi;  
w=2.0*pi*freq;  
X=w*L/1000.0;  
if (X<0.001) X=0.001; end;  
Z=sqrt(R*R+X*X);  
tauInv=R/X;  
loadAng=atan(X/R);  
k1=peakV/Z;  
k2=2.0*k1*sin(loadAng-fangRad)/(1.0-exp(-pi*tauInv));  
k3=k1*sin(loadAng-fangRad);  
if (fangRad<loadAng)  
    A=k2;  
    sw=1;  
else  
    A=k3;  
    sw=2;  
end;  
Ampavg=0;  
AmpRMS=0;  
for n=1:360;  
    theta=n/180.0*pi;  
    X(n)=n;  
    if (sw==1);  
    if (n<fangDeg);  
        cur=k1*sin(pi+theta-loadAng)  
            + A*exp(-tauInv*(pi+theta-fangRad));  
        vbr(n)=peakV*sin(theta+pi);  
        vind(n)=vbr(n)-R*cur;  
        iLoad(n)=cur;  
        vSCR(n)=peakV*sin(theta);  
        Ampavg=Ampavg+cur*1/360;  
        AmpRMS=AmpRMS+cur*cur*1/360;  
    elseif ((n>=fangDeg) & (n<(180+fangDeg)));  
        cur=k1*sin(theta-loadAng)+ A*exp(-tauInv*(theta-  
fangRad));  
        vbr(n)=peakV*sin(theta);  
        vind(n)=vbr(n)-R*cur;  
        iLoad(n)=cur;  
        vSCR(n)=0;  
        Ampavg=Ampavg+cur*1/360;  
        AmpRMS=AmpRMS+cur*cur*1/360;  
    else (n>=(180+fangDeg));  
        cur=k1*sin(theta-pi-loadAng)+ A*exp(-tauInv*  
(theta-pi-fangRad));  
        vbr(n)=peakV*sin(theta-pi);  
        vind(n)=vbr(n)-R*cur;  
        iLoad(n)=cur;
```

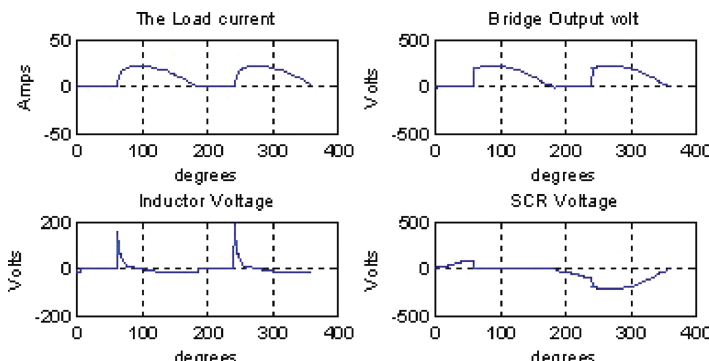
```
vSCR(n)=peakV*sin(theta);
Ampavg=Ampavg+cur*1/360;
AmpRMS=AmpRMS+cur*cur*1/360;
end;
else
if (n<fangDeg);
    cur=k1*sin(pi+theta-loadAng)+ A*exp
(-tauInv*(pi+theta-fangRad));
if (cur>0);
    vbr(n)=peakV*sin(theta+pi);
    vind(n)=vbr(n)-R*cur;
    iLoad(n)=cur;
    vSCR(n)=peakV*sin(theta);
    Ampavg=Ampavg+cur*1/360;
    AmpRMS=AmpRMS+cur*cur*1/360;
else;
    vbr(n)=0.0;
    vind(n)=0.0;
    iLoad(n)=0.0;
    vSCR(n)=peakV*sin(theta)/2.0;
end;
elseif ((n>=fangDeg) & (n<(180+fangDeg)));
    cur=k1*sin(theta-loadAng)+ A*exp(-tauInv*(theta-
fangRad));
if (cur>0);
    vbr(n)=peakV*sin(theta);
    vind(n)=vbr(n)-R*cur;
    iLoad(n)=cur;
    vSCR(n)=0;
    Ampavg=Ampavg+cur*1/360;
    AmpRMS=AmpRMS+cur*cur*1/360;
else;
    vbr(n)=0.0;
    vind(n)=0.0;
    iLoad(n)=0.0;
    vSCR(n)=peakV*sin(theta)/2.0;
end;
else (n>=(180+fangDeg));
    cur=k1*sin(theta-pi-loadAng)+ A*exp
(-tauInv*(theta-pi-fangRad));
    vbr(n)=peakV*sin(theta-pi);
    vind(n)=vbr(n)-R*cur;
    iLoad(n)=cur;
    vSCR(n)=peakV*sin(theta);
    Ampavg=Ampavg+cur*1/360;
    AmpRMS=AmpRMS+cur*cur*1/360;
end;
end;
end;
```

```

subplot(3,2,1),plot(X,iLoad),grid
title('The Load current')
xlabel('degrees')
ylabel('Amps')
subplot(3,2,2),plot(X,vbr),grid
title('Bridge Output volt')
xlabel('degrees')
ylabel('Volts')
subplot(3,2,3),plot(X,vind),grid
title('Inductor Voltage')
xlabel('degrees')
ylabel('Volts')
subplot(3,2,4),plot(X,vSCR),grid
title('SCR Voltage')
xlabel('degrees')
ylabel('Volts')

```

Test: For 220 V ac supply, 50 Hz, $R = 10$ ohms, $L = 3\text{Mh}$, delay angle = 60 degree, various plots for FW controlled rectifier are as:



Example A.4.12: Program to compute various performance parameters for full-bridge inverter

SOLUTION

```

%Program to compute various performance parameters for
full-bridge inverter
Vs = input('Enter input dc voltage in Volts');
Rl = input('Enter Load resistance in ohms');
L = input('Enter Load inductance in henry');

```

```
Ron = input('Enter forward resistance of switch ohms');
w = 2*50*pi;
R = Rl + 2*Ron;
q = w*L/R;
x = 2*q/pi;
IL = Vs/R*sqrt(1 - x*tanh(1/x));
IL2 = IL^2;
PL = IL2*Rl
Pxtr = 0.5*IL2*Ron
Ps = PL + 4*Pxtr
eta = PL/(PL + 4*Pxtr)
```

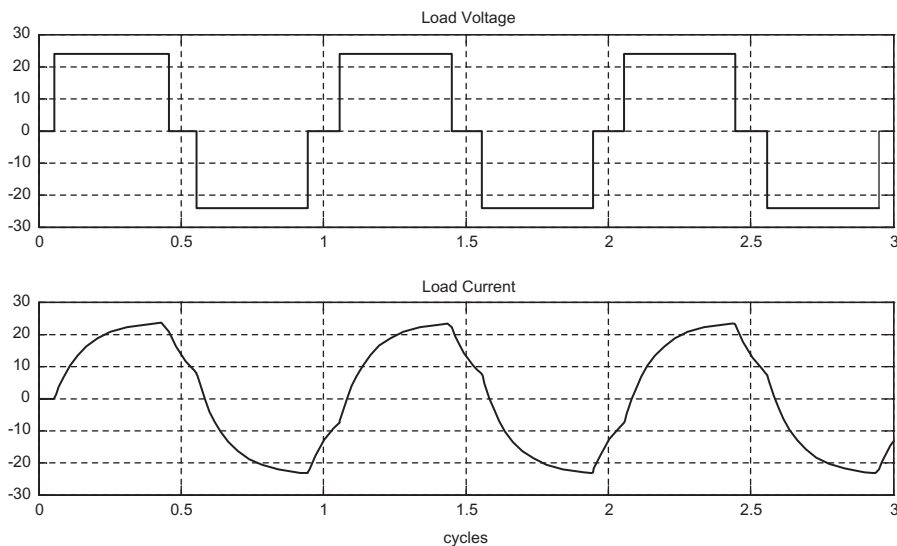
Test: For $V_s = 24$ V, $R_l = 1$ ohm, $L = 2$ mH, $R_{on} = 0.02$ ohm, various performance parameters for full-bridge inverter are: $P_L = 329.9671$, $P_{xtr} = 3.2997$, $P_s = 343.1658$, $\eta = 0.9615$

Example A.4.13: Program to simulate the full-bridge inverter with any degree of blanking or commutation time interval

SOLUTION

```
%Program to simulate the full-bridge inverter with any
degree of blanking or
%commutation time interval
Vs = input('Enter input dc voltage in Volts');
R = input('Enter Load resistance in ohms');
L = input('Enter Load inductance in henry');
f = input('Enter the value of frequency of ac in Hz');
alpha = input('Enter value of half the dead time (blank-
ing or commutation time)interval in degrees'); global
A B d
T = 360;
Lf = L*f;
A = -R/Lf;
d = alpha/T;
B = Vs/Lf;
x0 = 0;
[t, IL] = ode23('inverter', [0 3], x0);
u = 0.5*(sign(t - fix(t) - d) - sign(t - fix(t) - (0.5 - d)));
sign(t - fix(t) - (0.5 + d)) + sign(t - fix(t) - (1 - d)));
subplot(2,1,1), stairs(t, u*Vs), grid
title('Load Voltage')
subplot(2,1,2), plot(t, IL), grid
title('Load Current')
xlabel('cycles')
```

Test: For $V_s = 24$ V, $R_l = 1$ ohm, $L = 2$ mH, $f = 50$ Hz, half the dead time (blanking or commutation time)interval $\alpha=20$ degree:



REFERENCES

1. MATLAB 8.0 and Toolbox 8.1, *The MathWorks*, Natick, MA.
2. B. K. Bose, *Power Electronics and AC drives*, Prentice Hall, Englewood Cliffs, NJ, 1986.
3. M. H. Rashid, *Power Electronics: Circuits, Devices, and Applications*, Pearson Education, Singapore, 2004.
4. P. T. Krein, *Elements of Power Electronics*, Oxford University Press, New York, 2003.
5. K. Thorborg, *Power Electronics*, Prentice Hall International (UK), London, UK, 1988.
6. A. M. Trzynadlowski, *Introduction to Modern Power Electronics*, 3rd edition, John Wiley & Sons, Hoboken, NJ, 2010.
7. B. M. Wilamowski, J. D. Irwin, *Power Electronics and Motor Drives*, CRC Press, Boca Raton, FL, 2011.
8. F. Mazda, *Power Electronics Handbook*, Newnes, Oxford, 1997.
9. F. Blaabjerg, *Control of Power Electronic Converters and Systems*, Academic Publishers, London, UK, 2018.
10. S. N. Manias, *Power Electronics and Motor Drive Systems*, Academic Publishers, 2017.

Index

Note: Page numbers in italic and bold refer to figures and tables, respectively.

Page number followed by n refers to footnote.

A

AC-bus link interface, *see DC-AC converters*
AC microgrid, 679–680, 680
AC module configuration, PV system in, 646,
 646–647
AC motor, 608–607, 607
AC regulators, 657
AC ripple voltage, 233
AC static switches, 9
active islanding detection, 686–687
active torque, 459
active vectors, 442, 443
AC-to-AC converters, 458
AC-to-DC converters, 457, 457
AC voltage controllers (AC regulators), 8
 defined, 357
 on-off control/integral cycle control,
 357–360, 358
 phase control, 360–361
 single-phase, 358, 361–365
 three-phase full-wave, 366, 367
 voltage control methods, 357
AC voltage regulators, 8
adaptive filter (AF), 663
alloy diffused method, 48, 48
amorphous silicon cells, 611
amplitude modulation index, 320
anti-islanding, 686
armature voltage control method, 492
auxiliary thyristor (AT), 234
avalanche breakdown, 53
average load/output current, 112, 114, 117
average load/output voltage, 111–112, 114, 117,
 120, 122, 125, 131, 134
 maximum, 135
 normalized, 131–132, 135
average output voltage, 182, 184

B

battery-powered electric vehicles (BEVs), 591,
 593
 drivetrain topology, 594–595, 595
 features, 592
bearing currents, EV, 598
BEVs, *see battery-powered electric vehicles (BEVs)*
bidirectional battery chargers, 690, 690

bidirectional converter, 653
bidirectional DC-DC converters, 602–606
bidirectional DC power supplies, 401, 402
bifilar-wound motor, drive circuit, 585
bipolar drive circuits, 584–585, 585
bipolar HVDC structure, 626
bipolar junction transistors (BJTs), 4, 23–24, 217
 power MOSFETs *versus*, 29
 steady-state characteristics, 24, 24–25, 25
 switching characteristics, 25–27, 26
 turn-off time, 26–27
 turn-on time, 25–26
bipolar modulation technique, 649
BJTs, *see bipolar junction transistors (BJTs)*
BLDC (brushless DC) motor, 599,
 599–600
boost (step-up) converter, 251, 251–253, 293, 647,
 647–648, 677
braking mode, motor, 462
bridge-type-controlled rectifier
 with RL load, 122–125
 with R load, 121–122
bridge-type cycloconverter
 single-phase to single-phase step-down, 376,
 378–379
 single-phase to single-phase step-up, 376,
 377–378
brushless DC (BLDC) motor, 599, 599–600
buck-boost converter, 253–254, 253–256,
 293–294
buck (step-down) converter, 247–251, 248, 293
buck-type bidirectional converter, 602, 603
burst firing, 357

C

cascaded H-bridge multilevel inverter (CHBMI),
 408, 408–410
central inverter configuration, PV system in,
 646, 647
chargers, G2V, 690
chopper(s), 8, 217
 circuit operation, 217, 219
 classes, 218
 commutation, 218, 233–247
 control strategies, 220–222
 current-commutated, 240, 240–243,
 241, 242

- chopper(s) (*Continued*)
 input/output voltage levels, 217
 load-commutated, 244, 244–247, 245, 246
 operation principle, 218–219
 output voltage and current, 217
 step up/down, 222, 222–223
 type-A (step-down) analysis, 227–233
 voltage-commutated, 234–240, 235, 236, 237
- chopper configurations, 223, 224
 first-quadrant/type-A, 224, 224, 721–723
 four-quadrant/type-E, 226, 226–227
 second-quadrant/type-B, 224–225, 225,
 723–724
 two-quadrant type-A/type-C, 225, 225
 two-quadrant type-B/type-D, 225, 226
- chopper control
 DC series motor, 505, 506, 506–507, 507
 separately excited DC motors, 500–505, 501,
 502, 503, 504
- circuit turn-off time (t_0), 111, 114, 117,
 120–122, 124
- clamped inductive circuit, 429
- Class A chopper, 224, 224, 721–723
- Class B chopper, 224–225, 225, 723–724
- Class C chopper, 503, 724–725
- commutation, 37
 current, 234
 forced, 188, 189, 233–234; *see also forced commutation*
 load, 233–234
 switching technique, 446
 voltage, 234
- computer simulation, power electronics circuits, 11
 benefits, 12
 demerits, 12
 importance, 12
 tools, 13–14
- conergy NPC inverter, 652, 652
- configurable logic blocks (CLB), 553
- constant frequency system, 220, 220
- constant-power drive, 465, 465
- constant-speed drives, 457
- constant-torque drive, 464–465, 465
- constant V/f control, 519–521, 521
- contactless EV charging system, 705
- continuous conduction, 122–124, 123, 124n2, 218
 limits, 231–232
 mode, 647
 single-phase semiconverter, RL load,
 180–182, 214
- continuous constant load, 468
- continuous load current, 379, 380, 391
- continuous variable loads, 468
- controllable switches, 7, 17
- conventional PWM, 427
- converter(s), 457–458, 675; *see also specific converter*
 circuits/analysis, 624–625
 controlled matrix, 556
 system, 10
 coupled AC configuration, hybrid MG, 680
- CRF (current ripple factor), 648
- critical loads, 677
- CSC (current source converter), 653, 654
- CSIs, *see current source inverters (CSIs)*
- cuk regulator, 257–258, 257–260, 294
- current-commutated chopper, 234, 240, 240–243,
 241, 242, 292, 728–729
- current limit control (CLC), 222, 222
- current ratings, SCR, 50–51
- current ripple factor (CRF), 648
- current source converter (CSC), 653, 654
- current source inverters (CSIs), 297, 315
 single-phase, 315, 315–316
 three-phase, 316, 317
 two-level back-to-back, 653, 655
 versus VSIs, 317–318
- cycle selection, 357
- cycloconverters, 8; *see also specific cycloconverters*
 classifications, 375
 output voltage equation for, 384, 384–385
 single-phase to single-phase, 375–378, 376
 single-phase to single-phase step-down, 376,
 378–380
 three-phase to single-phase, 380–382, 381
 three-phase to three-phase, 382–384

D

- DC-AC converters, 678, 678
- DC-bus link interface, *see DC-DC converters*
- DC chopper, 8
- DC-DC converters, 677, 677
 bidirectional, 602–606
- DC machines, 487–490
- DC microgrid, 679, 679
- DC motors, 456, 606, 606, 608
 chopper control, 500–507
 phase-controlled rectifier control, 492–500
 separately excited, 491
 shunt/separately excited, 488–489, 489
 speed control, 492
 squirrel cage IM *versus*, 479
 three-phase half-controlled rectifier control,
 499, 499–500
- DC power-stations converter
 components, 625
- DC power supplies, 400–401, 401
 bidirectional, 401, 402
 resonant, 400–401, 401

- DC separately excited motor drive
 single-phase fully controlled rectifier control, 493, 493–494, 495
 single-phase half-controlled rectifier control, 495–497, 496, 497
 three-phase fully controlled rectifier control, 497, 497–499, 498
- DC series motor, 490
 basics, 489–490
 supply voltage on characteristics, 491
- DC shunt motor, 488–489, 489
- DC static switches, 9
- DC-to-AC converters, 297, 458
 classifications, 297–298
 performance parameters, 298–299
 VSIs, 299–314
- DC-to-DC converters, 218, 458
- DC transmission, 623–624, 624
- deadtime commutation, 446
- decoupled AC configuration, hybrid MG, 680
- delay time
 BJT, 25
 IGBT, 31
 power MOSFET, 28
 thyristor, 35–36
- Derating Factor (DRF), 66–67, 100
- DFIG (double-fed induction generator), 645, 645
- DIAC, 21, 22
- di/dt* protection, 72
- diode(s), 7, 17
 AC-DC converters, 405
 -clamped inductive load, 427
 -clamped inverter, 410–411
 rectifiers, 7
 reverse recovery characteristics, 19–21, 20
- direct-fed (DF) coil WPT system, 696, 696
- direct matrix converter (DMC)
 commutation methods in, 446
 three-phase to three-phase, 439–440, 440
- direct-torque control (DTC), 554, 555, 556
- discontinuous conduction, 119n1, 124–125, 125, 221
 RLE load and, 128, 128–129
 single-phase semiconverter, RL load, 183, 183–185, 184
- discontinuous load current, 376, 378, 379
- Displacement Factor (DF), 108
- distortion factor (DF), 298–299
- distributed generation (DG), 675; *see also microgrid (MG)*
 components, 676
 integration issues, 681–682
- distribution grid, 681
- DMC, *see direct matrix converter (DMC)*
- double-fed induction generator (DFIG), 645, 645
- DRF (Derating Factor), 66–67, 100
- drive circuits, stepper motors, 584–585
- drivetrain analysis
 BEVs, 594–595, 595
 FCVs, 596, 597
 parallel HEV, 595–596, 596
 series HEV, 594–595, 595
 series-parallel HEV, 596, 597
- dry friction, 466
- DTC (direct-torque control), 554, 555, 556
- dual active-bridge (DAB) converter, 435, 435–437, 436
- dual converters, 107, 135
 circulating current-type, 138, 138–139
 ideal, 136, 136–137
 noncirculating-type, 136
 practical, 137–139
 single-phase, 139–142, 140, 176
 three-phase, 142–144, 143
- duty cycle, 468
- dv/dt* protection, 69–71
- dv/dt* triggering, 53
- dwell-time calculations, 422–424, 423
- dynamic braking, 526, 526, 527
- dynamic torque, 470
- E**
- EAC (extinction angle control), 188–190, 214
- efficiency of rectification (η), 108
- 18-pulse AC-DC converters, 406, 407
- electric drives, 455
 advantages, 459–460
 block diagram, 456, 488
 characteristics, 460
 classifications, 461
 controller, 459
 electrical motors, 456–457
 elements, 455–456
 EM application in, 480–481
 four-quadrant operation, 463–464
 load torques, 459
 power modulator, 457–458
 rating, 474–477
 selection, 477–480
 sources, 458
 system, 456
- electric motor (EM), 461, 591
 application in electric drives, 480–481
 four-quadrant operation, 462
- electric vehicles (EVs), 688
 bearing currents, 598
 BEVs, 591, 592, 593–595, 595
 charging system, 705, 705
 G2V, 690
 hybrid, *see hybrid electric vehicles (HEVs)*
 motor drives selection for, 607–611
 power converter for, 601–606

- electric vehicles (EVs) (*Continued*)
 solar-based, 614–615, 615
 V2G, 688–689, 689
 vehicle dynamics, 598–600
 vibration, 598
- electronics workbench, 13
- engine-based HEV, 601, 601
- envelope voltage, 441
- equivalent system, 470
 load torque, 471
 moment, inertia, 471–472
 to rotational motor, 472–473
- EVs, *see* electric vehicles (EVs)
- extinction angle control (EAC), 188–190, 214
- extinction time, 232–233
- F**
- FACLF (fast-acting current-limiting fuse), 68–69, 69
- FACTS, *see* flexible AC transmission system (FACTS)
- fall time, GTO, 41
- fan-type load, 466
- fast-acting current-limiting fuse (FACLF), 68–69, 69
- fast Fourier transform (FFT), 562, 570
- FCMLI, *see* flying capacitor multilevel inverter (FCMLI)
- FD, *see* freewheeling/flywheeling diode (FD)
- field-flux control method, 492
- field-programmable gate arrays (FPGAs), 551
 advantages, 553
 control implementation on, 559, 561, 562
- filter modeling, 633, 633–634
- firing angle (α), 109
- firing/triggering circuits, SCR, 54, 54
 main features, 54
 optoisolators, 55
 pulse transformer, 55
 RC, 58–60
 R circuit, 55, 55–57, 57
 UJT relaxation oscillator, 61, 61–62
- FLDTC, *see* fuzzy-logic DTC (FLDTC)
- flexible AC transmission system (FACTS), 627
 modeling, 633–635
 STATCOM, 629, 630
 SVCs, 627
 system dynamic performance improvement, 635, 635–636, 637
- TCR, 627–628, 628
- TCSC, 629–631, 631
- TSC, 628, 628–629
- UPFC, 631–632, 632
- fluctuating energy flow, 614
- flux/electromagnetic torque, estimation, 556–557
- flyback converter, 431
- flyback HV SMPC, 432
- flyback-mode regulators, 391
- flyback-mode-type switching regulator, 393–394, 394
- flyback SMPS, 395, 396, 397, 402
- flying capacitor (FC), 411
- flying capacitor multilevel inverter (FCMLI), 411–412, 412, 412
- forced commutation, 233–234
 CSI, 654
 inverter, 297
 VSI, 654
- form factor (FF), 108
- forward-biased (FB) mode, 19
- Forward Blocking Mode (FBM), 34, 34, 69
- forward braking operation, 463–464
- Forward Conducting Mode (FCM), 34
- forward leakage current, 34
- forward-mode-type switching regulator, 392–393, 393
- forward voltage triggering, 53
- four-coil MIMO circuit, 699
- four-quadrant converter, 107
- four-quadrant operation
 electrical drive, 463–464
 EM, 462
 hoist drive, 463
- FPGAs, *see* field-programmable gate arrays (FPGAs)
- freewheeling/flywheeling diode (FD), 116–117, 179, 218
- frequency-controlled PRC, 434
- frequency modulation control, 220–221
- frequency modulation index, 415
- fuel cell, 611, 616
- fuel-cell-powered electrical drives, 616, 617
- fuel-cell vehicles (FCVs), 591, 593
 drivetrain, 596, 597
 engine-based, 601, 602
 features, 592
- full-bridge SMPS, 399–400, 400, 403
- full HEV, 594, 594
- full-power converter, 645–647, 646
- full-wave-controlled converters, 118, 118
- full-wave rectifier (FWR), 106
- fully controlled converter, 124
- fully controlled rectifiers, 106
- fuzzy-logic controllers, 552, 557–559, 558, 559, 560, 560
- fuzzy-logic DTC (FLDTC), 552–564, 563, 564
- G**
- G2V (grid-to-vehicle), 690, 690
- gate characteristics, thyristors, 38–40, 39
- gate-control circuit, 54

gate protection, 72
gate recovery time, 38
gate triggering, 51–52, 52
gate turn-off (GTO) thyristor, 40
 static V-I characteristics, 40, 41
 switching characteristics, 41, 42
GCC (grid-connected converters), 644–645
GCI (grid-connected inverter), 669–671
gear ratios, 471, 471
gravitational torque, 464
grid-connected converters (GCC), 644–645
grid-connected inverter (GCI), 669–671
grid-connected MG, 678, 686
grid-integrated WT and PV system, 644, 644–645
grid side converter, 653, 654
grid synchronization, 657–668, 682; *see also phase-locked loop (PLL)*
grid-to-vehicle (G2V), 690, 690
grid voltage, *i/p*, 568
group drive system, 461
GTO, *see gate turn-off (GTO) thyristor*

H

H5 SMA single-phase solar PV inverter, 649–650, 650
half-bridge parallel-resonant converter, 433
half-bridge SMPS, 398, 398–399, 403
half-controlled converter, 182
half-controlled rectifiers, 105–106
half-wave rectifier (HWR), 106, 110
harmonic analysis, 566, 570, 571
harmonic factor (HF), 109, 298
harmonic reduction, 334
H-bridge-based boosting PV converter, 648, 648
H-bridge inverter
 NPC, 651, 651–652
 single-stage, 649, 649
 two-stage boost, 648, 649
HERIC single-phase solar PV inverter, 650, 650–651
HEVs, *see hybrid electric vehicles (HEVs)*
high-voltage direct current (HVDC), 8, 13, 297, 625–626
hoist/hoisting load, 466–467, 472
holding current (I_H), 51
HVDC, *see high-voltage direct current (HVDC)*
hybrid electric vehicles (HEVs), 591; *see also electric vehicles (EVs)*
 characteristics, electric traction, 608, 608
 electric-propulsion systems, 607–608
 engine-based, 601, 601
 features, 592
 functions, 593–594, 594
 motor drives selection for, 607–611
 parallel, 593, 595–596, 596

power converter for, 601–606
series, 592, 594–595, 595
series-parallel, 591–592, 593, 596, 597
hybrid microgrid, 680, 681
hybrid modulation technique, 649
hybrid stepper motor, 583, 583–584
hysteresis current-control technique, 413, 413–415, 414
hysteresis modulation, 327

I

ideal dual converters, 136, 136–137
IGBTs, *see insulated-gate bipolar transistors (IGBTs)*
IM, *see induction motor (IM)*
impulse (surge) current rating, 50–51, 98
individual drive system, 461
induction drives, modeling/characteristics, 516–518
induction motor (IM), 456, 551, 608–609
 basics, 513–516, 514, 515
 braking, 524–526
 characteristics, 609
 controllers for, 551–552, 552
 drive parameters, 567
 drive under investigation, 553, 553–562
FLDTC-based MC-FED, 566, 572
integrated circuits, 552, 552–553
single-phase, 487
squirrel cage, 513
stator current, 567
three-phase, *see three-phase IM*
inductive-coupling-based wireless charging system, 702
inductive wireless power transfer (IWPT), 696, 700, 700–701
inertia torque, 470
infrared-emitting diode (IRED), 55
In-Phase Sinusoidal PWM (INSPSPWM), 418
input characteristics, BJT, 24, 24
input current vector, 442, 445, 445, 554, 554
input line/phase voltages, 441
insulated-gate bipolar transistors (IGBTs), 30, 436
 static V-I characteristics, 30
 switching characteristics, 30
 transfer characteristics, 30
 turn-off time, 31
 turn-on time, 30–31
integral cycle control (ICC), *see on-off control*
integrated circuits, 552, 552–553
intelligent module, 9
interline power flow controller (IPFC), 638, 638, 639
internal combustion engine (ICE) vehicle, 591, 593
inverse Park transform, PLL and, 661, 661–663
inversion operation, 195, 195

inversion process, 441
 inverters, 8, 297, 678; *see also specific inverter applications*, 297
 CSI, 297
 force-commutated, 297
 hysteresis current control, 413, 413–415, 414
 internal control, 319
 line-commutated, 297
 performance parameters, 298–299
 PWM, 298
 series-connected, 319
 square wave, 298
 VSI, 297
 inverting regulator, 253
 IPFC, *see interline power flow controller (IPFC)*
 islanding-mode control schemes, 678, 685
 islanding technique, 686–687
 isolated bidirectional DC-DC converters, 604, 604
 IWPT, *see inductive wireless power transfer (IWPT)*

L

latching current (I_L), 51
 LC-filters, 669, 669–670
 LCL-filters, 670, 670–671
 L-filters, 669, 669
 light-activated SCR (LASCR), 53
 light triggering, 53
 linear controllers, 413
 linear *versus* switching power supply, 392
 line-commutated converter, 105
 input side, quantities on, 108–109
 output side, quantities on, 107–108
 performance indices for, 107–110
 line-commutated inverters, 124, 195, 297
 live-shaft drive system, 461
 load(s)
 commutation, 233–234, 303
 conditions, 476
 continuous constant, 468
 continuous variable, 468
 critical, 677
 current, value, 115
 fan-type, 466
 hoisting, 466–467
 impact, 469
 inertia, 476–477
 MG, 677
 pulsating, 468
 short-time, 469
 short-time intermittent, 469
 textile loom, 468
 tier-1/2/3, 677
 torque, 466
 types, 677

load-commutated chopper, 244, 292–293, 727–728
 circuit diagram, 244
 commutating capacitor, 245–247
 current and voltage waveforms, 245
 design considerations, 245
 modes, working, 246
 operation modes, 244
 load torques, 459
 as angle, shaft displacement, 467
 effect, 491–492
 as position function, 466
 varying with time, 468, 468–469
 loop filter (LF), 658, 682
 lowest-order harmonic (LOH), 299

M

magnetic-resonance-based wireless charging system, 702
 magnetic resonance WPT system, 697
 dual and multiterminal, 700
 four-coil, 697
 multiterminal, 697–699
 three-coil, 698
 Mamdani-type fuzzy-logic controller, 557
 MATLAB (MATrix LABoratory), 14
 advantages, 712–713
 defined, 711
 uses, 711
 MATLAB/Simulink simulation
 Class A chopper, 721–723
 Class B chopper, 723–724
 Class C chopper, 724–725
 current-commutated chopper, 728–729
 IPSPWM method, 418
 load-commutated chopper, 727–728
 M-files, 713, 736–748
 POSPWM method, 417
 single-phase full-bridge VSI, 733–734
 single-phase full-wave-controlled rectifier, 716–720
 single-phase full-wave dual converter, 720–721
 single-phase fully controlled rectifier-fed separately excited DC motor drive, 735
 single-phase half-bridge VSI, 729–731
 single-phase half-wave-controlled rectifier, 713–716
 SPWM method, 416
 THISPWM method, 419
 three-phase 180-degree-mode VSI, 731–732
 voltage-commutated chopper, 726–727
 matrix converter (MC), 8–9, 437
 fed IM drive, DTC for, 554, 554–556, 556
 switching configuration, 555
 three-phase AC-AC, 437–439, 438
 maximum power point tracking (MPPT), 643, 646–647

- metal-oxide semiconductor field-effect transistors (MOSFETs), [7](#), [27](#), [391](#)
- M-files (MATLAB functions), [713](#), [736](#)–[748](#)
- microgrid (MG), [675](#), [676](#)
AC, [679](#)–[680](#), [680](#)
advantages, [675](#)
architecture, [679](#)–[681](#)
components, [676](#)
DC, [679](#), [679](#)
DG, *see* distributed generation (DG)
EVs and, *see* electric vehicles (EVs)
grid synchronization, [682](#)–[684](#)
hybrid, [680](#), [681](#)
islanding, [686](#)–[687](#)
loads, [677](#)
power electronics interface, *see* power electronics converters (PECs)
small-signal stability, [685](#)
stability, [684](#)–[686](#), [685](#), [686](#)
storage system in, [681](#)
transient stability, [685](#)–[686](#)
voltage stability, [684](#)
- micro HEV, [594](#), [594](#)
- microsources, [677](#)
- microwave-based wireless charging system, [702](#)
- midpoint cycloconverter, [375](#)–[377](#), [376](#), [382](#)
- mild HEV, [594](#), [594](#)
- MIMO, *see* multiple-input multiple-output (MIMO) circuit
- MISO, *see* multi-input single-output (MISO) circuit
- modulation index, [194](#), [321](#), [415](#)
- modulation techniques, [323](#)
delta, [327](#), [328](#)
harmonic-injected, [326](#)–[327](#), [327](#)
staircase, [325](#), [325](#)
stepped, [326](#), [326](#)
trapezoidal, [324](#), [324](#)–[325](#)
- moment of inertia, [469](#)
equivalent, [471](#)–[472](#)
retardation test, [473](#), [473](#)–[474](#)
- monocrystalline silicon cell, [611](#)
- monopolar HVDC structure, [625](#)
- MOS-controlled thyristors (MCTs), [4](#)
- MOSFETs (metal-oxide semiconductor field-effect transistors), [7](#), [27](#), [391](#)
- motoring mode, [462](#)
- motor load drive system, [469](#), [469](#)
- MPC, *see* multipulse converter (MPC)
- MPPT (maximum power point tracking), [643](#), [646](#)–[647](#)
- multielement resonant converters, [434](#), [434](#)
- multi-input single-output (MISO) circuit, [697](#), [699](#)
- multilevel-cascaded H-bridge VSI, [409](#)
- multilevel inverters, [407](#)–[408](#), [408](#)
CHBMI, [408](#), [408](#)–[410](#)
FCMLI, [411](#)–[412](#), [412](#), [412](#)
- NPC, [410](#)–[411](#)
- multilevel VSC, [407](#)–[408](#)
- multimotor drive system, [461](#)
- multiphase bidirectional DC-DC converters, [605](#), [605](#), [606](#)
- multiple-input multiple-output (MIMO) circuit, [697](#), [699](#)
- multiple PWM, [321](#)–[322](#), [322](#)
- multipulse converter (MPC), [405](#)–[407](#), [406](#)
- multispeed drive, [464](#)
- multistack variable-reluctance stepper motor, [582](#)
- multistring configuration, PV system in, [646](#), [647](#)
- multiterminal WPT system, [697](#)–[699](#)
- N**
- n*-coil relay circuit, [700](#)
- neutral point clamped (NPC)
H-bridge inverter, [651](#), [651](#)–[652](#)
multilevel inverter, [410](#)–[411](#)
topology, [651](#)
- Nikola Tesla, [695](#)
- nonisolated bidirectional DC-DC converter, [602](#)–[604](#), [605](#)
- nonlinear controllers, [413](#)
- nonradiative WPT technology, [701](#)
- normalized average output voltage, [131](#)–[132](#), [135](#)
- NPC, *see* neutral point clamped (NPC)
- npn* type semiconductor, [23](#), [23](#)
- O**
- 180-degree conduction-mode inverter, [305](#)–[310](#), [306](#), [307](#), [314](#)
- one-quadrant converter, [179](#)
- 120-degree mode VSI, three-phase, [310](#)–[314](#), [311](#), [312](#)
- online electric vehicle, WPT system in, [705](#)
- online simulation, [14](#)
- on-off control, [357](#)–[360](#), [358](#)
- optimum voltage vector, [445](#)
- optoisolators, [55](#)
- output characteristics
BJT, [24](#), [24](#), [25](#)
IGBT, [30](#)
power MOSFETs, [28](#), [28](#)
- output harmonics, reduction, [379](#), [380](#), [385](#)–[386](#)
- output line voltage, [447](#)
- output phase voltage, [447](#)
- output voltage vector, [445](#), [554](#)
- overcurrent, [68](#)–[69](#)
- overlap period/angle (μ), [144](#)–[147](#)
- overvoltage, [67](#)–[68](#)

P

parallel-connected SCRs, 65–66, 66
 parallel HEV, 593, 595–596, 596
 parallel-loaded resonant converter, 430
 parallel resonant converter (PRC), 433–434
 passive islanding detection, 687
 passive torque, 459
 peak inverse voltage (PIV), thyristor, 113–114, 120, 122
 PECs, *see power electronics converters (PECs)*
 permanent-magnet (PM) motors, 582, 582–583
 brushless motors, 609, 610
 PF, *see power factor (PF)*
 phase-angle control (PAC), 188
 phase control, 109, 110, 360–361
 phase-controlled line-commutated converter, 654
 phase-controlled rectifiers, 8, 107
 classifications, 105–107
 dual converters, 135–144
 line-commutated converter, performance indices for, 107–110
 overview, 105
 single-phase converters, 110–129
 source impedance, effects, 144–147
 three-phase converters, 129–135
 phase detector (PD), 658, 682
 phase displacement, 334
 phase-locked loop (PLL), 657, 678, 682, 682
 equations, 658–659
 inverse Park transform and, 661, 661–663
 linearized small-signal model, 659–660
 SOGI, 663–666
 SOGI-QSG, 666–668
 structure, 657, 658
 T/4 transport delay, 660–661, 661
 phase-opposition sinusoidal PWM (POSPWM), 417
 P-HEVs (plug-in HEVs), 591, 594, 594
 photovoltaic (PV) system
 array, 611–614, 613
 grid-integrated WT and, 644, 644–645
 grid requirements for, 656–657
 inverter, 648–652
 inverter design parameters for, 657
 topologies, 646, 646–647
 piece-wise linear electrical circuit simulation (PLECS), 13
 PIV (peak inverse voltage), thyristor, 113–114, 120, 122
 planar diffused method, 47, 48
 PLL, *see phase-locked loop (PLL)*
 plugging, 525, 526
 plug-in HEVs (P-HEVs), 591, 594, 594
 PM, *see permanent-magnet (PM) motors*
 pnp type semiconductor, 23, 23
 point of common coupling (PCC), 676

pole-amplitude modulation, 524
 pole-changing drive, 523
 polycrystalline silicon cells, 611
 power circuit diagrams, 488, 489
 power converter switching techniques
 inverters, hysteresis current control, 413, 413–415, 414
 PWM technique, 415–426
 power diodes, 17–19, 18
 reverse recovery characteristics, 19–21, 20
 working and V-I characteristics, 19
 power electronics, 3–4, 623, 687
 applications, 10–11
 block diagram, 4
 circuits, computer simulation, 11–14
 control, energy and, 4
 definition, 3
 demerits, 10
 modules, 9–10
 power generation, 640, 640
 power electronics converters (PECs), 7–9, 640, 677, 682, 687
 for AC motor drives, 606–607
 boost converter, 647, 647–648
 DC-AC converters, 678, 678
 DC-DC converters, 602–606, 677, 678
 for DC motor drives, 606
 for EVs, 601–606
 full-power converter, 645–647, 646
 interconnection with medium-voltage grid, 684
 for renewable energy integration, 643–652
 variable-speed DFIG, 645, 645
 power factor (PF), 109, 188
 EAC, 188–190
 input, 112–113, 385
 PWM control, 192–193, 193
 SAC, 190–192, 191
 SPWM, 194, 194–195
 power flow control mechanism, active/reactive, 626, 626
 power module, 9
 power MOSFETs, 7, 27
 versus BJT, 29
 circuit diagram, 28
 output characteristics, 28, 28
 switching characteristics, 28–29, 29
 transfer characteristics, 27, 28
 turn-off time, 28–29
 turn-on time, 28
 power semiconductor devices, 4, 5–6, 7, 10
 categorization, 18
 overview, 17
 power SIM (PSIM), 13
 power systems computer-aided design (PSCAD), 13
 power transfer efficiency (PTE), 704

- power transistors, characteristics, 23
 BJT, 23–27
 IGBT, 30–31
 power MOSFETs, 27–29
 practical dual converters, 137–139
 protection of SCR, 67, 68
 di/dt , 72
 dv/dt , 69–71
 gate, 72
 overcurrent, 68–69
 overvoltage, 67–68
 PSPICE tool, 13
 pulsating loads, 468
 pulse transformer, 55
 pulse-width modulation (PWM), 217, 221, 298, 320, 391, 551
 controls, 8–9, 192–193, 193, 215
 multiple, 321–322, 322
 single, 320, 321
 sinusoidal, 322–323, 323
 push-pull SMPS, 397, 397–398, 403
 PV, *see photovoltaic (PV) system*
 PV inverter, 648
 conergy NPC inverter, 652, 652
 H5 SMA single-phase solar, 649–650, 650
 H-bridge-based boosting PV converter, 648, 648
 HERIC single-phase solar, 650, 650–651
 NPC H-bridge inverter, 651, 651–652
 single-stage H-bridge inverter, 649, 649
 two-stage boost H-bridge inverter, 648, 649
 PWM, *see pulse-width modulation (PWM)*
 PWM techniques, 415
 IPSPWM, 418
 POSPWM, 417
 space vector, 440–445
 SPWM, 416, 416
 THISPWM, 418–419
 three-phase two-level SVPWM, 420–426
- Q**
- quadrant operation, drive, 462–463; *see also chopper configurations; four-quadrant operation*
 quadrature signal generator (QSG), 660, 662, 663, 664
 quasi-resonant converters, 430, 431
- R**
- radiative WPT technology, 701
 rectification process, 441
 rectifiers, 107; *see also specific rectifiers*
 controllability, 105–106
 diodes, 7
 fully controlled, 106
- half-controlled, 105–106
 half-wave, 110
 input waveform, 106
 output voltage waveform, pulses in, 106
 phase-controlled, 8
 phases, input voltage, 106
 quadrant operation, 106–107, 107
 semiconverter, 105–106
 single-phase one-pulse, 111
 single-quadrant, 106, 107
 two-quadrant, 106, 107
 uncontrolled, 105
 V-I characteristics, 106–107
 reference speed reversal, 562, 564, 564, 565
 regeneration, 124
 regenerative braking, 502, 502–503, 524–525, 525
 relay circuit, 700, 700
 renewable energy-generation system, 640, 640
 resistance-capacitance (RC) triggering circuit, 58
 full-wave circuit, 59, 59–60, 60, 99
 half-wave circuit, 58, 58–59, 99
 resistance (R) triggering circuit, 55, 55–57, 57, 99
 resonant converters, 426–434
 resonant DC power supplies, 400–401, 401
 resonant load converters, 429–430
 resonant pulse inverters, 400
 resonant switch converters, 430–431
 resonant transition converter, 432, 433
 reverse-biased (RB) mode, 19
 Reverse Blocking Mode (RBM), 34, 34
 reverse braking, 463
 reverse breakdown voltage, 34
 reverse recovery time, 19, 37
 Ripple Factor (RF), 108, 233
 rise time
 BJT, 26
 IGBT, 31
 power MOSFET, 28
 thyristor, 36
 root mean square (RMS), 108
 load current, 112
 load voltage, 112, 114, 117
 output voltage, 120, 122, 131, 135, 182
 rotor circuit
 adding resistance in, 521–522, 522
 voltage injection in, 523, 523, 533, 533–535
 rotor position sensors, 578
 rotor-resistance control, 532–533, 533
- S**
- SABER tool, 14
 SCRs, *see silicon-controlled rectifiers (SCRs)*
 second-order generalized integrator (SOGI), 663–666
 PLL, 667, 667, 668
 QSG, 666–667, 667

- self-controlled mode, 578, 579
 semiconverters, 179
 - asymmetrical, 179, 180
 - circuit, 180–181
 - quadrant operation, 179
 - rectifiers, 105–106
 - single-phase, *see* single-phase semiconverter, RL load
 - symmetrical, 179, 180
 - three-phase semiconverter with RL load, 186, 186–187
- separately excited DC motor, 488–489, 489
 series-connected inverters, 319
 series-connected SCRs, 63, 63, 64
 - dynamic equalizing circuit, 64–65
 - static equalizing circuit, 63–64
- series HEV, 592, 594–595, 595
 series-loaded resonant converter, 430
 series-parallel HEV, 591–592, 593, 596, 597
 series-parallel hybrid converter, 434
 series resonant converter (SRC), 434
 seven-segment switching sequence, 425, 425
 silicon-controlled rectifiers (SCRs), 4, 47, 377
 - alloy diffused, 48, 48
 - construction, 47
 - construction and structure, 48
 - converter- and inverter-grade, 38, 38
 - current ratings, 50–51
 - firing (triggering) circuits for, 54, 54–62
 - by gate triggering, requirements, 76–77
 - parallel-connected, 65–66, 66
 - planer diffused, 47, 48
 - protection, 67–72, 68
 - series and parallel operation, 62–66
 - series-connected, 63, 63–65, 64
 - specifications and ratings, 49
 - string efficiency, 66–67
 - transistors *versus*, 88–89
 - turn on, methods, 51–53
 - voltage ratings, 49–50, 50
- simulation, 12; *see also* computer simulation; power electronics circuits; MATLAB/Simulink simulation
 - online, 14
 - tools, 13–14
- Simulink, 13–14; *see also* MATLAB/Simulink simulation
- single-band hysteresis controller, 415, 415
 single-band hysteresis current control (SBHCC), 413
 single-input multiple-output (SIMO) circuit, 697, 698
- single-phase
 - AC voltage controllers, 358, 361–365
 - converters, 110–129
 - CSIs, 315, 315–316
 - DAB converter, 435, 435
 - dual converter, 139–142, 140, 176
 - full converter, 215
 - full-wave-controlled rectifier, 716–720
 - full-wave dual converter, 720–721
 - half-bridge inverter, VSI, 299, 300, 729–731
 - IM, 487
 - one-pulse rectifier, 111
 - TCR, 628
 - TSC, 628
 - two-pulse rectifier, 179
 - single-phase full-bridge inverter, VSI, 299–301, 301
 - Fourier analysis, 303–304
 - load voltage and current waveforms, 302
 - MATLAB, 733–734
 - with RL and RLC overdamped loads, 303
 - with RLC underdamped loads, 303
 - single-phase full-wave-controlled converter, 118
 - bridge-type-controlled rectifier with RL load, 122–125, 175
 - bridge-type-controlled rectifier with R load, 121, 121–122
 - mid-point rectifier with R load, 119, 119–120, 175
 - with RLE load and discontinuous conduction, 128, 128–129
 - single-phase fully controlled rectifier
 - fed separately excited DC motor drive, 735
 - with source/load inductance, 144–147, 145, 176
 - single-phase half-wave-controlled rectifier
 - with RLE load, 125–128, 126
 - with RL load, 113, 113–116, 174, 714–715
 - with RL load and FD, 116, 116–117, 175, 715–716
 - with R load, 110, 110–113, 174, 713–714, 716–717
 - single-phase inverters, voltage control, 318
 - AC output, external control, 318–319
 - input DC, 318, 319
 - internal control, 319
 - single-phase semiconverter, RL load
 - continuous conduction, 180–182, 214
 - discontinuous conduction, 183, 183–185, 184
 - single-phase to single-phase cycloconverter
 - bridge-type, 376, 377–378
 - midpoint, 375–377, 376
 - single-phase to single-phase step-down cycloconverter
 - bridge-type, 376, 378–379
 - midpoint, 376, 379, 380, 380
 - single-phase VSIs, 299
 - full-bridge inverter, 299–304, 301
 - half-bridge inverter, 299, 300
 - single PWM, 320, 321
 - single-quadrant converter, 105–106, 182
 - single-quadrant drive, 497
 - single-quadrant rectifier, 106

- single-speed drive, 464
single-stack variable-reluctance motor, 581, 581
single-stage H-bridge inverter, 649, 649
sinusoidal output voltage, 380, 381
sinusoidal pulse-width modulation (SPWM)
 technique, 322–323, 323, 415–416
 control, 194, 194–195, 215
 switching pulses, 416
six-phase generator, 655, 656
six-step bridge inverter, 306
slip power control, 535
 static Kramer drive, 543, 543
 static rotor-resistance control, 535–539, 539
 static Scherbius drive, 539–542, 540, 541, 542
slip regulators, 458
smart grid applications, 687, 688
smart-power, 9
SMPC (Switched Mode Power Conversion),
 432, 432
SMPS, *see* Switched-Mode Power Supply (SMPS)
snubber circuits, 67, 70, 427
 design, 70, 70–71, 100
 switching trajectory with, 429
softness factor/S-factor, 20
soft-switching inverters, 607
soft-switching topologies, 428
 flyback converter, 431
 multilevel resonant converters, 434
 phase-shift bridge, 432–433
 PRC, 433–434
 resonant load converters, 429–430
 resonant switch converters, 430–431
 SMPC, 432, 432
 trajectory, 430
SOGI, *see* second-order generalized integrator
 (SOGI)
solar-based EV, 614–615, 615
solar-based pump system, 615, 615–616
solar cells, 611
solar photovoltaic (SPV) technology, 611
solar-powered variable-speed drive, 614–616
solenoid-based WPT system, 706, 706
source impedance, 144–147
space vector algorithm, 442
space vector modulation, 328–333, 329, 333
space vector pulse-width modulation
 (SVPWM), 440–445, 443, 444,
 446, 551
speed control, DC motors, 492
speed-torque characteristics, 532
spiral-based WPT system, 706, 706–707, 707
spread time, thyristor, 36
SPWM, *see* sinusoidal pulse-width modulation
 (SPWM) technique
square wave inverters, 298
squirrel cage IM, 513
SRM (switched reluctance motor), 610, 611
STATCOM, *see* static synchronous compensator
 (STATCOM)
static Kramer drive, 543, 543
static rotor-resistance control, 535–539, 539
static Scherbius drive, 539–542, 540, 541, 542
static switches, 9
static synchronous compensator (STATCOM),
 627, 629, 630
 modeling, 634, 634–635
 voltage-current characteristic, 630
static VAR compensator, 627
static V-I characteristics; *see also* V-I
 characteristics
 GTO thyristor, 40, 41
 IGBT, 30
 thyristors, 33, 33–34
stator circuit, adding impedance, 521, 522
stator voltage control method, 527,
 527–528, 528
steady-state characteristics, 24, 24–25, 25
steady-state ripple, 231
step-down cycloconverter, 378
step load, transients, 568
stepper motor, 579–580
step-up cycloconverter, waveforms, 377
 continuous load current, 380
 discontinuous conduction, 379
step up/down chopper, 222, 222–223,
 291–292
storage time, GTO, 41
string configuration, PV system in, 646, 647
string efficiency, 66–67, 100
supply voltage, varying, 519, 520
SVPWM, *see* space vector pulse-width
 modulation (SVPWM)
Switched Mode Power Conversion (SMPC),
 432, 432
Switched-Mode Power Supply (SMPS)
 flyback, 395, 396, 397
 full-bridge, 399–400, 400
 half-bridge, 398, 398–399
 push-pull, 397, 397–398
 working, 391–394
switched-mode regulators, 247
 boost (step-up) converter, 251, 251–253
 buck-boost converter, 253–254,
 253–256
 buck (step-down) converter, 247–251, 248
 cuk regulator, 257–258, 257–260
switched reluctance motor (SRM), 610, 611
switching characteristics
 BJTs, 25–27, 26
 GTO, 41, 42
 IGBT, 30
 power MOSFETs, 28–29, 29
 thyristors, 35–38
switching circuits, 458

- switching frequency (SF), 413
 switching patterns, 330, 331, 332, 333
 switching pulses method
 IPSPWM, 418
 POSPWM, 417
 SPWM, 416
 THISPWM, 419
 switching sequence, 425
 switching states, 420, 421
 switching trajectory, 428
 switching waveforms, 428
 switch voltage/current waveforms, 431
 symmetrical angle control (SAC), 190–192, 191, 214
 synchronous generator, 655, 656
 synchronous motors, 456, 575–577, 576, 609
 speed control, 578
 speed-torque/torque-angle characteristics, 577
- T**
- T/4 transport delay, 662–663, 663
 tail time, GTO, 41
 TCSC, *see* thyristor-controlled series compensator (TCSC)
 temperature triggering, 53
 THD, *see* total harmonic distortion (THD)
 thermal runaway, 65
 third-harmonic injection sinusoidal PWM (THISPWM), 418–419
 three-coil
 MISO circuit, 699
 resonating WPT system, 702, 702–705
 SIMO circuit, 698
 three-phase
 AC-AC MC, 437–439, 438
 bridge-type cycloconverter, 383
 CSIs, 316, 317
 dual converters, 142–144, 143
 full converter, 133–135, 133, 176
 full-wave AC voltage controllers, 366, 667
 half-wave cycloconverter, 382
 motor, no-load current, 518
 180-degree-mode VSI, 731–732
 semiconverter, RL load, 186, 186–187, 214
 to single-phase cycloconverter, 380–382, 381
 six-pulse converter, 133
 to three-phase cycloconverter, 382–384, 383
 two-level SVPWM, 420–426
 three-phase converters, 129
 full converter, 133–135, 133
 with RL load, 129–132, 130, 175–176
 three-phase IM, 513
 equivalent circuit, 516
 modifying torque-speed characteristics, 519–524
 speed control, 527–535
 starting performance, 518–519
 three-phase three-level (TPTL), 410
 three-phase VSI bridge inverters, 304–305, 305
 180-degree mode, 305–310
 120-degree mode, 310–314
 three-pulse converter, 129
 thyristor-controlled series compensator (TCSC), 627, 629–631, 631
 thyristors, 7, 17, 297, 378, 497
 characteristics, 32, 32–33
 commutation methods, 105
 gate characteristics, 38–40, 39
 GTO, 40–42
 hard firing/overdriving, 37
 methods, 44
 static V-I characteristics, 33, 33–34
 switching characteristics, 35–38
 trigger circuit, 39
 turn-off time, 35, 37–38
 turn-on time, 35, 35–36
 two-transistor model, 42, 42–44, 44
 Thyristor-Switched Capacitor (TSC), 627–629
 time ratio control (TRC), 220–221
 toolboxes, MATLAB, 713
 torque-speed characteristic, 610, 611
 total harmonic distortion (THD), 298, 406, 426, 564
 TPTL-NPC MLI topology, 410, 411
 transfer characteristics
 IGBT, 30
 power MOSFETs, 27, 28
 transformer utilization factor (TUF), 109
 transient stability, 524
 transistor-controlled reactor (TCR), 627–628
 transistors *versus* SCR, 88–89
 trapezoidal modulation, 324, 324–325
 trapezoidal speed-time curve, 477
 TRC (time ratio control), 220–221
 TRIAC, 22, 22–23
 triangular factor, 324
 triangular speed-time curve, 476
 true synchronous mode, 578, 578
 TSC (Thyristor-Switched Capacitor), 627–629
 TUF (transformer utilization factor), 109
 turn-off snubber, 427, 429
 turn-off time
 BJTs, 26–27
 GTO, 41
 IGBT, 31
 power MOSFETs, 28–29
 thyristors, 35, 37–38
 turn on methods, SCR, 51
 dv/dt triggering, 53
 forward voltage triggering, 53

- gate triggering, 51–52, 52
light triggering, 53
temperature triggering, 53
turn-on snubber, 429
turn-on time
 BJTs, 25–26
 GTO, 41
 IGBT, 30–31
 power MOSFETs, 28
 thyristors, 35, 35–36
12-pulse AC-DC converters, 405–406, 406
24-pulse AC-DC converters, 406–407, 407
two-coil WPT, 695–696
two-level back-to-back CSI/VSI, 653, 655
two-level inverter, space vector, 421
two-quadrant converter, 106, 124
two-quadrant drive, 494
two-quadrant rectifier, 106, 107
2Q-ZVS-MR converter, 606
two-stage boost H-bridge inverter, 648, 649
two-transistor model, 42, 42–44, 44
type-A (step-down) chopper analysis
 with resistive load, 227, 227–228
 with RLE load, 228–233, 229
- U**
- UJT, *see* uni-junction transistor (UJT)
uncontrolled rectifiers, 105
unidirectional AC-DC converters, 405
unidirectional battery chargers, 690, 690
unidirectional buck converter, 602
unified power flow controller (UPFC), 627, 631, 632
unified power quality conditioners (UPQC), 639, 639–640
uniform pulse width modulation (UPWM), 321
uni-junction transistor (UJT), 61, 61–62, 99–100
uninterruptible power supplies (UPS), 297
unipolar drive circuits, 584, 584
unipolar modulation technique, 649
UPFC, *see* unified power flow controller (UPFC)
UPQC, *see* unified power quality conditioners (UPQC)
utility grid, 682, 686
- V**
- V2G, *see* vehicle-to-grid (V2G) interconnection
variable-frequency control method, 528–531, 531, 532
variable frequency system, 220, 221
variable-frequency variable-source (VFVS), 531
variable impedances, 458
- variable-reluctance motor, 580–581
 advantages, 582
 multistack, 582
 single-stack, 581, 581
variable-speed drives (VSDs), 457, 464, 551
vehicle-to-grid (V2G) interconnection, 688–689, 689
Very High Speed Integrated Circuit
 Hardware Description Language (VHDL), 559
- V-I characteristics
 DIAC, 22
 IGBT static, 30
 practical and ideal, 18
 rectifiers, 106–107
 thyristors static, 33, 33–34
 TRIAC, 22
 UJT, 61, 62
 working and, 19
- virtual test bed (VTB), 14
voltage-clamping (VC) device, 67–68, 68
voltage-commutated chopper, 234–240, 235, 236, 237, 292, 726–727
voltage-controlled oscillator (VCO), 658, 682
voltage injection, 523, 523
voltage ratings, SCR, 49–50, 50
voltage source converter (VSC), 407–408, 653, 654
voltage source inverters (VSIs), 297, 299, 554, 633
 versus CSIs, 317–318
 single-phase, 299–304
 three-phase, 304–314, 305
 three-phase two-level, 420
 two-level back-to-back, 653, 655
VSC, *see* voltage source converter (VSC)
VSDs, *see* variable-speed drives (VSDs)
VSIs, *see* voltage source inverters (VSIs)
- W**
- WebMATHEMATICA package, 14
wind turbine (WT), 644
 converter for DFIG, 645, 645
 full-power converter for, 645–647, 646
 grid converter for, 652–656
 grid-integrated PV and, 644, 644–645
 grid requirements for, 656–657
 inverter design parameters for, 657
wind turbine generators (WTGs), 656–657
wireless charging system, 695, 702
wireless power transfer (WPT) system, 695
 DF coil, 696, 696
 efficiency, 708, 708
 IWPT, 700, 700–701
 magnetic resonance, 697–700

wireless power transfer (WPT) system
(Continued)
model, 695–696
in online electric vehicle, 705
radiative and nonradiative, 701
solenoid-based, 706, 706
spiral-based, 706, 706–707, 707
three-coil resonating, 702, 702–705
two-coil, 695–696

wound-rotor induction-motor, 513, 535
WPT, *see* wireless power transfer (WPT) system
WT, *see* wind turbine (WT)
WTGs (wind turbine generators), 556–557

Z

zero-current switching (ZCS), 428–430, 430
zero-voltage switching (ZVS), 357, 428–430, 430